MAAP 3.0B Code Evaluation

Final Report

J. U. Valente and J. W. Yang

Safety and Risk Evaluation Division
Department of Nuclear Energy
Brookhaven National Laboratory
Upton, New York 11973

October 1992

Prepared for
U. S. Nuclear Regulatory Commission
Washington, DC 20555

FIN L-1499

Abstract

This report describes the NRC sponsored review of the MAAP code, version 3.0B. The primary objective of the review was to evaluate the MAAP code for its use in conjunction with activities related to performance of an IPE for operating reactors.

The review focuses on those aspects of an IPE that will be addressed with MAAP analyses, namely determination of success criteria, the timing of key events, and containment response to severe accident loads. An important finding of the review was that in general, MAAP is adequate for predicting thermal-hydraulic behavior prior to clad damage. However, as the MAAP models contain a number of simplifications, the utilities should provide justification for using MAAP if certain thermal-hydraulic conditions, listed in the report, are encountered.

The review confirmed that the utilities should not use MAAP for determining success criteria after clad damage. After clad damage MAAP should be used to provide the utility with a framework for obtaining an understanding of containment failure modes, the impact of phenomena and plant features, as well as operator actions. In this role, MAAP analyses should be supplemented with sensitivity studies to ensure that the utility staff have an appreciation of the uncertainties surrounding containment performance during a severe accident. The review of this aspect of MAAP's application to an IPE focused on the adequacy of the range of parameters previously recommended for the sensitivity analysis.

The ranges of parameters previously recommended for MAAP sensitivity analysis by MAAP developers were generally found to be adequate for reflecting the uncertainty surrounding severe accident issues. However, there are a number of areas where added or enhanced sensitivity cases beyond those previously recommended could provide the utility with a more complete appreciation of the conditions which may be encountered during a severe accident. These added or enhanced cases are described in the main text of this report and summarized in the executive summary.

Table of Contents

Table of Contents (Continued)

Executive Summary

Background and Objective

The Modular Accident Analysis Program (MAAP) computer code was developed as part of the industry response to the post TMI-2 NRC initiatives related to severe accidents at nuclear power reactors. This development effort, undertaken in conjunction with the Industry Degraded Core Rulemaking (IDCOR) Program, was directed at providing industry with the broad analytical capability necessary to predict the progression of severe accidents. An early version of the MAAP code was used to predict containment response and environmental source terms for several accident sequences in a number of Boiling Water Reactor (BWR) and Pressurized Water Reactor (PWR) plants as part of the IDCOR program. The results of these calculations and available experimental data formed the basis for several technical meetings between the NRC and IDCOR. As a result of these meetings, in which the predictions of MAAP were compared with calculations performed by NRC sponsored codes and experimental data, a number of NRC/IDCOR Technical Issues were developed. These issues identified areas of significant phenomena, which involve considerable uncertainty, and where differences between the NRC sponsored codes and MAAP were observed. These issues together with other considerations guided the development of subsequent revisions of the MAAP code and also NRC sponsored codes.

In the Commission policy statement on severe accidents in nuclear plants, issued on August 8, 1985, (50 FR 32138), the Commission concluded that systematic evaluations are beneficial in identifying plant-specific vulnerabilities to severe accidents that could be fixed with low-cost improvements. With that in mind, the Commission directed the staff to develop an approach to be implemented by utilities in performing plant specific evaluations. In response to the Commission directive, the staff issued to utilities Generic Letter 88-20 [E1], outlining the elements of the Individual Plant Examination (IPE) program. NUREG-1335 "Individual Plant Examinations Submittal Guidance" [E2] was subsequently issued to aid the utilities in formulating their response to the generic letter.

It is now evident that industry analysis of a particular plant response to severe accidents and the associated phenomena, performed as part of the IPE program, will in part be based on MAAP code calculations. The NRC staff therefore decided to undertake a review of the MAAP code using the assistance of Brookhaven National Laboratory (BNL). The review was intended to provide assurance that industry-generated IPEs, at least to the extent practicable, represent reasonable estimations of the progression of severe accident sequences and the plant response to these sequences. The current version of MAAP is sponsored by EPRI, with developmental activities being pursued by Fauske Associates Incorporated (FAI) and Gabor, Kenton, & Associates (GKA).

This report describes the NRC sponsored review of the MAAP code, version 3.0B [E3]. Specifically, revision 7.0 for BWRs and revision 17.0 for PWRs were reviewed. The primary objective of the review was to evaluate the MAAP code for its use in conjunction with activities related to performance of an IPE for operating reactors. Therefore, the review considered the guidance provided by GKA regarding sensitivity analyses for IPEs using MAAP 3.0B [E4]. MAAP was evaluated to provide assurance that IPEs will be analyzed with a methodology which adequately treats significant phenomena and reflects the uncertainty surrounding issues for which confirmatory research is planned or ongoing.

Review Approach

Chronologically, the review was performed in three phases. The study began with a review of the models used in MAAP based on the available documentation. Initially, the documentation supplied by the Electric Power Research Institute (EPRI) was for MAAP 3.0 and consisted of a two-volume User's Manual. In addition, there was an attachment consisting of descriptions of new subroutines added to MAAP 3.0 to create MAAP 3.0B. Subsequently, a new manual for MAAP 3.0B was issued. Three familiarization meetings between EPRI and NRC staff and its contractor, BNL, were convened. The first meeting concentrated on in-vessel phenomena, the second on ex-vessel severe accident progression and containment performance. The third emphasized the secondary containment models, and presented the MAAP Design Review [E5] performed under the sponsorship of EPRI. Responses to questions asked by NRC/BNL during these meetings were provided by Nuclear Management and Resources Council (NUMARC).

The second phase consisted of performing calculations with the MAAP and MELCOR [E6] codes for two severe accident sequences, a Loss of All Electric Power Sequence in a BWR (Peach Bottom) and a Small Break LOCA in a PWR (Zion). A meeting was held between industry representatives and NRC staff to determine how the numerical comparisons between MAAP and MELCOR were to be made. Subsequent meetings between Fauske and Associates, Incorporated (FAI) and BNL helped to standardize the input deck descriptions. MELCOR calculations were made by BNL staff. MAAP calculations were carried out by FAI and the results forwarded to BNL. A consensus was reached on further MAAP calculations that should be made (sensitivity runs) to help explain the differences observed in the MAAP-MELCOR base comparisons.

Consequently the third phase focused on performing a series of sensitivity calculations with MAAP, conducted by FAI, in order to assess the effect of varying a number of model parameters.

The assessment of the MAAP code relied on available state of the art information regarding severe accident phenomena. The BNL reviewers were familiar with past and ongoing efforts in the reactor safety community to refine understanding of the events which could potentially occur in a severe accident. Wherever possible, experimental data related to the particular phenomenon under consideration was included in the evaluation of the code modeling. Clearly however, there are still many aspects of severe accident conditions, and containment performance under these conditions, for which data is lacking. To some degree, sensitivity analyses can be used to account for uncertainty in basic modeling assumptions. The appropriateness of the range of these sensitivity analyses was again based on available data, and comparison against other modeling approaches. Comparing MAAP results with MELCOR calculations for the same initial conditions also helped in establishing sensitivity ranges, since MELCOR represents an attempt, independent from MAAP, to integrate available information into a consistent model for severe accidents.

Review Findings

The review focuses on those aspects of an IPE that will be addressed with MAAP analyses, namely determination of success criteria, the timing of key events and containment phenomena related to severe accidents. Utilities may wish to use MAAP to predict the time from accident initiation to the time of clad damage for the purposes of determining success criteria for quantification of the Level 1 (core damage frequency estimate) part of an IPE. Thus an important aspect of the review was to determine how well MAAP models the loss of coolant inventory for a range of initiating events (i.e., transients or LOCAs). An important finding of the review was that in general, MAAP is adequate for predicting thermal-hydraulic behavior prior to clad damage unless certain thermal-hydraulic conditions are encountered. These are:

1. The break location gives rise to a quasi-steady state two-phase flow condition (BWR/PWR).
2. The RPV water level and vessel flow conditions may expose the fuel to departure from nucleate boiling (DNB) conditions while MAAP continues to predict adequate core cooling (BWR).
3. The reactor has not scrammed (fuel stored energy will not be released) (BWR/PWR).
4. Clad temperature is above 1200°K (BWR/PWR).

(Additional details are provided in Section 2.1.) As the MAAP models contain a number of simplifications, the utilities should provide justification for using MAAP if these thermal-hydraulic conditions are encountered.

The review confirmed that the utilities should not use MAAP for determining success criteria after clad damage (e.g., to determine whether or not a core can be successfully reflooded after extensive fuel melting has occurred). Therefore, after clad damage MAAP should be used to provide the utility with a framework for obtaining an understanding of containment failure modes, the impact of phenomena and plant features, as well as operator actions. In this role, MAAP analyses should be supplemented with sensitivity studies to ensure that the utility staff has an appreciation of the uncertainties surrounding containment performance during a severe accident. Therefore, the review of this aspect of MAAP's application to an IPE focused on the adequacy of the range of parameters recommended [E4] for the sensitivity analysis.

It should be noted that, even with extreme variations of the parameters available in MAAP, some severe accident phenomena cannot be addressed. An example is the potential for local detonation which strongly depends on gas mixing, i.e., stratification and local concentration of detonable gases. Because of its fixed coarse containment nodalization and fixed flow paths, MAAP cannot address these issues. This is recognized in the MAAP guidance document. Another example is direct containment heating (DCH), which is not modelled for BWRs and is treated with a parametric model for PWRs. In accordance with GL88-20, quantification of DCH in an IPE is not required. Therefore, we have not judged the adequacy of the MAAP DCH model.

The ranges of parameters recommended [E4] for MAAP sensitivity analyses were generally found to be adequate for reflecting the uncertainty surrounding severe accident issues. However, there are a number of areas where added or augmented sensitivity cases (beyond those recommended in Reference E4) are recommended. These recommendations are based on an examination of available MAAP sensitivity analyses, limited comparison with MELCOR, and consideration of phenomenological uncertainties. We believe that these recommendations will provide the utility with a more complete appreciation of the conditions which may be encountered during severe accidents. However, the synergistic effects associated with severe accident behavior make it difficult to ensure that all important sensitivities can be forecast for the entire spectrum of severe accidents. These additional sensitivity cases are in the following six areas: [Note: other recommendations, insights, etc. are contained in Section 2]

1. In the area of in-vessel hydrogen generation, Reference E4 makes different recommendations for the BWR and PWR versions of MAAP. For the PWR version of MAAP, no blockage (FCRBLK=0) and single-sided clad oxidation were recommended. The PWR model, however, considers the effect of accumulated material on flow area and can thereby block flow. The PWR model also includes consideration of clad ballooning. These input options were judged to be adequate and no additional sensitivity cases were recommended for the PWR version of MAAP. However, for the BWR version, local blockage (FCRBLK=0) and single-sided clad oxidation were recommended. Clad ballooning is not modeled. Therefore, for the BWR version of MAAP it was considered prudent to (1) recommend a base case with single sided clad oxidation and no local blockage (FCRBLK = -1), (2) use the single sided clad oxidation with local blockage as a sensitivity case, and (3) add a second sensitivity case with no local blockage and double-sided clad oxidation to provide an upper bound on the potential for in-vessel hydrogen generation.

2. In-vessel core relocation is an area of significant uncertainty and Reference E4 recommends sensitivity cases to address this important issue. Sensitivity studies with the PWR version of MAAP for a model parameter, (which represents the eutectic heat of fusion of the core materials) showed that it can have a significant impact on debris distribution between the reactor core, the cavity, and the lower containment compartment after reactor vessel failure. One of the sensitivity cases, calculated in Reference E7 but not recommended in E4, showed that all of the core debris would be released from the vessel compared with about 70% of the core in the base case and that the time to containment failure was reduced by several hours [E7]. Because of the apparent

sensitivity of this parameter, a MAAP calculation should be performed using the upper value of the uncertainty range suggested in the MAAP sensitivity study [E7]. Limited sensitivity studies with the eutectic heat of fusion parameter, previously carried out with the BWR version of MAAP did not indicate as significant a sensitivity as was found for PWRs. Moreover, for BWRs, this sensitivity calculation is believed to be covered by other BWR recommended sensitivities. However, because (1) the eutectic heat of fusion is a true physical uncertainty, (2) not all BWR containment types and accident scenarios were investigated in detail to ascertain this parameter's quantitative significance, and (3) for the sake of consistency, this sensitivity calculation is also recommended for BWRs. A further sensitivity case regarding core relocation also applies to both BWRs and PWRs. Reference [E4] recommends that the core melt fraction necessary to transport all the core material from the vessel at RPV failure be varied as a sensitivity case for at least one sequence in IPEs performed for BWRs and PWRs. Given the potential sensitivity of this modeling assumption it is recommended that this sensitivity be performed for each of the representative sequences in an IPE in which the RPV fails before the containment does.

3. Sensitivity studies with the PWR version of MAAP [E7] showed that during sequences where the reactor coolant system (RCS) remains at high pressure, changing the in-vessel natural circulation configuration (controlled by an input model parameter) could shorten the time to containment failure by several hours. The MAAP guidance document states that "for most plants" (i.e., Westinghouse plants) the parameter should be set to zero; no uncertainty analysis is recommended. For "B&W plants and perhaps some others," the parameter should be set to one. An uncertainty analysis is recommended for a high pressure station blackout sequence. This general guidance is not adequate regardless of reactor design. We conclude that, absent a demonstration of the applicability of the natural circulation flow parameter chosen, all plants should perform the sensitivity case. Also, if calibration of the MAAP model against the Westinghouse two component tests indicate the presently-used range of parameters FAOUT and FWHL is not adequate, additional sensitivity studies may be required.

4. In the area of hydrogen combustion, Reference E4 makes several recommendations for sensitivity analyses related to auto-ignition, jet-burning, and the reliability of igniters. These recommendations are adequate for IPE application. However, no recommendations were made for the flame flux multiplier. This parameter influences combustion completeness, combustion duration, and therefore, the pressure rise due to combustion. Benchmark calculations reveal that due to the uncertainty of this parameter, the MAAP model underpredicted the combustion completeness and duration, relative to test data, in many cases. In a discussion of the MAAP combustion model for Advanced Light Water Reactors (ALWRs), Plys and Astleford [E8] suggested that if a sensitivity analysis is desired, the recommended value of the flame flux multiplier should be varied and the range of variation was provided. The flame flux multiplier should therefore be varie over this same range (see page 6-2) for those accident sequences in an IPE for which combustion plays an important role in primary containment failure. Combustion may be an important consideration in IPEs for BWRs with Mark III

sensitivity of this parameter, a MAAP calculation should be performed using the upper value of the uncertainty range suggested in the MAAP sensitivity study [E7]. Limited sensitivity studies with the eutectic heat of fusion parameter, previously carried out with the BWR version of MAAP did not indicate as significant a sensitivity as was found for PWRs. Moreover, for BWRs, this sensitivity calculation is believed to be covered by other BWR recommended sensitivities. However, because (1) the eutectic heat of fusion is a true physical uncertainty, (2) not all BWR containment types and accident scenarios were investigated in detail to ascertain this parameter's quantitative significance, and (3) for the sake of consistency, this sensitivity calculation is also recommended for BWRs. A further sensitivity case regarding core relocation also applies to both BWRs and PWRs. Reference [E4] recommends that the core melt fraction necessary to transport all the core material from the vessel at RPV failure be varied as a sensitivity case for at least one sequence in IPEs performed for BWRs and PWRs. Given the potential sensitivity of this modeling assumption it is recommended that this sensitivity be performed for each of the representative sequences in an IPE in which the RPV fails before the containment does.

3. Sensitivity studies with the PWR version of MAAP [E7] showed that during sequences where the reactor coolant system (RCS) remains at high pressure, changing the in-vessel natural circulation configuration (controlled by an input model parameter) could shorten the time to containment failure by several hours. The MAAP guidance document states that "for most plants" (i.e., Westinghouse plants) the parameter should be set to zero; no uncertainty analysis is recommended. For "B&W plants and perhaps some others," the parameter should be set to one. An uncertainty analysis is recommended for a high pressure station blackout sequence. This general guidance is not adequate regardless of reactor design. We conclude that, absent a demonstration of the applicability of the natural circulation flow parameter chosen, all plants should perform the sensitivity case. Also, if calibration of the MAAP model against the Westinghouse two component tests indicate the presently-used range of parameters FAOUT and FWHL is not adequate, additional sensitivity studies may be required.

4. In the area of hydrogen combustion, Reference E4 makes several recommendations for sensitivity analyses related to auto-ignition, jet-burning, and the reliability of igniters. These recommendations are adequate for IPE application. However, no recommendations were made for the flame flux multiplier. This parameter influences combustion completeness, combustion duration, and therefore, the pressure rise due to combustion. Benchmark calculations reveal that due to the uncertainty of this parameter, the MAAP model underpredicted the combustion completeness and duration, relative to test data, in many cases. In a discussion of the MAAP combustion model for Advanced Light Water Reactors (ALWRs), Plys and Astleford [E8] suggested that if a sensitivity analysis is desired, the recommended value of the flame flux multiplier should be varied and the range of variation was provided. The flame flux multiplier should therefore be varied over this same range (see page 6-2) for those accident sequences in an IPE for which combustion plays an important role in primary containment failure. Combustion may be an important consideration in IPEs for BWRs with Mark III

containments (or for the times when the other BWR containment types are de-inerted) and for PWRs with Ice Condenser containments and for some PWRs with large dry or subatmospheric containments.

5. Several recommendations were given in Reference E4 for MAAP sensitivity cases related to core/concrete/water interactions. These recommendations include consideration of items such as the amount of floor area the corium might occupy and the mode of heat transfer between the corium and an overlying water pool. These input options were found to be adequate for application of the PWR version of MAAP to an IPE. However, for BWRs, the effects on CCI from the corium spreading in the drywell, and from ablated concrete of vertical surfaces contacted by the corium pool, need special consideration. The MAAP user should ascertain if, for the representative sequences being analyzed, the volume of the corium would be sufficient to spill over onto the drywell floor. This is important for sunken (pedestal floor is lower than drywell floor) pedestal floors. If the drywell floor does receive corium, than we recommend a base case where the corium is restrained to a drywell floor area of 1/4 of the true drywell floor, and a sensitivity case where the corium is permitted to spread throughout the drywell floor. This applies to all BWR containment designs with the exception of a Mark II containment exposed to a low pressure RPV meltthrough. For the latter case, MAAP 3.0B already accounts for possible corium flow channeling based on the manways connecting the drywell and pedestal regions. It should be noted that reference E4 does presently recommend a sensitivity for a Mark I containment where the base case is assumed to be full drywell floor spreading of the corium and the sensitivity restricts the corium in the drywell to 1/4 of the drywell floor. We have recommended the base case to be the restricted corium flow case because it is generally consistent with the approach in NUREG/CR-5423, "The Probability of Liner Failure in a Mark I Containment," Theofanous, T.G., et al., August, 1991.

   In addition, we recommend that a modification to MAAP 3.0B Rev 7.0 (BWR version) be made to calculate the effect of allowing the full sidewall gases to react with the corium pool. BNL recommends the modelling enhancement be part of the base case (see Sections 3.3.2.4 and 6.2.1).

   For high pressure RPV meltthrough, MAAP 3.0B for BWR use does not include a Direct Containment Heating model. The BWR version of MAAP 3.0B is capable of performing a calculation of the containment response for a high pressure sequence and we have reviewed this model. However, we cannot judge its acceptability due to lack of relevant experimental data for BWRs to serve as the basis for an assessment. Rather, the NRC has in the past recommended, and continues to recommend, that utilities address high pressure RPV failure sequences according to the guidance in GL 88-20 and its supplements 1 and 3. In particular, NRC has emphasized enhancement of ADS reliability.

6. For ATWS scenarios in BWRs, BNL recommends that a sensitivity case be performed using the user-supplied power versus level curve option in MAAP. It is our belief that the uncertainty in any chosen power vs. level curve employed for the base case used in the IPE necessitates a detailed justification of the curve, such as a

detailed TRAC analyses. Otherwise, we recommend a sensitivity case be performed where the power vs. level curve is adjusted as discussed in Section 2.3.2, p. 2-6. Since ATWS scenarios are in general less significant for PWR plants than for BWRs, this sensitivity calculation is not requested for PWRs.

Conclusions

In summary, MAAP 3.0B was in general found adequate for determining success criteria from accident initiation to the time of clad damage unless certain thermal hydraulic conditions exist. These are:

1. The break location gives rise to a quasi-steady state two-phase flow condition (BWR/PWR).
2. The RPV water level and vessel flow conditions may expose the fuel to departure from nucleate boiling (DNB) conditions while MAAP continues to predict adequate core cooling (BWR).
3. The reactor has not scrammed (fuel stored energy will not be released) (BWR/PWR).
4. Clad temperature is above 1200°K (BWR/PWR).

The utilities should justify the use of MAAP if these thermal-hydraulic conditions are encountered during this time phase. MAAP 3.0B should not be used for determining success criteria after clad damage (e.g., to determine whether or not a core can be successfully reflooded after extensive fuel melting has occurred). After this time, MAAP should be used to provide the utility with an appreciation of the uncertainties surrounding containment performance during a severe accident. The MAAP sensitivity studies recommended [E4] for performing an IPE were in general found adequate. A relatively small number of additional sensitivity studies are recommended as described above and in Section 2.

References

E1. U.S. NRC, "Individual Plant Examinations for Severe Accident Vulnerabilities - 10CFR§50.54(f)," Generic Letter No. 88-20, November 23, 1988.

E2. U.S. NRC, "Individual Plant Examination: Submittal Guidance," Final Report, NUREG-1335, August 1989.

E3. MAAP3.0B Users Manual, Vol. 1 and Vol. 2, Fauske & Associates, Inc, March 1990.

E4. Kenton, M.A., and J.R. Gabor, "Recommended Sensitivity Analyses for an Individual Plant Examination Using MAAP 3.0B," Gabor, Kenton & Associates, Inc

E5. "MAAP Design Review," Jason Associates Corporation, October 1989.

E6. Summers, R.M et al, "MELCOR 1.8.0: A Computer Code for Nuclear Reactor Severe Accident Source Term and Risk Assessment Analyses," NUREG/CR-5531, Sandia National Laboratories, Albuquerque, NM, January 1991.

E7. Mendoza, Z.T. and J.M. Hall, "MAAP3.0B Sensitivity Analysis for PWR Station Blackout Sequences," NP-7192, Electric Power Research Institute, January 1991.

E8. Plys, M.G., and R.D. Astleford, "Modifications for the Development of the MAAP-DOE Code, Vol. III: A Mechanistic Model for Combustion Integrated Accident Analysis, Task 3.4.5," DOE/ID-10216, Vol. III, November 1988.

1 Introduction and Approach

1.1 Background

The Modular Accident Analysis Program (MAAP) computer code was developed as part of the industry response to the post TMI-2 NRC initiatives related to severe accidents at nuclear power reactors. This development effort, undertaken in conjunction with the Industry Degraded Core Rulemaking (IDCOR) Program, was directed at providing industry with the broad analytical capability necessary to predict the progression of severe accidents. An early version of the MAAP code was used to predict containment response and environmental source terms for several accident sequences in a number of Boiling Water Reactor (BWR) and Pressurized Water Reactor (PWR) plants as part of the IDCOR program. The results of these calculations and available experimental data formed the basis for several technical meetings between the NRC and IDCOR. As a result of these meetings, in which the predictions of MAAP were compared with calculations performed with NRC sponsored codes and experimental data, a number of NRC/IDCOR Technical Issues were developed. These issues identified areas of significant phenomena, which involve considerable uncertainty, and where differences between the NRC sponsored codes and MAAP were observed. These issues, together with other considerations, guided the development of subsequent revisions of the MAAP code and also the NRC sponsored codes.

In the Commission policy statement on severe accidents in nuclear plants issued on August 8, 1985, (50 FR 32138), the Commission concluded that systematic evaluations are beneficial in identifying plant-specific vulnerabilities to severe accidents that could be fixed with low-cost improvements. With that in mind, the Commission directed the staff to develop an approach to be implemented by utilities in performing plant specific evaluations. In response to the Commission directive, the staff issued to utilities Generic Letter 88-20 [1], outlining the elements of the Individual Plant Examination (IPE) program. NUREG-1335 "Individual Plant Examinations Submittal Guidance" [2] was subsequently issued to aid the utilities in formulating their response to the generic letter.

It is now evident that industry analysis of a particular plant response to severe accidents and the associated phenomena, performed as part of the IPE program, will in part be based on MAAP code calculations. The NRC staff therefore decided to undertake a review of the MAAP code using the assistance of Brookhaven National Laboratory (BNL). The review was intended to provide assurance that industry-generated IPEs, at least to the extent practicable, represent reasonable estimations of the progression of severe accident sequences and the plant response to these sequences. The current version of MAAP is sponsored by EPRI, with developmental activities being pursued by Fauske Associates Incorporated (FAI) and Gabor, Kenton, & Associates (GKA).

1.2 Objective

This report describes the NRC sponsored review of the MAAP code, version 3.0B [3]. The primary objective of the review was to evaluate the MAAP code for its use in conjunction with activities related to performance of an IPE for operating reactors. Therefore, the review also considered the guidance provided by GKA regarding sensitivity analyses for IPEs using MAAP 3.0B [4].

It should be noted that there are several revisions to MAAP 3.0B. The differences among revisions can significantly affect code predictions. Therefore, it is important for the utilities to clearly identify which revision of MAAP 3.0B was used when their IPE was conducted. BNL reviewed revision 7.0 for BWR plants and revision 17.0 for PWR plants. The comments in this report apply to these revisions but may not all be applicable for other revisions.

It should also be noted that MAAP 3.0B contains significant modifications and improvements relative to the early versions of MAAP used in the IDCOR program. An element of the review was therefore to assess how MAAP 3.0B addresses the NRC/IDCOR issues [5]. Another element of this program was to compare the analytical models in the MAAP 3.0B code with their counterparts in the NRC developed MELCOR [6] code.

MAAP was evaluated to provide assurance that IPEs will be analyzed, to the extent practicable, with a methodology which adequately treats significant phenomena and reflects the uncertainty surrounding issues for which confirmatory research is planned or ongoing. It must be emphasized that this review concentrated on evaluating MAAP 3.0B for its use as an IPE tool. This report therefore focuses on those aspects of an IPE that will be addressed with MAAP analyses, namely the timing of key events and containment response to severe accident conditions. Utilities may want to use MAAP to predict the time from accident initiation to the time of clad damage for the purposes of determining success criteria for quantification of the Level 1 (core damage frequency estimate) part of an IPE. Thus an important aspect of our review was to determine how well MAAP models the loss of coolant inventory for a range of initiating events (i.e., transients or LOCAs). We envision that MAAP will also be used to provide the utility with a framework for obtaining an understanding of and appreciation for containment failure modes, the impact of phenomena and plant features, as well as operator actions. In this role, MAAP analyses are expected to be supplemented with sensitivity studies to ensure that the utility staff has an appreciation of the uncertainties surrounding containment performance during a severe accident. Therefore, our review of this aspect of MAAP's application to an IPE focused on the adequacy of the range of parameters recommended [4] for the sensitivity analysis.

The purpose of the review was to evaluate the models in MAAP 3.0B and their sensitivity to parametric variations. A line by line review of MAAP coding was not performed.

1.3 Approach

Chronologically, the review was performed in three phases. The study began with a review of the models used in MAAP based on the available documentation. Initially, the documentation supplied by the Electric Power Research Institute (EPRI) was for MAAP 3.0 and consisted of a two-volume User's Manual. In addition, there was an attachment consisting of descriptions of new subroutines added to MAAP 3.0 to create MAAP 3.0B. Subsequently, a new manual for MAAP 3.0B was issued which contained many revisions to the previous documents and therefore, required additional evaluation.

Three familiarization meetings between EPRI and NRC staff and its contractor, BNL, were convened. The first meeting concentrated on in-vessel phenomena, the second on ex-vessel severe accident progression and containment performance. The third emphasized the secondary containment models, and presented the MAAP Design Review performed under the sponsorship of EPRI. Responses to questions asked by NRC/BNL during these meetings were provided by Nuclear Management and Resources Council (NUMARC). As a result of this phase BNL issued a number of draft technical evaluation reports (TERs) which addressed the modeling aspects of MAAP. Separate draft TERs were written for the BWR and PWR reviews. The information in these TERs is contained in Appendices A and B of this report.

The second phase consisted of performing calculations with the MAAP and MELCOR codes for two severe accident sequences, a Loss of All Electric Power Sequence in a BWR (Peach Bottom) and a Small Break LOCA in a PWR (Zion). A meeting was held between industry representatives and NRC staff to determine how the numerical comparisons between MAAP and MELCOR were to be made. Subsequent meetings between Fauske and Associates, Incorporated (FAI) and BNL helped to standardize the input deck descriptions. MELCOR calculations were made by BNL staff. MAAP calculations were carried out by FAI and the results forwarded to BNL. The results of the numerical comparisons were the subject of two additional draft BNL TERs which are documented in Appendices C and D. The results differed sufficiently so that a consensus was reached on further MAAP calculations that should be made (sensitivity runs) to help explain the differences observed in the MAAP-MELCOR base comparisons.

Consequently the third phase focused on performing a series of sensitivity calculations with MAAP in order to assess the effect of varying a number of model parameters. These calculations were detailed in another two draft BNL TERs, and the results are contained in Appendices E and F of this report.

The present report documents the findings of the above phases and makes a recommendation on the applicability of MAAP 3.0B for IPEs.

As the discussions in the subsequent sections of the report indicate, the assessment of the MAAP code relied on available state of the art information regarding severe accident phenomena. The BNL reviewers were familiar with past and ongoing efforts in the reactor safety community to refine understanding of the events which could potentially occur in a severe accident. Wherever possible, experimental data related to the particular phenomenon under consideration was included in the evaluation of the code modeling. Clearly however, there are still many aspects of severe accident conditions, and containment performance under these conditions, for which data is lacking. To some degree, sensitivity analyses can be used to account for uncertainty in basic modeling assumptions. The range of these sensitivity analyses as recommended in this report are again based on available data, and comparison against other modeling approaches. Comparing MAAP results with MELCOR calculations for the same initial conditions also helped in establishing sensitivity ranges, since MELCOR represents an attempt, independent from MAAP, to integrate available information into a consistent model for severe accidents.

1.4 Organization of the Report

Section 2 highlights the principal issues regarding the application of MAAP for IPE analysis: the use of MAAP for establishing success criteria prior to clad damage (Section 2.1), the application of MAAP for containment performance analysis (Section 2.2), and the application of MAAP in analyzing representative sequences expected to be found in an IPE (Section 2.3). This last section summarizes the additional sensitivity cases recommended for the performance of an IPE as a result of this review.

Section 3 discusses the technical issues for IPE severe accident analysis. This section deals principally with accident progression modeling and containment performance issues. The models in MAAP for various severe accident phenomena are considered and assessed based on current understanding of such phenomena. Comparable models in MELCOR are also discussed.

Section 4 is concerned with MAAP's modelling of fission product release and transport. The pertinent models in MAAP are described and some comparisons are drawn with MELCOR models. To some extent, fission product calculations will play a role in IPE assessments, as indicated in NUREG-1335 [2]. Some utilities may want to utilize MAAP to support their analyses in this area. Therefore this section is included for completeness.

The timing of significant events as calculated by MAAP and MELCOR for the same accident sequences is compared in Section 5. The two sequences considered are a Loss of All Electrical Power accident in a BWR Mark I plant, and a Small Break LOCA in a Westinghouse type PWR plant with a large dry containment.

Section 6 summarizes the results from a number of sensitivity calculations performed with MAAP for this review and from a previous study. This section, along with the model discussions of Section 3, provides the basis for the additional IPE sensitivity cases recommended in Section 2.3.

Section 7 summarizes the review and presents the conclusions.

The Appendices provide additional detail for the material presented in the main report. Appendices A and B state the findings of the literature review of documentation related to MAAP severe accident modelling. There are two appendices because there are separate PWR and BWR versions of MAAP. This duality in the appendices extends to the numerical comparisons documented in Appendices C and D, and the sensitivity calculations presented in Appendices E and F.

2 Accident Progression Issues for IPE Analysis

2.1 Use of MAAP for Success Criteria Before Clad Damage

Licensees are expected to make use of MAAP during their IPE analyses to determine the time from accident initiation until critical fuel temperatures are reached. The times for key events calculated by the code during this early phase of an accident will provide a guide for determining whether a particular recovery action, taken to reestablish core cooling, can be carried out before clad damage occurs. It is expected that MAAP calculations will also be used to determine how fast inventory is lost from the reactor coolant system (RCS) and what the flow requirements are for successful recovery. Therefore, an important focus of the review was on modeling in MAAP which is significant for core heatup and for RCS inventory loss during this phase of the accident.

The following limitations were found in the relevant models:

1. The fuel pin thermal model has a single temperature node, which represents thermal conditions for the fuel pellet, fuel cladding, and in the BWR version, fuel channel material. Since the capacitance of the fuel pin is large in comparison to the fuel cladding, the MAAP model will underpredict the clad heatup rate once clad oxidation power exceeds decay power.

2. For the MAAP versions reviewed, there is no two-phase critical flow model for Reactor Pressure Vessel (RPV) breaches. This could result in a large error in RPV inventory loss when the breach is in a volume containing a two-phase mixture or froth region.

3. Complicated flow patterns may occur in a BWR RPV under natural circulation conditions, but may not be predicted accurately with MAAP due to lack of a slip model outside the core region. MAAP utilizes a single pressure node for the entire RPV, but does attempt to predict natural circulation based on density-weighted water columns within and outside the core shroud. This model, however, may not be accurate enough under some conditions where slip and two-phase frictional multipliers can become important.

4. MAAP lacks a comprehensive heat transfer package for the core region. The code does not predict departure from nucleate boiling.

5. Fuel stored energy is a user-supplied value, which is released at a code-specified rate after scram. Power reductions alone (as may occur in an ATWS Scenario) will not release this energy.

Given the above, if the following conditions are predicted to occur during an accident, the utility performing the IPE should provide justification for using MAAP 3.0B to predict success criteria for the accident time phase before clad damage:

1. The break location gives rise to a quasi-steady state two-phase flow condition (BWR/PWR).
2. The RPV water level and vessel flow conditions may expose the fuel to departure from nucleate boiling (DNB) conditions while MAAP continues to predict adequate core cooling (BWR).
3. The reactor has not scrammed (fuel stored energy will not be released) (BWR/PWR).
4. Clad temperature is above 1200°K (BWR/PWR).

In order to establish success criteria for terminating an accident which has progressed beyond clad damage, complex thermal-hydraulic and chemical processes would need to be modeled in a computer code. This modeling would need to provide confident estimates of the time windows for action and of the flow rates sufficient for cooling that would be accurate enough for comparison with operator response time and equipment capability estimates. Based on these considerations, we believe MAAP should not be used for determining success criteria after clad damage, i.e., to determine whether a core can be successfully reflooded after fuel damage or if an accident can be arrested ex-vessel.

2.2 Application of MAAP for Containment Performance Analysis

The primary use of MAAP after clad damage is for predicting containment failure modes, and estimating the ranges of the challenges produced by severe accident phenomena. The range of significant containment loads can be gauged and an analyst can use the code to help in quantifying a containment event tree. Utilities can use the code to acquire an understanding of the advantages and disadvantages of particular plant features as well as operator actions. In this way, the application of the MAAP code can help in achieving the IPE objective of identifying specific vulnerabilities for a particular plant.

The users of the code are encouraged and expected to perform sensitivity studies for the containment performance part of the analysis. Therefore, the review concentrated here on the adequacy and appropriateness of the range of parameter variation called for in the MAAP Users Manual [3] and the MAAP IPE Guidance Document [4]. Comments regarding the suitability of the guidance provided in References 3 and 4 are found throughout this report.

While providing an understanding of containment failure modes and timing is the primary objective of an IPE analysis, knowledge regarding radioactive material release and transport through the reactor coolant system, the containment, and the auxiliary buildings may also be of interest [2]. It is possible that utility analysts may want to use MAAP calculations as part of their source term estimates. In anticipation of such use of the code, and for technical completeness, this review also addresses modeling issues in MAAP related to fission product release and transport. These issues are briefly discussed in Section 4 of this report.

2.3 Application of MAAP in Representative IPE Accident Sequences

2.3.1 Introduction

In order to enhance the value of this report as a reference for a reviewer of an IPE, recommendations are listed in this section regarding the use of MAAP, for particular representative sequences likely to be found in an IPE. The scope of the present examination of MAAP permitted a detailed investigation of the results obtained with MAAP for only two sequences: a small break LOCA sequence in a PWR plant, and a loss of all electric power sequence in a BWR plant. However, information from these two calculations, as well as the conclusions obtained from the examination of the important models in MAAP and sensitivity calculations performed by others [7], can be used as a basis for some general recommendations for the use of MAAP in analyzing different types of representative sequences.

IPE Reviewers should ensure that the utility submitting an IPE carried out the applicable sensitivity studies recommended in the GKA Guidance Document [4]. There is no reason to repeat those recommendations here. However, there are a number of areas where BNL feels that additional sensitivity cases or enhancements of cases recommended in the Guidance Document, clarification of the Guidance Document [4] or cautions are appropriate. The additional sensitivity cases are outlined below. The rationale for their application is provided in the discussion of the pertinent models in Section 3 and in the sensitivity analysis in Section 6 of this report.

In general, the representative sequences which will be chosen during the performance of an IPE can be placed in one of the following five accident classes.

- I Loss of Reactor Cooling resulting in failure of the Reactor Coolant System (RCS) when the containment is intact

- II Loss of Containment Cooling resulting in failure of the containment before RCS failure

- III Accelerated Loss of Reactor Cooling resulting in rapid failure of the RCS (possibly due to a large LOCA) before containment failure

IV Loss of Reactivity Control (i.e., ATWS) which can result in accelerated loss of containment before RCS failure

V Unisolated Bypass of the Containment (i.e., steamline breach outside primary containment or interfacing LOCAs)

2.3.2 Additional BWR Sensitivity Cases

Class I - Loss of Reactor Cooling (RCS Fails Before Containment)

The BWR Mark I sequence calculated with MAAP during this review (loss of all inventory makeup) falls into this category. Results from this case show that the generation of H_2 in-vessel and effects of core-concrete interaction (CCI) are the two major uncertainties. For in-vessel hydrogen generation in a BWR, BNL recommends a base case calculated with single-sided clad oxidation and no local blockage. BNL further recommends two sensitivity calculations: one with two-sided clad oxidation and no local blockage, and one with single-sided oxidation with local blockage. Discussions regarding this recommendation can be found in Sections 3.2.1 and 6.2.2.

Several recommendations were given in Reference 4 for MAAP sensitivity cases related to core/concrete/water interactions. These recommendations include consideration of items such as the amount of floor area the corium might occupy and the mode of heat transfer between the corium and an overlying water pool. These input options were found to be adequate for application of the PWR version of MAAP to an IPE. However, for BWRs, the effects on CCI from the corium spreading in the drywell, and from ablated concrete of vertical surfaces contacted by the corium pool, need special consideration. The MAAP user should ascertain, if for the representative sequences being analyzed, the volume of the corium would be sufficient to spill over onto the drywell floor. This is important for sunken (pedestal floor is lower than drywell floor) pedestal floors. If the drywell floor does receive corium, then we recommend a base case where the corium is restrained to a drywell floor area of 1/4 of the true drywell floor, and a sensitivity case where the corium is permitted to spread throughout the drywell floor. This applies to all BWR containment designs with the exception of a Mark I containment exposed to a low pressure RPV meltthrough. For the latter case, MAAP 3.0B already accounts for possible corium flow channeling based on the manways connecting the drywell and pedestal regions. It should be noted that Reference 4 does presently recommend a sensitivity for a Mark I containment where the base case is assumed to be full drywell floor spreading of the corium and the sensitivity restricts the corium in the drywell to 1/4 of the drywell floor. We have recommended the base case to be the restricted corium flow case because it is generally consistent with the approach in NUREG/CR-5423, "The Probability of Liner Failure in a Mark I Containment, "Theofanous, T.G. et al., August, 1991.

In addition, we recommend that a modification to MAAP 3.0B Rev 7.0 (BWR version) be made to calculate the effect of allowing the full sidewall gases to react with the corium pool. BNL recommends the modelling enhancement be part of the base case (see Sections 3.3.2.4 and 6.2.1). The sidewall gas reacions reduced the time to containment failure by several hours in the BWR Mark I calculations conducted for this review, and the percent reduction in total time is expected to be even larger for Class III accidents where the time to containment failure depends primarily on CCI effects (due to accelerated time to RPV failure in Class III versus Class I).

For high pressure RPV meltthrough, MAAP 3.0B for BWR use does not include a Direct Containment Heating model. The BWR version of MAAP 3.0B is capable of performing a calculation of the containment response for a high pressure sequence and we have reviewed this model. However, we cannot judge its acceptability due to lack of relevant experimental data for BWRs to serve as the basis for an assessment. Rather, the NRC has in the past recommended, and continues to recommend, that utilities address high pressure RPV failure sequences according to the guidance in GL 88-20 and its supplements 1 and 3. In particular, NRC has emphasized enhancement of ADS reliability.

In the GKA Guidance Document [4] on MAAP, the authors do recommend at least one sensitivity case where the required core melt fraction for total core relocation at RPV failure is 0.2 as opposed to the 0.9 base condition. If more corium is released from the RPV, CCI would be enhanced and hence, the time to containment failure would be reduced. Based on this consideration, BNL recommends that this sensitivity be performed for every sequence where the RPV fails before the containment, i.e., Class I and III. Another parameter, related to core relocation, whose variation was shown to have a significant impact on results in a previous PWR sensitivity study [7] is the eutectic heat of fusion. Limited sensitivity studies with this parameter carried out in the past with the BWR version of MAAP did not show as significant a sensitivity as was found for PWRs. Moreover, for BWRs this sensitivity is believed to be covered by other recommended sensitivities. However, because (1) the eutectic heat of fusion is a true physical uncertainty, and (2) not all BWR containment types and accident scenarios were investigated in detail to ascertain this paramter's quantitative significance, and (3) for the sake of consistency, this sensitivity calculation is also recommended for Class I and III accidents for BWRs. Additional comments on core relocation can be found in Sections 3.2.2, 6.1.1, and 6.2.3.

For sequences in which combustion can influence containment failure, sensitivity cases varying the flame flux multiplier parameter "FLPHI" should be provided as discussed in Sections 3.3.3 and 6.1.1.1.

Class II - Station Blackout with Initial RPV Makeup (Containment Fails Before RCS)

This class of accidents results in the containment failing before the RPV. BNL does not recommend any additional sensitivities beyond those outlined for Class I accidents. However, some cautions for IPE application should be observed:

1. If High Pressure Cooolant Injection, Reactor Core Isolation Cooling (HPCI/RCIC) or other non-electric powered pumps are utilized beyond containment failure, detailed justification is needed, including analyses showing that local temperature trips of pertinent equipment have been checked and are not exceeded and that Net Positive Suction Head (NPSH) and vortex limits are not violated.

2. Recommendation in the Guidance Document [4] on considerations for the effects on containment structural integrity by elevated containment temperature should be observed.

Class III - LOCA (Accelerated Failure of RCS Before Containment)

The accidents in this class are similar to class I accidents. A major difference is that the accident progression is accelerated because the RPV inventory is not just boiling off, but it is being released through a break. In addition, there can be much less water in the lower plenum at the time of lower core plate failure. BNL has no added recommended sensitivities for this class beyond those for Class I. The following caution should be observed:

- Small and intermediate size LOCAs (including Stuck Open Relief Valves) should be examined for break location and the possibility of sustained two-phase critical flow. (The versions of MAAP examined for this review do not have a two-phase critical flow model.)

Class IV - Anticipated Transients Without Scram (ATWS)

The sensitivity cases recommended for Class II apply for this class also. The following observation is also made:

If MAAP is used to estimate ranges of containment performance during ATWS events, the ATWS power curve used should be explicitly justified and some sensitivities run. There are large uncertainties in any power versus level correlation due to its dependence on core power shape, natural circulation, and void quality or slip assumptions in two-phase regions.

In the ATWS subroutine, MAAP employs a form of the Chexal-Layman correlation as an option. This correlation relates power to downcomer level and RPV pressure. In MAAP, core boil-up height, or froth level, is used along with RPV pressure. This correlation itself has uncertainty that is related to core power distribution and natural circulation considerations. The uncertainty is further increased because of the simplified thermal hydraulics MAAP employs to implement the correlations. Therefore the choice of the power-level correlation has to be justified. The three choices offered by MAAP are a standard Chexal-Layman correlation, another correlation where the effects of core inlet subcooling are considered, and a user-supplied power versus RPV downcomer level curve. BNL recommends that sensitivities be performed using the user-supplied curve method. The following guidance is suggested: The Chexal-Layman correlation would predict a power level of about 4% of original power for a core where the operators of a BWR have tripped the recirculation pumps, lowered water level to top of active fuel and depressurized the RPV to the point where the SRVs would reclose on spring return pressure. It is our belief that the uncertainty in this value is large, i.e., power could be as high as 8%. Therefore, without a detailed explicit justification in the IPE, such as a detailed TRAC calculation, BNL would recommend that a case be provided where the power vs. level curve employs an offset at the lowest power (water at TAF and RPV depressurized). The power at normal water level and RPV pressure condition could remain the same. (Half the power reduction can be attributed to depressurization and half to level control.) Figure 2.1 is a representation of the recommended sensitivity case. The suggested sensitivity considers that the uncertainty grows as the level in the downcomer drops. Figure 2.1 is not numerically exact, but is supplied to indicate that the recommendation is for an offset in the Chexal-Layman prediction at the lower water level by a factor of x, and no offset at the normal operating water level. In the figure, x was taken as two but the IPE submitter should justify the value he chooses. Detailed information on power versus level control in BWRs can be found in NSAC-70, " Reducing BWR Power by Water Level Control During an ATWS," Energy Incorporated and Nuclear Safety Analysis Center, August 1984.

Class V - Direct Bypass of Containment

There are no additional sensitivities or recommendations besides those for Class I for accidents in this class. We caution, however, that the failure that is assumed to cause the bypass should be examined to determine if it can trip or damage any system which is assumed to be active in this IPE sequence. Justification should be given for why each system is assumed to be available.

2.3.3 Additional PWR Sensitivity Cases

For PWR analysis with MAAP, a few additional sensitivity cases are also recommended:

1. As with BWRs, for accidents where H_2 combustion plays an important role in containment failure, BNL recommends a variation of the Flame Flux Multiplier modeling parameter "FLPHI." A discussion is provided in Sections 3.3.3 and 6.1.1.1.

2. For high pressure sequences such as station blackouts and small LOCAs, BNL recommends that, absent a demonstration of the applicability of the natural circulation flow parameter chosen, in addition to the natural circulation option chosen for the base case, the remaining other option should be used for a sensitivity case Also, the MAAP natural circulation model should be calibrated against the Westinghouse two component tests. If calibration against the tests indicates the presently used range of parameters FAOUT and FWHL is not adequate, additional sensitivity studies may be required. A discussion is provided in Sections 3.1.1 and 6.1.1.2.

3. To investigate the potential impact on containment failure time of the uncertainties of fuel relocation and debris distribution, BNL suggests that additional calculations varying the eutectic heat of fusion for accident classes I and III be performed. The fuel relocation model is discussed in Section 3.2.2. The basis for this recommendation is presented in Section 6.1.1.3.

4. A sensitivity case using a required core melt fraction of 0.2 for total core relocation at RPV failure, previously discussed for BWRs, is recommended for class I and III accidents in PWRs also. The basis for this recommendation is discussed in Sections 3.2.2 and 6.2.3.

The sensitivity studies recommended for BWRs in Section 2.3.2 related to in-vessel hydrogen generation, CCI, and ATWS were found to be unnecessary for application to PWRs.

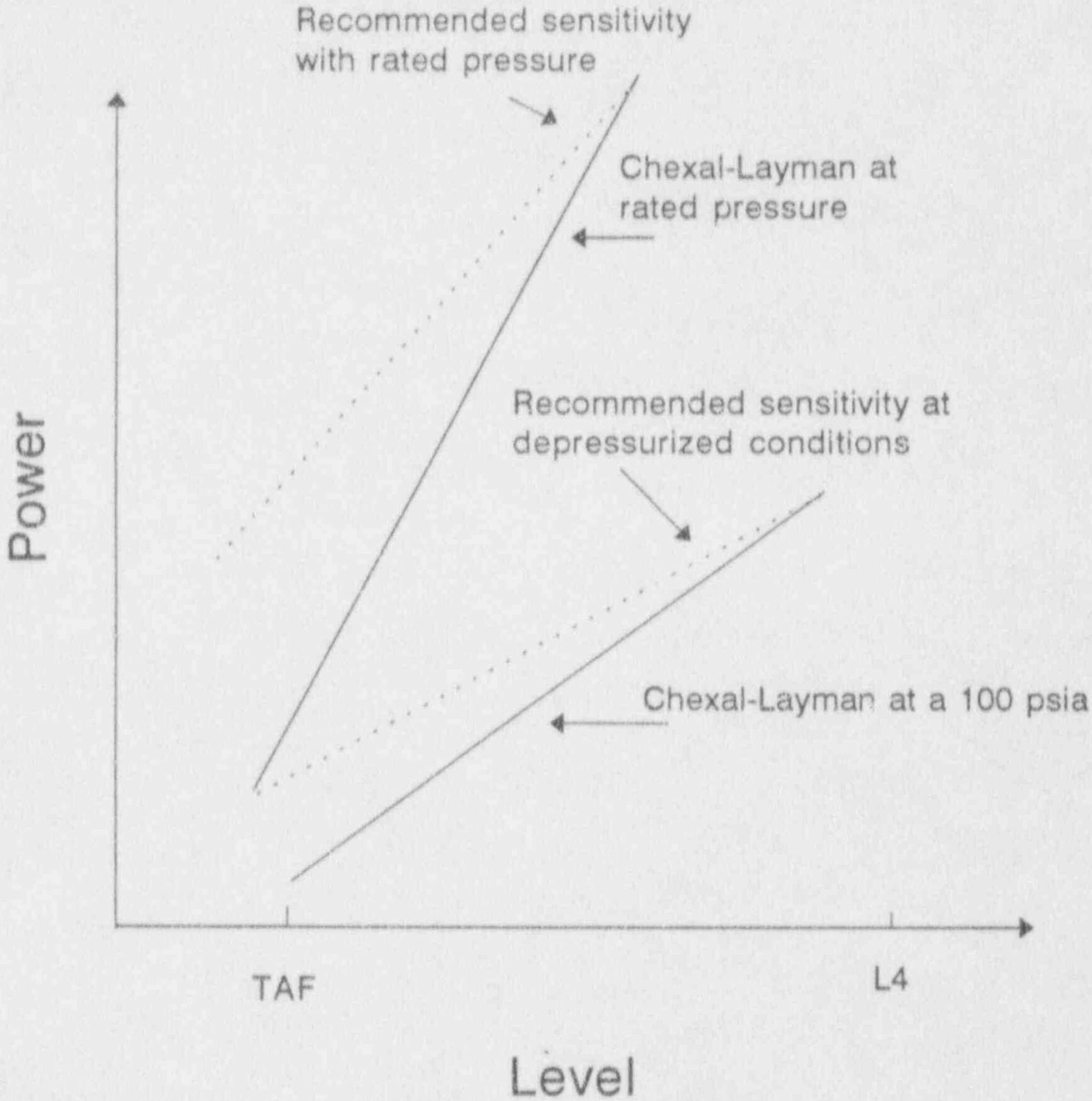
Recommended sensitivity
with rated pressure
Chexal-Layman at
rated pressure
Recommended sensitivity at
depressurized conditions
Chexal-Layman at a 100 psia
Power
TAF
L4
Level

Figure 2.1

3 Technical Issues for IPE Severe Accident Analysis

3.1 Accident Initiation to Fuel Damage

3.1.1 Reactor Coolant System Natural Circulation

3.1.1.1 Issue Discussion

This issue involves the effects of natural circulation in the reactor vessel and the reactor coolant system, and is primarily important for PWRs during high-pressure accident sequences. It is recognized that natural circulation flow induced by buoyancy forces under high pressures can cause a counter-current flow in the hot leg leading to the steam generators. The hot gases from the core can increase considerably the temperatures in the upper plenum of the reactor vessel, the hot leg, the steam-generator tubes, and other piping systems. The temperature could be high enough to challenge the structural integrity of the RCS. Therefore, there is a potential that natural circulation could lead to a failure of the steam generator-tubes or cause a hot leg/surge line failure before the bottom head of the reactor vessel has been penetrated by the relocated core debris.

Natural circulation flow in the reactor vessel could increase hydrogen generation by recirculating the steam from the upper plenum back to the core to react with the fuel cladding. The high temperature in the upper plenum could also potentially promote oxidation of structural materials, and generate more hydrogen.
The transport, deposition, and revaporization of fission products in the primary system strongly depend on temperatures and fluid movement, and hence, are affected by natural circulation in the primary system.

Because of the importance of natural circulation and its impact on reactor vessel failure, hydrogen production, and fission products, the analytical models and assumptions used in the MAAP code to predict the natural circulation flow are of particular concern.

3.1.1.2 MAAP and MELCOR Models

In the MAAP code, natural circulation flow is calculated using a one-dimensional, quasi-steady state momentum balance along predefined loops. There are three modeled loops in the PWR version of the code: 1) core-upper plenum circulation, 2) hot leg-steam generator circulation, and 3) PWR primary system circulation. These models include the U-tube type and once-through type steam-generators, and two different core-upper plenum designs by Westinghouse and B & W. A detailed discussion of these models is given in Section 4 of Appendix A.

MAAP 3.0B has provided parameters for natural circulation. The event flag, IEVNT 208, is used to model the condition that the coolant pump seals clear and unidirectional circulation occurs in the coolant loop. One parameter (FCDDC) is related to the efficiency of condensation in the cold leg but is currently not available in MAAP. One parameter (VFSEP) refers to the void fraction in the primary system, above which phase separation is assumed, and two-phase natural circulation stops. Two parameters (FAOUT and FWHL) are related to the hot leg-steam generator (U-tube) circulation flow. The flag to control the configuration of natural circulation is denoted by the parameter FNCBP. The rest of the parameters involve heat-transfer coefficients, friction factors, and a finite-difference scheme for numerical calculations. All the parameters, except IEVNT208 and FCDDC, were included in the MAAP sensitivity study [7] as discussed in Section 4 of Appendix E.

In addition to these model parameters, the MAAP blockage model plays an important role in natural circulation. The activation of the blockage model will reduce the natural circulation flow and limit the increase in temperature in the hot leg region. The MAAP IPE guidance document [4] recommends that the blockage model be deactivated for the base case to increase hydrogen generation. This recommendation would increase the potential for a temperature-induced failure in the hot leg or surge line.

MELCOR does not have any special models for natural circulation. However, because control volume and flow path topology are free, and multiple flow paths between the control volumes are allowed, the user can model natural circulation phenomena. The one-dimensional momentum equation that is solved for the flow path network has gravitational heads. However, the results depend on user-specified nodalization. MELCOR does not model counter-current flow in a flow path.

3.1.1.3 Verification and Assessment of the MAAP Model

Benchmarking calculations were performed for the model of the U-tube steam generator against the Westinghouse 1/7 scale test data [8]. The data was obtained from one low-pressure water test and four high-pressure SF_6 tests. Two model parameters were involved in the benchmark calculation, namely, the fraction of tubes carrying flow away from the hot leg (FAOUT) and the coefficient of the hot leg counter-current flow (FWHL). The results of the benchmark calculations show that values of 0.3 for FAOUT and 0.115 for FWHL yield the overall best agreement between the model and data [8]. The two values are recommended [4] to be used in the base case for IPEs. Additional tests have been carried out by Westinghouse with a two component system. To date, the MAAP model has not been calibrated against these more recent tests.

For once-through steam generators of the B & W type, results from a simple counter-current flow model were correlated with limited data to determine an empirical coefficient similar to FWHL. MAAP users should be aware that this model has not been fully verified due to the lack of test data.

The MAAP sensitivity study performed for the Zion plant for a station blackout sequence [7] indicated the importance of the parameter FNCBP, in-vessel natural circulation configuration, on containment failure time. However, the MAAP model has not been fully verified for all PWR designs. A specific criterion on the selection of this parameter is not provided by the MAAP guidance document. The selection of this parameter should depend on the relative flow area and resistance of the reactor vessel.

3.1.1.4 Conclusion

The natural circulation model provides the MAAP 3.0B code with an inherent capability for realistically treating this important phenomenon. However, there are uncertainties in the model in the areas of onset of phase separation, pre-defined flow paths in the RCS, flow redistribution in core channels, and counter-current flow in the hot leg.

For PWR IPE applications, we recommend that, absent a demonstration of the applicability of the option chosen, in addition to the natural circulation configuration option chosen for the base case, the other option should be used for a sensitivity case. Also, the MAAP natural circulation model should be calibrated against the Westinghouse two component tests. If calibration against the tests indicate the presently-used range of FAOUT and FWHL is not adequate, additional sensitivity studies may be required. See Section 6.1.2 for additional discussion.

3.2 Fuel Damage to Vessel Failure

3.2.1 Modeling of In-Vessel Hydrogen Generation

3.2.1.1 Issue Discussion

The amount of hydrogen that could be generated in the vessel during a severe accident is uncertain. The major factors in code modelling, which affect production, include the changes in reactive surface area by relocation; the amount of steam reaching the reactive surface; the material considered as part of the reactive or oxidized surface area; and the reaction of materials above and below the core.

Hydrogen production affects in-vessel and ex-vessel phenomena. Oxidation of zircaloy and stainless steel is exothermic, and hence, adds to the energy in the vessel and to the rise in temperature of the vessel's internal structures. These structures may experience oxidation themselves, which can cause their failure and relocation. The oxidation energy will influence in-vessel thermal hydraulics, and hence, the deposition, retention, and revaporization of radioactive vapor and aerosol material.

In some scenarios, hydrogen release will influence the pressurization of the containment and may cause rapid failure of some containment structures. Possible hydrogen burning can cause failure of equipment and enhance the driving force carrying radioactivity to the environment.

3.2.1.2 MAAP and MELCOR Models

MAAP models only zircaloy oxidation in the core region. For the BWR and PWR versions, the user can vary the reactive surface of the clad to simulate the entire range from single-sided up to two-sided oxidation. (In addition, the PWR MAAP version allows for a reactive surface area increase due to clad ballooning and fuel relocation.) For BWRs, "blockage" can be of three forms: full blockage which prevents oxidation in a channel once any one of the fuel nodes in the channel undergoes the onset of melting (node at eutectic temperature), local blockage where further oxidation in a node which has or is undergoing melting is prevented, and finally, the no blockage model. For the PWR code version, the user can choose between a blockage and no blockage model. The no blockage PWR and BWR models are similar. This model does not permit any oxidation cutoff due to the onset of melting. However, as a node is filled with molten material the reduced flow area limits the amount of steam available for oxidation.

Because there are no channels in a PWR to separate the axial flow streams as there are in a BWR, one could say that the PWR blockage model (HEATUP/PWR) is the same as the BWR local blockage model (HEATUP/BWR).

The PWR version allows for oxidation of the relocated zirconium in the plenum region. This feature is not found in the BWR version of MAAP. No in-vessel oxidation of steel located in the reactor pressure vessel (RPV) is performed by MAAP. However, once the molten steel is ejected to the cavity or pedestal area upon vessel failure it is free to oxidize during CCI. Sensitivity calculations were performed (see Section 6) to see what the effect would be of increasing the steel mass of the lower core plate to account for the possible relocation of other steel masses found throughout the RPV.

MELCOR's model for in-vessel hydrogen production is substantially different from MAAP's. MELCOR allows for oxidation of stainless steel as well as zircaloy in the core and lower plenum regions of the RPV. Further, MELCOR will vary the reactive surface during relocation. For conglomerate (molten) debris, the reactive surface is varied such that during the initial phases of candeling the reactive area grows. It then decreases because it is assumed that the region between the fuel rods becomes filled.

MELCOR also utilizes particulate debris where the user specified spherical diameter determines reactive surface area. Zircaloy can become part of the particulate debris if the clad failure criterion chosen by the user is a non-negligible fraction of its thickness. Typically, however, the clad is transported as conglomerate debris. MELCOR does have a provision to cut-off oxidation in channels which become completely blocked. This was not used in our studies with the code.

A very important difference between MAAP and MELCOR exists regarding the availability of steam to the core region once the lower core plate fails. In MAAP, this plate fails when the lowest core node becomes fully molten. At this time, all molten debris above the plate pours into the lower plenum. Because of modeling assumptions used, the time between the lower core plate's failure and ejection of the debris from the RPV is very short (on the order of seconds or tens of seconds). The result is that little water in the lower plenum is made available to the clad remaining in the core. MELCOR, on the other hand, will fail the lower plate when it reaches a user-specified yield temperature. If particulate debris rests on the plate at the time of failure, it will relocate via gravitational settling to the lower plenum where substantial steaming can occur if water is available. This steam is then made available to oxidize the material remaining in the core region. Since MELCOR does not allow any corium mass transfer across the user-supplied ring nodalization, there is typically substantial core material remaining above the lower core plate when the particulate debris first enters the lower plenum. (In the BWR studies, the conglomerate debris had frozen above the lower core plate and was not available for transport based on the support option chosen). This phenomenon results in substantial differences in the in-vessel hydrogen generation predicted between MELCOR and MAAP, and can be tied to the basic assumption of the physical form the corium takes (liquid vs. solid).

3.2.1.3 Verification and Assessment of the MAAP Model

As stated above, only Zr oxidation is considered in MAAP inside the vessel. The Cathcart equation is used in the MAAP oxidation model below 1850K and the Baker-Just relation is used above this temperature. BNL compared these correlations with others used in MELCOR, MELPROG, and SCDAP. At higher temperatures (above 1875K), the Baker-Just correlation (used in MAAP) predicts a higher oxidation rate than the Urbanic-Heidrick correlation (used in MELCOR), but a lower rate than the Prater-Courtright correlation (used in MELPROG and SCDAP).. At temperatures below 1800K, the Cathcart correlation agrees well with the Prater-Courtright correlation. The difference in reaction rate may not be very important, because hydrogen generation is often controlled by other factors, such as steam availability and clad surface temperature. During a degraded core accident, the steam availability could become the dominant factor. Without the restoration of a core injection system, hydrogen generation is often terminated due to steam starvation during a severe accident sequence.

Clad ballooning is not modelled in the BWR version of MAAP. In the PWR version, MAAP computes clad ballooning resulting from a pressure differential across the clad. However, there are limitations to this model also. It does not consider the effect of oxidation on the mechanical properties of the clad. Oxidation will form an embrittled layer on the clad, which is likely to limit ballooning and burst to a local area. Fuel pitch also should be considered as a constraint to limit the degree of ballooning.

The lack of an in-vessel steel oxidation model in MAAP is a limitation. Also, as previously noted, for the BWR version of MAAP there is no alteration of the surface area of core cells containing clad and exposed to oxidation during the relocation process in MAAP.

The FAI document FAI/88-41 "Status of Technical Issue Resolution," [9] compares results of the MAAP in-vessel hydrogen generation model against the Power Burst Facility-Severe Fuel Damage Tests (PBF-SFD). FAI claims good agreement between MAAP and PBF-SFD prior to fuel relocation. After this, however, FAI [9] finds "considerable numerical differences." However, if experimentally measured steaming rates are input into MAAP, "generally good agreement" for total hydrogen production is obtained. In addition, to obtain agreement in the BWR MAAP version the "fuel channel is assumed to remain open."

3.2.1.4 Conclusions

BNL recommends the use of the single sided, no blockage model in MAAP for the base case for BWRs as well as PWRs, because we believe that the issue of in-vessel hydrogen production remains highly uncertain and is traceable to the assumptions governing the physical form of the relocating corium.

Besides redefining the base case of the EPRI guidance document for BWRs, we recommend additional sensitivity cases: MAAP should be run with the local blockage model and single-sided clad oxidation to give a lower bound estimate of H_2 generation and zircaloy oxidation in the vessel. To estimate an upper bound, MAAP should also be run with no blockage and two-sided clad oxidation. Additional comments are found in Section 6.2.2.

For PWRs, no additional sensitivity runs beyond those suggested by the guidance document [4] are recommended.

3.2.2 Models for Core Slump, Core Collapse, and Reactor Vessel Failure

3.2.2.1 Issue Discussion

Core slump, involves the core relocation process, which has synergistic effects on many other thermal-hydraulic, material interaction and hydrogen-production phenomena. This issue relates to the geometry of the core during accident progression, which can affect core cooling and power distribution. Of concern are the criteria used to begin relocation, and the physical form taken by the relocating material.

While the core debris remains above the lower-core plate and until the core collapses, any water in the lower plenum region will be unavailable for fuel cooling or oxidization, except for possible swelling in the level induced by pressure reductions, such as through the actuation of safety relief valves. Criteria that should be used to model the collapse of the core and failure of the lower plate remain uncertain, as do the effects of lower plate failure on vessel integrity. In particular, the fraction of the core material transferred to the lower plenum when the plate fails is uncertain, and this fraction is tied to the physical form (liquid, solid, or slurry) of the relocated core material.

The amount and dispersal of corium in the lower plenum will influence the attack and failure of the lower vessel head. Again, the physical form of the debris will strongly govern the surface area available for cooling by any water remaining in the lower plenum. Also in question is whether the RPV will fail due to a creep failure of the lower head or via a penetration failure.

In addition to failure of the lower head, there is uncertainty regarding the upper-vessel temperatures which may cause components to fail or relocate, and the loss of the vessel's pressure boundary. These latter concerns involve natural circulation flows, which could carry the heat to these regions (see Section 3.1.1). Along with the potential failure of the components of the upper vessel, the issues of steel oxidation in-vessel and increased steel mass outside the vessel during core-concrete interaction (CCI) need to be considered.

3.2.2.2 MAAP and MELCOR Models

Details of the MAAP and MELCOR models of core-melt progression and vessel failure can be found in Appendices A and B. MAAP employs a simple single temperature eutectic model for core relocation. The eutectic melting temperature and latent heat of fusion are supplied by the user. Their dependency on mass composition, i.e., on the amounts of UO_2 and Zr, are not functional inputs. MAAP 3.0B, Rev. 7, for the BWR, also has a control-blade single melting temperature model with a melting temperature and relocation model different from that of the fuel's. The recommended temperature for fuel failure [4] is 2500 K. The molten corium follows a simplified candling freeze-flow transport to the support plate. When the lowest core node (the one adjacent to the lower-core plate) becomes fully molten, the plate is modeled as failed and all molten material above the plate flows through the failed region.

In the BWR version, all molten debris is transported to the lower plenum to attack all the control rod guide tubes within the one radial ring where the core plate has failed. Once the penetration fails, the molten debris is ejected. The present model usually results in very rapid failure of the penetration and ejection of the contents of the lower plenum. A temperature, supplied by the user, is the criterion for penetration failure.

In the PWR version of MAAP, once the core support-plate fails, all molten debris is relocated to the lower plenum, but the attack on the vessel is controlled by a delay time specified by the user. This parameter prevents failure of the vessel until a specified time after the support plate has failed.

In the BWR version, the amount of steel in the lower core plate is specified by the user, and this amount is available for ejection, as is any molten stainless steel from the control blades. In the PWR version, the user similarly controls the amount of steel that can be ejected.

Subsequent to vessel failure and molten material ejection in MAAP, all remaining solid debris can also be ejected, depending on a user supplied input. The user can specify the fraction of core which must be molten in order for the ejection of all solid debris to take place.

MELCOR has a relatively sophisticated relocation model. Fuel failure occurs when structural support provided by the cladding is lost, usually due to clad melting. The clad subsequently candles and built-in algorithms allow the UO_2 to be transported to the support plate. The support plate fails at a temperature supplied by the user. Solid debris is transported, based on gravitational settling and molten debris candles on the lower plenum structures. In the lower plenum, the debris attacks the lower vessel head as well as a penetration. If the penetration fails, only that amount of material within the user-specified radial ring of the failed penetration will be ejected. Ejection of the corium will not occur until additional MELCOR constraints, involving the corium being sufficiently molten to flow, are met.

In the MELCOR-MAAP BWR comparison, the times between failure of the lower core plate and vessel penetration failure are markedly different. For the MAAP runs, the time predicted was about 10 seconds, while it was about 1 hour for the MELCOR base case. In MELCOR, a substantial amount of water in the lower plenum is boiled off before the penetrations were predicted to reach their failure temperature. In the MELCOR sensitivity runs made with a larger number of radial rings, the time between plate and vessel failure is reduced to about 1 minute. The wide spread in the two MELCOR results is due, in part, to an error in MELCOR affecting lower-core plate attack (see Appendix F). It was observed, however, that MELCOR predicts a penetration which, if sufficiently surrounded by debris, will fail before the debris is quenched by the lower plenum water.

3.2.2.7 Verification and Assessment the MAAP Model

There is little experimental data available for verification of core relocation models. Fauske and Associates, Inc. [9] reference the LOFT FP-2 experiment and the TMI-2 accident, and cite the TMI data to argue that the upper plenum structure remains intact as MAAP has predicted.

The assumptions used in MAAP that core material will relocate as a eutectic liquid and that this liquid is formed at a specified temperature are approximations. As previously noted, the user specifies the eutectic melting temperature and the latent heat of fusion. By varying these parameters the influence of the uncertainties associated with the eutectic liquid approximation on time of vessel failure, hydrogen production, and ultimately time of containment failure can be characterized. Using a high eutectic temperature, for example, would delay the onset of core melt, possibly prolong the clad oxidation, and generate more hydrogen.

Another uncertainty of the core relocation process is the degree to which the structural integrity of the vessel internals is maintained once fuel relocation has begun and high RPV temperatures have been reached.

3.2.2.4 Conclusions

Core slump, collapse, and vessel failure phenomena remain uncertain. The uncertainty of how the core materials will relocate once the vessel itself fails can be addressed to some extent by using the core collapse criteria modelling parameter, in MAAP. This parameter allows the user to specify the fraction of the core which must be in a molten state in order for all core materials, i.e. solid and liquid, to be expelled from the vessel. For instance, when this parameter, called FMAXCP in MAAP/BWR and FCRDR in MAAP/PWR, is set equal to 0.1, a core melt fraction of 0.9 is needed before solid material remaining in the core region is expelled.

The MAAP Guidance Document [4] already recommends that a sensitivity study, using this parameter, be performed in order to characterize uncertainties related to fission product revaporization in a failed reactor vessel (see Section 4.4). BNL suggests that this study be enlarged by looking at the effect the variation of this parameter has on containment failure time, and that this sensitivity calculation be carried out for every sequence where the RPV fails before the containment.

In BWRs, for instance, the integrity of the reactor vessel upper intern ructures is likely to be compromised due to degraded yield strength caused by elevated temperatures once condi. causing core relocation are reached. In one calculation, MAAP predicted the outer shroud head would reach a peak temperature of 1300 K at about 9000 seconds. This temperature might be high enough for collapse; however, the temperature never reached the melting range. In general, however, the ability to retain structural support for the core once fuel relocation has begun and high RPV internal temperatures have been reached is uncertain. A substantial relocation of solid core debris cannot be ruled out. MAAP's modeling parameter FMAXCP allows the user to vary the amount of core required to have melted at the time of vessel failure to relocate all of the remaining core. While the geometry in PWRs is different, the possibility of solid debris relocation and expulsion still exists, and the PWR sensitivity study [7] showed that variation of the parameter influenced containment failure time significantly in PWRs.

Similar to the guidance in Reference 4, BNL suggests that for this sensitivity case the core melt fraction required for total core relocation at containment failure be set at 0.2 instead of the 0.9 value used for the base case.

BNL recommends a second sensitivity case to address core relocation uncertainties. The variation here should be on the latent heat of fusion of the eutectic mixture, parameter LHEU. This parameter influences both hydrogen production as well as the distribution of core materials throughout the reactor vessel, the cavity and the lower containment. This distribution will affect the amount of CCI taking place.

The PWR sensitivity study [7] showed that this could be an important parameter for containment failure time. One of the sensitivity cases, calculated in Reference 7 but not recommended in Reference 4, showed that all of the core debris would be released from the vessel compared with about 70% of the core in the base case and that the time to containment failure was reduced by several hours [7]. Because of the apparent sensitivity of this parameter, a MAAP calculation should be performed using the upper value of the uncertainty range suggested in the MAAP sensitivity study [7]. Limited sensitivity studies with the eutectic heat of fusion parameter, previously carried out with the BWR version of MAAP did not indicate as significant a sensitivity as was found for PWRs. Moreover, for BWRs, this sensitivity calcualtion is believed to be covered by other BWR recommended sensitivities. However, because (1) the eutectic heat of fusion is a true physical uncertainty, (2) not all BWR containment types and accident scenarios were investigated in detail to ascertain this parameter's quantitative significance, and (3) for the sake of consistency, this sensitivty calculation is also recommended for BWRs.

3.3 After Reactor Vessel Failure

3.3.1 Direct Containment Heating (DCH)

At the present time, Direct Containment Heating does not have to be quantified by the utilities performing an IPE. For completeness, a review of the DCH model in MAAP is included here.

3.3.1.1 Issue Discussion

This issue deals with the potential dispersal of molten core debris into the containment's atmosphere following release from the reactor vessel at high pressure, and the subsequent energy transfer from the dispersed core debris to the atmosphere, causing rapid pressurization. The severity of such an event could be further exacerbated by the burning of hydrogen. Hydrogen may be generated by direct oxidation of any metallic component during the dispersal process, or be simultaneously released from the reactor vessel into the containment.

Appendix 1 of the NRC IPE Generic Letter [1] listed the following uncertainties related to direct containment heating: 1) area of the vessel failure, 2) the amount of molten corium in the lower head at the time of failure, 3) the degree to which the corium fragments upon ejection, 4) the degree and extent to which a path from the lower cavity to the upper containment atmosphere is obstructed, 5) the amount of fragmented molten corium that could enter and interact with the atmosphere of the upper containment, and 6) the temperature of the cavity gas. Because of these uncertainties, NRC stated that parametric variations should be used to investigate the impact of these uncertainties on the containment response in future industry studies. Mitigation of the potential for high-pressure melt ejections (HPME) should be considered in the Severe Accident Management (SAM) program.

3.3.1.2 MAAP and MELCOR Model

MAAP 3.0 used a simplified parametric approach to treat DCH (PWR version only). A modified model was introduced in MAAP 3.0B [8]. The following are the basic assumptions used in MAAP 3.0B:

(1) The initial molten core debris consists of UO_2, Zr, ZrO_2, and steel;

(2) The oxidation of Zr, Fe, and Cr by steam and oxygen in the compartment are allowed;

(3) The order of oxidation is Zr, Cr, and Fe based upon availability of reactants;

(4) The order of reaction among oxidizing agents is, first - entrained water, second - steam in the destination compartment, and last - oxygen in the destination compartment;

(5) Available energy from the core debris includes the internal energy of each component plus energy produced by oxidation;

(6) Energy is first transferred to co-entrained water until either the debris is quenched or all the water is vaporized;

(7) A new, effective debris temperature is determined after the preceding chemical reactions and quenching have been evaluated. The new temperature then is used to determine energy transfer to gases in the destination compartment;

(8) Evolved hydrogen can burn if the gas concentrations or temperatures exceed the flammability threshold;

(9) Simultaneous entrainment of water and corium to the lower and upper containments is allowed.

The parametric characteristics of the MAAP DCH model are reflected in two user-specified model parameters: FCMDCH and FCMDA. The parameter FCMDCH refers to the fraction of debris that is transported from the reactor cavity as finely fragmented droplets. The parameter FCMDA refers to the fraction of debris that is transported to the upper compartment. The default values for FCMDCH and FCMDA in MAAP/PWR revision 17 are 0.1 and 0.4, respectively. The MAAP IPE guidance document [4] recommends selecting values of the two parameters based on the configuration of the cavity. It further recommends that an uncertainty analysis be performed for the parameter FCMDCH, but not for FCMDA.

The present version of the MELCOR code does not have a DCH model, and hence, no comparison could be made.

3.3.1.3 Verification and Assessment of the MAAP Model

At the second NRC MAAP Familiarization Meeting, FAI discussed their MAAP DCH benchmarking activities in two areas: (1) debris ejection from the cavity, and (2) debris disposition in the lower compartment after ejection. The experiments considered in the benchmarking activity include (1) ANL's fluid reactor cavity simulation, (2) ANL wood's metal tests with a simulated reactor cavity and lower compartment, (3) SNL tests on a Zion-like reactor cavity, (4) ANL's analysis of corium-water thermal interactions, (5) FAI wood's metal building-block tests, and (6) FAI's 20 Kg thermite tests, in a 5% scaled geometric model of the Zion reactor cavity, lower, and upper compartments. These experiments increased understanding of the DCH process and confirmed some of the basic assumptions used in the MAAP code. However, some of the major modifications to the MAAP 3.0B DCH model have not been verified (such as the simultaneous dispersal to both lower and upper compartments).

3.3.1.4 Conclusion

The MAAP DCH model is parametric. The accuracy of its predictions strongly depends on the boundary and initial conditions at the time of reactor vessel failure, and the user-specified model parameters. The conditions at the time of reactor vessel failure are determined by MAAP's treatment of melt progression in the reactor vessel. The values of the model parameters depend on the configuration of the specific cavity and containment of each plant. Therefore, uncertainty analysis is essential for the MAAP DCH model. For example, in addition to model parameters, the mass of steel structures modeled in the reactor vessel should be considered in uncertainty analysis, because the modified DCH model includes the oxidation of Fe and Cr.

3.3.2 Heat Transfer Models from Molten Core to Concrete/Containment

3.3.2.1 Issue Discussion

When the corium penetrates the lower vessel head and interacts with containment surfaces, there is uncertainty related to the amount of energy produced by the corium and the distribution of this energy. These issues can affect the time to containment failure, and the success of mitigating actions.

The source of energy includes the chemical oxidation reactions that occur as water and carbon dioxide are released from the concrete. Water in the concrete is either chemically bound or free to evaporate. Reactions that can take place and the phases of the reactants and products have much to do with the chemical energy produced. What chemical constituents are available to react depends on the stratification, or lack of it, in the corium pool.

Energy is transferred from the corium pool to the surroundings, including concrete, water, and atmospheric gases. Various approximations can be made regarding which heat transfer modes are dominant. Since heat transfer is a strong function of the available surface area, any assumption related to how far the corium debris spreads is also an important consideration.

3.3.2.2 MAAP and MELCOR Models

MAAP assumes that the debris is in liquid form, and hence, it will spread within the confines of its containment surroundings. In addition, levitation of the debris is modeled if failure of the reactor pressure vessel (RPV) occurs under high pressure. MAAP assumes all corium components are perfectly mixed, and this allows for the reduction of UO_2 by zirconium metal. Hence, ZrO_2 can be formed without the need for concrete ablation. The release of both evaporative and bound water occurs when the concrete is predicted to reach an ablation temperature [4] supplied by the user. The fraction of the energy transferred from the corium to the atmosphere is partly controlled by the convective heat transfer coefficient between the corium pool and its crust, also supplied by the user. The mode of heat transfer from the upper surface of the corium is a combination of radiation to the concrete walls and convection to the atmosphere. In the version of MAAP reviewed in this study, it was assumed that the gases (H_2O and CO_2) emitted from the side walls of the concrete being attacked by the corium will not react with the corium.

MELCOR assumes the debris is a mixture of solid and liquid but its ability to spread is controlled by a separate cavity structure which is user specified. MELCOR does not provide for levitation or entrainment of the debris caused by a high-pressure RPV blowdown. MELCOR assumes that the oxides are not in contact with the metals, and hence, zirconium oxidation occurs from the release of H_2O and CO_2 from the concrete. MELCOR allows for the release of free water from the concrete at a much lower temperature than that used in MAAP if the concrete degassing option is chosen. Otherwise, MELCOR simplistically assumes the simultaneous release of free and bound water. Unlike MAAP, MELCOR's heat transfer to the surrounding containment atmosphere considers radiative heating of the gas by the corium upper surface. Convective heat transfer to the gas is also modeled. The gases released from side-wall-concrete ablation are allowed to react with the corium. From the MAAP-MELCOR comparison we observed there was a large difference in chemical power predicted by the two codes [Appendix D].

3.3.2.3 Verification and Assessment of the MAAP Model

There are a number of experimental programs, which provide data for benchmarking in this area: SWISS, which measured the extent of concrete ablation when water was added above the corium; SURC (sustained urania/concrete) experiments; and the BETA experiments. MAAP gives good overall predictions of the depth of concrete ablation observed in the SWISS tests. There was considerable disagreement between MAAP calculations and SURC data. This was traced to an error in MAAP which has been corrected. The discrepancy observed between MAAP predictions and the BETA results was attributed to the aspect ratio of the tests. That is, the experiments were conducted with corium spreads that were deep and narrow, not shallow and wide as the MAAP authors believe would be more typical of accidents.

Items that could benefit from further study, include radiative heating of the atmosphere, modeled in MELCOR and not in MAAP, direct energy deposition in the atmosphere from airborne energy-producing fission products, and heating of slabs by deposited fission products.

Sensitivity cases which affect this issue are discussed in Section 6.2.1.

3.3.2.4 Conclusions

Uncertainties associated with CCI are many and it would be difficult to have sensitivity cases for every one of the large number of model assumptions that go into CCI's contribution to determining containment failure time. Comparison of MAAP and MELCOR calculations help to provide an estimated quantification of the uncertainty.

As stated in Section 2.3.2, several recommendations were given in Reference 4 for MAAP sensitivity cases related to core/concrete/water interactions. These recommendations include consideration of items such as the amount of floor area the corium might occupy and the mode of heat transfer between the corium and an overlying water pool. These input options were found to be adequate for application of the PWR version of MAAP to an IPE. However, for BWRs, the effects on CCI from the corium spreading in the drywell, and from ablated concrete of vertical surfaces contacted by the corium pool, need special consideration. The MAAP user should ascertain if, for the representative sequences being analyzed, the volume of the corium would be sufficient to spill over onto the drywell floor. This is important for sunken (pedestal floor is lower than drywell floor) pedestal floors. If the drywell floor does receive corium, then we recommend a base case where the corium is restrained to a drywell floor area of 1/4 of the true drywell floor, and a sensitivity case where the corium is permitted to spread throughout the drywell floor. This applies to all BWR containment designs with the exception of a Mark II containment exposed to a low pressure RPV meltthrough. For the latter case, MAAP 3.0B already accounts for possible corium flow channeling based on the manways connecting the drywell and pedestal regions. It should be noted that Reference 4 does presently recommend a sensitivity for a Mark I containment where the base case is assumed to be full drywell floor spreading of the corium and the sensitivity restricts the corium in the drywell to 1/4 of the drywell floor. We have recommended the base case to be the restricted corium flow case because it is generally consistent with the approach in NUREG/CR-5423, "The Probability of Liner Failure in a Mark I Containment," Theofanous, T.G., et al., August 1991.

In addition, we recommend that a modification to MAAP 3.0B Rev 7.0 (BWR version) be made to calculate the effect of allowing the full sidewall gases to react with the corium pool. BNL recommends the mode, ; enhancement be part of the base case (see Section 6.2.1).

For high pressure RPV meltthrough, MAAP 3.0B for BWR use does not include a Direct Containment Heating model. The BWR version of MAAP 3.0B is capable of performing a calculation of the containment response for a high pressure sequence and w have reviewed this model. However, we cannot judge its acceptability due to la of relevant experimental data 'WRs to serve as the basis for an assessment. Rather, the NRC has in the past recommended, and continues to recommend, that utilities address high pressure RPV failure sequences according to the guidance in GL 88-20 and its supplements 1 and 3. In particular, NRC has emphasized enhancement of ADS reliability.

3.3.3 Hydrogen Ignition and Burning

3.3.3.1 Issue Discussion

This issue addresses ignition criteria, the rate and completeness of combustion, gas transport by natural convection, and hydrogen recombination in the reactor cavity. There were substantial differences between models used in NRC sponsored codes and the models used in the early MAAP 2.0 and 3.0 codes. The differences influenced the pressure and temperature loads imposed on the containment structure and equipment predicted by the codes. However, the earlier MAAP 3.0 combustion model has been replaced by a new model in MAAP 3.0B [8] which uses a different approach to the flammability limit and completeness of combustion.

3.3.3.2 MAAP and MELCOR Models

The technical aspects of combustion involve combustion modes (e.g., deflagration, detonation, and diffusion flame), flammability limits, burn time, burn completeness, presence of ignition sources (deliberate or random), and mixing of gases in the containment. Most of the technical aspects are treated reasonably in MAAP 3.0B. Mixing in the containment depends on the containment nodalization, and the modeling of natural circulation in the containment. MAAP has a fixed coarse nodalization and pre-defined natural circulation loop. For a lumped-parameter code, MAAP's containment model can reasonably represent the major compartments of a containment. However, stratification within a compartment and local concentrations of gases cannot be addressed. The fixed and pre-defined coarse containment nodalization prevents the code from being used to perform sensitivity calculations in this area. MAAP 3.0B cannot be used to assess the potential for local detonation, which strongly depends on gas mixing in the containment. This is recognized in the MAAP guidance document [4].

MAAP models two types of deflagration; global (complete), and local (incomplete). A global burn involves the burning of all combustible gases in a compartment. A local burn is initiated by deliberate ignition systems (i.e., igniters) and may involve only a fraction of the gas volume in a compartment. The ignition of hydrogen-laden jets is modeled as a diffusion flame in the MAAP code. This type of burn refers to those circumstances when a very high temperature jet emerges from a potentially inerted region into a cooler, non-inerted region where it induces a burn.

In the MAAP 3.0B code, the flammability limits are determined by the construction of a combustion diagram. The domain of the diagram consists of both lean and rich flammability limits (LFL and RFL). A power law expression is developed for the flammability limit curve that is further modified for elevated temperatures. Limited experimental results have shown that high temperatures tend to cause the LFL to decrease and the RFL to increase. The flammability limit curves at various temperatures are used in the MAAP code for upward and downward flame propagations. The limits of upward flame propagation are for the global (complete) burn mode. At elevated temperatures, a very small fraction of hydrogen is required to induce a flame propagation. This situation leads to the autoignition model in the MAAP code which assumes that ignition occurs if the temperature of the mixture is above a critical autoignition temperature (model parameter TAUTO), and the inertant fraction is less than a specified value (model parameter XSTIA). The nominal autoignition temperature is 983K and the maximum inerting fraction is 0.75 in the MAAP code.

The MAAP code also applies an ignition criterion when active igniters are present. The ignition criterion is specified in terms of a mole fraction of hydrogen above (or below) the temperature- and steam-concentration-dependent limits. The user-specified ignition criterion is model parameter DXHIG, and the recommended value is zero. This model parameter can be used to represent the postulated unreliability of igniters.

The ignition of a hydrogen-laden jet is determined by comparing the temperature of the gas stream with the user-specified autoignition temperature TJBRN. The recommended value for TJBRN is 1060 K. Jet burning will not occur if the downstream compartment has less oxygen or more steam than would allow a premixed burn. The jet burn criterion is consistent with the flammability limit used in MAAP. Sensitivity analyses for jet-burning, autoignition, and the unreliability in igniters are recommended in the MAAP guidance document [4].

The burn time and combustion completeness are key parameters that determine the quantity of hydrogen reacted and the combustion rate, which, in turn, determine the rate of energy release and containment pressurization. In MAAP, the burn time and combustion completeness are obtained by solving the mass and momentum equations for a fireball. MAAP assumes that the spherical fireball expands at the speed of a laminar flame when buoyancy effects are small. When the fireball is large, its growth is modeled as a plume entraining unburned gases at a rate proportional to its upward velocity. The upward velocity is determined by considering the acceleration of the fireball due to buoyancy and drag forces. The analytical model involves several parameters, such as entrainment coefficient, speed of the laminar flame, the fireball's surface area, and drag coefficient. The uncertainties in these parameters are covered by a user-specified flame-flux multiplier, model parameter FLPHI. The recommended best estimate values of the flame flux multiplier are 2 and 10, respectively, for quiescent and turbulent conditions. BNL recommends performing an uncertainty analysis on the flame flux multiplier for the IPEs.

The combustion model in MELCOR assumes a discrete burn, which refers to the burning of combustible gases uniformly in a compartment only after the prescribed ignition or propagation criteria are met. These criteria are based on experimental data, determined in steam-saturated air at relatively low temperatures and pressures. The criteria depend only on the concentrations of gases: there is no temperature-dependency.

MELCOR does not model hydrogen combustion as a flame front; instead, it assumes that hydrogen burns uniformly in a compartment. The flame speed and completeness of combustion are determined by empirical correlations derived from a variety of experiments.

3.3.3.2 Verification and Assessment of the MAAP Model

The flame-flux multiplier is an important parameter because it attempts to encompass most of the uncertainties in MAAP's analytical solution of the fireball. This multiplier has been determined by benchmark calculation against four series of experiments (WNRE, EPRI/ACUREX, VGES, and NTS), all of which involved the burning of hydrogen by igniters in a pre-mixed atmosphere. Several injection tests were included in the EPRI/ACUREX experiments. FAI reported that the experimental data on pressure rise and completeness of combustion can be represented by using a flame-flux multiplier of 2 for quiescent conditions, and 10 for turbulent environments when the containment fans or sprays are turned on. When these values for the flame-flux multiplier are used, the MAAP combustion model agrees reasonably well with many experimental results. However, it also underpredicts the completeness and duration of burns observed in many of the experiments.

We note that all the tests involved in the benchmark experiments were performed at low temperatures and low pressures. The test environment differs from that expected in the containment during a severe accident. Furthermore, few tests were selected to represent the turbulence environment, and they only involved fans. Tests involving sprays (EPRI/ACUREX tests 2-4 and 2-9) are not reported in the benchmark calculation. Among these test cases of limited turbulence, many were performed in an atmosphere without any inert gases (steam or CO_2), which is unlikely to occur during a severe accident. Thus, there could be uncertainties in the recommended values of the flame-flux multiplier for severe accident analysis because of the differences between the conditions of the test and those expected in the containment.

3.3.3.3 Conclusion

The new model introduced into MAAP 3.0B is an improvement for describing combustion behavior. Because there is no sensitivity study of the new model on containment performance [7], and there is no direct comparison between the MAAP model and the NRC-developed model, we are unable to assess its impact on containment performance analysis.

The new model appears to be limited by the lack of flammability data at elevated temperatures and the uncertainty ascribed to the utilization of the flame-flux multiplier.

In the MAAP guidance document [4], there is no recommendation regarding variation of the multiplier parameter for uncertainty analysis. However, we recommend that the multiplier parameters be considered in an uncertainty analysis for BWR and PWR sequences in which combustion plays an important role in the containment's performance. The same values of the parameter recommended for uncertainty analysis for ALWRs [10] should be used for IPEs, as discussed in Section 6.1.1.

3.3.4 Containment Performance

3.3.4.1 Issue Discussion

This issue involves the mode of containment failure and the related size and location of failure. Two types of assumptions regarding the mode of containment failure have been used for severe accident risk estimates: catastrophic failure at some threshold pressure, or a leak-before-break mechanism. In a document related to NRC/IDCOR issues [5], the NRC staff stated that leakage criteria for penetrations have not been developed and verified. "It is, therefore, the staff position that until such time that the leakage criteria have been developed based on the results of separate effect experiments that have been conducted on electrical penetration assemblies, isolation valves, and steel and gasket materials, it should be assumed in severe accident analyses that the containment fails upon reaching the threshold pressure" [5].

The size and location of containment failure affect the consequences and the risk associated with severe accidents. The predictions of failure size and location depend on the details of accident evaluation. NRC staff [5] stated that, ". . .since rupture is often caused by highly localized phenomenon that may be difficult to anticipate, analyses with large containment failure sizes (e.g., values used in NRC risk studies) must be undertaken." For the failure location, NRC staff [5] stated that, ". . .for containments that are completely surrounded by an enclosure building where credit for deposition of fission product is assumed, several failure locations should be considered in the analyses to establish the most likely place for containment failure."

3.3.4.2 MAAP and MELCOR Models

In the MAAP code, two models can initiate containment failure. One is a simple model which uses a user-specified parameter, such as a threshold pressure, threshold temperature, or a temperature-dependent pressure limit as the failure criterion to initiate catastrophic failure. A more detailed model involves stress and strain analysis. In this model, containment failure is assumed to occur when the resultant stress equals the ultimate stress. This model can simulate a leak-before-break situation if the initial failure is in the steel liner. The MAAP IPE guidance document [4] recommends that the simple model be used for IPEs.

The failure location and size are user-specified in MAAP. Depending on the accident sequence, the failure location could be in the wetwell or drywell regions for BWRs, and in the upper or annular compartments for PWRs. The MAAP IPE guidance document [4] does not recommend any sensitivity study on failure location, except for a BWR Mark I containment. Based on a study of containment strength, Reference 4 recommends that utilities performing IPEs for BWRs with Mark I Containments should investigate both wetwell and drywell failures. For the failure size, the MAAP IPE guidance document [4] recommends a small leakage area (about 0.005 square meters) if the containment is experiencing slow pressurization, and a larger area (about 0.1 square meters) for rapid pressurization. However, Reference 4 states that plant-specific assessments are highly desirable.

MELCOR uses control functions to simulate containment failure. Failure can be initiated at a user-specified pressure, temperature, or time. The control function is equivalent to the simple model available in the MAAP code. Failure location and size also are user-specified in MELCOR.

3.3.4.3 Verification and Assessment of the MAAP Model

The MAAP containment failure model requires user-specified failure criteria - pressure or temperature, location, and area. These parameters are plant-specific and may be determined by containment specific stress analysis.

3.3.4.4 Conclusion

The MAAP containment-failure model is a parametric one based on user-specified events. All the input parameters are plant-specific and are subject to uncertainty. MAAP sensitivity analyses [7] showed that the containment failure time can be significantly affected by the estimated failure pressure and temperature. The MAAP guidance document [4] recommends that the determination of the type of sensitivity calculations needed should be based on the results of independent analyses which provide the best-estimate containment failure pressure for the plant analyzed. The uncertainty of failure pressure should also include the effect of temperature on the integrity of the containment [4].

4 Fission Product Release and Transport

Fission product calculations, while not the primary focus of IPE analysis, will play a role, as indicated in NUREG-1335.[2], in plant assessment. Some utilities may want to rely in part on MAAP calculations to support their analysis in this area. Therefore, this section describes the important models in MAAP related to fission product generation and transport. Comparisons with the corresponding MELCOR models or other available information are also made. Some observations and insights resulting from the BNL examination of the MAAP models in this area are also included in the discussion below.

4.1 Fission Product Release Prior to Vessel Failure

4.1.1 Issue Discussion

There are four concerns associated with this issue: the initial release of fission products from the fuel, the temperature required for relocation, tellurium retention by unoxidized zirconium, and the chemical form of iodine. Subsequent to meetings between NRC staff and industry several years ago, changes were made in MAAP to address the first three concerns.

The timing of the fission product release from the fuel can have a significant effect on the amount and timing of the release to the containment. The thermal hydraulic conditions in the vessel determine the degree of deposition and transport of the fission products.

The fuel failure temperature corresponds to the loss of structural integrity of the cladding and its ability to retain gaseous fission products. The temperature chosen for this phenomenon can also affect the environmental source term, as it affects vessel failure time.

Tellurium (Te) can be assumed to be released in-vessel or carried along with the zirconium as it is relocated. For severe accidents which result in failure of the reactor vessel and the containment, Te's contribution to the environmental source term depends on whether it is released in-vessel or ex-vessel as a result of CCI. Iodine's chemical form, whether it is in the form of CsI or elemental iodine, will affect its deposition and revaporization properties in the reactor pressure vessel and containment, and hence, its release to the environment.

4.1.2 MAAP and MELCOR Models

Unlike the PWR version of MAAP 3.0B, the BWR version does not have a gap release model. There is a fuel damage temperature, which is the criterion for the beginning of fission product release from the fuel, but MAAP does not model the release of fission products from the fuel-clad gap and plenum [11]. The recommended damage temperature is set at 1200 K in the BWR [4] version.

MAAP uses a eutectic temperature of 2500 K for the beginning of relocation of molten core materials [4]. This temperature is above the melting temperature of zircaloy, but below that of UO_2. The cladding and fuel are modeled as one temperature node in MAAP.

In the guidance document [4] for MAAP, the recommendation is to bind all Te to the unreacted zirconium and release it ex-vessel. Elemental iodine is not modelled in MAAP.

MELCOR has a gap release model with a release temperature of 1173 K. It employs a clad-melt temperature, which can be chosen as the eutectic melt temperature, if the user desires. Default values in MELCOR assume that the relocating molten material is a eutectic, consisting of 20% UO_2 and 80% Zr. In MAAP, all the UO_2 is assumed to form a eutectic with all the clad (in the BWR model, this includes the channel zircaloy). MELCOR allows elemental iodine to be tracked separately from CsI. MELCOR also makes provisions for Te retention by unoxidized zirconium [6], and modifies the release of Te in-vessel to account for this.

The U-Zr-O phase diagram [12] shows that where Zr in the clad is available to form a eutectic with UO_2, a slurry phase of liquid and solid U-Zr-O would exist from 2173 K to 2673 K. The time needed for full dissolution of UO_2 (zirconium attacking the UO_2 grain boundaries) would be a few minutes at 2500 K. At this temperature, however, a relatively large fraction of UO_2 would remain in a solid phase when a dissolution nearing 70% is obtained (a slurry with about 30% in solid form). In most cases, the failure of the vessel will occur earlier if earlier corium relocation is predicted. MAAP's assumption of an all-liquid corium may not allow as fast an attack on the lower support plate as would the assumption of a solid-liquid phase.

The guidance document [4] cautions that, under some conditions, the assumption that Te is released only outside the vessel can be non-conservative. However, it does not recommend varying the release model flag when MAAP is used for the IPE studies. No investigation was made on Te distribution in the MAAP-MELCOR comparisons.

Tellurium can be modelled in MAAP as being carried out of the vessel with the unoxidized zirconium. There is no quantitative justification given for performing sensitivity studies on the release of Te in-vessel for those cases where the assumption of all Te being released ex-vessel is considered non-conservative. Such cases would include those where containment failure occurs before vessel failure.

4.2 Release Model for Control Rod Materials

4.2.1 Issue Discussion

In PWR plants (with silver-indium-cadmium control rods), this issue relates to the fraction of the control rod material that would be released as an aerosol in the primary system during a core-melt accident.

For BWR plants, the issue relates to possible chemical reactions of the boron carbide (B_4C) control material that could increase hydrogen production and alter the chemical form of the fission product species, especially iodine.

4.2.2 MAAP and MELCOR Models

The MAAP-PWR model accounts for the release of control materials. The major assumptions used in the MAAP code are:

(1) The control rod materials (Cd, In, and Ag) and other structural materials (Sn and Mn) are lumped together as radioactivity-inert aerosols.

(2) These materials are released in their dominant chemical form when the node reaches the melting temperature of carbon steel.

(3) The releases are limited by their saturation densities at the model temperature.

(4) When the blockage model is used, the local flow is set to zero at the user-specified fuel eutectic temperature (2500 K). Therefore, structural materials are not released from the blocked nodes.

(5) When the blockage model is not used, the releases of structural materials are based on the conditions of flow and saturation.

(6) The user controls the saturation limitation through a model parameter which overrides the limitation. The impact of the blockage model on clad oxidation is, thus, separated from its impact on the release of fission products.

In MELCOR, fission products are grouped into 15 classes according to their properties. The control rod material cadmium (Cd) is added to group 11, and indium (In) and silver (Ag) are added to group 12. The release rates of fission products are computed by the empirical correlations of the CORSOR or CORSOR-M model. Both models consider the release rate of each material class as a function of temperature only. MELCOR also considers the effect of vapor pressure of each material class.

Neither MAAP nor MELCOR models the chemical reactions of B_4C.

In-pile tests in the Power Burst Facility (PBF) (SFO-1) and Annular Core Research Reactor (ACRR) (DF-3) under conditions typical of a reactor accident sequence, support control-rod modeling and relocation models leading to low aerosol production [5]. The test results agree qualitatively with the predictions of the MAAP model on control-rod aerosol release.

At present, the NRC and IDCOR models are in agreement, in so far as both models predict that the control material aerosols are not expected to have a significant effect on in-vessel fission product behavior. For BWRs, the effects of B_4C on hydrogen production and on the chemical form of iodine are minimal.

4.3 Model for Fission Product and Aerosol Deposition in the Primary System

4.3.1 Issue Discussion

The deposition of aerosols in the RPV depends on a number of removal processes. NRC code development in this area involves grouping the aerosols by size (sectional code). Such a tool is the computer code MAEROS [13], which is incorporated into the MELCOR code. To have a much faster running code, the utilities have sponsored an approach that does not explicitly track aerosol size groups, but uses empirical data to help establish decay constants. This model uses equations for steady-state and aging (aerosol mass concentration decay) time-periods. Concerns have been raised on the appropriateness of this model for the full spectrum of possible accident conditions.

4.3.2 MAAP and MELCOR Models

Details of these models can be found in Appendices A and B. As stated above, MELCOR uses a sectional code whereas MAAP employs aerosol mass-decay constants in a steady-state and aging-mass equation set.

Since early 1985, additional numerical and empirical comparisons have been made on a refined aerosol model. These comparisons included the AB2, 5, 6, and 7 tests [9]. Comparisons against the DEMONA test also were made. The MAAP developers claim good agreement during the source and decay periods [8], and that the model is conservative during the transition from source to decay.

Based on the literature review o.   MAAP model, we believe that specific groups of material aerosols may experience different source-to-decay transition times, than represented by MAAP. We believe grouping all material class elements and compounds into one mass group, as represented in MAAP has not been completely justified [14].

4.4 Revaporization of Fission Products in the Upper Plenum

4.4.1 Issue Discussion

Fission product aerosols and vapor deposited on cool vessel components can become resuspended due to revaporization. This issue focuses on the amount and timing of the revaporization. in particular, the effects of surface chemistry are considered importan'. The vapor pressures of the fission products may change because they have chemically combined with the steel of the in-vessel components.

The thermal-hydraulics in the vessel will affect deposition and revaporization. The energy carried by the fission products to heat the in-vessel components needs to be predicted, as do the flow currents.

4.4.2 MAAP and MELCOR Models

To address this concern in MAAP, there are three specific modelling assumptions. The fission-product energy carried by each material group is fixed as a time-independent fraction of the decay power. MAAP does not alter the vapor pressure of the fission products caused by chemical reactions on the surfaces of the in-vessel components. MAAP predicts the effects of natural circulation flow in and out of a vessel, for cases where the vessel has two flow paths in communication with the containment. This flow provides a strong driving force for removing the revaporizing fission products from the vessel.

MELCOR alters the fraction of power produced by each fission-product material group as a function of time. It does not allow any in-vessel chemical reactions with component material. Any circulation flow paths are determined by the conservation laws for the arrangement of the vessel's control volumes.

Sensitivity studies on revaporization uncertainties were performed in a past MAAP analysis [9], by altering the vapor pressure of the fission-product groups. This alteration resulted in a delayed release of the volatile fission products and the overall mass. The MAAP developers now recommend the inclusion of a new parameter [4] that will affect only the vaporization rate. It is not yet clear what form the new rate-equation will take.

The MAAP guidance document [4] recommends further sensitivity studies on the removal of the remaining core mass, once the vessel has suffered melt-through. The intention here is to affect the rate of heat-up of the in-vessel heat slabs by the deposition of fission product from the remaining core material. Normally, the user is directed to assume that when 90% of the original core mass has been removed from the core and the vessel has failed, the remaining 10% should be ejected. However, to see the effect on revaporization timing, a sensitivity study is recommended [4], whereby the heat supplied to the heat slabs is reduced by removing the remaining core material once 20% has melted out of the core region and the vessel has failed. This recommended sensitivity study is for both PWR and BWR IPE application.

The guidance document [4] recommendation for sensitivity cases regarding the fraction of molten core material existing at the time of vessel failure, and needed to expel all core material, is a good one and should be augmented to gauge the effect this variation has on containment failure time, as discussed in Section 3.2.2.

Some power factor concerns were found in the MAAP-MELCOR comparison as described in Appendix D.

4.5 Ex-Vessel Fission Product Release Modelling

4.5.1 Issue Discussion

This issue is related to the issue of "Heat Transfer Models From Molten Core to Concrete/Containment" discussed in Section 3.3.2. There, we discussed some of the uncertainties relating to the composition of the corium debris in the cavity or pedestal. In Sections 5 and 6, we mention the large difference associated with chemical power predicted by MAAP and MELCOR. The debris temperature and composition have a direct effect on the gases and fission products released during CCI. The problem is complicated by the uncertainty of the chemistry of the CCI material, which alters the reactions and the rates of those reactions.

4.5.2 MAAP and MELCOR Models

The number of compounds existing in the corium pool and the rates of chemical reactions that can occur will affect the release of fission products. In MAAP a homogenous pool of material with perfect mixing is assumed, and compounds that will contribute at least 1% or more to an element's total vapor pressure are considered [15]. An ideal solution behavior for most of the reactions is assumed, i.e., that the Gibb's free-energy of a reaction is unaffected by other compounds in the pool. As such, the energy states are unperturbed and the activity coefficients are set to unity. However, in MAAP 3.0B, a change was made to allow the user to alter the activity coefficients of a number of compounds: K_2O, SiO_2, SrO, and BaO.

In MELCOR the oxide and metal compounds are stratified. However, within each layer an ideal solution is assumed to obtain the equilibrium constants using Gibb's free-energy. One difference of this modeling is that while MAAP reduces UO_2 with Zr, these materials do not come into contact in the corium pool of MELCOR. Therefore, the oxidation of zirconium occurs when water or some other oxidizing agent is released from the concrete.

From the MAAP-MELCOR comparison, we observed that there was a large difference in chemical power predicted by the two codes. Further, MELCOR showed large differences in the temperature of the different stratified layers in the corium pool, which could have a significant effect on the vapor pressures of the fission products. MELCOR predicts as much as a 500 K increase from the light oxide to the metal layers.

There is uncertainty in both the physical stratification of metals and oxides as well as the thermodynamic properties of the corium mixed with concrete constituents. The effects on temperature also will affect the release of fission products from CCI. Section 3.3.2 discussed of some of the empirical studies that have been compared to MAAP.

The METOXA program is used in MAAP to determine the chemical reactions during CCI. It has been checked for consistency in a FAI publication [16]. The choice of the non-unity activity coefficients is supplied in the MAAP guidance document [4]. Admittedly this choice is not based on a large amount of empirical data.

Uncertainties in this area remain. As more information becomes available, it should be considered in the modelling.

4.6 Amount and Timing of the Suppression Pool Bypass

4.6.1 Issue Discussion

For some severe accidents in BWRs, steam and gases from the core debris percolate through the suppression pool. Under these circumstances, the water can retain a significant fraction of the aerosols and condensed vapors. This pool scrubbing is a very effective way of reducing the airborne fission products and thus reducing the potential source term. However, if the flow path bypasses the suppression pool, this important scrubbing action is also bypassed with the possibility of a much larger source term. Aerosol buildup sufficient to plug the flow paths is predicted to occur under some circumstances. A previous NRC review [9] of this issue involved consideration of the Vaughan plugging model. A particular concern was whether or not this model can correctly predict suppression pool bypass, and hence, the effectiveness of fission-product scrubbing. The issue has been extended to include plugging of containment leakage paths.

Technical Specifications for BWRs specify an allowable suppression pool bypass. Normal bypass from drywell to wetwell is not usually modeled in studies of source term. Instead, an estimate is made of the probability of gross bypass and the source term effects determined for this case.

4.6.2 MAAP and MELCOR Models

MAAP incorporated the Vaughan plugging model. MELCOR does not have an explicit model for predicting plugging of suppression pool bypass paths.

Earlier review by the NRC of MAAP [9] considered the IDCOR Technical Report 85.2 [17] (July 1985). After some changes were made, the Vaughan model was found acceptable for a driving pressure less than a few tenths of an atmosphere, and flow path areas less than 1 cm in diameter.

The IPE guidance document [4] concurs with the earlier agreement on the use of the Vaughan model. That is, for flow paths less than 1 cm in diameter and differential pressures across the flow path of less than a few tenths of an atmosphere, plugging is permitted. If the pressure increases, the plugged path will be reopened, but could be plugged again if the pressure drops below a few tenths of an atmosphere.

4.7 Secondary Containment Performance

4.7.1 Issue Discussion

Several parameters that can affect the size and makeup of the radiological source term to the environment involve the performance of the secondary containment, i.e., the reactor building for BWRs and the auxiliary building for PWRs. Residence time governs the sedimentation of aerosols. The size of the postulated break in the primary containment, the break's location, the potential for hydrogen burns and other fires, the configuration of forced and natural circulation flow-paths, and the production rate of CCI gases will affect residence time.

Secondary containment performance is measured in terms of a secondary containment decontamination factor (DF), which is defined as the mass of fission products released to the secondary containment divided by the mass of fission products released to the environment. In past comparisons [4], it was observed that MAAP could yield significantly larger DFs than the NRC-sponsored code models.

4.7.2 MAAP and MELCOR Models

Appendices A and B compare the aerosol models for MAAP and MELCOR. Essentially, MELCOR tracks multi-size aerosols while MAAP uses a method that determines an equivalent removal constant, and does not track aerosol size concentrations.

Either code will allow the user to model breaks of any size or location in the primary containment, or to simulate a containment bypass. Both codes contain models for H_2 burning, and neither code considers the effects of such a burn on equipment, or allows for material fires.

Both codes can simulate natural circulation and forced flows such as could exist if a standby ventilation system is used. As discussed in Section 3.3.2.2, both MAAP and MELCOR model CCI with its release of gases, but they use different chemical reactions.

Many of the models that contribute to secondary containment performance have been discussed under other issues. The exception is the reactor building model for natural circulation.

The MAAP developers conducted several experiments [18] to simulate natural circulation. The results of the development effort are represented in MAAP's reactor building or secondary containment model for flows between compartments.

The BWR MAAP-MELCOR comparison indicates that for CsI, MAAP predicts a DF for the RB more than an order of magnitude higher than MELCOR at 20,000 seconds, after the respective containment failure time. The CsI release fraction to the environment predicted by MAAP is .002 and the fraction of CsI retained in the reactor building is 0.066. MELCOR, on the other hand, predicts a CsI fraction distribution of 0.2 in the RB and 0.2 to the environment. These results indicate that MAAP arrives at a reactor building DF of 34, whereas MELCOR predicts a DF of 2.

It appears that MAAP predicts DFs for the Reactor Building that are more optimistic than those predicted by NRC-sponsored methods. Since the atmosphere, as well as the drywell liner, are hotter in MELCOR than MAAP when containment fails, more vapors would be expected to be airborne at the time of containment failure. This effect would lower the DF predicted by MELCOR in comparison with MAAP.

5 Numerical Comparison Studies

As part of the MAAP review, calculations were performed with MAAP and MELCOR for the same accident sequences. Results for a Loss of All Electric Power sequence in a BWR (Peach Bottom) and for a Small Break LOCA sequence in a PWR (Zion) were compared. MELCOR calculations were performed by BNL. Version 1.8.0 of the MELCOR code was used. MAAP calculations were carried out by FAI and forwarded to BNL. The results of these comparisons are discussed here; details of the calculations can be found in Appendices C and D.

5.1 PWR Numerical Comparison Study

For the small break LOCA sequence a break diameter of 2.5 inches was postulated. The small break LOCA sequence is characterized by a rapid depressurization of the primary system, rapid core uncovery and heat-up, and early failure of the reactor vessel. The sequence allows one to evaluate the effects of accumulator injection, break flow, and early release of hydrogen and fission products into containment. However, the potential for natural circulation in the primary system and direct containment heating at the time of vessel breach are reduced, due to the depressurization in the primary system.

In performing the MELCOR analysis, the selections of nodalization, numerical strategy, and many input parameters were based on best judgement. Although no systematic study of the code sensitivity was performed, we believe that this MELCOR analysis represents a reasonable description of the small break LOCA sequence for a PWR plant. The MAAP analysis was provided by Fauske & Associates, Inc. All the 78 model parameters used in the present MAAP analysis were those recommended by the Sensitivity Study Guidance Document [4]. Detailed discussions of the MAAP and MELCOR analyses of the primary system's thermal-hydraulics, fuel behavior, RPV penetration failure, as well as corium/concrete interaction, containment response, and fission product releases are presented in Appendix C.

Although both codes have approximately the same nodalization and initial inventories, detailed comparisons show the following differences between the two codes:

1) MAAP predicts an early phase separation at about 1000 seconds and the break flow contains only single-phase fluid. The accumulator water is injected directly into the reactor vessel and is not released through the break. MELCOR predicts a single-phase flow or two-phase mixture through the break, depending on the water level relative to the break location. The accumulator water injected into the broken leg is all released through the break.
2) MAAP predicts a relatively slow, discrete, natural circulation in the primary system. MELCOR shows a continuous natural circulation in the primary system, with a higher flow-rate. Flow reversals also are predicted by MELCOR.

3) The single-node of the core plate in the MAAP analysis yields a late failure of the core plate, at about 13500 seconds. MELCOR has four radial nodes for the lower core plate and predicts a rapid failure of the core plate in each radial node as debris is relocated on the plate. Failure times for the various radial rings are from 10790 to 11423 seconds.

4) MAAP models one penetration while MELCOR has four penetrations. The failure of the four penetrations extends over of approximately 3750 seconds.

5) MAAP predicts the ejection of debris into the reactor cavity immediately after penetration failure. The sequence of ejection is corium, water, and gas. MELCOR predicts the ejection of debris over a time period of 137 minutes. Water and steam are ejected immediately once the flow path (failure) is opened. Corium ejection has to satisfy the discharge criterion, i.e. total molten mass must be greater than 5000 kg and the melt fraction exceeds 0.1.

6) MAAP shows the start of hydrogen generation at 3230 seconds, and about 340 kg of hydrogen is generated before the penetration failure. The onset of hydrogen generation predicted by MELCOR is at 2200 seconds, and about 260 kg is generated before the penetration failure.

7) MAAP shows another 240 kg of hydrogen generated after reactor vessel failure due to steam entering from the reactor cavity into the failed reactor vessel through the penetration hole. This is not modeled in MELCOR. The buoyant-driven flow model used in MAAP to describe this steam ingress has not been verified experimentally.

8) MELCOR shows a 1.3% oxidation of steel in the reactor vessel. MAAP does not model steel oxidation in the reactor vessel.

9) MAAP predicts a complete dryout of water in the reactor cavity. MELCOR does not predict water dryout in the cavity. Continuous water recirculation between the cavity and lower compartment is predicted by MELCOR.

10) In the MAAP analysis, the water boil-off completely quenches the corium in the cavity. In the MELCOR analysis, the corium temperature stays above the solidus temperature.

11) Since the corium is quenched, the concrete ablation predicted by MAAP is delayed until 55,000 seconds. The ablation distances, both radially and axially are 0.8 m. MELCOR shows an immediate erosion of concrete as the corium is discharged into the cavity. The ablation distances are 1.40 m axially and 0.27 m radially.

12) MAAP-predicted gas releases (H_2, CO, CO_2, and steam) from corium-concrete interaction are less than the MELCOR results. However, in the MAAP analysis, the complete boil-off of water in the reactor cavity adds a large quantity of steam to the containment atmosphere, which results in faster pressurization and an earlier failure of the containment.

13) Both MAAP and MELCOR show that the containment is steam-inerted, and hydrogen combustion is not predicted.

14) The MELCOR concrete degassing model releases about 83,600 Kg of steam into the containment. Degassing is not modeled in MAAP unless concrete ablation temperatures are reached.

15) The containment pressurization rate predicted by MAAP is about 14 Pa/s during water boil-off, and is about 3.75 Pa/s after water dryout in the cavity region. MELCOR maintains a flooded cavity and the rate of containment pressurization is about 9.2 Pa/s.

16) MAAP shows a large retention of CsI in both the primary system (53%) and containment (45%); MELCOR shows about 25% retention in the primary system and 75% in the containment.

17) For all materials except the noble gases, the environmental release predicted by MAAP is much larger than the MELCOR predictions. This is due to the time of actuation of containment sprays. In MAAP, the containment spray is activated 13 hours before the initiation of corium-concrete interaction (see Table 5.1). Therefore, it has no impact on aerosol removal. While in MELCOR, the containment spray is actuated about 1 hour after the initiation of corium-concrete interaction, and can effectively remove aerosols released from the corium pool in the cavity region. Recirculation was not modelled.

Table 5.1 summarizes the timing of major events, and shows that MAAP predictions are characterized by a later time of core uncovery, core dryout, and fuel relocation than predicted by MELCOR. However, the MAAP predicted time of containment failure is about 3.5 hours earlier than that predicted by MELCOR. This is due to the faster pressurization rates predicted in MAAP because of the rapid steam generation from core debris cooling computed in MAAP but not in MELCOR.

Table 5.1 Summary of Major Events (Time in Seconds) (Zion SBLOCA Sequence)

	MELCOR	MAAP
Start of Break	0.0	0.0
Core Uncovery	1640	2,349
In-core 1 Kg H_2 Release	2,200	3,230
First Clad Failure	2,655	3,268
First Fuel Melting	2,825	3,779
Start of Fuel Relocation	2,655	5,250
Core Dryout	3,230/8,585	12,953
Accumulator On	3,362	3,671
Relocation to Lower Plenum	10,790 - 11,423	13,527
Penetration Failure	11,378 - 15,126	13,587
CCI Production of 1 Kg CO	11,540	54,870
Containment Sprays On	15,200	7,321
Containment Failure	104,496	92,718

5.2 BWR Numerical Comparison Study

The Loss of All Electric Power sequence modeled postulates an immediate loss of all injection and a subsequent boil-off of RCS inventory at high pressure.

In this section, we compare the times of the key events and conditions in the containment obtained with MAAP and MELCOR. Key event times are given in Table 5.2. We discovered that the MAAP base case employed the no local blockage model for hydrogen generation rather than the local blockage model recommended by the MAAP guidance document [4]. All other options used by MAAP were in accordance with the guidance document. However, no aerosol impaction in the Reactor Building is used in the MAAP runs. Details of this study can be found in Appendix D. Detailed comparison between the predictions of the two codes for the particular sequences modelled shows the following differences:

1. There is some difference in the time when the RPV water level drops to the Top of Active Fuel (TAF). This difference is investigated in Appendix D, and is primarily due to differences in water allocation in MAAP and MELCOR. Both codes start with the same amount of water in the RPV, but MAAP has more water in its lower plenum and less above TAF. This difference in timing of 500s continues throughout the rest of the accident sequence predictions. Removing it would mean that MELCOR's initiation of clad melting would be at 4500s (5000 - 500) compared to MAAP's prediction of 3900s.

2. MELCOR predicts earlier failure of the core support-plate than MAAP, yet later vessel failure. MAAP models an all liquid eutectic U-Zr-O and allows all molten corium in the core region to be relocated to the lower plenum once the core support-plate fails. Once in the lower plenum, the corium quickly attacks a lower head penetration and failure of the vessel is predicted within seconds of the lower core-plate failure. The MAAP model predicts minimal cooling of the molten debris in the lower plenum and much of the lower plenum's initial water inventory is also relocated at the time of vessel failure. However, in the MELCOR model, a mixture of solid and liquid debris is assumed and only the material located on the lower core plate ring, which fails, is allowed to be transported to the lower plenum. This is a far smaller amount of corium, (than predicted in MAAP) and for our case, involves only solid particulate debris, as the liquid debris solidified above the lower core plate. Corium remains in the lower plenum for more than 3000s before vessel failure. This allows steam produced in the lower plenum to continue to oxidize zirconium in the core region, where nearly all the zirconium remains during this time. The zirconium, which initially melted, was predicted to solidify during the candling process onto cooler regions in the core.

3. After vessel failure, MAAP ejects not only all the corium in the lower plenum, but all remaining core material in the core region, some of which may not have melted in this scenario. This latter action is modelled in

response to the input options recommended by the guidance document [4]. The ejected corium then begins to attack the concrete and to heat-up the containment. In MELCOR after failure of the RPV and depressurization of the RCS, corium is not ejected from the vessel until it has become sufficiently molten to create a slurry. After this slurry is predicted, the predominantly solid corium is allowed to exit the RPV. There is about a 5000s delay from the time of vessel failure until the corium is ejected. Only that mass of corium in the region of the penetration failure is predicted to be ejected in MELCOR. Additional penetrations will have to fail to cause the remaining corium in the lower plenum to be ejected. The amount of corium initially predicted to be ejected in MELCOR is only a fraction of that predicted by MAAP.

4. Concrete attack is predicted to occur sooner with MAAP than MELCOR after the corium is released from the RPV. In the base study, corium is assumed to occupy the entire drywell and cavity concrete floor area. In the MELCOR analysis, the corium was assumed to occupy approximately 40% of the floor area. One reason for these differences is that in MAAP, the RPV is pressurized at the time of vessel failure and the liquid corium is dispersed during vessel blowdown over a large floor area. In MELCOR, the RPV has depressurized at the time the corium is released and thus, the corium was assumed to be spread over a smaller floor area.

5. MAAP predicts a much later containment failure time than MELCOR. At the time of containment failure, MAAP predicts a release to the containment of much larger quantities of non-condensible gases but the containment's atmospheric temperature is below that of MELCOR's. MAAP predicts the containment fails at nearly the same pressure as predicted by MELCOR, but with an atmospheric temperature in the drywell about one-half of that of MELCOR's prediction. This difference is caused by the greater volume of non-condensible gases released by MAAP into the containment. MELCOR predictions of the drywell atmosphere show a number of temperature excursions resulting from discrete corium additions to the corium pool. These peaks subside as the heat structures absorb the energy.

The chemical power during CCI predicted by MELCOR is a much larger fraction of the total power in the corium pool than predicted in MAAP. In MELCOR the chemical power was predicted to exceed the decay power at certain times. The chemical power was always predicted in MAAP to be a small fraction of the decay power. The chemical power in MELCOR is primarily a result of the gases released from concrete ablation. A greater amount of these gases react with the corium pool to produce heat to raise the atmospheric drywell temperature in MELCOR than in MAAP. One modelling difference between the codes is that MELCOR allows the gases released from the side walls of the core-concrete interface to react with the corium pool, while MAAP does not.

Additional comparisons are shown in Table 5.3. The results of this numerical comparison prompted the selection of the sensitivity studies which are presented in Section 6.2.

Table 5.2 Key Event Times

Event	MAAP(s)	MELCOR(s)
Loss of all electrical power	0.0	100
Core uncovery (swollen level at TAF)	1900	2500
Collapsed water level at Bottom of Active Fuel	4600	5900
1 kg of hydrogen generated	2924	4000
Clad damage (clad perforation)	3147	3800
Initiation of clad melting	3920	4500
First fuel material relocation	3936	4500
First fuel material relocation to core support plate	4538	5100
Core support plate failure	7752	9800 (R1)* 6500 (R2) 15,500 (R3)
Vessel failure time	7765	9910 (R1) 12,077 (R2) 22,000 (R3)
Corium mass released from RPV	7765	14,900
Concrete attack starts (gas released)	8447	20,000
Containment failure	86,000	32,000
Start of burning in reactor building	86,000	32,000
Reactor building failure	86,000	32,000

Note: R1, R2, and R3 refer to radial nodes in the core region. R1 is the inner node and R3 is the outer node.

Table 5.3 Corium Effects in Containment

Event Description	MAAP	MELCOR
Mass ejected from RPV:	Nearly all at once	Gradual over time
Composition	Mostly liquid.	Mostly solid.
Temperature	≈2500 K	Initially much cooler < 2000°K but later material is close to 2500°K.
Core Release Sequence	Corium released followed by 100,000 kg of water and gas	Tens of thousands of kg of water ejected before corium.
Corium Distribution	Mostly liquid corium distributed throughout drywell and pedestal region.	Mostly solid debris contained within pedestal and part of drywell floor area.
Containment Atmosphere Heatup	No radiative heating of gases directly by the corium pool or crust.	Radiative heating of the containment atmosphere by corium pool or crust.
Total mass of H_2 produced in vessel at time of RPV failure	860 kg	1000 kg
Mass of H_2 produced in-vessel at time of RPV failure by stainless steel oxidation	0.0 kg	100 kg
Conditions at Time of Containment Failure:		
Wetwell Airspace Temp	344°K	370°K
DW Gas Temp	710°K	1300°K
DW Pressure	127 psia	130 psia
Mass of H_2 produced	1250 kg	1140 kg in vessel only
Mass of CO, CO_2, and H_2 in containment (DW and WW) and RPV	≈12,400 kg	≈7850 kg
DW Liner Temperature	700 K	1000 K

6 Sensitivity Studies

As pointed out in Section 1.3, a number of sensitivity calculations with MAAP were carried out as a result of the code comparison with MELCOR. The purpose of these calculations was to obtain a better understanding of the effect of varying a number of the modeling parameters in MAAP. In addition to the sensitivity cases performed as part of this study, a sensitivity study carried out previously for PWRs [7] was also considered. The results from both of these analyses provide a major part of the basis for the additional sensitivity cases recommended in this report for application of MAAP to IPEs. The discussion on sensitivity cases for PWRs is based principally on the calculations in Reference 7, while the BWR section is based mainly on the calculations carried out for the present study. It should also be noted that some of the sensitivity cases discussed under PWRs are also applicable to BWRs and vice-versa as indicated in Section 2.3. The main points are summarized below, additional details can be found in Reference 7 and in Appendices E and F.

6.1 PWR Sensitivity Studies

6.1.1 Previous PWR Sensitivity Study

The MAAP/PWR code has 78 model parameters and 10 plant specific input parameters which are subject to uncertainties and can be used to perform sensitivity studies. A comprehensive sensitivity study was performed for a station blackout sequence [7] for the Zion plant. The study included most of the MAAP model parameters and covered a wide variation in the parameter values. Only the DCH and combustion models were not included in the study. A detailed evaluation of the sensitivity study [7] and the sensitivity-study guidance document [4] is given in Appendix E.

The accident sequence selected for the sensitivity study (i.e., the station blackout event) leads to a late failure of the containment at about 37 hours. Variations of many of the parameters also resulted in the prediction of a late containment failure (i.e., the containment failure time varied by only several hours) rather than an early failure. The MAAP guidance document [4] recommends the best estimate values of the parameters, and their ranges, for sensitivity studies to be used in the IPEs. In general, the recommendations given in the guidance document are adequate for the IPEs. However, because of the importance of certain parameters and/or the lack of sensitivity analysis for some parameters, we recommend that the following also be considered in the IPEs:

6.1.1.1 Hydrogen Combustion

MAAP has 6 model parameters related to various aspects of combustion, such as deflagration, auto-ignition, jet-burning, and the reliability of the ignitors. The MAAP guidance document [4] has adequate recommendations for uncertainty analysis for most of the parameters, except the flame flux multiplier. This parameter (FLPHI) has a significant impact on combustion completeness, combustion duration, and therefore, the pressure rise due to combustion. Based on benchmark calculations, Reference 10 recommended that the parameter assume a value of 2 under quiescent conditions, and the value of 10 under turbulent conditions (i.e., when fans and sprays are activated). No recommendations are given in the MAAP guidance document [4] to change the multiplier parameter for uncertainty analysis. However, inspection of the benchmark calculation reveals that the MAAP model underpredicts the combustion completeness and duration relative to test data in many cases. In a discussion of the MAAP model for Advanced Light Water Reactors (ALWRs), Plys and Astleford [10] suggest that if a sensitivity analysis is desired, a minimum value of 1 and a maximum value of 3 for quiescent cases is recommended. For turbulent cases, the range of the parameter should be expanded to include from 3 to 12. We agree with the above recommendations and suggest that the same recommendations be applied to the IPEs for accident sequences in which combustion plays an important role on containment performance. Combustion may be an important consideration in IPEs for PWRs with Ice Condenser Containments and for some PWRs with large dry or subatmospheric containments. It could also be important for BWRs with Mark III containments.

6.1.1.2 In-Vessel Natural Circulation

Specific criteria for performing uncertainty analysis on the parameter FNCBP (in-vessel natural circulation configuration) should be provided in the MAAP guidance document. This parameter is used to select whether natural circulation flow from the upper plenum passes down the outer part of the core (FNCBP = 0) or down the core barrel/core baffle annulus (FNCBP = 1). The MAAP guidance document states that "for most plants" (i.e., Westinghouse plants) the parameter should be set to zero; no uncertainty analysis is recommended. For "B&W plants and perhaps some others," the parameter should be set to one; an uncertainty analysis is recommended for a high pressure station blackout sequence. The general guidance is not adequate. We conclude that, unless a demonstration of the applicability of the natural circulation flow parameter chosen can be provided, all plants should perform the sensitivity case as well as the base case. The MAAP sensitivity study for the Zion plant [7] reveals that when the parameter is changed from zero (default value) to one, the time to containment failure is reduced by 5 hours.

6.1.1.3 Latent Heat of Fusion of the Eutectic Mixture

The MAAP best estimate of the latent heat of fusion for the eutectic core material mixture is 250 KJ/kg and it is recommended for use in the IPEs [4]. No sensitivity analysis is recommended in Reference 4. The uncertainty estimate of this parameter in the MAAP code is in the range of 100 to 400 KJ/kg. The sensitivity study performed for the Zion plant for a station blackout sequence shows that the time to containment failure is reduced by 8 hours when the maximum value of the latent heat (400 KJ/kg) is used. The latent heat of the eutectic affects the melting and relocation of a fuel node [7], which in turn affects hydrogen production in-vessel as well as the debris

1

IMAGE EVALUATION TEST TARGET (MT-3)

150mm

6"

1

IMAGE EVALUATION TEST TARGET (MT-3)

150mm

6"

1

IMAGE EVALUATION TEST TARGET (MT-3)

150mm

6"

1

IMAGE EVALUATION TEST TARGET (MT-3)

1.0 1.1 1.25 1.4 1.6 1.8 2.0 2.2 2.5 2.8 3.2 3.6 4.0

150mm

6"

distribution (corium composition, state) in the reactor core, reactor cavity, and other locations after the reactor vessel breach. Therefore additional sensitivity cases varying the latent heat are recommended. This recommendation extends to BWRs also.

6.1.2 Additional PWR Sensitivity Study

Two sensitivity cases were performed as part of the current review effort. In one case, a large core support-plate mass was used to model additional steel to be included in the corium-concrete interaction. The results showed there was no impact on containment performance because of the steam limitation on steel oxidation. In the other case, a very low heat transfer between the debris and water was assumed to simulate a non-coolable debris bed when the depth of the debris exceeds 25 cm. This simulation resulted in a low boiloff rate for water in the cavity, plus an extended corium-concrete interaction in the cavity. The combined effect was to delay the predicted containment failure time significantly. Containment pressurization was predicted to be slower for a non-coolable debris bed configuration because a significant fraction of the decay heat goes to heating concrete. In a coolable configuration, all of the decay heat goes to boiling water which results in more rapid containment pressurization.

6.2 BWR Sensitivity Studies

As a result of the MAAP/MELCOR base-case comparison discussed in Section 5.2, a number of modelling differences were identified as possibly causing the large difference in predicted time to containment failure.

6.2.1 Core-Concrete Interaction

The major factor influencing containment failure time was found to be the extent of corium distribution across the drywell floor after reactor pressure vessel failure. Essentially, the sensitivity studies revealed that attaining the threshold ablation temperature had the largest effect on containment failure time. If the corium was assumed to be spread across the whole drywell floor, this threshold temperature was not reached for a large fraction of the concrete. Only the corium in the pedestal region (the drywell concrete floor immediately below the reactor vessel) was predicted to heat the concrete to the ablation temperature. FAI was requested to run a MAAP case where the area of the drywell floor (excluding the pedestal floor area) was reduced to one-quarter of the value assumed for the base-case. This made the concrete floor areas of MAAP and MELCOR essentially equal. The resulting time to containment failure predicted by MAAP dropped from 86,000s to 42,000s (no local blockage cases). However, the temperature in the drywell predicted by MAAP remained substantially below that predicted by MELCOR at the time of containment failure.

Large differences were observed between the rate of chemical energy produced by the MAAP and MELCOR calculations. The difference may be in part due to MELCOR's stratification of the components in the corium pool. In MAAP zirconium is allowed to oxidize by reducing uranium dioxide, while in MELCOR zirconium oxidizes from the H_2O and CO_2 released from the concrete. Further, MELCOR models the reaction of gases released from the side-walls which results in the generation of greater chemical energy. This last effect could cause the differences found between MAAP and MELCOR in the temperature of the containment gas at the time of containment failure, with MELCOR giving higher values (Appendix D).

BNL requested FAI to run MAAP allowing the side-wall gases to react with the corium pool. FAI performed the MAAP runs using an improved version of the BWR MAAP 3.0B version identified as Rev. 7.01. As can be seen in Table 6.1, the relative effect of this modeling assumption was much stronger when the corium is assumed to be spread over a smaller area of the drywell floor (cases 3 and 4). For these cases, the effect of the sidewall gas reaction effectively reduced the time between vessel failure and containment failure by 25%. Given the impact of this model assumption on the predicted containment performance BNL recommends that this option be used by utilities when performing an IPE.

6.2.2 In-Vessel Hydrogen Production

Table 6.1 Effect of Concrete Sidewall Gas Reaction on Containment Failure Time for the BWR Station Blackout Sequence Using MAAP 3.0B, Rev. 7.01

Case #	Sidewall Case Reaction	Spread of Corium on DW Floor	Time of Containment Failure (second)
1	None	Full	130,000
2	Full	Full	122,000
3	None	Quarter	53,000
4	Full	Quarter	42,000

Note: The time of vessel failure was predicted to be 10,000 seconds for these cases, which assumed the local channel blockage model. Also note that the times presented here are different than those of Section 5 where results with MAAP Rev 7.0 were given.

The sensitivity cases were performed with MAAP assuming various model options as indicated in Table 6.2 and the results were compared to MELCOR calculations. The initial MELCOR model had relatively coarse core nodalization. As a result the core debris was predicted to be retained in the vessel lower plenum for a relatively long time. The resulting steam generation caused a large amount of zirconium oxidation.

In a later version of MELCOR with finer core nodalization, a reduced time between lower plate failure and vessel failure resulted in less steam from the lower plenum being available for in-core oxidation. In addition, an estimate was made in which the failure temperature criteria of 2500K was reduced to 2200K. The amount of in-vessel hydrogen generation for these cases is given in Table 6.2.

It sho--ld also be noted that in the BNL BWR numerical comparisons of MAAP and MELCOR, errors were found in both computer codes which can greatly affect the results. In MELCOR, an error pertaining to debris relocation to the lower core support plate and lower plenum affected the availability of steam to oxidize the steel and zircaloy. In MAAP, an error in the channel blockage option flag resulted in MAAP employing the "no channel blockage" option when the "local blockage" option was requested. Table 6.2 correctly identifies the MAAP option employed by the code along with hydrogen generation comparisons.

Based on the sensitivity results in Table 6.2 and the discussion in Section 3.2.1, BNL recommends the use of the single-sided, no local blockage model for the base case because we believe that the issue of in-vessel hydrogen production remains highly uncertain and is traceable to the assumptions governing the mode of corium relocation. We recommend that for BWRs, MAAP be run with the local blockage model and single-sided clad oxidation to give a lower bound estimate of hydrogen generation and zircaloy oxidation in the vessel. It will also provide a different corium composition for CCI. To estimate an upper bound, MAAP should also be run with no blockage and two-sided oxidation.

Table 6.2 BWR MAAP-MELCOR Comparison of Hydrogen Generation

Condition	MELCOR(kg)	Condition	MAAP(kg)
1) MELCOR base case, 2500°K failure temp.	1000	MAAP base case, no local blockage, single-sided oxidation	860
2) MELCOR fine core nodalization, 2500°K failure temp.	600	MAAP, no local blockage, 2-sided oxidation	970
3) MELCOR **estimate** for 2200°K failure temp. in base run	500	MAAP estimate [19] for base case, with local blockage, single-sided oxidation	430

6.2.3 Core Collapse Criteria

In-vessel core relocation is an area of significant uncertainty and Reference 4 recommends sensitivity cases to address this important issue.

Several MAAP BWR runs were made to investigate the effects of varying the amount of stainless steel released with the corium at vessel failure. A large variation in containment failure times was predicted in these MAAP calculations. By varying the mass of the core support plate from 10,000 kg to 60,000 kg, (and hence the amount of steel assumed to relocate with the core debris to the cavity) the containment failure time increased from 73,000 seconds to 93,000 seconds. The contributing factor was largely the additional heat capacity of the corium (caused by the additional steel), which reduced the amount of concrete ablation by the core debris.

Another uncertainty involves integrity of the internal vessel structures. In one calculation MAAP predicted the outer shroud head would reach a peak temperature of 1300 K at about 9000 seconds. This temperature might be high enough for collapse; however, the temperature never reached the melting range. In general, however, the ability to retain structural support for the core once fuel relocation has begun and high RPV internal temperatures have been reached is uncertain. A substantial relocation of solid core debris cannot be ruled out. Given the uncertainty of retaining the structural integrity of the vessel internals after core melt and relocation, a sensitivity case should be considered which investigates this effect. As discussed in previous sections, MAAP has a modeling parameter which allows the user to vary the amount of core required to have melted at the time of vessel failure to relocate all of the remaining core. Presently, this is set to a required 90% melt fraction. Given the uncertainty noted above, BNL recommends that a sensitivity case with melt fraction reduced to 20% be performed for a wider range of accident sequences than currently recommended in Reference 4. The PWR sensitivity study [7] showed that this parameter was important for containment failure time calculations in PWRs also.

7 Conclusions

This report describes the NRC sponsored review of the MAAP code, version 3.0B [3]. The primary objective of the review was to evaluate the MAAP code for its use in conjunction with activities related to performance of an IPE for operating reactors. Therefore, the review considered the guidance provided by GKA regarding sensitivity analyses for IPEs using MAAP 3.0B [4]. MAAP was evaluated to provide assurance that IPEs will be analyzed with a methodology which adequately treats significant phenomena and reflects the uncertainty surrounding issues for which confirmatory research is planned or ongoing.

The review focuses on those aspects of an IPE that will be addressed with MAAP analyses, namely determination of success criteria, the timing of key events, and containment response to severe accident loads. Utilities may wish to use MAAP to predict the time from accident initiation to the time of clad damage for the purposes of determining success criteria for quantification of the Level 1 (core damage frequency estimate) part of an IPE. Thus an important aspect of the review was to determine how well MAAP models the loss of coolant inventory for a range of initiating events (i.e., transients or LOCAs). An important finding of the review was that in general, MAAP is adequate for predicting thermal-hydraulic behavior prior to clad damage. However, as the MAAP models contain a number of simplifications, the utilities should provide justification for using MAAP if certain thermal-hydraulic conditions are encountered. These conditions are:

1. The break location gives rise to a quasi-steady state two-phase flow condition (BWR/PWR).
2. The RPV water level and vessel flow conditions may expose the fuel to departure from nucleate boiling (DNB) conditions while MAAP continues to predict adequate core cooling (BWR).
3. The reactor has not scrammed (fuel stored energy will not be released (BWR/PWR).
4. Clad temperature is above 1200°K (BWR/PWR).

The review confirmed that the utilities should not use MAAP for determining success criteria after clad damage (e.g., to determine whether or not a core can be successfully reflooded after extensive fuel melting has occurred). Therefore, after clad damage MAAP should be used to provide the utility with a framework for obtaining an understanding of containment failure modes, the impact of phenomena and plant features, as well as operator actions. In this role, MAAP analyses should be supplemented with sensitivity studies to ensure that the utility staff have an appreciation of the uncertainties surrounding containment performance during a severe accident. Therefore, the review of this aspect of MAAP's application to an IPE focused on the adequacy of the range of parameters recommended [4] for the sensitivity analysis.

The ranges of parameters recommended [4] for MAAP sensitivity analysis were generally found to be adequate for reflecting the uncertainty surrounding severe accident issues. However, there are a number of areas where added or enhanced sensitivity cases (beyond those recommended in Reference 4) could provide the utility with a more complete appreciation of the conditions which may be encountered during a severe accident. These added or enhanced cases are described in the main text of this report and summarized in the executive summary.

8 References

1. U.S. NRC, "Individual Plant Examinations for Severe Accident Vulnerabilities - 10CFR§50.54(f)," Generic Letter No. 88-20, November 23, 1988.

2. U.S. NRC, "Individual Plant Examination: Submittal Guidance," Final Report, NUREG-1335, August 1989.

3. MAAP3.0B Users Manual, Vol. 1 and Vol. 2, Fauske & Associates, Inc, March 1990.

4. Kenton, M.A., and J.R. Gabor, "Recommended Sensitivity Analyses for an Individual Plant Examination Using MAAP 3.0B," Gabor, Kenton & Associates, Inc.

5. Letter from T.P. Speis (USNRC) to A. Buhl (International Technology), "Transmittal of NRC Technical Issue Positions for Issues 4, 12, 10, 13B, 15 and 16," November 26, 1986.

6. Summers, R.M., et al, "MELCOR 1.8.0: A Computer Code for Nuclear Reactor Severe Accident Source Term and Risk Assessment Analyses," NUREG/CR-5531, Sandia National Laboratories, Albuquerque, NM, January 1991.

7. Mendoza, Z.T. and J.M. Hall, "MAAP3.0B Sensitivity Analysis for PWR Station Blackout Sequences," NP-7192, Electric Power Research Institute, January 1991.

8. MAAP3.0B PWR Revision 17 Transmittal Documentation, FAI/91-13, Fauske & Associates, Inc., January 1991.

9. FAI/88-41, "Status of Technical Issue Resolution," Draft, Fauske & Associates, Inc., April 1988.

10. Plys, M.G., and R.D. Astleford, "Modifications for the Development of the MAAP-DOE Code, Vol. III: A Mechanistic Model for Combustion Integrated Accident Analysis, Task 3.4.5," DOE/ID-10216, Vol. III, November 1988.

11. MAAP 3.0B/BWR Review Comments Responses to Second Familiarization Meeting, April 2-3, 1990.

12. Hohorst, J.K., "SCDAP/RELAP5/MOD2 Code Manual, Vol. 4: MATPRO-A Library of Materials Properties for Light-water Reactor Accident Analysis," NUREG/CR-5273, EG&G Idaho, Inc., Idaho Falls, ID, February 1990.

13. Gelbard, F., MAEROS User Manual, NUREG/CR-1391, SAND 80-0822, SNL, December 1982.

14. Ng, R.N., Letter to Dr. C.G. Tinkler, May 9, 1991.

15. Ng, R.N, Letter to Dr. F. Eltawila, Evolution of MAAP Models Over the Last Few Years, March 18, 1991.

16. METOXA, "An Equilibrium Model for Fission Product Release During CCI," FAI/87-20, April 1987.

17. IDCOR Report 85.2

18. "MAAP Design Review," Jason Associates Corporation, October 1989.

19. Private Communication with Marty Plys, FAI.

APPENDIX A

PWR Model Descriptions

J.W. Yang

Table of Contents

Table of Contents

Table of Contents

1 Introduction

This appendix summarizes a review of the MAAP 3.0B/PWR code. [1] The work was performed under Tasks 1 to 4 of the MAAP Code Evaluation Program (FIN L-1499).

The primary objectives of the review are:

(1) To evaluate MAAP methodology and modeling of the significant phenomena and the sensitivity to parametric or mechanistic variations in the modeling: and

(2) To compare the analytical models and parameters used in the MAAP 3.0B/PWR code with their counterparts in the MELCOR code, sponsored by the NRC [2].

Part I RCS Thermal Hydraulics and Heat Transfer

2 Primary System

In the MAAP code, a primary system is considered as a "region", which includes all of what is usually considered as the primary system except for the pressurizer. The region subroutine PRISYS computes the thermodynamic properties and the rate of change of dynamic variables in the primary system. The nodalization, thermodynamics, water transport, gas transport, heat transfer, and heat structures of the system are discussed in this section.

2.1 Nodalization

The MAAP code is capable of modelling two primary system loops. A break in the primary system is modelled as one "broken" loop, and the remaining loop is used to represent the other intact loop or loops. For transient sequences, the broken loop can be defined as the loop containing the pressurizer. Each loop is represented by five nodes: hot leg, hot leg tubes, cold leg tubes, intermediate leg, and cold leg. The reactor vessel region has three nodes: downcomer, upper plenum, and dome. Thus, a total of 13 nodes is used to represent the primary system. The hydrogen mass fraction, gas temperature, and up to four structure temperatures are computed for each node. A detailed accounting of water inventory and tracking of hydrogen and fission product transport also are performed for each node.

Although the major elements of a PWR primary system are represented by the MAAP code, the fixed nodalization does not permit a user to perform a sensitivity study on the effect of finer nodalization. In many cases, such as natural circulation, the flow rate is sensitive to the local fluid density, and a finer nodalization would improve the code predictions. The 3.0B version of MAAP has a finer primary system nodalization than the 2.0 version. This finer nodalization improves MAAP code predictions as shown in the simulation of the first 174 minutes of the Three Mile Island Unit 2 accident [3]. Sharon et al. reported that "the changes to the nodalization and structure improve the resolution of the structure temperature calculation" [3].

Unlike the MAAP code, there are no predefined models and no specific nodalization built into the MELCOR code. The MELCOR code uses the control volume concept to represent the reactor system (except for the core region). Each of the nodes modeled in MAAP for the primary system can be represented by a control volume in the MELCOR code. The MELCOR code is composed of many packages; each models different aspects of reactor accident phenomenology. The Control Volume Thermodynamics (CVT) package evaluates the thermodynamic state within each control volume, and the Control Volume Hydrodynamics (CVH) package evaluates the mass and energy flows between control volumes. The flow rate of gases and water between two control volumes are determined in the Flow Paths (FP) package. Thus, a series of control volumes connected by flow paths can be defined to represent the entire primary system. MELCOR thus provides freedom to perform sensitivity studies entirely from code input, without modification to the code itself (MELCOR permits a maximum of 999 control volumes). In addition, the code can provide more detailed information within a control volume than MAAP. For example, MELCOR allows a maximum of 100 structures from the Heat Structure (HS) package to interact with the thermodynamics in each control volume.

2.2 Phase Mode

The MAAP3.0B/PWR code considers either a mixed. homogeneous two-phase flow or a separated gas and water flow in the primary system. When flow rates through breaks in the primary system or through the main coolant pumps are insufficient to sustain homogeneous flow, and when the coolant inventory drops to a level that prevents two-phase natural circulation, the phases are treated as separated. For the mixed phase, an overall average void fraction is assumed in the primary system. For separated phases, a constant collapsed water level is computed for the primary system, provided there is sufficient water in the primary system to permit communication between the water pools in the cold legs, the reactor vessel downcomer, and the core region. The water pools in the primary system are separated when the coolant inventory in the primary system decreases and prevents this communication. When this situation occurs, a separate mass and energy balance are calculated for each pool. The collapsed water levels in the hot leg, cold leg, and downcomer region are computed by subroutines HLLVL, CLLVL, and DCLVL, respectively. These subroutines perform a simple calculation based on the water mass of the nodals and their specific volume. (The level of the boiled water in the core region is determined by the subroutine VLEVEL and is discussed in the next section.)

The MELCOR code uses the CVH package to compute the phase mode for each control volume (i.e., each node in MAAP's nomenclature). The phase mode in MELCOR is based on the physical situation predicted for each control volume. An average void fraction for the entire primary system is not computed in the MELCOR code.

2.3 Thermodynamics

The thermodynamic states of the primary system (i.e., properties of water and gas, system pressure, and temperature) are computed according to the phase mode in the primary system. Auxiliary property subroutines, such as TFWATR for subcooled water, SWATER for superheated steam, and STMSIU and SATGAS for saturated steam, use correlations similar to those in Keenan's steam tables or are taken directly from these tables.

For the mixed phase mode, the system is considered either saturated or solid. In a saturated state, it is assumed that gases (steam and noncondensible gases) are in equilibrium with water; the system temperature, masses of water and steam are estimated by subroutine SATGAS, based on conservation of energy and mass. The saturation pressure is evaluated by function PSATW, in which $P=f(T)$ is computed by a correlation from Keenan's steam table. If the system is solid, the system pressure is set to the pressurizer pressure.

For the separated phase mode, a significant difference in temperature may exist between the water and gas regions. The temperature of each water pool in the primary system is treated separately by subroutine POOL, which calculates the mass and energy boiled from a superheated water pool to bring the temperature back to saturation. Calculations for gases are performed by subroutine PTCAL, in which all control volumes in the primary system are lumped together to estimate the average gas temperature and system pressure.

The local gas temperature and the rate of change of local temperature are computed for each node in the primary system by subroutines FLOW and CRATES. Using the flow rate determined by FLOW for flow paths connecting the primary system nodes, the subroutine CRATES computes the rate of change of gas temperature in each node, and then uses a fully implicit integration technique based on a first-order backward differentiation formula to advance the gas temperature. The local gas temperatures are slightly adjusted as necessary to make them consistent with the average temperature computed by PTCAL.

The local gas temperature is important for predicting natural circulation and the transport of fission products in the primary system. The calculation of local gas temperature involves an estimation of heat transfer between the gas and heat sinks in each node. Heat transfer to structures is discussed in next section.

In MELCOR, all thermodynamic properties are defined by an equation of state based on the volume, mass, and energy content of a control volume. There are two basic options available, selected by user input: equilibrium thermodynamics and non-equilibrium thermodynamics. Equilibrium thermodynamics assumes that the gas and water phases are in thermal and mechanical equilibrium (i.e., they have the same temperatures and pressures). The equilibrium state is reached by an instantaneous mass and energy transfer between the two phases. Non-equilibrium thermodynamics, on the other hand, assumes that neither thermal nor phase equilibrium is reached; while the pressures of the gas and water pool are equal, their temperatures may be different. Non-equilibrium thermodynamics would result in a substantial driving force for condensation or evaporation. All steam and water properties in MELCOR are taken from Keenan's and Keys' correlations. The thermodynamic data are consistent and satisfy Maxwell's relations. The Water Package evaluates specific heat, specific volume, enthalpy, entropy, and free energy at particular temperatures and pressures. The transport properties, such as thermal conductivity and viscosity of steam and water, are given by the Material Property package. The transport properties can be modified through user input.

2.4 Heat Structures

Sixteen structures in the reactor pressure vessel, hot leg, cold leg, and primary side of the steam generators are modeled in the MAAP code. These structures are considered as heat sinks only. The heat balance for the structures does not include any power source due to oxidation, but heat generation by the deposited fission products is considered. All structures, except the steam generator tubes, are represented as two-dimensional slabs. The tubes in a steam generator are treated as 1-D heat sinks.

Heat conduction in axial and radial directions is considered. The axial nodes are assumed to be equally spaced; the node height is specified by the user. Axial nodes that are equally spaced could introduce uncertainty in modeling axial heat conduction for those nodes near the gas-water interface, where a large axial temperature gradient is expected. Nodes above the water level will have higher temperatures and an excessively large quantity of heat conducted into the water unless a fine nodalization is used. Furthermore, when determining the average surface temperatures in the covered and uncovered regions, MAAP assumes that "partially covered nodes are treated either as covered or uncovered nodes, depending on their uncovered area fraction (if less than 1/2, considered covered)." (Subroutine PSEQPT, p.4 [1]) This assumption could cause the predicted structural heat transfer to the fluid to become uncertain, which, in turn, could affect the boil-off rate of water, if large nodalization is used.

The radial nodalization also assumes an equal node thickness. However, the number of nodes is calculated so that the resulting node thickness should be commensurate with the maximum problem time step allowed. The limitation of the radial node thickness is based on a consideration of numerical stability.

MAAP assumes all structures in the primary system are made of steel and remain in an intact, solid configuration. The oxidation, melting, and relocation of structures are not modeled.

MELCOR has a more general treatment for structures that are modeled by the Heat Structure (HS) Package. Structures can assume a rectangular, cylindrical, spherical, or hemispherical geometry; and may be composed of several different materials specified by the user. An internal (or surface) power source may be specified for a heat structure. Any spatial and time dependency of the power source also may be specified by the user. However, only one-dimensional heat conduction in the radial direction is represented in MELCOR. The nodalization is specified by the user and may be non-uniform, i.e., the distance between temperature nodes need not be the same. MELCOR does not model the oxidation, melting, and relocation of structural materials (which is consistent with MAAP modeling assumptions).

In the MAAP code, heat transfer to or from the primary system structures is computed by subroutine HTSHCR for the gas-covered region and by subroutines HTPSEQ and HTSBWL for the water-covered region.

In a gas-covered region, gas to structure radiation is treated by the gray-gas model with emissivities specified by the user for gas and structure. The gray-gas model is a first approximation for gas radiation. The effect of steam, which absorbs and transmits radiation at certain selective wavelengths, is not considered in the model. For natural convection, conventional correlations for laminar and turbulent flows are used for vertical, horizontal surfaces, and circular pipes. For forced convection, only correlations developed for internal pipe flows are used. A correction factor for the pipe length is included in the laminar flow equation. However, the forced convection correlations are not consistent with the assumption that all heat structures are rectangular slabs.

Heat transfer between water pools and heat structures in the primary system are determined by the conventional Dittus-Boelter correlation for turbulent flow in circular pipes. This correlation is valid if pumped flow is available in the primary system. When the water flow rate of the primary system is low, after the main coolant pumps are tripped, heat transfer is governed by natural circulation. Both laminar and turbulent correlations for natural circulation flows are available in the MAAP code. It is reported, in subroutine HTSBWL[1], that "numerical instabilities may arise if the predicted heat transfer coefficient can reduce the pool or the wall temperature below that of the other". When this situation occurs, the heat transfer coefficient is limited to a value required to equilibrate the temperatures of the water and the walls in one time step.

A more general treatment is provided in MELCOR for heat transfer to and from structures. Heat transfer correlations in MELCOR cover a broad range of flow conditions. For example, the correlations cover the internal pipe flow and the external flow over slabs; the transition region between laminar and turbulent flow, and combined natural and forced convection also are covered. In addition, the structure-to-gas radiation model has the option to include the equivalent band model, which estimates the absorption and transmission of thermal radiation in steam. A comparison of heat transfer correlations in MAAP and MELCOR is given in Table A.1.

2.5 Water Transport

In the MAAP code, water transport within the primary system is determined by the water volume in each node and the system average void fraction, when the flow is homogeneous, or when two-phase natural circulation is occurring. The average void fraction is determined from a mass balance on the primary system, including the pressurizer.

When the flow phases are separated, but water pools are still coupled, the communication between water pools is determined by the assumption of equal collapsed water levels in each node (subroutine WLEVEL). When water pools are decoupled due to the reduction of water inventory, MAAP computes water flows from the cold leg to the downcomer (subroutine DCOVFL), and from the downcomer to the core (subroutine MNOMTR). In subroutine DCOVFL, the quantity of water transport from the cold leg to the downcomer is determined by a mass balance using the volumes and water density in each region. All safety injections and break flows are included in the mass balance. In subroutine MNOMTR, the flow is determined from unequal static heads between the downcomer and the core. The current time step is used to compute the transport rate. These simple quasi-steady treatments satisfy the overall mass balance; however, they would not be valid during a transient when steam condensation, water entrainment, and counter-current flow are expected. These conditions could occur if ECCS is restored.

An important part of water transport is the break flow. The break flow, which directly affects the time to core uncovery, is a key parameter in severe accident analysis. The break flows of the primary system (subcooled water and two-phase mixture) are computed by considering the pressure difference across the break, the void fraction, and other fluid properties. In subroutine WFLOW, the ratio of the actual pressure across the break area is compared with the critical pressure ratio to decide whether or not the flow is choked. The critical pressure ratio is calculated by a simplified fit to the Henry-Fauske critical flow model. The model was developed for a one-component mixture flowing through convergent nozzles, and it is based on a lumped, non-equilibrium approach. A subcooled liquid, saturated liquid, two-phase mixture, and saturated vapor are all calculated by the Henry-Fauske model.

Table A.1 Comparison of Structure Heat Transfer in the Primary System

	MAAP	MELCOR
Structure Geometry	Rectangular Slab	Rectangular, Cylindrical, Spherical, and Hemispherical
Structural Material	Uniform	Non-uniform, user-specified
Heat Conduction	2-D (radial & axial)	1-D (radial)
Nodalization		
axial	Equal space	---
radial	Equal space	Non-uniform
Number of nodes		
axial	Fixed	---
radial	Fixed by the time step allowed	User-specified
Power Source	Due to fission product deposition	User-specified tabular functions allow time-space variation
Oxidation	No	No
Melting	No	No
Heat Transfer in Gas Covered Region		
Radiation	Gray-gas model	Gray-gas model or equivalent band model
Natural Convection		
Laminar and Turbulent	Yes	Yes
Transition	No	Yes
Forced Convection		
Laminar and Turbulent	Yes	Yes
Transition	No	Yes
Mixed Convection	No	Yes
Liquid film evaporation and condensation	No (yes for steam generator tubes)	Yes
Heat Transfer in Water Covered Region		
Natural Convection		
Laminar and Turbulent	Yes	Yes
Transition	No	Yes
Forced Convection		
Laminar and Turbulent	Turbulent Only	Yes
Transition	No	Yes
Mixed Convection	No	Yes

Subroutine WFLOW provides three formulas for calculating the flow rate. The first formula is for small void fraction ($\alpha \leq 0.001$), where the effects of friction and pipe length/diameter ratio are included. The other two formulas are for calculating the intermediate and large void fractions and the effect of pipe length is not considered. The inclusion of the length effect, when the upstream fluid is near saturation or subcooled (i.e., small void fraction), reflects the results of small scale tests, which showed a rapid increase of the critical flow with shortened pipe length [4]. Because the critical flow rate is sensitive to the pipe length and/or length/diameter ratio, users of the MAAP code must select the proper data for the conditions being analyzed.

In the MELCOR code, the flow velocity is first determined using the flow momentum equation (DVH and FP packages) for each flow path. The flow velocity is then compared with a calculated critical flow to determine if choking should be imposed. The test is bypassed if the flow rate is less than 20 M/S. The threshold is a sensitivity coefficient which can be changed by the user. The critical mass flux in MELCOR is based on the RETRAN model; it uses the Moody model for saturated (two-phase) water and the Henry-Fauske model for subcooled water, with a small interpolation region between them. The Moody model is based on non-homogeneous, equilibrium assumptions. MELCOR allows a discharge coefficient less than 1.0 to be applied to the flow rate to account for Vena Contractor effects.

Saha [4] reviewed the Moody and Henry-Fauske models and compared test data from small scale, steady-state critical flow experiments. The comparison with experimental data reveals that there are disagreements over the effect of pipe diameters on the critical flow rate. However, there is no discrepancy over the effect of pipe length. All experiments show that the critical flow rate increases significantly as the pipe length is shortened. However, it is not yet established whether or not the pipe length, or the pipe length/diameter ratio, or both should be the governing parameters. Saha concluded that both the length and the diameter, along with the upstream fluid conditions, are important in determining the critical flow rates. Experiments have shown that the critical flow rate also increases with decreasing upstream enthalpy, particularly for near-saturation and subcooled liquid conditions. However, the modified Henry-Fauske correlation used in the MAAP code for low void fraction flow includes a length/diameter ratio term and the Moody correlation used in MELCOR does not have any length and/or diameter corrections.

The effects of pipe length and diameter are attributed to thermal non-equilibrium phenomena. The Henry-Fauske model is based on the non-equilibrium assumptions, but uses a lumped parameter rather than a mechanistic approach. For this reason, Saha expressed some concern on applying the Henry-Fauske model to transient situations. Moody's model is based on thermal equilibrium assumptions, and it gives reasonably good predictions for pipes with large length/diameter ratios. For short pipes and low void fraction, the model under-predicts the critical flow rate.

2.6 Gas Transport

Gas transport in the primary system is computed from a quasi-steady momentum balance. The calculation involves the imbalance in static heads around the system, the change of nodal gas temperature, and all sources and sinks of gas.

Gas flowing out of the primary system through the PORVs or breaks is computed by subroutine GFLOW. A compressible adiabatic, critical flow model for a gas mixture containing steam and hydrogen is used. The gases are assumed ideal gases and the compressibility factor for steam is included. The actual pressure ratio across the open area is first computed and compared with the critical pressure ratio to check if the flow is choked. The mass flow rate is then given in terms of the sonic velocity with a multiplier. The multiplier is a function of pressure ratio and specific heat ratio.

In MELCOR, the procedure to compute gas flow rate is similar to that used for water flow. The momentum equation is first solved to determine the gas flow rate and compared with a critical flow to determine if choking should be imposed. The critical mass flux of a gaseous mixture is taken as the sonic flux at the minimum section of a flow path. A multiplier, which is a function of the specific heat ratio, is applied to the sonic mass flux. The multiplier represents the reduction in density because of expansion, and the reduction in sound speed because of cooling. Although the formula of critical mass flux used in MAAP and MELCOR are different, the results are about the same.

3 Core Heatup

3.1 General Core Model and Nodalization

In MAAP, the PWR reactor core is assumed to consist only of fuel rods and coolant flow channels; structural materials (such as grid plates) and control rods are not included. The pellets and clad in a fuel rod are lumped together and only an average fuel temperature is computed. Because there are no barriers in a PWR core, a uniform boiled-up water level is assumed across the core. During uncovery of the core, when the core and downcomer are hydraulically disconnected from the rest of the primary system, the core and downcomer have the same collapsed water level.

The core is divided into radial rings and axial rows. All nodal variables have a dimension of a maximum of 70 nodes. The maximum number of rings is 7, and the maximum number of rows is 20. (The maximum number of rows is actually 19 for the active fuel; the top row is used to represent the unfueled upper fission gas plena.) Any combination of rings and rows is acceptable, provided that the numbers do not exceed the maximum values. The normalized flow area for each ring and the normalized power for each ring and row are user-specified. The reactor lower plenum, which is excluded from the primary system nodalization, is lumped with the downcomer. There is no radial and axial nodalization in the lower plenum, which is treated as one volume.

In the core (COR) package of the MELCOR code, the reactor core includes the portion of the lower plenum directly beneath the core. Both the core and the lower plenum are divided into concentric radial rings and axial segments. A particular radial ring and axial segment designates a cell. The number of rings and segments are user-specified, and the maximum nodes allowed for the radial rings and axial segments are 9 and 49, respectively. The maximum axial segments in the lower plenum is 50. The larger number of axial nodes available in MELCOR should provide a better description of core relocation and interaction in the lower plenum. A comparison of the nodalization used in MAAP and MELCOR is shown in Figure A.1 and Table A.2.
In MELCOR, the fuel pellet, cladding and control rod are modeled separately as three components within individual COR cells. Other structural materials, such as a grid plate, also are allowed in each cell. A lumped parameter treatment is used for each of the above components within a cell; therefore, each component is represented by a single temperature. Six materials can be specified in the COR package. The materials are UO_2, Zircaloy, steel, Zircaloy oxide, steel oxide, and control rod poison (Ag-In-Cd alloy).

3.2 Heatup of Water Pool and Covered Fuel Nodes

The covered part of the core in MAAP extends from the bottom of the core to the location of the boiled-up level. The boiled-up level is determined by subroutine VLEVEL, in which a total mass balance is performed as the volumes of the core and lower plenum are accounted for. In determining the amount of water stored in the reactor core region, the lower plenum is assumed to be a hemisphere, and its free volume is computed as ($2/3\ \pi\ r^3$), where r is the radius of the lower plenum. This computation ignores the presence of support structures and instrument guide tubes in the lower plenum. Without considering the volumes occupied by the structural materials, the free volume and the amount of water stored in the lower plenum are overestimated. This would affect the predictions related to corium/lower head interaction.

In the covered part of the core, steam generation is computed by boiling and flashing. Boiling is caused by heat transfer from the covered fuel nodes to the water pool. Both the internal thermal resistance in the fuel rod and the external convective resistance at the fuel rod surface are considered in the heat transfer calculation. The convective heat transfer is computed "using Dittus-Boelter correlations if film boiling is assumed, otherwise a constant value, 1000, for nucleate boiling is used" (subroutine HEATUP, pg. 8) [1]. Neither the film boiling correlation nor the code logic to switch from film boiling to nucleate boiling is given in the user's manual [1].

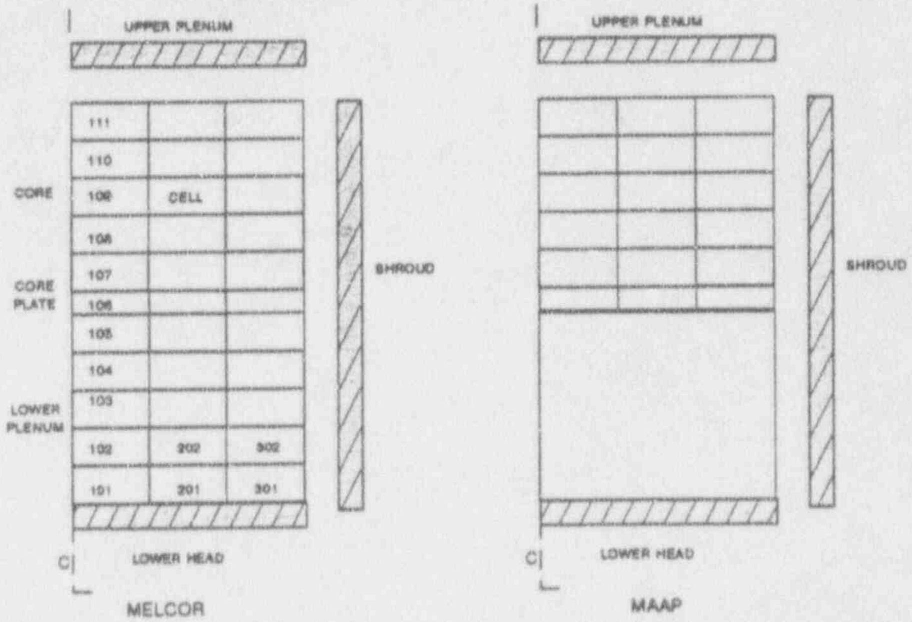

Figure A.1 Comparison of Core/Lower Plenum Nodalization

For a partially covered node, the decay heat of that fraction of the node under water level is used as the only heat source to the water pool, and no other heat transfer is computed. When the core is recovered, the heat transfer calculation is based on a consideration of two-phase hydrodynamic stability. This stability consideration assumes that a maximum steam velocity exists beyond which liquid droplets would be entrained in the gas stream and be carried out of the pool. A maximum boil-off rate is computed from this maximum steam velocity. The MAAP code assumes that heat transfer to the water pool based on this stability is an upper limit, and that heat transfer computed from convection or decay heat can not exceed this limit.

Steam generation by flashing is calculated in subroutines POOL and RATES, if the pressure in the primary system changes with time. These two subroutines compute the rate of mass that has to be released from a superheated water pool to maintain it at saturation. When performing these computations, a characteristic time is used to determine the rate of flashing. The characteristic time is simply the current timestep if the equilibrium thermodynamics model is used. However, the characteristic time is the greater of five times the current timestep, or 5 seconds, when the non-equilibrium thermodynamics model is used. According to the MAAP manual, the choices of time scales are based on stability considerations.

Thermal radiation is another potential source for steam generation. MAAP models the exchange of thermal radiation between gas and water pools (subroutine HTGPL). The model assumes that radiation heat transfer is directly related to the partial pressure of steam and the radiation path length. When the model is applied to the reactor core region, there is a large uncertainty in determining the radiation path length. The presence of fuel bundles with or without cladding ballooning would make it difficult to evaluate the radiation path length. It is noted that the MAAP radiation model does not include the downward axial radiation from fuel nodes to the water pool. This radiation heat transfer could be important when fuel nodes above the steam-water interface are highly oxidized and are at relatively high temperatures.

Table A.2 Comparison of Core Modeling

Model	MAAP	MELCOR
Maximum nodes in core Axial Radial Total	 20 7 70	 49 9 441
Maximum nodes in lower plenum Axial Radial	 1 1	 50 9
Fuel Rod	Lumped No axial conduction	Clad and pellet separated Gap conductance and axial conduction included
Control Rod	Not modeled	Lumped
Structural Material	Not modeled	Lumped
Material Represented	UO_2, Zr, ZrO_2	UO_2, Zr, ZrO_2 steel, steel oxide, and Ag-In-Col alloy
Zr Oxidation	Yes	Yes
Termination of Zr Oxidation	Onset of melting or blockage model chosen	User-specified cut-off temperature
Fe Oxidation	No	Yes
Termination of Fe Oxidation	--	No
Clad Ballooning	Yes	No
Clad Failure	Yes	No

Steam generation due to boiling and flashing is a very important source for the metal/water reaction (MWR) in the uncovered region above the water level. If steam generation is not properly computed, steam starvation often becomes the limiting mechanism for Zircaloy oxidation and severely restricts the predicted hydrogen generation.

In the MELCOR code, simplified nucleate and film boiling correlations are used to estimate the heat transfer from the covered fuel nodes to the water pool. Heat transfer between water and structural materials immersed in the pool also is modeled. Pool convection and boiling correlations are used to compute this heat transfer. At the water/gas interface, MELCOR computes mass and energy transfer according to a user-specified equilibrium or non-equilibrium thermodynamics model. When the equilibrium thermodynamics model is specified, mass and energy transfer between the water pool and gas is instantaneous. When the non-equilibrium thermodynamics model is specified, MELCOR calculates the energy exchange at the pool surface, the rate of evaporation or condensation there, and the rate of phase separation as bubbles rise to join the atmosphere.

3.3 Heatup of Uncovered Nodes

Modeling of the heatup of the uncovered fuel nodes is an important part of the analysis of a degraded core accident. The energy balance for the nodes in the core region includes consideration of decay heat, oxidation heat, convection, and radiation heat transfer. For the case of upper head injection, MAAP also models the heat loss to water sprayed into the top of the core. Before core melt and relocation, decay heat is related to those fission products associated with the fuel nodes. The decay heat only includes that portion of the decay heat associated with nonvolatile fission products after molten fuel relocation occurs. At this time, the energy of the molten corium also is included in the energy balance as a heat gain or loss. If corium is entering a node, it represents an energy gain, whereas if corium is leaving the node, it is an energy loss. A similar energy balance is performed in the MELCOR code.

A one-dimensional radiation model is used in MAAP to estimate radial heat transfer by radiation from the inner fuel assemblies to outer assemblies and from the outer assemblies to the core barrel. Two assumptions are involved in this model: view factors between two neighboring radial nodes are one and the emissivities of the surfaces also are unity. Both assumptions yield maximum radiation heat transfer. Fuel rod to gas radiation is not modeled in MAAP. Thus, the absorption, transmission, and emission of radiation by steam at high temperatures are not accounted for in MAAP.

Convective heat transfer is computed for a gaseous mixture of steam and hydrogen. Forced laminar and turbulent heat transfer correlations for fully developed flow in circular pipes are used. No natural convection heat transfer correlation is provided in MAAP. The thermal resistance due to internal conduction in the fuel rods is considered in the heat transfer calculation. The internal thermal resistance in a lumped pellet and clad node involves two approximations: (1) the effective radius of the fuel rod is 0.3 of the pellet radius, and (2) the thermal conductivity of the lumped node is represented by the thermal conductivity of UO_2. These approximations are considered to give a reasonable estimate of the fuel-to-clad heat transfer [HEATUP/PWR, pg. 8]. The appropriateness of these approximations at high temperatures when the clad is oxidized is uncertain. Oxidation of the clad would greatly reduce the thermal conductivity of the clad. (The thermal conductivity is about 42 and 2.5 w/m-K for Zr and ZrO_2, respectively.) In addition, clad ballooning at high temperatures and low pressures would increase the pellet-to-clad gap resistance. These factors could cause MAAP's heat conduction model to be inaccurate at high temperatures.

In MELCOR, the pellet and clad are not lumped together; radially average temperatures are computed separately. Radial conduction through the pellet-to-clad gap is calculated by an analytical expression, which includes the thermal radiation and gas conductance through the gap region. The user specifies the gap thickness to use in the model. Axial heat conduction is modeled for both the pellet and clad. In general, axial heat conduction is insignificant, except at the liquid-gas interface, where it can be important due to the very steep temperature gradient that exists in this region. This steep temperature gradient could induce a large axial heat conduction from the uncovered fuel nodes to the water pool and contribute to water boiloff. In addition, the separation of the pellet and the clad in the MELCOR code should provide a better estimate of the clad temperature, which is important for predicting the oxidation rate and the onset of clad failure. The lumped parameter treatment together with the estimate of the effective pellet radius modeled in the MAAP code could produce more uncertainty in the predicted fuel temperature. Because the decay heat and the oxidation heat are distributed uniformly over the lumped node, the clad temperature would be over-estimated before oxidation and under-estimated after oxidation occurs. The temperature uncertainty will, in turn, affect the hydrogen generation rate. (Although an interactive procedure is used in MAAP to estimate the clad surface temperature during core recovery, the validity of the procedure was not demonstrated.)

Convective heat transfer in MELCOR is treated for a wide range of flow conditions. Correlations for laminar and turbulent gas flow in both forced and natural convection are provided. The laminar forced convection correlations represent both developing and fully-developed flow in circular pipes and rod bundle arrays. The turbulent forced convection correlations are the same as that used in MAAP. The natural convection correlations are for flows in narrow vertical channels.

In MELCOR, thermal radiation is modeled among components (i.e., clad, control rod, and structure) within a cell and across cell boundaries. The radiation model considers intervening gray medium (i.e., steam) between surfaces. The emissivity of Zircaloy is computed as a function of temperature and oxide thickness, and the emissivity of steel is temperature-dependent. The emissivity of steam varies depending on the temperature of the steam and the optical depth. (The optical depth is the product of steam partial pressure and mean beam length; both are computed in the code.) The view factors used in the radiation model represent the effects of surface orientation and are specified by the user.

In summary, the MELCOR treatment of heat conduction, convection, and radiation in the uncovered region is much more rigorous than the treatment by the MAAP code. The treatment of the heat transfer in the uncovered region of the core is a very important component for analyzing the degraded core accident sequences. Separation of the clad and pellet, and the inclusion of control rod and structural materials in the core region (as modeled in MELCOR) will have some impact on the predicted core meltdown progression (relative to MAAP predictions).

3.4 Metal Oxidation and Hydrogen Generation

Zircaloy oxidation by steam becomes important at temperatures above 1300K. The oxidation rate laws used in MAAP are the Cathcart and Baker-Just solid-state diffusion correlations for temperatures less than 1850K and greater than 1875K, respectively. An interpolation between the two correlations is made between 1850K and 1875K. The two correlations are compared with other correlations used in MELCOR, MELPROG, and SCDAP in Figure A.2.

At higher temperatures (above 1875K), the Baker-Just correlation (used in MAAP) predicts a higher oxidation rate than the Urbanic-Heidrick correlation (used in MELCOR), but a lower rate than the Prater-Courtright correlation (used in MELPROG and SCDAP). At temperatures below 1800K, the Cathcart correlation agrees well with the Prater-Courtright correlation. The difference in reaction rate shown in Figure A.2 may not be very important, because hydrogen generation is often controlled by other factors, such as steam availability and clad surface temperature.

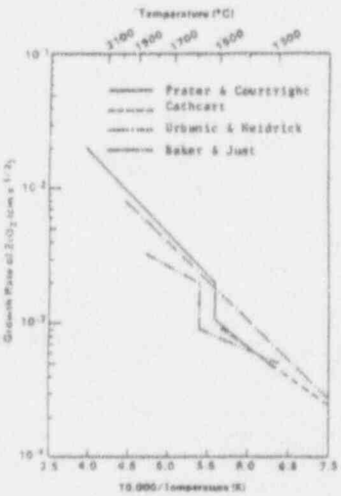

Code	Correlation
MAAP	Cathcart for T ≤ 1850°K Baker-Just for T > 1875°K (Interpolation 1850°K < T < 1875°K)
MELCOR	Urbanic-Heidrick
SCDAP	Prater-Courtright
MELPROG	Prater-Courtright

Figure A.2 Comparison of Growth Rate of ZrO_2

During a degraded core accident, the steam availability could become the dominant factor. Without the restoration of a core injection system, hydrogen generation is often terminated due to steam starvation during a severe accident sequence.

MAAP also allows (through user input) double-sided oxidation after the clad is predicted to burst. Because clad burst is often associated with flow blockage, which may restrict the steam supply, the double-sided oxidation options may not significantly affect the overall hydrogen production.

In MAAP, clad oxidation is terminated either due to blockage or the onset of melting when the block option is used. The eutectic melting temperature is specified by the model parameter No. 52, with a default value of 2500K. When a node temperature reaches the eutectic melting temperature, MAAP assumes that the flow area at that node is reduced to zero and no steam flow is available; hence, no further oxidation can occur.

Flow blockage also can be controlled by the model parameter No. 55, which specifies a minimum porosity (default value 0.1). When a node porosity is less than the minimum value, MAAP assumes the flow channel is completely blocked and the oxidation is terminated.

It should be emphasized that the termination of hydrogen generation due to melting as modeled in MAAP does not agree with some experimental evidence. For example, PBF tests [5,6] have shown that a large quantity of hydrogen was generated after the start of Zircaloy melting. Metallographic determination of local peak temperatures of the PBF debris after testing showed continued oxidation and hydrogen generation at temperatures higher than the Zircaloy melting point. These test data do not indicate a cutoff or diminished hydrogen production after the start of Zircaloy melting and fuel dissolution.

In MELCOR, clad oxidation is controlled by two user-specified oxidation cutoff temperatures to prevent oxidation below or above certain temperatures. The lower cutoff temperature (default = 1100K) prevents oxidation at temperatures that generate only minute quantities of hydrogen. The upper cutoff temperature (default = 9900K) can be used to limit the amount of oxidation for sensitivity analysis, such as blockage and melting.

In addition to Zircaloy, oxidation of stainless steel is another potential hydrogen source during a degraded core accident. MELCOR has a model for steel oxidation which is similar to the Zircaloy oxidation model. The steel is divided into four constituent elements (iron, chromium, nickel, and carbon), according to the mass fractions specified by the user on input data. Separate reaction equations for these elements are used to estimate the quantity of hydrogen generated and the reaction energy produced. A parabolic rate equation is used to estimate the reaction rate for steel. The steel oxidation rate equation used in MELCOR is compared to the Zircaloy oxidation rate equation used in MAAP (i.e., the Baker-Just and Cathcart correlations) in Figure A.3. The rate of oxidation of steel by steam is relatively small compared with the oxidation of Zircaloy at temperatures below 1400K. However, at higher temperatures and near the steel melting point, the rate of oxidation of steel exceeds that of Zircaloy. Recent studies showed that natural circulation in the primary system at high pressure could result in high structure temperatures in the upper plenum, hot leg, and surge line [7,8]. When this situation occurs, oxidation of stainless steel could occur in these regions, and additional hydrogen would be generated from this source.

The MELCOR steel oxidation model only applies to structures in the core region. No oxidation model is provided for structures in the upper plenum and primary system. MAAP does not have a steel oxidation model. Hence, both codes could underestimate hydrogen generation if conditions for steel oxidation exist in the primary system during a degraded core accident.

3.5 Clad Ballooning

Subroutine STRETH in MAAP computes clad ballooning caused by a pressure differential across the fuel cladding. The release of Xenon gas from a fuel pellet and the over-heating of the fuel rod are used to establish the internal gas pressure of the fuel rod based on the ideal gas law. Depending upon the internal gas pressure and the extent of the loss of pressure in the primary system, hoop stress is computed for each axial node. This is followed by the calculation of both elastic strain and plastic strain. The cladding behaves locally elastically, if the elastic strain is greater than the plastic strain. Otherwise, the cladding begins to deform plastically and the rate of plastic strain is computed, if the plastic strain is greater than the elastic strain. All strain correlations used in MAAP are from the handbook MATPRO. The following effects of clad ballooning are modelled in MAAP:

(1) Increasing the local fuel rod area for heat transfer and oxidation;

(2) Increasing the local flow resistance, and hence, decreasing the natural circulation flow rate of the upper plenum-to-core; and

(3) Diverting flow to less-ballooned channels.

The MAAP code also computes the temperature-dependent tangential stress as the burst stress using correlations from the handbook MATPRO. Clad failure at any axial node is assumed if the burst stress is greater than the hoop stress. Clad ballooning ceases when clad fails due to the burst stress, or when the clad reaches the Zircaloy melting temperature at 2150K.

However, the clad ballooning model in MAAP does not consider the effect of oxidation on the mechanical properties of the clad. Oxidation will form an embrittled layer on the clad, which is likely to limit the ballooning and burst to a local area. Fuel pitch also should be considered as a constraint to limit the degree of ballooning. Finally, the "effective pellet radius" (i.e., 30% of the pellet radius) in the MAAP fuel conduction model should be modified to include the clad deformation.

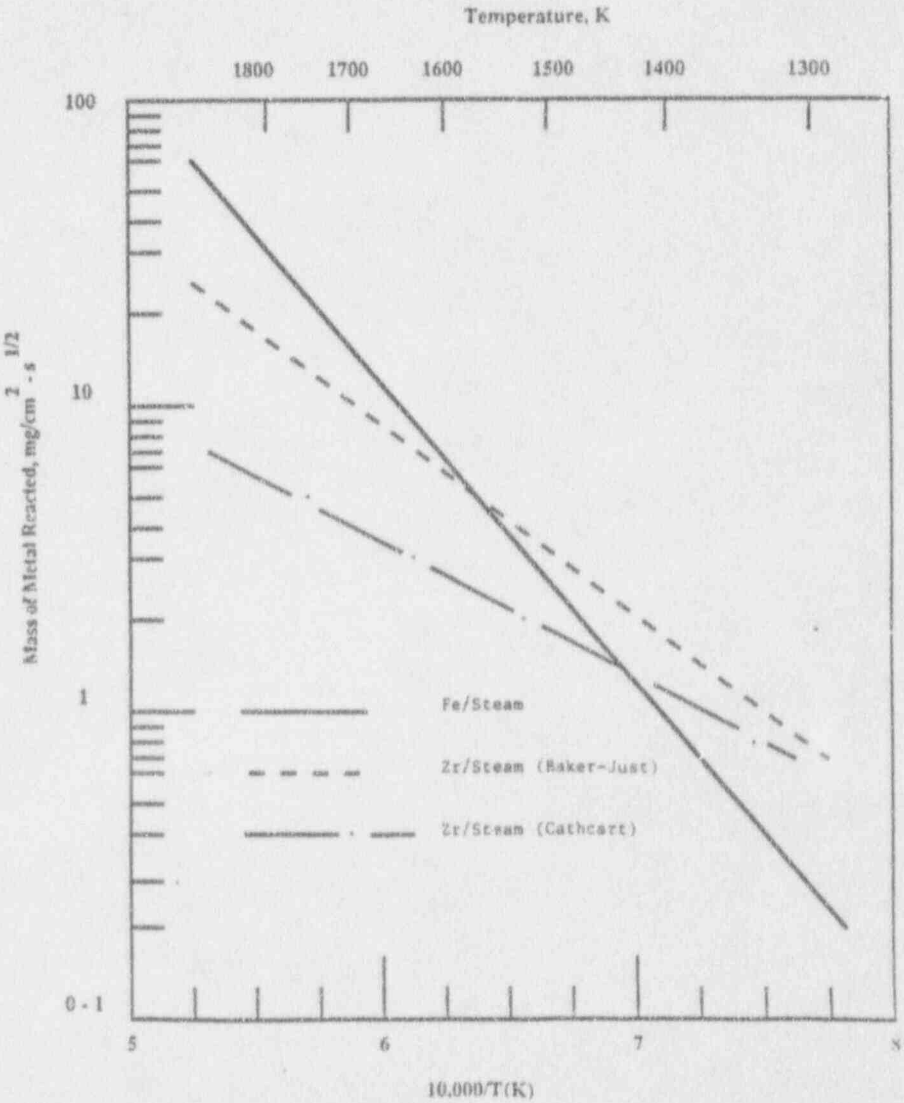

Figure A.3 Comparison of Fe/Steam Oxidation with Zr/Steam Oxidation

MELCOR does not model clad ballooning and burst; it only provides a specified time-and-space dependent blockage for flow channels that is specified by the user. The oxidation by residual steam on both the inner and outer surface of the clad, which is implemented in the MAAP code after clad burst, is not modeled in MELCOR.

4 Natural Circulation

Natural circulation flow in the primary system is an important mass and heat transfer process that can influence the progression of a severe accident sequence. The impact of various modes of natural circulation is important during different periods of a severe accident. The pre-dryout natural circulation of the primary system, during a sequence with loss of forced circulation, determines core cooling in the primary system and influences the time of core uncovery. The steam/gas natural circulation within a PWR reactor vessel and between the upper vessel head and the steam generators, during a high-pressure post-dryout/pre-melt period was recognized as a very important phenomenon with a strong influence on the accident sequence [7]. In some sequences, the energy redistribution could be of such a magnitude that the possibility of the primary system failing before fuel failure was considered [8].

Since MAAP 3.0B does not have a momentum equation which can handle natural circulation phenomena, additional models were introduced into the code to simulate the most important modes of natural circulation in the primary system. The impact of natural circulation is of greatest importance in high-pressure PWR sequences, and therefore, most of the models exist in the MAAP PWR code.

Accurate simulation of natural circulation phenomena requires a detailed multidimensional/multiphase model which needs a considerable amount of computing time. Usually such models are not suitable for simulating severe accidents that may extend for several hours. Therefore, simplified one-dimensional or space-independent models are used under these circumstances. These models should be able to give adequate predictions of energy redistribution and the flow field. However, an assessment of such models is necessary to validate their applicability to the severe accident analysis being performed.

There are three models for natural circulation in the MAAP 3.0B PWR code:

1. Core-Upper plenum circulation
2. Hot leg-Steam generator circulation
3. PWR primary system circulation

The basic characteristic of all the models is that they consider only a single-phase ideal gas, which is assumed to be a mixture of steam and noncondensibles. No phase change models are included. Natural circulation flow is calculated using a quasi-steady momentum balance along predefined loops. The acceleration pressure drop is neglected in all models.

4.1 Core - Upper Plenum Natural Circulation

This natural circulation is an important energy transfer mechanism during a high-pressure PWR transient. The MAAP 3.0B model allows a user to choose between two predefined flow patterns associated with different vessel geometries (Westinghouse or Babcock & Wilcox).

Total natural circulation flow is calculated in HEATUP/PWR, using the assumption that all up and all down flowing channels have the same friction pressure gradient, which is based on constant friction factor, f=0.1. This friction factor influences friction vs buoyancy pressure drop and the onset of natural circulation. A constant value for the factor seems to disregard the importance of the phenomenon, especially when it could be calculated using one of several correlations already present in the code.

The return flow occupies half of the total core flow area, although the upward flow has a non-returning component and a lower average density. A simplified continuity equation or experimental results could be used to obtain a better approximation of the flow area distribution.

The pressure drop of the horizontal flow is taken into account only in the fuel region (the pressure drop of the upper head flow is neglected). This is probably of secondary importance since an integrated momentum equation is used to calculate natural circulation flow, and the pressure drop in the upper plenum could be included in any other loop component.

It is assumed that downward flow turns sideways when its temperature equals that of the upward flow. It seems that an equal density criterion would have a better physical foundation for the sideward flow. Equal temperature is a good approximation if the upward and downward flow have the same composition (or are one component flows). The comparison, which is used to support the model, is done against single component experiments and is not sufficient for the model. A comparison against multicomponent flow experiments or numerical simulations would give a proper assessment of the model.

The horizontal flow area is assumed to have a constant height (0.5 m) regardless of the system's dimensions. The user can investigate this rough assumption by making sensitivity studies in which the cross flow friction factor could be changed.

The total core flow calculated in subroutine HEATUP/PWR is partitioned among parallel channels using the criterion on equal pressure drop (subroutine REMIX). The acceleration pressure drop is neglected in the momentum balance, which tends to overestimate the flow in a heated channel. MAAP also allows the user to disable the full two-dimensional, core flow model used in REMIX, and replace it with a simple model that splits the flow based only on the flow areas.

After reactor vessel failure, natural circulation between the upper plenum and the core is assumed to be replaced by overall uni-directional natural circulation patterns, which are set up around the coolant loops of the primary system.

4.2 Hot Leg - Steam Generator Natural Circulation

The model for energy transport from the upper head of the reactor vessel to the hot leg and steam generator tubes can significantly impact high-pressure severe accident sequences. This natural circulation phenomenon transfers energy to other parts of the primary system pressure boundary (the pressurizer surge line and steam generator tubes), making failure of the pressure boundary before the core melts and the lower plenum fails, a possibility. A simplified modeling of this counter-current flow in the hot leg and the two-way flow in the steam generator tubes is a difficult task. MAAP 3.0B has simple models for the natural circulation in both U-tube and once-through steam generators as discussed in Section 4.3.1.

4.2.1 Model for the U-Tube Steam Generator

The difference in temperature between the upper head of the reactor vessel and the inlet plenum of the steam generator gives rise to a counter-current flow in the hot leg. The flow is modeled using a correlation based on static momentum balance with a coefficient as a model parameter. The default value for the correlation coefficient was derived from the experiment.

The difference in the inlet and outlet plena temperatures of the steam generator gives rise to the flow-through steam generator tubes. The gas flows from the inlet plenum through a certain number of the U-tubes to the outlet plenum, and returns back to the inlet plenum through the rest of the tubes. Using the calculated heat transfer coefficients for the "out" and "back" tubes, a constant secondary temperature, and a linearized density change, the flow temperature can be calculated as a solution to the system of nonlinear equations.

The fraction of tubes, with flow in the "out" direction, is a user-input parameter. Benchmarking calculations show good agreement with test data, when the fraction of tubes carrying the outflow is taken between 0.25 and 0.45.

4.2.2 Model for Once-Through Steam Generators

The model for the natural circulation in the once-through steam generators neglects heat transfer between the primary and secondary side due to water seal, which prevents flow through the tubes. However, those temperature differences between the upper head of the reactor vessel and hot leg, and the hot leg and candy-cane give rise to counter-current flows in the hot leg and candy-cane. The model for the counter-current flow is similar to that used in the U-tube steam generator. It is assumed that the bulk of the heat is dissipated in the candy-cane.

4.3 Primary System Natural Circulation

4.3.1 Two-Phase Mixture Natural Circulation

A very simple model for natural circulation of both separated and homogeneous phases in the primary system exists in the MAAP code. The model is based on the assumption of a constant void fraction in the whole primary system. The average void fraction used as a set point for the switch between the homogeneous and stratified model in the primary system is a user-input parameter.

The same void fraction is used for a break flow calculation, which leads to a large uncertainty in the calculation for the primary coolant inventory. A user specified break area using experimental or design code results could be the answer to this problem.

In the separated mode, if the pools are connected, the flows are based on the constant collapsed water level in the primary system. If the pools are decoupled, the flow rate between them is calculated as an excess water mass divided by the time step (DCOVFL). Quasi-steady manometric balance is used to calculate downcomer-core flow rate.

The simple flow model is enhanced in steam generators to predict the phenomena for the natural circulation of the two-phase mixture such as phase separation and reflux-condensation heat transfer mode.

Although it may seem that the natural circulation flow model of the two-phase mixture in the primary system is oversimplified, the additional models introduced into the code may significantly improve the code's abilities of simulation. However, assessment through integral natural circulation tests is necessary to validate code applicability to severe accident analysis.

4.3.2 Natural Circulation of Gas in the Primary System

The natural circulation flow of the steam/noncondensibles mixture in the primary system influences mass and energy transport during a post-dryout phase of severe accidents. The model implemented in MAAP 3.0B calculates the average temperature of gas in PTCAL by lumping together all the control volumes. Gas temperatures and flows of local control volumes are calculated in subroutine FLOW using quasi-steady momentum balances over predefined flow loops and an ideal gas equation of state. The flow through the loop is set to zero if the flow path is blocked due to water.

4.4 MELCOR Natural Circulation

There are no special models for natural circulation in MELCOR 1.8.0. However, because the control volume and the topology of flow paths are user inputs, and multiple flow paths between control volumes are allowed, the user can model natural circulation phenomena during the severe accident. The one-dimensional momentum equation that is solved for the flow path network has gravitational heads. This equation is expected to give good results in the case of simulating simple, one-dimensional natural circulation. However, the results are dependent on user specified nodalization and modeling of multidimensional counter-current natural circulation during the severe accident could be only roughly approximated.

5 Accident Initiation, Intervention, and Operator Action

The MAAP code uses "event flags" to initiate an accident transient and to set up the intervention conditions for operator actions. These flags define the events that cause the accident. The flags cover a large range of potential accident initiators, including loss of electrical power, loss of main and auxiliary feed water, the availability of high pressure injection (HPI), low pressure injection (LPI), upper head injection (UPI), and charging pumps, stuck open PORVs in either the primary system and/or the steam generator system, a V sequence, and a break in the primary system. The flags are sufficient to represent all potential accident initiators that have been identified in current PRAs.

The intervention flags set up conditions by specifying limits for any set of key variables, or by declaring any of the event flags as key events for operator actions. There are 12 key variables which can be used as bases for intervention for PWRs. They involve pressures, temperatures, water levels, time, and others. The pressure controlled flags are:

Primary system pressure, and
Containment building pressure.

The temperature controlled flags are:

Lower compartment temperature, and
Hottest core node temperature.

The water-level controlled flags are:

Water level in the Pressurizer,
Water level in the RWST, and
Water level in the unbroken loop steam generator system.

The time controlled flags are:

Problem time, and
Delta time after the previous intervention has occurred.

The other flags are:

Average void fraction of the primary system,
Total hydrogen mass generated in accident,
User defined events.

Although most of the important variables are included in the intervention flags for potential operator action, there are still some variables which could be added to the above list. For example, the temperature in the containment annular region could be added as a base for potential operator action. There is important equipment, such as accumulators, pressurizer relief tank, vent ducts, and electrical cable panels, located in the annular region. An indication of high temperature in this region could allow the operator to initiate containment sprays or fans to lower the temperature. This operator action could be modeled by an intervention flag. (Note that the sprays and fans are only activated automatically by pressure setpoints in the MAAP code.) Another example is the temperature in the reactor cavity region, which could be used as an intervention flag to initiate cavity flooding. Cavity flooding is modeled in the MAAP code and has been considered as a potential severe accident management strategy [9]. The operator actions cited in the previous examples can be modeled by MAAP using time as the intervention flag. However, the timing would have to be determined by a previous analysis.

There are no equivalent intervention flags in the MELCOR code. MELCOR uses the control function defined in the Control Function Package (CF) to perform similar intervention and operator actions. The CF Package allows the user to define functions of elements in the MELCOR database, and make values of these functions available to other physical packages. The logical-or real-valued control functions may be used to initiate or control the operation of models or components as conditions change during a calculation. Examples of control functions are:

(1) The operation of pumps,
(2) The actuation of spray sources,

(3) The opening and closing of valves, and
(4) The initiation of trips.

Because the elements used in the MELCOR Control Functions are from the MELCOR database, the number of variables which can be used for intervention are much more than the 12 variables defined in the MAAP code for PWRs. It would be easier for MELCOR to simulate operator actions required by the Emergency Operation Procedures (EOPs) and any potential severe accident management strategies.

6 Engineered Safety Systems

MAAP models the passive and active emergency core cooling systems. The passive systems include the low pressure accumulator and the high pressure accumulator (i.e., upper head injection for ice-condenser plants). The active systems include charging pumps, safety injection pumps, and low pressure injection through the residual heat removal (RHR) pumps. For the containment, MAAP has a spray model and a fan cooler model. The suction and discharge of all engineered systems are summarized in Table A.3.

Table A.3 Engineered Safety Systems Modeled in MAAP

System	Suction		Discharge
	Injection	Recirculation	
UHI LP Accumulator	Accumulator Accumulator	No No	Upper head Cold leg or downcomer
Safety Injection CHP HPI LPI	RWST with external makeup	Sump and RHR HX	Cold leg or hot leg or downcomer
Containment Safety System Sprays	RWST with external makeup	Sump and RHR HX	Containment
Fan	---	Upper containment	Lower Containment

The actuation logic for the safety systems is defined in subroutine EVENTS. The use of two event flags is sufficient to model the three positions (on, off, automatic) of all engineered safety systems. The event flags also define water sources for the system; namely the RWST, sump, or accumulator. In addition, a condensate storage tank is defined for the auxiliary feedwater, and a cavity injection tank for cavity flooding. However, no alternate water source is specified in the subroutine EVENTS. In a study of candidate accident management strategies [9], several recommendations were made to ensure manual intervention upon failure of automatic switchover, and to ensure adequate heat removal by emergency connection of existing or alternate water sources. The water sources include the service water or firewater supply system. To model these potential accident management strategies, MAAP would have to include an alternate water source in subroutine EVENTS and in the parameter file.

All core injection systems are actuated by pressure setpoints given in the parameter file and can be changed by user's input. According to the Westinghouse PWR System Manual [10], the engineered safety features will be actuated by the four signals listed below, in addition to the manual operation:

(1) Low pressurizer pressure,
(2) High containment pressure,
(3) High steam line differential pressure, and
(4) High steam line flow - coincident with low steam line pressure or low-low average temperature.

The first two signals are modeled in MAAP by the automatic or intervention event flags. Presently, the last two signals cannot be simulated by MAAP.

The performance of the engineered safety systems are modeled in subroutine ENGSAF in MAAP. This subroutine computes water mass flow rate, energy flow rate, water temperature, the required net positive suction head for pumps, and the exit temperature of the heat exchangers. The pump flow rate can be specified by a 5-point pump curve. The ability to throttle the pump discharge and refill the RWST are two features of the MAAP model. These two features also are part of the accident management strategies recommended by Luckas et al. [9].

The restoration of the ECCS introduces many complex thermal hydraulic phenomena in the primary system. There will be steam condensation, entrainment, and counter-current flow in the downcomer. The core region above the quenching front will be either in the inverted annular flow regime (for high flooding rate), or the dispersed droplet regime (for low flooding rate). However, both regimes have poor heat transfer characteristics. The fuel rod will be subjected to a large temperature gradient in both the radial and axial directions. In a degraded core accident, complex corium/water interaction could occur. The present version of MAAP may not be able to simulate these phenomena.

7 Summary

Based on this preliminary review, it appears that the MAAP code can model all of the major elements of a PWR system and the important thermal-hydraulic phenomena. A large number of model parameters allows the user to perform sensitivity studies. The logic used in the code provides a convenient way to simulate accident initiation, intervention, and operator action. The following are some specific comments, which are discussed in more detail in the report:

(1) The fixed nodalization for the primary system and reactor core is restrictive.

(2) Inclusion of structural materials, other than steel should provide a more general treatment of structures.

(3) Control rod and structural materials can influence the progression of a degraded core accident. They are currently not included in the core heatup model in MAAP, neither are models for steel oxidation.

(4) The validity of the fuel rod heat conduction model has not been established for situations in which clad oxidation and ballooning have occurred.

(5) Adding a natural circulation model in the MAAP code is an improvement for treating this important phenomena. More benchmarking calculations under various conditions, such as two-component flow with mixed convection could help to validate this model.

8 Oxidation and Hydrogen Generation

The MAAP modeling of clad oxidation and hydrogen generation while the reactor core has an intact geometry is relatively straightforward and was reviewed in Section 3. During the core heatup, MAAP allows the clad oxidation to be modified when clad ballooning occurs. Ballooning has two potentially opposing effects on the extent of clad oxidation. It increases the surface area, which tends to enhance the oxidation, and reduces the area of the flow channels, limiting the amount of steam available for reaction. The net effect on clad oxidation depends on a balance between the two effects. MAAP allows for double-sided oxidation to simulate steam ingress after rupture of the clad.

In the uncovered region of the core, clad oxidation is terminated at the onset of fuel melting and flow channel blockage. When to terminate hydrogen generation represents a large uncertainty of the phenomenological modeling in MAAP. This assumption does not agree with experimental evidence. Data from several experimental programs demonstrated that hydrogen generation continues after melting and relocation [11]. In fact, experimental data suggests that a significant amount of hydrogen could be generated after Zircaloy melting and relocation.

In a region reflooded after the onset of melting, oxidation may continue if the user defeats the submerged blocking model with IEVNT = 1. Because a covered node is assumed to rapidly quench, this option does not significantly influence the predicted hydrogen generation. For an uncovered node there is also the option of defeating the blockage model (FCRBLK = O), which will effectively allow the oxidation to continue.

Hydrogen generation from the interaction of corium with water in the lower plenum of the reactor vessel is modeled in the PLH2 subroutine of the MAAP code. Any Zircaloy, which has not reacted previously in the core region, can be oxidized as it drains into the water pool, remaining in the lower plenum of the reactor vessel. The important features of the PLH2 model are summarized below:

(1) The entire mass of corium (i.e., uranium dioxide, metallic zirconium, zirconium oxide, and steel) is involved in the reaction. The corium is assumed to be in the form of particulates.

(2) Properties of the uranium dioxide, instead of the mixture properties, are used in the heat balance calculation to estimate the corium temperature and heat flux from the corium surface.

(3) A critical steaming rate (input) is used to estimate the total pool heat removal.

(4) The total corium surface area is estimated from the total pool heat removal, corium heat flux, and corium mass.

(5) The total corium surface area is assumed to consist of metallic zirconium which allows the metal/water reaction to take place.

(6) The corium quenching time is estimated by assuming that the surface cooling is limited by either a) surface heat transfer, or b) conduction within the particles. The time to reach the zirconium freezing point is assumed to be the maximum of the two quenching times.

(7) Metal oxidation and hydrogen generation are terminated at 1000 K.

The PLH2 model is not mechanistic and involves a large range of uncertainty caused by parameters such as corium mass, surface area, physical properties, and cooling rate.

In Section 3, we explained that MAAP does not consider potential hydrogen generation due to steel oxidation. Comparisons between steel oxidation and zircaloy oxidation show that the reaction rate of steel is higher at temperatures above 1450 K. The steel reaction is considerably higher when steel reaches its melting point. A 3000-Mwt PWR plant, such as Zion, contains about 3400 kg of stainless steel in the core region. After the onset of core melting, this amount of steel, if reacted, could produce about 160 kg of hydrogen based on the following reaction:

$$3Fe + 4H_2O \longrightarrow Fe_3O_4 + 4H_2$$

Thus, without modeling steel oxidation, MAAP could potentially underestimate the total hydrogen production.

In the MELCOR code, both Zircaloy and stainless steel oxidation are considered [2]. The metal oxidation is not terminated at the onset of melting and is allowed to continue during core relocation. Although MELCOR does not have a mechanistic treatment of metal water reactions (MWR) during core relocation, it estimates the hydrogen generation based on the quantity of steam and surface area available at that time. MELCOR defines a Zircaloy oxidation cut-off temperature for parametric studies. No cut-off temperature is defined for steel oxidation.

9 Core Melt

The core meltdown process during a degraded core accident is extremely complex. Much of the complexity is due to the composition of the reactor core. In a PWR core, UO_2 and Zircaloy make up about 94 Wt%. The remaining materials are primarily stainless steel, Inconel, control rods made of Ag-In-Cd material, and Al_2O_3 used in the burnable poison rods. All these materials have different melting temperatures, and complex chemical reactions can occur among the various components. A mechanistic treatment of the physical and chemical phenomena associated with core melt is not feasible for integrated system codes, such as MAAP and MELCOR. These codes must use a simplified approach to represent the major features of the core melt process. Before reviewing the MAAP code, a brief description of the core meltdown processes based on existing information available in the literature [11, 12, 13, 14] is presented. With this background, the MAAP code will be assessed and comparisons with the MELCOR code will be made.

Hofmann [12] suggested that core meltdown processes could be characterized by three temperature regimes. The first temperature regime is between 1473 K and 1673 K. During this temperature regime, the Ag-In-Cd alloy (control rods), which has a very low melting temperature (1073 K), is likely to be the first component to melt after core uncovery. Any mechanical rupture of the control rod cladding (stainless steel) will allow the molten Ag-In-Cd alloy to contact the Zircaloy guide tubes and even some of the Zircaloy cladding around the fuel rods. The contact would form low-temperature eutectic solutions and cause local damage in the core region well below the melting temperature of Zircaloy (approximately 2033 K). The relocation of the eutectic solutions may form a local blockage which would restrict flow and cause accelerated heat up of the core.

The second temperature regime is between 2073 K and 2273 K. If the Zircaloy clad has not been oxidized, then it will melt at about 2033 K and relocate downward along the fuel rod. If an oxide layer has formed on the outside surface of the clad, then relocation of any molten Zircaloy on the inside will be prevented, because the oxide layer will remain solid until the core reaches much higher temperatures (the melting point of ZrO_2 is 2973 K). Under these conditions, the molten Zircaloy will chemically dissolve the solid UO_2 pellet and ZrO_2 shell. The result is chemical dissolution (i.e., liquefaction) of UO_2 and ZrO_2 by the molten Zircaloy at about 1000 K below the melting points of UO_2 and ZrO_2.

The third temperature regime is between 2873 K and 3123 K. If a reactor core ever reaches this high temperature regime, the remaining UO_2, ZrO_2, and the (U, Zr) O_2 solid solution will start to melt. This melting will lead to complete meltdown of all remaining core materials.

In the MAAP code, the control rods and structural materials in the core region are not included in the core melt model. (They are considered for release and transport of fission products.) Therefore, the early formation of local blockage by the low-temperature eutectic solutions of control rods and structural materials, and their impact on the heatup rate of the core are not considered. Only the eutectic solution of UO_2, ZrO_2, and Zr is assumed in MAAP.

Melting of the undissolved Zr is not modeled. Core melting is determined by a user-specified eutectic temperature and a user-specified latent heat of melting. The two parameters control the timing of fuel melt and the rate of fuel melting. Because the onset of fuel melt is used to terminate clad oxidation, these two parameters significantly affect the in-vessel hydrogen generation, and therefore, must be selected carefully. Using a high eutectic temperature, for example, would delay the onset of core melt, prolong the clad oxidation, and generate more hydrogen. The values recommended by MAAP for the two parameters are:

	Best Estimate	Recommended Range Minimum	Maximum
Eutectic Melting Temperature, K	2500	2100	2800
Latent Heat, KJ/Kg	250	100	400

The MELCOR code does not consider any reactions of chemical dissolution and, hence, no eutectic solutions are modeled. Because MELCOR models fuel rods, control rods, and structural materials independently, and treats the cladding and fuel pellets separately, the code allows each material component to melt independently, based on the melting temperature of each material component. The latent heat is used to control the melting rate. The values recommended by MELCOR are given below:

	Melting Temperature, K	Latent Heat, KJ/Kg
UO_2	3113	273
Zr	2098	225
ZrO_2	2990	707
Stainless Steel	1770	268
Stainless Steel Oxide	1870	598

The above material properties can also be user-specified. Comparisons between the two codes show that the best estimated latent heat of the eutectic solution recommended by MAAP corresponds to the average value of UO_2 and Zr used in MELCOR. The minimum value recommended by MAAP is outside of the range of the individual materials used in MELCOR. The best estimate for the eutectic melting temperature recommended by MAAP is the average of the melting temperatures of Zr, ZrO_2, and UO_2 used in MELCOR. The minimum and maximum values of the eutectic temperature recommended by MAAP also are within the range used in MELCOR.

10 Core Relocation

As part of a review of experiments on core-melt progression, Wright [11] summarized the relocation behavior observed during the early and late phase melt progression. Three separate and distinct material relocation processes were found to occur during melt progression involving metallic melts, ceramic melts, and solid ceramic debris. These processes also occur at different local temperatures and times during accident sequences. Melt relocation was found to occur by noncoherent, noncoplanar rivulet flow.

In MAAP, the core relocation is treated by a very simple model. The molten material from a melting node runs downward until it reaches a node which is frozen or already completely full. The internal energies of the molten material and the still-frozen material are mixed which usually refreezes the molten material. There is no control of melt flow pattern and no computation of the refreezing rate. Since the materials contain decay heat, remelting and refreezing can occur repetitively as water boil-off and core meltdown proceed. Remelting and refreezing are based on an instantaneous energy balance calculation.

In MELCOR, the relocation model considers the downward flow of molten core materials and the subsequent refreezing of these materials as they transfer latent heat to cooler structures below. The model is semi-mechanistic, based on fundamental thermal and hydraulic principles, but incorporating user-specified refreezing heat transfer coefficients. By appropriate adjustment of these refreezing coefficients, the MELCOR model is adaptable to either film or rivulet flow. Because the code models the melting of each material independently whenever the melting temperature is reached, the relocation of each material also is treated independently. The code has six user-specified candling heat transfer coefficients for UO_2, Zr, ZrO_2, stainless steel, stainless steel oxide, and control poison material.

Molten mass is relocated downward in stepwise fashion until it has all refrozen on components in one or more lower cells as illustrated in Figure A.4. The material refrozen on a component becomes an integral part of that component. Molten material originating in one type of component refreezes in the same component type in the lower cells unless that component does not exist in those cells. If the originating component does not exist in a cell, the molten material refreezes on an alternate component referred to as particulate debris. If neither the originating component nor an alternate refreezing component is found in a cell, the molten material falls through to the next lower cell. The refreezing logic is summarized below:

Originating Component Type	CL	OS	PD
Primary Refreezing Component	CL	OS	PD
Alternate Refreezing Component	PD	PD	CL
	(Fallthrough)		

Note: CL = Cladding
OS = Other Structural Materials
PD = Particulate Debris

Formation of particulate debris is another feature of the MELCOR code. The model assumes that particulate debris is formed whenever the unoxidized metal thickness of an intact component reaches a user-defined minimum value. This assumption implies that the oxide layer on a component provides no structural strength to the component and the component is supported by the metallic layer. The default values of minimum thickness of unoxidized Zircaloy in cladding and the minimum thickness of unoxidized steel in "other structure" are both 0.1 mm. Whenever cladding in a cell fails, both fuel and cladding component masses in the cell are converted to particulate debris masses. The MAAP code does not have an equivalent model for the particulate debris bed; hence, no comparison with the MELCOR can be made.

MELCOR also has a model to hold up molten material by an oxide shell until it is breached. The model is controlled by two parameters: a critical oxide thickness and a critical temperature. The default values for these parameters are currently set so that the holdup model is effectively turned off. No hold up model is provided in the MAAP code.

11 Molten Pool Heat Transfer

MAAP models the axial and radial heat transfer from a molten pool in a core channel to the adjacent frozen nodes. The axial heat transfer between the molten pool and frozen materials above and below the pool is determined by the QCONHT subroutine. The basic assumptions are:

(1) The molten pool is fully mixed and can be represented by a single temperature.

(2) The heat transfer to the frozen materials above and below the pool is based on a constant heat transfer coefficient defined by the model parameter HTCMCR.

(3) The crusts above and below the pool have identical thickness and temperature. The temperature is equal to the eutectic melting temperature of the core material.

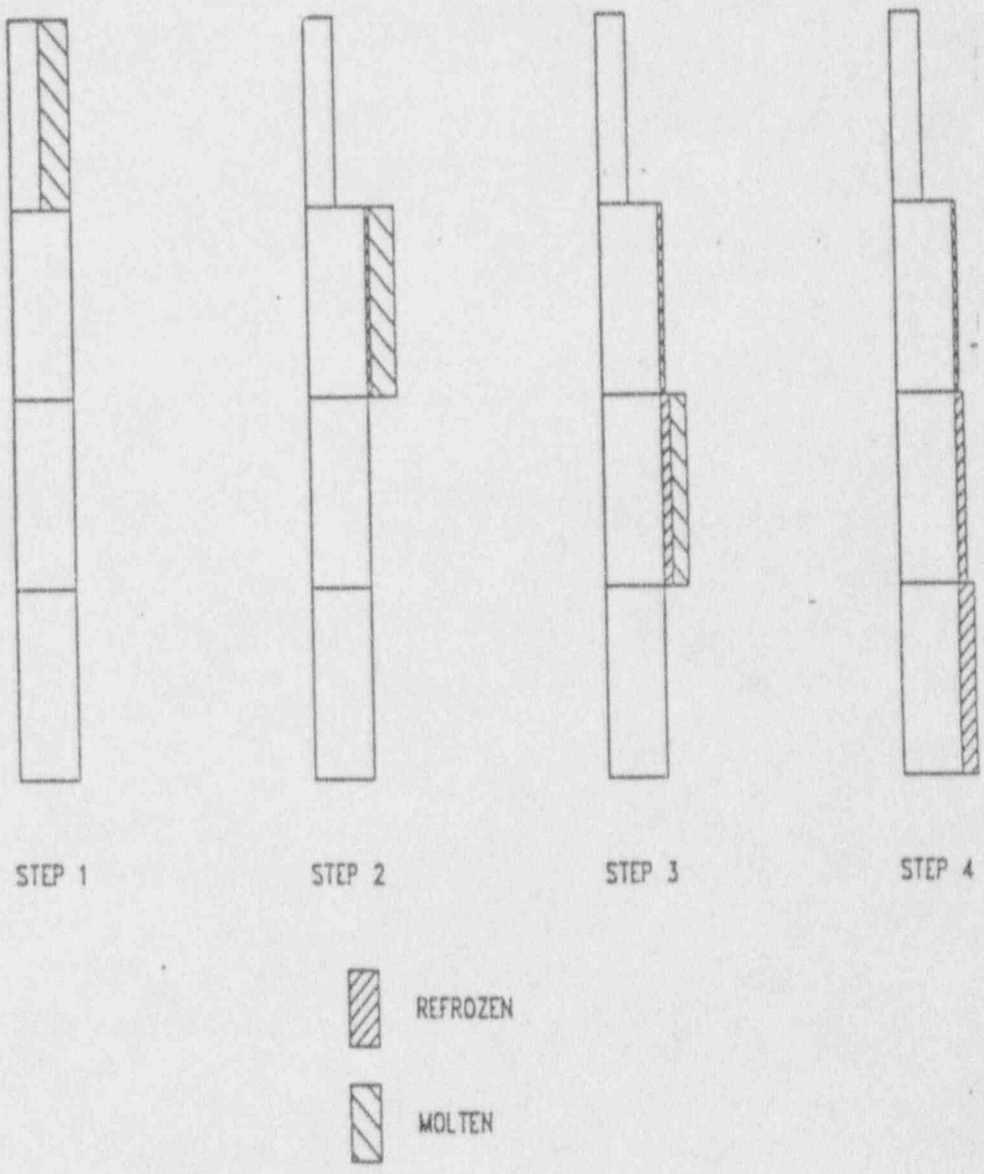

Figure A.4 ME. COR Candling Process Steps

These assumptions represent a simplified approach to modeling heat transfer mechanisms within a molten pool. Because the molten pool contains decay power, an internal temperature gradient in the pool is expected. The assumption of a single temperature in the pool implies that the heat transfer is not conduction-limited; it is controlled by convection at the interface. The default value of the model parameter HTCMCR is 1000 J/m^2-K-s, and the recommended ranges are 500 to 5000 J/m^2-K-s. No justification is given that the pool heat transfer will not become conduction-limited even when the maximum value of HTCMCR is used. The model also implies that the crust thickness does not present any thermal resistance to the overall heat transfer. The assumption of identical crust thickness and temperature above and below the pool ignores the possibility that some portion of the crust may be in contact with coolant, and could be thicker and have a lower temperature.

In an actual accident, the formation of the crust during core meltdown is expected to be a dynamic process. The thickness of the crust depends on a transient energy balance between the decay power in the molten pool and heat loss through the thickness of the crust to the adjacent medium. The thickness grows if heat loss is greater than the decay power. The growth of the crust layer would cause an increase of thermal resistance and retard the heat loss, which, in turn, would stop the crust growth and could eventually lead to the decay of crust thickness. On the other hand, a reduced crust thickness implies a reduced thermal resistance and would increase the heat loss, which, in turn, would lead to growth of the crust. This self-sustained oscillatory behavior of crust growth and decay has been reported in the literature [15]. However, MAAP's model does not reflect this physical process.

Radial heat transfer between a molten node and an unmolten node is computed by a simple model to replace the radial radiation model developed for a pair of unmolten nodes. The model uses a non-mechanistic treatment to limit the radial heat transfer.

MELCOR does not have an equivalent molten pool model.

12 Core Support Plate Interaction and Core Collapse

In the MAAP code, the corium/support plate interaction is modeled by assuming that the support plate is melted at the time the corium leaves the original core boundary. The mass melted is specified by the user, and the rate of steel melting is estimated by the energy convected from the corium. The melted steel is added to the corium pool of the lower plenum. Note that in the core region, the corium is assumed not to contain of any steel. Only in the lower plenum is steel included in the corium composition.

MAAP also models core collapse after reflood if the core has experienced extensive oxidation. The collapsing criterion is based on a fraction of clad oxidized (model parameter FEMBRT) specified by the user. The best estimate, and the recommended minimum and maximum values are 10%, 0%, and 100%, respectively. Once the channel collapses, the mass in the channel above moves downward to the lower portion of the channel. After reactor vessel breach, and when the core mass is down to a fraction of the original mass (model parameter FCRDR) specified by the user, the remainder of the core is dumped to the lower plenum in one time-step, and then dumped into the reactor cavity. The best estimate, and the recommended minimum and maximum values are 10%, 0%, and 100%, respectively.

MELCOR uses a different approach to model the interaction with support plate and core collapse. This approach is based on user specified logic processes instead of rate processes. As discussed in Section 10, MELCOR models the melting and relocation of each material component independently. The relocated molten material must freeze on a primary or alternate material component in the next cell. If no primary and alternate material components are found, the debris will fall through and eventually reach the support plate located in the lower plenum of the reactor.

The support of material components at any axial segment is controlled by a (ISUP) specified by the user. This flag determines whether material components in an axial segment are supported by components in the cell below or by lateral support. The parameter ISUP has two digits, and the logic is described as follows:

First Digit

= 1 Core plate ("other material component") will support particulate debris until the component reaches the failure temperature. (The default value of the failure temperature is 1273.15K).

= 0 The particulate debris will not be supported by the "other structure" at this level.

Second Digit

= 1 Intact components in the axial segment will remain in that cell until they melt or form particulate debris.

= 0 An intact component in the cell below must be present to support components in the current cell, otherwise these components will be relocated downward.

It is clear that the treatment presented in both the MAAP and MELCOR codes strongly depends on parameters specified by the user. Because the change of core geometry is controlled by these parameters, the selection of the parameter values will affect the timing and mode of core melt progression.

13 Lower Head Failure

The mode and timing of lower head failure during a severe accident has an important effect on subsequent phenomena that strongly influence containment performance, such as direct containment heating (DCH) and corium/concrete interactions. The complex corium/lower head interaction depends on the design of the lower reactor vessel region. In a PWR vessel, the lower internal structures consist of grid plates which support the fuel assemblies, and flow distributors which regulate the core inlet flow. Both the grid plates and flow distributors have holes 4 cm to 20 cm in diameter. The relocation rate could be limited if corium originating within the fuel assemblies passes through these holes before entering the lower head. In addition, many PWRs have bottom-entry instrument penetration nozzles; however, some PWRs do not have any penetrations through the lower head. The impact of these differences in the design of the lower vessel head on corium/lower head interactions will be discussed based on the available literature. With this background, the MAAP code will be assessed and comparisons with MELCOR will be made.

TMI-2 data suggested that core debris relocation into the lower vessel is unlikely to involve a coherent melt consisting of a large fraction of the core inventory [14]. Instead, a rate-limited relocation of the debris is more likely, starting with a local breach of a crust formed in the core region. In addition, the structures containing flow paths of varying sizes will intercept and redirect the streams or rivulets formed by the melting.

As the molten fuel falls through the water pool in the lower plenum, it may breakup due to hydrodynamic instability as shown by experiments and analysis performed at Argonne National Laboratory [16]. The breakup length depends on the initial jet and ambient water conditions. The breakup of the jet into droplets enhances heat transfer which may lead to solidification of the debris; this solidification would, in turn, produce a particulate bed rather than a molten pool on the bottom of the vessel. Particles formed by this process are expected to have a relatively larger size, and the resulting debris bed is likely to be coolable if sufficient water is present. However, if the interaction involves a steam explosion, then the particles would be relatively small, and the resulting debris bed may not be coolable.

Based on the configuration of corium in the lower plenum, several potential modes of lower head failure for the reactor vessel have been identified for light water reactors. Each failure mode is briefly discussed below:

(1) Jet Impingement

Ablation due to jet impingement is a potential cause of early vessel failure. The erosion of steel structures by a high temperature jet is characterized by a rapid ablation rate at the stagnation point of impingement. The ablation rate would be considerably reduced by the formation of a crust layer of urania. Due to the presence of a large number of penetrations in some reactor designs and the potential for jet breakup in the water pool, it is unlikely that a molten jet will directly attack the lower vessel head. However, penetration tubes may fail if they are hit by the jet.

(2) Plugging and Failure of Lower Head Penetrations

With a large number of penetrations in the lower head of some PWRs, it is likely that the core debris will first attack the penetration tubes. Failure of the tubes could allow molten material to flow down the tubes and refreeze to form a crust along the tube wall. If the temperature of the core debris is high enough, melting or creep rupture of the tube walls may occur. Data from the TMI-2 vessel show that wall failure occurred in several instrument penetration tubes and that many tubes were plugging by debris. In fact, some of the tubes were plugged in sections well outside the reactor vessel.

(3) Ejection of a Lower Head Penetration

Core melt attack on a penetration tube and the sustained heating from accumulated debris may cause tube penetration weld failure. Weld failure under high system pressure may result in tube ejection.

(4) Global Creep Rupture

In a PWR with no penetration tubes attached to the lower head, a direct contact between the core debris and the lower head wall will cause a substantial heating of the lower head. The heating, in conjunction with the stress induced by elevated system pressure and/or the weight of the core debris, may lead to lower head failure by a global creep rupture. Depending on the debris configuration and coolability, the average rise in the temperature of the vessel wall is likely to be relatively slow. The time-to-vessel failure is related to the system pressure, thickness of the vessel wall, the sensible and decay heats of the core debris, and the contact between the core debris and vessel wall. A depressurized reactor vessel should reduce the potential for creep rupture-induced vessel failure.

Given the above background, MAAP uses a very simplified approach for modeling corium/lower head interactions. MAAP does not consider rate-limited relocation of corium in the form of streams or rivulets into the lower plenum. MAAP considers the collapse of the support steel plate, together with the core debris accumulated above it, into the lower plenum. The remaining core mass is then dumped to the lower plenum in one time-step based on a parameter specified by the user as described in Section 12. For PWRs with in-core instrument tube penetrations, the failure of penetrations is usually assumed. The input parameter file specifies the number, time delay, and initial radius of failed penetrations. For PWRs without penetration tubes, the user specifies an effective time delay and initial radius of the breach area. The best estimate time delay suggested by MAAP is 60 seconds. The minimum and maximum values of the recommended ranges are 30 and 1000 seconds, respectively. The use of time delay to control the lower head failure is non-mechanistic and arbitrary. The time of lower head failure should depend on the state of corium in the lower head, the contact between corium and penetrations (or lower head wall), and the state of the primary system. These are accident sequence dependent and can not be generalized by a time-delay parameter.

MELCOR uses a more complex (but still parametric) treatment of the corium/lower head interaction than MAAP. MELCOR does not consider a massive core slump; it models the relocation of each material component into the lower plenum independently, according to the "logic process" described in Section 12. All components are allowed to freeze on "other structures" (primary refreezing component) or "particulate debris" (alternate refreezing component). The refreezing heat transfer coefficient specified by the user could simulate the rate-limited relocation. In the lower plenum, heat transfer between debris and lower head ($q_{d,h}$), between debris and penetration ($q_{d,p}$), and between penetration and lower head ($q_{p,h}$) are computed through simple energy balance equations. Figure A.5 illustrates heat flows in the lower head. The energy balance is performed for the bottom axial node of penetrations and top node of the lower head. The heat transfer coefficients, surface areas, and masses are parameters specified by the user for the energy balance calculations. In addition, MELCOR also considers convection heat transfer from the penetrations, debris and lower head to the fluids in the lower head. The outer boundary of the lower head is treated as adiabatic, but the internal heat conduction through the lower head wall is included.

In MELCOR, failure of the lower head is assumed to occur whenever the temperature of the penetration or innermost lower head node reaches a failure temperature specified by the user. The default value of the failure temperature is 1273 K. The user may also specify a logical control function to trigger lower head failure. For example, such a control function might refer to a table of differential failure pressures as a function of lower head temperature to simulate the effect of pressure loading on lower head strength at high temperatures.

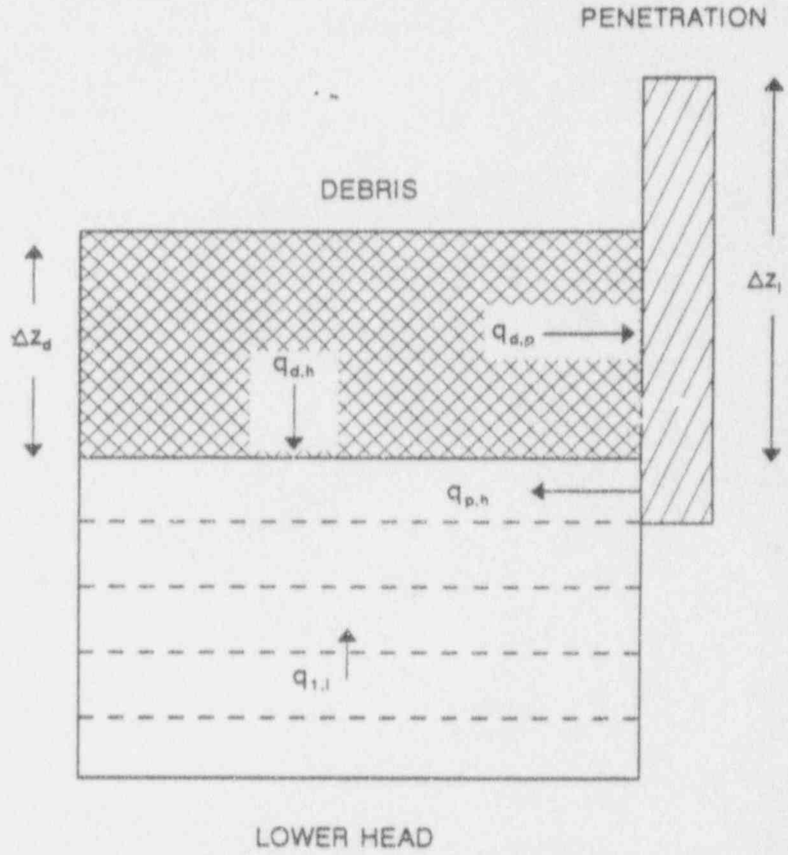

Figure A.5 MELCOR Lower Head Heat Balance

In summary, the complex corium/lower head interaction is not fully represented in either the MAAP or MELCOR code. Among the four potential failure modes, jet impingement and penetration ejection are not considered at all in either code. Only penetration failure and global rupture are represented by simple parametric models in the two codes. The lack of any heat transfer calculation between core debris, penetration and lower head wall, and the use of the time-delay parameter are major drawbacks of the MAAP code. The MELCOR model is more rigorous than the MAAP model. MELCOR not only performs heat transfer calculations between the various components in the lower head region, but also allows the user to implicitly consider the stress effect on global rupture. However, the largest uncertainty of the MELCOR model is the heat transfer coefficients specified by the user. Estimates of the heat transfer coefficients should be obtained by analyzing experimental data or mechanistic codes.

14 Corium Discharge

The quantity and rate of corium discharged from the reactor vessel have an important impact on the dissipation of corium and the ability for corium to cool in the containment. In MAAP, radial ablation of the failed penetrations and the discharge of corium and water are computed following the vessel failure. The velocity of corium discharge is determined by the sum of pressure difference across the opening and the static pressure head of water and corium in the vessel. No discharge coefficient is involved. The basic model for vessel ablation is that radial heat flux from the flowing molten corium supplies the sensible and latent heat to ablate the failed vessel penetration. The radial heat flux for vessel ablation is assumed to be proportional to the temperature difference between the melting point of the corium and the wall (steel). A heat transfer coefficient determined by the Colburn-Reynolds analogy between heat and momentum transfer is used to estimate the radial heat transfer. The ablation rate so determined is proportional to the discharge velocity. The ablating steel is added to the corium and discharged to the containment. When the corium is depleted, water remaining in the reactor vessel is discharged.

In MELCOR, logic processes are applied to restrict the debris discharge. After the penetration failure, the code requires that a total molten mass of 5000 Kg or a melt fraction of 10% is necessary before debris ejection can begin. The mass of each material available for discharge is controlled by a flag IDEJ specified by the user. In the default option (IDEJ=0), the masses of each material available for ejection are the total debris material masses, regardless of whether or how much they are melted. In the other option (IDEJ=1), all steel, Zircaloy, and UO_2 melted are available for ejection; the ZrO_2 and steel oxide available for ejection are the masses of these materials multiplied by the melt fraction of the metallic component of each material. Additionally, the mass of solid UO_2 available for ejection is the Zircaloy melt fraction times the mass of UO_2 that could be relocated with Zircaloy into the lower head. For the case of a gross failure of the lower head, all debris in the bottom cell is discharged immediately.

The discharge velocity in MELCOR is computed in a similar manner as in the MAAP code. The discharge velocity is determined by the pressure difference between the lower plenum and reactor cavity, and by the static pressure head of debris. The static pressure head of water, which is usually smaller than that of debris, is not included in the MELCOR code. However, MELCOR includes a discharge coefficient specified by the user to provide options to limit the discharge rate. The ablation rate also is computed by a simple energy balance similar to the treatment in the MAAP code. The heat transfer coefficient is given by a empirical correlation, which shows that the heat transfer coefficient is proportional to $V^{0.8}/X^{0.2}$, where V is the discharge velocity, and X is the penetration diameter or lower head thickness. This formulation suggests that the ablation rate will be reduced with the increase of failure size as the ablation continues.

15 Summary

The late in-vessel phase of a severe accident involves complex phenomena. Although the complexity can not be modeled mechanistically by system codes such as MAAP and MELCOR, both codes have attempted to use the parametric approach to represent the major features involved during this late phase of an accident. The major differences between MAAP and MELCOR are summarized in Table A.4

Based on this preliminary review, the parametric treatment in the MAAP code can be improved. The following are specific suggestions:

(1) Including control rod and structural materials in the analysis of oxidation, melting, relocation, and blockage formation could have a significant effect, particularly, for a partially degraded core accident.

(2) Rate-limited relocation would enhance the MAAP model.

(3) The potential for particulate debris bed formation in the core and the lower plenum regions could be important.

(4) The use of time-delay as the lower head failure criterion could be improved by replacement with an appropriate heat balance analysis.

(5) The pressure effect on lower head strength could influence lower head failure.

For the current models used in the MAAP code, sensitivity studies should be performed for IPES, and the selection of parameters specified by the user must be justified.

Table A.4 Comparison of In-Vessel Melt Progression

Phenomena	MAAP	MELCOR
Oxidation		
Zr Oxidation	Yes	Yes
Fe Oxidation	No	Yes
Core Region: Clad ballooning effect	Yes	No
2-side oxidation	Yes	No
Termination criteria	Fuel melting or flow blockage, if the blockage option is used	Zr: cut-off temperature (option), Fe: No
Lower Plenum Oxidation	Yes	Yes
Termination Criteria	1000 K	No
Core Melt		
Control Rod and Structures	No	Yes
Fuel Rod	Eutectic (UO_2-ZrO_2-Zr)	UO_2, ZrO_2, Zr
Core Relocation		
Material Relocated	Eutectic	Zr, ZrO_2, UO_2, steel, steel oxide, control poison material
Refreezing heat transfer coefficient	No	User-specified
Control of melt flow	No	By refreezing heat transfer coefficient
Particulate debris	Crudely modeled	Yes
Molten pool	Yes	No
Core Support Plate		
Mass of support plate melted	User-specified	Computed
Failure criteria	---	Failure temperature
Melted mass added to corium	Yes	Yes
Core Collapse		
Criteria	User-specified parameter	User-specified parameter

Table A.4 Comparison of In-vessel Melt Progression (Continued)

Phenomena	MAAP	MELCOR
Lower Head Failure		
Jet impingement	No	No
Penetration ejection	No	No
Penetration failure	Yes	Yes
Lower head rupture	Yes	Yes
Failure criteria	Time-delay	Failure temperature or pressure effect
Heat balance calculation	No	Yes
Discharge velocity		
discharge coefficient	No	Yes
static pressure head	Debris and water	Debris
constraints of discharge	None	5000 kg or 10% melt fraction (for penetration failure)
Material discharged	Molten debris and water	Molten and solid debris
Amount of mass discharged	1. Total mass of debris in the lower plenum 2. User can specify the fraction of original core mass below which the remaining core is discharged after vessel failure	1. Gross failure: total mass of debris 2. Penetration future: controlled by user-specified logic process
Ablation rate	Proportional to V V= discharge velocity	Proportional to $V^{0.8}/X^{0.2}$ X = failure diameter of lower head thickness

16 Primary Containment Nodalization and General Description

Four PWR plants were selected as reference plants and modeled with the MAAP/PWR code. The Zion, Oconee, and Calvert Cliffs plants were selected as representative of large dry containments, and Sequoyah represented ice condenser containments. The MAAP dry-containment model is divided into 4 regions: upper containment (A-compartment), lower containment (B-compartment), cavity (C-compartment), and the annulus region (D-compartment). These compartments are connected by flow paths to simulate forced and natural convection flow, and water drainage.

The lower compartment (B) and cavity (C) are connected by two flow paths; the instrument tunnel and the reactor vessel/shield wall annulus. Water and corium can be specified to flow through the tunnel only, but not through the annular passage. However, for plants with a flow area through the instrument tunnel, which is smaller than the area of the reactor vessel/shield wall annulus (i.e., reactors with no lower head penetrations), MAAP allows the debris and water to be dispersed directly to the upper compartment (A) whenever the calculated gas velocity exceeds the entrainment threshold (EVENT flag No. 53). This is done by setting the model parameter No. 13 FCMDA to be 1.

The MAAP model of the ice condenser plant has two compartments in addition to the 4 compartments in the dry containment model. The additional compartments are the ice condenser (I-compartment), and the upper plenum (U-compartment), located between the lower and upper compartments. Steam, hydrogen, and other gases can be specified for the connecting flow paths. The ice condenser compartment also provides water drainage to the lower compartment.

The flow paths defined in MAAP can be connected to form natural circulation loops. For dry containments, MAAP allows one loop between the lower and cavity compartments (loop BC) and another loop between the upper, lower, and annulus compartments (loop ABD). For ice condenser containments, a loop between the upper, lower, ice condenser, and upper plenum (loop ABIU) is added. The flow rate is determined using an equal-pressure approach, i.e., flow circulation results in pressure equilibrium among the various regions in the containment. Assessment of the pre-defined circulation loop could be made by comparing it with specifically developed containment codes, such as CONTAIN, which uses the implicit method to compute fluid flow without a pre-defined circulation loop.

Although the major regions of a PWR containment are represented by the MAAP code model, the fixed nodalization and pre-specified flow paths and flow materials do not permit a user to perform a sensitivity study on the effect of nodalization. In many cases, such as natural convection, the flow rate is sensitive to the local fluid density and a finer nodalization would improve the code's prediction. Hydrogen mixing is an example. Computer code simulation of the HDR experiments [17,18] demonstrated the importance of fine nodalization on predictions of hydrogen distribution in a large containment. An accurate prediction is essential to assess the potential mode of hydrogen combustion, such as a localized detonation. The fixed, four-compartment nodalization in MAAP may not be sufficient for adequate evaluation of hydrogen distribution under severe accident conditions.

Phenomena treated in various containment compartments are also fixed in the MAAP code as summarized in Table A.5:

(1) All the phenomena modeled in MAAP can be specified in the upper compartment (A);

(2) The containment sprays, DCH, and corium-concrete interactions cannot be specified in the annulus compartment (D);

(3) No metal equipment heat sink is modeled in the cavity (C) and annulus compartments (D).

Table A.5 Phenomena Modeled in Pre-Specified Containment Compartment (MAAP)

Compartment[1]	A	B	C	D	I	U
Containment Failure Location	Yes	No	No	Yes	No	No
Fan Suction[2]	Yes	No	No	No	No	No
Sprays	Yes	Yes	No	No	No	No
DCH	Yes	Yes	No	No	No	No
Corium-Concrete Interaction	Yes	Yes	Yes	No	No	No
Metal Equipment Heat Sink	Yes	Yes	No	No	No	No
Wall Heat Sink	Yes	Yes	Yes	Yes	No	No
H_2 and CO Combustion	Yes	Yes	Yes	Yes	No	Yes
Water Flashing and Rainout	Yes	Yes	Yes	Yes	Yes	Yes
Water Overflow	Yes	Yes	Yes	Yes	Yes	Yes

Based on PWR subroutine Index given in Volume I, Section 14 of Reference [1].

Note 1. A = upper compartment, B = lower compartment, C = cavity, D = annulus, I = ice condenser, U = upper plenum

2. MAAP 3.0B PWR, Revision 17 allows the user to specify fan cooler suction and discharge locations.

The phenomena allowed to occur in pre-specified compartments are reasonable in most cases. However, the exclusion of certain phenomena in some compartments, particularly in the annulus region, limits the flexibility of the code.

Unlike the MAAP code, there is no specific nodalization and no predefined models built into the MELCOR code. MELCOR uses the control volume concept to represent the containment system. Each of the compartments modeled in MAAP for the dry containment can be represented by a control volume in MELCOR. (The present version of MELCOR does not model the ice condenser plant.) In MELCOR, all phenomena can be imposed on any control volume by control functions; this flexibility allows many sensitivity studies to be made.

17 Corium Entrainment and Corium/Water Interaction

After failure of the reactor vessel, several subroutines (EXVIN, ENTRAN, PLH2, and PLSTM) are used to estimate the behavior of the corium and the production of steam and hydrogen during corium/water interactions. Each of the subroutines describes a different mode of corium interaction, represented by a different corium configuration ranging from droplets to a molten pool. At the second familiarization meeting we expressed concern about the basis for assuming these configurations and the related computational procedure. Each subroutine is discussed in the following sections.

17.1 Subroutine EXVIN

EXVIN computes the amount of steam produced during a steam explosion in the reactor cavity during the initial interaction between debris and water. The time for initiation of an explosion is determined when a column of corium contacts the cavity floor plus a user-specified delay time. The maximum quantity of corium involved in the steam explosion is assumed to be the mass which would be submerged in the water after the delay. It is assumed that the energy transfer to water will quench this debris to water saturation temperature. The amount of steam produced is calculated from the amount of energy released as the debris is cooled to the saturation temperature of the water. No succeeding explosions and no structural effects are involved in the calculation. The MAAP model does not calculate the dynamic force due to the conversion of thermal energy into mechanical energy which could threaten the integrity of the containment as reported in the studies of steam explosion. Hydrogen generation during a steam explosion is not modeled.

17.2 Subroutine ENTRAN

ENTRAN computes the flow rate of corium and water from the reactor cavity to the containment compartment due to the entrainment or flooding of water and corium in the high-speed stream of hydrogen and steam that is in the reactor vessel. A constant MAAP entrainment time (0.5 seconds) is used to determine the entrainment rate. We also expressed concern about the entrainment model at the second familiarization meeting. The questions and answer are given below [20]:

Question:

> The entrainment rate of corium and water from the reactor cavity to the containment lower compartment is controlled by the "entrainment time." A constant entrainment time (0.5 s) is used in the code. Should the entrainment time depend on the geometry and pressure in the cavity? Is the entrainment model also used for the DCH calculations?

Answer:

> While the true entrainment time does vary with geometry and pressure, a constant value is used to formulate a rate because the value of the rate is not influential on the transferred mass. This parameter should be set to a value lower than the blowdown time of the vessel to guarantee debris dispersal. It is used to formulate reaction rates from the total amount of material available for reaction, and heat transfer rates from energy transfer needed for equilibration. Thus, the same total change would occur, regardless of the selected time constant. In principle, the time constant could influence heat transfer or reactions during DCH, but this is not believed to be important for reasonable entrainment times.

In Reference [19], IDCOR stated that ". . .the transport of core material from the failed RPV to the containment floor is dependent on the shape and size of the cavity (and tunnel(s) where applicable) connecting the lower region of the RPV to the containment region. . ." Based on this position, IDCOR classified PWR reactor cavities into fourteen types according to geometry to express the degree of debris dispersal during a high-pressure melt ejection accident. The classification covers a wide variation in expected debris dispersal. For example, a type A configuration (such as Zion) would allow large dispersal, while a type D configuration (such as Surry) would retain essentially all of the debris in the cavity. Thus, the mass and rate of corium entrainment should depend on the specific cavity configuration of each plant. To apply the MAAP entrainment model to IPE, in which a plant-specific cavity configuration is involved, users should justify their selection of the entrainment parameter.

17.3 Subroutine PLH2

PLH2 computes hydrogen generation after corium/water contact in the reactor cavity. As described in Reference [20], PLH2 ". . .uses all the corium available at the time of vessel failure (even though some may remain in the vessel) and uses properties for corium in the lower head (even though EXVIN or JET may have been called). PLH2 is also called once in the lower compartment when debris can be entrained to it from the cavity. It is called after a small amount of debris is accumulated, but assumes that all debris in the cavity and lower compartment is available (even though it may not all be entrained) using properties for corium in the cavity (even though DCH may have been called). . ."

According to this description, the PLH2 computation involves a large uncertainty on the mass and properties of the corium, which would affect the prediction of hydrogen generation.

17.4 Subroutine PLSTM

PLSTM computes steam production due to the contact of debris with water after the debris relocates into the reactor cavity or is entrained into the upper and lower compartments. The corium configuration in the PLSTM model is assumed to be a molten pool with a crust layer at the corium/water interface. A major assumption is that the debris crust in contact with the water will crack and allow water ingress which results in the rapid removal of heat from the debris. However, the subroutine imposes several limitations on the heat flux from the debris to the water pool, namely, the rate of addition of water, the quenching rate of the corium, hydrodynamic stability, film boiling, and critical heat flux. Three user-specified parameters, i.e., Model parameters No. 8 (HTFB, film boiling heat transfer coefficient), No. 21 (FDROP, droplet critical flow parameter), and No. 33 (FCHF, Kutateladze critical superficial gas velocity) control the corium/water interaction.

Since debris quenching, steam generation, and containment pressurization are very sensitive to these parameters, the selection of the input values must be carefully made, and in the form of a sensitivity study.

17.5 Summary

As the above description shows, steam and hydrogen generation are computed by several subroutines independently. The quantity of corium involved in the corium/water interaction is controlled by the entrainment model. Each subroutine has its own assumptions related to the configuration, mass, and properties of the corium. The lack of interaction among these subroutines may cause inconsistencies in modeling the physical process occurring during corium/water interaction, which could affect the corium-concrete interaction, combustion, and containment pressurization.

In MELCOR, debris relocation outside the vessel, heat transfer, and oxidation due to corium/water interactions are modeled in the Fuel Dispersal Interaction (FDI) package. Eventually, three types of phenomena will be treated in this package: (1) the ejection of low-pressure molten fuel from the reactor vessel, (2) the ejection of high-pressure molten fuel from the reactor vessel (direct heating), and (3) steam explosion following a low-pressure ejection sequence. Currently, the FDI package can only treat a low-pressure ejection (the mixing phase before a steam explosion). Models for steam explosions and direct heating are not available presently in the MELCOR code.

During low pressure ejection, heat is transferred to the water pool from the molten fuel (if present in the associated control volume) as it fragments and falls to the cavity floor. Heat transfer normally occurs by radiation, but a convective lower bound is also included. If a water pool is in the control volume, all of the energy transfer from the molten fuel is used to boil water (there is no pool heatup, only boiling). If there is not a water pool in the control volume, material passes through FDI without any removal of energy.

The model described in the MELCOR/FDI package would provide a consistent treatment of corium configuration, and the initial and end states of corium for various corium and water interactions.

18 Corium-Concrete Interaction

Corium-concrete interactions are modeled in two different subroutines in the MAAP/PWR code, namely JET and DECOMP. Subroutine JET treats the decomposition of concrete directly under the reactor vessel when it is attacked by a corium jet discharged from the reactor vessel. Subroutine DECOMP provides a general treatment of the decomposition of concrete by a molten or solid corium pool. DECOMP is the main subroutine used to model corium-concrete interactions, which could take place in the upper, lower, and the cavity compartments. The MELCOR code does not have a model for concrete decomposition by direct jet impingement. However, MELCOR incorporates the CORCON-MOD2 model [21], which is equivalent to DECOMP in MAAP. Although DECOMP and CORCON both model the major phenomena related to corium-concrete interactions, there are significant differences in the assumptions and approximations used.

18.1 JET

JET computes the transient ablation rate of the concrete floor in the cavity compartment caused by direct contact with a jet of molten corium. The velocity of the corium stream impinging on the concrete surface is first determined. Then, a stagnation point heat transfer correlation is used to compute the rate of heat transfer from the corium jet to the concrete, which, in turn, determines the rates of concrete ablation and gas evolution.

Since both JET and DECOMP are used to model concrete decomposition, we expressed concern as to how computational procedures are used in the MAAP code for these two subroutines. In response to our questions, FAI provided the following description [20]:

> JET is called starting at vessel failure and until all the corium present in the vessel at failure has relocated to the containment, a duration of several seconds for high pressure failure to tens of seconds for low pressure failure. JET uses the instantaneous flowrate out the failure and corium properties in the lower head. It assumes the debris exits as a stream and contacts the floor in this manner, whether or not water is present in the cavity, maximizing jet erosion.
>
> DECOMP is called after corium contact with the floor and it assumes a pool of debris exists for heat transfer to concrete and to either overlying coolant or the surroundings. Thus, DECOMP could be called while JET is still being called and before entrainment occurs. A minimum debris mass must be present for DECOMP to be called, so after entrainment DECOMP may not be called until more melting in-vessel occurs.

The above description shows that JET and DECOMP are treated independently and simultaneously. This treatment is an attempt to maximize concrete erosion, but it could result in the same small area of concrete (that area in contact with the JET) being eroded in both subroutines.

We also raised questions about the presence of water in the cavity when subroutine JET is used.

Question:

> Is the JET subroutine limited to the dry cavity situation? No water/corium interaction and jet break-up are modeled in this subroutine.

Answer:

> JET is called during the initial corium release after vessel failure whether or not water is present. Jet erosion has no discernable impact on overall code results.

Depending on the ratio of jet length/diameter (i.e., the cavity depth and the size of the ablation hole in the vessel lower head), hydrodynamic instability could cause the jet to break up and prevent it from reaching the concrete floor. Thus, the JET model could be invalid for a flooded cavity configuration. Since the JET model does not play a significant role in the overall results of the code, we suggest that the subroutine be omitted (or modified) to avoid the inconsistencies discussed in this section.

18.2 DECOMP

MAAP assumes that corium-concrete interactions can occur simultaneously in more than one containment region. Hence, MAAP allows the DECOMP subroutine be called by the upper, lower, and cavity compartments. In MELCOR, corium-concrete interactions are modeled in the Cavity Package (CAV), which allows an arbitrary number of cavities to be defined (100 are permitted by the input records format). At present, all MELCOR analyses use a single cavity to model corium-concrete interaction. Thus, the ability of MELCOR to model corium-concrete interactions in a multiple-cavity configuration has not been tested.

18.2.1 Molten Pool Heat Transfer

DECOMP assumes that the molten corium pool is homogeneously mixed. The concrete slag caused by the melting of concrete is assumed to enter the debris pool immediately and mix with the core debris. The homogeneously mixed model implies that the debris has a single temperature, that there is uniform pool heat convection in all directions, and an equal thickness of the bottom and side crusts. (The top crust is treated separately.) The model also results in the same temperature profiles and erosion rates of concrete in both sideward and downward directions.

In the CORCON model used in MELCOR, a stratification model is assumed for the molten debris pool. It is assumed that the oxidic species and metallic species in the melt are mutually immiscible. Buoyancy forces are sufficient to separate the molten debris into two phases, even when there is vigorous mixing by gases from the decomposition of concrete. In addition to the two layers (metal/oxide), CORCON provides another oxidic layer on the top of debris melt. This less-dense oxidic layer is composed of ablation concrete oxides and steel oxides produced by chemical reactions with the concrete-decomposition gases. However, the three-layer configuration (oxide/metal/oxide) is not predicted to last for a long time. The bottom fuel oxide layer diluted by concrete oxides becomes less dense than the metal layer. At this point, it is assumed that the bottom oxide layer moves above the metal layer and forms a single oxide layer. The CORCON model predicts different temperatures in each of the layers in the molten pool, non-uniform heat transfer, and non-uniform crust thickness in the sideward and downward directions. Consequently, in CORCON the concrete decomposition and gas release rates are different in the downward direction than in the sideward direction.

The different assumptions used in the two codes gave rise to the following question (and answer) [illegible]:

Question:

> In the DECOMP subroutine, two assumptions are used to compute the erosion rate of the concrete cavity in the downward and radial directions. The two assumptions are (1) no stratification in the molten pool, and (2) a uniform rate of heat transfer. Please explain the rationale behind these assumptions.

Answer:

> No stratification is assumed in DECOMP because:
>
> 1) When Zr is present, it is soluble in the oxides,

2) It is unclear whether layers would exist for gas velocities of interest when Zr is oxidizing.

3) Heat transfer between such layers, would be highly effective and would not significantly alter the split between heat transfer to concrete versus the surroundings.

4) Chemical equilibrium should occur anyway. Briefly, we do not believe that stratification would have a significant impact on bottom-line results such as total concrete erosion and combustible gas generation.

Uniform sideward and downward heat transfer is assumed because heat transfer coefficients in either direction are nearly equal. The tough part of this problem is quantification of other heat transfer resistances: slag, crust, and gas. It is difficult to relate the unequal erosion observed in, for example, the BETA tests to a reactor case because 1) the height/diameter ratio is quite different, 2) the decay power will be in the oxide and not the metal, and stratification may not occur. Thus, this simplification is employed. Ultimately, this assumption should lead to a conservative answer for structural degradation by sideward erosion since the model apparently overpredicts sideward erosion.

Besides the BETA tests, Sandia (the developer of the CORCON code) cited other experimental evidence [22] to support the multiple-layer approach. The difference in heat transfer in the sideward and downward directions, as claimed by Sandia, is caused by the gas flow between the melt and the concrete. In the downward direction (i.e., on the concrete floor), gas is generated at the boundary and enters the melt, while on the side surfaces, gas forms a flowing film along the melt boundary.

In both DECOMP and CORCON, a quasi-steady model is used for heat transfer calculations. In DECOMP, the convective heat loss from the molten debris to its peripheral crust is determined by a heat transfer coefficient specified by the user, i.e., model parameter No. 12 HTCMCR. The best estimate, recommended minimum and maximum values are 1000, 500, and 5000 $W/m^{-2}\cdot K$, respectively. This heat transfer is equal in downward, upward, and sideward directions. In CORCON, the multi-layer model permits the code to compute separate temperatures for each layer. The heat transfer to the upper, bottom, and side surfaces are computed by different correlations. The presence of bubble agitation is included in the heat transfer correlations. The model parameters used in MAAP allow the heat transfer coefficient to be varied, so as to observe sensitivity to debris temperature. We note that the release of fission products is strongly affected by the temperature of the debris.

18.2.2 Effect of Water Layer

Both MAAP and MELCOR allow for a water layer on top of the debris pool in the DECOMP and CORCON subroutines. This water layer is assumed not to interact energetically with the molten materials, but rather, serve as an additional heat sink. The presence of a water pool is predicted to cool the top of the melt below the solidification temperature, forming a thin solid crust on the surface.

In DECOMP, the corium/water interaction is determined in subroutine PLSTM (Section 17 of this report). The model assumes that the debris crust in contact with water will crack and allow the ingress of water. The corium/water interaction could quench the debris. In CORCON, the possibility of crust cracking and water ingress are not modeled; the overlying water pool is modeled only as a heat sink. The heat transfer model in CORCON includes the full boiling curve based on standard pool-boiling correlations. No correction is made for the effects of gas injection at the melt/water interface. Also, the water pool does not have a significant influence on the temperature of the core debris. In a recent report, Powers et. al. [2?] stated that ". . .the data base now available on these simultaneous (corium/concrete/water) interactions does not support the belief that water will quench core debris. . .".

18.2.3 Corium-Concrete Contact and Heat Conduction in Concrete

One large difference between the DECOMP and CORCON models is the treatment of heat transfer at the corium-concrete interface and within the solid concrete. When core debris attacks the concrete, solidification of the melt and melting of the concrete occur at the interface. A thin thermal layer penetrates the solid concrete, within which complex decomposition reactions take place.

In DECOMP, a direct contact between the core debris and concrete is assumed. The interface temperature of the debris crust and the concrete is equal to the temperature of the concrete surface, which is the ablation temperature for concrete. (DECOMP assumes that concrete melting begins instantaneously upon contact with molten debris.) A one-dimensional heat conduction calculation is performed by subroutine HTWALL for temperature profiles in the solid concrete. Because the heat flux and temperature profiles are the same both downwards and sidewards, the erosion rate also is the same in these directions.

CORCON assumes that a stable gas film forms upon initial contact between the molten core debris and concrete. The concrete is separated from the debris by a gas film. The gas film model was modified in CORCON-MOD2, which is the version used in the current version of MELCOR. It is believed that under most conditions, gas release is usually far less than that required to form a stable gas film, and instead, intermittent debris/concrete contact occurs. Therefore, an interface temperature model was implemented in the CORCON-MOD2 code to describe heat transfer at the interface between the core debris and the concrete. The interface temperature predicted by CORCON is closer to the debris temperature than to the concrete surface temperature due to the higher thermal conductivity of the core debris.

The CORCON interface model also included the melting of the concrete and solidification of the core melt. The concrete slag is removed from the interface into the core melt by rising bubbles. The gas film model has been retained in the code but is only invoked when the gas velocity is sufficiently high.

CORCON does not consider heat conduction into the concrete nor decomposition in advance of the ablation front. Only one-dimensional steady-state ablation is computed.

18.2.4 Solid Pool Treatment

Both DECOMP and CORCON allow the formation of a solidified pool when the crust thickness fills the entire pool. In DECOMP, the treatment of heat transfer in a solidified pool is similar to that in a molten pool. The same heat conduction is calculated for the side walls and the lower bottom wall, resulting in equal erosion of these walls.

The equal concrete-erosion model in DECOMP is not applicable to a solidified debris pool. Because of the rigid surfaces of the debris, the molten concrete and released gases are likely to form a film between the debris and the uneroded cavity sidewalls. This film represents an additional thermal resistance and would reduce the rate of the erosion of the sidewall. Furthermore, the newly eroded concrete will not be able to mix with the rest of the debris and will probably be pushed to the top of the debris where it will form a growing crust. Since the concrete slag crust has no internal heating, it provides an effective insulating barrier to upward heat transfer. The insulation effect will influence the internal heat transfer in the solid debris pool. These phenomena are omitted in the DECOMP model. CORCON predicts a top oxide layer, which is a mixture of core and concrete oxides and is, thus, internally heated. This treatment, developed for a molten pool, is not valid for a solidified pool.

Another important feature related to solidified debris is mixing and stratification during the transition between molten and solidified debris. DECOMP assumes there is gross mixing while CORCON assumes stratification. For a conduction-limited solid debris, the most important property that affects the heat transfer process is thermal conductivity. Since thermal conductivity for the metallic and oxidic phases differ by at least an order of magnitude, the difference plays an important role in debris heat transfer. In the CORCON stratification model, the metallic layer has higher thermal conductivity but a lower decay power source. Hence, the metallic layer may solidify while the oxidic layer remains molten. The potential for a partially solidified layer and a molten layer can not be modeled by DECOMP.

18.2.5 Chemical Reactions

In DECOMP, the various oxidation processes are computed by the chemical equilibrium model in the METOXA subroutine. The model allows all reactions to proceed in parallel. Potential oxidation of chromium, a constitute of stainless steel, is omitted because at present, MAAP's mass balance equations do not include chromium.

In MELCOR, the chemical reactions are calculated with the latest version of the chemical equilibrium routine developed for CORCON. An entropy of mixing term is included in the chemical potential of each condensed-phase species, whose principal effect is to eliminate the strict sequential oxidation of metallic species. Chromium oxidation is included in MELCOR.

19 Combustion

MAAP models three types of combustion: global (complete), local (incomplete), and continuous burns. A global burn involves the burning of all combustible gases in a compartment. A local burn is initiated by deliberate ignition systems (i.e., igniters) and may involve only a fraction of the gas volume in a compartment. The ignition of hydrogen-laden jets is modeled as a "continuous" burn in the MAAP code. This type of burn refers to those circumstances when a very high temperature jet emerges from a potentially inerted region into a cooler, non-inerted region where it induces a burn. For example, a hot mixture of hydrogen-steam could enter the containment auxiliary building during an interfacing system LOCA (ISL) and cause a hydrogen burn in the auxiliary building. Another example is a hot hydrogen-steam jet from the reactor cavity region that enters into the containment lower region.

The combustion mode modeled in the MELCOR code is denoted as a discrete burn, in which combustible gases are uniformly burnt in a compartment only after prescribed ignition or propagation criteria are met.

19.1 Flammability Limits

In the MAAP 3.0B code, the flammability limits are determined by the construction of a combustion diagram. The domain of the diagram consists of both lean and rich flammability limits (LFL and RFL). A power law expression is developed for the flammability limit curve that is further modified for elevated temperatures. Limited experimental results have shown that high temperatures tend to cause the LFL to decrease and the RFL to increase. The flammability limit curves at various temperatures are used in the MAAP code for upward and downward flame propagations. The limits of upward flame propagation are used for the local (incomplete) burn mode, and the limits of downward flame propagation are for the global (complete) burn mode. At elevated temperatures, a very small fraction of hydrogen is required to induce a flame propagation. This situation leads to the autoignition model in the MAAP code which assumes that ignition occurs if the temperature of the mixture is above a critical autoignition temperature (Model parameter No. 71), and the inertant fraction is less than a specified value (Model parameter No. 72). The nominal autoignition temperature is 983K and maximum inerting fraction is 0.75 in the MAAP code.

The MAAP code also applies an ignition criterion when active igniters are present. The ignition criterion, specified as a mole fraction of hydrogen above (or below) the temperature- and steam-concentration-dependent limits, is an offset to the downward flammability limits. The user-specified ignition criterion is Model parameter No. 73, and the recommended value is zero.

The ignition of a hydrogen-laden jet is determined by comparing the temperature of the gas stream with the user-specified autoignition temperature TJBRN (Model parameter No. 60). The recommended value for TJBRN is 1060 K. Jet burning will not occur if the downstream compartment has less oxygen or more steam than would allow a premixed burn. The jet burn criterion is consistent with the flammability limit used in MAAP.

The ignition and propagation criteria used in the MELCOR code are based on experimental data determined in steam-saturated air at relatively low temperatures and pressures. The criteria are:

a. oxygen mole fraction ≥ 0.05,

b. inertant (steam and CO_2) mole fraction ≤ 0.55, and

c. combustible gas mole fraction must be

$$X_{H_2} + \frac{A}{B} X_{CO} \geq A$$

where,

	A		B
Ignition Limits	0.07	—	0.129
Propagation Limits			
Upward	0.041		0.125
Horizontal	0.06		0.138
Downward	0.09		0.15

These ignition limits are appropriate when modeling accident sequences with igniters operating. Without igniters, the limits are higher. The MELCOR code increases the ignition limits to A = 0.1 and B = 0.167 when the igniters are not operating. The propagation limits shown above depend on the spatial relationship of two compartments (i.e., whether the adjacent compartment is located above, below or on the same level as the burning compartment). The concentration limits specified for propagation apply to the adjacent compartments, not the compartment in which the burn originates. The low concentration limit in the upward direction implies that the upward propagation of the flame is much easier due to buoyancy. The criterion for downward propagation implies that the compartment could spontaneously ignite before downward propagation would occur.

In comparison, the ignition model in MELCOR is relatively simple; its flammability limits are independent of temperature and inertant fraction if the inertant fraction is less than 55%. The MAAP model requires the flammability limits to be determined by the flammability diagrams, which depend on both temperature and the inertant fraction. Since both models are empirical and there are few experiments at elevated temperatures, the validity of the MAAP model and the applicability of the MELCOR model at elevated temperatures must be determined.

We note that neither MELCOR nor MAAP model a hydrogen detonation. However, in the MELCOR code, a warning message is given in a computer printout, that a detonation is predicted in a containment compartment, if the following conditions are satisfied:

Molar fraction of H_2 > 0.14

Molar fraction of O_2 > 0.09

Molar fraction of steam < 0.30

The consequence of a hydrogen detonation is not modeled in the code.

19.2 Burn Time and Combustion Completeness

The burn time and combustion completeness are key parameters that determine the quantity of hydrogen reacted and the combustion rate, which, in turn, determine the rate of energy release and containment pressurization. In MAAP, the burn time and combustion completeness are obtained by solving the mass and momentum equations for a fireball. MAAP assumes that the spherical fireball expands at the speed of a laminar flame when buoyancy effects are small. When the fireball is large, its growth is modeled as a plume entraining unburned gases at a rate proportional to its upward velocity. The upward velocity is determined by considering the acceleration of the fireball due to buoyancy and drag forces. The analytical model involves several parameters, such as entrainment coefficient, speed of the laminar flame, the fireball's surface area, and drag coefficient. The uncertainties in these parameters are covered by a user-specified flame-flux multiplier, model parameter No. 74 FLPHI. The recommended best estimate, minimum, and maximum values of the flame flux multiplier are 2, 1, and 10, respectively.

MELCOR does not model hydrogen combustion as a flame front; instead, it assumes hydrogen burns uniformly in a compartment. Thus, during a burn, a compartment will consist of a homogeneous mixture of burned and unburned gases. The flame speed and combustion completeness are determined by empirical correlations which are derived from a variety of experiments that were performed in the Variable Geometry Experimental System (VGES), Fully Instrumented Test Series (FITS), and at the Nevada Test Site (NTS). No analytical solutions are involved in MELCOR combustion model. The flame speed correlations used in the MELCOR code are functions of the initial mole fraction of diluents and the initial mole fraction of combustible gases. The correlation does not depend on temperature.

In the MELCOR code, the burn time is calculated as the ratio of a characteristic length to the flame speed. The default value of the characteristic length (i.e., travel distance of the flame) is the cubic root of the compartment volume. The final mole fraction of combustible gases is determined by the combustion completeness model which uses empirical correlations. Combustion is assumed to be complete for combustible gas concentrations at or above 8%. The final combustible concentration may never be reached if the burn is oxygen-limited.

20 Direct Containment Heating (DCH)

In certain reactor accidents, the reactor core can be degraded while the reactor coolant system remains pressurized. In these accidents, molten core debris will relocate to the bottom of the reactor vessel and will start attacking the bottom head of the reactor vessel. When the latter is breached, core debris will be ejected under pressure. The ejected materials are likely to be dispersed out of the reactor cavity as fine droplets, quickly transferring thermal energy to the atmosphere. In addition, the metal components of the ejected core debris, mostly zirconium and steel, can react with atmospheric oxygen and steam to generate a large quantity of hydrogen and chemical energy. This complicated physical and chemical process is known as direct containment heating and may be a significant source of containment pressurization.

MAAP modeling of the DCH process is parametric to allow sensitivity studies. The flow rates of water, steam, and zirconium entrained from the cavity are adjusted for chemical reactions and heat transfer. The thermal and chemical equilibrium of corium entrained out of the cavity with water and gas is assumed.

MAAP PWR Revision 17 has added the oxidation of steel and the highly exothermic reaction of Zr with oxygen in the containment atmosphere. The Zr/O_2 reaction is particularly important for the upper compartment which is rich in oxygen.

The conditions inside the reactor vessel at the time of vessel failure are very important to the extent of containment pressurization due to DCH. These conditions are determined by the accident sequence and the in-vessel meltdown progression of the core. The kind of information needed to predict the magnitude of DCH are the reactor pressure vessel (RPV), the size of the bottom head failure, the melt mass available for release as well as its temperature and composition, the amount of hydrogen/steam dissolved in the melt, the available mass of water in the RPV, the pressure of the reactor coolant system (RCS) and the amount of hydrogen in the RCS at the time of vessel failure. The MAAP modeling of some important phenomena such as entrainment/deentrainment are overly simplified. In addition, the DCH subroutine is not called by the CCOMPT subroutine which means that DCH is not modeled for the cavity. This will under-predict the pressure difference between the cavity and the lower compartment during the blowdown time.

In the MAAP code, control material and fission products are added to the mass of debris in the lower plenum as debris leaves the core region, and are released at vessel failure with the bulk debris. The movement of these materials is performed in subroutines HEATFP (melting rate from the core) and PSFP (addition rate to the lower plenum).

The present version of MELCOR does not have a DCH model and, hence, no comparison can be made.

21 Containment Safeguard Systems

21.1 Containment Sprays

MAAP models containment sprays for the upper and lower compartments. Sprays are not allowed in the annulus region. The code assumes that droplets enter the compartment at an effective height at the terminal velocity and drift downward until either they evaporate or strike a water surface. Users can specify what fraction of the spray flow from the upper compartment proceeds unimpeded into the lower compartment. Using the user-specified nozzle height, initial droplet size, flow rate, and temperature, MAAP computes the mass and heat transferred from the droplets to the containment's atmosphere. If the droplets enter at a temperature below the dewpoint, moisture in the containment's atmosphere will condense on the droplets. If the temperature is higher than the dew point, droplets can be heated up and begin to evaporate. The heat and mass transfer by condensation, evaporation and convection are computed by empirical correlations. Only one droplet size can be specified by the user.

In MELCOR, the containment sprays can be modeled in any control volume (i.e., containment compartment) and be carried over to a lower compartment or collected in the containment spray sump. Droplets reaching the bottom of a control volume and not being carried over to other volumes or placed in the sump are put into the pool of the control volume. A distribution and frequency of droplet size may be input for every spray source. A maximum of 5 sizes can be specified. Empirical correlations also are used to estimate the heat and mass transfer between the droplets and containment's atmosphere.

The MELCOR model is more flexible than MAAP in the treatment of spray source volume, the distribution of droplet size, and the carry over to a lower volume. However, it is expected that differences in the spray models of the two codes will not have a significant effect on the thermal-hydraulics of the containment, but will affect the transport of fission products in the containment, particularly due to the treatment of droplet size distribution.

21.2 Fans

MAAP allows the user to specify the suction and discharge locations for fan coolers. The rates of flow and energy transport are computed by mass and heat balance. Cross flow and finned tubes are assumed for the fan cooler. The detailed calculations of heat and mass transfer involve film-wise condensation on the cooler outer surface, thermal resistance through the tube wall, and convection in the co-current internal flow.

In MELCOR, the suction and discharge of the air flow can be specified separately for any control volume. Heat and mass transfer also are computed for the heat exchangers. Although the details of computation differ from the MAAP code, the general approach of using the conservation laws are similar.

22 Containment Failure Model

In the MAAP code, the area and location of containment failure are user-specified. Failure can occur either in the upper compartment or the annulus region. Two models can initiate containment failure. A simple model uses a user-specified event, such as pressure or temperature, as the failure criterion. A more detailed model involves stress and strain analysis. In the latter model, the containment wall is divided into 3 regions: liner, tendons, and rebar. Initially, the elastic deformation caused by the rise in the containment's internal pressure is computed. After the yield stress is exceeded, the calculation uses a plastic deformation model. Containment failure is assumed when the resultant stress equals the ultimate stress. The failure is considered as a "leak-before-break" if the initial failure is in the liner. The failure is referred to as global failure if the initial failure is in the rebar or tendons. Local failure of a penetration also is considered. The detailed model has been used in the MAAP/PWR sensitivity studies [24]. The results show that the strain model is not conservative with regard to failure time. The failure time is important for the transport of fission products and offsite consequence analyses. The detailed failure model is not recommended for IPE applications [25].

MELCOR uses control functions to simulate containment failure. Failure can be initiated by user-specified pressure, temperature, or time. The area and location of failure are also user-specified. The control function is equivalent to the simple model available in the MAAP code.

23 Auxiliary Containment

The auxiliary containment model is a new addition to the MAAP code. It is very important for the analysis of containment bypass events. The model does not use the approach of fixed nodalization and the pre-defined circulation loop used in MAAP for the primary containment. Instead, a node and junction type model was constructed which allows the user to specify the number of control volumes and the junctions; a maximum of 9 and 50 are allowed, respectively. Multiple junctions, both vertical and horizontal, are allowed for each control volume. The model calculates forced, unidirectional, and counter-current natural circulation flows passing through these junctions. Thus, the MAAP model attempts to treat a very complex flow situation in a multiple region system.

For each control volume, thermal hydraulic properties and their rate of change are computed. Most of the phenomena which could occur in the primary containment are accounted for, such as combustion, sprays, heat transfer to walls, flashing, and rainout.

The most important part of the model is the determination of flow patterns. Three flow patterns are developed: the unidirectional flow (Bernouilli flow), purging flow and counter-current flow. Bernouilli flow alone is used for junctions where it exceeds the purging flow. A fraction of the countercurrent flow is superimposed on the Bernouilli flow for junctions where the purging flow exceeds the Bernouilli flow. The fraction is determined by a correlation to FAI data which equals zero when the purging and Bernouilli flows are equal and which equals one when the Bernouilli flow is zero. The Bernouilli flow is derived from a simple force balance and is based on the assumption that the gas density is uniform in the control volume, i.e., there is no stratification in the compartment. The model will introduce some error for situations in which a large variation in temperature and/or concentration results in a large variation in density. The other two flow models, purging flow and counter-current flow, are derived from empirical correlations.

The experimental base on which the flow models were developed involves a small-scale test apparatus. The test tank, which is essentially a two-volume system, is 0.55 in square and 0.762 in deep. Salty water and fresh water were used to create the density-driven flow through small openings in the partition located in the tank. The ratio of density difference to the average density is between 0.024 and 0.17. For ideal gases, the corresponding temperature difference will be in the range of 10 to 68 K for an average temperature of 400 K. This example illustrates the condition of the auxiliary building at which the empirical correlation could be applied. Other factors, such as geometric scale, multiple volumes, fluid properties, and the partition and opening configurations, must be considered when the MAAP model is applied to the auxiliary building under severe accident conditions.

We note that the experiments used a single-phase fluid (water) in an idealized quasi-steady condition. In the auxiliary building, the atmosphere is expected to contain a large fraction of steam which will condense. In addition, other processes, such as sprays and combustion, could occur in the building. (A hydrogen burn will create a temperature difference much larger than that used in experiments.) Since physical situations in the auxiliary building will differ from the idealized condition employed in the experiments, a scaling study is needed to verify these empirical correlations.

Using the control volume concept, MELCOR can model the auxiliary building in a similar manner to the primary containment. MELCOR does not have a model which can treat counter-current flow in a junction.

24 Ice Condenser Plant

The compartment nodalization and flow circulation loop of an ice condenser containment were discussed in Section 16. MAAP considers the ice condenser as a heat sink for pressure suppression. A simplified model is used to treat the steam condensation and ice melting. The following are the major assumptions used in the model:

1) Heat transfer to the ice condenser is fully effective and is not degraded until all the ice is melted. The presence of condensate film on heat transfer surface area and the decrease of surface area due to ice melting are ignored.

2) The temperature of the steam-air mixture leaving the top of the ice condenser compartment is constant, independent of flow conditions. We requested clarification of the implications of the constant temperature of the exit gas. The question and answer are given below [20]:

   Question:

   In the HICE subroutine, the temperature of the exit gas is fixed at 100°F. A fixed temperature implicitly determines the melting rate of the ice. What is the range of flow rate within which the assumption of a fixed exit temperature is valid? Is this temperature adequate during a very low or high blowdown rate of the primary system or under conditions where hydrogen burn occurs in the upper plenum?

   Answer:

   The ice condenser exit gas temperature is set to 100°F to reflect experimental data for high rates of blowdown flow. Since the melting rate of the ice is determined by the rate of steam condensation, it is relatively insensitive to selection of a lower exit temperature, which could result from lower flow rates. That is, the steam mole fraction at 100°F is roughly 5%, whereas its mole fraction would be considerably higher on entry, so that nearly all the steam is already condensed by the model. Therefore, reasonable variation in this exit temperature for lower flow rates would have negligible impact on the ice melt time. It is worth noting that the temperature of the condensate as it exits the ice condenser is assumed to be equal to the average of the inlet and outlet saturation temperatures (the latter is the exit gas temperature). The sensitivity of the melting rate to this assumption is also believed to be small.

3) The grid and structures used to hold up the ice blocks are not considered as heat sinks. The ice-condenser compartment will not play any role on containment response after the ice is completely depleted.

4) Flow area of the junction between the ice condenser and upper plenum compartments is a function of flow direction. The flow area representing the intermediate deck doors will close if the flow reverses. A bypass area which is provided in the design to equalize pressure difference will open. This is modeled by multiplying the normal forward-direction flow area by a user-specified factor when flow reverses. This treatment is also applied to the fan dust dampers.

5) Boiling of the water pool at the bottom of ice condenser by the dissolved fission product and the decay heat in the gas phase are modeled in MAAP.

Based on this description, the simplified model may give some uncertainties on the predicted rates of steam condensation and ice melting.

The present version of the MELCOR code does not have an ice condenser model. Hence, no comparison can be made.

25 Summary

Based on this preliminary review, the MAAP code appears to represent containment buildings and important related phenomena reasonably well. Some models contain parameters which allow the user to perform sensitivity studies. The following items are specific comments, which have been discussed in more detail in this report:

1) The fixed nodalization and pre-defined circulation loop for the primary containment are restrictive, particularly for an analysis of hydrogen distribution in the containment. The present structure of the code does not allow a user to identify the potential for a localized detonation, which is potentially an important issue affecting the performance of the PWR containment during severe accidents.

2) Various corium/water interactions are treated independently and inconsistently by several subroutines (EXVIN, ENTRAN, PLH2, and PLSTM). The treatment could predict an excessive generation of steam which will increase the containment's inertness and reduce the potential for combustion.

3) The logic for calculating concrete decomposition by subroutine JET is not consistent with subroutine DECOMP and the corium/water interaction subroutines (EXVIN, ENTRAN, PLH2, and PLSTM).

4) In treating corium-concrete interactions, there are four major differences between the subroutines DECOMP (MAAP) and CORCON (MELCOR): melt stratification, corium-concrete contact at interface, sideward and downward erosion of concrete, and heat conduction in solid concrete. These differences will affect the containment performance (such as combustion, pressurization rate and

basemat melt-through) and the release and transport of fission products in the containment. The two subroutines were examined carefully by the code comparison exercise.

5) For hydrogen and CO combustion, the differences between the MAAP and MELCOR treatments are the ignition criterion, burn time, and completeness of combustion. MAAP relies on an analytical model and MELCOR uses empirical correlations. Hydrogen combustion is an important issue for the PWR dry containment, as is considered by the NRC Generic Issue GI 121 [26]. The code predictions would affect the proposed hydrogen control in the PWR dry containment.

6) MAAP appears to have an adequate treatment of containment sprays and fans. However, in comparison with the MELCOR code, the restriction imposed by MAAP on the spray source compartment and the size distribution of the spray droplets may have some impact on the transport of fission products in the containment.

7) The detailed treatment of the auxiliary building is a good addition to the MAAP code. The auxiliary building model is important for containment bypass events. The model contains empirical correlations developed from small test apparatus under simplified conditions.

26 Fission Products Treatment in the PWR System

26.1 Fission Product Species

In the MAAP and MELCOR codes, fission products refer to both radioactive and non-radioactive nuclides generated by fuel fissioning and other non-radioactive material released from structures (control rods) or corium/concrete interaction. The initial masses of 27 specific fission products (22 from fuel and 5 from structures), in the form of chemical elements, are provided by the MAAP input file (Table A.6). The 22 elements from the fuel are lumped into 12 groups when they are released from the fuel rods. The 12 groups, most of which are chemical compounds, as shown in Table A.7, are treated separately as aerosols or vapors in the MAAP code. The 5 elements from the structures in Table A.6 are lumped together into group 1 in the MAAP code (aerosol of Table A.7). Any concrete aerosol generated by the corium/concrete interaction also is included in group 1 (aerosol of Table A.7).

In MELCOR, fission products are treated by the Radionuclide Package (RN). In this package, chemical elements of similar properties are grouped into 15 classes (Table A.8). Comparing Table A.8 with Table A.7 shows that MELCOR treats the fission products as elements, not compounds as treated in MAAP. The different chemical forms used in the two codes make a direct comparison of the source terms in the MAAP/MELCOR comparison exercise more complicated, because conversion of the species would have to be made. For example, CsI in class 2 and CsOH in class 6 of the MAAP species must be converted and combined in order to compare with Cs in class 2 of the MELCOR species. Although MELCOR permits the combination of two classes to form a new class upon release, such as Cs + I to CsI, all default properties have to be redefined for the new material class through the input file specified by the user.

Table A.6 Initial Core Fission Products in MAAP From Fuel

1. Xe	12. Mo
2. Kr	13. Tc
3. I	14. Ru
4. Rb	15. Sb
5. Cs	16. Te
6. Sr	17. Ce
7. Ba	18. Pr
8. Y	19. Nd
9. La	20. Sm
10. Zr	21. Np
11. Nb	22. Pu

From Structural Materials

1. Cd
2. In
3. Ag
4. Sn
5. Mn

Table A.7 Fission Product Species in MAAP

1. Noble Gases and Radioactivity Inert Aerosols
2. CsI + RbI
3. TeO_2
4. SrO
5. MoO_2
6. CsOH + RbOH
7. BaO
8. La_2O_3 + Pr_2O_3 + Nd_2O_3 + Sm_2O_3 + YO_3
9. CeO_2
10. Sb
11. Te_2
12. UO_2 + NpO_2 + PuO_2

MELCOR uses the VANESA model to compute the radionuclide release from the reactor cavity. Because VANESA models 25 species, mapping is employed between the 25 species defined in VANESA and the 15 material classes used in the RN package. Mapping also is performed between non-radioactive materials in the COR package (core), i.e., steel and steel oxide, and the material classes in the RN package. If the default class structure is used, the default mapping applies. However, if the default class structure is revised, mapping must be modified through the input records.

In MAAP, the total core inventory of the 27 elem .ts given in Table A.6 is specified by the user in the input file. The initial distribution of the masses is specified .a the core peaking factors. In MELCOR, the initial distribution of the masses of core fission products also can be specified in the input file to reflect the radial and axial power profiles in the core. In addition, MELCOR allows fission products to reside in the fuel-cladding gap.

26.2 Fission Product Transport

Fission product transport is closely coupled with the thermal-hydraulics. In any region of the primary system or containment, the rate of change of fission product depends on the volumetric flows and temperature of gases and the temperatures of structures in that region. On the other hand, the energy balance required in the thermal-hydraulic calculation needs information on the fission product decay heating. Therefore, the behavior of the fission products predicted by either MAAP or MELCOR strongly depends on the thermal-hydraulic behavior predicted by the codes.

In MAAP, the behavior of the fission product is a alyzed separately for the primary system, steam generators, pressurizer, quench tank and for the containment .pper, lower, annulus, and cavity compartments. Aerosol also is analyzed for the auxiliary building. In each region, aerosols and fission product vapors are transported along with the steam, hydrogen, and other gases. If a water pool is present in the region, as in the case of the containment, pool scrubbing is estimated, and the deposited aerosols are transported with water. However, pool scrubbing is not modeled for the annulus and ice condenser regions of the containment. Pool scrubbing also is not modeled for the primary system. MAAP permits fission products mixed in the corium to be transported with corium during core relocation, discharge from the reactor vessel, and entrainment in the containment. The quantity of fission products transported with corium is determined by the fractional volume of corium involved in these processes.

Table A.8 Material Classes in MELCOR

Class Name	Representative	Member Elements
1. Noble Gas	Xe	He, Ne, Ar, Kr, Xe, Rn, H, N
2. Alkali Metals	Cs	Li, Na, K, Rb, Cs, Fr, Cu
3. Alkaline Earths	Ba	Be, Mg, Ca, Sr, Ba, Ra, Es, Fm
4. Halogens	I	F, Cl, Br, I, At
5. Chalcogens	Te	O, S, Se, Te, Po
6. Platinoids	Ru	Ru, Rh, Rb, Re, Os, Ir, Pt, Au, Ni
7. Early Transition Elements	Mo	V, Cr, Fe, Co, Mn, Nb, Mo, Tc, Ta, W
8. Tetravalent	Ce	Ti, Zr, Hf, Ce, Th, Pa, Np, Pu, C
9. Trivalents	La	Al, Sc, Y, La, Ac, Pr, Nd, Pm, Sm, Eu, Gd, Tb, Dy, Ho, Er, Tm, Yb, Lu, Am, Cm, Bk, Cf
10. Uranium	U	U
11. More Volatile Main Group	Cd	Cd, Hg, Zn, As, Sb, Pb, Tl, Bi
12. Less Volatile Main Group	Sn	Ga, Ge, In, Sn, Ag
13. Boron	B	B, Si, P
14. Water	H_2	H_2O
15. Concrete	---	---

In MELCOR, aerosols and fission product vapors are transported between control volumes through flow paths in a similar manner as the MAAP model. However, fission product transport in any flow path can be disabled by a user-input record to simulate the potential blockage of aerosols in the flow path. The removal of aerosols and vapors by filters in any flow path also can be modeled in MELCOR. In MAAP, the filter is modeled only in the auxiliary building with DFs specified by the user.

26.3 Fission Product Decay Heating

MAAP tracks the energy associated with fission product decay. Each fission product species is assumed to decay at a rate proportional to that given by the ANSI decay curve. As the fuel node heats up and releases fission products, the associated decay heat energy moves out of the core into other parts of the primary system. In MAAP, each node in the primary system may have multiple heat sinks, which can be heated up by the deposited fission products. Masses of fission products which are deposited on each of the heat sinks, are tracked separately. Decay energy associated with the suspended fission products is assumed not to heat up the atmosphere in that node. The energy is converted to one of the heat sinks which has the largest surface area. The largest heat sink is selected to reduce the temperature rise due to fission product decay heating. Revaporization of volatile fission products is determined by the heat sink temperature.

In the containment, MAAP allows the decay energy of the suspended fission products to be added to the atmosphere energy in that compartment. This addition will serve to increase the containment temperature. The decay energy of deposited fission products is added to the single heat sink in the compartment. (In each compartment, MAAP only models one heat sink to receive the decay energy.) The surface area of the single heat sink in each containment compartment is specified by the user, and the aerosol settling area is provided by the floor area also specified by the user.

In MELCOR, the decay energy of each fission product species can be proportional to the ANSI decay curve or can be described in a tabular form provided in the input file. In each control volume, different treatments are applied to the decay energy provided by fission products in the atmosphere, in the water pool, and deposited on the surface structure:

(1) Decay energy provided by fission products in the atmosphere is divided among the atmosphere of that volume, surfaces in that volume, and the atmosphere and surfaces of other volumes. The split of the decay energy is determined by the user's input.

(2) Decay energy provided by fission products in a water pool is completely absorbed by the pool.

(3) Decay energy associated with fission products deposited on a structure is allocated to the structure, the atmosphere of the volume, other surfaces in the volume, and the atmosphere and surfaces of other volumes. The allocation can be specified by the user.

These treatments are an attempt by the MELCOR code to consider energy transfer by radiation among the atmosphere and structures of the volume and other volumes.

A comparison between the two codes on the way fission products are treated is summarized in Table A.9. The MELCOR treatment includes many parameters specified by the user for performing sensitivity studies.

27 In-Vessel Release

In the MAAP code, the fission product release from the fuel rod starts at the time of clad failure. There are two criteria for clad failure: a failure temperature specified by the user, or when the computed burst stress of the clad is greater than the hoop stress. The failure temperature is provided by model parameter No. 46, which has a default value of 1200 K. The stress analysis depends on the heat up rate of the fuel rod, and therefore is dependent on the accident sequence. Presently, it is not known which criterion will result in early cladding failure for a given accident sequence. Because the release time, relative to the failure time of the reactor vessel and the failure time of the containment, is important for the overall fission product deposition in the primary system and release to the containment, some comparative analysis should be performed to guide the selection of the two criteria for in-vessel release.

The releases of the volatile materials (noble gases, Cs, I, and Te) are estimated in MAAP by either the steam oxidation model or the empirical correlations recommended in NUREG-0772 [27]. The steam oxidation model assumes that the release of volatile fission products follow the kinetics of fuel oxidation when UO_2 is heated in steam. The model shows that the fractional release of all volatile fission products is a function of time and temperature. The correlations recommended in NUREG-0772 provide the fractional release rate coefficient (fraction/minute) as a function of temperature only. The correlations contain empirical constants which are derived from experimental data for temperatures greater than 1000°C. The two models have been compared with identical boundary conditions (core flows, temperatures, etc.), and the predicted release rates for Cs and I from the two models are reported to agree reasonably well [28].

Table A.9 Comparison of Fission Products Treatment

	MAAP	MELCOR
Initial Fission Products Masses	• Total core inventory of 25 elements are provided • Radial and axial distribution of masses are specified via peaking factors	• Initial masses are provided in COR and RN package • Radial and axial distribution of masses can be specified
Fission Products Species	• 12 classes (Most are chemical compounds, except noble gases and Sb)	• 15 elements (default) • A total of 20 elements can be user-specified • Chemical compound can be user-specified • Mapping is required
Fission Products Transport	• Fission Products in each region are transported along with the flow • Pool scrubbing is modeled in all containment compartments, except ice-condenser and annulus region • No pool scrubbing in primary system • No filter in any flowpath, except the auxiliary building	• F.P. in each control volume is transported along with the flow • Pool scrubbing is allowed in every flow path and control volume as user-specified • Filter is allowed in any flow path as user-specified
Fission Product Decay Heating		
F.P. Suspended in Atmosphere	• Allowed to heatup the atmosphere in containment • Not allowed to heatup the atmosphere in primary system (Heat is transferred to the largest heat sink)	• Allowed to heat up atmosphere and structures of the current volume and other volumes • Split energy is user-specified

	MAAP	MELCOR
F.P. Deposited on Structures	• Heat-up of the single structure in each region of the containment • Heat up of multiple structures in primary system	• Allowed to heat up the structure, atmosphere and other structures of the current volume, and atmosphere and structures of other volume • Split of energy is user-specified
F.P. Deposited in Water Pool	• Complete absorption by water pool	• Complete absorption by water pool

A separate treatment is used for the release of tellurium, because tellurium can be chemically bonded to the cladding when Zr is less than 70-90% oxidized. Therefore, MAAP provides an option to allow the tellurium to remain in the core region. The option is provided by the model parameter No. 51, FTEREL, specified by the user. With this parameter at zero, Te will remain in the core region, supply decay heat during the core heat up, and will be transported with Zr and molten fuel during core relocation into the containment. In the containment, Te is released from the melt as Zr is oxidized due to core/concrete interactions. When the model parameter is one, Te will be released according to either the steam oxidation model or the empirical correlations. Recently, a new model parameter No. 77, FTENUR was added for use in correlation with the NUREG-0772. FTENUR is defined as the oxidized Zircalloy mass fraction limit below which tellurium release rates are limited. FTENUR has a default value of 0.9 [29].

For non-volatile fission products, MAAP uses Kelly's correlations of the fractional release rate coefficient, which contain empirical constants for different fission product elements, similar to the correlations recommended in the NUREG-0772 report. The release of the non-volatile fission products also is limited by the transport of fluid flow computed by the MAAP code, i.e., the ability of the flow to carry the materials to the upper plenum. This limitation implies that the concentration of any element in the atmosphere can not be greater than the saturated concentration based on chemical equilibrium. A negative value of the model parameter No. 50, FPRAT, specified by the user will turn on the saturation limitation mechanisms, which reduces the release of nonvolatile fission products.

Although the control rod and structural materials are not considered when calculating the core thermal-hydraulics, MAAP does consider the release of In, Cd, Ag, Su, and Mn at the time the melting point of steel is reached in any node. The release of these materials is controlled by the saturation densities at the nodal temperature. MAAP accounts for the transport of these materials in the primary system and in the containment.

In MELCOR, the initial fission product masses are allocated to the fuel or the fuel-cladding gap. In the gap region, the fraction, not the mass, of the initial inventory is specified. The default values of the fraction of gap inventory used in MELCOR are obtained from the CORSOR model. For example, the amount of gap inventory is taken to be 5% of the initial mass of Cs, 1.7% of I, 3% of the noble gases, and 0.01% of Te. It should be noted that these values depend on the degree of irradiation of the fuel rod. Values provided by CORSOR are for highly irradiated rods and are not applicable to fresh rods.

MELCOR models the in-vessel release by two stages: gap release and fuel release. Fission products in the fuel-cladding gap are released at cladding failure defined by either a failure temperature specified by the user or the loss of intact cladding geometry. The default value of the failure temperature is 1170 K, which is comparable with the recommended failure temperature (1200 K) used in MAAP for fission product release. The loss of an intact cladding is determined by the model of the fuel melt in the COR package [2]. When any fuel node reaches the above release criterion, the entire gap inventory in the fuel rods of that radial ring is released instantly to the surrounding control volume. The subsequent release from fuel as it heats up is calculated on a node by node basis. The fission products from the fuel are released to the gap inventory when the cladding is intact, and are released to the surrounding control volume when the cladding fails.

The release rates of fission products from the fuel are computed according to the empirical correlations provided by the CORSOR or CORSOR-M model depending on the user's selection. These empirical correlations are the same as those reported in NUREG-0772, which also were used in the MAAP code. The CORSOR and CORSOR-M models consider the release rate of each material class as a function of temperature only. The surface-to-volume ratio of the material is not included. An option has been added in MELCOR to consider this ratio. A component surface-to-volume ratio specified by the user is compared to a base value, derived from the CORSOR experimental data (422.5 1/m). The computed release rate of the CORSOR or CORSOR-M model is increased or decreased by the ratio of the value specified by the user to the base value. The release rate calculated for each class by the CORSOR or CORSOR-M model applies to all core components (i.e., fuel, cladding, control rod, and particulate debris.)

The treatment of Te in MELCOR is slightly different than in the MAAP code. In MELCOR, the computed Te release of CORSOR or CORSOR-M is used when the amount of cladding oxidation is greater than a cut-off value (default=0.70). When the amount of cladding oxidation is less than the cut-off value, the release rate is multiplied by a multiplier (default=0.025). Recall that MAAP also provides the option such that the Te release rate is determined by the CORSOR-M correlations. However, the recommended default value is 0.9. [29].

MELCOR also considers the effect of the vapor pressure of each material class. No concentration of any element can be greater than the saturation concentration in the surrounding control volume. If the release mass is greater than the saturation value for the fission product vapor, the excess vapor mass is converted to aerosol mass. MAAP also uses the saturation concentration to limit the release of fission products, and there is no excess vapor mass.

Hobbins, et al., [30] pointed out that melt progression in the reactor core has important effects on fission product release as described below:

a. Burst release due to fuel microcracking during core reflooding can increase the release of the fission products.

b. Fuel liquification (i.e., dissolution of fuel pellet with molten zircaloy) destroys the crystal structure of the UO_2 pellet so that the release of fission products is much faster than the process of diffusion in a solid.

These effects are not considered in MAAP or in MELCOR. A comparison of the treatments in MAAP and MELCOR for the in-vessel release phase are summarized in Table A.10.

28 Ex-Vessel Release

The release of fission products during corium-concrete interaction is computed by the METOXA subroutine of the MAAP code. METOXA models vaporization of compounds from the molten corium pool. The compounds include those present in liquid form as corium constituents and those formed by chemical reactions between liquid corium constituents and the concrete decomposition products. A total of 23 reactions and element balances are modeled as the "basis set" in METOXA. Compounds not included in the basis set are considered in a set of auxiliary relations. The chemical reactions involve 30 x 6 condensed species and gases.

Table A.10 Comparisons of In-Vessel Release

	MAAP	MELCOR
Release Criteria		
1. User-specified Failure Temperature	Default = 1200 K	Default = 1170 K
2. Failure of Intact Cladding	Burst stress analysis	Clad melting analysis
Release Mode	Gap release and fuel release	Gap release and fuel release
Volatile materials release	1. Steam oxidation model 2. Empirical correlations (NUREG-0772) [27]	CORSOR or CORSOR-M model
Treatment of Te	User-specified option: 1. No release 2. Same as MELCOR model. The default valve of the cut-off parameter (FTENUR) is 90%	User-specified cut-off parameter: 1. Above 70% Zr oxidation: CORSOR or CORSOR-M model 2. Less 70% Zr oxidation reduced by a user-specified multiplier (0.025)
Non-volatile Material Release	Kelly's correlation	CORSOR or CORSOR-M model

The vaporization model in METOXA assumes chemical equilibrium for all chemical reactions between the liquid corium constituents and the concrete off-gas. Ideal fugacity is assumed for gases. Non-ideality of the liquid compound is expressed by the activity coefficients, which are temperature- and composition-dependent. Four activity coefficients, expressed as model parameters specified by the user, are provided by MAAP for sensitivity studies for the compounds SiO_2, SrO, BaO, and K_2O or Na_2O. The recommended minimum and maximum values for these coefficients cover a large range of uncertainty.

METOXA also assumes equal oxygen potential throughout the debris pool. This assumption implies that gas agitation will create enough interfacial contact between any phases to promote oxygen diffusion to equilibrium. There is no stratification or phase separation on oxygen potential.

The ex-vessel release is sensitive to the corium temperature and all other factors that influence the corium temperature, such as corium/water and corium-concrete interactions. Thus, the release of the ex-vessel fission products modeled in METOXA is coupled to the analysis performed by the DECOMP subroutine. In DECOMP, a single corium temperature is computed based on the uniform mixing model.

In MELCOR, the VANESA model has been implemented and coupled to CORCON during every time-step to estimate the release of fission products from the corium-concrete interaction. Two aerosol generation processes are addressed in VANESA. In addition to the vaporization release considered in MAAP, VANESA also includes the mechanical aerosol generation process.

A total of 27 species are considered in VANESA. Each species within the melt represents an element or group of elements presumed to have similar physical and chemical properties. Because CORCON assumes a multiple layer of the corium pool, each melt species is assigned to either the metallic or oxidic layer, depending upon the species' chemical characteristics. Furthermore, the oxygen potential of the oxidic layer is assumed to be the same as that calculated for the metallic layer. This assumption is equivalent to the assumption that oxygen transport between the oxidic and metallic phases is sufficiently rapid to compensate for various processes that would otherwise increase the oxygen potential of the oxidic layer.

In the VANESA vaporization model, chemical equilibrium between the gas phase and the condensed phase is assumed separately for the oxidic and metallic layers. The non-ideal effects are represented by the activity coefficient for the condensed phase and fugacity coefficient for the gas phase. However, the present version of VANESA used in MELCOR made the following approximations: (1) nearly all constituents of the metallic and oxidic phase of the core melt were assumed to be ideal, (2) Na_2O and K_2O were taken to be non-ideal and have an activity coefficient of 10^{-6}, (3) all gases and vapors are ideal. These approximations also are implemented in MAAP. (The recommended best estimate of Na_2O and K_2O activity coefficient also is 10^{-6}.)

The vaporization model considered in both MAAP and MELCOR provides the upper bound estimate of materials which are released from the core debris interacting with concrete. The kinetic factors which might prevent the vaporization process from reaching the equilibrium limit also is considered in VANESA. Because vaporization processes involve the transfer of a volatile constituent to the free surface of the vapor phase, VANESA considers the following rate processes:

(1) The volatile constituents of the condensed phase must migrate to the free surface;

(2) Once the constituent reaches the free surface, it must transfer into a vapor; and

(3) Vapor at a surface must be conducted away from the surface until the gas phase becomes locally saturated and net vaporization ceases.

Each of the above steps is a kinetic process that requires time. Because the steps are serially related any one of them can become rate-limiting. The kinetic processes are not modeled in MAAP. The inclusion of the kinetic model and the chemical equilibrium model is an important difference between the MELCOR and MAAP code.

Another important aspect of the VANESA model is the inclusion of mechanical aerosol generation, which refers to the dispersal of small droplets of melt into the containment atmosphere by gas bubbles rising through the melt. The process can occur in two ways: bursting of bubbles at the surface of the melt and the entrainment of the melt. When gas generation rate is low, gases pass through the melt as discrete bubbles. At the surface of the molten debris, the bubbles burst and throw the melt material upward in droplets of small dimension. As the rate of gas generation rises, entrainment of melt droplets at the surface of the melt can occur. Within the context of the VANESA model, only the uppermost portion of the core debris in the oxide layer participates in the mechanical aerosol production process. The particle size distribution, generation rate, and aerosol composition are considered in the VANESA model.

The mechanical aerosol generation is important during the time periods when 1) gas generation rates are high during the early transient stage of corium-concrete interaction, 2) the corium temperature is low so that the aerosol generation due to vaporization becomes insignificant at the late stage of a transient. At low temperatures in the corium, gas generation from the decomposition of concrete can still be high and the bubble bursting and/or entrainment can still be significant. The mechanical aerosol generation model is omitted in the MAAP code.

The comparisons of the ex-vessel release in MAAP and MELCOR are summarized in Table A.11.

Table A.11 Comparisons of Ex-Vessel Release

	MAAP	MELCOR
Vaporization Release		
Chemical Equilibrium	Yes	Yes
Gas Phase	Ideal fugacity	Ideal fugacity
Condensed Phases	Non-ideality by activity coefficient	Non-ideality by activity coefficient
Temperature-Dependent	Single corium temperature	Separate temperatures for oxidic and metallic layers
Oxygen Potential	Uniform	Uniform for all layers
Kinetic Rates	Omitted	Rate limitation considered
Mechanical Aerosol Generation	Omitted	Burst release and melt entrainment are modeled

29 Aerosol Dynamics

In MAAP, the removal rates of aerosol and vapor from the gas phase to surfaces or the revaporization rates of deposited materials are computed in subroutine FPTRAN. In this subroutine, the aerosol decay or removal constant is expressed by the instantaneous aerosol concentration of any species. Brownian and gravitational motions are modeled for aerosol agglomeration using the principle of similitude, which states that the determination of the size distribution function can be made universal by introducing suitable scale factors, i.e., using dimensionless parameters to express the aerosol density and the aerosol decay or removal constant. The principle of similitude used in MAAP is valid only for two limiting cases when only one of the deposition processes is operative. The two limiting cases are the aging of an initially specified aerosol, and a steady-state aerosol generated by a constant continuous source. These two cases can show how the shape of size distributions vary with time or with the aerosol source strength, i.e., aerosol concentration decay or buildup. For aerosol conditions that involve both the steady-state and decay (aging) regimes of aerosol behavior or more than one particle removal processes, MAAP uses an interpolation method between the two limiting cases and the "combining law" to represent the combining effect of the two major removal processes.

Similar treatment also is applied for particle deposition on surfaces covered by turbulent boundary layer (turbulent deposition), for deposition by inertial impaction and for particle removal by leaking, steam condensation, and thermophoresis. Empirical correlations of the removal rate constant as a function of aerosol mass density were developed for these mechanisms. It is noted that these dimensionless correlations involve many empirical constants. MAAP allows three of the empirical constants to be used as model parameters for sensitivity study. These parameters are:

	Best Estimate	Recommended Range	
		Minimum	Maximum
Collision Efficiency (No. 68)	0.33	0.33	1
Particle Collision Shape Factor (No. 38)	2.5	1	10
Aerosol Settling Shape Factor (No. 39)	1.0	1	15

The effect of such a large variation of these parameters has been investigated in the MAAP-3.0B Sensitivity Analysis [24], which shows that the upper bound of these parameters play an important role in the release of La, Sr, and Te, and on the DFs of Cs, I, and Te in the auxiliary building.

Water soluble aerosols also are modeled in MAAP to consider the condensational growth of hygroscopic nuclei in subsaturated or saturated steam environments. The model assumes:

(1) Particle size is uniform, and the aerosol behavior is monodisperse;

(2) Particle growth by condensation is more rapid than the growth by coagulation and particle removal by gravity is attained by each particle;

(3) The initial seed particle radius is empirically determined as 0.3 microns (model parameter No. 49);

(4) The criterion for choosing between the dry aerosol model and water soluble aerosol model is based on the relative values of the predicted removal constant. The larger removal constant is used for hygroscopic aerosol fallout.

The aerosol dynamics performed in subroutine FPTRAN is based on an aerosol size distribution determined by the local quantities in each control volume. However, if a group of control volumes are interconnected and the inter-mixing flows are large enough to result in effectively the same size distribution, the aerosol dynamics will be computed by the averaged quantities over the group members. The criterion of group formation is based on the product of the aerosol residence time and the removal rate. If the smaller product of all the control volumes in the group is less than 1, MAAP/PWR will take the following steps:

(1) All containment compartments are considered to be a group;

(2) All primary system nodes other than the reactor dome are considered to be a group, if recirculating flow paths in the primary system are not blocked by a water level.

MELCOR does not consider the formation of groups and does not use any averaged quantities to compute aerosol dynamics. All aerosol calculations are based on local quantities in a control volume.

MELCOR uses the MEAROS model to compute the aerosol behavior in the atmosphere of each control volume. MEAROS is a multisectional, multicomponent aerosol model, which evaluates the dynamic size distribution of each component. Different aerosol species, referred to as components, are specified such that the model can track the behavior of each species individually. A number of size classes, referred to as sections, are specified to represent the particle size distribution for the suspended aerosols. Each component can have an independent source size distribution and source rate. In MELCOR, up to 5 sections and 15 components can be specified. However, limited by the computational time, specification of only one component is recommended in the present version of the MELCOR code to achieve the best calculational time. Condensation and water can be one of the aerosol components; it is referred to as fog and its mass is calculated in the Control Volume Hydrodynamics (CVH) package. The input parameters specifying the aerosol size boundaries are the lower bound and upper bound aerosol diameters. The default values are 10^{-6} and 5×10^{-5} m, respectively. The initial mass of the aerosol water is put into the smallest aerosol section.

MELCOR treats three agglomeration processes: Brownian, gravitational, and turbulent agglomeration. The code allows many input parameters specified by the users to control these processes for sensitivity studies. The input parameters include the material density (default 1000 kg/m^3), aerosol dynamic shape factor (default 1.0), agglomeration shape factor (default 1.0), turbulence dissipation rate (default 0.001m^2/s^3), particle slip coefficient (default 1.37), and particle sticking coefficient (default 1.0).

In MELCOR, aerosol deposition and settling are treated as separate processes. Aerosols can directly deposit onto a surface (ceiling, wall, or floor) through deposition processes. Settling refers to large aerosols (formed by agglomeration) which fall onto horizontal surfaces in the control volume by gravity. There are four deposition processes: Brownian, gravitational, thermophoresis, and diffusiophoresis. Thermophoresis is the migration of aerosol particles to surfaces due to a temperature gradient in the gas boundary layer. Diffusiophoresis is the migration of aerosol particles to surfaces due to a concentration gradient.

In addition to structural surfaces, a water pool in any control volume is considered to be available for deposition and settling. Aerosols also can settle between control volumes through open flow paths, called "flowthroughs". The input parameters controlling the aerosol deposition processes are the thermal accommodation coefficient (default 1.0), particle slip coefficient (default 1.37), diffusion boundary layer thickness (default 10^{-5} m), and the ratio of the thermal conductivity of the gas to that for the particle (default 0.05).

Instead of the principle of similitude used in MAAP, aerosol dynamics in MELCOR is described by a set of ordinary differential equations. To integrate these equations forward in time, the kernel for agglomeration and the rate constants for aerosol deposition need to be known on the basis of size class used. When defined on the basis of size classes, the agglomeration kernel and the rate constants are referred to collectively as aerosol coefficients. The MELCOR/MEAROS model computes these aerosol coefficients. The pressure and temperature of the atmosphere are embedded in these coefficients and are fixed for a single set of coefficients. Because the calculation of these coefficients is time consuming, MELCOR only computes 4 sets of coefficients at points given by combinations of two temperatures and two pressures. Changing thermal-hydraulic conditions during the transient are accommodated by interpolating between these sets of coefficients. Thus, the two temperatures and two pressures should be chosen to bound the temperatures and pressures expected during the transient. This procedure imposes some constraints as summarized below:

(1) The aerosol material density is assumed to be the same for all components.

(2) The particle shape is constant.

(3) The degree of turbulent agglomeration is constant.

(4) Deposition rate is independent of particle composition. (The ratio of the thermal conductivity of air to that of the aerosol material is fixed.)

The MEAROS model for particle growth or decay due to water condensation or evaporation on the aerosols is not used in MELCOR. MELCOR uses the fog mass (aerosol water) calculations of the Control Volume Hydrodynamics (CVH) package to determine the amount of water present in the atmosphere. The model accounts both for the diffusivity of water vapor in air and for the conduction of heat associated with condensation or evaporation.

The comparisons of MAAP and MELCOR aerosol dynamics are summarized in Table A.12.

30 Engineering Safety Feature Models

30.1 Pool Scrubbing

Pool scrubbing refers to the removal of aerosols by several physical processes, which are involved in transporting gas-borne particles to the liquid interface (bubble surface) when steam/gas mixtures are bubbled through a water pool. The processes modeled in MAAP include gravitation, inertial impaction, Brownian diffusion, condensation, and thermophoresis. The term used to quantify the reduction is the decontamination factor (DF). In MAAP, pool scrubbing is considered for the upper, lower, and cavity compartments, and for the auxiliary building. In these regions, a water pool above the molten corium will remove a fraction of aerosols entrained by gases released from the corium-concrete interaction. A tube rupture in the steam generator and a pipe break in the primary system also can result in pool scrubbing of fission products and are modeled in MAAP. Pool scrubbing in the annulus compartment and ice-condenser region are not modeled in MAAP.

Table A.12 Comparisons of Aerosol Dynamics

	MAAP	MELCOR
Treatment Method	Numerical solution Aerosol decay or removal constant is related to aerosol concentration by the principle of similitude	MAEROS analytical model to determine aerosol coefficient
Aerosol Agglomeration	Brownian and gravitational	Brownian, gravitational, and turbulent
Aerosol Deposition Structures	All surfaces for condensation and gravitational settling Singe structure in each region of containment for thermophoresis Multiple structures in primary systems Structure orientation not specified Gravitational, inertial impact, turbulent, leakage, steam condensation, and thermophoresis	Multiple structures in each control volume Structure orientation specified Brownian, gravitational, thermophoresis, and diffusiophoresis
Aerosol Settling	On horizontal surfaces only	On horizontal surface only
Water Aerosol	Condensation and evaporation considered	Treated as fog in CVH package

The pool scrubbing model used in MAAP consists of the computation of DFs for the incoming aerosols and for condensable gases that form aerosols upon entering the pool. The total DF for the incoming aerosols is computed by engineering correlation of the results generated by SUPRA, coupled to the non-dimensional aerosol particle size distribution. The DFs depend on the following parameters:

(1) Gas injection mode: Two modes are modeled in MAAP for the PWR systems. A sparger is assumed for containment compartments involving corium-concrete interaction. A side vent is assumed for rupture of steam generator tubes and the auxiliary building for conservative consideration. (The DF associated with side vent injection is lowest.)

(2) Aerosol particle radius: MAAP/PWR sets the particle size as 0.01 microns for the sparger injection mode by assuming that the particles are formed by homogeneous nucleation. For the side vent injection mode, the aerosol particle mass distribution is computed by the subroutines AMDIST and ADJUST, which cover 10 particle sizes ranging 0.01 to 1 microns.

(3) System pressure: The range of system pressure covered by the model for the calculation of DF is 1 to 5 atm.

(4) Pool subcooling: The degree of pool subcooling covered by the model is up to 30K.

(5) Pool height: The maximum pool height covered by the model is 6 m for sparger injection and 1.8 m for side vent injection.

(6) Gas composition: The incoming gas composition is assumed to be hydrogen and steam for the sparger injection mode and a mixture of steam, air and hydrogen for side vent injection.

In view of the above parameters, the range of system pressure, pool subcooling, and pool height are adequate under most of the severe accident conditions. However, the assumed gas composition for the case of sparger injection (i.e., corium-concrete interaction) ignores the large quantity of CO_2 and CO released from the concrete decomposition. Since physical properties of CO_2 and CO are quite different than that of H_2, ignoring these gases would cause an uncertainty on the DF calculation.

For fission product vapors that have condensed to form aerosols upon entering a cold pool, the decontamination factors are computed by analytical models in the VAPRDF subroutine. The analytical models consider the effects of vapor condensation, inertial impaction and thermophoresis. In the inertial impaction model, MAAP assumes that a higher-velocity gas jet containing fine aerosol particles enters a pool of water. The entrainment of water at the gas-liquid interface forces water droplets into the submerged jet. The aerosol particles within the gas stream are collected by the water drops at a rate proportional to the relative velocity between the drops and the particles. The main features of the analytical model include the following:

(1) The behavior of the two-phase axisymmetric turbulent free jet is not affected by the incoming aerosol particles.

(2) After the initial expansion zone, a turbulent entrainment zone is defined based on a minimum gas velocity required for the liquid atomization process. The length of the entrainment region is determined by the mass and momentum equations involving correlations for the entrainment velocity, minimum gas velocity, and an entrainment coefficient.

(3) The average droplet size in the entrainment zone is computed using the volume-to-surface area approach and Weber number criterion. (The critical Weber number is taken as 6.)

(4) The aerosol particles are assumed to move with the jet velocity, and the droplet velocity is estimated by a force balance. The particle collection efficiency is proportional to the relative velocity between the particles and droplets.

These features are reasonable for the analytical model. The uncertainty of the computed DF depends on the assumptions and approximations related to the entrainment length, entrainment velocity, entrainment coefficient, droplet size, and velocity.

For the thermophoretic process, MAAP determines the decontamination factor by using the mass balance law and a thermophoretical deposition velocity related to the temperature gradient at the gas/liquid interface. Using the assumption that the particle concentration is proportional to the gas temperature, the DF is simplified as the ratio of initial gas temperature to the final gas temperature. It is noted that the assumption of the proportionality between the gas temperature and particle concentration was derived from an analysis involving the thermphoretic transport of small particles through a free convection boundary layer adjacent to a vertical surface [31]. The analysis is valid under two conditions: 1) natural convection boundary layer flow along a vertical surface, and 2) the product of thermophoretic transport coefficient and Prandtl number is unity. The first condition may not apply for the present pool scrubbing situation. The validity of the second condition has to be proven.

In MELCOR, the treatment of pool scrubbing is different than in MAAP. MELCOR only considers the removal of incoming aerosols in the pool; the thermophoretic process is not considered. MELCOR uses analytical models to compute the aerosol particle deposition velocity. In the model, the pool is divided into an entrance region and a bubble rise region. In the entrance region, it is assumed that the gas would attain thermal equilibrium with the pool water, and condensation would occur. Thus, an inlet scrubbing factor can be estimated on the basis of the fraction of the gas that condenses. It is assumed that the particles are swept along with the condensing steam. The DF is simply expressed as the ratio of mole fraction of noncondensables at the pool temperature and entrance pressure to the mole fraction of noncondensables before entering the pool.

In the bubble rise region, aerosol particle capture by gravitational settling, inertial impaction and Brownian diffusion are determined based on the mass and momentum conservation laws for spherical particles. Once bubbles begin to rise, evaporation will begin because the bubble pressure decreases with decreasing depth. Thus, water evaporation, which decrease aerosol removal at the gas-liquid interface also is considered in MELCOR. The net DF in the bubble rise region is the sum of aerosol removal rates by these mechanisms. The total decontamination factor for pool scrubbing is the product of the values for the entrance and bubble rise regions. The following are the restrictions of the pool scrubbing model in MELCOR:

(1) The submerged depth of the flow path must be greater than the "zero efficiency bubble rise height" in order to compute the pool scrubbing. The default value of the height specified by the user is 0.01m.

(2) Two bubble rise velocities must be specified by the user. One is the bubble rise velocity with respect to the liquid, which determines the driving force for inertial deposition in the bubble. The default value of this velocity is 0.2 m/s. The other velocity is the rise velocity of the bubble swarm used to determine the position of the bubble with respect to time and the resulting evaporation from the pool to the bubble. The default value of this velocity is 1.16 m/s.

(3) Spherical bubbles are normally assumed; however, a user can specify an elliptical shape for the rising bubbles. Elliptical correction factors are computed to modify the spherical bubble velocities. For spherical bubbles, the bubble diameter must be specified, and the default value is 0.005m. For elliptical bubbles, the major to minor axis is specified by the user, and the default value is 1.5.

The comparisons of pool scrubbing in MAAP and MELCOR are summarized in Table A.13.

Table A.13 Comparisons of Pool Scrubbing

	MAAP	MELCOR
Incoming Aerosol	Engineering correlation of SUPRA results. Parameters controlling DF are: 1. Gas injection mode 2. System pressure 3. Pool subcooling 4. Gas composition 5. Pool height	Analytical model. Pool has two regions. 1. Entrance region (vapor condensation effect) 2. Bubble rise region User-specified parameters required: bubble diameter, rise velocity, minimum pool height
Aerosol Formed by Condensable Gases		
Jet Entrainment	Analytical model involves entrainment region length, entrainment velocity, droplet size and velocity, etc.	Not modeled
Thermophoretical	Analytical model developed for natural convection boundary layer flow along a vertical surface	Not modeled

30.2 Containment Sprays

When available, containment sprays are an effective mechanism for removing fission products. An analytical model using the first-order rate equation is used in MAAP. This model shows that the rate of change of aerosol particle concentration due to containment sprays is governed by the size of the water droplet, concentration of the water droplet, relative velocity of the particles and water droplets, and the collection coefficient parameter. MAAP considers the collection coefficient parameter to be independent of the particle size distribution and species class. The spray absorption of elemental iodine is absent from the MAAP model.

MELCOR also uses the first order-rate equation to estimate the change of fission product mass in terms of a rate constant. The rate constant depends on the material class and droplet size, and is treated differently for vapors and aerosol particles. Aerosol removal by inertial impaction and interception, with diffusiophoresis effects are considered. Vapor removal by absorption using a stagnant film model to compute the absorption coefficient is included. The vapor removal model is important for the absorption of elemental iodine. The MELCOR code allows a partition coefficient specified by the user to limit the iodine absorption. The partition coefficient is defined as the ratio of the iodine concentration in the liquid droplets to the iodine concentration in the gas under equilibrium conditions. Using the partition coefficient, a user can simulate chemical solutions contained in the spray water for the control of iodine. For example, the partition coefficient can vary from 100,000 for the boric acid solution to 2,500 for the sodium thiosulfate solution.

Comparisons of the MAAP and MELCOR spray models are summarized in Table A.14.

Table A.14 Comparisons of Containment Spray Model

	MAAP	MELCOR
Aerosol Removal	First order rate equation	First order rate equation
Vapor absorption	Not modeled	Stagnant film model with partition coefficient for iodine vapor control

30.3 Ice Condenser

Removal of fission products in an ice condenser is important when early containment failure occurs and significant fission product inventory is lost from the primary system before the depletion of ice. In MAAP, aerosol removal by steam condensation and gravitational settling are modeled for the ice condenser and upper plenum compartments. The empirical models used to estimate the aerosol decay rate are the same as that used for other containment compartments as described in Section 28. Because conditions under which these empirical correlations were developed are different than that in the ice condenser region, the models may not be appropriate for the ice condenser. For example, in addition to the deposition on solid surface, there is retention by absorption in flowing liquid water film formed by the melting of ice and the condensation of steam. Diffusiophoretic deposition, which occurs as the result of steam condensation, and thermophoretic deposition, which is related to the large temperature difference between the gases entering and leaving, could be more important in the ice condenser region than in other containment regions.

MELCOR does not have an ice condenser model and therefore, no comparison can be made.

30.4 Filters

Filter systems are used as atmosphere cleanup systems in many ESF systems, such as the containment air recirculating system and the auxiliary building filter system. The filter systems are intended to trap iodine and aerosol particles from the air before they are released to the environment.

MAAP does not model filters in any flow path, except the auxiliary building. MELCOR has a simplified model to represent the removal of aerosol particles or fission product vapor in any flow path. The model requires the following parameters specified by the user:

(1) Flow path in which a filter is modeled,
(2) Type of filter, i.e., aerosol or vapor, but not both,
(3) Global DF, and
(4) Total mass loading.

31 Summary

Comparisons of the treatment of fission products by the MAAP and MELCOR codes are given in the summary tables presented at the end of each section of this report. These tables reveal large differences between the two codes. However, many differences between individual process may not make any significant impact on the overall behavior of the fission products. This behavior is strongly coupled with the thermal-hydraulic behavior predicted by the code. The release, transport, and removal of fission products are affected by the code predictions on fuel heatup, cladding failure, fuel melt, gas and structure temperatures, inter-compartment flow, natural circulation, and the corium/water and corium-concrete interactions. Thus, the fission product treatment should be reviewed on the basis of a complete examination of the MAAP and MELCOR codes. The MAAP/MELCOR comparison exercise, which presented an integrated fission product and thermal-hydraulic analysis, can be used as the basis of evaluation.

Finally, the following are comments based on this preliminary review:

(1) In the primary system, the decay energy associated with the suspended fission products is not used to heat up the atmosphere, but is converted to the heat sink with the largest surface area. This treatment would affect the temperature of the heat sink and the revaporization of volatile fission products.

(2) The omission of the mechanical aerosol generation in the ex-vessel release model could introduce uncertainties when gas generation rates are high during the early transient stage of corium-concrete interaction, and when the vaporization process becomes insignificant at the late stage of a transient.

(3) Adding absorption of iodine would enhance the containment spray model.

(4) The pool scrubbing model does not include the CO_2 and CO gases for the sparger injection mode (i.e. corium-concrete interaction). Because the properties of CO_2 and CO are different from that of H_2, the omission of CO_2 and CO would affect the empirically determined DF.

32 References

1. MAAP 3.0B Users Manual, Vol. 1 and Vol. 2, Fauske & Associates, Inc., March 16, 1990.

2. MELCOR 1.8.0: A Computer Code for Nuclear Reactor Severe Accident Source Term and Risk Assessment Analysis, NUREG/CR-5531, Sandia National Laboratory. January 1991.

3. Sharon, A. et al., "Simulation of the First 174 Minutes of the Three Mile Island Unit 2 Accident Using MAAP 3.0B," Nuclear Technology, Vol. 87, 1989, p. 1067.

4. Saha, P., "A Review of Two-Phase Steam-Water Critical Flow Models with Emphasis on Thermal Nonequilibrium," NUREG/CR-0417, Brookhaven National Laboratory, September 1978.

5. Cronenberg, A. W. et al., "An Assessment of Hydrogen Generation for the PBF Severe Fuel Damage Scoping and 1-1 Tests," NUREG/CR-4866, Idaho National Engineering Laboratory, April 1987.

6. Cronenberg, A. W., et al., "Zircaloy Oxidation and Hydrogen Generation Behavior During Severe Accidents," Proceedings 24th National Heat Transfer Conference, Pittsburgh, Pennsylvania, p. 301, August 1987.

7. USNRC, "Severe Accident Risks: An Assessment for Five U. S. Nuclear Plants, Summary Report," NUREG-1150, Second Draft for Peer Review, June 1989.

8. Bayless, P. D., "Analysis of Natural Circulation During a Surry Station Blackout Using SCDAP/RELAP5," NUREG/CR-5214, EG&G Idaho, Inc., October 1988.

9. Luckas, W. J., et al., "Assessment of Candidate Accident Management Strategies," NUREG/CR-5471, Brookhaven National Laboratory, March 1990.

10. Westinghouse PWR System Manual

11. Wright, R. W., "Experiments on In-Vessel Core-Melt Progression," International Seminar on Fission Product Transport Processes in Reactor Accidents, Dubrovnik, Yugoslavia, May 22-26, 1989.

12. Hofmann, P., et al., "Chemical Interactions of Reactor Core Materials Up to Very High Temperatures," KfK 4485, Kernforschungszentrum Karlsruhe GmbH, Karlsruhe, FRG.

13. Carlson, E. R. and B. A. Cook, "Chemical Interactions Between Core and Structural Materials," Proceedings of the First International Information Meeting on the TMI-2 Accident, p. 191, 1985.

14. Tolman, E. L., et al., "TMI-2 Core Bore Acquisition Summary Report," EGG-TMI-7385, Rev. 1, Idaho National Engineering Laboratory, February 1987.

15. Cheng, F. B., "Periodic Growth and Decay of a Frozen Crust Over a Heat Generating Liquid Layer," Journal of Heat Transfer, Vol. 103, 1981, p. 369.

16. Wang. S. K., et al., "Modeling of Thermal and Hydrodynamic Aspects of Molten Jet/Water Interactions," ANS proceedings of 1989 National Heat Transfer Conference, Philadelphia, PA, 1989.

17. Wolf, L., "Results of Preliminary Hydrogen Distribution Experiment at HDR and Future Experiments for Phase III," Proceedings of 16th Water Reactor Safety Information Meeting," Vol. 5, NUREG/CR-0097, U. S. NRC, March 1989.

18. Pong, L. T., "HECTR Assessment of Some HDR Experiments," ANS Proceedings of 1989 National Heat Transfer Conference, Philadelphia, PA, 1989.

19. IDCOR, "Technical Support for Issue Resolution," Technical Report 85.2, Fauske & Associates, Inc., Burr Ridge, IL, July 1985.

20. FAI Response to NRC Question Set 2: MAAP/PWR, October 1990.

21. Cole, Jr., R., K., et al., "CORCON-MOD2: A Computer Program Analysis of Molten-Core Concrete Interactions," NUREG/CR-3920, Sandia National Laboratory, August 1989.

22. Copus, E. R. and D. R. Bradley, "Interaction of Hot Solid Core Debris with Concrete," NUREG/CR-4558, Sandia National Laboratory, June 1986.

23. Powers, et. al., "Recent Advances in the Study of Core Debris Interactions with Concrete", ANS Transactions, Vol. 63, 1991, p. 261.

24. Mendoza, Z. T., and J. M. Hall, "MAAP-3.0B Sensitivity Analysis for PWR Station Blackout Sequences," NP-7192, EPRI, January 1991.

25. Kenton, M. A., and J. R. Gabor, "Recommended Sensitivity Analysis For An Individual Plant Examination Using MAAP 3.0B", Gabor, Kenton and Associates, Inc.

26. Ferrell, C. M. and L. Soffer, "Resolution of Unresolved Safety Issue A-48, Hydrogen Control Measures and Effects of Hydrogen Burns on Safety Equipment," NUREG-1370, U. S. Nuclear Regulatory Commission, September 1989.

27. U. S. Nuclear Regulatory Commission, "Technical Bases for Estimating Fission Product Behavior During LWR Accidents," NUREG/CR-0772, 1981.

28. IDCOR, "Technical Support for Issue Resolution," Technical Report 85.2, Fauske & Associates, Inc., Burr Ridge, IL, July 1985.

29. FAI/91-13, MAAP 3.0B PWR Revision 17, PWR 16.05 Changes, Attachment 9. Fauske & Associates, Inc., January 1991.

30. Hobbins, R. R., et al., "The Influence of Core Degradation Phenomena on In-Vessel Fission Product Behavior During Severe Accident," International European Nuclear Society/American Nuclear Society Meeting on Thermal Reactor Safety, Avignon, France, October 2, 1988.

31. Epstein, M., et al., "Thermophoretic Deposition of Particles in Natural Convection Flow from a Vertical Plate," J. of Heat Transfer, Vol. 107, 1985, p. 272.

APPENDIX B

BWR MODEL DESCRIPTIONS

J.U. Valente

Table of Contents

1 BWR Geometric Considerations

The geometry of the system modeled by MAAP consists of multiple connected regions with fixed topology. Multi-region nodalization is typically used to represent the containment and the auxiliary building. The primary system is modeled as a single pressure region but does contain many mass and energy nodes. Different types of BWR containment are built into the code -- Mark I, II, and III.

1.1 Nodalization of NSSS Thermal Hydraulics

The primary system has an internal nodalization structure consisting of mass and energy control volumes connected with flow paths and heat structures. Coarse fixed nodalization for the thermal-hydraulic model is built into the code.

Figure B.1 shows that the BWR Reactor Pressure Vessel (RPV) is nodalized into 8 control volumes representing:

1. Core.
2. Shroud Head.
3. Separator.
4. Upper Head.
5. Upper Downcomer.
6. Lower Downcomer.
7. Recirculation Loop.
8. Lower head.

Appropriate flow paths between primary system volumes also are modeled by the code. The location of the break in the primary system's pressure boundary is defined by the user.

The user cannot change the primary system nodalization in MAAP, but for most cases, the existing nodalization is sufficient. Problems may arise if natural circulation with two-phase flow becomes important for the accident sequence.

The MELCOR 1.8.0 code has no specific nodalization built into it and no predefined models for reactor system components except for the core. The system nodalization depends fully on the user, and consists of general control volumes, and flow paths. This format gives the user greater flexibility in system modeling, but also requires more input data. The approach used in MELCOR is found in some design-basis thermal-hydraulic codes. Simplifications deemed appropriate for severe accident analysis are left to the user, who usually chooses relatively coarse nodalization with a few control volumes.

1.2 Nodalization of the Fuel Region

The core region has further detailed modeling so that the behavior of the reactor core can be better predicted during and after uncovery. The existing model was developed as a simplification to obtain a fast-running code. Accordingly, the nodalization of the core is limited to a maximum of eight radial rings and ten axial planes. Radial rings have equal area fraction, and because the axial nodes are equally spaced, the subdivisions are of equal volume. The node boundaries are fixed in time and do not shift to coincide with physical demarcations, such as the height of the water and steam mixture in the coolant channel.

A further simplification of the code is the assumption of a single temperature node for the fuel-clad-channel model. The author's justification for this assumption is the anticipation that MAAP analysis will be used to predict decay power conditions when radial temperature gradients in the fuel rods are small.

In the BWR model, a single temperature node is used for the fuel rods and surrounding zircaloy channel at each core subdivision. Heat transfer by convection to the coolant and control blade heat sink are explicitly calculated, and a separate energy node is used for the control blade. MAAP calculates at each core subdivision in the BWR model:

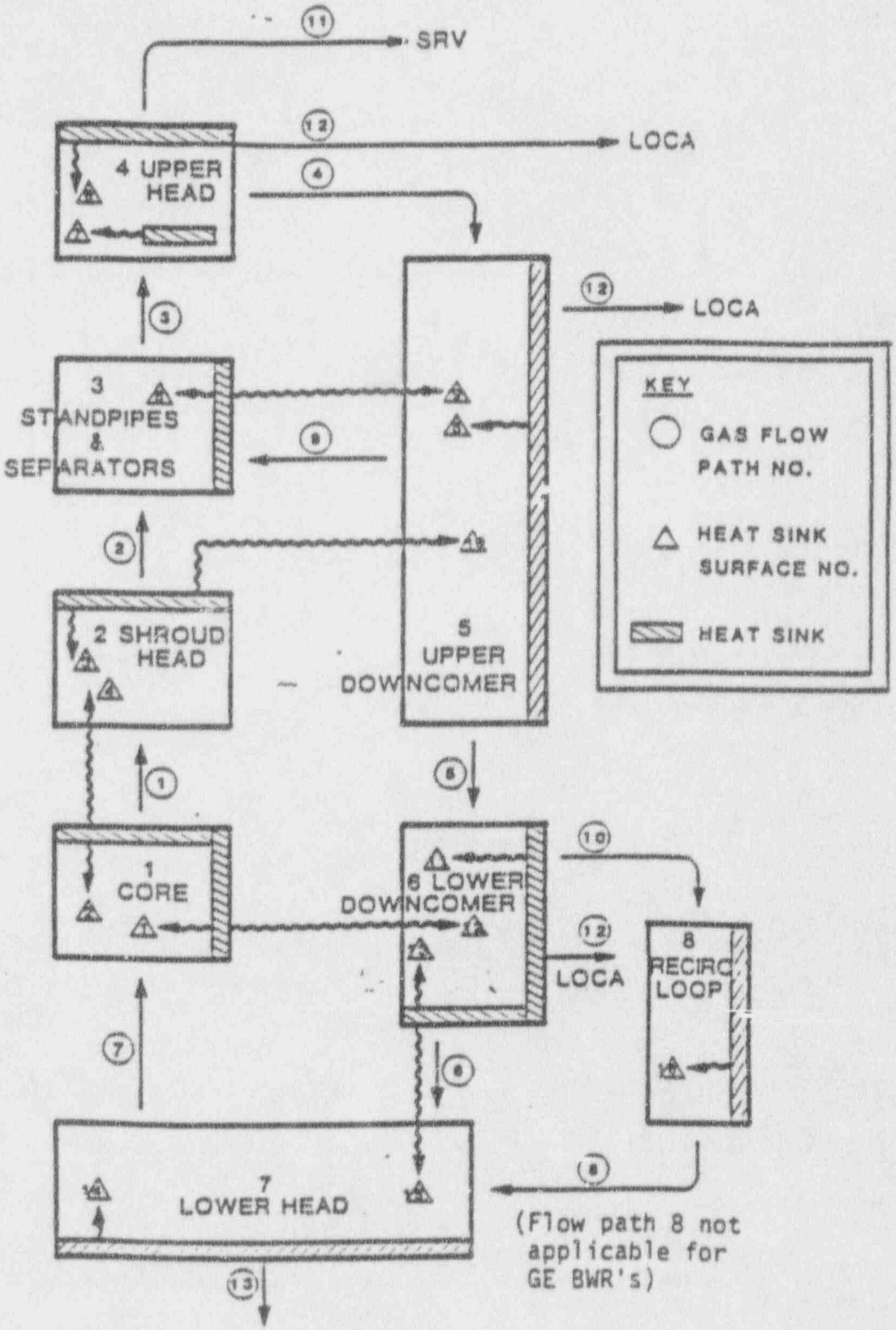

Figure B.1 MAAP 3.0B BWR Reactor Pressure Vessel (RPV) Nodalization

1. The total energy in the node.
2. The mass of fuel in the node.
3. The mass of zircaloy in the cladding.
4. The mass of zircaloy in the fuel channel segment (cans).
5. The mass of ZrO_2 in the cladding.
6. The mass of ZrO_2 in the fuel channel segment.
7. The energy in the associated control blade section.

The core model is much more elaborate in the MELCOR 1.8.0 code. Both core and lower plenum regions have a detailed, two-dimensional (r,z) subdivision. The number of radial rings in the core and lower plenum is limited to 9 and the maximum number of axial segments is 99 (a maximum of 50 in lower plenum). These divisions define individual core cells that are interfaced to principal thermal-hydraulic control volumes. Within each cell there are one or more types of components: (1) fuel pellet, (2) clad, (3) canister walls (for BWRs), (4) other structures, and (5) particulate debris. Each component may be composed of up to six materials: (1) UO_2, (2) zircaloy, (3) ZrO_2, (4) steel, (5) steel oxide, and (6) control rod poison, which may be either boron carbide (B_4C) or a silver-indium-cadmium alloy (Ag-In-Cd). Each component within a core cell has a separate temperature node. Heat transfer is modeled between components, between the outermost components in neighboring cells, and from the components and coolant. All thermal calculations are based on the internal energies of the materials. The mass and internal energy of each material in each component are tracked separately.

1.3 Heat Structures

Primary system heat sinks are modeled as two-dimensional heat slabs in MAAP 3.0B. The number and position of heat sinks in a BWR reactor pressure vessel is fixed and built into the code (See Figure B.1). The user defines (x,z) nodalization for each heat slab. In the BWR code, the following 11 heat sinks are modeled (associated boundary Thermal-hydraulic control volumes are given in parenthesis):

1. Core Shroud (Core - Lower downcomer).
2. Core Top Guide (Core - Shroud Head).
3. Shroud Head (Shroud Head - Upper Downcomer).
4. Standpipes & Separators (Separators - Upper Downcomer).
5. Upper Head (Upper Head).
6. Steam Dryers (Upper Head).
7. Upper Downcomer RPV Wall (Upper Downcomer, above top of the active fuel).
8. Lower Downcomer RPV Wall (Lower Downcomer, below TAF).
9. Recirculation Pipe (Recirculation piping).
10. Lower Head (Lower Head).
11. Shroud Support (Lower Downcomer - Lower Head).

The two-dimensional model improves the predictive capability of the fixed, relatively coarse nodalization.

The heat structure package in MELCOR 1.8.0 calculates heat conduction within an intact solid structure, and energy transfer across its boundary surfaces into control volumes. The modeling capabilities for the heat structures are general, and their number and position, geometric shape and nodalization are defined by the user. The heat structure is assumed to be solid and is represented by one-dimensional heat conduction with specified boundary conditions at each of its two boundary surfaces. The heat structure geometry could be rectangular cylindrical, spherical, or hemispherical. An internal spatial-and-time dependent power source may be specified for a heat structure. The greater flexibility of the MELCOR code is an advantage when compared with MAAP, but the MELCOR input file requires much more effort to prepare, and possibly greater nodalization because it is not two-dimensional.

2 Conservation Equations

In this section, we discuss the fundamental set of equations in MAAP and compare them to MELCOR's equations, including natural circulation. Discussion of component models, such as pumps and heat exchangers, will be covered in the section on the NSSS-ECCS interface.

MAAP uses the nodalization scheme outlined in the first section. Mass and energy are maintained for each thermal hydraulic node. These equations, taken together, regulate the flow and constituents of the flow between the nodes. There are no inertial terms in the MAAP equation set, and there is one thermodynamic pressure for the entire NSSS. Forced flows, as opposed to natural circulation flows, are based on assuring that whatever mass flow goes into a mass node, also comes out modified by any fluid source or sink. If the mass node is the core region, the quality of the exit flow, and hence, the mass split between the steam dome and downcomer region, is determined by the energy equation. Unless the vessel is flooded up beyond the separater dryer region, only dry stream is allowed to enter the steam dome. However, in simple terms, the mass equation is solved with feedwater fills and steamline flow or leaks. Distribution between regions is based on thermal hydraulic circuits which are hard-wired into the code.

This formulation lends itself to a fast-running code, which will monitor changes in flow at the vessel inlet and outlet, with the consequential effects on core cooling and core coverage. Being a source-term code, vessel inventory and fuel cooling are of prime importance during the early accident time-phase.

For the primary system regions, MAAP is, essentially, a homogeneous equilibrium model (HEM) code. However, the user does not directly specify the mass inventory of the Reactor Pressure Vessel (RPV). Instead, the code determines a core inventory based on a void fraction calculated from inlet-exit mass flows and energy generation. A drift flux model is used to determine both the core region's average void fraction and boiled-up water level.

To determine heatup of the fuel node, the code initially assumes that the nodes are covered and that all the fuel is at the coolant's saturation temperature. This state holds true until MAAP calculates that the collapsed water level outside the core shroud falls below the Top of Active Fuel (TAF). Once this occurs, MAAP begins to examine the energy balance of each fuel node, considering Zr oxidation, convection, radiation heat transport, and counter-current flow for quenching. However, the assumption of a lumped single-temperature fuel-clad-channel parameter remains. This assumption may have two limitations: underprediction of clad temperatures when the Zr-H_2O reaction is strong, and unrealistic estimates of the energy stored in the fuel and the resultant clad temperature, following node uncovery during an Anticipated Transients Without Scram scenario. The MAAP model does not release fuel stored energy until scram has occured.

MELCOR has a different modelling approach. Although it also lacks a multifluid slip model outside the core region, it allows the user to determine the number and location of the control volumes. MELCOR's control volumes solve the mass, momentum, and energy equations, including inertial effects. While the number of volumes can be much greater than the fixed regions of MAAP, the number is restricted by computational time.

These differences between MAAP and MELCOR can effect the prediction of some phenomena. Further, having a model which allows for different saturation temperatures throughout the RPV when flashing is possible can result in more accurate predictions. These differences in the models can be examined using the example of a station blackout. MAAP, with one state pressure throughout the vessel, might exhibit flashing in the lower plenum, with accompanying added steam flow into the core, whereas MELCOR might exhibit flashing only in the upper downcomer region. These differences could result in different predicted coolant flow rates to the core, with corresponding differences in core heatup and H_2 generation.

During a station blackout, after scram, the vessel inventory will tend to equilibrate in temperature. The actual response will depend on the operator's action in supplying inventory makeup. The operator should attempt to maintain a stable water level in the vessel with RCIC, but if that was not possible, then HPCI may automatically cycle between L2 and L8 (low and high RPV water levels). Therefore, when the safety relief valves (SRVs) are opened either due to high pressure or because of a forced operation brought on by the Heat Capacity Temperature Limit

(HCTL), one might observe a more accurate stratified or layered flash in MELCOR. The effect of this response would have to be reviewed in terms of vessel inventory and clad temperatures.

In the case of SRV actuation to prevent overpressure, the codes differ in the choking model used at saturated conditions (MELCOR using Moody; MAAP using Henry-Fauske), but these codes can be made nearly equivalent by the choice of contraction coefficient or flow area.

A concern may lie in the amount of mass which must be passed to allow reseating of a SRV. The quality of the flow passed by MAAP and MELCOR also should be reviewed. Whereas, MAAP is primarily HEM, it will pass only steam through the SRVs provided that the water level is below their elevation (perfect separator and dryer efficiency model function). Indeed, MAAP handles only single phase flow. On the other hand, MELCOR also does not have a slip model but it gives the user the option to have an atmosphere first flow junction. This option requires transport of all steam or atmosphere first before liquid. However, this protocol can also lead to problems, because there probably would be some water carryover through the SRVs and the blowdown inventory ratio quickly climbs as quality decreases. The use of MELCOR's separated flow could underpredict inventory loss. For MAAP and MELCOR, the same amount of energy would be required to boil-off the equivalent amount of liquid. Provided that the pressure used in MAAP is appropriately weighted for mass, and all other things are equal, MAAP should pass the same amount of mass to handle the pressurization as MELCOR. In this case, MELCOR must be configured to pass only steam through its SRVs. However, all things are not equal.

In terms of clad temperature, there may be no immediate concern while inventory makeup is available. Once this is lost and the water level has dropped to the bottom of the core, it is likely that both MAAP and MELCOR will predict lower plenum flashing during SRV opening. How the codes predict this flow split may be different. Because of MAAP's hard-wired flow circuits, all this flow may be forced into the core region, while MELCOR may direct some lower plenum inventory up through the jet pumps, which could have an effect on core cooling after the vessel inventory drops below the core. MAAP <u>may</u> overpredict the time before clad heatup during this phase, although the time difference may be very small and unimportant for some scenarios. The water left in the lower downcomer after vessel melt through can have a strong effect on fission products retained in the vessel, however.

Considering clad failure, the fluid model for MAAP allows a two-phase, core-covered height to be determined, using the drift-flux model. MELCOR calculates a two-phase pool region, but with a bubble-rise model where bubbles' density distribution and rise velocity are supplied by the user. MAAP also allows for different two-phase heights among the radial core zones. Also, MAAP calculates the rise in gas temperature up through the axial core while MELCOR uses a dz/dt approximation (what appears to be a linear averaged axial gas temperature) in the core control volume.

Three related items in a slow boil-off scenario can be compared. First, because MAAP lumps the fuel and clad together, it may underpredict the onset of clad failure. Now, this can be adjusted by the temperature input for fuel failure chosen by the user. Second, although MAAP calculates energies from the Zr-H_2O reaction, it does not track steel oxidation. This energy may be substantial for the control blades, which are steel tubes filled with boron carbide all in a steel cruciform sheath. However, before clad damage (at approximately 1700°F), there may be little oxidation of steel. Oxidation becomes important at higher temperatures. Thirdly, MAAP uses the blades as a heat sink to store and relinquish heat energy to the fluid but not to generate heat, though it does keep track of blade temperature. With the current concerns over loss of reactivity control, MAAP should incorporate a model to allow a user option for recriticality based on a loss of control material. MELCOR's model does not do this, but it is in a better position to incorporate one because it already determines the melting and relocation of control blades. Recent revisions to MAAP now allow for the relocation of the blade material based on a separate temperature.

Natural circulation flow in the primary system is an important means of mass and heat transfer that can alter a severe accident sequence. The impact of various modes of natural circulation is important during different periods of a severe accident. The natural circulation of the primary system before dryout, during a sequence with loss of forced circulation, determines core cooling in the primary system and influences the time of core uncovery. The natural circulation of gas between the core and internal structures of the RPV upper plenum could remove a substantial amount of energy from the core region during the period after dry-out, and could influence the time of core melt.

Because MAAP 3.0B does not have a momentum equation which can handle natural circulation phenomena, additional models were introduced into the code to simulate the most important modes of natural circulation in the primary system. Two modes of natural circulation are represented:

1. RPV natural circulation consisting of three loops.
2. Shroud head - Standpipe natural circulation.

In both models, natural circulation flow is calculated using a quasi-steady momentum balance along predefined loops.

In the RPV material circulation mode, there is a detailed model for natural circulation of gas (FLOW) and a very simple model for two-phase natural circulation of water. The latter is based on a manometric balance between collapsed levels in the core and downcomer (JPFLOW). This loop consists of the lower head, core, shroud head, and downcomer. The natural circulation flow of gas is calculated in the same way as in the PWR primary system except for the different nodalization, that is, it calculates the average gas temperature in PTCAL by lumping all the control volumes together. Local region gas temperatures and flows are calculated in the subroutine FLOW using quasi-steady momentum balances over predefined flow loops and an ideal gas equation of state. There are three flow loops: (1) core-shroud head-standpipes and separators-upper head-upper downcomer-lower downcomer-hyper lower head-core (2) standpipes & separators-upper head-upper downcomer-standpipes and separators, and (3) lower downcomer-recirculation loop-lower head-lower downcomer.

The coarse control volume mesh in MAAP 3.0B does not allow the natural circulation loop in the RPV to function if water is present in the lower part of the RPV. In that case, the thermal coupling between the core and the internals of the upper plenum is unrealistically low. Therefore, an additional model for natural circulation between the shroud head and separators region was introduced. It is assumed that the flow area is divided equally among up and down flows. Flow is calculated using a steady-state momentum balance, in which the gravity head is equated to the friction and acceleration pressure drop. If unidirectional flow calculated in subroutine FLOW is larger than this natural circulation flow, or if the water level is above TAF, natural circulation flow is set to zero.

There are no special models for natural circulation in MELCOR 1.8.0. However, because the topology of the control volume and flow paths is flexible, and multiple flow paths between control volumes are allowed, the user can model natural circulation phenomena during a severe accident. The one-dimensional momentum equation that is solved in MELCOR for a flow path network has gravitational heads included, in which the internal volume structure also is accounted for. This equation is expected to give good results for a simple simulation of one-dimensional natural circulation. However, the results depend on user-specified nodalization, and modeling of multidimensional counter-current natural circulation during the severe accident can be only roughly approximated.

3 Convergence Criteria and Time Step Control

Because there are no inertia terms, one might classify MAAP as quasi-steady. In many cases, MAAP smooths a change in a parameter over several time steps, thus, in a way, simulating inertia effects. This leads us into a review of the methodology for time-step selection. The user selects a maximum and minimum time-step in MAAP. In addition, the maximum allowable rates of change for mass, temperature, and pressure are supplied by the user. MAAP then calculates the rate of change of these parameters in two ways; instantaneously, based on the present values and governing equations, and averaged over a code-selected time step. The code picks the smaller absolute change predicted by these two methods, then compares these to the allowable change and, if the criteria for rates supplied by the user are met, uses the chosen size for the time step. If not, the code begins to adjust the size of the time step until the rates criteria are met. The documentation supplied with MAAP does not identify how the code chooses the initial time step when it performs its averaging (referred to as "prompt approximation"). Also, real oscillatory flows will not be predicted by MAAP (such as those produced by valve closings), just long-term trends.

MELCOR does not solve the three conservation equations simultaneously, but solves the momentum equation by velocity iteration and meets a hard-wired coded tolerance for velocity and pressure (9 percent for velocity and .05 percent for pressure). Smaller time-steps are chosen to meet this tolerance. MELCOR's authors have called these steps subcycles. The outer iteration then is the solution of the mass and energy equations using the selected velocities. Convergence again is determined, after a check to see that the equation of state pressures for each control volume obtained in this outer iteration agree within a hard-wired coded tolerance with the pressures calculated in the velocity subcycle calculation. If they do not, ultimately the momentum equation will be solved again with a tighter time-step size. Once the time step has met the requirements for conservation solution consistency, the variation of pressure and temperature over this time step is checked and must meet a tolerance of less than a 10 percent change in pressure and less than a 20 percent plus 1K change in temperature; again, all sequences are hard wired.

From these descriptions of MELCOR and MAAP, MAAP seems to offer greater user control. The method for variable rate control employed by MAAP needs better documentation in the manual, however. MAAP uses a different solution technique than the one explained for MELCOR. Although MAAP determines rates of change of key variables, there is no consistency check between something like an inner and outer loop on pressure for each control volume because only one pressure is used in the primary. Instead, once the time step is determined, based on a given estimate of the rates, MAAP determines the flow through the different flow loops (there are three closed and three open loops), and the change in pressure from the equation of state. The change in temperature is calculated from the known energy sources and flow rates. The equation set in MELCOR is far more ambitious because of the inclusion of inertia and tracking of pressure terms in each control volume. The need for accuracy is discussed elsewhere; the need for stability was our present concern.

BNL is concerned with MAAP's ability to model any real oscillations. LOCAs and simple transients may present no problems, but with the possible complexity of EOPs (Emergency Operating Procedures) the MAAP model may be cause for concern. For the source-term representative sequences, and for establishing success criteria, MAAP's approach may not be sufficient.

4 NSSS Heat Transfer Package

The energy balance in the NSSS requires models for heat transfer through the primary system's heat structures and between heat structures and the fluid that could exist in the primary system during postulated accident sequences. Since the magnitude of radiological release and the transport and deposition of fission products depends strongly on the temperature of the primary system, adequate heat transfer modeling is necessary for a source-term code.

Heat conduction is modeled in MAAP 3.0B in the form of two-dimensional, rectangular heat structures (the semi-infinite slab approximation). The primary system heat slabs are nodalized using equally spaced mesh. An implicit finite-difference iterative method is employed to solve the non-linear two dimensional heat conduction equation. If the structure's height is more than ten times its depth, axial heat conduction is ignored.

MELCOR 1.8.0 uses a finite-difference method to solve a one-dimensional heat conduction equation in rectangular, cylindrical, spherical, and hemispherical heat slabs. Temperature nodes must be located at the boundary surfaces and at interfaces between different materials, and they may be arbitrarily located within individual materials. Each surface has one of the following boundary conditions specified by the user:

1. Symmetry (adiabatic).
2. Convective with calculated heat-transfer coefficient.
3. Convective with calculated heat-transfer coefficient and a specified surface power function.
4. Convective with specified heat-transfer coefficient function.
5. Specified surface-temperature function.
6. Specified surface-heat flux function.

The convective heat-transfer coefficient is based on associated control volume thermal-hydraulic conditions.

An extremely wide range of multiphase heat-transfer regimes may be encountered in the core of reactors. The common way of predicting heat transfer in thermal-hydraulic analysis is by using a set of semi-empirical correlations developed for each convection regime that is expected in the primary system. An appropriate fluid-flow model also is required to determine the heat-transfer regime.

The coarse-control volume nodalization and simplified fluid-flow model used in MAAP 3.0B gives only a rough flow-regime differentiation. Therefore, the convective heat-transfer package is small and covers only basic types of convection.

The heat-transfer mode is determined only by the level of the steam/water mixture in the coolant channel and the location of the quench front, if the core sprays have been activated. The result is general heat-transfer cases that may apply to an individual node in the core region. If more than one case applies for an individual node (partially covered node), separate heat-transfer coefficients are calculated for each part of the node, and the results are averaged by the length fraction that corresponds to the individual heat-transfer case. The different heat-transfer cases are represented in the following:

1. Covered Node: For a node which has never been uncovered, it is assumed that its temperature will follow the temperature of the water pool. This assumption implies an infinite heat-transfer coefficient. If a node has been completely uncovered and becomes recovered, a possible temperature gradient through a steam film is assumed. A constant film boiling heat-transfer coefficient specified by the user calculates the heat-transfer resistance. When the temperature of a recovered node falls to within 10K of the pool temperature, the node status is changed to never uncovered and an infinite heat-transfer coefficient is assumed.

2. Uncovered Node: A convective heat-transfer coefficient in an uncovered node is calculated using the Dittus-Boelter correlation if the gas mixture flow is turbulent (Re > 2000). For laminar flow, a constant Nusselt number is assumed (Nu=3.7).

3. Quenching and Quenched Nodes: After activation of core sprays, the heat-transfer characteristics of an uncovered node is influenced by the movement of the quench front. The rate at which spray water flows downward is derived from a counter-current flooding limitation with K = 3.0 (K is Kutateladze number). After the quench front has passed through a node, an infinite heat-transfer coefficient is assumed.

For the control-blade heat sink, a constant heat-transfer coefficient is specified by the user. In the covered and quenched portion, the heat-transfer is augmented to maintain the temperature of the blade at the saturation temperature.

Convective heat-transfer from the heat structures in the primary system to the liquid and gas in the primary system is calculated using different correlations for forced and for natural circulation. For a covered node, the code uses the Dittus-Boelter correlation if the primary coolant pumps are running, and a natural circulation heat-transfer correlation recommended by McAdams when the main coolant pumps are tripped. To avoid numerical instabilities, MAAP limits the heat-transfer coefficient to half of the value required to equilibrate the water and the heat sink temperature in one time-step.

If the node is uncovered, a combined convective and radiative heat-transfer coefficient is calculated. The former is given as an average Nusselt number. In the case of natural circulation, the Nusselt number is correlated as a function of the Rayleigh number. The correlation parameters depend on heat-transfer surface orientation and Grashof number. For forced convection, the laminar Sieder-Tate Correlation is used for Reynolds numbers less than 2000, and a minimum Nusselt number of 2 is assumed if the Reynolds number is near zero. For Reynolds numbers greater than 6000, the Dittus-Boelter correlation is used. When the Reynolds number is between 2000 and 6000, an exponential interpolation between the laminar and turbulent correlation is used.

As with most of the other phenomena, heat-transfer is treated separately for the reactor core versus the other heat structures in MELCOR 1.8.0. The detailed COR Package calculates the thermal response of the structures in the core. The Heat Structure Package (HS) models the behavior of other heat structures, including the core shroud and upper plenum heat structures. All important heat-transfer processes are modeled in each core cell. However, since a simplified thermal-hydraulic model is used inside the core cells, detailed differentiation of convective heat-transfer modes is not possible. The MELCOR model has correlations for forced laminar and turbulent flow and natural circulation. For liquid covered components, simplified boiling curves calculate the heat-transfer coefficient. Most of the constants used in the MELCOR correlations have been implemented as sensitivity coefficients, thus allowing the user to change them.

In MELCOR, the heat-transfer model from the heat structures of the primary system has more convective modes. These are tied to the thermal-hydraulic conditions in control volumes. This heat-transfer package is very similar to those used in "design-basis" thermal-hydraulic codes.

For an accident involving core uncovery, radiative heat-transfer is important. The typical radial power profile in a LWR exhibits a significant reduction in power generation in the outer core region, which translates to a large radial temperature gradient representing a large potential driving force for radial radiative heat-transfer in the core. An approximate radial radiative heat-transfer model is incorporated in the MAAP/BWR code, which compares favorably with more detailed calculations. The model uses emissivity factors of one. Only fuel pins and channel walls are considered, and conduction heat resistance is considered only through the cans. The emissivity assumption allows more radial heat-transfer than can actually be transferred. On the other hand, the view factors are one to the adjacent nodes and zero to non-adjacent nodes, which reduces the radial transfer of radiation heat.

The radiative heat-transfer in the MELCOR core package is more mechanistic. Thermal radiation among components within core cells, across cell boundaries, and from components to steam is modeled as exchange of radiation between pairs of surfaces with an intervening gray medium. The surface emissivities are calculated for different components as a function of temperature and oxide thickness. The view factors used in the model are implemented as user-specified parameters.

The heat-transfer coefficient for radiation between the surface of a RPV heat structure and gas is calculated in MAAP 3.0B using emissivities specified by the user and the gray gas model. In MELCOR, two options are available. The user can choose between an equivalent band model or the gray gas model. The emissivities are calculated as a function of gas composition and radiation path length, which are user-specified.

5 Core-Materials Package

Most of the important differences between MAAP and MELCOR in the core materials package are closely related to the way the core and melt progression are modeled. As noted in Section 2, MELCOR has a more detailed model for core geometry (fuel pellets, gap, clad, channel, and control blades) than does MAAP. For this reason in MELCOR the core's material properties, such as the melt temperatures of the pure substances, are included. MELCOR tracks solid core debris with that which melts.

MAAP follows the temperature of the core with the fuel-clad channel as one temperature, and that of the control blade as another. The user supplies a fuel damage temperature and a fuel melt eutectic temperature. The default value for the fuel damage temperature in MAAP has been changed to 1173K, while that for MELCOR is 1200K, both these values are close to estimates of fuel damage for BWR prepressurized fuel.

In the BWR version of MAAP clad ballooning is not modelled; however, MELCOR allows the user to construct a model which is used primarily for H_2 generation. MELCOR's core thermal-hydraulic model does not allow segregation of the coolant at the core entrance to the channeled fuel assemblies as MAAP does, so ballooning will not affect the distribution of core-entrance flow among the core radial regions. However, the pressure drop in the core would be increased by the reduced flow area. MAAP can be corrected to account for the effect of the ballooning area on the surface area available for H_2 generation through an input parameter which allows multiplication of the available surface area for Zr oxidation. However, this change would be applied to all fuel clad surfaces and not just to those ballooning. Because clad strain is also a function of heat-up rate and not just temperature and pressure, the user will have to estimate this input parameter carefully.

The core-materials package in MAAP would appear to have sufficient tuning parameters to estimate the uncertainty in in-vessel hydrogen generation. However, the lack of a steel oxidation model during this phase is a deficiency which is discussed in Appendix F of this report. Still it may be satisfactory to estimate the uncertainty in hydrogen generation based on sensitivity runs which exhibit the differences produced by varying the reactive surface area of one material.

6 NSSS-ECCS Interface

The ECCS modeling capabilities in MAAP are flexible. Not only does the code handle nearly all the normal modes of ECCS operation, but it can simulate reconfigured modes of operation, such as the following:

1) Placing the HPCI or RCIC unit in the test mode to control reactor pressure, which can be simulated by appropriate modelling of the turbine steam flow and pump flow curves.

2) Using the fire water system in place of the service water system when operating the RHR in the Steam Condensing mode, which is simulated by a combination of modelling the RCIC system characteristics and RHR suppression pool cooling mode. This configuration maintains RPV inventory while removing the appropriate amount of steam from the RPV and still not overly heating the suppression pool water.

If a simulation is required of both normal and severe accident modes of ECCS operation in a single study, the turbine steam flow and pump characteristics in MAAP must be altered by the code user in conjunction with a change in parameter input. In MAAP, although RPV injection flow is affected by the vessel pressure, containment sprays are unaffected by containment pressure. This is realistic for normal ECCS spray operational modes, which take suction from the suppression pool, but may result in modeling difficulties when attempting to align a fire pump in a containment spray mode. Otherwise, MAAP's ability to model pump shut off heads is good.

Another area of consideration is NPSH (Net Positive Suchtion Head) and related topics, which are concerned with modelling of two-phase flow in pumps, especially during EOPs (Emergency Operating Procedures), which bypass CST (Condensate Storage Tank) to Suppression Pool transfer or the use of containment venting. As an example, NPSH requirements for HPCI can be modelled by setting a turbine trip of the HPCI turbine, based on a pre-selected Suppression Pool temperature, when the system's source of inventory is from the pool. This action would trip HPCI by an automatic trip. If HPCI had been manually actuated, the user could employ the operation intervention cards using the codes for pool temperature or pressure, and manually turn off HPCI. A similar ability would be desirable for the local ambient-temperature trip of HPCI (set at approximately 150°F). However, this ability is not available. This type of local trip is not unique to HPCI. A general work around for the user is to stop execution on time and manually trip the system after examining the conditions. This approach could be taken if there was sufficient physical parameter intervention logic. However, with the exception of the lack of operator intervention condition codes for the reactor building or secondary containment, MAAP covers most of the parameters tracked by the operator during severe accidents and covered in the EPGs.

MAAP assumes what the power source is for different systems, and when that source is lost, it will shed all of its system loads.

In general, MAAP has a user-friendly and very versatile control and trip system, which should allow effective simulation of system operations during normal conditions and severe accidents. MELCOR modelling of engineering safety function is based on the use of control block modules. Even pumps are modelled using control functions. Probably, most ECCS functions could be modelled with MELCOR, but it is much more laborious than MAAP. The control input of MELCOR can get very large.

7 Core Melt Progression and Vessel Failure Models and Analysis

Table B.1 compares the MAAP and MELCOR models for the Core Melt Progression (CMP) phase.

7.1 Adequate Core Cooling

The onset of fuel failure is brought about by the loss of adequate core cooling. In a design sense, this is usually defined to mean dropping the two-phase coolant level below the top of the active fuel; however, it is possible to have sufficient steam cooling of some upper regions of the core so that even the onset of pin perforation failure (around 1600°F) would not occur. The latter is a function of the core's power profile in a natural circulation flow domain. As was discussed in Section 3, MAAP predicts a two phase level for each of its axial core channels. Those regions which are above this level are considered uncovered and MAAP will determine the temperature of the gas (steam) as it travels further up the channel. The temperature of the fuel then is determined from the temperature of the surrounding gas and a known core cell power. MAAP can predict mass flow rates through the core using hydrostatic pressure differences between the inner and outer core shroud. Interestingly, MAAP 3.0B includes a simulation of counter current flow for its control volume arrangement by allowing the separator region to have simultaneous upward and downward flows with the shroud head region that lies below (see Figure B.1). Heat transfer properties and flow rates are affected by MAAP's calculation of hydrogen generation and mass distribution.

There are some major differences between MAAP and MELCOR. In MELCOR if the core is represented as two fluid volumes, lattice fuel region and the bypass region, a uniform pool height will be obtained for all the core fuel regardless, of the number of fuel cells employed. The dT/dZ algorithm takes over above the pool-atmosphere interface and performs an energy balance on the gas as it travels up a given core channel. Thus, MELCOR can track the gas temperature axially as MAAP does, but the transition between two phase and gas flow is channel-specific in MAAP but not in MELCOR. Thus, MELCOR could underpredict the fuel temperature in the hotter channels, and overpredict the time before fuel failure. However, MELCOR tracks the cladding temperature differently for the fuel and zircaloy channel, a feature that can become important for transients where fission power still allows for a pronounced temperature gradient in the fuel pin, or when clad oxidation is rapid. MELCOR uses these separate component temperatures to aid in predicting material melting (Section 5.3).

A natural circulation path can be set up with MELCOR between the upper vessel's internals and the shroud head, but this would necessitate the addition of more control volumes than is normally used (Figure B.2).

Based on this discussion, one might expect MAAP to predict the beginning of fuel heatup sooner than MELCOR during the boil-off phase of an accident which has insufficient vessel inventory makeup. The single core pool level estimated by MELCOR is an averaging tool. The greater nodalization of core components in MELCOR should be helpful in fast uncovery accidents, and in those which include fission power and recovery estimates. The MELPROG-TRAC study [1] pointed out the importance of modeling natural circulation. MAAP has added a model for heatup of the upper internals, and, in theory, MELCOR gives the user the flexibility to add whatever loops are wanted.

7.2 Oxidation and Hydrogen Generation

Three major items are discussed in this section: the material tracked for oxidation, the rate equations for oxidation, and the surface areas exposed to oxidation.

MAAP only follows Zr oxidation, using the Cathcart equation below 1850K and Baker-Just above this value. MAAP does not alter the surface area exposed to oxidation during the relocation process [5]. MELCOR follows both steel and Zr, using the Urbanic-Hendrick study for Zr [6]. The surface available for oxidation is altered during relocation. From the documentation, MELCOR alters the active surface for molten (conglomerate) debris. This debris contains Zr. There are no major differences in the Zircaloy oxidation-rate equations; however, the lack of a steel-oxidation model in MAAP is of concern. This is because a MELPROG-TRAC [1] study found that high temperatures may be experienced by the steel upper vessel internals. Also, we discussed in Chapter 2 our concern about the steel cruciform control blades and the potential for recriticality if recovery is attempted after loss of control material.

With the MAAP model, the user may be able to examine the uncertainty in the H_2 production and heat generation due to oxidation by using the two-side clad oxidation multiplier and bypassing the full channel melt-blockage model.

However, this cannot be accomplished and still leave a match between MELCOR and MAAP for steel and steel oxide leaving the vessel when it is breached. To illustrate the difference between the heat of reaction from steel oxidation vs that of zircaloy, MELCOR gives, at a reference temperature of 1500K, a value for energy release of 6.43 $\times 10^6$ J/kg of zircaloy reacted and 6.45 $\times 10^5$ J/kg for steel [7]. We note that zirconium has about twice the atomic

Table B.1 Melt Progression Model Comparison

	Adequate Core Cooling	Oxidation & H_2 Generation	Fuel Failure
MAAP 3.0B	Different two-phase fluid heights can be calculated for each axial channel Single lumped parameter temperature model Separate natural circulation paths have been added Shroud head and standpipe separators form flow loop with ½ standpipes used for upflow and the others downflow.	Zr oxidation only Cathcart ≤ 1850K Baker-Just > 1850K Channel Blockage Option Checks for steam starvation Checks for amount of Zr remaining which is unoxidized [Heatup p. 17] User surface multiplier available could be used for two sided clad oxidation. Areas for oxidation are unaltered by melt progression [Answer to Question 26 May 22 RNNG]	No gap release model Fuel failure is due to eutectic melting temperature being reached and this is user supplied
MELCOR 1.8	Core fluid control volumes overlaid by multiple core energy cells which yield different temperatures for each core component and melting temperatures for each material in a component. Pool level is the same for all axial channels in a fluid control volume Temperature of core components are effected by a dT/dZ algorithm which allows atmosphere temperature to increase axially Natural circulation can be modeled in the vessel by use of multiple control volumes	Steel, Zr oxidation Urbanic-Heidrick oxidation model for Zr In-vessel steel oxidation For particle debris it uses a user supplied particle size (COR-RM-54)) For conglomerate debris (molten material) uses coated areas	Material temperatures are tracked to determine melting When the unoxidized metal thickness reaches a user supplied value or melting temperature, the intact component fails. When the clad fails, any unoxidized solid metal (if failure was due to thickness) becomes part of the particulate debris. [p. 53 of COR-RM] A solid material transport option is available. This allows solid material which has not reached the above criteria, to be transported with molten material [p. 49 of COR-RM] Gap release due to either user supplied failure temperature or loss of intact fuel geometry

*Note - COR-RM = COR module reference manual.

Table B.1 Melt Progression Model Comparison (Continued)

Code	Core Melting	Relocation	Fuel Coolant Interactions/ Debris Cooling
MAAP	Eutectic Melting default 2500K No axial core heat transfer Control blade eutectic melting temperature of 1500K Axial heat transfer only in a channel of molten corium	Molten material can travel one axial cell per time step [p. 18, Heatup] It is possible that hydraulic pressure from upflowing steam will prevent molten material from slumping downward. Under these conditions steam flow will continue Lower tie plate fails when lowest core node becomes fully molten	Convective heat transfer is permitted between molten corium in a core node to any coolant, but heat transfer coefficient is user supplied [QCONHT] Relocation geometric effects on heat transfer are not considered
MELCOR	Material Melt Defaults SS - 1700K SS oxide - 1870K Zr - 2098K B_4C - 2620K ZrO_2 - 2990K UO_2 - 3113K Axial and radial core heat transfer	Conglomerate material has melting and freezing rates calculated and can occupy interstitial volume Relocation of molten debris is through a candling model Particulate solid debris material can be formed when - structure can no longer support it or - solid material transport option is employed Relocation of solid debris is by gravity Lower tie plate fails when temperature reaches a user supplied failure temperature	Relocation effects flow and heat transfer surfaces for particulate debris. User supplies a particle spherical diameter Conglomerate debris does not effect heat transfer model presently [p. 50 of COR-RM], however, it does effect material volume of core cell fluid volume and hence level and pressure drop [p. 47 of COR-RM]

Table B.1 Melt Progression Model Comparison (Continued)

	Vessel Attack	Core Debris Ejection	Recovery
MAAP	Flow of molten debris to lower plenum is constrained by either 1) Velocity of steam leaving the region 2) Velocity no greater than that which would release all molten material to plenum in one-time step [FLOWCP] Molten corium on upper control rod drive support goes to heating any water in the lower plenum Molten corium in lower control rod support goes to heat a head penetration which will fail when it reaches user supplied temperatures User supplies initial vessel hole size and maximum ablated size	Molten material ejected with the heaviest material first [VFAIL] Hydrodynamic flow	MAAP is able to distinguish between quenching from above vs reflooding from below
MELCOR	Particulate debris falls by gravity to lower head Conglomerate debris will candle on support structure such as control rod drive supports, and if these are already melted or unavailable, the conglomerate debris will candle onto particulate debris Detailed 1-D heat transfer failure due to melting <u>or</u> loss of yield strength minimum thickness <u>or</u> control logic for failure supplied [illegible] user The lower head has [illegible] temperature nodes. When inner node reaches failure temperature then ejection can begin and ablation is possible. When outer node reaches failure temperature, entire cell area becomes flow area	Detailed two option model 1. All debris in bottom axial segment are ejected 2. From the bottom axial segment eject - Molten steel, Zr and UO_2 - Steel oxide and control poisons available multiplied by steel melt fraction - ZrO_2 and solid UO_2 available multiplied by zircaloy melt fraction Before ejection is permitted the following constraints must be met: A total molten mass of 5000kg or melt fraction of 0.1 Hydrodynamic flow	No quenching model Areas for heat transfer and cooling are effected by relocation of debris

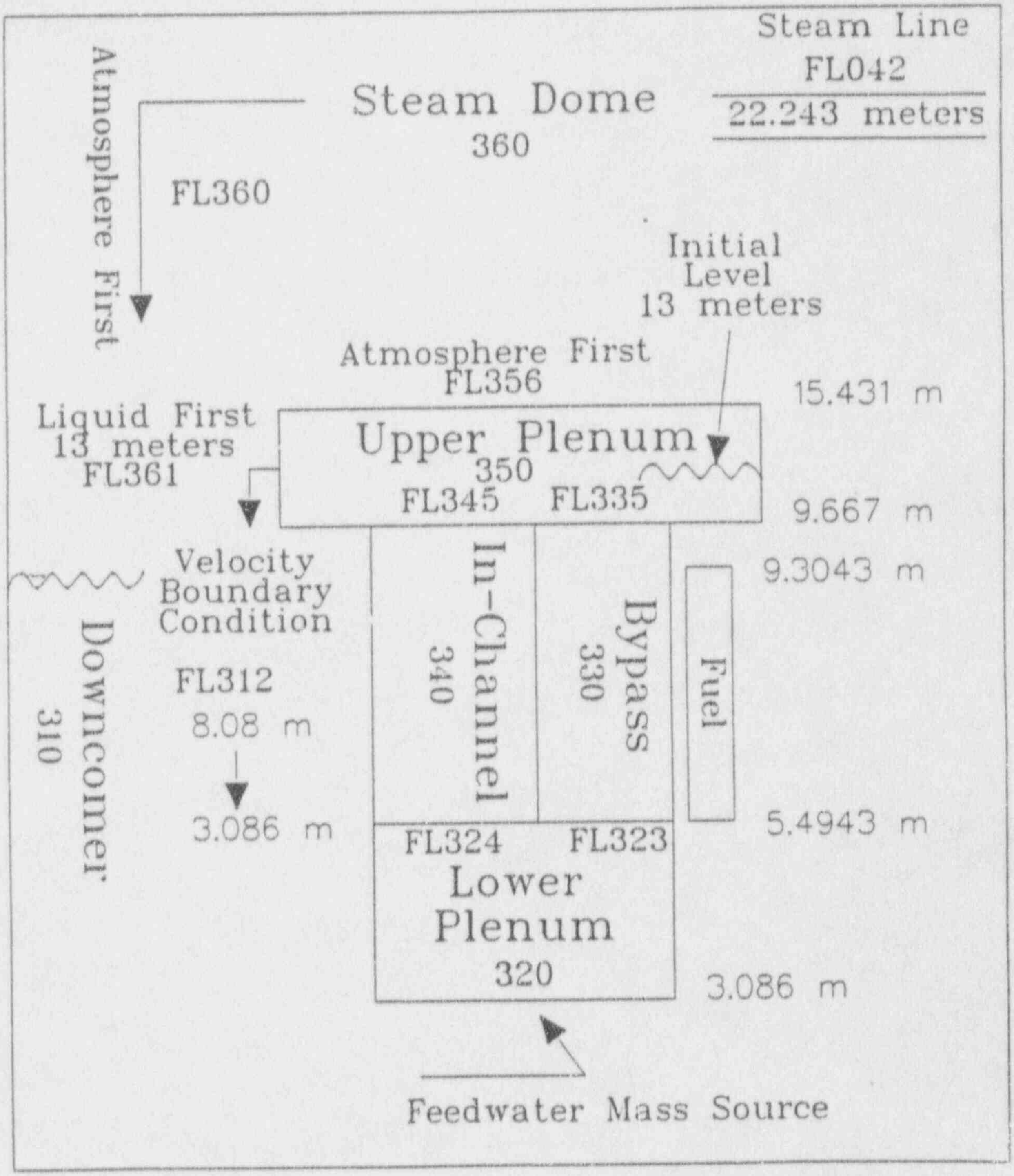

Figure B.2 MELCOR 1.8 BWR Reactor Pressure Vessel (RPV) Nodalization

weight of iron and also, that close to the melting temperature of steel (≈1400 C) iron's oxidation rate can be greater than that of zircaloy [7].

7.3 Fuel Failure

MAAP uses a very simple fuel-failure model. First, although MAAP has no gap release model, the user supplies a fuel-damage temperature (default = 1200K). At this value, fission products begin to be released from the fuel materials. Then, to handle the loss of an intact fuel geometry, a fuel-failure temperature associated with a U-Zr-O eutectic melt-temperature also is supplied by the user. When it is reached, this temperature starts the melting of the fuel and its relocation.

MELCOR uses a minimum thickness criteria for the unoxidized metal in the cladding or a failure temperature for fuel failure. The thickness value also is supplied by the user and is based on the loss of structural support. Hence, when this value is reached, relocation of solid or particulate debris begins. As applied to the cladding, the thickness of the zircaloy wall can be reduced by oxidation. If melting has occurred, MELCOR has a user option to include the transport of some of the solid material with the molten material (conglomerate debris). Gap release of fission products can be accomplished by exceeding clad damage temperature given by the user [9], or when the fuel loses its intact geometry.

The first effect of clad damage is the release of fission product gases. A fuel damage temperature is used in both codes to indicate the onset of clad damage. MELCOR, unlike MAAP, has a gap release model. That is the gap acts as a reservoir for storing gases before the cladding is damaged. MELCOR's damage temperature is measured against the clad temperature node itself. MAAP uses the fuel-clad-channel lumped temperature node. MELCOR has a fuel-to-clad gap conductance along with the ability to allow the user to alter its value during the heatup phase.

Fuel relocation affects the core's geometry, mass and the energy source distribution. Once fuel failure has occurred, the energy source from decay power will be redistributed in MAAP. If the channel flow-blockage model is chosen, and the necessary conditions have been reached to permit blockage, steam starvation and the loss of H_2 generation in that axial channel will occur. With relocation of the hot corium, attack on the lower tie plate and vessel will begin.

In MELCOR, clad relocation will begin at clad failure, or melting temperature. At fuel failure the transport of particulate or solid debris begins along with its effects on geometry changes.

7.4 Core Melting

The entry condition for core melting in MAAP is the eutectic temperature supplied by the user (discussed in Section 7.3). MELCOR allows separate melt temperatures for each material in each core component; each component has its own temperature node. Molten debris is called conglomerate debris in MELCOR. Neither code has a mechanistic Zr-U-O mixture model as will be the case in the next version of MAAP [10] (the MELCOR revision 1.8 documentation states that this will be incorporated). Table B.1 shows the default values used by the codes.

The use of Zr-U-O mechanistic mixture modelling is preferable to the simplified approach described above. MELCOR allows greater user flexibility in representing the melting and freezing phenomena along with the resulting location of the core materials before and after vessel breach. Preferential solidification or removal of core debris from the corium flow during failure of the vessel will affect the response in the containment. Recovery success also will be affected by material melt characteristics since they will affect heat transfer and flow properties.

7.5 Relocation and Blockage

Debris relocation can alter heat sources, and change heat-transfer surfaces, flow areas, and oxidation surfaces. As debris relocates, it can cause flow blockages and displace water.

MAAP has a relatively simple relocation model. Relocation begins when the eutectic melt temperature is reached. The debris will relocate only as a molten material except when the vessel head fails. The debris moves downward, moving only one axial cell in a time step. At each time-step, the relative amounts of molten and solid material are determined by assuming thermal equilibrium. This assumption is simplistic. Heat transfer would determine how much of this flowing molten material would freeze, and it might be possible for greater relocation. It is possible for a node to become frozen solid; in which case, if a channel blockage model option is chosen by the MAAP user, the code prevents any further steam flow, and oxidation also is prevented in the fuel axial channel. When the lowest node in the channel becomes fully molten, the lower tie-plate for that radial ring fails. The molten corium throughout the core then enters the lower plenum. When the material remaining in the core region drops below a fraction specified by the user, (all relocatable core material remaining in the core region) will exit the vessel along with the core material which is in the lower plenum at the time of vessel failure. Present default for this parameter is 0.1 or a core melt fraction of 90%.

In the MELCOR relocation model, the rate of downward flow is governed by thermal-hydraulic considerations and the model includes a heat-transfer coefficient supplied by the user to determine the freezing of the relocated molten material. Besides conglomerate debris, MELCOR calculates solid debris, called particulate debris, which is created when the structural support for the solid material is lost. If the core melts at the midplane first, and fuel failure occurs in a center cell node, all the fuel above that node may also be relocated provided there is sufficient free volume available in the receiving nodes. If the receiving node is fully evacuated of fuel, and the nodes above are not damaged, they will all move down in a step fashion.

MELCOR has detailed algorithms to describe how these two types of debris can occupy free volume spaces. The particulate debris relocates by gravity; the solid debris particles can fill any unoccupied free volume.

Molten material also can occupy such free volume plus a volume called the interstitial volume which cannot be occupied by solid debris. This interstitial volume is controlled by the user by means of porosities.

Flow blockage is possible in MELCOR when the molten debris occupies all remaining cell volume and freezes. There is a user-controlled method to stop oxidation on a cell-by-cell basis. In MELCOR, the lower tie-plate fails when its temperature reaches a value set by the user.

The synergistic effects of relocation are important. Relocation can alter the time-to-vessel-failure, and the thermal and physical constituents of the material ejected from the vessel.

7.6 Fuel Coolant Interaction/Debris Cooling

To model convection between the molten debris and the coolant in a core region, both MAAP and MELCOR employ a convective heat-transfer coefficient set by the user. However, the relocation model of MELCOR adjusts flow areas and heat surfaces to account for the heat transfer from and cooling of, particulate debris. Since MAAP has no model for solid debris, it retains the uncovered-node-heat-transfer correlations for gas cooling during heatup. During relocation if the core node becomes molten, another heat-transfer correlation supplied by the user is evoked (see Table B.1). This is the same convective heat transfer coefficient used in the molten corium pool to crust heat transfer when the corium enters the containment.

7.7 Vessel Attack

When the lower tie-plate fails, MAAP's lowest axial node in its hottest radial ring is fully molten. Above this node rests several other molten nodes and, possibly, some intact fuel in the highest axial nodes of the core. When the tie-plate fails, there will be a large quantity of molten corium running down the control rod guide tubes in that radial region corresponding to the core plate failure location [11]. The MAAP subroutine "FLOWCP" constrains the velocity of this molten material either to be no greater than that which would transport all the molten debris to the lower plenum in one time step, or to the velocity of steam leaving this region. The minimum value is used. The velocity of steam is determined from the following equation found in subroutine FLOWCP:

$$v_r = \frac{\sigma\,[T_{CM}^4 - T_W^4]}{\rho_g\,[h_g - h_W]}$$

Where:

σ	=	Stefan - Boltzmann constant
T_{CM}	=	Corium temperature
T_W	=	Lower plenum water temperature
ρ_g	=	Saturated steam density at primary system pressure
h_g	=	Specific enthalpy of saturated steam
h_W	=	Specific enthalpy of lower plenum water

For an RPV pressure of 1100 psia, v_r is about 450 ft/hr or .1 ft/sec. The corium flow area is that area between the control-rod guide tubes (CRGT).

With the entry of the corium into the lower plenum, heat transfer to the CRGT begins and that fraction of the corium which covers the upper part of the tube heats any water in the lower plenum. The corium surrounding the lower CRGTs is used to heat the steel penetration to its failure temperature. The user can set a time constraint on failure of the lower head, based on the time from failure of the tie plate. The MAAP documentation shows that the lower plenum fills with molten corium from the bottom up. Quoting from the subroutine FREEZE:

> "If the corium pool has risen above the transition from lower to upper CRD tubes, the thickness and mass of the corium crust on the submerged sections of the upper CRDT's are calculated."

These events can result in early failure of the lower head with a large amount of water still in the vessel at the time of failure.

At the time of failure of the lower tie-plate, MELCOR may have a mixture of molten and solid debris which will fall into the lower plenum. The lower plenum is usually modelled in MELCOR as a cell grid. This format means that debris relocation will follow a similar methodology as in the core regions, relocating down the axial cells, and there will be no radial spreading to adjacent radial cells. Candling will occur on support structures such as CRGTs. Particulate debris will fall to the lower head, where it will begin to attack the penetrations of the lower head. The penetrations will fail on reaching a temperature supplied by the user. The user can have the MELCOR code predict lower head failure when the inner-surface temperature-node of the lower head reaches a failure temperature, or a minimum solid thickness of steel remains, or by using the control logic modules of MELCOR to establish a unique failure mode.

For both MAAP and MELCOR, the initial size of the penetration failure is permitted to grow by ablation. One feature of MELCOR is that when the outer surface temperature node of the bottom head has reached melting temperature, the flow area becomes that of the lowest lower plenum cell area.

MELCOR and MAAP have quite different relocation and freezing models in the lower plenum. Again, MELCOR is more mechanistic, but vessel failure still has great uncertainty associated with it. The time from lower tie plate to head failure was found (see Appendix D) to be a major difference between these codes.

MELCOR treats oxidation in the lower plenum as it does in the core cells; MAAP does not predict any oxidation in this region.

7.8 Ejection of Core Debris

Once the lower head has failed, the debris is discharged into the containment. In MAAP, all molten debris is ejected and its rate of ejection is a function of the breach size and the vessel's pressure. The user through the input parameter "FMAXCP" can direct the code to eject core solid debris based on the core's melt fraction. After the corium is expelled, any water in the vessel is then ejected.

MELCOR has a more complicated model because its debris can be molten as well as solid. Once the criteria for head failure have been reached, MELCOR checks to see whether a total debris melt fraction of 0.1 or a total molten mass of 5000 kg has been attained. One of these two criteria must be satisfied before MELCOR ejects the core debris. The user has two options for predicting what is the ejection sequence (see Table B.1). The relocation model employed in the core is also used in the lower plenum cells, so that when a full lower cell begins to empty, the material in the upper cells can begin to locate downward.

In MELCOR, there is no radial mixing of debris so that penetration failure must occur in each radial ring in order to eject debris from that ring. However, once a penetration has failed, one user option would be to have all debris ejected from the lowest axial cell of the radial ring effected. The other option (see Table B.1) results in the ejection of all molten debris together with some fraction of solid debris.

The MAAP model (which may have water remaining in the vessel at head failure and assumes that the corium is ejected before the water) should result in a relatively conservative estimate of direct containment heating (DCH). The water-steam mixture leaving the vessel could produce the levitation velocities needed to force droplets of molten corium out of a containment cavity below the vessel. MAAP does not create multiple head failures to remove the molten debris as MELCOR does. MAAP may, however, be too optimistic in removing as much of the corium from the vessel as it does. Mechanistically, some solid debris may exist and may remain in the vessel's lower plenum after initial blowdown. If more material leaves the vessel, there will be less remaining to continually heatup the remaining intact fuel or core debris, and revaporization of fission products. Further, the sequence of ejection of vessel material can be very important, and there is some question as to whether water and gas can blow by the corium through the head failure.

7.9 Recovery

Success criteria for arresting the in-vessel melt progression is intimately tied to modeling recovery. Being able to match the cooling requirements to energy production has to be modeled carefully. Recovery is a function of both decay heat and energy release from chemical oxidation. A function of a successful recovery is the requirement for getting the coolant to the intact or degraded core configuration.

MAAP has separate models for core spray or quenching, and for reflooding from below. The latter can enhance steam flow up through the core and possibly enhance oxidation. MELCOR has no quenching model. However, MELCOR will handle material reconfiguration more mechanistically than MAAP and alter the oxidation process and location (see Sections 7.2, 7.5, and 7.6).

For the above reasons, MAAP cannot handle recovery.

8 BWR Containment Models and Analysis

As with other MAAP models, the configuration of the containment control volume is fixed. Figure B.3 is a MAAP representation of a Mark II primary containment. MELCOR affords the user greater flexibility, and Figure B.4 is one representation of a Mark II containment. However, these models are not substantially different. MELCOR has an explicit representation of the downcomers, while MAAP models the dynamics that may occur in the downcomers, but does not represent them in a separate control volume. The MELCOR model also has an upper and lower cavity control volume while MAAP models only the upper cavity. This modeling difference could be important if the corium preferentially relocates to the lower cavity, because communication between this region and the rest of the wetwell is typically through manways. Nine Mile Unit II has downcomers in the pedestal region and other Mark IIs have floor drains, which could allow this type of preferential mass transport. This arrangement would affect pressurization, local corium power density, and corium quenching. Both MAAP and MELCOR have provisions for modelling of pressure-suppression bypass, wetwell to drywell vacuum breakers, containment venting, sprays, and containment failure.

For each of the following major models discussed in this chapter, we have summarized the differences between MAAP and MELCOR in Table B.2.

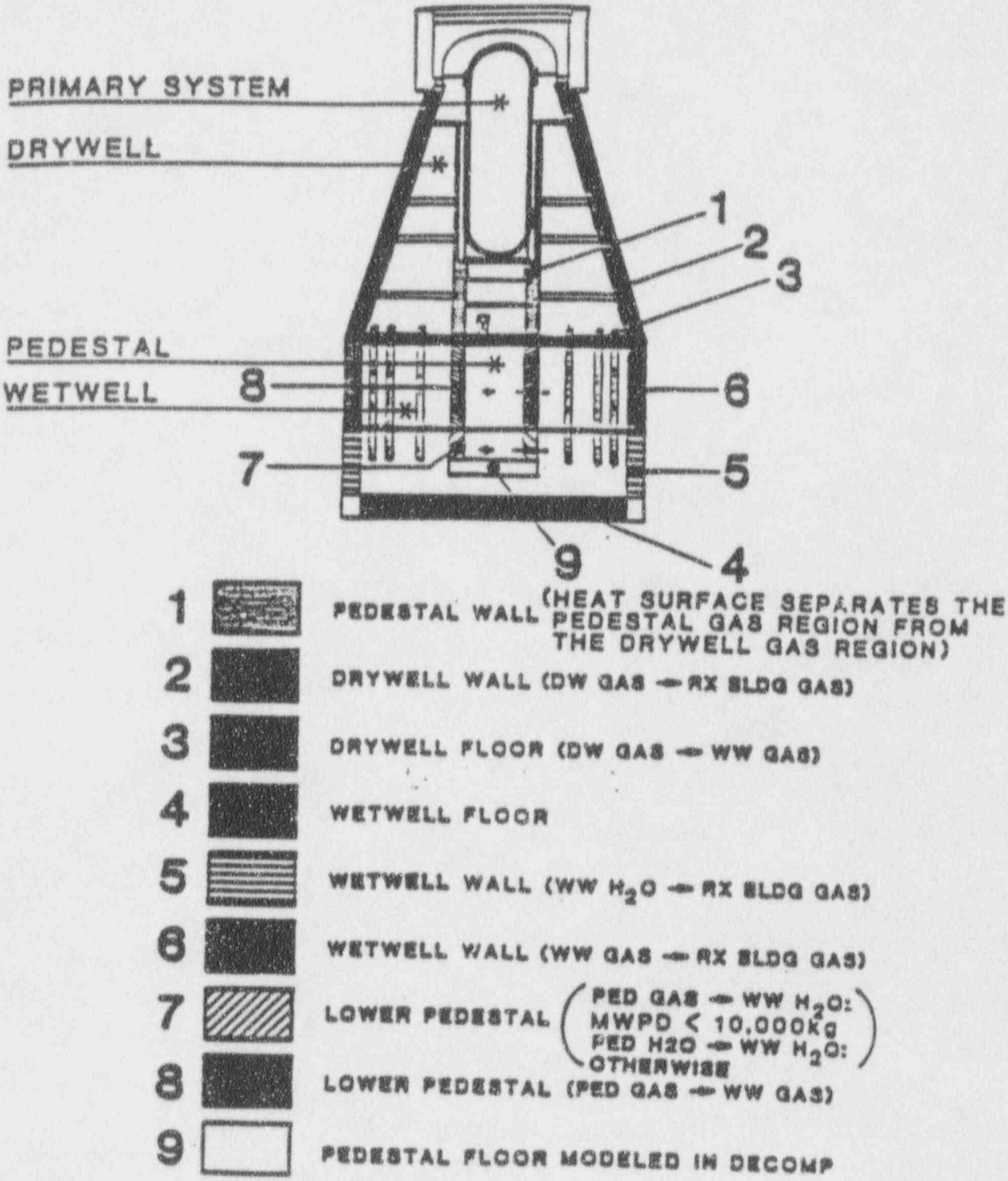

Figure B.3 Susquehanna Mark II Containment

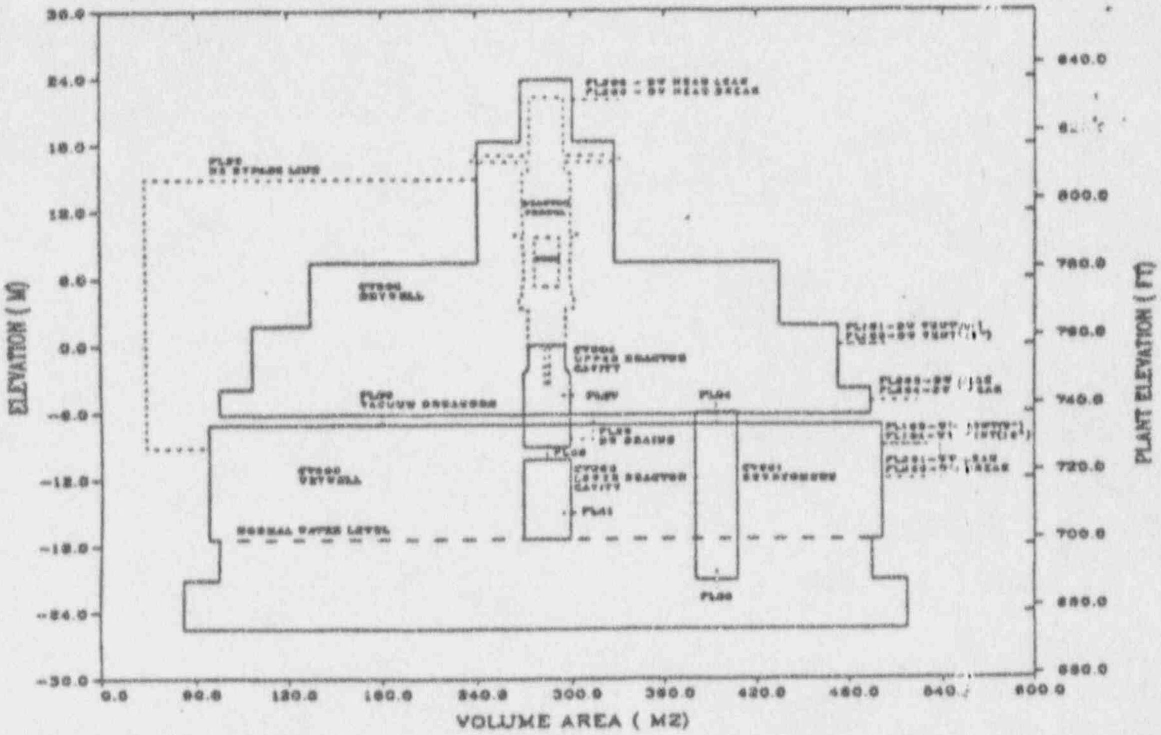

Figure B.4 LaSalle MELCOR Containment System

8.1 Direct Containment Heating (DCH)

Presently, MELCOR has no DCH model. MAAP models DCH in the PWR version, but not in the BWR version. The PWR DCH model is more of a parametric study tool than a detailed model. The corium is assumed to be in thermal equilibrium with the cavity's atmosphere, and the energy addition rate is limited essentially by the mass flow into the cavity from the RPV. The CONTAIN code [17] includes a consideration of heat transfer time constants on energy transfer.

MAAP has a model [ENTRAN] for the transport of molten corium out of the pedestal region and into the drywell if the RPV blowdown force is sufficient to levitate the molten mass. Such transport spreads the corium with its energy into a larger volume.

8.2 Steam Explosion

Steam explosions are difficult to predict. While MELCOR has no steam explosion model, MAAP attempts to simulate this phenomena. MAAP requires water to be present on the pedestal floor before vessel failure [EXVIN]. It will then track the amount of corium contained in a cylinder whose radius is related to the RPV's breach size, and whose height is the water height in the pedestal region. If there is at least 1 kg of water and 1 kg of corium present, then the corium is assumed to transfer energy to the water until it is cooled .o the saturation temperature of the water. Recent modifications to EXVIN now allow the user control over the energy transfer rate. No structural damage is assumed.

The MAAP model is parametric in nature. This classification is justified by the amount of corium assumed to interact with the water, its energy transfer rate, and the restriction to one explosion only in the pedestal region. However, the user can employ the model to evaluate the effect of energy stored in the corium (at or close to the

Table B.2 Containment Phenomena Model Comparison

	MAAP	MELCOR
DCH	Not modeled	Not modeled
Steam Explosion	Parametric study model available A geometrically derived amount of corium is assumed to equilibriate to the water saturation temperature within one time step. Reaction occurs in the pedestal region.	Not modeled
Core-Concrete Interaction	One homogeneous layer of corium modeled Ideal solution used (activity coefficients set to one) except for four compounds Sidewalls and bottom of CCI crucible are ablated equally CCI gases released from sidewalls are not permitted to react with corium debris H_2O, H_2, O_2, N_2, CO, and CO_2 are tracked. Utilizes a single melt temperature	Uses CORCON MOD2 models Allows for a maximum of three layers - metal, heavy oxides, light oxides Each phase (metal and oxides) is treated as ideal solutions. Cr tracked Different attack rates for CCI crucible sides and bottom Sidewall gas reacts with debris but at different temperatures than bottom gases Suppresses all gaseous releases other than H_2O, H_2, CO_2, and CO. Utilizes a liquidus-solidus transition temperature unique for each layer
Combustion	Detonation is not modeled Ignition - user controlled as offset of code supplied flammability map Inerting values supplied as a concentration at autoignition temperature. This results in reduction of flammability map. Propagation modeled as a spherical flame front which terminates on reaching a ceiling. Code checks concentrations to determine if downward propagations occur. Combustion completeness - Determined by concentration (burn is complete if concentration was large enough for downward propagation) and/or distance to ceiling.	Detonation not modeled but ouput indicates if detonation conditions are reached. Ignition - user supplied input Inerting - user supplied limits for H_2O and CO_2 Propagation - up, down, and sideward determined by flow paths in burning control volume. Flame can propagate to an adjacent control volume. Combustion Completeness - takes form of: 1) User input constants 2) User created function 3) Default is HECTR 1.5 Flame speed is determined by the solution of mass and momentum equation Flame speed takes form of: 1) User input constant 2) User created function 3) Default is HECTR 1.5

user's supplied eutectic melt temperature of the corium), and the various amounts of water available in the pedestal region on the performance of the containment.

8.3 Core-Concrete Interaction (CCI)

The various modelling options used during CCI are discussed in the following sections.

8.3.1 Material Location and Physical Properties

MAAP assumes that the corium melt is homogenous and that the crust has the same composition as the bulk molten pool. The material properties of the debris in the MAAP model are also homogeneous, with a single melt temperature. The internal energy of the pool is determined by tracking the composition of UO_2, Zr, ZrO_2, carbon steel, and concrete. In this manner, the solid-to-liquid fusion energies of the pool constituents are incorporated into the determination of the energy of the molten pool. Other properties such as conductivity, viscosity, and density are composition weighted.

MELCOR uses the CORCON MOD2 model for CCI and allows the debris pool to be composed of a metal layer sandwiched between two (heavy and light) oxide layers. MELCOR has a range of melting temperatures for each layer or mixture. At temperatures below the solidus and above the liquidus, each layer has its enthalpy or internal energy weighted by the material's composition. However, between the liquidus and solidus temperature, a linear extrapolation of enthalpy is used (see Figure B.5). For comparison, a mechanical mixture model is shown in this figure. MAAP uses a mechanical mixture model.

Neither model is exact. The presence of such a large mixture of elements produces a complicated phase diagram (map). This complexity affects the containment analysis in how the debris pool energy is allocated. How this energy will be used in increasing the atmospheric temperature of the containment, ablating concrete, or being retained to produce a phase change is of primary interest.

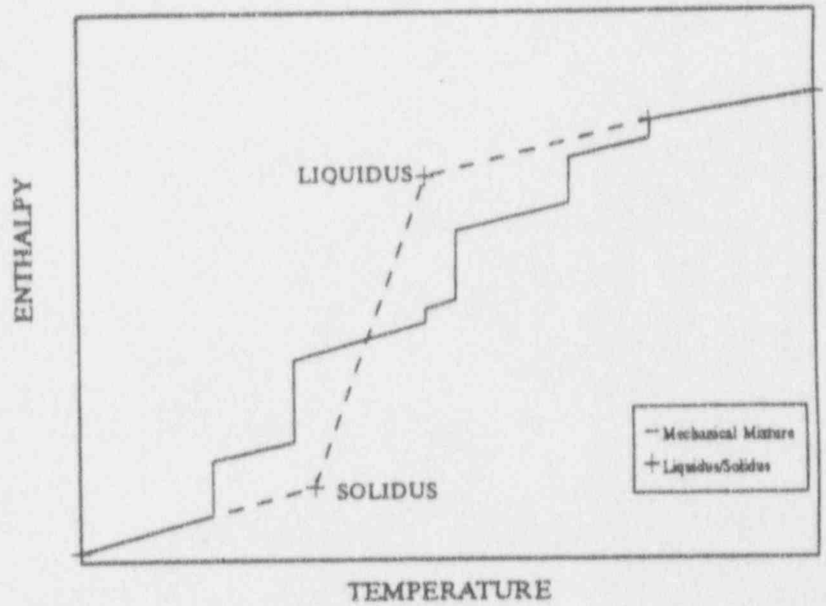

Figure B.5 Two Phase Construction for Mixture

8.3.2 Heat Transfer and Energy Generation Model

Because MAAP uses single-value melting temperatures for the debris and concrete, it simplifies the modeling of heat transfer. The heat source resulting from oxidation is volumetrically distributed in the debris (including the crust). The user supplies a convective heat transfer coefficient between the molten corium and the crust. This coefficient is used to determine the heat flux to the concrete because it affects the corium crust thickness. From this determination, a concrete temperature profile is obtained in subroutine HTWALL.

MAAP also tracks the heat into and out of the crust layer (always assumed to be at least 1 mm thick); the model assumes that there is a parabolic temperature profile in the crust. MAAP assumes heat transfer is the same to the side and bottom surfaces. However, radiative and convective heat transfer must be considered for the top surface. Knowing the heat transfer into the crust from the molten debris, the energy generated in the crust, and the heat transferred from the crust to the concrete, MAAP can determine whether or not the thickness of the crust will grow.

The situation is far more complicated in MELCOR, and we will not give details here. Considering the fact that the energy source in the debris is not uniform but distributed according to the mixture layers the metal layer produces much of the energy from the oxidation reaction, and the heavy oxide layer contains much of the decay heat. Users of CORCON have noted the presence of only a thin oxide crust because of the high rate of heat generation within the layer. Further complicating matters with MELCOR is the formation of crusts in the metallic layer, and a non-uniform heat transfer to the sides and bottom of the debris pool.

Heat transfer to the concrete is very important because it inputs concrete ablation which in turn reflects the formation of gases, pressurization of the containment, and aerosol fission products. A closer look is recommended at the way MAAP handles this, including the effects of varying the convective heat transfer term over an order of magnitude (1000-10,000 W/m^2) [19]. Some results are given in Appendix F. Possibly, a homogenized energy source, as used in MAAP is not conservative because, in reality, the energy may be concentrated at the bottom of the corium pool where the heavy oxides may gravitate.

8.3.3 Chemical Reactions in the Debris Pool

MAAP uses the subroutine METOXA to determine the chemical reactions and their energies. Other computer codes were used to formulate the necessary data for METOXA. First, the chemical equilibrium code EQUUS identified the important reactions, which were then separated into basis and auxiliary reactions. A numerical solution is first attempted on the basis reactions, and used to converge with the auxiliary reactions. An iterative process is used until the equilibrium conditions are established for a given time-step. The equilibrium constants used in this solution scheme are based on a functional fit to the Gibb's free energy functions of the reactants and products, similar to that used in VANESA. By and large, MAAP's model assumes an ideal solution of reactants and products, such that the presence of other chemical reactions does not effect the Gibb's free energy functions in determining the equilibrium constants. To correct for this non-realistic assumption, MAAP allows the user to adjust the activity coefficients of four compounds. However, MAAP does not allow the gases coming off the sides of the CCI pool to react.

MELCOR allows the gases released from the sides of the CCI pool to react. MELCOR uses the CORCON MOD2 model for chemical reactions, which also solves for the minimization of the Gibb's function. Each phase is treated as an ideal solution. Because most of the chemical reactions result from metal oxidation, MAAP and MELCOR would give different locations of this energy source with MELCOR having these reactions concentrated in the metal layer. This concentration could cause the reactants to heat up and alter the equilibrium constants and the volatile mass released. If the heavy oxide layer is the primary interface with the concrete, this chemical reaction energy will have to be transferred to the concrete if the energy is to affect the ablation process. With MAAP, the chemical energy will immediately have an effect on ablation because the metals are homogenized throughout the CCI pool. Therefore, it is not clear which model will be conservative in terms of ablation. In MAAP and MELCOR the evaporative water in the concrete undergoing ablation is released at the same temperature as the bonded water in MAAP. However, MELCOR does have an option for early evaporative water release for heat slabs.

8.3.4 Gas Transport and Generation

As discussed, the MAAP code does not allow for the reaction of gases released from CCI, if they are released from the sides of the CCI pool. Also, the MAAP model will create a pool which has straight sides due to the uniform heat transfer coefficient used on the sides and bottom. The surface area for CCI then will be governed by this geometry, and by the swelling of molten debris, which occurs as the gases lower the density of the corium.

In MELCOR, a larger surface area may be obtained for CCI because the shape of the CCI pool can be irregular. Also, MELCOR allows for the interaction of gases released from the side walls even though they are assumed not to form droplets, but to flow as a film up the sidewalls. MELCOR also allows for swelling of the corium.

8.4 Debris Spread and Coolability

There is a unique Mark II component model in MAAP for debris spread and coolability. The drywell floor has downcomers connecting the drywell and wetwell mounted within it. However, the corium would be first relocated to the pedestal floor region before being allowed to flow out to the drywell floor. MAAP's subroutine DCFAIL attempts to simulate this flow and the progressively larger flow area available to the wetwell as the corium spreads (as the corium covers more downcomers). Although the model is simple, it is an improvement over a fixed downcomer flow area, and its effect on CCI and spray effectiveness should be clear. The use of the control theory model of MELCOR would allow the user to simulate this effect also.

We now discuss the interaction of the corium with the suppression pool water in a Mark II downcomer. MAAP establishes a quenching zone [QUENCH], so that the entire suppression pool is not required to reach saturation before the corium will produce steaming. The control theory blocks or an increased number of control volumes would have to be used in MELCOR to construct such a simulation. We believe that the phenomena simulated in MAAP are real and have an effect on pressure response of the containment.

Another unique model in MAAP dealing with debris spread, which was discussed in the earlier section on DCH, involves high pressure blowdown of the RPV. MAAP's corium entrainment model [ENTRAN] allows for the removal of corium from the pedestal region by levitating steam and H_2 gas from the highly pressurized RPV. Our concern is that this model assumes that all the mass in the pedestal can be removed in 0.5 second if the conditions for levitation exist for that length of time. This flow rate may be too large, and although the debris added to the drywell atmosphere surface area will affect the short-term rate of pressurization in a conservative way, it may not conservatively handle CCI and its longer term pressurization rate. This will be seen in Appendix F where MAAP produced a shorter time to containment failure when the corium was restrained from spreading throughout the drywell.

Both MAAP and MELCOR model the cooling effects of a pool of water above the corium-debris pool. MAAP permits the user to adjust the critical heat flux multiplier (FCHF) to permit sensitivity studies.

To handle natural circulation in the pedestal region, MAAP allows flow to enter the lower opening of this region to remove heat before passing up and out through the upper openings in the pedestal. Additional drywell control volumes would have to be included in MELCOR to simulate this natural circulation.

8.5 Combustion

The major items to be considered under the topic of combustion are the following:

- ignition
- propagation
- degree of burn completion
- flame speed

MAAP includes lean and rich flammability limits (LFL and RFL) with a dependence on gaseous temperature. Functionally, an increase in temperature lowers the fuel requirements for LFL and raises them for RFL. Because combustion is permissible between these limits, the rise in temperature increases the (combustible mixture) range for flammability. The determination of ignition is based on a user-supplied offset of the LFL and RFL, thereby reducing the acceptable mixture required to a subset of the flammability regime. Figure B.6 gives an example of the LFL, RFL, and the ignition offset.

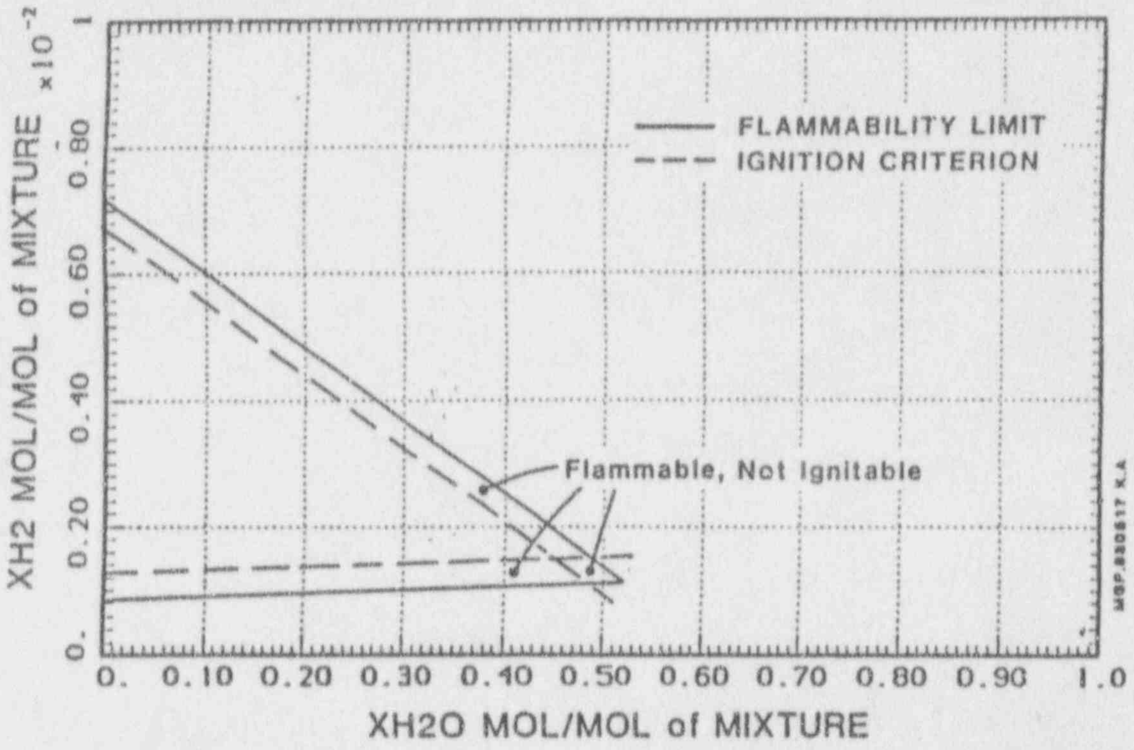

Fig . B.6 H_2-AIR-H_2O Ignition Example

An inerting gas, such as N_2, H_2O, or CO_2 also can affect the flammability and ignition regimes. MAAP uses values given by the user for both a concentration of inert gases that prevent ignition at an autoignition temperature and the autoignition temperature; in effect, this reduces the flammability regime further.

Modelers of IPEs must be careful to not always assume combustion close to the LFL, assuming this to be conservative. A greater pressure increase could be obtained if ignition was not allowed until the RFL was reached. In summary, ignition in MAAP is based on a regime developed from an offset of a flammability regime. Flammability is a function of gas temperature and the mole fraction of its constituents.

Ignition in MELCOR is determined by a an input value supplied by the user. This value is compared to a code-calculated value which is a function of both H_2 and CO mole fractions. Tests also are made to determine whether there are acceptable amounts of O_2 and of the inerting gases of CO_2 and H_2O. The limits for these gases also are user-supplied and compared to code-calculated values.

In MELCOR, the user supplies the fuel ignition concentration and the requirements for oxygen concentration. The user further supplies a requirement for the concentration of inert gases to prevent ignition. MELCOR's ignition criteria is not temperature-dependent, except in the user's prethought in choosing the limits supplied.

MAAP has different LFL and RFL limits for directing propagation, which also affect the degree of burn completion. All downward propagation burns are assumed to be 100% complete [FLAMM]. If the burns are incomplete, their burn time is decided in MAAP from the time it takes the spherical flame front to contact the ceiling of the volume within which the burning occurs. Contact with the ceiling stops the combustion. The velocity of the flame front is determined from the solution of the momentum equation, which considers buoyancy and drag.

MELCOR allows the user to input a constant for burn completeness, use a concentration dependent correlation or employ a control function relationship which the user supplies. The propagation follows the flow paths. Up, down, and horizontal paths, therefore, are dependent on the configuration of the control volumes. As with combustion completeness, MELCOR offers the same three options for flame speed: a user-supplied value, a control function, or a concentration-dependent correlation.

Both MAAP and MELCOR afford strong user control over ignition. For flame speed, MAAP allows a tunable parameter called the "flame flux multiplier", which controls combustion rate. MELCOR users can supply their own flame speed. For propagation, MAAP users are able to assure a downward complete burn by setting the ignition criteria such that the fuel concentration is higher than that necessary for a downward propagation flame; if it is not, the size of the volume and the distance to the control volume ceiling limits burn completeness. MELCOR users have full latitude in choosing burn completeness, and propagation is even permitted across control volumes.

There is a large degree of versatility in the combustion models employed by MAAP and MELCOR. However, it is the pressure that results from the burn and the remaining constituents of the gas mixture which are important. MAAP will not calculate a detailed pressurization rate but only an average value based on the burn completion and duration of combustion. MELCOR adjusts the burning rate.
MAAP's flammability regime should help its calculations because they are temperature-dependent.

8.6 Engineered Safety Features and Alternate Systems

MAAP is much more user friendly in modeling the ECCS than MELCOR, having specific, standard models for each major system. In MELCOR, the user would have to use control theory and a control volume-junction structure to accomplish a similar task. The pump models in MAAP include the effect of backpressure on their flow if the discharge is to the RPV, but not if it is to the containment.

Probably the most important Emergency Core Cooling System (ECCS) for the containment is the containment spray mode of the Residual Heat Removal System. Both MAAP and MELCOR have a spray model. MELCOR uses the HECTR code. Both models assume that the droplets are spherical, that they fall at terminal velocity, and are isothermal. Further, the models allow for condensation and evaporative mass transfer as well as for aerosol washout. Unfortunately, sprays do not remain as sprays for long in containments congested with equipment. With increased control volume nodalization, MELCOR might be able to be adjusted to address this concern. Similarly, the user input on droplet size is a parameter in MAAP that also may be used to improve the results.

Containment Venting should not be a problem for either code in terms of mass flow, though MELCOR would have inertia effects and MAAP would not. However, the effect of this difference should be small over the time phase of venting.

With respect to the pressure-suppression downcomer clearance, MAAP has no true inertia model. However, the flow between the drywell and wetwell will be smoothed if the Bernouli flow rates yield flows greater than those which would equalize drywell and wetwell differential pressure in less than 2 seconds, or 2 global time-steps. In effect, this procedure tries to accommodate the lack of inertia in the Bernouli equation. Wetwell and drywell vacuum breakers also are easily modeled by these codes.

Containment failure is usually modeled on pressure or temperature criteria. MAAP has a containment strain failure model for the Mark III containment design that can be used. Because of the complexity of containment design, it would be better to perform detailed auxiliary (non-MAAP) calculations to equate containment failure to a specified failure temperature or pressure. There will always be an uncertainty related to containment failure or breach size. Typically, the user would perform a parametric study of the release of fission product or the consequences versus a spectrum of failure or breach sizes.

A gas combustion front can be either subsonic, or sonic to supersonic in velocity; this characteristic defines the difference between a deflagration and a detonation. While MAAP does not consider detonation, MELCOR will send a message to the output file if conditions for detonation have been reached. This is the extent of detonation modeling in these codes. The pressure spike from detonation can be larger than that for deflagration, but its duration is much shorter [21]. The effect on electrical and mechanical penetrations from a local detonation are neglected.

9 Fission Product Release and Transport Models and Analysis

9.1 Classification and Grouping

MAAP tracks 22 specific fission product (FP) species (elements and compounds) which are grouped into 12 chemically similar groups (Table B.3). The initial mass of the 22 species are user supplied and are grouped, conserving their total number of moles, into the 12 chemical groups. On the other hand, MELCOR allows the user to create up to 20 material classes, though typically only 15 are used (Table B.4). These groups are based on chemical properties and allow for the assignment of the periodic table of elements. Interestingly, for each of these material classes, MELCOR distinguishes between radioactive mass and fission product mass. When a mass is released from the fuel in MELCOR, it is assigned to the appropriate material class, based upon its release in elemental form. However, the mass increment becomes part of the radioactive mass of that material class. MELCOR then assumes the elemental form will take on compound forms, for example, Cs becomes CsOH. The mass of this compound form then becomes part of the fission product mass of that material class. The properties of the fission products will be those of the material class. The user can, if desired, specify unique material classes for compounds, such as CsI. Tables B.3 and B.4, however, show that in Table B.3, only Cs takes on dual material classes in MAAP in the form of CsI and CsOH. Therefore, any concern that MELCOR may not correctly represent the appropriate characteristics (vapor pressure, for example) for the fission product <u>compounds</u>, based on elemental grouping, may not be a problem.

Whether sufficient numbers of fission product compounds are tracked in MAAP is hard to judge without first seeing whether the inclusion of more compounds, such as in MELCOR, would alter the predicted dose produced by the consequence code. In WASH 1400 [23], 25 elements were tracked, compared to 22 in MAAP. MELCOR's input follows the material classes for initialization of mass distribution. Hence, if it is planned to include more individual fission products in the material class, it would be wise to check MELCOR's Decay Heat Package. Here, MELCOR uses tabular look-up functions to determine the amount of decay heat produced at any given time by the material classes. This information is based on tracking 29 elements over time from a representative ORIGEN run. The end result is that MELCOR supplies a time dependent decay power to each class such that the fraction of the <u>total</u> decay power assigned to each class may vary in time. MELCOR thus has a varying shape and amplitude function for decay power.

MAAP, on the other hand, fixes the decay power fraction for each of its FP groups or classes and varies only the magnitude as a function of time. Decay power has a fixed shape and varying amplitude function.

9.2 Sources

In MAAP, no fission products are released from the fuel matrix until fuel damage is predicted to occur; this is usually associated with clad damage. In MAAP and MELCOR, a fuel damage temperature is supplied by the user. In MELCOR, however, fission products located in the gap before clad damage will be released upon reaching this fuel damage temperature. This format is more realistic than that in MAAP, which has a delay time associated with the release from the fuel matrix to the gap. MELCOR also will allow for fuel damage if the criteria for fuel failure has been reached. This point is dependent on minimum Zr thickness of the clad, or Zr melting temperature.

Once damage occurs, fission product release occurs for MAAP and MELCOR. MAAP classifies the fission product groups into volatile and non-volatile categories and applies different criteria to them. For volatile fission products, their release histogram from the fuel is governed solely by an exponential functional relationship of the form:

$$K(t) = Ae^{BT}$$

Table B.3 MAAP Fission Product Species

1. Nobles	7. BaO
2. CsI	8. La_2O_3 + Pr_2O_3 + Nd_2O_3 + Sm_2O_3 + Y_2O_3
3. TeO_2	9. CeO_2
4. SrO	10. Sb
5. MoO_2	11. Te_2
6. CsOH	12. UO_2 + NpO_2 + PuO_2

Table B.4 Material Classes in MELCOR

Class Name	Representative	Member Elements
1. Noble Gas	Xe	He, Ne, Ar, Kr, Xe, Rn, H, N
2. Alkali Metals	Cs	Li, Na, K, Rb, Cs, Fr, Cu
3. Alkaline Earths	Ba	Be, Mg, Ca, Sr, Ba, Ra, Es, Fm
4. Halogens	I	F, Cl, Br, I, At
5. Chalcogens	Te	O, S, Se, Te, Po
6. Platinoids	Ru	Ru, Rh, Pb, Re, Os, Ir, Pt, Au, Ni
7. Early Transition Elements	Mo	V, Cr, Fe, Co, Mn, Nb, Mo, Tc, Ta, W
8. Tetravalent	Ce	It, Zr, Hf, Ce, Th, Pa, Np, Pu, C
9. Trivalents	La	Al, Sc, Y, La, Ac, Pr, Nd, Pm, Sm, Eu, Gd, Tb, Dy, Ho, Er, Tm, Yb, Lu, Am, Cm, Bk, Cf
10. Uranium	U	U
11. More Volatile Main Group	Cd	Cd, Hg, Zn, As, Sb, Pb, Tl, Bi
12. Less Volatile Main Group	Sn	Ga, Ge, In, Sn, Ag
13. Boron	B	B, Si, P
14. Water	H_2O	H_2O
15. Concrete	---	---

Where:

K(t)	=	fractional release rate as a function of time
A & B	=	constants depending on fission products and piecewise dependent on temperature
T	=	temperature of the fuel

The non-volatiles use an Arrhenius formulation:

$$K(t) = K_o e^{-(Q/RT)}$$

Where:

K_o&Q	=	constants supplied for each fission product
R	=	universal gas constant
T	=	temperature of fuel

Another limitation on the release rate for the non-volatiles is that they can not exceed their individual vapor-saturation pressure. One could argue that they would be released as aerosols, which is what effectively occurs with the volatile fission products, but the constants employed by MAAP must not be tuned for this. This omission can have a major effect on their release if the channel fuel blockage model [25] is employed, since gas flow blockage could greatly affect the attainment of saturation pressure. We note that MAAP does not allow the presence of any aerosols in the core region, but for the volatiles MAAP will transport the vapors to the upper plenum where, if supersaturation conditions exist, they will create aerosols.

There are user options in dealing with Te; one option may either release the Te as a volatile or assume it to be transported out of the core with the corium melt, combined with the unoxidized Zr. Te would then be released in the containment as the Zr metal is oxidized during CCI. The other option would release the Te in the core after a user-supplied input value for the oxidized fraction of Zr has been exceeded. This latter option is in agreement with the NUREG 772/Kelly model.

The other major source of release of fission products to the gas stream occurs during CCI. Here, MAAP employs the METOXA subroutine group to determine the chemical equilibrium of the elements and compounds supplied by the corium and steel laden concrete. The gases are assumed to be liberated from the corium pool. Some gases would be tracked in the 12 fission-product groups; these would be added to the gas medium. MAAP developers argue that the volatility of some of the fission products is not well understood in such a corium pool as is present during CCI. Therefore, they allow for the effect of a non-ideal solution on the oxide forms of Sr and Ba as well as on Si, K, and Na. The user then can control their release rates by using activity coefficients.

There are two substantial differences from MAAP that are associated with MELCOR; both involve aerosols. The first deals with the release of aerosols from the core region. MELCOR does not limit release due to vapor pressure in the core for the non-volatiles while MAAP does. For the volatiles, although MAAP has no limitation on mass removal based on vapor pressure, it assumes vapor is transported to the region above the core and checks there for supersaturated conditions to create aerosols. However, the total core-release conditions are considered for the volatiles released and supersaturation conditions may not exist, while they might in the more active core nodes. Hence, MELCOR may predict aerosol formation when MAAP may not.

The second major difference is aerosol release from CCI. MELCOR, which uses a modified VANESA, predicts aerosol release. MAAP will not release vapor beyond its saturation pressure in the melt. The bulk of the aerosols released are expected to be of non-radioactive mass, which will have an effect on radioactive aerosols when these non-radioactive aerosols join them in the containment. However, it cannot be said that MAAP is conservative in its predictions because even though the removal rates from the containment atmosphere may be less in MAAP, there also is less of an aerosol source term and only some of this is radioactive. The timing of the containment breach and the core-concrete interaction conditions have synergistic effects on aerosol release to the environment.

9.3 Transport

In MAAP, aerosols and vapors are carried with the bulk gaseous flow. This flow is usually laden with H_2, H_2O, CO, CO_2, and N_2. In general, deposited fission products flow with the medium they are deposited in, which can be water or the corium. This statement is true for the containment. For the core, water transport of liquid fission products is not modeled. Fission products still bound up with the corium when they leave the vessel are transported with the exiting corium.

The fission product groups carry decay energy (discussed in Section 9.1). MAAP makes a distinction in energy deposition, however, based on analysis of the containment or the RPV. In the containment regions, FPs in gases heat their transport medium, and deposited vapors and aerosols heat a water pool if there is one in the control volume or the region they are in. If a water pool is not present, then they directly heat a heat slab.

For the RPV, the airborne vapors and aerosols as well as deposited vapors and aerosols heat a pre-selected heat sink.

MAAP's and MELCOR's transport mechanisms are essentially the same for vapors and aerosols. Those fission products, which are contained within the mixture or pool region of the control volumes, are transported with the mixture whether or not the control volumes are within the core or containment. MAAP's failure to transport pool deposited FP in the vessel may be a concern if in-vessel recovery actions are attempted. Transport of the FPs, which are retained in the fuel, whether liquid or solid, are relocated with the fuel; this happens while relocation is occurring in-vessel as well as at the time of vessel breach.

Table B.5 summarizes the way MAAP and MELCOR transmit the decay heat from fission products. For airborne fission products, MAAP has different criteria for the containment and vessel regions. For the vessel, this heat can only be deposited on a heat slab. In the containment, the air will be heated. In MELCOR, the user directs what fraction of the airborne FP heat in a control volume will go to the air or surface. In MAAP there are no FPs directly heating the vessel water, and, in a containment region, deposited fission products heat the water if present or a heat slab. MELCOR retains within a pool the heat produced by fission products deposited there. Also, in MELCOR, any fission products deposited on a heat slab can be directed to heat any heat slab or control volume gas.

From the above discussion, MELCOR offers far greater tunability in directing fission product heat. This flexibility can be of great importance in affecting FP transport and transition. MAAP is more limited, especially in the vessel. Presently, this limitation is most troublesome for cases involving in-vessel recovery actions, or very slow vessel uncovery (for example, having inadequate inventory make-up to the vessel). This latter case could allow substantial water to remain in the vessel during fission product release from the fuel.

9.4 Transition

In MAAP, fission product vapors follow their thermodynamic properties of condensation and evaporation. That is, they will condense within the gaseous medium to form aerosols if they become supersaturated. They will also condense on cool heat slabs to form liquids. Revaporization from the heat slabs also is permitted.

MAAP's modeling of aerosol transition, primarily its removal from gaseous transport, has removed the explicit tracking of the size dependence of aerosols. Essentially, MAAP classifies a time frame as either one of steady-state aerosol generation, or aging with no source. The simple mass balance equation for the airborne aerosol is then:

$$\frac{dm}{dt} = -\lambda m + m_p$$

Table B.5 Fission Product Release and Trasnport Models

	MAAP	MELCOR
Classification and Grouping	Tracks 22 FP elements grouped into 12 material groups. For BWR version, structural material such as Zr is not released from core material [FPGRP] The 12 material groups can take on four forms: Vapor Aerosol Deposited in water pools Retained in core or corium Total decay power (amplitude function) is calculated and is time dependent but the distribution of this gross power amongst the twelve material groups (shape function) does not vary with time	Nearly the full periodic table of the elements are assigned to material groups User can create up to twenty material groups though fifteen is standard. Compounds use the elemental properties of only one of the constituents. Within each material group, MELCOR tracks the mass of the radioactive material and fission product mass Release fractions from fuel are a function of the material group they are within Decay power is modelled as both a time dependent amplitude and shape function based on tabular look-up
Sources a) Fuel	No gap release but start of release from fuel matrix on user-supplied clad failure temperature Each tracked fission product has its own release model constants. The release model used is a function of whether the isotope is classified as volatile or non-volatile. a) The volatile fission products can use either $K(t) = A\exp(BT)$ or Cubicciotti's model (user option) b) The non-volatiles use an Arrhenius formulation $K(t) = K_o\exp(-Q/RT)$ Fission products are released as vapors only (no aerosols). Their release can be either: diffusion from the fuel matrix melting or mass transfer the from the core region limited. Te, at user option, can be released in-vessel or out of vessel during CCI	Gap release on user supplied temperature or at time of fuel failure which is based on clad zircaloy metal (unoxidized) thickness User has option of choosing CORSOR or CORSOR-M model for FP release from fuel The CORSOR model is of the form: $K(t) = A\exp(BT)$, while the CORSOR-M model is an Arrhenius formulation The release constants are functions of the material group (same constant for each element in a given material group) Non-radioactive materials, including cladding, canister and control rods follow same release rates as the radioactive FP in their material class [RM-RM-6] Fission products can be released as vapors or aerosols if saturation conditions are exceeded [RN-RM-7] Te release in-vessel can be reduced by the presence of non-oxidized Zr

Table B.5 Fission Product Release and Transport Models (Continued)

	MAAP	MELCOR
b) CCI	During CCI, oxidation and reduction reactions occur which cannot only result in chemical changes but alter the major release of the FP from the corium pool Documentation appears to support the release only of vapors within the pool "Once the FP leaves the core or core debris, its chemical state as given by the 12 FP groups is frozen" Ba and Sr are two of the major radioactive aerosols one might expect from CCI; these have user input activity coefficients for tunability	During CCI, a modified VANESA model has been incorporated. This includes: aerosol generation rates concentration of aerosols in gaseous release from the pool Aerosols and vapors are released from the pool. Most aerosols are non-radioactive aerosols, however, these non-radioactive aerosols can have an effect on the aerosol removal mechanisms in the containment.
Transport	Aerosols and vapors are transported with H_2O and H_2. Deposited fission products transport with water between containment regions. This is not done between reactor vessel regions. Fission products in the corium, exit vessel with the corium In containment: -airborne FP heat the air -deposited FP heat a water pool if present, otherwise a selected heat slab In-vessel regions: -airborne and deposited FP heat an individual heat sink	Aerosols and vapors are transported with H_2O and H_2 FP products in the water pool for a control volume are transported with the pool Fission products in the core material are transported with it during relocation. This could be in solid or liquid form. In any control volume: airborne FP have user supplied split of this heat between the atmosphere or surface of any volume. A water pool is classified as a surface. decay heat from FP deposited on any heat slab can be directed to any heat slab or control volume gas phase fission products deposited in a water pool directly heat that pool

Table B.5 Fission Product Release and Transport Models (Continued)

	MAAP	MELCOR
Transition	FAI developed aerosol mass conservation equation utilizing decay terms. Does not track particle (aerosol size) Separate mass conservation equation not written for each chemical component Aerosol decay constants exist for: -settling -diffusion phases (steam condensation) -thermophoresis -impaction -hydroscopic aerosol modeling considered to enhance settling Combining laws for decay constants are employed Aerosols created from super saturated vapors User input includes two shape factors used in the decay constants and aerosol seed radius used in the hydroscopic aerosol model Spray removal model Pool scrubbing model based on functional fit to SUPRA numerical experiments Aerosols evaporate to keep a vapor saturated, MAAP handles revaporization	Uses MAEROS which is a sectional aerosol code - it tracks particle size Separate mass conservation equation written for each chemical component Coagulation due to: -Brownian Motion -gravity -turbulence Particle deposition due to: -settling -diffusion -thermophoresis Particle growth due to condensation of water vapor on particles User can set all material classes to a single component in the solution of the MAEROS sectional solutions. This would accelerate the solution time [RM-RN-p.7] Aerosols created from supersaturated vapors Resuspensions of aerosols deposited on surfaces are not predicted in MELCOR Spray model based on the HECTR code is employed. It removes both aerosols and vapors Pool scrubbing model exists for aerosols only Filter model removes aerosols and vapors. Could be used in Reactor Building of BWR TRAP-MELT2 code equations are utilized to determine condensation and evaporation of vapors from aerosols and heat structures Aerosols created from supersaturated vapors

Where:

m	=	mass of aerosol
m_p	=	source term
$-\lambda m$	=	removal term with λ being the decay constant

Then, for the steady-state formulation we have:

$$\frac{dm}{dt} = 0 = -\lambda m + m_p$$

and for the aging state with no source:

$$\frac{dm}{dt} = -\lambda m$$

MAAP solves these equations by using the formulations previously discussed (Section 9.2) to determine "m_p" and by determining the decay constant "λ". MAAP determines the decay constants for a variety of removal mechanisms by determining a functional relationship for "λ", based on numerical experiments which used a size-dependent solution for aerosol behavior. The exact solution of λ is determined by solving for two-dimensionless scaling parameters "Λ" and "M", which depend on the geometric and physical properties of the aerosol material, such as its viscosity, the height of the volume containing aerosol, the density of aerosol particles, and temperature. In addition, there are two user-supplied aerosol shape factors that have defaults supplied by the MAAP developers.

The aerosol physics model also employs combining and interpolation laws. If more than one removal mechanism is occurring, the model has combining laws to determine the appropriate decay constant for the mass conservation equation. Interpolation is used to treat conditions between steady-state and aging. Log-log plots are presented by the MAAP developers to compare the accuracy of their interpolation schemes to more detailed aerosol codes products and equipment. From these comparisons, it appears that the MAAP model can do well when there is a well-defined demarcation between times when a strong source exists and then ceases. In a severe accident, there would be times of strong sources mixed with times of weak source. It is not explicitly clear what the degree of accuracy would be when these conditions were reviewed on a linear time plot. MAAP has a model for hydroscopic aerosols, which can result in greater sedimentation rates than their dry aerosol model. This wet-aerosol sedimentation rate can be controlled by the user's choice of the particle size of the initial seed (dry aerosol).

MAAP has two other special aerosol removal mechanisms. The first is water spray entrainment. This model determines the reduction in gaseous suspended aerosols as a function of the radius of water spray droplets, their settling velocity, and collection efficiency; this last is determined by experiment. This model must be used with an assumption about the size of the droplets of spray because containment sprays will impinge on drywell equipment.

Pool scrubbing is the second special component of the mechanism for removal of aerosol. The MAAP model also includes pool scrubbing of vapors, which when passed through a pool, are anticipated to condense into liquid aerosols and also be removed. MAAP's models are based on a functional fit to numerical experiments performed with the SUPRA code, using the following parameters:

1) Mode of gas injection (such as downcomers and side vents)

2) Geometry (height of pool)

3) Gas condition (steam mass fraction and composition)

4) Pool conditions (subcooled, pressure)

5) Aerosol characteristics (size)

We have suggested that MAAP does not keep track of the particle size of the aerosol during its transition or removal from the atmospheric calculation. So, to correctly use the SUPRA data, MAAP looks up a interpolated table for a predefined spectrum of particle sizes, which are functions of viscosity, gas temperature, mass generation rate, and user-tunable shape factors. MAAP effectively calculates a decontamination factor for each particle size and then mass-averages these to get a total DF.

The characteristics of the aerosol model in the MELCOR code can be found in Table B.5. It is interesting that the MELCOR mass conservation equations for aerosol are general ones. They are not limited to the steady-state and aging regimes. Further, they are sectionalized into size groups for aerosols, and give the user the flexibility to separately track different compositions. Because MAAP appears to solve the aerosol mass equation for only one large composition of all tracked groups, it would be interesting to see whether MELCOR would yield similar results by just using only one composition, as in MAAP, and then comparing this to a case where multiple mass equations (based on multiple compositions) were employed. Our particular concern is that MAAP may not correctly determine the release functions of aerosol fission products which have different dominant times of production. If there was a late production of a given FP aerosol, which is released into an atmosphere of an aging aerosol environment, then MAAP would shift to a steady-state continuous-source solution [$dm/dt = 0 = -\lambda m + m_{product}$], not considering the potential of the new source of single composition on a size section, quite different from an aerosol atmosphere which had been aging for some time. MAAP would simply remove the new component using the same decay constant as the aged aerosol. However, MAAP would remove it on a rate commensurate with its relative mass composition in the total aerosol atmosphere. The end result may be an overprediction of the removal rate of the newly predirected aerosol's versus what a sectional code such as MELCOR would yield.

10 References

1. R.J. Henninger, et al., MELPROG/TRAC: Update and Applications," Fourteenth Water Reactor Safety Information Meeting, 1986.

2. D.L. Hagrman, "Materials Properties Models for Severe Core Damage Analysis," Informal Report, EGG-CDD-5801, May 1982.

3. A. Sheron, et al., "Modification for the Development of the MAAP-DOE Code, Vol. V: A Model for Recovery of a Badly Degraded Core WBS 3.4.7," DOE/ID-10216, Vol. V, December 1988.

4. Deleted.

5. R.N. Ng, Letter to C.G. Tinkler, May 22, 1990, Answer to Question 26.

6. V.F. Urbanic, et al., "High-Temperature Oxidation of Zircaloy-2 and Zircaloy-4 in Steam," Journal of Nuclear Materials, 75 (1978) p. 251-261.

7. R.M. Summers, "Core (COR) Package Reference Manual," Part of MELCOR documentation package, Version 1.8.0, p. COR-RM-35, February 17, 1989.

8. "LWR H_2 Manual," NUREG/CR-2726, August 1983.

9. R.M. Summers, "Core (COR) Package Reference Manual," Version 1.8.0, p. COR-RM-6, February 17, 1989.

10. M.G. Plys, et al., "DOE Modifications to the MAAP Code, Volume VI: Core Melt Progression Modeling and Benchmarking," Task 3.4.8, DOE/ID-10216, Vol. VI, August 1989.

11. R.N. Ng, letter to C.G. Tinkler, May 22, 1990, Answer to Question 9.

12. J.U. Valente, et al., "MAAP 3.0B Review," TER #1, May 1, 1990.

13. R.K. Cole, et al., "CORCON - Mod 2: A Computer Program for Analysis of Molten Core Concrete Interactions," NUREG/CR-3920, August 1984, p. 40.

14. ibid, p. 14.

15. J.U. Valente, "MAAP 3.0B/BWR Review, Technical Evaluation Report 2, core Melt Progression," August 1990.

16. "MAAP 3.0B Users Manual," subroutine FLAMM.

17. D.C. Williams, et al., "CONTAIN Analysis of Direct Containment Heating Events in the Surry Plant," ANS Thermal-Hydraulic Division Proceedings of the ANS/ENS International Meeting, October 31 - November 4, 1988, Washington, D.C.

18. R.K. Cole, et al., "CORCON - Mod 2: NUREG/CR-3920, August 1984.

19. "MAAP 3.0B Users Manual," subroutine DECOMP, p. 25.

20. ibid, subroutine DECOMP, p. 10

21. ibid, MAAP Appendix 3B/P, "Introduction to Combustion," p. 1.

22. J.U. Valente, "MAAP 3.0B/BWR Review, Technical Evaluation Report 2, Core Melt Progression," August 1990.

23. "Reactor Safety Study - An Assessment of Accident Risks in 25 Commercial Nuclear Power Plants," WASH-1400 (NUREG-75/014), October 1975.

24. J.U. Valente, "MAAP 3.0B/BWR Review, Technical Evaluation Report 3, Severe Accident Containment Modeling," October 1990.

25. J.U. Valente, "MAAP 3.0B/BWR Review, Technical Evaluation Report 2, Core Melt Progression," August 1990.

26. J.U. Valente and D. Mirkovic, "MAAP 3.0B Review", May 1990 and Ref. 2 and 3 above.

27. K.Y. Suh, "MELCOR Modifications for the Development of the MAAP-DOE Code, Vol. VII: A Best-Estimate Correlation of In-Vessel Fission Product Release for Severe Accident Analysis, WBS 3.4.8," DOE/ID-10216, Vol. VII, January 1989.

28. M.A. McCartney, M.G. Plys, "Modifications for the Development of the MAAP-DOE Code, Volume I: A Mechanistic Model for Core-Concrete Interactions and Fission Product Release in Integrated Accident Analysis, Task 3.4.3," DOE/ID-10216, Vol. I, Nov. 1988.

APPENDIX C

PWR MELCOR/MAAP Comparative Analysis

J.W. Yang and S. Nimnual

Table of Contents

1 Introduction

This appendix summarizes the MELCOR analysis, as well as the comparison with a MAAP analysis, of a small break LOCA accident sequence for the Zion plant. The work was performed under Task 5 of the MAAP Code Evaluation Program. Task 5 calls for Brookhaven National Laboratory to perform a comparative analysis with the MELCOR and MAAP codes. The MAAP analysis utilizing MAAP 3.0B, Revision 17.0, was provided by Fauske & Associates, Inc. Version 1.8.0 of the MELCOR code was used.

BNL started the MELCOR analysis by using a Zion input deck prepared previously, in an unrelated 1988 study, for the steady-state calculation of a station blackout sequence. This input deck was updated for the latest version of the MELCOR code and was modified to simulate a small break LOCA transient. Considerable changes were made to input parameters related to the control volume thermohydraulics, flow paths, and heat structures. Nodalizations in the primary system and containment were expanded. Because the MELCOR code has not been systematically tested for the PWR systems, BNL encountered many problems related to numerical instability. These problems were successfully eliminated by improving the time-step control, by nodalization, and by selecting proper input parameters. Due to the limited time allocated for this project, BNL has not systematically tested its numerical strategies and has not evaluated the uncertainties of the predicted results.

2 Description of Accident Sequences

The accident sequence selected for the analysis was a small break LOCA. The basic assumptions defining the sequence are listed below:

1. The break size is 2.5 inches in diameter.
2. The break location is at the intermediate leg with an elevation of 6.37m above the reference elevation of the bottom of the reactor vessel.
3. There is no power scram delay time.
4. Coolant pumps are immediately turned off, and no pump coastdown is modeled.
5. No feed water is provided to the secondary side of the steam generators.
6. Accumulators are activated when the primary system pressure reduces to 4.137 Mpa, and are stopped when the pressure increases above 4.2 Mpa.
7. Failure of both high-pressure and low-pressure core injection is assumed.
8. Containment sprays are activated when the containment pressure reaches 0.262 Mpa, and terminated when the pressure is below this level.
9. The refueling water storage tank provides water for the containment sprays. The initial water mass in the tank is assumed to be 127,000 Kg (i.e. 10% of normal capacity). The reduced water mass was assumed to limit the spray operation to enhance containment pressurization and the potential for hydrogen combustion.
10. The recirculation mode of containment spray operation was assumed to be not operational.
11. A 15.2 cm high curb is located at the opening of the tunnel section of the reactor cavity compartment to limit the quantity of water flowing back to the cavity.

The small break LOCA sequence is characterized by a rapid depressurization of the primary system, rapid core uncovery and heat-up, and early failure of the reactor vessel. The sequence allows us to evaluate the effects of accumulator injection, break flow, and early release of hydrogen and fission products into containment. However, the potential for natural circulation in the primary system and direct containment heating at the time of vessel breach are reduced due to the depressurization in the primary system.

3 Basic Modeling

3.1 MELCOR

The 4-loop Zion plant was modeled as a 2-loop system in the MELCOR analysis. The three intact loops were lumped together to represent the unbroken (UB) loop and the loop which contains the small pipe break was referred to as the broken (BK) loop. The pressurizer was assumed to be located in the BK-loop. Each loop was represented by five control volumes: the hot leg, the rising tubes and down tubes in the steam generator, the intermediate leg, and the cold leg. The reactor vessel was modeled as four control volumes: the upper plenum, core, lower plenum, and downcomer. The flow bypass channel was lumped together with the lower plenum. Thus, a total of 14 control volumes were used to represent the primary system and the reactor core. In addition, the pressurizer, quench-tank, accumulators, the secondary side of the steam generators, and the turbine room were modeled separately as additional control volumes. Zion has four accumulators in each of the four coolant loops. Three accumulators were connected to the cold leg of the UB-loop, and one accumulator was connected to the BK-loop. The turbine room was modeled as the control volume, which receives steam released from the secondary side of the steam generators. A total of 24 flow paths, including the release from the quench tank and the break flow from the intermediate leg to the lower compartment of the containment, were modeled for these control volumes. A schematic diagram of the control volumes and flow paths is shown in Figure C.1.

In MELCOR, the reactor core includes the region of the lower plenum directly beneath the core. Both the core and lower plenum are divided into concentric radial rings and axial segments. A particular radial ring and axial segment designates a cell. This analysis has six axial segments and four rings in the core regions, i.e. 24 cells. The active fuel was distributed in five axial segments. The top axial segment, which does not contain fuel, represents the unheated section of the fuel rod. The fuel pellet, cladding, control rod and structural materials were treated separately as different components within each cell. Each component is represented by a single temperature.

Six axial segments and four radial rings were used to model the lower plenum region. Three of the axial segments represent the lower core plate, mixer, and bottom support plate. The core and lower head nodalization is illustrated in Figure C.2. Four penetration tubes, one in each radial ring, were modeled in the present analysis. The penetration tubes were attached to the lower vessel head, which has four nodes that are used to estimate the thermal response after the core debris relocates into the lower plenum. The penetrations or the lower head failed when temperature of a penetration or the innermost lower head node reached the failure temperature specified by the user (1273 K).

The containment was divided into four control volumes: the reactor cavity, the upper, lower, and annulus compartments. These compartments were connected by two flow paths between the reactor cavity and the lower compartment: the instrument tunnel and the reactor vessel/shield wall annular passage. Containment sprays were modeled in the upper compartment. The spray water was split into the lower and annulus compartments and collected in the sumps. Failure of the upper compartment was assumed when the containment pressure reached 1.027 Mpa, 149 psia, the failure pressure specified by the user. The failure area was assumed to be 0.65 m^2. The analysis also assumed a leakage in the annular compartment when the containment pressure reached 0.44 Mpa, as specified by the user. The leakage area was assumed to be 0.495 cm^2.

In summary, the Zion plant was represented by 27 control volumes, 32 flow paths, and 119 heat structures, as shown in Tables C.1 to C.3. Table C.1 shows the altitude, volume, height and flow area of each control volume. The characteristics of each flow path, such as elevation of junctions, initial fraction of open area, path orientation, and flow conditions, are summarized in Table C.2. The nodalization, geometry, altitude, orientation, and surface boundary conditions of each structure are given in Table C.3. In Table C.3, the degassing model was applied to some containment concrete structures. This model allows the concrete structure to release water vapor and carbon dioxide when the structure reaches the user-specified temperatures. The degassing model increases the containment pressurization rate as additional gases are released to the containment.

3.2 MAAP

The nodalization used in MAAP to represent the Zion plant are shown in Figures C.3 and C.4. A comparison with the nodalization used in MELCOR reveals the following differences:

1. MAAP divides the upper region of the reactor vessel into two nodes: upper dome and upper plenum; MELCOR considers this region as one control volume.
2. MAAP lumps the downcomer and the lower plenum as one node; MELCOR separates these two regions into two control volumes.

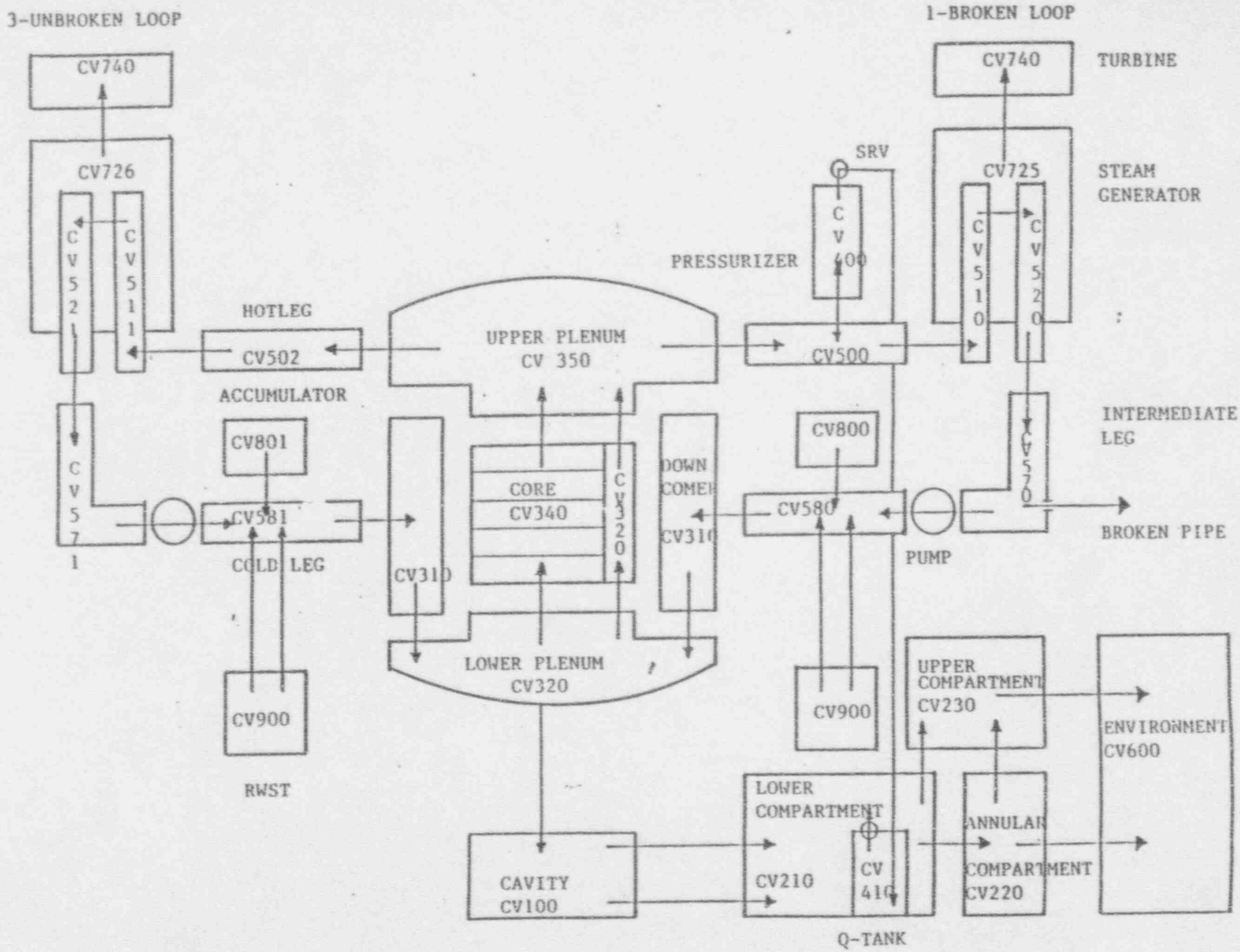

Figure C.1 Zion Control Volume Schematic (two-loop) for MELCOR Simulation of S-LOCA

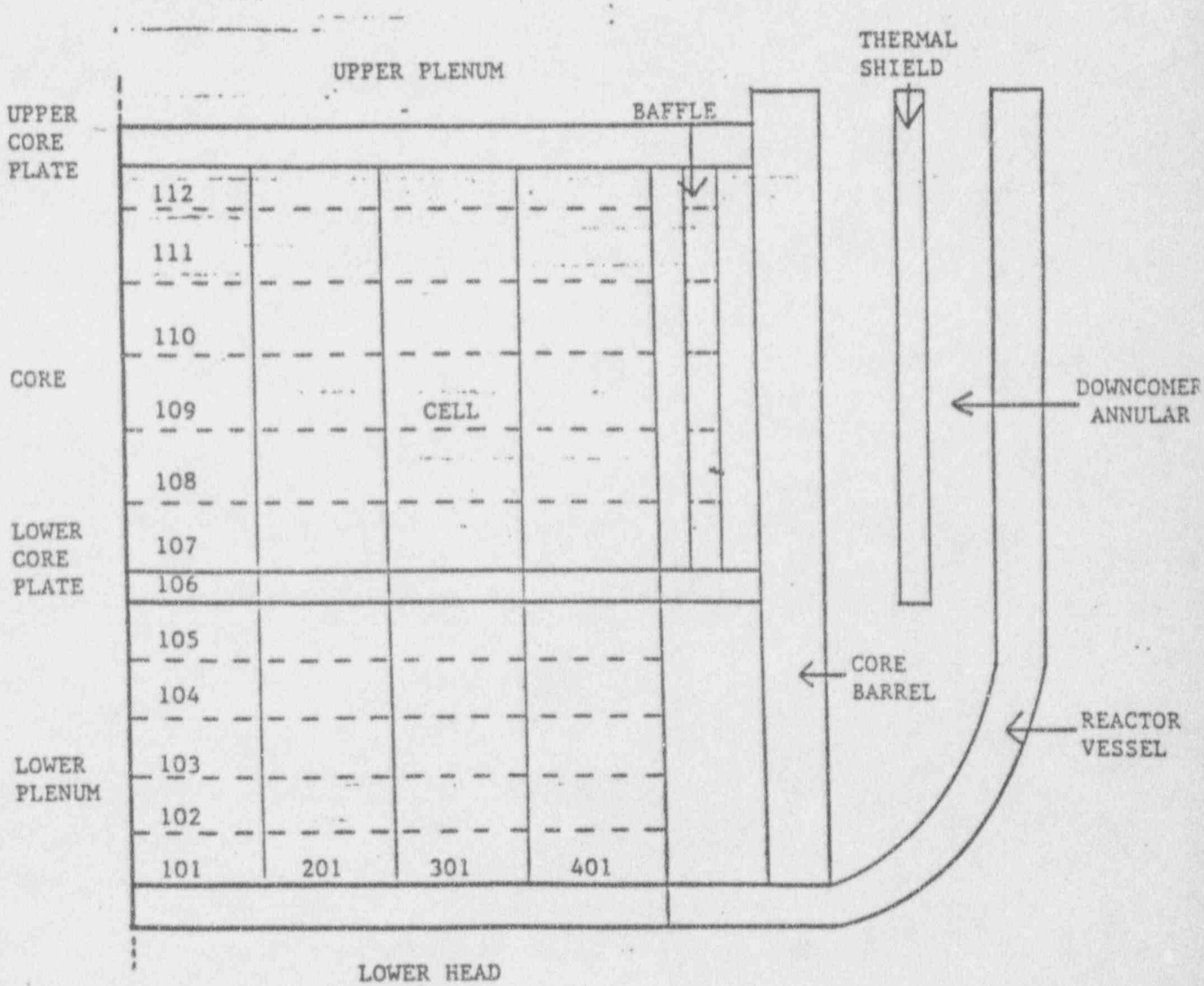

Figure C.2 Core/Lower Plenum Nodalization

Table C.1 Control Volumes Modeled in MELCOR Analysis

CV100 NAME ——> CAVITY

ALTITUDE	VOLUME	HIGHT	AREA
-6.043	0.0		
0.0	162.60	6.043	26.9170942
7.975	217.00	7.975	6.8137931

CV210 NAME ——> LOW-COMP

ALTITUDE	VOLUME	HIGHT	AREA
2.533	0.0		
15.093	12100.	12.560	963.375796

CV220 NAME ——> ANN-COMP

ALTITUDE	VOLUME	HIGHT	AREA
2.533	0.0		
15.093	9716.	12.560	773.089172

CV230 NAME ——> UPP-COMP

ALTITUDE	VOLUME	HIGHT	AREA
15.093	0.0		
67.150	58900.	52.057	1131.45206

CV310 NAME ——> DOWNCOMER

ALTITUDE	VOLUME	HIGHT	AREA
1.3272	0.000		
3.1012	5.5998	1.7740	3.15659526
10.483	26.6868	7.3818	2.85662034

CV320 NAME ——> LOWER-PLENUM

ALTITUDE	VOLUME	HIGHT	AREA
0.1445	0.0000		
0.6211	1.4842	0.4766	3.11414184
1.0976	5.4836	0.4765	8.39328437
1.3272	7.9255	0.2296	10.635453
3.1012	23.7349	1.7740	8.91172492
7.1592	32.5611	4.0580	2.17501232

CV340 NAME ——> CORE-CHANNEL

ALTITUDE	VOLUME	HIGHT	AREA
3.1012	0.0		
7.1592	19.937	4.0580	4.91301134

CV350 NAME ——> UPPER-PLENUM

ALTITUDE	VOLUME	HIGHT	AREA
7.1592	0.00		
10.483	36.89	3.3238	11.0987424
10.61	37.53	0.127	5.03937008
11.209	46.614	0.599	15.1652755
11.584	51.487	0.375	12.9946667
11.958	55.378	0.374	10.3983957
12.333	57.957	0.375	6.88266667
12.708	58.884	0.375	2.472

CV400 NAME ——> PRESSURIZER

ALTITUDE	VOLUME	HIGHT	AREA
8.324	0.0000		
12.559	0.98826	4.235	0.233355372
13.626	3.531	1.067	2.38307404
26.46	49.415	12.834	3.5751909
27.526	51.958	1.066	2.38555347

CV410 NAME ——> Q-TANK

ALTITUDE	VOLUME	HIGHT	AREA
1.0088	0.000		
2.4231	25.485	1.4143	18.019515
3.8373	50.97	1.4142	18.0207891
3.8473	50.971	0.0100	0.1
27.526	52.472	23.6787	0.0633903044

CV500 NAME ——> HOT-1LEG

ALTITUDE	VOLUME	HIGHT	AREA
7.9557	0.0000		
8.324	1.6952	0.3683	4.60276948
8.6923	3.3867	0.3683	4.59272332
10.100	3.5403	1.4077	0.109114158

CV502 NAME ——> HOT-3LEG

ALTITUDE	VOLUME	HIGHT	AREA
7.9557	0.0000		
8.324	5.0802	0.3683	13.7936465
8.6923	10.16	0.3683	13.7925604
10.10	10.621	1.4077	0.327484549

CV510 NAME ——> SG1-TRISE

ALTITUDE	VOLUME	HIGHT	AREA
8.8117	0.0000		
9.3405	0.5789	0.5288	1.09474281
9.8692	2.0466	0.5287	2.77605447
10.398	3.9454	0.5288	3.59077156
10.399	3.9464	0.001	1
21.403	15.291	11.004	1.03095238

CV511 NAME ——> SG3-TRISE

ALTITUDE	VOLUME	HIGHT	AREA
8.8117	0.0000		
9.3405	1.7367	0.5288	3.28422844
9.8692	6.1398	0.5287	8.32816342
10.398	11.836	0.5288	10.7719365
10.399	11.839	0.001	3
21.403	45.873	11.004	3.09287532

CV520 NAME ——> SG1-TDOWN

ALTITUDE	VOLUME	HIGHT	AREA
8.8117	0.0000		
9.3405	0.5789	0.5288	1.09474281
9.8692	2.0466	0.5287	2.77605447
10.398	3.9154	0.5288	3.59077156
10.399	3.9464	0.001	1
21.403	15.291	11.004	1.03095238

CV521 NAME ——> SG3-TDOWN

ALTITUDE	VOLUME	HIGHT	AREA

Table C.1 Control Volumes Modeled in MELCOR Analysis (Continued)

CV100 NAME ——> CAVITY

ALTITUDE	VOLUME	HIGHT	AREA
-6.043	0.0		
0.0	162.68	6.043	26.9170942
7.975	217.03	7.975	6.8137931

CV210 NAME ——> LOW-COMP

ALTITUDE	VOLUME	HIGHT	AREA
2.533	0.0		
15.033	12100.	12.560	963.375796

CV220 NAME ——> AIRI-COMP

ALTITUDE	VOLUME	HIGHT	AREA
2.533	0.0		
15.093	9710.	12.560	773.089172

CV230 NAME ——> UPP-COMP

ALTITUDE	VOLUME	HIGHT	AREA
15.093	0.0		
67.150	58900.	52.057	1131.45206

CV310 NAME ——> DOWNCOMER

ALTITUDE	VOLUME	HIGHT	AREA
1.3272	0.000		
3.1012	5.5998	1.7740	3.15659526
10.483	26.6868	7.3818	2.85662034

CV320 NAME ——> LOWER-PLENUM

ALTITUDE	VOLUME	HIGHT	AREA
0.1445	0.0000		
0.6211	1.4842	0.4766	3.11414104
1.0976	5.4836	0.4765	8.39328437
1.3272	7.9255	0.2296	10.635453
3.1012	23.7349	1.7740	8.91172492
7.1592	32.5611	4.0580	2.17501232

CV340 NAME ——> CORE-CHANNEL

ALTITUDE	VOLUME	HIGHT	AREA
3.1012	0.0		
7.1552	19.937	4.0500	4.91301134

CV350 NAME ——> UPPER-PLENUM

ALTITUDE	VOLUME	HIGHT	AREA
7.1592	0.00		
10.483	36.89	3.3238	11.0987424
10.61	37.53	0.127	5.03937008
11.209	46.614	0.599	15.1652755
11.584	51.487	0.375	12.9946667
11.958	55.376	0.374	10.3983957
12.333	57.957	0.375	6.88266657
12.708	58.884	0.375	2.472

CV400 NAME ——> PRESSURIZER

ALTITUDE	VOLUME	HIGHT	AREA
8.324	0.0000		
12.559	0.98826	4.235	0.233355372
13.626	3.531	1.067	2.38387404
26.46	49.415	12.834	3.5751909
27.528	51.958	1.068	2.38555347

CV410 NAME ——> Q-TANK

ALTITUDE	VOLUME	HIGHT	AREA
1.0088	0.000		
2.4231	25.485	1.4143	18.019515
3.8373	50.97	1.4142	18.0207891
3.8473	50.971	0.0100	0.1
27.528	52.472	23.6787	0.0633903044

CV500 NAME ——> HOT-1LEG

ALTITUDE	VOLUME	HIGHT	AREA
7.9557	0.0000		
8.324	1.6952	0.3683	4.60276548
8.6923	3.3867	0.3683	4.59272332
10.100	3.5403	1.4077	0.109114158

CV502 NAME ——> HOT-3LEG

ALTITUDE	VOLUME	HIGHT	AREA
7.9557	0.0000		
8.324	5.0802	0.3683	13.7936465
8.6923	10.16	0.3683	13.7925604
10.10	10.621	1.4077	0.327484549

CV510 NAME ——> SG1-IRISE

ALTITUDE	VOLUME	HIGHT	AREA
8.8117	0.0000		
9.3405	0.5789	0.5288	1.09474281
9.8692	2.0466	0.5287	2.77605447
10.398	3.9454	0.5288	3.59077156
10.399	3.9464	0.001	1
21.403	15.291	11.004	1.03095238

CV511 NAME ——> SG3-IRISE

ALTITUDE	VOLUME	HIGHT	AREA
8.8117	0.0000		
9.3405	1.7367	0.5288	3.28422844
9.8692	6.1398	0.5287	8.32816342
10.398	11.836	0.5288	10.7719365
10.399	11.839	0.001	3
21.403	45.873	11.004	3.09287532

CV520 NAME ——> SG1-IDOWN

ALTITUDE	VOLUME	HIGHT	AREA
8.8117	0.0006		
9.3405	0.5789	0.5288	1.09474281
9.8692	2.0466	0.5287	2.77605447
10.398	3.9454	0.5288	3.59077156
10.399	3.9464	0.001	1
21.403	15.291	11.004	1.03095238

CV521 NAME ——> SG3-IDOWN

ALTITUDE	VOLUME	HIGHT	AREA

Table C.1 Control Volumes Modeled in MELCOR Analysis (Continued)

ALTITUDE	VOLUME	HIGHT	AREA
8.8117	0.0		
9.3405	1.7367	0.5288	3.28422844
9.8692	6.1398	0.5287	0.32816342
10.398	11.836	0.5288	10.7719365
10.399	11.839	0.001	3
21.403	45.873	11.004	3.09287532

CV570 NAME ---> INTERM-1LEG

ALTITUDE	VOLUME	HIGHT	AREA
5.5833	0.0000		
5.9770	0.3005	0.3937	0.763271527
6.3707	1.8360	0.3937	3.9001778
7.9748	2.1429	1.6041	0.191322237
8.5822	3.7288	0.6074	2.61096477
8.8117	6.2000	0.2295	10.767756

CV571 NAME ---> INTERM-3LEG

ALTITUDE	VOLUME	HIGHT	AREA
5.5833	0.0000		
5.9770	0.9015	0.3937	2.28981458
6.3707	5.5080	0.3937	11.7005334
7.9748	6.4287	1.6041	0.57396671
8.5822	11.1864	0.6074	7.8328943
8.8117	18.6000	0.2295	32.303268

CV580 NAME ---> COLD-1LEG

ALTITUDE	VOLUME	HIGHT	AREA
7.9748	0.0000		
8.3240	1.5500	0.3492	4.43871707
9.5758	3.1000	1.2518	1.23821697

CV581 NAME ---> COLD-3LEG

ALTITUDE	VOLUME	HIGHT	AREA
7.9748	0.0000		
8.3240	4.6500	0.3492	13.3161512
9.5758	9.3000	1.2518	3.7146589

CV725 NAME ---> SECOND-SG1

ALTITUDE	VOLUME	HIGHT	AREA
10.4706	0.0		
21.8928	78.454	11.4220	6.8935738
29.4365	168.2	7.5439	11.8964992

CV726 NAME ---> SECOND-SG3

ALTITUDE	VOLUME	HIGHT	AREA
10.4706	0.0		
21.8926	229.38	11.4220	20.0805463
29.4365	498.60	7.5439	35.6897626

CV740 NAME ---> TURBINE

ALTITUDE	VOLUME	HIGHT	AREA
-10.0	0.0		
10.0	1.0E10	20.0	500000000

CV600 NAME ---> ENVIRONMENT

ALTITUDE	VOLUME	HIGHT	AREA
-20.0	0.0		
100.0	1.0E9	120.0	8333333.33

CV800 NAME ---> ACC1-TANK

ALTITUDE	VOLUME	HIGHT	AREA
20.0	0.0		
45.0	2.5E6	25.0	100000

CV801 NAME ---> ACC3-TANK

ALTITUDE	VOLUME	HIGHT	AREA
20.0	0.0		
45.0	7.5E6	25.0	300000

CV900 NAME ---> RWS-TANK

ALTITUDE	VOLUME	HIGHT	AREA
20.0	0.0		
45.0	2.5E9	25.0	100000000

otal number of lines in the source ---> 6634

Table C.2 Flow Paths Modeled in MELCOR Analysis

MELCOR - FLOW PATHS INPUT

I	Num	Name	FrmV / To V	Z From / Z To	Opn F	Area / Length	Z OpnFr / Z OpnTo	Typ Act	Bub Fr / Bub To	Fric For / Fric Rvs	Chok F / Chok R	Vinit A / Vinit P	Valve	Pump	Time
1	362	SRV-QTANK	400	22.0	0.0	0.0476	Deflt	0	No	1.86	1.0	0.0	CF100		
			410	1.1		32.596	Deflt	0	SPARC	1.86	1.0	0.0	CF100		
2	021	Q-TANK-DISC	410	3.8373	0.0	0.14138	Deflt	0	No	1.0	1.0	0.0	CFTrp		
			210	3.8373		2.8285	Deflt	0	No	1.0	1.0	0.0	20		
3	150	CAV-BYPASS	100	0.0	1.0	0.5	0.80	3	SPARC	0.2	1.0	0.2			
			210	7.97		1.06	0.80	0	SPARC	0.2	1.0	0.0			
4	151	CAV-TUNNEL	100	-2.94	1.0	5.8	2.72	3	SPARC	0.2	1.0	0.2			
			210	4.042		6.83	2.72	0	SPARC	0.2	1.0	0.0			
5	215	LOW-ANNUL	210	4.32	1.0	19.0	3.5682	3	No	0.2	1.0	0.2			
			220	4.32		12.8648	3.5682	0	No	0.2	1.0	0.0			
6	225	ANN-UPPER	220	15.093	1.0	502.0	12.64	0	No	0.2	1.0	0.2			
			230	15.093		30.88	12.64	0	No	0.2	1.0	0.0			
7	226	LOW-UPPER	210	15.093	1.0	100.0	5.6419	0	No	0.2	1.0	0.2			
			230	15.093		30.88	5.6419	0	No	0.2	1.0	0.0			
8	031	VESSEL-BREACH	320	0.1445	0.0	0.01	Deflt	3	No	1.0	1.0	0.0	CF50		
			100	6.0		0.1445	Deflt	0	No	1.0	1.0	0.0	CF50		
9	014	CONT-RUPTURE	230	50.0	0.0	0.6503	Deflt	3	No	1.0	1.0	0.0	CF60		
			600	50.0		1.07	Deflt	0	No	1.0	1.0	0.0	CF60		
10	056	CTMT-FAIL	220	11.0	0.0	4.952E-5	Deflt	0	No	1.0	1.0	0.0	CF40		
			600	11.0		1.07	Deflt	0	No	1.0	1.0	0.0	CF40		
11	312	AN-LP	310	1.3272	1.0	3.784	0.015	0	No	2.449	1.0	8.9516			
			320	1.3272		0.0563	0.015	0	No	2.449	1.0	8.9516			
12	324	LP-CH	320	3.1012	1.0	4.987	0.015	0	No	9.96	1.0	4.6865			
			340	3.1012		3.5074	0.015	0	No	9.96	1.0	4.6865			
13	335	BP-UP	320	7.1592	1.0	2.174	0.015	0	No	16.108	1.0	7.417			
			350	7.1592		4.8034	0.015	0	No	16.108	1.0	7.417			
14	345	CH-UP	340	7.1592	1.0	4.987	0.015	0	No	3.51	1.0	5.292			
			350	7.1592		4.8034	0.015	0	No	3.51	1.0	5.292			
15	400	SURGE-LINE	500	8.324	1.0	0.0634	Deflt	0	No	30.0	1.0	0.0			
			400	8.324		31.659	Deflt	0	No	30.0	1.0	0.0			
16	500	RPV-HOTLEG1	350	8.324	1.0	0.4261	Deflt	3	No	0.1614	1.0	0.0			
			500	8.324		8.2296	Deflt	0	No	0.1614	1.0	14.363			
17	502	RVP-HOTLEG3	350	8.324	1.0	1.2784	Deflt	3	No	0.1614	1.0	0.0			
			502	8.324		8.2296	Deflt	0	No	0.1614	1.0	14.362			
18	510	HOTLG-SGRISE1	500	10.10	1.0	0.4261	Deflt	0	No	0.0245	1.0	0.0			
			510	10.10		15.944	Deflt	0	No	0.0245	1.0	13.9			
19	511	HOTLG-SGRISE3	502	10.10	1.0	1.2783	Deflt	3	No	0.0245	1.0	0.0			
			511	10.10		12.591	Deflt	0	No	0.0245	1.0	13.5			
20	520	SGRISE-DOWN-1	510	20.8	1.0	1.0311	Deflt	0	No	0.613	1.0	0.0			
			520	20.8		17.666	Deflt	0	No	0.613	1.0	5.538			
21	521	SGRISE-DOWN-3	511	20.8	1.0	3.0933	Deflt	0	No	0.613	1.0	0.0			
			521	20.8		17.666	Deflt	0	No	0.613	1.0	5.538			
22	578	SCDOWN-INTM1	520	8.8117	1.0	0.48695	Deflt	3	No	0.05709	1.0	0.0			
			570	8.8117		11.0334	Deflt	0	No	0.05709	1.0	0.0			
23	577	SGDOWN-INTM3	521	8.8117	1.0	1.4609	Deflt	3	No	0.05709	1.0	0.0			
			571	8.8117		11.0334	Deflt	0	No	0.05709	1.0	0.0			
24	579	PIPE-BREAK	570	6.3707	1.0	0.0032	0.06	3	No	0.05709	1.0	0.0			
			210	6.3707		4.6054	0.06	0	No	0.05709	1.0	0.0			
25	580	INTM-1COLD	570	7.9748	1.0	0.48695	Deflt	3	No	0.05709	1.0	0.0		FANA	
			580	7.9748		9.7827	Deflt	0	No	0.05709	1.0	11.405			
26	581	INTM-3COLD	571	7.9748	1.0	1.4609	Deflt	3	No	0.05709	1.0	0.0		FANA	
			581	7.9748		9.7827	Deflt	0	No	0.05709	1.0	11.405			
27	590	COLD-1DC	580	8.324	1.0	0.3832	Deflt	3	No	0.73	1.0	0.0			
			310	8.324		9.2864	Deflt	0	No	0.73	1.0	8.9497			

Table C.2 Flow Paths Modeled in MELCOR Analysis (Continued)

28	591	COLD-3DC	581	8.324	1.0	1.1496	Deflt	3	No	0.73	1.0	0.0		
			310	8.324		9.2864	Deflt	0	No	0.73	1.0	8.9497		
29	730	SG1-STOUT	725	29.4365	0.0	0.5837	0.8621	0	SPARC	1.0	1.0	0.0	CF735	
			740	10.0		36.5980	0.8621		SPARC	1.0	1.0	0.0	CF735	
30	731	SG3-STOUT	726	29.4365	0.0	1.7511	2.5863	0	SPARC	1.0	1.0	0.0	CF745	
			740	10.0		36.5980	2.5863		SPARC	1.0	1.0	0.0	CF745	
31	800	ACC-1	800	20.0	0.0	0.0081	0.1	2	No	0.5	1.0	0.0	CFTrp	
			580	7.9748		18.3	0.5	0	No	0.5	1.0	0.0	808	
32	801	ACC-3	801	20.0	0.0	0.0243	0.1	2	No	0.5	1.0	0.0	CFTrp	
			581	7.9748		18.3	0.5	0	No	0.5	1.0	0.0	858	
33	900	HPI-1	900	20.0	0.0	0.0081	0.1	2	No	0.0	1.0	0.0	CFTrp	FANA
			580	7.9748		30.0	0.5	1	No	0.0	1.0	0.0	908	----
34	901	HPI-2	900	20.0	0.0	0.0243	0.1	2	No	0.0	1.0	0.0	CFTrp	FANA
			581	7.9748		30.0	0.5	1	No	0.0	1.0	0.0	918	----
35	950	CHARGE-PUMP1	900	20.0	0.0	0.0046	0.1	2	No	0.0	1.0	0.0	CFTrp	FANA
			580	7.9748		30.0	0.5	1	No	0.0	1.0	0.0	958	----
36	951	CHARGE-PUMP2	900	20.0	0.0	0.0138	0.1	2	No	0.0	1.0	0.0	CFTrp	FANA
			581	7.9748		30.0	0.5	1	No	0.0	1.0	0.0	968	----

<u>Note:</u>

- Z = Elevation, m
- Open F = Fraction of flow path open
- Z open = "From and To" junction flow path opening height, m
- Type Act = Type of flow path (0 = normal vertical flow, 3 = normal horizontal flow)
- Bub = "From and To" junction bubble rise switch (0 = no bubble, 1 = SPARC model)
- FMC = "Forward and Reverse" loss coefficient
- Chok = "Forward and Reverse" choked flow discharge coefficient
- Vint = Initial atmosphere and pool velocity, M/S

Table C.3 Heat Structures Modeled in MELCOR Analysis

MELCOR - HEAT STRUCTURE INPUT
Problem Title ---) 'ZION SMALL PIPE BREAK 2.5 " @ INTERMEDIATE LEG'

Heat Structure									Boundary Surface (Left/Right)						Radiation	
!	Number	Name	Nod	Geo	Altit.	Orien	Mult	S	Vol	Cond	Flow	Area	Chr.L	DZ	Emiss	Rad Mod
1	10001	CONTAINMENT CYL	7	CYLN	2.533	Vert	1.0	N	220	1	EXT	1402.0	16.0	12.56	0.0	No Rad
										0		---	---	---	0.0	No Rad
2	20001	CONTAINMENT CYL	7	CYLN	15.093	Vert	1.0	N	230	1	EXT	6007.0	49.2	47.711	0.0	No Rad
										0		---	---	---	0.0	No Rad
3	10002	CONTAINM DOME	7	RECT	62.804	Horz	1.0	N	230	1	EXT	1011.61	42.672	42.672	0.0	No Rad
										0		---	---	---	0.0	No Rad
4	10003	CONTAINM FLOOR1	8	RECT	2.2282	Horz	1.0	N		0		---	---	---	0.0	No Rad
									210	1	EXT	897.50	20.15	20.15	0.0	No Rad
5	20003	CONTAINM FLOOR2	8	RECT	2.2282	Horz	1.0	N		0		---	---	---	0.0	No Rad
									220	1	EXT	535.31	13.05	13.05	0.0	No Rad
6	10004	REACTOR CAVITY	5	CYLN	-6.043	Vert	1.0	N	100	1	EXT	305.24	6.94	14.0	0.0	No Rad
										0		---	---	---	0.0	No Rad
7	10055	CAVITY FLOOR	5	RECT	-6.043	Horz	1.0	N	100	1	EXT	37.9	6.94	6.94	0.0	No Rad
										0		---	---	---	0.0	No Rad
8	10005	CRANE WALL	8	RECT	2.533	Vert	1.0	N	210	1	EXT	1202.5	25.12	12.56	0.0	No Rad
									220	1	EXT	1202.5	25.12	12.56	0.0	No Rad
9	20005	CRANE WALL	8	RECT	15.093	Vert	1.0	N	230	1	EXT	227.40	4.75	2.3752	0.0	No Rad
									230	1	EXT	227.40	4.75	2.3752	0.0	No Rad
10	10006	OPERATING DECK	9	RECT	10.0776	Horz	1.0	N	230	1	EXT	232.2575	20.515	20.515	0.0	No Rad
									230	1	EXT	232.2575	20.515	20.515	0.0	No Rad
11	10007	SHIELD WALLS	7	RECT	2.533	Vert	1.0	N	210	1	EXT	273.45	7.09	12.56	0.0	No Rad
									210	1	EXT	273.45	7.09	12.56	0.0	No Rad
12	20007	SHIELD WALLS	7	RECT	15.093	Vert	1.0	N	230	1	EXT	51.71	1.34	2.3752	0.0	No Rad
									230	1	EXT	51.71	1.34	2.3752	0.0	No Rad
13	10008	REFUELING CANAL	4	RECT	10.61	Vert	1.0	N	210	1	EXT	857.36	4.308	4.483	0.0	No Rad
										0		---	---	---	0.0	No Rad
14	20008	REFUELING CANAL	4	RECT	15.093	Vert	1.0	N	230	1	EXT	629.09	3.161	3.2894	0.0	No Rad
										0		---	---	---	0.0	No Rad
15	10009	STEEL STRUCT. I	4	RECT	10.0776	Horz	4.0	N	230	1	EXT	580.644	4.00	40.193	0.0	No Rad
									230	1	EXT	580.644	4.00	40.193	0.0	No Rad
16	10010	STEEL STRUCT 2	5	RECT	3.0	Vert	4.	N	210	1	EXT	560.90	8.0	12.09	0.0	No Rad
									210	1	EXT	560.90	8.0	12.09	0.0	No Rad
17	20010	STEEL STRUCT 2	5	RECT	3.0	Vert	4.	N	220	1	EXT	560.90	8.0	12.09	0.0	No Rad
									220	1	EXT	560.90	8.0	12.09	5.0	No Rad
18	10011	RPV UP-CYL	7	CYLN	7.4096	Vert	1.0	N	310	1	INT	44.1809	3.0004	3.0004	0.0	No Rad
										0		---	---	---	0.0	No Rad
19	10012	RPV LOW-CYL	7	CYLN	1.3272	Vert	1.0	N	310	1	INT	69.3814	5.0259	5.0259	0.0	No Rad
										0		---	---	---	0.0	No Rad
20	10015	UPPLEN COLUMNS	2	CYLN	7.1592	Vert	109.0	N	350	1	EXT	3.321	0.1651	5.5480	0.0	No Rad
									[illegible]	1	EXT	3.321	0.1905	5.5480	0.0	No Rad
21	10016	UPPLEN PLATE	6	RECT	10.403	Horz	1.0	N	350	1	EXT	15.1652	4.3942	4.3942	0.0	No Rad
									350	1	EXT	15.1652	4.3942	4.3942	0.0	No Rad
22	10017	UPPER HEAD	7	HSUP	10.[illegible]	----	1.0	N	350	1	INT	31.5	2.2392	2.2392	0.0	No Rad
										0		---	---	---	0.0	No Rad
23	10018	THERMAL SHIELD	4	CYLN	3.1012	Vert	1.0	N	310	1	INT	57.825	0.1524	4.572	0.0	No Rad
									310	1	EXT	59.832	0.2286	4.572	0.0	No Rad
24	50013	COR BARREL-UP	4	CYLN	7.1592	Vert	1.0	N	350	1	INT	39.0536	0.415	3.32	0.0	No Rad
									310	1	EXT	41.0950	0.5207	3.32	0.0	No Rad
25	40013	COR BARREL-3	4	CYLN	3.1012	Vert	1.0	N	320	1	INT	47.9245	4.058	4.058	0.0	No Rad
									310	1	EXT	49.3016	4.058	4.058	0.0	No Rad
26	30013	COR BARREL-2	4	CYLN	1.3272	Vert	1.0	N	320	1	INT	20.9507	1.774	1.774	0.0	No Rad
									310	1	EXT	21.5877	1.774	1.774	0.0	No Rad
27	20013	COR BARREL-1	4	CYLN	6.1445	Vert	1.0	N	320	1	INT	13.9675	1.1027	1.1027	0.0	No Rad

Table C.3 Heat Structures Modeled in MELCOR Analysis (Continued)

									320	1	EXT	14.3922	1.1027	1.1027	0.0	No Rad
28	10043	COR BAFFLE-6	4	CYLN	3.1012	Vert	1.0	N	340	1	INT	0.5379	0.0508	0.0508	0.0	No Rad
									320	1	EXT	0.5555	0.0508	0.0508	0.0	No Rad
29	10044	COR BAFFLE-7	4	CYLN	3.1520	Vert	1.0	N	340	1	INT	7.7456	0.73152	0.73152	0.0	No Rad
									320	1	EXT	7.8336	0.73152	0.73152	0.0	No Rad
30	10045	COR BAFFLE-8	4	CYLN	3.88352	Vert	1.0	N	340	1	INT	7.7456	0.73152	0.73152	0.0	No Rad
									320	1	EXT	7.8336	0.73152	0.73152	0.0	No Rad
31	10046	COR BAFFLE-9	4	CYLN	4.61504	Vert	1.0	N	340	1	INT	7.7456	0.73152	0.73152	0.0	No Rad
									320	1	EXT	7.8336	0.73152	0.73152	0.0	No Rad
32	10047	COR BAFFLE-10	4	CYLN	5.34656	Vert	1.0	N	340	1	INT	7.7456	0.73152	0.73152	0.0	No Rad
									320	1	EXT	7.8336	0.73152	0.73152	0.0	No Rad
33	10048	COR BAFFLE-11	4	CYLN	6.07808	Vert	1.0	N	340	1	INT	7.7456	0.73152	0.73152	0.0	No Rad
									320	1	EXT	7.8336	0.73152	0.73152	0.0	No Rad
34	10049	COR BAFFLE-12	4	CYLN	6.8096	Vert	1.0	N	340	1	INT	3.1640	0.2988	0.2988	0.0	No Rad
									320	1	EXT	3.1646	0.2988	0.2988	0.0	No Rad
35	10054	UPPER COREPLATE	3	RECT	7.1004	Horz	1.0	N	340	1	EXT	11.099	3.7592	3.7592	0.0	No Rad
									350	1	EXT	11.099	3.7592	3.7592	0.0	No Rad
36	20054	LOWER COREPLATE	3	RECT	3.1012	Horz	1.0	N	320	1	EXT	11.099	3.4087	0.0508	0.0	No Rad
									340	1	EXT	11.099	3.4087	0.0508	0.0	No Rad
37	30054	LOWER COREPLATE	3	RECT	1.3272	Horz	1.0	N	320	1	EXT	11.099	3.4087	0.2235	0.0	No Rad
									320	1	EXT	11.099	3.4087	0.2235	0.0	No Rad
38	10019	PIPE HOTLEG	4	CYLN	7.9557	Horz	1.0	N	500	1	INT	19.0441	0.7366	8.2296	0.0	No Rad
										0		---	---	---	0.0	No Rad
39	10021	LUMP HOTLEG PIPE	4	CYLN	7.9557	Horz	3.0	N	502	1	INT	19.0441	0.7366	8.2296	0.0	No Rad
										0		---	---	---	0.0	No Rad
40	10022	SG INLET PLEN	5	HSLW	8.8117	----	1.0	N	510	1	INT	7.9173	1.5875	1.5875	0.0	No Rad
										0		---	---	---	0.0	No Rad
41	10025	SG OUTL PLEN	5	HSLW	8.8117	----	1.0	N	520	1	INT	7.9173	1.5875	1.5875	0.0	No Rad
										0		---	---	---	0.0	No Rad
42	10026	LUMPSG INL PLEN	5	HSLW	8.8117	----	3.0	N	511	1	INT	7.9173	1.5875	1.5875	0.0	No Rad
										0		---	---	---	0.0	No Rad
43	10029	LMPSG OUT PLEN	5	HSLW	8.8117	----	3.0	N	521	1	INT	7.9173	1.5875	1.5875	0.0	No Rad
										0		---	---	---	0.0	No Rad
44	10030	PIPE-INTERM	4	CYLN	5.5833	Horz	1.0	N	570	1	INT	12.5537	0.7879	9.4756	0.0	No Rad
										0		---	---	---	0.0	No Rad
45	10031	LUMP PIPE-INTER	4	CYLN	5.58433	Horz	3.0	N	571	1	INT	12.5537	0.7874	9.4756	0.0	No Rad
										0		---	---	---	0.0	No Rad
46	10032	PIPE COLDLEG	4	CYLN	7.98	Horz	1.0	N	580	1	INT	6.36	0.7874	8.08	0.0	No Rad
										0		---	---	---	0.0	No Rad
47	10033	LUMP PIPE COLDLEG	4	CYLN	7.98	Horz	3.0	N	581	1	INT	6.36	0.7874	8.08	0.0	No Rad
										0		---	---	---	0.0	No Rad
48	10034	TUBESHEET-IN	5	RECT	10.4706	Horz	1.0	N	510	1	INT	2.9274	1.5875	1.5875	0.0	No Rad
									725	1	EXT	2.9274	1.5875	1.5875	0.0	No Rad
49	10035	TUBESHEET-OUT	5	RECT	10.4706	Horz	1.0	N	520	1	INT	2.9274	1.5875	1.5875	0.0	No Rad
									725	1	EXT	2.9274	1.5875	1.5875	0.0	No Rad
50	10036	LUMP HTUBESH-IN	5	RECT	10.4706	Horz	3.0	N	511	1	INT	2.9274	1.5875	1.5875	0.0	No Rad
									726	1	EXT	2.9274	1.5875	1.5875	0.0	No Rad
51	10037	LUMP TUBESH-OUT	5	RECT	10.4706	Horz	3.0	N	521	1	INT	2.9274	1.5875	1.5875	0.0	No Rad
									726	1	EXT	2.9274	1.5875	1.5875	0.0	No Rad
52	10038	VBARR SG-SEP	4	RECT	8.8117	Vert	1.0	N	510	1	INT	3.9587	1.5875	1.5875	0.0	No Rad
									520	1	EXT	3.9587	1.5875	1.5875	0.0	No Rad
53	10039	LUMP-VBAR-SGSEP	4	RECT	8.8117	Vert	3.0	N	511	1	INT	3.9587	1.5875	1.5875	0.0	No Rad
									521	1	EXT	3.9587	1.5875	1.5875	0.0	No Rad
54	10050	SURGE LINE	2	CYLN	8.325	Horz	1.0	N	400	1	INT	13.9114	0.2842	15.581	0.0	No Rad
										0		---	---	---	0.0	No Rad
55	10051	PRESSURIZER	4	CYLN	12.5	Vert	1.0	N	400	1	INT	100.54	2.1336	15.	0.0	No Rad
										0		---	---	---	0.0	No Rad
56	10052	RELIEF LINE	2	CYLN	1.15	Vert	1.0	N	410	1	INT	14.5515	0.1421	26.37	0.0	No Rad
										0		---	---	---	0.0	No Rad
57	10053	RELIEF TANK	4	CYLN	0.9072	Horz	1.0	N	410	1	INT	72.32	2.0285	0.1382	0.0	No Rad
										0		---	---	---	0.0	No Rad

Table C.3 Heat Structures Modeled in MELCOR Analysis (Continued)

58	10060	PRESS FLOOR	4	RECT	12.432	Horz	1.0	N	400	1	INT	3.575	2.1336	2.1336	0.0	No Rad
										0		---	---	---	0.0	No Rad
59	10061	ENV FLOOR	2	RECT	-20.	Horz	1.0	N	600	1	EXT	1.E7	3.16E3	3.16E3	0.0	No Rad
										0		---	---	---	0.0	No Rad
60	10062	RWST-FLOOR	2	RECT	20.	Horz	1.0	N	900	1	EXT	100.0	F.0	11.0	0.0	No Rad
										0		---	---	---	0.0	No Rad
61	20062	HPI-LINE	2	CYLN	20.0	Horz	1.0	N	900	1	INT	11.9695	0.1270	30.0	0.0	No Rad
										0		---	---	---	0.0	No Rad
62	30062	HPI-LINE-LUMP	2	CYLN	20.0	Horz	3.0	N	900	1	INT	11.9695	0.1270	30.0	0.0	No Rad
										0		---	---	---	0.0	No Rad
63	60062	ACC1-FLOOR	2	RECT	20.	Horz	1.0	N	800	1	EXT	100.0	5.0	11.0	0.0	No Rad
										0		---	---	---	0.0	No Rad
64	70062	ACC2-FLOOR	2	RECT	20.	Horz	1.0	N	801	1	EXT	100.0	5.0	11.0	0.0	No Rad
										0		---	---	---	0.0	No Rad
65	80062	ACC1-LINE	2	CYLN	20.0	Horz	1.0	N	800	1	INT	11.9695	0.1270	18.3	0.0	No Rad
										0		---	---	---	0.0	No Rad
66	90062	ACC2-LINE-LUMP	2	CYLN	20.0	Horz	3.0	N	801	1	INT	11.9695	0.1270	18.3	0.0	No Rad
										0		---	---	---	0.0	No Rad
67	10063	TURBINE-FLOOR	2	RECT	-10.	Horz	1.0	N	740	1	EXT	1.E7	3.16E3	3.16E3	0.0	No Rad
										0		---	---	---	0.0	No Rad
68	20063	TURBINE-LINE	2	CYLN	10.48	Vert	1.0	N	725	1	INT	35.05	0.3048	18.9	0.0	No Rad
										0		---	---	---	0.0	No Rad
69	30063	TURB-LINE-LUMP	2	CYLN	10.48	Vert	3.0	N	725	1	INT	35.05	0.3048	18.9	0.0	No Rad
										0		---	---	---	0.0	No Rad
70	20023	SG-BOT-SHELL	5	CYLN	10.4706	Vert	1.0	N	725	1	INT	112.1574	10.8632	10.8632	0.0	No Rad
										0		---	---	---	0.0	No Rad
71	30023	SG-UP-SHELL	5	CYLN	21.3338	Vert	1.0	N	725	1	INT	81.5092	5.9063	5.9063	0.0	No Rad
										0		---	---	---	0.0	No Rad
72	40023	SG-SEC-DOME	5	HSUP	27.2401	----	1.0	N	725	1	INT	30.3112	2.1968	2.1968	0.0	No Rad
										0		---	---	---	0.0	No Rad
73	20027	SG-BOT-SHELL	5	CYLN	10.4706	Vert	3.0	N	725	1	INT	112.1574	10.8632	10.8632	0.0	No Rad
										0		---	---	---	0.0	No Rad
74	30027	SG-UP-SHELL	5	CYLN	21.3338	Vert	3.0	N	725	1	INT	81.5092	5.9063	5.9063	0.0	No Rad
										0		---	---	---	0.0	No Rad
7f	.0027	SG-SEC-DOME	5	HSUP	27.2401	----	3.0	N	725	1	INT	30.3112	2.1968	2.1968	0.0	No Rad
										0		---	---	---	0.0	No Rad
76	40001	SG-RISE-TUBE-1	4	CYLN	10.4706	Vert	3388.	N	510	1	INT	0.0642	0.9939	0.9939	0.0	No Rad
									725	1	EXT	0.0642	0.9939	0.9939	0.0	No Rad
77	40002	SG-RISE-TUBE-2	4	CYLN	11.4645	Vert	3388.	N	510	1	INT	0.0642	0.9939	0.9939	0.0	No Rad
									725	1	EXT	0.0642	0.9939	0.9939	0.0	No Rad
78	40003	SG-RISE-TUBE-3	4	CYLN	12.4584	Vert	3388.	N	510	1	INT	0.0642	0.9939	0.9939	0.0	No Rad
									725	1	EXT	0.0642	0.9939	0.9939	0.0	No Rad
79	40004	SG-RISE-TUBE-4	4	CYLN	13.4523	Vert	3388.	N	510	1	INT	0.0642	0.9939	0.9939	0.0	No Rad
									725	1	EXT	0.0642	0.9939	0.9939	0.0	No Rad
80	40005	SG-RISE-TUBE-5	4	CYLN	14.4462	Vert	3388.	N	510	1	INT	0.0642	0.9939	0.9939	0.0	No Rad
									725	1	EXT	0.0642	0.9939	0.9939	0.0	No Rad
81	40006	SG-RISE-TUBE-6	4	CYLN	15.4401	Vert	3388.	N	510	1	INT	0.0642	0.9939	0.9939	0.0	No Rad
									725	1	EXT	0.0642	0.9939	0.9939	0.0	No Rad
82	40007	SG-RISE-TUBE-7	4	CYLN	16.4340	Vert	3388.	N	510	1	INT	0.0642	0.9939	0.9939	0.0	No Rad
									725	1	EXT	0.0642	0.9939	0.9939	0.0	No Rad
83	40008	SG-RISE-TUBE-8	4	CYLN	17.4279	Vert	3388.	N	510	1	INT	0.0642	0.9939	0.9939	0.0	No Rad
									725	1	EXT	0.0642	0.9939	0.9939	0.0	No Rad
84	40009	SG-RISE-TUBE-9	4	CYLN	18.4218	Vert	3388.	N	510	1	INT	0.0642	0.9939	0.9939	0.0	No Rad
									725	1	EXT	0.0642	0.9939	0.9939	0.0	No Rad
85	40010	SG-RISE-TUBE-10	4	CYLN	19.4157	Vert	3388.	N	510	1	INT	0.0642	0.9939	0.9939	0.0	No Rad
									725	1	EXT	0.0642	0.9939	0.9939	0.0	No Rad
86	40011	SG-RISE-TUBE-11	4	CYLN	20.4096	Vert	3388.	N	510	1	INT	0.0642	0.9934	0.9934	0.0	No Rad
									725	1	EXT	0.0642	0.9934	0.9934	0.0	No Rad
87	50001	SG-DOWN-TUBE-1	4	CYLN	10.4706	Vert	3388.	N	520	1	INT	0.0642	0.9939	0.9939	0.0	No Rad
									725	1	EXT	0.0642	0.9939	0.9939	0.0	No Rad
88	50002	SG-DOWN-TUBE-2	4	CYLN	11.4645	Vert	3388.	N	520	1	INT	0.0642	0.9939	0.9939	0.0	No Rad

Table C.3 Heat Structures Modeled in MELCOR Analysis (Continued)

									726	1	EXT	0.0642	0.9939	0.9939	0.0	No Rad
89	50003	SG-DOWN-TUBE-3	4	CYLN	12.4584	Vert	3388.	N	520	1	INT	0.0642	0.9939	0.9939	0.0	No Rad
									725	1	EXT	0.0642	0.9939	0.9939	0.0	No Rad
90	50004	SG-DOWN-TUBE-4	4	CYLN	13.4523	Vert	3388.	N	520	1	INT	0.0642	0.9939	0.9939	0.0	No Rad
									725	1	EXT	0.0642	0.9939	0.9939	0.0	No Rad
91	50005	SG-DOWN-TUBE-5	4	CYLN	14.4462	Vert	3388.	N	520	1	INT	0.0642	0.9939	0.9939	0.0	No Rad
									725	1	EXT	0.0642	0.9939	0.9939	0.0	No Rad
92	50006	SG-DOWN-TUBE-6	4	CYLN	15.4401	Vert	3388.	N	520	1	INT	0.0642	0.9939	0.9939	0.0	No Rad
									725	1	EXT	0.0642	0.9939	0.9939	0.0	No Rad
93	50007	SG-DOWN-TUBE-7	4	CYLN	16.4340	Vert	3388.	N	520	1	INT	0.0642	0.9939	0.9939	0.0	No Rad
									725	1	EXT	0.0642	0.9939	0.9939	0.0	No Rad
94	50008	SG-DOWN-TUBE-8	4	CYLN	17.4279	Vert	3388.	N	520	1	INT	0.0642	0.9939	0.9939	0.0	No Rad
									725	1	EXT	0.0642	0.9939	0.9939	0.0	No Rad
95	50009	SG-DOWN-TUBE-9	4	CYLN	18.4218	Vert	3388.	N	520	1	INT	0.0642	0.9939	0.9939	0.0	No Rad
									725	1	EXT	0.0642	0.9939	0.9939	0.0	No Rad
96	50010	SG-DOWN-TUBE-10	4	CYLN	19.4157	Vert	3388.	N	520	1	INT	0.0642	0.9939	0.9939	0.0	No Rad
									725	1	EXT	0.0542	0.9939	0.9939	0.0	No Rad
97	50011	SG-DOWN-TUBE-11	4	CYLN	20.4096	Vert	3388.	N	520	1	INT	0.0642	0.9934	0.9934	0.0	No Rad
									725	1	EXT	0.0642	0.9934	0.9934	0.0	No Rad
98	60001	SG-RISE-TUBE-L1	4	CYLN	10.4706	Vert	10164.	N	511	1	INT	0.0642	0.9939	0.9939	0.0	No Rad
									726	1	EXT	0.0642	0.9939	0.9939	0.0	No Rad
99	60002	SG-RISE-TUBE-L2	4	CYLN	11.4645	Vert	10164.	N	511	1	INT	0.0642	0.9939	0.9939	0.0	No Rad
									726	1	EXT	0.0642	0.9939	0.9939	0.0	No Rad
100	60003	SG-RISE-TUBE-L3	4	CYLN	12.4584	Vert	10164.	N	511	1	INT	0.0642	0.9939	0.9939	0.0	No Rad
									726	1	EXT	0.0642	0.9939	0.9939	0.6	No Rad
101	60004	SG-RISE-TUBE-L4	4	CYLN	13.4523	Vert	10164.	N	511	1	INT	0.0642	0.9939	0.9939	0.0	No Rad
									726	1	EXT	0.0642	0.9939	0.9939	0.0	No Rad
102	60005	SG-RISE-TUBE-L5	4	CYLN	14.4462	Vert	10164.	N	511	1	INT	0.0642	0.9939	0.9939	0.0	No Rad
									726	1	EXT	0.0642	0.9939	0.9939	0.0	No Rad
103	60006	SG-RISE-TUBE-L6	4	CYLN	15.4401	Vert	10164.	N	511	1	INT	0.0642	0.9939	0.9939	0.0	No Rad
									726	1	EXT	0.0642	0.9939	0.9939	0.0	No Rad
104	60007	SG-RISE-TUBE-L7	4	CYLN	16.4340	Vert	10164.	N	511	1	INT	0.0642	0.9939	0.9939	0.0	No Rad
									726	1	EXT	0.0642	0.9939	0.9939	0.0	No Rad
105	60008	SG-RISE-TUBE-L8	4	CYLN	17.4279	Vert	10164.	N	511	1	INT	0.0642	0.9939	0.9939	0.0	No Rad
									726	1	EXT	0.0642	0.9939	0.9939	0.0	No Rad
106	60009	SG-RISE-TUBE-L9	4	CYLN	18.4218	Vert	10164.	N	511	1	INT	0.0642	0.9939	0.9939	0.0	No Rad
									726	1	EXT	0.0642	0.9939	0.9939	0.0	No Rad
107	60010	SG-RISE-TUBE-L10	4	CYLN	19.4157	Vert	10164.	N	511	1	INT	0.0642	0.9939	0.9939	0.0	No Rad
									726	1	EXT	0.0642	0.9939	0.9939	0.0	No Rad
108	60011	SG-RISE-TUBE-L11	4	CYLN	26.4096	Vert	10164.	N	511	1	INT	0.0642	0.9934	0.9934	0.0	No Rad
									726	1	EXT	0.0642	0.9934	0.9934	0.0	No Rad
109	70001	SG-DOWN-TUBE-L1	4	CYLN	10.4706	Vert	10164.	N	521	1	INT	0.0642	0.9939	0.9939	0.0	No Rad
									726	1	EXT	0.0642	0.9939	0.9939	0.0	No Rad
110	70002	SG-DOWN-TUBE-L2	4	CYLN	11.4645	Vert	10164.	N	521	1	INT	0.0642	0.9939	0.9939	0.0	No Rad
									726	1	EXT	0.0642	0.9939	0.9939	0.0	No Rad
111	70003	SG-DOWN-TUBE-L3	4	CYLN	12.4584	Vert	10164.	N	521	1	INT	0.0642	0.9939	0.9939	0.0	No Rad
									726	1	EXT	0.0642	0.9939	0.9939	0.0	No Rad
112	70004	SG-DOWN-TUBE-L4	4	CYLN	13.4523	Vert	10164.	N	521	1	INT	0.0642	0.9939	0.9939	0.0	No Rad
									726	1	EXT	0.0642	0.9939	0.9939	0.0	No Rad
113	70005	SG-DOWN-TUBE-L5	4	CYLN	14.4462	Vert	10164.	N	521	1	INT	0.0642	0.9939	0.9939	0.0	No Rad
									726	1	EXT	0.0642	0.9939	0.9939	0.0	No Rad
114	70006	SG-DOWN-TUBE-L6	4	CYLN	15.4401	Vert	10164.	N	521	1	INT	0.0642	0.9939	0.9939	0.0	No Rad
									726	1	EXT	0.0642	0.9939	0.9939	0.0	No Rad
115	70007	SG-DOWN-TUBE-L7	4	CYLN	16.4340	Vert	10164.	N	521	1	INT	0.0642	0.9939	0.9939	0.0	No Rad
									726	1	EXT	0.0642	0.9939	0.9939	0.0	No Rad
116	70008	SG-DOWN-TUBE-L8	4	CYLN	17.4279	Vert	10164.	N	521	1	INT	0.0642	0.9939	0.9939	0.0	No Rad
									726	1	EXT	0.0642	0.9939	0.9939	0.0	No Rad
117	70009	SG-DOWN-TUBE-L9	4	CYLN	18.4218	Vert	10164.	N	521	1	INT	0.0642	0.9939	0.9939	0.0	No Rad
									726	1	EXT	0.0642	0.9939	0.9939	0.0	No Rad
118	70010	SG-DOWN-TUBE-L10	4	CYLN	19.4157	Vert	10164.	N	521	1	INT	0.0642	0.9939	0.9939	0.0	No Rad
									726	1	EXT	0.0642	0.9939	0.9939	0.0	No Rad

Table C.3 Heat Structures Modeled in MELCOR Analysis (Continued)

119	70011	SG-DOWN-TUBE-L11	4	CYLN	20.4096	Vert	10164.	N	521	1	INT	0.0642	0.9934	0.9934	0.0 No Rad
									726	1	EXT	0.0642	0.9934	0.9934	0.0 No Rad

MELCOR - HEAT STRUCTURE GAS SOURCES INPUT

	Heat Structure Gas Source							
	Number	Release Surface	Nod	Gas Name	Density	Ht.of React	T low	T upp
1	11001	10001 (left)	4	H2O-VAP	96.14	1.808E6	360.0	380.0
2	12001	10001 (left)	4	CO2	409.0	6.912E6	500.0	520.0
3	21001	20001 (left)	4	H2O-VAP	96.14	1.808E6	360.0	380.0
4	22001	20001 (left)	4	CO2	409.0	6.912E6	500.0	520.0
5	11002	10002 (left)	4	H2O-VAP	96.14	1.808E6	360.0	380.0
6	12002	10002 (left)	4	CO2	409.0	6.912E6	500.0	520.0
7	11003	10003 (right)	7	H2O-VAP	93.6	1.809E6	360.0	380.0
8	12003	10003 (right)	7	H2O-VAP	46.8	6.912E6	500.0	520.0
9	13003	10003 (right)	7	CO2	409.0	6.912E6	500.0	520.0
10	21003	20003 (right)	7	H2O-VAP	93.6	1.808E6	360.0	380.0
11	22003	20003 (right)	7	H2O-VAP	45.8	6.912E6	500.0	520.0
12	23003	20003 (right)	7	CO2	409.0	6.912E6	500.0	520.0
13	11005	10005 (left)	7	H2O-VAP	96.14	1.808E6	360.0	380.0
14	12005	10005 (left)	7	CO2	409.0	6.912E6	500.0	520.0
15	21005	20005 (left)	7	H2O-VAP	96.14	1.808E6	360.0	380.0
16	22005	20005 (left)	7	CO2	409.0	6.912E6	500.0	520.0
17	11006	10006 (left)	7	H2O-VAP	96.14	1.808E6	360.0	380.0
18	12006	10006 (left)	7	CO2	409.0	6.912E6	500.0	520.0
19	11007	10007 (left)	6	H2O-VAP	96.14	1.808E6	360.0	380.0
20	12007	10007 (left)	6	CO2	409.0	6.912E6	500.0	520.0
21	21007	20007 (left)	6	H2O-VAP	96.14	1.808E6	360.0	380.0
22	22007	20007 (left)	6	CO2	409.0	6.912E6	500.0	520.0

Note:

S = Internal power source distribution in the heat structure.

cond = Boundary condition type;
0 for a symmetry (insulated)
1 for a convective boundary condition

FLOW = Type of flow over boundary surface of heat structure

Radiation = Boundary surface radiation data;
Emiss for emissivity of the surface
Rad Mod for radiation mode of the surface;
"EQUIV BAND" or GRAY GAS A" or no radiation applied.

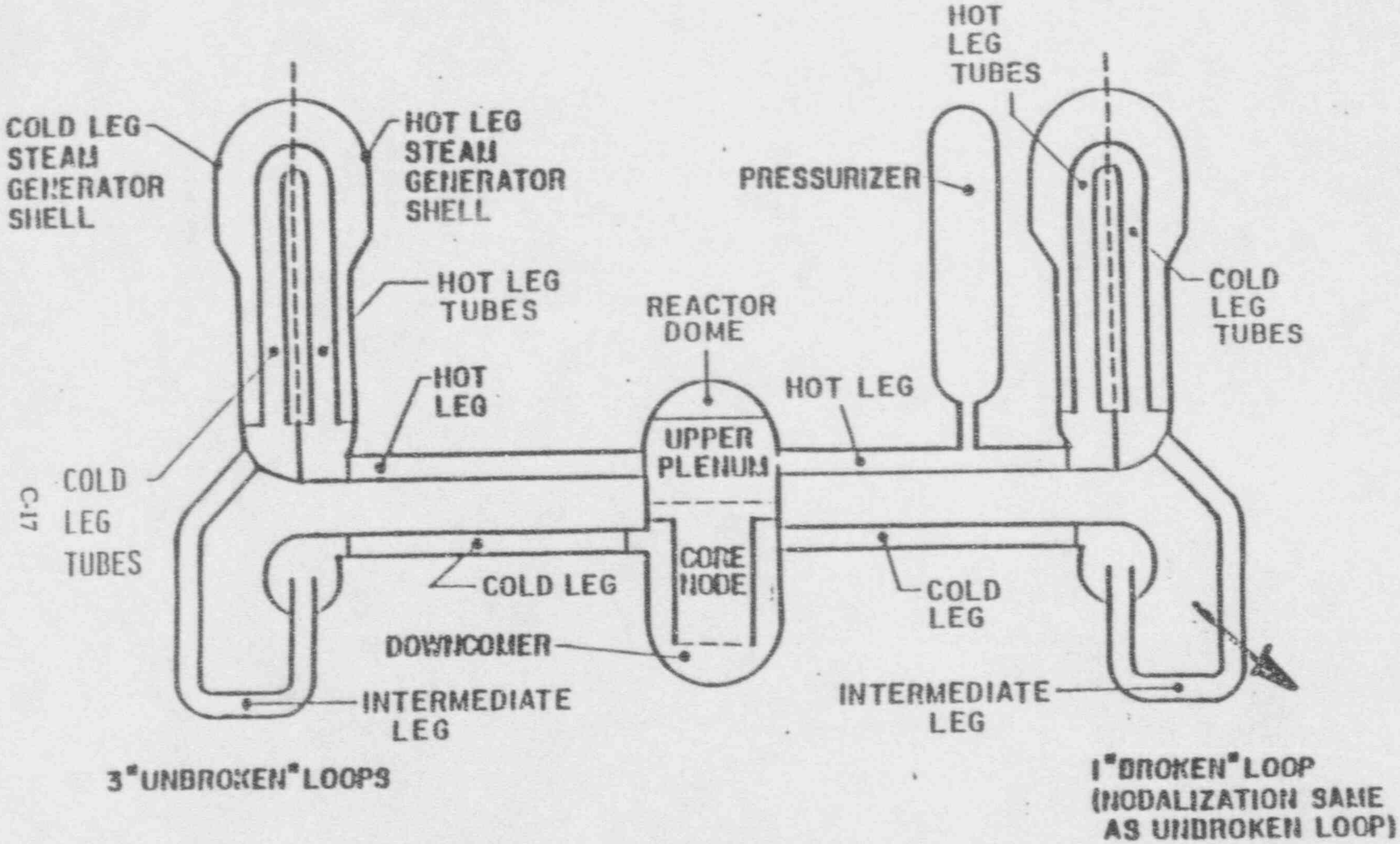

Figure C.3 Primary System Nodalization Used in MAAP

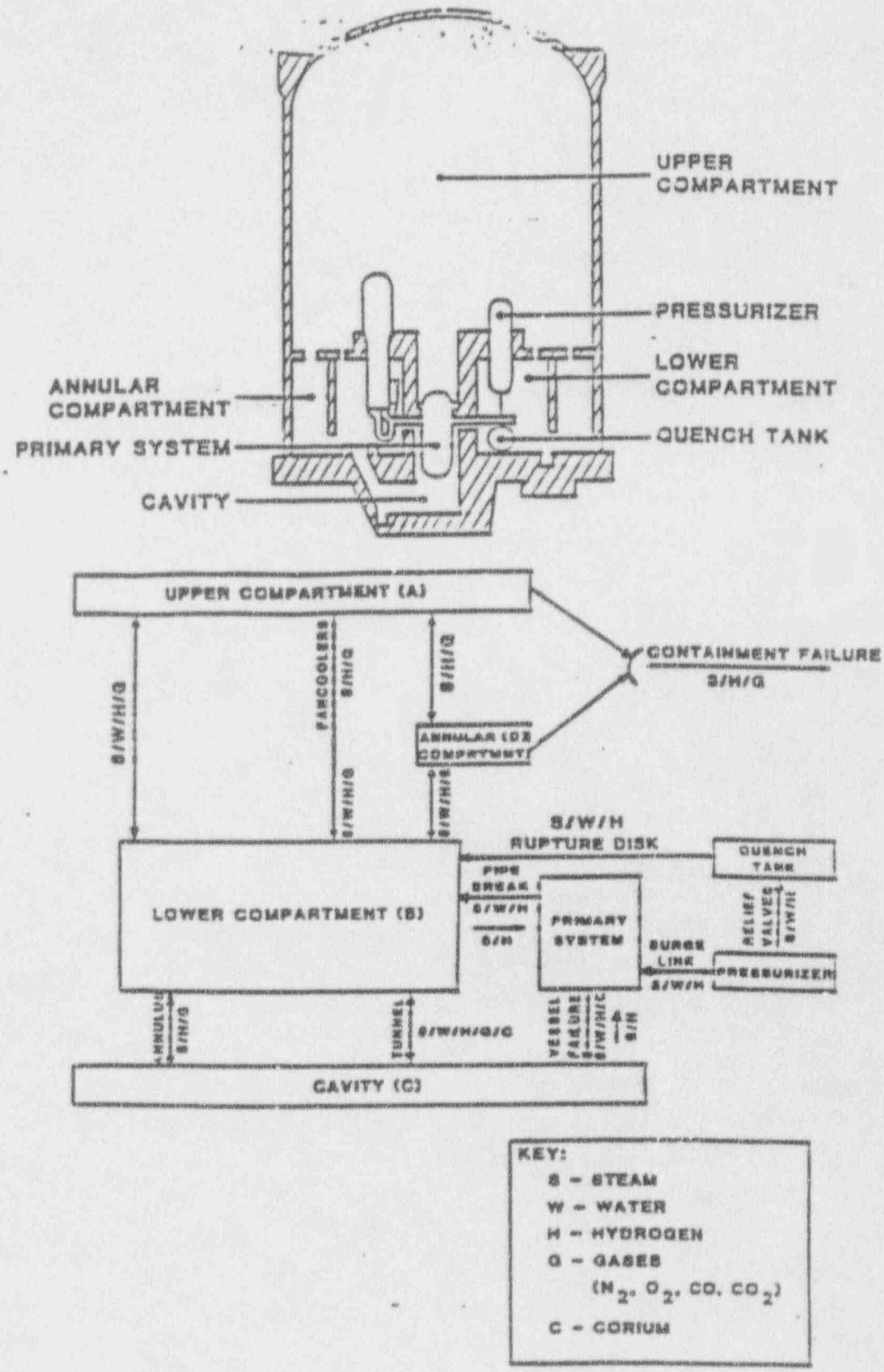

Figure C.4 Containment Nodalization Used in MAAP

3. MAAP does not consider the bypass channel in the core region; MELCOR includes it in the lower plenum region.
4. MAAP has a more detailed modeling of the second side of the steam generators; MELCOR uses a single nodalization for the secondary side of the steam generator.
5. MAAP connects the accumulators directly to the downcomer (i.e. lower plenum); MELCOR connects the accumulators to the cold leg.
6. MAAP represents the auxiliary building by four nodes; the auxiliary building is not modeled in the MELCOR analysis.

MAAP uses fixed nodalization for the primary system and containment. The user can specify the nodalization only in the auxiliary building. MELCOR does not have any specific nodalization; the nodalization used in the analysis was selected mainly to match that used in the MAAP analysis. However, considerations were given to reduce the computing time and the potential for numerical instability. A systematic study on the effect of nodalization on MELCOR predictions has not been performed.

MAAP also has a different treatment of the reactor core than MELCOR. MAAP assumes that the PWR core consists of only fuel rods and coolant flow channels. Structures and control rods are not included. The pellet and clad are lumped together and are represented by a single average temperature. In the analysis, MAAP divided the core into 7 radial rings and 10 axial segments. This nodalization is finer than that used in MELCOR. However, in the lower plenum, only one node is considered in the MAAP analysis. A single penetration is modeled in the lower plenum.

MAAP also models the containment failure and leakage in the annular compartments as MELCOR does. The failure area, leakage area, and the failure pressure in MAAP are the same as that in MELCOR. However, MAAP uses normal containment leakage throughout the analysis.

MAAP/PWR has 78 input model parameters. The values of these parameters, recommended by the Sensitivity Study Guidance Document [1], were used in the MAAP analysis.

4 Initial Conditions

The initial inventory of water, UO_2, Zr, structural materials, fission product materials, and the radial and axial power distributions in the core region, used in MAAP and MELCOR are compared in this section to ensure that the analysis is based on similar initial conditions.

The initial water inventory in the primary system and its distribution in the reactor vessel and coolant loops are given below:

	MELCOR	MAAP
Primary System	229,150 Kg	224,540 Kg
Reactor Vessel	100,870	111,400
Loop	128,280	113,100

Although the total water mass in the MELCOR analysis is only about 2% more than that used in the MAAP analysis, MELCOR has about 10% less water in the reactor vessel and 12% more in the coolant loop. The difference in the water distribution is caused by differences in the water density computed by the initial pressures and temperatures specified for the primary system. MAAP assumed a uniform pressure and temperature distribution in the primary system, while MELCOR assumed a variation of pressures and temperatures based on the normal operating conditions. However, the small difference in the initial water distribution may not have a significant effect on a transient behavior, as the flow will be reestablished based on the transient mass and energy balance.

In the pressurizer, both codes have the same total mass:

	MELCOR	MAAP
Water	10,523 Kg	10,413 Kg
Steam	3,426	3,542
Total	13,949	13,955

In the secondary side of the steam generators, MELCOR has less inventory as shown below:

	MELCOR	MAAP
Water/Unit	33,560 Kg	37,000 Kg
Steam/Unit	3,560	4,460

The 10% smaller inventory of water in MELCOR would affect the decay energy removal from the primary system.

A comparison of the core inventory is given below:

	MELCOR		MAAP	
	Kg	%	Kg	%
UO_2	98,250	78.6	98,250	82.9
Zr	20,207	16.0	20,207	17.1
Stainless Steel	2,450	2.0		
Control Rod	4,280	3.4		
Total	125,195	100.0	118,457	100.0

Both codes have the identical inventory of UO_2 and Zr. The MAAP code does not model the stainless steel and control rod. These materials are included in the MELCOR analysis as additional heat sinks and are included in the core debris. Because of the small quantity (5.4%) of these materials, they are not expected to significantly affect the overall core meltdown.

In the lower plenum, MELCOR models structures in three axial nodes. The total masses are given below:

Axial Node	Structure	Mass, Kg
6	Lower Core Plate	3,712
5	Diffuser	2,784
3	Bottom Support Plate	16,332

In MAAP, the mass of the lower core plate (3,712 Kg) is specified in the parameter file for the core support plate. Masses of the other two structures (diffuser and bottom support plate) are not included in the MAAP analysis. All materials in the core and lower plenum regions modeled in both MELCOR and MAAP can be relocated downward during the core meltdown phase and can be ejected to the cavity at or after penetration failure.

Because of differences in nodalization, the axial and radial power distributions modeled in the two codes cannot be compared directly. In MAAP, the active fuel has a length of 3.56 m (140.2 in) and is divided into 9 segments. The peaking factor of each axial segment is user-specified. In MELCOR, the active fuel has a length of 3.6576 m (144 in) and is divided into 5 segments. The MELCOR input file specifies the relative power density of these axial segments. To compare with MAAP, the specified relative power densities that are specified by MELCOR are normalized and converted into peaking power factors as shown in Figure C.5. The comparison in Figure C.5 shows that there are differences in the axial peaking power factors used in the two codes.

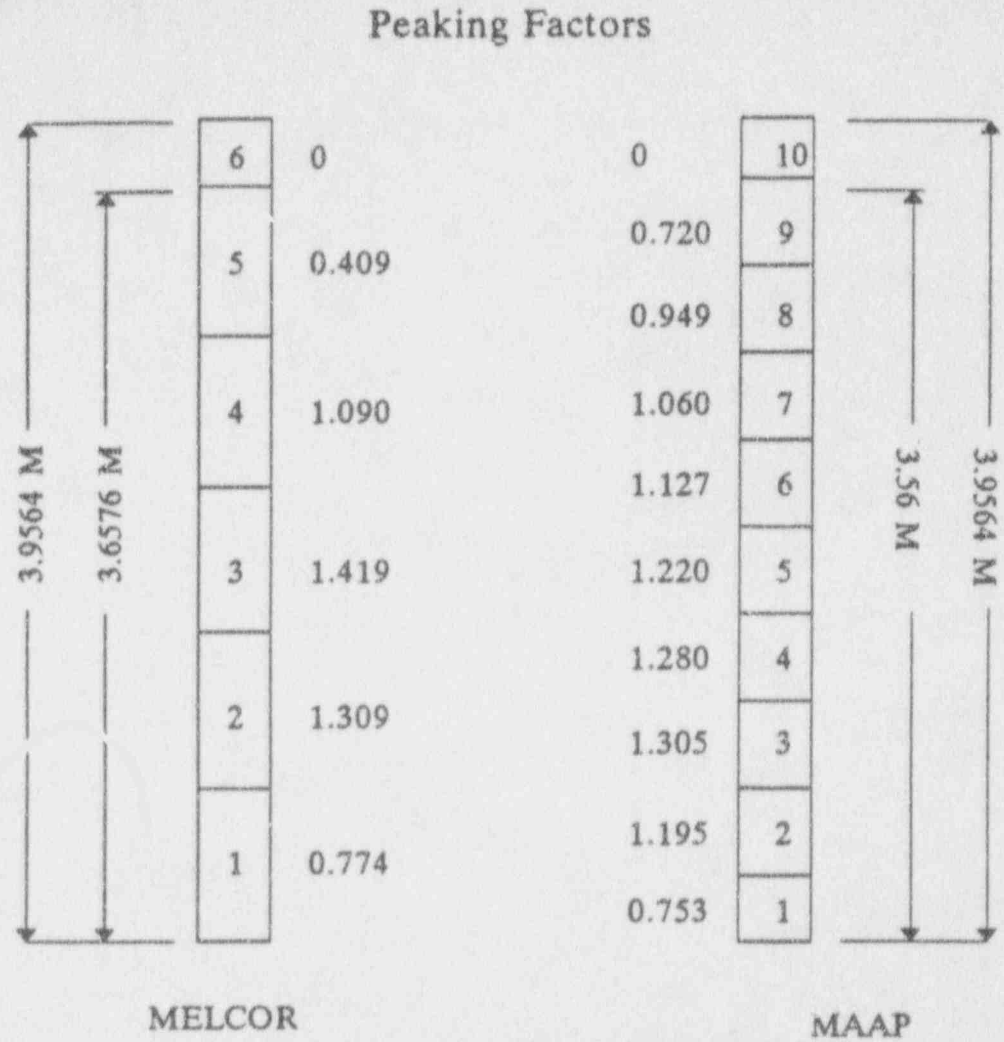

Figure C.5 Nodalization and Peaking Factor of Fuel Rod

For the radial power distribution, MELCOR requires the input of volume fraction and power fraction for each of the radial rings. The power fractions of the 4 radial rings used in the analysis of MELCOR are converted into radial peaking factors as shown in Table C.4. The analysis of MAAP has 7 radial rings. The volume fractions and radial peaking factors of these are compared in Table C.4. The radial power distribution modeled in the two codes is approximately comparable. For example, the radial ring No. 1 in MELCOR is approximately equivalent to the combination of rings No. 1 and 2 in MAAP. The radial ring No. 2 in MELCOR is approximately equivalent to the sum of rings No. 3, 4, and 5 in MAAP.

The axial and radial nodalization and power distribution are expected to affect the timing and behavior of fuel melting and relocation.

Tables C.5 and C.6 show the fission product inventory used in MELCOR and MAAP, respectively. Because the two codes use different classifications for the fission product groups, the masses are not directly compared. In MELCOR, Cs (Class 2) and I (Class 4) are combined together to form CsI and CsOH. The CsI group is referred to as Class 16 in MELCOR and can be compared to Class 2 in MAAP. The CsOH group is referred to as Class 2 in MELCOR and can be compared to Class 6 in MAAP.

Table C.4 Radial Power Distribution

MELCOR

Radial Ring	Volume Fraction	Power Fraction	Peaking Factor
1	0.16	0.1758	1.136
2	0.48	0.5232	1.127
3	0.17	0.1561	0.949
4	0.19	0.1449	0.788
Total	1.0	1.0	4.0

MAAP

		Peaking Factor	
Radial Ring	Volume Fraction	Input	Normalized
1	0.081	1.0974	1.146
2	0.102	1.0900	1.138
3	0.143	1.140	1.190
4	0.160	1.05	1.096
5	0.169	0.904	0.944
6	0.170	0.762	0.796
7	0.175	0.660	0.689
Total	1.0	6.7034	7.0

Note: Ring No. 1 is the inner ring.
Ring No. 4 (or No. 7) is the outer ring.

Table C.5 Fission Product Inventory in MELCOR

Class Name		Representative	Core Inventory, Kg
1.	Noble Gas	Xe, Kr	345.0
2.	Alkali Metals	Cs	192.3
3.	Alkaline Earths	Ba, Sr	151.4
4.	Halogens	I	14.9
5.	Chalcogens	Te	30.3
6.	Platinoids	Ru	212.9
7.	Early Transition Elements	Mo	251.1
8.	Tetravalent	Ce	443.1
9.	Trivalents	La	411.1
10.	Uranium	U	86,000
11.	More Volatile Main Group	Cd	1.0
12.	Less Volatile Main Group	Sn	5.7
13.	Boron	B	0
14.	Water	H_2O	0
15.	Concrete	--	0

Note: In MELCOR, Cs (Class 2) and I (Class 4) are combined together to form CsI and CsOH. The CsOH group is referred to as Class 2, and CsI as Class 16.

Table C.6 Fission Product Inventory in MAAP

	Fission Product Species	Core Inventory, Kg
1.	Noble Gases and Radioactivity Inert Aerosols	345.0
2.	CsI + RbI	31.8
3.	Te O_2	0
4.	SrO	78.7
5.	MoO_2	267.5
6.	CsOH + RbOH	213.4
7.	BaO	97.2
8.	La_2O_3 + Pr_2O_3 + Nd_2O_3 + Sn_2O_3 + 1/2 O_3	530.6
9.	CeO_2	229.2
10.	Sb	1.05
11.	Te_2	32.8
12.	UO_2 + NpO_2 + PuO_2	98,937

5 Discussion of Results

5.1 Primary System Thermohydraulics

MELCOR Analysis

The primary system pressure is illustrated in Figure C.6. The major features of the pressure plot are as follows: a) a rapid depressurization from 15.6 Mpa to about 7.5 Mpa within about 1000 seconds as a result of the sudden opening of the break area; b) a gradual decrease of pressure from about 1000 seconds to about 3200 seconds due to the continuous loss of coolant and water boil-off; c) an increase of pressure due to the activation of accumulators from about 3200 seconds to 4500 seconds; d) a small rise in presures followed by a decrease between 4500 to 10,500 seconds due to reheating in the core region after terminating accumulator injection and continuous loss of coolant; e) a spike in pressure at about 11,000 seconds caused by fuel relocation into the lower plenum, followed by rapid depressurization and penetration failure. Each of these features will be discussed in more detail.

Figure C.7 shows that MELCOR predicted water flowing out of the break area initially at about 144,000 Kg. This quantity of water occupies about 230 m^3 to 190 m^3 when water density is evaluated at 15.6 Mpa and 7.5 Mpa, respectively. Consequently, there is a rapid decrease of water level in the upper plenum and in the core region as shown in Figures C.8 to C.9. In the upper plenum, the water is depleted completely at about 460 seconds. At the same time, water in the core region decreases to a level near the bottom of the active fuel (4 M). However, the water levels are quickly recovered as a result of flow recirculation in the reactor vessel and in the coolant loops. Figure C.10 shows a pattern of natural circulation in the reactor vessel, i.e, flow moves downward from the upper plenum through the bypass channel to the lower plenum, and then from the lower plenum, flow moves upward through the core channels to the upper plenum. A positive downward flow from the downcomer to the lower plenum also is shown in Figure C.10, although a large flow oscillation is predicted in this region.

ZION SMALL BREAK 2.5" AT INTERMEDIATE LEG

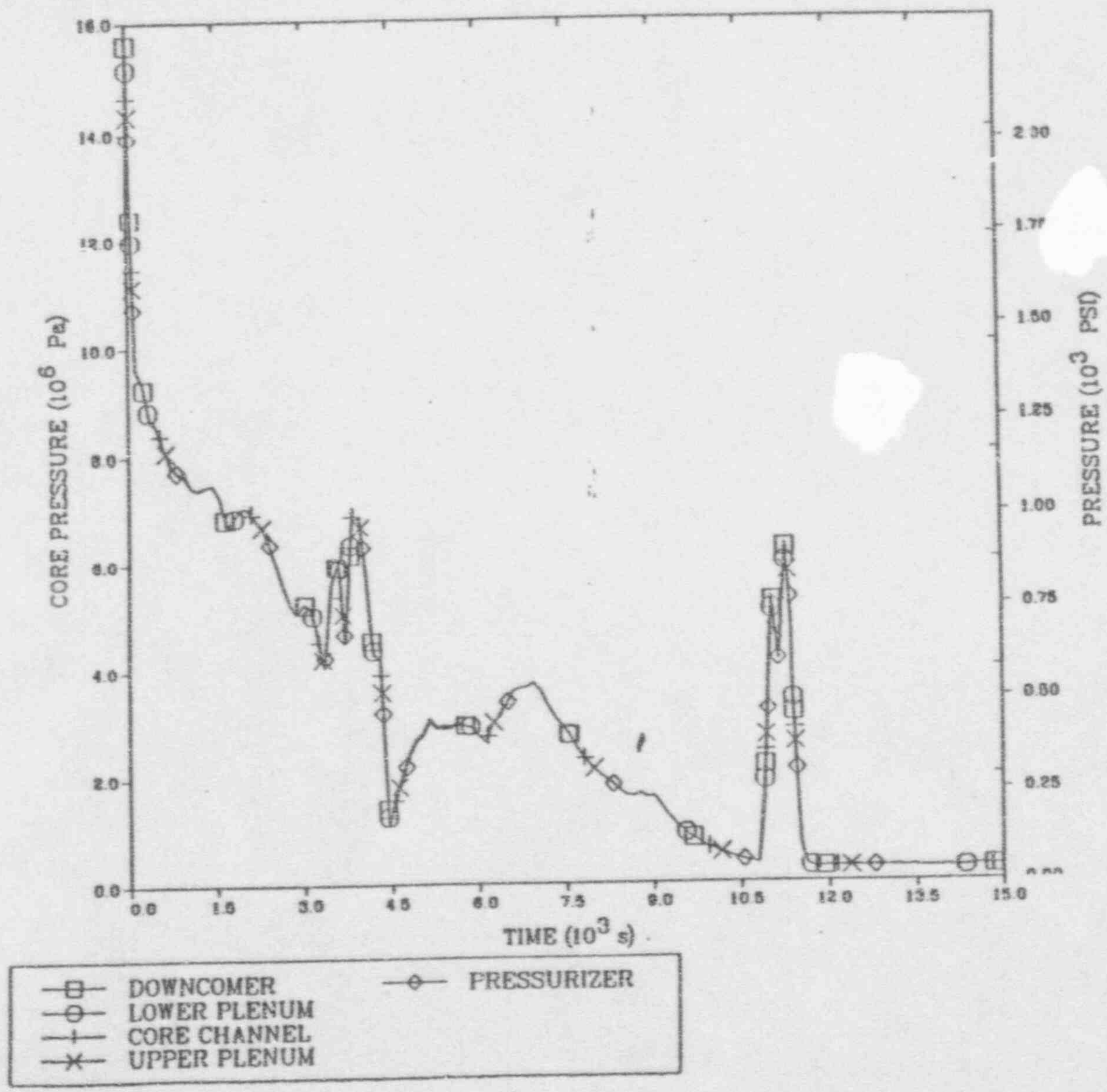

Figure C.6 MELCOR Predicted Reactor Vessel Pressure

ZION SMALL BREAK 2.5" AT INTERMEDIATE LEG

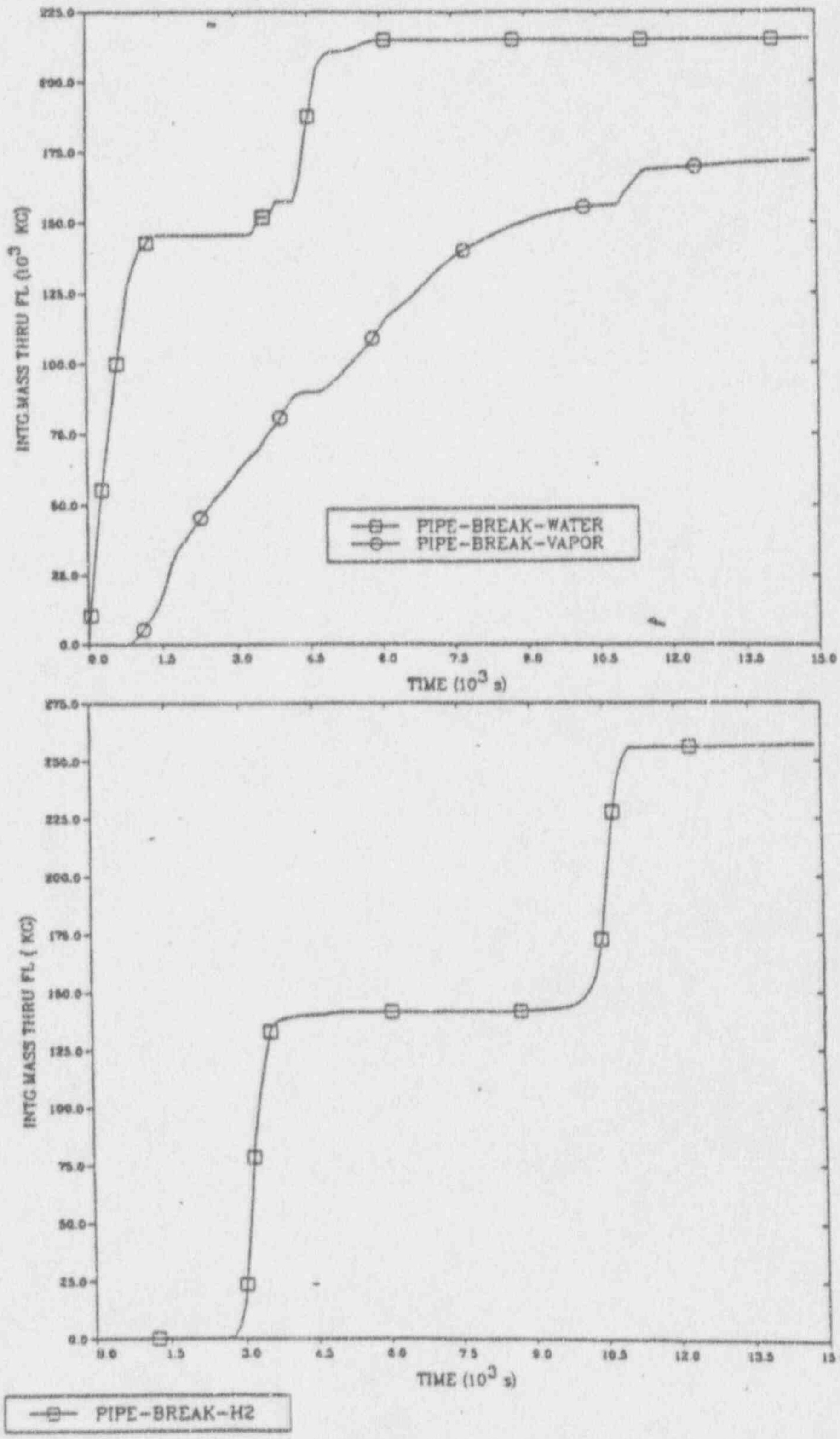

Figure C.7 MELCOR Predicted Break Flow

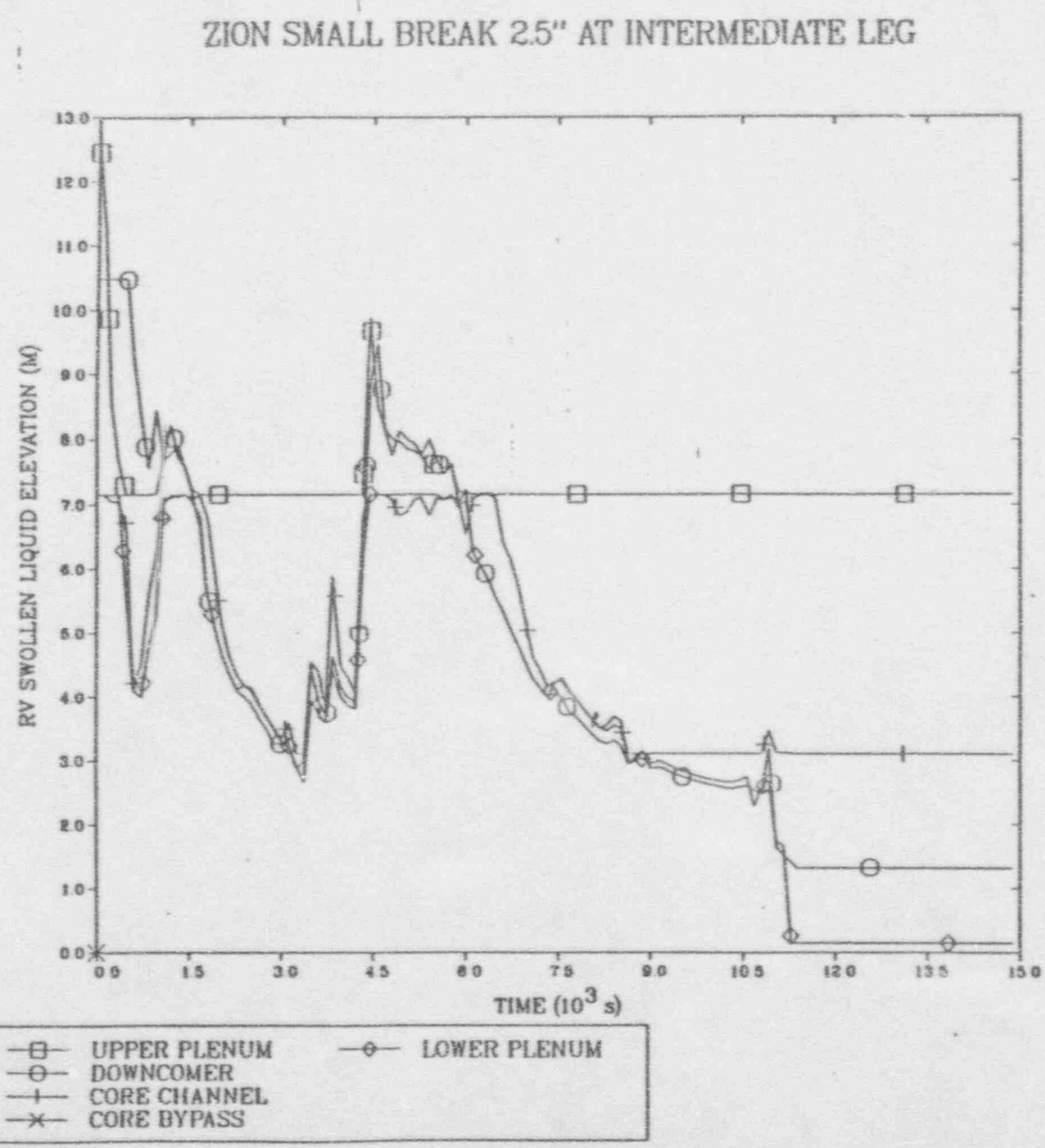

Figure C.8 MELCOR Predicted Swollen Liquid Elevation in Reactor Vessel

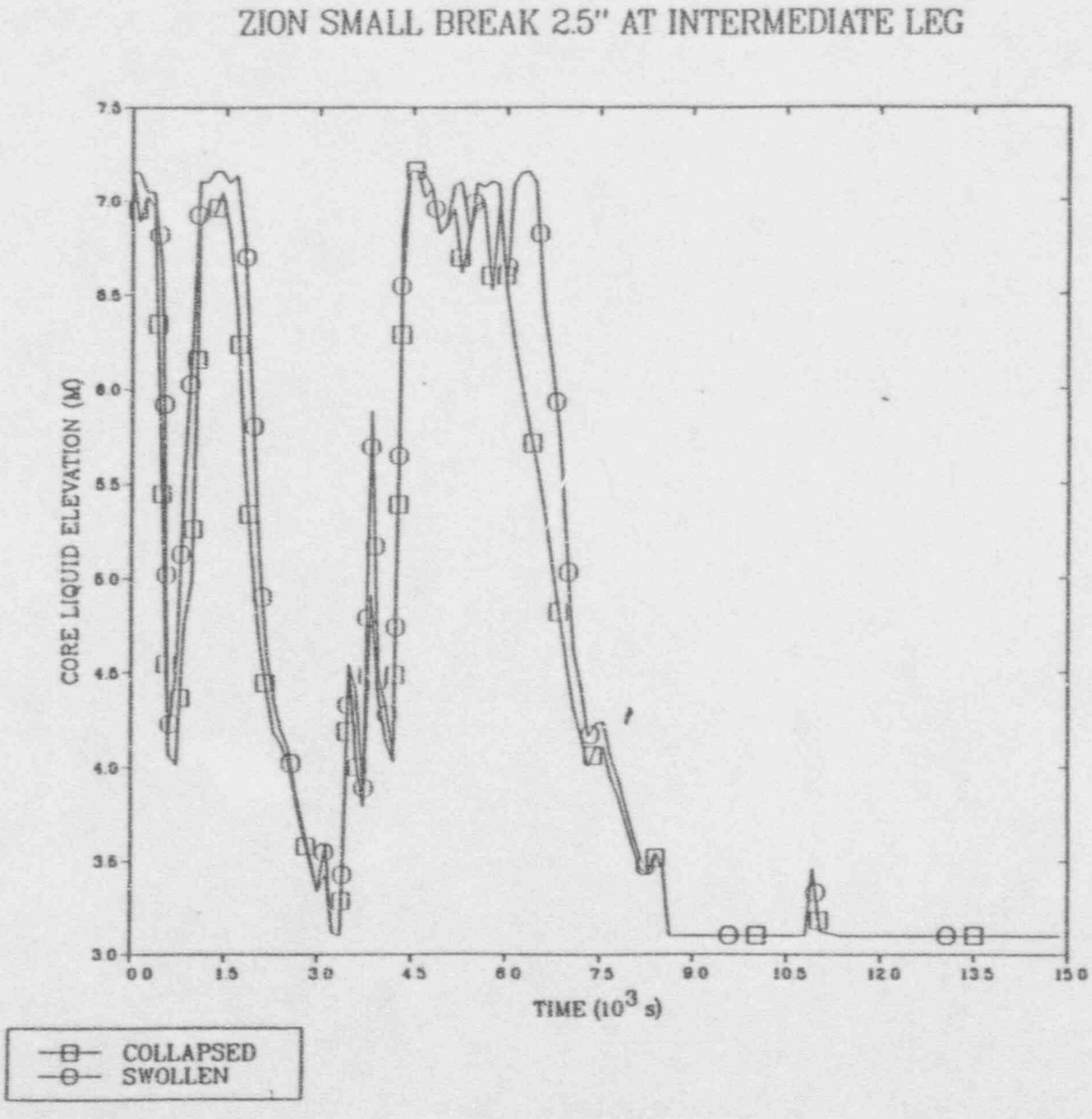

Figure C.9 MELCOR Predicted Swollen Core Liquid Level

ZION SMALL BREAK 2.5" AT INTERMEDIATE LEG

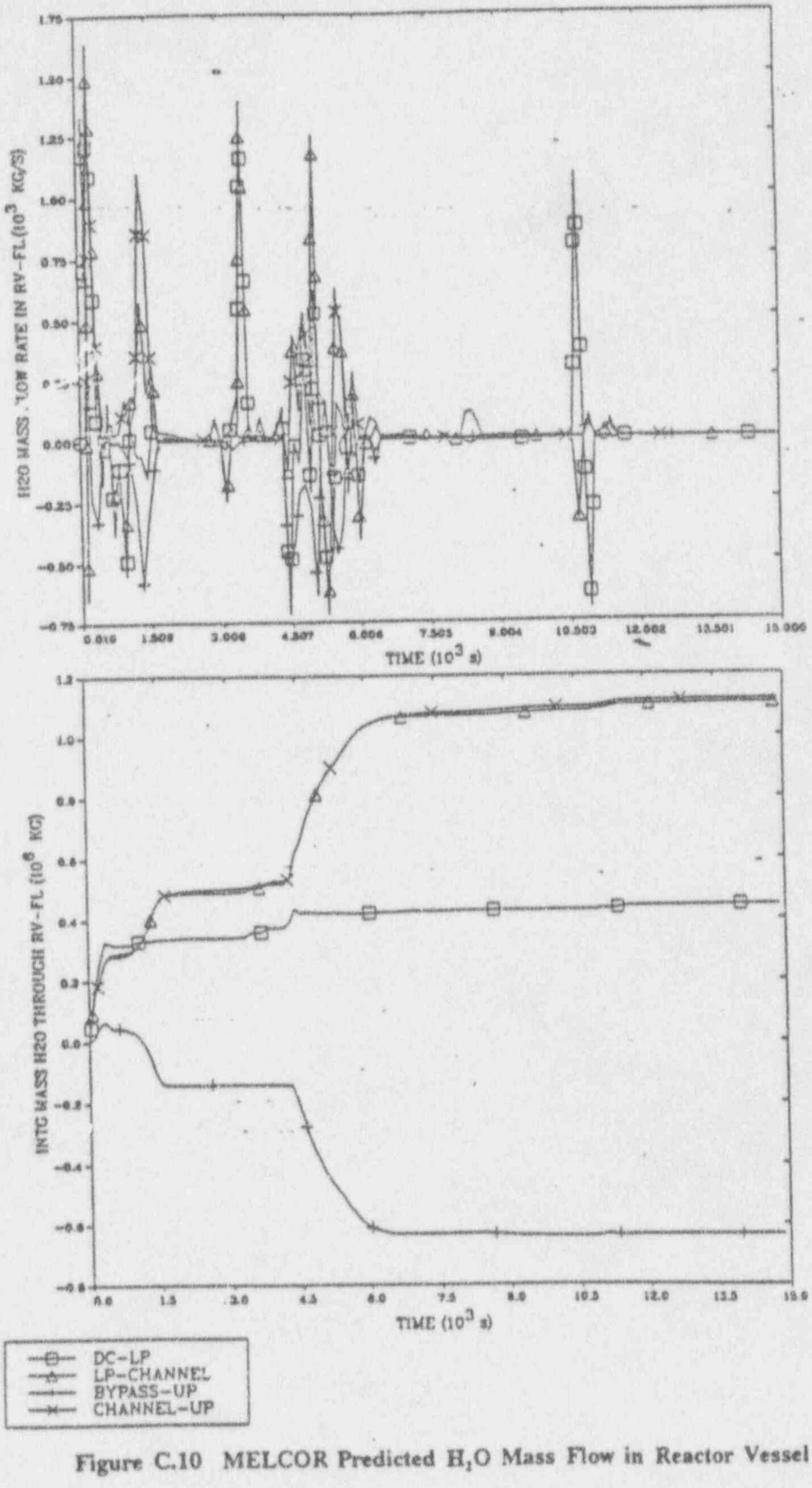

Figure C.10 MELCOR Predicted H_2O Mass Flow in Reactor Vessel

The flow pattern in the unbroken loop is shown in Figure C.11. MELCOR predicted a large flow oscillation during the first 1500 seconds. There are two periods during which flow reversal in the loop was predicted. The flow reversal implies that due to the quick depressurization in the reactor vessel and loss of water inventory in the upper plenum, water in the UB-loop was drained back to the upper plenum. However, the integrated mass flow show that there is no net flow reversal in the UB-loop.

In the BK-loop, MELCOR predicted a reversed flow from the downcomer through the cold leg and intermediate leg to the break area as shown by the negative flows in Figure C.12. Figure C.12 also reveals a large flow oscillation in the broken loop.

The natural circulation flow in the reactor vessel and flow reversal in the coolant loops discussed here result in a rapid core recovery at about 750 seconds, as shown in Figure C.9. However, the water level in the core region cannot be maintained because of the continued loss of water inventory through the break area. At about 3200 seconds, the water level is reduced below the bottom of active fuel elevation.

With the sudden addition of water from the accumulator in the uncovered core region and a rapid generation of steam, MELCOR predicted a spike in temperature around 3200 seconds as shown in Figure C.13. The extremely high atmospheric temperature (4500 K) is unrealistic and is probably caused by the numerical scheme used in MELCOR. Another high temperature period in the core and upper plenum regions between 7500 to 11,000 seconds is caused by the core dryout before fuel relocates into the lower plenum.

The accumulators are activated at about 3360 seconds when the primary system pressure is reduced to 4.275 Mpa. Figure C.14 shows that about 38,000 Kg of water is discharged into the cold leg of the BK-loop and about 114,000 Kg to the cold leg of the UB-loop in 1140 seconds. The water added to the UB-loop flows to the downcomer and into the lower plenum, while the water added to the BK-loop is released through the break. The increase of water break flow in Figure C.7, water level spike in Figure C.8 and C.9, and the increase of mass flow in the coolant loops in Figures C.10 to C.12, are evidence that the accumulators activate at about 3360 seconds. The activation of the accumulators reflooded the core.

Comparison with MAAP

Thermohydraulics in the primary system and core region predicted by MAAP are shown in Figure C.15 to C.19. Comparisons with the predictions by MELCOR show differences on pressures, temperatures, and behavior of flow.

Figures C.15 illustrates the primary system pressure, water level in the core region, and the accumulator injection rate. Similar to MELCOR predictions, MAAP predicted an initial decrease of system pressure to about 8.2 Mpa. The pressure remains at this level to about 1500 seconds, and then starts to decrease until 3670 seconds, when the accumulators are activated. The cyclic operation of the accumulators causes a slight oscillation of the system pressure. The pressure becomes stable at about 8000 seconds, when the accumulator water injection is terminated and the core is recovered. At about 10,000 seconds, pressure starts to decrease and the primary system is completely depressurized at 13,587 seconds, when failure of the penetration tubes in the lower plenum is predicted.

Comparisons between the MELCOR predicted pressure (Figure C.6), water level (Figure C.9), accumulator water injection (Figure C.14), and the MAAP results reveal the following differences:

1. The MELCOR code predicted two pressure spikes due to accumulator water injection at 3400 seconds and fuel relocation into the lower plenum at 11,000 seconds. These were not predicted by MAAP. Calculations by MAAP showed that the primary system was depressurized throughout the entire transient.

2. MELCOR predicted that initial core uncovery and recovery within the first 1000 seconds were not predicted by MAAP. Although a large quantity of water was released through the break, MAAP calculations showed that the water level in the reactor vessel was unaffected for about 2000 seconds.

ZION SMALL BREAK 2.5" AT INTERMEDIATE LEG

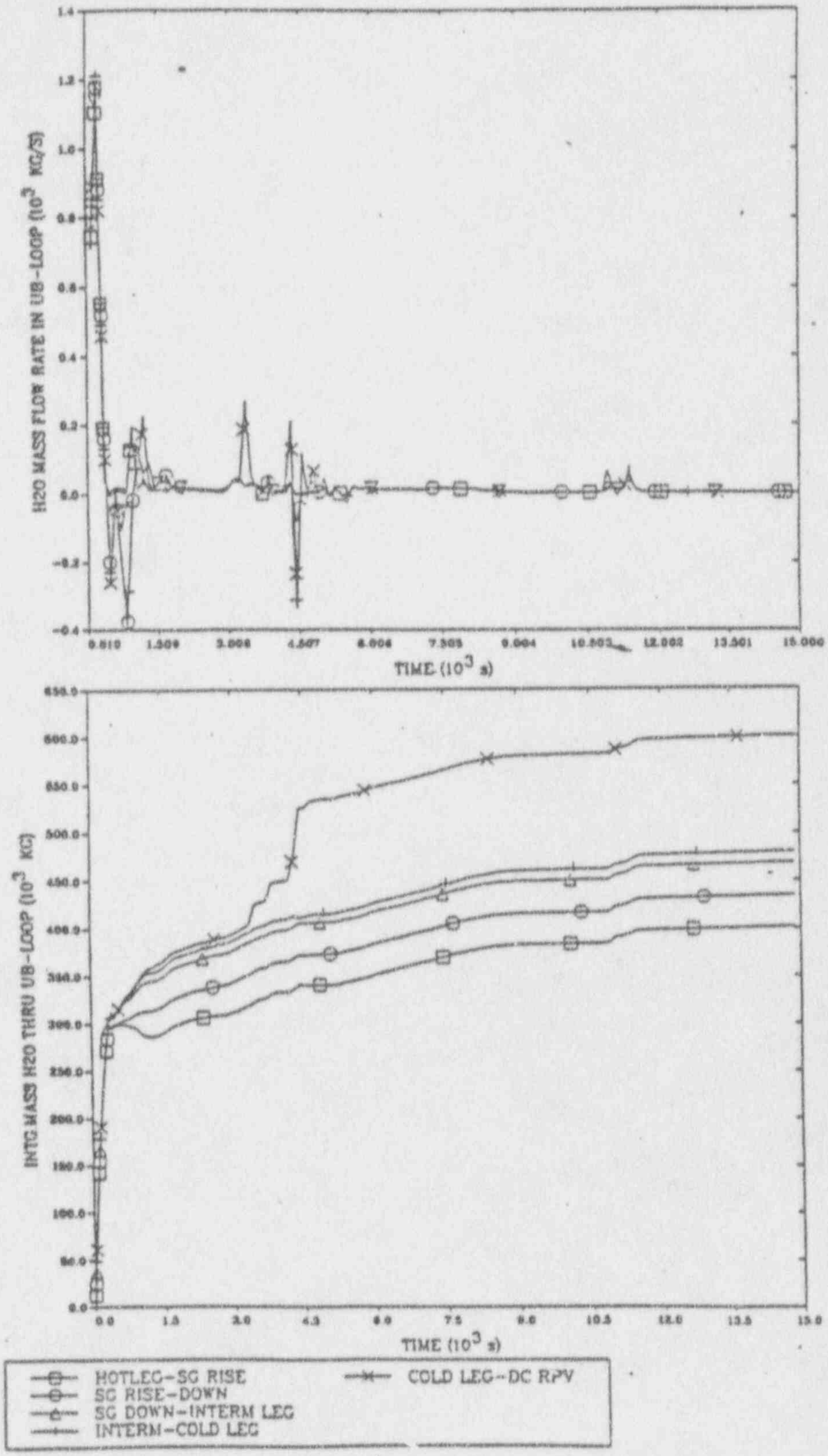

Figure C.11 MELCOR Predicted H_2O Mass Flow in the Unbroken Loop

ZION SMALL BREAK 2.5" AT INTERMEDIATE LEG

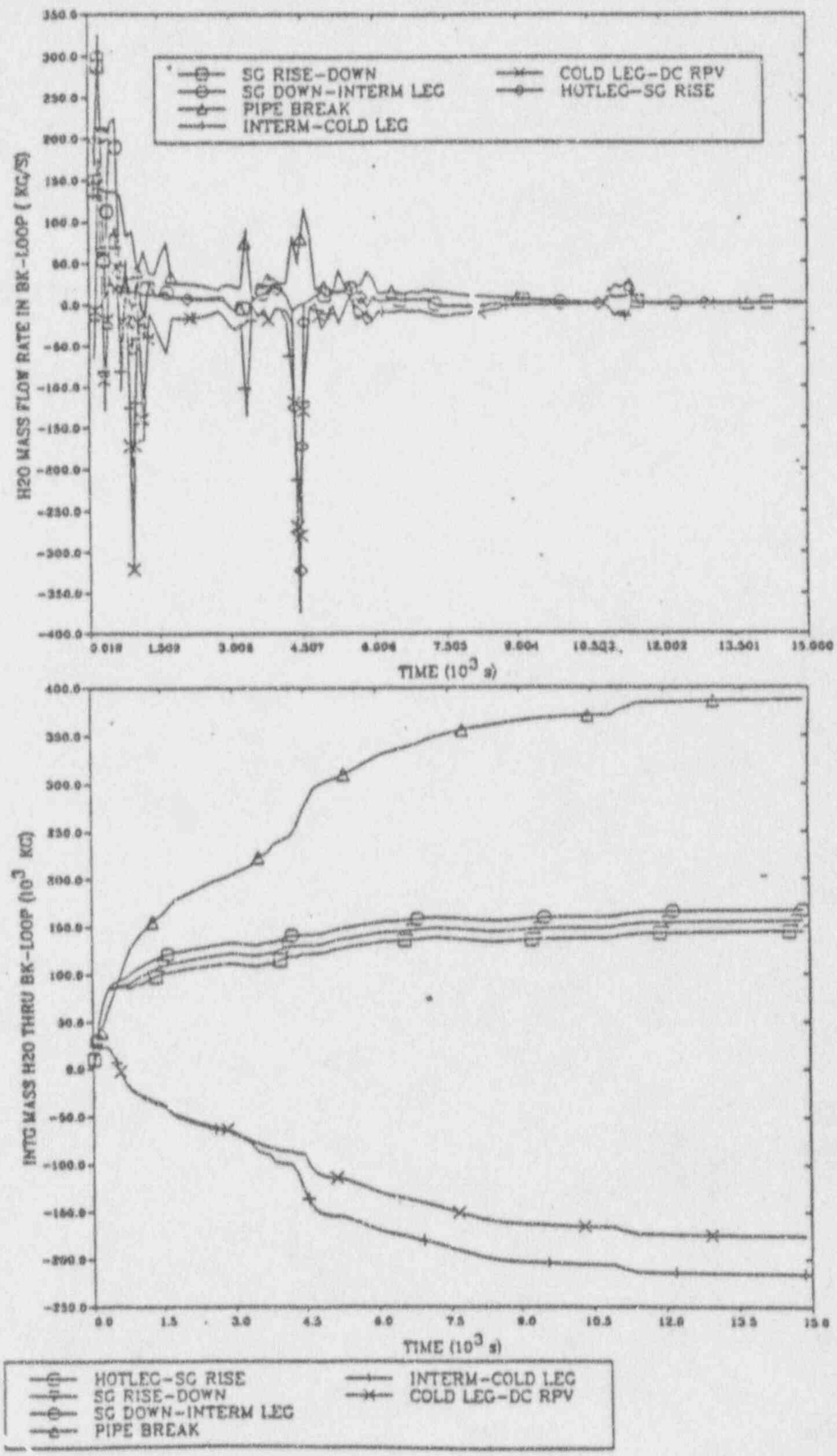

Figure C.12 MELCOR Predicted H_2O Mass Flow in the Broken Loop

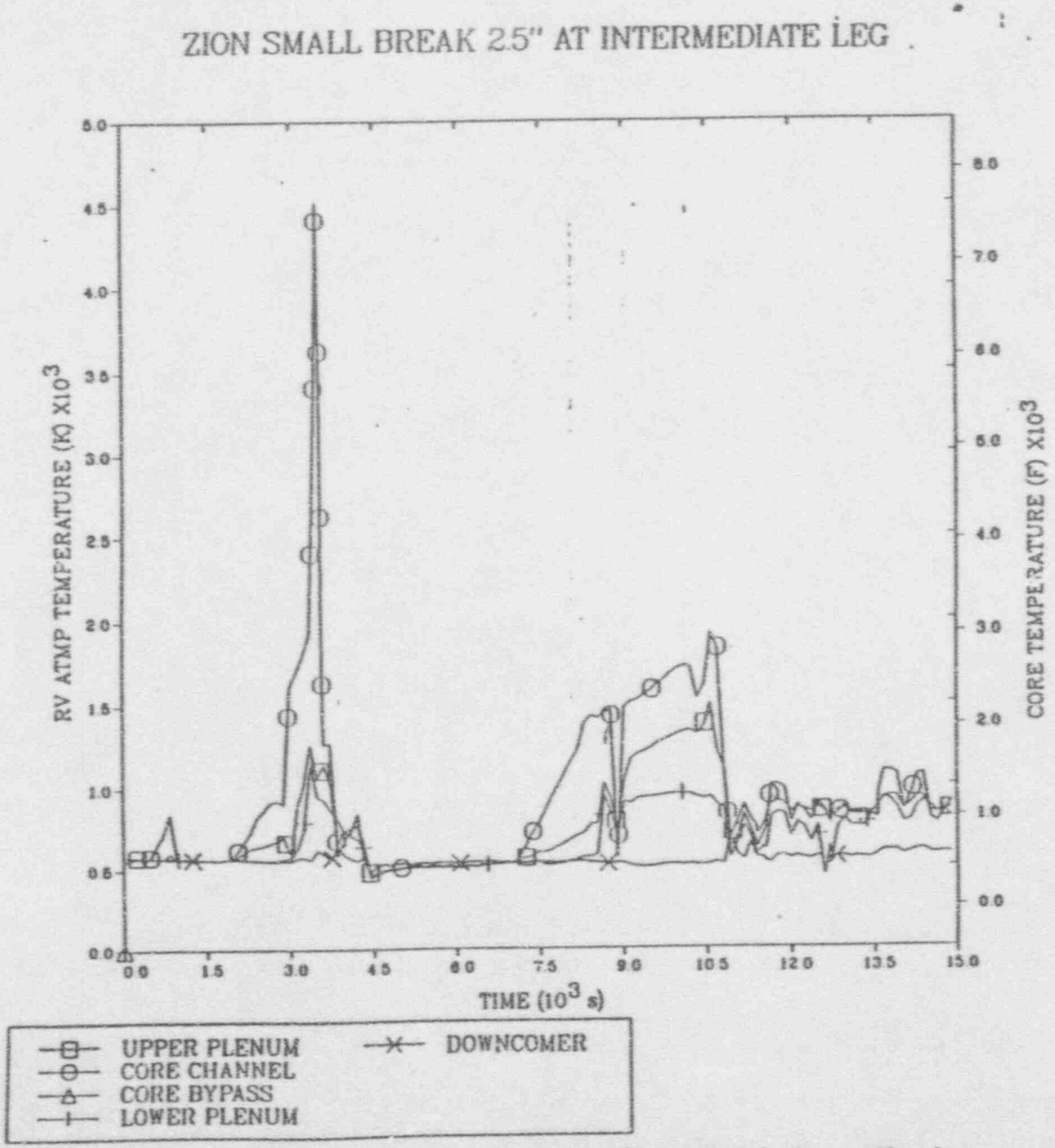

Figure C.13 MELCOR Predicted Atmosphere Temperature in Reactor Vessel

ZION SMALL BREAK 2.5" AT INTERMEDIATE LEG

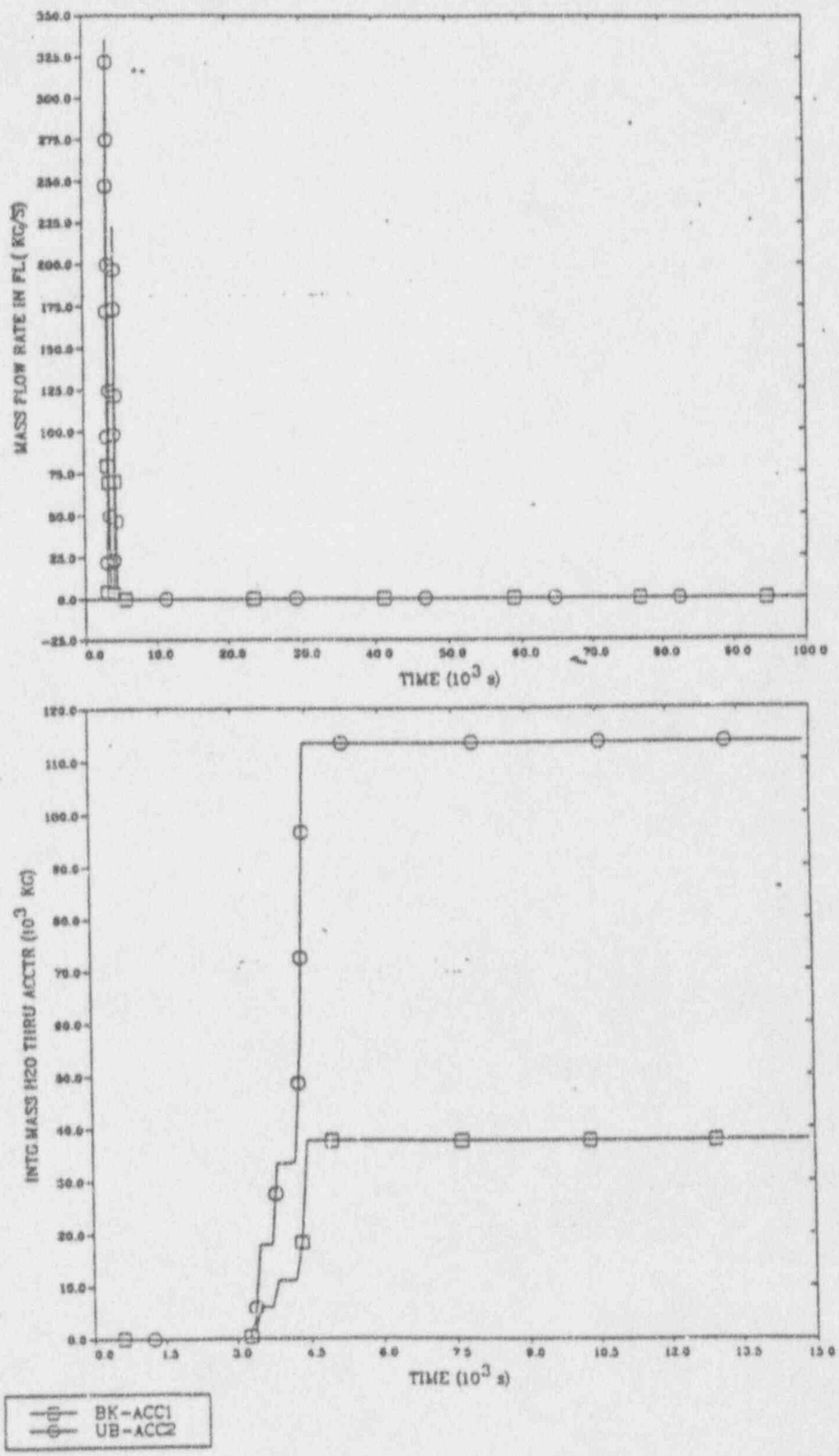

Figure C.14 MELCOR Predicted Accumulator Flow

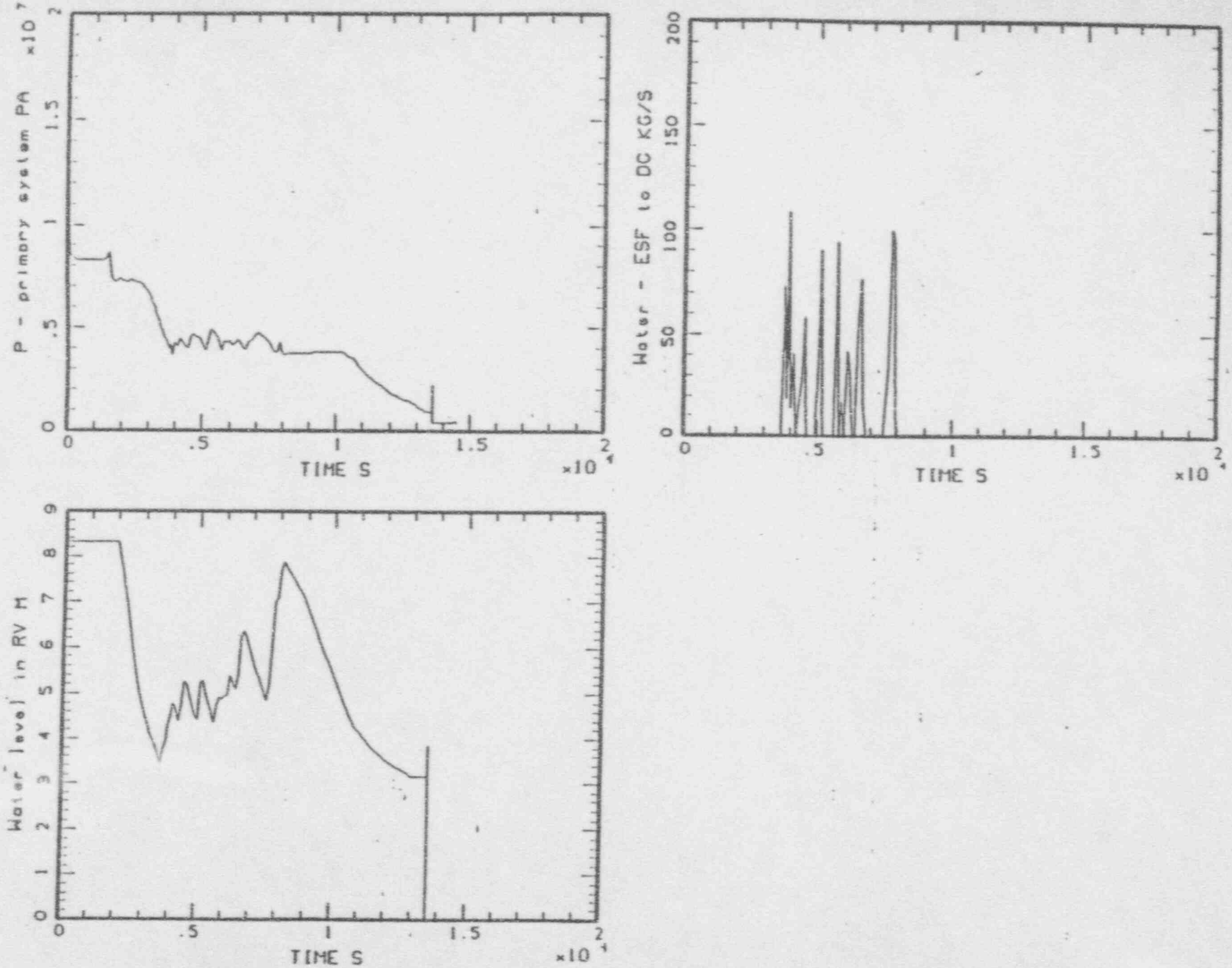

Figure C.15 MAAP Predicted System Pressure, Core Water Level, and Accumulator Water Injection Rate

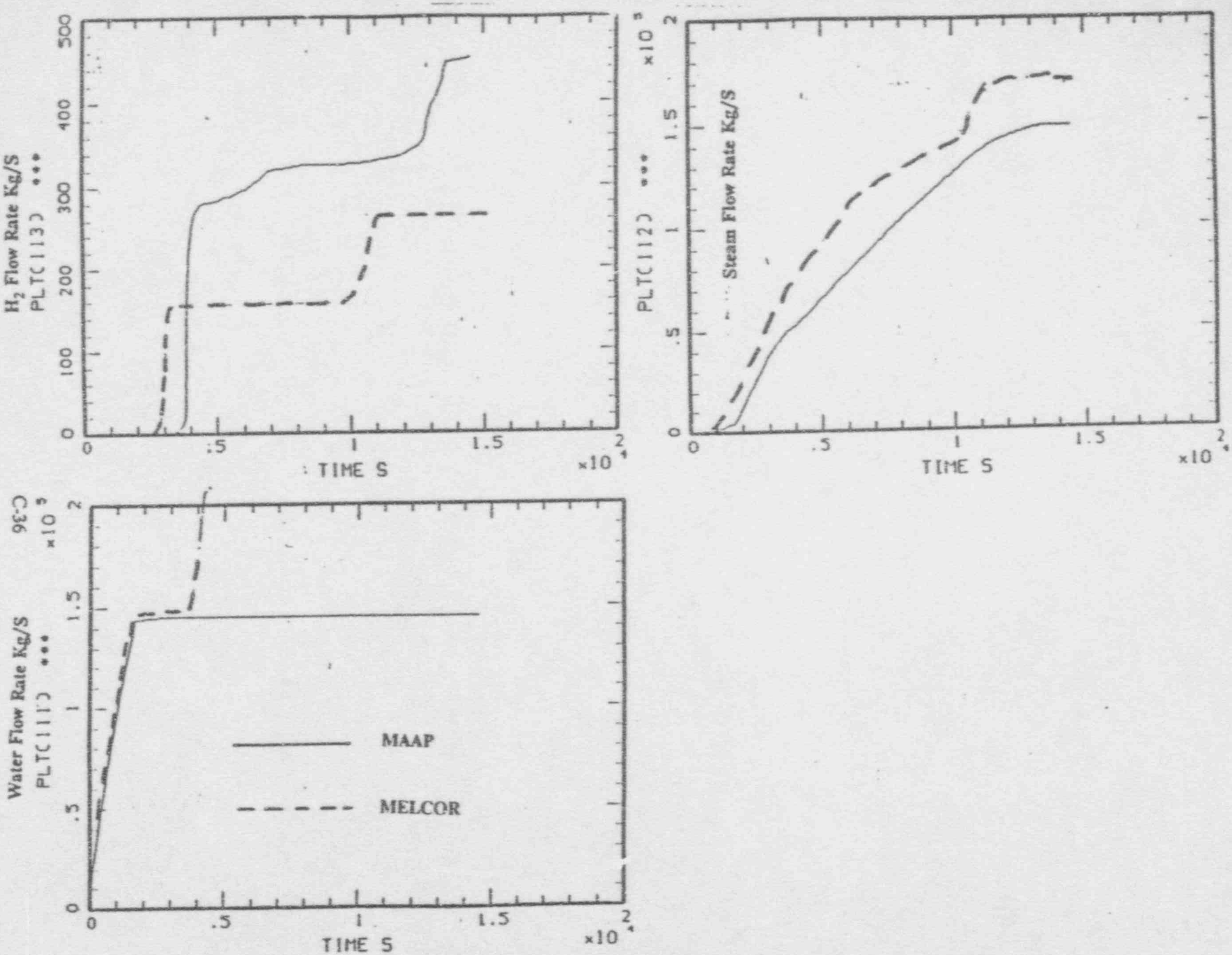

Figure C.16 MAAP Predicted Break Flow Rate

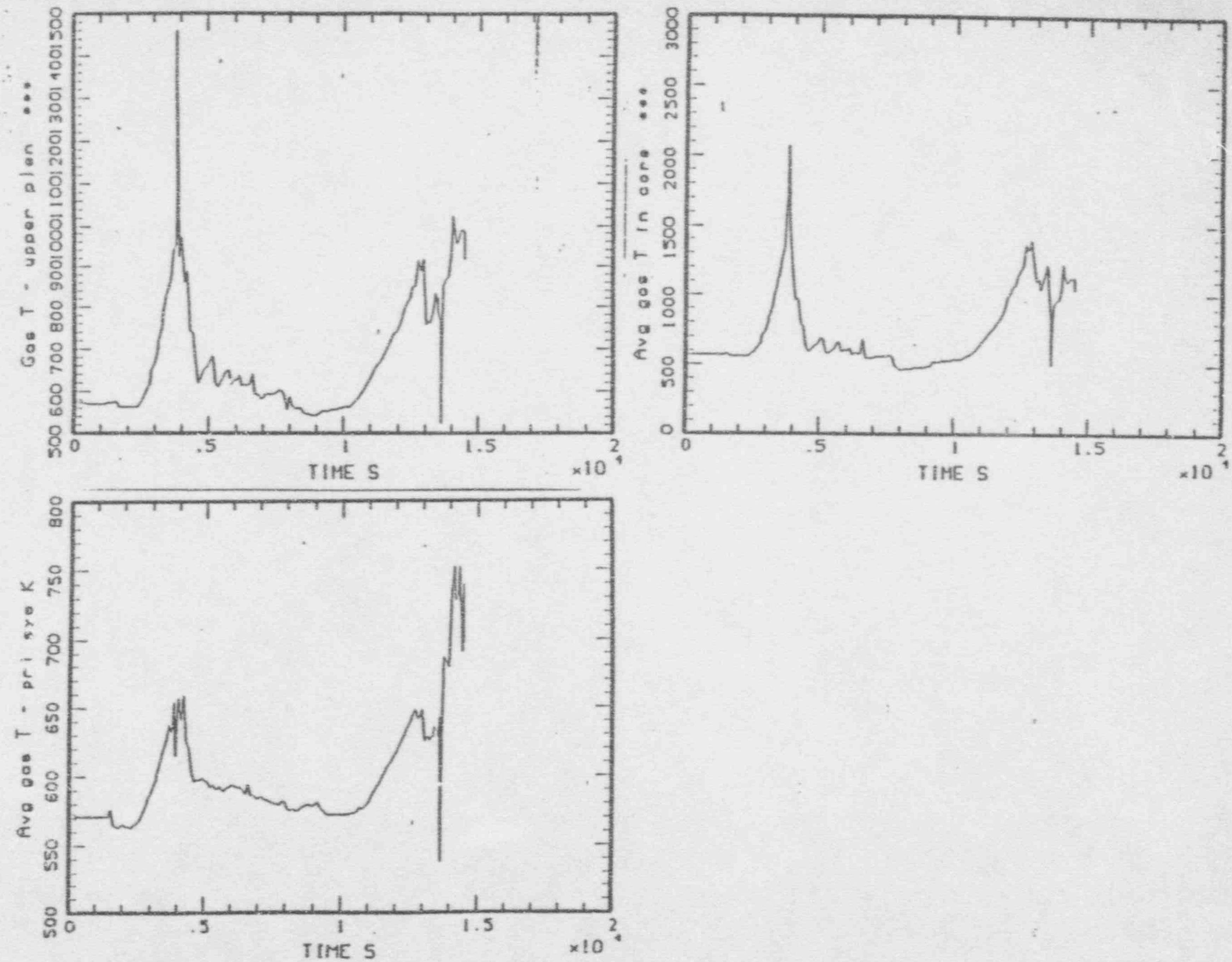

Figure C.17 MAAP Predicted Gas Temperature In Primary System

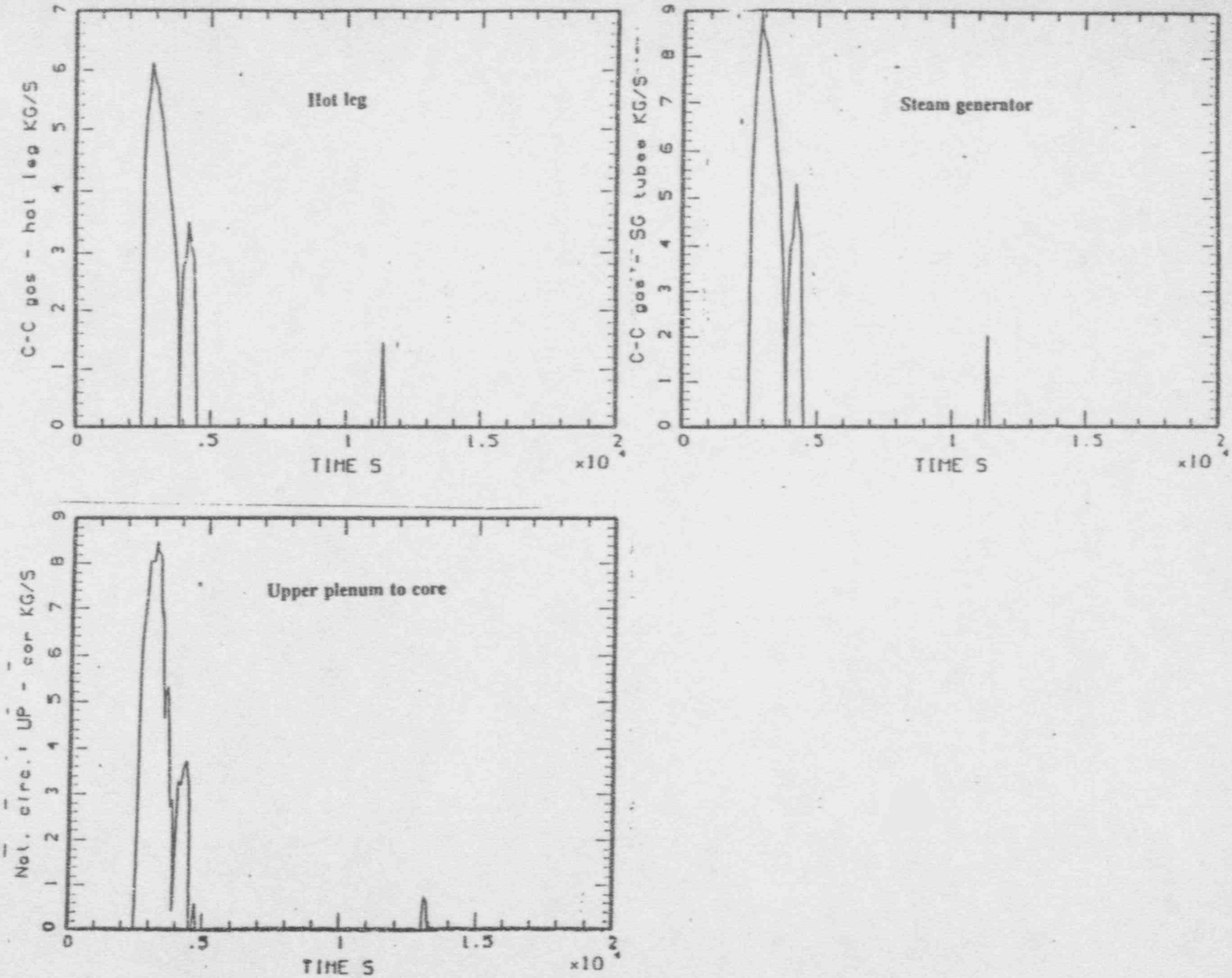

Figure C.18 MAAP Predicted Natural Circulation Flow

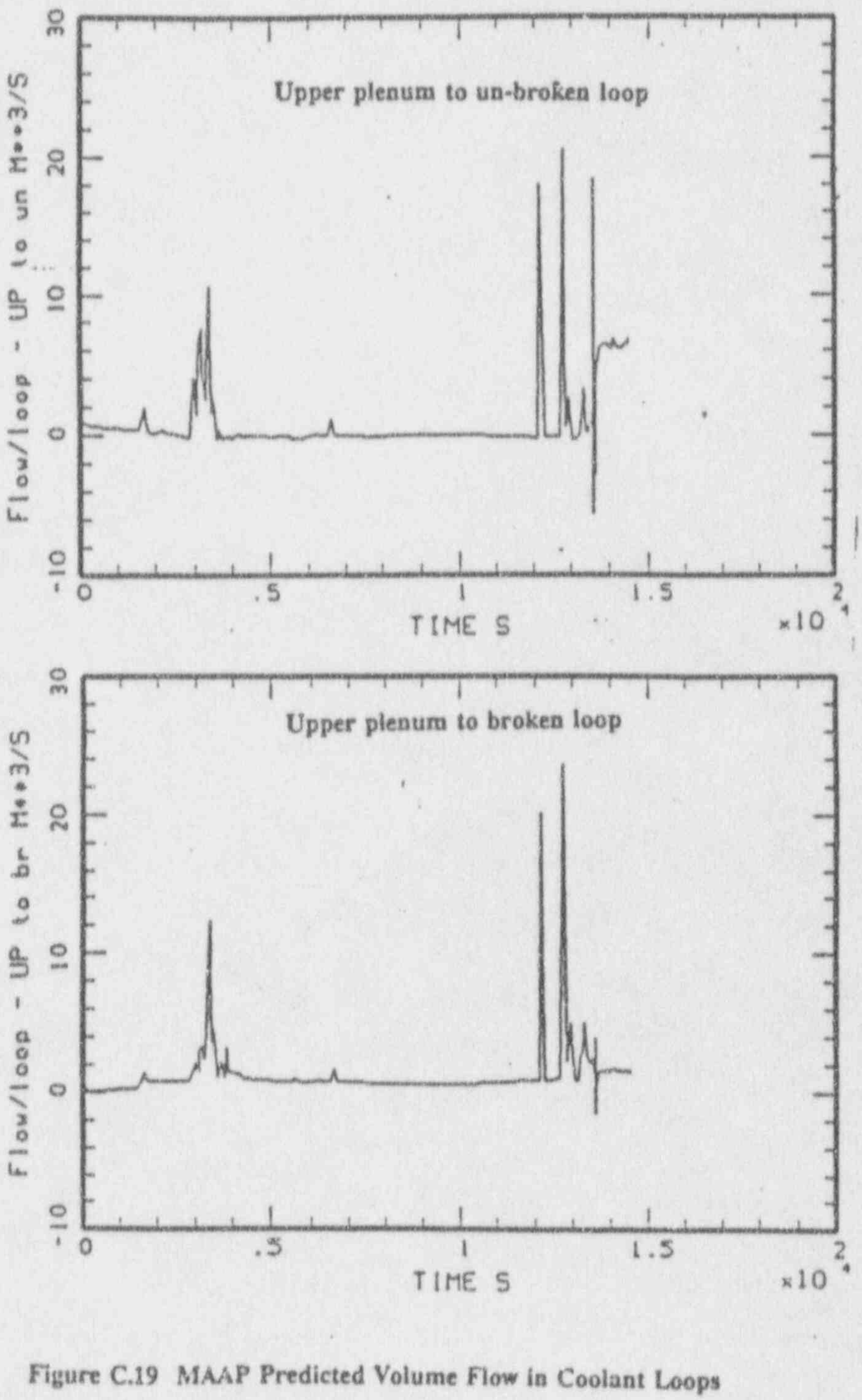

Figure C.19 MAAP Predicted Volume Flow in Coolant Loops

3. Both MELCOR and MAAP showed a complete core recovery after accumulator water was added into the reactor vessel. However, the MELCOR predicted water level (10 m) is about 2 meters higher than that predicted by MAAP (8 m).

4. In the analysis of MELCOR, the accumulators were operated for about 1100 seconds and the maximum injection rate is 325 Kg/s. In the analysis of MAAP, the accumulators were operated for 4500 seconds with the maximum injection rate at 100 Kg/s.

The break flows predicted by MAAP are shown in Figure C.16 in comparison with the MELCOR results given in Figure C.7. The total water flows predicted by the two codes agree well before the accumulators activate. In the analysis of MELCOR, the accumulator water injected into the broken loop is released through the break; while in the analysis of MAAP, all accumulator water is added directly to the reactor vessel lower plenum. MELCOR's calculation showed that hydrogen was released in two stages: about 138 Kg during the early heatup and another 122 Kg during core debris relocation into the lower plenum. The total hydrogen released is about 260 Kg. Contrary to MELCOR, MAAP's calculation showed a large release of about 280 Kg of hydrogen during the early heatup. Another 60 Kg was gradually released during the transient before the reactor vessel failure at 13,587 seconds. A total of 340 Kg of hydrogen is released. Note that in the analysis of MELCOR, the break flow consists of a mixture of water, steam, and hydrogen before 6000 seconds. After the water level was reduced below the break elevation at 6000 seconds, only the gaseous mixture (steam and hydrogen) was released through the break. In the analysis of MAAP, phase separation started early and the break flow contains mainly the gaseous mixture

The gas temperatures predicted by MAAP are shown in Figure C.7. A peak core temperature (2000 K) is predicted at about 3700 seconds after the onset of fuel melting before the accumulators are activated. Once the accumulator water is added to the core and the core is reflooded, gas temperature is maintained at about 600 K. The low core temperature will not increase system pressure. We should point out that the peak core temperature (2000 K) predicted by MAAP is much lower than the unrealistic temperature (4500 K) predicted by MELCOR (Figure C.14).

Figure C.18 and Figure C.19 present some natural circulation flows provided by MAAP. Figure C.18 shows the natural circulation flows from the upper plenum to the core region, counter-current flows in the hot leg and in the steam generator tubes. Figure C.19 shows flow from the upper plenum to the UB-loop and BK-loop. Both figures show two distinguishable time periods of natural circulation. The first (between 2500 to 4500 S) approximately corresponds to the time of core uncovery and accumulator water injection. The second starts at about 11500 S: the cause of the development of natural circulation has not been identified. Comparisons with the MELCOR predictions (Figures C.10 to C.12) reveal that:

(a) The continuous flow circulation in the reactor vessel and loops predicted by MELCOR are not indicated by MAAP;
(b) The negative flow (i.e., reversal flow) predicted by MELCOR is not indicated by MAAP;
(c) The natural circulation flow rates predicted by MELCOR are much higher than MAAP's predictions.

5.2 Fuel Relocation and Reactor Vessel Failure

MELCOR Analysis

In MELCOR, several important assumptions, which affect fuel behavior during core meltdown and the timing of major events, are made.

1. Holdup of molten material by an oxide shell is turned off by using the default values of the sensitivity coefficients C1131.
2. A particulate debris is formed when the unoxidized Zr thickness in an intact cladding reaches 10^{-6} m. This assumption implies that a very thin layer of the unoxidized Zr will be sufficient to support the fuel. The same criterion is applied to the unoxidized steel thickness in structures.
3. The porosity and diameter of the particulate debris are 0.4 and 0.0125 m, respectively.
4. The relocation of core material in all core cells is governed by two assumptions: a) the particulate debris will not be supported by the "other structure" at this level, and b) an intact component in the

cell below must be present to support components in the current cell, otherwise these components will be relocated downward.

5. For the axial cell No. 6 (i.e., lower core plate at the bottom of the active fuel), we assumed that the plate will support particulate debris until the steel reaches the failure temperature (1273 K). The intact steel will remain in that cell until it melts or forms a particulate debris.
6. The default values specified by the input parameter COR0007 for transporting secondary materials during candling were used. The default values specify that the quantity of UO_2 relocated with the molten Zr is 20% of the molten Zr. The quantity of ZrO_2 relocated with the molten Zr is directly proportional to the existing fraction of ZrO_2 to Zr.
7. The candling heat transfer coefficients, which specify the refreezing of the molten core materials, are 300 W/m^2-K.
8. In the lower plenum, the failure of the lower head is assumed to occur whenever the temperature of the penetrations or the innermost node of the lower head reaches 1273 K.
9. Heat transfer coefficients from debris to penetrations, and from debris to the lower head are assumed to be 500 W/m^2-K.
10. The relocation of materials in all cells in the lower plenum is governed by two assumptions: a) particulate debris will not be supported by steel, and b) intact steel will remain until it melts or forms particulate debris.
11. There are four penetrations, one in each radial ring. The initial diameter of the penetrations is 0.1084 m.
12. The discharge coefficient for ejecting debris through the failed penetration opening is 1.0.
13. The default value of the corium discharge flag is used (i.e. IDEJ = 0). This value implies that the masses of each material available for ejection are total debris masses, regardless of whether or how much they are melted. Note that after penetration failure, MELCOR requires that a total molten mass of 5000 Kg, or a melt fraction of 10% is necessary before debris can be ejected.

Based on these assumptions, fuel melting and relocation predicted by MELCOR are summarized in this section. Figure C.20 shows the clad and fuel temperatures in the inner ring of the core. Clad in the middle and upper axial segments (Cells 109 to 112) melts at about 2655 seconds. The melting of the metallic Zr relocates molten Zr. As the model of holdup the molten material is turned off in this analysis. With the removal of metallic Zr, the fuel loses its support; thus particulate debris consisting of UO_2 and ZrO_2 is formed in these cells. The fuel temperature in Figure C.20 shows that UO_2 remains as solid material. The melting of clad and formation of particulate debris in the lower segments of the core (i.e. Cells 108 and 107) are delayed by about 7800 seconds.

In the inner ring, there are about 15,720 Kg of UO_2 and 2,990 Kg of Zr in the five active fuel nodes. Another 244 Kg of Zr is in the unheated top node. The detailed relocation of these core materials from the top cell in the core region (112) to the bottom cell in the lower plenum (101) is illustrated in Figure C.21. The core materials in the top three Cells (112, 111 and 110) fall through directly to Cells 109 to 106. Since clad failure is delayed for Cells 107 and 108, the intact components permit the holdup of the particulate debris on Cells 109 to 107. According to the MELCOR logic process for relocating material, the lower core plate (Cell 106) can support the particulate debris and hold up steel by refreezing molten steel moved to this cell. Before the complete relocation of core material into the lower plenum at about 10,790 seconds, Figure C.21 shows that all UO_2 (about 15,720 Kg) are accumulated in Cells 106 to 109, all Zr and ZrO_2 (about 3650 Kg) in the core region are accumulated in Cells 107 and 106. In the lower plenum, all core debris are accumulated in the three lower cells (101 to 103). The code predicted penetration failure at about 12,706 seconds. However, according to the logic process, which restricts the debris discharge, ejection of debris starts at about 15,240 seconds as shown in Figure C.21.

Similar fuel and clad temperatures, and material relocation behavior are predicted for the other radial rings. Table C.7 summarizes the core relocation, penetration failure and debris ejection in all radial rings. The time duration between the onset of relocation to the complete relocation into the lower plenum varies from 132 to 145 minutes in the four radial rings. It should be pointed out that the input parameters required for the lower head analysis and the modeling of the lower head represent one of the largest uncertainties of the MELCOR code. No parametric study has been performed to assess the uncertainty of the lower head analysis.

ZION SMALL BREAK 2.5" AT INTERMEDIATE LEG

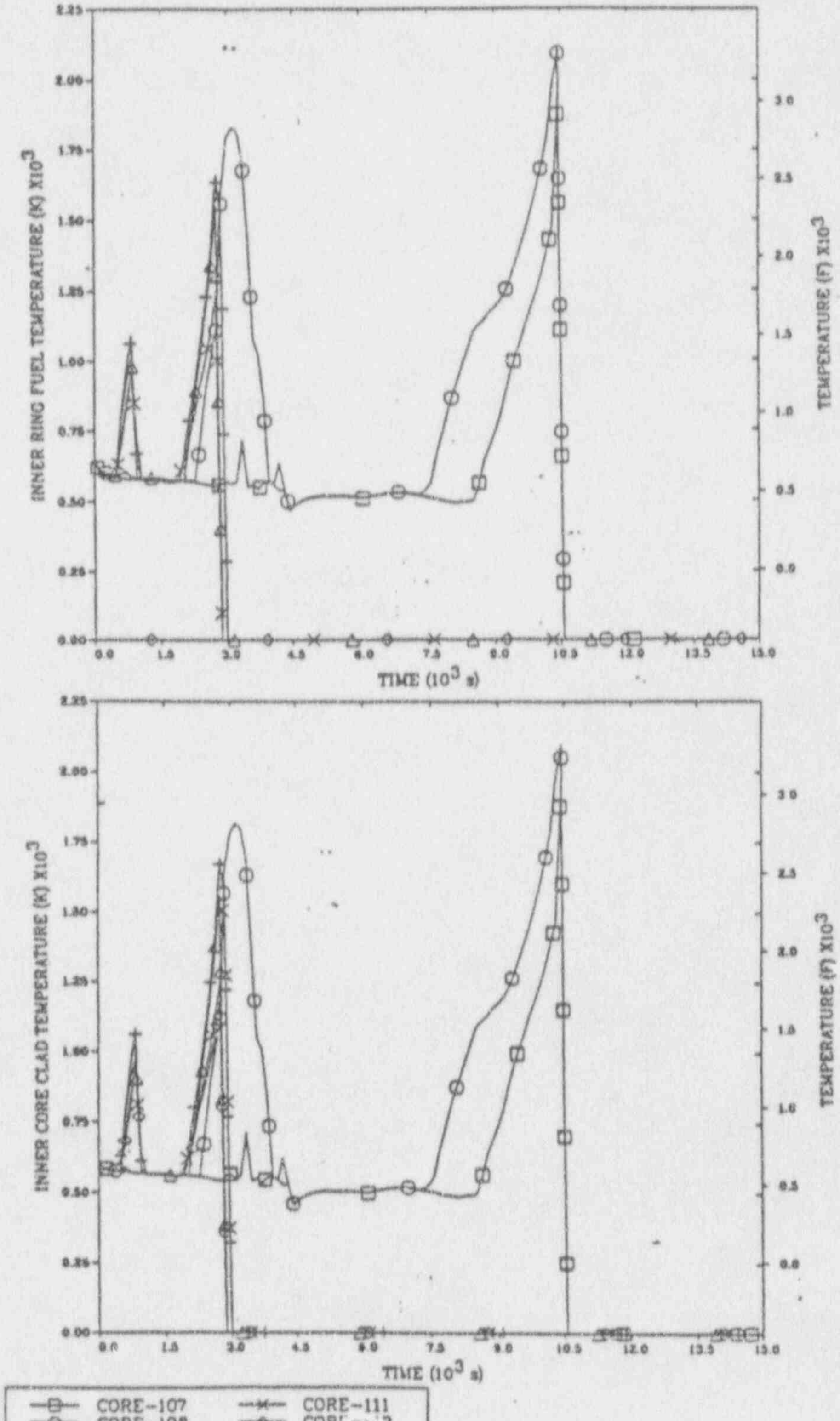

Figure C.20 MELCOR Predicted Clad and Fuel Temperature in the Inner Ring

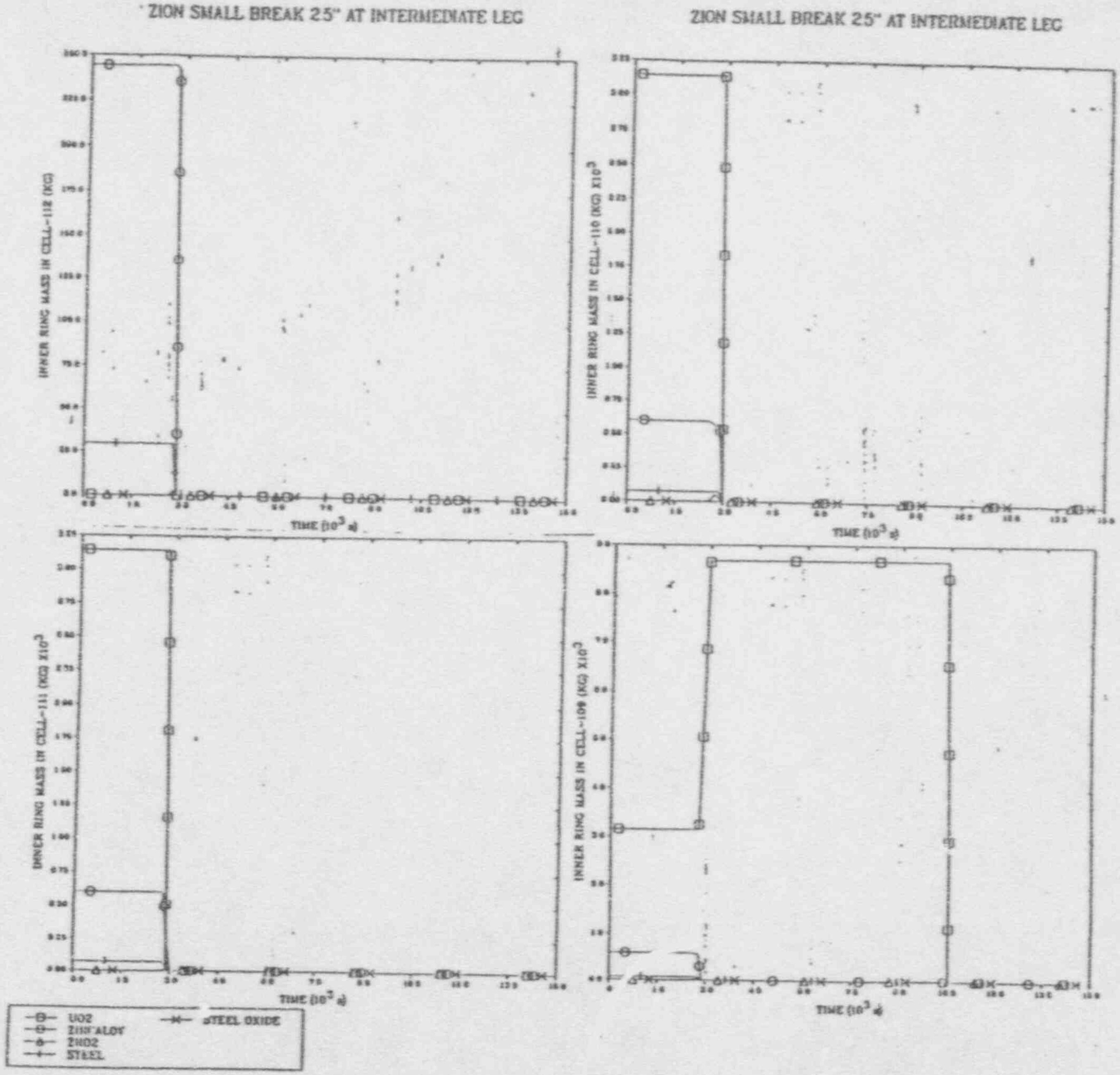

Figure C.21 MELCOR Predicted Core Relocation in the Inner Ring

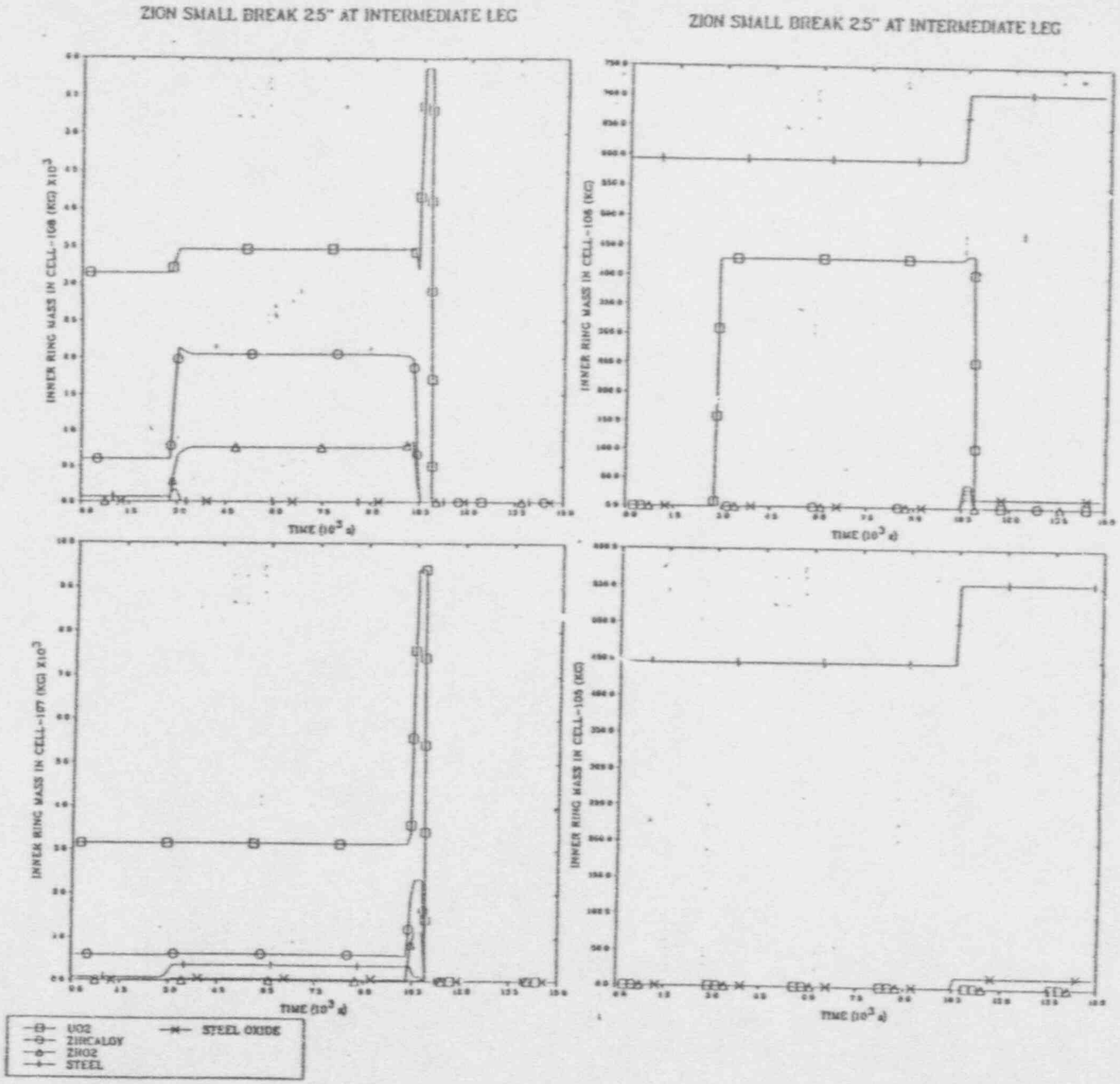

Figure C.21 MELCOR Predicted Core Relocation in the Inner Ring (Continued)

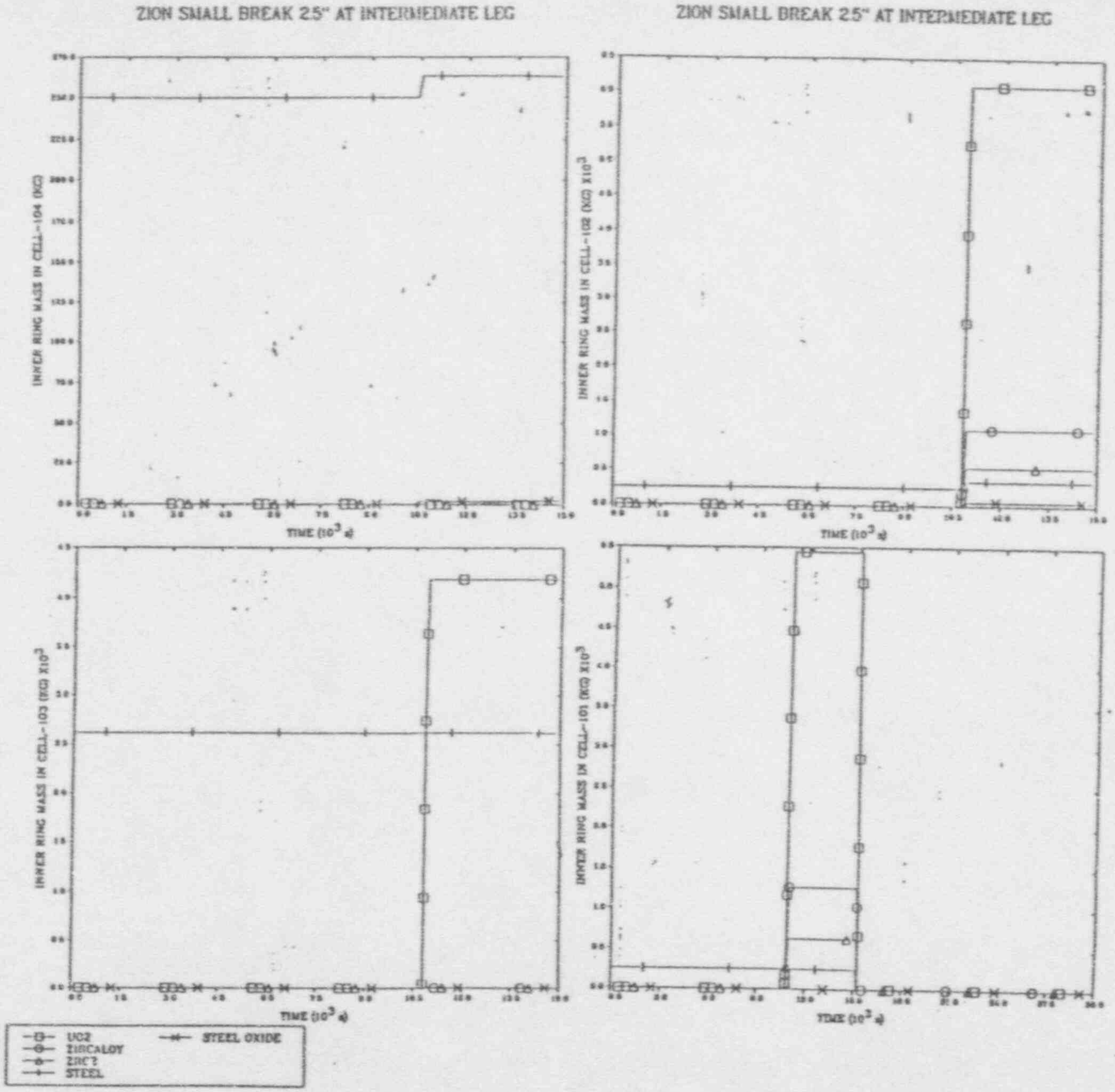

Figure C.21 MELCOR Predicted Core Relocation in the Inner Ring (Continued)

Table C.7 Summary of Fuel Relocation and Vessel Failure

MELCOR

Radial Ring	Start of Relocation	Failure of Core Plate	Time Duration[1]	Penetration Failure	Debris Discharge
1	2,655 s	10,790 s	135 min	12,706 s	15,240 s
2	2,655	11,135	141	11,376	13,443
3	2,710	11,423	145	11,544	11,640 - 21,961
4	2,885	10,790	132	15,126	19,320 - 20,641

MAAP

Radial Ring	Fuel Failure	Debris Relocation to Bottom Node	Time Duration[2]	Penetration Failure[3]	Debris Discharge
1	3,778 s	5,614 s	30 min	13,587 s	13,587 s
2		5,566			
3		5,250			
4		12,163			
5		12,963			
6		--			
7		13,473			

Note:
1. Time Duration = Time between the start of relocation to the core plate failure.
2. Time Duration = Time between fuel failure to the debris relocation to the bottom node of the core.
3. MAAP predicted the failure of core support plate at 13,527 s.
Penetration failure is determined by a user-specified time delay of 60 seconds.

The temperatures of penetrations and the innermost node of the lower head are shown in Figures C.22 to C.23, respectively. The failure temperature of the structural materials is 1273 K. Figure C.23 shows that after the penetration failure, the surface of the lower head in the inner ring also reaches the failure temperature. It appears that there is a potential for a direct failure of lower head wall. The debris mass in the lower head is shown in Figure C.24. After the onset of relocation of core materials due to the failure of the core plate at about 10,790 seconds, a total of 125,000 Kg of debris mass is accumulated in the lower head. Figure C.24 illustrates that, starting from 12,000 seconds, all debris mass is ejected from the lower plenum in 10,000 seconds.

Comparison With MAAP

Figures C.25 and C.26, respectively, show the fuel temperatures and UO_2 masses for each of the 10 axial nodes in the inner ring predicted by MAAP. The top node (the node with no fuel pellets) is referred to as Node 10, and the bottom node as Node 1. The major features of these two plots are described below:

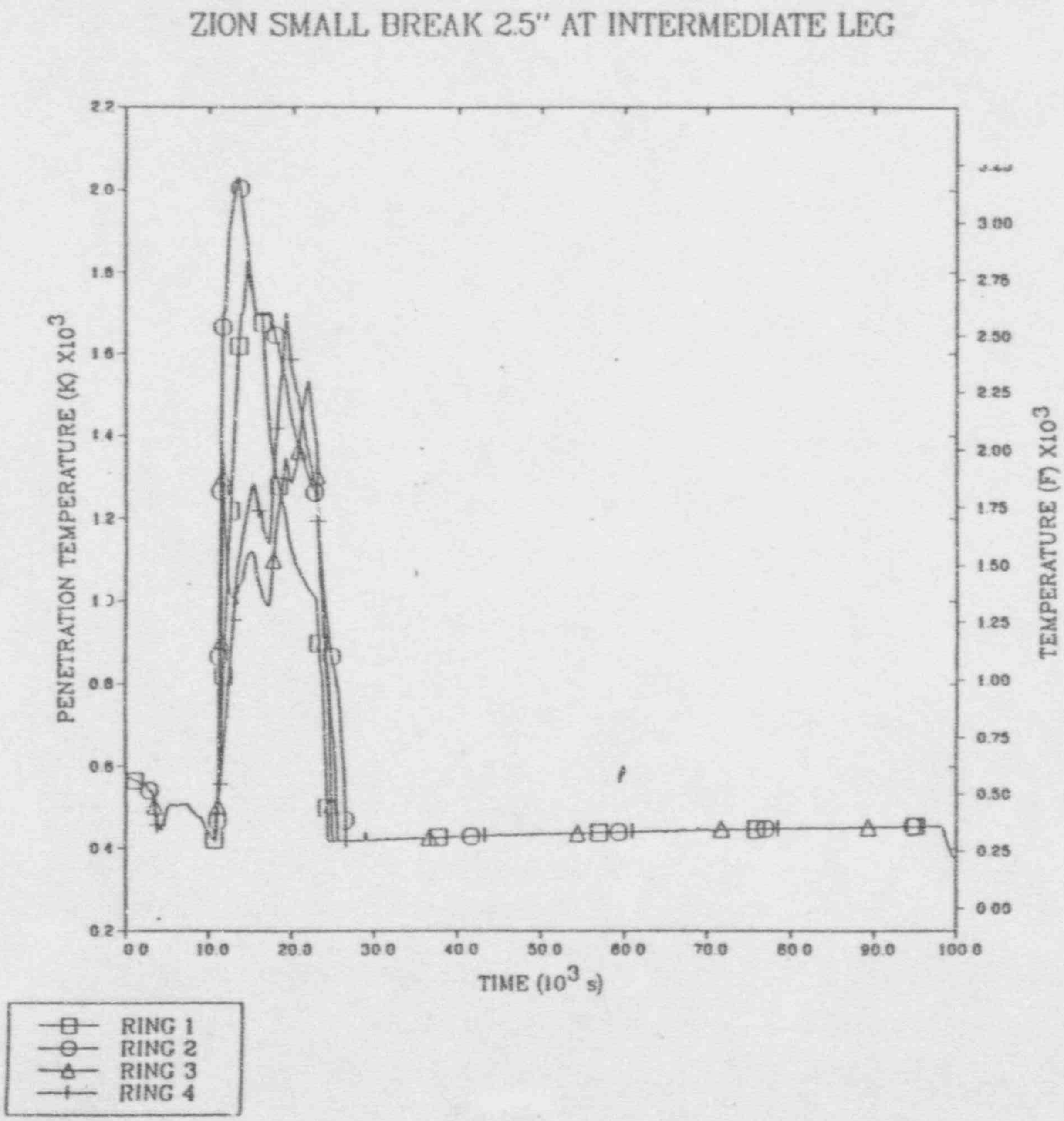

Figure C.22 MELCOR Predicted Penetration Temperatures

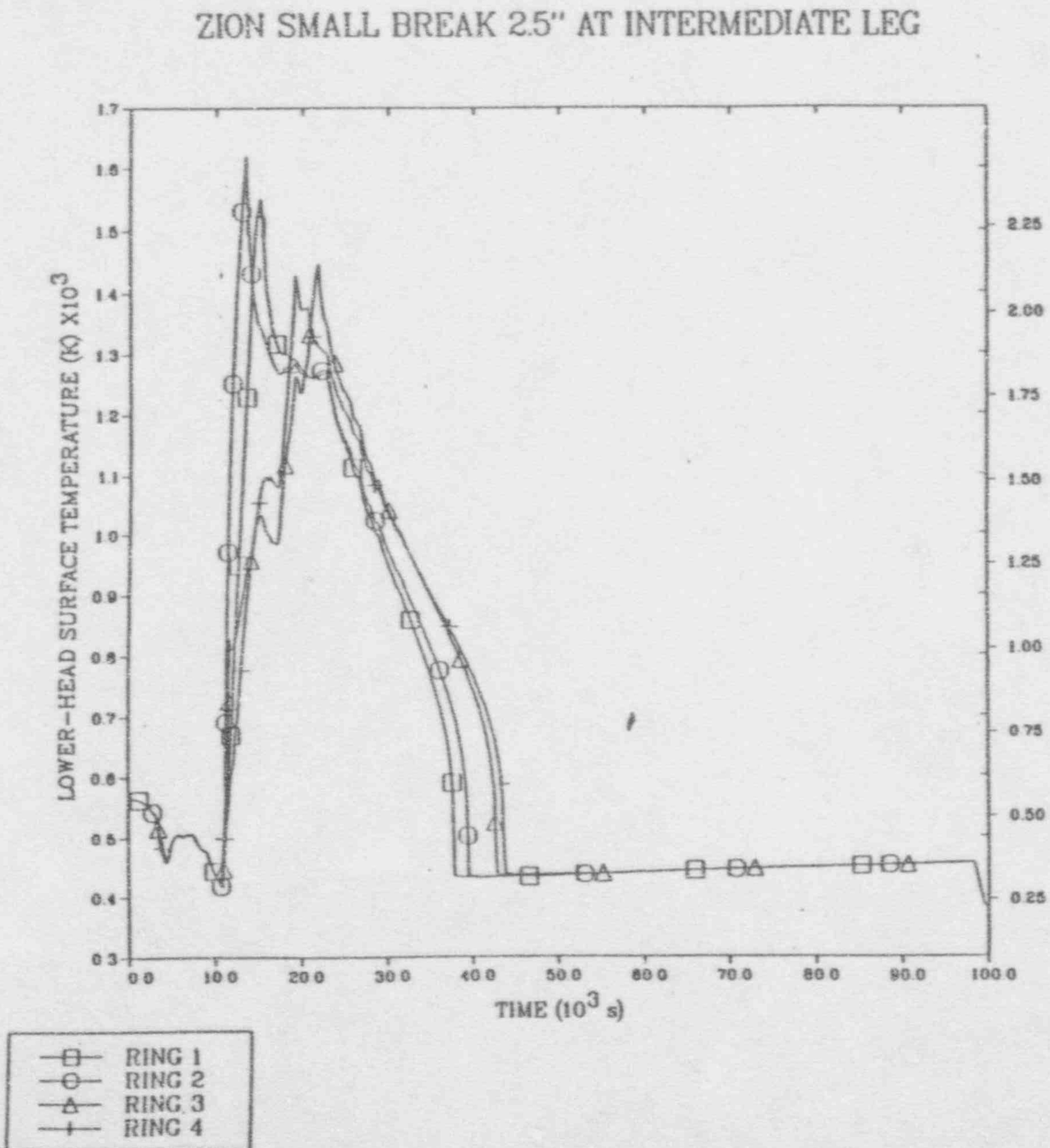

Figure C.23 MELCOR Predicted Lower Head Surface Temperatures

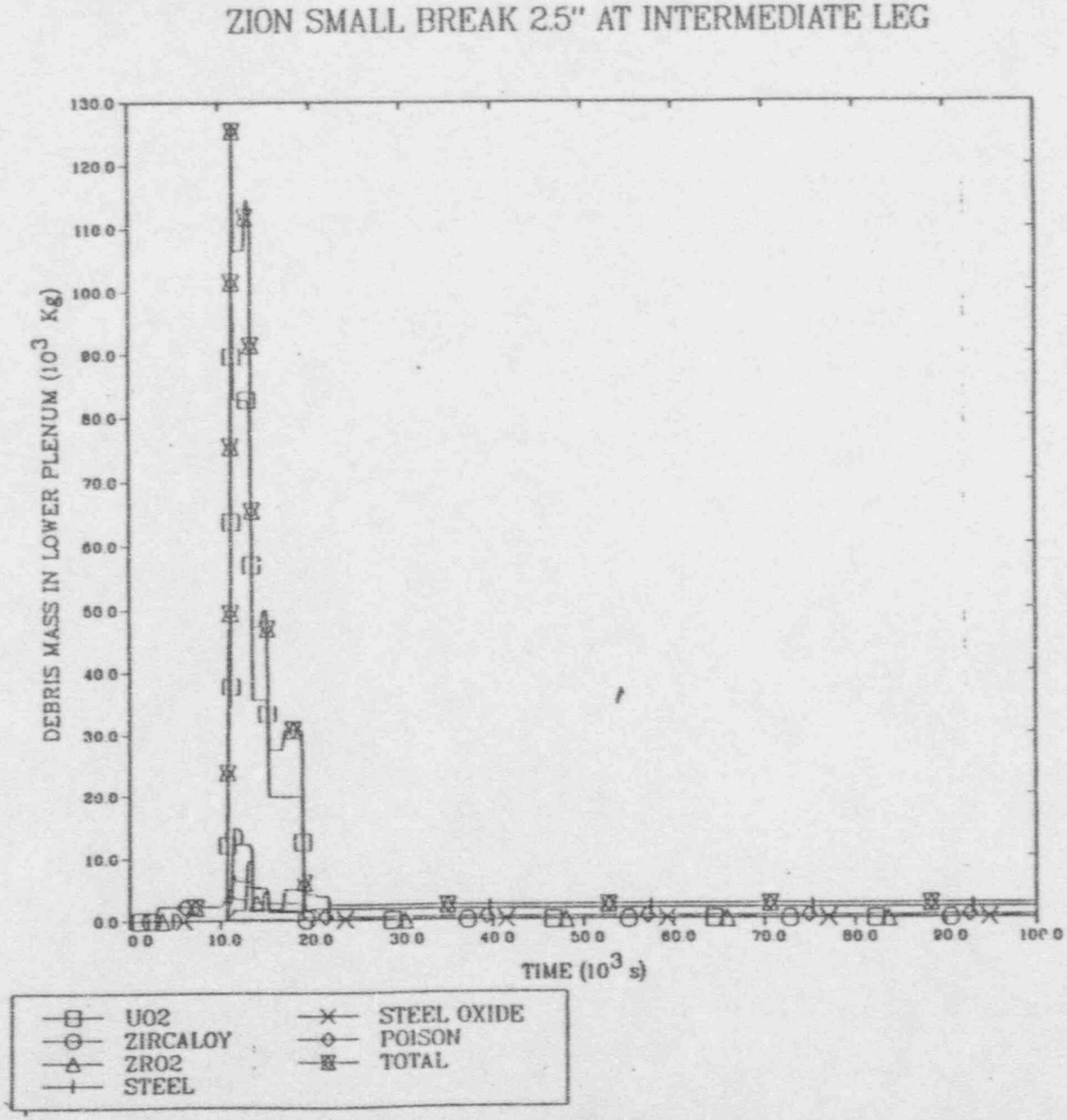

Figure C.24 MELCOR Predicted Debris Mass in Lower Plenum

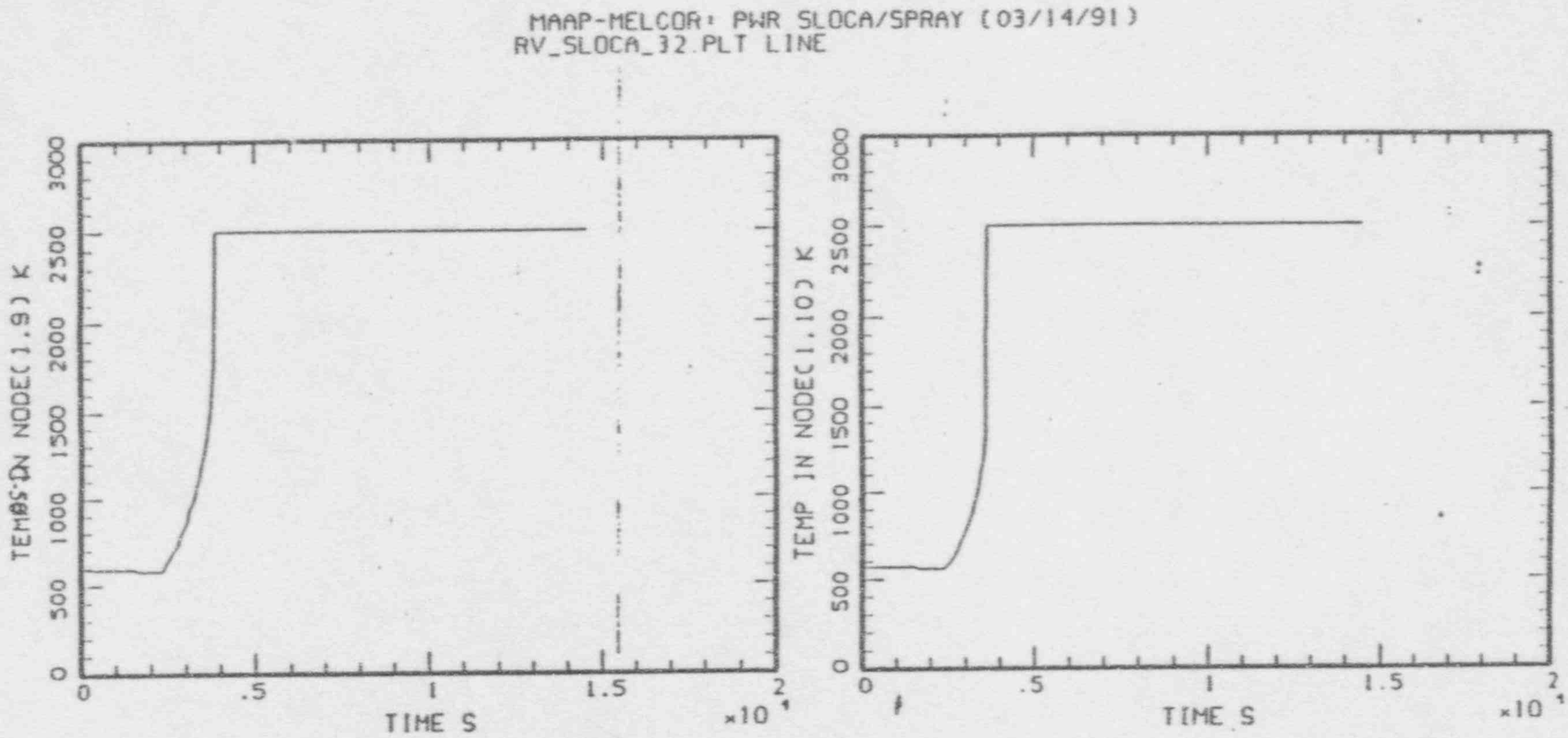

Figure C.25 MAAP Predicted Fuel Rod Temperature

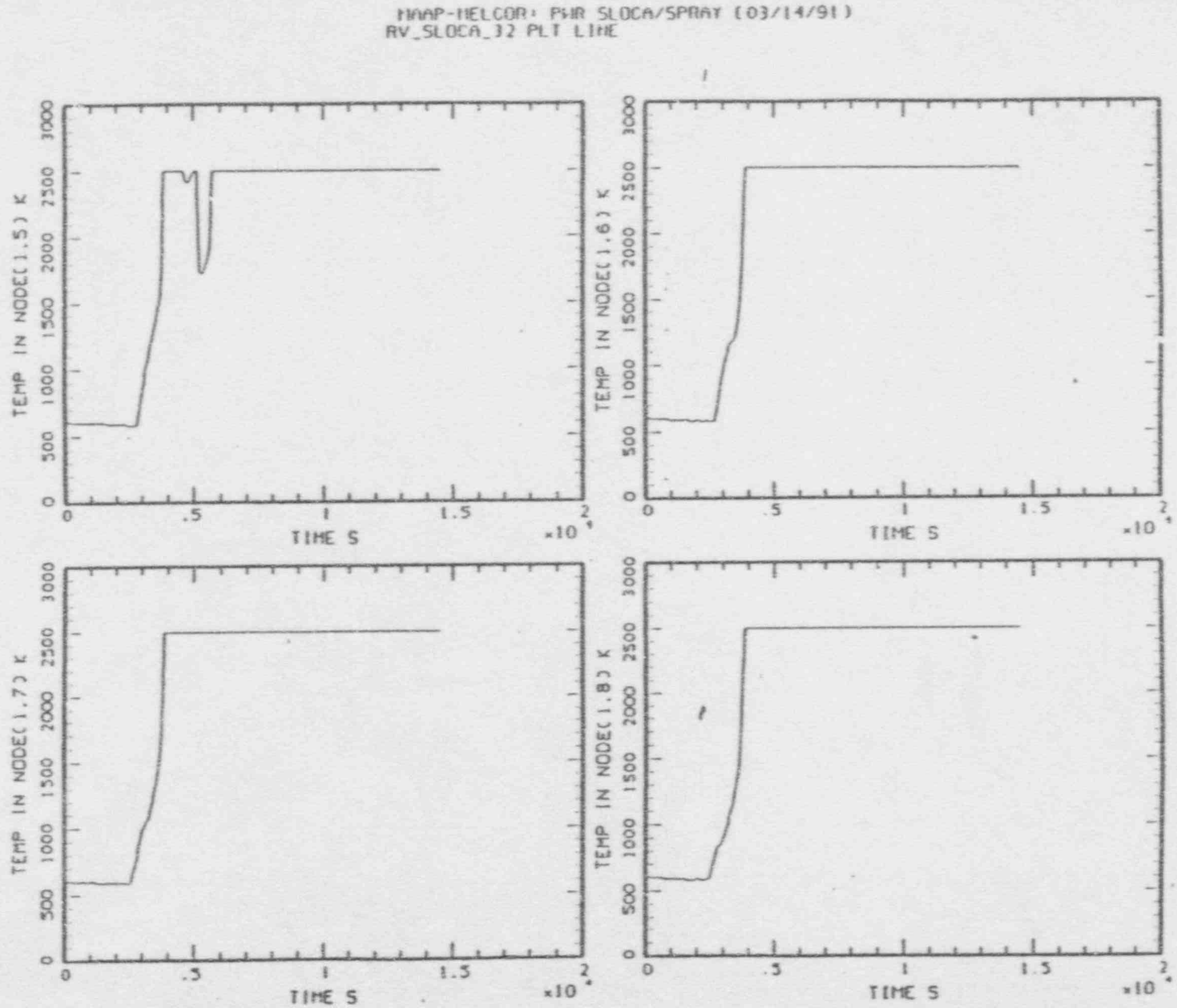

Figure C.25 MAAP Predicted Fuel Rod Temperature (Continued)

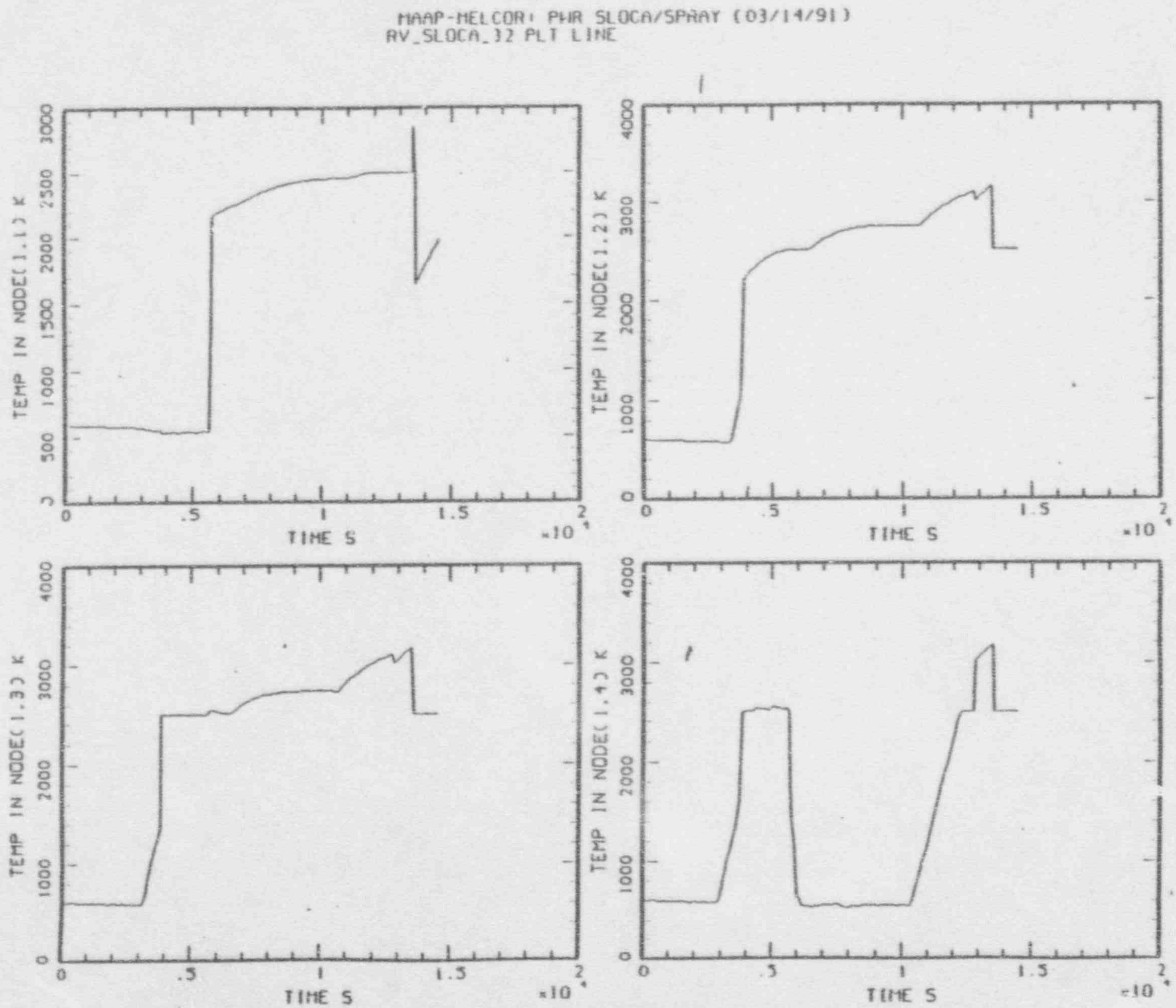

Figure C.25 MAAP Predicted Fuel Rod Temperature (Continued)

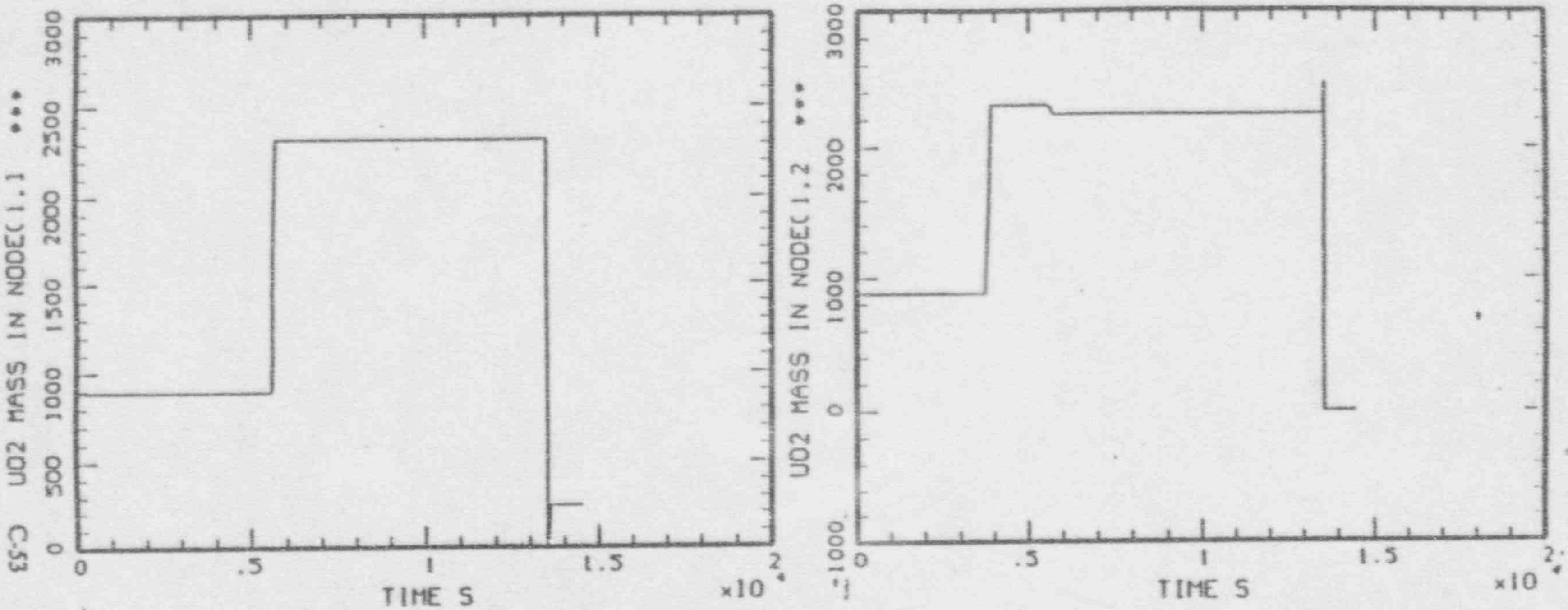

Figure C.26 MAAP Predicted Fuel Rod Relocation

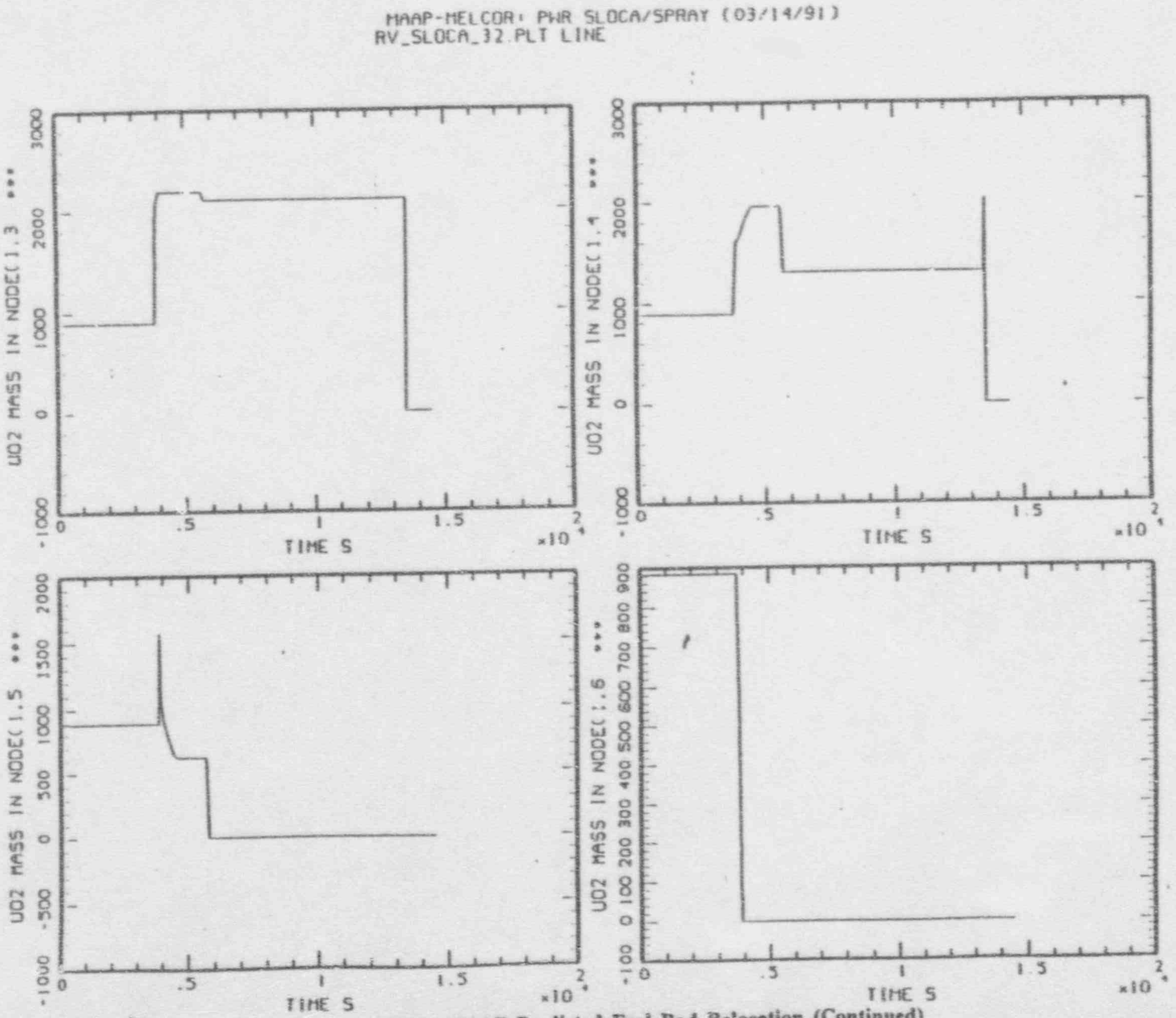

Figure C.26 MAAP Predicted Fuel Rod Relocation (Continued)

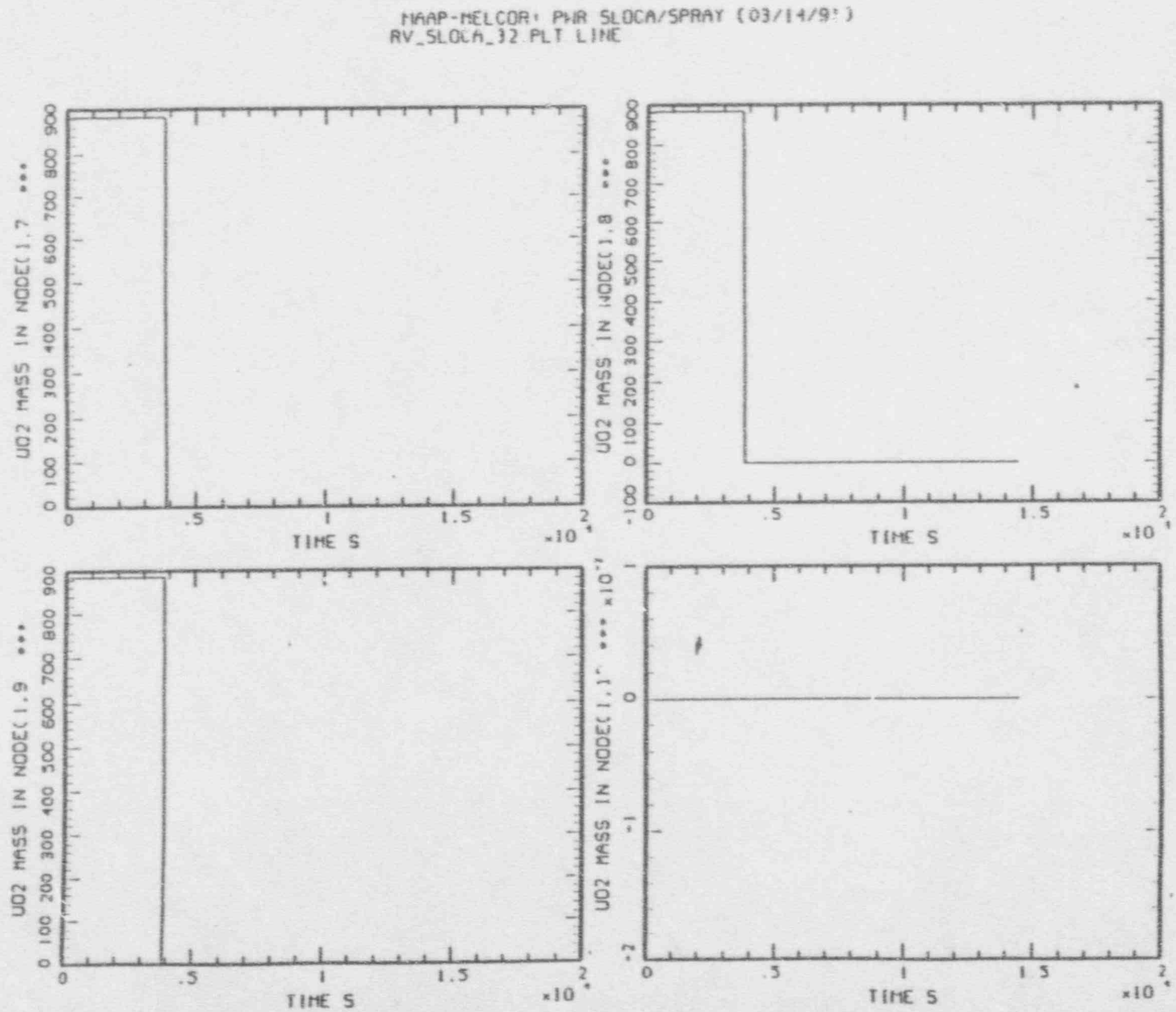

Figure C.26 MAAP Predicted Fuel Rod Relocation (Continued)

a. For the upper half segment of the fuel rod (i.e., Nodes 6 to 10), heating-up starts early, at about 2400 seconds. In about 25 minutes (i.e., at 3900 seconds), the fuel reaches the melting temperature (2500 K) and is immediately relocated to the lower part of the core (i.e., Nodes 1 to 4).
b. The middle segment of the fuel (Nodes 4 and 5) is subjected to melting, freezing and remelting due to the repeated flooding by the accumulator, at about 3670 seconds. The relocation of these nodes is delayed to about 5800 seconds for Node 5, and 13,500 seconds for Node 4.
c. The accumulation of molten debris in the lower segment of the core (Nodes 1,2, and 3) forms a super-heated molten pool. The debris temperature reaches 3200 K.
d. MAAP predicted the failure of the core support plate at 13,527 seconds. All core debris, including the mass of the support plate, is relocated into the lower plenum.

No plots of temperatures and masses in other radial rings are provided by MAAP. Only the time of debris relocation to the bottom node is provided by MAAP for each of the 7 radial rings. The relocation time is compared in Table C.7; the relocation in the outer rings (Rings 4 to 7) is considerably delayed. The delay of relocation in the outer rings causes the late failure of the penetration tube in the lower plenum.

The corium mass predicted by MAAP in the lower head is about 71,000 Kg. The mass is immediately discharged to the reactor cavity at the time of penetration failure as shown in Figure C.27.

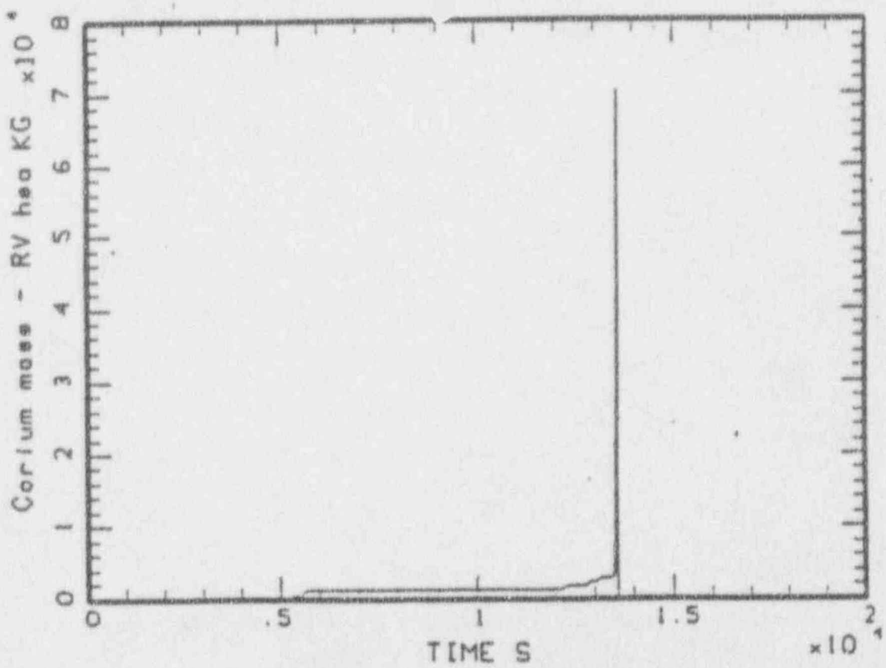

Figure C.27 MAAP Predicted Corium Mass in Lower Head

The comparisons between the predictions by MELCOR and MAAP are summarized below:

a. Both MAAP and MELCOR predicted an early activation of accumulators, which causes the delay of the relocation of core debris to the bottom nodes of the core.
b. MELCOR separates the lower core plate into radial zones, and predicts the failure of the core plate in each radial zone separately. The predicted failure time is between 10,790 to 11,423 seconds. MAAP treats the core plate as a single node, and predicted a late failure of the core plate at 13,527 seconds.
c. MELCOR has 4 radial rings and 4 penetrations in the lower plenum. Each penetration failure is determined by a thermal analysis of the individual penetration. The failure time of the 4 penetrations extended from 11,376 seconds to 15,126 seconds. MAAP has only one penetration in the lower plenum. The penetration failure is specified by a delay time (i.e., 60 seconds) after the relocation of corium into the lower plenum. The MAAP predicted penetration failure time is 13,587 seconds, about 37 minutes later than the failure of the first penetration predicted by MELCOR.

d. MELCOR predicted the ejection of debris into the reactor cavity in 172 minutes (from 11,640 s to 21,960 s). MAAP predicted the ejection of debris into the reactor cavity immediately after the penetration failure.

e. The quantity of debris accumulated in the lower plenum predicted by MELCOR (120,000 Kg) is much greater than that predicted by MAAP (78,000 Kg).

5.3 In-Vessel Oxidation

MELCOR Analysis

MELCOR predicted that cladding oxidation starts at about 2200 seconds. Most of the oxidation is completed at about 10,000 seconds and a total of 260 Kg of hydrogen is generated as shown in Figure C.28. The quantity of hydrogen corresponds to the oxidation of 29% of the active cladding. Almost all of the hydrogen generated in the reactor vessel flows out to the containment through the break area as illustrated in Figure C.7 in Section 5.1. The integrated mass flow through the break area also shows a large quantity of steam during hydrogen release. This implies that the hydrogen generation is not terminated by steam starvation. The termination of hydrogen generation predicted by MELCOR is related to its core relocation model. It is known that the prediction of hydrogen generation during core relocation is uncertain, because of the uncertainties in the Zr surface area, the Zr temperature, and the steam distribution. In MELCOR, oxidation of conglomerate debris (i.e., material that has melted and resolidified onto other components) is modeled using variable surface areas to match the assumed configurations of the debris. Oxidation of the corresponding intact surfaces is reduced to reflect shielding by that debris.

Figures C.29 and C.30 shows the masses of the oxidic and metallic Zr and steel predicted by MELCOR. The mass of steel oxide is about 1.3% of the total steel inventory (28,286 Kg). The oxidation of steel in the core and lower plenum region predicted by MELCOR would not contribute significantly to total hydrogen generation.

Comparison with MAAP

Figure C.31 shows hydrogen generation due to cladding oxidation predicted by MAAP. Hydrogen is generated at about 3230 seconds, approximately 1,000 seconds later than that predicted by MELCOR. About 340 Kg of hydrogen is produced in about 300 seconds. Figure C.16 in Section 5.1 also shows that hydrogen generation as predicted by MAAP is not terminated by steam starvation.

In Figure C.31, a large quantity of hydrogen (about 240 Kg) is generated after the reactor vessel fails. This is caused by the steam entering from the reactor cavity into the failed reactor vessel through the penetration hole. Because the oxidation of steel is not modeled in MAAP, this hydrogen is generated by the oxidation of metallic Zr. The quantity of metallic Zr remaining in the reactor vessel is not provided by MAAP.

5.4 Corium/Concrete Interaction

MELCOR Analysis

In the analysis of MELCOR the four penetrations fail from 11,378 to 15,126 seconds, as discussed in Section 5.2. The debris discharge starts at 11,640 seconds and terminates about 22,000 seconds. All the discharged debris is located in the reactor cavity, because MELCOR does not have an entrainment model to carry the debris to other compartments. When the debris ejection ends, the cavity has about 200,000 Kg of debris, as shown in Figure C.32. More debris is added to the cavity due to the erosion of concrete. At the end of 100,000 seconds, the total mass of debris is about 256,000 Kg. In addition to this mass, there is a layer of water on the top of the debris pool, as shown in Figure C.33. About 150,000 Kg of water is in the cavity at the time of vessel failure.

The MELCOR analysis shows that water is continuously transported into the reactor cavity. The water transport into the containment is important for the corium/concrete interaction and the retention of the fission products. The sources of water in containment are the water released from the pipe break and the penetration holes, and the

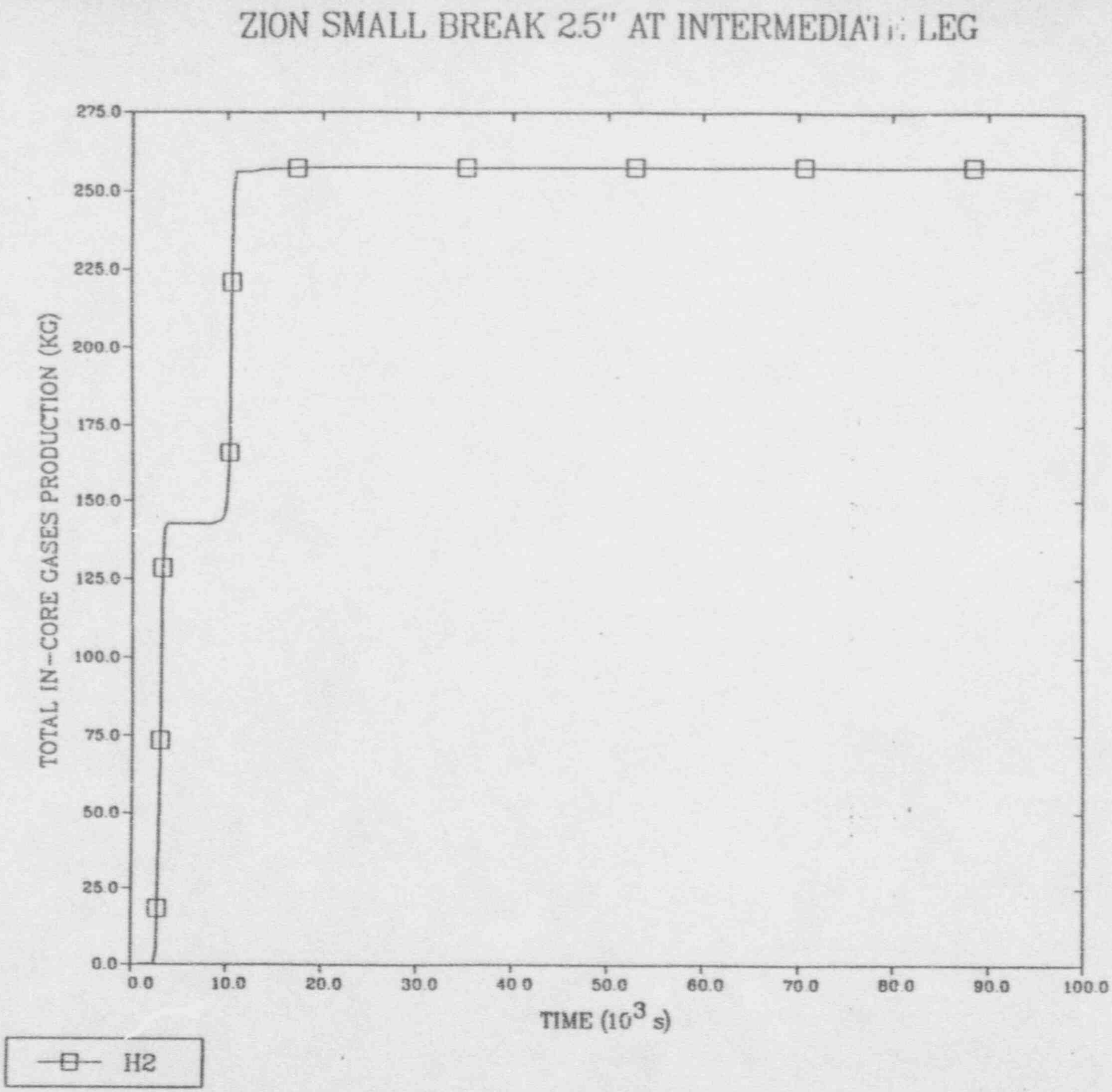

Figure C.28 MELCOR Predicted In-Vessel Hydrogen Generation

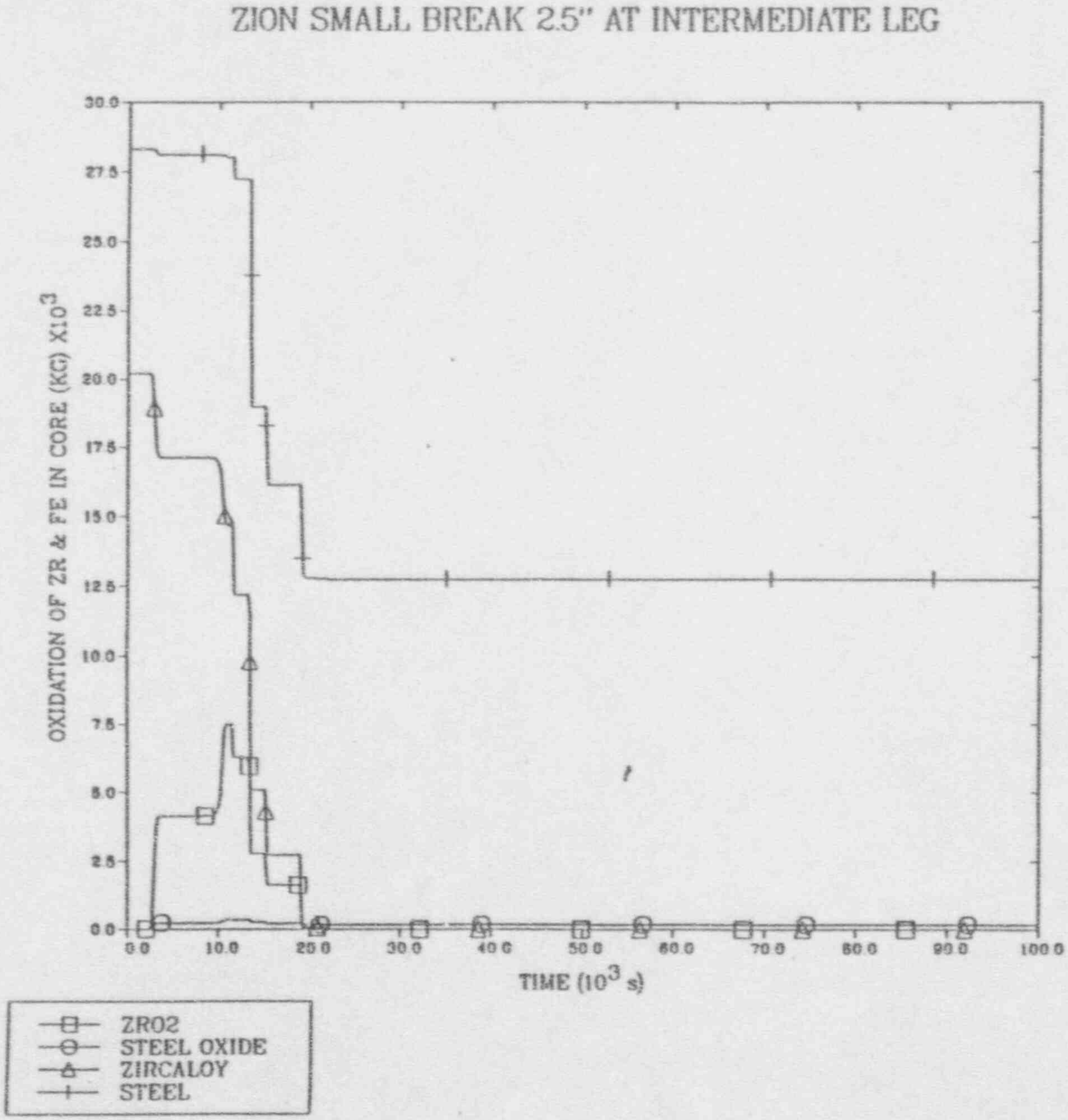

Figure C.29 MELCOR Predicted Oxidation of Zr and Steel in Core

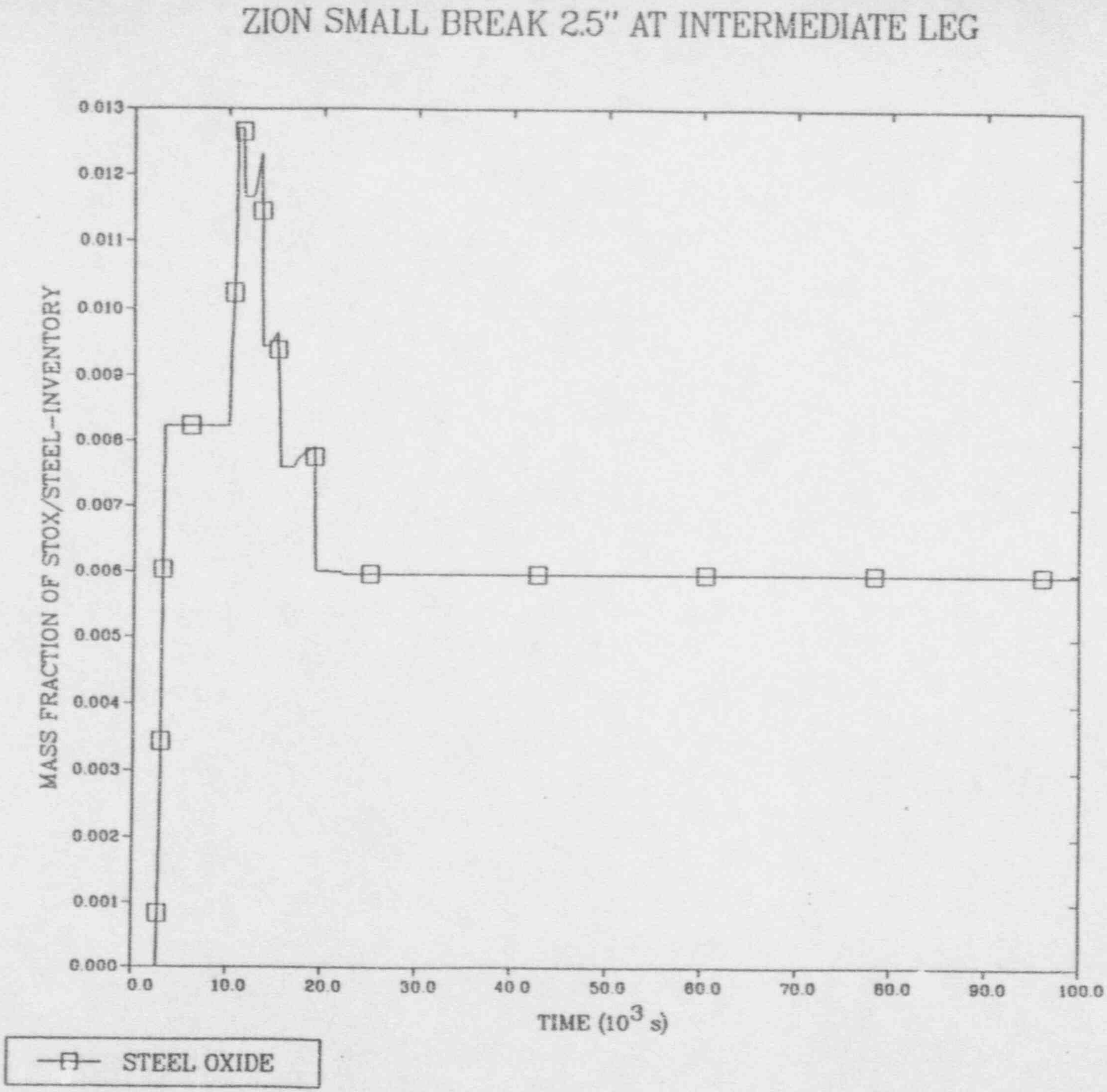

Figure C.30 MELCOR Predicted Mass Ratio of Steel Oxide

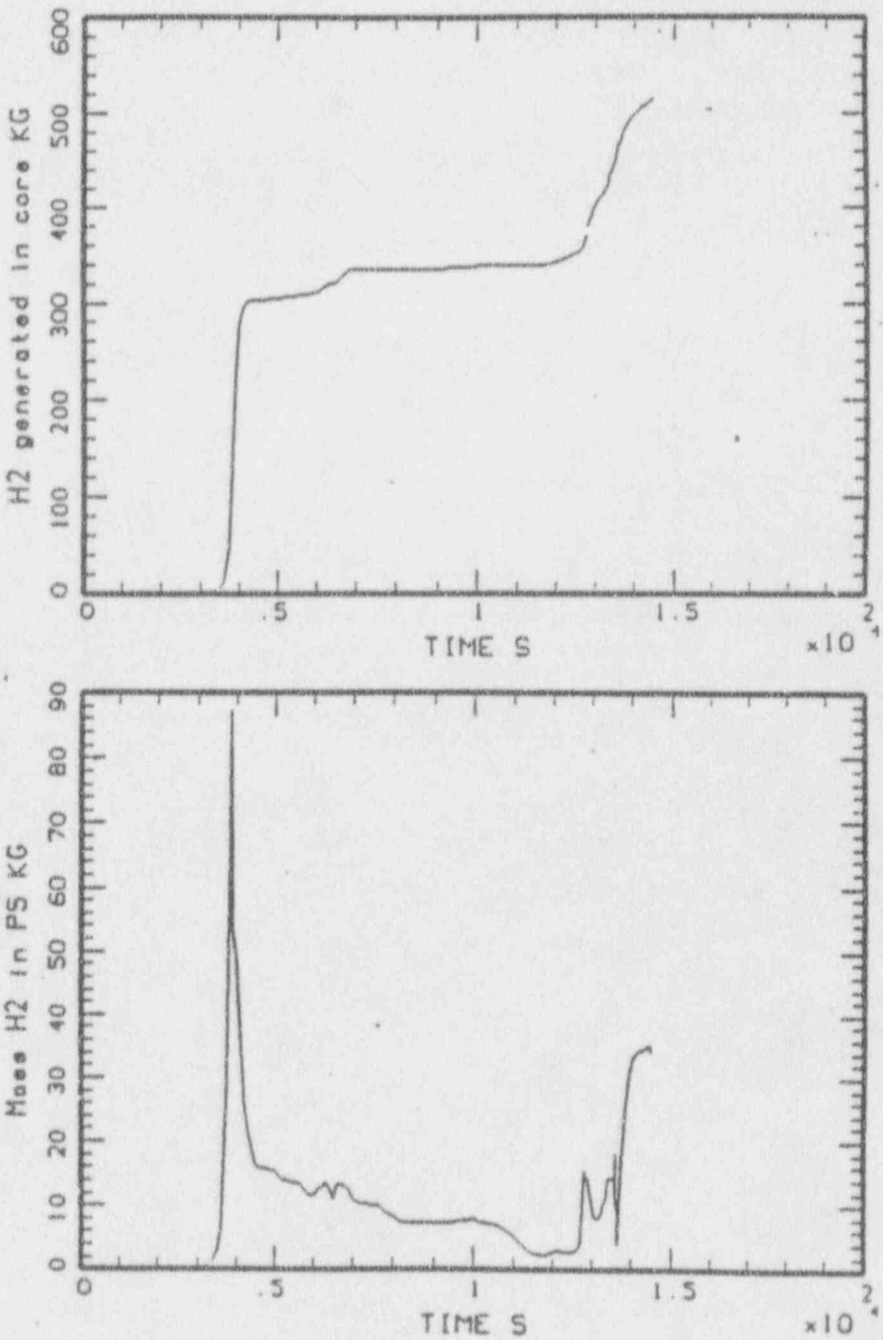

Figure C.31 MAAP Predicted In-Vessel Hydrogen Generation

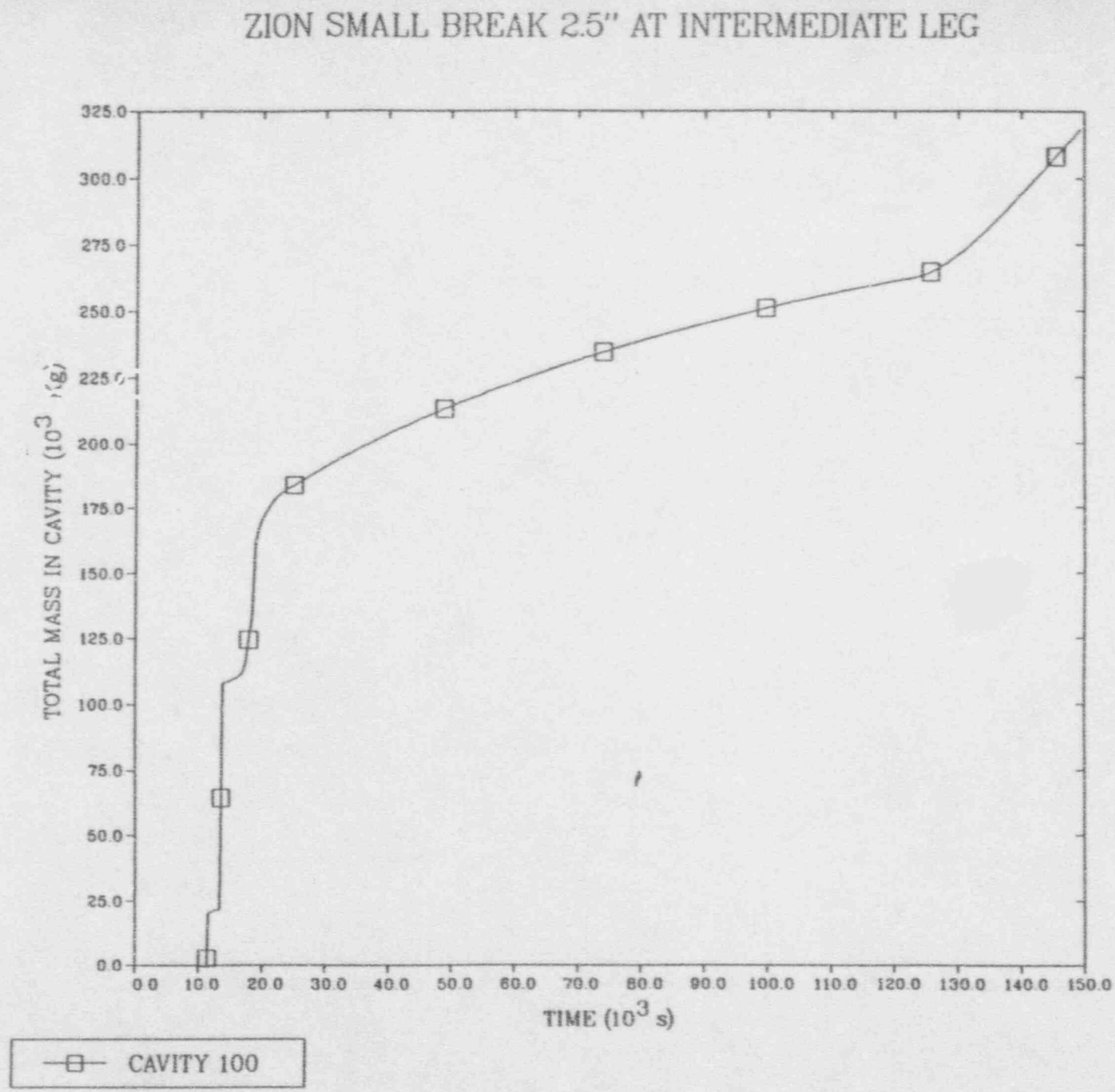

Figure C.32 MELCOR Predicted Mass in Reactor Cavity

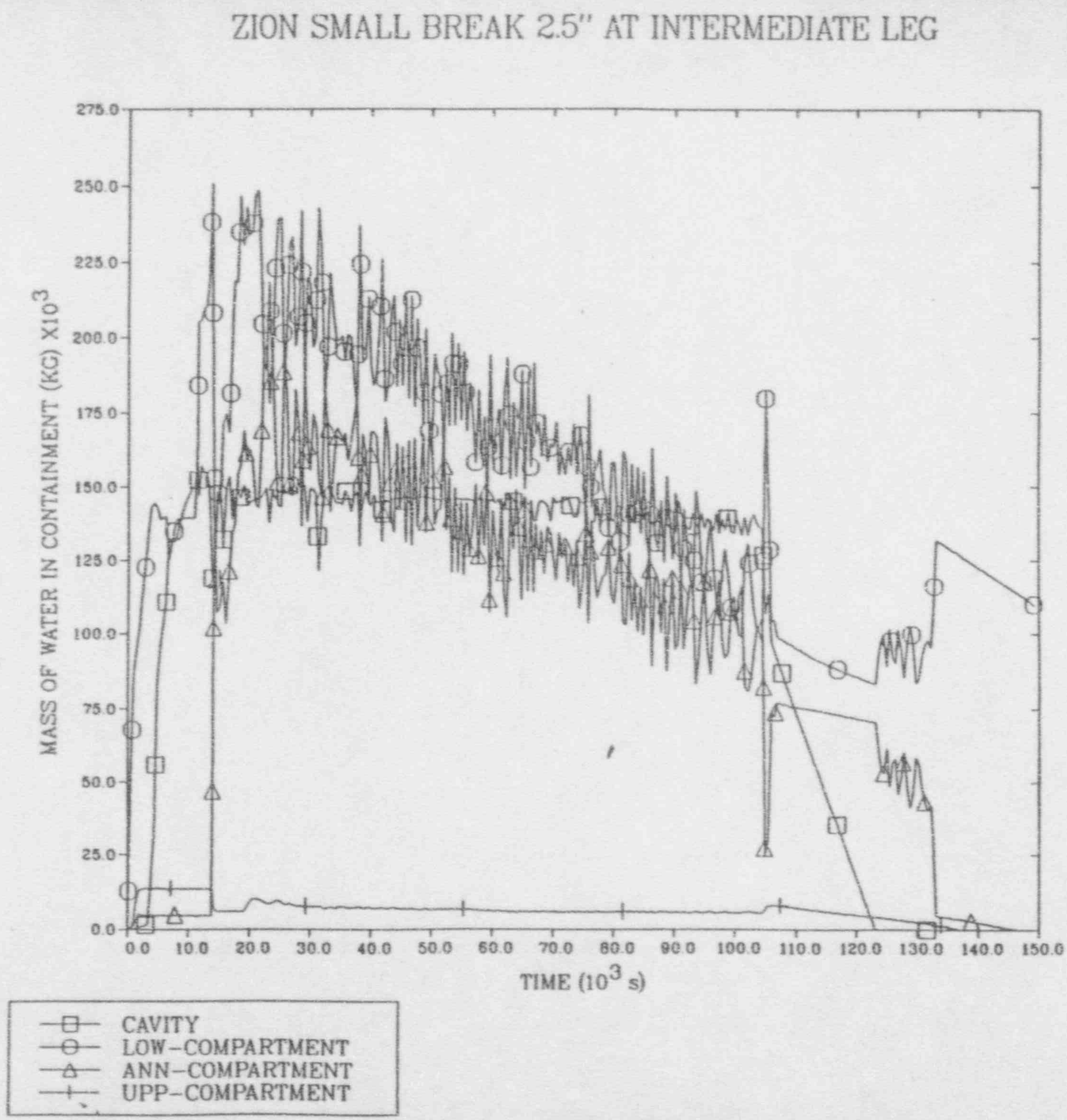

Figure C.33 MELCOR Predicted Water Mass in Containment

condensation of vapor released from the reactor vessel and the concrete structure. Sprays activated at 15,200 seconds also add about 127,000 Kg of water into the containment. Figure C.34 shows the integrated water flows in each compartment; the following are noted from the figure:

(a) A large quantity of water flows from the upper compartment into the lower compartment. At the end of 100,000 seconds before the containment failure, a total of 290,000 Kg of water has flowed into the lower plenum.

(b) Initially water flows from the upper compartment into the annulus region. The flow is nearly terminated at about 14,000 seconds.

(c) There is a continuous exchange of water flow between the lower compartment and the annulus region. After about 55,000 seconds, the decrease of the integrated flow from the lower compartment into the annulus shows a reversal from the annulus to the lower compartment.

(d) The cavity and the lower compartment are connected by two flow paths: the instrument tunnel and the bypass channel. Figure C.34 shows an interesting water circulation between the two regions; the water flows from the cavity into the lower compartment through the bypass channel (the positive flow in Figure C.34), and flows back to the cavity through the instrument tunnel (the negative flow in Figure C.34). The water circulation maintains a flooded cavity for the entire transient.

The transient flow rates in these flow paths connecting the various compartments of the containment are shown in Figure C.35. The water flow is characterized by a large oscillation of the flow rate. Between the upper/lower and upper/annulus regions, the flow rate is relatively small. However, between the annulus and the lower compartment, the flow rate is in the order of hundred Kg/s, showning a strong exchange of water between these two regions.

According to the CORCON model, core debris in the cavity region has three layers: light oxidic, metallic, and heavy oxidic layers as shown in Figure C.36. The light oxidic layer is composed of ablation concrete oxides and steel oxides produced by chemical reaction with the concrete-decomposition gases. Figure C.36 shows that the thickness of this light oxidic layer grows rapidly as the thermal erosion of concrete becomes significant at about 20,000 seconds, when the heavy oxidic layer at the bottom is diluted by concrete oxides and moves upward to form a single oxide layer. Figure C.36 also shows that during the entire transient, the temperature of the debris is above the solidus temperature (1420 K for the limestone and common sand type concrete).

The downward and radial erosion distances predicted by CORCON are given in Figure C.37. At 100,000 seconds (i.e., near the time of containment failure), the maximum erosion distances are 1.44 m and 0.27 m in the axial and radial directions, respectively. Based on these erosion rates, the total releases of H_2, CO, H_2O, and CO_2 predicted by MELCOR at the time of containment failure (104,500 seconds) are 575, 16,000, 580, and 1440 Kg, respectively (Figure C.38).

Comparison with MAAP

Figure C.39 shows the corium mass and temperature, ablation distance, and water mass in the cavity region predicted by MAAP. Comparisons with MELCOR's predictions provide the following:

a) The initial water mass in the reactor cavity (170,000 Kg) predicted by MAAP is comparable to that predicted by MELCOR (150,000 Kg). However, MAAP predicted a gradual boil-off of the water in the cavity at a rate of about 50 Kg/s.
Water dryout occurs at about 42,000 seconds. The water boil-off rate predicted by MELCOR is only 1.12 Kg/s. No dryout in the cavity is predicted by MELCOR.

b) The initial temperature of corium (2500 K) predicted by MAAP is the same as that predicted by MELCOR (2500 K). However, MAAP has a much stronger corium/water interface heat transfer, which results in a complete quench of the corium at about 16,000 seconds. The corium starts to reheat at about 44,000 seconds, as water in the cavity is completely depleted. The temperature of corium rapidly reaches to 2500K at which the concrete ablation is initiated. During the entire transient of concrete ablation, the temperature of corium remains above 2000K. On the contrary, the corium temperature predicted by MELCOR remains slightly higher than the solidus temperatures.

c) Because of the quench of corium, concrete ablation is delayed until 55,000 seconds. Because MAAP has equal ablation in both radial and axial directions, the erosion depths in both directions are 0.8 m at the end of 120,000 seconds. On the other hand, MELCOR predicted an immediate erosion of concrete as

ZION SMALL BREAK 2.5" AT INTERMEDIATE LEG

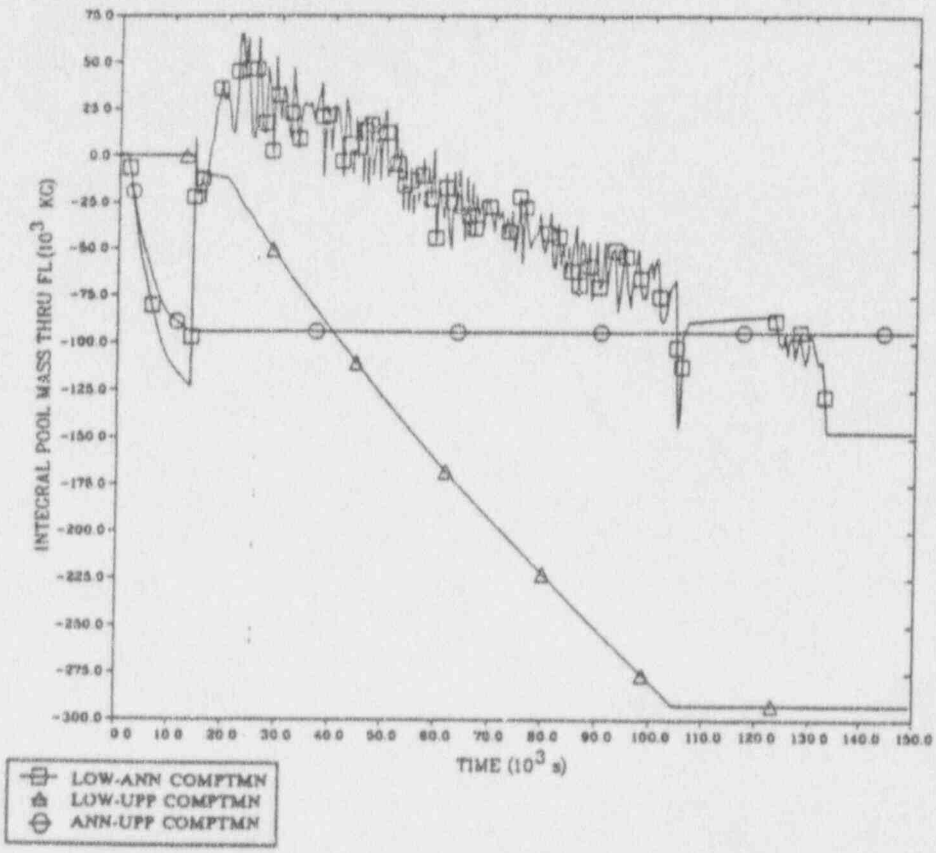

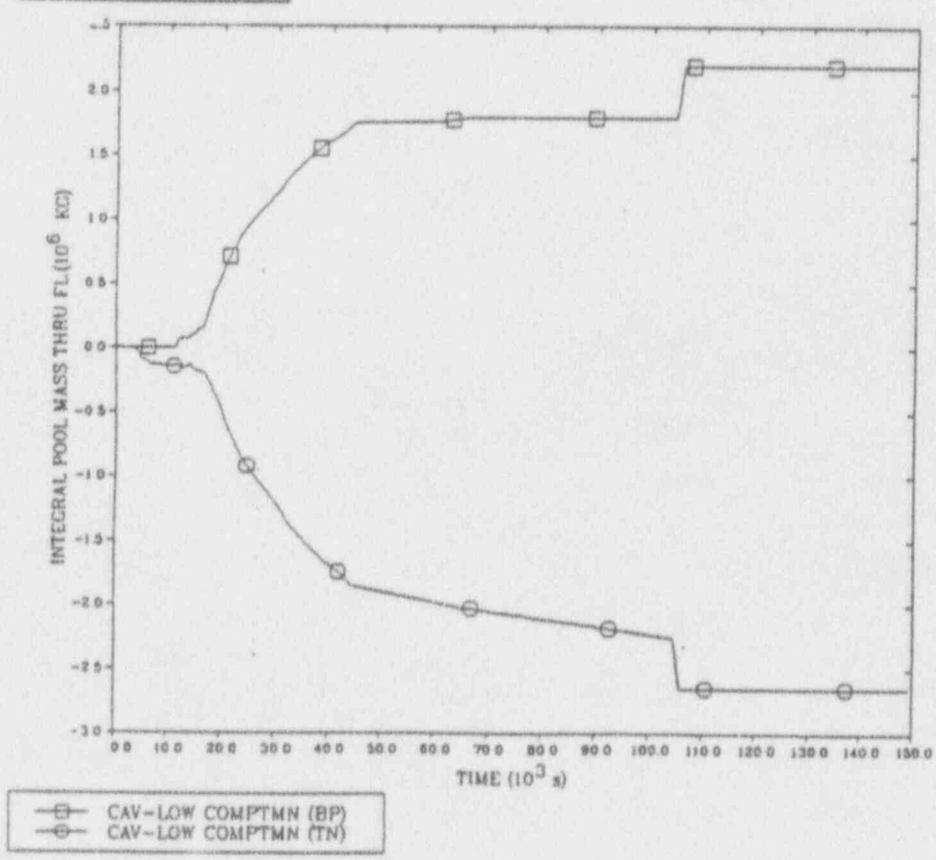

Figure C.34 MELCOR Predicted Water Flow in Containment

ZION SMALL BREAK 2.5" AT INTERMEDIATE LEG

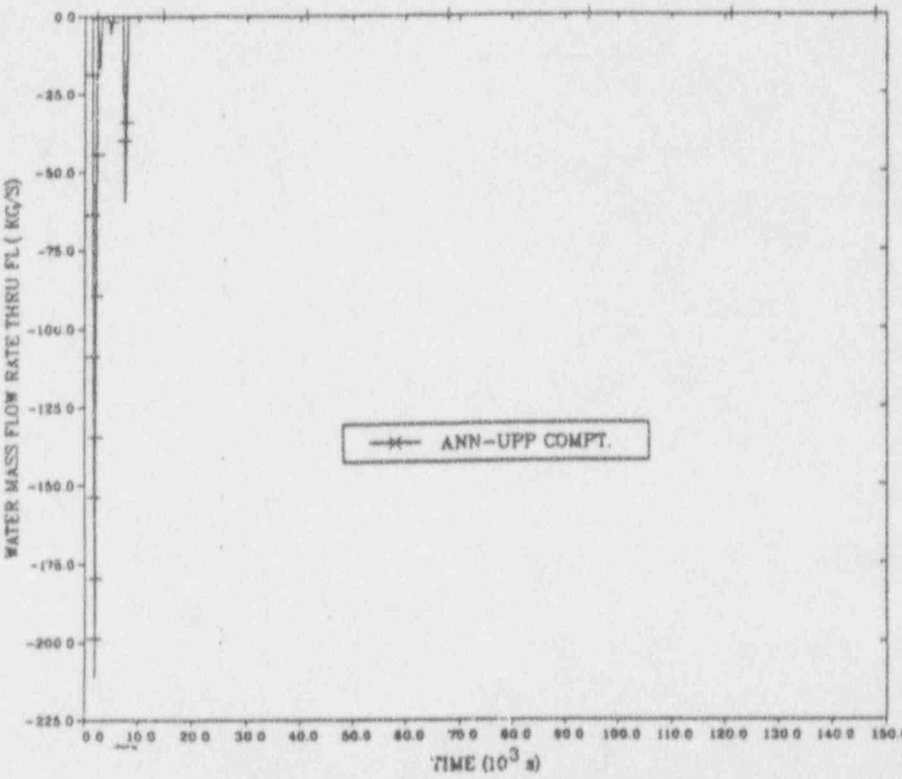

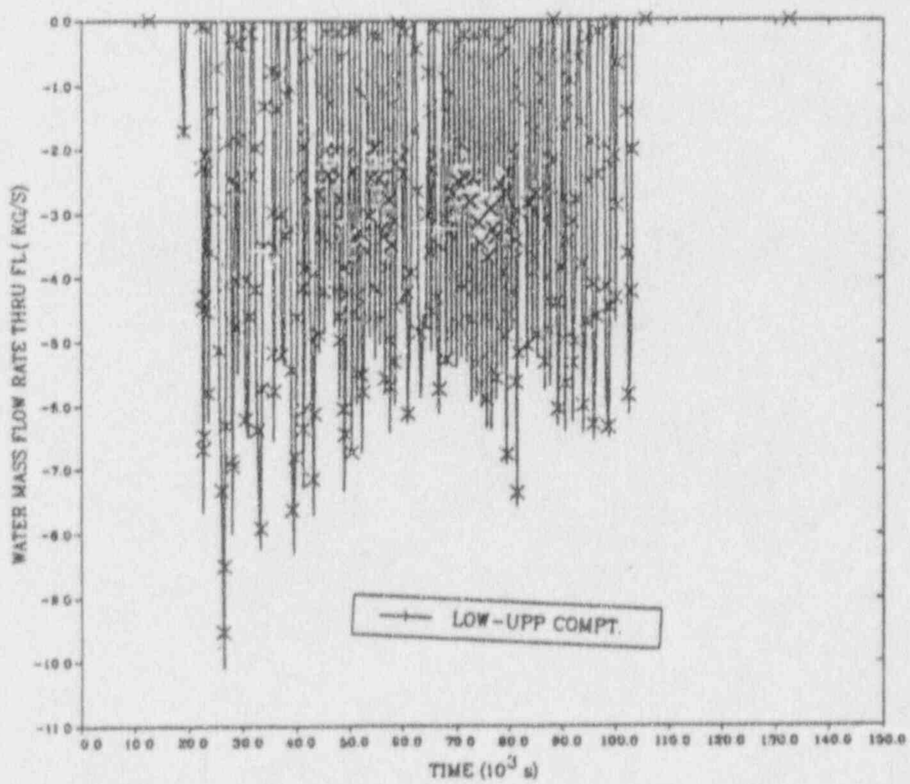

Figure C.35 MELCOR Predicted Water Flow Rate in Containment

ZION SMALL BREAK 2.5" AT INTERMEDIATE LEG

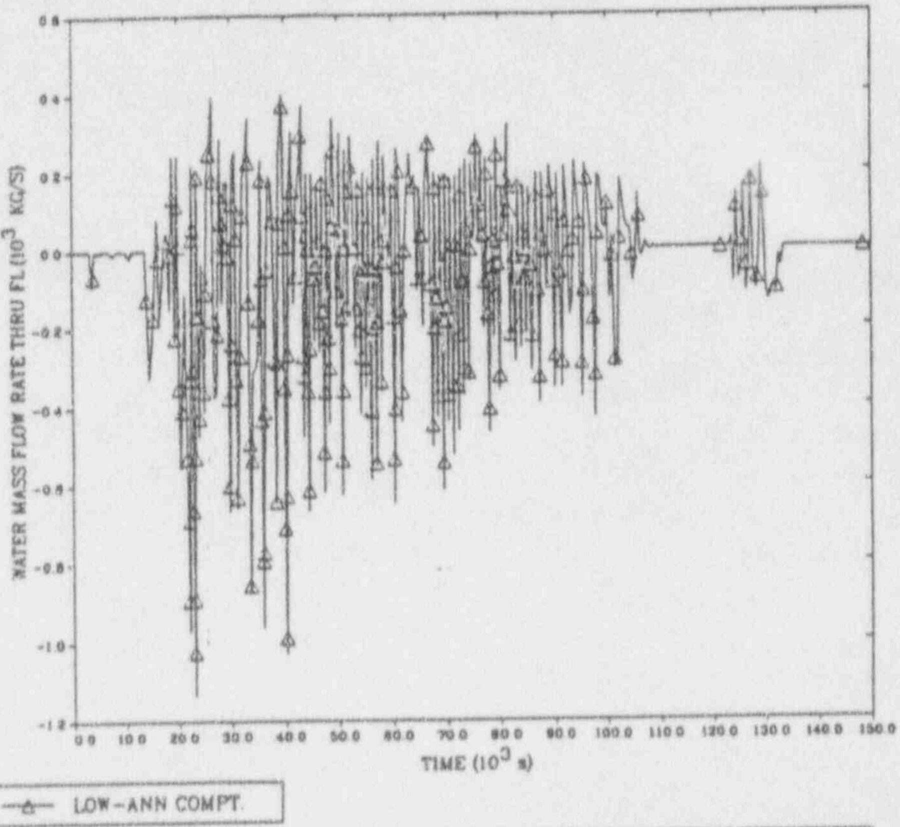

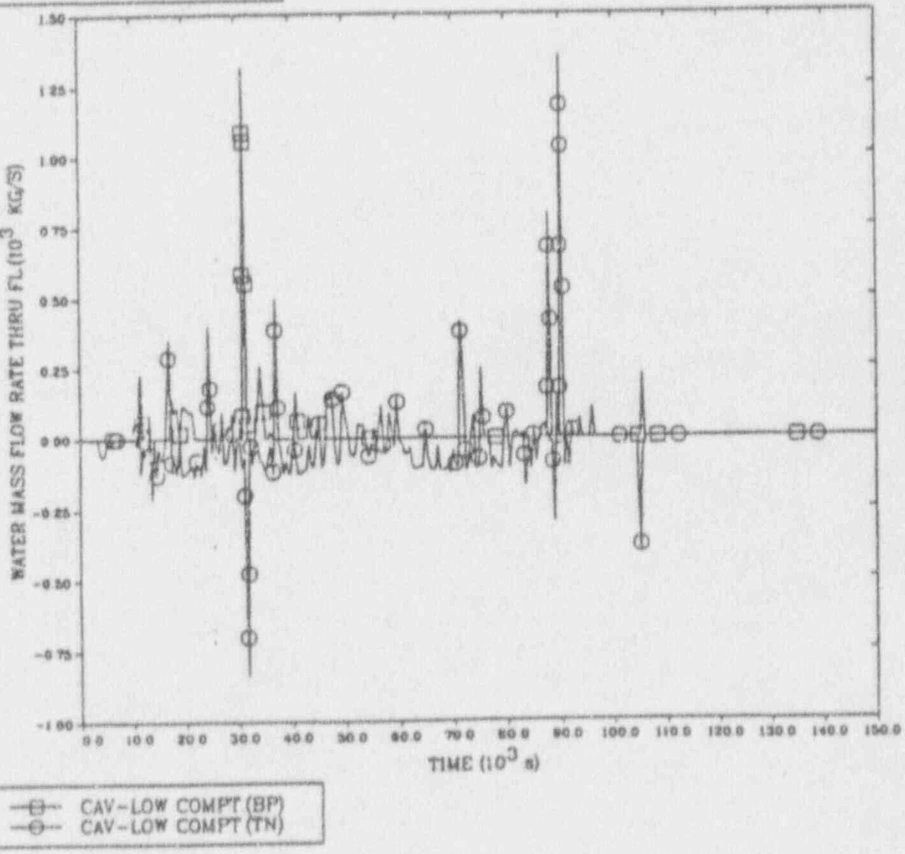

Figure C.35 MELCOR Predicted Water Flow Rate in Containment (Continued)

ZION SMALL BREAK 2.5" AT INTERMEDIATE LEG

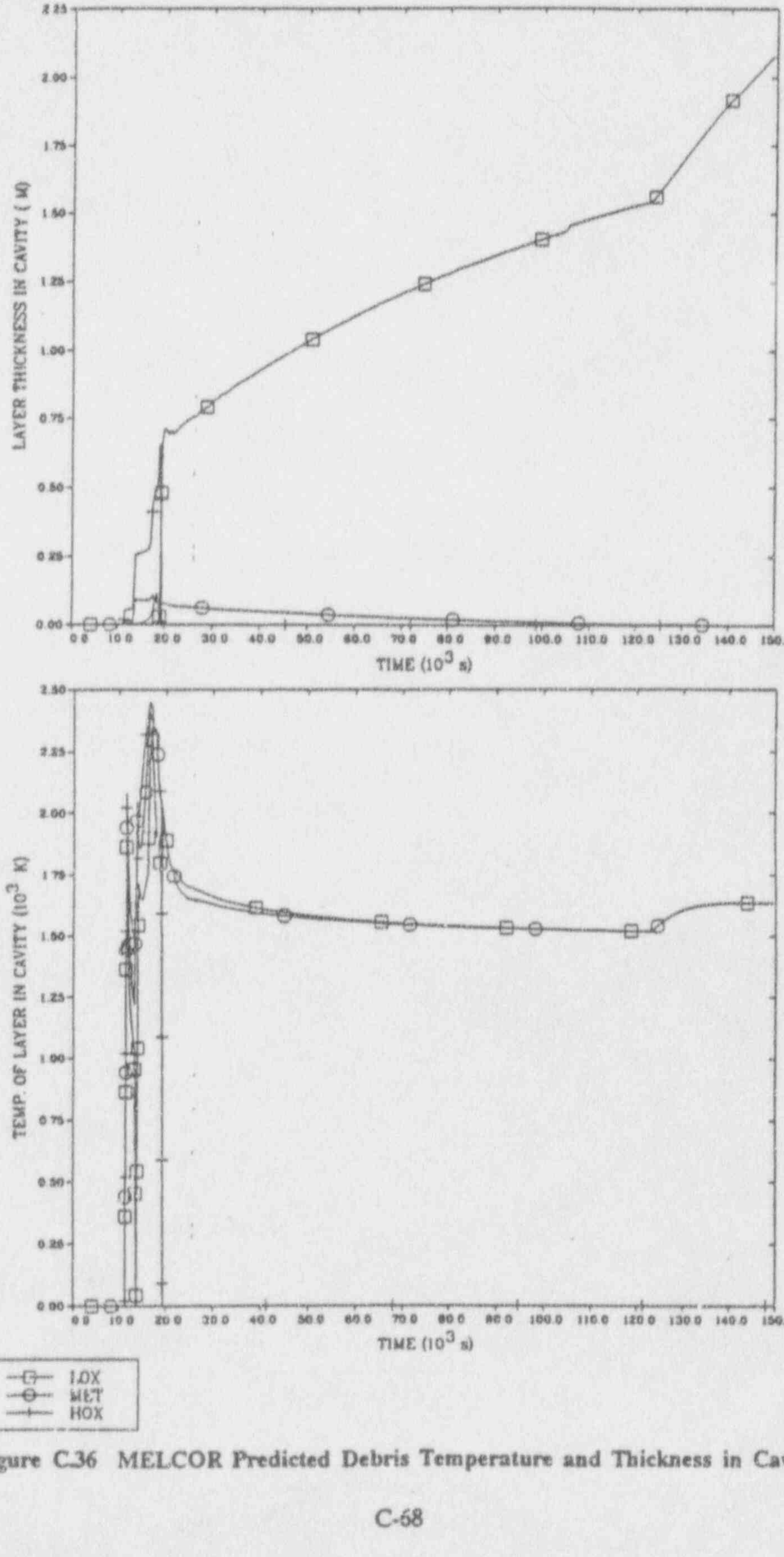

Figure C.36 MELCOR Predicted Debris Temperature and Thickness in Cavity

ZION SMALL BREAK 2.5" AT INTERMEDIATE LEG

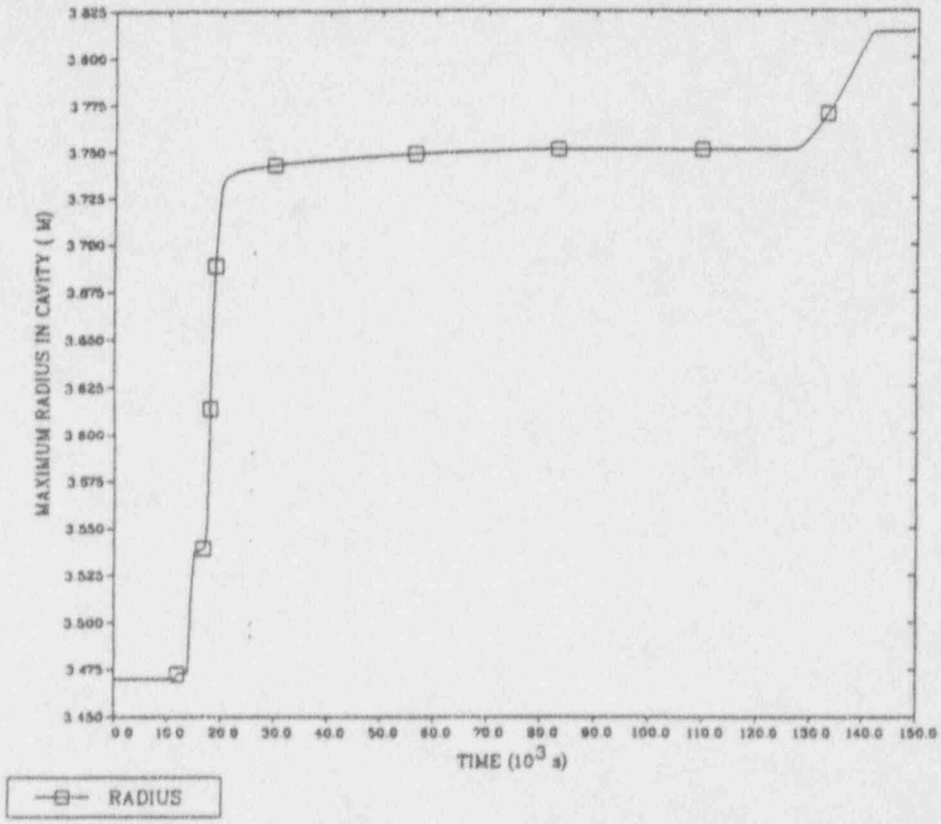

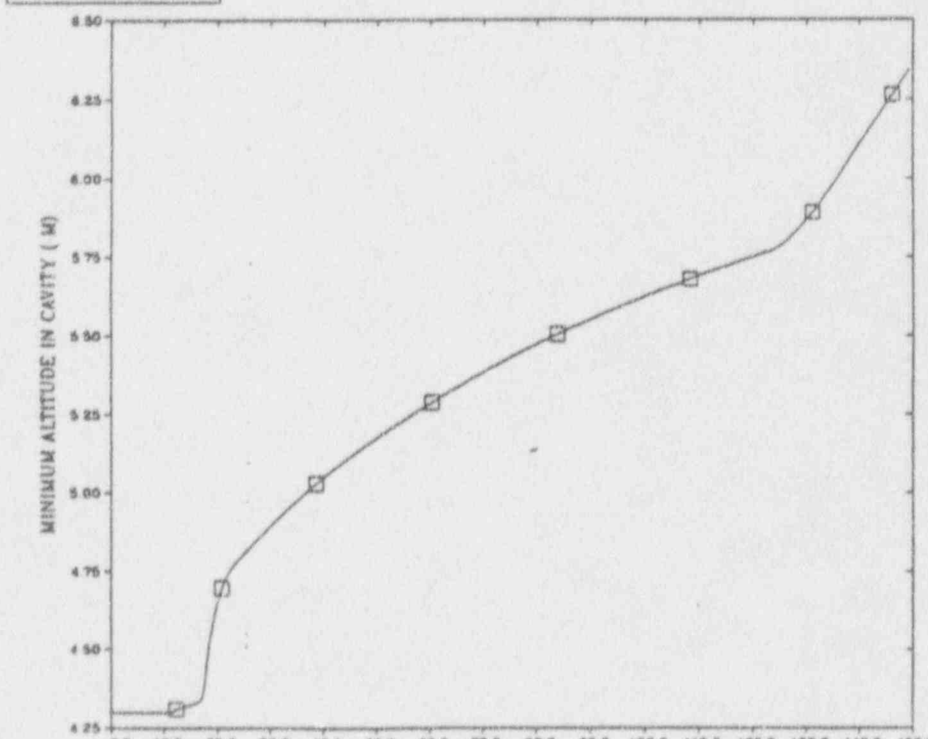

Figure C.37 MELCOR Predicted Concrete Erosion Distance

ZION SMALL BREAK 2.5" AT INTERMEDIATE LEG

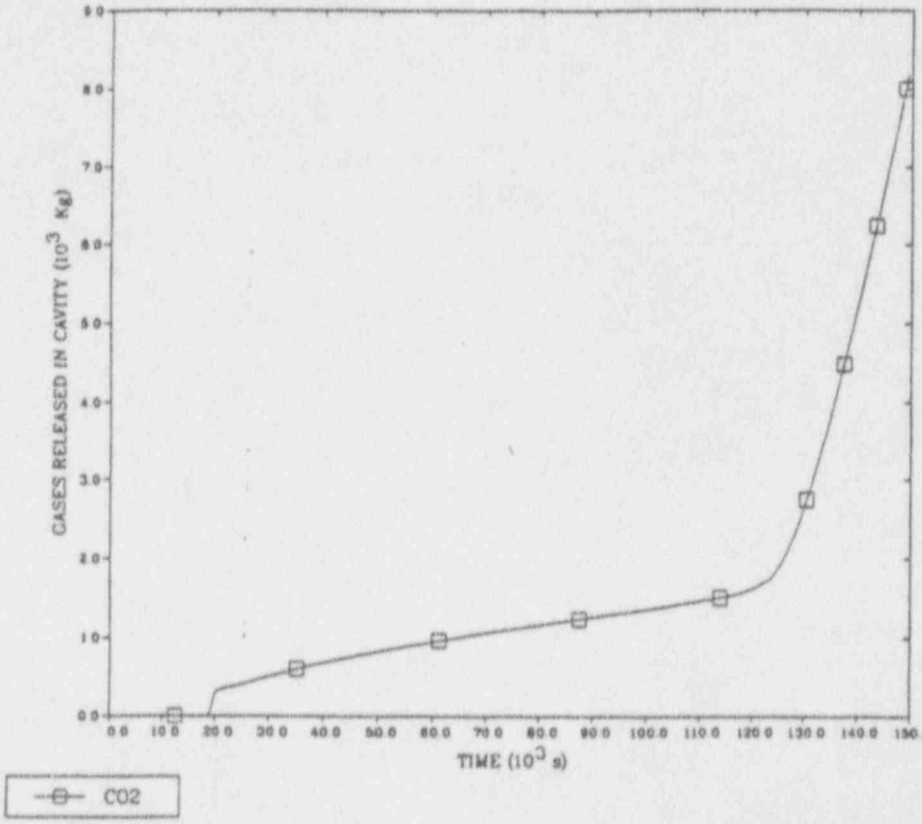

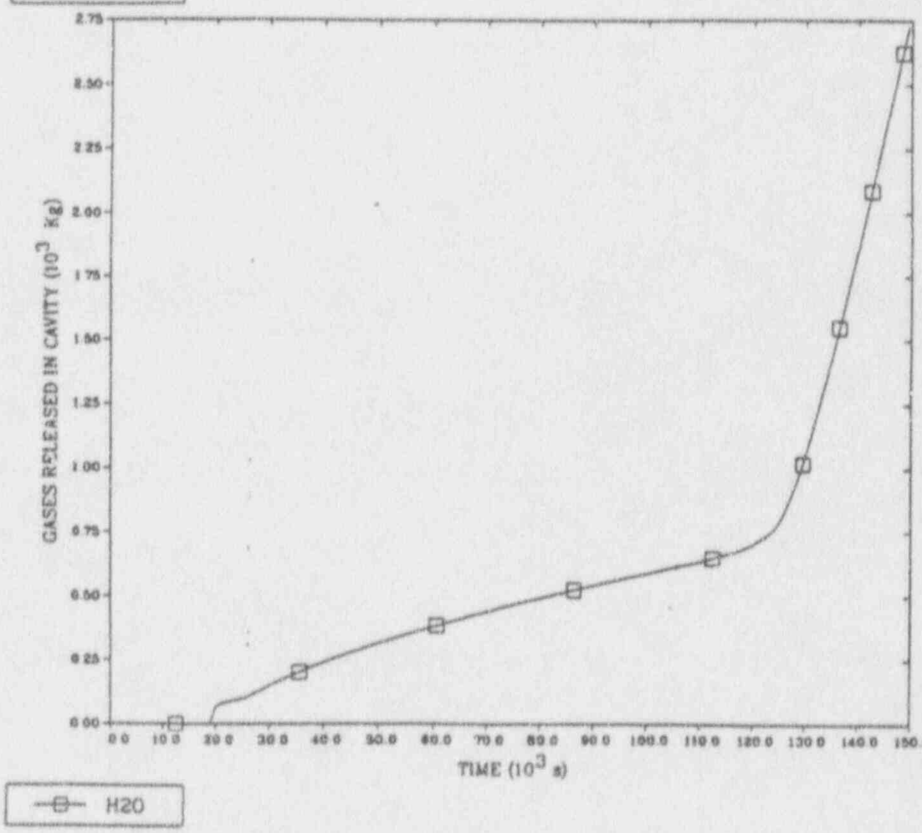

Figure C.38 MELCOR PRedicted Gas Release From Corium-Concrete Interaction

ZION SMALL BREAK 2.5" AT INTERMEDIATE LEG

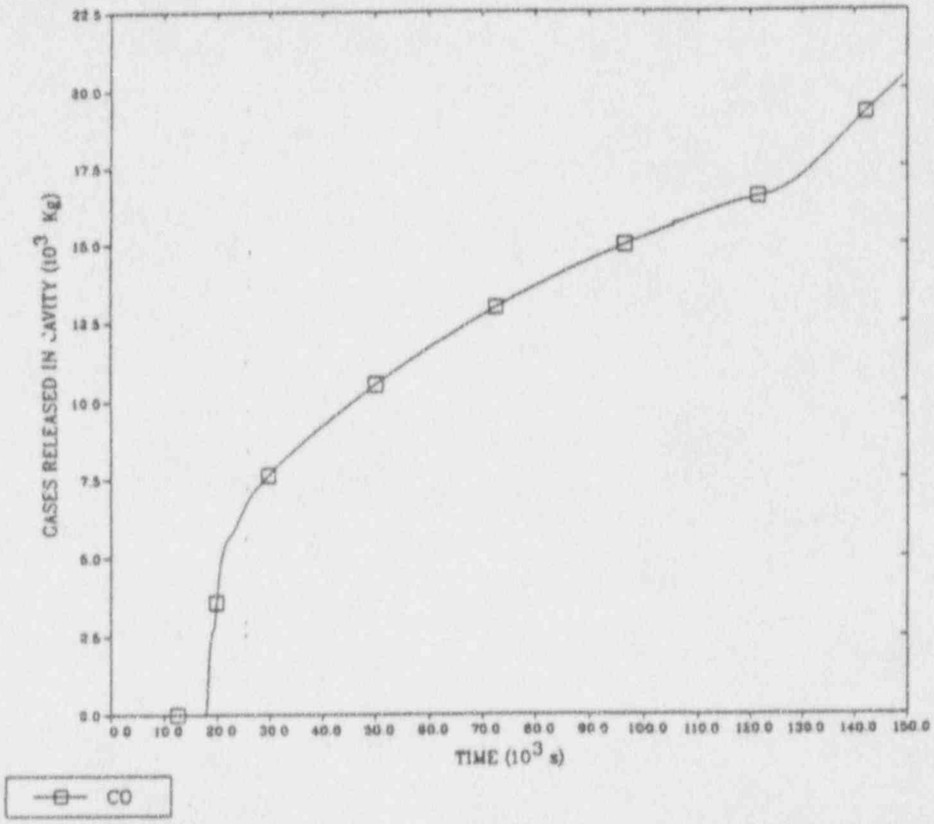

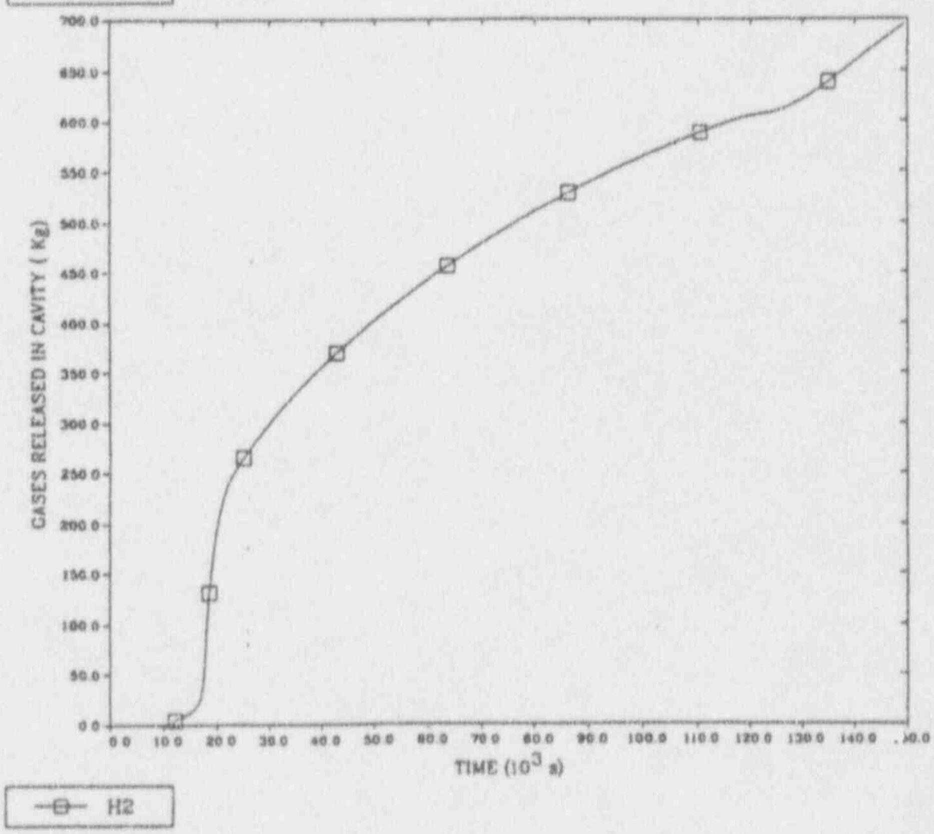

Figure C.38 MELCOR Predicted Gas Release From Corium-Concrete Interaction (Continued)

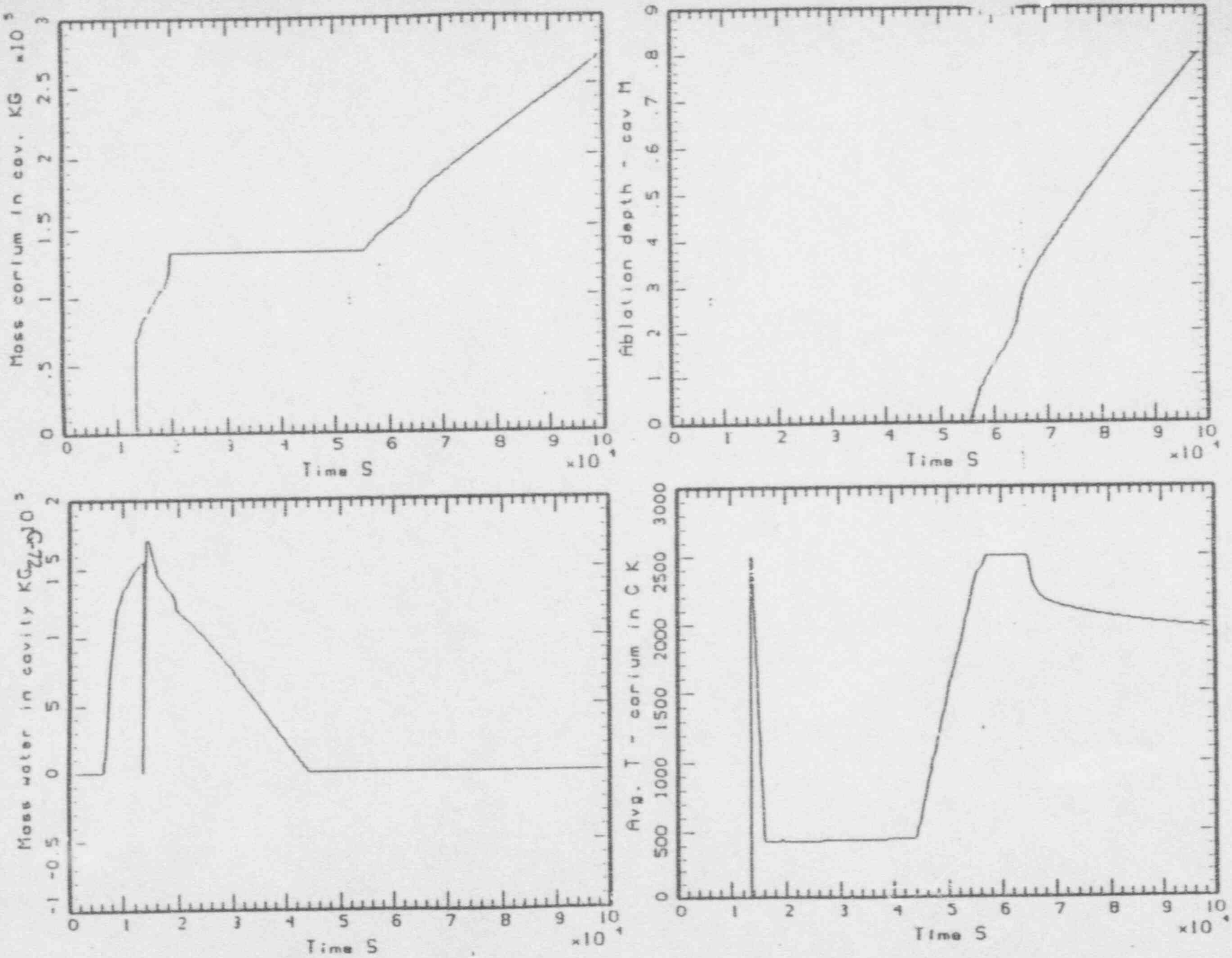

Figure C.39 MAAP Predicted Corium Mass, Water Mass, Corium Temperature, and Ablation Distance

the corium is discharged into the cavity. The maximum erosion distance in the axial direction (1.44 m) is much larger than that predicted by MAAP. In the radial direction, the maximum erosion distance predicted by MELCOR is only 0.27 m.

Figure C.40 shows the total releases of steam, H_2, CO, and CO_2 predicted by MAAP. Because of the dryout of water in the cavity and a high corium temperature, MAAP predicts a strong gas release. The following comparison shows the total gas release at the time of containment failure:

	MAAP	MELCOR
Cavity Condition	Dry	Wet
Ablation Initiation, S	54,870	11,540
Containment Failure, S	92,718	104,500
H_2, Kg	350	575
Steam, Kg	1,400	580
CO, Kg	9,000	16,000
CO_2, Kg	5,600	1,440

The time duration of gas release (from the initiation of ablation to containment failure) predicted by MAAP is much shorter than that predicted by MELCOR.

The dry cavity configuration predicted by MAAP is caused by the water distribution predicted by the code in the various compartments of the containment and water flow between these compartments. Figure C.41 shows the water masses in the upper, lower, annulus, and cavity regions, and Figure C.42 shows the water flow between these compartments. Comparisons with the results from the analysis of MELCOR given in Figures C.33 to Figure C.35 indicate that a) the water mass predicted by MAAP in each of the compartment is much less than that predicted by MELCOR and b) the continuous and oscillating water flow pattern predicted by MELCOR between each compartment is not predicted by MAAP. These differences are related to the modeling of containment structures and vapor condensation from these structures. The degassing model in MELCOR also contributes to the containment water inventory.

MAAP also predicted the entrainment of 10 Kg of corium into the lower compartment. This small quantity of corium has no effect on concrete interaction as shown in Figure C.43.

5.5 Containment Behavior

MELCOR Analysis

In Section 2 of this appendix, we state that the operation of sprays is assumed when the containment pressure reaches 0.26 Mpa. The operation is limited by the amount of water in the refueling water storage tank (i.e. 250,000 Kg, about 10% of the normal capacity). Figure C.44 shows that the containment sprays were operated from 15,200 to 18,800 seconds, according to the MELCOR analysis. During this time period, the containment pressure is maintained at 0.26 Mpa as shown in Figure C.45. After the sprays are terminated, the containment pressure increases steadily due to the release of gases from the corium/concrete interaction. At 104,996 seconds, the pressure reaches the estimated containment capacity (1.027 Mpa or 149 psia), and loss of containment integrity is assumed to occur at this time.

Figure C.45 shows that the reactor cavity, which is the source compartment, has a pressure slightly higher than that in the other compartments. The average pressurization rate is about 9.2Pa/s. Figure C.45 also shows that the containment is inerted during the transient as indicated by the partial pressure of steam. The inertness is further illustrated by molar fractions of gases in each compartment as given in Figure C.46. In all compartments, the atmosphere is dominated by steam. During the debris ejection and the initial corium-concrete interaction, the reactor cavity has very high fractions of H_2 and CO, above 28% and 25%, respectively. However, no combustion was predicted because the atmosphere is inerted by the presence of a high fraction of steam.

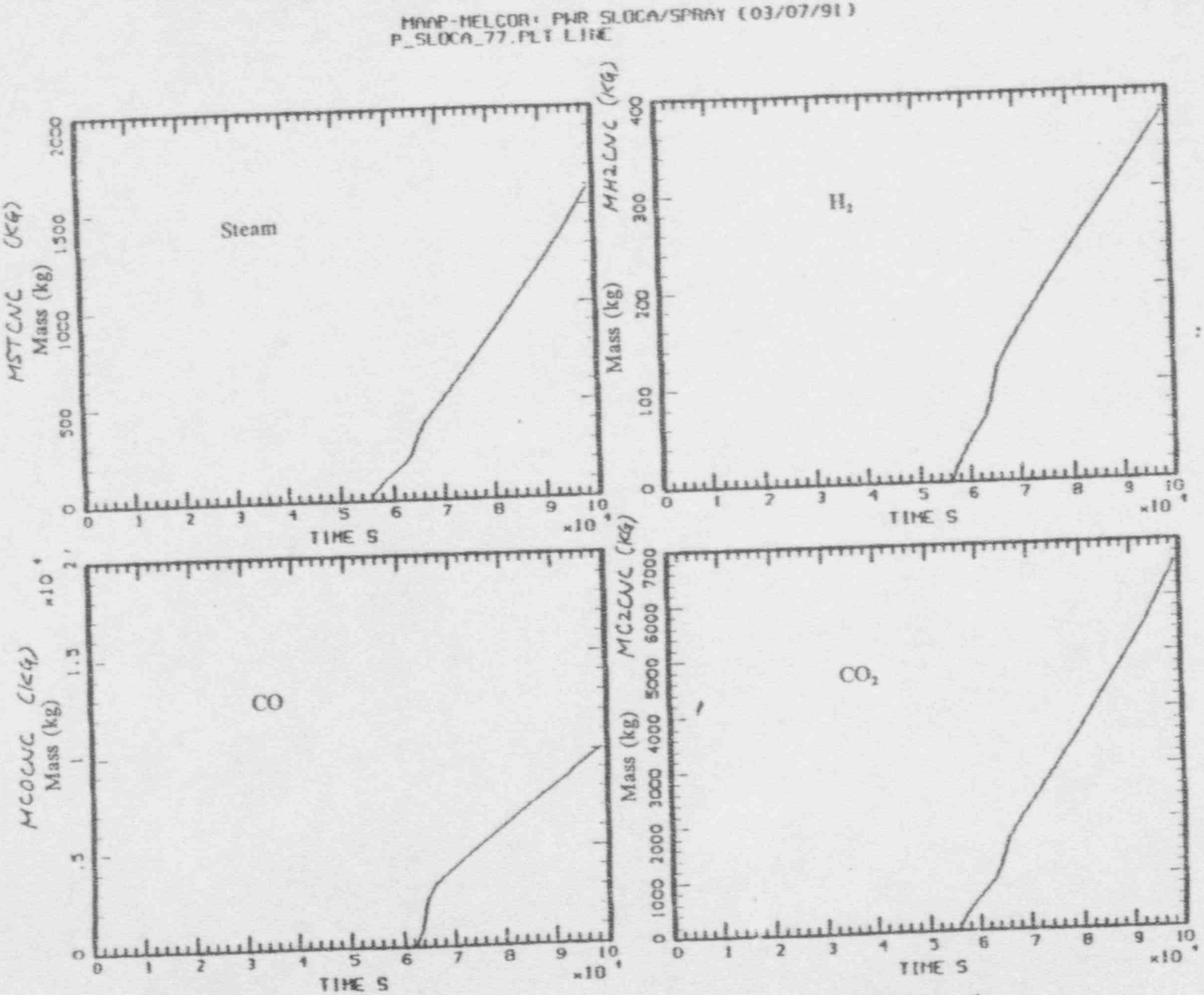

Figure C.40 MAAP Predicted Gas Release From Corium-Concrete Interaction

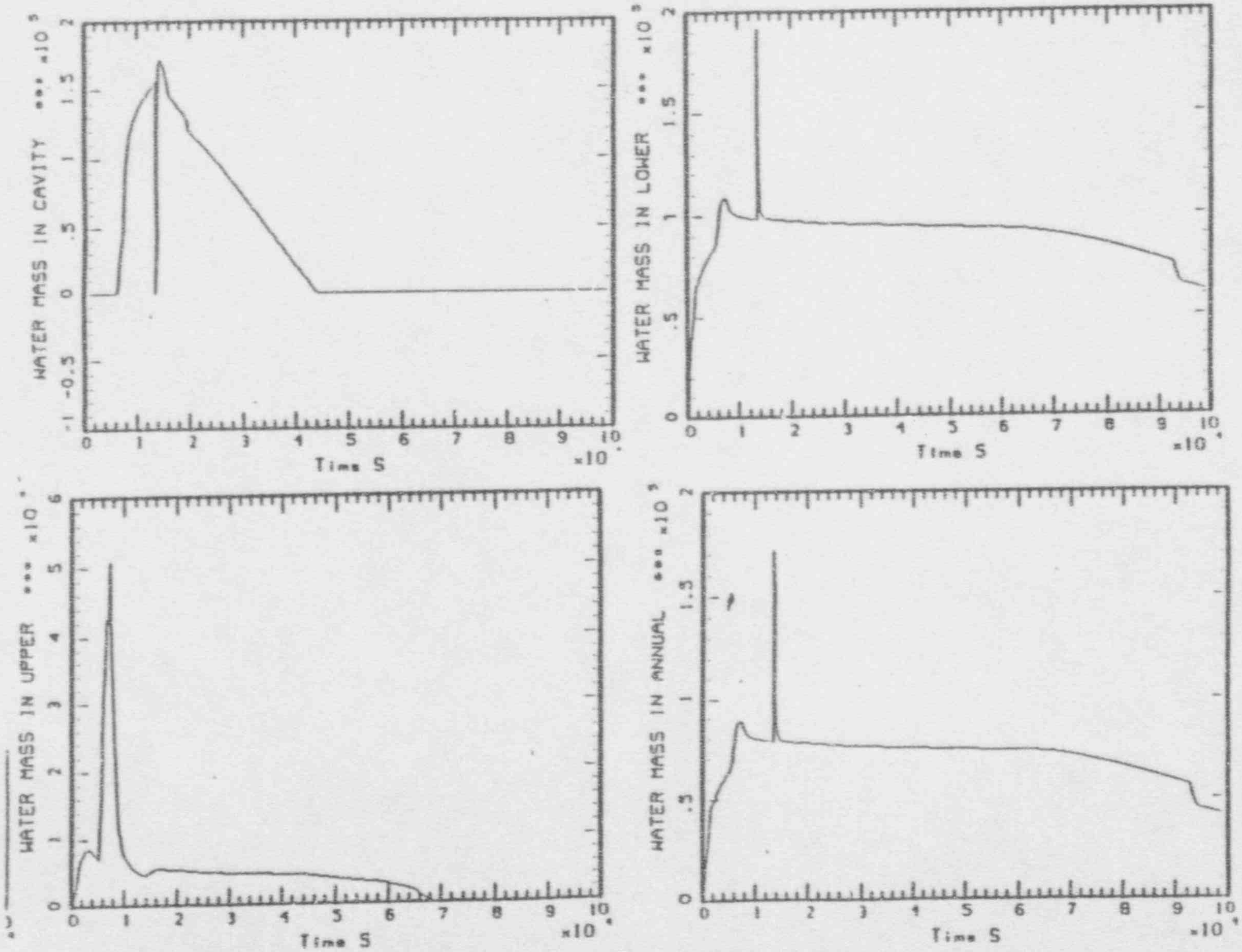

Figure C.41 MAAP Predicted Water Mass in Containment

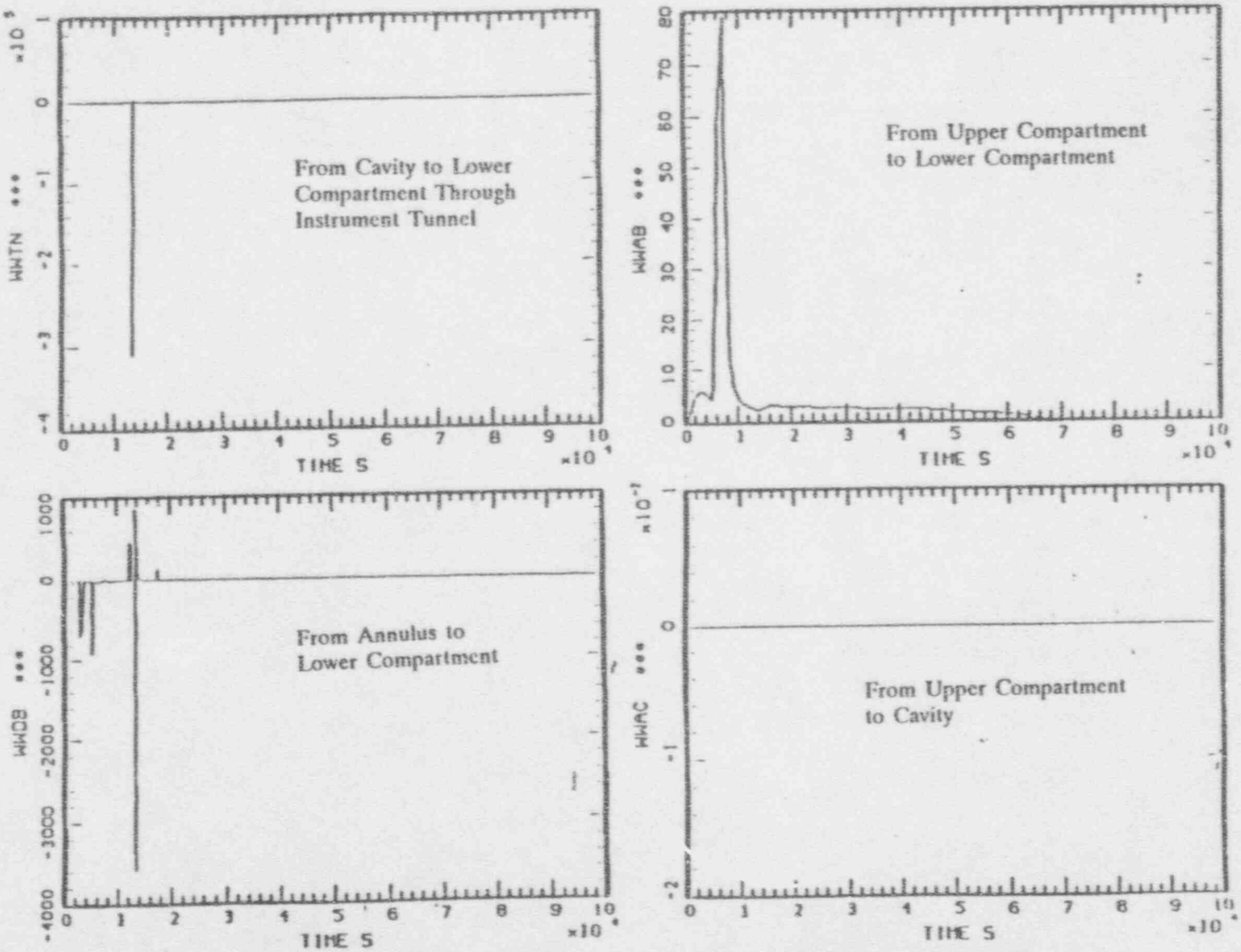

Figure C.42 MAAP Predicted Water Flow Rate in Containment

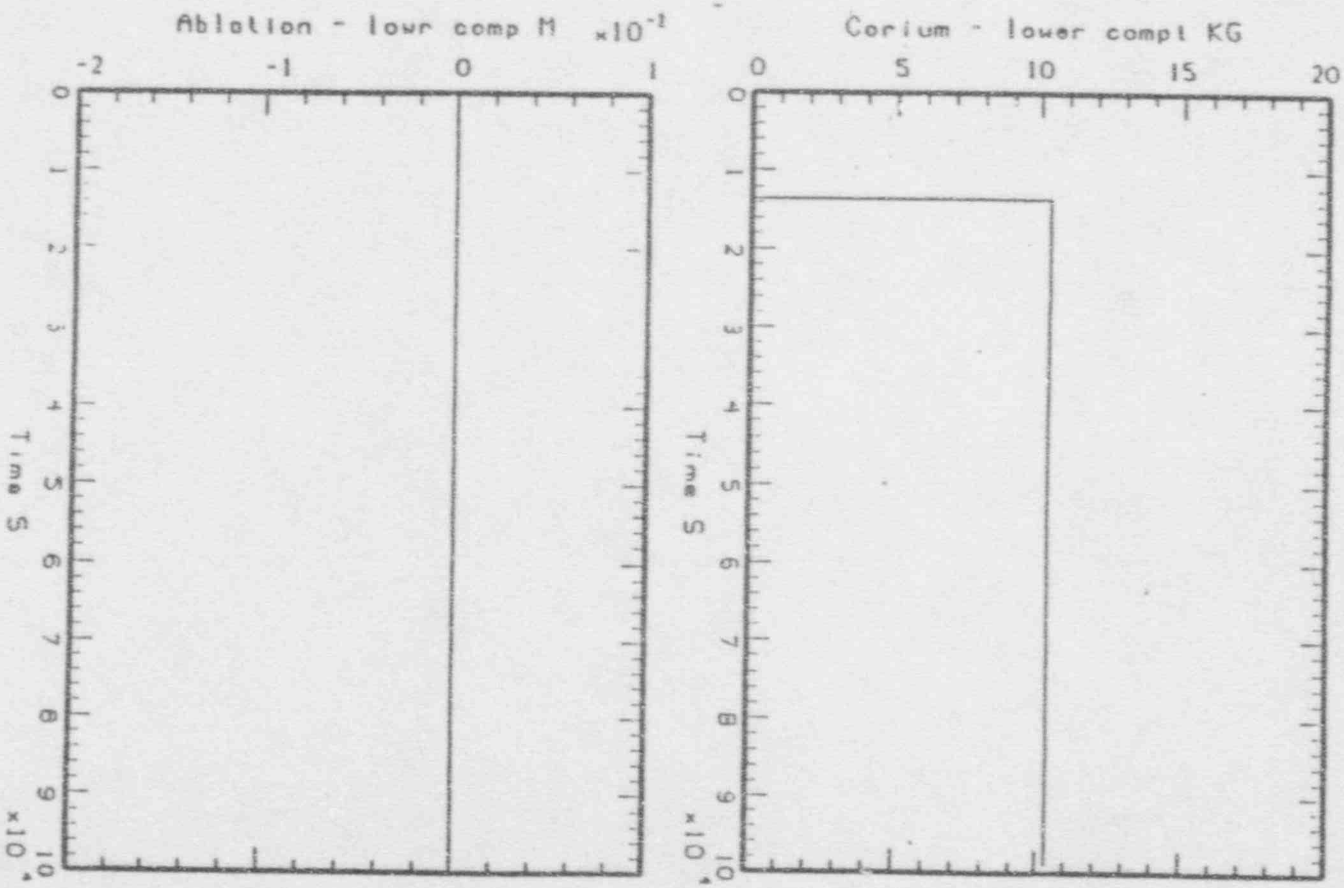

Figure C.43 MAAP Predicted Corium Mass and Ablation in Lower Compartment

ZION SMALL BREAK 2.5" AT INTERMEDIATE LEG

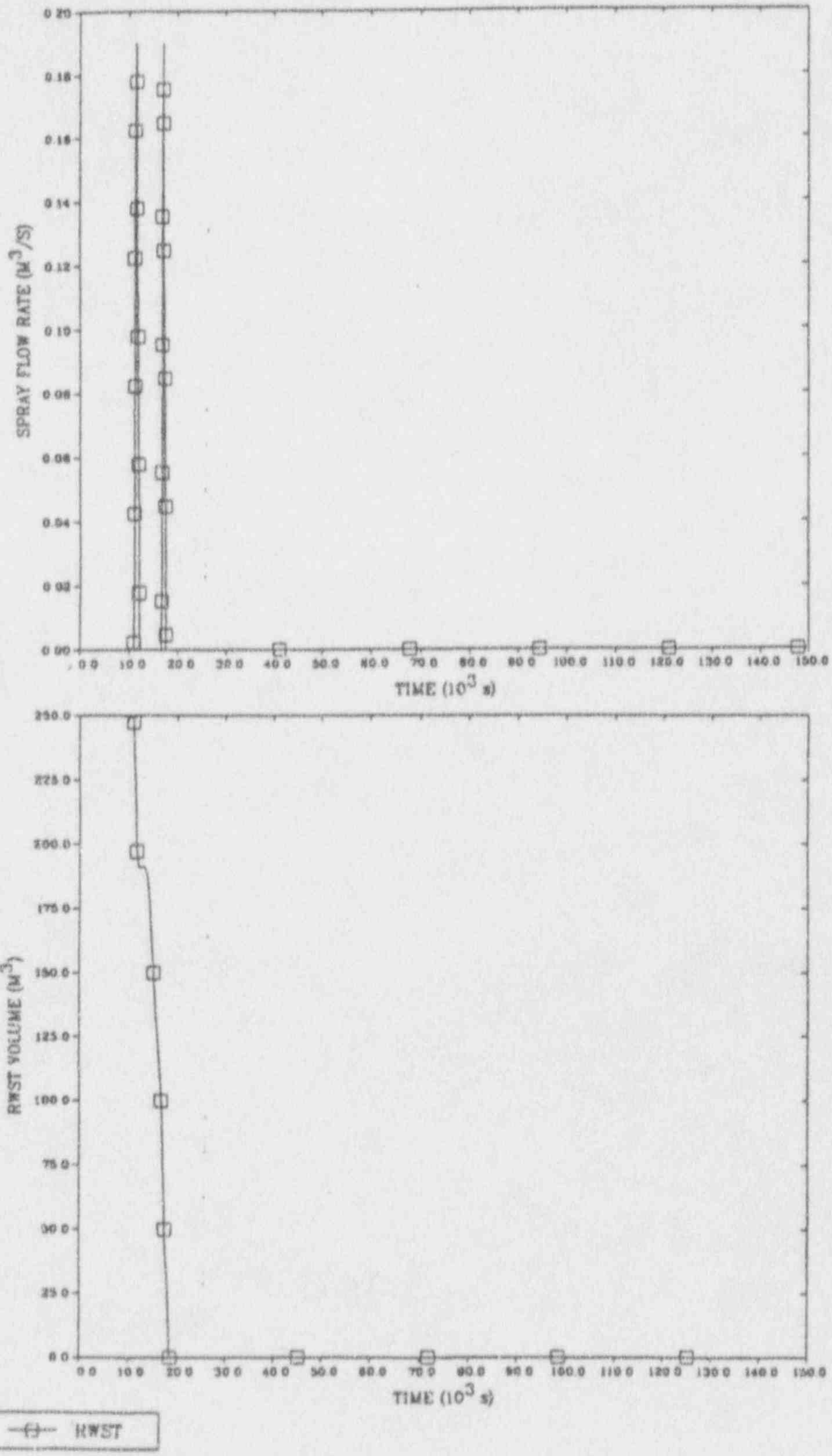

Figure C.44 MELCOR Predicted Containment Sprays

ZION SMALL BREAK 2.5" AT INTERMEDIATE LEG

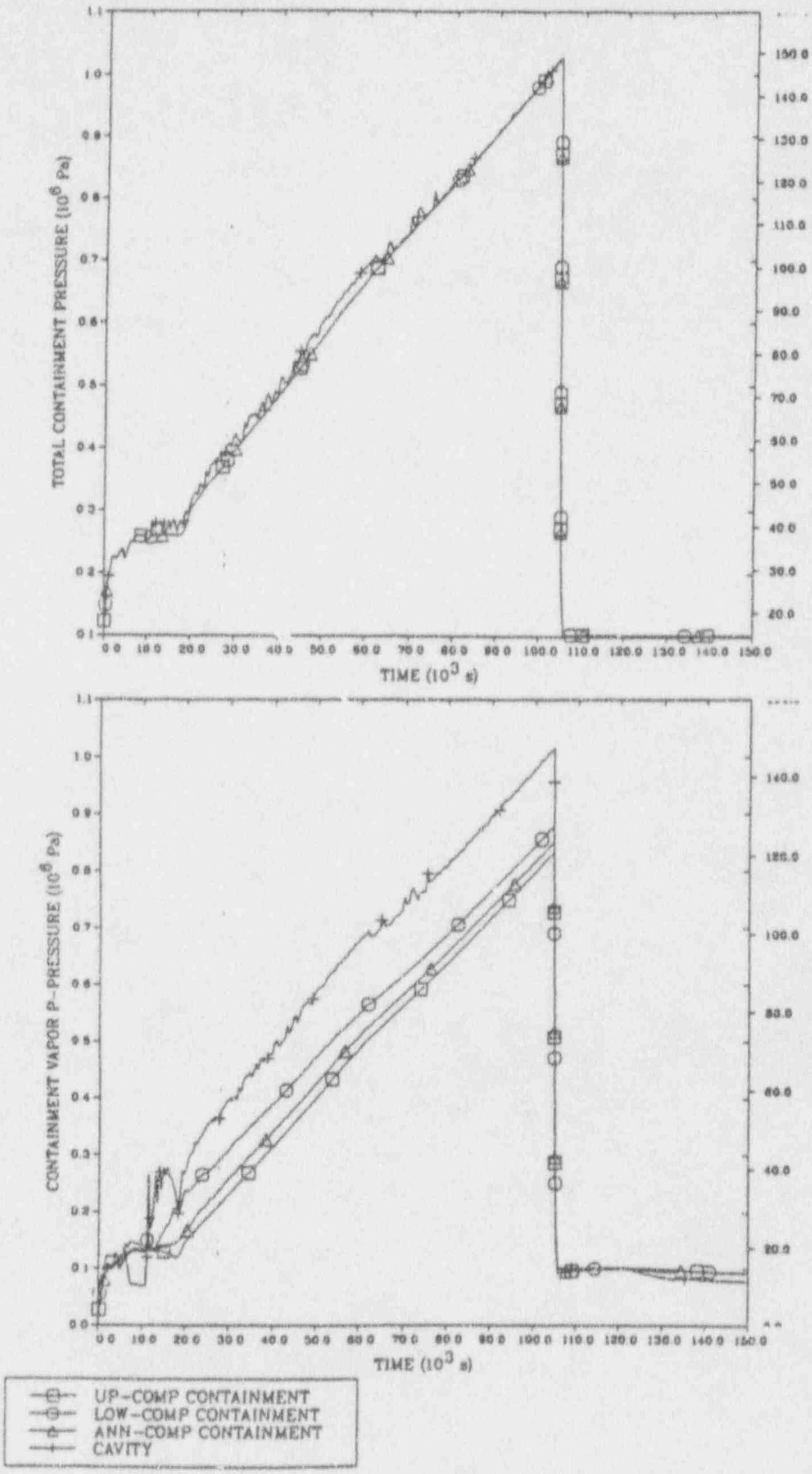

Figure C.45 MELCOR Predicted Containment Pressure

ZION SMALL BREAK 2.5" AT INTERMEDIATE LEG

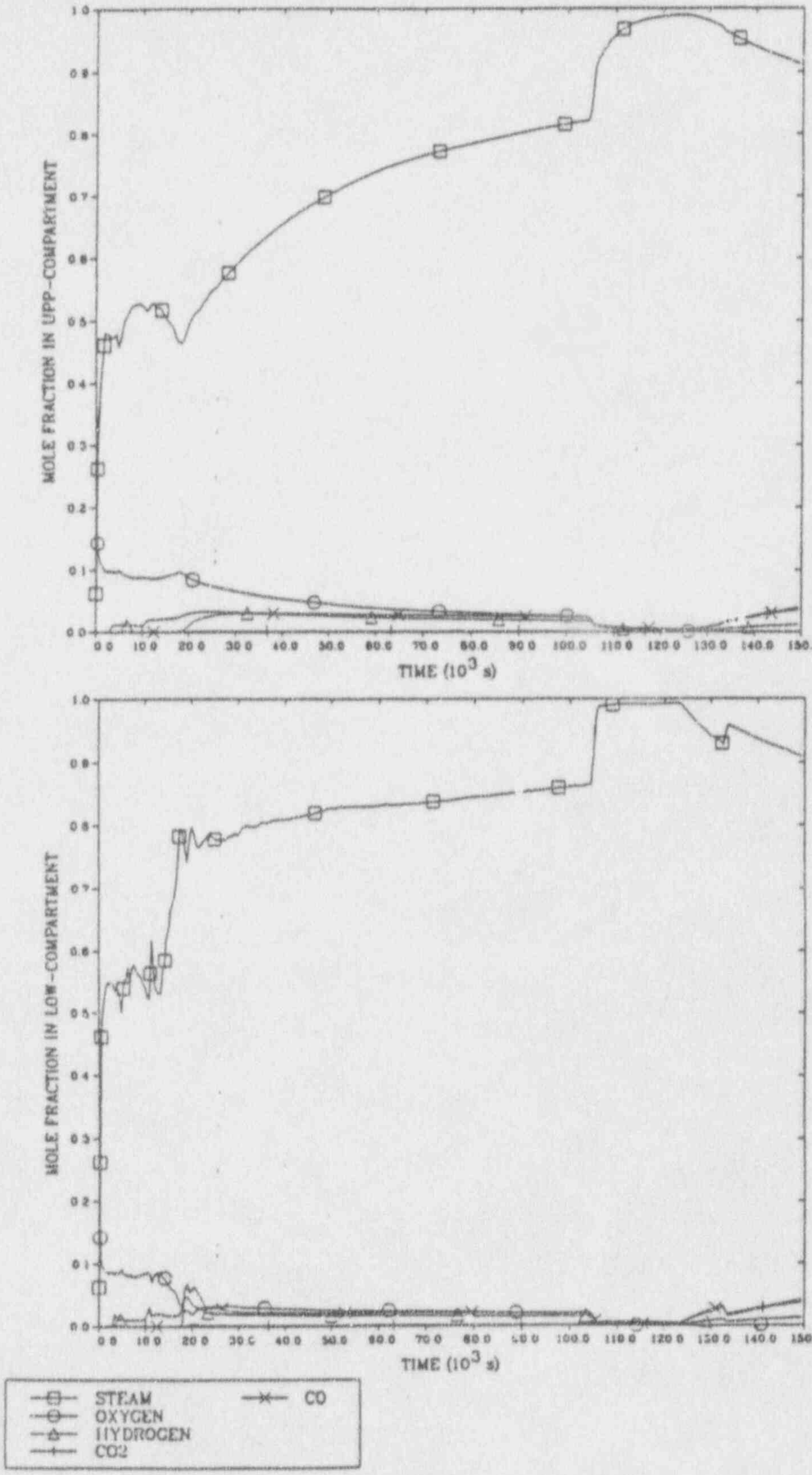

Figure C.46 MELCOR Predicted Gas Molar Fractions in Containment

ZION SMALL BREAK 2.5" AT INTERMEDIATE LEG

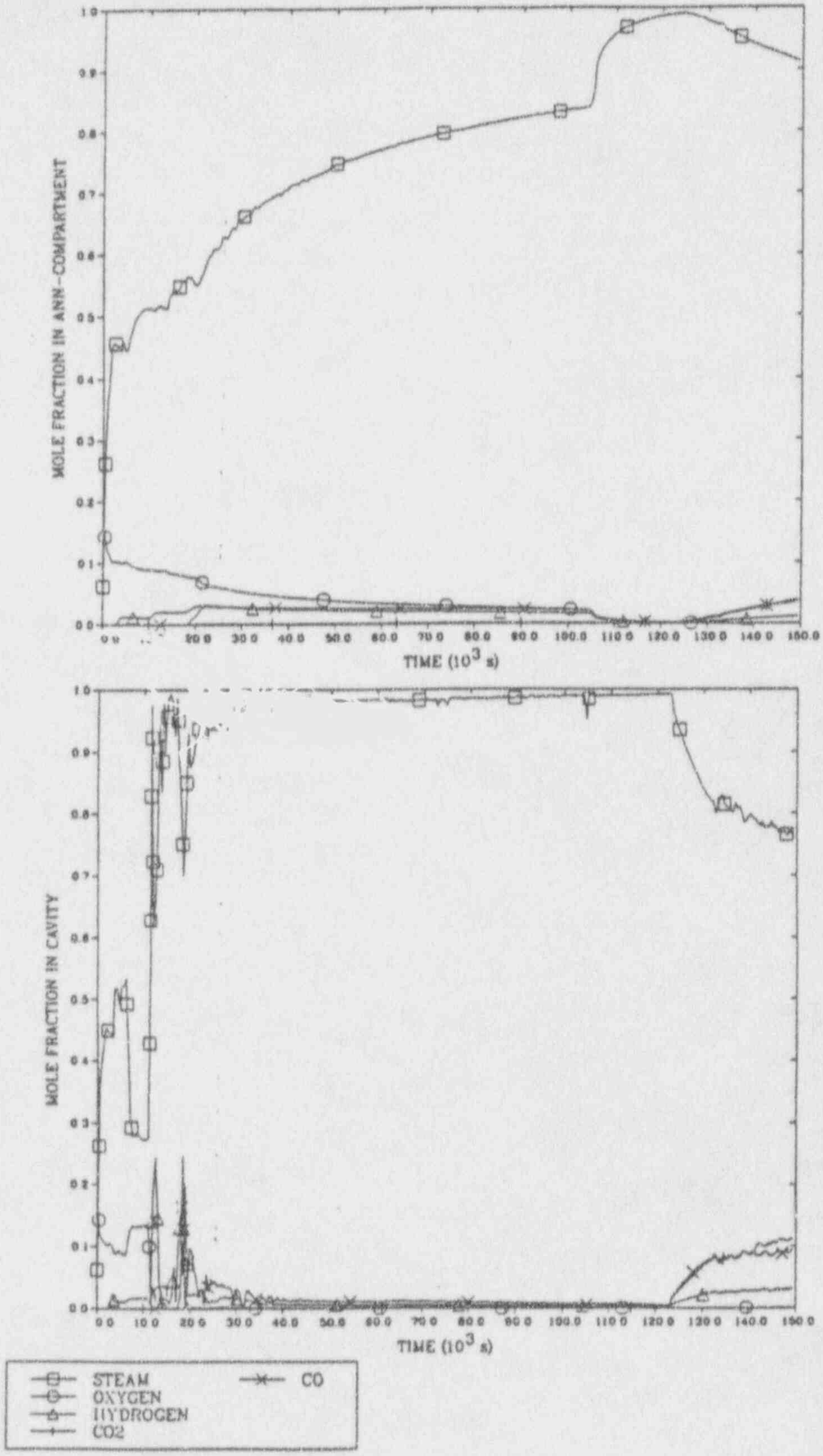

Figure C.46 MELCOR Predicted Gas Molar Fractions in Containment (Continued)

Figure C.47 shows containment atmosphere and water temperatures predicted by MELCOR. Temperatures in the containment are close to the saturation temperature before the containment failure. We do not expect the relatively low temperature to threaten the containment integrity.

The degassing model in MELCOR permits the release of water vapor and CO_2 from the concrete structures over a degassing temperature range specified by the user. In the analysis, the values of the temperature range are 360 to 380 K for the free water vapor, and 500 to 520 K for the chemically bounded water vapor and CO_2. Based on the containment temperature shown in Figure C.47, only the free water vapor would be released during the transient (Figure C.48) and the release of CO_2 is not expected (Figure C.49). The total quantity of water vapor released from all concrete structures is about 83,600 Kg (Figure C.48). The quantity of water vapor released is much more than the amount of steam released due to the corium/concrete interaction in the cavity (about 2100 Kg). Because of the large surface area of some structures, such as the crane wall of the crane compartment, a large amount of steam is released.

The steam masses in the four compartments of the containment are shown in Figure C.50. The total steam mass before the containment failure is about 344,000 Kg. We will discuss the balance of steam mass later in this section when we compare MELCOR's predictions with MAAP's predictions.

The containment pressure predicted by MAAP is given in Figure C.51. The containment is initially subjected to a higher pressurization rate of about 14 Pa/s due to the water boil-off in the reactor cavity. After the water depletes at about 42,000 seconds, the containment pressurization rate is reduced to about 3.75 Pa/s. Containment failure is predicted at 92,718 seconds, which is about 5,628 seconds (i.e., 1.6 hours) sooner than that predicted by MELCOR.

Figure C.52 shows the molar fractions of gases predicted by MAAP in the four compartments of the containment. Similar to MELCOR's results, MAAP predicts a steam dominated containment. In the cavity region, the steam fraction reaches 100% during the water boil-off. Figure C.52 does not show peak fractions of H_2 (28%) and CO (25%) predicted by MELCOR in the cavity region.

The containment temperatures predicted by MAAP are shown in Figure C.53. The temperatures in the upper, lower, and annulus compartments are comparable to those predicted by MELCOR. Because of the dryout in the cavity, MAAP predicted a much higher temperature in the cavity compartment. This high temperature should generate a strong buoyancy force to enhance the flow mixing in the containment.

Finally, Figure C.54 shows the steam mass in the containment predicted by MAAP. The steam mass is used for the overall mass balance and is compared with the MELCOR results as shown in Table C.8. The steam mass in each compartment of the containment predicted by MAAP can be compared to that predicted by MELCOR. However, there is a large difference in the steam sources; for example, MAAP does not have the large quantity of vapor due to degassing of the concrete structures. According to the MAAP analysis, the complete water boil-off in the cavity at about 44,000 seconds provides a larger steam source to the containment. It is noted that steam sources given in Table C.8 do not include the vaporization of containment spray water and water pools in various containment compartments. The continuous boiling in the reactor cavity as predicted by the MELCOR code is not included in Table C.8.

5.6 Fission Product Release

MELCOR models the in-vessel release by two stages: gap release and fuel release. Fission products in the fuel-cladding gap are released at cladding failure defined by a user-specified temperature (1170 K). The subsequent release from the fuel is determined by the fuel heat-up rate, according to the CORSOR-M model. The cladding failure time for the four radial rings predicted by MELCOR are:

Ring 1	2655 s
Ring 2	2655
Ring 3	2710
Ring 4	2885

ZION SMALL BREAK 2.5" AT INTERMEDIATE LEG

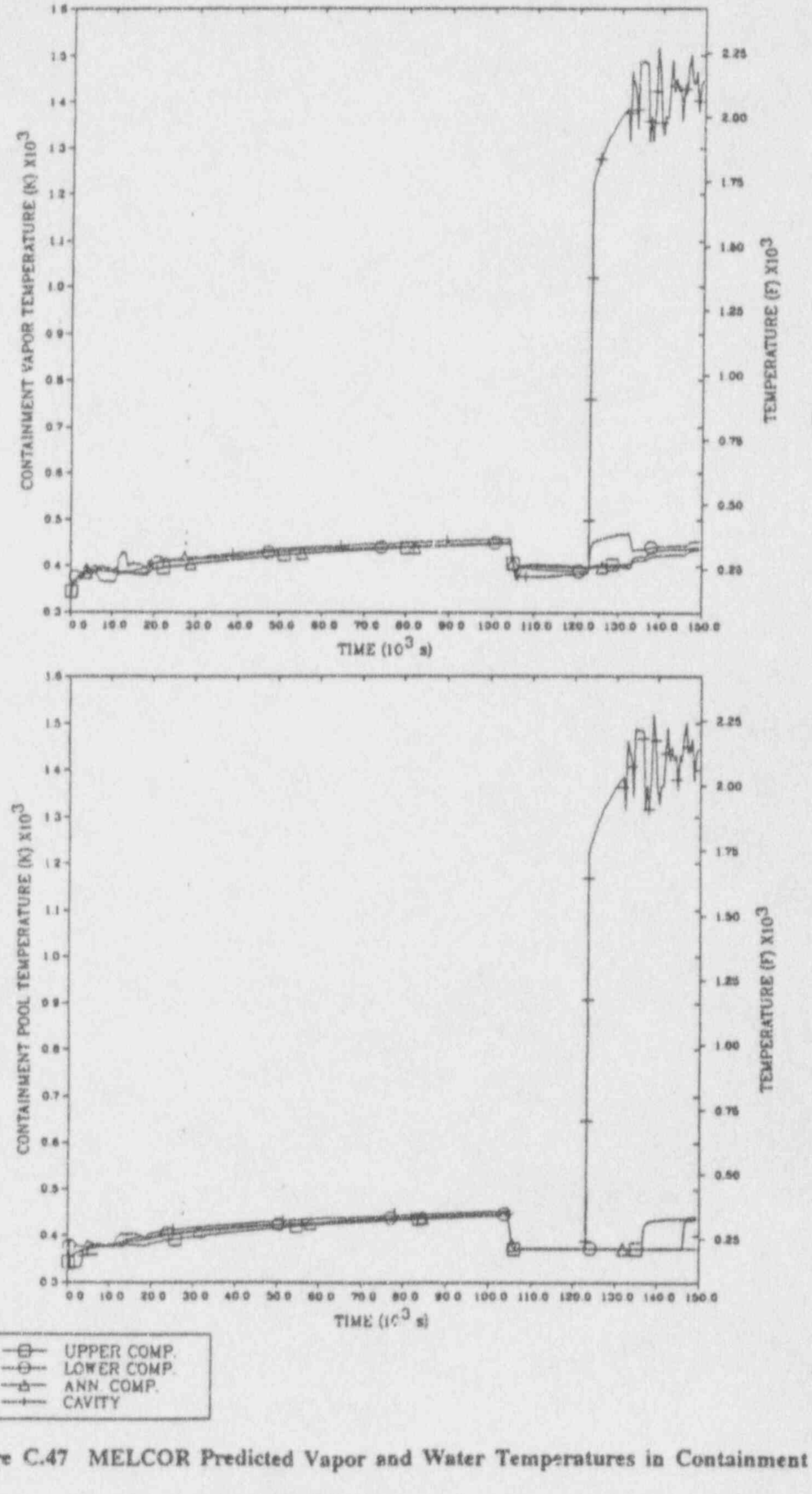

Figure C.47 MELCOR Predicted Vapor and Water Temperatures in Containment

ZION SMALL BREAK 2.5" AT INTERMEDIATE LEG

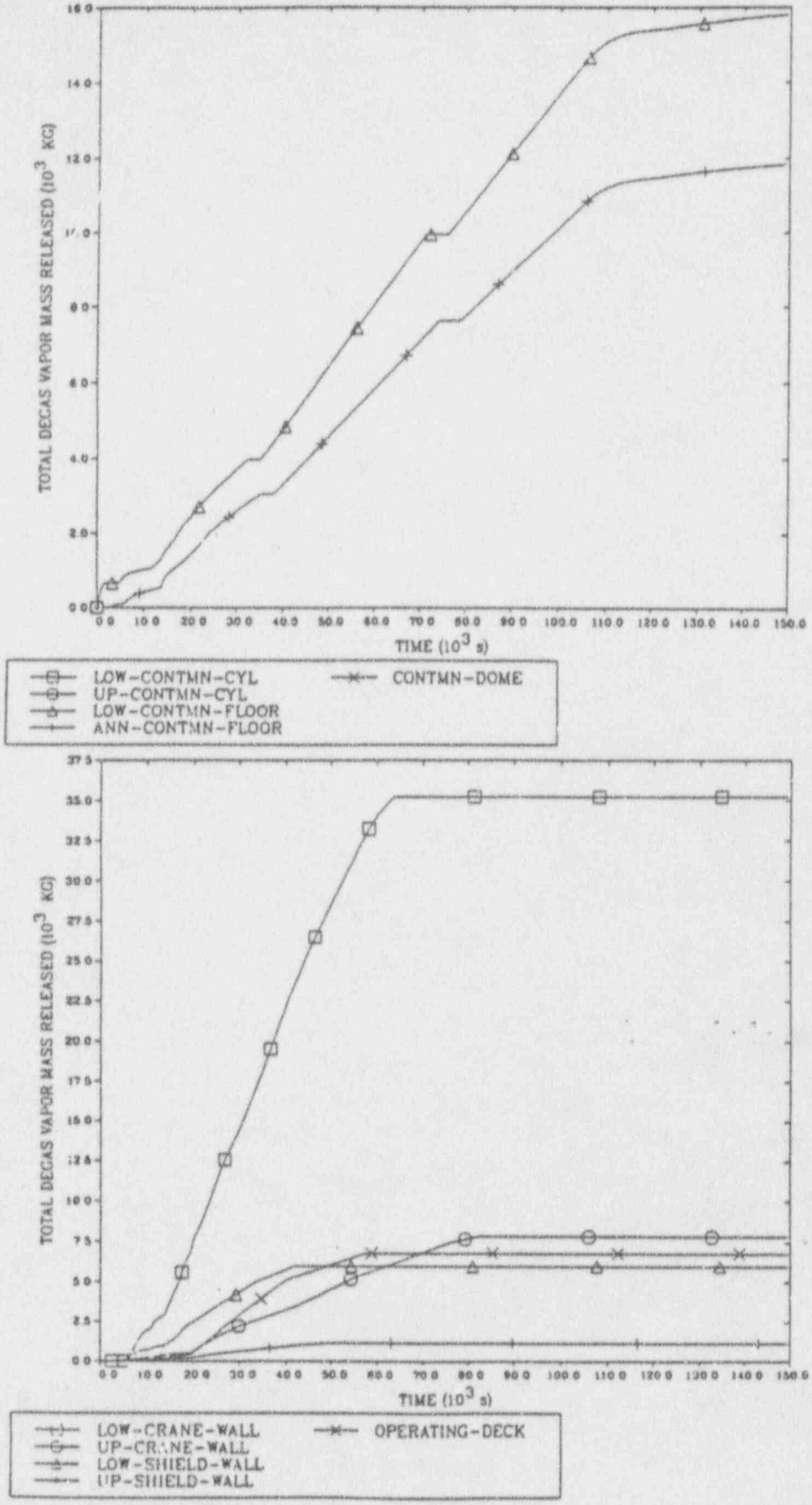

Figure C.48 MELCOR Predicted Degassing of Water Vapor From Concrete Structures

ZION SMALL BREAK 2.5" AT INTERMEDIATE LEG

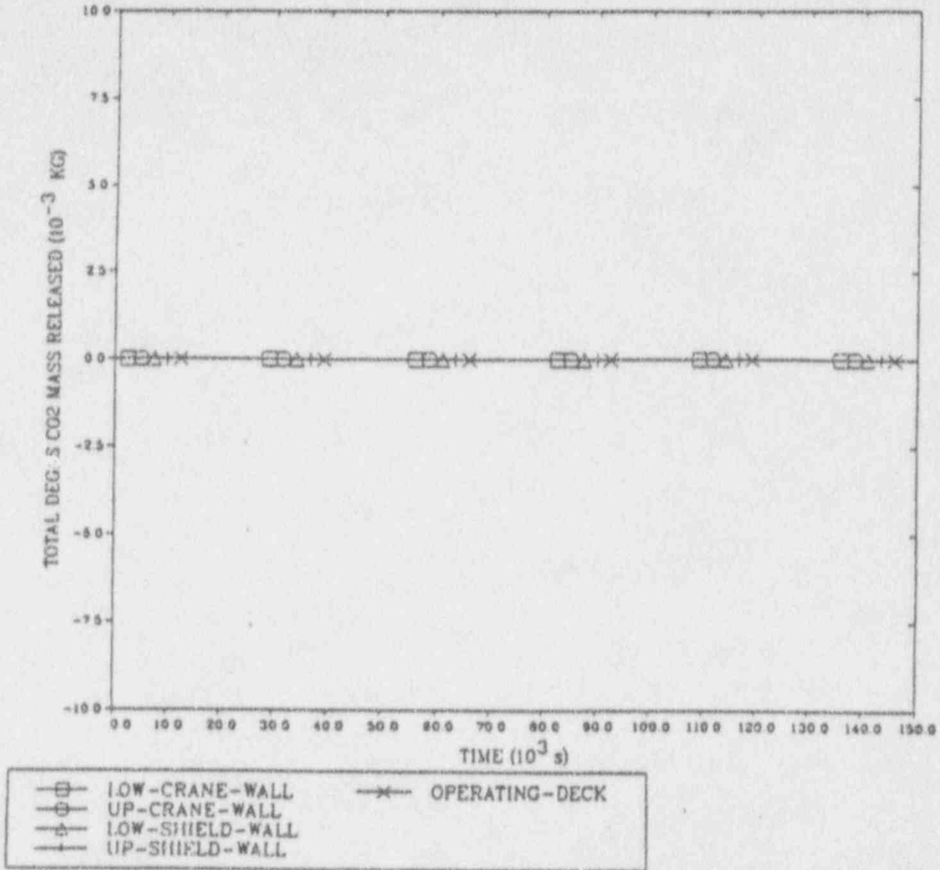

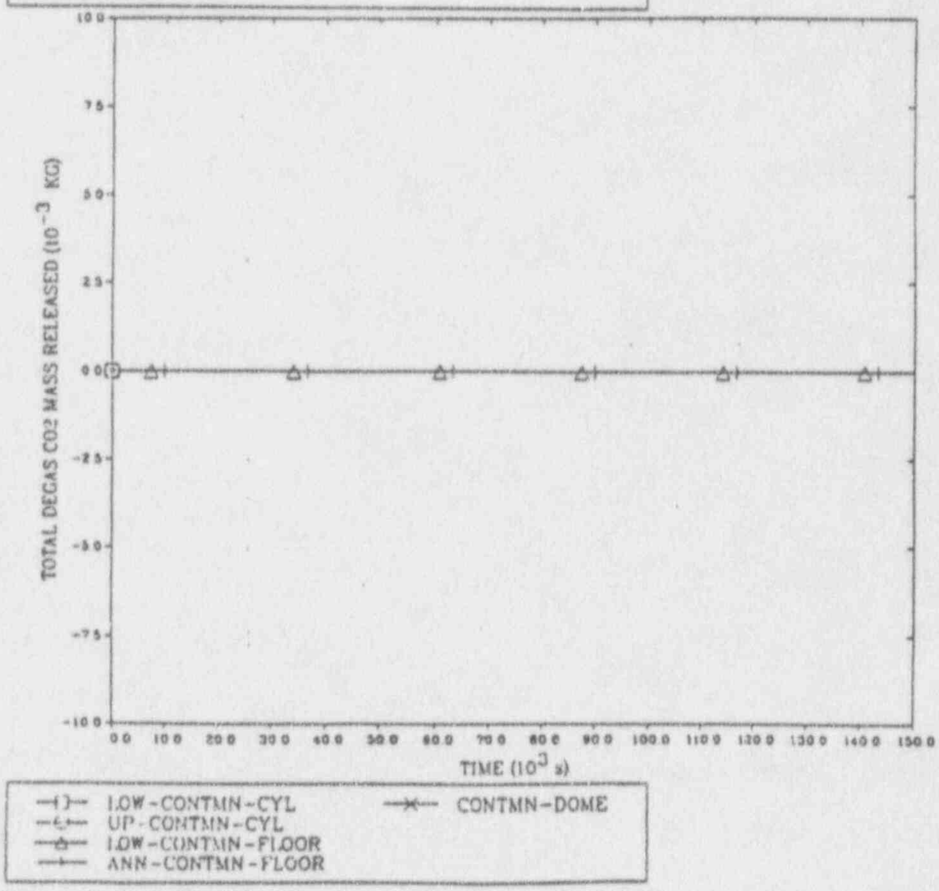

Figure C.49 MELCOR Predicted Degassing of CO_2 From Concrete Structures

ZION SMALL BREAK 2.5" AT INTERMEDIATE LEG

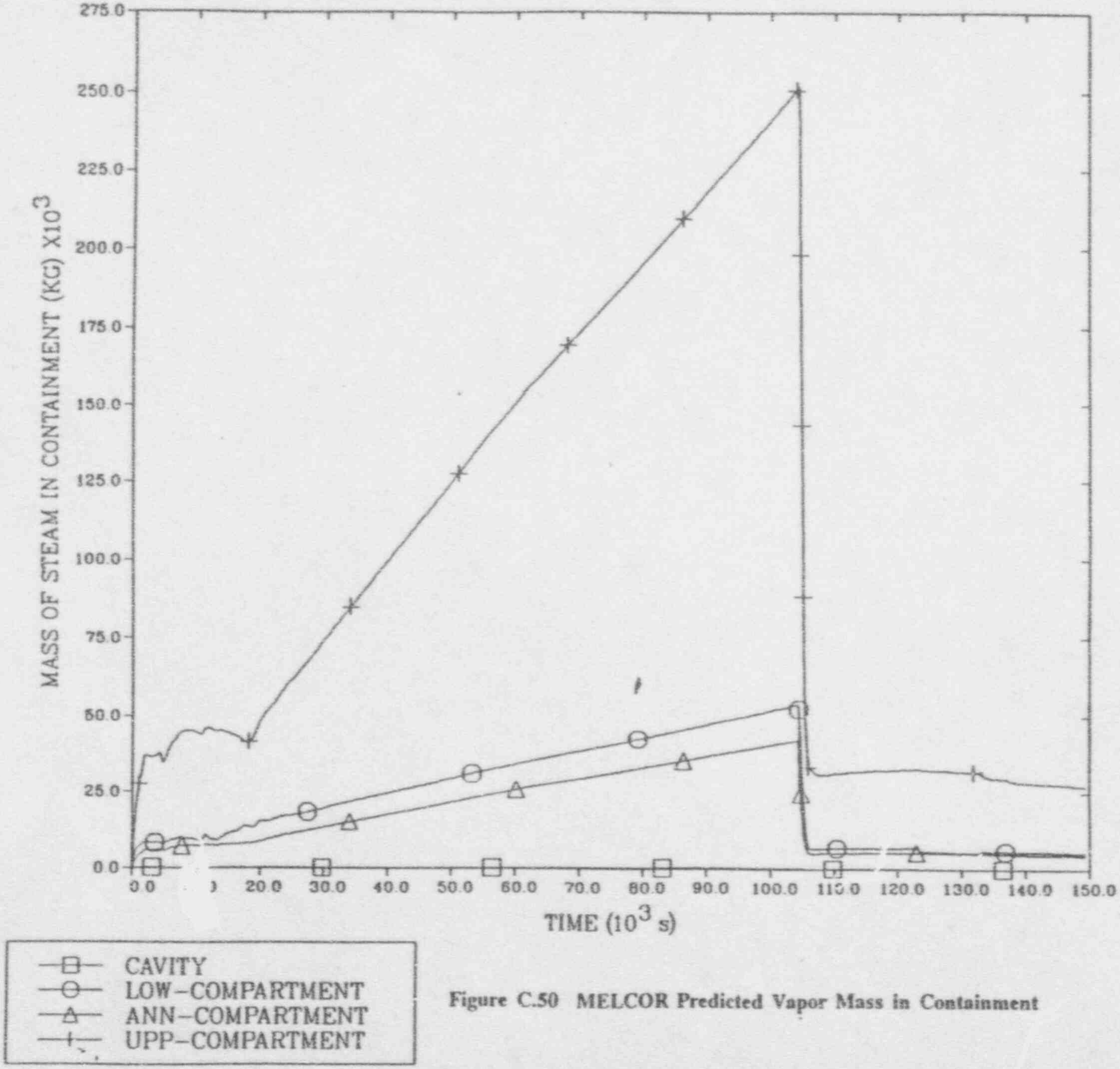

Figure C.50 MELCOR Predicted Vapor Mass in Containment

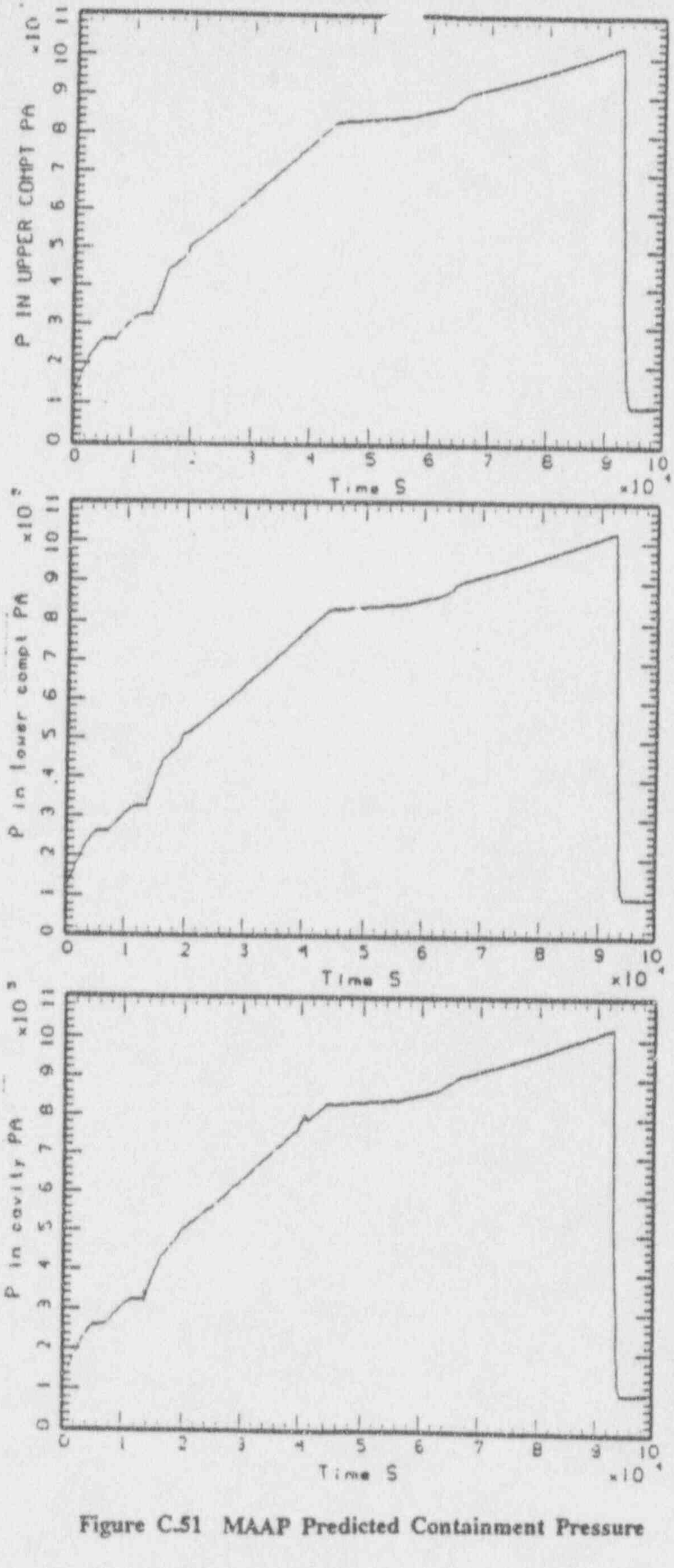

Figure C.51 MAAP Predicted Containment Pressure

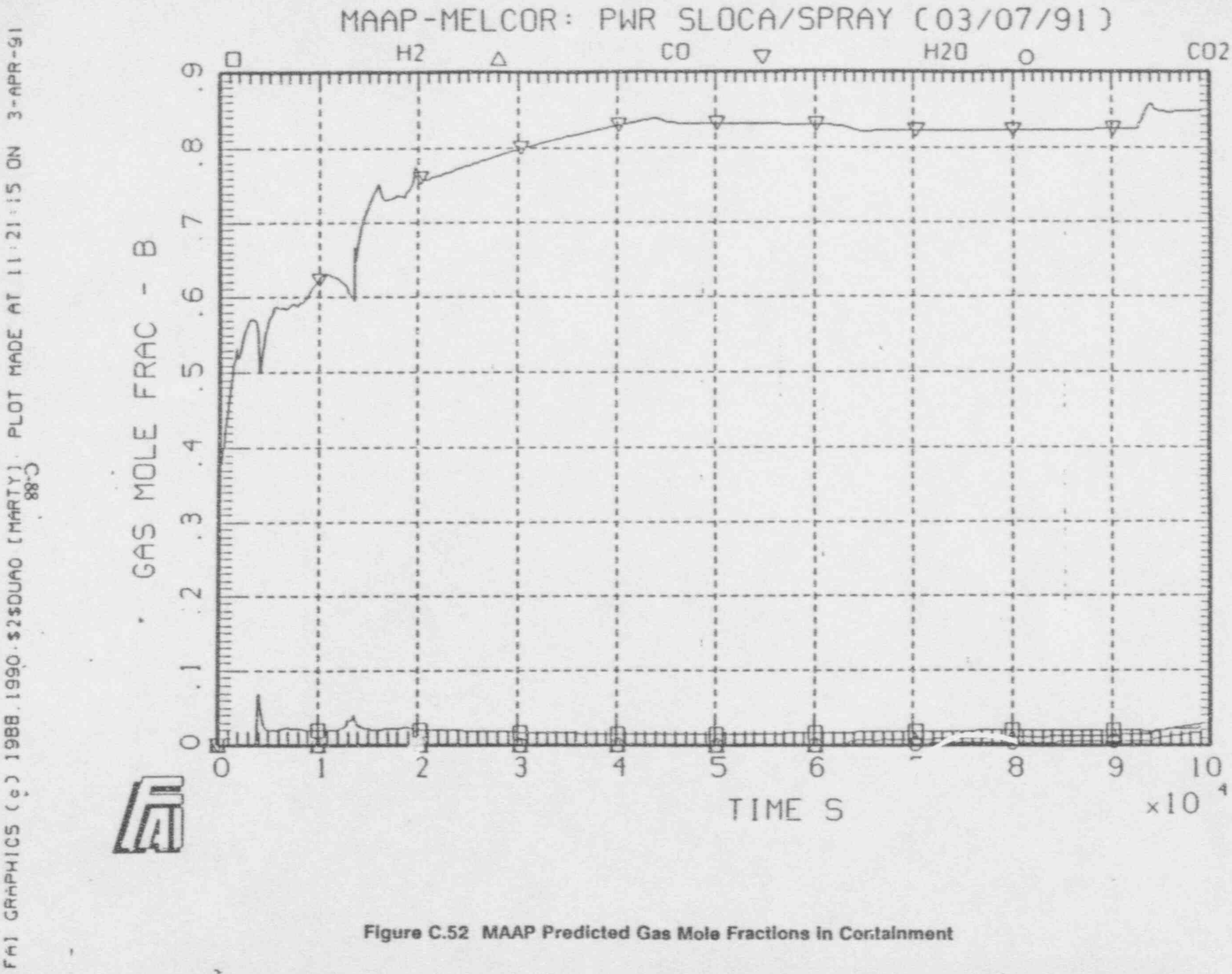

Figure C.52 MAAP Predicted Gas Mole Fractions in Containment

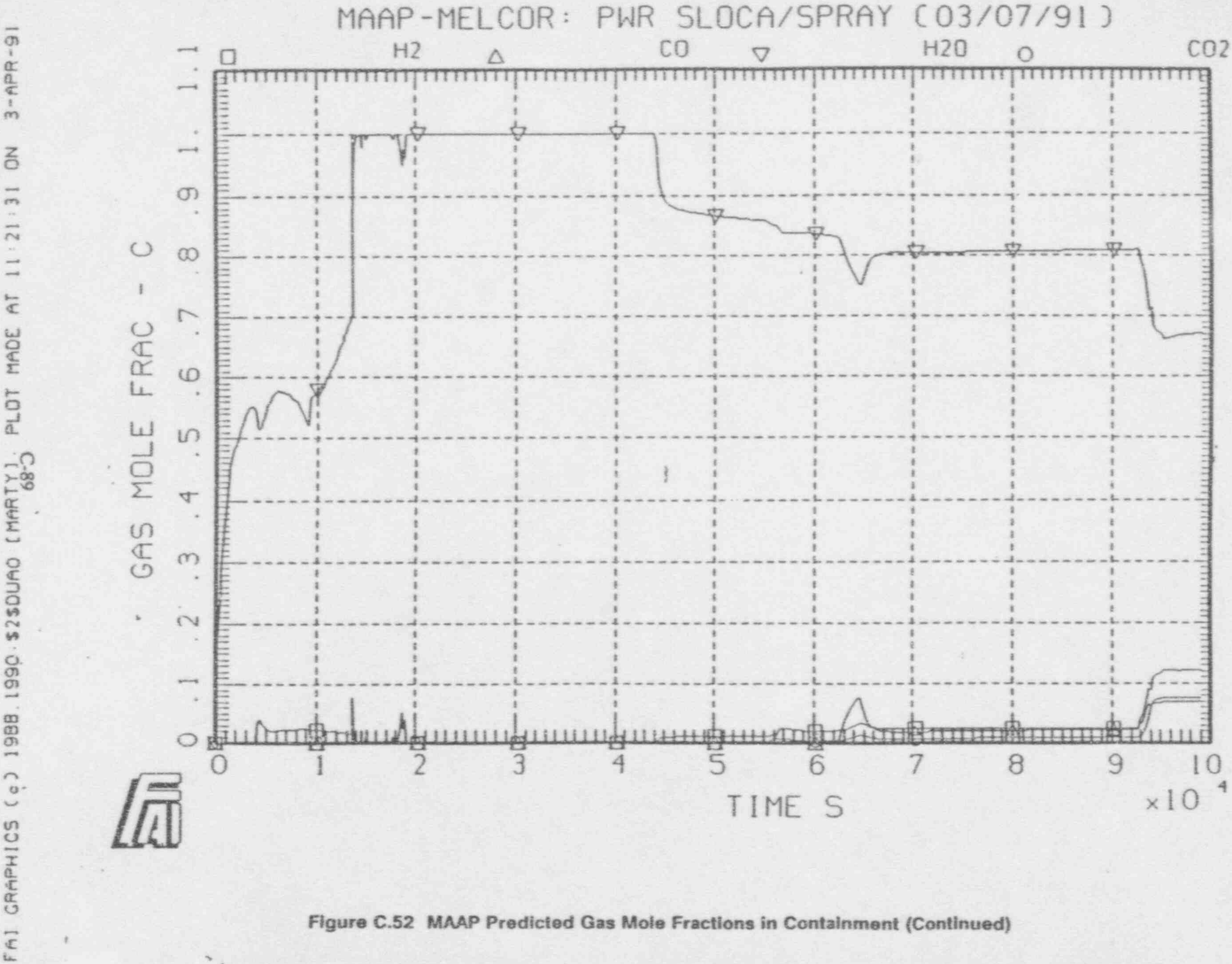

Figure C.52 MAAP Predicted Gas Mole Fractions in Containment (Continued)

Figure C.52 MAAP Predicted Gas Mole Fractions In Containment (Continued)

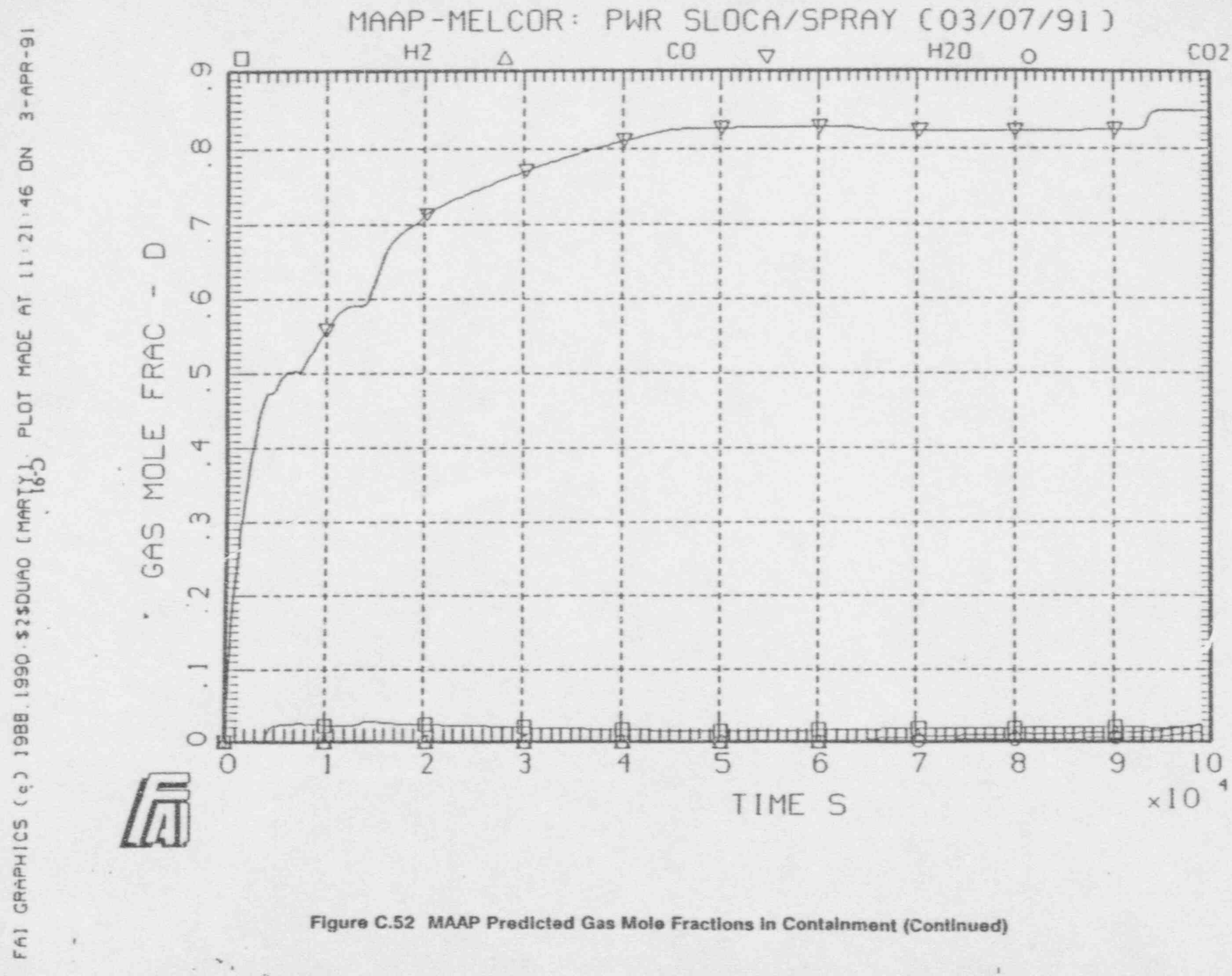

Figure C.52 MAAP Predicted Gas Mole Fractions in Containment (Continued)

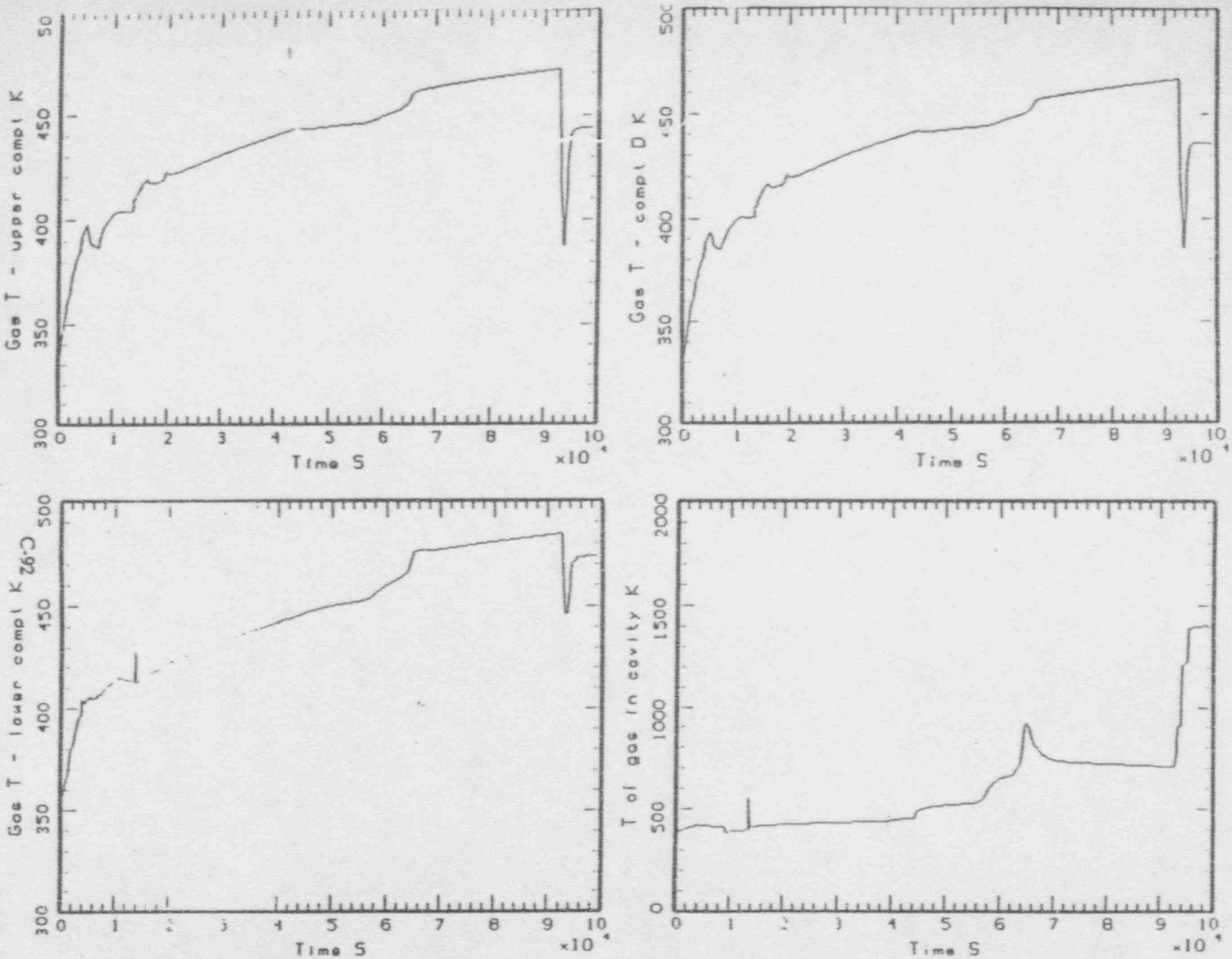

Figure C.53 MAAP Predicted Temperatures In Containment

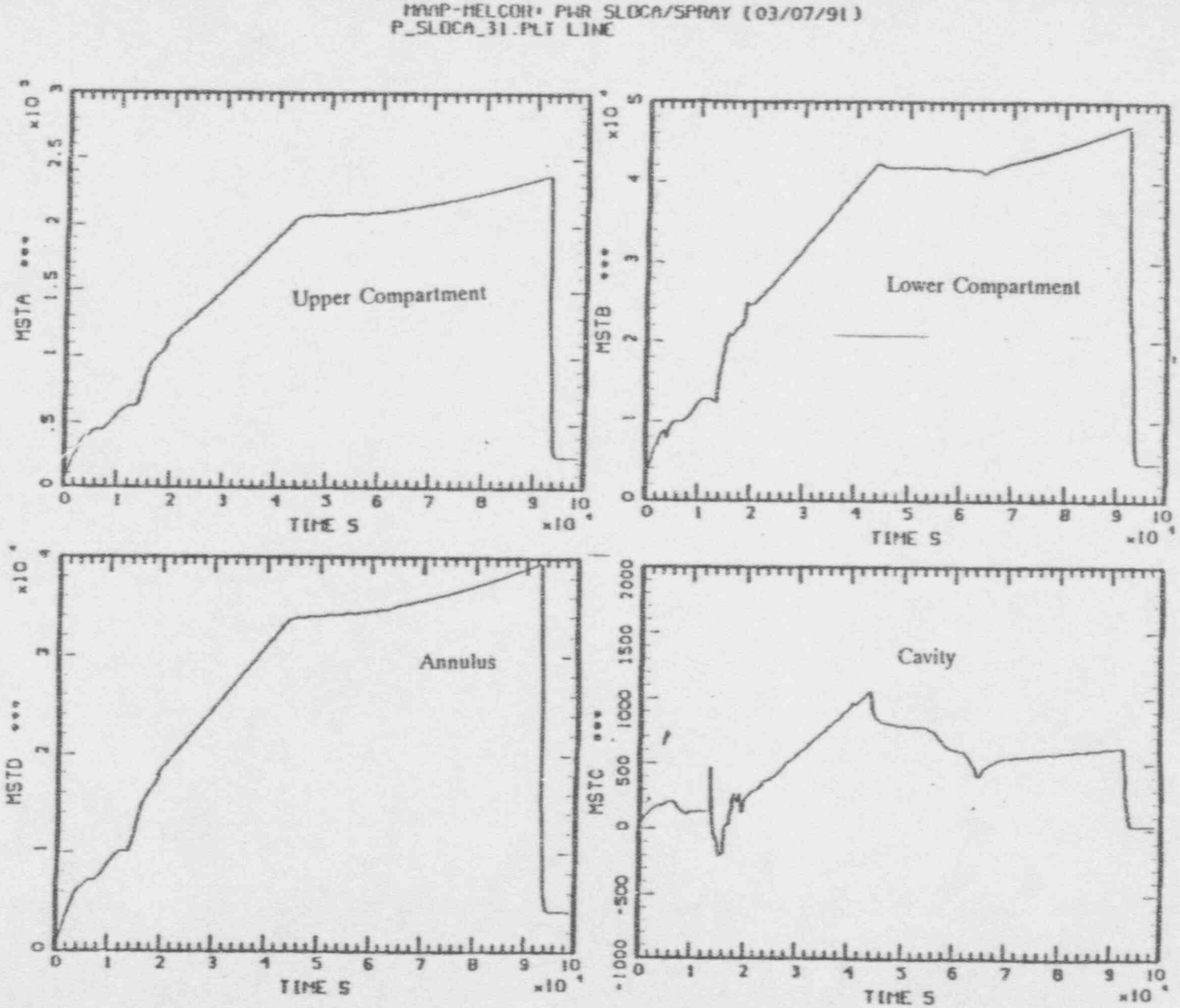

Figure C.54 MAAP Predicted Steam Mass in Containment

Table C.8 Comparison of Steam Mass Balance in Containment

	MAAP	MELCOR
Steam Content, Kg at the Time of Containment Failure		
Upper	240,000	250,000
Lower	47,000	56,000
Annulus	39,000	36,000
Cavity	600	0
TOTAL	326,600	342,000
Steam Sources, Kg (Released at Various Times During the Transient)		
Degassing	-	83,600
Break Flow	150,000	170,000
Corium/Concrete Interaction	170,000	-
TOTAL	320,000	253,600

Figure C.55 shows the fission products released in core. Major releases are the noble gases, CsOH, CsI, and Ba. The release of control rod materials and Te are relatively small. The release and deposition of the total radioactive materials, and the sum of radioactive and non-radioactive materials are shown in Figures C.56 and C.57, respectively. About 28% of all radioactive materials are deposited on heat structures.

Table C.9 summarizes the fractional distribution of radioactive materials in the core, the cavity (i.e. corium), the reactor coolant system, the reactor building (containment), and the environment. The distribution is given at 100,000 seconds, about 28 minutes after containment failure. Table C.9 shows that a large fraction of Ru, Mo, Ce, La, and U are retained in the corium in the reactor cavity region. The CsOH and CsI are mainly distributed in the reactor coolant system and containment. Revaporization could cause the portion in the reactor coolant system to be released to the containment later during the transient. A considerable fraction of the control rod material (Cd and Sn) also is retained in the reactor coolant system and containment.

MAAP only provided the fractional distribution for CsI and SrO; the comparisons are shown in Table C.10. For CsI, MAAP shows 53% and 45% retainment in the primary system and containment respectively, and MELCOR shows about 25% and 75% retainment in the primary system and containment. The environmental release of CSI predicted by MAAP is two orders of magnitude higher than that predicted by MELCOR. For SrO, MAAP shows that nearly all the materials are retained in the cavity, while MELCOR shows that a considerable fraction also is retained in the containment. The environmental release of SrO predicted by MAAP is one order of magnitude higher than that predicted by MELCOR.

Plots of the environmental release of the 12 groups of fission product are provided by MAAP as shown in Figure C.58. These releases are compared with the MELCOR predictions in Table C.11. For all materials, except the noble gases, the environmental release predicted by MAAP is much larger than MELCOR's predictions. MELCOR shows extremely small releases for Mo, Ce, La, and U groups. This extremely low release is partially related to the large quantities of water in the cavity as predicted by MELCOR. In the MAAP analysis, the interaction of corium-concrete starts after the cavity water has depleted. Another important factor which affects the environment release is the time of actuation of containment sprays. In MAAP, the containment sprays were activated 13 hours before the initiation of corium/concrete interaction. Therefore, it has no impact on aerosol removal. In MELCOR, the containment sprays were actuated about 1 hour after the initiation of corium/concrete interaction, and can effectively remove aerosols released from the corium pool in the cavity region.

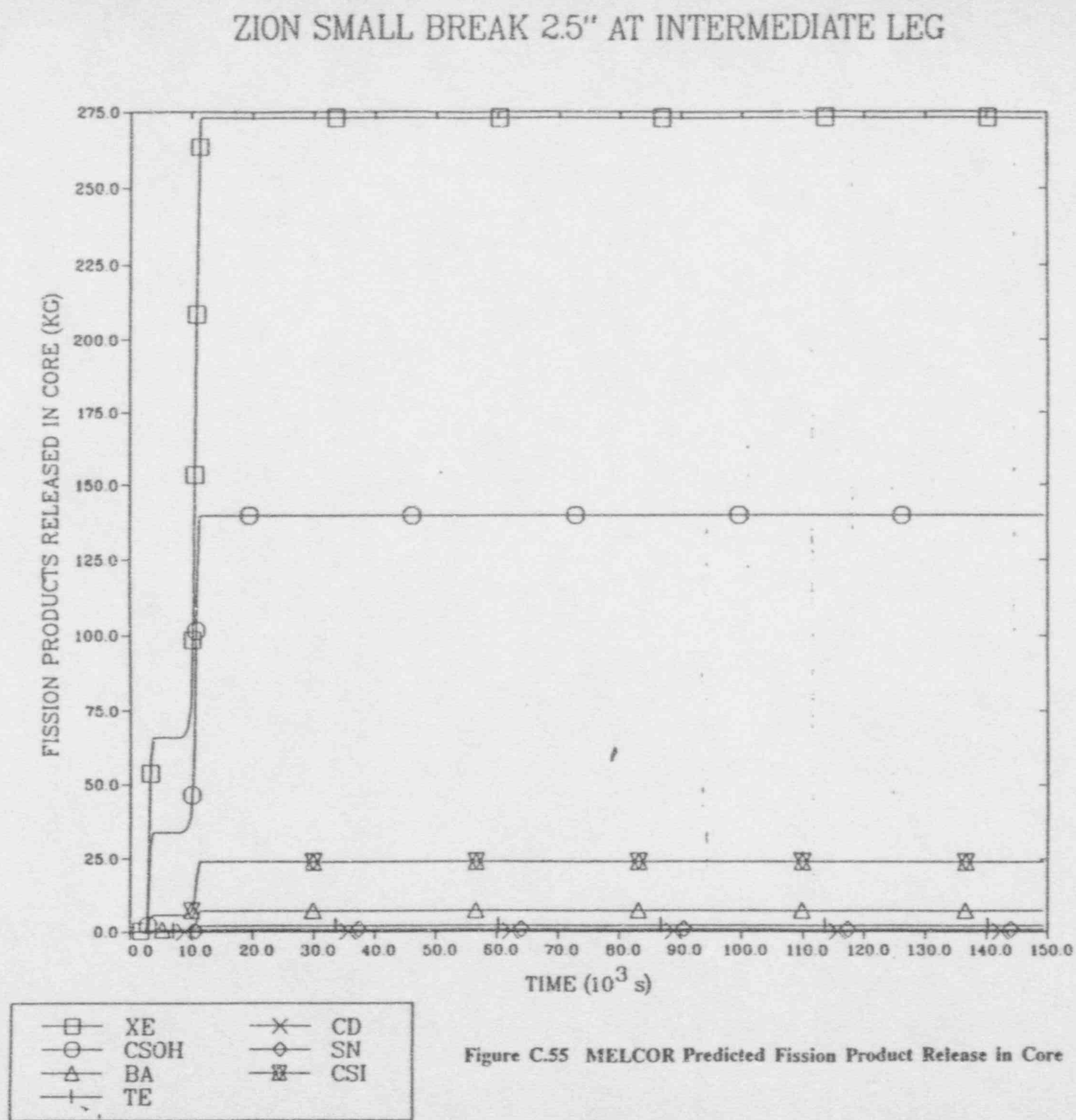

Figure C.55 MELCOR Predicted Fission Product Release in Core

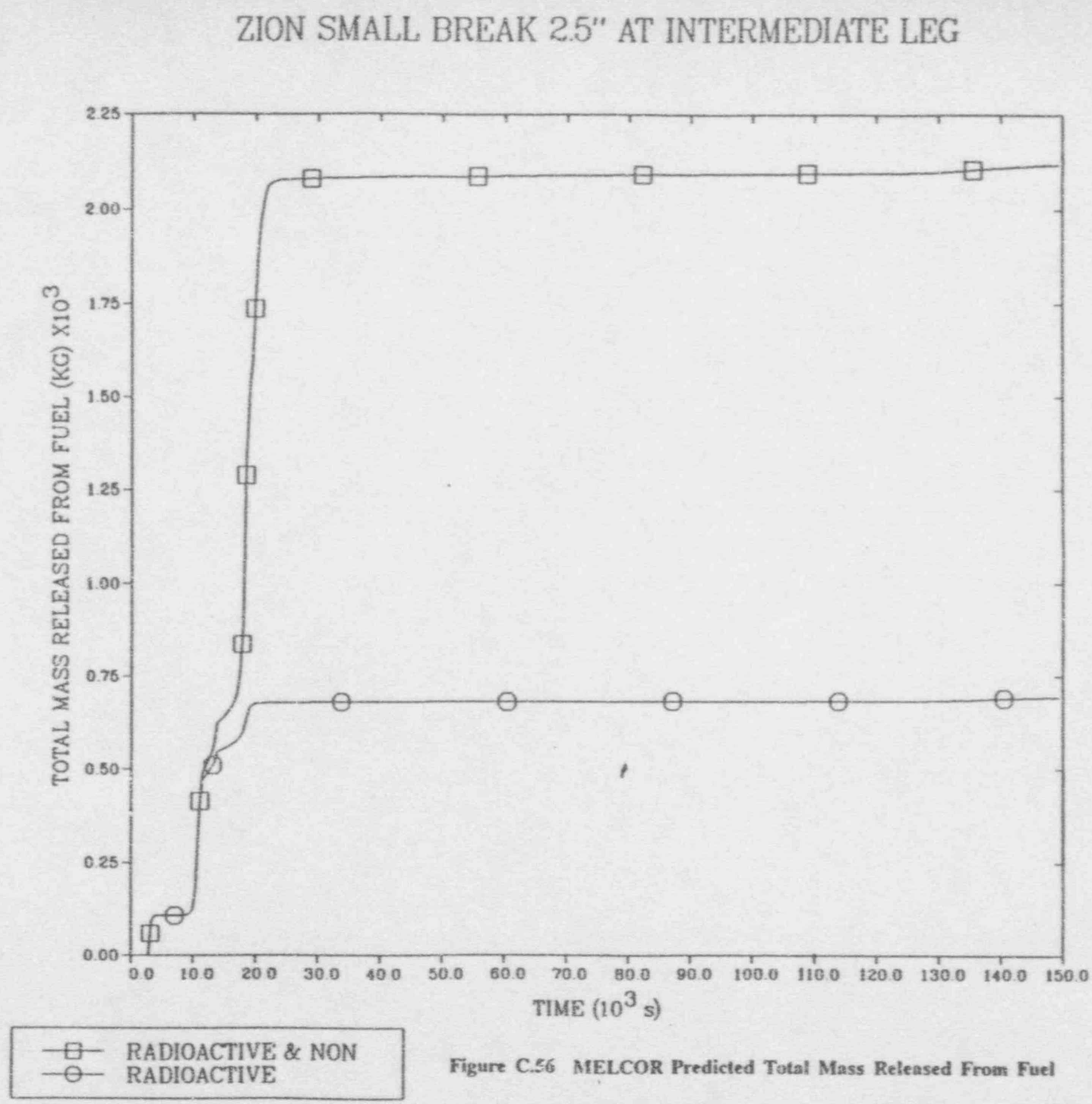

Figure C.56 MELCOR Predicted Total Mass Released From Fuel

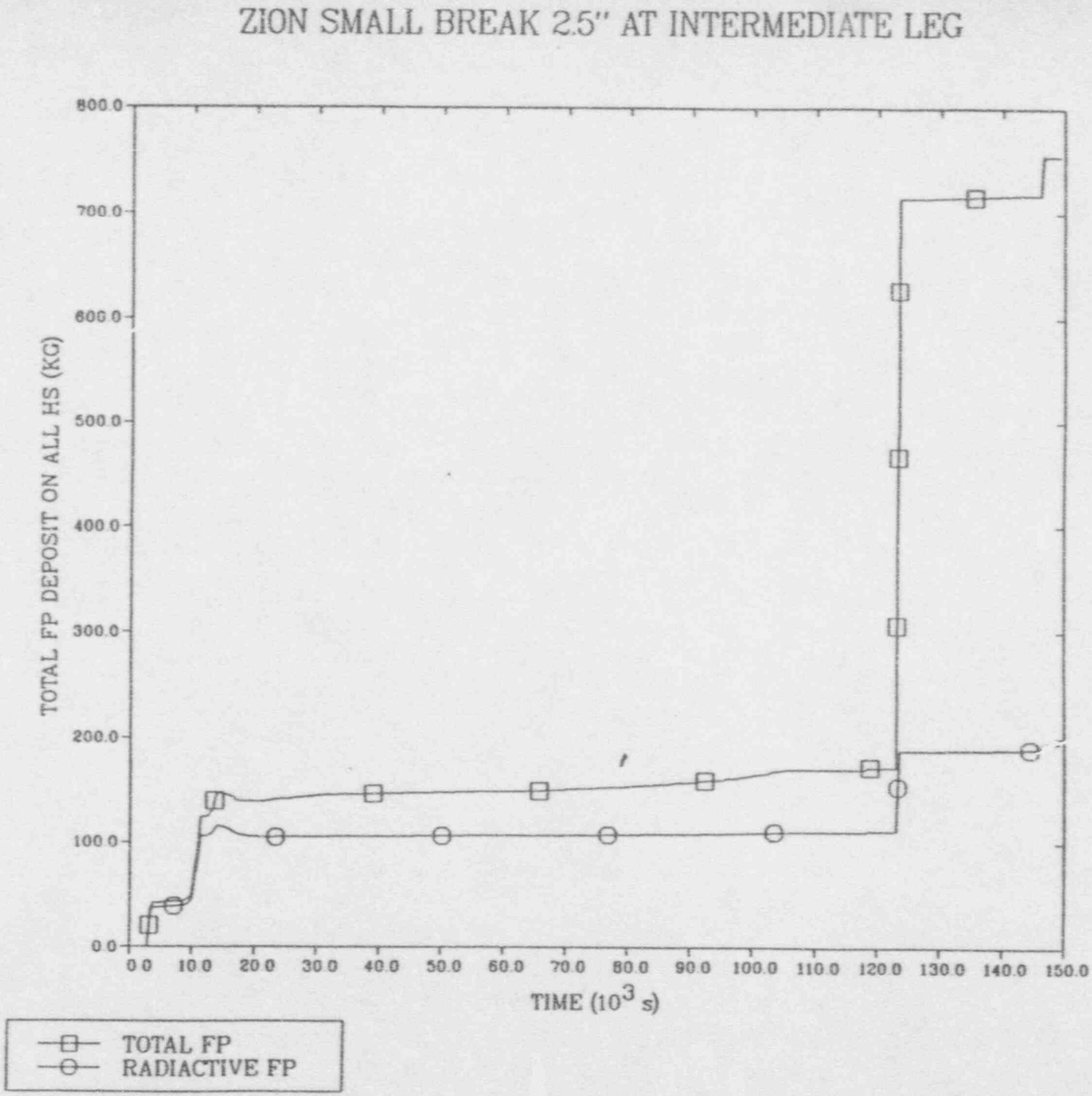

Figure C.57 MELCOR Predicted Total Mass Deposition on Heat Structures

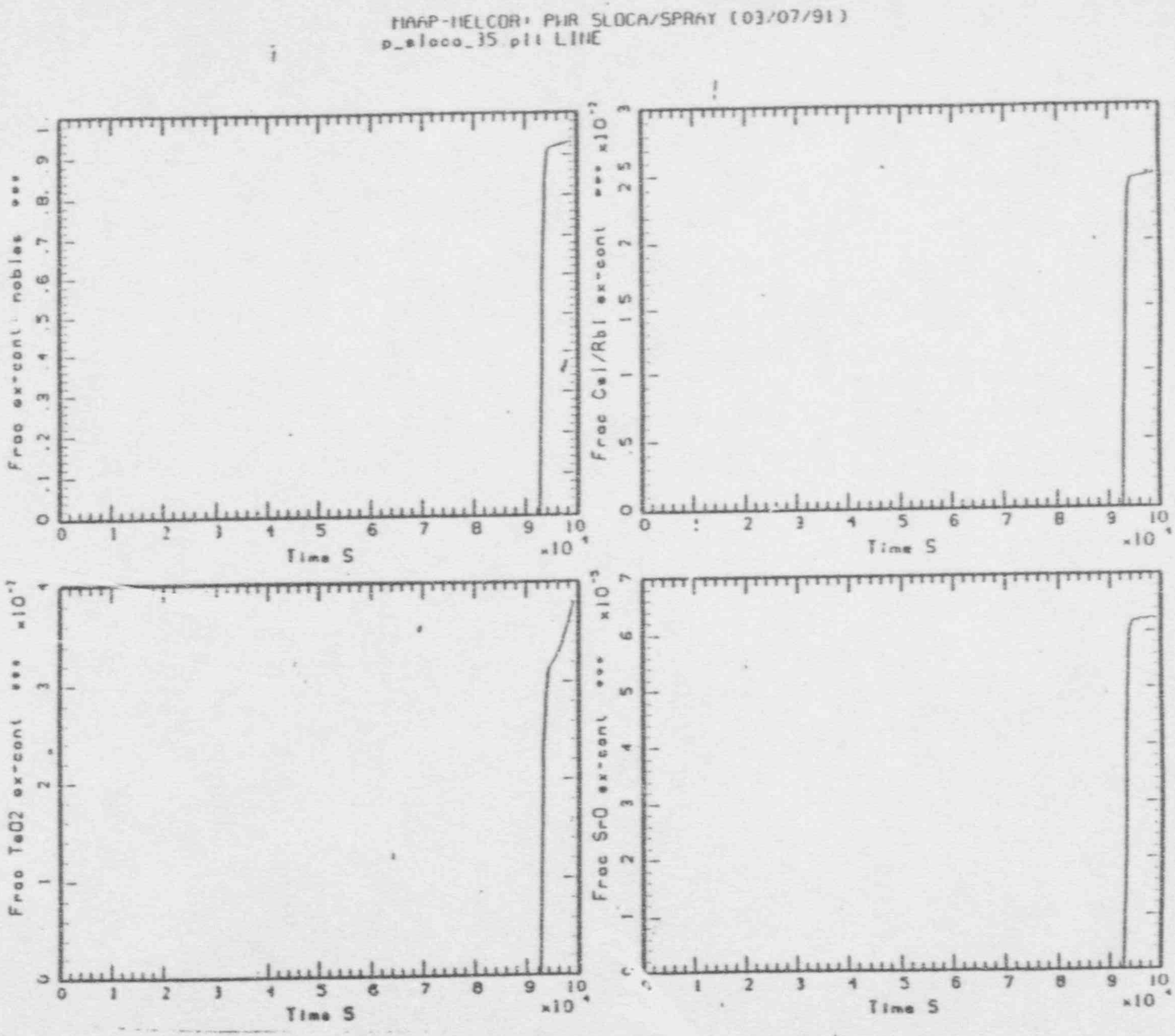

Figure C.58 MAAP Predicted Environmental Release

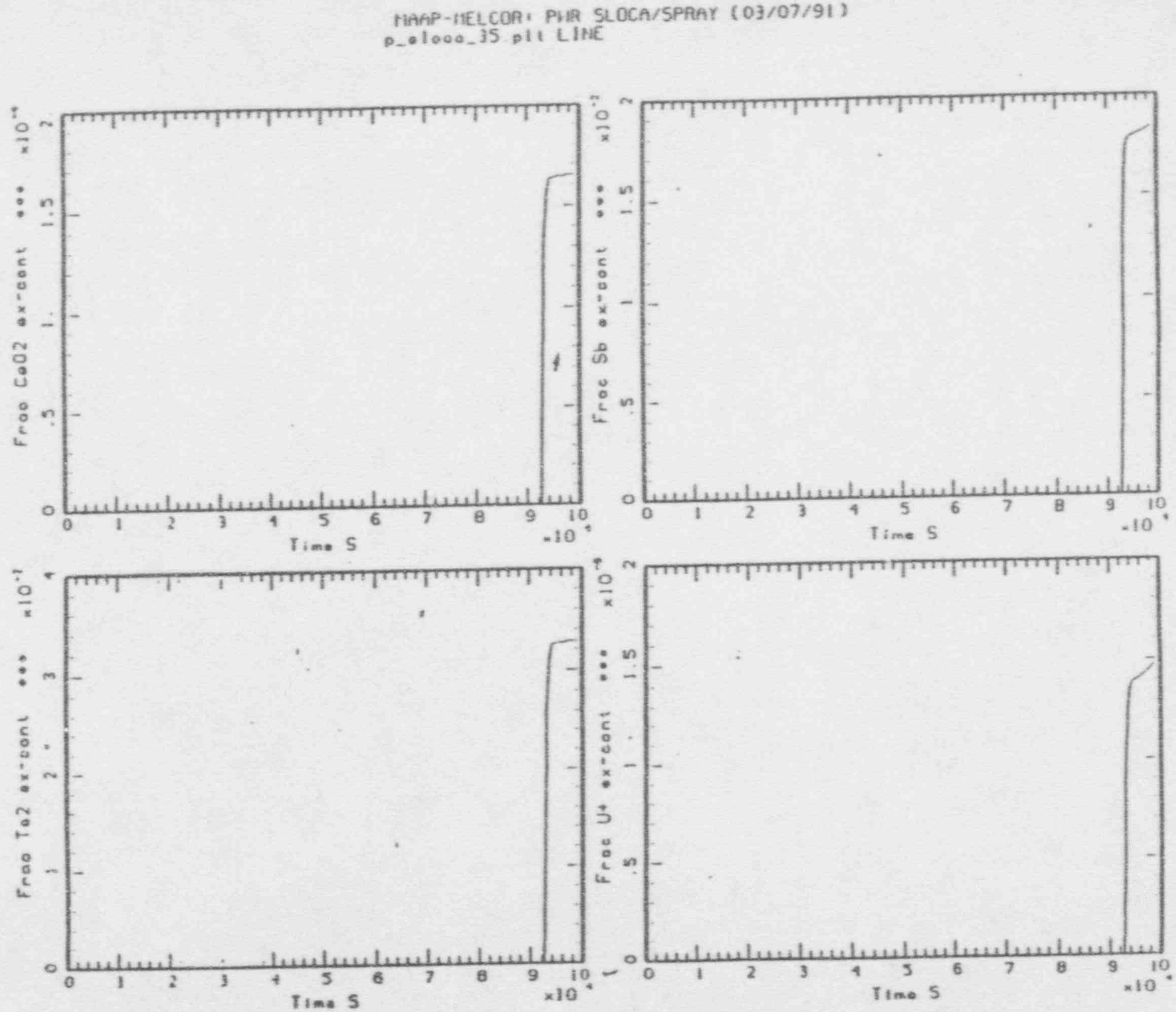

Figure C.58 MAAP Predicted Environmental Release (Continued)

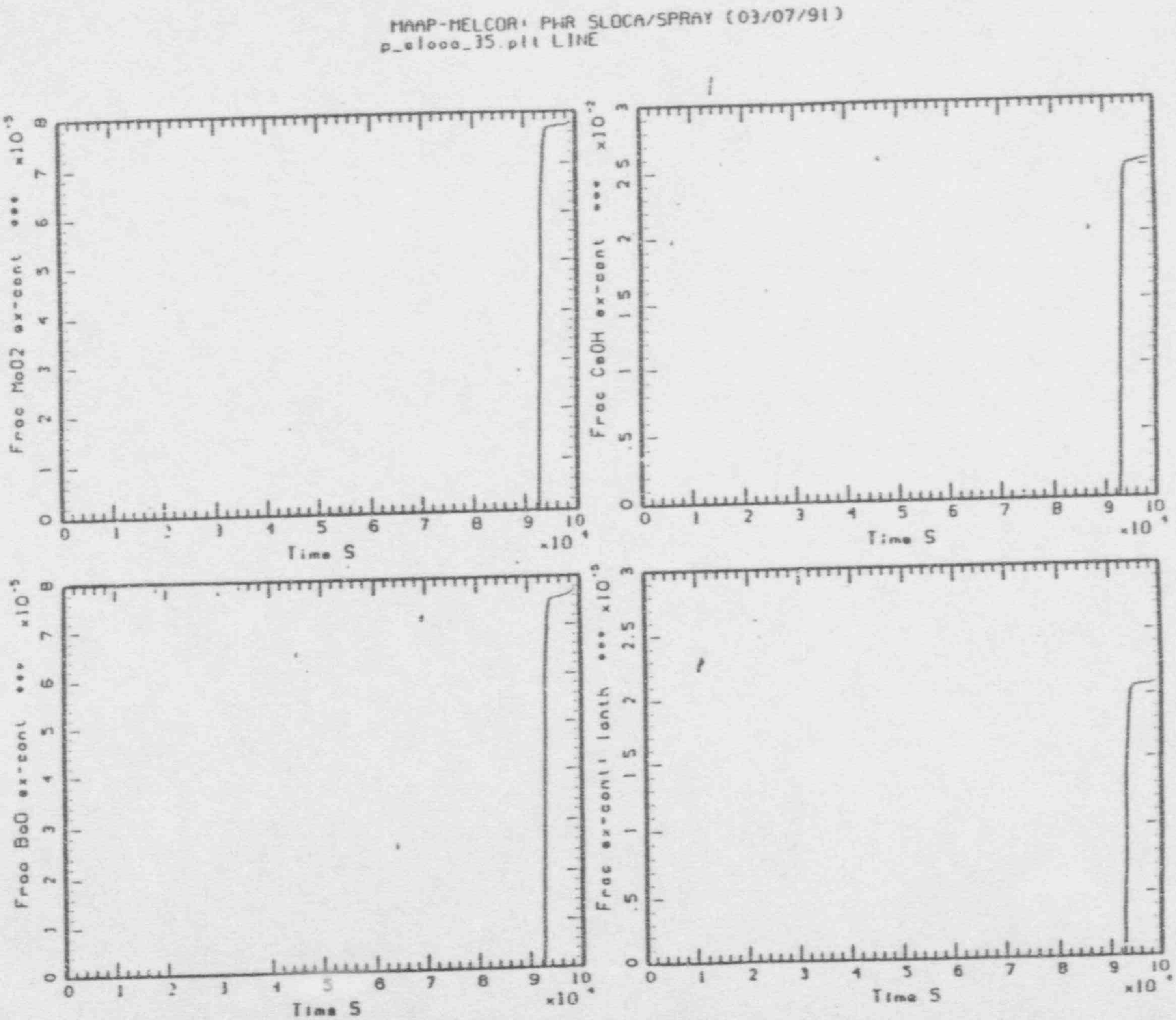

Figure C.58 MAAP Predicted Environmental Release (Continued)

Table C.9 MELCOR Predicted Fractional Distribution of Radioactive Materials

RADIOACTIVE RADIONUCLIDE FRACTIONAL DISTR

CLASS	CORE	CAVITY	RCS	RB	TB	ENVIRON
1	0.691E-19	0.000E+00	0.280E-03	0.359E-01	0.000E+00	0.964E+00
2	0.723E-19	0.767E-14	0.387E+00	0.613E+00	0.000E+00	0.238E-04
3	0.717E-19	0.609E+00	0.244E-01	0.367E+00	0.000E+00	0.100E-05
4	0.144E-15	0.000E+00	0.539E-05	0.355E-01	0.000E+00	0.964E+00
5	0.101E-18	0.380E+00	0.305E-01	0.589E+00	0.000E+00	0.140E-03
6	0.651E-19	0.997E+00	0.560E-03	0.212E-02	0.000E+00	0.169E-07
7	0.749E-19	0.913E+00	0.160E-01	0.705E-01	0.000E+00	0.587E-06
8	0.775E-19	0.100E+01	0.169E-04	0.722E-04	0.000E+00	0.903E-08
9	0.719E-19	0.993E+00	0.124E-03	0.650E-02	0.000E+00	0.797E-08
10	0.699E-19	0.100E+01	0.213E-04	0.109E-03	0.000E+00	0.817E-08
11	0.775E-19	0.739E+00	0.580E-01	0.203E+00	0.000E+00	6.259E-05
12	0.876E-19	0.707E+00	0.585E-01	0.234E+00	0.000E+00	0.124E-04
13	0.000E+00	0.000E+00	0.000E+00	0.000E+00	0.000E+00	0.000E+00
14	0.000E+00	0.000E+00	0.000E+00	0.000E+00	0.000E+00	0.000E+00
15	0.000E+00	0.000E+00	0.000E+00	0.000E+00	0.000E+00	0.000E+00
16	0.242E-26	0.353E-08	0.253E+00	0.746E+00	0.000E+00	0.126E-03

Note:

Class 1 = Xe, Kr	Class 9 = La
Class 2 = CsOH	Class 10 = U
Class 3 = Ba, Sr	Class 11 = Cd, Sb
Class 4 = I	Class 12 = Sn
Class 5 = Te	Class 13 = N/A
Class 6 = Ru	Class 14 = N/A
Class 7 = Mo	Class 15 = N/A
Class 8 = Ce	Class 16 = CsI

Table C.10 Comparison of Fractional Mass Distribution

	MELCOR	MAAP
CSI		
Core	0.0	0.0
Cavity	0.35(-8)*	0.69(-4)
Primary System	0.25	0.53
Containment	0.75	0.45
Environment	0.13(-3)	0.29(-1)
Sr/SrO		
Core	0.0	0.0
Cavity	0.61	0.987
Primary System	0.24(-1)	0.43(-2)
Containment	0.37	0.94(-2)
Environment	0.10(-5)	0.62(-4)

*0.35(08) = 0.35×10^{-8}

Table C.11 Comparison of Fractional Release to Environment

Class	MELCOR		MAAP	
1	Noble Gas	0.96	0.93	Noble Gas
2	CsOH	0.24(-4)	0.255(-1)	CsOH
3	Ba, Sr	0.10(-5)	0.62(-4) 0.78(-4)	SrO BaO
5	Te	0.14(-3)	0.38(-1) 0.33(-1)	TeO_2 Te_2
7	Mo	0.59(-6)	0.78(-4)	MoO_2
8	Ce	0.90(-8)	0.16(-3)	CeO_2
9	La	0.80(-8)	0.21(-4)	La
10	U	0.82(-8)	0.15(-5)	U
11	Sb, Cd	0.26(-5)	0.185(-1)	Sb
16	CsI	0.13(-3)	0.25(-1)	CsI/RbI

6 Summary

Detailed discussions of the analyses of MAAP and MELCOR's primary system thermohydraulics, fuel behavior, penetration failure, corium-concrete interaction, containment response, and fission product releases were presented. In analyzing MELCOR, we selected nodalization, numerical strategy, and many input parameters based on our best judgement. Although no systematic study of the code sensitivity was performed, we believe that the present analysis of MELCOR represents a reasonable description of the small break LOCA sequence for a PWR plant. The MAAP analysis was provided by Fauske & Associates, Inc. All 78 model parameters used in this analysis are recommended by the Sensitivity Study Guidance Document.

Although both codes have about the same nodalization and initial inventories, detailed comparisons show the following differences between the two codes:

1) MAAP predicts an early phase separation at about 1000 seconds and the break flow contains only single-phase fluid. The accumulator water is injected directly into the reactor vessel and is not released through the break. MELCOR predicts a single-phase flow or two-phase mixture through the beak, depending on the water level relative to the break location. The accumulator water injected into the broken leg is released through the break.
2) MAAP predicts a relatively slow, discrete, natural circulation in the primary system. MELCOR shows a continuous natural circulation in the primary system, with a higher flow-rate. Flow reversals also are predicted by MELCOR.
3) The single-node of the core plate in the MAAP analysis yields a late failure of the core plate, at about 13500 seconds. MELCOR has four radial nodes for the lower core plate and predicts a rapid failure of the core plate in each radial node as debris is relocated on the plate. Failure times for the various radial rings are from 10790 to 11423 seconds. Radial ring 1 is the inner ring and 4 the outer ring.
4) MAAP models one penetration while MELCOR has four penetrations. The failure of the four penetrations extends over of approximately 3750 seconds.
5) MAAP predicts the ejection of debris into the reactor cavity immediately after penetration failure. The sequence of ejection is corium, water, and gas. MELCOR predicts the ejection of debris over a time period of 137 minutes. Individual modelling packages exist in MELCOR for tracking corium, water, and gas.

6) MAAP shows the start of hydrogen generation at 3230 seconds, and about 340 kg of hydrogen is generated before the penetration failure. The onset of hydrogen generation predicted by MELCOR is at 2200 seconds, and about 260 kg is generated before the penetration failure.
7) MAAP shows another 240 kg of hydrogen generated after reactor vessel failure due to steam entering from the reactor cavity into the failed reactor vessel through the penetration hole. This is not modeled in MELCOR. The buoyance-driven flow model used in MAAP to describe this steam ingress has not been verified experimentally.
8) MELCOR shows a 1.3% oxidation of steel in the reactor vessel. MAAP does not model steel oxidation.
9) MAAP predicts a complete dryout of water in the reactor cavity. MELCOR does not predict water dryout in the cavity. Continuous water recirculation between the cavity and lower compartment is predicted by MELCOR.
10) In the MAAP analysis, the water boil-off completely quenches the corium in the cavity. In the MELCOR analysis, the corium temperature stays above the solidus temperature.
11) Since the corium is quenched, the concrete ablation predicted by MAAP is delayed until 55,000 seconds. The ablation distances, both radially and axially are 0.8 m. MELCOR shows an immediate erosion of concrete as the corium is discharged into the cavity. The ablation distances are 1.40 m axially and 0.27 m radially.
12) MAAP-predicted gas releases (H_2, CO, CO_2, and steam) from corium-concrete interaction are less than the MELCOR results. However, in the MAAP analysis, the complete boil-off of water in the reactor cavity adds a large quantity of steam to the containment atmosphere, which results in faster pressurization and an early failure of the containment.
13) Both MAAP and MELCOR show that the containment is steam-inerted, and hydrogen combustion is not predicted.
14) The MELCOR concrete degassing model contributes about 83,600 Kg of steam into the containment. Degassing is not modeled in MAAP unless concrete ablation temperatures are reached.
15) The containment pressurization rate predicted by MAAP is about 14 Pa/s during water boil-off, and is about 3.75 Pa/s after water dryout in the cavity region. MELCOR maintains a flooded cavity and the rate of containment pressurization is about 9.2 Pa/s.
16) MAAP shows a large retention of CsI in both the primary system (53%) and containment (45%); MELCOR shows about 25% retention in the primary system and 75% in the containment.
17) For all materials except the noble gases, the environmental release predicted by MAAP is much larger than the MELCOR predictions. This is due to the time of actuation of containment sprays. In MAAP, the containment spray is activated 13 hours before the initiation of corium-concrete interaction (see Table 5.1). Therefore, it has no impact on aerosol removal. In MELCOR, the containment spray is actuated about 1 hour after the initiation of corium-concrete interaction, and can effectively remove aerosols released from the corium pool in the cavity region.

Table C.12 summarizes the timing of major events and shows that MELCOR's predictions are characterized by earlier core uncovery, core dryout, fuel relocation, and penetration failure. On the other hand, MELCOR predicted the time of containment failure at 104,496 seconds, about 3.2 hours later than that predicted by MAAP at 92,718 seconds.

Table C.12 Summary of Major Events (Time in Seconds)

	MELCOR	MAAP
Start of Break	0.0	0.0
Core Uncovery	1640	2,349
In-Core 1 Kg H_2 Release	2,200	3,230
First Clad Failure	2,655 - 2,855	3,268
Fuel Melting	2,825	3,779
Start of Fuel Relocation	2,655	5,250
Core Dryout	3,230/8,585	12,953
Accumulator On	3,362	3,671
Relocation to Lower Plenum	10,790 - 11,423	13,527
Penetration Failure	11,378 - 15,126	13,587
CCI Production of 1 Kg CO	11,540	54,870
Containment Sprays On	15,200	7,321
Containment Failure	104,496	92,718

7 Reference

1. Kenton, M.A., and J.R. Gabor, "Recommended Sensitivity Analysis for an Individual Plant Examination Using MAAP 3.0B," Gabor, Kenton & Association, Inc.

Appendix D

BWR MELCOR/MAAP Comparative Analysis

J.U. Valente, L. Neymotin

Table of Contents

1 Introduction

The objective of this study is to determine the suitability of using the MAAP 3.0B Rev 7 (BWR), severe accident computer code for Individual Plant Evaluation (IPE). The task discussed in this appendix involves the predictions of both MAAP and MELCOR 1.8.0 for a Station Blackout with battery failure initiated at 100% rated power conditions. The plant chosen was a BWR 4 with a Mark I containment.

Previous work on this project reviewed the documentation on models used in MAAP and compared it to that of MELCOR [1]. The results of the numerical experiments reported in this appendix use insights from this previous work. To fulfill this project's objective, we compare MELCOR and MAAP's basic modelling assumptions, such as the physical nature of corium.

To assure that differences in predictions are not due to differences in representation of the plant's configuration, the input decks of both codes were reviewed for consistency. This configuration, as well as the phenomenological modelling options used in each code, are discussed in Section 3. Section 2 describes the accident sequence being studied, and the significant figures of merit (such as time to containment failure, etc.). Section 4 contains the results and analyses obtained with both MAAP and MELCOR, and Section 5 presents our conclusions and recommendations.

For documentation purposes, Attachments A and B contain the input decks used in BNL's study for MAAP and MELCOR. The MAAP input deck was supplied by FAI and reviewed by BNL.

2 Description of Accident Sequence

We chose a Station Blackout where the batteries are lost at time zero along with AC power as the accident scenario. Before this accident initiation, the plant had been operating at full power. The loss of AC would result in closure of the Main Steam Isolation Valves (MSIV), and the loss of feedwater flow quickly thereafter. All pumps driven by AC power are lost, and with the loss of DC power, all motorized valve control for the steam driven HPCI and RCIC also is unavailable. No inventory makeup results in boil-off of the reactor vessel through the safety relief valves (SRVs), with the vessel isolated, the core shutdown, and the containment sealed. No operator intervention is assumed, and the vessel will remain pressurized until its failure. This condition could result in Direct Containment Heating (DCH); however, DCH is not modelled by either computer code. MAAP allows entrainment of molten debris in the pedestal region to the drywell by the high velocity water/gas jet exiting the RPV. This will be discussed in subsequent sections.

Once boil-off begins, a key parameter is the beginning of core uncovery. Once this occurs, fuel heatup will begin and will be accelerated by clad oxidation. We have, as a significant figure of merit (SFM), the time when the codes predict that more than 1 kg of H_2 has been produced. The release of fission products will occur when the temperature for clad damage is reached. However, MELCOR will then release its fuel-clad gap inventory, while MAAP will begin to release fission product gases from the pellet. Failure criteria used by the codes are given in Table D.1. The first relocation of core material will occur in MAAP when the control blade reaches a eutectic temperature of 1500K, while MELCOR uses the stainless steel melting temperature of 1700K. Fuel relocation begins when the MAAP code predicts a core node reaching a 2500K eutectic temperature. In MELCOR, two criteria are employed; either the clad reaches 2500K or its thickness becomes less than 10^{-6}m. As shown in the following sections, the time of relocation is very important, especially for MELCOR, because it can predict relocation to occur when water is still above the lower core support plate. Further, MELCOR can predict solid debris relocation. This means that at the time of clad failure, the UO_2 debris can fall to the core support plate. The version of MELCOR used in this study is 1.8.0 CZ, with an additional correction for UO_2 mass relocation from the vessel to the cavity. There is an error in this version, which we discovered, but left uncorrected, which affects solid debris relocations. With a high intact component porosity chosen for the core fuel cells, no solid debris is expected to be transported past intact fuel cells. However, in the MELCOR run of record, this is not the case, and as much as 10 tons have been relocated to the core support plate level in the inner two rings, with most of the solid debris being held about 5 ft. above this.

Table D.1 Failure Criteria

Failure Mode	Limit	
	MAAP	MELCOR
Clad damage	1200K	1173K
Core Support Plate Failure	Lowest core node fully molten at 2500K	Plate at 1273K
C. Blade Relocation	1500K	SS melt 1700K
Fuel relocation	2500K	Zr reaches 2500K or Zr clad thickness < 10^{-6} m
RPV penetration failure	carbon steel melt temp ≥ 1700K (FREEZE)*	1273K
RPV lower head failure	----	1273K outer node
Concrete Ablation Temp	1500K	1500
Containment Failure	temperature dependent pressure failure limits	temperature dependent pressure failure limits

*(FREEZE) notation refers to a subroutine or module.

Also, the code incorrectly relocates all solid debris in a given ring to below the core support plate once this structure has failed. This relocation occurs regardless of whether or not the debris is supported by the core support plate. Then, depending on the quantity of water there, it is possible to quench this initial debris and delay the failure of the core support plate. Relocation also affects the surface area available for hydrogen generation.

Melt progression has been highlighted as a major difference between these two codes [1], and it manifests itself strongly in the time to core support plate failure, the mass of corium which falls into the lower plenum when the plate fails, and the time to vessel failure. These will be discussed further in Section 4. It should be remembered that in MAAP all molten debris, above the lower core support plate is relocated to the lower plenum when the support plate fails. In MELCOR, the lower plenum is relocated on a radial ring by ring basis. The amount of mass first transported to the lower plenum then is different, and this difference will have a long-term effect on the release of corium from the vessel. Once the lower tie plate fails, all molten debris is transported to the lower plenum in MAAP, but not in MELCOR. In effect, this raises the amount of mass that drops into the lower plenum. If the mass is large enough, it would be able to transform all the lower plenum water to steam based on the heat capacitance of the corium, provided it stayed in the lower plenum long enough before vessel failure. While the former condition is true for MAAP, the latter is not and the vessel fails containing a large amount of lower plenum water. Conversely, MELCOR will drop only a relatively small amount of debris into the lower plenum. If small, it could result in steam cooling of the material remaining in the core. This cooling could substantially delay the time to vessel failure.

Once the vessel has failed, the ejection of the material is characterized by its sequence, amount, temperature, composition, physical state, and timing. These factors are a major difference between MAAP and MELCOR and will set the stage for their predictions of containment failure time. The amount of non-condensibles ejected from the vessel, as well as the amount produced during CCI will strongly affect this time. Due to the different physical state of the ejected corium (amount of solid and molten debris) and the sequence of ejection, the debris in MAAP will spread over a much larger concrete surface area. With MELCOR, there will be a substantial delay from the time of vessel failure to the ejection of debris due to the debris' non-molten state. With MELCOR a very large fraction of solid debris is ejected. Debris in MELCOR would have undergone a substantial cooling in the lower plenum, while with MAAP the vessel will fail with a large amount of lower plenum water remaining.

MAAP and MELCOR may give very different predictions of containment pressure and temperature histograms. In Appendix B [1], we discussed that the models for CCI are very different for the two codes. Because CCI is a function of concrete heating, the corium spread models of MAAP and MELCOR will influence the competition of the atmosphere above the debris and the concrete below it for the debris heat energy. Still we can assume that there will be some height of debris above the concrete, where the heat transfer coefficients out of the debris will be limiting the energy released to the atmosphere. Even if the mass, area, composition, and debris temperature were the same for MAAP and MELCOR, the fact that MAAP modeling does not allow the H_2O and CO_2 from the sidewalls of the concrete being attacked from interacting with the corium should result in a lower amount of H_2 released, and most likely, a greater amount of CO_2 than that calculated with MELCOR. There is a greater amount of CO_2 than H_2O in the concrete. Although the containment is assumed to be inerted in our study, the H_2 can undergo burning when it is released to the reactor building, which is rich in oxygen. The heat slabs modelled will have a major effect on the containment response, and we spent extra effort to assure that the heat slabs are correctly represented in the input of the two codes.

Both non-condensible mass and heat added to the gas will increase pressure. Containment failure pressure is temperature-dependent. This factor is accounted for in both code predictions of containment failure. We did not determine the failure criteria for electrical or hot and cold mechanical penetrations.

For fission products, we looked at the differences in the release timing from the fuel. Also, the decontamination factor associated with the various volumes will play a major role. We spent extra effort in matching deposition areas of MAAP and MELCOR because sedimentation is the primary mechanism for aerosol removal.

3 Model Description

3.1 Approach to Setting up the Comparative Input Decks

The starting point consisted of existing MAAP and MELCOR decks representing Peach Bottom, which is a BWR/4 with a steel Mark I containment. A concerted effort was made to assure that plant features were fairly represented in the two input decks. We then adjusted the MAAP input deck to reflect that of the MELCOR deck. If questions arose regarding the MELCOR value, it was examined and an acceptable value was chosen. This resolution process worked well for plant configuration items such as masses and geometric arrangements. A different approach was used for the unique modelling options used in the two codes. These include items such as the number of core cells, or the MAAP options used for core blockage of steam flow. MELCOR also required a choice of modelling options to be made. Among the more important was whether to permit intact fuel within a given radial core ring to relocate once the core support plate failed. Another option determined what was ejected from the vessel at the time of breach.

Therefore, the compatibility of the input decks was determined using the following three steps. (Examples of the first two are given above.)

1) Match of plant configurational inputs.
2) Choices of the model parameters: In MAAP, this meant following the recommendation of the user's guidance documents [3,4]. In MELCOR, this meant using the deck as received and reviewed by the BNL team.

3) Changes to the recommended model parameters. The number of changes were small. In MELCOR, an additional containment failure mode based on the temperature of the containment drywell liner was added. In MAAP, a similar temperature-dependent containment failure mode was employed.

All changes in MELCOR's deck for this study are commented on with dates from 10/90-4/91. The choice of input parameters in MAAP are commented on to the extent their value was based on a MELCOR value. Listings of the input decks are in Appendices A and B.

3.2 Core Modelling

3.2.1 MAAP Core Modelling

The core is divided into 5 rings and 10 axial segments. In addition, there is an unheated fuel length at the top of the core of .33 meters. The total height of the fuel region is 3.81 m. Each core node or cell contains fuel pellets, clad, Zr channel, and control blade. (The blades are idealized to 150".) The total internal masses of the core region are given in Table D.2.

Table D.2 Core Masses

Active Fuel Cells	MAAP 5 Radial x 10 Axial	MELCOR 3 Radial x 5 Axial
UO_2 (kg)	1.685×10^5	1.685×10^5
Zr (kg)	7.1×10^4	7.1×10^4
Stainless Steel (SS) (kg)	9.68×10^3	1.2×10^4
B_4C (kg)	1.79×10^3	1.79×10^3

3.2.2 MELCOR Core Modelling

MELCOR's core is part of a grid structure of cells, which extends from the vessel lower head to the unheated portion of the fuel rods (fuel gas plenum region). The axial number of cells is 12, of which axial cells 1 to 5 are in the vessel lower plenum; cell 6 is the core support plate; and cells 7 to 11 are UO_2 containing fuel nodes. Cell 12 does not contain fuel. In addition, there are 3 radial rings, so the total number of core cells is (12 - 6) x 3 = 18.

Fifteen of these bear fuel. Unlike MAAP's core model, MELCOR is modelled for this study with different masses UO_2 and other core material based on cell location. All fuel containing core cells are .7620m in length. The fuel gas plenum is .3627m (CORZ1201). The mass content of a center ring fuel cell is 14995 kg of UO_2, 3153 kg of

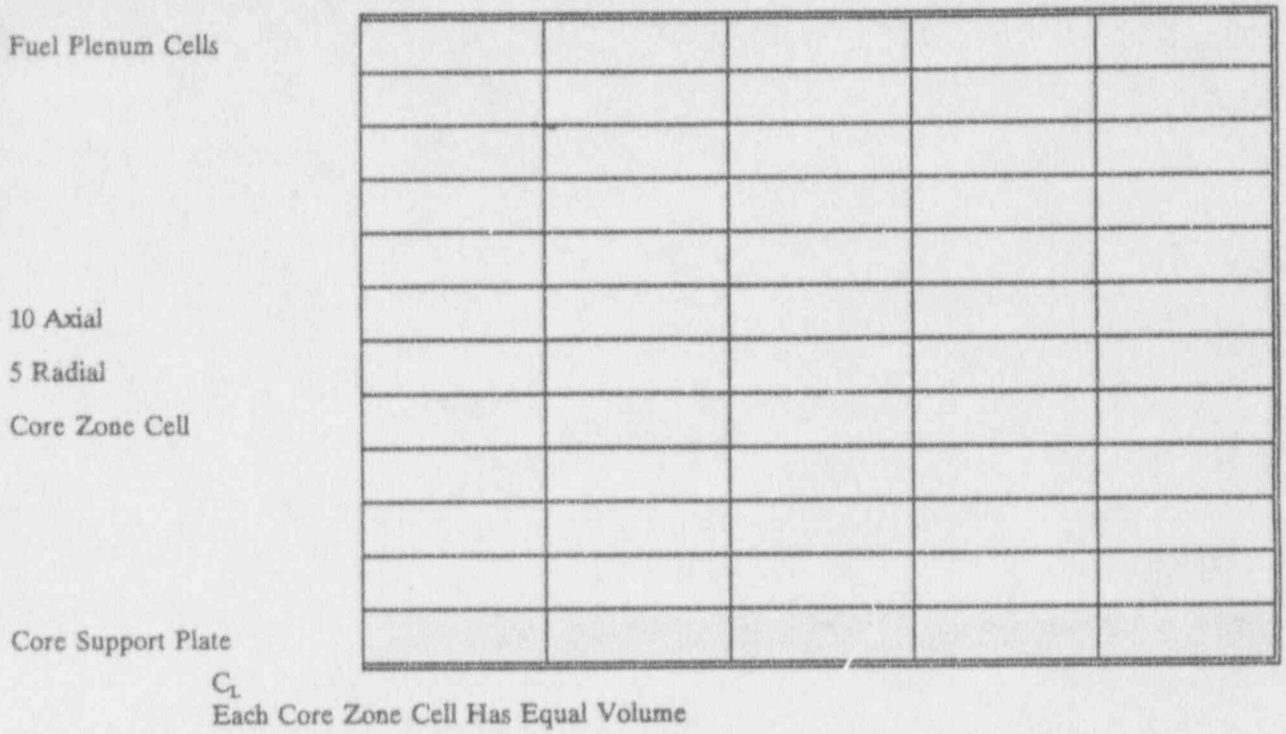

Figure D.1 MAAP Core Grid

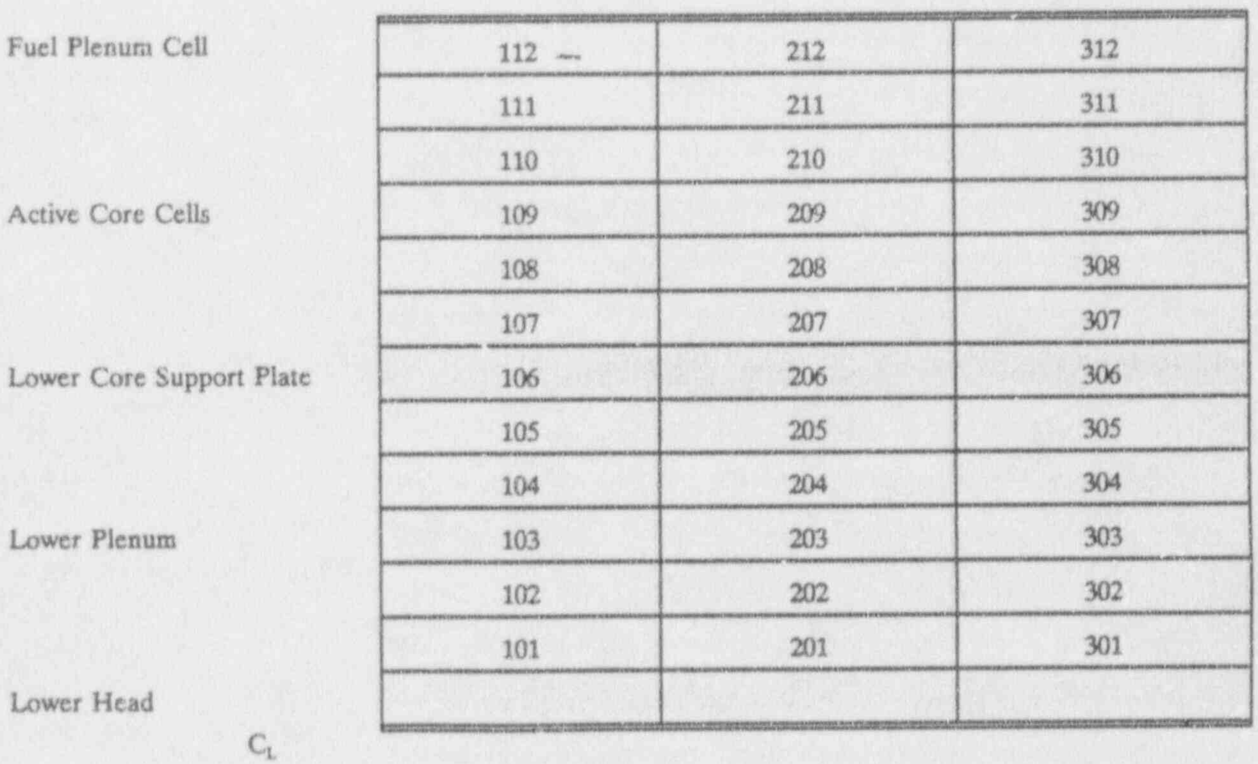

Figure D.2 MELCOR Core Grid Structure

clad Zr, 1077 kg of control blade SS, 158.9 kg of B_4C, and 2339 kg of Zr channel material. Summing over all 15 fueled core cells yields the values supplied in Table D.2.

Table D.2 shows the good agreement between the two input decks. The mass of stainless steel (SS) posed some unique problems. In MAAP, when relocation occurs, only the SS represented in the core region and the lower core support plate will be ejected from the vessel. In MELCOR, the SS in the upper and lower fuel tie plate, the core support plate, and the control rod guide tubes can be ejected. As shown in Table D.3, there is a substantial difference in the amount of SS which the two codes may relocate to the pedestal region. In addition, there are 75 tons of lower head material; some of which is ablated and relocated to the pedestal.

Table D.3 Relocatable Steel Masses

	MAAP (kg)	MELCOR (kg)
Active Fuel Cell	9.68×10^3	1.2×10^4
Upper Fuel Tie Plate and Top Guide	N/A	2.4×10^4
Lower Fuel Tie Plate and Core Support Plate	2.4×10^4	1.5×10^4
CRD Tubes	N/A	2.1×10^4
Total	3.368×10^4	7.2×10^4

3.3 Initial RPV Inventory and Control Volume

The values of the RPV Inventory and Control Volume for MELCOR and MAAP were matched. MELCOR has some unique problems associated with attaining a stable 100% power configuration. A stable case with approximately 259,000 kg of water (liquid and vapor) was used, and duplicated in the MAAP code.

Figures D.3 and D.4 show the arrangement of the RPV control volume. MAAP uses eight volumes, while MELCOR was configured with six. MAAP uses separate volumes for the upper and lower downcomers, as well as the recirculation loop. MELCOR combines these into a single volume and uses a volume vs. elevation table to account for the geometry.

As indicated in Table D.4, the distribution of the RPV volumes was modelled fairly closely. One difference is in the standpipe and separator region, but since MELCOR and MAAP match initial water (liquid and gas) inventory,

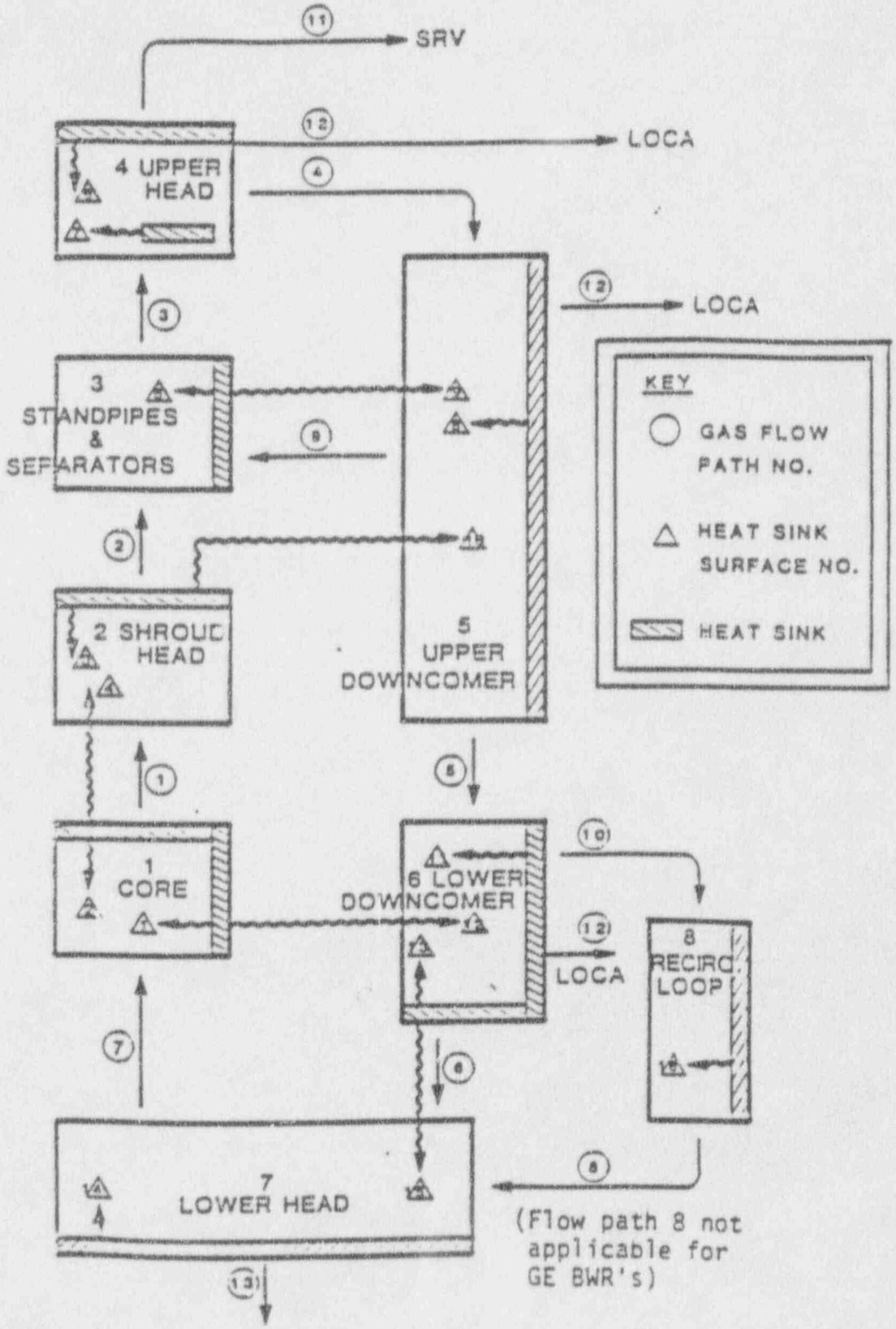

Figure D.3 MAAP RPV Control Volume and Heat Slab Locations

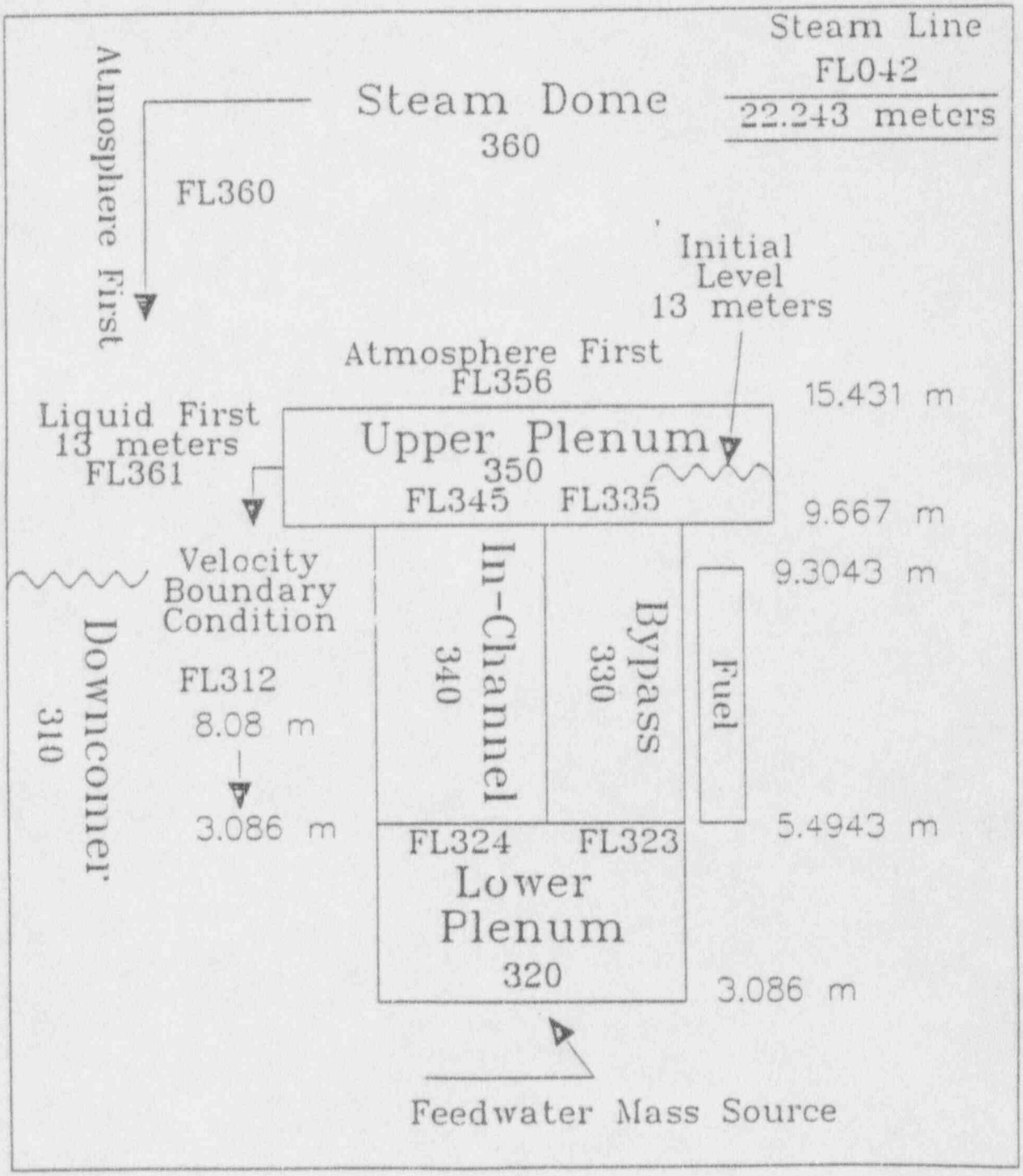

Figure D.4 MELCOR RPV Control Volume Locations this should only result in a small difference in the initial liquid RPV inventory. The biggest discrepancy lies in the location of liquid water above and below the top of active fuel (TAF). This discrepancy will be discussed at length in Section 4.1.

Table D.4 RPV Values

Volume Description	MAAP (m^3)	MELCOR (m^3)
Core	33.3	33.3 m^3
Upper Plenum	27.3	44.9
Standpipes and Separators	44.9	
Steam Dome	217	218.6
Upper Downcomer	141	183.8 Amt below jet pumps = 41
Lower Downcomer	41	
Lower Plenum	115	103.5
Recirc Loop	4.6	Included in downcomers

3.4 RPV Heat Slabs

The heat sinks employed by MAAP for the reactor pressure vessel and its internals can be found in the Primary System's input block of the parameter file. For MELCOR, this data can be found in the heat structure card images designated "HS". Table D.5 breaks down these slabs and their masses. Figure D.3 gives the location of these slabs in MAAP.

Nearly all of the differences in the mass of the heat slabs are due to the difference in the lower head mass. In MELCOR, a value of 7.5×10^4 kg was used for the heat-up and failure of this component, but not in the heat slab input description (see Table D.5).

3.5 Containment Configuration and Initial Conditions

Both MAAP and MELCOR were modelled using a three control volume containment. Figure D.5 is a drawing of a Mark I steel containment. In MAAP, the drywell, wetwell, and pedestal cavity are modelled as separate control volumes. In MELCOR, besides a drywell and wetwell, the downcomers connecting these two regions are a separate control volume. During corium ejection, the receiving volume is the pedestal cavity in MAAP, and the drywell in MELCOR. However, in MELCOR, the CORCON model is used, and this essentially places a core

Table D.5 RPV Heat Slabs

Item Description	Number	MAAP mass (kg)	MELCOR mass (kg)
Shroud	1	1.6×10^4	2.68×10^4
Shroud Head	2	2.0×10^4	
Standpipes and Separators	3	5.0×10^4	
Upper Head	4	5.2×10^4	5.3×10^4
Upper Downcomer	5	2.38×10^5	
Lower Downcomer	6	1.59×10^5	
Lower Head	7	7.5×10^4	3.2×10^4
Recirc Loop	8	2×10^4	
Shroud Support	9	2×10^4	
RPV Cylinder	10		4.0×10^5
Separator and Shroud Head	11		6.96×10^4
Dryers	12	4.27×10^4	4.27×10^4
Shroud Lower Plenum Extension	13		1.5×10^4
Total		6.9×10^5	6.4×10^5

catcher in the drywell thermal-hydraulic control volume. In Table D.6, we note that the total free volume is maintained. For comparison, the MAAP drywell and pedestal volumes were set equal to MELCOR's drywell and downcomer volumes. Very little of MELCOR's downcomer volume is occupied by liquid. Table D.6 also compares the heat slab masses used in MAAP and MELCOR. Figure D.6 and D.7 give a schematic of the heat slab locations used in MAAP and MELCOR.

We note that the agreement is very good for the heat slabs (Table D.6). One difference is in the way heat loss from the RPV vessel to the drywell is handled. In MAAP, one supplies a heat loss from the vessel at time zero (for our case 1 MW), while MELCOR uses the RPV surface area and a heat transfer coefficient supplied by the user (in our case h = 6.62 W/m^2, so the initial heat loss is also ≈ .66 MW). However, MELCOR's RPV mass also is available for dynamic effects as the accident progresses. This may involve slightly greater heat transfer to the drywell during the heat-up and relocation of fuel. Based on a conversation with Fauske and Associates, Inc., input parameter "QCO" (the 1 MW value) is used to get a heat transfer coefficient between the vessel and drywell, and hence, the two codes are in fair agreement.

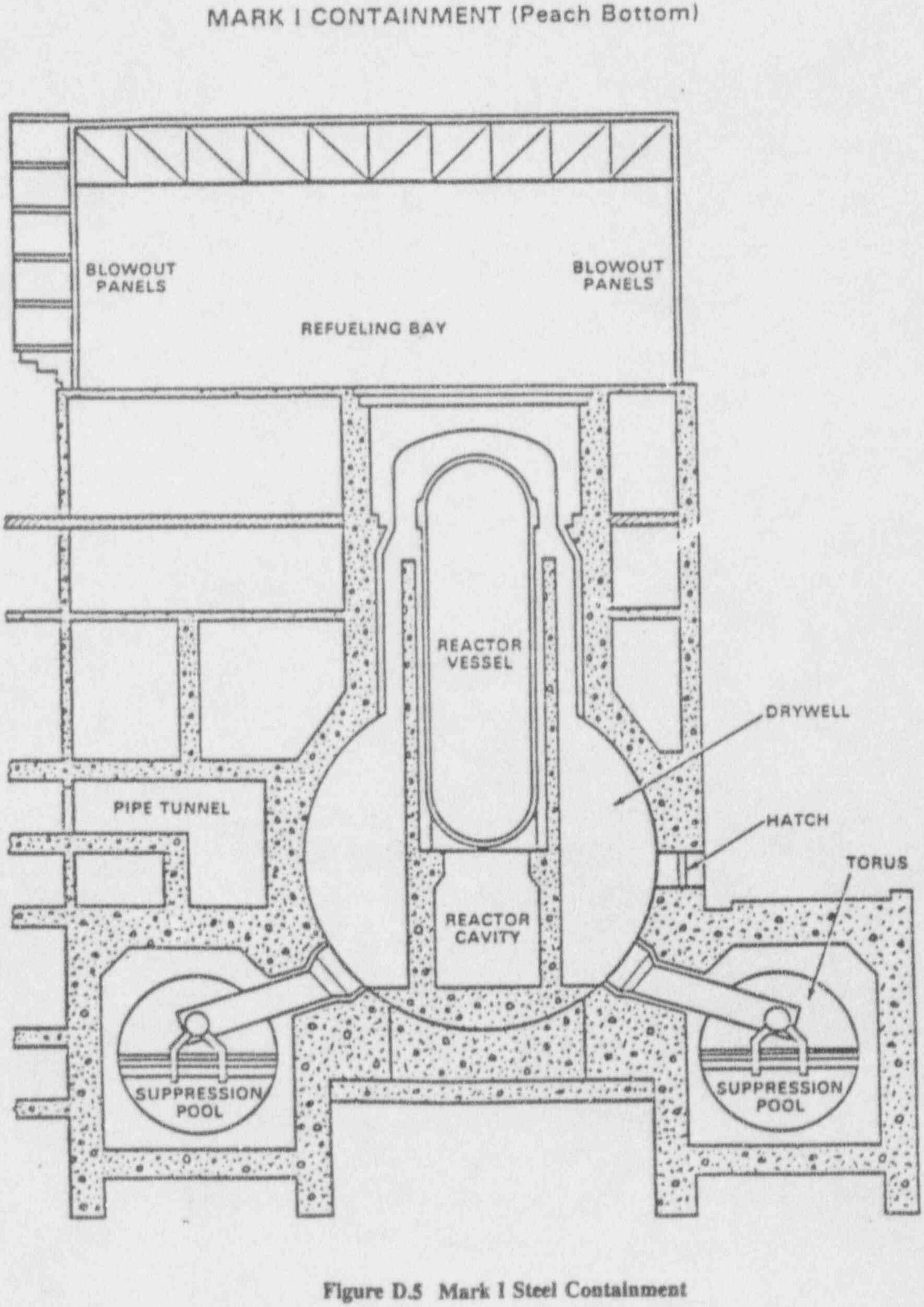

Figure D.5 Mark I Steel Containment

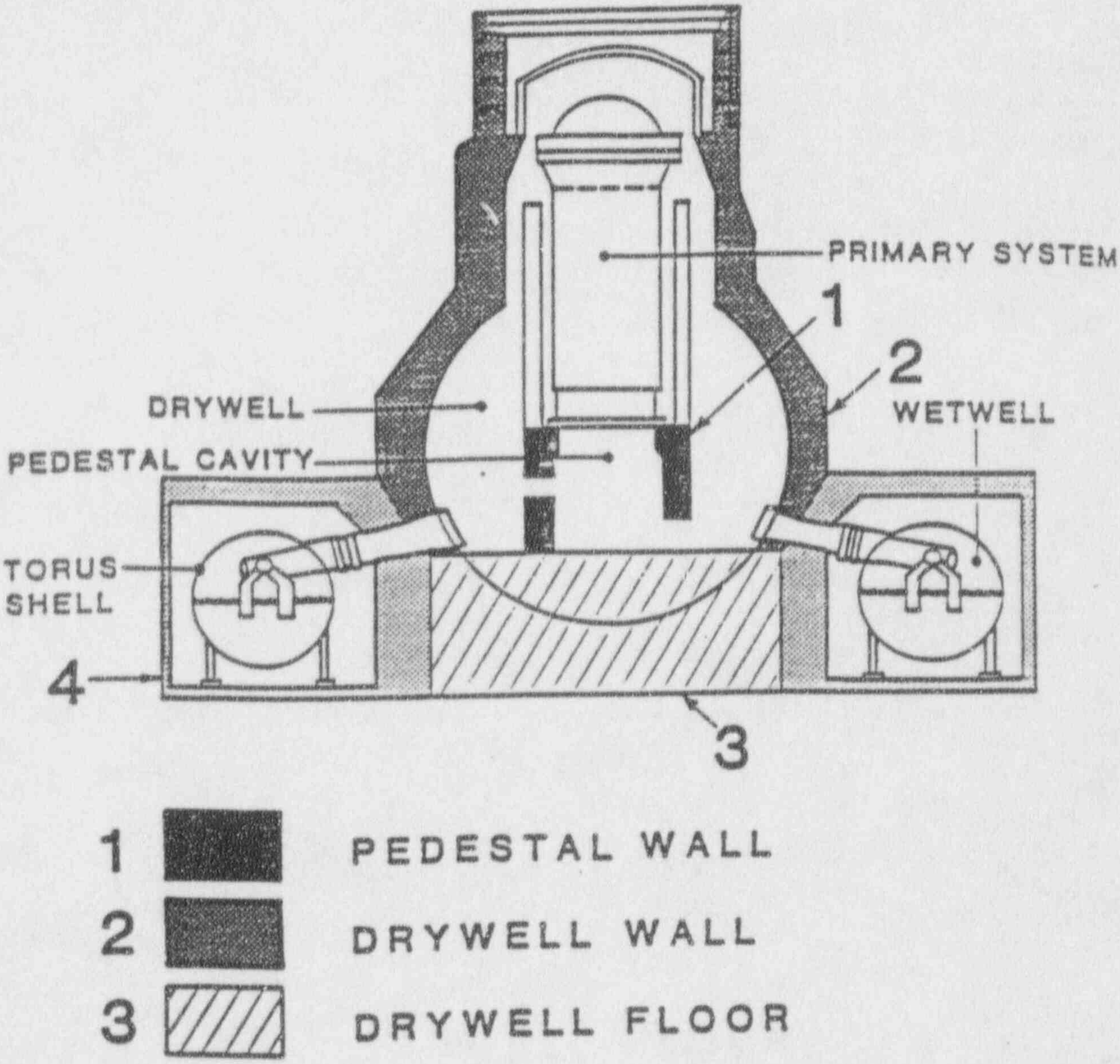

Figure D.6 MAAP Containment Heat Slab Configuration

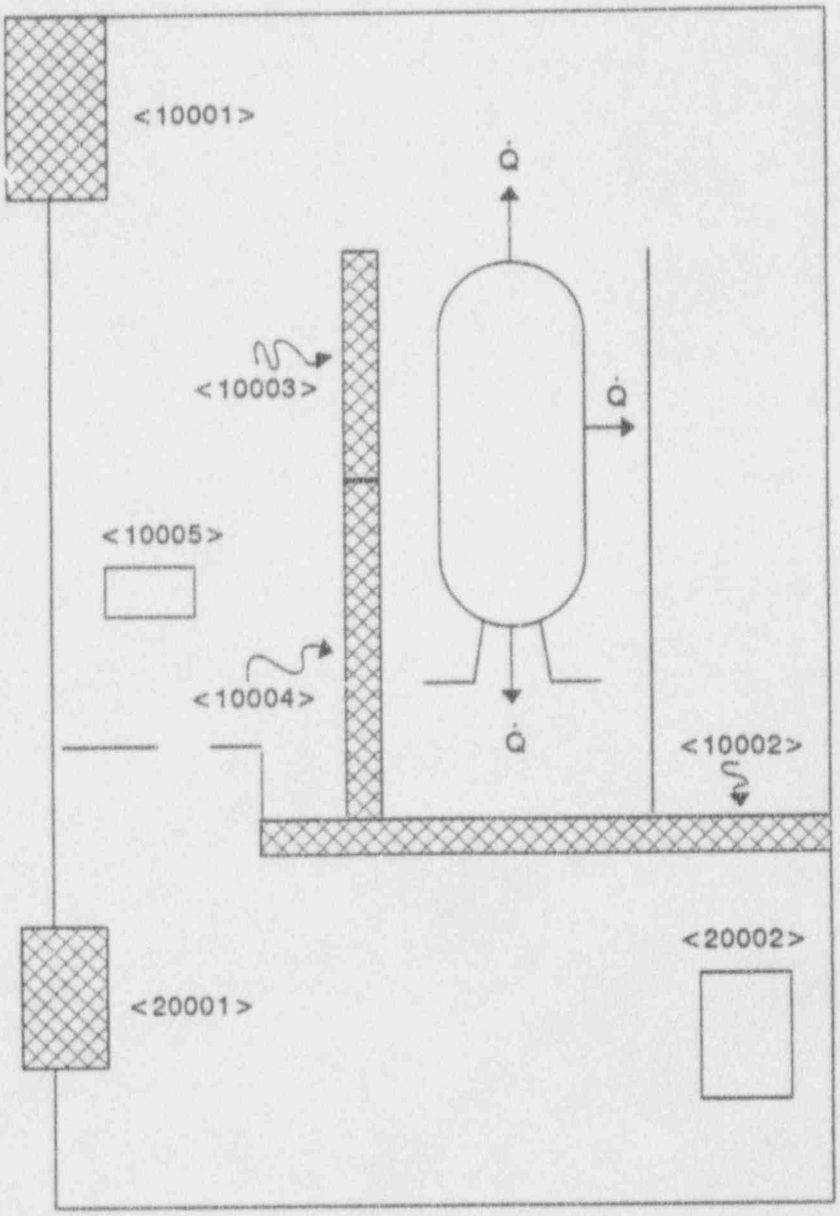

<xxxxx> = Heat Slab Designated in MELCOR

Figure D.7 MELCOR Containment Heat Slab Configuration

Table D.6 Containment Configuration

	MAAP	MELCOR
Volumes		
Drywell	4560 m^3	4235 m^3
Wetwell	7132.5 m^3	7132.5 m^3
Pedestal	240 m^3	N/A
Downcomer	N/A	565 m^3
Masses		
Liquid Water	3.5×10^6 kg	3.5×10^6 kg

Heat Slabs	MAAP Area	MAAP Thickness	MELCOR Area	MELCOR Thickness
Drywell Wall (+ concrete with 1" gap)	1736 m^2	.0286 m	1736 m^2	.0286 m
Drywell Wall Concrete		1.57		1.57
Drywell Floor	132	1.44	132	1.44
Drywell EQ	801	.017	801	.01747
Wetwell Wall	1584	.01588	1584	.01588
Wetwell EQ	4188	.017	4188	.01747
Pedestal Wall Upper	1105	.4055	767	.349
Pedestal Wall Lower			337	.533
Pedestal EQ	67.8	.0586		
RPV Surfaces			420	≈.13

The MAAP and MELCOR inputs were compared to assure that the initial pressures, temperatures, and relative humidities in the control volumes, which make up the containment, were compatible (see Table D.7). In addition, the containments are both inerted.

Table D.7 Containment Control Volume Initial Condition

	MAAP			MELCOR		
	Pressure	Temperature	Relative Humidity	P	T	RH
Drywell	0.1 MPa	330K	.5	.1 MPa	330K	.5
Wetwell	0.1 MPa	305	.5	.1 MPa	330	.5
Pedestal	0.1 MPa	330	.5	N/A		
Downcomers	N/A			.1 MPa	330 gas /305 liquid	.5
Wetwell Pool		305			305	

3.6 Reactor Building Configuration and Initial Conditions

Both MAAP and MELCOR use the same 8-volume reactor building model (Figure D.9). The volume of each of the control volumes were compared and their values are shown in Figure D.9 in cubic meters. The reactor building's air atmosphere will support hydrogen combustion. Both codes model containment failure to occur along the boundary with the reactor building torus room (Volume 401 in Figure D.9). The temperature of the reactor building is at 295K, and atmospheric pressure.

Because of the important role the reactor building plays in attenuating the radiological release from the containment, a large amount of detail was incorporated into its heat slab structure. Six surfaces, including the external wall of the reactor building, primary containment wall, ceiling, floor, internal wall, and miscellaneous steel are modeled in each reactor building volume in the MELCOR deck. The number of heat slabs available for each reactor building control volume in MAAP is limited to the outer wall, floor, and internal walls. The last of these was used to simulate the miscellaneous steel used in MELCOR. Also, impaction was not used in the MAAP run for reactor building volumes. Impaction modelling is recommended when using MAAP for IPEs. A comparison of the modeling used in the Reactor Building for representative Reactor Building control volumes is given in Table D.8.

The floor areas are equal, which is important because they are the aerosol settling areas. The important difference is the surface area and thickness of the steel representations as it affects heat transfer. A vertical orientation was used in MELCOR for all surfaces except the floors. In MAAP more steel mass is spread over a larger surface area with a smaller thickness then in MELCOR. This should decrease MAAP's heat removal time constant when

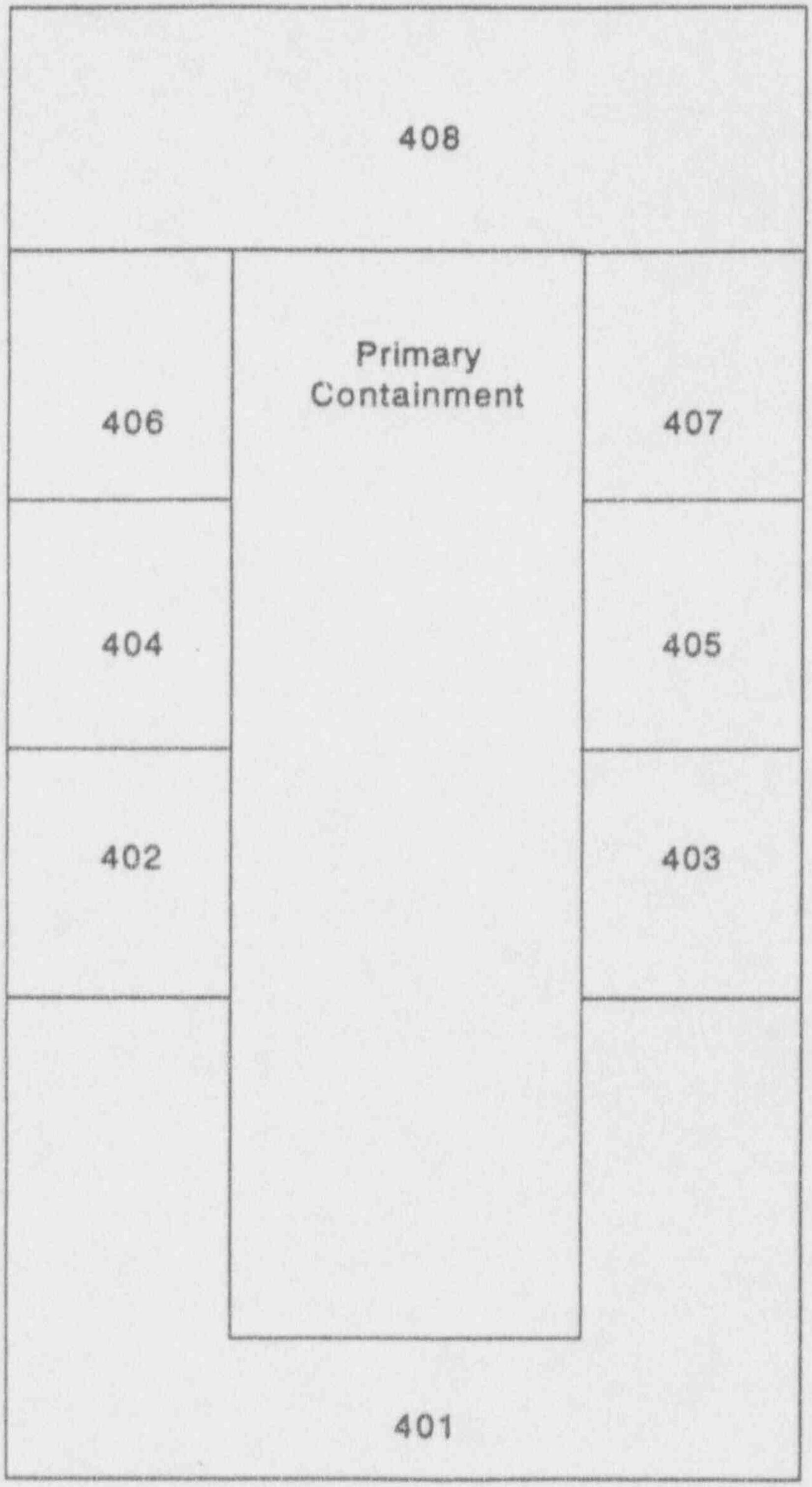

Figure D.9 MAAP and MELCOR 8-Volume Reactor Building

Table D.8 Reactor Building Heat Slabs

	MAAP			MELCOR		
Control Volume and Slab Description	Surface Area (m^2)	Thickness (m)	Mat	Surface Area (m^2)	Thickness (m)	Mat
401/Torus Room						
Floor	1166		C	1166	.75	C
Outer Wall	2264	2.65	C	1391	.5	C
Misc. Steel						
Inner Walls	0.0		S	805	.75	C
P.C. Wall						
Ceiling				1166	.75	C
402/Typical EQ Room						
Floor	588		C	588	1.15	C
Outer Wall	1556	1.57	C	671	.9	C
Misc. Steel				167	.0127	S
Inner Walls	921.8	0.0042	S	950	0.35	C
P.C. Wall				315	1.5	C
Ceiling				588	0.6	C
408/Refueling Deck						
Floor	1362		C	1362	.23	C
Outer Wall	1362	.23	C	3063	.00254	S
Misc. Steel				356	.0127	S
Inner Wall	9804	.0056	S			
Ceiling				1661	.0254	C

C = Concrete, S = Steel, Rooms 402 to 407 inclusive are equipment rooms

the containment fails, possibly reducing flow out of the Reactor Building failure location, which is in the Refueling Bay volume.

In MAAP the outer wall and internal walls of the MELCOR model are combined in the outer wall slab. Although the surface areas seem close, the thickness is much greater in MAAP, and hence, the total heat capacitance will be larger. Because concrete slabs react relatively slowly in terms of heat transfer, the effects of this difference may not be all that great over containment blowdown time. However, both the effects on aerosols and vapor condensation must be considered. Vapor condensation should occur on all surfaces regardless of orientation.

3.7 Fission Product Groups

MELCOR tracks 103 decay heat elements in 16 fission product classes. However, only 29 of these elements contribute any significant amount of heat, and their masses essentially constitute the total mass of the radionuclide groups. MAAP requires the user to supply 22 elemental masses of which 19 are made part of the 12 groups of fission products. The other three elements, Zr, Nb, and Ru, are always part of the core material (see FPGRP subroutine description in the MAAP User Manual). The masses determined for the 29 fission product elements of MELCOR were used in the MAAP input. Specifically, there were 20 common elements, which are primary contributors to decay power in MELCOR, and are mass input elements in MAAP. Sm and Pu masses also were included in MAAP, but not considered as major decay power elements in MELCOR, and hence, they were not mass contributors to MELCOR's Decay Heat Fission Product Class. Table D.9 shows the elemental mass as employed by the two codes.

Table D.9 Radioactive Masses

Element	MAAP (kg)	MAAP and MELCOR (kg)	MELCOR (kg)
Sm	53.8		
Pu	743		
As			0.01
Se			5
Br			1.97
Rh			35
Pd			89
Ag			4.7
Sm			3.9
Ba			121
Nd			315
Pm			12.9
U			1.3×10^5
Xe		429.36	
Kr		34.349	
I		18.963	
Rb		32.202	
Cs		236.15	
Sr		85.872	
Ba		121.65	
Y		42.936	
La		107.34	
Zr		311.29	
Nb		3.578	
Mo		275.51	
Tc		71.56	
Ru		182.48	
Sb		1.3954	
Te		35.78	
Ce		243.30	
Pr		93.028	
Nd		314.86	

3.8 Model Options

3.8.1 Core Concrete Interaction

In MELCOR CORCON's default values for limestone, common sand concrete are used. This composition is duplicated in MAAP. The CORCON crucible or core-catcher used in MELCOR is approximately twice the floor surface area used in MAAP's pedestal volume. This was a modification made late in the study to simulate the spreading of corium on to one-quarter of the drywell floor area. MAAP allows the corium to be entrained out of this pedestal region by the water-gas jet as well as spill over or out the pedestal-drywell man ways. These model options chosen for MAAP and MELCOR are consistent with their RPV core ejection models.

3.8.2 Core Models

MAAP uses a "no core blockage/local node cut-off" model and single-sided Zr clad oxidation. The effect of this option is to prevent oxidation in a cell node, if it is completely full of corium. However, MAAP 3.0B rev 7.0 contained an error which resulted in no core blockage as well as no local node cut off when the previously mentioned option was chosen. In MELCOR, a core support plate failure model is chosen which, when failure of the plate occurs at 1273K, allows core debris, relocated on the failed core support plate ring, to pass to the lower plenum. Also, the corium default ejection model chosen in MELCOR permits ejection from the vessel of all debris (solid and liquid), which exists in the lower plenum's bottom axial segment at the time of penetration failure, provided the liquification of the debris meets the constraints explained in Appendix B.

3.8.3 Burn Model

MAAP assumes that conditions for ignition and flammability are the same (zero effect of the ignition and flammability limits [1]). MAAP uses an auto ignition temperature for H_2 burns of 983K and has an inerting steam mole fraction of .75. MELCOR uses the default values applied when no ignition source is available, as would be the scenario for a station blackout plus loss of DC. This scenario requires an H_2 mole fraction greater than or equal to 0.1, and an O_2 mole fraction greater than or equal to 0.05. The combined H_2O and CO_2 mole fraction must be less than or equal to 0.55.

3.8.4 Aerosol Model

Five aerosol sizes are used in the MELCOR calculation. In MAAP an Aerosol Multiplier (FAERDC) equal to 3.0 is used. This will result in a slower transition to a lower aerosol equilibrium steady state airborne mass, if a change in aerosol pressure occurs, than a FAERDC equal to 8.0 (a previously recommended value). This smaller value should decrease a compartment's DF.

4 Discussion of Results

The outcome of this comparative numerical experiment is described in terms of four accident time phases. Table D.10 lists some of the key event times. Those times after the core support plate fails are particularly noteworthy. Note that for MELCOR three different values are listed for core plate failure times because corium flow across radial rings is not permitted in the MELCOR model. In MAAP, once the core support plate has failed, all molten material is relocated to the lower plenum. All the corium flows out of the vessel at once.

One other observation should be made at this time: the MELCOR model prevents the debris in the lower plenum from being ejected at the time of vessel failure. This ejection is prevented because there is a constraint in the code, which requires at least 5000 kg of molten mass or a melt fraction of 0.1 (COR-RM-64).

4.1 Vessel Mass and Energy Considerations from Accident Initiation to Clad Damage (Plot 1)

Although MAAP and MELCOR began with nearly the same water inventory, there is a relatively large difference (approximately 8 min.) in time to core uncovery (TAF), which grows to about 20 min. by the time the level reaches the bottom of the core. The latter is affected by corium relocation, and the former can be attributed to a mismatch of the initial water inventory location. Table D.4, and Figures D.3 and D.4 should be referred to in order to follow this discussion. Basically, MELCOR's Steam Dome and MAAP's Upper Head have equal volumes. MELCOR's Upper Plenum and MAAP's Standpipes and Separators also have equal volume (44.9m^3). Gas and liquid phases exist in the core and higher volumes. The lower downcomer, recirculation loop and lower head volume can be assumed to contain only liquid water at accident initiation. However, by comparing the inventories in these volumes and remembering that the total primary system inventory is the same in both codes, we can infer the liquid water distribution above the core region. MAAP has a 115m^3 volume in its Lower Plenum, vs. only 103.5m^3 for MELCOR's comparative volume shown in Figure D.4. This means that a full 11.5m^3 of liquid water is located below the core region in MAAP that must be above the core region in MELCOR. Further, even though MAAP and MELCOR input represent the same volume for their cores, MELCOR's core is a separated volume. MELCOR's core has a pool covered by an atmosphere, while in MAAP a two-phase representation is used. These configurations translate to be roughly equivalent to 1m^3 of liquid water that would be above TAF in MAAP and below TAF in MELCOR. Further, MAAP has 4.6m^3 of liquid water represented in its recirculation loop. MELCOR represents this in its downcomer volume but MELCOR's downcomer volume equals that of MAAP's. Therefore, MAAP has another 4.6m^3 of liquid water below TAF that has been modelled in MELCOR

Table D.10 Key Event Times

Event	MAAP(s)	MELCOR(s)
Loss of all electrical power	0.0	100
Core uncovery (swollen level at TAF)	1900	2500
Collapsed water level at BAF	4600	5900
1 kg of hydrogen generated	2924	4000
Clad damage (clad perforation)	3147	3800
Initiation of clad melting	3920	4500
First fuel material relocation	3930	4500
First fuel material relocation to core support plate	4538	5100
Core support plate failure	7752	9800 (R1) 6500 (R2) 15,500 (R3)
Vessel failure time	7765	9910 (R1) 12,000 (R2) 22,000 (R3)
Cavity receives mass	7765	14,900
Concrete attack (gas released)	8447	20,000
Containment failure	86,000	32,000
Start of burning in reactor building	86,000	32,000
Reactor building failure	86,000	32,000

Note: R1, R2, and R3 refer to redial rings in the core region. R1 is the inner ring and R3 is the outer ring.

as above TAF. Adding these differences in liquid water placement results in MAAP having about $15m^3$ of liquid water volume below TAF that MELCOR has above. With a density of 739.4 kg/m^3 and a latent heat of evaporation of $1.5x10^3$ kJ/kg, the required energy to convert $15m^3$ of liquid to steam is $1.7x10^{10}$J. Other differences which may affect the predicted times to TAF are: main steam isolation valve and feedwater flow dynamics, fuel stored energy, and other heat slab effects.

In MAAP both MSIV flow and feedwater flow are modelled to stop at time zero. In MELCOR feedwater flow is ramped to zero in one-hundredth of a second. However, in MELCOR 3 seconds are allowed for the MSIVs to close, losing approximately $250m^3$ of steam inventory. This inventory would be relieved due to SRV actuation in

MAAP. Therefore, this loss of steam in MELCOR will simply relieve RPV pressure earlier than in MAAP. This should have little effect on the time for the water level to reach TAF. The MSIV discharge is akin to an early SRV actuation.

Stored fuel energy will be considered next. In MAAP 5 full power seconds [5] are used to represent the stored energy in the fuel. The equivalent average temperature for the fuel in MELCOR can be determined. Using Table D.2 for UO_2 mass, we have $\approx 1.685 \times 10^5$ kg. With a specific heat of approximately 300J/kgK [5], the stored energy is 5.06×10^7 J/K. One full power second is 3.293×10^9 W-sec or 3.293×10^9 joules. Therefore, in MAAP 1.65×10^{10} joules represent the stored energy in the fuel. The fuel temperature in MELCOR above saturation would have to be 326K to match this. A review of the UO_2 temperature plots in MELCOR would show approximately 900K at steady state instead of the $\approx$891K as expected by MAAP.

In MAAP the RPV heat slabs have more mass than in MELCOR. These slabs absorb heat because the saturation temperature rises after the MSIV closes due to increased RPV pressure. Table D.5 shows the difference in slab mass, a difference of $.5 \times 10^5$ kg. The increase in saturation temperature between 1000 and 1100 psia is approximately 5K. With a steel specific heat of .11 Btu/#F or 460 J/kgC, we obtain a stored energy difference of 1.15×10^8 joules. That is, the heat slabs in MAAP would be available to cool the inventory by 1.15×10^8 joules more than those in MELCOR. The difference in heat loss through the RPV walls is 880 Mw-sec over 2000 sec, or 8.8×10^8 J. This is because the loss in MAAP is 1 MW vs. .66 MW for MELCOR.

At 2% of full power 6.6×10^7 joules/sec are produced. Table D.11 represents the energy differences discussed above in terms of time at 2% of full power. Table D.10 shows that MAAP predicts water to drop to TAF 500 seconds before MELCOR. Hence, much of the difference can be attributed to the $15m^3$ or nearly 12,000 kg of water that MAAP has in the lower plenum and that MELCOR has above the core.

Table D.11 RPV Mass and Energy Summary

Description of Difference	MAAP vs. MELCOR	
Lower plenum water	decrease by $\approx$ 256s	$= 1.7 \times 10^{10}$ J
Fuel stored energy	essentially equal	
Slab stored energy	increase by $\approx$ 3s	$= 1 \times 10^8$ J
RPV heat losses over 2000s	increase by $\approx$ 27s	$= 8.8 \times 10^8$ J
Totals	decrease by 226s	

We should make one more point before leaving this discussion on accident time phase. Because MAAP has the clad and fuel pellets as part of a single temperature node, we expect that while decay power, and not clad oxidation is driving the energy source in any given core cell, MAAP will give a higher clad temperature than a multinode fuel model, such as contained in MELCOR. This will drive the cladding to an earlier time of enhanced oxidation, and result in early hydrogen generation. We observed this in MAAP's prediction of 1 kg of hydrogen generated about 1000 sec after TAF uncovery. We compared this prediction to MELCOR's prediction of 1500 sec. This may also be effected by the finer core axial nodalization present in MAAP as well.

Once the cladding's oxidation becomes the primary heat source, MELCOR should heat its clad up faster than MAAP. The fuel nodalization scheme in MAAP should result in a slower temperature rise in the clad as it couples its temperature to the UO_2. This will result in a longer time for clad oxidation before it relocates. We expected to observe a longer time differential between clad damage to clad melt for MAAP than MELCOR. However, this differential is only marginal as shown in Table D.10. We attribute the reason to the much smaller fuel cell size used in MAAP or differences in equations on clad oxidation rates.

4.2 Core Heatup to Vessel Ejection (Plots 2-32)

We enter this time phase defined as the time of clad damage with a 550-sec difference between MAAP and MELCOR. As we progress to clad melting, and initiation of relocation, the two codes essentially maintain this difference. There is no increase in divergence from the initiation of relocation to the time of fuel relocation to the core support plate. In MAAP, before material relocates to the core support plate, the node above the plate would have to receive some molten eutectic material. MELCOR has no such constraint. Instead, solid debris from cell 110 (Figure D.2) will have relocated to the support plate as soon as this cell's structural integrity has been lost. This is due to the error in version CZ as we discussed earlier. Thus, while MAAP's relocating material is undergoing a candling process on its way to the support plate, MELCOR's solid debris is undergoing gravitational settling.

A consequence of these models is that it is entirely possible for water to be above the support plate in MELCOR at the time of first relocation of solid debris there. However, this consequence is very unlikely in MAAP, certainly with a given radial ring, because if water had been present, it would have arrested the melt progression to this lowest node. A review of the core level vs. time plot in MELCOR (Plot 27) clearly shows that there was water (2500 kg.) present above the core plate at the time of solid debris relocated there. This water is rapidly boiled off; Table D.10 shows that all water in the core is boiled-off at 5500 sec, that is 550 sec after the first relocation of core debris.

In MAAP, no water remains in any fuel channels at 4600 seconds (Plot 25), which nearly coincides with the first relocation to the plate that occurs at 4538 s. Note that in MAAP, the presence of liquid water above the core plate does not mean that there is water in the hottest channel. In MELCOR, if there is liquid water above the core plate, there is liquid water also in the hottest channel.

Once the lowest fuel cell in MAAP becomes fully molten (2500K), at 7752 s, more than 3200 seconds after first fuel relocation to this cell, the core support plate fails. The relocation in MELCOR begins with cell 110 reaching its clad melt temperature of 2500K. The conglomerate (molten) debris, which is mostly Zr clad, carries with it about 20% (by mass) of UO_2 in solid form. This initially is transported down to cell 109, where it refreezes. The remaining solid UO_2 from cell 110 is supposed to remain in cell 110, because the porosity of the intact fuel cells was input at 0.99. The UO_2 remains in the cell to simulate that the solid debris size is too large in its assumed particle size to be transported past an intact fuel cell. However, because of the error in the MELCOR code, about 10 tons of the 15 tons of UO_2 initially in cell 110 is transported to the core support plate, where the water boils off. Cell 111 cannot be transported to the compacted cell 110 because it has not yet reached its failure temperature, and because cell 110 is not fully empty of material. If cell 110 were fully empty, cell 111 material would be transported with its geometry intact to cell 110. Because cell 110 has particulate debris, cell 111 relocates after its clad reaches 2500K at around 5500s. The conglomerate debris from cell 111 travels to cell 109, and its particulate debris travels to cell 110. The non-fuel bearing cell 112 will be free to be transported to cell 111, when all component masses have evacuated that cell or when the material in cell 112 melts.

The water boil-off produced by the relocation of some of the particulate debris from cell 110 is insufficient to quench all of the intact core and may have shortened the time to failure of cell 210 because of increased steam availability for oxidation heatup of that cell. After an initial dip in Zr temperature, cell 110 rapidly heats up and fails at about 6000s. Again because of a code error, some of this cell's particulate debris is relocated to the core support plate. However, with no or little water remaining above this structure, to cool the 10 tons of UO_2 from cell 210 relocated there, ring two's support plate quickly attains its yield strength temperature of 1200K at 6500s. This results in the relocation of all particulate debris in the core region of ring two. This is another error (caused by the same mechanism as the first error that we discovered) in MELCOR. MELCOR should have transported only the particulate debris available on the lower core support plate at the time of its failure instead of all the particulate debris in ring two. All the particulate debris in ring two includes that in cell 210 and cell 211, because these cells had reached their failure criteria. This would mean that about 30 tons of UO_2 are initially transported to the lower plenum region when the core support plate of ring two fails. This debris begins the boil-off of the lower plenum water. At about 8000s, cell 109 reaches its failure temperature. At 9800s, the core support plate of ring one attains its yield temperature, and the particulate debris from this core's ring (about 45 tons) are transported to the lower plenum, which has been sufficiently boiled dry by the mass relocation of ring two to the region. The result is rapid failure of a vessel penetration in ring one at 10,000s. At 12,000s, a vessel penetration of ring two fails. It takes beyond 21,000s before any additional fuel cells fail, with the last cells, those in ring three, relocating at 26,500s, when the lower support melts.

In MAAP, when the plate fails, all molten debris flows down the break location and combines within one radial zone of the lower plenum. It then boils the water in this region and attacks the lower head penetrations. From Plot 26, this happens at 7752 sec. Because this material is fully molten with a eutectic melt temperature of 2500K, it is no surprise that the lower head fails quickly thereafter. The melting temperature of steel is only about 1700K. Also, because of the melt progression, there is little time for the water to boil-off in the plenum region in MAAP. Therefore, at time of vessel failure, much of the water in the lower plenum is ejected.

Although MELCOR first fails its center ring penetration at 10,000 s (Plot 30), we note that ejection does not occur until approximately 15,000 s, when the debris, previously cooled by the water in the lower plenum, heats up to the extent that either 5000 kg or 0.1% of the corium is molten. This modeling criteria results in a condition, where, even though MELCOR fails a vessel penetration only about 2,000 seconds after MAAP, the first time core material exits the vessel is nearly 7,000 seconds after MAAP. We also should note that because of the options selected in the MAAP model, when the vessel fails, the entire core and molten lower core support plate steel are ejected.

Before discussing the effects of corium ejection on the containment response, a word about in-vessel hydrogen generation is appropriate. Approximately 860 kg of H_2 is predicted to be produced in-vessel by MAAP before vessel failure (Plot 31). All corium is ex-vessel after vessel failure. In MELCOR, approximately 1000 kg are predicted before vessel failure. Although nearly all the Zr in MAAP reaches 2500K before being ejected, in MELCOR some fuel cells are relocated before reaching 2500K.

Several items effect hydrogen production:

- Water availability
- Time at elevated temperature
- Surface area
- Stainless steel oxidation

The surface area for oxidation used in MAAP and MELCOR for our case does not consider double-sided clad surfaces. However, the similarity ends there. MAAP uses a fixed geometry for each fuel cell until there is no longer any Zr remaining in that cell. MELCOR uses a complicated geometry algorithm on the fuel cells, which experience conglomerate debris mass addition or removal. First, MELCOR increases the available area for oxidation on mass addition, and then decreases it as the conglomerate debris begins to reduce interstitial volume. Particulate debris is assumed to take on a spherical form with a one-inch diameter; however, this form does not affect Zr, but only UO_2.

Because the fuel cell temperature nodes of MAAP include a lumped parameter assumption for the UO_2, clad, and channel material, we anticipate that if the nodalizations of the core were equal for the codes, MAAP's cladding would remain at an elevated temperature for a longer period than MELCOR's.

In MELCOR's hydrogen production, about 100 kg is produced by stainless steel oxidation. This production is not modelled in MAAP. We believe that another reason for the hydrogen differences between the codes is the availability of the water for oxidation. There are two essential features here. The first involves the total amount of water which is made available to the Zr for oxidation. MELCOR boils-off a greater inventory of water before vessel failure.

The second feature, however, is just as important. This feature involves the temperature of the Zr at the time of water availability. In MELCOR, part of the water made available to the Zr includes that from SRV actuation. The Zr can either be quenched or heated-up through rapid oxidation because of the presence of water, its flow rate and the temperature of the Zr. In many of the cell Zr temperature plots, after the lower core support plate fails at around 6500s, there is an initial cooling of the core Zr. However, after this cooling occurs, a heatup occurs during the time before vessel failure at 10000s.

As an example, a study of the Zr temperature of cell 209 shows a quench just after 6500s. When the first lower core support plate fails (ring 2), the temperature then recovers, because the mass of the relocated material of ring two is not enough to sustain rapid water boil-off from the lower plenum. Its stored energy is too small and it reverts to decay power boil-off. During this time, the Zr in cell 209 again heats up and because sufficient oxidizing water is available, hydrogen is produced. Another cycle is reached on the failure of ring one's support plate, but because more mass is relocated into the lower plenum when this ring fails than that of ring 2, a greater core quench is observed. It then takes a longer time to get the Zr in cell 209 to elevated temperatures, and under these conditions, there is no longer any water in the lower plenum for boil-off.

A review of the H_2 produced in the core for MELCOR shows that nearly 80% of H_2 is produced between the time the first lower core support plate fails and the vessel failure.

In MAAP, all hydrogen is produced before core support plate failure, and hence, only the water above this plate and some relocated there on SRV actuations is available for the H_2 production.

In summary, there have been cases where MELCOR predicts less H_2 produced in-vessel than MAAP because of small input changes. This happens when the relocation of material in ring one is sufficient to cause that rings lower support plate to fail first, and the remaining core is then quenched. Therefore, rings two or three do not experience fuel failure until well after the vessel itself fails. In those cases where MELCOR predicts more H_2 than MAAP, the first fuel relocation in ring one occurs later than in the low H_2 case, and it is insufficient to fail the ring one lower support plate before some fuel in ring two relocates to the core plate, and ring two's support plate fails. The two cases in MELCOR do not have a different heat-up rate for ring one's support plate. Instead, the different phenomena is tied to the temperature of the clad in some of the fuel cells of ring two. In the low H_2 case, ring two cells are quenched by the water boiled-off by the relocated mass of ring one, while in the high H_2 case, the temperature of the clad is sufficiently high in the second ring to experience only a momentary quench before the amount of cooling water becomes insufficient. Thereafter, oxidation heatup drives ring two cells to fail and rapidly attacks ring two's lower support plate. Nearly 400 kg of additional H_2 is produced after ring two's core support plate fails.

Finer core nodalization in MELCOR and also in MAAP should affect H_2 production. Further, the correction of the relocation model in MELCOR should have a major effect.

In MAAP increasing the number of rings should result in a more rapid failure of the core support plate, which may reduce the time to vessel failure and reduce H_2 production.

In MELCOR a finer nodalization should decrease the time for first fuel relocation to the core support plate, which should help cool the remaining intact fuel and decrease H_2 production. Correcting the relocation model, however, should have the opposite effect because no relocation of particle debris to the lower plenum will occur until the lower cells in a ring fail.

4.3 Containment (Plots 31, 33-58)

The significant figure of merit during this accident time phase is the time to containment failure. Table D.10 shows a surprising difference in time between the MAAP and MELCOR predictions. MAAP predicts failure due to a temperature degraded failure pressure of 130 psia at 86,000 seconds. MELCOR predicts failure at 32,000 seconds because of a temperature affected pressure as well. However, the pressure at the time of MELCOR's failure also is 130 psia. MELCOR's drywell wall temperature at this time is close to 1000K. MAAP's wall temperature is about 700K when it reaches drywell pressure failure. There is a greater rise in drywell temperature in MELCOR than in MAAP.

Starting with the ejection from the failed vessel's penetration, MAAP and MELCOR take very divergent paths. MAAP's corium is essentially molten at 2500K. Further, after it has been ejected, a large jet of water and gas levitates a large fraction of it into the drywell and out of the pedestal region (Plots 36 and 41). MAAP's pedestal is actually a sump. After the effects of entrainment, about 80% of the corium remains on the drywell floor and the rest is in the pedestal area. The large lower plenum water mass also cools the corium. Except for the initial time of dispersion, the corium temperature in the drywell (Plot 36) remains just below the ablation temperature for concrete (1500K). This would imply the very large drywell floor heat slab along with the water from the RPV effectively cools the corium which has been transferred from the pedestal region. This will effect the amount of CCI gases produced, leaving only the pedestal region for CCI. Here, looking at the plot of corium temperature versus time (Plot 41), we see that this fraction of the ejected core material produces concrete attack (see Table D.12). We should keep in mind that the evaporative water is released at 1500K in MAAP. Further, outgasing of the pedestal heat slabs is modelled in MAAP. Outgassing of non-corium covered concrete heat slabs were not modelled in MELCOR. MELCOR also does not release evaporative water until concrete ablation temperature is reached for the concrete in contact with corium.

MELCOR predicts gradual ejection of the corium, and because the initial amount of corium was cooled by the lower plenum water, it is actually much cooler than 2500K (see Plot 54), and most of it is solid debris. Being solid, the corium would not be entrained by the exiting gas, and it remains within the region below the vessel. Here it heats the concrete to ablation. To simulate a degree of corium spread, the cavity volume has been enlarged to include an increase in floor area that is equal to that of one-quarter of the drywell floor. This enlargement doubles the cavity floor area over that as compared to the pedestal area. Further, there will be an effect on the cavity side wall area exposed to the corium. There is an initial doubling of the contact surface for CCI, which decreases to about a factor of 1.5 when all the corium is ejected.

A review of MAAP's corium distribution (Plots 36 and 41) shows that of the total 270,000 kg of corium at vessel failure, entrainment forces nearly all of the corium into the drywell until about 90,000 kg settles back into the pedestal, leaving 180,000 kg in the drywell. The corium temperature of the drywell (see Plot 36) shows a very quick cool down to below the ablation temperature of the concrete. The corium's contribution to containment pressurization then is based on capacitance and decay energy heat transfer by convection to the atmosphere, and radiative heat transfer to the heat slabs. There also is direct heating of the atmosphere by fission products contained in the atmosphere. The drywell floor is competing for the corium energy even though it does not reach ablation temperature.

In MAAP's pedestal region, the 90 tons of corium stay above the concrete ablation temperature, which results in the release of H_2 and CO. The rate of concrete attack can be found in Plot 42, where after 50,000 s, almost one-half of a meter has been decomposed. The global H_2 and CO mass release plots (Plot 31) show that there is a gradual addition of non-condensable mass to the containment. The free water in the concrete, which represents nearly 1/2 of the total amount of water, is freed at the same temperature as the ablation temperature.
Over 10,000 seconds from the time MAAP's cavity received the corium, the addition of H_2 and CO mass to the atmosphere are about 350 kg H_2 and no CO. In comparison to this, we see from MELCOR's total gas release from cavity (Plot 55) a negligible release of noncondensibles (15,000-25,000s). The next 10,000 seconds, however, are significant. In this time period (17,000 - 27,000 for MAAP), there is little further release of gas as the concrete is being heated to ablation in the pedestal. In MELCOR, this period is from 25,000 to 35,000 seconds. During

Table D.12 Corium Effects in Containment

Event Description	MAAP	MELCOR
Mass ejected from RPV	Nearly all at once	Gradual over time
Composition	Mostly liquid.	Mostly solid.
Temperature	≈2500 K	Initially much cooler < 2000K but later ejected material is close to 2500K.
Ejection Sequence	100,000 kg of cooler liquid water and gas follow eject on top of previously ejected corium.	Tens of thousands of kg of water ejected before corium.
Distribution	Mostly liquid corium is distributed throughout drywell and pedestal region.	Being mostly solid debris it is contained within a pedestal-like volume and .25 of drywell.
Heatup	No radiative heating of gases directly by the corium pool or crust.	Radiative heating of the containment atmosphere by corium pool or crust.
Wetwell Airspace Temp at TOF*	344°K	370°K
DW Gas Temp at TOF	710°K	1300°K
DW Pressure at TOF	127 psia	130 psia
Mass of H_2 produced at TOF	1250 kg	1140 kg in vessel only
Mass of H_2 produced in vessel at time of RPV failure.	860 kg	1000 kg
Mass of H_2 product in-vessel at time of RPV failure by stainless steel	0.0 kg	100 kg
Mass of CO, CO_2, and H_2 in containment (DW and WW) and RPV at TOF	≈12,400 kg	≈7850 kg
DW Liner Temperature	700 K	1000 K
Concrete ablation distance — Vertical	.7m ≈ 100 to Pedestal Region	0.9 m — Cavity Volume
Horizontal	.7	0.25 m
Decay power as percent of total power	90 - 100%	10 - 100%

*TOF = Time of Failure (Containment)

Note: MAAP predicts about 4 Pa/s DW pressurization rate after RPV vessel blowdown. MELCOR's DW pressurization rate is not at all linear due to the discrete additions of corium from the vessel to the corium pool in the cavity.

this time, MELCOR predicts containment failure and produces nearly an additional 13,000 kg of non-condensibles. Only 8000 kg were necessary to cause containment failure.

Therefore, we should appreciate that in MELCOR non-condensibles are produced at a faster rate than in MAAP. One look at how 270 tons of corium at a density of approximately 10,000 kg/m^3 would be spread is revealing. The exposed concrete area in MELCOR is 68.5m^2. In MAAP, with a pedestal wall height of about 0.46m and corium of 90 tons, we have within the pedestal, a contact area of 34m^2, and in the drywell region another 112m^2. This yields a concrete attack area in MAAP of nearly 150m^2, more than double that of MELCOR's, and the height of the corium in MAAP's drywell is only 0.2 meters. MAAP does not predict sufficient heat flux for the corium in the drywell to bring the concrete to ablation temperature. The result is a very slow rate of attack in the pedestal region.

The mass addition rate, however, is only part of the difference in containment failure time between MAAP and MELCOR predictions. How the source energy is transferred also is important. Besides the additional area of direct contact concrete in MAAP, the gas or atmosphere is heated differently in MAAP. As has been discussed, in MELCOR radiative heat transfer from the corium to the gas is used, which results in a very quick rise in drywell temperature (see Plot 50). This stands in sharp contrast to the temperature histogram obtained with MAAP (see Plot 35). The linearized rise rate in MELCOR is 3.0K/min from the time of corium ejection to containment failure. The corresponding rate in MAAP is about 0.3K/min, which occurs even though far more corium is ejected earlier in MAAP than in MELCOR and over a greater surface area.

In MAAP the slabs are heated by radiation from the corium and then the atmosphere by convection and radiation from the slabs. The drywell wall is a single node, and for a Mark I, this involves a large mass. The need to heat this mass before the atmosphere responds to the radiation from the corium is non-conservative because it will underpredict containment pressurization. This difference in modelling on the outcome should be quantified. Recall that there is a containment concrete wall separated by a 1" air gap in both MAAP and MELCOR models. Also, the energy absorbed by the drywell floor heat slabs should be compared before any conclusion regarding the differences related to the energy release in the CCI models of MAAP and MELCOR can be drawn. A comparison of the drywell wall and atmosphere temperatures for the two codes shows a very big difference (Plots 50 and 49), with MELCOR showing a difference of 300 K between wall and atmosphere temperature at the time of containment failure. The convective heat transfer between the atmosphere and wall shows how low this parameter is (Plot 51). Remember also, that MELCOR has a multi-node, drywell wall heat slab, a high atmosphere heat-up rate, and the enhancement of the atmosphere's absorptivity because of aerosols. In contrast, MAAP shows an atmosphere and drywell steel liner temperature which nearly duplicate each other (Plots 45 and 35).

Neither code has a rigorous radiative heat transfer circuit from the corium to the slabs and atmosphere. The beam length assumption that MELCOR uses for the atmosphere, and whether the absorptivity error is acceptable should also be confirmed. For large partial pressure of steam, CO_2, and aerosols concentration, a difference in beam length of 10 meters may have a small effect on the overall absorptivity of the drywell's atmosphere.

4.4 Fission Product Response Including Revaporization Concerns (Plots 59-60)

For MELCOR, we can present at the this time only plots of total radioactive masses released from fuel, deposited on all control volume slabs, and released to the environment to determine an effective total DF. We will present this for time of fuel relocation, time of vessel failure, time of containment failure, and at 24,000 seconds after containment failure. The first of these represents release from clad perforation before first relocation. From Table D.9, the total radioactive mass is 3,230 kg plus 1.3×10^5 kg of UO_2. From Table D.13, we see that MELCOR predicts a decontamination factor by the slabs of slightly greater than 2.

The MAAP data takes a different form. The only ex-containment release fraction supplied is for CsI (Plot 60). This shows a release fraction of .05 at the time of containment failure, growing to nearly .2 about 30,000 seconds after this.

Table D.13 Radionuclide Tracking for MELCOR

Times→	4,750	15,000	36,000	60,000
Total radioactive mass (kg) released from fuel	5	170	1,000	1,100
[illegible]ted on slabs	0	5	500	600
In containment atmosphere				
Aerosols	--	3	1	--
Vapor	--	95	300	40
In.containment pool				
Aerosols	2	25	39	39
Pool	--	--	--	--
In environment				
Vapor	--	--	--	375
Aerosol	--	--	--	14.5
Total				390

The DF (decontamination factor) that MAAP yields for this one element, not including any DF afforded by the reactor building, would be about 5. This is better than double the average of all radionucleate DF afforded by MELCOR, and MELCOR's number includes the effect of the RB.

MAAP and MELCOR models differ in decay power distribution between the radioactive isotopes.

As part of the MAAP-MELCOR comparison, a review of the heat produced by the fission product material groups for both computer codes was performed. CsI and CsOH are of particular interest. Table D.14 shows that MAAP has a fixed power factor for those compounds of 15.1% and 10.0%, respectively. That is their fraction of total decay power. For MELCOR, the corresponding power factors are determined for CsI by noting that all of the I will combine with an equal number of moles of Cs. Thus, the power factor for CsI would be slightly higher than that for I alone or group 4 in Table D.15. MAAP predicts a higher power factor than MELCOR for CsI for nearly all time periods except approximately two hours after scram (7458 s in Table D.15).

For CsOH, MELCOR simply augments the Cs of Class 2 with hydrogen and oxygen. Therefore, the power factors for Cs should be used for comparison against MAAP's value of 10%. Again, MAAP's predictions are on the high side, by as much as an order of magnitude at the time of containment failure for the BWR Peach Bottom Loss of all Power case. This finding means that MAAP would be expected to have revaporized these compounds earlier than MELCOR, and that they may have been removed from the gaseous phase because of deposition in the containment by the time containment failed.

Table D.14 Power Factors of the MAAP Fission Product Group

Fission Product Group		Power Factor
1.	Noble Gas	2.8
2.	CsI	15.1
3.	TeO_2	1.9
4.	SrO	6.2
5.	MoO_2	5.0
6.	CsOH	10.0
7.	BaO	--
8.	La_2O_3	--
9.	CeO_2	--
10.	Sb	--
11.	Te_2	1.92
12.	$UO_2 + NpO_2 + PuO_2$	--

*Taken from MAAP 3.0B Subroutine CMHEAT

Table D.15 Power Factors of the MELCOR Fission Product Group*

Fission Product Group		Representative	Initial Mass (kg)	Power Fraction at 600s	7458s	20,000s	30,000s	MAAP Equivalent Group
1.	Noble Gas	Xe	464	7.4	7.1	3.9	2.8	1
2.	Alkali Metals	Cs	268	9.9	1.6	0.9	1.0	6
3.	Alkaline Earths	Ba	208	10.0	11.0	11.4	11.1	4,7
4.	Halogens	I	21	13.0	16.0	12.1	11.0	2
5.	Chalcogens	Te	41	5.3	8.0	9.2	10.2	3,11
6.	Platinoids	Ru	307	2.8	4.0	4.6	4.7	
7.	Transition Metals	Mo	351	9.8	5.2	5.8	6.2	5
8.	Tetravalents	Ce	594	8.8	20.7	29.4	29.3	9,12
9.	Trivalents	La	571	24.0	24.3	23.3	22.5	8
10.	Uranium	U	$1.3x10^5$	4.5	0.5	0.2	0.3	12
11.	More Volatile	Cd	1.4	3.5	1.4	0.9	0.7	10
12.	Less Volatile	Sm	8.6	0.7	0.5	0.2	0.1	
13.	Boron	B	--					
14.	Water	N_2O	--					
15.	Concrete	--	--					
16.	CsI	CsI	$1x10^{-6}$					

*Compiled from MELCOR Sensitivity Run 177, 4/26/91

5 Summary

Using MELCOR for comparative purposes, shows that the two codes' representations of physical models are different from the time of core relocation. Modelling the relocated material as an eutectic liquid leads to much of the difference. Because of this, the attack of the lower core support plate and the subsequent failure of the lower head are seen in this study to be performed with greater mass and higher specific energy content in the MAAP representation than in MELCOR. The MAAP model of lower head attack has some physical justification if one believes that a large mass (here nearly the entire core) would flow down the control rod drive guides, and attack the penetrations with a surface area equal to that of a few CRD tubes (only those tubes in the initially failed region). One would expect a rapid failure of a penetration whose melt temperature is 1700K, when surrounded by a large quantity of corium whose initial temperature is 2500K. Some questions remain, however:

- Should relocation only occur for molten debris?
- Should all debris be molten?
- Is it appropriate to assume a fuel cell is in equilibrium with any corium debris which might enter it, thus not permitting transport of the liquid debris to the cells below until the cell in question has reached the eutectic temperature?
- Is it correct to assume that all molten debris as it exists in the core will flow to the lower plenum once a core support plate failure occurs?
- Why must the entire lower cell become fully molten to produce a lower core support plate failure?
- Why must the lower core support plate fail to allow progression of a liquid corium to the lower plenum?

These and other questions arise if one attempts to associate a physical meaning to the MAAP model. MAAP's predicted failure times up to vessel failure are conservative with respect to MELCOR. By using the molten debris model, and not allowing blow-by of the lower plenum water and RPV gases, entrainment out of the lower plenum region is considered in MAAP. This results in the water cooling the corium while a large fraction of the corium (more than 70%) is spread over the drywell floor. The size of the drywell floor and the water cooling that the corium experiences result in this drywell corium not having enough energy to produce concrete ablation. The result is a much reduced gas addition rate to the drywell atmosphere when compared with MELCOR results. Further, the heatup rate of the gas in the drywell is much less than predicted in MELCOR, even though the surface area of the corium exposed to the atmosphere is greater. MAAP's approximation for a transparent (absorptivity of zero) atmosphere with heating of the gas by convection from the drywell liner and pedestal heat slab may not be conservative.

Any use of a severe accident code for IPE work should require a plant specific review of the temperature and pressure containment failure modes. If a criteria on temperature-dependent pressure failure had not been included here, the difference in the times to containment failure predicted by MAAP or MELCOR would be much greater.

At this time, the radiological consequences have not been fully reviewed and we will withhold comment in this area.

6 References

1. Valente, J. et al., MAAP 3.0B Code Evaluation, Final Report, May 1992.

2. Kenton, M.A. and Gabor, J.R., "Recommended Sensitivity Analyses for an Individual Plant Examination Using MAAP 3.0B," Gabor, Kenton, and Associates, Inc.

3. BWR Mark I MAAP Users Guide, Fauske and Associates, Inc. May 1989.

4. MAAP 3.0B BWR Rev. 7 Transmittal Documentation, FAI/91-12, January 1991.

5. Hohorst, J.K., SCADAP/RELAP5/MOD2 Code, Vol. 4, NUREG/CR-5273, p. 2.2-9, February 1990.

6. Ibid., p. 4.3-2.

7. Cole, R.K., et al., "CORCON-Mod 2; A Computer Program for Analysis of Molten-Core Concrete Interactions," NUREG/CR-3920, p. 39, August 1984.

APPENDIX C - Plots

```
*************************************************************************
*************************************************************************
***     Reactor:                  Peach Bottom BWR 4/MK 1
***     Sequence:                 Long Term Station Blackout Without Depressurization
***     Compartments:     RPV(6), DW(1), WW(1), SC(9), ENV(1)
*************************************************************************
*************************************************************************
***  MODIFICATIONS SUMMARY
***
***  MOD NAME DATE        DESCRIPTION
***
***   0  CJS  02/24/88 - FRESH START - STRIPPED OLD HISTORY
***                      FROM PB6G.DAT, ADDED NEW DECAY HEAT TABLE,
***                      VENT DOWNCOMER MODEL, RADIATIVE HEAT TRANSFER,
***                      PUMP AND CRD LEAKAGE, RELTRAC CONTROL FUNCTIONS,
***                      CONTAINMENT VENT PATHS, NEW RS INPUT.
***   1  IEM  12/01/88   REMOVED RELTRAC CF'S AS SEPARATE FILE RELTRC.DAT;1.
***   2  IEM  02/16/88   MODIFIED SEVERAL INPUT PARAMETERS IN COR PKG.
*************************************************************************
*************************************************************************
* LN 7.27.90 Filenames are changed
* TITLE      SB-LT-W/O-DEP
TITLE     'Peach-Bottom'
JOBID      'SBO-Time0'
* CRTOUT
* OUTPUTF
* RESTARTF
* DIAGF
DTTIME    0.1
*************************************************************************
*************************************************************************
*** NON-CONDENSIBLE GASES PACKAGE
*************************************************************************
***         GAS   MATERIAL NUMBER
NCG000      O2        4
NCG001      N2        5
NCG002      H2        6
NCG003      CO        7
NCG004      CO2       8
NCG005      CH4       9
*************************************************************************
*************************************************************************
*** CONTROL VOLUME HYDRODYNAMICS PACKAGE
*************************************************************************
***         CV 100 is the Drywell
***
CV10000   DRYWELL   2   2   2
CV100A0   2
* MAAP value for pressure, 1.041e5, 12.10.90
* Relative humidity 50 % (JV) 02.01.91
CV100A1   PVOL    1.041E5        PH2O   8630.0
* CV100A1   PVOL    1.0108E5       PH2O   0.0
* MAAP value for atmosphere temperature, 12.10.90
CV100A2   TATM    330.0  TPOL    300.0
CV100A3 MFRC.1 0.                MFRC.3 0.0
* Inerted containment (JV) 02.01.91
CV100A4 MFRC.5 1.0          MFRC.4 0.0
* CV100A4 MFRC.5 .7671       MFRC.4 .2329
* previously CV100A0 3
* CV100A3   MASS.1  0.0       MASS.2  0.0
* CV100A4   MLFR.5 .7671     MLFR.4  0.2329
***
***         ALTITUDE   VOLUME
CV100B1     -9.093       0.
CV100B2     -8.636       6.106
CV100B3     -8.331      46.376
CV100B4     23.496    4236.0
***
***         Agrees with ORNL MARCON input (floor area = 1422.1 ft**2, height to
***         lower lip of vent lines = 1.0 ft, total free volume = 166605 ft**3
***         JLS  11/19/85
***         Corrected units conversion error for elevation of lower lip
***         and added sump volume to table
***         SED   9/12/86
***         Corrected for the addition of the vent/downcomer volume CV150
***         CJS  2/24/88
*************************************************************************
***         CV 150 is the Downcomer Volume
***
***    ...  check initial atm. & liq.  temperatures, pressures, PH2O.LN
*           content of phases ...  in all compartments
CV15000   VENT/DOWNCOMER   2   2   2
CV150A0   3
* Relative humidity 50 % (JV) 02.01.91
CV150A1   PVOL    1.041E5     PH2O  8630.0
* CV150A1   PVOL    1.041E5     PH2O  0.0
CV150A2   TATM    330.0       TPOL  305.0
* wetwell volume, ln 12.10.90
CV150A3   ZPOL    -11.86      VFOG    0.0
* CV150A3   ZPOL    -11.435        VFOG    0.0
* Inerted containment (JV) 02.01.91
```

```
CV150A4   MLFR.5  1.0       MLFR.4  0.0
* CV150A4   MLFR.5  0.7671       MLFR.4  0.2329
***
***        ALTITUDE   VOLUME
CV150B1     -12.81       0.0
CV150B2     -10.63      82.0
CV150B3      -9.07     257.0
CV150B4      -5.59     565.0
********************************************************************************
***        CV 200 is the Wetwell
***   ...  check initial atm. & liq.  temperatures, pressures, PH2O. LW
CV20000   WETWELL   2   2   3
CV20003   47.33  *  CV area for velocity calculation
CV200A0   3
* Relative humidity 50 % (JV) 02.01.91
CV200A1   PVOL    1.041E5          PH2O  2410.0
* CV200A1   PVOL    1.041E5          PH2O  -1.0
CV200A2   TATM    305.0   TPOL    305.0
* wetwell volume, ln 12.10.90
CV200A3   ZPOL   -11.86        VFOG    0.0
* CV200A3   ZPOL   -11.435     VFOG    0.0
CV200A4   MLFR.5  1.00
***
***        ALTITUDE   VOLUME
CV200B1     -16.38       0.0
CV200B2     -15.16     572.7
CV200B3     -13.33    2114.3
CV200B4     -12.81    2629.6
CV200B5     -12.11    3298.1
CV200B6     -11.76    3647.5
CV200B7     -11.50    3898.0
CV200B8     -10.63    4837.2
CV200B9     -10.28    5088.3
CV200BA      -9.07    6033.7
CV200BB      -8.46    6547.6
CV200BC      -6.93    7132.5
* wetwell volume, ln 12.10.90
* FSAR total volume based on averages of two numbers (from - to)
* is very close:  7233 m3, we leave the original value
* The average liquid volume is 3549 m3 (FSAR). This value corresponds to
* the initial water level of 11.86 m (the original was -11.435 m
* at 7h 50' )
***
***        Data corrected for addition of CV150 and expanded to include
***        entire instrumentation volume table - CJS 2/24/88
********************************************************************************
***        SIX-VOLUME PRIMARY SYSTEM FROM MARCON VOLUME/ALTITUDE TABLES
********************************************************************************
***        CV 310 is the Reactor Pressure Vessel Annulus
***
* 01.16.91:  equilibrium option, no vapor - level lower:  worked!
CV31000   ANNULUS  1  2  1    *  NON-EQ TH, VERT FLOW, PRI CV
* CV31000   ANNULUS  2  2  1    *  NON-EQ TH, VERT FLOW, PRI CV
* Time0:  switching to 3, 11.01.90
CV310A0   3                      *  P/T/X DATA
CV310A1   PVOL      7.03E6   *  1030 PSI
* 01.14.91 initial level from 9.0 to 13.0 meters (target 14.5 meters)
* Raise the water inventory to match MAAP and design
* Instability develops...
CV310A2   ZPOL      13.0       * meters
* CV310A3   TPOL    5?7.0        *  DEG K
* CV310A2   PH2O    -1.0          *  PH2O = PVOL
* CV310A3   TATM    -1.0          *  TATM = T(SAT) AT PH2O
* time0:  TPOL 55?.0 originally
* CV310A4   TPOL    547.0        *  DEG K
* CV310A5   MFRC.1   0.8884084  *  MFRC POOL, 89296.5 LBS H2O
* CV310A6   MFRC.2   0.0         *  MFRC FOG
* CV310A7   MFRC.3   0.1115916  *  MFRC STEAM, 11216.4 LBS H2O
***
***        ALTITUDE   VOLUME
CV310BA      3.086     0.0000 * BOTTOM OF SHROUD BAFFLE
CV310BM      8.080    41.0323 * JET PUMP THROAT
CV310BP      9.152    51.5666
CV310BV     10.460    61.1004 * BOTTOM OF SHROUD DOME
CV310B0     11.242    74.3757 * TOP OF SHROUD DOME
CV310B9     15.431   1?3.7962 * TOP OF SEPARATORS
*
* 10.19.90 time0:  Feedwater Flow (quantity per unit time, cvh-UG-17)
* Inject into Lower Plenum instead of downcomer (condensation
* for non-equilibrium case 11.05.90)
CV3?0C1   MASS.1    320    3
CV3?0C2   TE        321    9
*
CF32?00   FW-MASSFLOW    TAB-FUN   1   1.    0.
CF32003   320
CF32010   1.    0.        TIME
*
TF32000   FW-MASSFLOW   5   1.      0.
TF32011   0.     1670.0  10.    1670.0  100.    1670.0   *
TF32013   100.01  0.      1.E6  0.
*
```

```
* sensitivity:  drop temperature to bypass alfa=0.4 problem,
* core uncovery.  11.15.90, original Tfv=464.35 K
CF32100  FW-TEMP   EQUALS  1  1.   0.     *
CF32101  464.35
CF32110  0.       464.35  TIME
*
* CV320C0 MASS.1 320 2 * tabular function:  flow rate, kg/s
* CV320C1 TE 321 5 * tabular function:  temperature, K
*
* flow
* TF32000 WFW 3 1.0 0.0
* TF32010 0.0  1670.0  100.0 1670.0 100.01 0.0
* temperature
* TF32100 TFW 3 1.0 0.0
* TF32110 0.0 464.35   5.0   464.35   100.0 464.35
*
*********************************************************************************
***       CV 320 is the Reactor Pressure Vessel Lower Plenum
***       including the internal volume of the jet pumps
***
CV32000   LOWER-PLENUM  2 2 1 *  NON-EQ TH, VERT FLOW, PRI CV
CV320A0   3                    *  P/T/X DATA
CV320A1   PVOL     7.03E6   *  1030 PSI
CV320A2   ZPOL     5.4943   *  Pool elevation
* CV320A2   PH2O    -1.0          *  PH2O = PVOL
* CV320A3   TATM    -1.0          *  TATM = T(SAT) AT PH2O
* CV320A4   TPOL   547.0         *  DEG K
* CV320A5   MFRC.1   1.000        *  MFRC POOL, 166093.9 LBS H2O
* CV320A6   MFRC.2   0.0          *  MFRC FOG
* CV320A7   MFRC.3   0.0          *  MFRC STEAM
***
***       ALTITUDE   VOLUME
CV320B1     0.000     0.0000  * BOTTOM OF RPV
CV320B2     1.2964   11.4064
CV320B3     2.2757   34.7348
CV320B4     3.2560   61.3489
CV320B5     4.2363   81.8691
CV320B6     5.2166   99.2356
CV320B7     5.4943  103.4594  * BOTTOM OF ACTIVE FUEL
*********************************************************************************
***       CV 330 is the Reactor Pressure Vessel By-Pass
***
* Time0:  change to recommended:  CV330A0 3, previously 2
* CV33000   BY-PASS  2  2  1    *  NON-EQ TH, VERT FLOW, PRI CV
* CV330A0   2                    *  P/T/X DATA
* CV330A1   PVOL     7.03E6   *  1030 PSI
* CV330A2   PH2O    -1.0         *  PH2O = PVOL
* CV330A3   TATM    -1.0         *  TATM = T(SAT) AT PH2O
* CV330A4   TPOL   558.0       *  DEG K
* CV330A5   MFRC.1   0.9944445 *  MFRC POOL, 41700.1 LBS H2O
* CV330A6   MFRC.2   0.0         *  MFRC FOG
* CV330A7   MFRC.3   0.0055555 *  MFRC STEAM, 233.1 LBS H2O
***
* equilibrium
CV33000   BY-PASS  2  2  1    *  NON-EQ TH, VERT FLOW, PRI CV
CV330A0   3                    *  P/T/X DATA
CV330A1   PVOL     7.03E6   *  1030 PSI
CV330A2   ZPOL   9.667       *  Pool elevation
CV330A3   VOID   0.0         *  Initial Void
***
***       ALTITUDE   VOLUME
CV330B7     5.4943    0.0000  * BOTTOM OF ACTIVE FUEL
CV330B8     6.2563    4.7889
CV330B9     7.0183    9.5779
CV330BA     7.7803   14.3668
CV330BB     8.5423   18.9546
CV330BC     9.3043   23.4455
CV330BD     9.667    25.7814  * TOP OF CORE TOP GUIDE
*********************************************************************************
***       CV 340 is the Reactor Pressure Vessel Channel
***
* Time0:  change to recommended:  CV340A0 3, previously 2
* some input is commented out ...
* non-equilibrium
* equilibrium 11.06.90
CV34000   CHANNEL  2  2  1    *  NON-EQ TH, VERT FLOW, PRI CV
CV340A0   3                    *  P/T/X DATA
* sensitivity:  drop initial pressure, keep liquid in, 11.02.90 ...
CV340A1   PVOL     7.03E6   *  1030 PSI
CV340A2   ZPOL     9.667    *  Pool elevation
* initial void, 11.02.90
CV340A3   VOID     0.0      *  Initial void
* CV340A2   PH2O    -1.0         *  PH2O = PVOL
* CV340A3   TATM    -1.0         *  TATM = T(SAT) AT PH2O
* CV340A4   TPOL   558.0       *  DEG K
* CV340A5   MFRC.1   0.9944445 *  MFRC POOL, 53860.8 LBS H2O
* CV340A6   MFRC.2   0.0         *  MFRC FOG
* CV340A7   MFRC.3   0.0055555 *  MFRC STEAM, 300.7 LBS H2O
***
***       ALTITUDE   VOLUME
CV340B7     5.4943    0.0000  * BOTTOM OF ACTIVE FUEL
```

```
CV340B8     6.2563    6.1869
CV340B9     7.0183   12.3739
CV340BA     7.7803   18.5608
CV340BB     8.5423   24.4793
CV340BC     9.3043   30.2791
CV340BD     9.667    33.2959  * TOP OF CORE TOP GUIDE
*******************************************************************************
* 10.30.90 time0  liquid-steam mixture
***         CV 350 is the Reactor Pressure Vessel
***         Shroud Dome, Pipes, and Separators
* Time0:  change to recommended:  CV350A0 3, previously 2
* some input is commented out ...
* equilibrium
***
CV35000     SHROUD-DOME  2 2 1  *  NON-EQ TH, VERT FLOW, PRI CV
CV350A0     3                   *  P/T/X DATA
CV350A1     PVOL      7.03E6   *  1030 PSI
* Code interpretation of input, p.  CVH-UG-15
* 11.07.90
CV350A2     ZPOL      13.000     *  Pool elevation
CV350A3     VOID      0.0        *
* CV350A2     PH2O      -1.0        *  PH2O = PVOL
* CV350A3     TATM      -1.0        *  TATM = T(SAT) AT PH2O
* CV350A4     TPOL    558.0        *  DEG K
* CV350A5     MFRC.1    0.95        *  MFRC POOL
* CV350A6     MFRC.2    0.0         *  MFRC FOG
* CV350A7     MFRC.3    0.05        *  MFRC STEAM
***
***         ALTITUDE    VOLUME
CV350BA      9.667      0.0000 * TOP OF CORE TOP GUIDE
CV350BD     10.460     17.9923 * BOTTOM OF SHROUD DOME
CV350BH     11.062     27.2877 * TOP OF SHROUD DOME
CV350BR     15.431     44.9011 * TOP OF SEPARATORS
*******************************************************************************
***         CV 360 is the Reactc. Pressure Vessel
***         Dryer Region and Steam Dome
***
CV36000     STEAM-DOME   2 2 1  *  NON-EQ TH, VERT FLOW, PRI CV
CV360A0     3                   *  P/T/X DATA
CV360A1     VOID   0.999   *
CV360A2     PVOL      7.03E6   *  1030 PSI
* CV360A2     PH2O      -1.0        *  PH2O = PVOL
* CV360A3     TATM      -1.0        *  TATM = T(SAT) AT PH2O
* CV360A4     TPOL    558.0        *  DEG K
* CV360A5     MFRC.1    0.0         *  MFRC POOL
* CV360A6     MFRC.2    0.0         *  MFRC FOG
* CV360A7     MFRC.3    1.000       *  MFRC STEAM, 18796.2 LBS H2O
***         ALTITUDE    VOLUME
CV360BA     15.431      0.0000 * TOP OF SEPARATORS
CV360BC     16.439     30.5896 * BOTTOM OF MAIN STEAM LINE
CV360BE     17.018     89.1637 * TOP OF MAIN STEAM LINE
CV360BR     22.243    218.5968 * TOP OF RPV
***
* 10.22.90 time0:  steamline connected to a huge sink volume
* Valve closes on time:  CF 43
CV42000 SL-SINK   2  2  1
CV420A0 3
CV420A1 PVOL  7.01E06      RNUM 1.0
CV420A2 VPOL  0.0          VFOG 0.0
***         ELEV  VOL
CV420B1  -17.2      0.
CV420B2    45.          1.E10
*
FL04200 SL-PATH     360     420     22.243     22.243
FL04201  1.589  0.5   1.0
FL04202  3   0   0   0
FL04203  1.0   1.0
FL042S1  1.589   0.5   1.422
FL042V0  -43  43 43
*
CF04300 MSIV TAB-FUN 1 1.0 0.0
CF04303 43
CF04310 1.0 0.0 TIME
* close in 3 seconds
TF04300  MSIV 3 1.0 0.0
TF04311  0.0 1.0    100.0 1.0   103.0 0.0
*******************************************************************************
***         CV 401 is the Torus Room
***
CV40100 'TORUS RM'        2  2  4        *  NON-EQ TH, VERT FLOW, CONT CV
CV401A0 2                                *  P/T/X DATA
CV401A1 PVOL 100000.              PH2O  0.0
CV401A2 TATM 295.0          TPOL 295.0
CV401A3 MFRC.1 0.                     MFRC.3 0.0
CV401A4 MFRC.5 .7671       MFRC.4 .2329
***         ELEV        VOL
CV401B1  -17.2           0.
CV401B2   -4.1       5426.
*******************************************************************************
***         CV 402 is the Southern half of the 135 Level
***
```

```
CV40200 LEV-135-SOUTH     2  2  4
CV402A0 2
CV402A1 PVOL  100000.           PH2O  0.0
CV402A2 TATM  295.0         TPOL 295.0
CV402A3 MFRC.1 0.                    MFRC.3 0.0
CV402A4 MFRC.5 .7671       MFRC.4 .2329
***         ELEV     VOL
CV402B1    -4.1        0.
CV402B2     5.1     5154.
*****************************************************************************
***        CV 403 is the Northern half of the 135 Level
***
CV40300 LEV-135-NORTH     2  2  4
CV403A0 2
CV403A1 PVOL  100000.           PH2O  0.0
CV403A2 TATM  295.0         TPOL 295.0
CV403A3 MFRC.1 0.                    MFRC.3 0.0
CV403A4 MFRC.5 .7671       MFRC.4 .2329
***         ELEV     VOL
CV403B1    -4.1        0.
CV403B2     4.5     5154.
*****************************************************************************
***        CV 404 is the Southeast quadrant of the 165 Level
***
CV40400 LEVEL-165-SE    2  2  4
CV404A0 2
CV404A1 PVOL  100000.           PH2O  0.0
CV404A2 TATM  295.0         TPOL 295.0
CV404A3 MFRC.1 0.                    MFRC.3 0.0
CV404A4 MFRC.5 .7671       MFRC.4 .2329
***         ELEV     VOL
CV404B1     5.1        0.
CV404B2    14.2     2356.
*****************************************************************************
***        CV 405 is the remainder of the 165 Level
***
CV40500 LEVEL-165-MAIN  2  2  4
CV405A0 2
CV405A1 PVOL  100000.           PH2O  0.0
CV405A2 TATM  295.0         TPOL 295.0
CV405A3 MFRC.1 0.                    MFRC.3 0.0
CV405A4 MFRC.5 .7671       MFRC.4 .2329
***         ELEV     VOL
CV405B1     5.1        0.
CV405B2    13.6     7066.
*****************************************************************************
***        CV 406 is the Southeast quadrant of the 195 Level
***
CV40600 LEVEL-195-SE    2  2  4
CV406A0 2
CV406A1 PVOL  100000.           PH2O  0.0
CV406A2 TATM  295.0         TPOL 295.0
CV406A3 MFRC.1 0.                    MFRC.3 0.0
CV406A4 MFRC.5 .7671       MFRC.4 .2329
***         ELEV     VOL
CV406B1    14.2        0.
CV406B2    26.1     2452.
*****************************************************************************
***        CV 407 is the remainder of the 195 Level
***
CV40700 LEVEL-195-MAIN  2  2  4
CV407A0 2
CV407A1 PVOL  100000.           PH2O  0.0
CV407A2 TATM  295.0         TPOL 295.0
CV407A3 MFRC.1 0.                    MFRC.3 0.0
CV407A4 MFRC.5 .7671       MFRC.4 .2329
***         ELEV     VOL
CV407B1    14.2        0.
CV407B2    25.5     4866.
*****************************************************************************
***        CV 408 is the Refueling Bay
***
CV40800 REFUELING-BAY   2  2  7
CV408A0 2
CV408A1 PVOL  100000.           PH2O  0.0
CV408A2 TATM  295.0         TPOL 295.0
CV408A3 MFRC.1 0.                    MFRC.3 0.0
CV408A4 MFRC.5 .7671       MFRC.4 .2329
***         ELEV     VOL
CV408B1    26.1        0.
CV408B2    45.0    31048.
*****************************************************************************
***        CV 409 is the Turbine Building
***
CV40900 TURBINE-BUILDING  2  2  5
CV409A0 2
CV409A1 PVOL  100000.           PH2O  0.0
CV409A2 TATM  295.0         TPOL 295.0
CV409A3 MFRC.1 0.                    MFRC.3 0.0
CV409A4 MFRC.5 .7671       MFRC.4 .2329
***         ELEV     VOL
```

```
CV409B1     5.1         0.
CV409B2    21.9    148826.
*****************************************************************************
***      CV 410 is the Environment
***
CV41000 ENVIRONMENT   2  2  6
CV410A0 2
CV410A1 PVOL  100000.          PH2O  0.0
CV410A2 TATM  296.0        TPOL 296.0
CV410A3 MFRC.1 0.                   MFRC.3 0.0
CV410A4 MFRC.5 .7671      MFRC.4 .2329
***        ELEV  VOL
CV410B1  -17.2      0.
CV410B2    46.           1.E10
*****************************************************************************
*****************************************************************************
*** FLOW PATH PACKAGE INPUT
*****************************************************************************
*****      MSL/SRV Flow Path
*****      From RPV MSL outlet to T-Quencher in Wetwell
*****
FL36200  STEAM-LINE-SRV  360  200  16.73  -15.01
FL36201  0.1319   47.15   0.0   0.6614   0.2794
FL36202  0  0  0  1  *  VERT, ACTIVE, NO BUBBLES, BUBBLES
FL36203  5.0  5.0
FL362V0  -1  105  105
FL362S1  0.1319   47.15   0.4511   5.E-6
***
***        BROWNS FERRY, DIVIDE SRV'S INTO FOUR MONOTONE GROUPS
***        REC  07/01/86
***
***        CF105 GIVES FRACTION OPEN OF THE MSL/SRV FLOW PATH (FL362)
***        IT IS THE SUM OF 4 CONTROL FUNCTIONS, EACH GIVING THE NUMBER
***        OF VALVES OPEN IN ONE SUBSET WITH MONOTONE OPEN/CLOSE
***        CHARACTERISTICS
***
CF10500   SRV   ADD    4    0.0604  0.0  *SF = 0.604 = 0.7855/13
CF10511   1.        0.      CFVALU.101           *NUMBER OPEN IN GROUP 1
CF10512   1.        0.      CFVALU.102           *NUMBER OPEN IN GROUP 2
CF10513   1.        0.      CFVALU.103           *NUMBER OPEN IN GROUP 3
CF10514   1.        0.      CFVALU.104           *NUMBER OPEN IN GROUP 4
***
CF10100   SRV-1  HYST   1    1.0      0.0  *GROUP 1, SRVS 1,6,9
CF10101   0.0                              *INITIAL VALUE
CF10103   -11   -21                        *LOAD/UNLOAD TF NUMBERS
CF10110   1.0   0.0     CFVALU.99
***
***        TF011 GIVES THE NUMBER OF VALVES IN GROUP 1
***        WHICH ARE OPEN AS A FUNCTION OF RISING PRESSURE DIFFERENCE
***
TF01100  SRV-LOAD-1     6    1.0      0.0
***
***       PRESSURE  NUMBER OPEN
TF01110  7.68759E6  0.0
TF01111  7.68760E6  1.0   *SRV 1 (1115 PSI)
TF01160  7.79101E6  1.0
TF01161  7.79102E6  2.0   *SRV 6 (1130 PSI)
TF01190  7.84617E6  2.0
TF01191  7.84618E6  3.0   *SRV 9 (1138 PSI)
***
***        TF021 GIVES THE NUMBER OF VALVES IN GROUP 1
***        WHICH ARE OPEN AS A FUNCTION OF FALLING PRESSURE DIFFERENCE
***
TF02100  SRV-UNLOAD-1   6    1.0      0.0
***
***       PRESSURE  NUMBER OPEN
TF02110  7.25322E6  0.0
TF02111  7.25323E6  1.0   *SRV 1 (1052 PSI)
TF02160  7.32217E6  1.0
TF02161  7.32218E6  2.0   *SRV 6 (1062 PSI)
TF02190  7.39112E6  2.0
TF02191  7.39113E6  3.0   *SRV 9 (1072 PSI)
***
CF10200   SRV-2  HYST   1    1.0      0.0  *GROUP 2, SRVS 2,3,7,8,12
CF10201   0.0                              *INITIAL VALUE
CF10203   -12   -22                        *LOAD/UNLOAD TF NUMBERS
CF10210   1.0   0.0     CFVALU.99
***
***        TF012 GIVES THE NUMBER OF VALVES IN GROUP 2
***        WHICH ARE OPEN AS A FUNCTION OF RISING PRESSURE DIFFERENCE
***
TF01200  SRV-LOAD-2    10    1.0      0.0
***
***       PRESSURE  NUMBER OPEN
TF01220  7.70827E6  0.0
TF01221  7.70828E6  1.0   *SRV 2 (1118 PSI)
TF01230  7.72206E6  1.0
TF01231  7.72207E6  2.0   *SRV 3 (1120 PSI)
TF01270  7.79791E6  2.0
TF01271  7.79792E6  3.0   *SRV 7 (1131 PSI)
TF01280  7.82848E6  3.0
```

```
TF012B1  7.82549E6  4.0    *SRV 8 (1135 PSI)
TF012C0  7.89443E6  4.0
TF012C1  7.89444E6  5.0    *SRV 12 (1145 PSI)
***
***       TF022 GIVES THE NUMBER OF VALVES IN GROUP 2
***       WHICH ARE OPEN AS A FUNCTION OF RISING PRESSURE DIFFERENCE
***
TF02200  SRV-UNLOAD-2   8    1.0     0.0
***
***       PRESSURE  FRACTION OPEN
TF02220  7.10154E6  0.0
TF02221  7.10155E6  1.0    *SRV 2 (1030 PSI)
TF02230  7.18428E6  1.0
TF02271  7.18429E6  3.0    *SRVS 3+7 (1042 PSI)
TF02280  7.24633E6  3.0
TF02281  7.24634E6  4.0    *SRV 8 (1051 PSI)
TF022C0  7.26012E6  4.0
T"022C1  7.26013E6  5.0    *SRV 12 (1053 PSI)
***
CF10300   SRV-3  HYST   1    1.0     0.0  *GROUP 3, SRVS 4,5,10,11
CF10301   0.0                              *INITIAL VALUE
CF10303   -13   -23                        *LOAD/UNLOAD TF NUMBERS
CF10310   1.0   0.0     CFVALU.99
***
***       TF013 GIVES THE NUMBER OF VALVES IN GROUP 3
***       WHICH ARE OPEN AS A FUNCTION OF RISING PRESSURE DIFFERENCE
***
TF01300  SRV-LOAD-3     8    1.0     0.0
***
***       PRESSURE  NUMBER OPEN
TF01340  7.75654E6  0.0
TF01341  7.75655E6  1.0    *SRV 4 (1125 PSI)
TF01350  7.76343E6  1.0
TF01351  7.76344E6  2.0    *SRV 5 (1126 PSI)
TF013A0  7.85996E6  2.0
TF013A1  7.85997E6  3.0    *SRV 10 (1140 PSI)
TF013B0  7.86685E6  3.0
TF013B1  7.86686E6  4.0    *SRV 11 (1141 PSI)
***
***       TF023 GIVES THE NUMBER OF VALVES IN GROUP 3
***       WHICH ARE OPEN AS A FUNCTION OF FALLING PRESSURE DIFFERENCE
***
TF02300  SRV-UNLOAD-3   8    1.0     0.0
***
***       PRESSURE  NUMBER OPEN
TF02340  6.99123E6  0.0
TF02341  6.99124E6  1.0    *SRV 4 (1014 PSI)
TF02350  7.05328E6  1.0
TF02351  7.05329E6  2.0    *SRV 5 (1023 PSI)
TF023A0  7.11533E6  2.0
TF023A1  7.11534E6  3.0    *SRV 10 (1032 PSI)
TF023B0  7.30838E6  3.0
TF023B1  7.30839E6  4.0    *SRV 11 (1060 PSI)
***
CF10400   SRV-4  HYST   1    1.0     0.0  *GROUP 4, SRV 13
CF10401   0.0                              *INITIAL VALUE
CF10403   -14   -24                        *LOAD/UNLOAD TF NUMBERS
C"10410   1.0   0.0     CFVALU.99
***
***       TF014 GIVES THE NUMBER OF VALVES IN GROUP 4
***       WHICH ARE OPEN AS A FUNCTION OF RISING PRESSURE DIFFERENCE
***
TF01400  SRV-LOAD-4     2    1.0     0.0
***
***       PRESSURE  NUMBER OPEN
TF014D0  7.90822E6  0.0
TF014D1  7.90823E6  1.0    *SRV 13 (1147 PSI)
***
***       TF024 GIVES THE NUMBER OF VALVES IN GROUP 4
***       WHICH ARE OPEN AS A FUNCTION OF FALLING PRESSURE DIFFERENCE
***
TF02400  SRV-UNLOAD-4   2    1.0     0.0
***
***       PRESSURE  NUMBER OPEN
TF024D0  6.99812E6  0.0
TF024D1  6.99813E6  1.0    *SRV 13 (1015 PSI)
***
***       CF99  gives the pressure difference between the primary system
***       and the drywell
***
CF09900  PDIF  ADD  2  1.  0.
CF09910  1.0  0.0  CVH-P.360  *  PRESSURE IN STEAM DOME
CF09911 -1.0  0.0  CVH-P.100  *  PRESSURE IN DRYWELL
******************************************************************************
***       Wetwell/Drywell vacuum breaker Flow Path
***       From the Wetwell through the vacuum breakers
***         to the Vent Lines (effectively to the Drywell)
***
FL02100  WET-DRY-VACBV   200   100   -10.13   -6.61
FL02101  1.86   0.5   0.0   0.445   2.06
FL02102  3  0  0  0  *  HORIZ, ACTIVE, ATMOS/ATMOS, ATMOS/ATMOS
```

```
FL02103  1.0  1.0
FL021V0  -1    2    2
FL021S1  1.86   0.5   0.445   5.E-6
***
***     CF001, CF002, and TF030 open and close the
***       vacuum relief valves at 0.5 psi (3447 Pa)
***       differential pressure between the wetwell
***       and the drywell
***
***         CF002 = SF*TF030 where SF = 1.0
***         TF030 = function (CF001)
***         CF001 = P.CV200 - P.CV100
***
CF00200  VAC-RV    TAB-FUN   1   1.00   0.00
CF00203  30
CF00210  1.00     0.00    CFVALU.001
***
***         CF200 = wetwell pressure - drywell pressure
***
CF00100  VAC-RV-DP     ADD   2   1.00   0.00
CF00110   1.00  0.00  CVH-P.200
CF00111  -1.00  0.00  CVH-P.100
***
TF03000  VAC-RV-AREA   4   1.00   0.00
***
***       FRACTION OPEN    PRESSURE
TF03010  0.00               0.00
TF03011  3.444E+03          0.00
TF03012  3.447E+03          1.00
TF03013  2.000E+04          1.00
*****************************************************************************
***        Vent Lines/Vent Header/Downcomers
***        From the Drywell to the Wetwell
***
FL01200  VENT-OPENING  100  150  -6.7   -6.7
FL01201  26.6   13.1    1.0   0.73   0.73
FL01202  0  0  0  0
FL01203  6.7  6.7
FL012S1  26.6   13.1    1.31   5.E-6
*******
FL02000  DOWNCOMEREX   150   200    -12.81     -12.81
FL02001  26.6   3.9   1.0   0.001    0.001
FL02002  0   0   0   1
FL02003  1.0   1.0
FL020S1  26.6    3.9   1.31   5.0E-6
*****************************************************************************
*****    Pump Seal Leakage Taken From Downcomer Vol 310 (45 % )
*****
FL37000  LEAKAGE-DOWN   310  100  6.838   -6.0
FL37001  2.783E-6   0.15   1.0
FL37002  3  0  0  0
FL37003  1.0  1.0
FL370S1  2.783E-6    0.15   0.001631
*****************************************************************************
*****    CRD Seal Leakage Taken From Lower Plenum (55 % )
*****
FL37100  LEAKAGE-LP   320  100    0.1     -6.0
FL37101  3.399E-6   0.15   1.0
FL37102  0  0  0  0
FL37103  1.0  1.0
FL371S1  3.399E-6    0.15   0.001804
*****************************************************************************
***       RPV FLOW PATHS
***
***  FLOW PATH ZFM AND ZTO CONSISTENT WITH HEIGHTS AND BOTTOM OF CONTROL VOLUMES
***  HYDRAULIC DIAMETERS AND FRICTION FACTORS CONSISTENT WITH LASALLE DECK
***  JMM  01/16/86
*****************************************************************************
* 12.11.90 Open flow path for transient (after VELOCITY bounda y
* closes the FL312 path, VELOCITY=0.0)
FL31100  DC-LP     310     320  8.080 3.086 * 8.080 M = open flow a. ~a
FL31101  0.6782  4.9936   1.0     0.1524   0.1524  *  DC-LP
FL31102    0        0           0          0  *  DC-LP
FL31103  0.0785   17.0     *
FL31104   0.0      0.0      *  Initial velocity
FL311S1  0.6782  4.9936  .27783  5.0E-06  18.0  *
FL311V1  -313  313  313
* open downcomer after steady state is completed, 12.12.90
*
CF31300 DC-VALVE TAB-FUN 1 1.0 0.0
CF31303 313
CF31310 1.0 0.0 TIME
* open in 4 seconds
TF31300  DC-VALVE 3 1.0 0.0
TF31311  0.0 0.0    100.0 0.0    104.0 1.0
*
***PATH  FLNAME  KCVFM  KCVTO   ZFM      ZTO
FL31200  AN-LP     310     320  8.080 3.086 * 8.080 M = JET PUMP THROAT
FL31201  0.6782  4.9936   1.0     0.1524   0.1524  *  AN-LP
* 10.19.90 time0: pump model
* FL312P0  QUICK-CF 312
```

```
* CF31200 PUMP-HEAD EQUALS 1 0.0 1.2E06 * Pa
* CF31210 1.0 0.0 TIME
* 10.24.90: following SANDIA, Carmel, 10.22.90
FL312T1  2 312
*
CF31200 JPUMP-VELOCITY TAB-FUN 1 1.0 0.0
CF31203 312
CF31210 1.0 0.0 TIME
* 12869-1670 kg/s, density at 547 K is 761 kg/m3, area 0.6782
* velocity 21.7 m/s
* velocity boundary condition is not working right ...
* 11.16.90 sensitivity:  flow drops by about 23 % .  Increase velocity ...
* from 21.7 to 26.7    Core uncovers ...
* 11.29.90 increase velocity to 26.7 from time 0.0
* 11.30.90 increase velocity to 28.3 to get SS flow more exact
* 01.16.91 equilibrium downcomer:  flow increased.  Drop velocity...
* from 28.3 to 22.96 based on flow overprediction
TF31200 JPUMP-VELOCITY 4 1.0 0.0
* reduce velocity over 4 seconds
TF31211 0.0 22.4   1.0 22.4   100.0 22.4  104.0  0.0
* end of the "jet pump model"
* Connection of steam dome to the downcomer, 11.09.90
* close the connection:  downcomer-to-dome steam flow 300 kg/s
* severe overpressurization, code stops
FL36000  DOME-DOWNC  360     310     15.431  15.431
FL36001  13.9    0.5      1.0    .19    .19           *  From GG deck
FL36002  1   0   0   0                                *  DM-DC
* 11.16.90 J. Valente increase by 100 times ...
* FL36003  0.11 0.11                                   *  DM-DC
FL36003  11.0 11.0                                    *  DM-DC
FL360S1  13.9 0.5  0.74  5.E-6                        *  DM-DC
*
FL32300  LP-BP    320     330     5.4943   5.4943
FL32400  LP-CH    320     340     5.4943   5.4943
FL34500  CH-SH    340     350     9.667    9.667
FL33500  BP-SH    330     350     9.667    9.667
FL35600  SH-SD    350     360    15.431   15.431
* 10.18.90 time0:  steam separators to downcomer ..   check initial
* water level elevation
* 01.16.91:  inject carry-over water at 9 meters (origin.lly 13 m) no...
FL36100  SS-AN       360     310    13.000    13.000
***
***PATH  FLARA   FLLEN   FLOPO   FLHGTF   FLHGTT      FLNAME
FL32301  6.1502  1.9050   .01289 0.1524   0.0254  *  LP-F/
* 11.07.90 Note initial opening 0.61748
FL32401  7.9428  1.9050   .61748 0.1524   0.1016  ·· LP-CH
* 10.23.90 time0
* steady-state (see Carmel's Memo, October 22, 1990, Sandia)
* opening areas:  1.0
* 11.26.90 Full height junction, JV
* FL33501  6.1502  1.9050   1.0     4.2       2.2      *  BP-SH
* FL34501  7.9428  1.9050   .61748 4.2       2.2      *  CH-SH
* 11.29.90 reduced junction heights
FL33501  6.1502  1.9050   1.0     0.1       2.2      *  BP-SH
FL34501  7.9428  1.9050   .61748 1.2       2.2      *  CH-SH
*
FL35601  4.7763  4.1885   1.0     5.0       5.0      *  SH-SD
FL36101 26.1069  5.3492   1.0
***
***PATH  SAREA   SLEN     SHYD    SRGH      SLAM      FLNAME
* segment area equal to flow area ...  11.14.90
* org FL312S1  0.0339  4.9936  .27783  5.0E-06  16.0  *  AN-LP
FL312S1  0.6782  4.9936  .27783  5.0E-06  16.0  *
FL323S1  6.1502  1.9050  .05841  5.0E-06  16.0  *  LP-BP
FL324S1  7.9428  1.9050  .01359  5.0E-06  16.0  *  LP-CH
FL335S1  6.1502  1.9050  .05841  5.0E-06  16.0  *  BP-SH
FL345S1  7.9428  1.9050  .01359  5.0E-06  16.0  *  CH-SH
FL356S1  4.7763  4.1885  .00878  5.0E-06  16.0  *  SH-SD
FL361S1 26.1069  5.3492  .73944  5.0E-06  16.0  *  SS-AN
***
***PATH  FRICFO   FRICRO     FLNAME   DF      DT
FL31203  0.0785   17.0     *  AN-LP    0.2078  5.3066
* 11.19.90 increase velocity to 27.1 from time 0.0 (orig.  21.7)
* 01.16.91 equilibrium downcomer:  flow increased.  Dr~ velocity...
* from 28.3 to 22.4  based on flow overprediction
FL31204  22.4     22.4    *  Initial velocity
* 10.26.90 time0:  bypass entrance form loss coefficients ...  check
* bypass
*
FL32303  0.5188   4.97    *  LP-BP    5.0201  2.7983
*
FL32304  16.000  16.000   *  initial velocities, 11.02.90
* 10.26.90 time0:  in-channel entrance form loss coefficients ...  check
FL32403  10.216   13.267  *  LP-CH    5.0201  3.1801
FL32404   0.0     3.4000  *  initial velocities 11.02.90
* 10.26.90 time0:  core exit form loss coefficients
* bypass exit
FL33503  50.0     0.5     *  BP-SH    2.7983  4.3326
FL33504  0.25     0.25    *  BP-SH    initial velocity
* core exit
FL34503  5.6885   5.6885  *  CH-SH    3.1801  4.3326
```

```
FL34504 0.0      3.4    * CH-SH    initial velocity
* exit from steam separators
FL35603 12.565  5.0475 * SH-SD    2.4660 6.3557
* Following GG deck, 11.01.90 Time0.  Removed 11.06.90 overpressurization
* 35604 10.0  0.0        * velocity
* FL36103 0.11     0.11    * SD-AN    6.3557 5.7654
* Time0:  Follow GG deck, 11.09.90, initial velocity
FL36104 0.50     0.60    * SD-AN    initial velocity
***
***PATH  KFLGFL  XACTFL   IBUBF   IBUBT   FLNAME
FL31202   0       0        0        0  *  AN-LP
FL32302   0       0        0        0  *  LP-BP
FL32402   0       0        0        0  *  LP-CH
* 11.20.90 liquid only
FL33502   0       0        0        0  *  BP-SH
* 11.20.90 liquid only
FL34502   0       0        0        0  *  CH-SH
FL35602   1       0        0        0  *  SH-SD
* 10.19.90 time0:  steam separators to downcomer
* 11.16.90 J. Valente:  general junction instead of liquid only (2)
* 01.15.90 General...  instability develops
FL36102   2       0        0        0  *  SS-AN Liquid First
* second path from core (steam only):  "steam sucker", 11.20.90
* FL34600  CH-SH2   340    350    9.500    9.667
* FL34601  7.9428  1.9050   .61748 0.15     0.15    *  CH-SH2
* FL346S1  7.9428  1.9050  .01359  5.0E-06  16.0  *  CH-SH2
* FL34603  5.6665   5.6665  *  CH-SH2   3.1601  4.3326
* FL34602   1       0       0        0  *  CH-SH2
*********************************************************************************
***       SECONDARY CONTAINMENT FLOW PATHS
*********************************************************************************
* failure area is changed to 0.1 from 0.102 m2   12.13.90
FL40000    'CONT FAIL'   100  401  -5.0    -5.0
FL40001    .1    0.001 0.0             * INITIALLY CLOSED
FL40002    3 * HORIZONTAL FLOW PATH
FL40003    0.593   0.593
FL40050    .1    0.001  1.0
FL400V0    150  145  145
***
***        CF150 opens the flow path from the drywell to the reactor
***        building at containment failure, CF145 sets the fraction open
***
CF14500    CONT-BRK  EQUALS  1  0.0  1.0
CF14510    1.0  0.0  TIME
***
* failure pressure is changed to .908 MPa from 0.910 MPa  12.13.90
CF15000    'FAIL THRESH' T-O-F  1  1.  0.
* 03.01.9\ JV adjust to have both pressure and temperature failure
* modes ...
* CF15003    -1.E9    992.0
* CF15010     1.0    0.0    HS-TEMP.1000101
* 4.15.91 JV: replacing temperature falure limit by the OLD limit
* on drywell atmosphere pressure.  Done after adding drywell wall
* concrete heat slab model.
CF15003     -1.E9  9.08E5
CF15010     1.  0.  CVH-P.100
***
*
***        NAME                FROM     TO      ZFROM        ZTO
FL40100 TORUS-135             401     402      -4.7        -4.1
FL40200 135-165-SHAFT         402     404       4.5         5.1
FL40300 135-SO-NO             402     403        .2          .2
FL40400 LEAK-135-SO           402     410        .2          .2
FL40500 NO-135-TURB           403     409        .2         6.2
FL40600 LEAK-135-NO           403     410        .2          .2
FL40700 165-195-SHAFT         404     406      13.6        14.2
FL40800 165-SE-MAIN           404     405       9.35        9.35
FL40900 LEAK-165-SE           404     410       9.35        9.35
FL41000 LEAK-165-MAIN         405     410       9.35        9.35
FL41100 195-SE-REFUEL         406     408      25.5        26.1
FL41200 195-SE-MAIN           406     407      19.85       19.85
FL41300 LEAK-195-SE           406     410      19.85       19.85
FL41400 LEAK-195-MAIN         407     410      19.85       19.85
FL41500 NO-REFUEL-ENV         408     410      34.9        34.9
FL41600 LEAK-REFUEL           408     410      35.55       35.55
FL41700 LEAK-TURB             409     410      13.5        13.5
***
***        AREA      LENGTH   FLOPO    HGTF    HGTTO
FL40101    8.6        .86      1.              .3      .3
FL40201   33.2       3.32      1.              .3      .3
FL40301   25.                 2.5       1.           .3      .3
FL40401    0.025     .0025     1.              .1      .1
FL40501    2.8        .28      0.              .3      .3
FL40601    0.025     .0025     1.              .1      .1
FL40701   33.2       3.32      1.              .3      .3
FL40801   43.8       4.38      1.              .3      .3
FL40901    0.025     .0025     1.              .1      .1
FL41001    0.025     .0025     1.              .1      .1
FL41101   33.2       3.32      1.              .3      .3
FL41201   74.6       7.46      1.              .3      .3
FL41301    0.025     .0025     1.              .1      .1
```

```
FL41401   0.025      .0025    1.          .1       .1
FL41501  22.3       2.23      0.          .3       .3
FL41601   0.109      0.0109   1.          .1       .1
FL41701   0.29       0.0109   1.          .1       .1
***
***       TYPE   ACTIVE   IBUBF   IBUBTO
FL40102    1       0        0       0
FL40202    1       0        0       0
FL40302    4       0        0       0
FL40402    4       0        0       0
FL40502    1       0        0       0
FL40602    4       0        0       0
FL40702    1       0        0       0
FL40802    4       0        0       0
FL40902    4       0        0       0
FL41002    4       0        0       0
FL41102    1       0        0       0
FL41202    4       0        0       0
FL41302    4       0        0       0
FL41402    4       0        0       0
FL41502    4       0        0       0
FL41602    4       0        0       0
FL41702    4       0        0       0
***
***       FRICFO     FRICREV
FL40103     .5         .5
FL40203     .5         .5
FL40303     .5         .5
FL40403    1.                    1.
FL40503     .5         .5
FL40603     .5         .5
FL40703     .5         .5
FL40803     .5         .5
FL40903    1.                    1.
FL41003    1.                    1.
FL41103     .5         .5
FL41203     .5         .5
FL41303    1.                    1.
FL41403    1.                    1.
FL41503     .5         .5
FL41603    1.                    1.
FL41703    1.                    1.
***
***       SAREA      SLEN    SHYD     SRGH   SLAM
FL401S1   8.5        .01      1.
FL402S1  33.2        .01      1.
FL403S1  25.                  .01      1.
FL404S1   0.025      .01      1.
FL405S1   2.5        .01      1.
FL406S1   0.025      .01      1.
FL407S1  33.2        .01      1.
FL408S1  43.8        .01      1.
FL409S1    .025      .01      1.
FL410S1    .025      .01      1.
FL411S1  33.2        .01      1.
FL412S1  74.5        .01      1.
FL413S1   0.025      .01      1.
FL414S1   0.025      .01      1.
FL415S1  22.3        .01      1.
FL416S1    .109      .01      1.
FL417S1    .29       .01      1.
***
***                  VALVES  -
***       TRIP NO.   CF-ON-FORWARD  CF-ON-REVERSE
FL405V1     110           111            111
FL415V1     140           141            141
***
***       TABULAR AND CONTROL FUNCTIONS FOR VALVE INPUT
***
CF10900  405-DP     ADD    4  1.    0.
CF10910   1.         0.    CVH-P.403
CF10911  -1.         0.    CVH-P.409
CF10912 -42.18  0.     CVH-RHOA.403
CF10913  10.79  0.     CVH-RHOA.409
***
CF11000  405-TRIP  T-O-F  1  1.    0.
CF11003  -1.85  1551.3
CF11010  1.    0.    CFVALU.109
***
CF11100  405-FRAC  HYST    1   1.    0.
CF11103  -410    -400
CF11110  1.    0.    CFVALU.109
***
TF40000  405-UNLOAD  1  1.    0.
TF40010  0.           1.
***
TF41000  405-A-DP  5 1.  0.
TF41010  1551.3  0.1
TF41011  1637.5  0.1857
TF41012  1723.7  0.7429
TF41013  1809.9  0.8357
```

```
TF41014  1896.0  1.
***
CF13900  415-DP     ADD    4  1.    0.
CF13910   1.         0.    CVH-P.408
CF13911  -1.         0.    CVH-P.410
CF13912 -86.33  0.     CVH-RHOA.408
CF13913 511.1   0.     CVH-RHOA.408
***
CF14000  413-TRIP  T-O-F  1  1.     0.
CF14003  -1.E6  2184.6
CF14010  1.   0.    CFVALU.139
***
CF14100  415-FRAC  HYST    1   1.    0.
CF14103  -440   -400
CF14110  1.    0.    CFVALU.139
***
TF44000  415-A-DP  5 1.  0.
TF44010  2184.6  0.1
TF44011  2274.3  0.2
TF44012  2394.0  0.8
TF44013  2513.7  0.9
TF44014  2633.4  1.
*********************************************************************
*********************************************************************
*** HEAT SLAB PACKAGE INPUT
*********************************************************************
***    HS NAMES
***
***SLAB         NAME
HS10001001  DRYWELL-LINER
HS10002001  DRYWELL-FLOOR
HS10003001  UP-REAC-PED
HS10004001  LO-REAC-PED
HS10005001  DRYWELL-STEEL
HS20001001  WETWELL-LINER
HS20002001  WETWELL-STEEL
HS31001001  RPV-CYLINDER
HS32001001  LOWER HEAD
***  TOP GUIDE COMBINED WITH CORE CELL STEEL MASS (RMS  6/04/86)
HS35003001  SEPARATORS * INCLUDES SHROUD DOME (RMS  6/04/86)
HS36001001  DRYERS
HS36002001  UPPER-HEAD
******************************************************************
***    HS MATERIALS
***
***SLAB          MATERIAL       INT      NAME
HS10001201    'CARBON STEEL'    4  *  DRYWELL-LINER
* 4.12.91 Adding containment liner gap and concrete model
* JV & LN
HS10001202     'AIR'              6  *  Liner Gap
HS10001203     'CONCRETE'        11  *  Drywell Wall
HS10002201      CONCRETE         10  *  DRYWELL-FLOOR
HS10003201      CONCRETE          7  *  UP-REAC-PED
HS10004201      CONCRETE          7  *  LO-REAC-PED
HS10005201     'CARBON STEEL'   3  *  DRYWELL-STEEL
HS20001201     'CARBON STEEL'   4  *  WETWELL-LINER
HS20002201     'CARBON STEEL'   3  *  WETWELL-STEEL
HS31001201     'CARBON STEEL'   6  *  RPV-CYLINDER
HS32001201     'CARBON STEEL'   5  *  LOWER-HEAD
HS36003201    'STAINLESS STEEL' 4  *  SEPARATORS
HS36001201    'STAINLESS STEEL' 1  *  DRYERS
HS36002201     'CARBON STEEL'   5  *  UPPER-HEAD
******************************************************************
***    HS GEOMETRIES
***
***SLAB        NO. T  GEOMETRY          INITIAL      NAME
***            NODES  SL CY SP HB RT   N  Y  I
* 4.12.91 Adding containment liner gap and concrete model
* JV & LN
HS10001000    12     1                 0         *  DRYWELL-LINER
* HS10001000     5     1                 0         *  DRYWELL-LINER
HS10002000    11     1                 0         *  DRYWELL-FLOOR
HS10003000     8     1                 0         *  UP-REAC-PED
HS10004000     8     1                 0         *  LO-REAC-PED
HS10005000     4     1                 0         *  DRYWELL-STEEL
HS20001000     5     1                 0         *  WETWELL-LINER
HS20002000     4     1                 0         *  WETWELL-STEEL
HS31001000     7        2              0         *  RPV-CYLINDER
HS32001000     6        2              0         *  LOWER-HEAD, MODELLED AS CYLINDER
HS36003000     5     1                 0         *  SEPARATORS
HS36001000     2     1                 0         *  DRYERS
HS36002000     6                    5  0         *  UPPER-HEAD
******************************************************************
***    HS ELEVATIONS/ORIENTATIONS
***
***SLAB       ELEVATION  ORIENTATION          NAME
***                      VT  HZ  UT
HS10001002      -8.635  1.0                *  DRYWELL-LINER
HS10002002      -8.635  0.0                *  DRYWELL-FLOOR
HS10003002      -0.991  1.0                *  UP-REAC-PED
HS10004002      -8.635  1.0                *  LO-REAC-PED
```

```
HS10005002     -8.635  1.0                  * DRYWELL-STEEL
* 03.01.91 JV
HS20001002    -14.82   1.0                  * WETWELL-LINER
* HS20001002     -11.660  1.0                * WETWELL-LINER
HS20002002    -13.18   1.0                  * WETWELL-STEEL
HS31001002      3.1856 1.0                  * RPV-CYLINDER
HS32001002      1.2964                      * LOWER-HEAD (TOP OF STUB TUBES)
HS35003002     10.92   1.0                  * SEPARATORS
HS36001002     16.18   1.0                  * DRYERS
HS36002002     19.0343 1.0                  * UPPER-HEAD
*****************************************************************************
***   HS D/T FORMATS
***
***SLAB       LOC T   FORMAT   LOCATION          NAME
***           DATA    D/T N-N  L/I BOUNDRY
HS10001100     -1     1          0.0     * DRYWELL-LINER
HS10002100     -1     1          0.0     * DRYWELL-FLOOR
HS10003100     -1     1          0.0     * UP-REAC-PED
HS10004100     -1     1          0.0     * LO-REAC-PED
HS10005100     -1     1          0.0     * DRYWELL-STEEL
HS20001100     -1     1          0.0     * WETWELL-LINER
HS20002100     -1     1          0.0     * WETWELL-STEEL
HS31001100     -1     1          3.1856  * RPV-CYLINDER
HS32001100     -1     1          2.5797  * LOWER-HEAD (RAD OF SHROUD)
HS35003100     -1     1          0.0     * SEPARATORS
HS36001100     -1     1          0.0     * DRYERS
HS36002100     -1     1          3.1856  * UPPER-HEAD
*****************************************************************************
***   HS D/T DATA
*****************************************************************************
***   DRYWELL-LINER
***
***   SLAB       DISTANCE  NODE
***                        NO.
HS10001102     0.00305    2
HS10001103     0.00914    3
HS10001104     0.01524    4
HS10001105     0.03858    5
* 4.12.91 Adding containment liner gap and concrete model
* JV & LN, additional nodes for air and concrete
HS10001106     0.04128    6
HS10001107     0.05398    7
HS10001108     0.07938    8
HS10001109     0.10478    9
HS10001110     0.6       10
HS10001111     1.0       11
HS10001112     1.62      12
***
***          TEMPERATURE
***
* MAAP value for floor temperature, 12.10.90
HS10001805    330.00      5
*
* 4.12.91 Adding containment liner gap and concrete model
* JV & LN, additional nodes for air and concrete
HS10001812    330.00      12
*****************************************************************************
***   DRYWELL-FLOOR
***
***   SLAB       DISTANCE  NODE
***                        NO.
HS10002102     0.00305    2
HS10002103     0.00914    3
HS10002104     0.02134    4
HS10002105     0.04572    5
HS10002106     0.09144    6
HS10002107     0.18288    7
HS10002108     0.36576    8
HS10002109     0.67056    9
HS10002110     1.00584   10
HS10002111     1.44250   11
***
***          TEMPERATURE
* MAAP value for temperature, 12.10.90
HS10002811    330.00      11
* adjusting for radiant HT between DW floor and DW atmosph.  02.14.91 (JV)
* Removed on 02.15.91:  almost doubles the execution time ...
*              EMISWL    MODEL        PATHL
* HS10002401     1.0    'GRAY GAS A'  8.3
* HS10002801    391.77        1
* HS10002802    391.49        2
* HS10002803    390.94        3
* HS10002804    389.83        4
* HS10002805    387.60        5
* HS10002806    383.44        6
* HS10002807    375.10        7
* HS10002808    358.44        8
* HS10002809    341.77        9
* HS10002810    330.56       10
* HS10002811    319.27       11
*****************************************************************************
```

```
***    UP-REAC-PED
***
***     SLAB       DISTANCE  NODE
***                          NO.
HS10003102       0.00305    2
HS10003103       0.00914    3
HS10003104       0.02134    4
HS10003105       0.04572    5
HS10003106       0.09144    6
HS10003107       0.18288    7
HS10003108       0.34930    8
***
***            TEMPERATURE
HS10003801      391.77       1
HS10003802      391.49       2
HS10003803      390.94       3
HS10003804      389.83       4
HS10003805      387.60       5
HS10003806      383.44       6
HS10003807      376.10       7
HS10003808      369.19       8
******************************************************************************
***    LO-REAC-PED
***
***     SLAB       DISTANCE  NODE
***                          NO.
HS10004102       0.00305    2
HS10004103       0.00914    3
HS10004104       0.02134    4
HS10004105       0.04572    5
HS10004106       0.10668    6
HS10004107       0.24384    7
HS10004108       0.53340    8
***
***            TEMPERATURE
HS10004801      391.77       1
HS10004802      391.49       2
HS10004803      390.94       3
HS10004804      389.83       4
HS10004805      387.60       5
HS10004806      382.05       6
HS10004807      369.55       7
HS10004808      343.16       8
******************************************************************************
***    DRYWELL-STEEL
***
***     SLAB       DISTANCE  NODE
***                          NO.
HS10005102       0.00305    2
HS10005103       0.00762    3
HS10005104       0.01747    4
***
***            TEMPERATURE
HS10005804      380.38        4
******************************************************************************
***    WETWELL-LINER
***
***     SLAB       DISTANCE  NODE
***                          NO.
HS20001102       0.00305    2
HS20001103       0.00601    3
HS20001104       0.01219    4
HS20001105       0.01588    5
***
***            TEMPERATURE
* 12.10.90 initial temperature for wetwell and its downcomer
* HS20001805     358.16        5
HS20001805      305.00       5
******************************************************************************
***  WETWELL-STEEL
***
***SLAB            DISTANCE  NODE
***                          NO.
HS20002102       0.00305    2
HS20002103       0.00795    3
HS20002104       0.01747    4
***
***            TEMPERATURE
* 12.10.90 initial temperature for wetwell and its downcomer
HS20002804      305.00       4
* HS20002804     358.16        4
******************************************************************************
***    RPV-CYLINDER
***
***     SLAB       DISTANCE  NODE
***                          NO.
HS31001102        3.1886    2  *  3.1856 M = LOC OF NODE 1
HS31001103        3.1926    3
HS31001104        3.2006    4
HS31001105        3.2156    5
HS31001106        3.2556    6
```

```
HS31001107        3.3412    7  * 3.3412 M - 3.1856 M = 0.1556 M = 6.125 IN
***
***          TEMPERATURE
HS31001807     559.00       7
*****************************************************************************
***    LOWER-HEAD
***
***    SLAB      DISTANCE  NODE
***                        NO.
HS32001102        2.5807    2  * 2.5797 M = LOC OF NODE 1
HS32001103        2.5837    3
HS32001104        2.5907    4
HS32001105        2.6157    5
HS32001106        2.6963    6  * 2.6963 M - 2.5797 M = 0.1176 M = 4.63 IN
***
***          TEMPERATURE
HS32001806     550.00       6
*****************************************************************************
***    TOP-GUIDE COMBINED WITH CORE CELL STEEL MASS
***    SHROUD-DOME COMBINED WITH SEPARATORS
***
***    SEPARATORS
***
***    SLAB      DISTANCE  NODE
***                        NO.
HS35003102        0.0030    2
HS35003103        0.0069    3
HS35003104        0.0119    4
HS35003105        0.0186    5  * MARCON INPUT (0.0453 FT)
***
***          TEMPERATURE
HS35003805     559.00       5
*****************************************************************************
***    DRYERS
***
***    SLAB      DISTANCE  NODE
***                        NO.
HS36001102      1.83E-03    2  * MARCON INPUT (0.00599 FT)
***
***          TEMPERATURE
HS36001802     559.00       2
*****************************************************************************
***    UPPER-HEAD
***
***    SLAB      DISTANCE  NODE
***                        NO.
HS36002102        3.1856    2  * 3.1856 M = LOC OF NODE 1
HS36002103        3.1926    3
HS36002104        3.2006    4
HS36002105        3.2256    5
HS36002106        3.2872    6  * 3.2872 M - 3.1856 M = 0.1016 M = 4 IN
***
***          TEMPERATURE
HS36002806     559.00       6
*****************************************************************************
***    HS INTERNAL POWER SOURCES
***
***SLAB       INT POW       NAME
***           SOURCE
***            N  Y
HS10001300   -1         *  DRYWELL-LINER
HS10002300   -1         *  DRYWELL-FLOOR
HS10003300   -1         *  UP-REAC-PED
HS10004300   -1         *  LO-REAC-PED
HS10005300   -1         *  DRYWELL-STEEL
HS20001300   -1         *  WETWELL-LINER
HS20002300   -1         *  WETWELL-STEEL
HS31001300   -1         *  RPV-CYLINDER
HS32001300   -1         *  LOWER HEAD
HS35003300   -1         *  SEPARATORS
HS36001300   -1         *  DRYERS
HS36002300   -1         *  UPPER-HEAD
*****************************************************************************
***    HS LEFT/INSIDE BOUNDARY CONDITIONS
***
***SLAB       TYPE        VOL  COEF.     CRT POOL     POOL  ATM      NAME
***           SYM CONV         FLOW      FRACTION     ONLY  ONLY
***                            TYPE      POOL ATM
HS10001400     1          100  'EXT'     1.0  1.0  *          X      DRYWELL-LINER
HS10002400     1          100  'EXT'     0.0  1.0  *                 DRYWELL-FLOOR
HS10003400     1          100  'EXT'     1.0  1.0  *          X      UP-REAC-PED
HS10004400     1          100  'EXT'     1.0  1.0  *          X      LO-REAC-PED
HS10005400     1          100  'EXT'     1.0  1.0  *          X      DRYWELL-STEEL
* JV 03.01.91:  covering slab to reduce deposition area
HS20001400     1          200  'EXT'     0.5  0.5  *    X     X      WETWELL-LINER
* HS20001400      1         200  'EXT'     0.0  0.0  *    X           WETWELL-LINER
HS20002400     1          200  'EXT'     1.0  1.0  *          X      WETWELL-STEEL
HS31001400     1          310  'EXT'  .40593 .40593 *                RPV-CYLINDER
HS32001400     1          320  'EXT'     1.0  1.0  *          X      LOWER HEAD
HS35003400     1          350  'EXT'     1.0  1.0  *          X      SEPARATORS
HS36001400     1          360  'EXT'     1.0  1.0  *          X      DRYERS
```

```
HS36002400      1       360  'EXT'      1.0  1.0  *          X     UPPER-HEAD
**********************************************************************************
***   HS RIGHT/OUTSIDE BOUNDARY CONDITIONS
***
***SLAB      TYPE         VOL   COEF.   CRT POOL     POOL  ATM    NAME
***          SYN CONV           FLOW    FRACTION     ONLY  ONLY
***                             TYPE    POOL ATM
HS10001600   0                                   *                DRYWELL-LINER
HS10002600   0                                   *                DRYWELL-FLOOR
HS10003600   0                                   *                UP-REAC-PED
HS10004600   0                                   *                LO-REAC-PED
HS10005600   0                                   *                DRYWELL-STEEL
HS20001600    1          401    'EXT'   1.           1.    *          X     WETWELL-LINER
HS20002300   0                                   *                WETWELL-STEEL
HS31001600       6120    100    'EXT'   1.0  1.0  *          X    RPV-CYLINDER
HS32001600       5120    100    'EXT'   1.0  1.0  *          X    LOWER HEAD
HS35003600       1       310    'EXT'   1.0  1.0  *          X    SEPARATORS
HS36001600   0                                   *                DRYERS
HS36002600       5120    100    'EXT'   1.0  1.0  *          X    UPPER-HEAD
**********************************************************************************
***        HS LEFT/INSIDE AREAS/LENGTHS
***
***    SLAB      AREA     CH L        AX L            NAME
HS10001500  1735.60    29.55       29.55       *  DRYWELL-LINER
*
HS10002500    132.12   11.80       11.80       *  DRYWELL-FLOOR
HS10003500    767.36   15.20       15.20       *  UP-REAC-PED
HS10004500    337.24    7.50        7.50       *  LO-REAC-PED
HS10005500    800.58   29.55       29.55       *  DRYWELL-STEEL
* 03.01.91 JV
HS20001500  3168.00     5.92        5.92       *  WETWELL-LINER
* HS20001500  1584.00     2.96        2.96       *  WETWELL-LINER
*
HS20002500  4188.53     5.182       5.182      *  WETWELL-STEEL
HS31001500    317.224  12.245      12.245      *  RPV-CYLINDER
HS32001500     33.141   2.04463     2.04463    *  LOWER HEAD
HS35003500    472.43    3.99        3.99       *  SEPARATORS
HS36001500   2945.03    2.23        2.23       *  DRYERS
HS36002500     63.762   3.1856      3.1856     *  UPPER-HEAD
**********************************************************************************
***        HS RIGHT/OUTSIDE AREAS/LENGTHS
***
***    SLAB      AREA     CH L        AX L            NAME
* 03.01.91 JV
HS20001700  3168.00     5.92        5.92       *  WETWELL-LINER
* HS20001700  1584.00     2.96        2.96       *  WETWELL-LINER
*
HS31001700    332.716  12.245      12.245      *  RPV-CYLINDER
HS32001700     34.652   2.04463     2.04463    *  LOWER HEAD
HS35003700    472.43    3.99        3.99       *  SEPARATORS
HS36002700     67.894   3.2872      3.2872     *  UPPER-HEAD
**********************************************************************************
***  ADDITIONAL HEAT STRUCTURES FOR CORE/LP SHROUD
**********************************************************************************
* LOWER PLENUM SHROUD - LOWER PLENUM TO DOWNCOMER HEAT TRANSFER
*
HS32004000  5            2             1
HS32004001  'LP SHROUD4'
HS32004002  3.084        1.0
HS32004100 -1            2             2.5797
HS32004101  0.00508       1
HS32004102  0.01016       1
HS32004103  0.01524       1
HS32004104  0.02032       1
HS32004200 -1
HS32004201  'STAINLESS STEEL'          4
HS32004300 -1
HS32004400  1            320           'EXT'        0.2           0.2
HS32004500  18.645       1.1503        1.1503
HS32004600  1            310           'EXT'        0.2           0.2
HS32004700  19.012       1.1503        1.1503
HS32004800 -1
HS32004801  561.0        5
*
HS32005000  5            2             1
HS32005001  'LP SHROUD5'
HS32005002  4.2363       1.0
HS32005100 -1            2             2.5797
HS32005101  0.00508       1
HS32005102  0.01016       1
HS32005103  0.01524       1
HS32005104  0.02032       1
HS32005200 -1
HS32005201  'STAINLESS STEEL'          4
HS32005300 -1
HS32005400  1            320           'EXT'        0.2           0.2
HS32005500  15.889       0.9803        0.9803
HS32005600  1            310           'EXT'        0.2           0.2
HS32005700  16.202       0.9803        0.9803
HS32005800 -1
HS32005801  561.0        5
```

```
*
HS32006000  5           2           1
HS32006001  'LP SHROUD6'
HS32006002  5.2166      1.0
HS32006100 -1           2           2.5797
HS32006101  0.00508     1
HS32006102  0.01016     1
HS32006103  0.01524     1
HS32006104  0.02032     1
HS32006200 -1
HS32006201  'STAINLESS STEEL'       4
HS32006300 -1
HS32006400  1           320         'EXT'       0.2         0.2
HS32006500  4.501       0.2777      0.2777
HS32006600  1           310         'EXT'       0.2         0.2
HS32006700  4.590       0.2777      0.2777
HS32006800 -1
HS32006801  561.0       5
*
* CORE SHROUD - CORE BYPASS TO DOWNCOMER HEAT TRANSFER
*
HS33007000  5           2           1
HS33007001  'CORE SHROUD7'
HS33007002  5.4943      1.0
HS33007100 -1           2           2.5797
HS33007101  0.00508     1
HS33007102  0.01016     1
HS33007103  0.01524     1
HS33007104  0.02032     1
HS33007200 -1
HS33007201  'STAINLESS STEEL'       4
HS33007300 -1
HS33007400  1           330         'EXT'       0.2         0.2
HS33007500  12.351      0.762       0.762
HS33007600  1           310         'EXT'       0.2         0.2
HS33007700  12.594      0.762       0.762
HS33007800 -1
HS33007801  561.0       5
*
HS33008000  5           2           1
HS33008001  'CORE SHROUD8'
HS33008002  6.2563      1.0
HS33008100 -1           2           2.5797
HS33008101  0.00508     1
HS33008102  0.01016     1
HS33008103  0.01524     1
HS33008104  0.02032     1
HS33008200 -1
HS33008201  'STAINLESS STEEL'       4
HS33008300 -1
HS33008400  1           330         'EXT'       0.2         0.2
HS33008500  12.351      0.762       0.762
HS33008600  1           310         'EXT'       0.2         0.2
HS33008700  12.594      0.762       0.762
HS33008800 -1
HS33008801  561.0       5
*
HS33009000  5           2           1
HS33009001  'CORE SHROUD9'
HS33009002  7.0183      1.0
HS33009100 -1           2           2.5797
HS33009101  0.00508     1
HS33009102  0.01016     1
HS33009103  0.01524     1
HS33009104  0.02032     1
HS33009200 -1
HS33009201  'STAINLESS STEEL'       4
HS33009300 -1
HS33009400  1           330         'EXT'       0.2         0.2
HS33009500  12.351      0.762       0.762
HS33009600  1           310         'EXT'       0.2         0.2
HS33009700  12.594      0.762       0.762
HS33009800 -1
HS33009801  561.0       5
*
HS33010000  5           2           1
HS33010001  'CORE SHROUD10'
HS33010002  7.7803      1.0
HS33010100 -1           2           2.5797
HS33010101  0.00508     1
HS33010102  0.01016     1
HS33010103  0.01524     1
HS33010104  0.02032     1
HS33010200 -1
HS33010201  'STAINLESS STEEL'       4
HS33010300 -1
HS33010400  1           330         'EXT'       0.2         0.2
HS33010500  12.351      0.762       0.762
HS33010600  1           310         'EXT'       0.2         0.2
HS33010700  12.594      0.762       0.762
HS33010800 -1
```

```
HS33010801  561.0        5
*
HS33011000  5            2            1
HS33011001  'CORE SHROUD11'
HS33011002  8.5423       1.0
HS33011100 -1            2            2.5797
HS33011101  0.00508       1
HS33011102  0.01016       1
HS33011103  0.01524       1
HS33011104  0.02032       1
HS33011200 -1
HS33011201  'STAINLESS STEEL'          4
HS33011300 -1
HS33011400  1            330          'EXT'        0.2          0.2
HS33011500  12.351       0.762        0.762
HS33011600  1            310          'EXT'        0.2          0.2
HS33011700  12.594       0.762        0.762
HS33011800 -1
HS33011801  561.0        5
* 11.28.90 Introducing the 6th axial cell at the top of the core
HS33012000  5            2            1
HS33012001  'CORE SHROUD12'
HS33012002  9.3043       1.0
HS33012100 -1            2            2.5797
HS33012101  0.00508       1
HS33012102  0.01016       1
HS33012103  0.01524       1
HS33012104  0.02032       1
HS33012200 -1
HS33012201  'STAINLESS STEEL'          4
HS33012300 -1
HS33012400  1            330          'EXT'        0.2          0.2
HS33012500  12.351       0.3627       0.3627
HS33012600  1            310          'EXT'        0.2          0.2
HS33012700  12.594       0.3627       0.3627
HS33012800 -1
HS33012801  561.0        5
*****************************************************************************
*****       TF120 specifies the dependence on temperature
*****       of the heat transfer coefficient for the insulated
*****       exterior of the reactor pressure vessel.    TF120
*****       specifies a constant heat transfer coefficient of
*****       6.62 W/M**2/deg K.
*****
TF12000     'RPV/DRYWELL HTC'   2      1.0      0.0
TF12010     273.15   6.62    5000.0   6.62
*****************************************************************************
*****  SECONDARY CONTAINMENT SURFACES
*****************************************************************************
*****  TORUS ROOM SURFACES
*****
HS04001000 15 1 0 0              * NO. NODES, TYPE, NO SS INIT, TRANS ITER
HS04001001 CENTRAL-COLUMN        *
HS04001002 -17.2  1.                    * BOTTOM ALTITUDE, ORIENTATION
HS04001100 -1 1 0.                        * NODALIZATION FLAGS, INSIDE RADIUS
HS04001102  .001    2            *
HS04001103  .003    3
HS04001104  .007    4
HS04001105  .015    5
HS04001106  .023    6
HS04001107  .039    7
HS04001108  .071    8
HS04001109  .135    9
HS04001110  .263   10
HS04001111  .500   11
HS04001112  .750   12
HS04001113 1.00    13
HS04001114 1.50    14
HS04001115 2.0     15
HS04001201 CONCRETE    14           * MATERIAL TYPE, MESH INTERVAL
HS04001300 0                        * SOURCE TYPE, FLAG, SOURCE MULTIPLIER
HS04001400 1     401  'EXT' 1.    1.      * LHS BC TYPE, ASSOC CV, POOL HT FLAGS
HS04001500 801.     6.9  6.9          * LHS AREA, CHARAC LENGTH, AXIAL LENGTH
HS04001600 0                        * RHS BC TYPE, ASSOC CV, POOL HT FLAGS
HS04001801 311.     15                * INITIAL TEMPERATURE, NODE NO.
*
HS04002000 11 1 0 0              * NO  NODES, TYPE, NO SS INIT, TRANS ITER
HS04002001 TORUS-ROOM-WALLS      *
HS04002002 -17.2    1.                  * BOTTOM ALTITUDE, ORIENTATION
HS04002100 -1 1 0.                        * NODALIZATION FLAGS, INSIDE RADIUS
HS04002102  .001    2            *
HS04002103  .003    3
HS04002104  .007    4
HS04002105  .015    5
HS04002106  .023    6
HS04002107  .039    7
HS04002108  .071    8
HS04002109  .135    9
HS04002110  .263   10
HS04002111  .500   11
HS04002201 CONCRETE    10           * MATERIAL TYPE, MESH INTERVAL
```

```
HS04002300 0                               * SOURCE TYPE, FLAG, SOURCE MULTIPLIER
HS04002400 1    401  'EXT'  1.    1.         * LHS BC TYPE, ASSOC CV, POOL HT FLAGS
HS04002500 1391.  8.9  8.9                 * LHS AREA, CHARAC LENGTH, AXIAL LENGTH
HS04002600 2210 -1   'EXT'                 * RHS BC TYPE, ASSOC CV, POOL HT FLAGS
HS04002801 311.     11                       * INITIAL TEMPERATURE, NODE NO.
*
HS04003000 15 1 0 0                    * NO. NODES, TYPE, NO SS INIT, TRANS ITER
HS04003001 FLOOR                       *
* USED VERTICAL ORIENTATION TO ELIMINATE POOL HEAT TRANSFER
HS04003002 -17.2    1.                         * BOTTOM ALTITUDE, ORIENTATION
HS04003100   -1   1 0.                       * NODALIZATION FLAGS, INSIDE RADIUS
HS04003102  .001    2                  *
HS04003103  .003    3
HS04003104  .007    4
HS04003105  .015    5
HS04003106  .023    6
HS04003107  .039    7
HS04003108  .071    8
HS04003109  .135    9
HS04003110  .263   10
HS04003111  .500   11
HS04003112  .750   12
HS04003113 1.00    13
HS04003114 1.50    14
HS04003115 2.0     15
HS04003201 CONCRETE    14                * MATERIAL TYPE, MESH INTERVAL
HS04003300 0                             * SOURCE TYPE, FLAG, SOURCE MULTIPLIER
HS04003400 1     401  'EXT'  1.    1.        * LHS BC TYPE, ASSOC CV, POOL HT FLAGS
HS04003500 1166.  15.    5.                         * LHS AREA, CHARAC LENGTH, AXIAL LENGTH
HS04003600 2210 -1   'EXT'               * RHS BC TYPE, ASSOC CV, POOL HT FLAGS
HS04003801 301.     15                     * INITIAL TEMPERATURE, NODE NO.
*
HS04005000 13 1 0 0                    * NO. NODES, TYPE, NO SS INIT, TRANS ITER
HS04005001 CEILING                     *
HS04005002 -4.7      0.                        * BOTTOM ALTITUDE, ORIENTATION
HS04005100 -1 1 0.                               * NODALIZATION FLAGS, INSIDE RADIUS
HS04005102  .001    2                  *
HS04005103  .003    3
HS04005104  .007    4
HS04005105  .015    5
HS04005106  .023    6
HS04005107  .039    7
HS04005108  .071    8
HS04005109  .135    9
HS04005110  .263   10
HS04005111  .500   11
HS04005112  .750   12
HS04005113 1.16    13
HS04005201 CONCRETE    12                  * MATERIAL TYPE, MESH INTERVAL
HS04005300 0                               * SOURCE TYPE, FLAG, SOURCE MULTIPLIER
HS04005400 1     401  'EXT'  1.    1.          * LHS BC TYPE, ASSOC CV, POOL HT FLAGS
HS04005500 1166.  11.     11.                         * LHS AREA, CHARAC LENGTH, AXIAL LENGTH
HS04005600 0                               * RHS BC TYPE, ASSOC CV, POOL HT FLAGS
HS04005801 311.     13                       * INITIAL TEMPERATURE, NODE NO.
*
*****    LEVEL-135-SOUTH SURFACES
*****
HS04006000 13 1 0 0                    * NO. NODES, TYPE, NO SS INIT, TRANS ITER
HS04006001 EXTWALL                     *
HS04006002 -4.1  1.                            * BOTTOM ALTITUDE, ORIENTATION
HS04006100 -1 1 0.                               * NODALIZATION FLAGS, INSIDE RADIUS
HS04006102  .001    2                  * LOCATION, NODE NO.
HS04006103  .003    3
HS04006104  .007    4
HS04006105  .015    5
HS04006106  .023    6
HS04006107  .039    7
HS04006108  .071    8
HS04006109  .135    9
HS04006110  .263   10
HS04006111  .500   11
HS04006112  .750   12
HS04006113  .900   13
HS04006201 CONCRETE    12                  * MATERIAL TYPE, MESH INTERVAL
HS04006300 0                               * SOURCE TYPE, FLAG, SOURCE MULTIPLIER
HS04006400 1     402  'EXT'  1.    1.          * LHS BC TYPE, ASSOC CV, POOL HT FLAGS
HS04006500  671.  7.5  7.5                 * LHS AREA, CHARAC LENGTH, AXIAL LENGTH
HS04006600 4200 410  'EXT'  1.    1.           * RHS BC TYPE, ASSOC CV, POOL HT FLAGS
HS04006700  671.  7.5  7.5                 * RHS AREA, CHARAC LENGTH, AXIAL LENGTH
HS04006801 301.     13                       * INITIAL TEMPERATURE, NODE NO.
*
HS04007000 14 1 0 0                    * NO. NODES, TYPE, NO SS INIT, TRANS ITER
HS04007001 PRIM-CONT-WALLS             *
HS04007002 -4.1      1.                        * BOTTOM ALTITUDE, ORIENTATION
HS04007100 -1 1 0.                               * NODALIZATION FLAGS, INSIDE RADIUS
HS04007102  .001    2                  *
HS04007103  .003    3
HS04007104  .007    4
HS04007105  .015    5
HS04007106  .023    6
HS04007107  .039    7
```

```
HS04007108  .071   8
HS04007109  .135   9
HS04007110  .263  10
HS04007111  .500  11
HS04007112  .750  12
HS04007113 1.00   13
HS04007114 1.50   14
HS04007201 CONCRETE    13                 * MATERIAL TYPE, MESH INTERVAL
HS04007300 0                              * SOURCE TYPE, FLAG, SOURCE MULTIPLIER
HS04007400 1    402  'EXT'  1.    1.        * LHS BC TYPE, ASSOC CV, POOL HT FLAGS
HS04007500 315.    7.5  7.5                * LHS AREA, CHARAC LENGTH, AXIAL LENGTH
HS04007600 0                              * RHS BC TYPE, ASSOC CV, POOL HT FLAGS
HS04007801 301.       14                   * INITIAL TEMPERATURE, NODE NO.
*
HS04008000 11 1 0 0               * NO. NODES, TYPE, NO SS INIT, TRANS ITER
HS04008001 INT-WALLS              *
HS04008002 -4.1      1.                      * BOTTOM ALTITUDE, ORIENTATION
HS04008100 -1 1 0.                             * NODALIZATION FLAGS, INSIDE RADIUS
HS04008102  .001   2              *
HS04008103  .003   3
HS04008104  .007   4
HS04008105  .015   5
HS04008106  .023   6
HS04008107  .039   7
HS04008108  .071   8
HS04008109  .135   9
HS04008110  .263  10
HS04008111  .350  11
HS04008201 CONCRETE    10                 * MATERIAL TYPE, MESH INTERVAL
HS04008300 0                              * SOURCE TYPE, FLAG, SOURCE MULTIPLIER
HS04008400 1    402  'EXT'  1.    1.        * LHS BC TYPE, ASSOC CV, POOL HT FLAGS
HS04008500  960.  7.5  7.5                * LHS AREA, CHARAC LENGTH, AXIAL LENGTH
HS04008600 0                              * RHS BC TYPE, ASSOC CV, POOL HT FLAGS
HS04008801 301.      11                    * INITIAL TEMPERATURE, NODE NO.
*
HS04009000 12 1 0 0               * NO. NODES, TYPE, NO SS INIT, TRANS ITER
HS04009001 CEILING                *
HS04009002  4.5      0.                      * BOTTOM ALTITUDE, ORIENTATION
HS04009100 -1 1 0.                             * NODALIZATION FLAGS, INSIDE RADIUS
HS04009102  .001   2              *
HS04009103  .003   3
HS04009104  .007   4
HS04009105  .015   5
HS04009106  .023   6
HS04009107  .039   7
HS04009108  .071   8
HS04009109  .135   9
HS04009110  .263  10
HS04009111  .500  11
HS04009112  .6    12
HS04009201 'CARBON STEEL'     2        * MATERIAL TYPE, MESH INTERVAL
HS04009202 CONCRETE   11
HS04009300 0                              * SOURCE TYPE, FLAG, SOURCE MULTIPLIER
HS04009400 1    402  'EXT'  1.    1.        * LHS BC TYPE, ASSOC CV, POOL HT FLAGS
HS04009500  588.  11.       5.                         * LHS AREA, CHARAC LENGTH, AXIAL LENGTH
HS04009600 0                              * RHS BC TYPE, ASSOC CV, POOL HT FLAGS
HS04009801 301.      12                    * INITIAL TEMPERATURE, NODE NO.
*
HS04010000 13 1 0 0               * NO. NODES, TYPE, NO SS INIT, TRANS ITER
HS04010001 FLOOR
* USED VERTICAL ORIENTATION TO ELIMINATE POOL HEAT TRANSFER
HS04010002 -4.1      1.                              * BOTTOM ALTITUDE, ORIENTATION
HS04010100 -1 1 0.                                     * NODALIZATION FLAGS, INSIDE RADIUS
HS04010102  .001   2
HS04010103  .003   3
HS04010104  .007   4
HS04010105  .015   5
HS04010106  .023   6
HS04010107  .039   7
HS04010108  .071   8
HS04010109  .135   9
HS04010110  .263  10
HS04010111  .500  11
HS04010112  .75   12
HS04010113 1.15   13
HS04010201 CONCRETE    12                 * MATERIAL TYPE, MESH INTERVAL
HS04010300 0                              * SOURCE TYPE, FLAG, SOURCE MULTIPLIER
HS04010400 1    402  'EXT'  1.    1.        * LHS BC TYPE, ASSOC CV, POOL HT FLAGS
HS04010500  588.  11.       5.                         * LHS AREA, CHARAC LENGTH, AXIAL LENGTH
HS04010600 0                              * RHS BC TYPE, ASSOC CV, POOL HT FLAGS
HS04010801 301.      13                    * INITIAL TEMPERATURE, NODE NO.
*
HS04011000  2 1 0 0               * NO. NODES, TYPE, NO SS INIT, TRANS ITER
HS04011001 MISC-STEEL
HS04011002 -6.1  1.                               * BOTTOM ALTITUDE, ORIENTATION
HS04011100 -1 1 0.                                  * NODALIZATION FLAGS, INSIDE RADIUS
HS04011102  .0177  2
HS04011201 'CARBON STEEL'     1        * MATERIAL TYPE, MESH INTERVAL
HS04011300 0                              * SOURCE TYPE, FLAG, SOURCE MULTIPLIER
HS04011400 1    402  'EXT'  1.    1.        * LHS BC TYPE, ASSOC CV, POOL HT FLAGS
HS04011500 166.9 3.        3.                         * LHS AREA, CHARAC LENGTH, AXIAL LENGTH
```

```
HS04011600 1    402  'EXT'  1.    1.       * RHS BC TYPE, ASSOC CV, POOL HT FLAGS
HS04011700 166.9 3.          3.
HS04011801 305.4 2                         * INITIAL TEMPERATURE, NODE NO.
*
*****   LEVEL-135-NORTH SURFACES
*****
HS04012000 13 1 0 0                        * NO. NODES, TYPE, NO SS INIT, TRANS ITER
HS04012001 EXTWALL
HS04012002 -4.1  1.                                   * BOTTOM ALTITUDE, ORIENTATION
HS04012100 -1 1 0.                                     * NODALIZATION FLAGS, INSIDE RADIUS
HS04012102  .001    2                      * LOCATION, NODE NO.
HS04012103  .003    3
HS04012104  .007    4
HS04012105  .015    5
HS04012106  .023    6
HS04012107  .039    7
HS04012108  .071    8
HS04012109  .135    9
HS04012110  .263   10
HS04012111  .500   11
HS04012112  .750   12
HS04012113  .900   13
HS04012201 CONCRETE    12                 * MATERIAL TYPE, MESH INTERVAL
HS04012300 0                              * SOURCE TYPE, FLAG, SOURCE MULTIPLIER
HS04012400 1    403  'EXT'  1.    1.        * LHS BC TYPE, ASSOC CV, POOL HT FLAGS
HS04012500  671.  7.5  7.5                * LHS AREA, CHARAC LENGTH, AXIAL LENGTH
HS04012600 4200 410  'EXT'  1.    1.        * RHS BC TYPE, ASSOC CV, POOL HT FLAGS
HS04012700  671.  7.5  7.5                * RHS AREA, CHARAC LENGTH, AXIAL LENGTH
HS04012801 301.    13                      * INITIAL TEMPERATURE, NODE NO.
*
HS04013000 14 1 0 0                        * NO. NODES, TYPE, NO SS INIT, TRANS ITER
HS04013001 PRIM-CONT-WALLS
HS04013002 -4.1    1.                                * BOTTOM ALTITUDE, ORIENTATION
HS04013100 -1 1 0.                                     * NODALIZATION FLAGS, INSIDE RADIUS
HS04013102  .001    2
HS04013103  .003    3
HS04013104  .007    4
HS04013105  .015    5
HS04013106  .023    6
HS04013107  .039    7
HS04013108  .071    8
HS04013109  .135    9
HS04013110  .263   10
HS04013111  .500   11
HS04013112  .750   12
HS04013113 1.00    13
HS04013114 1.50    14
HS04013201 CONCRETE    13                  * MATERIAL TYPE, MESH INTERVAL
HS04013300 0                               * SOURCE TYPE, FLAG, SOURCE MULTIPLIER
HS04013400 1    403  'EXT'  1.    1.          * LHS BC TYPE, ASSOC CV, POOL HT FLAGS
HS04013500 315.     7.5  7.5                * LHS AREA, CHARAC LENGTH, AXIAL LENGTH
HS04013600 0                               * RHS BC TYPE, ASSOC CV, POOL HT FLAGS
HS04013801 301.       14                     * INITIAL TEMPERATURE, NODE NO.
*
HS04014000 11 1 0 0                        * NO. NODES, TYPE, NO SS INIT, TRANS ITER
HS04014001 INT-WALLS
HS04014002 -4.1    1.                                  * BOTTOM ALTITUDE, ORIENTATION
HS04014100 -1 1 0.                                       * NODALIZATION FLAGS, INSIDE RADIUS
HS04014102  .001    2
HS04014103  .003    3
HS04014104  .007    4
HS04014105  .015    5
HS04014106  .023    6
HS04014107  .039    7
HS04014108  .071    8
HS04014109  .135    9
HS04014110  .263   10
HS04014111  .350   11
HS04014201 CONCRETE    10                  * MATERIAL TYPE, MESH INTERVAL
HS04014300 0                               * SOURCE TYPE, FLAG, SOURCE MULTIPLIER
HS04014400 1    403  'EXT'  1.    1.          * LHS BC TYPE, ASSOC CV, POOL HT FLAGS
HS04014500  948.  7.5  7.5                 * LHS AREA, CHARAC LENGTH, AXIAL LENGTH
HS04014600 0                               * RHS BC TYPE, ASSOC CV, POOL HT FLAGS
HS04014801 301.    11                        * INITIAL TEMPERATURE, NODE NO.
*
HS04015000 12 1 0 0                        * NO. NODES, TYPE, NO SS INIT, TRANS ITER
HS04015001 CEILING
HS04015002  4.5    0.                                  * BOTTOM ALTITUDE, ORIENTATION
HS04015100 -1 1 0.                                       * NODALIZATION FLAGS, INSIDE RADIUS
HS04015102  .001    2
HS04015103  .003    3
HS04015104  .007    4
HS04015105  .015    5
HS04015106  .023    6
HS04015107  .039    7
HS04015108  .071    8
HS04015109  .135    9
HS04015110  .263   10
HS04015111  .500   11
HS04015112  .6     12
HS04015201 'CARBON STEEL'     2      * MATERIAL TYPE, MESH INTERVAL
```

```
HS04015202 CONCRETE   11
HS04015300 0                                 * SOURCE TYPE, FLAG, SOURCE MULTIPLIER
HS04015400 1    403  'EXT'  1.    1.           * LHS BC TYPE, ASSOC CV, POOL HT FLAGS
HS04015500  587.  11.       5.                          * LHS AREA, CHARAC LENGTH, AXIAL LENGTH
HS04015600 0                                 * RHS BC TYPE, ASSOC CV, POOL HT FLAGS
HS04015801 301.     12                         * INITIAL TEMPERATURE, NODE NO.
*
HS04016000 13 1 0 0                          * NO. NODES, TYPE, NO SS INIT, TRANS ITER
HS04016001 FLOOR
* USED VERTICAL ORIENTATION TO ELIMINATE POOL HEAT TRANSFER
HS04016002 -4.1     1.                                     * BOTTOM ALTITUDE, ORIENTATION
HS04016100 -1 1 0.                                           * NODALIZATION FLAGS, INSIDE RADIUS
HS04016102  .001   2
HS04016103  .003   3
HS04016104  .007   4
HS04016105  .015   5
HS04016106  .023   6
HS04016107  .039   7
HS04016108  .071   8
HS04016109  .135   9
HS04016110  .263  10
HS04016111  .500  11
HS04016112  .75   12
HS04016113 1.15   13
HS04016201 CONCRETE    12                    * MATERIAL TYPE, MESH INTERVAL
HS04016300 0                                 * SOURCE TYPE, FLAG, SOURCE MULTIPLIER
HS04016400 1    403  'EXT'  1.    1.           * LHS BC TYPE, ASSOC CV, POOL HT FLAGS
HS04016500  587.  11.       5.                          * LHS AREA, CHARAC LENGTH, AXIAL LENGTH
HS04016600 0                                 * RHS BC TYPE, ASSOC CV, POOL HT FLAGS
HS04016801 301.     13                         * INITIAL TEMPERATURE, NODE NO.
*
HS04017000  2 1 0 0                          * NO. NODES, TYPE, NO SS INIT, TRANS ITER
HS04017001 MISC-STEEL
HS04017002 -4.1     1.                                     * BOTTOM ALTITUDE, ORIENTATION
HS04017100 -1 1 0.                                           * NODALIZATION FLAGS, INSIDE RADIUS
HS04017102  .0127  2
HS04017201 'CARBON STEEL'      1             * MATERIAL TYPE, MESH INTERVAL
HS04017300 0                                 * SOURCE TYPE, FLAG, SOURCE MULTIPLIER
HS04017400 1    403  'EXT'  1.    1.           * LHS BC TYPE, ASSOC CV, POOL HT FLAGS
HS04017500 166.9 3.         3.                          * LHS AREA, CHARAC LENGTH, AXIAL LENGTH
HS04017600 1    403  'EXT'  1.    1.           * RHS BC TYPE, ASSOC CV, POOL HT FLAGS
HS04017700 166.9 3.         3.
HS04017801 305.4 2                           * INITIAL TEMPERATURE, NODE NO.
*
*****   LEVEL-165-SE SURFACES
*****
HS04018000 13 1 0 0                          * NO. NODES, TYPE, NO SS INIT, TRANS ITER
HS04018001 EXTWALL
HS04018002  5.1     1.                                     * BOTTOM ALTITUDE, ORIENTATION
HS04018100 -1 1 0.                                           * NODALIZATION FLAGS, INSIDE RADIUS
HS04018102  .001   2
HS04018103  .003   3
HS04018104  .007   4
HS04018105  .015   5
HS04018106  .023   6
HS04018107  .039   7
HS04018108  .071   8
HS04018109  .135   9
HS04018110  .263  10
HS04018111  .500  11
HS04018112  .750  12
HS04018113  .90   13
HS04018201 CONCRETE    12                    * MATERIAL TYPE, MESH INTERVAL
HS04018300 0                                 * SOURCE TYPE, FLAG, SOURCE MULTIPLIER
HS04018400 1    404  'EXT'  1.    1.           * LHS BC TYPE, ASSOC CV, POOL HT FLAGS
HS04018500  345.  8.3  8.3                   * LHS AREA, CHARAC LENGTH, AXIAL LENGTH
HS04018600 4200 410  'EXT'  1.    1.           * RHS BC TYPE, ASSOC CV, POOL HT FLAGS
HS04018700  345.  8.3  8.3                   * RHS AREA, CHARAC LENGTH, AXIAL LENGTH
HS04018801 301.     13                         * INITIAL TEMPERATURE, NODE NO.
*
HS04019000 15 1 0 0                          * NO. NODES, TYPE, NO SS INIT, TRANS ITER
HS04019001 PCWALL
HS04019002  5.1     1.                                     * BOTTOM ALTITUDE, ORIENTATION
HS04019100 -1 1 0.                                           * NODALIZATION FLAGS, INSIDE RADIUS
HS04019102  .001   2
HS04019103  .003   3
HS04019104  .007   4
HS04019105  .019   5
HS04019106  .023   6
HS04019107  .039   7
HS04019108  .071   8
HS04019109  .135   9
HS04019110  .263  10
HS04019111  .500  11
HS04019112  .750  12
HS04019113 1.00   13
HS04019114 1.50   14
HS04019115 1.70   15
HS04019201 CONCRETE    14                    * MATERIAL TYPE, MESH INTERVAL
HS04019300 0                                 * SOURCE TYPE, FLAG, SOURCE MULTIPLIER
HS04019400 1    404  'EXT'  1.    1.           * LHS BC TYPE, ASSOC CV, POOL HT FLAGS
```

```
HS04019500 153.    8.3  8.3              * LHS AREA, CHARAC LENGTH, AXIAL LENGTH
HS04019600 0                             * RHS BC TYPE, ASSOC CV, POOL HT FLAGS
HS04019601 301.      15                    * INITIAL TEMPERATURE, NODE NO.
*
HS04020000 11 1 0 0                      * NO. NODES, TYPE, NO SS INIT, TRANS ITER
HS04020001 INTWALL
HS04020002  5.1    1.                              * BOTTOM ALTITUDE, ORIENTATION
HS04020100 -1 1 0.                                   * NODALIZATION FLAGS, INSIDE RADIUS
HS04020102  .001   2
HS04020103  .003   3
HS04020104  .007   4
HS04020105  .015   5
HS04020106  .023   6
HS04020107  .039   7
HS04020108  .071   8
HS04020109  .135   9
HS04020110  .263  10
HS04020111  .450  11
HS04020201 CONCRETE   10                 * MATERIAL TYPE, MESH INTERVAL
HS04020300 0                             * SOURCE TYPE, FLAG, SOURCE MULTIPLIER
HS04020400 1    404  'EXT'  1.    1.       * LHS BC TYPE, ASSOC CV, POOL HT FLAGS
HS04020500 1652.  8.3  8.3                * LHS AREA, CHARAC LENGTH, AXIAL LENGTH
HS04020600 0                             * RHS BC TYPE, ASSOC CV, POOL HT FLAGS
HS04020601 301.     11                    * INITIAL TEMPERATURE, NODE NO.
*
HS04021000 11 1 0 0                      * NO. NODES, TYPE, NO SS INIT, TRANS ITER
HS04021001 CEILING
HS04021002 13.6    0.                              * BOTTOM ALTITUDE, ORIENTATION
HS04021100 -1 1 0.                                   * NODALIZATION FLAGS, INSIDE RADIUS
HS04021102  .001   2
HS04021103  .003   3
HS04021104  .007   4
HS04021105  .015   5
HS04021106  .023   6
HS04021107  .039   7
HS04021108  .071   8
HS04021109  .135   9
HS04021110  .263  10
HS04021111  .500  11
HS04021201 'CARBON STEEL'      2         * MATERIAL TYPE, MESH INTERVAL
HS04021202 CONCRETE   10
HS04021300 0                             * SOURCE TYPE, FLAG, SOURCE MULTIPLIER
HS04021400 1    404  'EXT'  1.    1.       * LHS BC TYPE, ASSOC CV, POOL HT FLAGS
HS04021500  291.  11.       5.                      * LHS AREA, CHARAC LENGTH, AXIAL LENGTH
HS04021600 0                             * RHS BC TYPE, ASSOC CV, POOL HT FLAGS
HS04021601 301.     11                    * INITIAL TEMPERATURE, NODE NO.
*
HS04022000 12 1 0 0                      * NO. NODES, TYPE, NO SS INIT, TRANS ITER
HS04022001 FLOOR
* USED VERTICAL ORIENTATION TO ELIMINATE POOL HEAT TRANSFER
HS04022002  5.1    1.                              * BOTTOM ALTITUDE, ORIENTATION
HS04022100 -1  1 0.                                  * NODALIZATION FLAGS, INSIDE RADIUS
HS04022102  .001   2
HS04022103  .003   3
HS04022104  .007   4
HS04022105  .015   5
HS04022106  .023   6
HS04022107  .039   7
HS04022108  .071   8
HS04022109  .135   9
HS04022110  .263  10
HS04022111  .500  11
HS04022112  .800  12
HS04022201 CONCRETE   11                 * MATERIAL TYPE, MESH INTERVAL
HS04022300 0                             * SOURCE TYPE, FLAG, SOURCE MULTIPLIER
HS04022400 1    404  'EXT'  1.    1.       * LHS BC TYPE, ASSOC CV, POOL HT FLAGS
HS04022500  261.  11.       5.                      * LHS AREA, CHARAC LENGTH, AXIAL LENGTH
HS04022600 0                             * RHS BC TYPE, ASSOC CV, POOL HT FLAGS
HS04022601 301.     12                    * INITIAL TEMPERATURE, NODE NO.
*
HS04023000  2 1 0 0                      * NO. NODES, TYPE, NO SS INIT, TRANS ITER
HS04023001 STEEL
HS04023002  5.1    1.                              * BOTTOM ALTITUDE, ORIENTATION
HS04023100 -1 1 0.                                   * NODALIZATION FLAGS, INSIDE RADIUS
HS04023102  .0127  2
HS04023201 'CARBON STEEL'      1         * MATERIAL TYPE, MESH INTERVAL
HS04023300 0                             * SOURCE TYPE, FLAG, SOURCE MULTIPLIER
HS04023400 1    404  'EXT'  1.    1.       * LHS BC TYPE, ASSOC CV, POOL HT FLAGS
HS04023500   7.9  3.        3.                      * LHS AREA, CHARAC LENGTH, AXIAL LENGTH
HS04023600 1    404  'EXT'  1.    1.       * RHS BC TYPE, ASSOC CV, POOL HT FLAGS
HS04023700   7.9  3.        3.
HS04023801 301.  2                        * INITIAL TEMPERATURE, NODE NO.
*
*****   LEVEL-165-MAIN SURFACES
HS04024000 13 1 0 0                      * NO. NODES, TYPE, NO SS INIT, TRANS ITER
HS04024001 EXTWALL
HS04024002  5.1    1.                              * BOTTOM ALTITUDE, ORIENTATION
HS04024100 -1 1 0.                                   * NODALIZATION FLAGS, INSIDE RADIUS
HS04024102  .001   2
HS04024103  .003   3
HS04024104  .007   4
```

```
HS04024105  .015   5
HS04024106  .023   6
HS04024107  .039   7
HS04024108  .071   8
HS04024109  .136   9
HS04024110  .263  10
HS04024111  .500  11
HS04024112  .750  12
HS04024113  .90   13
HS04024201 CONCRETE   12                 * MATERIAL TYPE, MESH INTERVAL
HS04024300 0                             * SOURCE TYPE, FLAG, SOURCE MULTIPLIER
HS04024400 1    405  'EXT'  1.    1.        * LHS BC TYPE, ASSOC CV, POOL HT FLAGS
HS04024500 1030.  8.3  8.3               * LHS AREA, CHARAC LENGTH, AXIAL LENGTH
HS04024600 4200 410  'EXT'  1.    1.        * RHS BC TYPE, ASSOC CV, POOL HT FLAGS
HS04024700 1030.  8.3  8.3               * RHS AREA, CHARAC LENGTH, AXIAL LENGTH
HS04024801 301.     13                    * INITIAL TEMPERATURE, NODE NO.
*
HS04025000 15 1 0 0                      * NO. NODES, TYPE, NO SS INIT, TRANS ITER
HS04025001 PCWALL
HS04025002  5.1    1.                                 * BOTTOM ALTITUDE, ORIENTATION
HS04025100 -1 1 0.                                       * NODALIZATION FLAGS, INSIDE RADIUS
HS04025102  .001    2
HS04025103  .003    3
HS04025104  .007    4
HS04025105  .019    5
HS04025106  .023    6
HS04025107  .039    7
HS04025108  .071    8
HS04025109  .135    9
HS04025110  .263   10
HS04025111  .500   11
HS04025112  .750   12
HS04025113 1.00    13
HS04025114 1.50    14
HS04025115 1.70    15
HS04025201 CONCRETE   14                 * MATERIAL TYPE, MESH INTERVAL
HS04025300 0                             * SOURCE TYPE, FLAG, SOURCE MULTIPLIER
HS04025400 1    405  'EXT'  1.    1.        * LHS BC TYPE, ASSOC CV, POOL HT FLAGS
HS04025500 457.     8.3  8.3             * LHS AREA, CHARAC LENGTH, AXIAL LENGTH
HS04025600 0                             * RHS BC TYPE, ASSOC CV, POOL HT FLAGS
HS04025801 301.        15                 * INITIAL TEMPERATURE, NODE NO.
*
HS04026000 11 1 0 0                      * NO. NODES, TYPE, NO SS INIT, TRANS ITER
HS04026001 INTWALL
HS04026002  5.1    1.                                 * BOTTOM ALTITUDE, ORIENTATION
HS04026100 -1 1 0.                                       * NODALIZATION FLAGS, INSIDE RADIUS
HS04026102  .001    2
HS04026103  .003    3
HS04026104  .007    4
HS04026105  .015    5
HS04026106  .023    6
HS04026107  .039    7
HS04026108  .071    8
HS04026109  .135    9
HS04026110  .263   10
HS04026111  .450   11
HS04026201 CONCRETE    10                * MATERIAL TYPE, MESH INTERVAL
HS04026300 0                             * SOURCE TYPE, FLAG, SOURCE MULTIPLIER
HS04026400 1    405  'EXT'  1.    1.        * LHS BC TYPE, ASSOC CV, POOL HT FLAGS
HS04026500  950.  8.3  8.3               * LHS AREA, CHARAC LENGTH, AXIAL LENGTH
HS04026600 0                             * RHS BC TYPE, ASSOC CV, POOL HT FLAGS
HS04026801 301.     11                    * INITIAL TEMPERATURE, NODE NO.
*
HS04027000 11 1 0 0                      * NO. NODES, TYPE, NO SS INIT, TRANS ITER
HS04027001 CEILING
HS04027002 13.6     0.                                * BOTTOM ALTITUDE, ORIENTATION
HS04027100 -1 1 0.                                       * NODALIZATION FLAGS, INSIDE RADIUS
HS04027102  .001    2
HS04027103  .003    3
HS04027104  .007    4
HS04027105  .015    5
HS04027106  .023    6
HS04027107  .039    7
HS04027108  .071    8
HS04027109  .135    9
HS04027110  .263   10
HS04027111  .500   11
HS04027201 'CARBON STEEL'      2         * MATERIAL TYPE, MESH INTERVAL
HS04027202 CONCRETE    10
HS04027300 0                             * SOURCE TYPE, FLAG, SOURCE MULTIPLIER
HS04027400 1    405  'EXT'  1.    1.        * LHS BC TYPE, ASSOC CV, POOL HT FLAGS
HS04027500  874.  11.      5.                         * LHS AREA, CHARAC LENGTH, AXIAL LENGTH
HS04027600 0                             * RHS BC TYPE, ASSOC CV, POOL HT FLAGS
HS04027801 301.     11                    * INITIAL TEMPERATURE, NODE NO
*
HS04028000 12 1 0 0                      * NO. NODES, TYPE, NO SS INIT, TRANS ITER
HS04028001 FLOOR
* USED VERTICAL ORIENTATION TO ELIMINATE POOL HEAT TRANSFER
HS04028002  5.1    1.                                 * BOTTOM ALTITUDE, ORIENTATION
HS04028100 -1  1 0.                                      * NODALIZATION FLAGS, INSIDE RADIUS
HS04028102  .001    2
```

```
HS04028103  .003   3
HS04028104  .007   4
HS04028105  .015   5
HS04028106  .023   6
HS04028107  .039   7
HS04028108  .071   8
HS04028109  .135   9
HS04028110  .263  10
HS04028111  .500  11
HS04028112  .600  12
HS04028201 CONCRETE    11                 * MATERIAL TYPE, MESH INTERVAL
HS04028300 0                              * SOURCE TYPE, FLAG, SOURCE MULTIPLIER
HS04028400 1    405  'EXT'  1.    1.         * LHS BC TYPE, ASSOC CV, POOL HT FLAGS
HS04028500  784.  11.       5.                        * LHS AREA, CHARAC LENGTH, AXIAL LENGTH
HS04028600 0                              * RHS BC TYPE, ASSOC CV, POOL HT FLAGS
HS04028801 301.     12                     * INITIAL TEMPERATURE, NODE NO.
*
HS04029000  2 1 0 0                       * NO. NODES, TYPE, NO SS INIT, TRANS ITER
HS04029001 STEEL
HS04029002  5.1   1.                                   * BOTTOM ALTITUDE, ORIENTATION
HS04029100 -1 1 0.                                       * NODALIZATION FLAGS, INSIDE RADIUS
HS04029102  .0127  2
HS04029201 'CARBON STEEL'      1          * MATERIAL TYPE, MESH INTERVAL
HS04029300 0                              * SOURCE TYPE, FLAG, SOURCE MULTIPLIER
HS04029400 1    405  'EXT'  1.    1.         * LHS BC TYPE, ASSOC CV, POOL HT FLAGS
HS04029500 23.8  3.         3.                          * LHS AREA, CHARAC LENGTH, AXIAL LENGTH
HS04029600 1    405  'EXT'  1.    1.         * RHS BC TYPE, ASSOC CV, POOL HT FLAGS
HS04029700 23.8  3.         3.
HS04029801 301.  2                        * INITIAL TEMPERATURE, NODE NO.
*
***** LEVEL-195-SE SURFACES
*****
HS04030000 12 1 0 0                       * NO. NODES, TYPE, NO SS INIT, TRANS ITER
HS04030001 EXTWALL
HS04030002 14.2    1.                                  * BOTTOM ALTITUDE, ORIENTATION
HS04030100 -1 1 0.                                       * NODALIZATION FLAGS, INSIDE RADIUS
HS04030102  .001   2
HS04030103  .003   3
HS04030104  .007   4
HS04030105  .015   5
HS04030106  .023   6
HS04030107  .039   7
HS04030108  .071   8
HS04030109  .135   9
HS04030110  .263  10
HS04030111  .500  11
HS04030112  .600  12
HS04030201 CONCRETE    11                 * MATERIAL TYPE, MESH INTERVAL
HS04030300 0                              * SOURCE TYPE, FLAG, SOURCE MULTIPLIER
HS04030400 1    406  'EXT'  1.    1.         * LHS BC TYPE, ASSOC CV, POOL HT FLAGS
HS04030500  588.  5.1  5.1               * LHS AREA, CHARAC LENGTH, AXIAL LENGTH
HS04030600 4200 410  'EXT'  1.    1.         * RHS BC TYPE, ASSOC CV, POOL HT FLAGS
HS04030700  588.  5.1  5.1               * RHS AREA, CHARAC LENGTH, AXIAL LENGTH
HS04030801 301.     12                     * INITIAL TEMPERATURE, NODE NO.
*
HS04031000 14 1 0 0                       * NO. NODES, TYPE, NO SS INIT, TRANS ITER
HS04031001 PCWALL
HS04031002 14.2    1.                                  * BOTTOM ALTITUDE, ORIENTATION
HS04031100 -1 1 0.                                       * NODALIZATION FLAGS, INSIDE RADIUS
HS04031102  .001   2
HS04031103  .003   3
HS04031104  .007   4
HS04031105  .015   5
HS04031106  .023   6
HS04031107  .039   7
HS04031108  .071   8
HS04031109  .135   9
HS04031110  .263  10
HS04031111  .500  11
HS04031112  .750  12
HS04031113 1.0    13
HS04031114 1.5    14
HS04031201 CONCRETE    13                 * MATERIAL TYPE, MESH INTERVAL
HS04031300 0                              * SOURCE TYPE, FLAG, SOURCE MULTIPLIER
HS04031400 1    406  'EXT'  1.    1.         * LHS BC TYPE, ASSOC CV, POOL HT FLAGS
HS04031500 288.      5.1  5.1            * LHS AREA, CHARAC LENGTH, AXIAL LENGTH
HS04031600 0                              * RHS BC TYPE, ASSOC CV, POOL HT FLAGS
HS04031801 301.       14                   * INITIAL TEMPERATURE, NODE NO.
*
HS04033000 11 1 0 0                       * NO. NODES, TYPE, NO SS INIT, TRANS ITER
HS04033001  FLOOR
* USED VERTICAL ORIENTATION TO ELIMI[illegible]OL HEAT TRANSFER
HS04033002 14.2   1.                                   * BOTTOM ALTITUDE, ORIENTATION
HS04033100 -1     1 0.                                 * NODALIZATION FLAGS, INSIDE RADIUS
HS04033102  .001   2
HS04033103  .003   3
HS04033104  .007   4
HS04033105  .015   5
HS04033106  .023   6
HS04033107  .039   7
HS04033108  .071   8
```

```
HS04033109  .135   9
HS04033110  .263  10
HS04033111  .500  11
HS04033201 CONCRETE     10                    * MATERIAL TYPE, MESH INTERVAL
HS04033300 0                                  * SOURCE TYPE, FLAG, SOURCE MULTIPLIER
HS04033400 1     406  'EXT'  1.     1.            * LHS BC TYPE, ASSOC CV, POOL HT FLAGS
HS04033500 245.     11.     11.                               * LHS AREA, CHARAC LENGTH, AXIAL LENGTH
HS04033600 0                                  * RHS BC TYPE, ASSOC CV, POOL HT FLAGS
HS04033801 301.     11                         * INITIAL TEMPERATURE, NODE NO.
*
HS04034000 10 1 0 0                           * NO. NODES, TYPE, NO SS INIT, TRANS ITER
HS04034001 CEILING
HS04034002 25.5     0.                                       * BOTTOM ALTITUDE, ORIENTATION
HS04034100 -1 1 0.                                             * NODALIZATION FLAGS, INSIDE RADIUS
HS04034102  .001   2
HS04034103  .003   3
HS04034104  .007   4
HS04034105  .015   5
HS04034106  .023   6
HS04034107  .039   7
HS04034108  .071   8
HS04034109  .135   9
HS04034110  .150  10
HS04034201 'CARBON STEEL'      2              * MATERIAL TYPE, MESH INTERVAL
HS04034202 CONCRETE     9
HS04034300 0                                  * SOURCE TYPE, FLAG, SOURCE MULTIPLIER
HS04034400 1     406  'EXT'  1.     1.            * LHS BC TYPE, ASSOC CV, POOL HT FLAGS
HS04034500 245.     11.     11.                               * LHS AREA, CHARAC LENGTH, AXIAL LENGTH
HS04034600 0                                  * RHS BC TYPE, ASSOC CV, POOL HT FLAGS
HS04034801 301.     10                         * INITIAL TEMPERATURE, NODE NO.
*
HS04035000  2 1 0 0                           * NO. NODES, TYPE, NO SS INIT, TRANS ITER
HS04035001 STEEL
HS04035002 14.2     1.                                       * BOTTOM ALTITUDE, ORIENTATION
HS04035100 -1 1 0.                                             * NODALIZATION FLAGS, INSIDE RADIUS
HS04035102  .0127  2
HS04035201 'CARBON STEEL'      1              * MATERIAL TYPE, MESH INTERVAL
HS04035300 0                                  * SOURCE TYPE, FLAG, SOURCE MULTIPLIER
HS04035400 1     406  'EXT'  1.     1.            * LHS BC TYPE, ASSOC CV, POOL HT FLAGS
HS04035500  4.5  3.          3.                               * LHS AREA, CHARAC LENGTH, AXIAL LENGTH
HS04035600 1     406  'EXT'  1.     1.            * RHS BC TYPE, ASSOC CV, POOL HT FLAGS
HS04035700  4.5  3.          3.
HS04035801 301.  2                            * INITIAL TEMPERATURE, NODE NO.
*
***** LEVEL [illegible]-MAIN SURFACES
*****
HS04036000 12 1 0 0                           * NO. NODES, TYPE, NO SS INIT, TRANS ITER
HS04036001 EXTWALL
HS04036002 14.2     1.                                       * BOTTOM ALTITUDE, ORIENTATION
HS04036100 -1 1 0.                                             * NODALIZATION FLAGS, INSIDE RADIUS
HS04036102  .001   2
HS04036103  .003   3
HS04036104  .007   4
HS04036105  .015   5
HS04036106  .023   6
HS04036107  .039   7
HS04036108  .071   8
HS04036109  .135   9
HS04036110  .263  10
HS04036111  .500  11
HS04036112  .600  12
HS04036201 CONCRETE     11                    * MATERIAL TYPE, MESH INTERVAL
HS04036300 0                                  * SOURCE TYPE, FLAG, SOURCE MULTIPLIER
HS04036400 1     407  'EXT'  1.     1.            * LHS BC TYPE, ASSOC CV, POOL HT FLAGS
HS04036500 1222.  5.1  5.1                     * LHS AREA, CHARAC LENGTH, AXIAL LENGTH
HS04036600 4200 410   'EXT'  1.     1.            * RHS BC TYPE, ASSOC CV, POOL HT FLAGS
HS04036700 1222.  5.1  5.1                     * RHS AREA, CHARAC LENGTH, AXIAL LENGTH
HS04036801 301.     12                         * INITIAL TEMPERATURE, NODE NO.
*
HS04037000 14 1 0 0                           * NO. NODES, TYPE, NO SS INIT, TRANS ITER
HS04037001 PCWALL
HS04037002 14.2     1.                                       * BOTTOM ALTITUDE, ORIENTATION
HS04037100 -1 1 0.                                             * NODALIZATION FLAGS, INSIDE RADIUS
HS04037102  .001   2
HS04037103  .003   3
HS04037104  .007   4
HS04037105  .015   5
HS04037106  .023   6
HS04037107  .039   7
HS04037108  .071   8
HS04037109  .135   9
HS04037110  .263  10
HS04037111  .500  11
HS04037112  .750  12
HS04037113 1.0    13
HS04037114 1.5    14
HS04037201 CONCRETE     13                    * MATERIAL TYPE, MESH INTERVAL
HS04037300 0                                  * SOURCE TYPE, FLAG, SOURCE MULTIPLIER
HS04037400 1     407  'EXT'  1.     1.            * LHS BC TYPE, ASSOC CV, POOL HT FLAGS
HS04037500 950.     5.1  5.1                   * LHS AREA, CHARAC LENGTH, AXIAL LENGTH
HS04037600 0                                  * RHS BC TYPE, ASSOC CV, POOL HT FLAGS
```

```
HS04037801 301.      14                    * INITIAL TEMPERATURE, NODE NO.
*
HS04039000 11 1 0 0                   * NO. NODES, TYPE, NO SS INIT, TRANS ITER
HS04039001  FLOOR
* USED VERTICAL ORIENTATION TO ELIMINATE POOL HEAT TRANSFER
HS04039002 14.2   1.                                  * BOTTOM ALTITUDE, ORIENTATION
HS04039100 -1     1 0.                               * NODALIZATION FLAGS, INSIDE RADIUS
HS04039102  .001   2
HS04039103  .003   3
HS04039104  .007   4
HS04039105  .015   5
HS04039106  .023   6
HS04039107  .039   7
HS04039108  .071   8
HS04039109  .135   9
HS04039110  .263  10
HS04039111  .500  11
HS04039201 CONCRETE    10              * MATERIAL TYPE, MESH INTERVAL
HS04039300 0                           * SOURCE TYPE, FLAG, SOURCE MULTIPLIER
HS04039400 1    407  'EXT'  1.    1.        * LHS BC TYPE, ASSOC CV, POOL HT FLAGS
HS04039500 307.     11.    11.                        * LHS AREA, CHARAC LENGTH, AXIAL LENGTH
HS04039600 0                           * RHS BC TYPE, ASSOC CV, POOL HT FLAGS
HS04039801 301.     11                   * INITIAL TEMPERATURE, NODE NO.
*
HS04040000 10 1 0 0                    * NO. NODES, TYPE, NO SS INIT, TRANS ITER
HS04040001 CEILING
HS04040002 25.5    0.                                 * BOTTOM ALTITUDE, ORIENTATION
HS04040100 -1 1 0.                                      * NODALIZATION FLAGS, INSIDE RADIUS
HS04040102  .001   2
HS04040103  .003   3
HS04040104  .007   4
HS04040105  .015   5
HS04040106  .023   6
HS04040107  .039   7
HS04040108  .071   8
HS04040109  .135   9
HS04040110  .150  10
HS04040201 'CARBON STEEL'     2        * MATERIAL TYPE, MESH INTERVAL
HS04040202 CONCRETE    9
HS04040300 0                           * SOURCE TYPE, FLAG, SOURCE MULTIPLIER
HS04040400 1    407  'EXT'  1.    1.        * LHS BC TYPE, ASSOC CV, POOL HT FLAGS
HS04040500 307.     11.    11.                        * LHS AREA, CHARAC LENGTH, AXIAL LENGTH
HS04040600 0                           * RHS BC TYPE, ASSOC CV, POOL HT FLAGS
HS04040801 301.     10                   * INITIAL TEMPERATURE, NODE NO.
*
HS04041000  2 1 0 0                    * NO. NODES, TYPE, NO SS INIT, TRANS ITER
HS04041001 STEEL
HS04041002 14.2     1.                                * BOTTOM ALTITUDE, ORIENTATION
HS04041100 -1 1 0.                                      * NODALIZATION FLAGS, INSIDE RADIUS
HS04041102  .0127  2
HS04041201 'CARBON STEEL'     1        * MATERIAL TYPE, MESH INTERVAL
HS04041300 0                           * SOURCE TYPE, FLAG, SOURCE MULTIPLIER
HS04041400 1    407  'EXT'  1.    1.        * LHS BC TYPE, ASSOC CV, POOL HT FLAGS
HS04041500 13.3  3.          3.                       * LHS AREA, CHARAC LENGTH, AXIAL LENGTH
HS04041600 1    407  'EXT'  1.    1.        * RHS BC TYPE, ASSOC CV, POOL HT FLAGS
HS04041700 13.3  3.          3.
HS04041801 301.  2                     * INITIAL TEMPERATURE, NODE NO.
*
*****  REFUELING BAY SURFACES
HS04042000  6 1 0 0                    * NO. NODES, TYPE, NO SS INIT, TRANS ITER
HS04042001  EXTWALL
HS04042002 26.1     1.                                * BOTTOM ALTITUDE, ORIENTATION
HS04042100 -1 1 0.                                      * NODALIZATION FLAGS, INSIDE RADIUS
HS04042102  .0002  2
HS04042103  .0004  3
HS04042104  .0008  4
HS04042105  .0015  5
HS04042106  .00254 6
HS04042201 'CARBON STEEL'     5        * MATERIAL TYPE, MESH INTERVAL
HS04042300 0                           * SOURCE TYPE, FLAG, SOURCE MULTIPLIER
HS04042400 1    408  'EXT'  1.    1.        * LHS BC TYPE, ASSOC CV, POOL HT FLAGS
HS04042500 3063.  16.    16.                          * LHS AREA, CHARAC LENGTH, AXIAL LENGTH
HS04042600 0                           * RHS BC TYPE, ASSOC CV, POOL HT FLAGS
HS04042801 301.      6                   * INITIAL TEMPERATURE, NODE NO.
*
HS04043000  6 1 0 0                    * NO. NODES, TYPE, NO SS INIT, TRANS ITER
HS04043001  CEILING
HS04043002 45.0    0.                                 * BOTTOM ALTITUDE, ORIENTATION
HS04043100 -1 1 0.                                      * NODALIZATION FLAGS, INSIDE RADIUS
HS04043102  .002   2
HS04043103  .004   3
HS04043104  .008   4
HS04043105  .015   5
HS04043106  .0254  6
HS04043201 'CARBON STEEL'     5        * MATERIAL TYPE, MESH INTERVAL
HS04043300 0                           * SOURCE TYPE, FLAG, SOURCE MULTIPLIER
HS04043400 1    408  'EXT'  1.    1.        * LHS BC TYPE, ASSOC CV, POOL HT FLAGS
HS04043500 1661.  16.    16.                          * LHS AREA, CHARAC LENGTH, AXIAL LENGTH
HS04043600 0                           * RHS BC TYPE, ASSOC CV, POOL HT FLAGS
HS04043801 301.      6                   * INITIAL TEMPERATURE, NODE NO.
*
```

```
HS04044000 10 1 0 0                          * NO. NODES, TYPE, NO SS INIT, TRANS ITER
HS04044001  FLOOR
* USED VERTICAL ORIENTATION TO ELIMINATE POOL HEAT TRANSFER
HS04044002 26.1     1.                                           * BOTTOM ALTITUDE, ORIENTATION
HS04044100 -1 1 0.                                                  * NODALIZATION FLAGS, INSIDE RADIUS
HS04044102  .001    2
HS04044103  .003    3
HS04044104  .007    4
HS04044105  .015    5
HS04044106  .023    6
HS04044107  .039    7
HS04044108  .071    8
HS04044109  .135    9
HS04044110  .230   10
HS04044201 CONCRETE     9                    * MATERIAL TYPE, MESH INTERVAL
HS04044300 0                                 * SOURCE TYPE, FLAG, SOURCE MULTIPLIER
HS04044400 1    408  'EXT'  1.    1.            * LHS BC TYPE, ASSOC CV, POOL HT FLAGS
HS04044500 1362.  16.    16.                                 * LHS AREA, CHARAC LENGTH, AXIAL LENGTH
HS04044600 0                                 * RHS BC TYPE, ASSOC CV, POOL HT FLAGS
HS04044801 301.     10                        * INITIAL TEMPERATURE, NODE NO.
*
HS04045000  2 1 0 0                          * NO. NODES, TYPE, NO SS INIT, TRANS ITER
HS04045001  STEEL
HS04045002 26.1     1.                                       * BOTTOM ALTITUDE, ORIENTATION
HS04045100 -1 1 0.                                              * NODALIZATION FLAGS, INSIDE RADIUS
HS04045102  .0127  2
HS04045201 'CARBON STEEL'      1            * MATERIAL TYPE, MESH INTERVAL
HS04045300 0                                * SOURCE TYPE, FLAG, SOURCE MULTIPLIER
HS04045400 1     408  'EXT'  1.    1.          * LHS BC TYPE, ASSOC CV, POOL HT FLAGS
HS04045500 356.       3.      3.                                 * LHS AREA, CHARAC LENGTH, AXIAL LENGTH
HS04045600 1     408  'EXT'  1.    1.          * RHS BC TYPE, ASSOC CV, POOL HT FLAGS
HS04045700 356.       3.      3.
HS04045801 301.     2                        * INITIAL TEMPERATURE, NODE NO.
*
***** TURBINE BUILDING SURFACES
HS04046000  6 1 0 0                          * NO. NODES, TYPE, NO SS INIT, TRANS ITER
HS04046001  EXTWALL
HS04046002  5.1     1.                                       * BOTTOM ALTITUDE, ORIENTATION
HS04046100 -1 1 0.                                              * NODALIZATION FLAGS, INSIDE RADIUS
HS04046102  .0002  2
HS04046103  .0004  3
HS04046104  .0008  4
HS04046105  .0015  5
HS04046106  .00254 6
HS04046201 'CARBON STEEL'      5            * MATERIAL TYPE, MESH INTERVAL
HS04046300 0                                * SOURCE TYPE, FLAG, SOURCE MULTIPLIER
HS04046400 1     409  'EXT'  1.    1.          * LHS BC TYPE, ASSOC CV, POOL HT FLAGS
HS04046500 ' 37.      16.  16.                                * LHS AREA, CHARAC LENGTH, AXIAL LENGTH
HS04046600 0                                * RHS BC TYPE, ASSOC CV, POOL HT FLAGS
HS04046801 301.       6                      * INITIAL TEMPERATURE, NODE NO.
*
HS04047000  6 1 0 0                          * NO. NODES, TYPE, NO SS INIT, TRANS ITER
HS04047001  CEILING
HS04047002 21.9     0.                                       * BOTTOM ALTITUDE, ORIENTATION
HS04047100 -1 1 0.                                              * NODALIZATION FLAGS, INSIDE RADIUS
HS04047102  .002    2
HS04047103  .004    3
HS04047104  .008    4
HS04047105  .015    5
HS04047106  .0254   6
HS04047201 'CARBON STEEL'      5            * MATERIAL TYPE, MESH INTERVAL
HS04047300 0                                * SOURCE TYPE, FLAG, SOURCE MULTIPLIER
HS04047400 1     409  'EXT'  1.    1.          * LHS BC TYPE, ASSOC CV, POOL HT FLAGS
HS04047500 8807.  16.    16.                              * LHS AREA, CHARAC LENGTH, AXIAL LENGTH
HS04047600 0                                * RHS BC TYPE, ASSOC CV, POOL HT FLAGS
HS04047801 301.       6                      * INITIAL TEMPERATURE, NODE NO.
*
HS04048000  6 1 0 0                          * NO. NODES, TYPE, NO SS INIT, TRANS ITER
HS04048001  FLOOR
* USED VERTICAL ORIENTATION TO ELIMINATE POOL HEAT TRANSFER
HS04048002  5.1     1.                                       * BOTTOM ALTITUDE, ORIENTATION
HS04048100 -1 1 0.                                              * NODALIZATION FLAGS, INSIDE RADIUS
HS04048102  .2      5
HS04048103  .23     6
HS04048201 CONCRETE     5                   * MATERIAL TYPE, MESH INTERVAL
HS04048300 0                                * SOURCE TYPE, FLAG, SOURCE MULTIPLIER
HS04048400 1     409  'EXT'  1.    1.          * LHS BC TYPE, ASSOC CV, POOL HT FLAGS
HS04048500 8807.  16.    16.                              * LHS AREA, CHARAC LENGTH, AXIAL LENGTH
HS04048600 0                                * RHS BC TYPE, ASSOC CV, POOL HT FLAGS
HS04048801 301.       6                      * INITIAL TEMPERATURE, NODE NO.
*
HS04049000  2 1 0 0                          * NO. NODES, TYPE, NO SS INIT, TRANS ITER
HS04049001  STEEL
HS04049002  5.1     1.                                       * BOTTOM ALTITUDE, ORIENTATION
HS04049100 -1 1 0.                                              * NODALIZATION FLAGS, INSIDE RADIUS
HS04049102 .0127   2
HS04049201 'CARBON STEEL'      1            * MATERIAL TYPE, MESH INTERVAL
HS04049300 0                                * SOURCE TYPE, FLAG, SOURCE MULTIPLIER
HS04049400 1     409  'EXT'  1.    1.          * LHS BC TYPE, ASSOC CV, POOL HT FLAGS
HS04049500 356.       3.      3.                                 * LHS AREA, CHARAC LENGTH, AXIAL LENGTH
HS04049600 1     409  'EXT'  1.    1.          * RHS BC TYPE, ASSOC CV, POOL HT FLAGS
```

```
HS04049700 356.     3.     3.
HS04049601 301.   2                              * INITIAL TEMPERATURE, NODE NO.
*****************************************************************************
***** TABULAR FUNCTION INPUT FOR HEAT SLABS
*****
TF20000 'RHS HT COEF' 1 1.  0.  * NAME, NO. PAIRS, MUL CONST, ADD CONST
TF20010 0.  6.0                  * TIME, HEAT TRANSFER COEFFICIENT
*
TF21000 'RHS T - 286' 1 1.  0.  * NAME, NO. PAIRS, MUL CONST, ADD CONST
TF21010 0.  286.                                 * TIME, RHS TEMPERATURE
*****************************************************************************
*****************************************************************************
*** CORE PACKAGE INPUT
*****************************************************************************
*          BROWNS FERRY AND PEACH BOTTOM INPUT ADAPTED FROM THE
*          MELCOR CORE INPUT DECK CONSTUCTED FOR LASALLE
*
*            LASALLE C-LATTICE SPACINGS CHANGED TO
*            D-LATTICE SPACINGS WHICH ARE APPROPRIATE
*            FOR BROWNS FERRY AND PEACH BOTTOM
*
*            CORE NODALIZATION CHANGED FROM 3 RADIAL RINGS AND
*            6 AXIAL LAYERS TO 3 RADIAL RINGS AND 5 AXIAL LAYERS
*****************************************************************************
***  GENERAL CORE INPUT
*****************************************************************************
* 11.28.90 Introducing the 6th axial cell at the top of the core
*          NRAD     NAXL      NTLP      NCVOL   NLH     NPNTOT
COR00000  3         12        6         3       5       3
* COR00000  3         11        6         3       5       3
*
* adjusting LH parameters 02.14.91 (JV)
*          RFUEL    RCLAD     DRGAP     PITCH   DXCAN   DXSS    DXLH
COR00001  .005207  .0061341  .0001143 .016     .00254  .0012   .1894
* COR00001  .005207  .0061341  .0001143 .016     .00254  .0012   .2254
*
*          IRTYP    MCRP
COR00002  BWR      B4C
*
*          FCNCL    FSSCN    FCELR    FCELA    FLPUP
COR00003  0.50     0.95     0.30     0.15     0.95    * CHNGED FROM DFLT VALS 1-22-90
*
* 10.22.90 time0:  fission power
*          NTPCOR
* COR00004  101
COR00004  101  -88
*
*          HFRZFU   HFRZZR   HFRZSS   HFRZZX   HFRZSI   HFRZCP
COR00005  4000.0   4000.0   4000.0   4000.0   4000.0   4000.0
*
*          NTUOZR   MTZZZR   MTSXSS   MTCPSS   FUOZR    FZXZR    FSXSS    FCPSS
COR00007  1        2        2        2        0.2      1.0      1.0      0.0
*
*          DRCLMN   DRSSMN
COR00008  1.0E-06  1.0E-06
*
*          HDBPN    HDBLH      TPFAIL    CDISPN
* adjusting LH and penetration heat transfer coefficients 02.14.91 (JV)
COR00009  1200.0   1200.0     1273.15   1.0
* COR00009  600.0    600.0      1273.15   1.0
*
*          XFE      XCR       XNI       XCAR
COR00010  0.74     0.18      0.08      0.0
*
*          CELL ELEVATIONS AND POROSITIES
*          Z        DZ        PORIN    PORDP
CORZ0101  0.0      1.2954    0.                 0.3
CORZ0201  1.2954   0.9803    0.                 0.3
CORZ0301  2.2757   0.9803    0.                 0.3
CORZ0401  3.2560   0.9803    0.                 0.3
CORZ0501  4.2363   0.9803    0.                 0.3
CORZ0601  5.2166   0.2777    0.99     0.3
* 11.28.90 Introducing the 6th axial cell at the top of the core
CORZ0701  5.4943   0.7620    0.99     0.3
CORZ0801  6.2563   0.7620    0.99     0.3
CORZ0901  7.0183   0.7620    0.99     0.3
CORZ1001  7.7803   0.7620    0.99     0.3
CORZ1101  8.5423   0.7620    0.99     0.3
CORZ1201  9.3043   0.3627    0.99     0.3
*
*          CELL CROSS-SECTIONAL BOUNDARY AREAS
*          ASCELA
CORR0101  7.648
CORR0201  7.287
CORR0301  2.251
*
*          BOUNDARY HEAT STRUCTURES
CORZ0102  32001
CORZ0202  32001  1
CORZ0302  32001
CORZ0402  32004
```

```
CORZ0602  32006
CORZ0602  32006 11
CORZ0702  33007
CORZ0802  33008
CORZ0902  33009
CORZ1002  33010
CORZ1102  33011
* 11.28.90 Introducing the 6th axial cell at the top of the core
CORZ1202  33012
*
CORR0102  36003
CORR0202  36003
CORR0302  36003
*****************************************************************************
*          LOWER PLENUM AND CORE INPUT
*****************************************************************************
* CRD HOUSING - *** NOTE *** ALL MASS INPUT WITH PENETRATION INPUT
* CR GUIDE TUBES (185)
* CORE SUPPORT STRUCTURE (FUEL SUPPORT PIECES, CORE PLATE,
*   AND FUEL ASSEMBLY NOSE PIECES)
*
* R A     IREFN   ICVHC   ICVHB
COR10101  -1      320     320  *  LOWER PLENUM:  CRD HOUSING
COR20101  101
COR30101  101
*
COR10201  -1      320     320  *  LOWER PLENUM:  CR GUIDE TUBES
COR20201  102
COR30201  102
*
COR10301  102
COR20301  202
COR30301  302
*
COR10401  102     320     320
COR20401  202
COR30401  302
*
COR10501  102     320     320
COR20501  202
COR30501  302
*
COR10601  -1      320     320  *  LOWER PLENUM:  CORE SUPPORT STRUCTURES
COR20601  106
COR30601  106
*
COR10701  -1      340     330  *  CORE
COR20701  107
COR30701  107
*
COR10801  107
COR20801  207
COR30801  307
*
COR10901  107
COR20901  207
COR30901  307
*
COR11001  107
COR21001  207
COR31001  307
*
COR11101  107
COR21101  207
COR31101  307
* 11.28.90 Introducing the 6th axial cell at the top of the core
COR11201  107
COR21201  207
COR31201  307
*
*            XMFU     XMCL     *XMSS*    XMCP      XMCN
COR10102     0.0      0.0       0.0      0.0       0.0   *  CRD HOUSING
*
COR10202     0.0      0.0     2336.25    0.0       0.0   *  CR GUIDE TUBES
COR2\/202    -1.E3    -1.E3    2226.            -1.E3    -1.E3
COR30202    -1.E3    -1.E3     487.75   -1.E3     -1.E3
COR10602     0.0      0.0     6675.0     0.0       0.0   *  CORE SUPPORT
COR20602    -1.E3    -1.E3    6360.0    -1.E3     -1.E3  *  STRUCTURES
COR30602    -1.E3    -1.E3    1965.0    -1.E3     -1.E3
*
COR10702  14996.      3153.          1077.        156.9   2339.        *  CORE
COR20702  14287.      3004.          1026.        151.4   2229.
COR30702   4414.       925.           317.         46.6    686.5
* 11.28.90 Introducing the 6th axial cell at the top of the core
* no fuel in the top cell
* Adjusting Zr mass in the top cell:  01.11-12, 1991 meeting with FAI
* 01.24.91
COR11202      0.          -1.E3    10744.        0.0   1169.5  * top cell
COR21202      0.          -1.E3    10237.        0.0   1114.5
COR31202      0.          -1.E3     3163.        0.0    344.25
* COR11202      0.          -1.E3    10744.        0.0     -1.E3 * top cell
```

```
* COR21202      0.        -1.E3    10237.        0.0     -1.E3
* COR31202      0.        -1.E3     3163.        6.0     -1.E3
*
*    TOP GUIDE INCLUDED WITH AXIAL LEVEL 12 STEEL MASS
*old TOP GUIDE INCLUDED WITH AXIAL LEVEL 11 STEEL MASS
*
* 11.19.90 time0:  TFU, TCL, TSS originally 564.0
*          TFU      TCL      TSS      TCN
COR10103   558.0    558.0    558.0    558.0  *  CRD HOUSING
COR10203   558.0    558.0    558.0    558.0  *  CR GUIDE TUBES
COR10603   548.0    548.0    548.0    548.0  *  CORE SUPPORT STRUCTURES
COR10703   558.0    558.0    558.0    558.0  *  CORE
*
*          DHYCL    DHYSS    DHYDP    DHYCNC   DHYCNB
COR10104  1.0      1.0      0.0254    1.0      1.0   *  CRD HOUSING
COR10204  1.0      0.3      0.0254    1.0      1.0   *  CR GUIDE TUBES
COR10604  1.0      0.15     0.0254    1.0      1.0   *  CORE SUPPORT STRUCTURES
COR10704  0.005    0.003    0.0254    0.005    0.003 *  CORE
*
*          ASCELR   AFLOWC   AFLOWB
COR10105  12.70    7.648    0.0     *  CRD HOUSING
COR20105  17.75    7.287    0.0
COR30105  19.04    2.251    0.0
*
COR10205  9.61     7.348    0.0     *  CR GUIDE TUBES
COR20205  13.43    7.001    0.0
COR30205  14.41    2.163    0.0
*
COR10605  2.72     4.8171   0.0     *  CORE SUPPORT STRUCTURES
COR20605  3.80     4.3992   0.0
COR30605  4.08     1.3692   0.0
*
COR10705  7.47     3.53775 1.066   *  CORE
COR20705  10.44    3.3708  1.0176
COR30705  11.20    1.0414  0.3144
*
*           ASFU     ASCL     ASSS     ASCN
COR10106    0.0      0.0      0.0      0.0   *  CRD HOUSING
*
COR10206    0.0      0.0    141.64     0.0   *  CR GUIDE TUBES
COR20206   -1.E3    -1.E3   134.96    -1.E3
COR30206   -1.E3    -1.E3    41.7     -1.E3
*
COR10606    0.0      0.0     66.75     0.0   *  CORE SUPPORT STRUCTURES
COR20606   -1.E3    -1.E3    63.6     -1.E3
COR30606   -1.E3    -1.E3    19.65    -1.E3
*
COR10706  820.4     639.2   203.4    138.9   *  CORE
COR20706  800.7     609.0   193.9    132.3
COR30706  184.7     188.2    59.9     40.9
*****************************************************************************
*       LOWER HEAD INPUT
*****************************************************************************
* time0:  561 to 548.0
*          IRS      IRE      EMLH     TLH      ASLH     ICVLH    ICVCAV
* adjusting mass of LH 02.14.91 (JV)
CORLHD01  1        1        3.34E04  548.0    7.648    320      100
CORLHD02  2        2        3.18E04  548.0    7.287    320      100
CORLHD03  3        3        0.98E04  548.0    2.251    320      100
* CORLHD01  1        1        13670.0  548.0    7.648    320      100
* CORLHD02  2        2        13025.0  548.0    7.287    320      100
* CORLHD03  3        3         4024.0  548.0    2.251    320      100
*****************************************************************************
*          LOWER HEAD PENETRATIONS INPUT
*****************************************************************************
*          ALL PENETRATIONS ARE CRD HOUSINGS AND STUB TUBES
*          GEOMETRIC VALUES ARE ESTIMATES
* initial LP penetration diameter:  from 0.1 : to 0.223 m (0.039 m2)
*          IPNREF   INP      EMPN     TPN      ASPN     AXPN     DFLPN
* adjusting masses, HT coefficients, areas of penetrations 02.14.91 (JV)
* ASSUMING A CONTROL ROD GUIDE TUBE THICKNESS OF 7.66E-3 meters
CORPEN01  -1       1        67.0     548.0    1.11     3.25E-2 0.223
CORPEN02  -1       2        67.0     548.0    1.11     3.25E-2 0.223
CORPEN03  -1       3        67.0     548.0    1.11     3.25E-2 0.223
* CORPEN01  -1       1         940.0   548.0    24.43    0.675    0.223
* CORPEN02  -1       2         895.5   548.0    23.28    0.648    0.223
* CORPEN03  -1       3         276.7   548.0     7.19    0.169    0.223
*
*          DTDZ MODEL INPUT - VOLUME INLET SPECIFICATIONS
*
*          CV       SOURCE
CORTIN00  320      320      *LOWER PLENUM, LOWER PLENUM
CORTIN01  330      320      *BYPASS, LOWER PLENUM
CORTIN02  340      320      *CORE, LOWER PLENUM
*
* CANISTER BREACH FLOW PATH - NOT CURRENTLY USED
*
*FL39100    'CAN BREACH'   340  330  7.3993  7.3993
*FL39101    0.1319  1.0  0.0                * INITIALLY CLOSED
*FL39102    3 * HORIZONTAL FLOW PATH
*FL39103    5.0     5.0
```

```
*FL391B0   0.1319  1.0  0.4511
***        ADDED VALVE AND CF IN CASE WE WANT TO OPEN THIS UP
***        RED  9/10/86
*FL391V0    81   145   145
*
*CF08100   'CAN FAIL THRESH' T-O-F  1  1.  0.
*CF08103    -1.E9  1.E5
*CF08110   1.  0.  HS-TEMP-33007-1
*
* MAIN STEAM LINE BREACH FLOW PATH - NOT CURRENTLY USED
*
*FL39600   'MSL BREACH'   360  100  16.73  16.73
*FL39601   0.1319  1.0  0.0               * INITIALLY CLOSED
*FL39602   3 * HORIZONTAL FLOW PATH
*FL39603   5.0     5.0
*FL396B0   0.1319  1.0  0.4511
***        ADDED VALVE AND CF IN CASE WE WANT TO OPEN THIS UP
***        RED  9/10/86
*FL396V0    82   145   145
*
*CF08200   'MSL FAIL THRESH' T-O-F  1  1.  0.
*CF08203    -1.E9  1.E5
*CF08210   1.  0.  HS-TEMP-36002-1
*
* VESSEL BREACH INPUT
*
* initial breach area is 0.039 m2, 12.13.90 (originally 0.01 m2)
FL39900   'VESSEL BREACH'   320  100  0.0      -0.2254
FL39901   0.039 0.2254  0.0                * INITIALLY CLOSED
FL39902   3                                * HORIZONTAL FLOW PATH
FL39903   1.0      1.0
FL399B0   0.039  0.2254  0.1128
FL399V0   -1  130  130
*
* initial breach area is 0.039 m2, 12.13.90 (originally 0.01 m2)
CF13000   'VESSEL BREACH'  DIVIDE  2  1.0  0.0
CF13010   0.0  0.039    COR-ABRCH
CF13011   1.0  0.0      COR-ABRCH
*
* FLOW BLOCKAGE INPUT
*
CF09100  'FLAREA-1'  MIN  2  1.0  0.0
CF09110  0.0  2.18248  COR-AFLMIN.103.111
CF09111  1.0  0.0      COR-AFLMIN.103.111
*
CF09200  'FLAREA-2'  MIN  2  1.0  0.0
CF09210  0.0  2.07949  COR-AFLMIN.203.211
CF09211  1.0  0.0      COR-AFLMIN.203.211
*
CF09300  'FLAREA-3'  MIN  2  1.0  0.0
CF09310  0.0  0.64249  COR-AFLMIN.303.311
CF09311  1.0  0.0      COR-AFLMIN.303.311
*
CF09400  'FLAREA-T'  ADD  3  1.0  0.0
CF09410  1.0  0.0        CFVALU.091
CF09411  1.0  0.0        CFVALU.092
CF09412  1.0  0.0        CFVALU.093
* Time0:  drop core blockage, 11.02.90
* CF09500   'FRAC-AREA'  DIVIDE  2  1.0  0.0
* CF09502  3  0.03  0.61748
* CF09510  0.0  7.9428   CFVALU.094
* CF09511  1.0  0.0      CFVALU.094
* FL324V0    -1   95  95                       * CF FOR FLOW BLOCKAGE
*
*****************************************************************************
*****************************************************************************
*** DECAY HEAT PACKAGE
*****************************************************************************
***  SPECIFY A BWR
DCHREACTOR   BWR
*
*          SET REACTOR SHUTDOWN TIME TO -28200 SEC = -470.0 MIN,
*          THE START TIME OF THE MARCON BROWNS FERRY
*          STATION BLACKOUT CALCULATION
*
* DCHSHUT    0      -28200.0   * INMADNI JULY 19, 1988
DCHSHUT    0       100.0
*
*          INPUT MARCON TOTAL DECAY HEAT DATA
*          AS TABULAR FUNCTION TF077
*
*          TABULAR FUNCTION TF077 GIVES DECAY HEAT AS A FRACTION
*          OF THERMAL POWER AT SHUTDOWN VS TIME SINCE SHUTDOWN
*
*          THE ORIGINAL SOURCE FOR THE DEFAULT DECAY HEAT DATA
*          IN MARCON IS ERIC HASKIN'S SANDIA-ORIGEN RUN C3
*
*          THE NORMALIZED DECAY POWER CURVE WAS CHANGE TO MATCH THAT
*          OF THE LASALLE CALCULATION ON 10-27-87 BY CJS.
*
*          THERMAL POWER AT SHUTDOWN = 3293 MW
```

```
*
* 10.24.90 time0:  steady state power table
* Total power - decay (6 % ) = 3293*.94=3095.42
* 1 sec ramp, 11.06.90
* 15 sec ramp, 11.15.90, same, later uncovery ...
CF06800 CORE-POWER TAB-FUN 1 1.0 0.0
CF06803 68
CF06810 1.0 0.0 TIME
TF06800  CORE-POWER 4 1.0 0.0
* reduced power 11.19.90 to 2000 MWt.  Core uncovered ...
TF06811  0.0 0.0 1.0 3095.42E06 100.0 3095.42E06   100.1 0.0
*
*
DCHDECPOW      TF.77
TF07700   'DECAY HEAT'  44  3293.0E06  0.0
*
*        TIME SINCE         DECAY HEAT
*         SHUTDOWN      (FRACTION SHUTDOWN
*                          THERMAL POWER)
TF07711  0.00000E+00  6.00000E-02
TF07712  1.00000E+00  5.71500E-02
TF07713  1.50000E+00  5.55200E-02
TF07714  2.00000E+00  5.43700E-02
TF07715  3.00000E+00  5.20400E-02
TF07716  4.00000E+00  5.04000E-02
TF07717  6.00000E+00  4.80700E-02
TF07718  8.00000E+00  4.61900E-02
TF07719  1.00000E+01  4.47300E-02
TF07720  1.50000E+01  4.20500E-02
TF07721  2.00000E+01  4.01500E-02
TF07722  3.00000E+01  3.75600E-02
TF07723  4.00000E+01  3.57200E-02
TF07724  6.00000E+01  3.31300E-02
TF07725  8.00000E+01  3.13700E-02
TF07726  1.00000E+02  3.00000E-02
TF07727  1.50000E+02  2.77700E-02
TF07728  2.00000E+02  2.61900E-02
TF07729  3.00000E+02  2.42800E-02
TF07730  4.00000E+02  2.29300E-02
TF07731  6.00000E+02  2.10200E-02
TF07732  8.00000E+02  1.96500E-02
TF07733  1.00000E+03  1.85900E-02
TF07734  1.50000E+03  1.66200E-02
TF07735  2.00000E+03  1.52200E-02
TF07736  3.00000E+03  1.35400E-02
TF07737  4.00000E+03  1.23500E-02
TF07738  6.00000E+03  1.06700E-02
TF07739  8.00000E+03  9.81500E-03
TF07740  1.00000E+04  9.15200E-03
TF07741  1.50000E+04  8.19300E-03
TF07742  2.00000E+04  7.51200E-03
TF07743  3.00000E+04  6.76400E-03
TF07744  4.00000E+04  6.23200E-03
TF07745  6.00000E+04  5.48400E-03
TF07746  8.00000E+04  5.03900E-03
TF07747  1.00000E+05  4.6[illegible]300E-03
TF07748  1.50000E+05  4.14100E-03
TF07749  2.00000E+05  3.74900E-03
TF07750  3.00000E+05  3.27500E-03
TF07751  4.00000E+05  2.94000E-03
TF07752  6.00000E+05  2.46600E-03
TF07753  8.00000E+05  2.18700E-03
TF07754  1.00000E+06  1.97100E-03
*        END OF DECAY HEAT TABLE
*******************************************************************************
*******************************************************************************
*** TRANSFER PROCESS PACKAGE INPUT
*******************************************************************************
*   'IN' TRANSFER PROCESS FOR CORE PACKAGE
*            NMSIN    NTHRM
TPIN10100    5        9
TPIN10200    5        9
*
*    'OUT' TRANSFER PROCESS FOR FDI PACKAGE
*            NMSOT    NPOTDI   IOTMTX
TPOT10100    5        101      UIN.103
TPOT10200    5        102      DEF.1
*
*     COR-CAV TRANSLATION MATRIX
*     *** NOTE *** CONTROL POISON MASS IS NOT CONSERVED
*            NROW     NCOL
TPN1030000   5        6
*            NROW/NCOL  VALUE
TPN1030001   1/1        1.0      * UO2 MASS
TPN1030002   2/2        1.0      * ZRO2 MASS
TPN1030003   3/3        1.0      * STEEL MASS
TPN1030004   4/4        1.0      * ZR MASS
TPN1030005   5/5        1.0      * STEEL OXIDE MASS
*
*           TRANSFER PROCESS INPUT - RADIONUCLIDE MASS
*           NMSIN  NTHRM
```

```
TPIN60100   16      1
TPIN60200   16      1
*           NMSOT  NPOTOI  IOTNTI
TPOT60100   16      601    DEF.1
TPOT60200   16      602    DEF.1
*****************************************************************************
*****************************************************************************
*** CAVITY PACKAGE INPUT
* LaSalle deck from Sandia has a more updated version of CAVITY model
* Use it for PB later...  12.12.90 LN
* Properties were adjusted to MAAP 12.12.90:  CA C4 C2 C1
* C5+C6=0.047 C3
*****************************************************************************
***       CONTROL VOLUME NUMBER
CAV0000    100               'CAVITY 1'
* 02.11.91 changing to limestone concrete with iron rebar (JV)
CAV00C0    LIMESTONE/CS
CAV00C1    FE                .135
* 02.11.91 original composition with FAI modifications
* CAV00C0    NONSTAND                    * PEACE BOTTOM CONCRETE
* CAV00C1    AL2O3            0.036     * FROM R.M.HARRINGTON PRESENTATION
* CAV00C2    CAO              0.313     * APRIL 29, 1986, 'OTHER' INCLUDED
* CAV00C3    CO2              0.212     * WITH AL2O3
* CAV00C4    SIO2             0.368     * modified to MAAP 12.12.90
* CAV00C5    H2OEVAP          0.033
* CAV00C6    H2OCHEM          0.014
* CAV00C7    FE                .135
*
CAV00CA    TABLCT     1500.
CAV00CB    TINCT       300.
CAV00CC    EMISCT     .6
CAV00CD    DENSCT     2340.
CAV00CE    TSOLCT     1690.
CAV00CF    TLIQCT     1875.
*
* cavity geometry
CAV00G0    CORCON     2                    * FLAT BOTTOM CYLINDER
*
*           NRAYS      RO       ZO
CAV00G1       35       0.0      1.
* MAAP data:  only Radius and height were modified 12.11.90
*         ZT   RAD  HIT  RADC  RW  HRB   NBOT NCORN
* JV, NRC requested inclusion of 1/6 of drywell floor, 4.16.91
CAV00G2  2.    4.184 8.228 0.1  7.0  1.524  25    3
* CAV00G2  2.      3.047 8.228 0.1  7.0  1.524  25    3
* CAV00G2  2.      2.06 .457  0.1  7.0  1.524  25    3
*         NEXTRA REXTRA ZEXTRA
CAV00GA   40   6.4828  1.99
CAV00GB   20   6.4828  0.
CAV00TP  101
CAV00U1  EMISS.OX    0.5
CAV00U2  EMISS.MET   0.5
CAV00U3  EMISS.SUR   0.8
*****************************************************************************
*****************************************************************************
*** FDI PACKAGE INPUT
*****************************************************************************
*          CV    CAV   TPIN    TPOUT
*FDI0100  100     0    102      101
*
*            ZBOT       ZTOP
*FDI0102    -9.093      0.
*****************************************************************************
*****************************************************************************
***  BURN PACKAGE INPUT
*****************************************************************************
BUR000 0
*      XH2IGN   XCOIGN  XH2IGY  XCOIGY  XO2IG  XMSCIG
*BUR001
* changing after the meeting with FAI on 02.08.91 (BNL): JV
* no igniters after SBO...
*       CVNUM  IGNTR    CDIM    TFRAC
BUR101  401     0       17.6     .5
BUR102  402     0       11.2     .5
BUR103  403     0       17.3     .5
BUR104  404     0       13.3     .5
BUR105  405     0       19.2     .5
BUR106  406     0       13.5     .5
BUR107  407     0       16.9     .5
BUR108  408     0       31,4     .5
BUR109  409     0       53.0     .5
* BUR101  401      1       17.6     .5
* BUR102  402      1       11.2     .5
* BUR103  403      1       17.3     .5
* BUR104  404      1       13.3     .5
* BUR105  405      1       19.2     .5
* BUR106  406      1       13.5     .5
* BUR107  407      1       16.9     .5
* BUR108  408      1       31.4     .5
* BUR109  409      1       53.0     .5
*****************************************************************************
```

```
*****************************************************************************
***  RADIONUCLIDE PACKAGE INPUT
*****************************************************************************
*****************************************************************************
* SWW  4/15/86 - USE DEFAULT RADIONUCLIDES PLUS CSI CLASS # 16
*
DCHDEFCLS0 ALL
*
*  CSI CLASS
DCHNEM0100 CI 1.0E-6
DCHNEM0101 0.  8.3807E5  6.12 6.6913E5 61.2 4.6653E5 612.  3.2606E5
DCHNEM0102 3600.  2.2396E5 7200.  1.7296E5 14400.  1.1438E5 36000.  .70876E5
DCHCLS0160 CSI
DCHCLS0161 CI
*
DCHCLSNORM YES
*****************************************************************************
RN1000 0
RN1001 5 1 16 14 13 0 0
RN1100 1.0E-6 50.E-6 1000.
*
* 03.01.91 JV
RNFP000   -2
*R*I*F ACOEFF.DAT
*********************************************************************************
RNCFDM      5  1.0000E-06  5.0000E-05  1.0000E+03
RNCFPT   1.0000E+05  2.0000E+07  2.7300E+02  2.0000E+03
RNCF001       1.0186E-03  4.5704E-05  1.6010E-03  3.1139E-06  8.8671E-05
RNCF002       3.3591E-03  2.3637E-02  1.1002E-02  3.4453E-02  8.2611E-03
RNCF003       2.0706E-02  7.1868E-02  1.1065E-02  1.7239E-02  6.4472E-02
RNCF004       1.5567E-01  9.8779E-02  3.7445E-02  9.4339E-02  2.1376E-02
RNCF005       5.2564E-02  1.8671E-01  2.1614E-02  4.2597E-02  1.3262E-01
RNCF006       3.9979E-01  9.2094E-02  4.5294E-02  7.7244E-02  1.6000E-01
RNCF007       3.4325E-01  9.7787E-02  3.7490E-02  2.1379E-02  2.1615E-02
RNCF008       9.5940E-02  6.2653E-02  4.2604E-02  1.9007E-01  1.3281E-01
RNCF009       4.0707E-01  1.8059E-11  6.3623E-09  8.4610E-05  7.7807E-12
RNCF010       4.9788E-09  3.8412E-04  3.4583E-12  4.1557E-09  1.7920E-03
RNCF011       1.5606E-12  3.7259E-09  8.4712E-03  7.0929E-13  3.5163E-09
RNCF012       4.0293E-02  2.4117E+09  5.1547E+08  1.0886E+08  2.2867E+07
RNCF013       5.6715E+09  1.2307E+09  2.6165E+08  5.5126E+07  1.1568E+07
RNCF014       1.0690E-03  2.3609E-06  5.1650E-04  8.4633E-07  2.3460E-05
RNCF015       9.3519E-04  3.0642E-02  6.8176E-03  1.1491E-02  2.3907E-03
RNCF016       5.4290E-03  1.9898E-02  1.7873E-03  3.3378E-03  1.0807E-02
RNCF017       4.1805E-02  2.0290E-01  3.5836E-02  3.9735E-02  9.4563E-03
RNCF018       1.8697E-02  5.3887E-02  4.5296E-03  9.7530E-03  3.4876E-02
RNCF019       1.1019E-01  2.7268E-01  2.9951E-02  2.3681E-02  4.4965E-02
RNCF020       9.4660E-02  2.0397E-01  3.5860E-02  9.4586E-03  4.5297E-03
RNCF021       4.0252E-02  1.8721E-02  9.7544E-03  5.4822E-02  3.4924E-02
RNCF022       1.1216E-01  7.4037E-11  4.2289E-08  4.4019E-05  2.3089E-11
RNCF023       3.6148E-08  1.4874E-04  8.5045E-12  2.9178E-08  5.8708E-04
RNCF024       3.4739E-12  2.2514E-08  2.5421E-03  1.5020E-12  1.7688E-08
RNCF025       1.1577E-02  1.6779E+09  4.3603E+08  1.0102E+08  2.2115E+07
RNCF026       3.2359E+09  9.3301E+08  2.3060E+08  5.2099E+07  1.1278E+07
RNCF027       2.4442E-03  1.3032E-04  3.0622E-03  1.0443E-05  1.8333E-04
RNCF028       4.8955E-03  5.7416E-02  3.3716E-02  6.9061E-02  2.9606E-02
RNCF029       4.6288E-02  1.0892E-01  4.1140E-02  4.9651E-02  8.2112E-02
RNCF030       2.0608E-01  2.0771E-01  1.0100E-01  2.0964E-01  7.1334E-02
RNCF031       1.2951E-01  3.0400E-01  7.9284E-02  1.0757E-01  2.1503E-01
RNCF032       5.2917E-01  1.7301E-01  1.3223E-01  1.6454E-01  2.4790E-01
RNCF033       4.3662E-01  2.1013E-01  1.0113E-01  7.1345E-02  7.9288E-02
RNCF034       2.1270E-01  1.2969E-01  1.0788E-01  3.0893E-01  2.1535E-01
RNCF035       5.3852E-01  1.6144E-11  1.6771E-11  7.6764E-05  7.3802E-12
RNCF036       1.6714E-11  3.6696E-04  3.3745E-12  1.6687E-11  1.7545E-03
RNCF037       1.5431E-12  1.8675E-11  8.3892E-03  7.0653E-13  1.6670E-11
RNCF038       4.0114E-02  2.5090E+09  5.2477E+08  1.0975E+08  2.2962E+07
RNCF039       6.0829E+09  1.2682E+09  2.6523E+08  5.5468E+07  1.1600E+07
RNCF040       9.3078E-04  3.2930E-05  7.4056E-04  1.9923E-08  3.8960E-05
RNCF041       1.1768E-03  2.3664E-02  8.7336E-03  1.6760E-02  5.5964E-03
RNCF042       9.6204E-03  2.5797E-02  5.9960E-03  7.9483E-03  1.6127E-02
RNCF043       4.8696E-02  1.2839E-01  3.3266E-02  5.5121E-02  1.5854E-02
RNCF044       2.9493E-02  7.3077E-02  1.3027E-02  1.9733E-02  4.7357E-02
RNCF045       1.3034E-01  1.5294E-01  3.9562E-02  3.8608E-02  6.0208E-02
RNCF046       1.1019E-01  1.2932E-01  3.3296E-02  1.8856E-02  1.3027E-02
RNCF047       5.5862E-02  2.9522E-02  1.9736E-02  7.4264E-02  4.7424E-02
RNCF048       1.3259E-01  3.2865E-11  6.3990E-11  2.1316E-05  1.4982E-11
RNCF049       6.1997E-11  1.0165E-04  6.8414E-12  6.1072E-11  4.8547E-04
RNCF050       3.1266E-12  6.0645E-11  2.3201E-03  1.4293E-12  6.0450E-11
RNCF051       1.1091E-02  2.5048E+09  5.2436E+08  1.0971E+08  2.2948E+07
RNCF052       6.0457E+09  1.2666E+09  2.6607E+08  5.5453E+07  1.1599E+07
*
*ESF(POOL SCRUBBING INPUT) FOR FL362 & FL020
*
RN2PLS01  362    0.005   1.0   0.20   1.16
RN2PLS02  020    0.005   1.0   0.20   1.16
*
*CAVITY POOL SCRUBBING
*
RN2PLS03 1000    0.005   1.0   0.20   1.16
*
RNCLS0100 16
RNCLS0101 2 1.0  *CS
```

```
RNCLS0102 4 0.5  *I2
*
*   FUEL INVENTORIES
*
RNFP000 -1 * CORSOR W/ S/V RATIO
*
*   RADIAL RING 1
*
RNFPN10700 1
RNFPN10701 0 .177 .534
*
RNFPN10800 1
RNFPN10801 0 .230 .534
*
RNFPN10900 1
RNFPN10901 0 .230 .534
*
RNFPN11000 1
RNFPN11001 0 .222 .534
*
RNFPN11100 1
RNFPN11101 0 .141 .534
* 11.28.90 Introducing the 6th axial cell at the top of the core
* RNFPN11200 1
RNFPN11201 0 0.0  0.0
*
*   RADIAL RING 2
*
RNFPN20700 1
RNFPN20701 0 .177 .420
*
RNFPN20800 1
RNFPN20801 0 .230 .420
*
RNFPN20900 1
RNFPN20901 0 .230 .420
*
RNFPN21000 1
RNFPN21001 0 .222 .420
*
RNFPN21100 1
RNFPN21101 0 .141 .420
* 11.28.90 Introducing the 6th axial cell at the top of the core
* RNFPN21200 1
RNFPN21201 0 0.0  0.0
*
*   RADIAL RING 3
*
RNFPN30700 1
RNFPN30701 0 .177 .046
*
RNFPN30800 1
RNFPN30801 0 .230 .046
*
RNFPN30900 1
RNFPN30901 0 .230 .046
*
RNFPN31000 1
RNFPN31001 0 .222 .046
*
RNFPN31100 1
RNFPN31101 0 .141 .046
* 11.28.90 Introducing the 6th axial cell at the top of the core
* RNFPN31200 1
RNFPN31201 0 0.0  .0
*
*   GAP RADIONUCLIDES
*
*   RADIAL RING 1
*
RNGAP10700 1173.
RNGAP10701 2 .05       1.0  *CS
RNGAP10702 4 .017      1.0  *I
RNGAP10703 1 .03       1.0  *XE
RNGAP10704 5 .0001     1.0  *TE
RNGAP10705 3 .000001  1.0  *BA,SR
*
RNGAP10800 1173.
RNGAP10801 -107 1.  1.
*
RNGAP10900 1173.
RNGAP10901 -107 1.  1.
*
RNGAP11000 1173.
RNGAP11001 -107 1.  1.
*
RNGAP11100 1173.
RNGAP11101 -107 1.  1.
* 11.28.90 Introducing the 6th axial cell at the top of the core
RNGAP11200 1173.
RNGAP11201 2 .0        1.0  *CS
```

```
RNGAP11202 4 .0        1.0  *I
RNGAP11203 1 .0        1.0  *IE
RNGAP11204 5 .0        1.0  *TE
RNGAP11205 3 .0        1.0  *BA,SR
*
*     RADIAL RING 2
*
RNGAP20700 1173.
RNGAP20701 -107 1.  1.
*
RNGAP20800 1173.
RNGAP20801 -107 1.  1.
*
RNGAP20900 1173.
RNGAP20901 -107 1.  1.
*
RNGAP21000 1173.
RNGAP21001 -107 1.  1.
*
RNGAP21100 1173.
RNGAP21101 -107 1.  1.
* 11.28.90 Introducing the 6th axial cell at the top of the core
RNGAP21200 1173.
RNGAP21201 2 .0        1.0  *CS
RNGAP21202 4 .0        1.0  *I
RNGAP21203 1 .0        1.0  *IE
RNGAP21204 5 .0        1.0  *TE
RNGAP21205 3 .0        1.0  *BA,SR
*
*     RADIAL RING 3
*
RNGAP30700 1173.
RNGAP30701 -107 1.  1.
*
RNGAP30800 1173.
RNGAP30801 -107 1.  1.
*
RNGAP30900 1173.
RNGAP30901 -107 1.  1.
*
RNGAP31000 1173.
RNGAP31001 -107 1.  1.
*
RNGAP31100 1173.
RNGAP31101 -107 1.  1.
* 11.28.90 Introducing the 6th axial cell at the top of the core
RNGAP31200 1173.
RNGAP31201 2 .0        1.0  *CS
RNGAP31202 4 .0        1.0  *I
RNGAP31203 1 .0        1.0  *IE
RNGAP31204 5 .0        1.0  *TE
RNGAP31205 3 .0        1.0  *BA,SR
*
RNVMCL01 25 16
*************************************************************************
*         DEPOSITION SURFACES
*************************************************************************
*            IDS    SIDE     TYPE
* 02.11.91 changing to sedimentation area type to WALL, JV
RNDS000      10001   LHS     WALL          * DRYWELL-LINER
* RNDS000     10001   LHS     FLOOR          * DRYWELL-LINER
*
RNDS001      36002   RHS     FLOOR         * UPPER-HEAD
RNDS002      20001   LHS     FLOOR         * WETWELL-LINER
RNDS003      32001   LHS     FLOOR         * LOWER-HEAD
RNDS004      36002   LHS     CEILING       * UPPER-HEAD
RNDS005       4003   LHS     FLOOR         *
RNDS007       4010   LHS     FLOOR         *
RNDS009       4016   LHS     FLOOR         *
RNDS011       4022   LHS     FLOOR         *
RNDS013       4028   LHS     FLOOR         *
RNDS016       4033   LHS     FLOOR         *
RNDS018       4039   LHS     FLOOR         *
RNDS019       4044   LHS     FLOOR         *
RNDS021       4048   LHS     FLOOR         *
*************************************************************************
*         SETTLING AREAS
*************************************************************************
*              IVOLF    IVOLT      ELEV     AREA
RNSET000        310      320      5.4943    .6782        * AN-LP
RNSET001        330      320      5.4943    .0793        * BP-LP
RNSET002        340      320      5.4943   4.908         * CH-LP
RNSET003        350      340      9.667    5.366         * SH-CH
RNSET004        360      350     15.431    4.7763        * SD-SH
RNSET005        410      410      0.01      1.                     * ENV-ENV
RNSET006        402      401     -4.1      8.6           * FL401
RNSET007        404      402      8.1      33.2          * FL402
RNSET008        406      404     14.2      33.2          * FL407
RNSET009        408      406     26.1      33.2          * FL411
RNSET010        150      .00     -9.0      36.0          *
* 10.23.90 time0:  steamline huge sink volume
```

```
* Fake RN settling area, required by RN package
RNSET011     420     420     22.243  22.0        * ENV-ENV
*****************************************************************************
*** PLOT VARIABLES FOR RN CLASSES IN WETWELL & ENVIRONMENT
*****************************************************************************
CF90100  NG-200  EQUALS  1   1.      0.
CF90110   1.      0.     RN1-CVCLT-1-2.200
*
CF90200  CS-200  EQUALS  1   1.      0.
CF90210   1.      0.     RN1-CVCLT-2-2.200
*
CF90300  BA-200   EQUALS  1   1.      0.
CF90310   1.      0.     RN1-CVCLT-3-2.200
*
CF90400  I-200  EQUALS  1   1.      0.
CF90410   1.      0.     RN1-CVCLT-4-2.200
*
CF90500  TE-200  EQUALS  1   1.      0.
CF90510   1.      0.     RN1-CVCLT-5-2.200
*
CF90600  CI-200  EQUALS  1   1.      0.
CF90610   1.      0.     RN1-CVCLT-16-2.200
*
CF91100  NG-410  EQUALS  1   1.      0.
CF91110   1.      0.     RN1-CVCLT-1-2.410
*
CF91200  CS-410  EQUALS  1   1.      0.
CF91210   1.      0.     RN1-CVCLT-2-2.410
*
CF91300  BA-410   EQUALS  1   1.      0.
CF91310   1.      0.     RN1-CVCLT-3-2.410
*
CF91400  I-410  EQUALS  1   1.      0.
CF91410   1.      0.     RN1-CVCLT-4-2.410
*
CF91500  TE-410  EQUALS  1   1.      0.
CF91510   1.      0.     RN1-CVCLT-5-2.410
*
CF91600  CI-410  EQUALS  1   1.      0.
CF91610   1.      0.     RN1-CVCLT-16-2.410
*
CF92100  NG-100  EQUALS  1   1.      0.
CF92110   1.      0.     RN1-CVCLT-1-2.100
*
CF92200  CS-100  EQUALS  1   1.      0.
CF92210   1.      0.     RN1-CVCLT-2-2.100
*
CF92300  BA-100   EQUALS  1   1.      0.
CF92310   1.      0.     RN1-CVCLT-3-2.100
*
CF92500  TE-100  EQUALS  1   1.      0.
CF92510   1.      0.     RN1-CVCLT-5-2.100
*
CF92400  I-100  EQUALS  1   1.      0.
CF92410   1.      0.     RN1-CVCLT-4-2.100
*
CF92600  CI-100  EQUALS  1   1.      0.
CF92610   1.      0.     RN1-CVCLT-16-2.100
*
*****************************************************************************
*****************************************************************************
*** MATERIAL PROPERTIES PACKAGE
*****************************************************************************
***            Property               Units
***
***            temperature            K
***            density                kg/m**3
***            heat capacity          J/kg-K
***            thermal conductivity   W/m-K
*****************************************************************************
***           Material 2 is concrete
***
MPMAT00200    CONCRETE
***
***           PROPERTY    TAB FUNC
MPMAT00201      RHO         4
MPMAT00202      CPS         5
MPMAT00203      THC         6
***
***           Density of concrete
***
TF00400      'RHO CONCRETE'   2   1.00   0.0
***
***           TEMPERATURE     RHO
TF00412         200.00      2522.60
TF00413        5000.00      2522.60
***
***           Heat capacity of concrete
***
TF00500      'CPS CONCRETE'   2   1.00   0.0
***
```

```
* concrete properties to MAAP, 12.12.90
***            TEMPERATURE       CPS
TF00512          200.00        903.0
TF00513         5000.00        903.0
* TF00512          200.00        1299.97
* TF00513         5000.00        1299.97
***
***            Thermal conductivity of concrete
***
TF00600      'THC CONCRETE'   2   1.00   0.0
***
***            TEMPERATURE       THC
TF00612          200.00          1.524
TF00613         5000.00          1.524
*****************************************************************************************
***            Material 3 is carbon steel
***
MPMAT00300   'CARBON STEEL'
***
***            PROPERTY    TAB FUNC
***
MPMAT00301      RHO          7
MPMAT00302      CPS          8
MPMAT00303      THC          9
***
***            Density of carbon steel
***
TF00700      'RHO CARBON STEEL'   2   1.00   0.0
***
***            TEMPERATURE       RHO
TF00712          273.15       7833.0
TF00713         5000.00       7833.0
***
***            Heat capacity of carbon steel
***
TF00800      'CPS CARBON STEEL'   2   1.00   0.0
***
***            TEMPERATURE       CPS
TF00812          273.15        465.0
TF00813         5000.00        465.0
***
***            Thermal conductivity of carbon steel
***
TF00900      'THC CARBON STEEL'  10   1.00   0.0
***
***            TEMPERATURE       THC
TF00910          273.15         55.0
TF00911          373.15         52.0
TF00912          473.15         48.0
TF00913          573.15         45.0
TF00914          673.15         42.0
TF00915          873.15         35.0
TF00916         1073.15         31.0
TF00917         1273.15         29.0
TF00918         1473.15         31.0
TF00919         9973.15         31.0
***
MPMAT00500     ZIRCALOY
*
MPMAT00501     ENH   82
MPMAT00502     TMP   83
MPMAT00550     MLT   2500.0
* 01.15.91 JV: melting temperature 2100 K, sensitivity.  Bombed in CORE
* MPMAT00550     MLT   2100.0
*
TF08200    EZIRC   17   1.0
TF08211    300.0      0.
TF08212    400.0    21915.
TF08213    640.0   105110.
TF08214   1090.0   263960.
TF08215   1093.0   265275.5
TF08216   1113.0   276195.5
TF08217   1133.0   288245.5
TF08218   1153.0   301565.5
TF08219   1173.0   316935.5
TF08220   1193.0   332795.5
TF08221   1213.0   346665.5
TF08222   1233.0   357565.5
TF08223   1248.0   363753.
TF08224   2098.0   666353.
TF08225   2500.0   809465.
TF08226   2500.01  1034465.
TF08227   3598.0   1425353.
*
TF08300    TZIRC   17   1.0
*
TF08311        0.              300.0
TF08312      21915.            400.0
TF08313     105110.            640.0
TF08314     263960.           1090.0
TF08315     265275.5   1093.0
```

```
TF08316     276196.5    1113.0
TF08317     288245.5    1133.0
TF08318     301585.5    1153.0
TF08319     316935.5    1173.0
TF08320     332796.5    1193.0
TF08321     346685.5    1213.0
TF08322     357565.5    1233.0
TF08323     363753.          1248.0
TF08324     666353.          2098.0
TF08325     809465.          2500.0
TF08326    1034465.          2500.01
TF08327    1426363.          3598.0
*
* 4.12.91 Adding containment liner gap and concrete model
* JW & LN, additional nodes for air and concrete
MPMAT10000     'AIR'
MPMAT10001    RHO  45
MPMAT10002    CPS  44
TF04400        CPAI 2 1.0
TF04411         273.15 1000.0
TF04412        5000.0 1000.0
*
TF04500        RHAI 2 1.0
TF04511         273.15 1.1
TF04512        5000.0 1.1
*
MPMAT00700     'URANIUM DIOXIDE'
MPMAT00701    ENH  72
MPMAT00702    TMP  73
MPMAT00703    CPS  71
MPMAT00750    MLT  2800.0
*
TF07200     EUO2    31    1.0
TF07211      300.0          33143.
TF07212      400.0          58419.
TF07213      500.0          85883.
TF07214      600.0         114638.
TF07215      700.0         144257.
TF07216      800.0         174517.
TF07217      900.0         205288.
TF07218     1000.0         236492.
TF07219     1100.0         268080.
TF07220     1200.0         300023.
TF07221     1300.0         332309.
TF07222     1400.0         364947.
TF07223     1500.0         397973.
TF07224     1600.0         431455.
TF07225     1700.0         465502.
TF07226     1800.0         500266.
TF07227     1900.0         535945.
TF07228     2000.0         572782.
TF07229     2100.0         611064.
TF07230     2200.0         651111.
TF07231     2300.0         693275.
TF07232     2400.0         737927.
TF07233     2500.0         785450.
TF07234     2600.0         836232.
TF07235     2700.0         890656.
TF07236     2800.0         949096.
TF07237     2800.01       1223096.
TF07238     2900.0        1285906.
TF07239     3000.0        1353422.
TF07240     3113.0        1435764.
TF07241     3513.0        1636964.
*
TF07300     TUO2    31    1.0
TF07311       33143.            300.0
TF07312       58419.            400.0
TF07313       85883.            500.0
TF07314      114638.            600.0
TF07315      144257.            700.0
TF07316      174517.            800.0
TF07317      205288.            900.0
TF07318      236492.          1000.0
TF07319      268080.          1100.0
TF07320      300023.          1200.0
TF07321      332309.          1300.0
TF07322      364947.          1400.0
TF07323      397973.          1500.0
TF07324      431455.          1600.0
TF07325      465502.          1700.0
TF07326      500266.          1800.0
TF07327      535945.          1900.0
TF07328      572782.          2000.0
TF07329      611064.          2100.0
TF07330      651111.          2200.0
TF07331      693275.          2300.0
TF07332      737927.          2400.0
TF07333      785450.          2500.0
TF07334      836232.          2600.0
TF07335      890656.          2700.0
```

```
TF07336    849096.        2800.0
TF07337    1223096.       2800.01
TF07338    1285906.       2900.0
TF07339    1353422.       3000.0
TF07340    1436764.       3113.0
TF07341    1636964.       3613.0
*
TV07100    CPUO2  31     1.0
TF07111     273.15     230.22
TF07112     400.0      265.84
TF07113     500.0      282.07
TF07114     600.0      292.36
TF07115     700.0      299.67
TF07116     800.0      305.31
TF07117     900.0      309.98
TF07118    1000.0      314.03
TF07119    1100.0      317.69
TF07120    1200.0      321.15
TF07121    1300.0      324.59
TF07122    1400.0      328.24
TF07123    1500.0      332.40
TF07124    1600.0      337.43
TF07125    1700.0      343.76
TF07126    1800.0      351.84
TF07127    1900.0      362.14
TF07128    2000.0      375.09
TF07129    2100.0      391.08
TF07130    2200.0      410.45
TF07131    2300.0      433.45
TF07132    2400.0      460.23
TF07133    2500.0      490.88
TF07134    2600.0      525.4
TF07135    2700.0      563.71
TF07136    2800.0      605.67
TF07137    2800.01     503.0
TF07138    2900.0      503.0
TF07139    3000.0      503.0
TF07140    3113.0      503.0
TF07141    5000.0      503.0
*
*
```

```
mÞÞÞÞÞ0m C:\>a;
d command or file name

;44m¯¯41mÞÞÞ0m
mÞÞÞÞÞ0m C:\>a:

;44m¯¯41mÞÞÞ0m
mÞÞÞÞÞ0m
t ready error reading drive A
ort, Retry, Fail? r
\>dir

'olume in drive A has no label
irectory of  A:\

R_MEL  PAR   165007   4-08-91   3:55p
L_SBO  INP     3818   3-11-91   8:45a
      2 File(s)   1288192 bytes free

;44m¯¯41mÞÞÞ0m
mÞÞÞÞÞ0m A:\>type bwr_mel.apr
le not found

;44m¯¯41mÞÞÞ0m
mÞÞÞÞÞ0m A:\>type bwr_mel.par
************************************************************************
                                                                      **
      Peach Bottom Atomic Power Station "LIKE" Parameter File         **
                  BWR Mark I Containment                              **
                                                                      **
       BWR  MAAP 3.0B   PARAMETER FILE  vs  MELCOR INPUT DECK         **
                    REVISION DATE: 04/08/91                           **
************************************************************************

*************************************************************************


   (1) **USE_MELCOR_DATA** = USE MELCOR VALUE

*************************************************************************


   (2) **USE_MAAP_DATA** = USE MAAP VALUE

*************************************************************************


   (3) **CHANGE_MELCOR** = ADD/CHANGE DATA TO MELCOR

*************************************************************************


   (4) **KEEP_ITS_OWN** = KEEP ITS OWN VALUES

*************************************************************************


   (5) **NOT_IN_MELCOR** = DATA NOT USED IN MELCOR

*************************************************************************
```

```
PRIMARY SYSTEM
******************************************************************==BEGIN==
*
**01    8.862D0      AFLCOR      FLOW AREA OF REACTOR CORE
****** 7.9795        CV340BX      (33.2925/(9.667-5.4943))
1       7.9795D0     **USE_MELCOR_DATA**
*
**02    11.8D0       ALSH        AVERAGE FLOW AREA IN LOWER DOWNCOMER
****** 8.2859        CV310BX      (61.1004/(10.460-3.086))
2       8.2859D0     **USE_MELCOR_DATA**
*
**03    2.D0         AFLBYP      TOTAL CORE BYPASS FLOW AREA
****** 6.1786        CV330BX      (25.7814/(9.667-5.4943))
3       2.D0         **KEEP_ITS_OWN**         POSSIBLY DIFFERENT DEFINITIONS?
*
**04    20.0D0       AUSH        FLOW AREA IN UPPER DOWNCOMER
****** 19.2845       CV350BX      (44.9011/(15.431-9.667))
4       19.2845      **USE_MELCOR_DATA**
*
5       1.35D5       HCRD        SPECIFIC ENTHALPY OF CRD INLET FLOW
****** NOT USED IN MELCOR
*05                  **NOT_IN_MELCOR**
*
6       8.171D5      HFW         SPECIFIC ENTHALPY OF FEEDWATER
****** NOT USED IN MELCOR
*06                  **NOT_IN_MELCOR**
*
**07    1.586D5      MU2COR      TOTAL MASS OF UO2 IN CORE
****** 1.685D5       CORX0702      5*(14995+14287+4414)
7       1.685D5      **USE_MELCOR_DATA**
*
8       7.64D2       NASS        NUMBER OF FUEL ASSEMBLIES IN REACTOR CORE
****** NOT USED IN MELCOR
*                    **NOT_IN_MELCOR**
*
9       6.4D1        NPINS       NUMBER OF RODS IN ONE FUEL ASSEMBLY
****** NOT USED IN MELCOR
*                    **NOT_IN_MELCOR**
*
**10    1.85D2       NCRD        NUMBER OF CRD TUBES IN THE LOWER PLENUM
****** 1.85D2        CORXXX01    CR GUIDE TUBES (185)
0       1.85D2       **KEEP_ITS_OWN**
*
1       5.0D0        NQFPS       SENSIBLE ENERGY STORED IN FUEL AT BEGINNING OF
****** NOT USED IN MELCOR
*                    **NOT_IN_MELCOR**
*
2       3.0D0        TDMSIV      DELAY TIME FOR MSIV CLOSURE ONCE THE CLOSURE SIG
****** NOT USED IN MELCOR
*                    **NOT_IN_MELCOR**
*
3       3.5D0        TDSCRM      DELAY TIME FOR FULL SCRAM ONCE THE SCRAM SIGNAL
****** NOT USED IN MELCOR
*                    **NOT_IN_MELCOR**
*
4       3.0D7        TIRRAD      TOTAL EFFECTIVE IRRADIATION TIME FOR CORE
****** NOT USED IN MELCOR
*                    **NOT_IN_MELCOR**
*
*
*       CRD PUMPS VS REACTOR PRESSURE (15-30)
```

```
*     NOT FOUND IN MELCOR       CRD PUMPS ARE LOST IF AC POWER FAILS (SBO)
*                    **NOT_IN_MELCOR**
*
    7.D-3       WVCRDI  CRD FLOW RATE  PUMP HEAD-FLOW CURVE FOR CRD VOL FLOW
    1.12D-2     WVCRDI  CRD FLOW RATE  PRESSURE PRIM SYS.(PPS) VS CRD VOLUMETRIC
    1.12D-2     WVCRDI  CRD FLOW RATE  FLOW (WVCRD)
    1.12D-2     WVCRDI  CRD FLOW RATE
    1.12D-2     WVCRDI  CRD FLOW RATE
    1.12D-2     WVCRDI  CRD FLOW RATE
    1.12D-2     WVCRDI  CRD FLOW RATE
    1.12D-2     WVCRDI  CRD FLOW RATE
    6.894D6     PCRD   PPS FOR CRD PUMP
    1.0134D5    PCRD   PPS FOR CRD PUMP
    1.0134D5    PCRD   PPS FOR CRD PUMP
    1.0134D5    PCRD   PPS FOR CRD PUMP
    1.0134D5    PCRD   PPS FOR CRD PUMP
    1.0134D5    PCRD   PPS FOR CRD PUMP
    1.0134D5    PCRD   PPS FOR CRD PUMP
    1.0134D5    PCRD   PPS FOR CRD PUMP
*
       2275.D0   WFWMAX MAXIMUM FEEDWATER FLOW RATE OBTAINABLE (RUN OUT)
****** NOT USED IN MELCOR
*                **NOT_IN_MELCOR**
*
       4.42D2    WBPMAX MAXIMUM MAIN TURBINE BYPASS FLOW RATE
****** NOT USED IN MELCOR
*                **NOT_IN_MELCOR**
*
       1.4D-1    NXCORE EXIT CORE QUALITY AT TIME = 0.0SEC(TYPICAL .14)
****** NOT USED IN MELCOR
*                **NOT_IN_MELCOR**
*
**34   5.26D0       XDCORE      REACTOR CORE DIAMETER TO INNER SHROUD WALL
****** 5.1594       HS32001100       (2*2.5797)
       5.1594       **USE_MELCOR_DATA**
*
**35   22.23D0      XHRV        INTERIOR HEIGHT OF REACTOR VESSEL FROM TOP OF
****** 22.243       CV360BR
       22.243       **USE_MELCOR_DATA**
*
**36   3.188D0      XRRV        INTERIOR RADIUS OF REACTOR VESSEL
****** 3.1856       HS31001100
       3.1856       **USE_MELCOR_DATA**
*
**37   48.11D0      ZBJET       ELEVATION AT BOTTOM OF DOWNCOMER
****** 3.086        CV310BA
       48.276       **USE_MELCOR_DATA**       (ZBV+3.086)
*
**38   46.29D0      ZBRDT       ELEVATION AT THE BOTTOM OF THE CRD TUBES, WITHIN
****** 1.2954       HS32001002
       46.4854      **USE_MELCOR_DATA**       (ZBV+1.2954)

**39   58.19D0      ZBSEP       ELEVATION AT BOTTOM OF STEAM SEPARATORS
****** 10.92        HS35003002
       56.11        **USE_MELCOR_DATA**       (ZBV+10.92)

**40   45.19D0      ZBV         ELEVATION AT BOTTOM OF REACTOR VESSEL
****** 0.00         CV320B1                SET ZBV = 0.0   IN MELCOR
       45.19D0      **KEEP_ITS_OWN**       SET ZBV = 45.19 IN MAAP
```

```
**41    50.65D0      ZCPL       ELEVATION AT CORE PLATE
****** 5.4943       CV320B7
1       50.6843      **USE_MELCOR_DATA**       (ZBV+5.4943)
*
**42    53.40D0      ZTJET      ELEVATION AT TOP OF JET PUMPS
****** 8.080        CV310BM
2       53.27D0      **USE_MELCOR_DATA**       (ZBV+8.080)
*
**43    0.65D0       AJET       TOTAL JET PUMP AREA
****** 0.6782       FL31201
3       0.6782       **USE_MELCOR_DATA**
*
**44    54.43D0      ZTOAF      ELEVATION AT TOP OF ACTIVE FUEL
****** 9.667        CV330BD
4       54.857       **USE_MELCOR_DATA**       (ZBV+9.667)
*
**45    60.35D0      ZTSEP      ELEVATION AT TOP OF STEAM SEPARATORS
****** 15.431       CV310B9
5       60.621       **USE_MELCOR_DATA**       (ZBV+15.431)
*
6       59.49D0      ZWNORM     ELEVATION AT NORMAL DOWNCOMER WATER LEVEL
****** NOT USED IN MELCOR
*                    **NOT_IN_MELCOR**
*
**47    62.00D0      ZLOCA      ELEV OF BREAK, PUMP AND CRD SEAL LEAKAGES
****** 6.838        FL37001    PUMP SEAL LEAKAGE ELEV
7       52.028       **USE_MELCOR_DATA**       (ZBV+6.838)
*
**48    .0093D0      ALOCA      AREA OF BREAK FOR LOCA & V-SEQUENCES (SEQUENC
****** 6.182D-6     FL37000+FL37100           PUMP & CRD SEAL LEAKAGE AREAS
8       6.182D-6     **USE_MELCOR_DATA**       (2.783D-6+3.399E-6)
*
9       60.00D0      ZWL8       ELEVATION OF LEVEL 8 TRIP (HIGH DOWNCOMER WATER
****** NOT USED IN MELCOR
*                    **NOT_IN_MELCOR**
*
**50    49.19        SET ZSRR=ZBJET FOR PLANTS WITH INTERNAL RECIRC PUMPS XDRR=0.
****** 6.838        FL37001    PUMP SEAL LEAKAGE ELEV
0       52.028       **USE_MELCOR_DATA**       (ZBV+6.838)
*
1       58.87D0      ZSCRAM     LEVEL 2 TRIP FOR SCRAM
****** NOT USED IN MELCOR
*                    **NOT_IN_MELCOR**
*
2       7.342D6      PSCRAM     HIGH REACTOR PRESSURE SCRAM SETPOINT
****** NOT USED IN MELCOR
*                    **NOT_IN_MELCOR**
*
**53    1.D4         MCSPT      MASS OF CORE SUPPORT PLATE
****** 1.5D4        CORX0702                (NUREG/CR-2940 = 9297 KG)
3       24000.0      **USE_MAAP_DATA**       PER MEETING WITH BNL ON 02/11/91
*
4       3.6D3        TDSLC      TIME IT TAKES REACTOR TO SHUT DOWN AFTER THE INIT
****** NOT USED IN MELCOR
*                    **NOT_IN_MELCOR**
*
*
* RECIRC PUMP COASTDOWN CURVE (55-70)
* ---------------------------
****** NOT USED IN MELCOR
```

```
*                   **NOT_IN_MELCOR**         (55-70)
*
5   0.D0        TIRR(1) TIME AFTER PUMP TRIP VS. FRAC OF INIT RECIC PUMP FLOW
6   2.D0        TIRR(2)
7   4.D0        TIRR(3)
8   6.D0        TIRR(4)
9   8.D0        TIRR(5)
0   10.D0       TIRR(6)
1   12.D0       TIRR(7)
2   14.D0       TIRR(8)
3   1.D0        FWRR(1)
4   .77D0       FWRR(2)
5   .62D0       FWRR(3)
6   .53D0       FWRR(4)
7   .45D0       FWRR(5)
8   .34D0       FWRR(6)
9   .34D0       FWRR(7)
0   0.D0        FWRR(8)
*
*
* STANDBY LIQUID CONTROL SYSTEM (71-92)       ACTUATED MANUALLY ONLY (258)
* ------------------------------
****** NOT USED IN MELCOR
*                   **NOT_IN_MELCOR**
*
1   1.46D5      HSLC              INLET ENTHALPY OF SLC FLOW
2   0.D0        PSLC(1)           VESSEL PRESSURE POINTS FOR SLC FLOW CURVE
3   1.D7        PSLC(2)
4   1.D7        PSLC(3)
5   1.D7        PSLC(4)
6   1.D7        PSLC(5)
7   1.D7        PSLC(6)
8   1.D7        PSLC(7)
9   1.D7        PSLC(8)
0   1.72D-3     WVSLC(1)          SLC VOLUMETRIC FLOW RATE
1   1.72D-3     WVSLC(2)
2   1.72D-3     WVSLC(3)
3   1.72D-3     WVSLC(4)
4   1.72D-3     WVSLC(5)
5   1.72D-3     WVSLC(6)
6   1.72D-3     WVSLC(7)
7   1.72D-3     WVSLC(8)
*
*
8       0.D0        TDRPT         DELAY TIME FOR RECIRC PUMP TRIP ONCE TRIP SIGNA
****** NOT USED IN MELCOR
*                   **NOT_IN_MELCOR**
*
9       54.79D0     ZLMSIV        LOW WATER LEVEL FOR MSIV CLOSURE
****** NOT USED IN MELCOR
*                   **NOT_IN_MELCOR**
*
0       57.64D0     ZLRPT         LOW WATER LEVEL FOR RECIRC PUMP TRIP
****** NOT USED IN MELCOR
*                   **NOT_IN_MELCOR**
*
1       7.886D6     PHRPT         HIGH VESSEL PRESSURE SETPOINT FOR RECIRC PUMP
****** NOT USED IN MELCOR
*                   **NOT_IN_MELCOR**
```

```
2       1.1513D5    PDWSCM      HIGH DRYWELL PRESSURE SCRAM SIGNAL
****** NOT USED IN MELCOR
*                   **NOT_IN_MELCOR**
*
*
* FUEL INPUT (93-107)
* ----------
****** NOT USED IN MELCOR
*                   **NOT_IN_MELCOR**        (93-107)
*
3       .0299D0     FENRCH    NORMAL FUEL ENRICHMENT
****** NOT USED IN MELCOR
*                   **NOT_IN_MELCOR**
*
4       20000.D0    EXPO      AVERAGE EXPOSURE IN MWD/TONNE
****** NOT USED IN MELCOR
*                   **NOT_IN_MELCOR**
*
5       .6D0        FCR       PRODUCTION OF U239 TO ABSORPTION IN FUEL
****** NOT USED IN MELCOR
*                   **NOT_IN_MELCOR**
*
6       1.3D0       FFAF      RATIO OF FISSILE ABSORPTION TO TOTAL FISSION
****** NOT USED IN MELCOR
*                   **NOT_IN_MELCOR**
*
7       6.96D-1     FQFR1     FISSION POWER FRACTION OF U235 AND PU241
****** NOT USED IN MELCOR
*                   **NOT_IN_MELCOR**
*
8       2.238D-1    FQFR2     FISSION POWER FRACTION OF PU239
****** NOT USED IN MELCOR
*                   **NOT_IN_MELCOR**
*
9       8.D-2       FQFR3     FISSION POWER FRACTION OF U238
****** NOT USED IN MELCOR
*                   **NOT_IN_MELCOR**
*
)0      .3048D0     XPCRDT    PITCH OF CRD TUBES
****** NOT USED IN MELCOR
*                   **NOT_IN_MELCOR**
*
*101    .2755D0     XDCRDT    OUTER DIAMETER OF CRD TUBES
****** .273         PER ROC WITH J. VALENTE (BNL) ON 02/14/91
)1      .273        **USE_MELCOR_DATA**
*
)2      55.D0       NINST     NUMBER OF INSTRUMENT TUBES
****** NOT USED IN MELCOR
*                   **NOT_IN_MELCOR**
*
*103    .00419D0    XTHCRD    THICKNESS OF CRD TUBE WALL
****** 7.557D-3     PER ROC WITH J. VALENTE (BNL) ON 02/14/91
)3      7.557D-3    **USE_MELCOR_DATA**
*
)4      .0508D0     XDINST    OUTER DIAMETER OF INSTRUMENT TUBE
****** NOT USED IN MELCOR
*                   **NOT_IN_MELCOR**
*
)5      .075D0      XDRIVE    LOWER CRD DRIVE OUTER DIAMETER, THIS IS THE DIAME
****** NOT USED IN MELCOR
```

```
*                    **NOT_IN_MELCOR**
*
)6      1.0051D-3   VWCRD      SPECIFIC VOLUME OF CRD WATER
****** NOT USED IN MELCOR
*                    **NOT_IN_MELCOR**
*
)7      1.0051D-3   VWSLC      SPECIFIC VOLUME OF SLC WATER
****** NOT USED IN MELCOR
*                    **NOT_IN_MELCOR**
*
*
* ADS INPUT
* ---------
*
)8   .75834D6       PADSC      DRYWELL PRESSURE THAT WILL LEAD TO CLOSURE OF AD
****** NOT USED IN MELCOR
*                    **NOT_IN_MELCOR**
*
)9   .62046D6       PADSO      DRYWELL PRESSURE THAT WILL RE-OPEN ADS VALVES AS
****** NOT USED IN MELCOR
*                    **NOT_IN_MELCOR**
*
**110  .21437D0     XTRV       THICKNESS OF LOWER VESSEL HEAD
****** .1894        COR00001  PER ROC WITH J. VALENTE (BNL) ON 02/14/91
10     .1894D0      **USE_MELCOR_DATA**
*
*
* FEEDWATER PUMP COASTDOWN CURVE (111-126)
* ------------------------------
****** NOT USED IN MELCOR
*                    **NOT_IN_MELCOR**
*
11  0.D0        TIFWCD TIME SINCE MSIV CLOSURE SIGNAL VS. FEEDWATER
12  0.D0               COASTDOWN MASS FLOW RATE
13  0.D0               8 TIME POINTS,8 FLOW RATES
14  0.D0
15  0.D0
16  0.D0
17  0.D0
18  0.D0
19  0.D0         WFWCD
20  0.D0
21  0.D0
22  0.D0
23  0.D0
24  0.D0
25  0.D0
26  0.D0
*
27      5.96D6      PLMSIV     LOW RPV PRESSURE FOR MSIV CLOSURE
****** NOT USED IN MELCOR
*                    **NOT_IN_MELCOR**
*
**128  62.35D0      ZMSL       ELEVATION AT CENTER LINE OF THE MAIN STEAM LINE
****** 16.73        FL36200
28      61.92D0     **USE_MELCOR_DATA**        (ZBV+16.73)
*
* ATWS POWER (129-144)
* ----------
****** NOT USED IN MELCOR
```

```
*                   **NOT_IN_MELCOR**
*
29  -1.0        XATWS(1)   DOWNCOMER LEVELS
30  3.901D0     XATWS(2)
31  5.426D0     XATWS(3)
32  6.950D0     XATWS(4)
33  8.474D0     XATWS(5)
34  10.00D0     XATWS(6)
35  11.52D0     XATWS(7)
36  13.05D0     XATWS(8)
37  .10         FQATWS(1)  FRACTION OF TOTAL POWER
38  .18         FQATWS(2)
39  .27         FQATWS(3)
40  .30         FQATWS(4)
41  .36         FQATWS(5)
42  .40         FQATWS(6)
43  .40         FQATWS(7)
44  .40         FQATWS(8)
*
* INCREASED RPV NODALIZATION INPUT
* --------------------------------
*       NOTE: MAAP DOES NOT HAVE HEAT SINK FOR CRD TUBES AND HOUSINGS.
*             MAAP USES CRD TUBES TO CALCULATE FREE WATER VOLUME AND
*             CORIUM/CRD TUBES HEAT TRANSFER IN SUBR FREEZE AND ICRUST.
*             MELCOR: MCRD = 45680 KG
*
**145   52.7D3       MCS    MASS OF CORE SHROUD FROM TOP OF ACTIVE FUEL TO
****** 16.4D3        HS32004XXX..HS33011XXX    (101.787*0.02032*7930)
45      16.4D3       **USE_MELCOR_DATA**       (NUREG/CR-2940 = 53000 KG)
*
**146   5.4D3        MTG       MASS OF CORE TOP GUIDE
****** 24144         CORX1102       (10744+10237+3163)
46      5.4D3        **USE_MAAP_DATA**       (NUREG/CR-2940 = 6893 KG)
*
**147   20.D3        MSH       MASS OF SHROUD HEAD
****** 20.D3         HS35003500       INCLUDED IN SEPARATORS
47      20.D3        **USE_MAAP_DATA**  **USE_MELCOR_DATA**
*
**148   48.4D3       MSP        MASS OF STANDPIPES AND SEPARATORS
****** 69.7D3        HS35003500, INCLUDE SHROUD DOME  (472.43*0.0186*7930)-20.D3
48      49.7D3       **USE_MELCOR_DATA**
*
**149   42.D3        MDR        MASS OF STEAM DRYERS
****** 42.7D3        HS36001500       (2945.03*1.83E-3*7930.0)
49      42.7D3       **USE_MELCOR_DATA**
*
**150   89.D3        MUH        MASS OF RPV UPPER HEAD
****** 52.4D3        HS36002500      0.5*((4/3)*PI*(3.2872**3-3.1856**3))*7833.0
50      52.4D3       **USE_MELCOR_DATA**
*
**151   214.2D3      MUW        MASS OF RPV WALL FROM MAIN STEAM LINE ELEVATION
****** 238.0D3       HS31001500      60%*PI*(3.3412**2-3.1856**2)*15.87*7833.0
51      238.0D3      **USE_MELCOR_DATA**
*
**152   198.D3       MLW        MASS OF RPV WALL FROM TAF TO BOTTOM OF DOWNCOMER
****** 158.6D3       HS31001500      40%*PI*(3.3412**2-3.1856**2)*15.87*7833.0
52      158.6D3      **USE_MELCOR_DATA**
*
53      20.D3        MRR        MASS OF RECIRC DISCHARGE PIPING
****** NOT USED IN MELCOR
```

```
*                   **NOT_IN_MELCOR**
*
**154   75.D3       MLH        MASS OF RPV LOWER HEAD
****** 30719.       CORLHDOX       (13670+13025+4024)
54      75.D3       **USE_MAAP_DATA**     PER ROC WITH J.VALENTE/BNL ON 02/14/91
*
55      20.D3       MSS        MASS OF SHROUD SUPPORT
****** NOT USED IN MELCOR
*                   **NOT_IN_MELCOR**
*
56      12.0        XZRR       LENGTH OF RECIRC PIPE MODELED
****** NOT USED IN MELCOR
*                   **NOT_IN_MELCOR**
*
*157    .70         XDRR       ID OF RECIRC PIPE
****** NOT USED IN MELCOR
57      .70         **NOT_IN_MELCOR** SET XDRR=0.0 FOR PLANTS WITH INTERNAL RECI
*
**158   2000.0      ASEP       TOTAL SURFACE AREA OF ALL STANDPIPES + SEPARATORS
****** 944.86       HS35003500,HS35003700      (472.43+472.43)
58      944.86      **USE_MELCOR_DATA**
*
59      13.2        AGSEP      TOTAL GAS FLOW AREA OF ALL STANDPIPES
****** NOT USED IN MELCOR
*                   **NOT_IN_MELCOR**
*
**160   2000.0      ADR        SURFACE AREA OF STEAM DRYERS
****** 2945.03      HS36001500
60      2945.03     **USE_MELCOR_DATA**
*
61      .20         AUDSS      FLOW AREA FOR UPPER DOWNCOMER TO SEPARATORS FLOW
****** NOT USED IN MELCOR
*                   **NOT_IN_MELCOR**
*
62      5.0         AUHUD      FLOW AREA FOR UPPER HEAD TO UPPER DOWNCOMER FLOW
****** NOT USED IN MELCOR
*                   **NOT_IN_MELCOR**

**163   56.43       ZBSTAN     ELEVATION AT BOTTOM OF STANDPIPES (AVERAGE VALUE)
****** 10.46        CV350BD
63      55.65       **USE_MELCOR_DATA**       (ZBV+10.46)

**164   42.0        VSHED      TOTAL VOLUME INSIDE SHROUD HEAD
****** 27.2877      CV350BH
4       27.2877     **USE_MELCOR_DATA**

*165    45.0        VSEP       TOTAL VOLUME INSIDE STANDPIPES+SEPARATORS
****** 44.9011      CV350BR
5       44.9011     **USE_MELCOR_DATA**

*166    67.29       ZTV        ELEVATION AT TOP OF RPV
****** 22.243       CV360BR
6       67.433      **USE_MELCOR_DATA**       (ZBV+22.243)

 RPV HEAT LOSSES
 ---------------
7       1.D6        QCO        TYPICAL RPV CONVECTION LOSSES AT TIME ZERO
****** NOT USED IN MELCOR
                    **NOT_IN_MELCOR**
```

```
58      8.D0          FINPLT    .GE.2 = REFLECTIVE INSULATION, FINPLT=# OF PLATES
****** NOT USED IN MELCOR
*                     **NOT_IN_MELCOR**
*
59      .102          XTINS  THICKNESS OF INSULATION
****** NOT USED IN MELCOR
*                     **NOT_IN_MELCOR**
*
73      130.0         NSEP   NUMBER OF STEAM SEPARATORS
****** NOT USED IN MELCOR
*                     **NOT_IN_MELCOR**
*
* ISOLATION (ISO) CONDENSER (174-179)
* ------------------------
****** NOT USED IN MELCOR
*                     **NOT_IN_MELCOR**      **NOT_FOR_PEACH_BOTTOM**
*
74  430.D0      VWY315 VOLUME OF ISOLATION CONDENSER WATER
75  300.D0      TWY315 TEMPERATURE OF ISO CONDENSER WATER
76  1.D10       PHY315 HIGH RPV PRESSURE SIGNAL FOR ISO CONDENSER
78  -1.D10      ZLY315 LOW RPV WATER LEVEL ELEVATION TO INITIATE
79  65.0D6      QMY315 MAXIMUM COOLING CAPACITY ; 65 MW FOR 2-LOOP
*
*
*PRESSURE SETPOINT CURVE  (180-195)       FOR ISO CONDENSER
****** NOT USED IN MELCOR
*                     **NOT_IN_MELCOR**      **NOT_FOR_PEACH_BOTTOM**
*
30  0.0D0       TSY315(1) TIME SINCE ACTUATION FOR PRESSURE REGULATION
31  1.0D10      TSY315(2)
32  1.0D10      TSY315(3)
33  1.0D10      TSY315(4)
34  1.0D10      TSY315(5)
35  1.0D10      TSY315(6)
36  1.0D10      TSY315(7)
37  1.0D10      TSY315(8)
38  70.0D5      PSY315(1) PRESSURE REGULATION SETPOINT
39  70.0D5      PSY315(2)
90  70.0D5      PSY315(3)
91  70.0D5      PSY315(4)
92  70.0D5      PSY315(5)
93  70.0D5      PSY315(6)
94  70.0D5      PSY315(7)
95  70.0D5      PSY315(8)
*
96      0.D0          VRRMIN    MINIMUM VOLUME OF WATER IN RECIRC LOOP REQUIRED
****** NOT USED IN MELCOR
*                     **NOT_IN_MELCOR**
*
97      20.0          NJET      NUMBER OF JET PUMPS
****** NOT USED IN MELCOR
*                     **NOT_IN_MELCOR**
*
98      0.01          XTJET     AVERAGE THICKNESS OF JET PUMP WALL
****** NOT USED IN MELCOR
*                     **NOT_IN_MELCOR**
*
99      57.33         ZSPARG    CENTERLINE ELEVATION OF HPCI/RCIC SPARGER
****** NOT USED IN MELCOR
*                     **NOT_IN_MELCOR**
```

```
*
00      .01D0       XSPARG    HPCI/RCIC SPARGER DROPLET DIAMETER
****** NOT USED IN MELCOR
*                   **NOT_IN_MELCOR**
*
01      15.0D0      TD315     TIME RPV PRESSURE MUST BE ABOVE THE HIGH
****** NOT USED IN MELCOR
*                   **NOT_IN_MELCOR**
*
02      55.43       ZSPRCS    CENTERLINE ELEVATION OF LPCS/HPCS SPARGER
****** NOT USED IN MELCOR
*                   **NOT_IN_MELCOR**
*
03      .001D0      XSPRCS    HPCS/LPCS MEAN SPRAY DROPLET DIAMETER
****** NOT USED IN MELCOR
*                   **NOT_IN_MELCOR**
*
*************************************************************************
HEATUP
*******************************************************************==BEGIN==
*
**01    3.81D0      XZFUEL    LENGTH OF ACTIVE FUEL
****** 4.1727       CV330B7,D      (9.667-5.4943)
1       3.81D0      **USE_MAAP_DATA**
*
**02    5.21D-3     XRFUEL    RADIUS OF FUEL PELLET
****** 5.207D-3     COR00001
2       5.207D-3    **USE_MELCOR_DATA**
*
**03    8.13D-4     XTCLAD    THICKNESS OF FUEL CLADDING
****** 8.128D-4     COR00001
3       8.128D-4    **USE_MELCOR_DATA**
*
**04    3.5D4       MZRCAN    TOTAL MASS OF ZR IN ASSEMBLY CANS
****** 2.6282D4     CORX0702       5*(2339+2229+688.5)       MZRTOTAL=74000 KG
**04    39290.0     **USE_MELCOR_DATA**       PER MEETING WITH BNL ON 02/08/91
**      PER ROC WITH J. VALENTE/BNL ON 03/06/91              MZRTOTAL=71420 KG
4       36710.0     **USE_MELCOR_DATA**
*
5       0.0         MBCR      NOT USED
****** NOT USED IN MELCOR
*                   **NOT_IN_MELCOR**
*
**06    3.048D-3    XZRCAN    FUEL BUNDLE WALL THICKNESS
****** 2.54D-3      COR00001
6       2.54D-3     **USE_MELCOR_DATA**
*
*
* CORE PEAKING FACTORS  (07-83)  CHANGE IN MAAP:
* --------------------                 IH * JH = 5 * 10,    FPEAK(IH,JH)
****** FAXED FROM LEV NEYMOTIN (BNL) TO TOBY WU (FAI) ON 01/29/91
*                   **USE_MELCOR_DATA**  (07-83)
*
7   1.063D0          FPEAK(1,1) PEAKING FACTOR FOR NODE (1,1)
3   1.063D0          FPEAK(2,1) PEAKING FACTOR FOR NODE (2,1)
9   0.919D0          FPEAK(3,1) PEAKING FACTOR FOR NODE (3,1)
)   0.878D0          FPEAK(4,1) PEAKING FACTOR FOR NODE (4,1)
1   0.507D0          FPEAK(5,1) PEAKING FACTOR FOR NODE (5,1)
5   1.063D0          FPEAK(1,2) PEAKING FACTOR FOR NODE (1,2)
5   1.063D0          FPEAK(2,2) PEAKING FACTOR FOR NODE (2,2)
```

7	0.919D0	FPEAK(3,2)	PEAKING FACTOR FOR NODE (3,2)
8	0.878D0	FPEAK(4,2)	PEAKING FACTOR FOR NODE (4,2)
9	0.507D0	FPEAK(5,2)	PEAKING FACTOR FOR NODE (5,2)
3	1.382D0	FPEAK(1,3)	PEAKING FACTOR FOR NODE (1,3)
4	1.382D0	FPEAK(2,3)	PEAKING FACTOR FOR NODE (2,3)
5	1.195D0	FPEAK(3,3)	PEAKING FACTOR FOR NODE (3,3)
6	1.140D0	FPEAK(4,3)	PEAKING FACTOR FOR NODE (4,3)
7	0.658D0	FPEAK(5,3)	PEAKING FACTOR FOR NODE (5,3)
1	1.382D0	FPEAK(1,4)	PEAKING FACTOR FOR NODE (1,4)
2	1.382D0	FPEAK(2,4)	PEAKING FACTOR FOR NODE (2,4)
3	1.195D0	FPEAK(3,4)	PEAKING FACTOR FOR NODE (3,4)
4	1.140D0	FPEAK(4,4)	PEAKING FACTOR FOR NODE (4,4)
5	0.658D0	FPEAK(5,4)	PEAKING FACTOR FOR NODE (5,4)
9	1.382D0	FPEAK(1,5)	PEAKING FACTOR FOR NODE (1,5)
0	1.382D0	FPEAK(2,5)	PEAKING FACTOR FOR NODE (2,5)
1	1.195D0	FPEAK(3,5)	PEAKING FACTOR FOR NODE (3,5)
2	1.140D0	FPEAK(4,5)	PEAKING FACTOR FOR NODE (4,5)
3	0.658D0	FPEAK(5,5)	PEAKING FACTOR FOR NODE (5,5)
7	1.382D0	FPEAK(1,6)	PEAKING FACTOR FOR NODE (1,6)
8	1.382D0	FPEAK(2,6)	PEAKING FACTOR FOR NODE (2,6)
9	1.195D0	FPEAK(3,6)	PEAKING FACTOR FOR NODE (3,6)
0	1.140D0	FPEAK(4,6)	PEAKING FACTOR FOR NODE (4,6)
1	0.658D0	FPEAK(5,6)	PEAKING FACTOR FOR NODE (5,6)
5	1.334D0	FPEAK(1,7)	PEAKING FACTOR FOR NODE (1,7)
6	1.334D0	FPEAK(2,7)	PEAKING FACTOR FOR NODE (2,7)
7	1.153D0	FPEAK(3,7)	PEAKING FACTOR FOR NODE (3,7)
8	1.101D0	FPEAK(4,7)	PEAKING FACTOR FOR NODE (4,7)
9	0.635D0	FPEAK(5,7)	PEAKING FACTOR FOR NODE (5,7)
3	1.334D0	FPEAK(1,8)	PEAKING FACTOR FOR NODE (1,8)
4	1.334D0	FPEAK(2,8)	PEAKING FACTOR FOR NODE (2,8)
5	1.153D0	FPEAK(3,8)	PEAKING FACTOR FOR NODE (3,8)
6	1.101D0	FPEAK(4,8)	PEAKING FACTOR FOR NODE (4,8)
7	0.635D0	FPEAK(5,8)	PEAKING FACTOR FOR NODE (5,8)
1	0.847D0	FPEAK(1,9)	PEAKING FACTOR FOR NODE (1,9)
2	0.847D0	FPEAK(2,9)	PEAKING FACTOR FOR NODE (2,9)
3	0.732D0	FPEAK(3,9)	PEAKING FACTOR FOR NODE (3,9)
4	0.699D0	FPEAK(4,9)	PEAKING FACTOR FOR NODE (4,9)
5	0.404D0	FPEAK(5,9)	PEAKING FACTOR FOR NODE (5,9)
9	0.647D0	FPEAK(1,10)	PEAKING FACTOR FOR NODE (1,10)
0	0,847D0	FPEAK(2,10)	PEAKING FACTOR FOR NODE (2,10)
	0.732D0	FPEAK(3,10)	PEAKING FACTOR FOR NODE (3,10)
2	0.699D0	FPEAK(4,10)	PEAKING FACTOR FOR NODE (4,10)
	0.404D0	FPEAK(5,10)	PEAKING FACTOR FOR NODE (5,10)

07	1.067D0	FPEAK(1,1)	PEAKING FACTOR FOR NODE (1,1)
08	.960D0	FPEAK(2,1)	PEAKING FACTOR FOR NODE (2,1)
09	.853D0	FPEAK(3,1)	PEAKING FACTOR FOR NODE (3,1)
10	.572D0	FPEAK(4,1)	PEAKING FACTOR FOR NODE (4,1)
11	.191D0	FPEAK(5,1)	PEAKING FACTOR FOR NODE (5,1)
15	1.445D0	FPEAK(1,2)	PEAKING FACTOR FOR NODE (1,2)
16	1.300D0	FPEAK(2,2)	PEAKING FACTOR FOR NODE (2,2)
17	1.156D0	FPEAK(3,2)	PEAKING FACTOR FOR NODE (3,2)
18	.774D0	FPEAK(4,2)	PEAKING FACTOR FOR NODE (4,2)
19	.258D0	FPEAK(5,2)	PEAKING FACTOR FOR NODE (5,2)
23	1.561D0	FPEAK(1,3)	PEAKING FACTOR FOR NODE (1,3)
24	1.405D0	FPEAK(2,3)	PEAKING FACTOR FOR NODE (2,3)
25	1.249D0	FPEAK(3,3)	PEAKING FACTOR FOR NODE (3,3)
26	.836D0	FPEAK(4,3)	PEAKING FACTOR FOR NODE (4,3)
27	.279D0	FPEAK(5,3)	PEAKING FACTOR FOR NODE (5,3)

```
*31   1.600D0    FPEAK(1,4) PEAKING FACTOR FOR NODE (1,4)
*32   1.440D0    FPEAK(2,4) PEAKING FACTOR FOR NODE (2,4)
*33   1.280D0    FPEAK(3,4) PEAKING FACTOR FOR NODE (3,4)
*34   .857D0     FPEAK(4,4) PEAKING FACTOR FOR NODE (4,4)
*35   .286D0     FPEAK(5,4) PEAKING FACTOR FOR NODE (5,4)
*39   1.613D0    FPEAK(1,5) PEAKING FACTOR FOR NODE (1,5)
*40   1.452D0    FPEAK(2,5) PEAKING FACTOR FOR NODE (2,5)
*41   1.290D0    FPEAK(3,5) PEAKING FACTOR FOR NODE (3,5)
*42   .864D0     FPEAK(4,5) PEAKING FACTOR FOR NODE (4,5)
*43   .288D0     FPEAK(5,5) PEAKING FACTOR FOR NODE (5,5)
*47   1.639D0    FPEAK(1,6) PEAKING FACTOR FOR NODE (1,6)
*48   1.475D0    FPEAK(2,6) PEAKING FACTOR FOR NODE (2,6)
*49   1.312D0    FPEAK(3,6) PEAKING FACTOR FOR NODE (3,6)
*50   .878D0     FPEAK(4,6) PEAKING FACTOR FOR NODE (4,6)
*51   .293D0     FPEAK(5,6) PEAKING FACTOR FOR NODE (5,6)
*55   1.575D0    FPEAK(1,7) PEAKING FACTOR FOR NODE (1,7)
*56   1.418D0    FPEAK(2,7) PEAKING FACTOR FOR NODE (2,7)
*57   1.260D0    FPEAK(3,7) PEAKING FACTOR FOR NODE (3,7)
*58   .843D0     FPEAK(4,7) PEAKING FACTOR FOR NODE (4,7)
*59   .281D0     FPEAK(5,7) PEAKING FACTOR FOR NODE (5,7)
*63   1.548D0    FPEAK(1,8) PEAKING FACTOR FOR NODE (1,8)
*64   1.394D0    FPEAK(2,8) PEAKING FACTOR FOR NODE (2,8)
*65   1.239D0    FPEAK(3,8) PEAKING FACTOR FOR NODE (3,8)
*66   .830D0     FPEAK(4,8) PEAKING FACTOR FOR NODE (4,8)
*67   .277D0     FPEAK(5,8) PEAKING FACTOR FOR NODE (5,8)
*71   1.170D0    FPEAK(1,9) PEAKING FACTOR FOR NODE (1,9)
*72   1.053D0    FPEAK(2,9) PEAKING FACTOR FOR NODE (2,9)
*73   .936D0     FPEAK(3,9) PEAKING FACTOR FOR NODE (3,9)
*74   .627D0     FPEAK(4,9) PEAKING FACTOR FOR NODE (4,9)
*75   .209D0     FPEAK(5,9) PEAKING FACTOR FOR NODE (5,9)
*79   .781D0     FPEAK(1,10)PEAKING FACTOR FOR NODE (1,10)
*80   .703D0     FPEAK(2,10)PEAKING FACTOR FOR NODE (2,10)
*81   .625D0     FPEAK(3,10)PEAKING FACTOR FOR NODE (3,10)
*82   .419D0     FPEAK(4,10)PEAKING FACTOR FOR NODE (4,10)
*83   .140D0     FPEAK(5,10)PEAKING FACTOR FOR NODE (5,10)
*
7       0.33D0       XCHIM     UNHEATED FUEL LENGTH AT TOP OF CORE
****** NOT USED IN MELCOR
*                    **NOT_IN_MELCOR**
*
8       1.D-7        XIZROX    INITIAL CLADDING OXIDE THICKNESS
****** NOT USED IN MELCOR
*                    **NOT_IN_MELCOR**
*
*   NEW DATA FOR REVSION 6.06 - CONTROL BLADES
*
9       1785.5       MBCBLA   MASS OF B4C IN ALL CONTROL BLADES
0       9680.0       MSSBLA   MASS OF STAINLESS STEEL IN ALL CONTROL BLADES
1       0.74         MFFESS   FRACTION OF FE IN STAINLESS STEEL
2       0.18         MFCRSS   FRACTION OF CR IN STAINLESS STEEL
3       0.08         MFNISS   FRACTION OF NI IN STAINLESS STEEL
4       1500.0       TCBMP    MELTING POINT OF CONTROL BLADE
*
*
*************************************************************************
ENGINEERED SAFEGUARDS (GE  BWRS)   (01-108)
*******************************************************************==BEGIN==
****** NOT USED IN MELCOR
*                    **NOT_IN_MELCOR**  (01-108)
*
```

```
   2.D0        NLPCI1 NUMBER OF LPCI PUMPS IN LOOP 1
   2.0D0       NLPCI2 NUMBER OF LPCI PUMPS IN LOOP 2
   0.0D0       NLPCI3 NUMBER OF LPCI PUMPS IN LOOP 3
   4.0D0       NLPCSP NUMBER OF LPCS PUMPS
   0.0D0       NOT USED
   100.D0      VMNCST MIN. WATER VOLUME IN CONDENSATE STORAGE TANK TO SWITCH
   1.0051D-3 VWCST  SPECIFIC VOLUME OF CST WATER
*
* HPCI PUMP HEAD-FLOW CURVE  (08-23)      [AC, D/G, BATT]
* -------------------------
****** NOT USED IN MELCOR
*                  **NOT_IN_MELCOR**
*
   8.124D6    PHPCI(1)      PUMP CURVES FOR ECCS
   8.D6       PHPCI(2)      PHPCI VS VOLUMETRIC FLOW
   6.8D6      PHPCI(3)   WHERE: PHPCI=PPS-PDW
   5.1D6      PHPCI(4)
   3.06D6     PHPCI(5)
   1.7D6      PHPCI(6)
   1.134D6    PHPCI(7)
   4.17D5     PHPCI(8)
   .31567D0   WVHPCI(1) WHERE: WVHPCI=HPCI VOLUMETRIC FLOW
   .31567D0   WVHPCI(2)
   .31567D0   WVHPCI(3)
   .31567D0   WVHPCI(4)
   .31567D0   WVHPCI(5)
   .31567D0   WVHPCI(6)
   .31567D0   WVHPCI(7)
   .31567D0   WVHPCI(8)
*
* LPCI PUMP HEAD-FLOW CURVE   (ALSO USED FOR DRYWELL AND WETWELL SPRAYS AND
* -------------------------     POOL COOLING)  (24-39)
****** NOT USED IN MELCOR
*                  **NOT_IN_MELCOR**
*
   2.172D6    PLPCI(1)    WHERE: PLPCI=PPS-PDW
   2.123D6    PLPCI(2)
   1.916D6    PLPCI(3)
   1.66D6     PLPCI(4)
   1.4788D6   PLPCI(5)
   1.065D6    PLPCI(6)
   7.894D5    PLPCI(7)
   1.01342D5  PLPCI(8)
   0.D0       WVLPCI(1)   WHERE: WVLPCI=LPCI VOLUMETRIC FLOW
   6.313D-2   WVLPCI(2)
   1.894D-1   WVLPCI(3)
   2.525D-1   WVLPCI(4)
   3.47D-1    WVLPCI(5)
   4.48D-1    WVLPCI(6)
   5.05D-1    WVLPCI(7)
   6.31D-1    WVLPCI(8)

 LPCS PUMP HEAD-FLOW CURVE  (40-55)      [AC, D/G]
 -------------------------
 ***** NOT USED IN MELCOR
                   **NOT_IN_MELCOR**

   2.099D6    PLPCS(1)    WHERE: PLPCS=PPS-PDW
   2.03D6     PLPCS(2)
   1.961D6    PLPCS(3)
```

```
3   1.892D6    PLPCS(4)
4   1.824D6    PLPCS(5)
5   1.479D6    PLPCS(6)
6   8.928D5    PLPCS(7)
7   1.01342D5  PLPCS(8)
8   0.D0       WVLPCS(1)  WHERE: WVLPCS=LPCS VOLUMETRIC FLOW
9   .041D0     WVLPCS(2)
0   .063D0     WVLPCS(3)
1   .078D0     WVLPCS(4)
2   .0915D0    WVLPCS(5)
3   .1355D0    WVLPCS(6)
4   .1895D0    WVLPCS(7)
5   .246D0     WVLPCS(8)
*
* HPCS PUMP HEAD-FLOW CURVE  (56-71)      [AC, D/G]
* -------------------------
****** NOT USED IN MELCOR
*                   **NOT_IN_MELCOR**
*
6   0.0        PHPCS(1)   WHERE: PHPCS=PPS-PDW
7   0.0        PHPCS(2)
8   0.0        PHPCS(3)
9   0.0        PHPCS(4)
0   0.0        PHPCS(5)
1   0.0        PHPCS(6)
2   0.0        PHPCS(7)
3   0.0        PHPCS(8)
4   0.0        WVHPCS(1)  WHERE: WVHPCS=HPCS VOLUMETRIC FLOW
5   0.0        WVHPCS(2)
6   0.0        WVHPCS(3)
7   0.0        WVHPCS(4)
8   0.0        WVHPCS(5)
9   0.0        WVHPCS(6)
0   0.0        WVHPCS(7)
1   0.0        WVHPCS(8)
*
* RCIC PUMP HEAD-FLOW CURVE  (72-87)      [AC, D/G, BATT]
* -------------------------
****** NOT USED IN MELCOR
*                   **NOT_IN_MELCOR**
*
2   7.0D6      PRCIC(1)     WHERE: PRCIC=PPS-PDW
3   6.0D6      PRCIC(2)
4   5.0D6      PRCIC(3)
5   4.0D6      PRCIC(4)
6   3.0D6      PRCIC(5)
7   2.0D6      PRCIC(6)
8   1.134D6    PRCIC(7)
9   4.17D5     PRCIC(8)
0   .03788D0   WVRCIC(1)    WHERE: WVRCIC=RCIC VOLUMETRIC FLOW
1   .03788D0   WVRCIC(2)
2   .03788D0   WVRCIC(3)
3   .03788D0   WVRCIC(4)
4   .03788D0   WVRCIC(5)
5   .03788D0   WVRCIC(6)
6   .03788D0   WVRCIC(7)
7   .03788D0      WVRCIC(8)
*
* SYSTEM ACTUATION SET POINTS  (88-108)
* -------------------------
```

```
***** NOT USED IN MELCOR
                    **NOT_IN_MELCOR**

   57.66D0    ZLHPCI      LOW WATER LEVEL SETPOINT TO INITIATE HPCI (ON).
   1.1513D5   PSHPCI      HIGH DRYWELL PRESSURE SET POINT TO TRIP HPCI OFF.
   25.D0      TDHPCI      TIME DELAY FOR HPCI
   4.205D5    PHHPCI      MINIMUM VESSEL PRESSURE TO TRIP HPCI OFF, DUE TO
   -1.D10     ZLHPCS      LOW WATER LEVEL SETPOINT TO INITIATE HPCS (ON).
   1.D10      PSHPCS      HIGH DRYWELL PRESSURE SET POINT TO TRIP HPCS OFF.
   0.D0       TDHPCS      TIME DELAY FOR HPCS
   54.79D0    ZLLPCI      LOW WATER LEVEL SETPOINT TO INITIATE LPCI (ON).
   1.1513D5   PSLPCI      HIGH DRYWELL PRESSURE SET POINT TO TRIP LPCI OFF.
   24.D0      TDLPCI      TIME DELAY FOR LPCI
   -1.D10     PLLPCI      RPV-WETWELL PRESSURE TO CLOSE ADS IF OPEN
   54.79D0    ZLLPCS      LOW WATER LEVEL SETPOINT TO INITIATE LPCS (ON).
)0 1.1513D5   PSLPCS      HIGH DRYWELL PRESSURE SET POINT TO TRIP LPCS OFF.
)1 12.D0      TDLPCS      TIME DELAY FOR LPCS
)2 -1.D10     PLLPCS      RPV-WETWELL PRESSURE TO RE-OPEN CLOSED ADS
)3 57.66D0    ZLRCIC      LOW WATER LEVEL SETPOINT TO INITIATE RCIC (ON).
)4 1.1513D5   PSRCIC      HIGH DRYWELL PRESSURE SET POINT TO TRIP RCIC OFF.
)5 30.D0      TDRCIC      TIME DELAY FOR RCIC
)6 4.205D5    PHRCIC      MINIMUM VESSEL PRESSURE TRIP RCIC OFF. DUE TO
)7 1.3514D5   HCST        ENTHALPY OF CST
)8 290.D0     WSWHX       SERVICE WATER FLOW RATE (KG/S) PER RHR HTX
*
*
* SAFETY/RELIEF VALVES  (109-118,123-127,164-168,270-274)
* -------------------
* (109-118,123-127,164-168,270-274)   **USE_MAAP_DATA**
*
*109  .8605D-2  ASRV1  FLOW AREA OF RELIEF VALVE TYPE #1
*110  .8605D-2  ASRV2  FLOW AREA OF RELIEF VALVE TYPE #2
*111  .8607D-2  ASRV3  FLOW AREA OF RELIEF VALVE TYPE #3
*112  .8597D-2  ASRV4  FLOW AREA OF RELIEF VALVE TYPE #4
*113  -.8659D-2 ASRV5  FLOW AREA OF SAFETY VALVE TYPE #5
***** 0.1319        FL36201
9     0.01014
0     0.01014
1     0.01014
2     0.01014
3     0.01014


*114  1.0D0       NSRV1  NUMBER OF TYPE #1 RELIEF VALVES
*115  1.0D0       NSRV2  NUMBER OF TYPE #2 RELIEF VALVES
*116  6.0D0       NSRV3  NUMBER OF TYPE #3 RELIEF VALVES
*117  3.0D0       NSRV4  NUMBER OF TYPE #4 RELIEF VALVES
*118  2.D0        NSRV5  NUMBER OF TYPE #5 RELIEF VALVES
***** 3       CF10100
***** 5       CF10200
***** 4       CF10300
***** 1       CF10400
4     3.0D0
5     4.0D0
6     4.0D0
7     1.0D0
8     1.D0


      ADS VALVES  (119-122)
```

```
****** NOT USED IN MELCOR
*                    **NOT_IN_MELCOR**         (119-122)
*
19  0.D0       NADS1  NUMBER OF ADS VALVES IN GROUP 1
20  0.D0       NADS2  NUMBER OF ADS VALVES IN GROUP 2
21  3.D0       NADS3  NUMBER OF ADS VALVES IN GROUP 3
22  4.D0       NADS4  NUMBER OF ADS VALVES IN GROUP 4
*
*
23  7.84618D6  PSRV1  PRESSURE SETPOINT FOR #1 RELIEF VALVE
24  7.89444D6  PSRV2  PRESSURE SETPOINT FOR #2 RELIEF VALVE
25  7.86686D6  PSRV3  PRESSURE SETPOINT FOR #3 RELIEF VALVE
26  7.90823D6  PSRV4  PRESSURE SETPOINT FOR #4 RELIEF VALVE
27  8.6003D6  PSRV5  PRESSURE SETPOINT FOR #5 RELIEF VALVE
*
*
* ADS LOGIC  (128-130)
* ---------
****** NOT USED IN MELCOR
*                    **NOT_IN_MELCOR**
*
28     54.79D0     ZLADS     LOW WATER LEVEL FOR ADS INITIATION
****** NOT USED IN MELCOR
*                    **NOT_IN_MELCOR**
*
29     115.13D3    PSADS     HIGH DRYWELL PRESSURE SET POINT FOR ADS
****** NOT USED IN MELCOR
*                    **NOT_IN_MELCOR**
*
30     105.D0      TDADS     TIME DELAY FOR ADS ACTUATION
****** NOT USED IN MELCOR
*                    **NOT_IN_MELCOR**
*
31     366.33D0    TCHPCI    INLET TEMP LIMIT TO TRIP HPCI OFF.
****** NOT USED IN MELCOR
                     **NOT_IN_MELCOR**

2      27.88D0     ZCLHPS    PUMP CENTER LINE ELEVATION FOR HPCS
***** NOT USED IN MELCOR
                     **NOT_IN_MELCOR**

3      27.88D0     ZCLLPI    PUMP CENTER LINE ELEVATION FOR LPCI
***** NOT USED IN MELCOR
                     **NOT_IN_MELCOR**

4      27.88D0     ZCLLPS    PUMP CENTER LINE ELEVATION FOR LPCS
***** NOT USED IN MELCOR
                     **NOT_IN_MELCOR**

5      366.33D0    TCRCIC    INLET TEMP LIMIT TO TRIP RCIC OFF.
***** NOT USED IN MELCOR
                     **NOT_IN_MELCOR**

6      300.D0      TWSW      SERVICE WATER TEMP (RHR HEAT EXCHANGERS,TCOLD)
***** NOT USED IN MELCOR
                     **NOT_IN_MELCOR**

7      1.D0        TDDG1     HPCS DELAY TIME FOR DIESEL LOADING
***** NOT USED IN MELCOR
                     **NOT_IN_MELCOR**
```

```
*
38     11.D0        TDDG2     LPCI DELAY TIME FOR DIESEL LOADING
****** NOT USED IN MELCOR
*                   **NOT_IN_MELCOR**
*
39     11.D0        TDDG3     LPCS DELAY TIME FOR DIESEL LOADING
****** NOT USED IN MELCOR
*                   **NOT_IN_MELCOR**
*
40     0.0          NOT USED
****** NOT USED IN MELCOR
*                   **NOT_IN_MELCOR**
*
41     0.0          NOT USED
****** NOT USED IN MELCOR
*                   **NOT_IN_MELCOR**
*
42     0.0          NOT USED
****** NOT USED IN MELCOR
*                   **NOT_IN_MELCOR**
*
*
* ALTERNATE INJECTION OR DRYWELL SPRAY FROM OUTSIDE WATER SOURCE  (143-163)
* ---------------------------------------------------------------
****** NOT USED IN MELCOR
*                   **NOT_IN_MELCOR**
*
43  1.35D5     HWHPSW ENTHALPY OF ALT INJECTION OR SPRAY
44  1.D-3      VWHPSW SPEC VOL OF ALT INJECTION OR SPRAY
45  1.D10      PHPSW(1) PPS VS. VOLUMETRIC FLOW FOR  ALT INJECTION
46  1.D10      PHPSW(2)
47  1.D10      PHPSW(3)
48  1.D10      PHPSW(4)
49  1.D10      PHPSW(5)
50  1.D10      PHPSW(6)
51  1.D10      PHPSW(7)
52  1.D10      PHPSW(8)
53  .284D0     WVHPSW(1)
54  .284D0     WVHPSW(2)
55  .284D0     WVHPSW(3)
56  .284D0     WVHPSW(4)
57  .284D0     WVHPSW(5)
58  .284D0     WVHPSW(6)
59  .284D0     WVHPSW(7)
50  .284D0     WVHPSW(8)
*
51  1.D10      PDWSPR DRYWELL PRESSURE SETPOINT TO INITIATE MARK III
52  1.D10      PWWSPR WETWELL PRESSURE SETPOINT TO INITIATE MARK III
53  0.D0       TDSPR  TIME DELAY FOR MARK III CONTAINMENT SPRAYS
*
* SRV DEAD BANDS
* -------------
54  2.413D5    PDSRV1 DEAD BAND FOR SRV#1
55  2.413D5    PDSRV2 DEAD BAND FOR SRV#2
56  2.413D5    PDSRV3 DEAD BAND FOR SRV#3
57  2.413D5    PDSRV4 DEAD BAND FOR SRV#4
58  2.413D5    PDSRV5 DEAD BAND FOR SRV#5
*
* HPCI AND RCIC STEAM FLOW TO TURBINES VS PRESSURE POINTS APPEARING  (169-207)
* -----------------------------------------------------------------
```

```
****** NOT USED IN MELCOR
*                    **NOT_IN_MELCOR**
*
69  7.48D6     PTURHP(1)  PPS-PWW VS. STEAM FLOW TO HPCI TURBINE
70  7.928D5    PTURHP(2)
71  7.928D5    PTURHP(3)
72  7.928D5    PTURHP(4)
73  7.928D5    PTURHP(5)
74  7.928D5    PTURHP(6)
75  7.928D5    PTURHP(7)
76  7.928D5    PTURHP(8)
77  23.D0      WSTHPI(1)
78  12.D0      WSTHPI(2)
79  12.D0      WSTHPI(3)
80  12.D0      WSTHPI(4)
81  12.D0      WSTHPI(5)
82  12.D0      WSTHPI(6)
83  12.D0      WSTHPI(7)
84  12.D0      WSTHPI(8)
85  7.7D6      PTURRI(1)  PPS-PWW VS. STEAM FLOW TO RCIC TURBINE
86  1.013D6    PTURRI(2)
87  1.013D6    PTURRI(3)
88  1.013D6    PTURRI(4)
89  1.013D6    PTURRI(5)
90  1.013D6    PTURRI(6)
91  1.013D6    PTURRI(7)
92  1.013D6    PTURRI(8)
93  3.5D0      WSTRCI(1)
94  1.0D0      WSTRCI(2)
95  1.0D0      WSTRCI(3)
96  1.0D0      WSTRCI(4)
97  1.0D0      WSTRCI(5)
98  1.0D0      WSTRCI(6)
99  1.0D0      WSTRCI(7)
00  1.0D0      WSTRCI(8)
01  1.1355D6   PHTURH   HIGH HPCI TURBINE EXHAUST PRESSURE IN THE WETWELL
02  3.77D5     PHTURR   HIGH RCIC TURBINE EXHAUST PRESSURE IN THE WETWELL
*
03  0.D0       NOT USED
04  3.202D6    PHLPCI HIGH RPV PRESSURE TO INITIATE LPCI (ON).
05  3.202D6    PHLPCS HIGH RPV PRESSURE TO INITIATE LPCS (ON).
06  33.64D0    ZHISP  HIGH SUPP. POOL LEVEL FOR HPCI/HPCS/RCIC SUCTION
07  0.D0       ZLSPR  LOW WATER LEVEL FOR INITIATION OF AUTO
*
*
* RHR HEAT EXCHANGERS  (208-224)
* ------------------
****** NOT USED IN MELCOR
*                    **NOT_IN_MELCOR**
*
08  0.D0       NTHX   NUMBER OF TUBES IN RHR HTX
09  0.D0       NBHX   NUMBER OF BAFFLES IN RHR HTX
10  0.D0       XIDTHX TUBE ID FOR RHR HTX
11  0.D0       XTTHX  TUBE WALL THICKNESS FOR RHR HTX
12  0.D0       XTCHX  TUBE CENTER TO CENTER SPACING FOR RHR HTX
13  0.D0       XSHX   SHELL LENGTH FOR RHR HTX
14  0.D0       RGFOUL FOULING FACTOR FOR RHR HTX
15  0.D0       KTHX   THERMAL CONDUCTIVITY FOR TUBE WALL (RHR HTX)
16  0.D0       XBCHX  BAFFLE CUT LENGTH FOR RHR HTX
17  0.D0       XIDSHX SHELL ID FOR RHR HTX
```

```
18  0.D0        XSTHX  BUNDLE TO SHELL GAP LENGTH FOR RHR HTX
19  .654D0      NTUHX1 NTU FOR RHR HTX #1
20  .654D0      NTUHX2 NTU FOR RHR HTX #2
21  2.D0        NHX1   NUMBER OF RHR LOOP #1 HTX
22  2.D0        NHX2   NUMBER OF RHR LOOP #2 HTX
23  1.D0        FHX    TYPE OF RHR HTX(1=STRAIGHT TUBE,2=U TUBE)
*
*224   21.6D3        TDBATT BATTERY OPERATION TIME FOLLOWING STATION BLACK-OUT
****** NOT USED IN MELCOR  (LOCK OFF HPCI & RCIC IN THE INPUT DECK AFTER 6 HRS)
24     28.8D3        **USE_MAAP_DATA**  8 HRS       (6 HRS = 21.6D3)
*
* PUMP NPSH CURVES  (233-253)
* ----------------
****** NOT USED IN MELCOR
*                    **NOT_IN_MELCOR**
*
33  0.D0        ZHDLPI NPSH CURVE FOR LPCI VS. FLOW (ABOVE)
34  0.D0               (METERS)
35  0.D0
36  7.808D0
37  7.9768D0
38  8.213D0
39  8.375D0
40  8.796D0
41  0.D0        ZHDLPS NPSH CURVE FOR LPCS VS. FLOW (ABOVE)
42  7.969D0
43  8.024D0
44  8.076D0
45  8.134D0
46  8.381D0
47  9.116D0
48  10.64D0
49  27.88D0     CENTER LINE ELEVATION FOR RCIC PUMP
50  27.88D0     CENTER LINE ELEVATION FOR HPCI PUMP
*
51  0.0         NOT USED
52  0.0         NOT USED
53  0.0         NOT USED
*
* DRYWELL GAS COOLERS  (254-269)
* -------------------
****** NOT USED IN MELCOR
*                    **NOT_IN_MELCOR**
*
*
54  305.D0      TGDWHX(1)  COOLING CURVE FOR DRYWELL COOLERS
55  446.D0      TGDWHX(2)  TEMP IN DRYWELL VS. HEAT LOSS RATE (J/S)
56  500.D0      TGDWHX(3)
57  600.D0      TGDWHX(4)
58  700.D0      TGDWHX(5)
59  800.D0      TGDWHX(6)
0   900.D0      TGDWHX(7)
1   950.D0      TGDWHX(8)
2   0.D0        QGDWHX(1)  HEAT LOSS RATE FOR DRYWELL COOLERS (J/S)
3   2.D6        QGDWHX(2)
4   2.D6        QGDWHX(3)
5   2.D6        QGDWHX(4)
6   2.D6        QGDWHX(5)
7   2.D6        QGDWHX(6)
8   2.D6        QGDWHX(7)
9   2.D6        QGDWHX(8)
```

```
*
70  7.68760D6  PSRVL1  LOW END PRESSURE SETPOINT FOR #1 RELIEF VALVE
71  7.70828D6  PSRVL2  LOW END PRESSURE SETPOINT FOR #2 RELIEF VALVE
72  7.75655D6  PSRVL3  LOW END PRESSURE SETPOINT FOR #3 RELIEF VALVE
73  7.90823D6  PSRVL4  LOW END PRESSURE SETPOINT FOR #4 RELIEF VALVE
74  8.4279D6  PSRVL5  LOW END PRESSURE SETPOINT FOR #5 RELIEF VALVE
*
*
*****************************************************************************
*   SHUTDOWN COOLING SYSTEM (SCS)  (275-296)       [AC]
**********************************************************************==BEGIN==
****** NOT USED IN MELCOR
*                    **NOT_IN_MELCOR**
*
75  3.0        NSCSP               NUMBER OF SHUTDOWN COOLING SYSTEM (SCS) PUMPS
34  4.259D-1   WVSCS(1)            CONSTANT SCS VOLUMETRIC FLOWRATE
92  0.0        TDSCS               TIME DELAY FOR SCS OPERATION ONCE A
93  2.082D-1   WRBCC               REACTOR BUILDING CLOSED COOLING WATER
94  2.94D2     TWRBCC              RBCCW WATER TEMP (SCS HEAT EXCHANGERS,
95  4.498D2    TCSCS               RPV DOWNCOMER WATER TEMPERATURE WHICH WILL
96  1.289D5    PHSCS               RPV PRESSURE PERMISSIVE FOR SCS OPERATION.
*
*****************************************************************************
*   SCS HEAT EXCHANGERS  (297-310)      OPERATE WHEN SCS PUMPS ARE ON [AC]
**********************************************************************==BEGIN==
****** NOT USED IN MELCOR
*                    **NOT_IN_MELCOR**
*
97  2.368D3    NTSCHX              NUMBER OF TUBES IN THE SCS HEAT EXCHANGER
98  1.0D1      NBSCHX              NUMBER OF BAFFLES IN THE SCS HEAT EXCHANGER
99  1.656D-2   XIDTSC              SCS HEAT EXCHANGER TUBE INNER DIAMETER
00  1.245D-3   XTTSC               SCS HEAT EXCHANGER TUBE WALL THICKNESS
01  2.54       XTCSC               SCS HEAT EXCHANGER TUBE CENTER TO CENTER
02  6.518      XSSC                SCS HEAT EXCHANGER SHELL LENGTH
03  3.522D-4   RGFSC               SCS HEAT EXCHANGER FOULING FACTOR
04  1.73D1     KTSC                SCS HEAT EXCHANGER THERMAL CONDUCTIVITY FOR
05  3.1D-1     XBCSC               SCS HEAT EXCHANGER BAFFLE CUT LENGTH
06  1.5494     XIDSSC              SCS HEAT EXCHANGER SHELL INNER DIAMETER
07  2.445D-1   XSTSC               SCS HEAT EXCHANGER BUNDLE TO SHELL GAP
08  0.0        NTUSC               SCS HEAT EXCHANGER NTU.
09  3.0        NHXSC               NUMBER OF SCS HEAT EXCHANGERS
10  2.0        FSCHX               TYPE OF SCS HEAT EXCHANGERS,
*
*****************************************************************************
*
*@@@REV 7, PARAMETER SECTION *ADDITIONAL (#24) IS NEW
* IT CONTIAINS ADDITONAL (NEW) ENGINEERED SAFEGUARDS INPUTS
*
ADDITIONAL ENGINEERED SAFEGUARDS
*
* ---------------
* INJECTION LOGIC
* ---------------
*
    60.0   ZHHPCI        ELEVATION OF HIGH DOWNCOMER WATER LEVEL TO TRIP OFF
                         HPCI
    60.0   ZHRCIC        ELEVATION OF HIGH DOWNCOMER WATER LEVEL TO TRIP OFF
                         RCIC
    60.0   ZHHPCS        ELEVATION OF HIGH DOWNCOMER WATER LEVEL TO TRIP OFF
                         HPCS
```

```
*
4   59.49  ZWSHCD         DESIRED WATER LEVEL FOR CONTROLING HPCI & RCIC FLOW
*
5   0.34D6 PLIMSP(1)      TABLE FOR HEAT CAPACITY TEMPERATURE LIMIT CURVE( HCTL )
6   0.34D6 PLIMSP(2)
7   0.41D6 PLIMSP(3)
8   0.69D6 PLIMSP(4)
9   1.79D6 PLIMSP(5)
0   3.10D6 PLIMSP(6)
1   4.83D6 PLIMSP(7)
2   7.42D6 PLIMSP(8)
3   3.78D2 TLIMSP(1)
4   3.67D2 TLIMSP(2)
5   3.64D2 TLIMSP(3)
6   3.61D2 TLIMSP(4)
7   3.55D2 TLIMSP(5)
8   3.50D2 TLIMSP(6)
9   3.44D2 TLIMSP(7)
0   3.37D2 TLIMSP(8)
*
1   62.0   ZHFW           HIGH WATER LEVEL TO TRIP FEEDWATER
*
* ----
* RWCU
* ----
*
2   3.0     NRWCU        NUMBER OF REACTOR WATER CLEANUP PUMPS( 0.0 - 4.0, 3.0 )
3   0.43    WVRWCU       CONSTANT RWCU VOLUMETRIC FLOW RATE FOR EACH PUMP
*                        ( 0.41 - 0.44, 0.43)
4   0.0     TDRWCU       TIME DELAY FOR RWCU OPERATION ONCE AN INITIATION SIGNAL
*                        RECEIVED( 0.0 - 30.0, 0.0 )
5   1000.   NTRCHX       NUMBER OF TUBES IN ONE RWCU HEAT EXCHANGER
*                        ( 0.0 - 3000.0, 1000. )
6   10.     NBRCHX       NUMBER OF BAFFLES IN ONE RWCU HEAT EXCHANGER
*                        ( 0.0 - 15.0, 10. )
7   0.01656 XIDTRC       RWCU HEAT EXCHANGER TUBE INNER DIAMETER
*                        ( 0.0 - 0.0254, 0.01656 )
8   0.001245 XTTRC       RWCU HEAT EXCHANGER TUBE WALL THICKNESS
*                        ( 0.0 - 1.65D-3, 1.245D-3 )
9   0.0254 XTCRC         RWCU HEAT EXCHANGER TUBE CENTER TO CENTER SPACING
*                        ( 0.0 - 0.032, 0.0254 )
0   6.518   XSRC         RWCU HEAT EXCHANGER SHELL LENGTH( 0.0 - 16.2, 6.518 )
1   3.522D-4 RGFRC       RWCU HEAT EXCHANGER FOULING FACTOR
*                        ( 0.0 - 1.0D-3, 3.522D-4 )
2   17.3    KTRC         RWCU HEAT EXCHANGER TUBE WALL THERMAL CONDUCTIVITY
*                        ( 0.0 - 18.0, 17.3 )
3   0.31    XBCRC        RWCU HEAT EXCHANGER BAFFLE CUT LENGTH( 0.0 - 0.5, 0.31 )
4   1.5494 XIDSRC        RWCU HEAT EXCHANGER SHELL INNER DIAMETER
*                        ( 0.0 - 2.0, 1.5494 )
5   0.02    XSTRC        RWCU HEAT EXCHANGER BUNDLE TO SHELL GAP LENGTH
*                        ( 0.0 - 0.05, 0.02 )
6   0.0     NTURC        NTU FOR HEAT EXCHANGER( 0.0 - 1.5, 0.0 )
7   2.0     FRCHX        TYPE OF RWCU HEAT EXCHANGER( 1.0 - 2.0, 2.0 )
*                           1 = STRAIGHT TUBE, 2 = U TUBE
8   0.0     ZLRWCU       RWCU TRIP OFF LEVEL
*
*
* --------------
* DRYWELL COOLER
* --------------
```

```
*
9   3.0     NFN           NUMBER OF DRYWELL COOLERS ( 3 )
0   20.0    WVFNO         VOLUMETRIC FLOW RATE OF EACH DRYWELL COOLER ( 20 )
1   5.0     TDFAN         TIME DELAY FOR DRYWELL COOLERS ( 5 )
2   1200.   NTFC          NUMBER OF TUBES IN EACH DRYWELL COOLER ( 1200 )
3   180.    ATFC          OUTSIDE AREA OF ALL TUBES IN EACH DRYWELL COOLER ( 180 )
4   1500.   AFINFC        AREA OF ALL FINS IN EACH DRYWELL COOLER ( 1500 )
5   0.5     FFINFC        DRYWELL COOLER FIN EFFICIENCY ( 0.5 )
6   0.001   RGFLHX        DRYWELL COOLER INSIDE FOULING FACTOR ( 0.001 )
7   0.05    XDFNFC        DRYWELL COOLER FIN DIAMETER ( 0.05 )
8   0.001   XTTFC         DRYWELL COOLER TUBE THICKNESS ( 0.001 )
9   240.    KTFC          DRYWELL COOLER THERMAL CONDUCTIVITY ( 240 )
0   10.     AFLMNF        MINIMUM FLOW AREA THROUGH DRYWELL COOLER ( 10 )
1   0.015   XIDTFC        DRYWELL COOLLER TUBE INSIDE DIAMETER ( 0.015 )
2   5.0     NREGFC        NUMBER OF NODES USED TO MODEL EACH DRYWELL COOLER ( 5 )
3   310.    TCWHX         INLET COOLING WATER. I.E. SERVICE WATER TEMPERATURE TO
*                         DRYWELL COOLER ( 310 )
4   110.    WCWFC         INLET COOLING WATER FLOW RATE TO EACH DRYWELL COOLER
*                         ( 110 )
5   8.D5    PHDWDC        HIGH DRYWELL PRESSURE TO TRIP DRYWELL COOLER( 8.D5 )
*
*
******************************************************************************
*
*@@@REV 7, PARAMETER SECTION *ISOLATION  (#30) IS NEW
* IT CONTIAINS INPUT PARAMETERES FOR ISOLATION CONDESER
*
ISOLATION CONDENSER
*
1   -1.     VOLIC         VOLUME OF ISOLATION CONDENSER
2   81583.  MWICI         INITIAL MASS OF WATER IN ISOLATION CONDENSER
3   300.    TWICI         INITIAL WATER TEMPERATURE IN ISOLATION CONDENSER
4   0.0     PPSIC(1)      TABLE OF PRESSURE VS. HEAT TRANSFER RATE IN ISOLATION
5   1.D5    PPSIC(2)      CONDENSER
6   1.D6    PPSIC(3)
7   8.D6    PPSIC(4)
    9.D6    PPSIC(5)
    1.D7    PPSIC(6)
    2.D7    PPSIC(7)
    3.D7    PPSIC(8)
    0.0     QIC1(1)
    0.0     QIC1(2)
    6.8D7   QIC1(3)
    7.56D7  QIC1(4)
    7.57D7  QIC1(5)
    7.58D7  QIC1(6)
    7.59D7  QIC1(7)
    7.60D7  QIC1(8)
    2.29    ZWMAKE        WATER LEVEL TO WHICH THE MAKE-UP WATER FILLS THE IC
    0.0     WWMAKE        FLOW RATE OF MAKE-UP WATER
    1.25D5  HWMAKE        ENTHALPY OF MAKE-UP WATER
    48.1    AIC           FLOOR AREA OF THE ISOLATION CONDENSER
    1.01D5  PICI          INITIAL PRESSURE INSIDE THE ISOLATION CONDENSER
    0.01    ARUPIC        TUBE RUPTURE AREA
    1.00    XZTUB         HEIGHT OF THE TUBES ABOVE THE FLOOR OF IC
    0.1     AVEN          AREA OF THE ISOLATION CONDENSER VENT

******************************************************************************
   NOTES FOR THE FOLLOWING SECTIONS:
```

```
*        1) SEDIMENTATION
*             SEDIMENTATION AREA IS THE TOTAL HORIZONTAL AREA IN THE
*             PARTICULAR REGION IN WHICH AEROSOLS CAN SETTLE. A GOOD
*             APPROXIMATION IS  2 * FLOOR AREA.
*        2) IMPACTION
*             IN ORDER FOR IMPACTION TO BE EFFECTIVE THE TARGET MUST BE
*             OF A RELATIVELY SMALL WIDTH  (<.01 [M])  TYPICALLY THIS IS USED
*             TO MODEL THE IMPACTION ON GRATING WITHIN THE PLANT. FOR EXAMPLE
*             A SECTION OF GRATING 1 [M2] IN AREA COULD BE MADE UP OF
*             .003 [M] WIDE STRIPS OF STEEL SPACED .1 [M] APART. THE TOTAL
*             IMPACTION AREA WOULD THERFORE BE (.003 [M] * 1 [M] * 10 STRIPS)
*             = .03 [M2]. THE GRATE DIAMETER (OR WIDTH) IS .003 [M] AND
*             THE GAS FLOW  AREA THROUGH THE GRATE IS (1 [M2] - .03 [M2])
*             = .97 [M2].
*****************************************************************************
*
*****************************************************************************
DRYWELL
*********************************************************************==BEGIN==
*
**01    .5D0          RELHDW    INITIAL RELATIVE HUMIDITY IN DRYWELL
****** 0.5            PER MEETING WITH BNL ON 02/08/91
1       0.5           **KEEP_ITS_OWN**
*
**02    4841.D0       VOLDW     FREE VOLUME OF DRYWELL
****** 4235           CV100B4                   (4841-281)
2       4560.D0       **USE_MELCOR_DATA**       PER MEETING WITH BNL ON 02/08/91
*
**03    36.55D0       ZDWF      ELEVATION AT DRYWELL FLOOR
****** -8.635         HS10002002
3       36.555        **USE_MELCOR_DATA**      (ZBV-8.635)
*
**04    84.D0         ADWF      AREA OF DRYWELL FLOOR
****** 132.0          PER CONFERENCE CALL WITH BNL ON 02/11/91
4       132.0         **USE_MELCOR_DATA**
*
**05    37.24D0       ZWDWWW    ELEVATION OF DRYWELL-WETWELL WALL
****** -5.59          CV150B4
5       39.60D0       **USE_MELCOR_DATA**      (ZBV-5.59)
*
6       0.D0          NIGDW     NUMBER OF IGNITERS IN THE DRYWELL (MARK III ONLY)
****** NOT USED IN MELCOR
                      **NOT_IN_MELCOR**
*
        0.D0          XIGDW     AVERAGE DISTANCE FROM IGNITERS TO CEILING (MARK II
****** NOT USED IN MELCOR
                      **NOT_IN_MELCOR**

        0.D0          ACHDW     FLOOR BURN AREA
****** NOT USED IN MELCOR
                      **NOT_IN_MELCOR**

09      557.0         ASEDDW    AEROSOL SEDIMENTATION AREA
****** 1735.80        HS10001500
09      132.0         **USE_MAAP_DATA**      PER ROC WITH BNL ON 02/11/91
        99.5          **USE_MELCOR_DATA**    PER ROC WITH J.VALENTE/BNL ON 02/25/91

*10     0.0093        ADWLEK    DRYWELL VENT OR FAILURE AREA
****** 0.102          FL40001
        0.10          **USE_MELCOR_DATA**       AGREE WITH BNL 12/13/90
```

```
*
1      10.0          AIMPDW    DRYWELL TOTAL IMPACTION AREA
****** NOT USED IN MELCOR
*                    **NOT_IN_MELCOR**
*
2      .003          XDIMDW    DRYWELL MINIMUM GRATE DIAMETER (OR THICKNESS)
****** NOT USED IN MELCOR
*                    **NOT_IN_MELCOR**
*
3      50.0          AGRADW    DRYWELL FLOW AREA THRU GRATE
****** NOT USED IN MELCOR
*                    **NOT_IN_MELCOR**
*
4      1.D-3         XDDROP    SPRAY DROPLET DIAMETER
****** NOT USED IN MELCOR
*                    **NOT_IN_MELCOR**
*
5      14.02D0       XHSPDW    SPRAY FALL HEIGHT IN DRYWELL
****** NOT USED IN MELCOR
*                    **NOT_IN_MELCOR**
*
**16   9.0794D5      PCFAIL    CONTAINMENT FAILURE PRESSURE
****** 9.1D5         CP15003
6      9.08D5         **USE_MELCOR_DATA**      AGREE WITH BNL 12/13/90
*
7      10.5          XRBRDW    CHARACTERISTIC RADIUS OF DRYWELL FOR H2 BURNS
****** NOT USED IN MELCOR
*                    **NOT_IN_MELCOR**
*
8      30.74         XHBRDW    CHARACTERISTIC HEIGHT OF DRYWELL FOR H2 BURNS
****** NOT USED IN MELCOR
*                    **NOT_IN_MELCOR**
*
***********************************************************************
WETWELL
*******************************************************************==BEGIN==
*
**01   28.65D0       ZWWF      ELEVATION AT WETWELL FLOOR
****** -16.38        CV401B1
1      28.81D0       **USE_MELCOR_DATA**      (ZBV-16.38)
*
**02   .169D0        AVB       FLOW AREA THROUGH VACUUM BREAKERS
****** 0.155         FL02101      (1.86/12)
2      0.155         **USE_MELCOR_DATA**
*
3      12.0D0        NVB       NUMBER OF VACUUM BREAKERS
****** NOT USED IN MELCOR
*                    **NOT_IN_MELCOR**
*
**04   3.447D3       PSETVB    PRESSURE SETPOINT FOR VACUUM BREAKERS
****** 3.447D3       TF03012
       3.447D3       **KEEP_ITS_OWN**
*
5      2.757D3       PDVB      DEAD BAND FOR VACUUM BREAKERS
****** NOT USED IN MELCOR
*                    **NOT_IN_MELCOR**
*
**06   7419D0        VOLWW     FREE VOLUME OF WETWELL (MARK II AND MARK III ONLY
****** 7132.5        CV200BC
6      7132.5        **USE_MELCOR_DATA**
```

```
*
**07   1.D0         RELHWW    RELATIVE HUMIDITY IN WETWELL
****** PER ROC WITH LEV NEYMOTIN (BNL) ON 01/31/91
7      0.5          **USE_MELCOR_DATA**
*
8      0.D0         NIGWW     NUMBER OF IGNITERS IN THE WETWELL (MARK III ONLY)
****** NOT USED IN MELCOR
*                   **NOT_IN_MELCOR**
*
9      0.D0         XIGWW     AVERAGE DISTANCE FROM IGNITERS TO CEILING (MARK II
****** NOT USED IN MELCOR
*                   **NOT_IN_MELCOR**
*
0      0.D0         ACHWW     FLOOR BURN AREA
****** NOT USED IN MELCOR
*                   **NOT_IN_MELCOR**
*
1      0.D0         AWWF      AREA OF WETWELL FLOOR (MARK II)
****** NOT USED IN MELCOR
*                   **NOT_IN_MELCOR**
*
*12    929.0        ASEDWW    AEROSOL SEDIMENTATION AREA
****** 1584.0       HS20001500
2      1584.0       **USE_MELCOR_DATA**
*
3      .0093        ACVENT    WETWELL VENT OR FAILURE AREA (COMPT B FOR MARK III
****** NOT USED IN MELCOR
*                   **NOT_IN_MELCOR**
*
4      10.0         AIMPWW    WETWELL TOTAL IMPACTION AREA
****** NOT USED IN MELCOR
*                   **NOT_IN_MELCOR**
*
5      .003         XDIMWW    WETWELL MINIMUM GRATE DIAMETER (OR THICKNESS)
****** NOT USED IN MELCOR
*                   **NOT_IN_MELCOR**
*
6      50.0         AGRAWW    WETWELL FLOW AREA THRU GRATE
****** NOT USED IN MELCOR
*                   **NOT_IN_MELCOR**
*
7      3.66D0       XHSPWW    SPRAY FALL HEIGHT IN WETWELL
****** NOT USED IN MELCOR
*                   **NOT_IN_MELCOR**
*
8      0.D0         ZCFAIL    ELEVATION OF CONTAINMENT VENT IN WETWELL (MII ONL
****** NOT USED IN MELCOR
*                   **NOT_IN_MELCOR**
*
*19    28.8D0       ZSRVD     AVERAGE ELEVATION OF SRV DISCHARGE IN SUPP POOL
****** -15.01       FL36200
       30.18        **USE_MELCOR_DATA**       (ZBV-15.01)

       0            PCFM3  FAILURE PRESSURE OF CONTAINMENT OR ZERO
****** NOT USED IN MELCOR
                    **NOT_IN_MELCOR**

       21.3         XRCONT       CONTAINMENT RADIUS
****** NOT USED IN MELCOR
                    **NOT_IN_MELCOR**
```

```
*
2      425.          NHOOPW     NUMBER OF TENDONS IN HOOP DIRECTION IN THE LENG
****** NOT USED IN MELCOR
*                    **NOT_IN_MELCOR**
*
3      .01399        XTREHW     VOLUME OF REBAR PER UNIT AREA OF OUTER WALL (EQ
****** NOT USED IN MELCOR
*                    **NOT_IN_MELCOR**
*
4      .0156         XTREZW     VOLUME OF REBAR PER UNIT AREA OF OUTER WALL (EQ
****** NOT USED IN MELCOR
*                    **NOT_IN_MELCOR**
*
5      .06E0         XDHOPW     DIAMETER OF HOOP TENDONS
****** NOT USED IN MELCOR
*                    **NOT_IN_MELCOR**
*
6      50.           ZWCYL      HEIGHT OF THE CYLINDRICAL PART OF THE WETWELL W
****** NOT USED IN MELCOR
*                    **NOT_IN_MELCOR**
*
7      .3            XDZFW      DISPLACEMENT IN AXIAL DIRECTION WHICH IS SUFFIC
****** NOT USED IN MELCOR
*                    **NOT_IN_MELCOR**
*
8      .3            XDRFW      SAME AS 27 FOR THE RADIAL DIRECTION
****** NOT USED IN MELCOR
*                    **NOT_IN_MELCOR**
*
9      1.0           NTENZ      NUMBER OF TENDONS IN AXIAL DIRECTION
****** NOT USED IN MELCOR
*                    **NOT_IN_MELCOR**
*
0      1.0           XDTENZ     DIAMETER OF TENDONS IN AXIAL DIRECTION
****** NOT USED IN MELCOR
*                    **NOT_IN_MELCOR**
*
1      4.72          XRBRWW     CHARACTERISTIC RADIUS OF WETWELL FOR H2 BURNS
****** NOT USED IN MELCOR
*                    **NOT_IN_MELCOR**
*
2      4.72          XHBRWW     CHARACTERISTIC HEIGHT OF WETWELL FOR H2 BURNS
****** NOT USED IN MELCOR
*                    **NOT_IN_MELCOR**
*
***********************************************************************
PEDESTAL        (01-22)
*****************************************************************==BEGIN==
****** NOT USED IN MELCOR       === ADD A CONTROL VOLUME FOR PEDESTAL
*                    **NOT_IN_MELCOR**         (01-22)
*
1      2.917D1       APDF     AREA OF PEDESTAL FLOOR
2      4.5D0         APDVT    AREA OF PEDESTAL-DRYWELL OPENING
*
**03   2.40D2        VOLPD    VOLUME OF PEDESTAL
****** 240.0         PER MEETING WITH BNL ON 02/08/91
3      240.0         **USE_MAAP_DATA**
*
**04   36.55D0       ZWPDDW ELEVATION OF WALL BETWEEN PED AND DRYWELL
****** -8.635        HS10004002
```

```
****** 02/18/91, TO PREVENT CORIUM SPILL OVER TO DW, ZWPDDW=(ZPDF+1.063)=37.16
4      36.555       **USE_MELCOR_DATA**
*
**05   36.35D0      ZPDF       ELEVATION AT PEDESTAL FLOOR
****** -9.093       CV100B1        (HS10004002) ?
5      36.097       **USE_MELCOR_DATA**
*
6   .5D0       RELHPD INITIAL RELATIVE HUMIDITY IN PEDESTAL
7   0.D0       NIGPD  NUMBER OF IGNITERS IN THE PEDESTAL
8   0.D0       XIGPD  AVERAGE DISTANCE FROM IGNITERS TO CEILING
9   0.D0       ACHPD  FLOOR BURN AREA
0   0.D0       XWPDVT WIDTH OF PEDESTAL DOOR (MARK II ONLY)
*
1   0.D0       ADCPD  AREA OF A PEDESTAL DOWNCOMER IF ANY
****** NOT USED IN MELCOR
*                   **NOT_IN_MELCOR**
*
2   0.D0       NDCPD  NUMBER OF DOWNCOMERS IN PEDESTAL IF ANY
****** NOT USED IN MELCOR
*                   **NOT_IN_MELCOR**
*
3   2.D0       XHPDDW DISTANCE BETWEEN UPPER AND LOWER VENTS FOR
****** NOT USED IN MELCOR
*                   **NOT_IN_MELCOR**
*
4   32.50      ASEDPD AEROSOL SEDIMENTATION AREA
****** NOT USED IN MELCOR
*                   **NOT_IN_MELCOR**
*
5   3.0        AIMPPD PEDESTAL TOTAL IMPACTION AREA
6   .003       XDIMPD PEDESTAL MINIMUM GRATE DIAMETER (OR THICKNESS)
7   30.0       AGRAPD PEDESTAL FLOW AREA THRU GRATE
8   1.D10      ZWPDWW PEDESTAL-WETWELL OVERFLOW ELEVATION
9   2.917D1    APSUMP AREA OF PEDESTAL SUMP
0   36.35D0    ZPSUMP ELEVATION AT BOTTOM OF PEDESTAL SUMP
1    3.86      XRBRPD CHARACTERISTIC RADIUS OF PEDESTAL CAVITY FOR H2 BURNS
2    8.84      XHBRPD CHARACTERISTIC HEIGHT OF PEDESTAL CAVITY FOR H2 BURNS
*
*************************************************************************
TORUS AND MARK II WETWELL
*******************************************************************==BEGIN==
*
1      4.72D0    XRTOR  MINOR RADIUS OF TORUS (MI ONLY)
****** NOT USED IN MELCOR
*                   **NOT_IN_MELCOR**
*
2      106.7D0   XLTOR  CIRCUMFERENCE OF TORUS (MI ONLY)
****** NOT USED IN MELCOR
*                   **NOT_IN_MELCOR**
*
3      .292D0    ADC    AREA OF DOWNCOMER (MI AND MII ONLY)
****** NOT USED IN MELCOR
*                   **NOT_IN_MELCOR**
*
       96.D0     NDC    NUMBER OF DOWNCOMERS (MI AND MII ONLY)
****** NOT USED IN MELCOR
*                   **NOT_IN_MELCOR**
*
5      0.D0      VSSTOR VOLUME OCCUPIED BY VENT HEADER AND VENT PIPES IN
****** NOT USED IN MELCOR
```

```
*                    **NOT_IN_MELCOR**
*
**06   32.D0      ZBDC   ELEVATION AT BOTTOM OF DOWNCOMER (MI AND MII ONLY)
****** -12.81     CV150B1
5      32.38      **USE_MELCOR_DATA**      (ZBV-12.81)
*
**07   34.74D0    ZTDC   ELEVATION AT TOP OF DOWNCOMER (MI AND MII ONLY)
****** -10.53     CV150B2
7      34.66      **USE_MELCOR_DATA**      (ZBV-10.53)
*
**08   28.8D0     ZBTOR  ELEVATION AT BOTTOM OF TORUS (MI ONLY)
****** -16.38     CV200B1
3      28.81      **USE_MELCOR_DATA**      (ZBV-16.38)
*
**09   0.0168D0   XTOP   THICKNESS OF TORUS SHELL (MI ONLY)
****** 0.01588    PER ROC WITH J.VALENTE/BNL ON 02/25/91
)      0.01588    **USE_MELCOR_DATA**
*
)      5072.D0    ATR    AREA OF TORUS ROOM WALL (MI ONLY)
****** NOT USED IN MELCOR
*                    **NOT_IN_MELCOR**
*
**11   101342.D0    PTR    PRESSURE IN TORUS ROOM (MI ONLY)
****** 101310       CV401A1
1      101342.D0    **USE_MAAP_DATA**
*
**12   1.5D4      VOLTR  FREE VOLUME OF TORUS ROOM (MI ONLY)
****** 5426       CV401B2
2      5426       **USE_MELCOR_DATA**
*
**13   34.747D0   ZVBTOR CENTER LINE ELEVATION OF VACUUM BRKRS(MI AND MII)
****** -10.13     FL02100
3      35.06      **USE_MELCOR_DATA**      (ZBV-10.13)
*
       .015D0     XTHDC  THICKNESS OF DOWNCOMER PIPE (MII ONLY)
****** NOT USED IN MELCOR
*                 **NOT_IN_MELCOR**
*
*****************************************************************
SUPPRESSION POOL(MARKIII ONLY)
*****************************************************************

*****************************************************************
COMPTA (MARKIII-MIDDLE WETWELL COMPARTMENT)
*****************************************************************

*****************************************************************
COMPTB (MARKIII-UPPER WETWELL COMPARTMENT)
*****************************************************************

*****************************************************************
NITIAL CONDITIONS
*******************************************************==BEGIN==

*01   3.293D9    QPOWER      CORE POWER
***** 3.293D9    TF07700
      3.293D9    **KEEP_ITS_OWN**

*02   7.033D6    PPSO        INITIAL PRESSURE IN PRIMARY SYSTEM
***** 7.5207D6   CV3X0A1
```

```
2       7.033D6    **USE_MAAP_DATA**
*
**03    1.041D5    PPDO          INITIAL PRESSURE IN PEDESTAL
****** 1.97D5      CV150A1
3       1.041D5    **USE_MAAP_DATA**
*
**04    1.041D5    PDWO          INITIAL PRESSURE IN DRYWELL
****** 1.97D5      CV150A1
4       1.041D5    **USE_MAAP_DATA**
*
**05    1.041D5    PWWO          INITIAL PRESSURE IN WETWELL
****** 1.97D5      CV200A1
5       1.041D5    **USE_MAAP_DATA**
*
**06    33.22D0    ZSPDWO        INIT.ELEV. OF WATER LEVEL IN DW SIDE OF SUPP.POOL
****** -11.435     CV150A3                   VWMELCOR=3549.0
6       33.31      **USE_MELCOR_DATA**       PER MEETING WITH BNL ON 02/08/91
*
**07    33.22D0    ZSPWWO        INIT.ELEV. OF WATER LEVEL IN WW SIDE OF SUPP.POOL
****** -11.435     CV200A3                   VWMELCOR=3549.0
7       33.31      **USE_MELCOR_DATA**       PER MEETING WITH BNL ON 02/08/91
*
**08    3.3D2      TGPDO         INITIAL TEMPERATURE IN PEDESTAL
****** 393.37      CV150A2
8       3.3D2      **USE_MAAP_DATA**
*
**09    3.3D2      TGDWO         INITIAL TEMPERATURE IN DRYWELL
****** 393.37      CV250A2
9       3.3D2      **USE_MAAP_DATA**
*
**10    3.05D2     TGWWO         INITIAL TEMPERATURE IN WETWELL
****** 368.5       CV200A2
)       3.05D2     **USE_MAAP_DATA**
*
**11    3.05D2     TWSPO         INITIAL TEMPERATURE OF SUPPRESSION POOL WATER
****** 372.8       CV200A2
1       3.05D2     **USE_MAAP_DATA**
*
2       59.49D0    ZWSHO         INITIAL ELEVATION OF WATER IN THE SHROUD
****** NOT USED IN MELCOR
*                  **NOT_IN_MELCOR**
*
3       0.D0       MWCBO         MASS OF WATER IN UPPER POOL (MARKIII ONLY)
****** NOT USED IN MELCOR
*                  **NOT_IN_MELCOR**
*
1       591.D0     VCSTO         VOLUME OF WATER IN CONDENSATE STORAGE TANK
****** NOT USED IN MELCOR
*                  **NOT_IN_MELCOR**
*
***********************************************************************
TSINKS
*******************************************************************==BEGIN==

*01     189.D0     AHS1          AREA OF WALL #1 PEDESTAL-DRYWELL WALL
***** 337.24       HS10004500                HS10003500+HS10004500
        1104.62    **USE_MELCOR_DATA**       (337.24+767.38)

*02     1507.D0    AHS2          AREA OF WALL #2 DRYWELL WALL
***** 1735.8       HS10001500
```

```
2       1735.8     **USE_MELCOR_DATA**
*
**03    0.D0       AHS3         AREA OF WALL #3 DRYWELL FLOOR
****** 132.12      HS10002500
3       132.12     **USE_MELCOR_DATA**
*
**04    5073.D0    AHS4         AREA OF WALL #4 TORUS ROOM WALL (MI ONLY)
****** 4528.       HS0400X500       (805+1391+1166+1166)
4       4528.      **USE_MELCOR_DATA**
*
**09    1.3D0      KHS1         THERMAL CONDUCTIVITY OF WALL #1
****** 1.524       TF00612
)       1.524      **USE_MELCOR_DATA**
*
**10    1.3D0      KHS2         THERMAL CONDUCTIVITY OF WALL #2
****** 1.524       TF00612
)       1.524      **USE_MELCOR_DATA**
*
**11    1.3D0      KHS3         THERMAL CONDUCTIVITY OF WALL #3
****** 1.524       TF00612
1       1.524      **USE_MELCOR_DATA**
*
**12    1.3D0      KHS4         THERMAL CONDUCTIVITY OF WALL #4
****** 1.524       TF00612
2       1.524      **USE_MELCOR_DATA**
*
**17    1.32D0     XHS1         THICKNESS OF WALL #1
****** 0.4055      ((337.24)(0.5334)+(767.38)(0.3493))/(337.24+767.38)
7       0.4055     **USE_MELCOR_DATA** HS10003500,HS10004500,HS10003108,HS1000410
*
**18    1.83D0     XHS2         THICKNESS OF WALL #2
****** 1.5667      HS040XX11X       (1.5+1.5+1.7+1.7+1.5+1.5)/6
3       1.5667     **USE_MELCOR_DATA**
*
**19    1.D0       XHS3         THICKNESS OF WALL #3
****** 1.4425      HS10002111
        1.4425     **USE_MELCOR_DATA**

*20     1.07D0     XHS4         THICKNESS OF WALL #4
***** 1.415        HS0400X11X       (2+0.5+2+1.16)/4
)       1.415      **USE_MELCOR_DATA**

        0.D0       XLHSI1       INNER LINER THICKNESS FOR WALL #1
***** NOT USED IN MELCOR
                   **NOT_IN_MELCOR**

*26     2.713D-2   XLHSI2       INNER LINER THICKNESS FOR WALL #2
***** 0.02858      HS10001105
        0.02858    **USE_MELCOR_DATA**

        0.D0       XLHSI3  INNER LINER THICKNESS FOR WALL #3
***** NOT USED IN MELCOR
                   **NOT_IN_MELCOR**

        0.D0       XLHSI4  INNER LINER THICKNESS FOR WALL #4
***** NOT USED IN MELCOR
                   **NOT_IN_MELCOR**

        0.D0       XLHSO1  OUTER LINER THICKNESS FOR WALL #1
***** NOT USED IN MELCOR
```

```
*              **NOT_IN_MELCOR**
*
4      0.D0      XLHSO2  OUTER LINER THICKNESS FOR WALL #2
****** NOT USED IN MELCOR
*                **NOT_IN_MELCOR**
*
5      0.D0      XLHSO3  OUTER LINER THICKNESS FOR WALL #3
****** NOT USED IN MELCOR
*                **NOT_IN_MELCOR**
*
5      0.D0      XLHSO4  OUTER LINER THICKNESS FOR WALL #4
****** NOT USED IN MELCOR
*                **NOT_IN_MELCOR**
*
**41   2300.D0   DHS1    DENSITY OF WALL #1
****** 2522.60   TF00412
1      2522.60   **USE_MELCOR_DATA**
*
**42   2300.D0   DHS2    DENSITY OF WALL #2
****** 2522.60   TF00412
2      2522.60   **USE_MELCOR_DATA**
*
**43   2300.D0   DHS3    DENSITY OF WALL #3
****** 2522.60   TF00412
3      2522.60   **USE_MELCOR_DATA**
*
**44   2300.D0   DHS4    DENSITY OF WALL #4
****** 2522.60   TF00412
4      2522.60   **USE_MELCOR_DATA**
*
**49   880.D0    CPHS1   SPECIFIC HEAT FOR WALL #1
****** 1299.97   TF00512
9      1299.97   **USE_MELCOR_DATA**
*
**50   880.D0    CPHS2   SPECIFIC HEAT FOR WALL #2
****** 1299.97   TF00512
)      1299.97   **USE_MELCOR_DATA**
*
**51   880.D0    CPHS3   SPECIFIC HEAT FOR WALL #3
****** 1299.97   TF00512
       1299.97   **USE_MELCOR_DATA**

 *52   880.D0    CPHS4   SPECIFIC HEAT FOR WALL #4
 ***** 1299.97   TF00512
       1299.97   **USE_MELCOR_DATA**

 *57   0.D0      MEQPD   MASS OF EQUIPMENT IN PEDESTAL
 ***** 3.1D4     HS32001XXX      (0.1176*33.141*7833)
 *****           PER ROC WITH J.VALENTE/BNL ON 02/18/91
       3.1D4     **USE_MELCOR_DATA**       MELCOR=MASS OF LOWER-HEAD

 *58   1.9D6     MEQDW   MASS OF EQUIPMENT IN DRYWELL
 ***** 1.095D5   PER CONFERENCE CALL WITH BNL ON 02/11/91
       1.095D5   **USE_MELCOR_DATA**

 *59   5.5682D4  MEQWW   MASS OF EQUIPMENT IN WETWELL
 ***** 4.3D5     PER CONFERENCE CALL WITH BNL ON 02/11/91
       4.3D5     **NOT_IN_MELCOR**

 *62   0.D0      AEQPD   AREA OF EQUIPMENT IN PEDESTAL
```

```
****** 67.793     HS32001500,HS32001700      (33.141+34.652)
******            PER ROC WITH J.VALENTE/BNL ON 02/18/91
2      67.793     **USE_MELCOR_DATA**      MELCOR=LOWER-HEAD
*
**63   1.5D3      AEQDW   AREA OF EQUIPMENT IN DRYWELL
****** 801.0      PER CONFERENCE CALL WITH BNL ON 02/11/91
3      801.0      **USE_MELCOR_DATA**
*
**64   20.D0      AEQWW   AREA OF EQUIPMENT IN WETWELL
****** 3141.0     PER CONFERENCE CALL WITH BNL ON 02/11/91      (75% * 4188.0)
1      3141.0     **USE_MELCOR_DATA**
*
**67   50.D0      HTOUTW  HEAT TRANSFER COEFF. AT OUTER WALL
****** 6.08       TF20010
7      6.08       **USE_MELCOR_DATA**
*
*
*      (68-83) NOT USED IN MELCOR,  INNER LINER TO WALL GAP RESISTANCE
****** NOT USED IN MELCOR
*                 **NOT_IN_MELCOR**       **SET RGAPI?=0**  (68-83)
*
3   0.D0      RGAPI1  INNER LINER TO WALL GAP RESISTANCE #1
*
*69   1.D0      RGAPI2  INNER LINER TO WALL GAP RESISTANCE #2
**69   0.D0      RGAPI2  INNER LINER TO WALL GAP RESISTANCE #2
****** PER ROC WITH J. VALENTE/BNL ON 03/07/91, 1" GAP INSTALLED
9      0.67
*
)   0.D0       RGAPI3  INNER LINER TO WALL GAP RESISTANCE #3
1   0.D0       RGAPI4  INNER LINER TO WALL GAP RESISTANCE #4
2   0.D0       RGAPI5  INNER LINER TO WALL GAP RESISTANCE #5
3   0.D0       RGAPI6  INNER LINER TO WALL GAP RESISTANCE #6
4   0.D0       RGAPI7  INNER LINER TO WALL GAP RESISTANCE #7
5   0.D0       RGAPI8  INNER LINER TO WALL GAP RESISTANCE #8
5   0.D0       RGAPO1  OUTER LINER TO WALL GAP RESISTANCE #1
7   0.D0       RGAPO2  OUTER LINER TO WALL GAP RESISTANCE #2
3   0.D0       RGAPO3  OUTER LINER TO WALL GAP RESISTANCE #3
)   0.D0       RGAPO4  OUTER LINER TO WALL GAP RESISTANCE #4
)   0.D0       RGAPO5  OUTER LINER TO WALL GAP RESISTANCE #5
    0.D0       RGAPO6  OUTER LINER TO WALL GAP RESISTANCE #6
!   0.D0       RGAPO7  OUTER LINER TO WALL GAP RESISTANCE #7
    0.D0       RGAPO8  OUTER LINER TO WALL GAP RESISTANCE #8

 *84   5.3232D4  MEQWWS  MASS EQUIP. WETWELL (SUBMERGED)
 ***** 1.43D5     PER CONFERENCE CALL WITH BNL ON 02/11/91
       1.43D5     **USE_MELCOR_DATA**

 *85   1.D2       AEQWWS  AREA EQUIP. WETWELL (SUBMERGED)
 ***** 1047.0     PER CONFERENCE CALL WITH BNL ON 02/11/91      (25% * 4188.0)
       1047.0     **USE_MELCOR_DATA**


       XTGAP1-XTAGP8  (86-93, 95-99) NOT USED IN MELCOR
 ***** NOT USED IN MELCOR
                  **NOT_IN_MELCOR**       **SET XTGAP?=0**  (86-93,95-99)

    0.D0       XTGAP1  GAP THICKNESS FROM LINER TO WALL FOR  #1
    0.D0       XTGAP2  GAP THICKNESS FROM LINER TO WALL FOR  #2
    0.D0       XTGAP3  GAP THICKNESS FROM LINER TO WALL FOR  #3
    0.D0       XTGAP4  GAP THICKNESS FROM LINER TO WALL FOR  #4
```

```
0   0.D0       XTGAP5  GAP THICKNESS FROM LINER TO WALL FOR  #5
1   0.D0       XTGAP6  GAP THICKNESS FROM LINER TO WALL FOR  #6
2   0.D0       XTGAP7  GAP THICKNESS FROM LINER TO WALL FOR  #7
3   0.D0       XTGAP8  GAP THICKNESS FROM LINER TO WALL FOR  #8
*
4   10.0       ZEQDW  AVERAGE HEIGHT OF DRYWELL WALL
****** NOT USED IN MELCOR
*                **NOT_IN_MELCOR**
*
5   10.0
6   10.0
7   10.0
8   10.0
9   10.0
*
************************************************************************
MODEL PARAMETERS FOR BWR  (01-64)
****************************************************************==BEGIN==
**   NOTE: MODEL PARAMETERS WERE CHANGED PER GKA'S REPORT, "RECOMMENDED
**         SENSITIVITY ANALYSES FOR AN IPE USING MAAP 3.0B", DATED ??/??/??
**               >>>CHANGES WERE MADE ON 03/06/91<<<
*
1   .005D0     FRCOEF  FRICTION COEFFICIENT FOR CORIUM AS IT IS DISCHARGED
2   .10D0      FMAXCP  ONCE THE CORE FRACTION MELTS TO A VALUE BELOW
3   50.D0      HTBLAD  FUEL CHANNEL TO CONTROL BLADE HEAT TRANS. COEFF
4   300.D0     HTFB    NON-RADIATIVE FILM BOILING HEAT TRANS. COEFF.
*
**05   10.D0      FDF1    DF FOR WATER POOLS OVER CORE DEBRIS (EXCLUDING
****** 05 NOT USED PER REV 7
*
*
6   0.02D0     FEFFDR  DROP COLLECTION EFFICIENCY FOR SPRAY SWEEP-OUT
*
**07   1500.D0    TCLMAX  CLAD FAILURE TEMP TO BEGIN FISSION PRODUCT REL
****** 1173.      RNGAPXXX00
**07   1173.      **USE_MELCOR_DATA**
7      1200.0     **USE_MAAP_DATA**       CHANGED PER GKA REPORT ON 03/06/91
*
*@@@REV 7, PARAMETER 12 REDEFINED
**12   .9D0       FTENUR  UNOXIDIZED ZR MASS FRACTION LIMIT.
2      .1D0       CHANGED PER REV 7 ON 03/06/91
*
3   1.0D       SCALFP  FISSION PRODUCT RELEASE RATES DIVIDED BY THIS VALUE
4   1.D3       HTCMCR  CORIUM-CRUST HEAT TRANSF. COEFF. USED IN DECOMP
5   0.05D0     XCMX    MINIMUM CORIUM THICKNESS ON DRYWELL FLOOR AND PED
5   0.0?D0     XDCMSP  PARTICLE SIZE (DIAMETER) FOR CORIUM AS IT FALLS
*@@@REV 7, PARAMETER 17 ALTERED FOR NEW EXVIN MODEL
7  1.D-1       TDSTX - TIME DELAY AFTER CORIUM CONTACTS FLOOR TO TRIGGER
3   1.53D0     FCHTUR  CHURN-TURBULENT CRITICAL FLOW PARAMETER
)   3.7D0      FDROP   DROPLET CRITICAL FLOW PARAMETER
)   3.D0       FFLOOD  FLOODING FLOW PARAMETER
.   1.35D0     FSPAR   PARAMETER FOR BOTTOM-SPARGED STEAM VOID FRACTION
2   2.D0       FVOL    PARAMETER FOR VOLUME SOURCE VOID FRACTION MODEL
3   5.D-1      TTENTR  ENTRAINMENT EFFECTIVE EMPTYING TIME
*
.   .90D0      EW      EMISSIVITY OF WATER
*
**25   .85D0      EWL     EMISSIVITY OF WALL
****** PER ROC WITH J. VALENTE/BNL ON 02/15/91, EWL=0.8
****** PER ROC WITH J. VALENTE/BNL ON 02/18/91, EWL=0.85 FOR RECORD
```

```
5      0.85       **USE_MAAP_DATA**       **USE_MELCOR_DATA**
*
**26   .85D0      ECM      EMISSIVITY OF CORIUM
****** PER ROC WITH J. VALENTE/BNL ON 02/15/91, ECM=0.5
****** PER ROC WITH J. VALENTE/BNL ON 02/18/91, ECM=0.85 ?OR RECORD
5      0.85       **USE_MAAP_DATA**       **USE_MELCOR_DATA**
*
7    .6D0      EG       EMISSIVITY OF GAS
*
**28   .85D0      EEQ      EMISSIVITY OF EQUIPMENT
****** PER ROC WITH J. VALENTE/BNL ON 02/15/91, EEQ=0.8
****** PER ROC   TH J. VALENTE/BNL ON 02/18/91, EEQ=0.85 FOR R CORD
8      0.85          **USE_MELCOR_DATA**
*
9    0.5D0     FOVER    FRACTION OF CORE SPRAY FLOW ALLOWED TO BYPASS CORE
0    1.D0      NPF      NUMBER OF PENETRATIONS FAILED IN LOWER HEAD AT TIME
1    ?.D0      FCDCDW   DOWNCOMER PERIMETER PER METER FROM PEDESTAL DOOR
*
**32   0.14D0     FCHF     COEFFICIENT FOR CHF CORRELATION IN PLSTM
2      0.1        CHANGED PER GKA REPORT ON 03/06/91
*
**33   .75D0      FCDBRK  DISCHARGE COEFF  IENT FOR PIPE BREAK
3      0.7        CHANGED PER GKA REPORT ON 03/06/91
*
4    .33D0     FENTR    NUMBER TO MULTIPLY KUTATELADZE CRITERION BY TO
*
5    1.00      SCALU    SCALING FACTOR FOR ALL BURNING VELOCITIES
6    1.00      SCALH    SCALING FACTOR FOR HT COEFFICIENTS TO PASSIVE
*
**37   2.0D0      FUMIN   CLADDING SURFACE MULTIPLIER TO ACCOUNT FOR POTENTIAL
****** PER ROC WITH J.VALENTE/BNL ON 02/25/91
7      1.0        **USE_MAAP_DATA**       GKA RECOMMENDED VALUE
*
8    2.5       GSHAPE  PARTICLE COLLISION GAMMA SHAPE FACTOR
9    1.0       FSHAPE  CH1 SETTLING SHAPE FACTOR
*
**40   8.0        FAERI   RATIO OF AIRBORNE AEROSOL MASS TO THE MASS WHICH
****** PER ROC WITH J.VALENTE/BNL ON 02/25/91
**40   8.0        **USE_MAAP_DATA**       GKA RECOMMENDED VALUE = 3.0
0      3.0        CHANGED PER GKA REPORT ON 03/06/91
*
**41   0          FPRAT   1=NUREG-0772 FP RELEASES; 0=CUBICCIOTTI STEAM OX MODEL
****** PER ROC WITH J.VALENTE/BNL ON 02/25/91
1      -2         **USE_MAAP_DATA**       NEW VALUE FOR REV 7
*
2    1.0       FCSIVP  GROUP 2 (CSI) & GRUOP 6 (CSOH) VAPOR PRESSURE
3    0         FTEREL 0=TE BOUND UP IN ZIRCALLOY,1=NOT BOUND UP
*
**44   2.D5    PPLUG  PRESSURE DIFFERENCE TO BLOW OPEN PLUG IF LEAK PATH HAS
****** NOT IN MELCOR
**44   0.01    **USE_MAAP_DATA**      INTENTIIONALLY TO REMOVE PLUGGIN MODEL
**             PER ROC WITH J.VALENTE/BNL ON 02/25/91
1      0.5D5   **USE_MAAP_DATA**      GKA RECOMMENDED VALUE
*
**45   .02     XHLEAK WIDTH OF LEAK PAT
****** NOT IN MELCOR
**45   2.0     **USE_MAAP_DATA**      INTENTIIONALLY TO REMOVE PLUGGING MODEL
**             PER ROC WITH J.VALENTE/BNL ON 02/25/91
5      .02     **USE_MAAP_DATA**      PUT PLUGGING MODEL BACK
*
```

```
6   50000.      DKPLUG MOREWITZ COEFF FOR PLUGGING
7   2500.0      TEUTEC (TEU) CORE NODE EUTECTIC TEMPERATURE FOR MELTING NODE
8   2.5D5       LHEU   LATENT HEAT OF FUSION OF EUTECTIC
9   3.D-7       XRSEED SEED RADIUS FOR HYGROSCOPIC FORMATION
0   0.D0        TIDCF  IF EVENT CODE 216 IS SET TO 1 TO FAIL PEDESTAL
1   0.1         ASTRN  STRAIN INDUCED CONTAINMENT FAILURE AREA
2   0.1         AOVPR  GROSS OVER-PRESSURE CONTAINMENT FAILURE AREA
3   1060.0      TJBRN  JET BURN TEMP: IF GAS JET OUT OF PEDESTAL EXCEEDS
4   0.01D0      FASI   ACTIVITY COEFFICIENT FOR SIO2 IN METOXA EQUILIBRIUM
5   0.05D0      FASR   ACTIVITY COEFFICIENT FOR SRO
6   0.05D0      FABA   ACTIVITY COEFFICIENT FOR BAO
7   1.D-8       FAKO   ACTIVITY COEFFICIENT FOR K2O
*
**58   1.0      FCRBLK =1  CORE BLOCKAGE/LOCAL NODE CUT-OFF
****** PER ROC WITH J.VALENTE/BNL ON 02/25/91
******          MAAP 3B REV 7 = 0.0 (NO BLOCKAGE), GKA = 1.0 (BLOCKAGE FOR SBO)
8      0.0      **USE_MAAP_DATA**
*
9   .33         FEO    PRUPACHER-KLETT COLLISION EFFICIENCY
0   18.0        FNUDRP NUSSELT NO. WHICH GOVERNS HEAT CONDUCTION INTO
1    983.      TAUTO AUTOIGNITION TEMPERATURE FOR H2 BURNS
2    0.75       XSTIA STEAM MOLE FRACTION TO INERT A H2-AIR-H2O MIXTURE
3    0.00       DXHIG OFFSET H2 MOLE FRACTION FOR DEFINITION OF IGNITION
4    2.0        FLPHI FLAME FLUX MULTIPLIER (BETWEEN 1.0 AND 10.0)
*
*************************************************************************
CONCRETE PROPERTIES - USE CORCON-2 DATA
*****************************************************************==BEGIN==
*
**01   1500.      TCNMP       CONCRETE MELTING TEMPERATURE
****** 1750.      CAV00CA
1      1500.      **USE_MAAP_DATA**
*
**02   1159.7     LHDEC       REACTION ENERGY FOR CONCRETE DECOMPOSITION
****** PER ROC WITH J.VALENTE/BNL 02/26/91, REVISED AS REV 7
2      1.15D6     **USE_MAAP_DATA**
*
*03    580.0      LHCN        LATENT HEAT FOR CONCRETE MELTING
****** PER ROC WITH J.VALENTE/BNL 02/26/91, REVISED AS REV 7
3      0.56D6     **USE_MAAP_DATA**
*
**04   0.358      MFCN(1)     SIO2
****** 0.036      CAV00C4
4      0.358      **USE_CORCON_DATA**
*
**05   0.313      MFCN(2)     CAO
****** 0.454      CAV00C2
5      0.313      **USE_CORCON_DATA**
*
**06   0.036      MFCN(3)     AL2O3
****** 0.094      CAV00C1
6      0.036      **USE_CORCON_DATA**

       .0122      MFCN(4)     K2O
 ***** NOT USED IN MELCOR
                  **USE_CORCON_DATA**

       .0008      MFCN(5)     NA2O
 ***** NOT USED IN MELCOR
                  **USE_CORCON_DATA**
```

```
*
9       0.0069    MFCN(6)     MGO+MNO+TIO2
****** NOT USED IN MELCOR
*                 **USE_CORCON_DATA**
*
0       0.0144    MFCN(7)     FE2O3 -> FEO+O2
****** NOT USED IN MELCOR
*                 **USE_CORCON_DATA**
*
**11    0.        MFCN(8)     FE        MAAP HAS REBAR
****** 0.135      CAV00C7               MELCOR DOESN'T HAVE REBAR
1       0.        **KEEP_ITS_OWN**      MELCOR USES FE AS REBAR
*
2       0.0001    MFCN(9)    CR2O3
****** NOT USED IN MELCOR
*                 **USE_CORCON_DATA**
*
**13    0.047      MFCN(10)   H2O
****** 0.059       CAV00C5+CAV00C6
3       0.047      **USE_MAAP_DATA**
*
**14    0.212     MFCN(11)    CO2
****** 0.357      CAV00C3
4       0.212     **USE_CORCON_DATA**
*
5       0.        MFCN(12)    O2
****** NOT USED IN MELCOR
*                 **NOT_IN_MELCOR**
*
6       600.0     DCSRCN      DENSITY OF REBAR IN CONCRETE
****** NOT USED IN MELCOR
*                 **NOT_IN_MELCOR**
*
**17    903.0     CPCN0       SPECIFIC HEAT OF CONCRETE
****** 1299.97    TF00512
****** PER ROC WITH J.VALENTE/BNL ON 02/26/91, REVISED AS REV 7
7       1000.0    **USE_MAAP_DATA**
*
*
* 18-31 ARE FOR MARK III ONLY
*       (18-31)   **NOT_IN_MELCOR**      **NOT_FOR_PEACH_BOTTOM**
*
8     3.E11     PTEN   ELASTIC YOUNGS MODULUS FOR TENDONS
9     1.99E11   PEREB  ELASTIC YOUNGS MODULUS FOR REBAR
0     3.97E9    PEPTEN PLASTIC YOUNGS MODULUS FOR TENDONS
1     1.4E9     PEPREB PLASTIC YOUNGS MODULUS FOR REBAR
2     9.7E8     PSSPH  PRESTRESS ON HOOP TENDONS
3     1.01E9    PSSPZ  PRESTRESS ON AXIAL TENDONS
4     1.53E9    PSSYHT TENDON YIELD STRESS
5     4.137E8   PSSYHR REBAR YIELD STRESS
6     1.65E9    PSSFHT TENDON ULTIMATE STRESS
7     6.2E8     PSSFHR REBAR ULTIMATE STRESS
8     1.99E11   PEL    ELASTIC YOUNGS MODULUS FOR LINER
9     1.4E9     PEPL   PLASTIC YOUNGS MODULUS FOR LINER
0     4.137E8   PSSYHL LINER YIELD STRESS
1     6.2E8     PSSFHL LINER FAILURE STRESS
*
*
*****************************************************************************
FISSION PRODUCTS
```

```
*******************************************************************==BEGIN==
*
* INITIAL FISSION PRODUCT MASSES IN CORE REGION  (1-25)
****** NOT USED IN MELCOR
*                    **NOT_IN_MELCOR**
*
**01    387.0          Xe
****** 429.36          FAX FROM BNL TO FAI ON 10/19/90
1       429.36         **USE_MELCOR_DATA**
*
**02    25.7           Kr
****** 34.349          FAX FROM BNL TO FAI ON 10/19/90
2       34.349         **USE_MELCOR_DATA**
*
**03    16.6           I
****** 18.963          FAX FROM BNL TO FAI ON 10/19/90
3       18.963         **USE_MELCOR_DATA**
*
**04    23.3           Rb
****** 32.202          FAX FROM BNL TO FAI ON 10/19/90
4       32.202         **USE_MELCOR_DATA**
*
**05    207.0          Cs
****** 236.15          FAX FROM BNL TO FAI ON 10/19/90
5       236.15         **USE_MELCOR_DATA**
*
**06    62.7           Sr
****** 85.872          FAX FROM BNL TO FAI ON 10/19/90
6       85.872         **USE_MELCOR_DATA**
*
**07    105.0          Ba
****** 121.65          FAX FROM BNL TO FAI ON 10/19/90
7       121.65         **USE_MELCOR_DATA**
*
**08    36.2           Y
****** 42.936          FAX FROM BNL TO FAI ON 10/19/90
8       42.936         **USE_MELCOR_DATA**
*
**09    98.3           La
****** 107.34          FAX FROM BNL TO FAI ON 10/19/90
9       107.34         **USE_MELCOR_DATA**
*
**10    267.0          Zr
****** 311.29          FAX FROM BNL TO FAI ON 10/19/90
10      311.29         **USE_MELCOR_DATA**
*
**11    0.10           Nb
****** 3.578           FAX FROM BNL TO FAI ON 10/19/90
        3.578          **USE_MELCOR_DATA**
*
 *12    237.0          Mo
 ***** 275.51          FAX FROM BNL TO FAI ON 10/19/90
        275.51         **USE_MELCOR_DATA**

 *13    58.8           Tc
 ***** 71.560          FAX FROM BNL TO FAI ON 10/19/90
        71.560         **USE_MELCOR_DATA**

 *14    172.0          Ru
 ***** 182.48          FAX FROM BNL TO FAI ON 10/19/90
```

```
4       182.48          **USE_MELCOR_DATA**
*
**15    0.10            Sb
****** 1.3954           FAX FROM BNL TO FAI ON 10/19/90
5       1.3954          **USE_MELCOR_DATA**
*
**16    34.9            Te
****** 35.78            FAX FROM BNL TO FAI ON 10/19/90
6       35.78           **USE_MELCOR_DATA**
*
**17    208.0           Ce
****** 243.30           FAX FROM BNL TO FAI ON 10/19/90
7       243.30          **USE_MELCOR_DATA**
*
**18    80.4            Pr
****** 93.028           FAX FROM BNL TO FAI ON 10/19/90
8       93.028          **USE_MELCOR_DATA**
*
**19    271.0           Nd
****** 314.86           FAX FROM BNL TO FAI ON 10/19/90
9       314.86          **USE_MELCOR_DATA**
*
0       53.8            Sm
****** NOT USED IN MELCOR
*                       **NOT_IN_MELCOR**
*
**21    0.10            Np
****** 39.358           FAX FROM BNL TO FAI ON 10/19/90
1       39.358          **USE_MELCOR_DATA**
*
2       743.0           Pu
****** NOT USED IN MELCOR
*                       **NOT_IN_MELCOR**
*
3    0.D0       NOT USED
4    0.D0       NOT USED
5    0.D0       NOT USED
*
* STRUCTURAL MATERIAL MASS IN CORE REGION
*
**26    1050.      SN
****** 895.        CORX0702       0.0145*(5*(3153+3004+928+2339+2229+688.5))
6       895.       **USE_MELCOR_DATA**
*
**27    432.       MN             69824=SUM OF XMSS IN MELCOR
*****   432        CORXXX02       0.62%=(432/69824)
7       432.       **USE_MAAP_DATA**
*
**28    17000.     B4C
****** 1785.5      CORX0702       5*(158.9+151.4+46.8)
8       1785.5     **USE_MELCOR_DATA**
*
9       0.0         NOT USED
****** NOT USED IN MELCOR
*                   **NOT_IN_MELCOR**
*
0       0.0         NOT USED
****** NOT USED IN MELCOR
*                   **NOT_IN_MELCOR**
*
```

```
1       0.D0        FDFSP       DRYWELL VENTS DECON. FACTOR
****** NOT USED IN MELCOR
*                   **NOT_IN_MELCOR**
*
2       0.D0        FDFRV       SRV DECON. FACTOR
****** NOT USED IN MELCOR
*                   **NOT_IN_MELCOR**
*
*@@@REV 7, PARAMETERS 33 - 44 ADDED
* PERCENT DECAY POWER IN MAAP FISSION PRODUCT GROUPS
3    0.028D0     FP GRP #1,  NOBLES
4    0.151D0     FP GRP #2,  CSI
5    0.0194D0    FP GRP #3,  TEO2
6    0.062D0     FP GRP #4,  SRO
7    0.05D0      FP GRP #5,  MOO2
8    0.1D0       FP GRP #6,  CSOH
9    0.D0        FP GRP #7,  BAO
0    0.D0        FP GRP #8,  LA2O3
1    0.D0        FP GRP #9,  CEO2
2    0.D0        FP GRP #10, SB
3    0.0194D0    FP GRP #11, TE2
4    0.D0        FP GRP #12, UO2
*
*
************************************************************************
CONTROL CARDS  (01-329)
*********************************************************************==BEGIN==
****** NOT USED IN MELCOR
*                   **NOT_IN_MELCOR**
*
    1            IBWR   PLANT TYPE
    1=MARK I, 2=MARK II, 3=MARK III
    49           IRSTW  UNIT NUMBER TO WRITE RESTART FILE (MAIN)
    50           IHUW   UNIT NUMBER TO WRITE RESTART FILE (HEATUP)
    40           IPOUT  UNIT NUMBER TO WRITE PROGRAM OUTPUT FILE

*05    1         IPLT1  UNIT NUMBER FOR THE FIRST PLOT FILE (OTHER SEQUENTIAL)
*****            1 = USE A8 FORMAT,  2 = USE A15 FORMAT
       2         CHANGED PER REV 7 ON 03/18/91

    600          IPTSMX MAXIMUM NUMBER OF PLOTTED POINTS
    6            IPTSPK MAXIMUM NUMBER OF PLOT POINTS TRACED FOR FULL
    150          IPTSAV NUMBER OF POINTS SAVED FOR VARIABLE PLOT
    1            ISUMM  SUMMARY DATA(0=ALL EVENTS,1=SHORTER LIST)
    14           ISUM   SUMMARY FILE NUMBER
    1            IRUNG  1 = 1ST ORDER R-K, 2 = 2ND ORDER R-K
    1            IFREEZ 1= DO FREEZE FRONT CALC. (0=NO CALC.)
    0            IRET   WRITE RETAIN PLOT FILE (NOT USED)
    10           IFPPLT RETAIN PLOT FILE UNIT NUMBER (NOT USED)

*25    5         IH     NUMBER OF RADIAL NODES
***** 3          COR00000
       5         **USE_MAAP_DATA**

26     10        JH     NUMBER OF AXIAL NODES
***** 5          COR00000       (11-6)
       10        **USE_MAAP_DATA**

36    0            IBANG  0=HPCI,HPCS,RCIC REGULATE LEVEL L2-L8
3  1             IINERT 0=CONTAINMENT NOT INERTED,1=CONTAINMENT INERTED
```

```
54  1           IILPCI LPCI INJECTION: 1=LOWER PLENUM, 0=DOWNCOMER
*
*155   9        INODRB NUMBER OF REACTOR BLDG NODES + ENVIRONMENT
****** 9        CV401...CV409 + CV410
55     9        **USE_MELCOR_DATA**
*
56  13          IAUXW  FILE TO WRITE AUX CODE INFO
57  0           IAUXR  FILE TO READ AUX CODE INFO
*158  1           IPLMAP =0, USE OLD ARCHIC HARDWIRD PLOT ROUTINES AND APLOT
27  1           JNTGRT = 1 : UTILIZE CONSISTENT TIMESTEPS BETWEEN
28  0           ITDLIM = 1 : UTILIZE USER-INPUT CRITICAL PARAMETERS
29  0           [illegible]PT  = 1 : SORT OUT INTEGRATION DIAGNOSTIC FIGURES OF MERIT
*
36  1           IEMBAL = 1 : PRINT MASS & ENERGY BALANCE DATA ON TABULAR OUTPUT
37  1           ICRBAL = 1 : PRINT CORE BALANCE DATA ON TABULAR OUTPUT
*
*************************************************************************
AUX BLDG/REACTOR BLDG INPUT  (01-312, EXCEPT 273,274,277,278)
*****************************************************************==BEGIN==
*               **USE_MELCOR_DATA**
*
*               TOTAL FREE VOLUME
1     5426.     CV401B2
2     5154.     CV402B2
3     5154.     CV403B2
4     2356.     CV404B2
5     7066.     CV405B2
6     2425.     CV406B2
7     4866.     CV407B2
8    31048.     CV408B2
9   148825.     CV409B2
*
*
*               FLOOR AREA
1     1166.     HS04003500
2      588.     HS04010500
3      587.     HS04016500
4      261.     HS04022500
5      784.     HS04028500
6      245.     HS04033500
7      307.     HS04039500
8     1362.     HS04044500
9     8807.     HS04048500
*
*
*               ONE-SIDED OUTER WALL AREA
1       2264.0      805.     HS04001500
2       1556.0      671.     HS04006500
3       1554.0      671.     HS04012500
4       1351.0      345.     HS04018500
5       2047.5     1030.     HS04024500
6        668.0      588.     HS04030500
7       1393.0     1222.     HS04036500
8       1362.0     3063.     HS04042500
9       8807.0     8137.     HS04046500
*
*
*               OUTER WALL THICKNESS
1       2.6458       2.      HS04001115
2       1.5656       .9      HS04006113
```

```
3        1.5661          .9      HS04012113
4        1.1956          .9      HS04018113
5        1.4829          .9      HS04024113
6        1.3448          .6      HS04030112
7        1.6919          .6      HS04036112
8        0.2300      .00254      HS04042106
9        0.2300      .00254      HS04046106
*
*
*                 THERMAL CONDUCTIVITY OF OUTER WALL
1       1.524     HS04001201 & TF00612
2       1.524     HS04006201 & TF00612
3       1.524     HS04012201 & TF00612
4       1.524     HS04018201 & TF00612
5       1.524     HS04024201 & TF00612
6       1.524     HS04030201 & TF00612
7       1.524     HS04036201 & TF00612
8       1.524     HS04043201 & TF00912
9       1.524     HS04046201 & TF00912
*
*
*                 SPECIFIC HEAT OF OUTER WALL
1     1299.97     HS04001201 & TF00512
2     1299.97     HS04006201 & TF00512
3     1299.97     HS04012201 & TF00512
4     1299.97     HS04018201 & TF00512
5     1299.97     HS04024201 & TF00512
6     1299.97     HS04030201 & TF00512
7     1299.97     HS04036201 & TF00512
8     1299.97     HS04043201 & TF00812
9     1299.97     HS04046201 & TF00812
*
*
*                 HEIGHT OF OUTER WALL
          8.9     HS04001500
          7.5     HS04006500
63          7.5     HS04012500
          8.6     CV403B2-CV403B1
          8.3     HS04018500
          8.3     HS04024500
          5.1     HS04030500
          5.1     HS04036500
         16.0     HS04042500
         16.0     HS04046500


                  DENSITY OF OUTER WALL
      2522.60     HS04001201 & TF00412
      2522.60     HS04006201 & TF00412
      2522.60     HS04012201 & TF00412
      2522.60     HS04018201 & TF00412
      2522.60     HS04024201 & TF00412
      2522.60     HS04030201 & TF00412
      2522.60     HS04036201 & TF00412
      2522.60     HS04043201 & TF00712
      2522.60     HS04046201 & TF00712


                FORCED VOLUMETRIC VENTILATION FLOW OUT OF NODE

      0.0
```

```
2  0.0
3  0.0
4  0.0
5  0.0
6  0.0
7  0.0
8  0.0
9  0.0
*
*
*                FORCED VOLUMETRIC VENTILATION FLOW INTO NODE
1  0.0
2  0.0
3  0.0
4  0.0
5  0.0
6  0.0
7  0.0
8  0.0
9  0.0
*
*
*                AEROSOL SETTLING AREA = FLOOR AREA
01   1166.       HS04003500
02    588.       HS04010500
03    587.       HS04016500
04    261.       HS04022500
05    784.       HS04028500
06    245.       HS04033500
07    307.       HS04039500
08   1362.       HS04044500
09   8807.       HS04048500
*
*
*                IMPACTION AREA       **NOT_IN_MELCOR**
*                ONE QUARTER OF AVERAGED VERTICAL FLOW AREA
11      0.0        (8.6/4)
12      0.0        ((8.6+33.2)/2/4)
13      0.0
14      0.0        ((33.2+33.2)/2/4)
15      0.0
16      0.0        ((33.2+33.2)/2/4)
17      0.0
18      0.0        ((33.2+33.2)/2/4)
19      0.0
*
*
*111       2.10        (8.6/4)
*112       5.23        ((8.6+33.2)/2/4)
*113       0.0
*114       8.30        ((33.2+33.2)/2/4)
*115       0.0
*116       8.30        ((33.2+33.2)/2/4)
*117       0.0
*118       8.30        ((33.2+33.2)/2/4)
*119       0.0
*
*
*                MINIMUM GRATE DIAMETER FOR AEROSOL DEPOSITION BY IMPACTION
21  0.0
```

```
22   0.0
23   0.0
24   0.0
25   0.0
26   0.0
27   0.0
28   0.0
29   0.0
*
*
*               GRATE FLOW AREA FOR IMPACTION
31   0.0
32   0.0
33   0.0
34   0.0
35   0.0
36   0.0
37   0.0
38   0.0
39   0.0
*
*
*               AUX BUILDING SPRAY MASS FLOW RATE
41   0.0
42   0.0
43   0.0
44   0.0
45   0.0
46   0.0
47   0.0
48   0.0
49   0.0
*
*
*               SPRAY FALL HEIGHT
51   0.0
52   0.0
53   0.0
54   0.0
55   0.0
56   0.0
57   0.0
58   0.0
59   0.0
*
*
*               NODE NO. THAT THE VOL IN NODE 1 RECEIVES ITS INLET VENT.
1    10
2    10
3    10
4    10
5    10
6    10
7    10
8    10
9    10


                FLAG TO INDICATE HOW WATER ACCUMULATED IN A NODE IS DRAINED
                1 = INSTANTLY DRAINS ALL WATER FROM NODE #
```

```
*              0 = WATER DRAINS THRU THE SAME JUNCTIONS USED FOR GAS TRANSFER
71    0
72    0
73    0
74    1
75    1
76    1
77    1
78    0
79    0
*
*
*        ???   ELEVATION OF FLOOR OF NODE 1 WITH RESPECT TO GROUND LEVEL
81    -17.2
82     -4.1
83     -4.1
84      5.1
85      5.1
86     14.2
87     14.2
88     26.1
*189      5.1
89     4.5
*
*
*              CO2 MASS FLOWRATE FROM FIRE SUPPRESSION SYSTEM
91     0.
92     0.
93     0.
94     0.
95     0.
96     0.
97     0.
98     0.
99     0.
*
*
*              TOTAL AREA OF INTERNAL WALL
01     0.      NODE 1
02     921.8      NODE 2
03     920.8      NODE 3
04     306.8      NODE 4
05     921.6      NODE 5
06     254.0      NODE 6
07     333.6      NODE 7
08    9804.0      NODE 8
09   34244.0      NODE 9
*
*
*              THICKNESS OF INTERNAL WALL(S)
11     0.0
12     0.0042
13     0.0042
14     0.0032
15     0.0032
16     0.0031
17     0.0033
18     0.0056
19     0.0073
*
```

```
*
*                THERMAL CONDUCTIVITY OF INTERNAL WALL(S)       CARBON STEEL
*                **USE_MELCOR_DATA**        TF00911       52 W/M/K
21     52.0
22     52.0
23     52.0
24     52.0
25     52.0
26     52.0
27     52.0
28     52.0
29     52.0
*
*
*                SPECIFIC HEAT OF INTERNAL WALL(S)       CARBON STEEL
*                **USE_MELCOR_DATA**        TF00812       465 J/KG/K
31     465.0
32     465.0
33     465.0
34     465.0
35     465.0
36     465.0
37     465.0
38     465.0
39     465.0
*
*
*                HEIGHT OF INTERNAL WALL(S)
*
41       8.9     HS04001500
42       7.5     HS04006500
43       8.6     CV403B2-CV403B1
44       8.3     HS04018500
45       8.3     HS04024500
46       5.1     HS04030500
47       5.1     HS04036500
48      16.0     HS04042500
49      16.0     HS04046500
*
*
*                DENSITY OF INTERNAL WALL(S)             CARBON STEEL
*                **USE_MELCOR_DATA**        TF00712       7833 KG/M**3
51     7833.0
52     7833.0
53     7833.0
54     7833.0
55     7833.0
56     7833.0
57     7833.0
58     7833.0
59     7833.0


                 NODE NO. ON THE OTHER SIDE OF THE OUTER WALL(S)
 1      1
 2      2
 3      3
 4      4
 5      5
 6      6
```

```
67      7
68      8
69      9
*
71      0.        MSPRB0 INITIAL MASS OF WATER AVAILABLE FOR FIRE SPRAYS
****** NOT USED IN MELCOR
*                  **NOT_IN_MELCOR**
*
72      0.        MC2RB0 INITIAL MASS OF CO2 IN FIRE SUPPRESSION SYSTEM
****** NOT USED IN MELCOR
*                  **NOT_IN_MELCOR**
*
**273   295.0     INITIAL REACTOR BUILDING GAS TEMP
****** 299.8      CV405A2
73      295.0     **USE_MAAP_DATA**
*
**274   295.0     SPRAY WATER TEMPERATURE
****** 299.8      CV405A2
74      295.0     **USE_MAAP_DATA**
*
75     .001        SPRAY DROPLET DIAMETER
****** NOT USED IN MELCOR
*                  **NOT_IN_MELCOR**
*
**276   .10        INITIAL RELATIVE HUMIDITY IN REACTOR BUILDING
****** 0.0         PER ROC WITH LEV NEYMOTIM (BNL) ON 02/12/91
*       0.0        **USE_MELCOR_DATA**
*
**277   295.0      AMBIENT OUTSIDE TEMPERATURE
****** 299.8       CV410A2
77      295.0      **USE_MAAP_DATA**
*
**278   1.E5       AMBIENT PRESSURE
****** 101326.     CV410A1
78      1.E5       **USE_MAAP_DATA**
*
79     347.0    DAMPER CLOSING TEMPERATURE
80     1.E10    SPRAY INITIATION TEMPERATURE
81     1.E10    CO2 INITIATION TEMPERATURE
82     1.E10    TOTAL AEROSOL MASS REQUIRED TO TEAR OUT SGTS FILTERS
83     100.0    SGTS FILTER DF
84     6.2      XRBRRB(1) CHARACTERISTIC RADIUS OF NODE 1 FOR H2 BURNS
85     7.8      NODE 2
86     4.2      NODE 3
87     20.8     NODE 4
88     10.1     NODE 5
89     14.7     NODE 6
90     14.5     NODE 7
91     7.5      NODE 8
 2     24.2     NODE 9
 4     6.1      XHBRRB(1) CHARACTERISTIC HEIGHT OF NODE 1 FOR H2 BURNS
 5     202.     NODE 2
 6     25.7     NODE 3
 7     17.3     NODE 4
 8     8.5      NODE 5
 9     6.1      NODE 6
 0     6.1      NODE 7
 1     4.0      NODE 8
 2     14.2     NDOE 9
 4     0.D0     XIGRB  AVERAGE ELEVATION OF IGNITERS ABOVE FLOOR
```

```
05     0.D0     NODE 2
06     0.D0     NODE 3
07     0.D0     NODE 4
08     0.D0     NODE 5
09     0.D0     NODE 6
10     0.D0     NODE 7
11     0.D0     NODE 8
12     0.D0     NODE 9
*
*
TOPOLOGY
*
*    1       2       3       4      5       6         7        8
* NODE1, NODE2, V1-H0, ELEV, WIDTH, HEIGHT, LENGTH, AREA
*                                                            A = (A/(KLOSS)**0.5)
JNCTION 1-2
   1       2        1     13.1    3.31    3.31      0.86     12.164
JNCTION 2-4
   2       4        1      8.6    6.50    6.50      3.32     46.959
JNCTION 2-3
   2       3        0      4.3    5.64    5.64      2.50     35.361
JNCTION 3-9
   3       9        1      8.6    1.89    1.89      0.28      3.960
UNCTION 4-6
   4       6        1      8.5    6.50    6.50      3.32     46.959
UNCTION 4-5
   4       5        0      4.25   7.47    7.47      4.38     61.952
UNCTION 6-8
   6       8        1     11.3    6.50    6.50      3.32     46.959
UNCTION 6-7
   6       7        0      5.65   9.75    9.75      7.46     105.516
UNCTION 2-10
   2       10       0      4.3    0.178   0.178     0.0025   0.025
JNCTION 3-10
   3       10       0      4.3    0.178   0.178     0.0025   0.035
JNCTION 4-10
   4       10       0      4.25   0.178   0.178     0.0025   0.025
JNCTION 5-10
   5       10       0      4.25   0.178   0.178     0.0025   0.025
JNCTION 6-10
   6       10       0      5.65   0.178   0.178     0.0025   0.025
JNCTION 7-10
   7       10       0      5.65   0.178   0.178     0.0025   0.025
JNCTION 8-10
   8       10       0      8.8   5.33   5.33         2.23    31.542
JNCTION 8-10A
   8       10       0      9.45   0.373   0.373     0.0109   0.109
JNCTION 9-10
   9       10       0      8.4    0.607   0.607     0.0109   0.29
NTAINMENT INTERFACE
  -5.0
ID
*
*********************************************************************
LTMAP
EQ 1.0 300.0
*********************************************************************
*
                        MAAP BWR PLOT FILES
*********************************************************************
*
```

```
LOTFIL 41  /  PRIMARY SYSTEM
*===> FIGURES OF MERIT FOR MAAP-MELCOR COMPARISON
PS,TGPS,TWPS,TSATPS,TWLP,TWSH,MFSTPS,MFH2PS,MFO2PS,MFN2PS,MFCOPS,MFC2PS
WJET,XWCOR,XWSH,XW(1),XW(2),XW(3),XW(4),XW(5)
*  PRIMARY SYSTEM HEAT SINK IN PLOT FILE #46
LCMLP,TLCMLP
*===> FIGURES OF MERIT FOR MAAP-MELCOR COMPARISON
CORE,WCORI,WSTBRK,WFLSH,WFLLP,WFLPS
WLOCA,MWSH,WJETO,MWLPP,MWPSP,MSTPSP,MU2CT,XHCMLP,MCRUST
IMRAT,QDECAY,WWRV,WWSV
*****************************************************************
*
LOTFIL 42  /  HEATUP
*===> FIGURES OF MERIT FOR MAAP-MELCOR COMPARISON
110P,T15P,MH2GLO
CRN(1,1),TCRN(1,2),TCRN(1,3),TCRN(1,4),TCRN(1,5),TCRN(1,6),TCRN(1,7)
CRN(1,8),TCRN(1,9),TCRN(1,10)
U2N(1,1),MU2N(1,2),MU2N(1,3),MU2N(1,4),MU2N(1,5),MU2N(1,6),MU2N(1,7)
U2N(1,8),MU2N(1,9),MU2N(1,10)
*===> FIGURES OF MERIT FOR MAAP-MELCOR COMPARISON
SCOR,WH2COR,MWBYP,TCORO
ECCSS,WECCSI,WSTRV,PDWWW,VLCSTP,TLCMLP,UCMLP
*****************************************************************
*
LOTFIL 43  /  DRYWELL
*===> FIGURES OF MERIT FOR MAAP-MELCOR COMPARISON
DW,TGDW,TWDW,MWDW,XWDW,MCMTDW,TCMDW,MU2DW
CMDW(1),MCMDW(2),MCMDW(3),MCMDW(4),MCMDW(5),MCMDW(6),MCMDW(7),MCMDW(8)
FO2DW,NFC2DW,NFSTDW,NFCODW,NFH2DW,NFN2DW,XCNDWP,MH2GLO,MCOGLO
*===> FIGURES OF MERIT FOR MAAP-MELCOR COMPARISON
CRITP,FQTOT,QRVDW
*****************************************************************
*
LOTFIL 44  /  PEDESTAL AND WETWELL
*===> FIGURES OF MERIT FOR MAAP-MELCOR COMPARISON
PD,TGPD,TWPD,MWPD,XWPD,MCMTPD,TCMPD,MU2DP
FO2PD,NFC2PD,NFSTPD,NFCOPD,NFH2PD,NFN2PD,XCNPDP
CMPD(1),MCMPD(2),MCMPD(3),MCMPD(4),MCMPD(5),MCMPD(6),MCMPD(7),MCMPD(8)
*
WW,TGWW,MCMTWW,TCMWW,MU2WW
FO2WW,NFC2WW,NFSTWW,NFCOWW,NFH2WW,NFN2WW
CMWW(1),MCMWW(2),MCMWW(3),MCMWW(4),MCMWW(5),MCMWW(6),MCMWW(7),MCMWW(8)
*===> FIGURES OF MERIT FOR MAAP-MELCOR COMPARISON
WSP,TWSP,TSATWW,XSPWW,XSPDW,TETSP,TGTRP,THS2P(1)
*****************************************************************
*
LOTFIL 45  /  FISSION PRODUCT RELEASES
*===> FIGURES OF MERIT FOR MAAP-MELCOR COMPARISON
FPTC,MFPTP,FMCSIP,FMCSID,FMCSIW,FMCSIR
FPRIN(1),MFPRIN(2),MFPRIN(3),MFPRIN(4),MFPRIN(5),MFPRIN(7),MFPRIN(8)
FPRIN(9),MFPRIN(10),MFPRIN(11),MFPRIN(12)
FPREX(1),MFPREX(2),MFPREX(3),MFPREX(4),MFPREX(5),MFPREX(7),MFPREX(8)
FPREX(9),MFPREX(10),MFPREX(11),MFPREX(12)
*===> FIGURES OF MERIT FOR MAAP-MELCOR COMPARISON
FREL(1),FREL(2),FREL(3),FREL(4),FREL(5),FREL(6),FREL(7),FREL(8)
FREL(9),FREL(10),FREL(11),FREL(12)
*****************************************************************

LOTFIL 46  /  RPV & CONTAINMENT HEAT SINKS
PHSF(1),TPHSF(2),TPHSF(3),TPHSF(4),TPHSF(5),TPHSF(6),TPHSF(7)
```

```
[PHSF(8),TPHSF(9),TPHSF(10),TPHSF(11),TPHSF(12),TPHSF(13)
[PHSF(14),TPHSF(15),TPHSF(16)
THS1P(1),THS2P(1),THS3P(1)
TCNPD(1),TCNDW(1)
TSIHS1,TSOHS1,TSIHS2,TSOHS2,TSIHS3,TSOHS3,TSIHS4,TSOHS4,TGDW
TGCR,TGSH,TGSS,TGUH,TGUD,TGLD,TGLH,TGRR
*****************************************************************
*
PLOTFIL 47   / MASS & ENERGY BALANCE
*====> FIGURES OF MERIT FOR MAAP-MELCOR COMPARISON
MH2OPT,MH2OPB,MH2OER,UTOTT,UPSB,UPSE
MHOCNT,MCNB,MCNE,UCNTT,UCNTB,UCNTER
MFW,MSTSLO,MH2OZR,WSTSRV,UFW,USLO,UPSHS,UH2OZR,UFPDEC
UPSCT,UPSCNT,UPSLOS,UDKCNT,UCNABL,UHSTOT
*====> FIGURES OF MERIT FOR MAAP-MELCOR COMPARISON
*
*****************************************************************
*
* NOTE: IF YOU ARE NOT MODELING AUXILIARY BUILDINGS, (EG., INODRB=0
*       IN *CONTROL SECTION) COMMENT THE NEXT EIGHT LINES WITH **
PLOTFIL 48  /  AUXILARY BUILDING
ZWRB(1),ZWRB(2)
TGRB(1),TGRB(2),TGRB(3),TGRB(4),TGRB(5),TGRB(6),TGRB(7),TGRB(8),TGRB(9)
PRB(1),PRB(2),PRB(3),PRB(4),PRB(5),PRB(6),PRB(7),PRB(8),PRB(9)
WRB(1),WRB(2),WRB(3),WRB(4),WRB(5),WRB(6),WRB(7),WRB(8),WRB(9),WRB(10)
FMSGTP(1),FMSGTP(2),FMSGTP(3),FMSGTP(4),FMSGTP(5),FMSGTP(6)
FMENVP(1),FMENVP(2),FMENVP(3),FMENVP(4),FMENVP(5),FMENVP(6)
NFH2RB(1),NFO2RB(1),NFCORB(1),NFC2RB(1),NFSTRB(1),NFN2RB(1)
NFH2RB(2),NFO2RB(2),NFCORB(2),NFC2RB(2),NFSTRB(2),NFN2RB(2)
NFH2RB(3),NFO2RB(3),NFCORB(3),NFC2RB(3),NFSTRB(3),NFN2RB(3)
NFH2RB(4),NFO2RB(4),NFCORB(4),NFC2RB(4),NFSTRB(4),NFN2RB(4)
NFH2RB(5),NFO2RB(5),NFCORB(5),NFC2RB(5),NFSTRB(5),NFN2RB(5)
NFH2RB(6),NFO2RB(6),NFCORB(6),NFC2RB(6),NFSTRB(6),NFN2RB(6)
NFH2RB(7),NFO2RB(7),NFCORB(7),NFC2RB(7),NFSTRB(7),NFN2RB(7)
NFH2RB(8),NFO2RB(8),NFCORB(8),NFC2RB(8),NFSTRB(8),NFN2RB(8)
NFH2RB(9),NFO2RB(9),NFCORB(9),NFC2RB(9),NFSTRB(9),NFN2RB(9)
*FMTOTP(1),FMTOTP(2),FMTOTP(3),FMTOTP(4),FMTOTP(5),FMTOTP(6)
*
*****************************************************************
*
PLOTFIL 77      /MORE PLOT VARIABLES OF INTEGRAL M & E FOR NEW OUTPUT
HWPS,HWSH,HWLP,MWCOR,MWSH,MWLP,TGPS,TGSH,TGLH
*
*****************************************************************
*
PLOTFIL 78      /MORE PLOT VARIABLES OF INTEGRAL M & E FOR NEW OUTPUT
XUCPD,XLCPD,XUCDW,XLCDW,TCMPD,TCMPPD,TCMIPD,TCMDW,TCMPDW,TCMIDW
FXCNPD,FXCNDW,XCNPD,XCNDW
*
*****************************************************************
*
PLOTFIL 79      /MORE PLOT VARIABLES OF INTEGRAL M & E FOR NEW OUTPUT
PLT(250),PLT(251),PLT(252),PLT(253),PLT(254),PLT(255)
PLT(111),PLT(112),PLT(113),PLT(114),PLT(151),PLT(152),PLT(115)
PLT(121),PLT(122),PLT(123),PLT(124),PLT(161),PLT(162)
PLT(131),PLT(132),PLT(133),PLT(134),PLT(171),PLT(172)
PLT(141),PLT(181)
PLT(198),PLT(199)
PLT(201),PLT(202),PLT(203),PLT(204),PLT(208),PLT(209)
PLT(212),PLT(213),PLT(214),PLT(219)
```

```
LT(221),PLT(222),PLT(223),PLT(224),PLT(228),PLT(229)
CSP(1),MCSP(2),MCSP(3),MCSP(4),MCSP(5),MCSP(6),MCSP(7),MCSP(8)
*
*
ND
*
**********************************************************************
EVTMES
 1  T  TYPE 1 RELIEF VALVE OPEN
 1  F  TYPE 1 RELIEF VALVE CLOSED
 2  T  TYPE 2 RELIEF VALVE OPEN
 2  F  TYPE 2 RELIEF VALVE CLOSED
 3  T  TYPE 3 RELIEF VALVE OPEN
 3  F  TYPE 3 RELIEF VALVE CLOSED
 4  T  TYPE 4 RELIEF VALVE OPEN
 4  F  TYPE 4 RELIEF VALVE CLOSED
 5  T  ADS PERMISSIBLE-LP PUMP ON
 6  T  ADS SIGNAL-LOW WATER,HIGH DW PRESSURE
 7  T  HPCI ON
 7  F  HPCI OFF
 8  T  VESSEL FAILED
 9  T  HIGH VESSEL PRESSURE SCRAM
10  T  SCRAM SIGNAL RECIEVED
11  T    SHROUD WATER SATURATED
11  F    SHROUD WATER SUBCOOLED
12  T    LOWER PLENUM WATER SATURATED
12  F    LOWER PLENUM WATER SUBCOOLED
13  T  LPCI LOOP 2 ON
13  F  LPCI LOOP 2 OFF
14  T  RHR HTX. #1 ON
14  F  RHR HTX. #1 OFF
15  T  RHR HTX. #2 ON
15  F  RHR HTX. #2 OFF
16  T  CORE PLATE FAILURE
17  T  CALL HEATUP
17  F  NO LONGER CALLING HEATUP
18  T  HIGH WATER LEVEL IN SUPP. POOL
18  F  NO LONGER HIGH LEVEL IN SP
19  T  FEEDWATER PUMP TRIPPED
19  F  FEEDWATER ON
20  T  ADS ON
20  F  ADS OFF
21  T  CORIUM CONTACTING PEDESTAL FLOOR
22  T  EX-VESSEL STEAM EXPLOSION IN PEDESTAL
23  T  INITIATION SIGNAL RECVD FOR LPCI #2
23  F  INITIATION SIGNAL LOST FOR LPCI #2
24  T  SUCTION PRESS LIMIT REACHED ON LPCI #2
25  T  DIESEL LOADING PERMISSIBLE FOR HPCS
26  T  HPCS ON
26  F  HPCS OFF
27  T  LPCI LOOP 1 ON
27  F  LPCI LOOP 1 OFF
 8  T  LPCS ON
 8  F  LPCS OFF
 9  T  RCIC ON
 9  F  RCIC OFF
 0  T  CORE UNCOVERED
 0  F  CORE COVERED
 1  T  SHROUD WATER LEVEL < ELEVATION AT TOP OF JET PUMP
 1  F  SHROUD WATER LEVEL > ELEVATION AT TOP OF JET PUMP
```

32	T	DIESEL LOADING PERMISSIBLE FOR LPCI
33	T	DIESEL LOADING PERMISSIBLE FOR LPCS
34	T	HP INJECTION SUCTION FROM SUPPRESSION POOL
34	F	HP INJECTION SUCTION FROM CST
35	T	CORIUM IN LOWER PLENUM QUENCHED
35	F	CORIUM IN LOWER PLENUM NOT QUENCHED
36	T	CORIUM PRESENT IN LOWER PLENUM
36	F	CORIUM NOT PRESENT IN LOWER PLENUM
37	T	LOW WATER LEVEL IN CST
37	F	NORMAL WATER LEVEL IN CST
38	T	CORIUM AND WATER PRESENT IN LOWER PLENUM
38	F	CORIUM AND WATER NOT PRESENT IN LOWER PLENUM
39	T	LEVEL 8 HIGH WATER LEVEL
39	F	RESET LEVEL 8 TRIP
40	T	INITIATION SIGNAL RECVD FOR HPCI
40	F	INITIATION SIGNAL LOST FOR HPCI
41	T	INITIATION SIGNAL RECVD FOR HPCS
41	F	INITIATION SIGNAL LOST FOR HPCS
42	T	INITIATION SIGNAL RECVD FOR LPCI #1
42	F	INITIATION SIGNAL LOST FOR LPCI #1
43	T	INITIATION SIGNAL RECVD FOR LPCS
43	F	INITIATION SIGNAL LOST FOR LPCS
44	T	INITIATION SIGNAL RECVD FOR RCIC
44	F	INITIATION SIGNAL LOST FOR RCIC
45	T	HPCI TRIPPED OFF
46	T	SUCTION PRESS LIMIT REACHED ON HPCS
47	T	SUCTION PRESS LIMIT REACHED ON LPCI #1
48	T	SUCTION PRESS LIMIT REACHED ON LPCS
49	T	RCIC TRIPPED
49	F	RESET RCIC TRIP
50	T	LPCI #1 TO DRYWELL SPRAYS - OPEN
50	F	LPCI #1 TO DRYWELL SPRAYS - CLOSED
51	T	LPCI #2 TO DRYWELL SPRAYS - OPEN
51	F	LPCI #2 TO DRYWELL SPRAYS - CLOSED
52	T	LPCI #1 TO WETWELL SPRAYS - OPEN
52	F	LPCI #1 TO WETWELL SPRAYS - CLOSED
53	T	LPCI #2 TO WETWELL SPRAYS - OPEN
53	F	LPCI #2 TO WETWELL SPRAYS - CLOSED
54	T	LPCI #1 TO VESSEL - OPEN
54	F	LPCI #1 TO VESSEL - CLOSED
55	T	LPCI #2 TO VESSEL - OPEN
55	F	LPCI #2 TO VESSEL - CLOSED
56	T	LPCI #1 TO SUPPRESSION POOL - OPEN
56	F	LPCI #1 TO SUPPRESSION POOL - CLOSED
57	T	LPCI #2 TO SUPPRESSION POOL - OPEN
57	F	LPCI #2 TO SUPPRESSION POOL - CLOSED
58	T	LPCI LOOP 3 ON
58	F	LPCI LOOP 3 OFF
59	T	INITIATION SIGNAL RECVD FOR LPCI #3
59	F	INITIATION SIGNAL LOST FOR LPCI #3
60	T	SUCTION PRESS LIMIT REACHED ON LPCI #3
61	T	TYPE 5 SAFETY VALVES OPEN
61	F	TYPE 5 SAFETY VALVES CLOSED
62	T	MSIV CLOSED
62	F	MSIV OPEN
63	T	LOSS OF AC POWER (LOCKED)
64	T	REACTOR SCRAMMED
65	T	RECIRC PUMP TRIPPED
66	T	TURBINE STOP VALVES CLOSED
66	F	TURBINE STOP VALVES OPEN

67	T	LP PUMP PERMISSIBLE FOR WETWELL SPRAYS
68	T	WETWELL SPRAYS(MARKIII) ON
68	F	WETWELL SPRAYS(MARKIII) OFF
69	T	HPSW INJECTION ON
69	F	HPSW INJECTION OFF
70	T	PERMISSIBLE FOR RPT
71	T	CRD PUMP ON
71	F	CRD PUMP OFF
75	T	WATER IN CORE SATURATED
75	F	WATER IN CORE SUBCOOLED
76	T	CORIUM ENTRAINED IN PEDESTAL
76	F	CORIUM NO LONGER ENTRAINED IN PEDSTAL
77	T	WATER ENTRAINED IN PEDESTAL
77	F	WATER NO LONGER ENTRAINED IN PEDESTAL
78	T	LOW LEVEL TRIP FOR HPCI
78	F	RESET LOW LEVEL TRIP FOR HPCI
79	T	HIGH DRYWELL PRESSURE FOR HPCI
79	F	RESET HIGH DW PRESS. FOR HPCI
80	T	LOW LEVEL TRIP FOR HPCS
80	F	RESET LOW LEVEL TRIP FOR HPCS
81	T	HIGH DRYWELL PRESSURE FOR HPCS
81	F	RESET HIGH DW PRESS. FOR HPCS
82	T	LOW LEVEL TRIP FOR RCIC
82	F	RESET LOW LEVEL TRIP FOR RCIC
83	T	HIGH DRYWELL PRESSURE FOR RCIC
83	F	RESET HIGH DW PRESS. FOR RCIC
84	T	LOW LEVEL TRIP FOR LPCI
84	F	RESET LOW LEVEL TRIP FOR LPCI
85	T	HIGH DRYWELL PRESSURE FOR LPCI
85	F	RESET HIGH DW PRESS. FOR LPCI
86	T	LPCI FLOW > 0
86	F	LPCI FLOW = 0
87	T	LPCS FLOW > 0
87	F	LPCS FLOW = 0
88	T	DRYWELL VENT OPEN
88	F	DRYWELL VENT CLOSED
89	T	FIRST CALL TO ICRUST
90	T	LOW LEVEL TRIP FOR LPCS
90	F	RESET LOW LEVEL TRIP FOR LPCS
91	T	HIGH DRYWELL PRESSURE FOR LPCS
91	F	RESET HIGH DW PRESS. FOR LPCS
92	T	HIGH RCIC TURBINE EXHAUST
92	F	NO LONGER HIGH RCIC TURB. EXHAUST
93	T	LOW WATER TRIP FOR ADS
93	F	RESET LOW WATER TRIP FOR ADS
94	T	HIGH DRYWELL PRESSURE TRIP FOR ADS
94	F	RESET HIGH DRYWELL PRESSURE TRIP FOR ADS
95	T	PEDESTAL DOWNCOMER HAS FAILED
95	F	PEDESTAL DOWNCOMER NOT FAILED
96	T	AUX CONDENSER ON
96	F	AUX CONDENSER OFF
97	T	HIGH RPV PRESS INITIATION FOR ISO COND
97	F	NO HIGH RPV PRESS INITIATION FOR ISO COND
98	T	RX BLDG FIRE SPRAYS ON
98	F	RX BLDG FIRE SPRAYS OFF
99	T	RX BLDG CO2 FIRE SUPPRESSION ON
99	F	RX BLDG CO2 FIRE SUPPRESSION OFF
100	T	H2 BURNING IN RX BLDG
100	F	H2 NOT BURNING IN RX BLDG
101	T	BURNING IN PEDESTAL

1	F	BURNING OVER IN PEDESTAL
2	T	CORIUM TEMP. ABOVE CONTRETE MELTING IN PD
2	F	CORIUM TEMP. BELOW CONCRETE MELTING IN PD
3	T	WATER IN PEDESTAL
3	F	NO WATER IN PEDESTAL
4	T	WATER SATURATED IN PEDESTAL
4	F	WATER NO LONGER SATURATED IN PEDESTAL
5	T	CORIUM QUENCHED IN PEDESTAL
5	F	CORIUM NOT QUENCHED IN PEDESTAL
6	T	CORIUM AND WATER PRESENT IN PEDESTAL
6	F	NO CORIUM OR NO WATER PRESENT IN PD
7	T	CORIUM TEMP < CORIUM MELTING POINT IN PD
7	F	CORIUM TEMP > CORIUM MELTING POINT IN PD
8	T	FIRST CALL TO FREEZE
9	T	WETWELL VENT OPEN
9	F	WETWELL VENT CLOSED
0	T	RCIC SUCTION FROM SUPPRESSION POOL
0	F	RCIC SUCTION FROM CST
1	T	PRIMARY SYSTEM COUPLED
1	F	PRIMARY SYSTEM NOT COUPLED
2	T	MWLP G.T. MWMIN
2	F	MWLP L.E. MWMIN
3	T	ADS VALVES OPEN DUE TO LOW DRYWELL PRESSURE
3	F	ADS VALVES CLOSED DUE TO HI DRYWELL PRESSURE
4	T	ADS VALVES OPEN DUE TO HI RPV PRESSURE
4	F	ADS VALVES CLOSED DUE TO LOW RPV PRESSURE
5	T	START TO CALL FISSION PRODUCT MODELS
5	F	FISSION PRODUCT MODELS NOT CALLED
6	T	BURNING IN DRYWELL
6	F	BURNING OVER IN DRYWELL
7	T	CORIUM TEMP. ABOVE CONCRETE MELTING IN DW
7	F	CORIUM TEMP. BELOW CONCRETE MELTING IN DW
8	T	REVERSE FLOW THROUGH SUPPRESSION POOL VENTS
8	F	NORMAL FLOW RESTORED IN SUPPRESSION POOL VENTS
9	T	WATER IN DRYWELL
9	F	NO WATER IN DRYWELL
0	T	PDW > PPD
0	F	PDW < PPD
1	T	WATER TEMP. ABOVE SATURATION IN DRYWELL
1	F	WATER TEMP. BELOW SATURATION IN DRYWELL
2	T	CORIUM QUENCHED IN DRYWELL
2	F	CORIUM NOT QUENCHED IN DRYWELL
3	T	CORIUM AND WATER PRESENT IN DRYWELL
3	F	CORIUM AND WATER NOT IN DRYWELL
4	T	CORIUM TEMP < CORIUM MELTING POINT IN DW
4	F	CORIUM TEMP > CORIUM MELTING POINT IN DW
5	T	LOW DWNCMR - L PLEN PATH OPEN FOR CIRC
5	F	LOW DWNCMR - L PLEN PATH NOT OPEN FOR CIRC
6	T	UP DWNCMR - SEP PATH OPEN FOR CIRC
6	F	UP DWNCMR - SEP PATH NOT OPEN FOR CIRC
7	T	RECIRC LOOP OPEN FOR CIRC
7	F	RECIRC LOOP NOT OPEN FOR CIRC
3	T	TEMP LIMIT REACHED ON HPCI SUCTION
3	F	TEMP LIMIT NOT REACHED ON HPCI SUCTION
9	T	HIGH TURB EXHAUST FOR HPCI
9	F	RESET HIGH TURB EXHAUST FOR HPCI
0	T	LOW RPV PRESSURE FOR HPCI
0	F	RESET LOW RPV PRESSURE FOR HPCI
1	T	BURNING IN WETWELL
1	F	BURNING OVER IN WETWELL

```
2  T  CORIUM TEMP > CONCRETE MELTING IN WETWELL
2  F  CORIUM TEMP < CONCRETE MELTING IN WETWELL
3  T  VACUUM BREAKERS OPEN
3  F  VACUUM BREAKERS CLOSED
4  T  WATER IN SUPP. POOL
5  T  SUPPRESSION POOL SATURATED
5  F  SUPPRESSION POOL NO LONGER SATURATED
6  T  CORIUM QUENCHED IN WETWELL
6  F  CORIUM TEMP. ABOVE WATER SATURATION IN WW
7  T  CORIUM AND WATER PRESENT IN WETWELL
8  T  CORIUM TEMP < CORIUM MELTING POINT IN WW
8  F  CORIUM TEMP > CORIUM MELTING POINT IN WW
9  T  RX BLDG FIRE WATER DEPLETED
9  F  RX BLDG FIRE WATER NOT DEPLETED
0  T  SUPP POOL LEVEL BELOW VENT PIPE
0  F  SUPP POOL LEVEL ABOVE VENT PIPE
1  T    TOP VENT OPEN (MIII)
2  T    TOP VENT COVERED (MIII)
3  T    TOP VENT OPEN & MID VENT COVERED (MIII)
4  T    MID VENT OPEN & BOTTOM VENT COVERED (MIII)
5  T    BOTTOM VENT OPEN (MIII)
6  T  MWCA > 0 KG.
6  F  MWCA = 0 KG.
7  T  BURNING IN MIDDLE CONTAINMENT (MIII)
7  F  BURNING OVER IN MIDDLE CONTAINMENT (MIII)
8  T  MWCB > 0 KG.
8  F  MWCB = 10 KG.
9  T  BURNING IN UPPER CONTAINMENT (MIII)
9  F  BURNING OVER IN UPPER CONTAINMENT (MIII)
0  T  RX BLDG CO2 SUPPRESSION DEPLETED
0  F  RX BLDG CO2 SUPPRESSION NOT DEPLETED
1  T  RX BLDG DAMPERS CLOSED
1  F  RX BLDG DAMPERS OPEN
2  T  DRYWELL PURGE SYSTEM ON
2  F  DRYWELL PURGE SYSTEM OFF
3  T  LOCA SIGNAL FOR UPPER POOL DUMP
4  T  UPPER POOL DUMP ACTIVATED
5  T  CONTAINMENT PURGE ON
5  F  CONTAINMENT PURGE OFF
@@@REV 7, ADD MISSING EVENT MESSAGE #156
6  T  IGNITERS HAVE POWER
6  F  IGNITERS DO NOT HAVE POWER
7  T  DRYWELL PURGE PERMISSIBLE
8  T  END OF UPPER POOL DUMP
9  T  BATTERY POWER UNAVAILABLE
9  F  BATTERY POWER AVAILABLE
0  T  LOW LEVEL FOR SCRAM
1  T  HIGH DRYWELL PRESSURE FOR SCRAM
2  T  HIGH DRYWELL PRESSURE FOR SPRAYS
3  T  HIGH WETWELL PRESSURE FOR SPRAYS
4  T  HIGH SUPP. POOL TEMP. FOR RCIC
5  T  LOW RPV PRESSURE FOR RCIC
6  T  CORIUM IN WETWELL      r error writing device PRN
ort, Retry, Ignore, Fail? r

6  F  CORIUM NOT IN WETWELL
8  T  DRYWELL LEAK HAS PLUGGED
8  F  DRYWELL LEAK NOT PLUGGED
9  T  PLUGGED LEAK PATH BLOWN OPEN
9  F  PLUGGED LEAK PATH NOT BLOWN OPEN
```

```
70  T  CORE RADIAL REGION 1 HAS BLOCKED
70  F  CORE RADIAL REGION 1 NOT BLOCKED
71  T  CORE RADIAL REGION 2 HAS BLOCKED
71  F  CORE RADIAL REGION 2 NOT BLOCKED
72  T  CORE RADIAL REGION 3 HAS BLOCKED
72  F  CORE RADIAL REGION 3 NOT BLOCKED
73  T  CORE RADIAL REGION 4 HAS BLOCKED
73  F  CORE RADIAL REGION 4 NOT BLOCKED
74  T  CORE RADIAL REGION 5 HAS BLOCKED
74  F  CORE RADIAL REGION 5 NOT BLOCKED
*@@@REV 7, ADD NEW EVENT CODE MESSAGES 175 THRU 178, 180 THRU 188
75  T  INITIATION SIGNAL RECEIVED FOR DRYWELL COOLERS
75  F  INITIATION SIGNAL LOST FOR DRYWELL COOLERS
76  1  REACTOR WATER CLEANUP SYSTEM( RWCU ) ON
76  0  REACTOR WATER CLEANUP SYSTEM( RWCU ) OFF
77  1  INITIATION SIGNAL RECEIVED FOR RWCU
77  0  INITIATION SIGNAL LOST FOR RWCU
78  1  TRIGGER SIGNAL RECEIVED FOR HPCI
78  0  TRIGGER SIGNAL LOST FOR HPCI
79  T  SGTS FILTER AEROSOL LOADING EXCEEDED
79  F  SGTS FILTER AEROSOL LOADING NOT EXCEEDED
80  1  TRIGGER SIGNAL RECEIVED FOR HPCS
80  0  TRIGGER SIGNAL LOST FOR HPCS
81  1  TRIGGER SIGNAL RECEIVED FOR RCIC
81  0  TRIGGER SIGNAL LOST FOR RCIC
82  1  HIGH LEVEL TRIP FOR FEED WATER
82  0  RESET HIGH LEVEL TRIP FOR FEED WATER
83  1  LPCI #1 TO RAD WASTE - OPEN
83  0  LPCI #1 TO RAD WASTE - CLOSE
84  1  LPCI #2 TO RAD WASTE - OPEN
84  0  LPCI #2 TO RAD WASTE - CLOSE
85  1  HIGH WATER LEVEL RESET SIGNAL RECEIVED FOR HPCI
85  0  HIGH WATER LEVEL RESET SIGNAL NOT RECEIVED FOR HPCI
86  1  HIGH WATER LEVEL RESET SIGNAL RECEIVED FOR RCIC
86  0  HIGH WATER LEVEL RESET SIGNAL NOT RECEIVED FOR RCIC
87  1  HIGH WATER LEVEL RESET SIGNAL RECEIVED FOR HPCS
87  0  HIGH WATER LEVEL RESET SIGNAL NOT RECEIVED FOR HPCS
88  1  DRYWELL COOLERS ON
88  0  DRYWELL COOLERS OFF
90  T  CONT FAILED IN WW DUE TO STRAIN
91  T  CONT FAILED IN WW DUE TO OVERPRESSURE
92  T  CONT FAILED IN CA DUE TO STRAIN
93  T  CONT FAILED IN CA DUE TO OVERPRESSURE
94  T  CONT FAILED IN CB DUE TO STRAIN
95  T  CONT FAILED IN CB DUE TO OVERPRESSURE
96  T  SHUTDOWN COOLING ON
96  F  SHUTDOWN COOLING OFF
*@@@REV 7, ADD MISSING EVENT MESSAGE #197
* NOTE EVENT CODE 197 IS SET ONLY FOR ONE TIMESTEP IN WHICH
* EITHER THE REACTOR VESSEL OR CONTAINMENT FAILED.
97  T  EITHER REACTOR VESSEL OR CONTAINMENT JUST FAILED
*@@@REV 7, ADD NEW EVENT CODE MESSAGE #198
* NEW EVENT CODE FOR AUTODT PLOT SCALING
98  T  AUTOMATIC PLOT SCALING IS ON
98  F  EQUALLY SPACED PLOT SCALING IS ON
99  T  CONTAINMENT FAILURE
00  T  HPCI MAN ON
00  F  HPCI NOT MAN ON
01  T  HPCI LOCKED OFF
01  F  HPCI NOT LOCKED OFF
```

2	T	LPCI LOOP 1 MAN ON
2	F	LPCI LOOP 1 NOT MAN ON
3	T	LPCI LOOP 1 LOCKED OFF
3	F	LPCI LOOP 1 NOT LOCKED OFF
4	T	HPCS MAN ON
4	F	HPCS NOT MAN ON
5	T	HPCS LOCKED OFF
5	F	HPCS NOT LOCKED OFF
6	T	LPCS MAN ON
6	F	LPCS NOT MAN ON
7	T	LPCS LOCKED OFF
7	F	LPCS NOT LOCKED OFF
8	T	FEEDWATER MAN ON
8	F	FEEDWATER NOT MAN ON
9	T	FEEDWATER MAN OFF
9	F	FEEDWATER NOT LOCKED OFF
0	T	RCIC MAN ON
0	F	RCIC NOT MAN ON
1	T	RCIC LOCKED OFF
1	F	RCIC NOT LOCKED OFF
2	T	TURBINE STOP VALVE CLOSED
2	F	TURBINE STOP VALVE OPEN
3	T	TURBINE BYPASS CLOSED
13	F	TURBINE BYPASS OPEN
14	T	MSIVS MAN OPEN
14	F	MSIVS NOT MAN OPEN
15	T	MSIVS LOCKED CLOSED
15	F	MSIVS NOT LOCKED CLOSED
16	T	PEDESTAL DOWNCOMER FAILED
16	F	PEDESTAL DOWNCOMER NOT FAILED
17	T	SRV #1 MAN OPEN
17	F	SRV #1 NOT MAN OPEN
8	T	SRV #1 LOCKED CLOSED
8	F	SRV #1 NOT LOCKED CLOSED
9	T	SRV #2 MAN OPEN
9	F	SRV #2 NOT MAN OPEN
0	T	SRV #2 LOCKED CLOSED
0	F	SRV #2 NOT LOCKED CLOSED
1	T	SRV #3 MAN OPEN
1	F	SRV #3 NOT MAN OPEN
2	T	SRV #3 LOCKED CLOSED
2	F	SRV #3 NOT LOCKED CLOSED
3	T	SRV #4 MAN OPEN
3	F	SRV #4 NOT MAN OPEN
4	T	SRV #4 LOCKED CLOSED
4	F	SRV #4 NOT LOCKED CLOSED
5	T	ADS MAN OPEN
5	F	ADS NOT MAN OPEN
6	T	ADS LOCKED CLOSED
6	F	ADS NOT LOCKED CLOSED
7	T	RHR HTX #1 MAN ON
7	F	RHR HTX #1 NOT MAN ON
[illegible]	T	RHR HTX #1 LOCKED OFF
8	F	RHR HTX #1 NOT LOCKED OFF
9	T	RHR HTX #2 MAN ON
9	F	RHR HTX #2 NOT MAN ON
0	T	RHR HTX #2 LOCKED OFF
0	F	RHR HTX #2 NOT LOCKED OFF
1	T	LPCI LOOP 2 MAN ON
1	F	LPCI LOOP 2 NOT MAN ON

1

IMAGE EVALUATION TEST TARGET (MT-3)

150mm

6"

1

IMAGE EVALUATION TEST TARGET (MT-3)

150mm

6"

1

IMAGE EVALUATION TEST TARGET (MT-3)

150mm

6"

1

IMAGE EVALUATION TEST TARGET (MT-3)

150mm

6"

32 T LPCI LOOP 2 LOCKED OFF
32 F LPCI LOOP 2 NOT LOCKED OFF
33 T LPCI LOOP 1 TO DRYWELL SPRAYS-MAN ON
33 F LPCI LOOP 1 TO DRYWELL SPRAYS-NOT MAN ON
34 T LPCI LOOP 1 TO DRYWELL SPRAYS-LOCKED OFF
34 F LPCI LOOP 1 TO DRYWELL SPRAYS-NOT LOCKED OFF
35 T LPCI LOOP 2 TO DRYWELL SPRAYS-MAN ON
35 F LPCI LOOP 2 TO DRYWELL SPRAYS-NOT MAN ON
36 T LPCI LOOP 2 TO DRYWELL SPRAYS-LOCKED OFF
36 F LPCI LOOP 2 TO DRYWELL SPRAYS-NOT LOCKED OFF
37 T LPCI LOOP 1 TO WETWELL SPRAYS-MAN ON
37 F LPCI LOOP 1 TO WETWELL SPRAYS-NOT MAN ON
38 T LPCI LOOP 1 TO WETWELL SPRAYS-LOCKED OFF
38 F LPCI LOOP 1 TO WETWELL SPRAYS-NOT LOCKED OFF
39 T LPCI LOOP 2 TO WETWELL SPRAYS-MAN ON
39 F LPCI LOOP 2 TO WETWELL SPRAYS-NOT MAN ON
40 T LPCI LOOP 2 TO WETWELL SPRAYS-LOCKED OFF
40 F LPCI LOOP 2 TO WETWELL SPRAYS-NOT LOCKED OFF
*@@@REV 7, EVENT MESSAGE #241 CLARIFIED
41 T LPCI LOOP 1 ALIGNED TO VESSEL
41 F LPCI LOOP 1 NOT ALIGNED TO VESSEL
42 T LPCI LOOP 1 TO VESSEL-LOCKED OFF
42 F LPCI LOOP 1 TO VESSEL-NOT LOCKED OFF
*@@@REV 7, EVENT MESSAGE #243 CLARIFIED
43 T LPCI LOOP 2 ALIGNED TO VESSEL
43 F LPCI LOOP 2 NOT ALIGNED TO VESSEL
44 T LPCI LOOP 2 TO VESSEL-LOCKED OFF
44 F LPCI LOOP 2 TO VESSEL-NOT LOCKED OFF
45 T LPCI LOOP 1 TO SUPPRESSION POOL-MAN ON
45 F LPCI LOOP 1 TO SUPPRESSION POOL-NOT MAN ON
46 T LPCI LOOP 1 TO SUPPRESSION POOL-LOCKED OFF
46 F LPCI LOOP 1 TO SUPPRESSION POOL-NOT LOCKED OFF
47 T LPCI LOOP 2 TO SUPPRESSION POOL-MAN ON
47 F LPCI LOOP 2 TO SUPPRESSION POOL-NOT MAN ON
48 T LPCI LOOP 2 TO SUPPRESSION POOL-LOCKED OFF
48 F LPCI LOOP 2 TO SUPPRESSION POOL-NOT LOCKED OFF
49 T SUCTION FOR HP INJ MAN LINED UP TO SUPP POOL
49 F SUCTION FOR HP INJ NOT MAN LINED TO SUPP POOL
50 T LOSS OF AC POWER
50 F AC POWER RESTORED
51 T LOSS OF DIESEL POWER
51 F DIESEL POWER RESTORED
53 T NO H2 OR CO BURNING ALLOWED
53 F H2 AND CO BURNING ALLOWED
54 T SUCTION FOR RCIC MAN LINED UP TO SUPP POOL
54 F SUCTION FOR RCIC NOT MAN LINED TO SUPP POOL
55 T REACTOR MAN SCRAMMED
56 T BREAK IN PRIMARY SYSTEM (LOCA)
56 F NO BREAK IN PRIMARY SYSTEM
57 T ATWS RUN
58 T SLC INJECTION BEGUN
59 T LPCI LOOP 3 MAN ON
59 F LPCI LOOP 3 NOT MAN ON
60 T LPCI LOOP 3 LOCKED OFF
60 F LPCI LOOP 3 NOT LOCKED OFF
61 T SRV #5 MAN OPEN
61 F SRV #5 NOT MAN OPEN
62 T SRV #5 LOCKED CLOSED
62 F SRV #5 NOT LOCKED OFF
63 T VACUUM BREAKERS-MAN OPEN

63 F VACUUM BREAKERS-NOT MAN OPEN
64 T VACUUM BREAKERS-LOCKED CLOSED
64 F VACUUM BREAKERS-NOT LOCKED CLOSE
65 T DRYWELL PURGE MAN ON
65 F DRYWELL PURGE NOT MAN ON
66 T DRYWELL PURGE LOCKED OFF
66 F DRYWELL PURGE NOT LOCKED OFF
67 T UPPER POOL DUMP MAN OPEN
67 F UPPER POOL DUMP NOT MAN OPEN
68 T UPPER POOL DUMP LOCKED CLOSED
68 F UPPER POOL DUMP NOT LOCKED CLOSED
69 T CONTAINMENT PURGE MAN OPEN
69 F CONTAINMENT PURGE NOT MAN OPEN
70 T CONTAINMENT PURGE LOCKED CLOSED
70 F CONTAINMENT PURGE NOT LOCKED CLOSED
71 T 0 LPCS PUMPS ON
71 F DEFAULT LPCS PUMPS ON
72 T 2 LPCS PUMPS ON
72 F DEFAULT LPCS PUMPS ON
73 T 4 LPCS PUMPS ON
73 F DEFAULT LPCS PUMPS ON
74 T HPSW INJECTION MAN ON
74 F HPSW INJECTION NOT MAN ON
75 T HPSW INJECTION LOCKED OFF
75 F HPSW INJECTION NOT LOCKED OFF
77 T CRD PUMP MAN ON
77 F CRD PUMP NOT MAN ON
78 T CRD PUMP LOCKED OFF
78 F CRD PUMP NOT LOCKED OFF
79 T OPEN DRYWELL VENT
80 T CLOSE DRYWELL VENT
81 T STEAM BREAK OUT OF CONTAINMENT - OPEN
81 F STEAM BREAK OUT OF CONTAINMENT - CLOSED
82 T OPEN WETWELL VENT
83 T CLOSE WETWELL VENT
84 T DRYWELL COOLERS ON
84 F DRYWELL COOLERS OFF
85 T AUX CONDENSER MAN ON
85 F AUX CONDENSER NOT MAN ON
86 T AUX CONDENSER MAN OFF
86 F AUX CONDENSER NOT MAN OFF
88 T SHUTDOWN COOLING MAN ON
88 F SHUTDOWN COOLING NOT MAN ON
89 T SHUTDOWN COOLING MAN OFF
89 F SHUTDOWN COOLING NOT MAN OFF
96 T BAR GRAPH DISPLAYS ON
96 F BAR GRAPH DISPLAYS OFF
97 T HEAT-UP DISPLAY STATUS ON
97 F HEAT-UP DISPLAY STATUS OFF
98 T VESSEL DISPLAY STATUS ON
98 F VESSEL DISPLAY STATUS OFF
99 T CONTAINMENT DISPLAY STATUS ON
99 F CONTAINMENT DISPLAY STATUS OFF
00 T RESET CUMULATIVE FIGURE OF MERITS
@@@REV 7, ADD NEW EVENT CODE MESSAGES #301 THRU 311
01 1 LPCI LOOP 1 TO RAD WASTE - MAN ON
01 0 LPCI LOOP 1 TO RAD WASTE - NOT MAN ON
02 1 LPCI LOOP 1 TO RAD WASTE - LOCKED OFF
02 0 LPCI LOOP 1 TO RAD WASTE - NOT LOCKED OFF
03 1 LPCI LOOP 2 TO RAD WASTE - MAN ON

```
)3  0  LPCI LOOP 2 TO RAD WASTE - NOT MAN ON
)4  1  LPCI LOOP 2 TO RAD WASTE - LOCKED OFF
)4  0  LPCI LOOP 2 TO RAD WASTE - NOT LOCKED OFF
)5  1  ISOLATION CONDENSER TUBE RUPTURED
)5  0  ISOLATION CONDENSER TUBE NOT RUPTURED
)9  1  DRYWELL PURGE CLOSES UPON CONT. ISOLATION
)9  0  DRYWELL PURGE DOES NOT CLOSE UPON CONT. ISOLAICN
.0  1  SECOND DRYWELL PURGE LINE AVAILABLE
.0  0  SECOND DRYWELL PURGE LINE NOT AVAILABLE
.1  1  HEAT CAPACITY TEMPERATURE LIMIT( HCTL ) - ON
.1  0  HEAT CAPACITY TEMPERATURE LIMIT( HCTL ) - OFF
ID

***************************************************************************
IMING DATA
***************************************************************************
   20.D0      TDMAX  MAXIMUM ALLOWED TIME STEP
   1.D-3      TDMIN  MINIMUM ALLOWED TIME STEP
   4.D-2      FMCHMX MAXIMUM MASS CHANGE FRACTION FOR INTEGRATION
   5.D-2      FUCHMX MAXIMUM ENERGY CHANGE FRACTION FOR INTEGRATION
   1.D-1      MDFPMN MIN FISSION PROD MASS ALLOWED TO CONTROL TIME STEP
***************************************************************************

INTEGRATION
 CATEGORY 1 -- GAS MASSES & TEMPERATURES
  R  MGPS      FMGPS      0.04   1.E1   1.E10
  R  TGPS      FTGPS      0.05   1.E2   1.E4
  R  MGPD      FMGPD      0.04   1.E1   1.E10
  R  TGPD      FTGPD      0.05   1.E2   1.E4
  R  MGDW      FMGDW      0.04   1.E1   1.E10
  R  TGDW      FTGDW      0.05   1.E2   1.E4
  R  MGWW      FMGWW      0.04   1.E1   1.E10
  R  TGWW      FTGWW      0.05   1.E2   1.E4
  R  MGCA      FMGCA      0.04   1.E1   1.E10
  R  TGCA      FTGCA      0.05   1.E2   1.E4
  R  MGCB      FMGCB      0.04   1.E1   1.E10
  R  TGCB      FTGCB      0.05   1.E2   1.E4
 CATEGORY 2 -- WATER MASSES, ETC.
  R  MWPD      FMWPD      0.04   1.E4   1.E10
  R  MWDW      FMWDW      0.04   1.E4   1.E10
15  MSPDW = mass of water in wetwell downcomers (not used)
  R  MSPWW     FMSPWW     0.04   1.E2   1.E10
  R  MWCOR     FMWCOR     0.04   1.E3   1.E10    FALSE  8
  R  MWOSH     FMWOSH     0.04   1.E3   1.E10
  R  MWJET     FMWJET     0.04   1.E2   1.E10
  R  XROF      FXROF      0.04   1.E-3  1.E3
  R  MWAC      FMWAC      0.04   1.E10  1.E15
 CATEGORY 3 -- CRUST THICKNESSES
 CATEGORY 4 -- HARDWIRED AS IN ORIGINAL INTGRT
D
***************************************************************************
SEREVT

1       MH2GLO    >        1.0
1  TRUE     MORE THAN 1 KG H2 GENERATED

2       T110P      >=       1173.0
2  TRUE     CLAD FAILURE

3       T110P      >=       2500.0
```

```
03  TRUE    FUEL MELTING
*
04      XCNDWP    >       0.001
04  TRUE    CONCRETE ATTACK IN DRYWELL
*
05      XCNPDP    >       0.001
05  TRUE    CONCRETE ATTACK IN PEDESTAL
*
06      PDW       >       9.08E5
06  TRUE    DRYWELL PRESSURE  >  9.08E5 PA
*
07      TGDW      >       922.0
07  TRUE     DRYWELL TEMP  >  922.0 K (1200 F)
*
21      MBLAD(1,1)      >      230.3
21  TRUE       BLADES RELOCATE TO NODE(1,1)
*
22      MBLAD(2,1)      >      230.3
22  TRUE       BLADES RELOCATE TO NODE(2,1)
*
23      MBLAD(3,1)      >      230.3
23  TRUE       BLADES RELOCATE TO NODE(3,1)
*
24      MBLAD(4,1)      >      230.3
24  TRUE       BLADES RELOCATE TO NODE(4,1)
*
25      MBLAD(5,1)      >      230.3
25  TRUE       BLADES RELOCATE TO NODE(5,1)
*
31      MU2N(1,1)      >      3371.0
31  TRUE       FUEL RELOCATE TO NODE(1,1)
*
32      MU2N(2,1)      >      3371.0
32  TRUE       FUEL RELOCATE TO NODE(2,1)
*
33      MU2N(3,1)      >      3371.0
33  TRUE       FUEL RELOCATE TO NODE(3,1)
*
34      MU2N(4,1)      >      3371.0
34  TRUE       FUEL RELOCATE TO NODE(4,1)
*
35      MU2N(5,1)      >      3371.0
35  TRUE       FUEL RELOCATE TO NODE(5,1)
*
41      XW(1)      <      0.191
41  TRUE       BOILED UP WATER LEVEL IN REGION 1   <  0.191 M
*
42      XW(2)      <      0.191
42  TRUE       BOILED UP WATER LEVEL IN REGION 2   <  0.191 M
*
43      XW(3)      <      0.191
43  TRUE       BOILED UP WATER LEVEL IN REGION 3   <  0.191 M
*
44      XW(4)      <      0.191
44  TRUE       BOILED UP WATER LEVEL IN REGION 4   <  0.191 M
*
45      XW(5)      <      0.191
45  TRUE       BOILED UP WATER LEVEL IN REGION 5   <  0.191 M
*
ELECT ALL
```

```
12 PDW > 112.7 PSI AND TSIHS2 > 900. F
12 TRUE CNTMNT FAILED DUE TO PDW > 112.7 PSIA, TSIHS2 > 900 F
12 ACTION 4

13 PDW >  89.7 PSI AND TSIHS2 > 1000. F
.3 TRUE CNTMNT FAILED DUE TO PDW > 89 7 PSIA, TSIHS2 > 1000 F
.3 ACTION 4

14 PDW >  71.7 PSI AND TSIHS2 > 1100. F
14 TRUE CNTMNT FAILED DUE TO PDW > 71.7 PSIA, TSIHS2 > 1100 F
14 ACTION 4

15 TSIHS2 > 1200. F
.5 TRUE CNTMNT FAILED DUE TO TSIHS2 > 1200 F
.5 ACTION 4

   ACTION 4
     EVENT 279 TRUE
   END

*************************************************************
)G ON ALL
ID

,0,0                / NO MORE LOCAL PARAMETER CHANGE
                    / 0=INITIAL MAAP RUN, 1=RESTART MAAP RUN
.0000E+00           / PROBLEM START TIME, SEC
1.400E+04           / PROBLEM END TIME, SEC
.200E+03           / OUTPUT-RESTART FILE PRINT INTERVAL, SEC
56                  / BREAK (LOCA) IN PUMP SEAL AND CRD SEAL

15                  / MSIV LOCKED CLOSED
                    / TRUE
50                  / LOSS OF AC POWER
                    / TRUE
51                  / LOSS OF DIESEL POWER
                    / TRUE
                    / NO (MORE) INITIATOR(S), INTERVENTION CONDITION(S) FOLLOW
                    / INTERVENE WHEN THE FOLLOWING EVENT CODE(S) CHANGE
)                   / CORE UNCOVERED, &
                    / NO (MORE) INTERVENTION(S), OPERATOR ACTION(S) FOLLOW
                    / NO (MORE) OPERATOR ACTION(S), INTERVENTION(S) FOLLOW
                    / INTERVENE WHEN THE FOLLOWING EVENT CODE(S) CHANGE
                    / VESSEL FAILED
                    / NO (MORE) INTERVENTION(S), OPERATOR ACTION(S) FOLLOW
                    / NO (MORE) OPERATOR ACTION(S), INTERVENTION(S) FOLLOW
                    / INTERVENE ON DRYWELL TEMPERATURE OF
 2.0                / K, (1200 F) &
                    / NO (MORE) INTERVENTION(S), OPERATOR ACTION(S) FOLLOW
 9                  / OPEN DRYWELL VENT (CONTAINMENT FAILURE)
                    / TRUE &
 00                 / MAKE LOCAL PARAMETER CHANGE OF
 10,9.29E-4         / M2, DRYWELL FAILURE AREA (4.8 INCH DIA)
 0,0                / NO MORE LOCAL PARAMETER CHANGE
                    / NO (MORE) OPERATOR ACTION(S), INTERVENTION(S) FOLLOW
                    / INTERVENE ON ELAPSED TIME
 6000E+04           / SEC (10 HRS), &
                    / NO (MORE) INTERVENTION(S), MAAP EXECUTION ENDS

 ;44m‾‾41mÞÞÞ0m
```

```
ND
*

7;44m ‾41mÞÞÞ0m
1mÞÞÞÞÞ0m A:\>type bnl_sbo.inp
                    / 0=INTERACTIVE, 1=BATCH, 2=BATCH WITH SENSITIVITY OPTION
AP-MELCOR: BWR SBO (03/10/91)
                    / 0=USE PARAMETER DEFAULTS, 1=USE SUPPLIED PARAMETER FILE
5                   / PARAMETER FILE I/O NUMBER
                    / 0=NO PARAMETER FILE LISTING, 1=LIST PARAMETER FILE
                    / 0=NO LOCAL PARAMETER CHANGE, 1=LOCAL PARAMETER CHANGE(S)
,224,0.0            / NO BATTERY AVAILABLE
0,327,1             / INTEGRATOR ITERATION
0,328,0             / HARD-WIRED TIMESTEP CONTROL VARIABLES
5,58,0.             / NO BLOCKAGE

CHF    = 0.1
CDBRK  = 0.7
JMIN   = 1.0
AERDC  = 3.0
PRAT   = -2
PLUG   = 0.5E5

*****************************************************************
8

01 ZWSH > 52.028 M
01 TRUE LEAKAGE FROM PUMP SEAL AND CRD SEAL
 1 ACTION 1

   ACTION 1
     ALOCA = 6.182D-6 M**2
     ZLOCA = 52.028 M
   END

02 ZWSH < 52.0 M
02 TRUE LEAKAGE FROM CRD SEAL ONLY
02 ACTION 2

   ACTION 2
     ALOCA = 3.399D-6 M**2
     ZLOCA = 45.29 M
   END

03 EVENT 8  TRUE      ! VESSEL FAILURE
03 TRUE NO BREAK IN PS WHEN VESSEL FAILED
03 ACTION 3

   ACTION 3
     EVENT 256 FALSE
   END

.0 PDW > 159.7 PSI
.0 TRUE CNTMNT FAILED DUE TO PDW > 159.7 PSIA
.0 ACTION 4

.1 PDW > 126.7 PSI AND TSIHS2 > 800. F
.1 TRUE CNTMNT FAILED DUE TO PDW > 126.7 PSIA, TSIHS2 > 800 F
.1 ACTION 4
```

```
13 PDW >  89.7 PSI AND TSIHS2 > 1000. F
13 TRUE CNTMNT FAILED DUE TO PDW > 89.7 PSIA, TSIHS2 > 1000 F
13 ACTION 4

14 PDW >  71.7 PSI AND TSIHS2 > 1100. F
14 TRUE CNTMNT FAILED DUE TO PDW > 71.7 PSIA, TSIHS2 > 1100 F
14 ACTION 4

15 TSIHS2 > 1200. F
15 TRUE CNTMNT FAILED DUE TO TSIHS2 > 1200 F
15 ACTION 4

   ACTION 4
     EVENT 279 TRUE
   END

**************************************************************
)G ON ALL
ID

,0,0               / NO MORE LOCAL PARAMETER CHANGE
                   / 0=INITIAL MAAP RUN, 1=RESTART MAAP RUN
.0000E+00          / PROBLEM START TIME, SEC
4.400E+04          / PROBLEM END TIME, SEC
.200E+03          / OUTPUT-RESTART FILE PRINT INTERVAL, SEC
56                 / BREAK (LOCA) IN PUMP SEAL AND CRD SEAL

15                 / MSIV LOCKED CLOSED
                   / TRUE
50                 / LOSS OF AC POWER
                   / TRUE
51                 / LOSS OF DIESEL POWER
                   / TRUE
                   / NO (MORE) INITIATOR(S), INTERVENTION CONDITION(S) FOLLOW
:                  / INTERVENE WHEN THE FOLLOWING EVENT CODE(S) CHANGE
)                  / CORE UNCOVERED, &
                   / NO (MORE) INTERVENTION(S), OPERATOR ACTION(S) FOLLOW
                   / NO (MORE) OPERATOR ACTION(S), INTERVENTION(S) FOLLOW
:                  / INTERVENE WHEN THE FOLLOWING EVENT CODE(S) CHANGE
                   / VESSEL FAILED
                   / NO (MORE) INTERVENTION(S), OPERATOR ACTION(S) FOLLOW
                   / NO (MORE) OPERATOR ACTION(S), INTERVENTION(S) FOLLOW
                   / INTERVENE ON DRYWELL TEMPERATURE OF
:2.0               / K, (1200 F) &
                   / NO (MORE) INTERVENTION(S), OPERATOR ACTION(S) FOLLOW
'9                 / OPEN DRYWELL VENT (CONTAINMENT FAILURE)
                   / TRUE &
)00                / MAKE LOCAL PARAMETER CHANGE OF
 10,9.29E-4        / M2, DRYWELL FAILURE AREA (4.8 INCH DIA)
 0,0               / NO MORE LOCAL PARAMETER CHANGE
                   / NO (MORE) OPERATOR ACTION(S), INTERVENTION(S) FOLLOW
                   / INTERVENE ON ELAPSED TIME
 6000E+04          / SEC (10 HRS), &
                   / NO (MORE) INTERVENTION(S), MAAP EXECUTION ENDS

 ;44m 41mÞÞÞ0m
 mÞÞÞÞÞ0m A:\>
 ;44m 41mÞÞÞ0m
 mÞÞÞÞÞ0m A:\>
 ;44m 41mÞÞÞ0m
```

APPENDIX C - Plots

ZWV	Water Level in RV
TS1HS1	T OF INNER PD WALL
TS1HS2	T OF INNER DW WALL
TS1HS3	T OF DRYWELL FLOOR
TS1HS4	T OF TORUS ROOM WALL
THS1P(1)	T OF INNER PD WALL
THS2P(1)	T OF INNER DW WALL
THS3P(1)	T OF DRYWELL FLOOR
TCNPD(1)	T OF CONCRETE IN PD
TCNDW(1)	T OF CONCRETE IN DW
TWPS	WATER TEMP IN PS
TSATPS	SAT TEMP IN PS
TLCMLP	CORIUM TEMP IN LP
T11OP	MAX CORE NODE TEMP
UCMLP	CORIUM ENERGY IN LP
TWDW	WATER TEMP IN DW
MWDW	WATER MASS IN DW
MCMTDW	CORIUM MASS IN DW
MCMDW(1)	U OF MASS OF CORIUM IN DW
MCMDW(2)	UO2 MASS OF CORIUM IN DW
MCMDW(3)	C MASS OF CORIUM IN DW
MCMDW(4)	ZR MASS OF CORIUM IN DW
MCMDW(5)	ZRO2 MASS OF CORIUM IN DW
MCMDW(6)	CR MASS OF CORIUM IN DW
MCMDW(7)	CR203 MASS OF CORIUM IN DW
MCMDW(8)	FE MASS OF CORIUM IN DW
NF02DW	MOLE FRAC 02 IN DW
NFSTDW	MOLE FRAC STEAM IN DW
NFN2DW	MOLE FRAC N2 IN DW
TWPD	WATER TEMP IN PD
MWPD	WATER MASS IN PD
XWPD	WATER HEIGHT IN PD
MCMTPD	CORIUM MASS IN PD
NF02PD	MOLE FRAC 02 IN PD
NFC2PD	MOLE FRAC CO2 IN PD
NFSTPD	MOLE FRAC STEAM IN PD
NFC0PD	MOLE FRAC CO IN PD
NFN2PD	MOLE FRAC N2 IN PD
MCMPD(1)	U MASS OF CORIUM IN PD
MCMPD(2)	UO2 MASS OF CORIUM IN PD
MCMPD(3)	C MASS OF CORIUM IN PD
MCMPD(4)	ZR MASS OF CORIUM IN PD
MCMPD(5)	ZR02 MASS OF CORIUM IN PD
MCMPD(6)	CR MASS OF CORIUM IN PD
MCMPD(7)	CR203 MASS OF CORIUM IN PD

MCMPD(8)	FE MASS OF CORIUM IN PD
MCMTWW	CORIUM MASS IN WW
NFN2WW	MOLE FRAC N2 IN WW
MCMWW(1)	U MASS OF CORIUM IN WW
MCMWW(2)	UO2 MASS OF CORIUM IN WW
MCMWW(3)	C MASS OF CORIUM IN WW
MCMWW(4)	ZR MASS OF CORIUM IN WW
MCMWW(5)	ZRO2 MASS OF CORIUM IN WW
MCMWW(6)	CR MASS OF CORIUM IN WW
MCMWW(7)	CR203 MASS OF CORIUM IN WW
MCMWW(8)	FE MASS OF CORIUM IN WW
MFPREX(1)	MASS NOBLES EX-VSL
MFPREX(2)	MASS CSI/RBI EX-VSL
MFPREX(3)	MASS TEO2 EX-VSL
MFPREX(4)	MASS SRO EX-VSL
MFPREX(5)	MASS MOO2 EX-VSL
MFPREX(6)	MASS CSOH EX-VSL
MFPREX(7)	MASS BAO EX-VSL
MFPREX(8)	MASS LANTHANDS EX-VSL
MFPREX(9)	MASS CEO2 EX-VSL
MFPREX(10)	MASS SB EX-VSL
MFPREX(11)	MASS TE2 EX-VSL
MFPREX(12)	MASS UO2+ EX-VSL
MFPRIN(1)	MASS NOBLES IN-VSL
MFPRIN(2)	MASS CSI/RBI IN-VSL
MFPRIN(3)	MASS TE02 IN-VSL
MFPRIN(4)	MASS SRO IN-VSL
MFPRIN(5)	MASS M002 IN-VSL
MFPRIN(6)	MASS CSOH IN-VSL
MFPRIN(7)	MASS BAO IN-VSL
MFPRIN(8)	MASS LANTHANDS IN-VSL
MFPRIN(9)	MASS CEO2 IN-VSL
MFPRIN(10)	MASS SB IN-VSL
WWDCCR	WATER FLOW RATE FROM DC TO CORE
WSTCR	STEAM FLOW RATE FROM CORE
XWB	WATER HEIGHT IN B COMPT

Table 4-3

DESCRIPTION OF BWR PLOT FILES

First Plot File - Primary System (Default File #41)

TIME	Time since accident initiation.
PPS	Pressure in the primary system.
QCORE	Total core power.
TGPS	Average temperature of gas in the primary system.
TWLP	Temperature of water in the lower plenum.
TWSH	Temperature of water in the shroud.
WCORI	Core inlet flow rate.
WSTBRK	Steam flow rate through the break (lower plenum).
WFLSH	Flashing rate in the shroud.
WFLLP	Flashing rate in the lower plenum.
WFLPS	Flashing rate in the core.
MGLOBE	Global mass balance on water.
WWLOCA	Water flow rate through LOCA.
MWSH	Mass of water in the shroud.
WJETO	Total flow rate from downcomer to lower plenum.
MWLPP	Mass of water in the lower plenum.
MWPSP	Mass of water in the core.
MSTPS	Mass of steam in the primary system.
MU2CT	Mass of UO_2 in the core.
MLCMLP	Mass of molten corium in the lower plenum.
XHCMLP	Height of corium in the lower plenum.
MCRUST	Mass of corium in frozen crust (lower plenum).
XWJET	Height of water in the jet pumps (ref. to bottom of vessel).
XWCOR	Height of water in the core (ref. to bottom of vessel).
XWSH	Height of water in the shroud (ref. to bottom of vessel).
TIMRAT	Ratio of accident time to CPU time.
QDECAY	Decay power.
WWBRK	Flowrate of water through the lower head failure.

Table 4-3 (Continued)

DESCRIPTION OF BWR PLOT FILES

Second Plot File - Heatup (Default File #42)

TIME	Time since accident initiation.
WSCOR	Steam flow rate out of the core.
WH2COR	Hydrogen flow rate out of the core.
MWBYP	Mass of water in the core bypass region.
TCORO	Temperature of core outlet gases.
XW(1)	Boiled up water level in radial region 1 (ref. co bottom of core).
XW(2)	Boiled up water level in radial region 2 (ref. to bottom of core).
XW(3)	Boiled up water level in radial region 3 (ref. to bottom of core).
XW(4)	Boiled up water level in radial region 4 (ref. to bottom of core).
XW(5)	Boiled up water level in radial region 5 (ref. to bottom of core).
T11OP	Maximum temperature in core.
T15P	Average core temperature.
WECCSS	Core spray flow rate.
WECCSI	ECCS injection flow rate.
WSTRV	Flow rate of steam through the relief valves.
XHLPCI	Net positive suction head at LPCI pump.
XHLPCS	Net positive suction head at LPCS pump.
XHHPCS	Net positive suction head at HPCS pump.
XHRCIC	Net positive suction head at RCIC pump.
XHHPCI	Net positive suction head at HPCI pump.
PDWWW	Pressure difference between drywell and wetwell.
VLCSTP	Volume of water in the condensate storage tank.

Table 4-3 (Continued)

DESCRIPTION OF BWR PLOT FILES

Fourth Plot File - Pedestal and Wetwell (Default File #44)

TIME	Time since accident initiation.
NFH2WW	Mole fraction of H_2 in the wetwell.
PWW	Pressure in the wetwell.
TFLWW	Flame temperature in the wetwell.
TGWW	Temperature of gas in the wetwell.
TCMWW	Temperature of corium in the wetwell.
NFO2WW	Mole fraction of O_2 in the wetwell.
NFC2WW	Mole fraction of CO_2 in the wetwell.
NFSTWW	Mole fraction of steam in the wetwell.
NFCOWW	Mole fraction of CO in the wetwell.
MU2WWP	Mass of UO_2 in the wetwell.
PPD	Pressure in the pedestal.
TCMPD	Temperature of corium in the pedestal.
TGPD	Temperature of gas in the pedestal.
MU2PDP	Mass of UO_2 in the pedestal.
NFH2PD	Mole fraction of H_2 in the pedestal.
XCNPDP	Concrete ablation thickness in the pedestal.
MWPDPP	Mass of water in the pedestal.
MWSP	Mass of water in the suppression pool.
TWSP	Temperature of water in the suppression pool.
XSPWW	Level of water on the wetwell side of the suppression pool.
XSPDW	Level of water on the drywell side of the suppression pool (downcomer).
TETSP	Temperature of torus shell (Mark I).
THS2P(1)	Temperature of gas in torus room (Mark I).
THS2(1)	Temperature of heat sink #2 (node 1).

Table 4-3 (Continued)

DESCRIPTION OF BWR PLOT FILES

Fifth Plot File (Continued)

FMCSID	Fraction of CsI in the drywell and pedestal.
FMCSIW	Fraction of CsI in the wetwell.
FMCSIR	Fraction of CsI released from containment.
MFPREX(3)	Mass of Group 3 fission products released ex-vessel.
MFPREX(4)	Mass of Group 4 fission products released ex-vessel.
MFPREX(5)	Mass of Group 5 fission products released ex-vessel.
MFPREX(6)	Mass of Group 6 fission products released ex-vessel.
MFPREX(7)	Mass of Group 7 fission products released ex-vessel.
MFPREX(8)	Mass of Group 8 fission products released ex-vessel.
MFPREX(9)	Mass of Group 9 fission products released ex-vessel.
MFPREX(10)	Mass of Group 10 fission products released ex-vessel.
MFPREX(11)	Mass of Group 11 fission products released ex-vessel.
MFPREX(12)	Mass of Group 12 fission products released ex-vessel.

Table 4-3 (Continued)

DESCRIPTION OF BWR PLOT FILES

Seventh Plot File - Mark III Only (Default File #47)

TIME	Time since accident initiation.
NFH2CA	Mole fraction of H_2 in compartment A.
PCA	Pressure in compartment A.
TFLCA	Flame temperature in compartment A.
TGCA	Temperature of gas in compartment A.
NFO2CA	Mole fraction of O_2 in compartment A.
NFC2CA	Mole fraction of CO_2 in compartment A.
NFSTCA	Mole fraction of steam in compartment A.
HFCOCA	Mole fraction of CO in compartment A.
NFH2CB	Mole fraction of H_2 in compartment B.
PCB	Pressure in compartment B.
TFLCB	Flame temperature in compartment B.
TGCB	Temperature of gas in compartment B.
NFO2CB	Mole fraction of O_2 in compartment B.
NHC2CB	Mole fraction of CO_2 in compartmant B.
NFSTCB	Mole fraction of steam in compartment B.
NFCOCB	Mole fraction of CO in compartment B.
MWCBP	Mass of water in compartment B.

Table 4-3 (Continued)

DESCRIPTION OF BWR PLOT FILES

Auxiliary Building Output File (Continued)

WRB9	Same from node 9 to 10.
WRB10	Same from node 10.
FMTOTP1	Fraction of the fission product group 1 released from the primary containment.
FMTOTP2	Same for group 2.
FMTOTP3	Same for group 3.
FMTOTP4	Same for group 4.
FMTOTP5	Same for group 5.
FMTOTP6	Same for group 6.
FMSGTP1	Fraction of fission product group 1 drawn into the SGTS.
FMSGTP2	Fraction of fission product group 2 drawn into the SGTS.
FMSGTP3	Fraction of fission product group 3 drawn into the SGTS.
FMSGTP4	Fraction of fission product group 4 drawn into the SGTS.
FMSGTP5	Fraction of fission product group 5 drawn into the SGTS.
FMSGTP6	Fraction of fission product group 6 drawn into the SGTS.
FMENVP1	Fraction of fission product group 1 released to the environment (not through SGTS*).
FMENVP2	Fraction of fission product group 2 released to the environment (not through SGTS*).
FMENVP3	Fraction of fission product group 3 released to the environment (not through SGTS*).
FMENVP4	Fraction of fission product group 4 released to the environment (not through SGTS*).

---

*Note that the fractional releases from the SGTS system to the environment are obtained by multiplying the fraction of each group drawn into the SGTS system by the assumed filter efficiency.

MELCOR: High Pressure SBO (LN, 04/17/91)

Plot 1-8

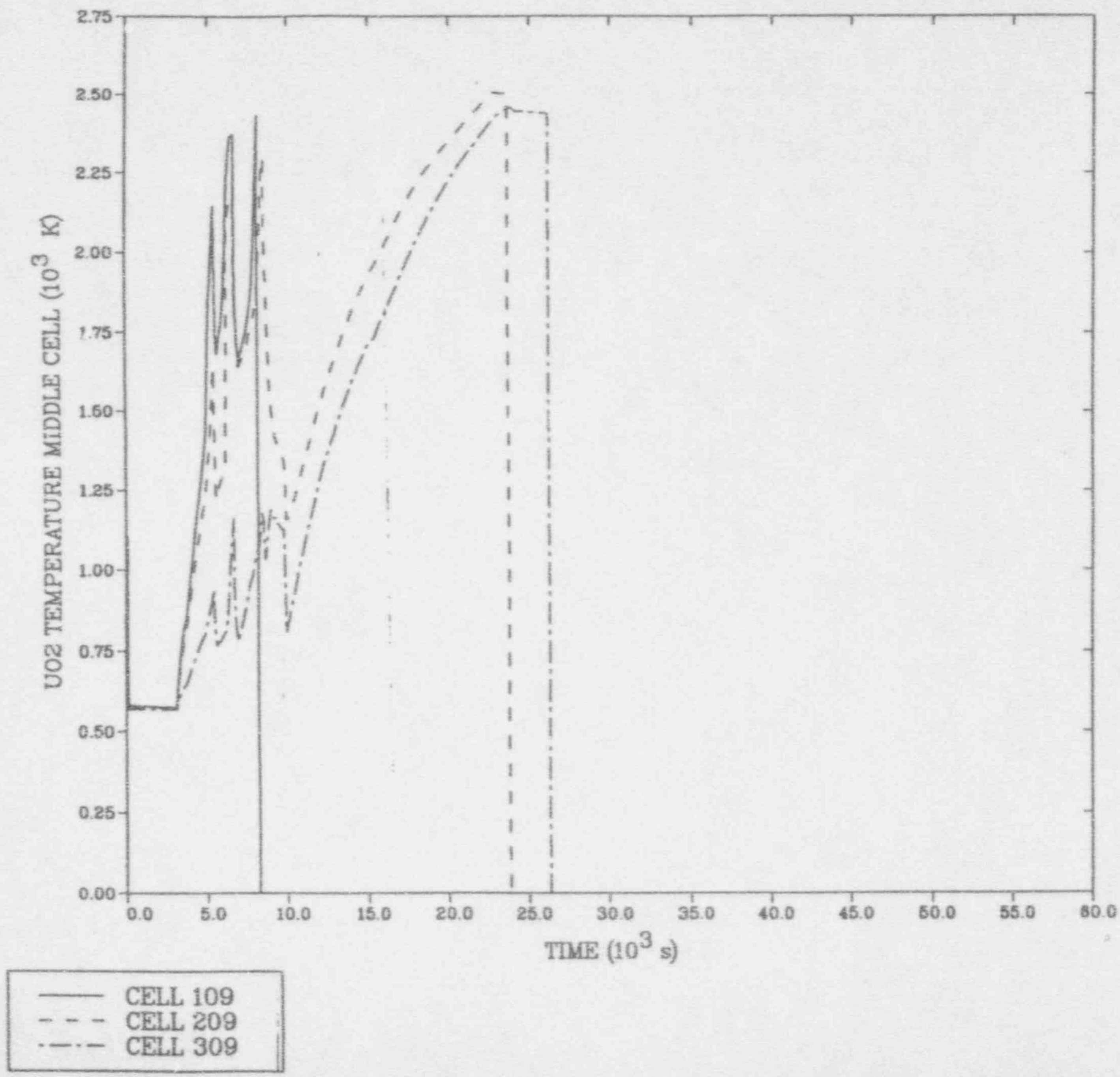

MELCOR: High Pressure SBO (LN, 04/17/91)

PLOT 2

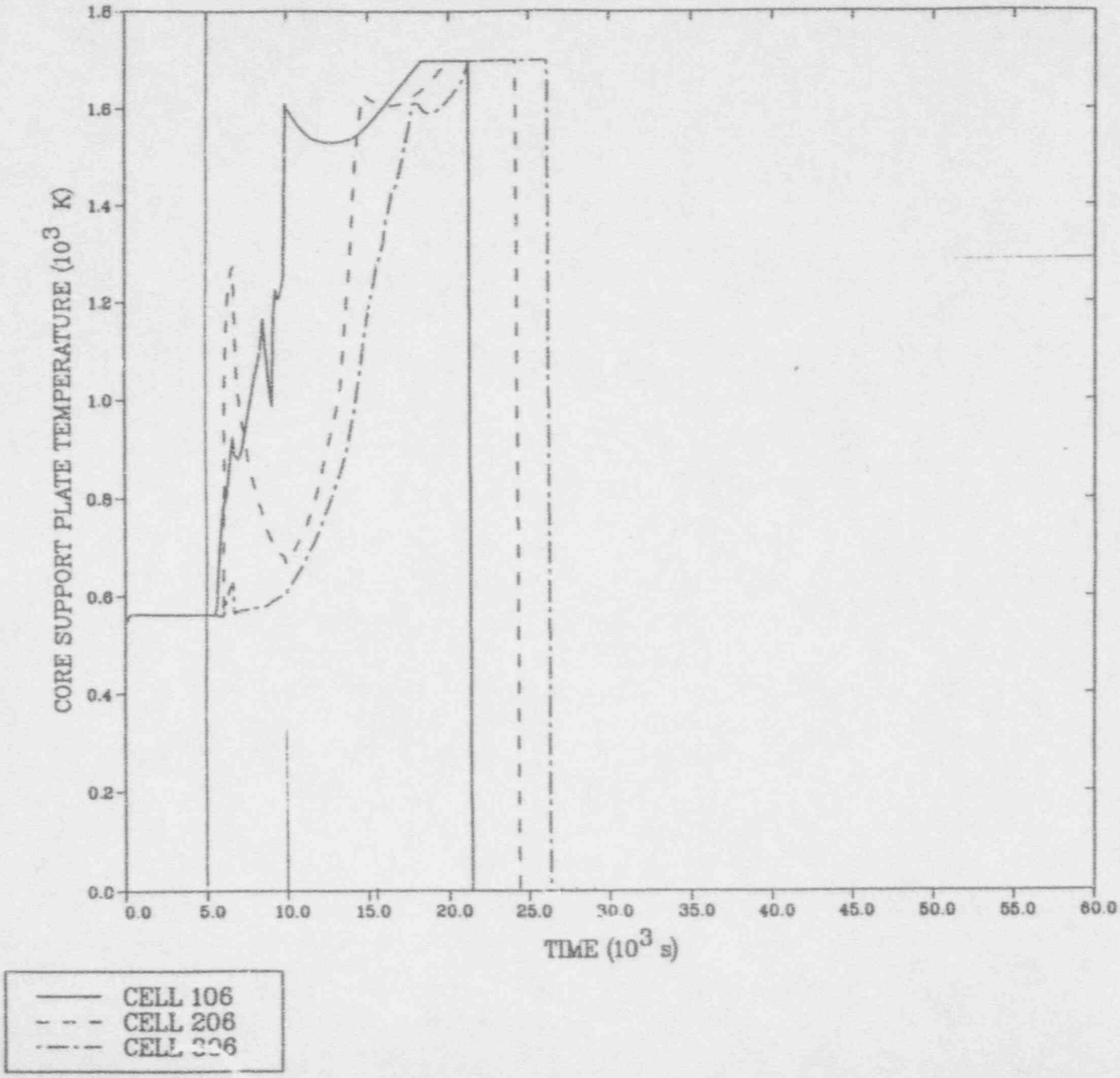

MELCOR: High Pressure SBO (LN, 04/17/91)

P 3

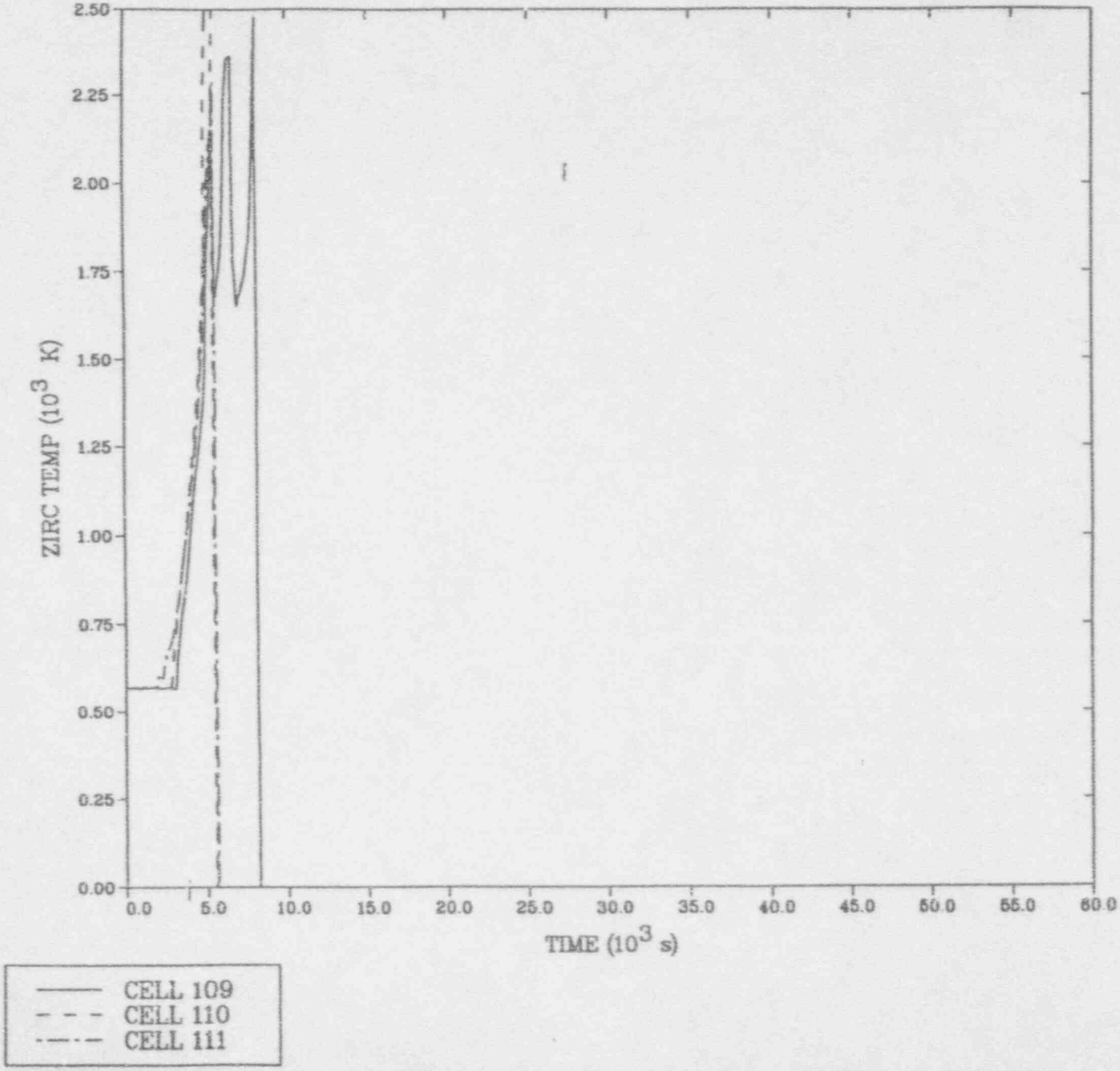

F-4

MELCOR: High Pressure SBO (LN, 04/17/91)

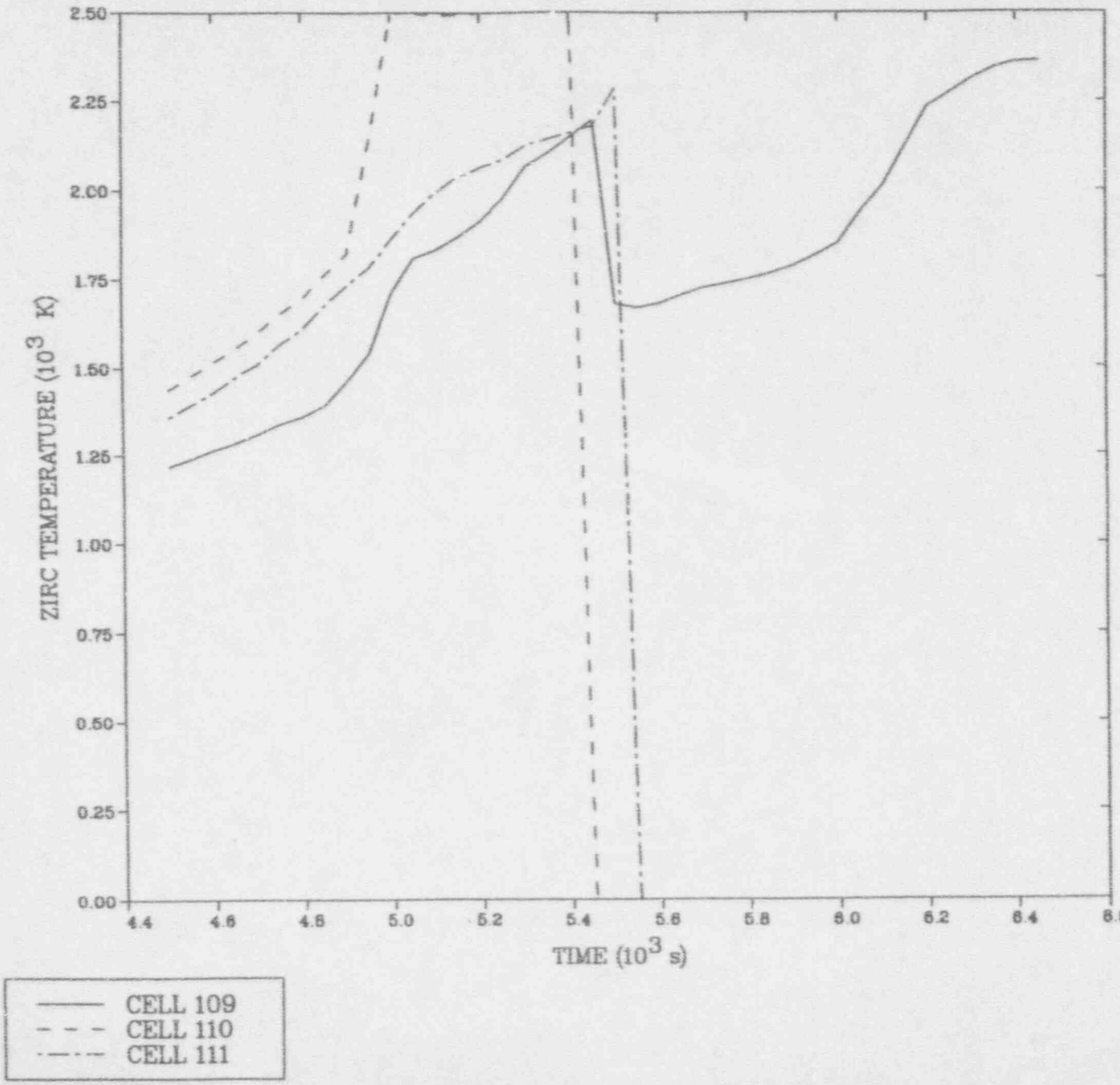

MELCOR: High Pressure SBO (LN, 04/17/91)

P 5

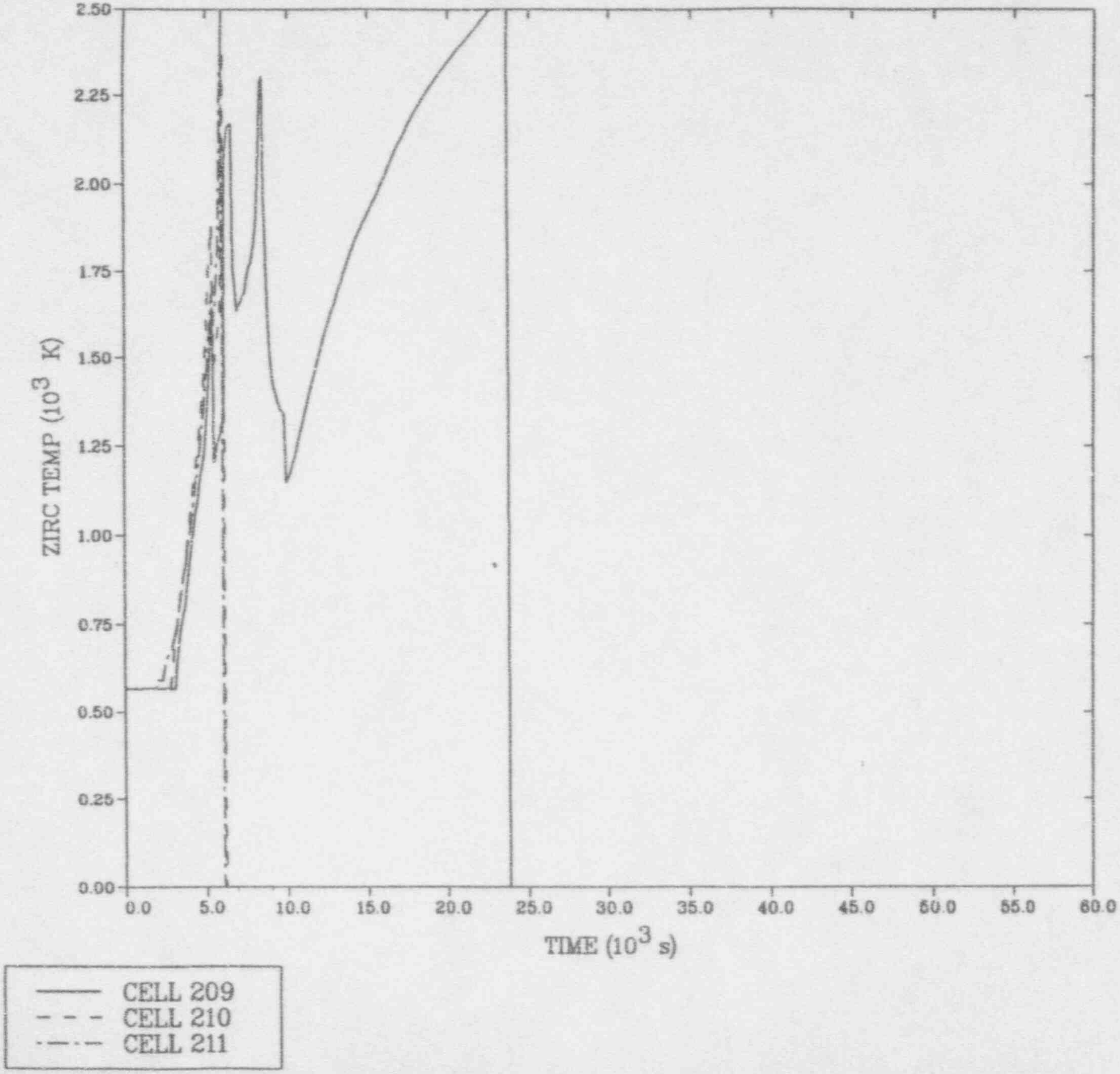

MELCOR: High Pressure SBO (LN, 04/17/91)

7 6

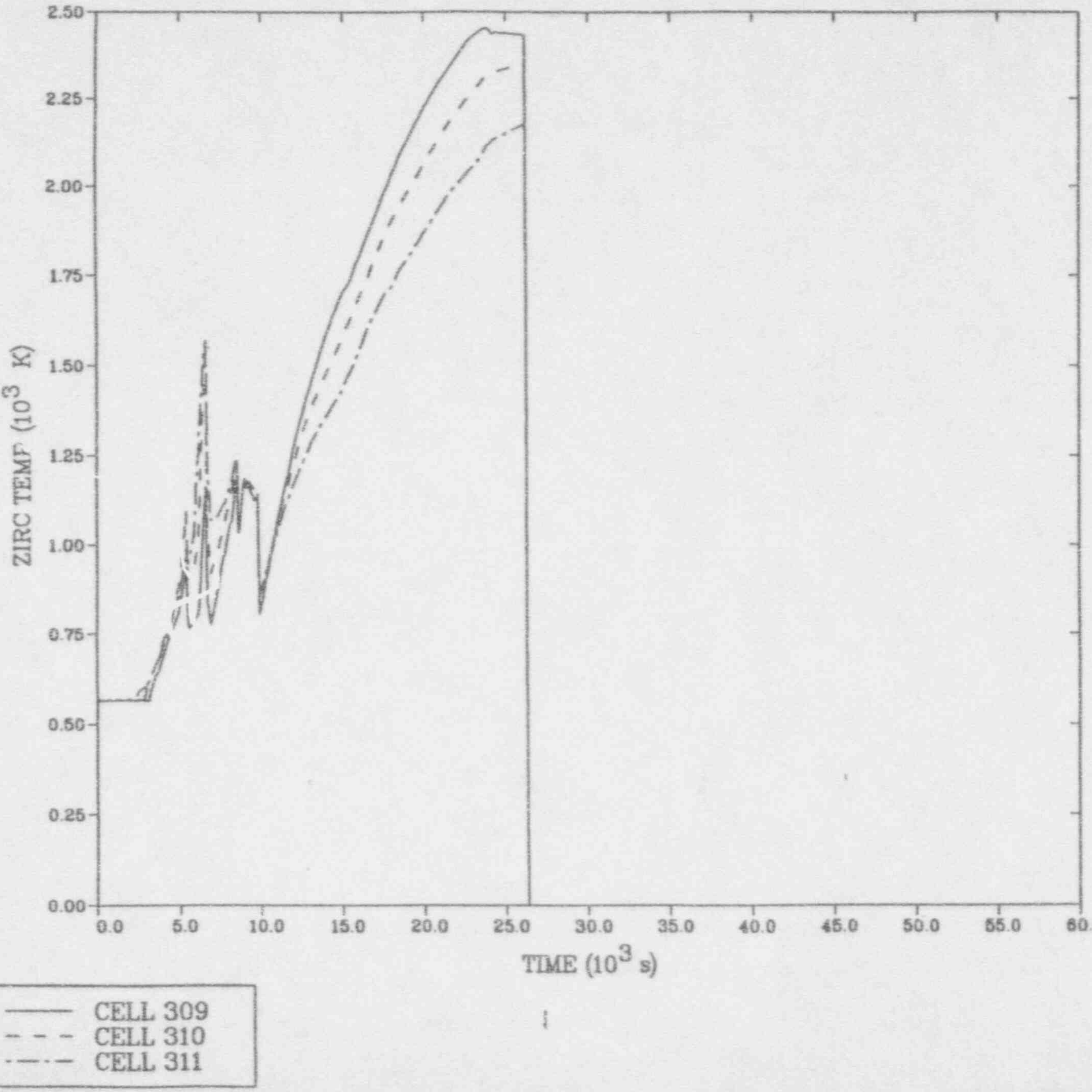

MELCOR: High Pressure SBO (LN, 04/17/91)

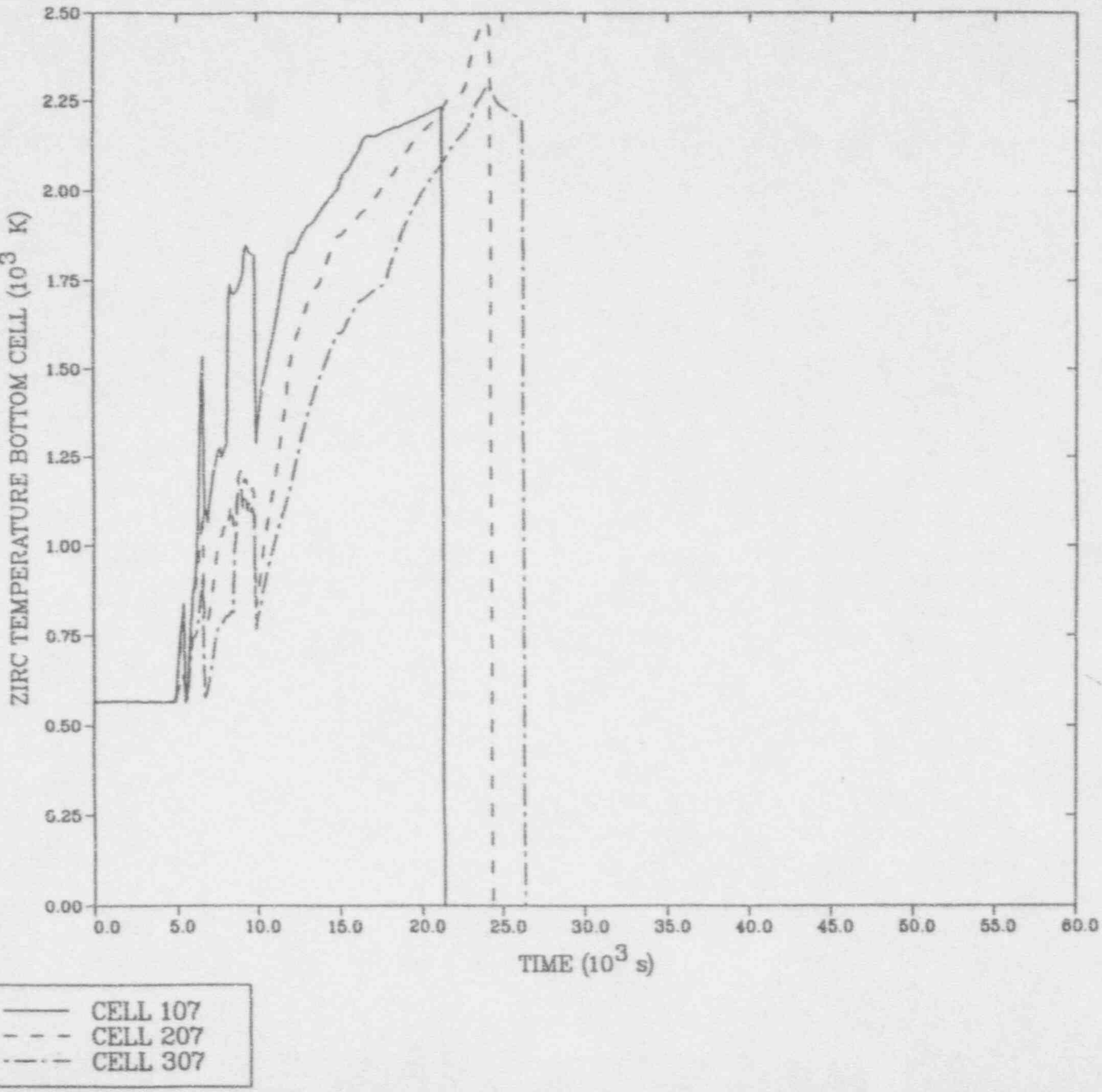

MELCOR: High Pressure SBO (LN, 04/17/91)

Plot 1 + 3

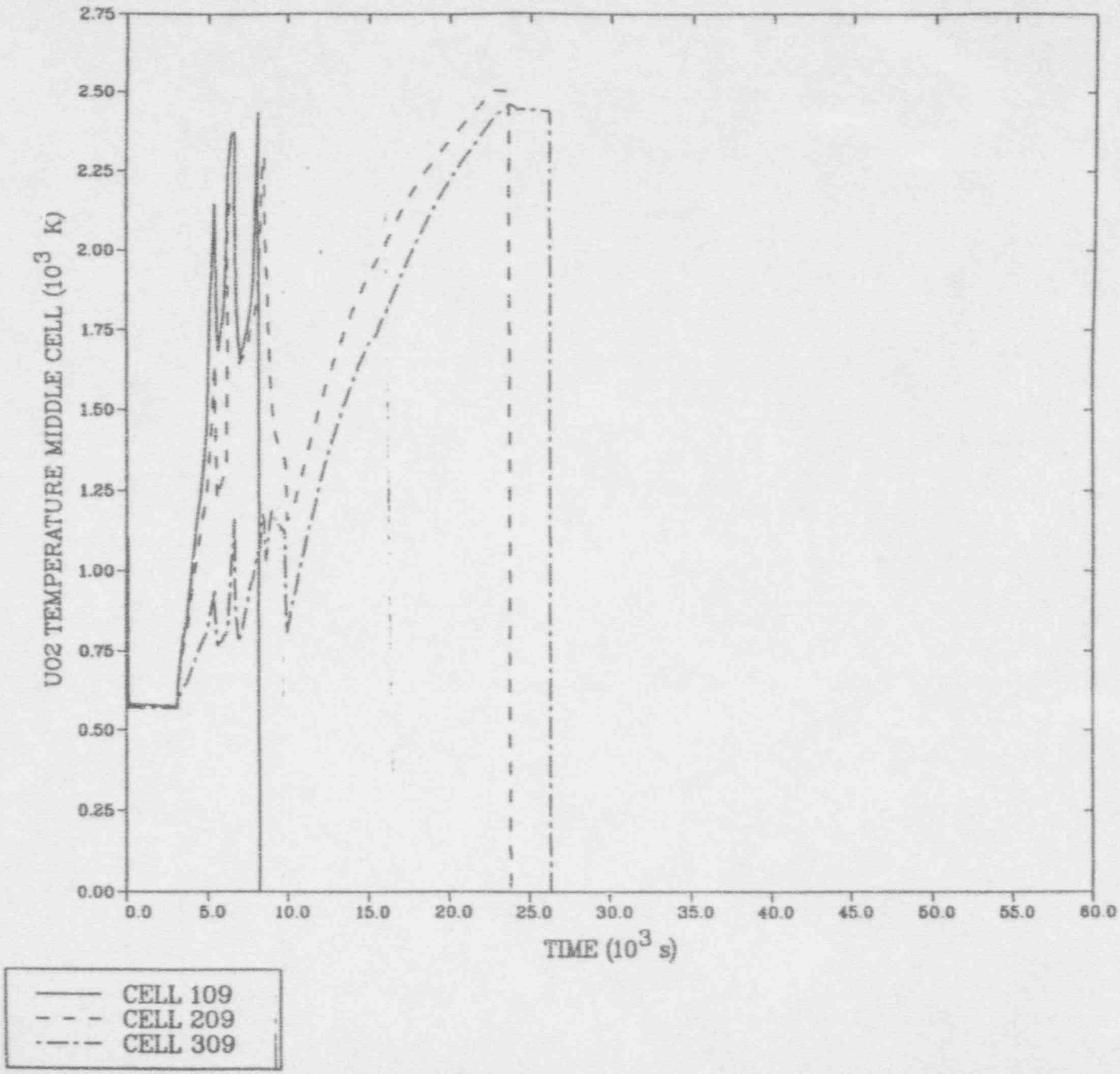

MELCOR: High Pressure SBO (LN, 04/17/91)

P 9

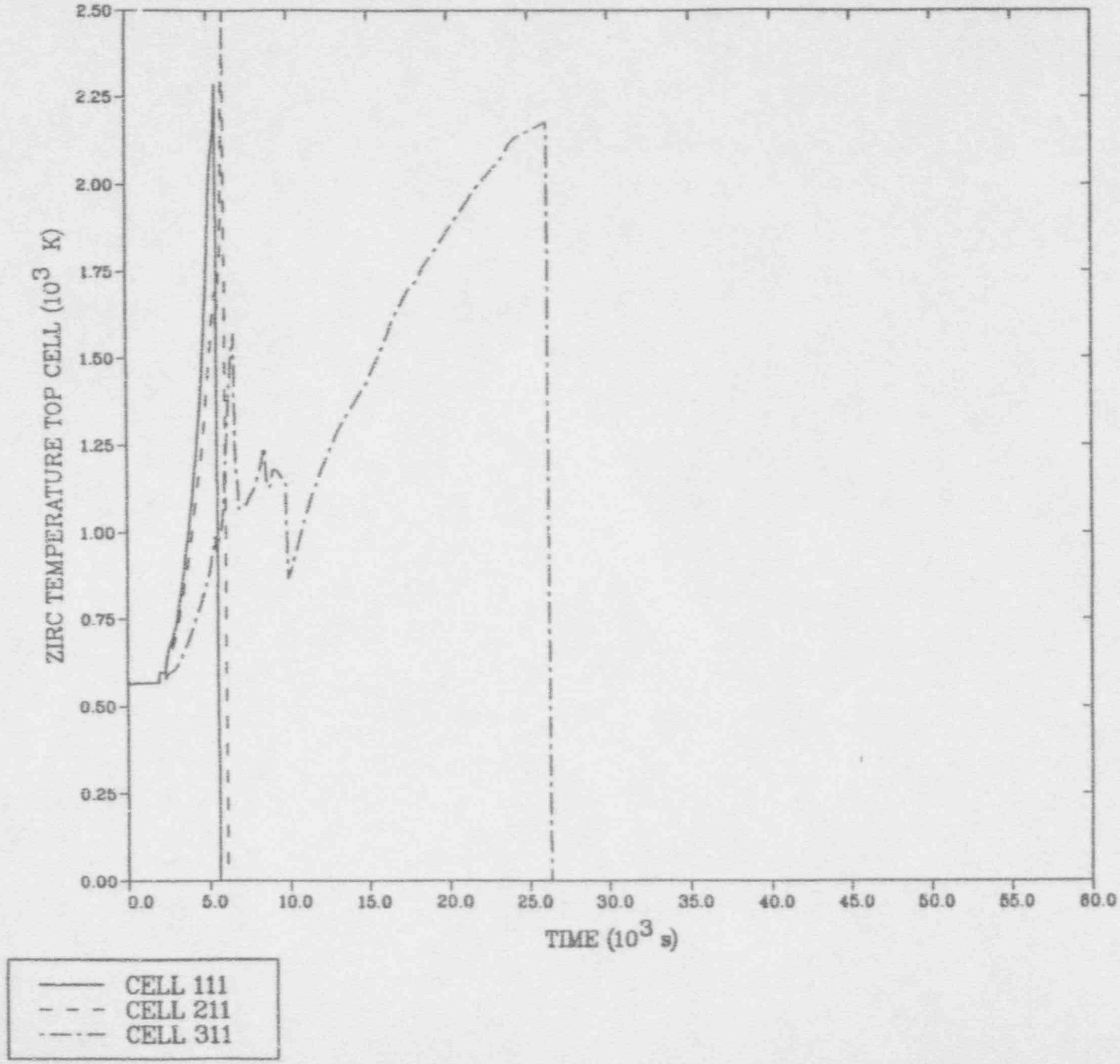

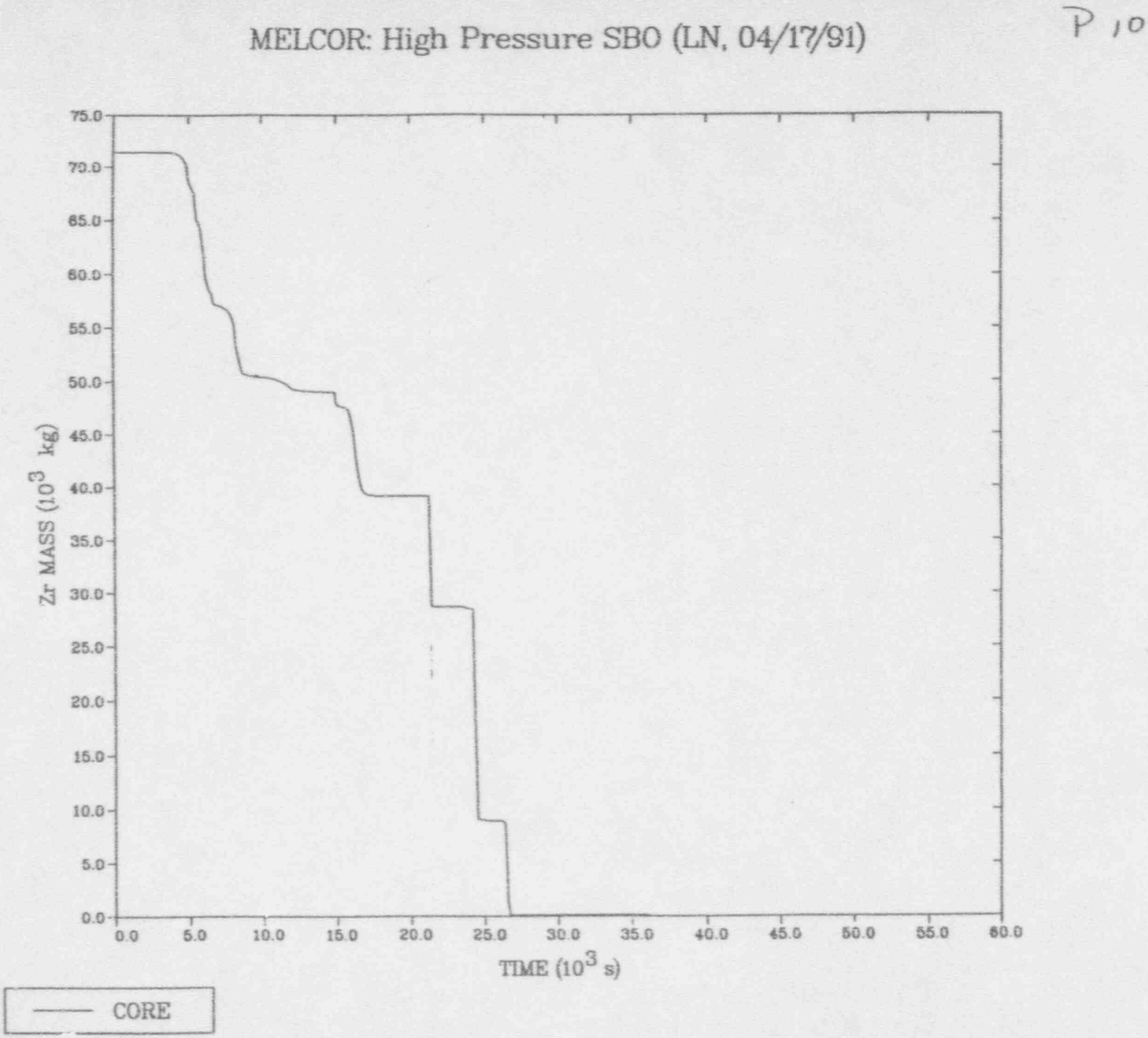
MELCOR: High Pressure SBO (LN, 04/17/91)
Zr MASS (10^3 kg)
TIME (10^3 s)
CORE
P 10

MELCOR: High Pressure SBO (LN, 04/17/91)

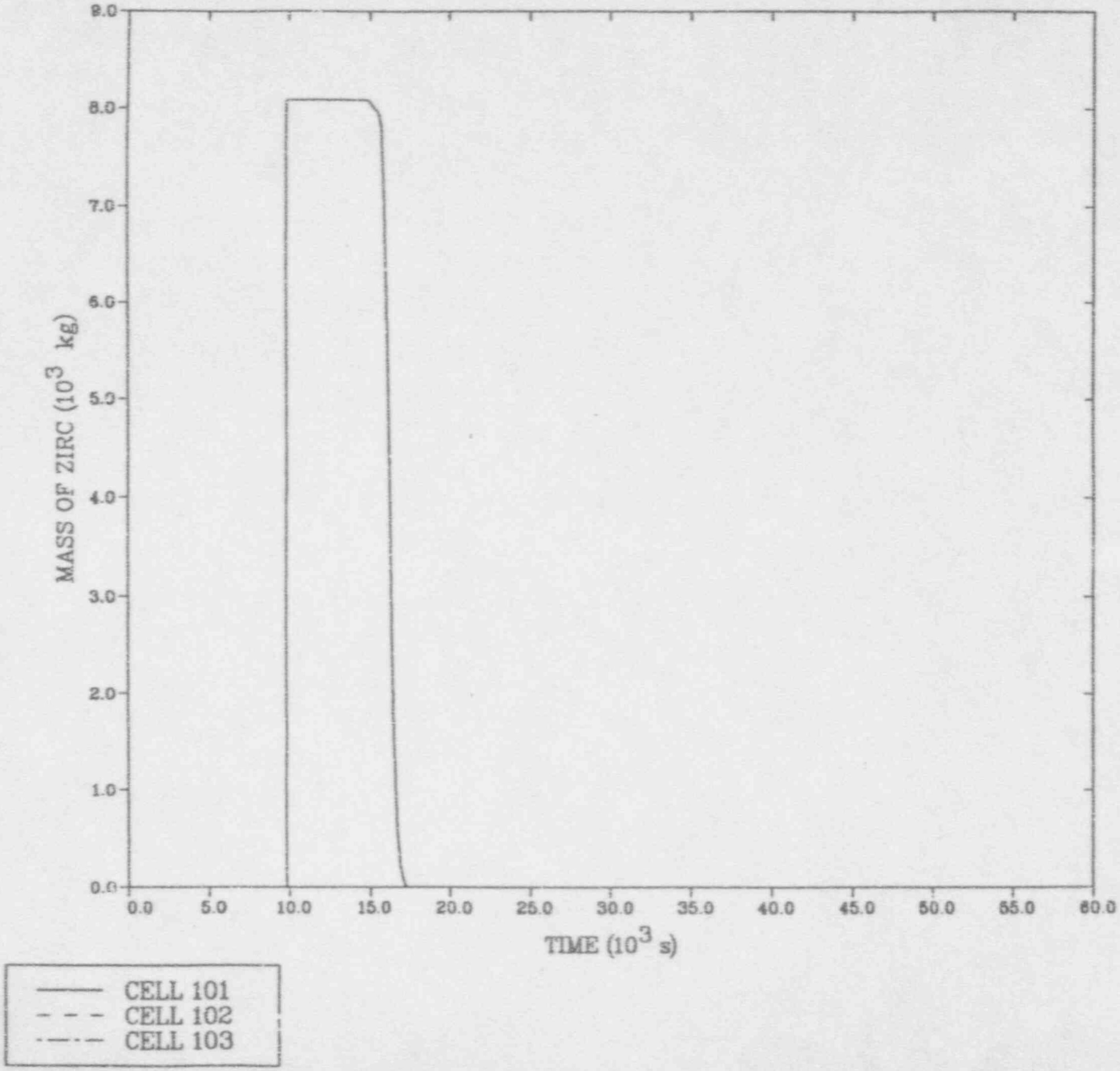

MELCOR: High Pressure SBO (LN, 04/17/91)

P 12

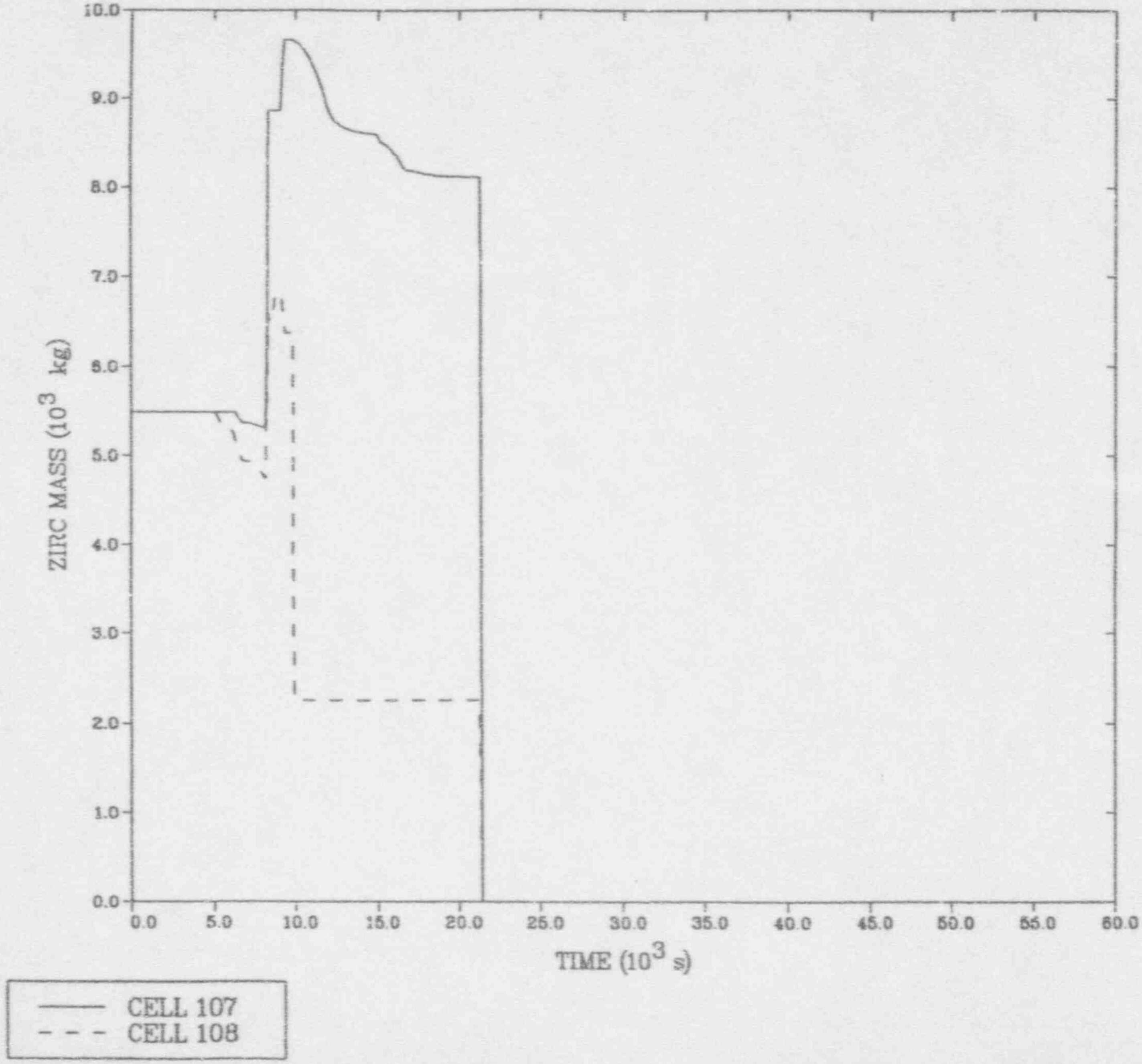

MELCOR: High Pressure SBO (LN, 04/17/91)

P 13

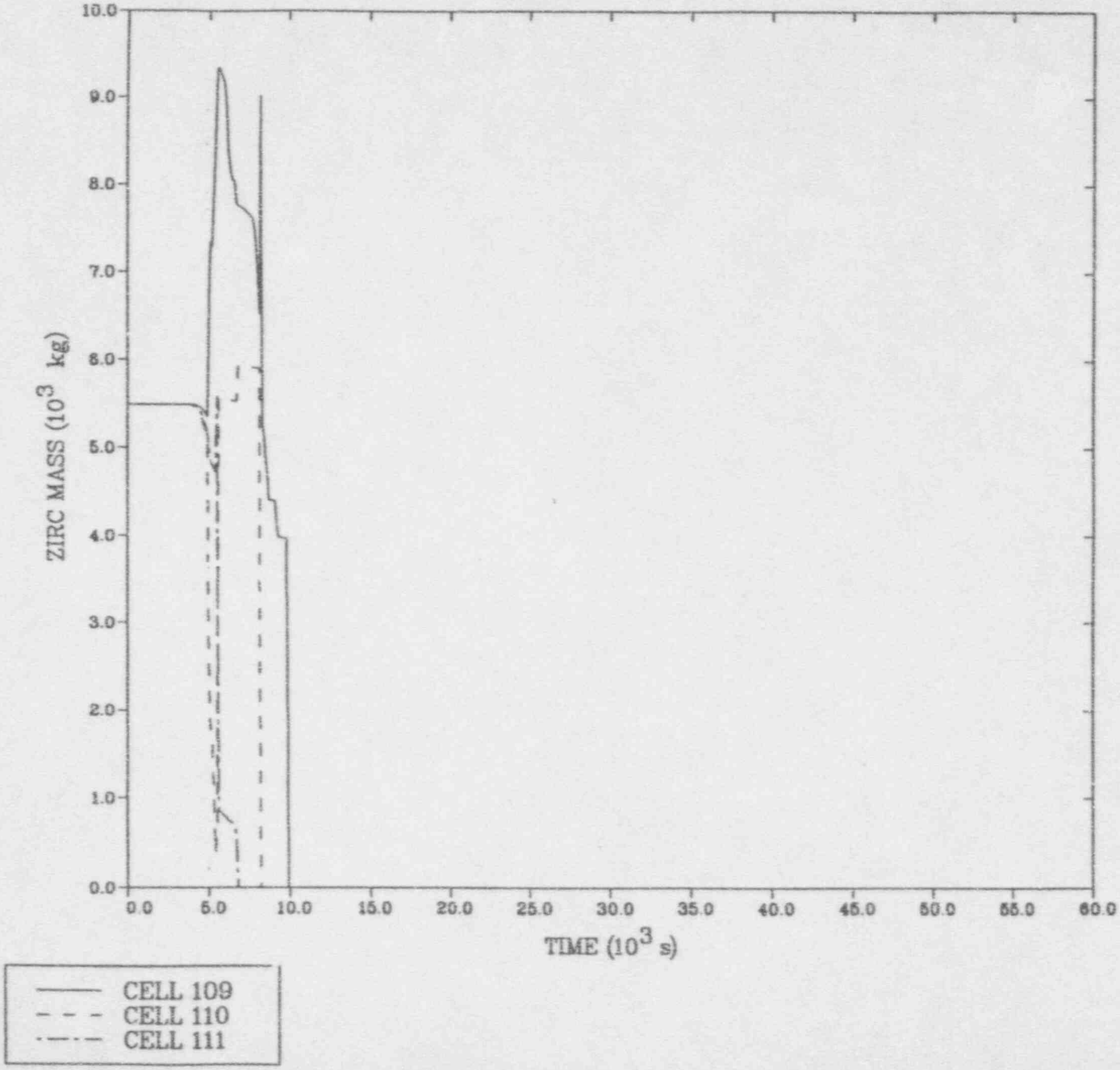

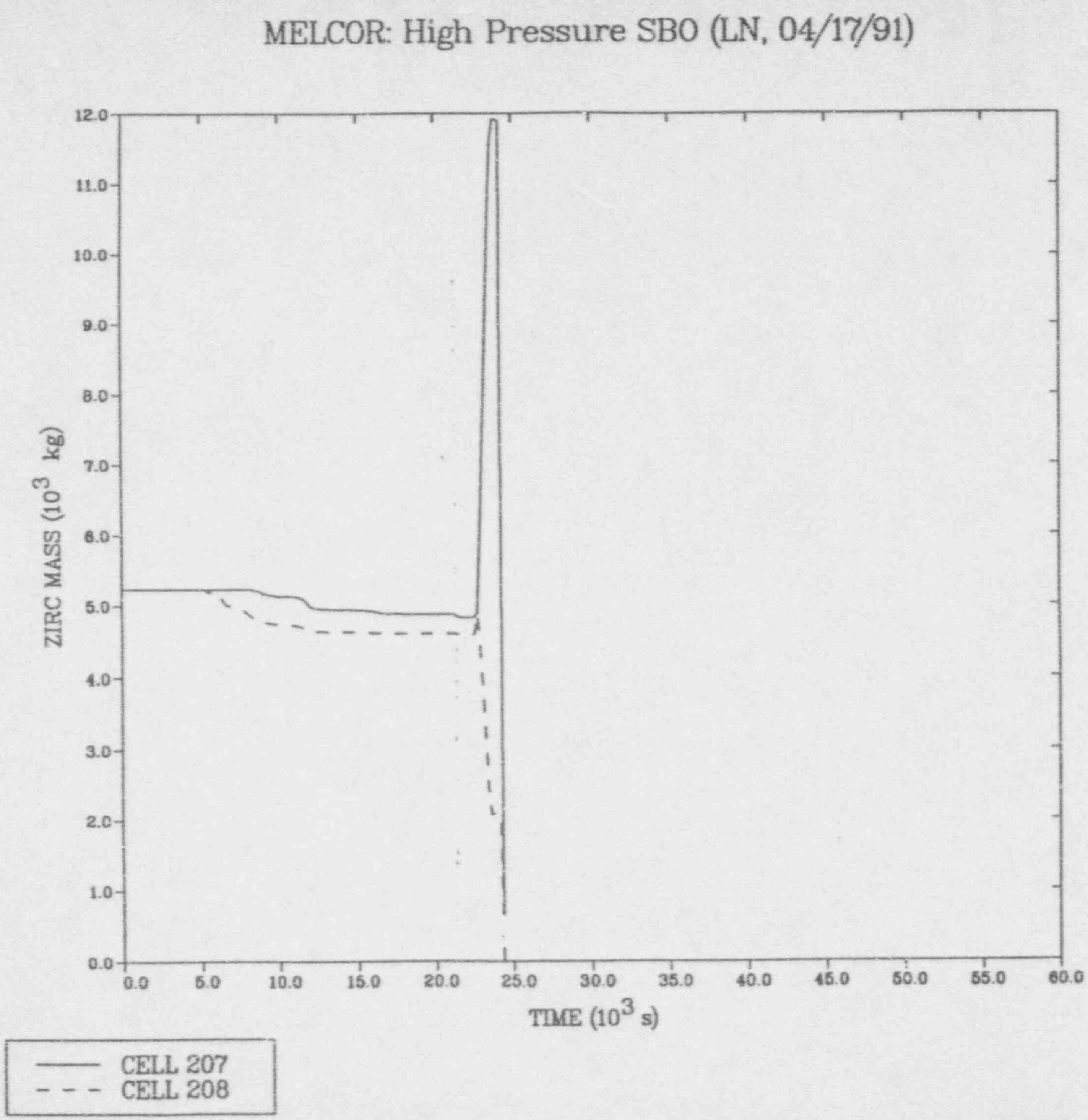

MELCOR: High Pressure SBO (LN, 04/17/91)
ZIRC MASS (10^3 kg)
0.0
1.0
2.0
3.0
4.0
5.0
6.0
7.0
8.0
9.0
10.0
11.0
12.0
0.0
5.0
10.0
15.0
20.0
25.0
30.0
35.0
40.0
45.0
50.0
55.0
60.0
TIME (10^3 s)
CELL 207
CELL 208

MELCOR: High Pressure SBO (LN, 04/17/91)

P 15

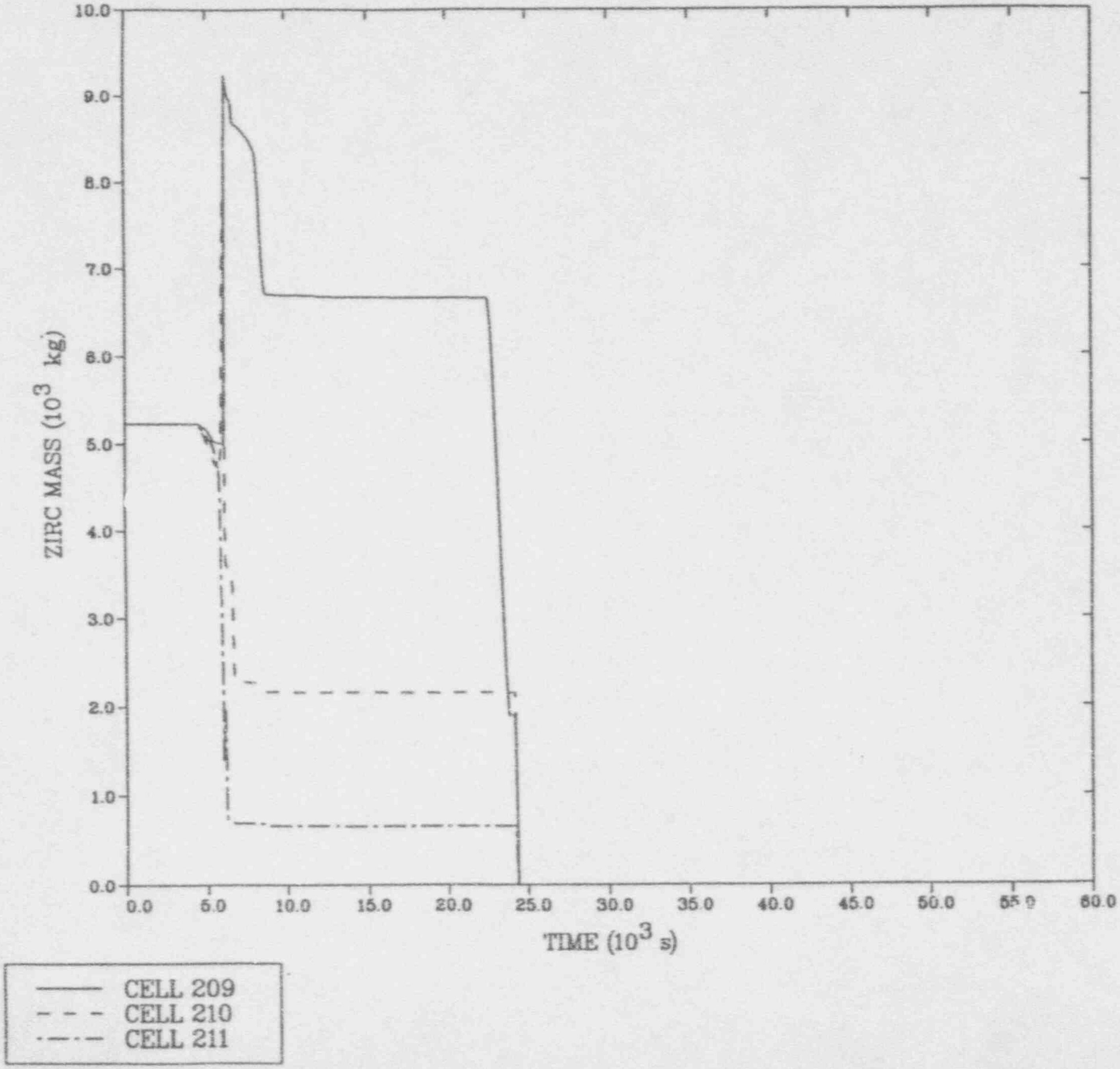

MELCOR: High Pressure SBO (LN, 04/17/91)

P 16

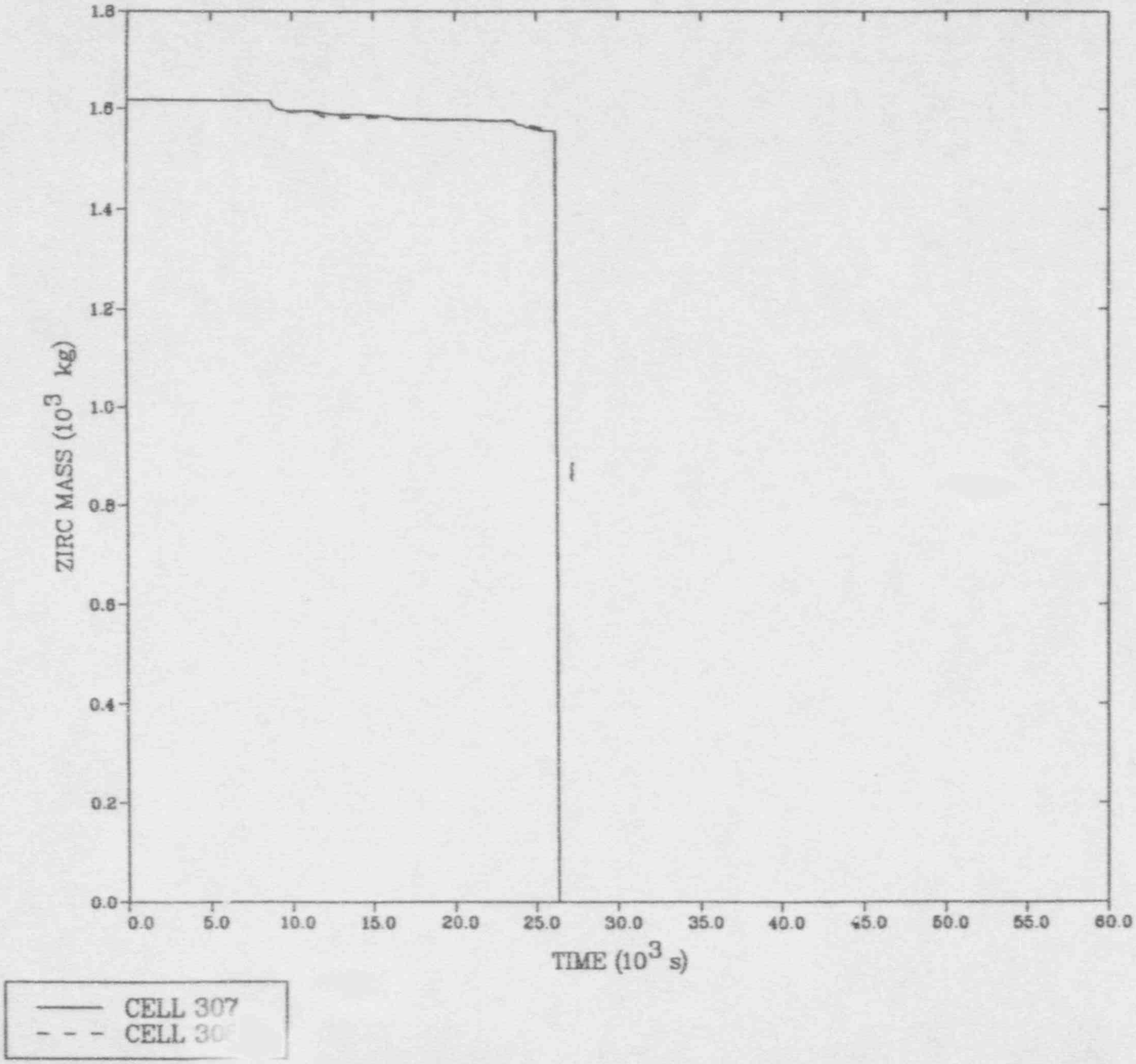

MELCOR: High Pressure SBO (LN, 04/17/91)

P 17

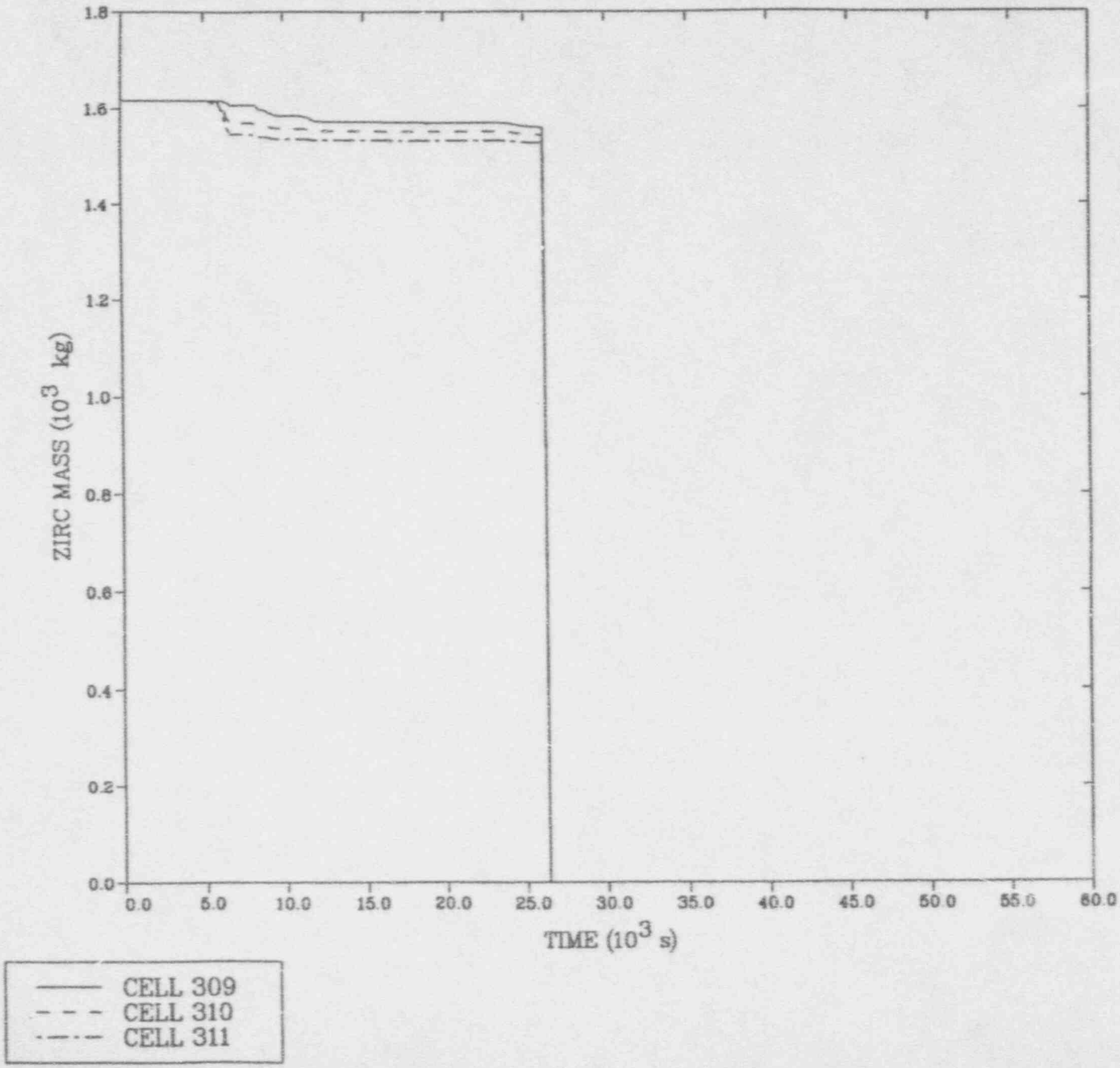

MELCOR: High Pressure SBO (LN, 04/17/91)

P 18

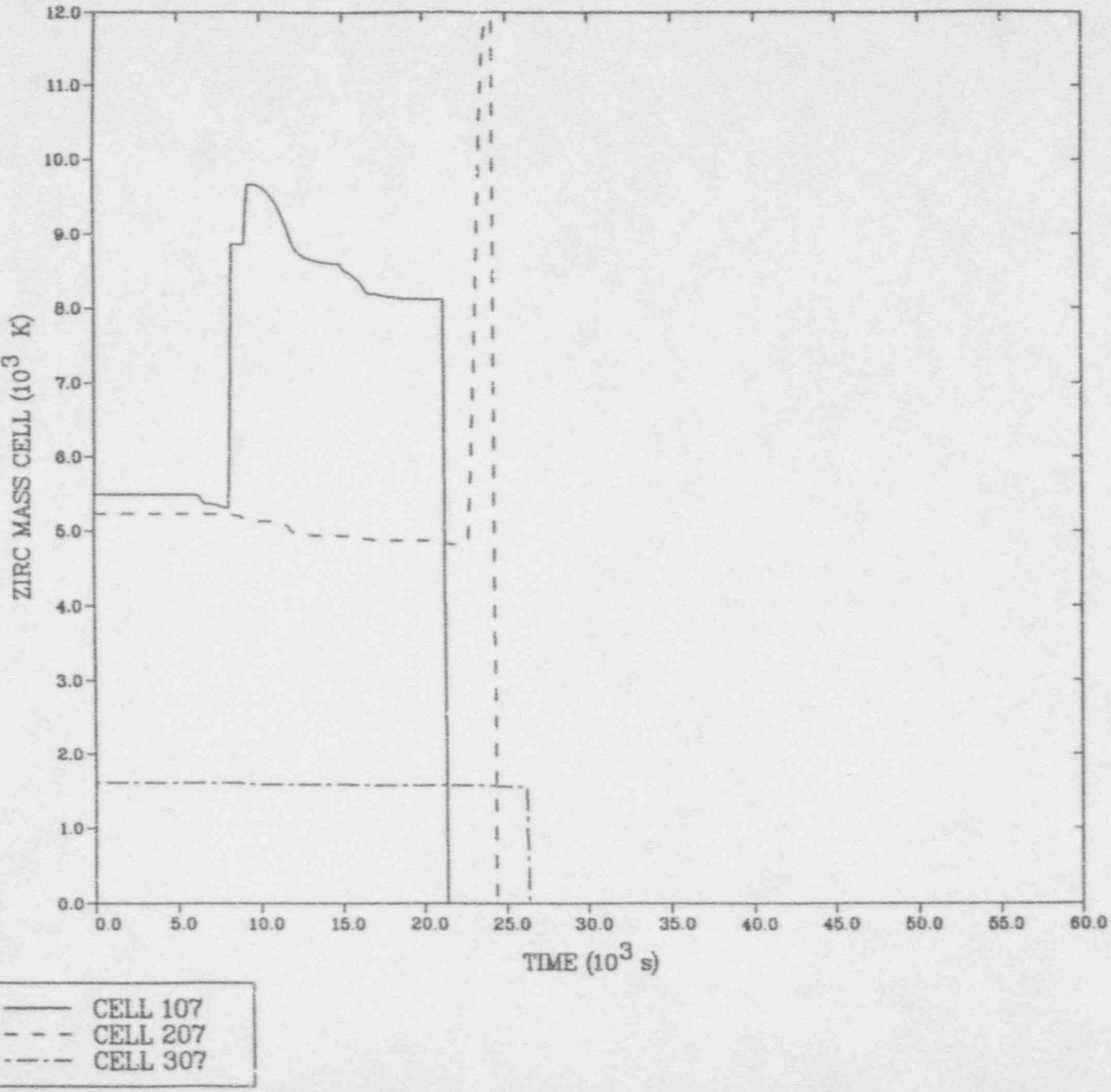

MELCOR: High Pressure SBO (LN, 04/17/91)

P 17

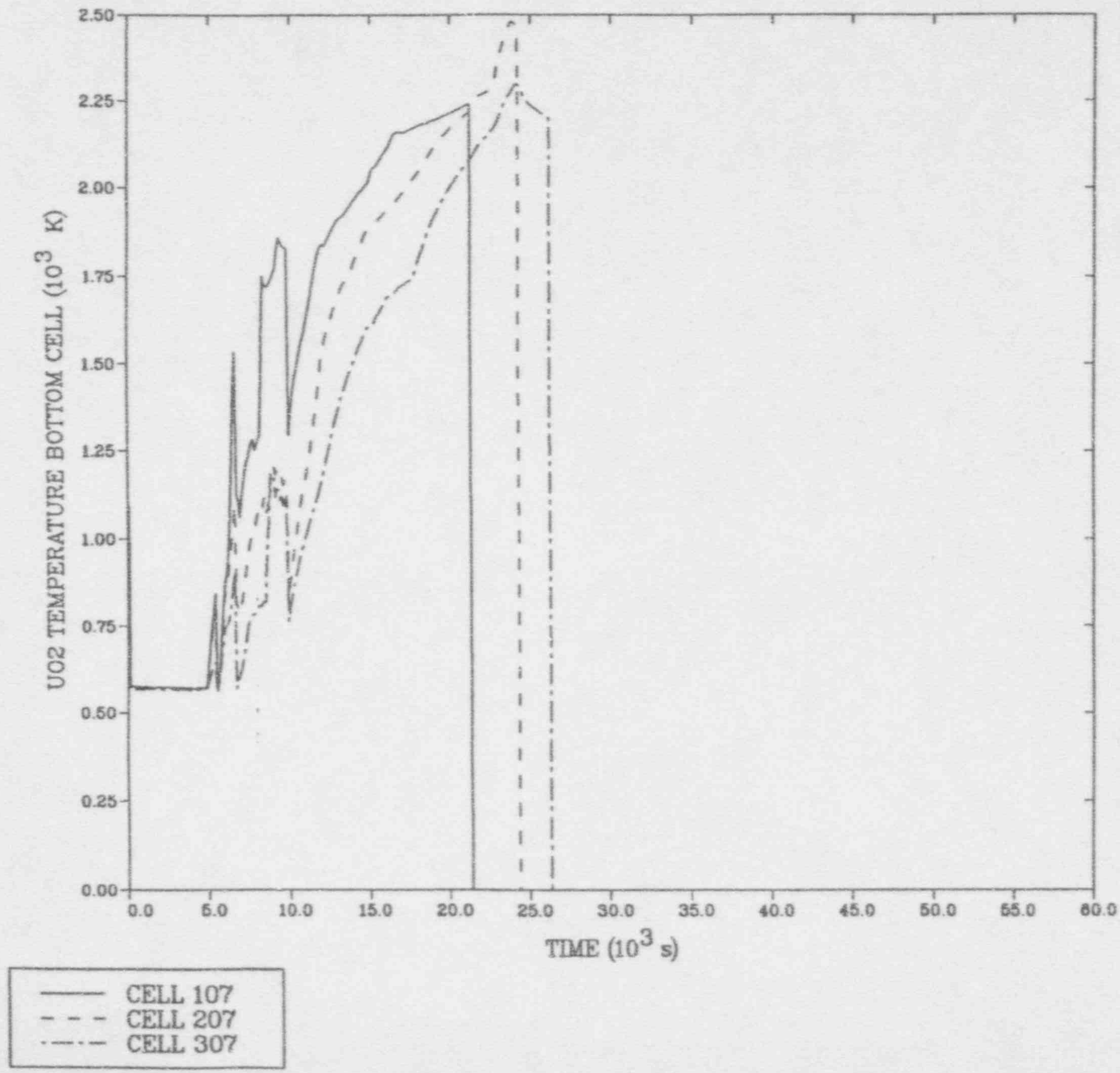

F 20

MELCOR: High Pressure SBO (LN, 04/17/91)

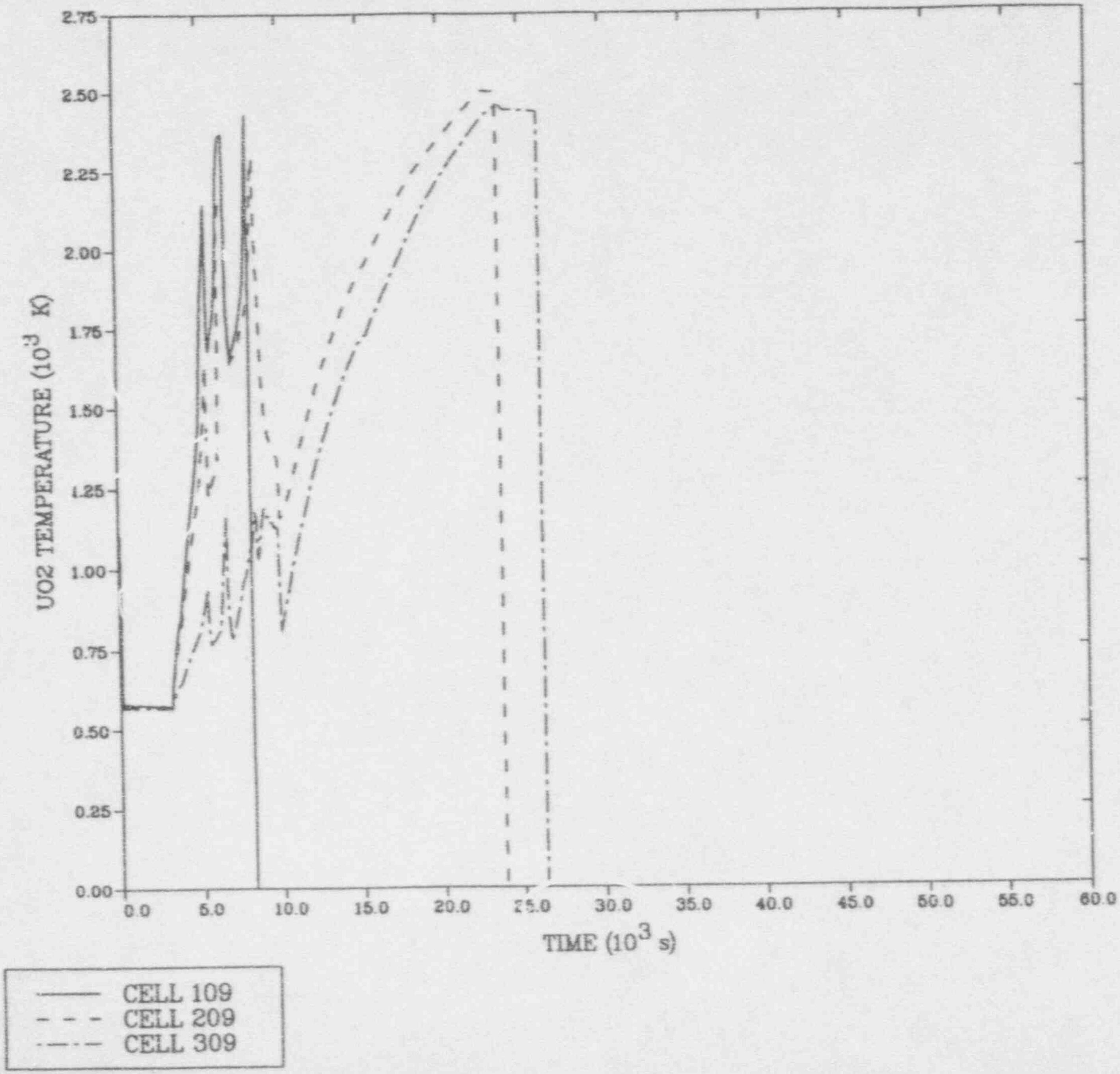

MELCOR: High Pressure SBO (LN, 04/17/91) P22

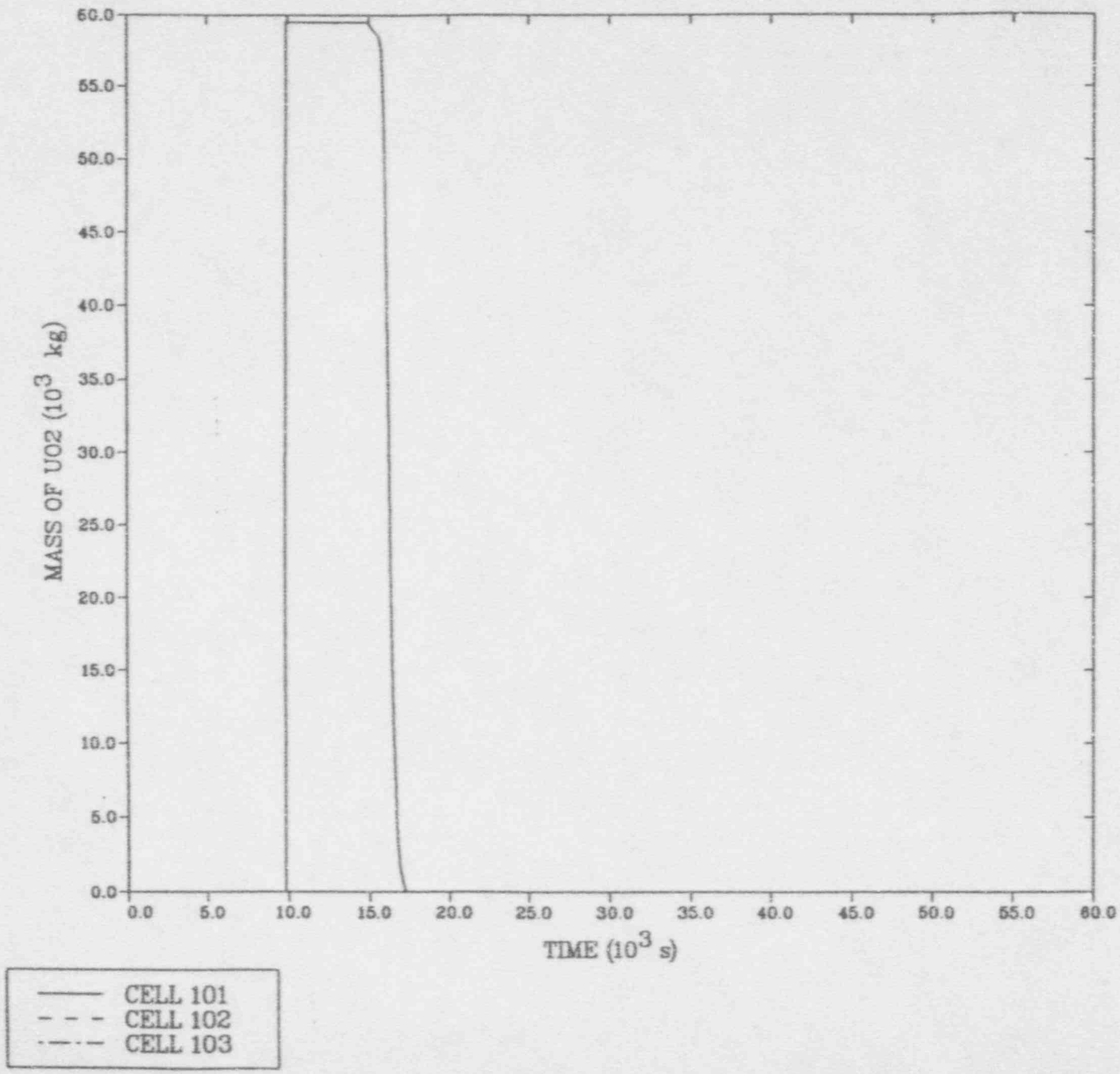

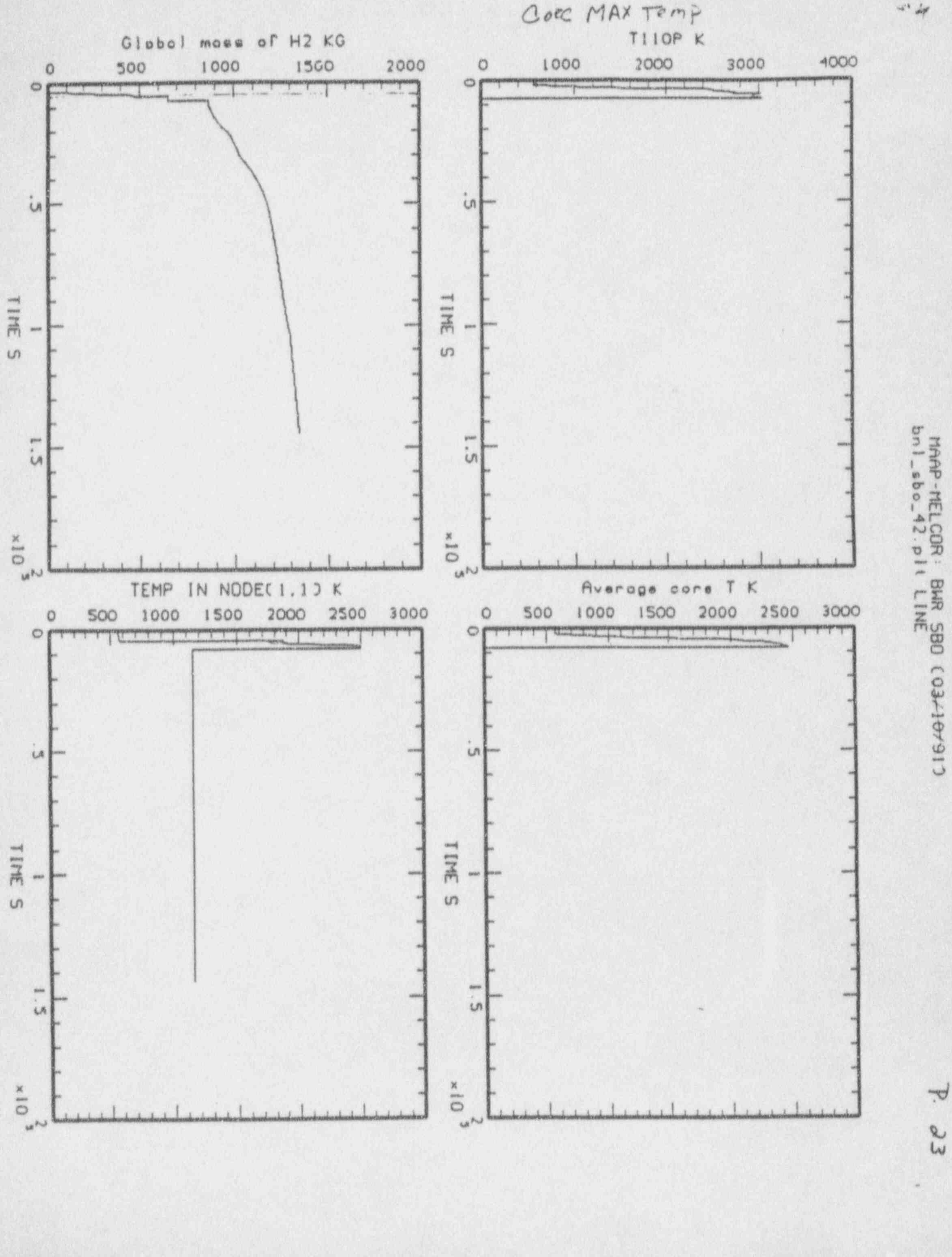

Core MAX Temp
Global mass of H2 KG
TIME S
T110P K
TEMP IN NODE(1,1) K
Average core T K
MAAP-MELCOR: BWR SBO (03/10/91)
bnl_sbo_42.plt LINE

P. 23

MAAP-MELCOR: BWR SBO (03/10/91)
bnl_sbo_41.p:' LINE

P 24

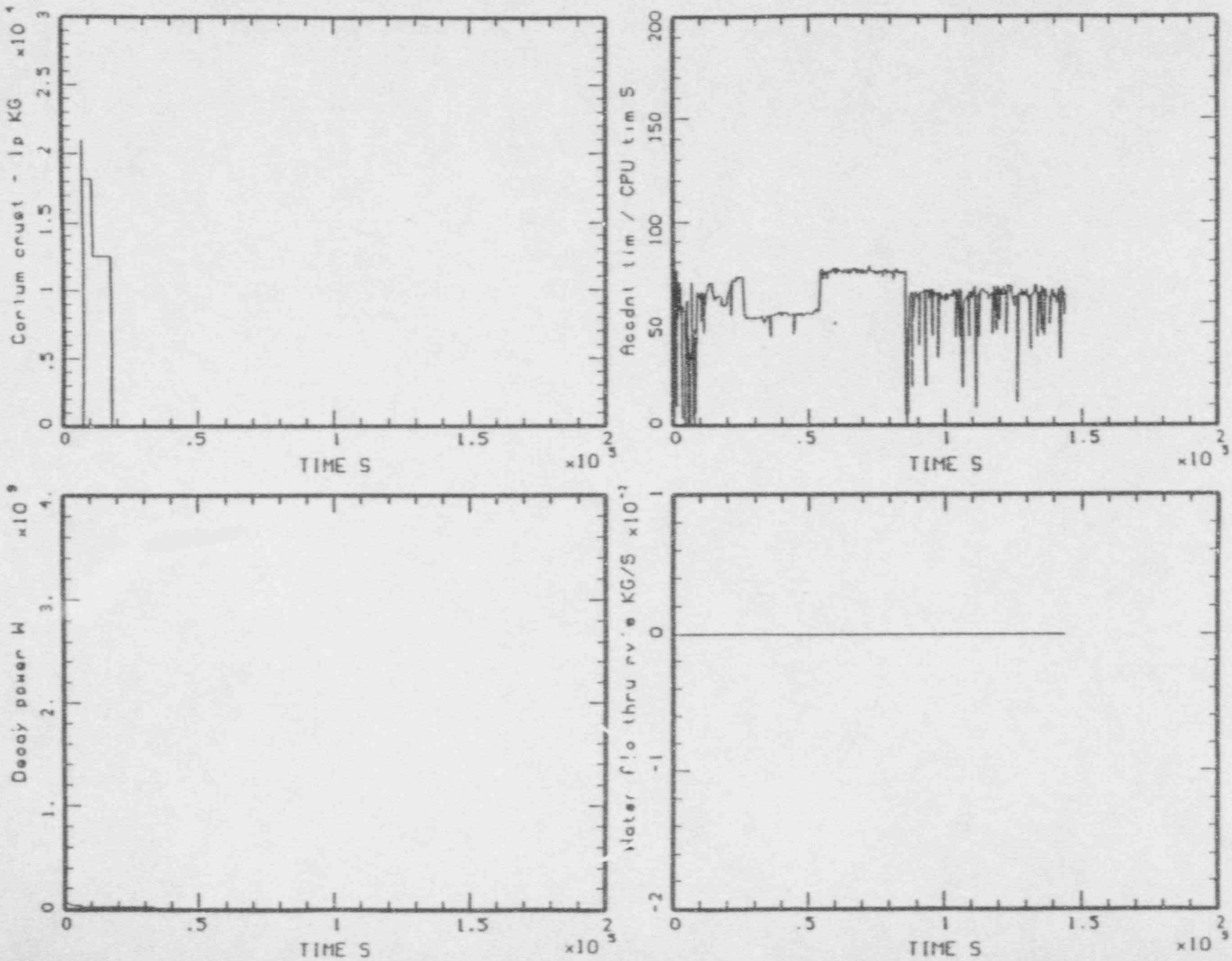

P 25

MAAP-MELCOR: BWR SBO (03/10/91)
bnl_sbo_41.plt LINE

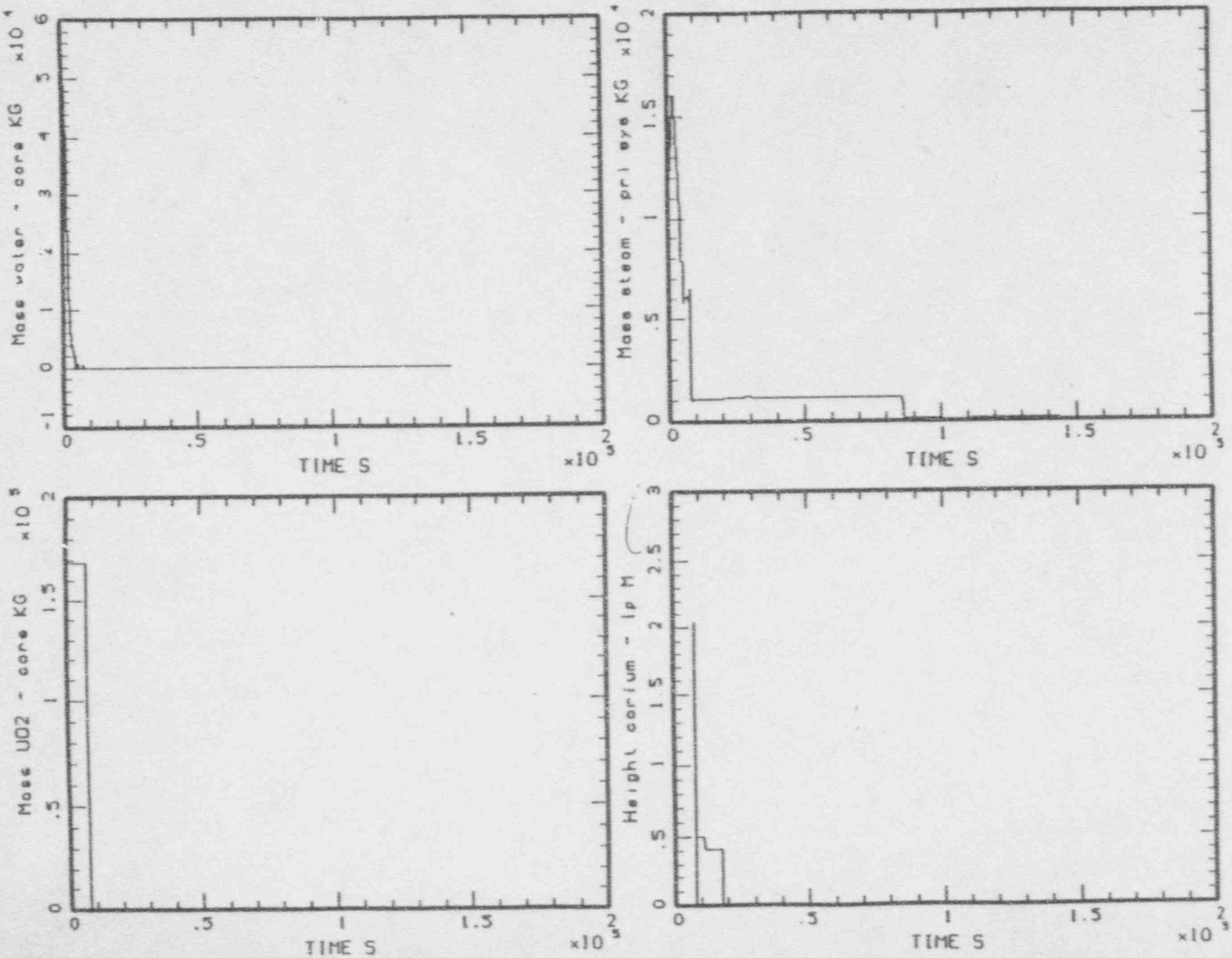

MAAP-MELCOR: BWR SBO (03/10/91)
bnl_sbo_41.plt LINE

P 26.

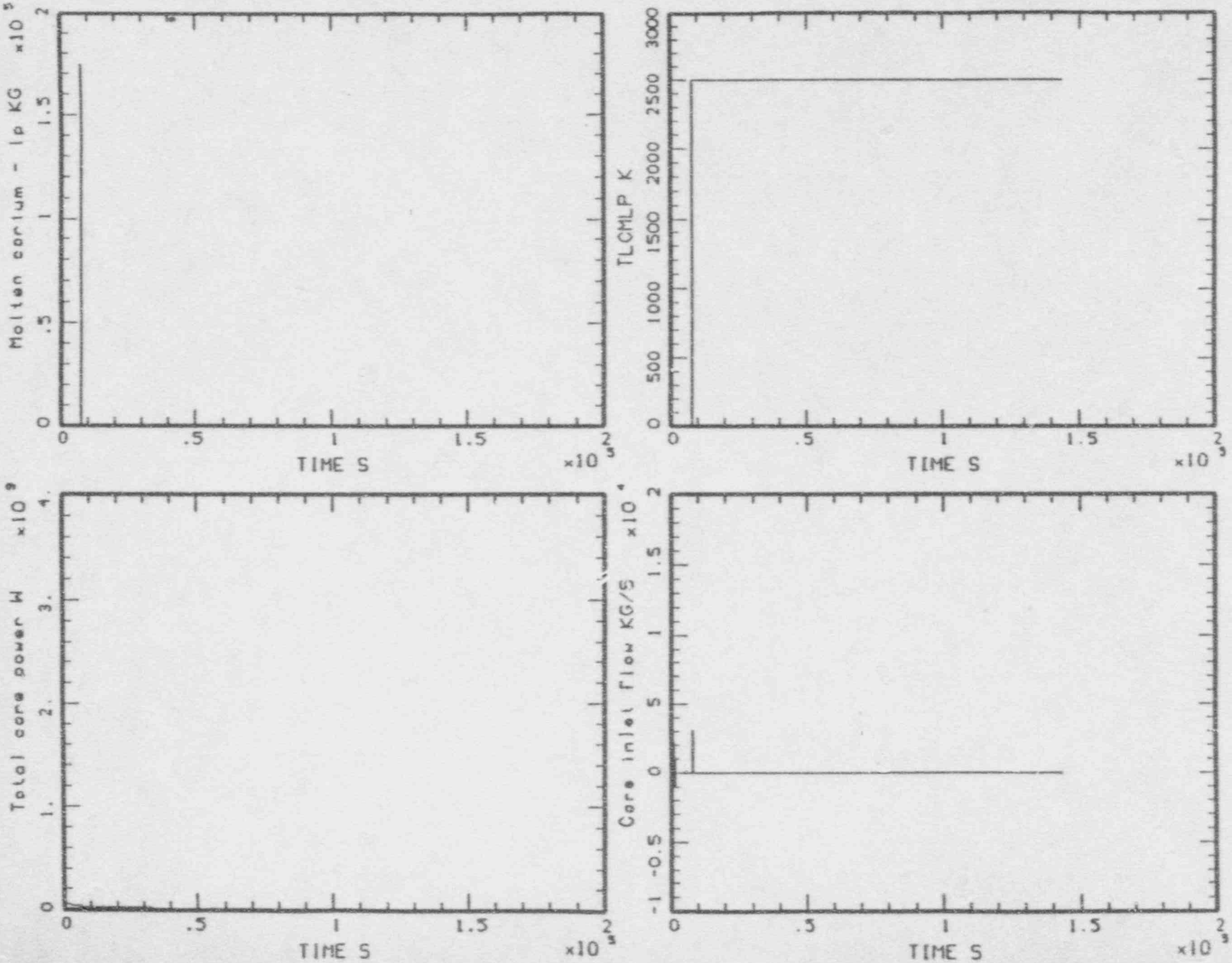

MELCOR: High Pressure SBO (LN, 04/17/91)

P 27

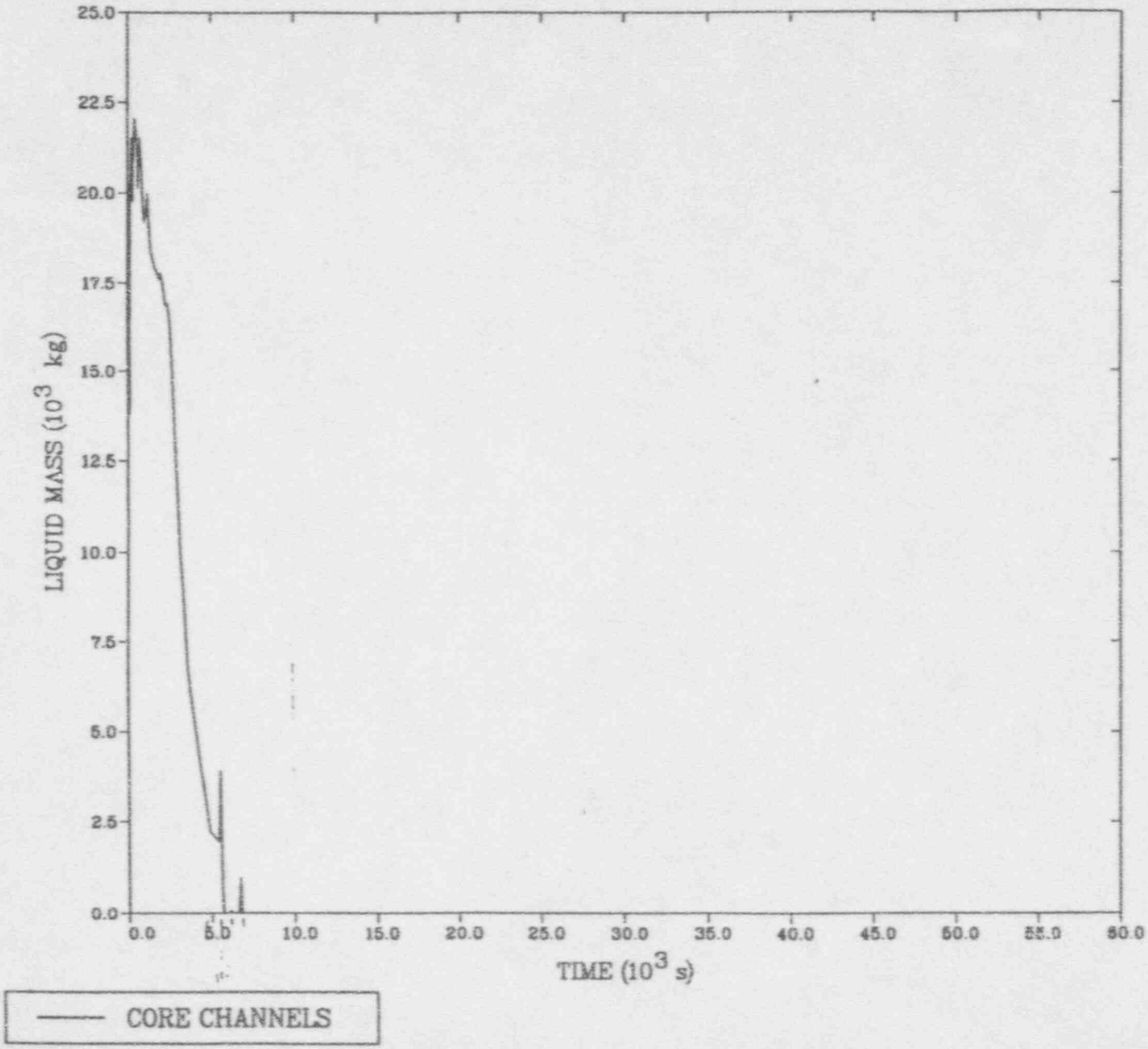

MELCOR: High Pressure SBO (LN, 04/17/91)

P 28

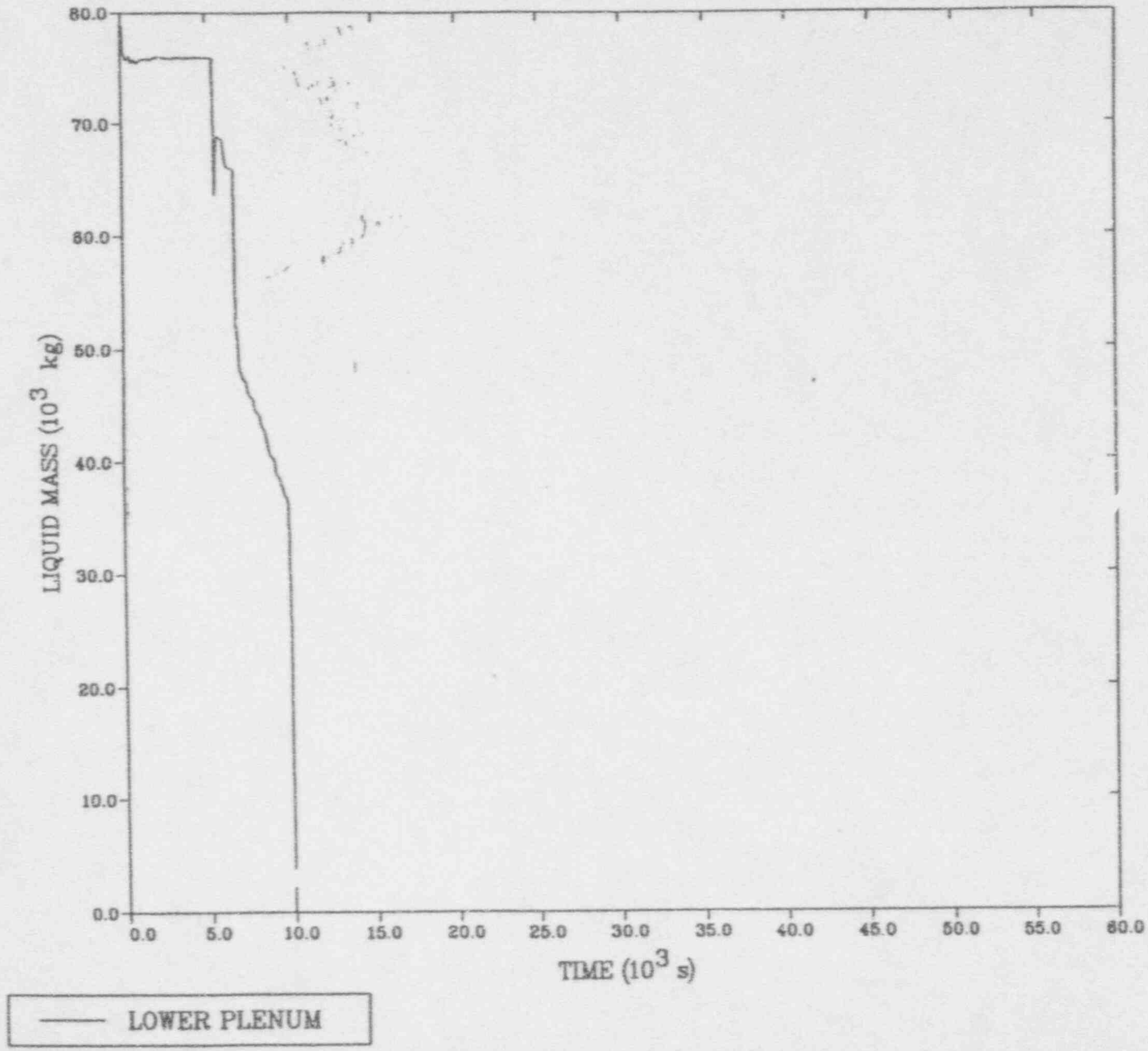

MELCOR: High Pressure SBO (LN, 04/17/91)

P 29

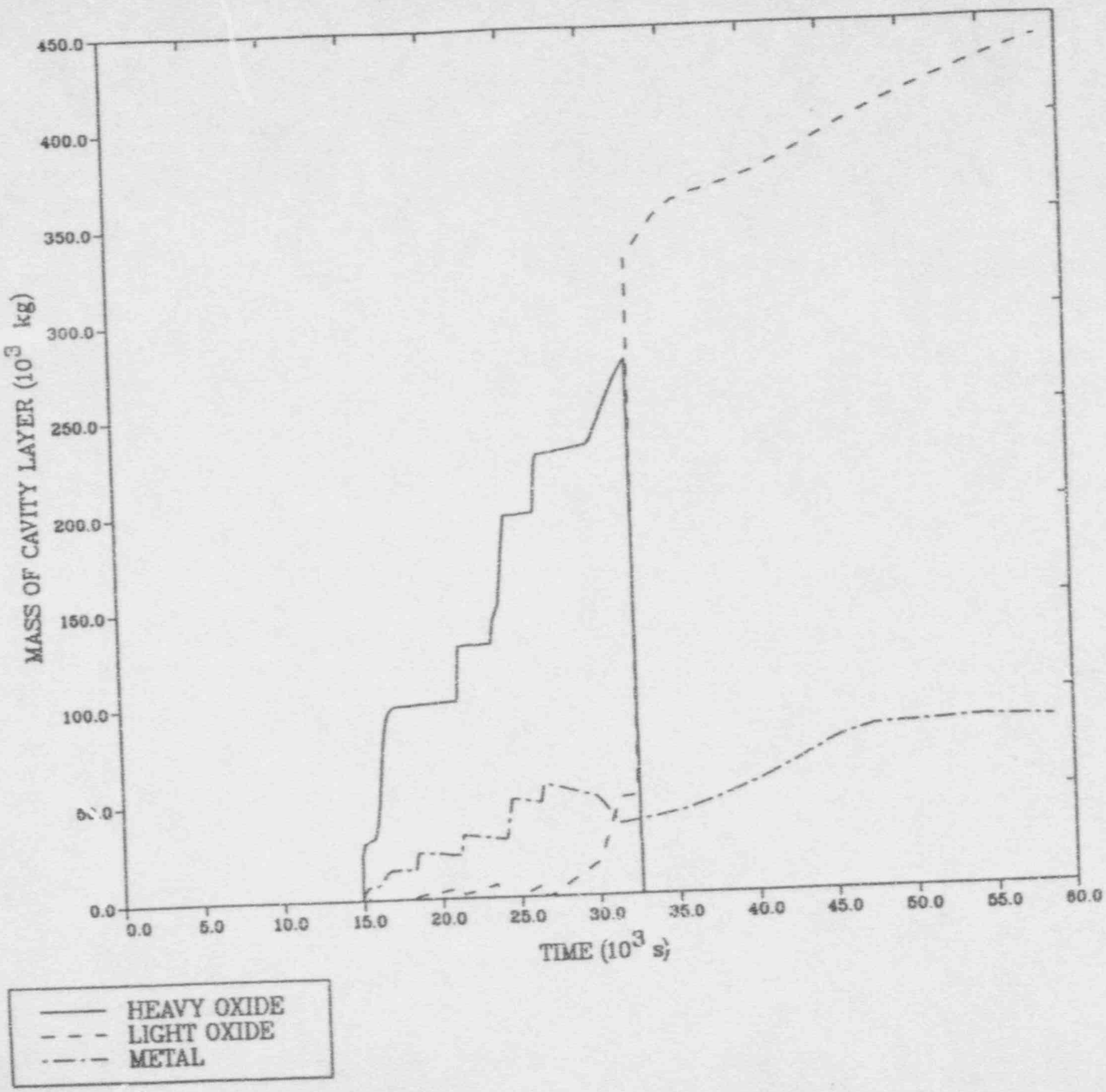

MELCOR: High Pressure SBO (LN, 04/17/91)

P 30

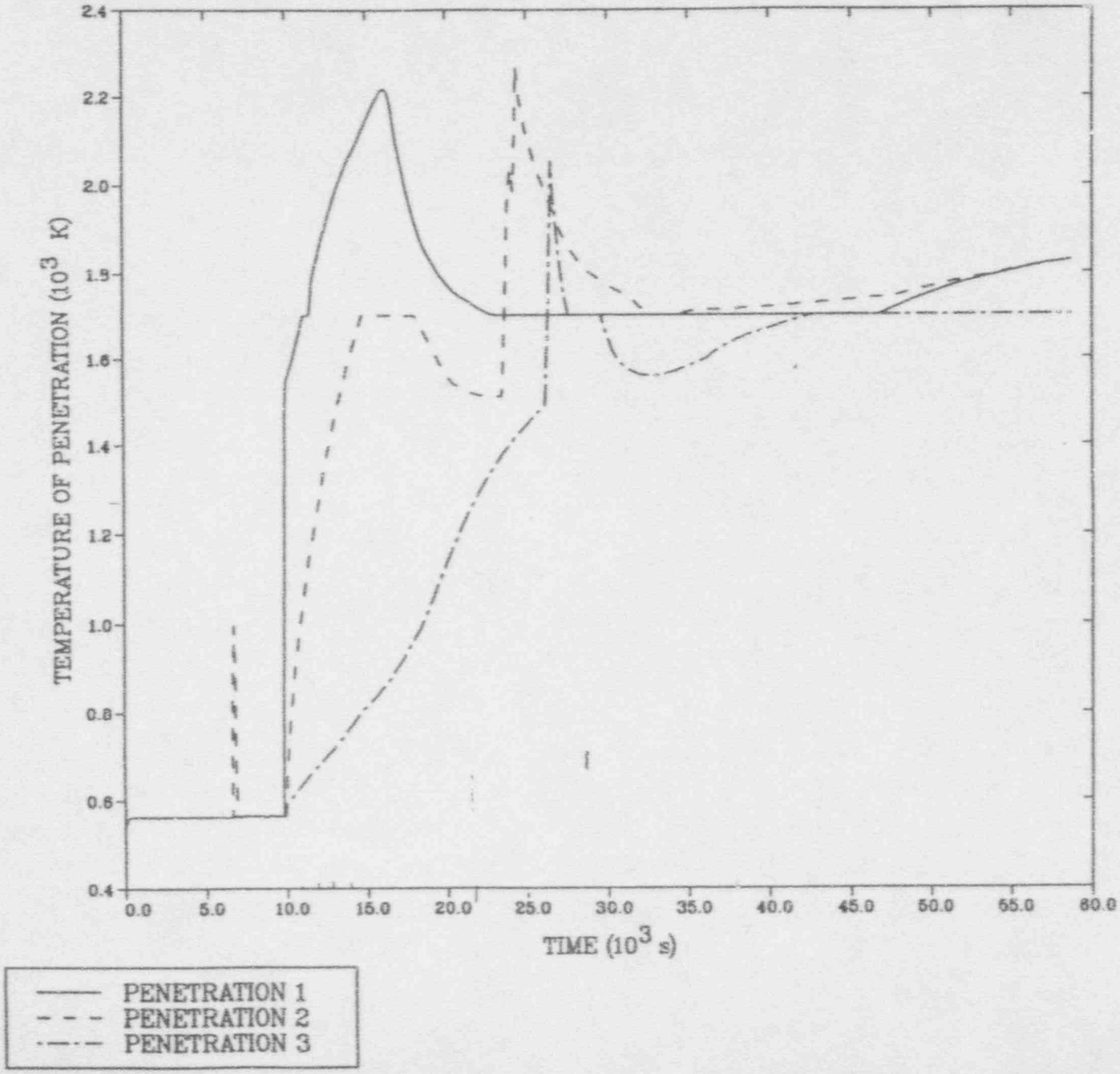

MAAP-MELCOR: BWR SBO (03/10/91)
bnl_sbo_43.plt LINE

P 31

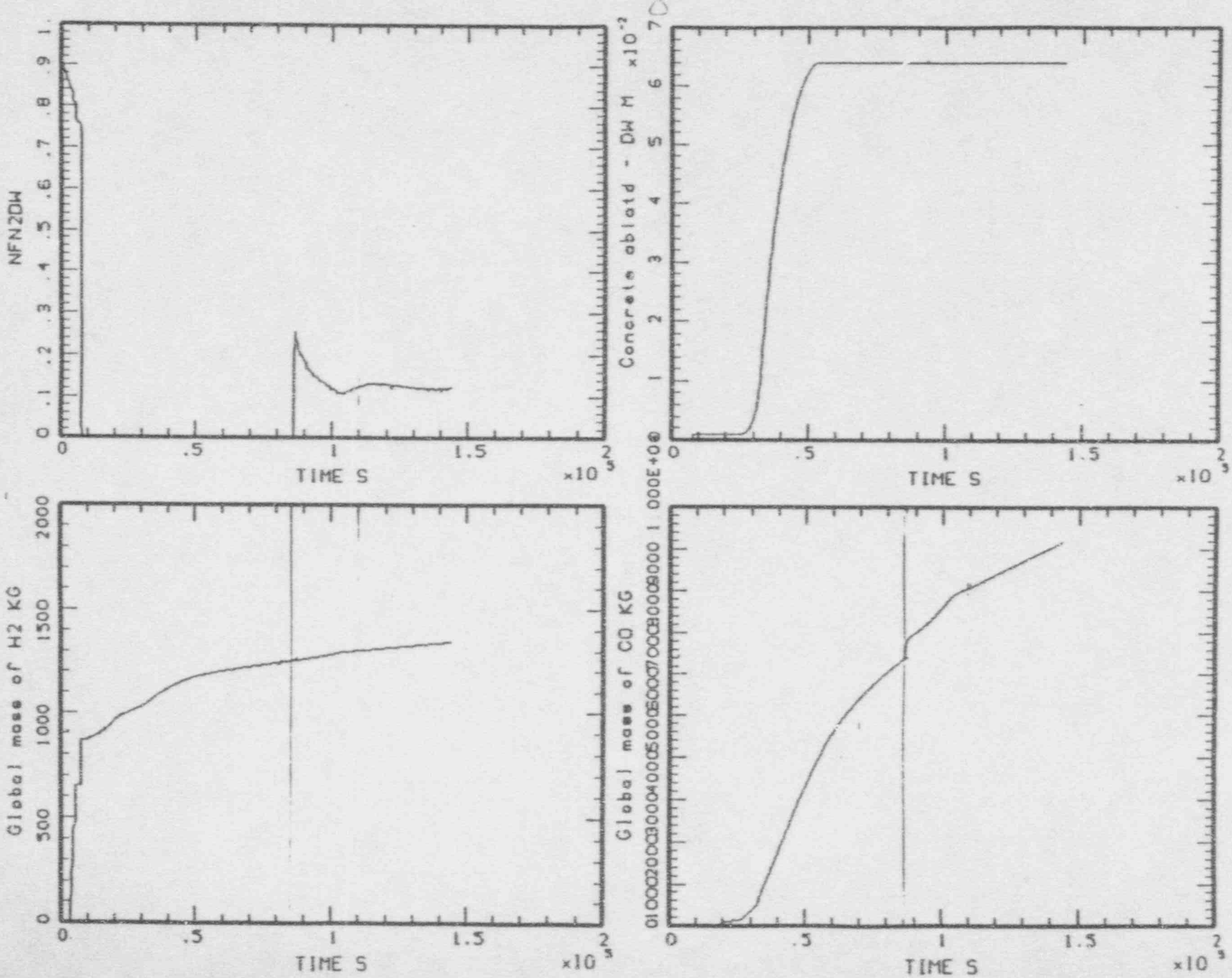

MELCOR: High Pressure SBO (LN, 04/17/91)

P 32

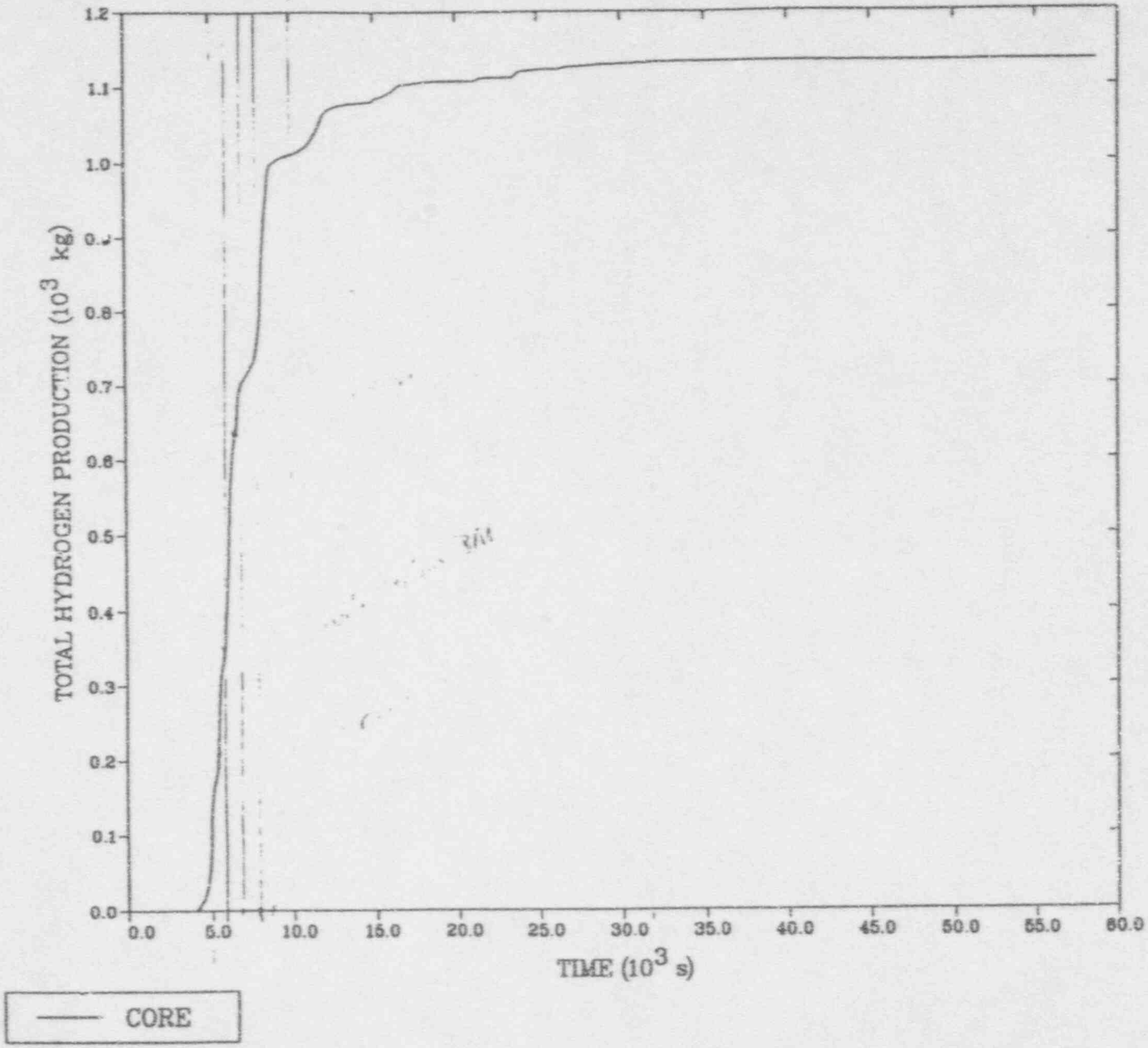

MAAP-MELCOR: BWR SBO (03/10/91)
bnl_sbo_41.plt LINE

P 33

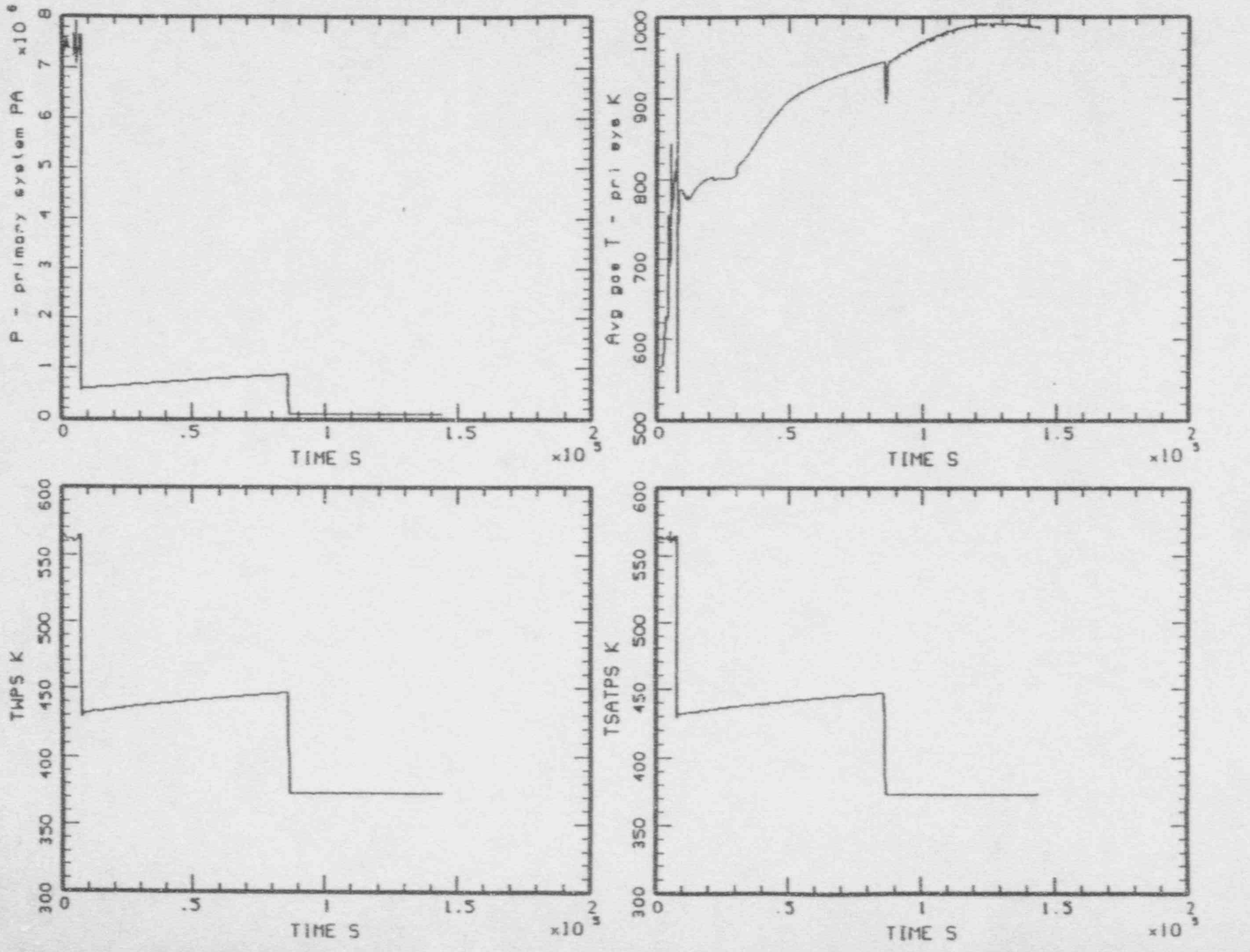

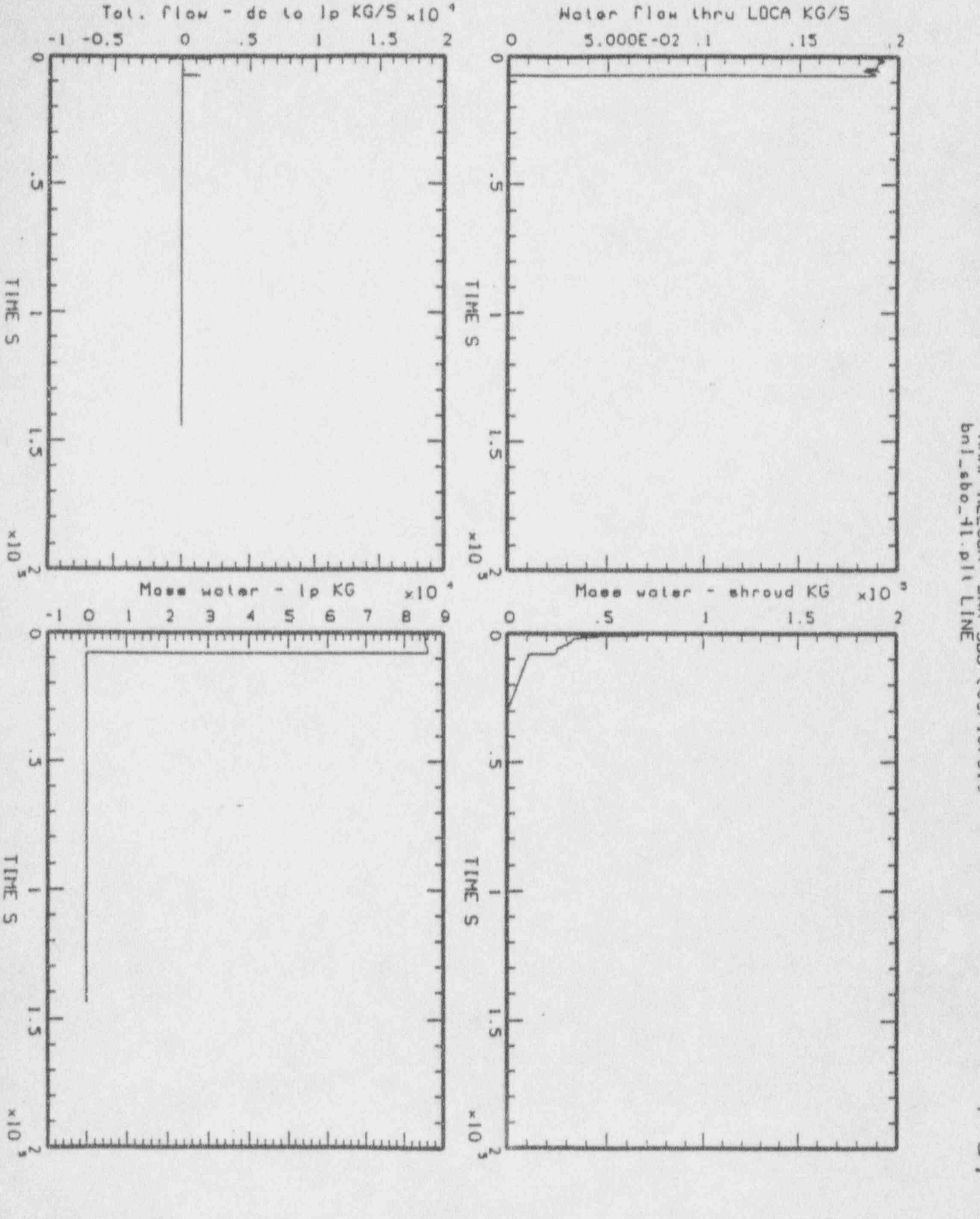
MAAP-MELCOR: BWR SBO (03/10/91)
bnl_sbo_41.pl; LINE
Tot. flow - dc to lp KG/S x10^4
Water flow thru LOCA KG/S
Mass water - lp KG x10^4
Mass water - shroud KG x10^3
TIME S
x10^5

P 34

MAAP-MELCOR: BWR SBO (03/10/91)
bnl_sbo_43.plt LINE

P 35

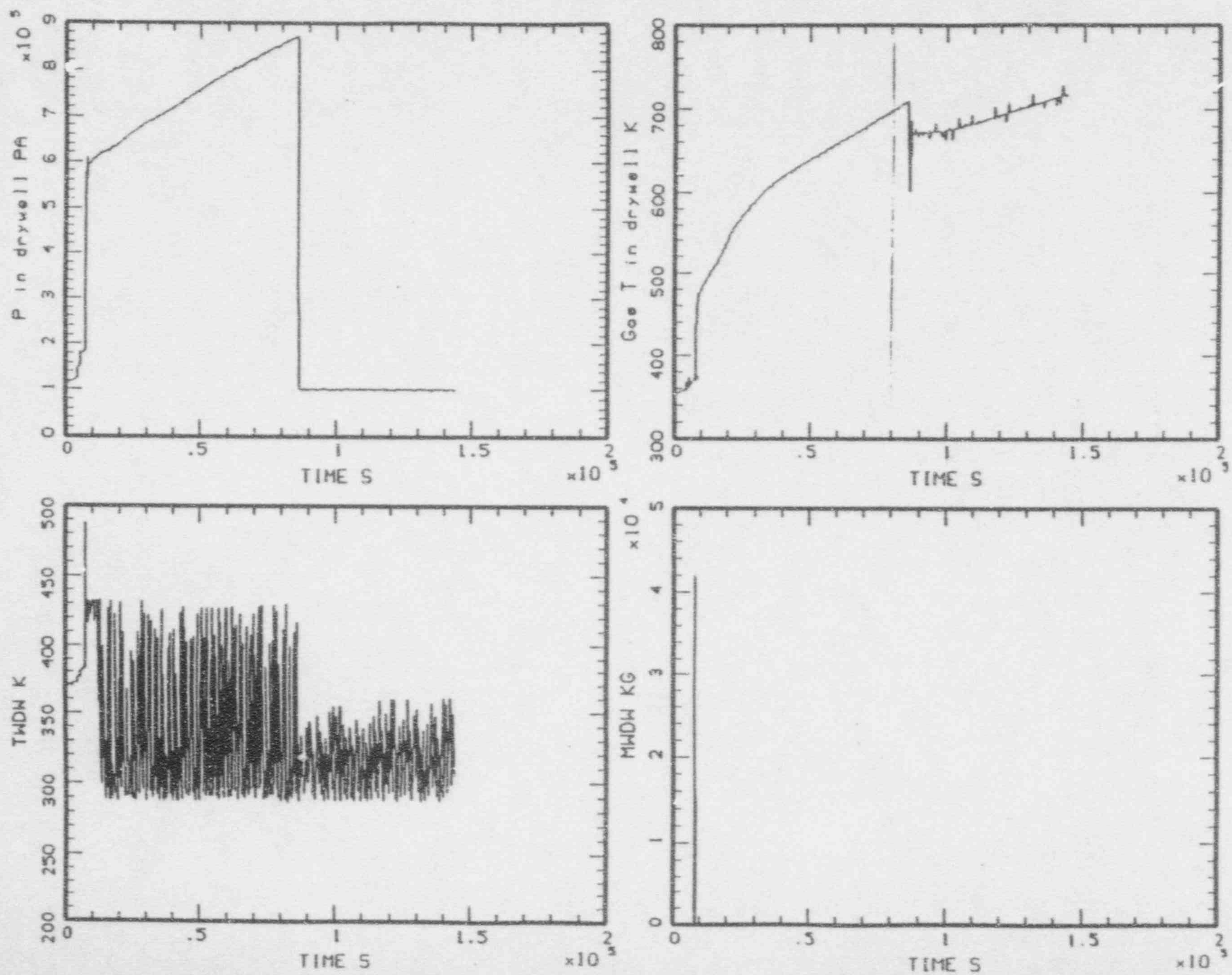

P 36

MAAP-MELCOR: BWR SBO (03/10/91)
bnl_sbo_43.plt LINE

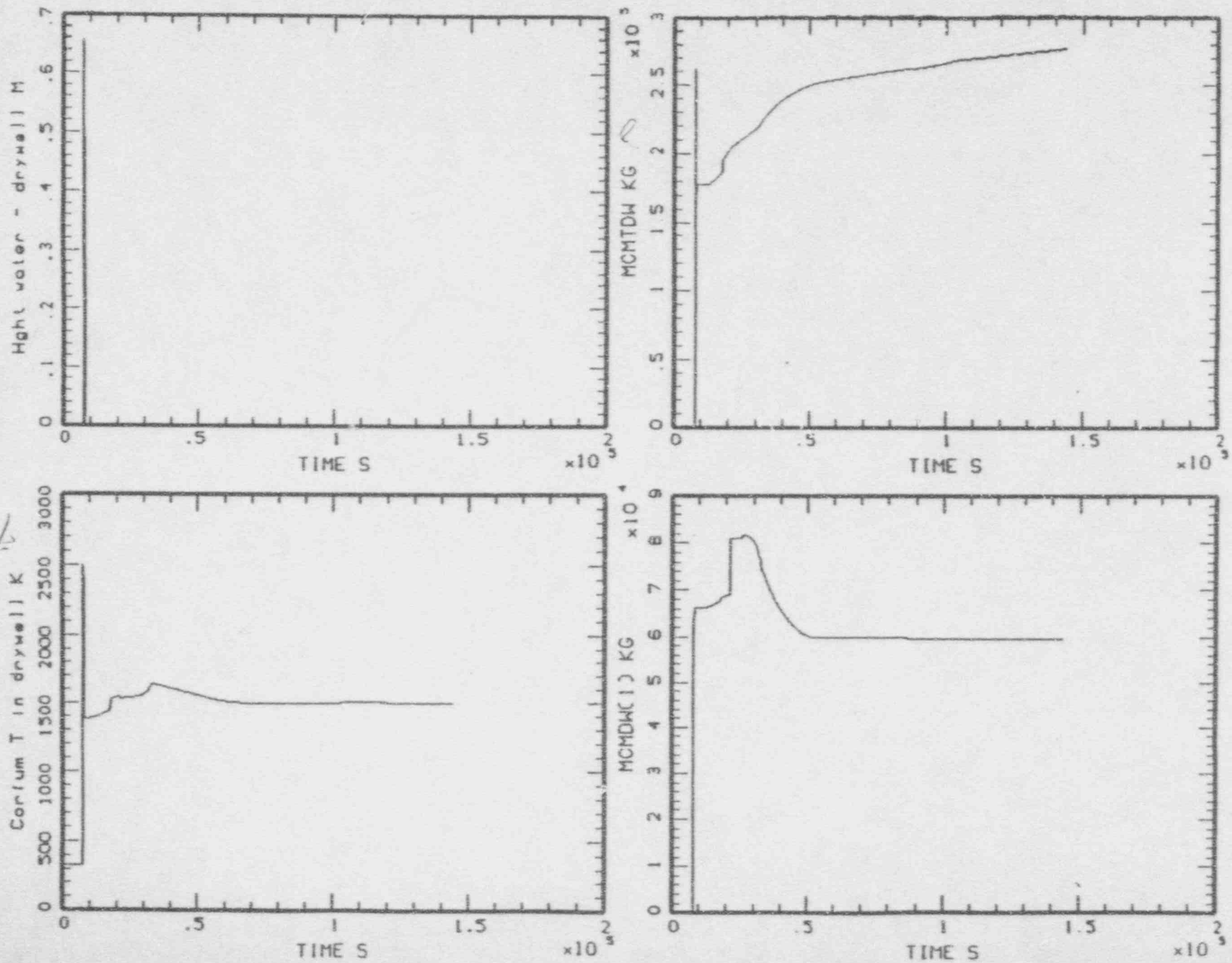

P 37

MAAP-MELCOR: BWR SBO (03/10/91)
bnl_sbo_43.pl: LINE

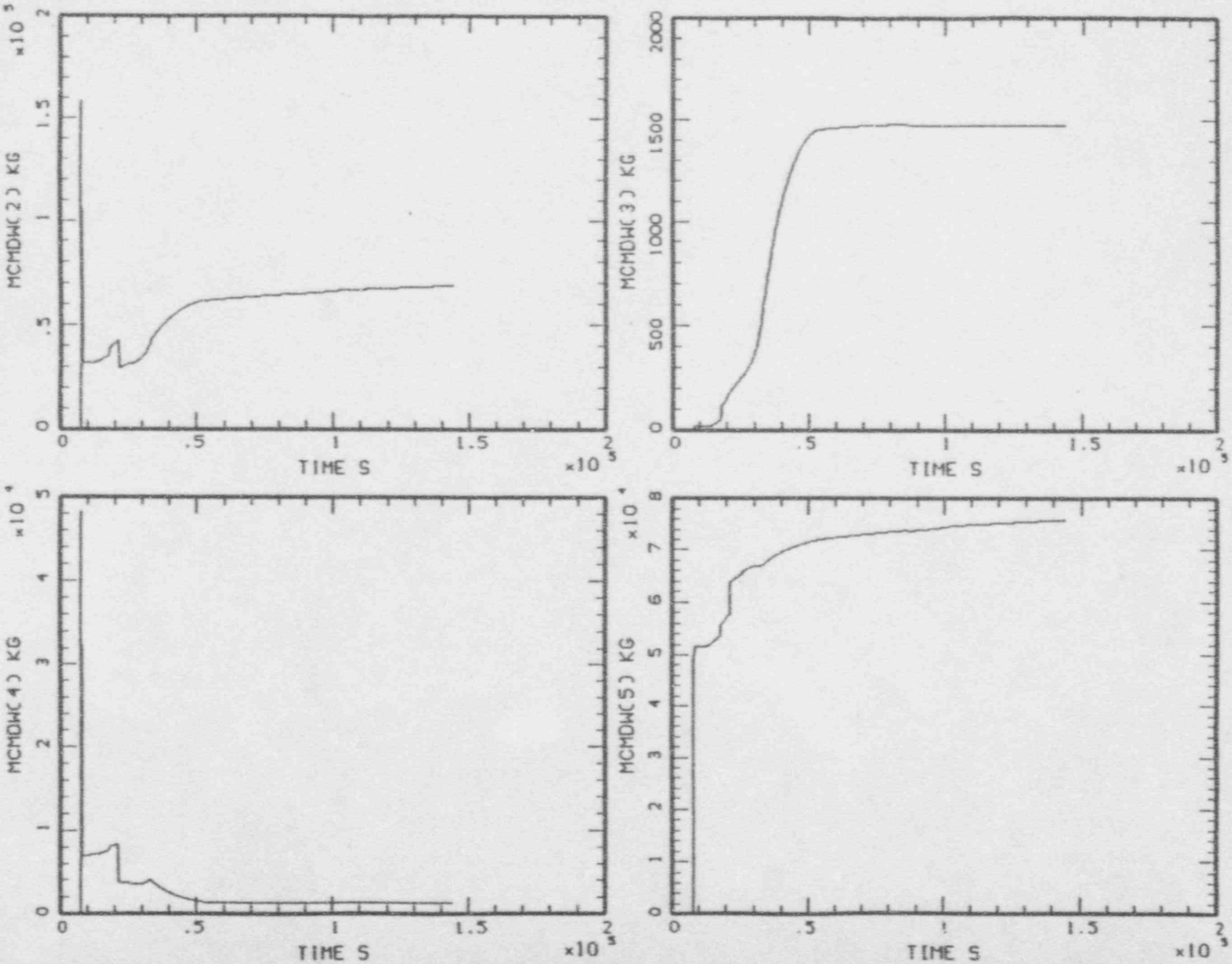

MAAP-MELCOR: BWR SBO (03/10/91)
bnl_sbo_43.plt LINE

P 38

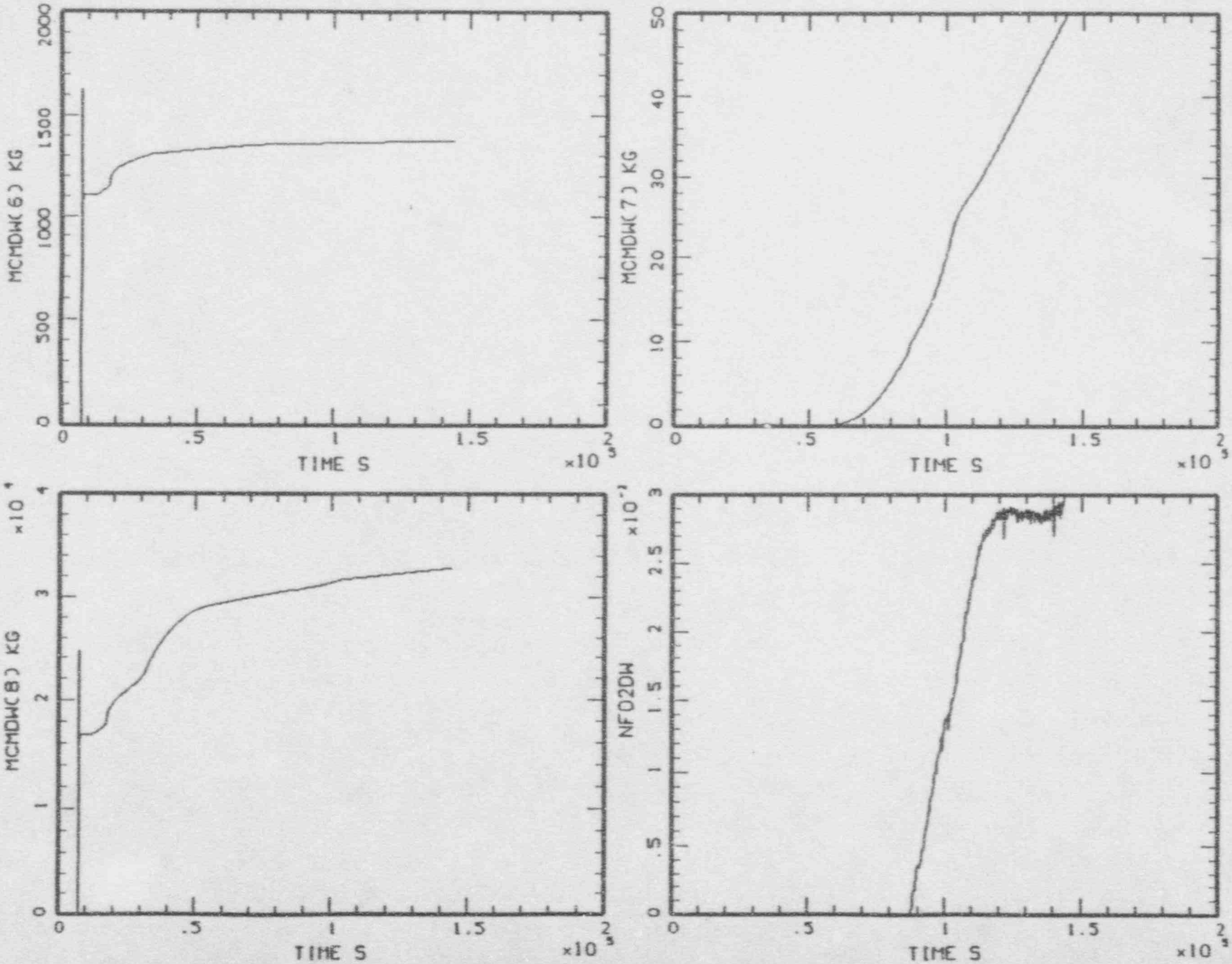

MAAP-MELCOR: BWR SBO (03/10/91)
bnl_sbo_43.plt LINE

P 39

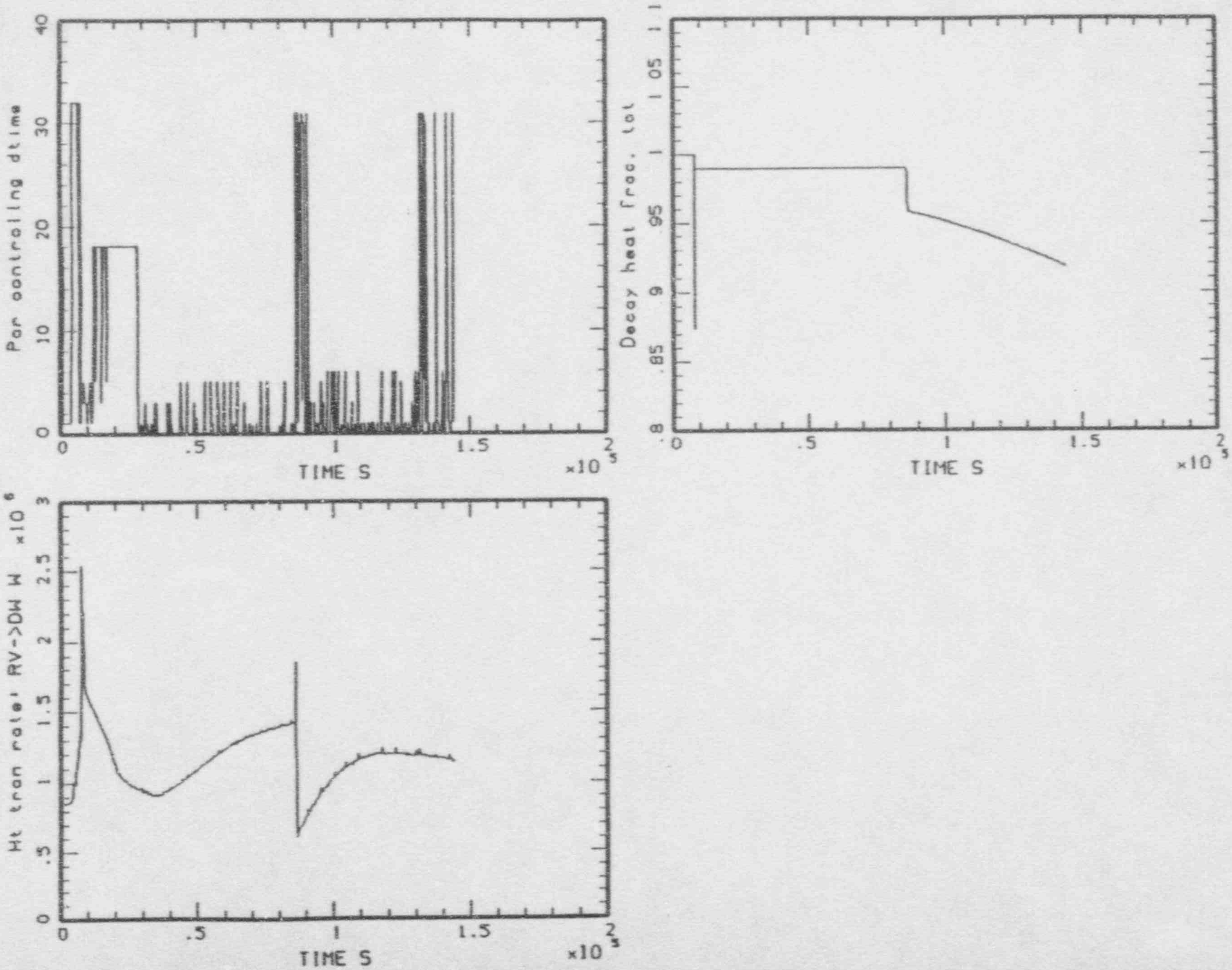

MAAP-MELCOR: BWR SBO (03/10/91)
bnl_sbo_44.plt LINE

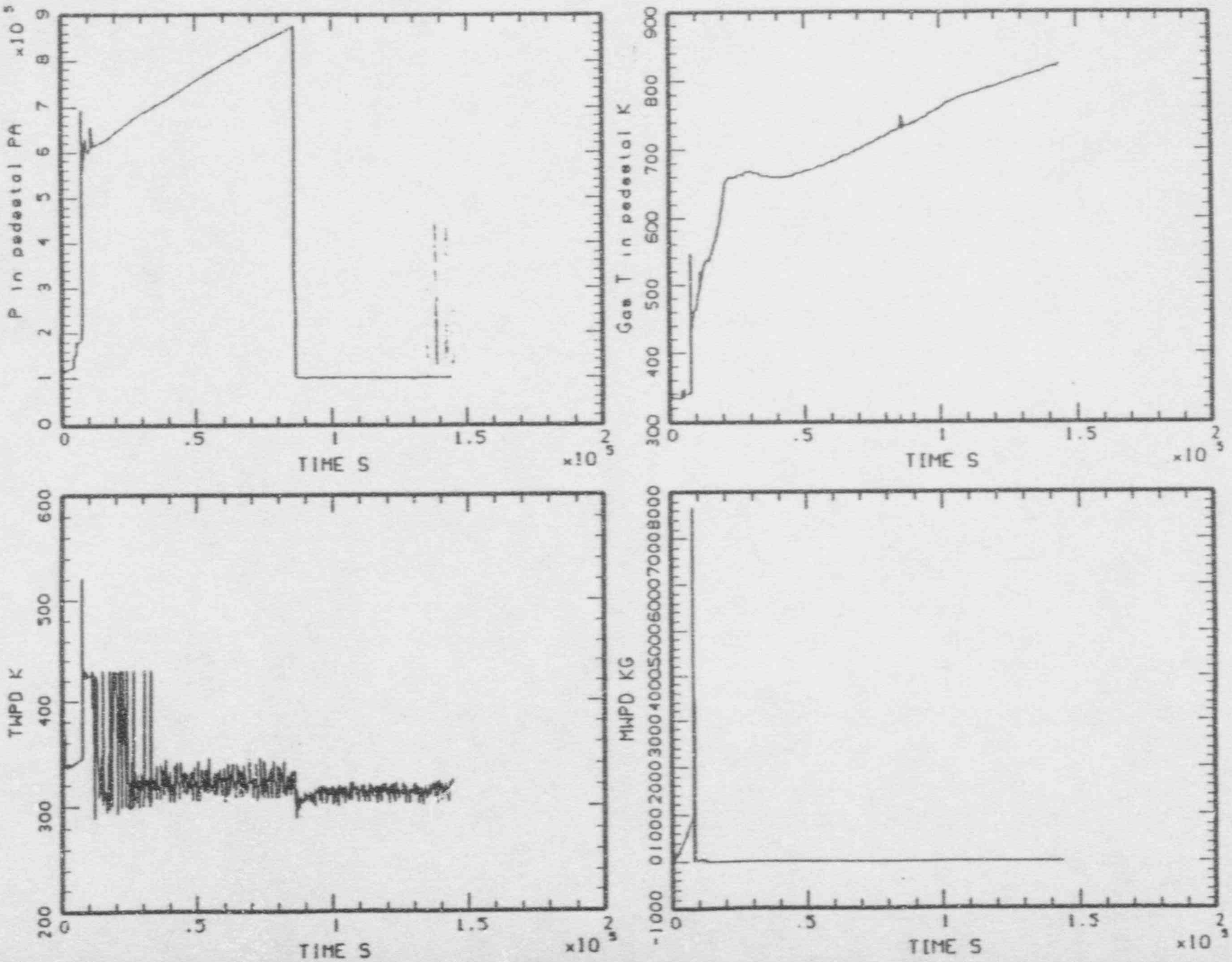

P41

MAAP-MELCOR: BWR SBO (03/10/91)
bnl_sbo_44.plt LINE

P41

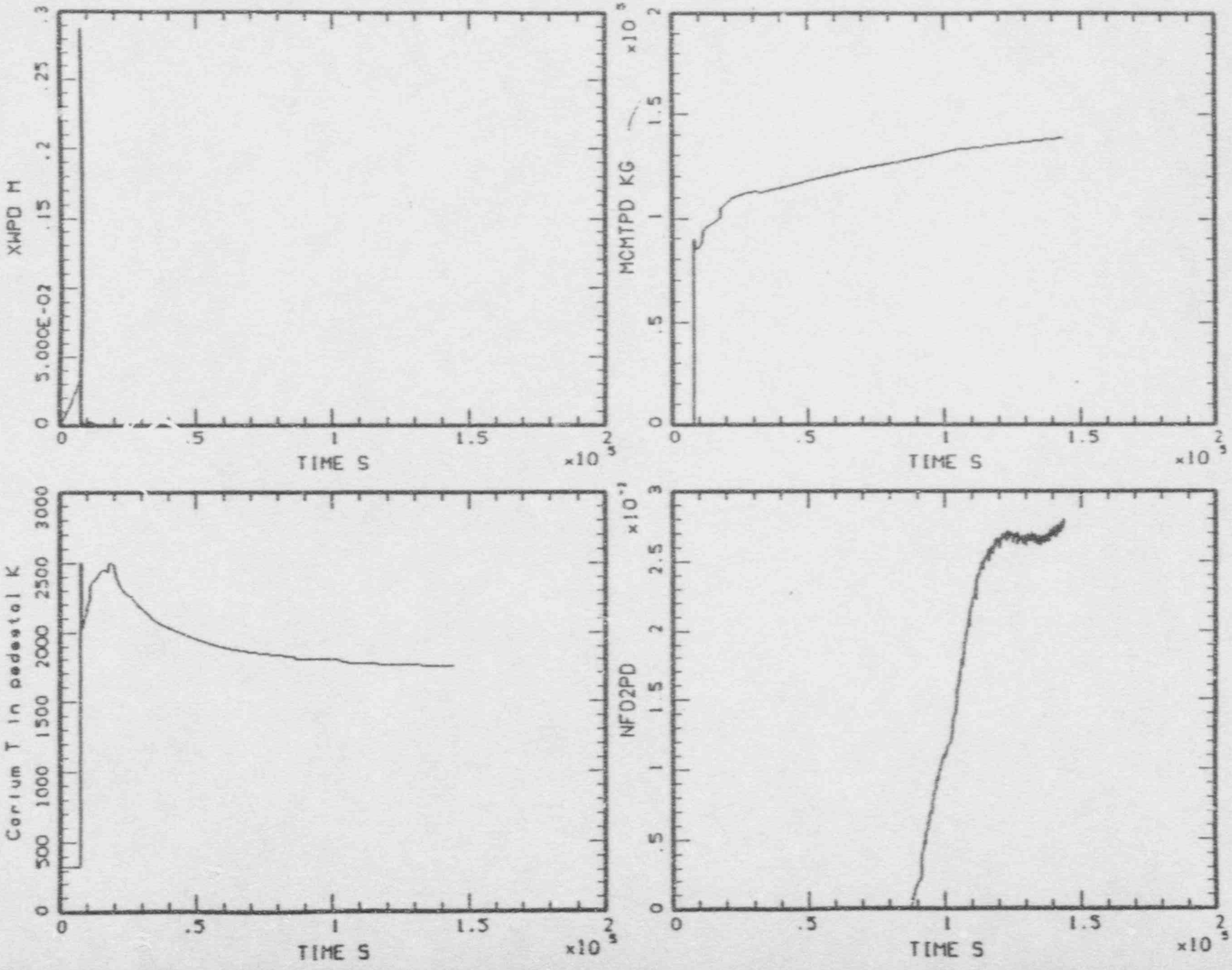

P 42

MAAP-MELCOR: BWR SBO (03/10/91)
bnl_sbo_44.plt LINE

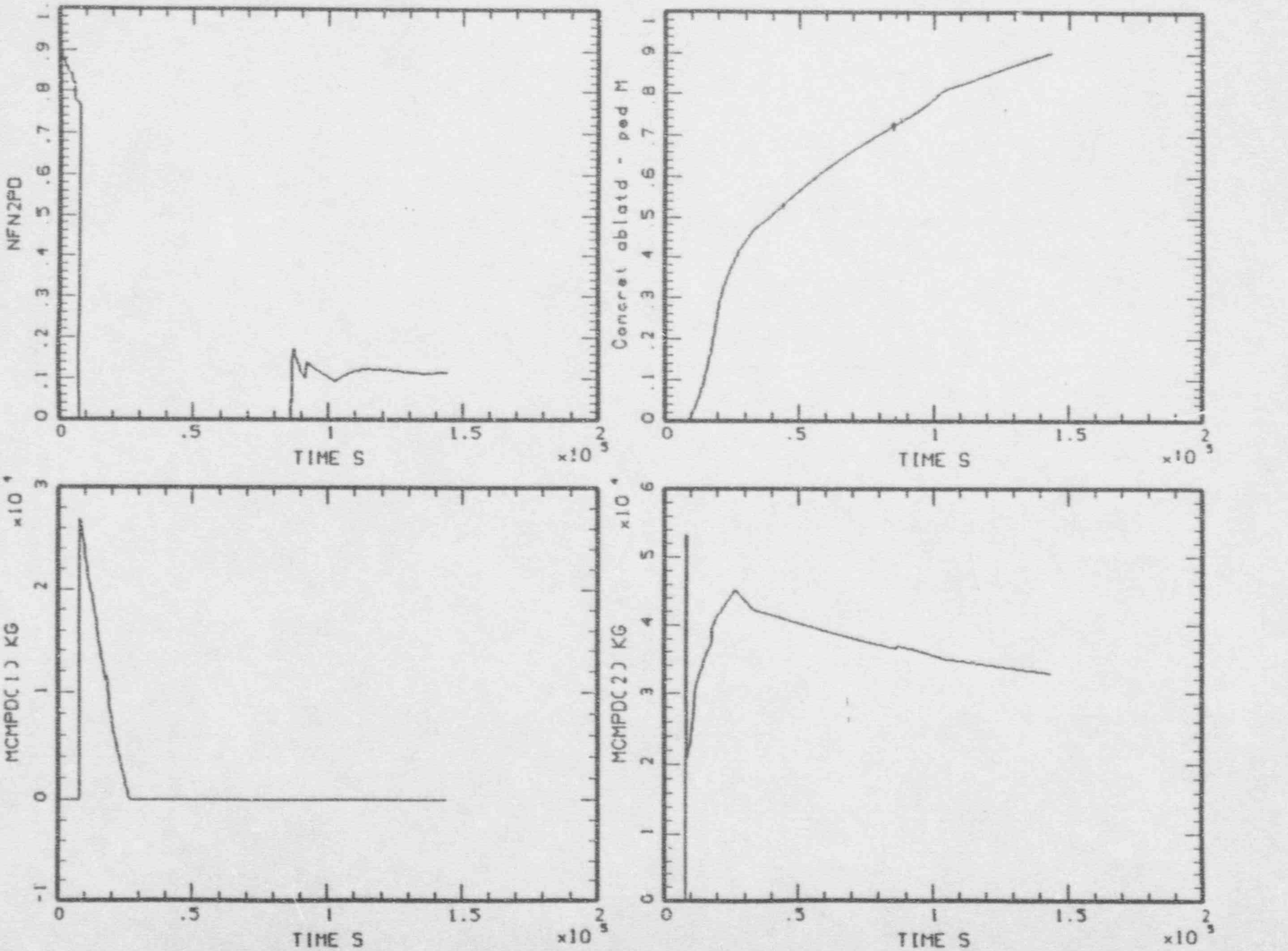

~~743~~

P43

MAAP-MELCOR: BWR SBO (03/10/91)
bnl_sbo_44.plt LINE

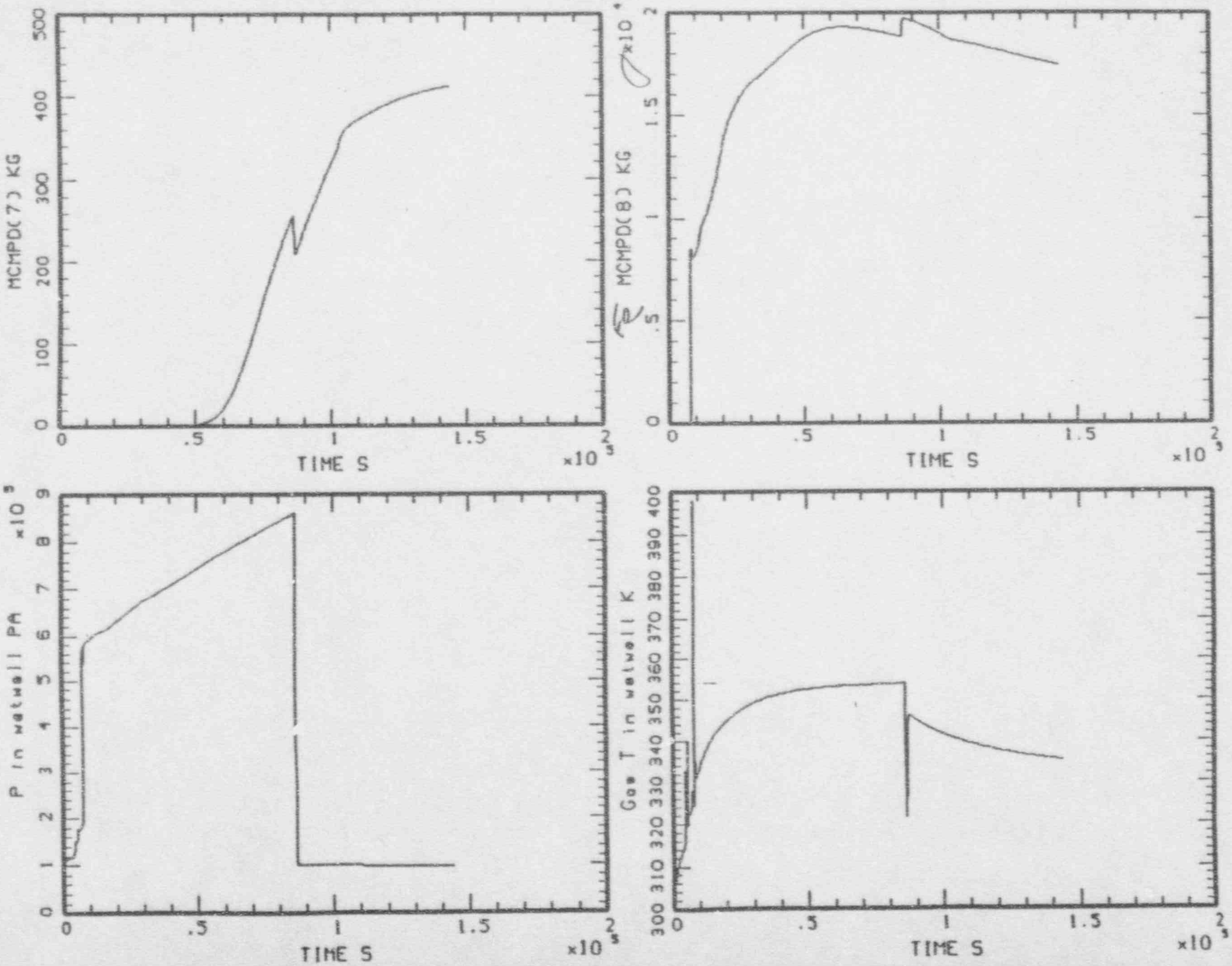

P44

MAAP-MELCOR: BWR SBO (03/10/91)
bnl_sbo_44.plt LINE

P 44

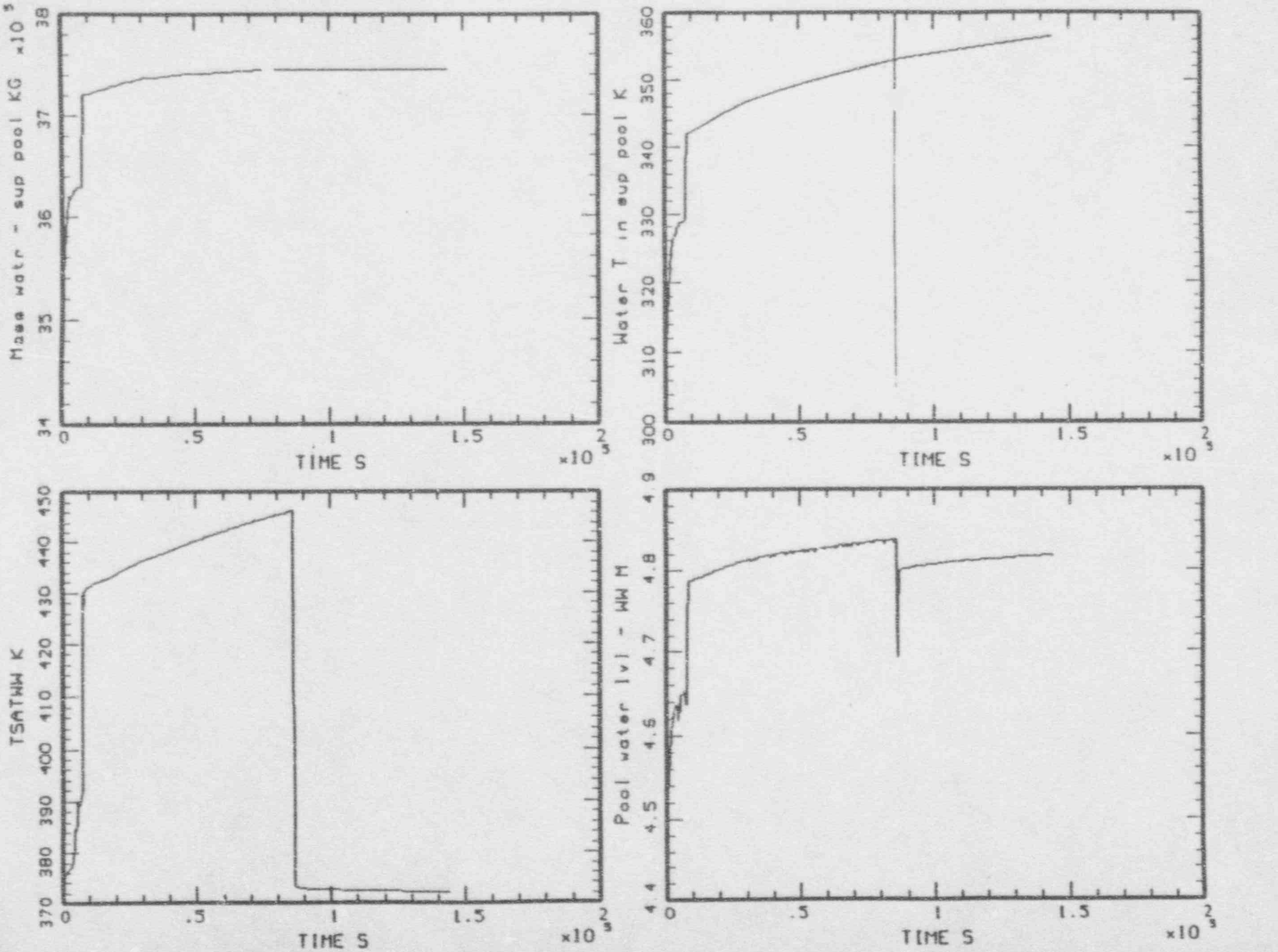

P45

MAAP-MELCOR: BWR SBO (03/10/91)
bnl_sbo_44.plt LINE

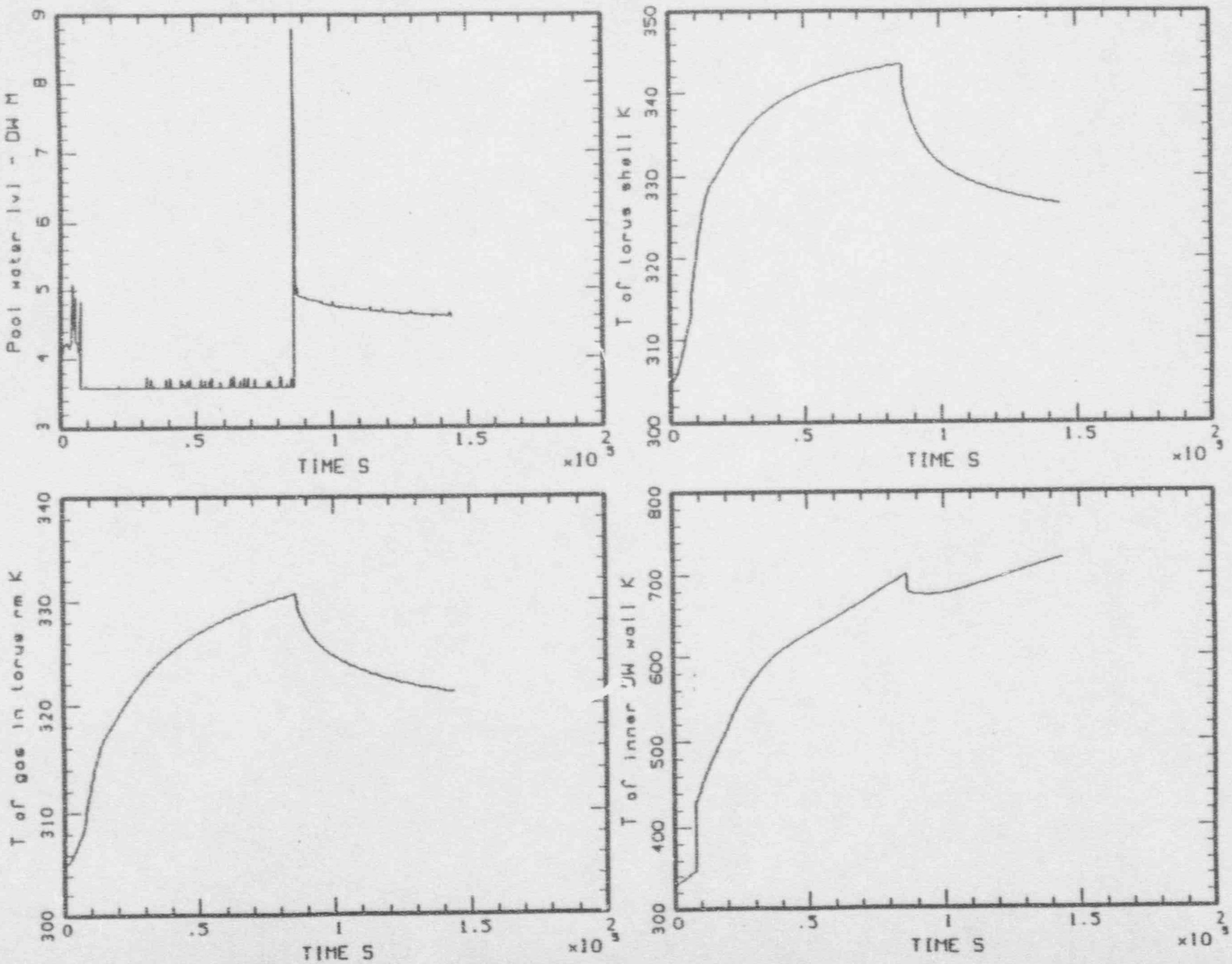

MELCOR: High Pressure SBO (LN, 04/17/91)

P 46

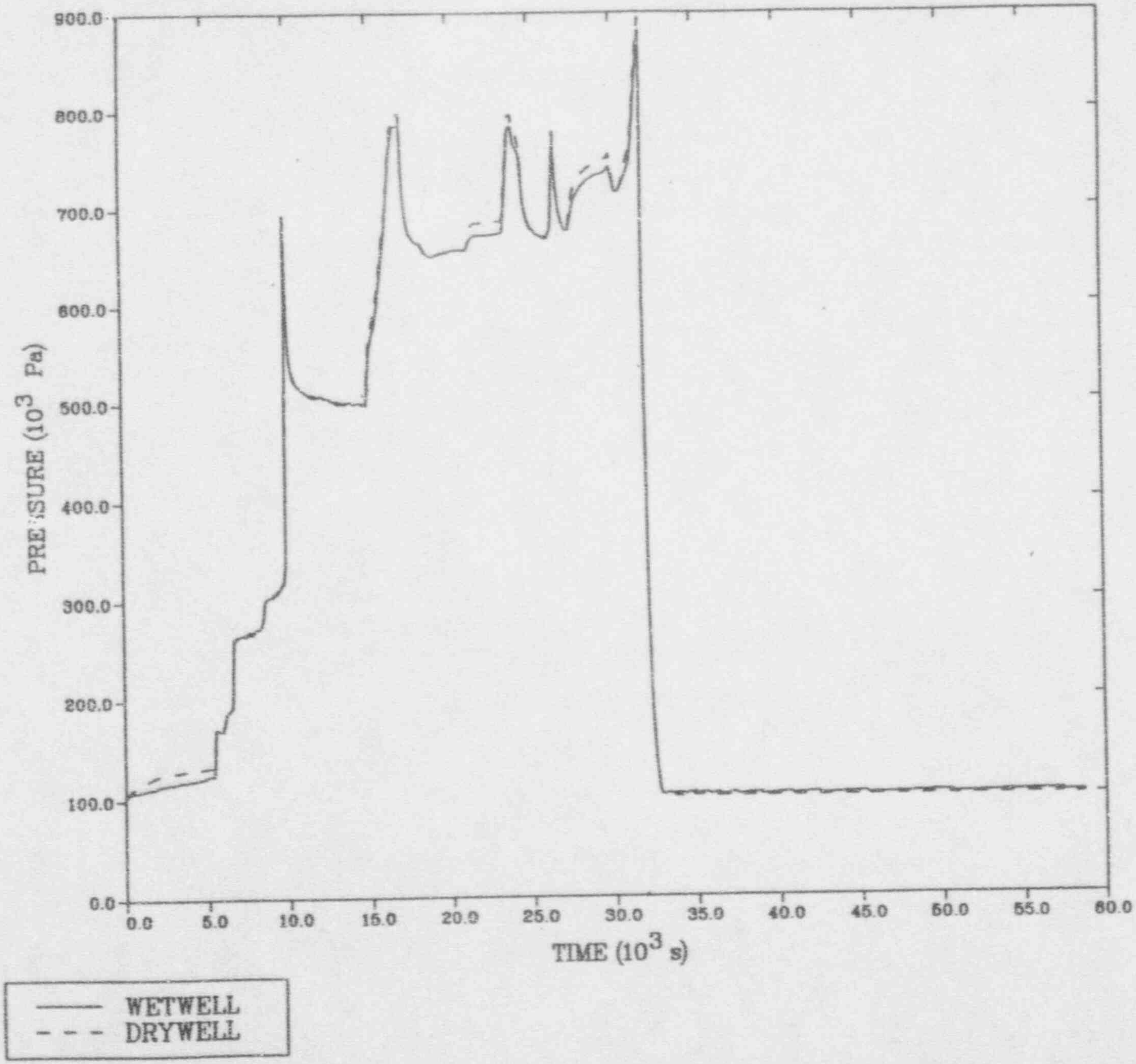

MELCOR: High Pressure SBO (LN, 04/17/91)

P 47

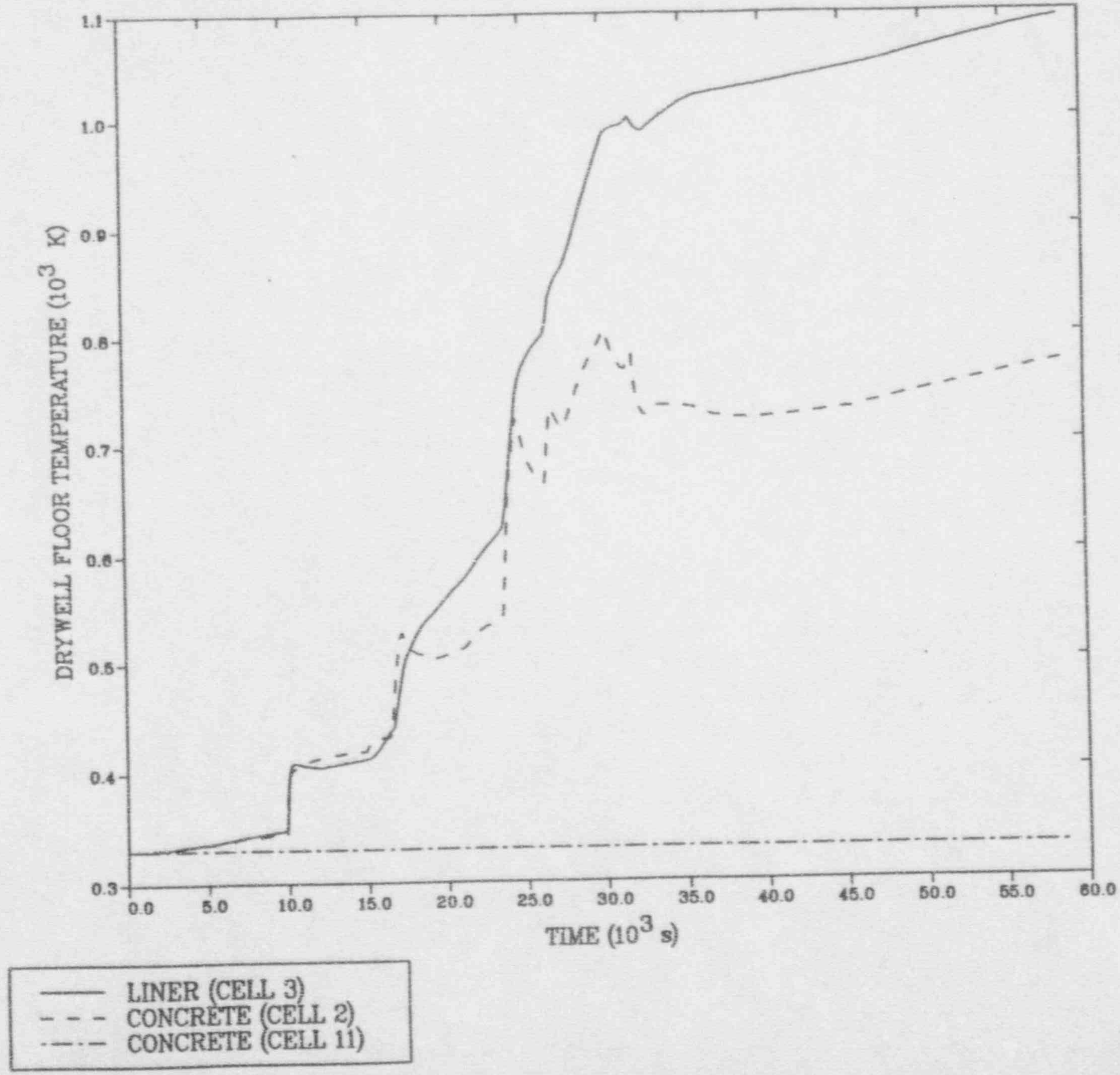

MELCOR: High Pressure SBO (LN, 04/17/91)

P 48 & P 49

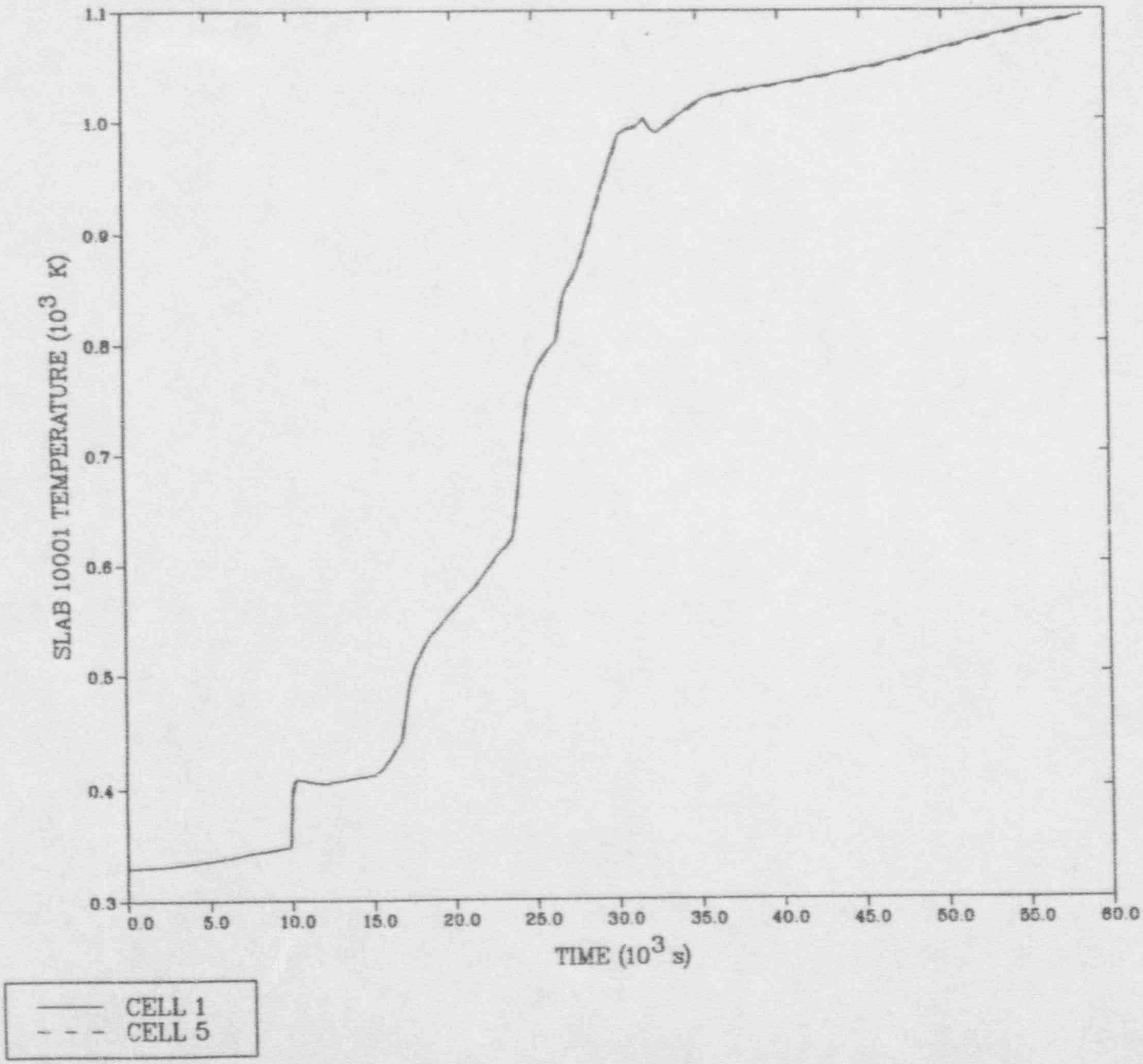

MELCOR: High Pressure SBO (LN, 04/17/91)

P 50

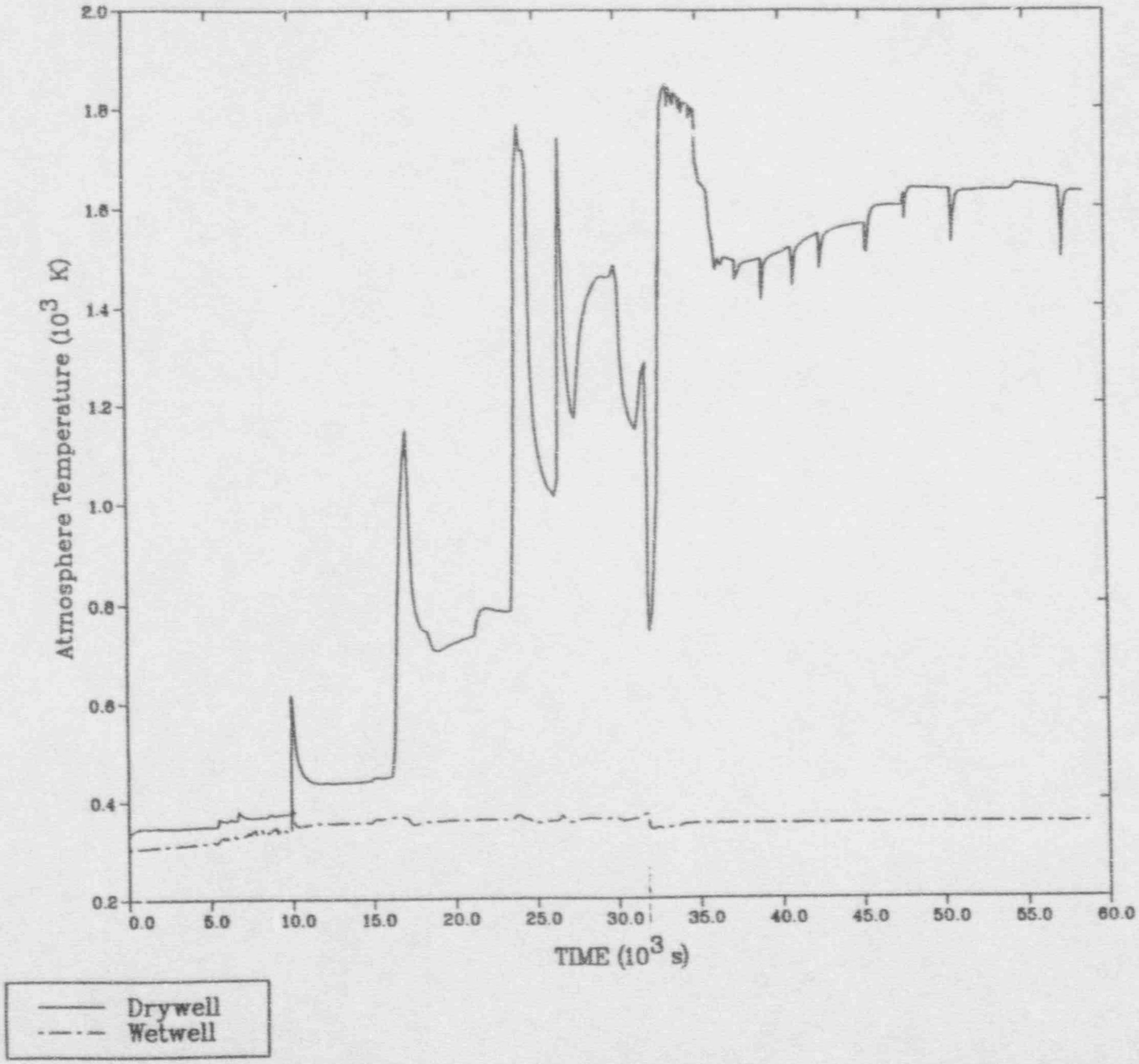

P 51

MELCOR: High Pressure SBO (LN, 04/17/91)

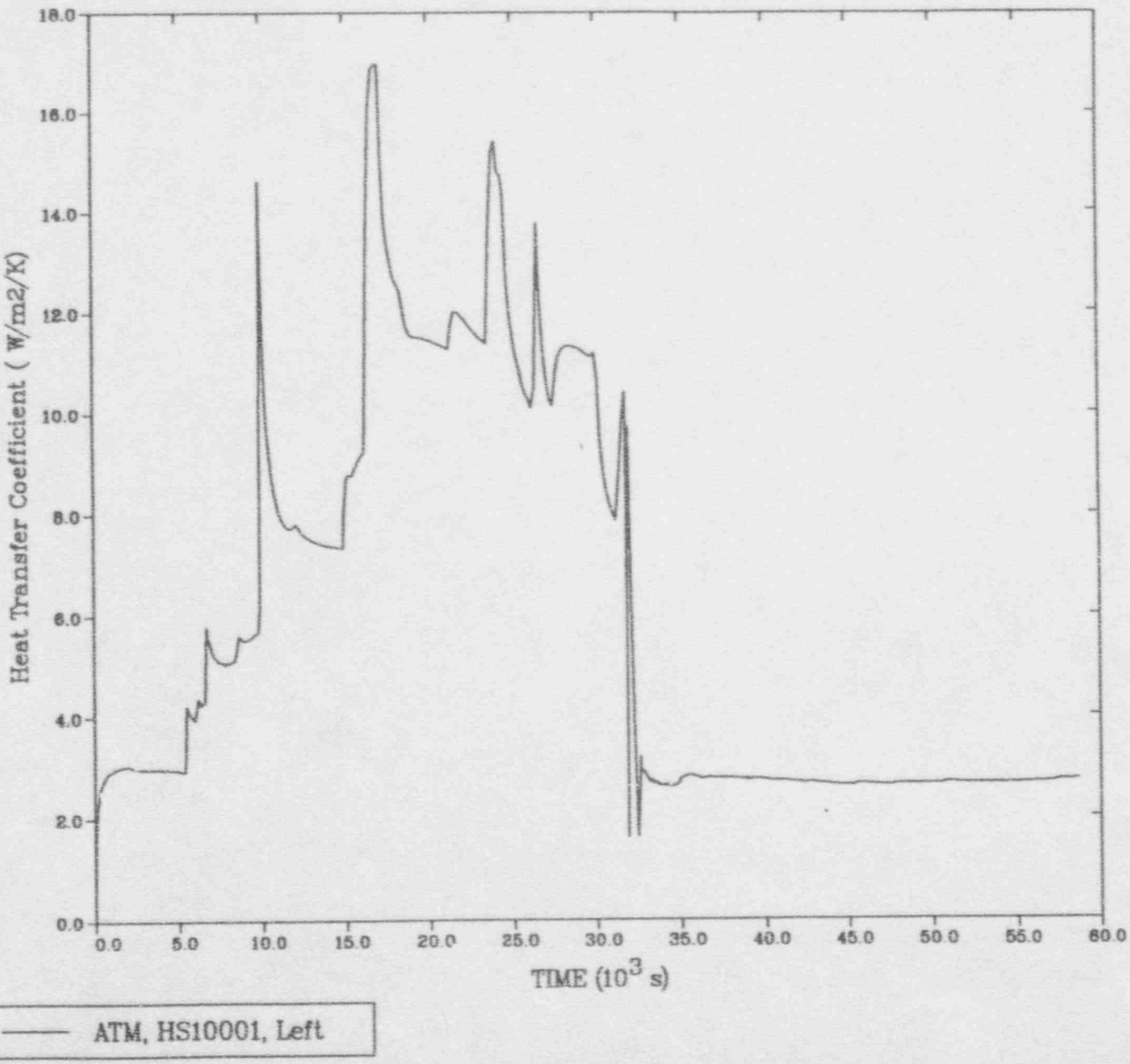

MELCOR: High Pressure SBO (LN, 04/17/91)

P52

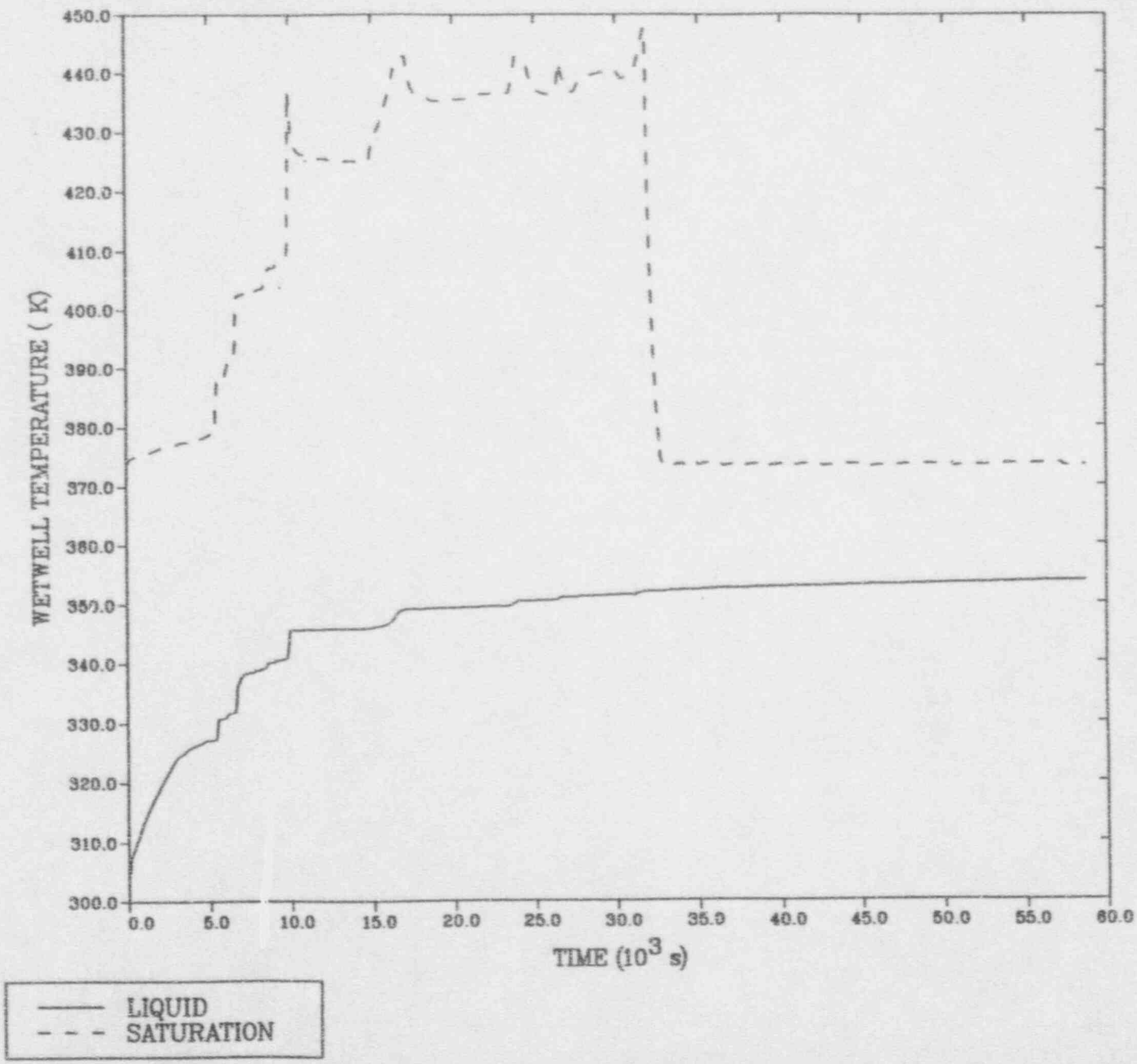

MELCOR: High Pressure SBO (LN, 04/17/91)

P 53

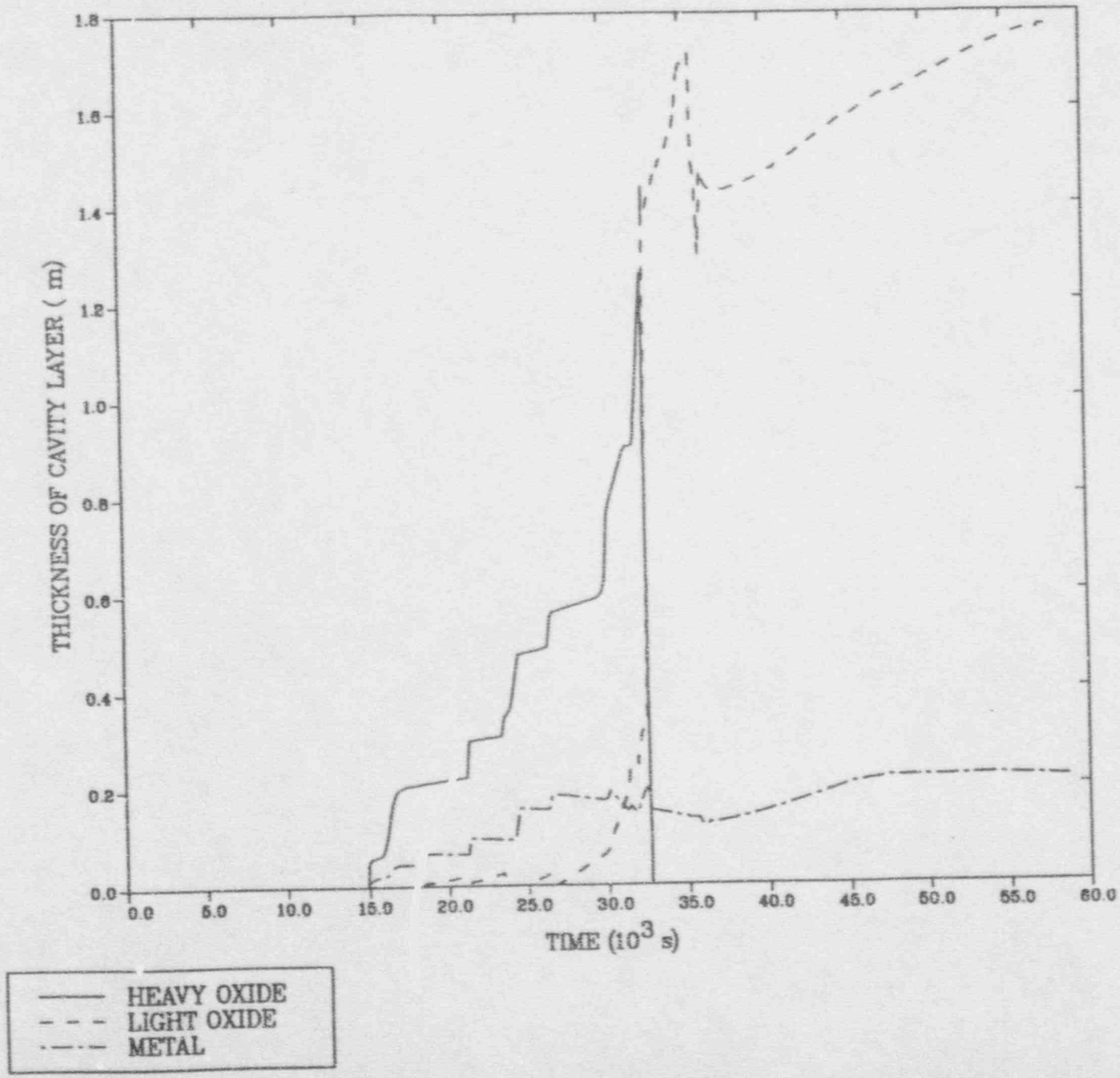

P 54

MELCOR: High Pressure SBO (LN, 04/17/91)

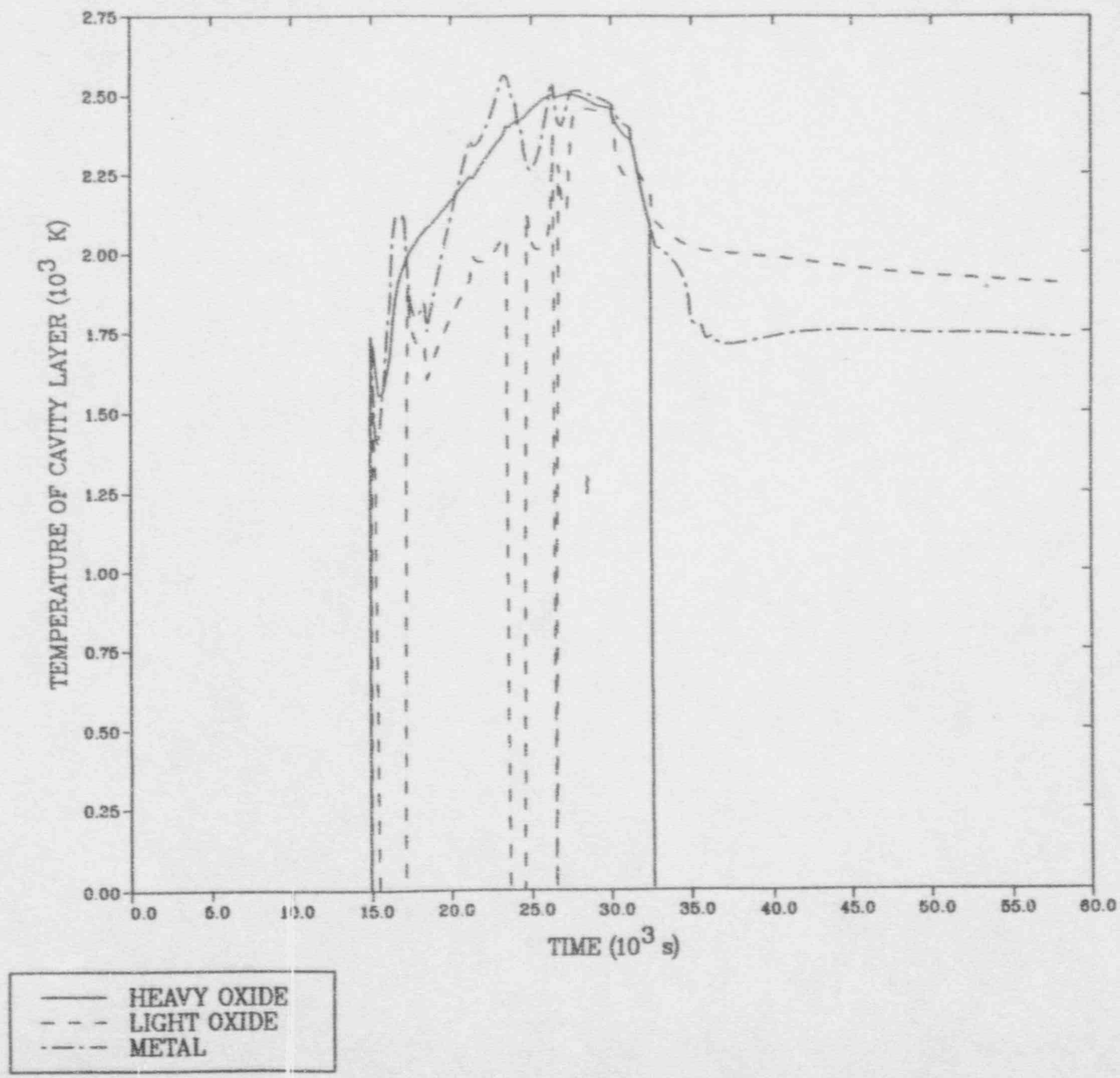

MELCOR: High Pressure SBO (LN, 04/17/91)

P 55

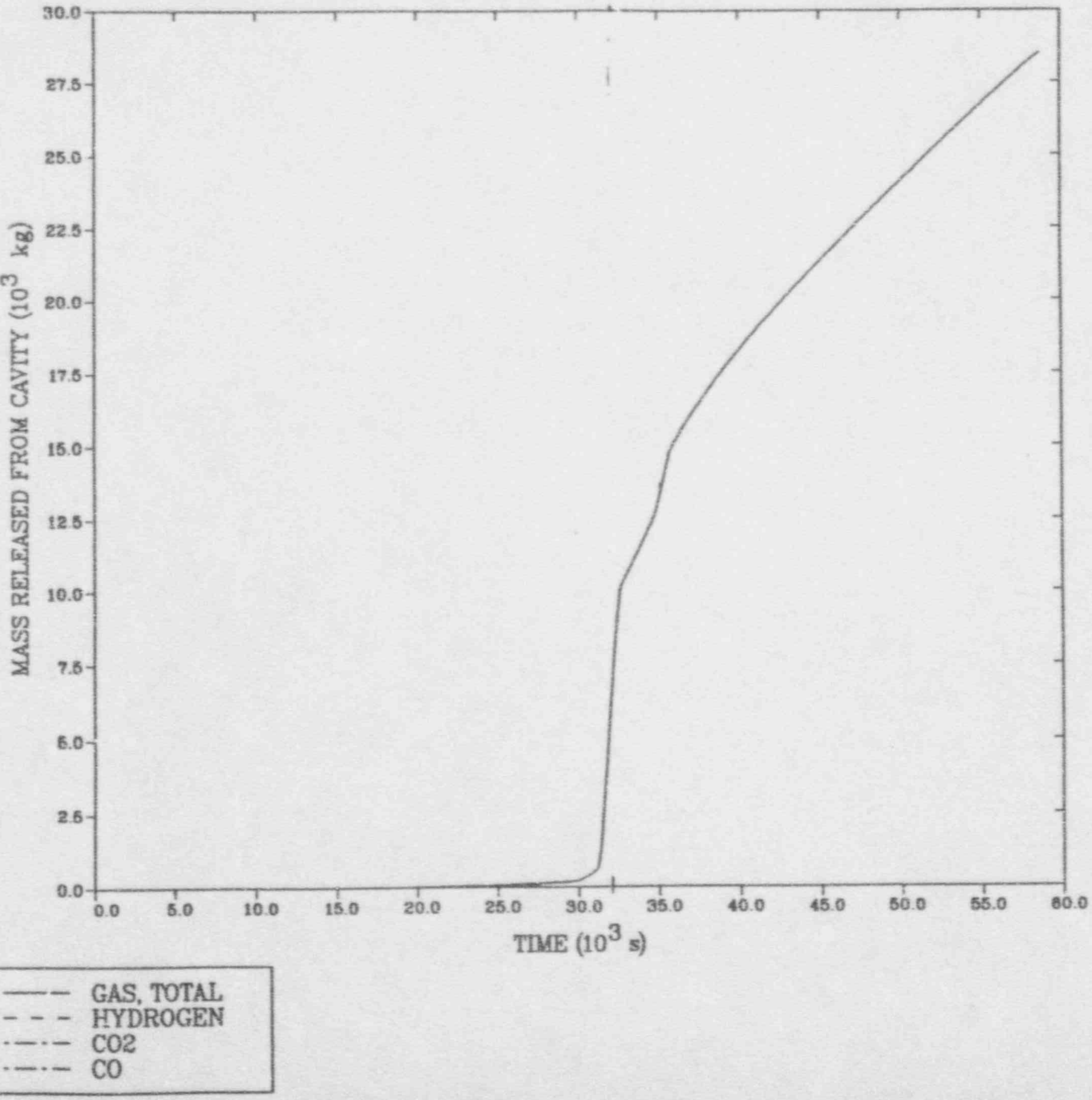

MELCOR: High Pressure SBO (LN, 04/17/91)

P 56

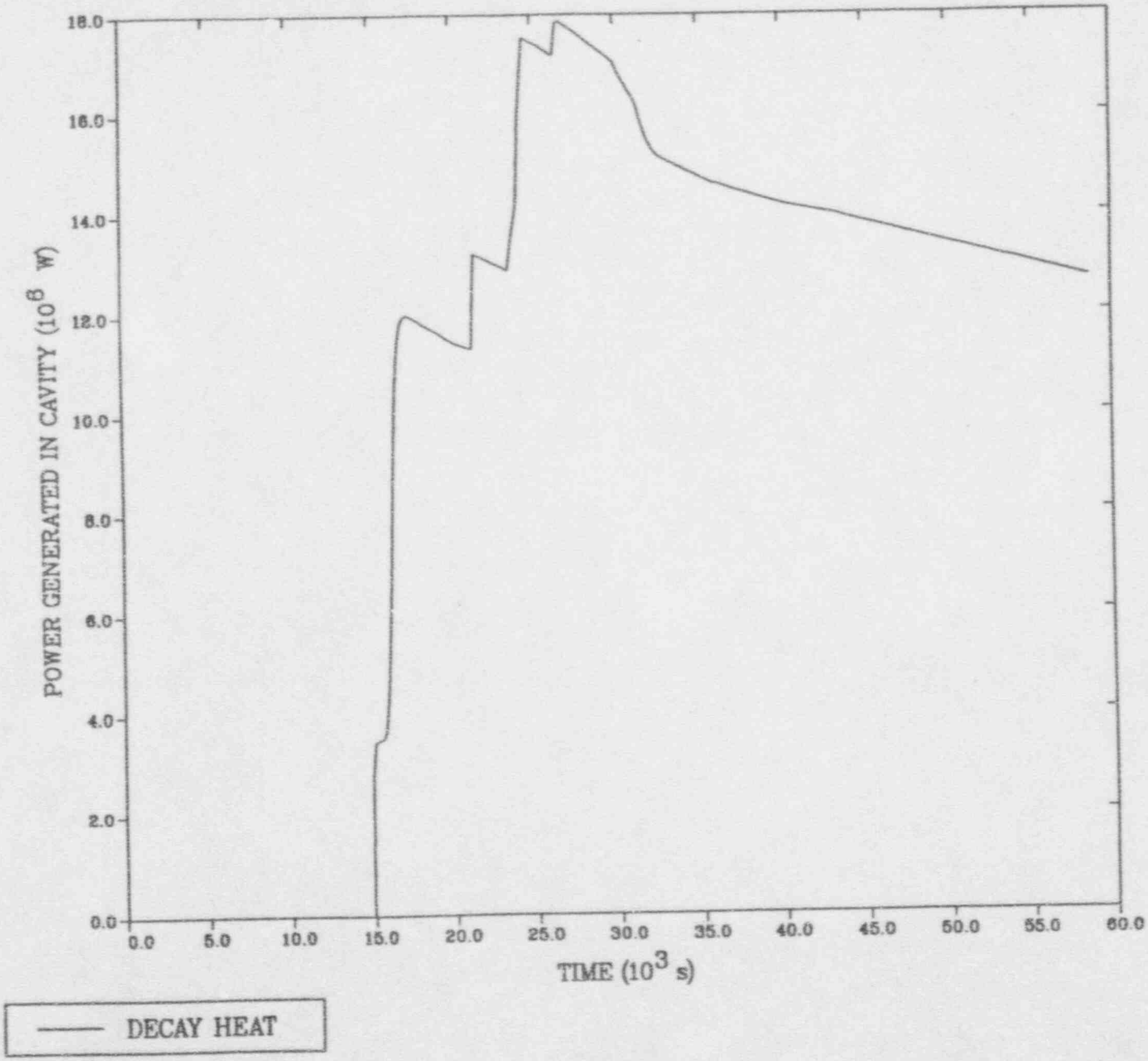

MELCOR: High Pressure SBO (LN, 04/17/91)

P 57

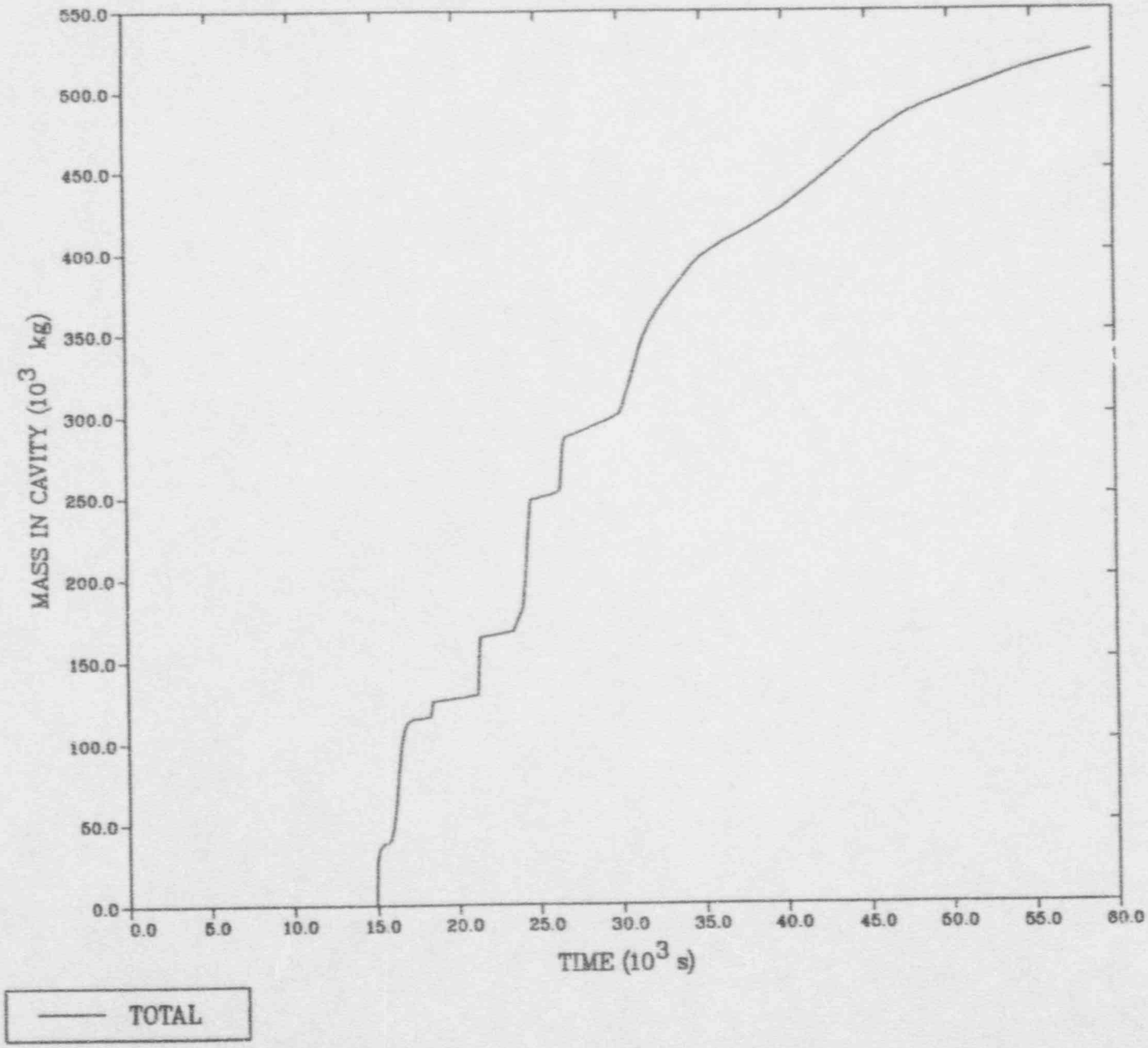

MELCOR: High Pressure SBO (LN, 04/17/91)

P 58

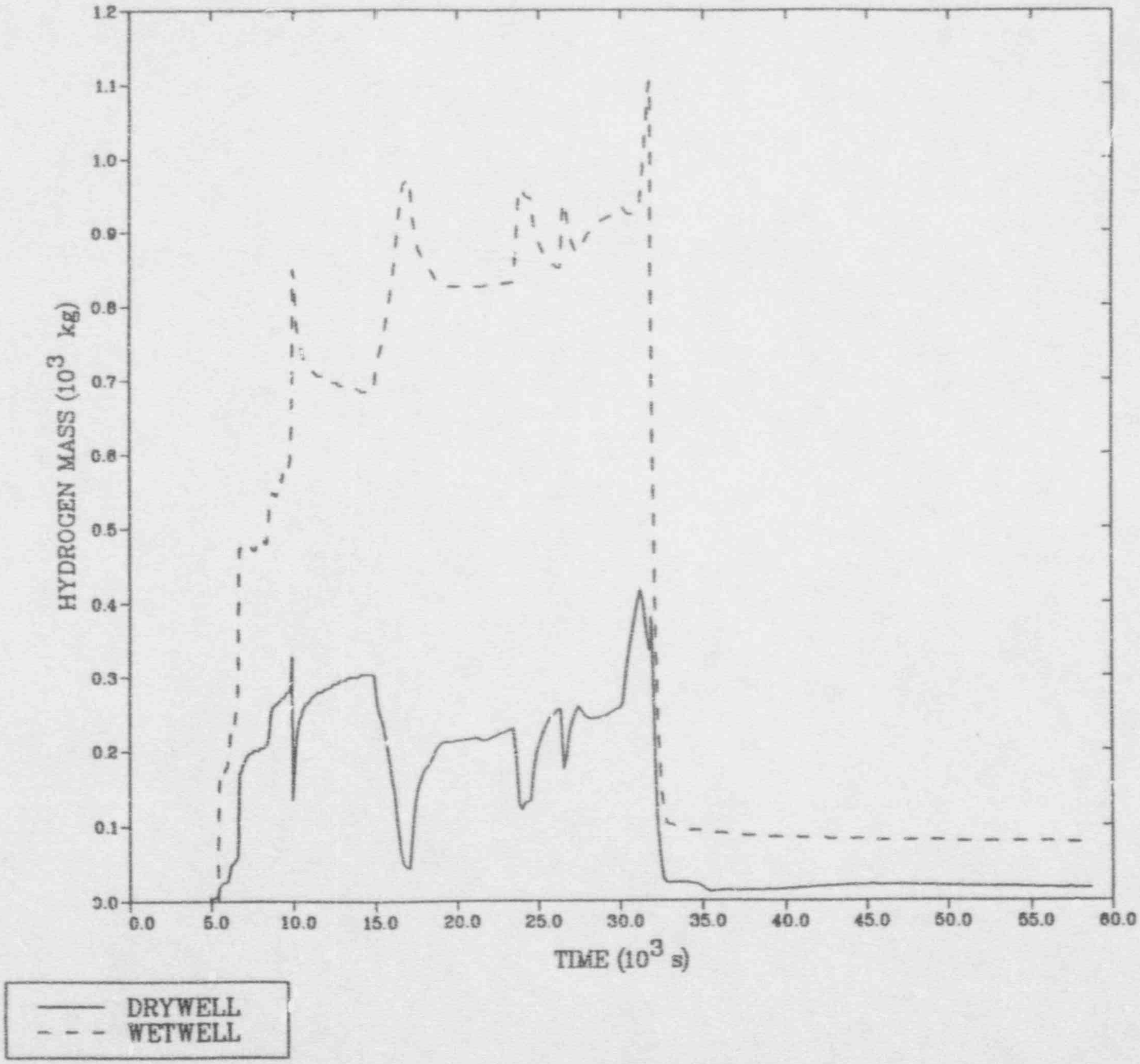

P 59a

MAAP-MELCOR: BWR SBO (03/10/91)
bnl_sbo_45.plt LINE

P 59

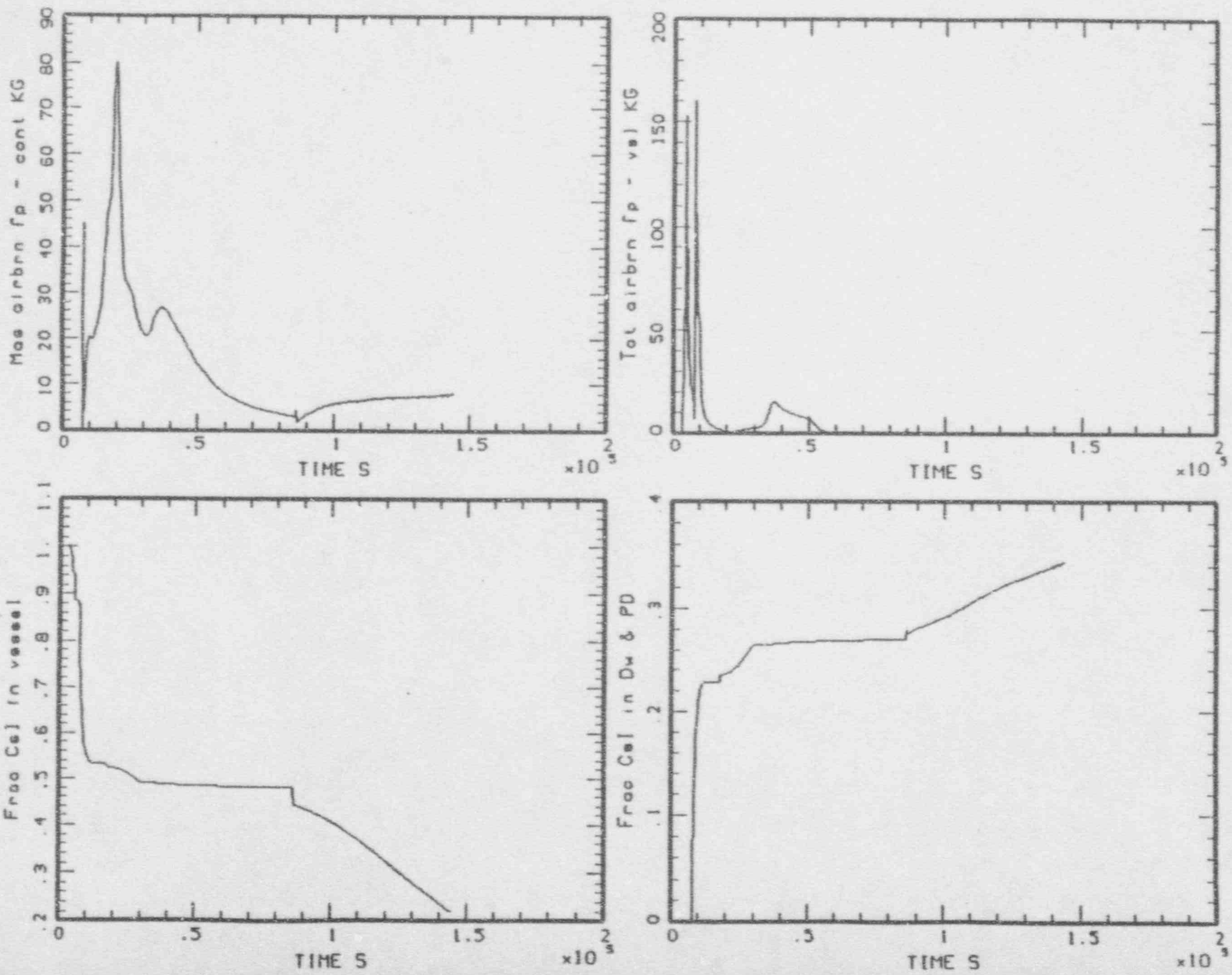

P60

MAAP-MELCOR: BWR SBO (03/10/91)
bnl_sbo_45.plt LINE

P 60

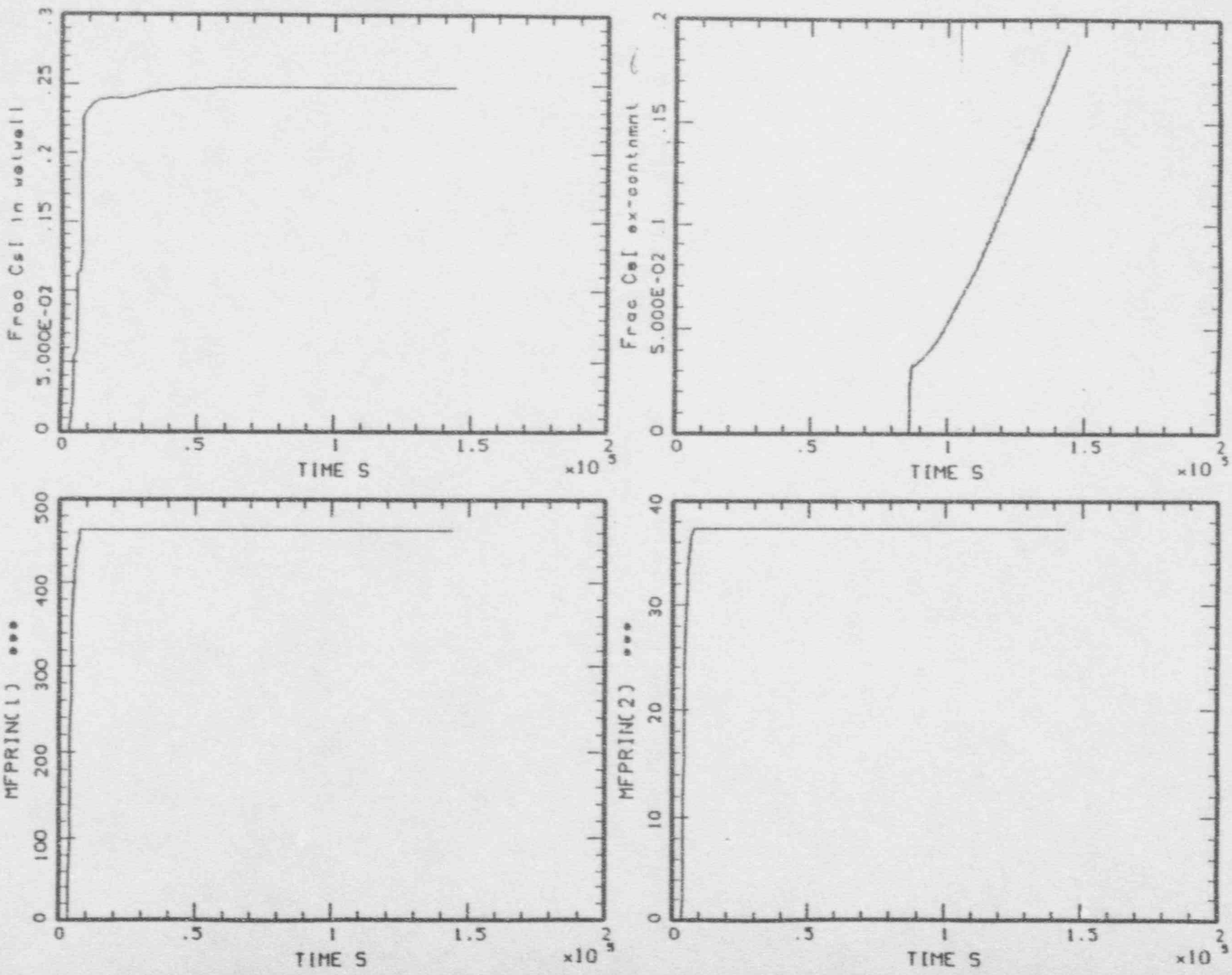

APPENDIX E

ASSESSMENT OF MAAP/PWR PARAMETERS

J.W. Yang

Table of Contents

1 Introduction

This appendix summarizes an assessment of MAAP/PWR modeling and input parameters. The work was performed under Task 6 of the MAAP Code Evaluation Program, which requires Brookhaven National Laboratory to perform a comprehensive review of those key input parameters and model assumptions which influence MAAP's calculations. In accordance with the NRC IPE guidance documents (NUREG-1335 [1] and Generic Letter No. 88-20 [2]) and discussions at the MAAP review meetings, this assessment focuses on those parameters which have significant effects on the mechanisms of containment failure and its timing. These parameters are important for assessing potential strategies for accident management and improvements in containment performance. The parameters reviewed in this appendix are grouped according to the following phenomenological issues: containment failure mode, in-vessel hydrogen generation and core-melt progression, primary system natural circulation, debris dispersal and distribution in the containment, coolability of debris in the containment, and hydrogen/carbon monoxide combustion.

The review of the parameters is based on the MAAP 3.0B PWR sensitivity study [3] and the IPE guidance document [4]. The results of recent MAAP analyses for a small break LOCA sequence also are discussed.

2 Containment Failure Mode

Postulated containment failure modes can be grouped into two types: catastrophic failure, or "leak-before-break". Presently, the majority of risk assessments have assumed the catastrophic-failure mode, in which the containment is predicted to fail suddenly at a threshold pressure. The MAAP 3.0B code has two methods to predict containment failure. The first method requires the user to specify the failure pressure (PCF), location, and failure area (ACFPR). The second method involves a time-dependent strain analysis.

Several sensitivity analyses have been performed assuming a catastrophic failure mode for a station blackout sequence [3]. The failure pressure, which directly affects the timing of containment failure, was varied from 0.3 Mpa to about 1.13 Mpa. The results are given below:

Case	Failure Pressure, Mpa	Failure Time, Hr.
TMLB-0 (Base)	1.03	36.8
-VF	0.3	4.0
-70LL	0.6	15.9
-70L	0.93	27.8
-70H	1.13	49.1

These analyses show that the failure time of containment is extremely sensitive to the assumed failure pressure. In a recent MAAP analysis for a small break LOCA sequence, it was shown that the pressurization rates for containment are about 14 Pa/s and 3.8 Pa/s for a flooded and dry cavity, respectively. These pressurization rates imply that by varying the failure pressure by 0.1 Mpa (i.e., 14.5 psi), the failure time could be altered by about 7,100 and 26,300 seconds for the flooded and dry cavity, respectively.

The failure pressure depends on the design of the containment and can be estimated by a plant-specific structural analysis or by adapting existing analyses from similar plants. In either case, there will be an uncertainty range associated with the predicted threshold pressure. For example, in NUREG-1150 [5], the range of failure pressure for two plants based on the 5th-95th percentile is:

Zion: 108-180 psig

Surry: 95-150 psig

The extremes of these pressure ranges could cause the predicted time of containment failure to vary by several hours if the MAAP code is used.

In the NRC Generic Letter No. 80-20 [2], it recommends:

1. the use of existing structural analyses to determine the ultimate pressure capacity of the containment, and
2. the development of a plant-specific probability distribution function of failure likelihood for the range of failure pressures.

In response to the NRC's recommendation, the MAAP guidance document [4] states that

1. the best-estimate containment failure pressure should be taken from outside analyses;
2. the determination of the type of sensitivity calculations needed should be based on the results of these analysis, and
3. additional calculations could be performed to estimate the effects of a lower failure pressure.

The recommendations given in MAAP guidance document in general agree with that of NRC. In view of the sensitivity of failure time to failure pressure as indicated by the MAAP uncertainty analysis [3], it is appropriate to consider the uncertainty range of failure pressure for IPEs.

The MAAP guidance document [4] also recommends considering the effect of temperature on containment failure. It states that the effect of temperature ". . .can be simulated in MAAP by reducing the containment failure pressure to a small value when high temperatures are reached." The lower failure pressures included in the sensitivity study [3] can be considered as a mechanism for simulating the effect of temperature.

The assumed size of failure would not affect the failure time of the containment, but would affect the source term. Based on the concept of leak-before-break, a smaller area of leakage is expected when there are low pressurization rates in the containment. The leakage area becomes larger when the pressurization rate becomes higher. In the sensitivity study [3], a variation of the area of the leak between 0.0005 to 0.05 m^2 was considered. (The area for the base case is 0.02 m^2). The failure pressure of the containment (the time at which leakage starts) was not changed. The results show that the failure size has a strong effect on the fractions of Sr, La, and Te released from the containment, and on the decontainment factors (DFs) in the auxiliary building. The range of failure size involved in the sensitivity study covers the range of leakage area estimated by the NRC's Containment Performance Working Group [6]. Because the failure size depends on the design of the containment (concrete vs. steel-shell) and penetrations, it is plant-specific. For example, a larger area would be appropriate for a steel-shell containment, particularly for high pressurization rates.

For PWR dry containments, failure location in the primary containment (i.e., upper or annulus region) will not play an important role either on the performance of the containment or on the source term. However, for an ice-condenser plant, a failure in the lower compartment would cause the fission products to bypass the ice condenser. (The failure location for the ice-condenser plant is not discussed in the MAAP guidance document [4]). We suggest that, for the case in which containment fails before the ice is depleted, sensitivity studies involving the failure of the lower compartment should be performed for the IPEs, based on considerations of the offsite consequences and the probability of the accident sequence.

In the auxiliary building, the failure area, location, and the general nodalization have a strong effect on the natural circulation pattern predicted by MAAP. The natural circulation would, in turn, affect the retention of the fission product. Because of the uncertainties involved in using the auxiliary building model, the MAAP guidance document suggests sensitivity studies [4] for those sequences in which the performance of the auxiliary building is clearly dominant.

The other containment failure model in the MAAP code is based on a time-dependent strain analysis. The MAAP guidance document does not recommend this failure model because of the NRC's recommendation that outside analyses of containment failure pressure should be developed. It is interesting that the strain model was included in the sensitivity study [3]; it showed that the containment had not failed at the end of the calculation (72 hours). (The containment is predicted to fail at 36.8 hours for the base case). Hence, the strain model predicts unrealistically long times to containment failure and, therefore, should not be used for IPEs.

3 In-Vessel Hydrogen Generation and Core Melt Progression

In the MAAP 3.0B/PWR code, hydrogen generation and melt progression are controlled by six model parameters and one input parameter specified by the user (MCSPO) as shown in Table E.1. The six model parameters are included in the sensitivity study for the station blackout sequence [3], and MCSPO was included in the recent MAAP analysis for a small break LOCA sequence [Appendix C]. The uncertainty analysis recommended for these parameters are included in Table E.1.

Table E.1 MAAP Input Parameters Involved With H_2 Generation and Core Melt Progression

Model Parameter No/Name	Sensitivity Study, Ref. [3]		Guidance Document, Ref. [4]	
	Base Case	Variation	Best Estimate	Uncertainty Analysis
5 FAOX	1	2	1	None
12 HTCMCR	1000 W/M^2-K	500, 5000	1000	None
46 TCLMAX	2100 K	1200	1200	None
47 LHEU	250 Kj/Kg	100, 400	250	None
52 TEU	2500 K	2100, 2800	2500	None
67 FCRBLK	1	0	0	Note 2
MCSPO (specified by the user)	-	-	Note 1	None

Description of Parameter:

FAOX = Cladding oxidation surface multiplier
HTCMCR = Heat-transfer coefficient between molten debris and a frozen crust
TCLMAX = Clad rupture temperature
LHEU = Latent heat assumed for U-Zr-O eutectic
TEU = Melting temperature assumed for U-Zr-O eutectic
FCRBLK = 1 for activation of the blockage model; 0 for no blockage model.
MCSPO = Total steel mass to be consumed by core debris as it flows to the lower plenum

Note 1: Mass of lower core support plate
Note 2: Activation of the blockage model for one station blackout sequence in which it is assumed that seal LOCAs will be small or non-existent, and that hot leg rupture does not occur. This is based on the consideration of RPV depressurization and fission product release.

Table E.2 summarizes the effects of the model parameters reported in the sensitivity study, which shows that these parameters do not have any significant effect on the time of reactor vessel failure. However, the containment failure time can be delayed or advanced by varying these parameters. The most important parameter which affects hydrogen generation is the blockage model. In the sensitivity study [3], the activation of the blockage model is assumed for the base case (FCRBLK = 1), and the predicted cladding oxidation is 25%. When the blockage model was deactivated (FCRBLK = 0), the cladding oxidation increased to 41%. Recent MAAP analysis for the

Zion plant of a small break LOCA sequence yields a 38% cladding oxidation with the blockage model deactivated. Deactivation gives an estimate of a hydrogen generation similar to the predictions from other computer codes such as MELCOR. The MAAP guidance document recommends deactivating the blockage model.

Table E.2 Significant Effects of MAAP Input Parameters Described in Table E.1

Model Parameter No/Name	Value Used	RPV Failure Time, Hr.	Containment Failure Time, Hr.	% Cladding Oxidation (in-vessel)
(Base Case)	-	4.0	36.8	25
5 FAOX	2	3.92	45.4	28
12 HTCMCR	5000	3.99	42.0	25
47 LHEU	100	4.05	45.5	22
47 LHEU	400	4.11	28.8	38
52 TEU	2100	3.96	39.6	16
52 TEU	2800	4.29	31.9	47
67 FCRBLK	0	4.19	34.6	41

See Table 1 for descriptions of model parameters.

It is interesting to note, that in Table E.2, the containment failure could occur 5 hours earlier if the high melting temperature of the eutectic (2800 K) is used, and 8 hours earlier if the high value of the latent heat of the eutectic (400 KJ/Kg) is used. Hofmann et. al.,[5] reported that the liquefaction of UO_2 and ZrO_2 by molten Zircaloy could occur at a temperature between 2033 K to 2273 K. The high value (2800 K) used in the sensitivity study probably overestimates the melting temperature of the eutectic, and therefore, the predicted early containment failure may not be realistic. The latent heat of the eutectic has a large uncertainty at present. For the individual constituents of the core, UO_2, Zr, and ZrO_2, the latent heats are 273, 225, and 707 KJ/Kg, respectively. The best estimate of latent heat assumed for the eutectic in the MAAP code is 250 KJ/Kg; the estimated minimum and maximum values are 100 and 400 KJ/Kg, respectively. Therefore, the best estimate and maximum values are within the range of the latent heats for individual constituents. The maximum value (400 KJ/Kg) considered in the sensitivity study is reasonable, and within the range of uncertainty.

In MAAP/PWR code, the latent heat affects the melting and freezing of a fuel node and its relocation process. The MAAP sensitivity analysis [3] reveals that varying this parameter changes the distribution of UO_2 (the largest component of core debris) in the reactor vessel, the reactor cavity and the containment lower compartment after the reactor vessel breach. The impact of the latent heat on containment failure time could be the result of debris distribution after the reactor vessel failure.

The MAAP guidance document [4] states that the selection of no blockage as the base case will serve to demonstrate the impact of uncertainties in the core melt progression modeling on the overall plant response. It does not recommend to vary any one of these parameters listed in Table E.1 for IPEs. We recognize that the sensitivity analyses [3] were obtained from a base case in which the blockage model was activated. The results may not be valid when the assumption of no blockage is used in the IPEs. However, in view of its impact on the containment failure time, we suggest that one additional calculation be performed using the maximum latent heat value (400 KJ/Kg), so that the potential of an earlier failure of the containment is not over-looked.

The parameter MCSPO is not a model parameter, but an input variable specified by the user. MCSPO represents the mass of steel which is consumed by core debris as it flows to the lower plenum. The MAAP guidance document suggests that the mass of the core support plate is considered as the best estimate of the parameter MCSPO. In the MAAP code, the mass of the core support plate is the only structure modeled in the lower plenum. Because the lower plenum of a PWR contains many more structures than the core support plate, a MAAP analysis could underestimate the quantity of steel that might be in the core debris. The steel mass can have two effects:

(1) The oxidation of steel during direct containment heating (DCH): MAAP has modified its DCH model to include the reaction of steam and air with steel. Depending on the quantity of steel, the oxidation of steel could provide a source of energy and of hydrogen equal to that of the oxidation of zircaloy.

(2) The long-term effect on containment pressurization and hydrogen generation: The steel structure in the lower plenum which could be included in the core debris, is similar in mass to the steel reinforcement in the concrete. A large quantity of steel in the core debris could affect the corium/concrete interaction.

A sensitivity study of steel mass on DCH was not performed in the MAAP analysis but a study of its effect on containment pressurization is included in the small break LOCA calculation. Here, the mass of the core support-plate was increased from 3,712 Kg (base case) to 23,578 Kg to include the masses of the diffuser and bottom plate. This additional steel increases the initial corium mass in the reactor cavity by about 15% as shown in Figure E.1(a). Because the steel mass does not contain any decay power, increasing the mass of the corium slightly reduces its temperature when the corium is reheated after the depletion of water, as shown in Figure E.1(b). Consequently, the concrete ablation distance and containment pressure are slightly reduced (Figures E.1(c) and (d)). The results given in Figure E.1 reveal that the addition of about 20,000 Kg of steel to the corium does not enhance the oxidation process. No additional oxidation heat is generated to increase the temperature of the corium, and no additional non-condensable gases are released to pressurize the containment (Figure E.2). It was reported [8] that, for the present case, oxidation of the steel is limited by the availability of steam released from the concrete. For both the base case and the sensitivity analysis, all steam released from the concrete is consumed.

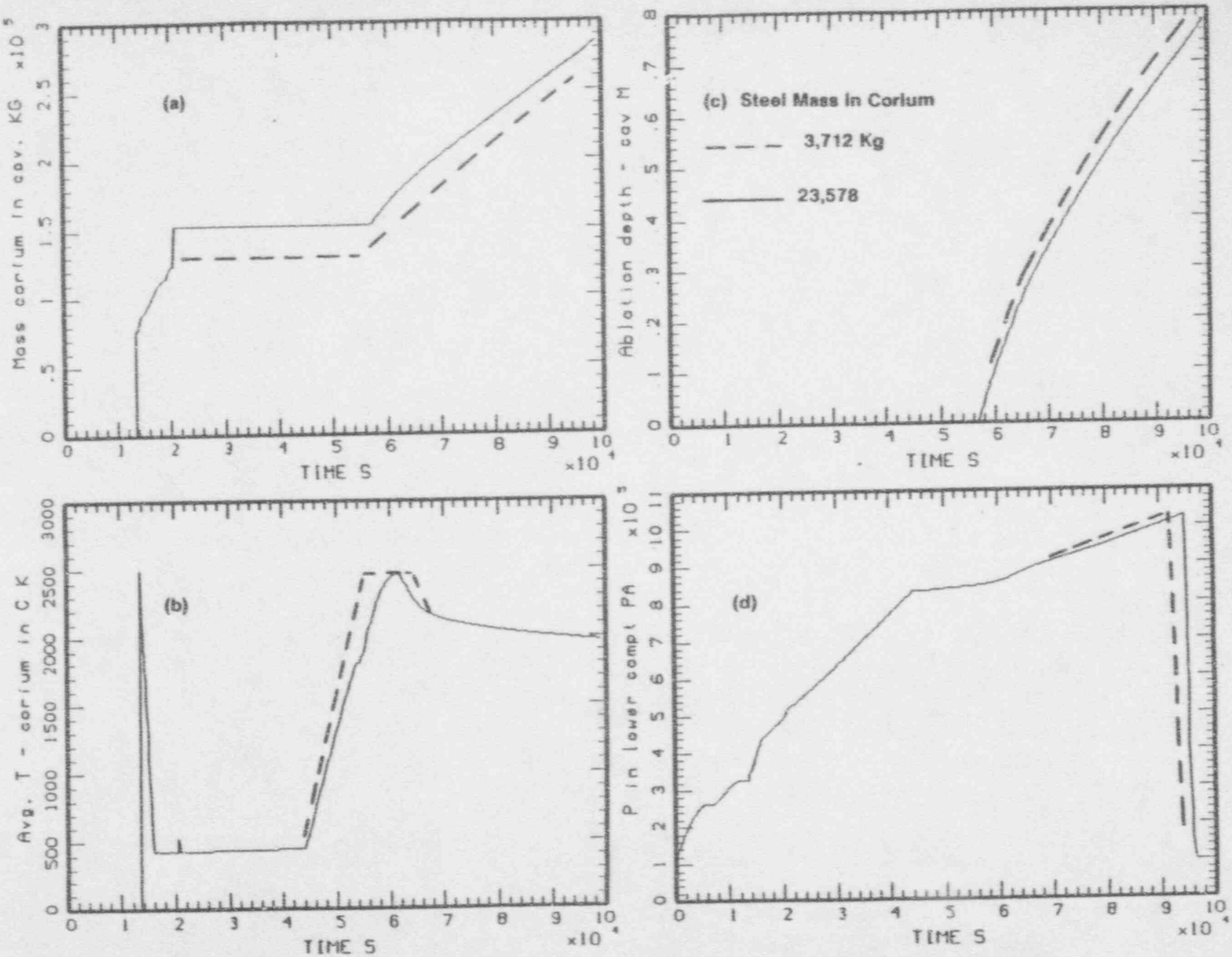

Figure E.1 Effect of Corium Steel Mass on Corium Temperature, Containment Pressure, and Ablation Depth

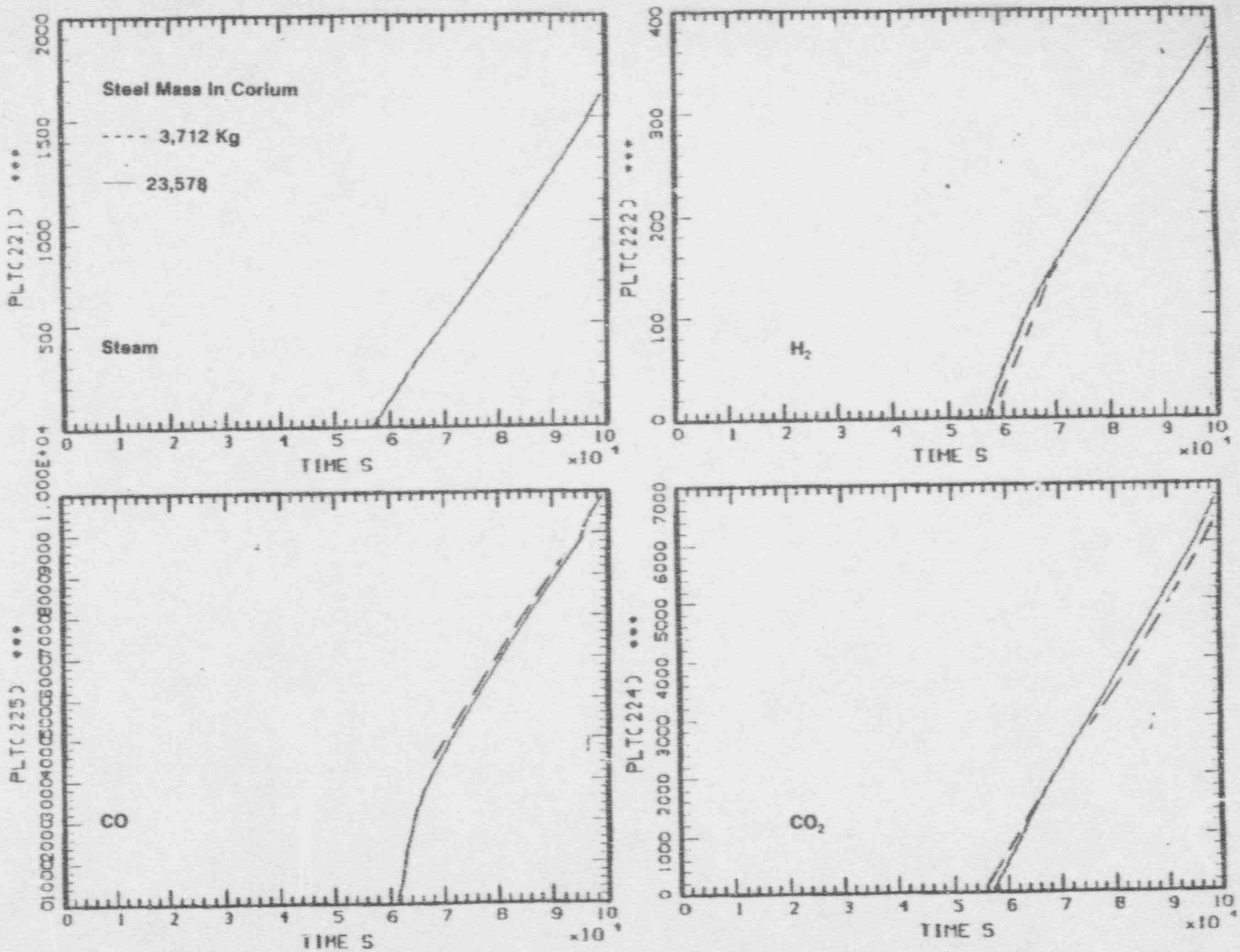

Figure E.2 Effect of Corium Steel Mass on CCI Gas Releases

4 Primary System Natural Circulation

Natural circulation is important for PWR high-pressure sequences because it plays an important role in removing decay power from the core region to the rest of the primary system. Depending on the magnitude of the circulation flow, the removal of the decay power could cause a temperature-induced failure of the hot leg or surge line.

In the MAAP code, the flow of natural circulation is calculated with a simplified one-dimensional, quasi-steady momentum balance along predefined loops. Table E.3 lists the model parameters involved in computing the flow of natural circulation for a Westinghouse-type PWR system with a U-tube steam generator geometry. Some parameters, such as FAOUT (fraction of tubes carrying flow away from the hot leg in counter-current flow calculations) and FWHL (hot leg counter-current flow coefficient) were determined by the EPRI/Westinghouse 1/7 scale experiments. In the MAAP guidance document [4], no uncertainty analysis is recommended for these two parameters.

Table E.3 Model Parameters for Natural Circulation

Model Parameter	Sensitivity Study, Ref [3]		Guidance Document, Ref. [4]	
No/Name	Base Case	Variation	Best Estimate	Uncertainty Analysis
59 VFSEP	0.6	0.25	0.6	None
9 HTSTAG	850 W/M^2-k	100,5000	850	None
10 FAOUT	0.3	0.1, 0.5	0.3	None
54 FNCBP	0	1	0, 1	0 (B&W)
53 FFRICR	0.1	0.05, 0.2	0.1	None
57 FFRICX	-0.25	0.1, 1, 0.25, -0.1, -1	0.25	None
75 FWHL	0.115	-	0.115	None
56 NSAMP	10	1, 20	10	None

Descriptions of Parameters:

VFSEP:	Void fraction in the primary system above which the phases separate and two-phase natural circulation stops.
HTSTAG:	Heat transfer coefficient between naturally circulating water and the surface of steam generator tubes.
FAOUT:	For counter-current flow calculations, fraction of tubes carrying flow away from the hot leg.
FNCBP:	Flag to denote the configuration of natural circulation assumed in core.
FFRICR:	Friction factor for axial flow in core.
FFRICX:	Friction factor for cross flow in core.
FWHL:	Coefficient used to calculate the counter-current flow in the hot leg.
NSAMP:	Coefficient used to smooth out numerical oscillations

For a once-through steam generator of a B & W type, MAAP uses a simple model which considers the counter-current flow in the candy-cane section of the hot leg. An empirical constant, similar to FWHL, is included in the model, which was correlated with limited experimental data. No sensitivity study has been reported for the once-through steam generator. The natural circulation flow in the hot leg is expected to be much smaller in the once-through steam generator design; its role in accident progression may not be significant.

The most important factor for natural circulation is the blockage model (FCRBLK), whose activation will reduce the natural circulation flow and limit the increase in temperature in the hot-leg region. The MAAP guidance document recommends that the blockage model is deactivated for the base case to increase hydrogen generation. This recommendation would increase the potential for a temperature-induced failure in the hot leg or surge line. Thus, for high-pressure sequences, the MAAP guidance document suggests that calculations are performed with and without induced hot-leg failure. This approach would cover some of the uncertainties in the modeling of core melt.

The effects of the model parameters for natural circulation reported in the sensitivity study [3] are summarized in Table E.4. These parameters have little effect on the predicted failure time of the reactor vessel and the quantity of hydrogen generated. However, some parameters affect the time of containment failure. There are two cases in which the containment fails earlier by about 5 to 6 hours.

The first case, which causes an early containment failure, involves the friction factor for cross flow in the core (FFRICX = 0.25). This value is recommended as the best estimate in the MAAP guidance document. The approach would predict an early containment failure time. The second case involves the natural circulation configuration (FNCBP) between the core and upper plenum. For FNCBP = 0 (base case for Westinghouse-type design), the return flow of natural circulation passes along the peripheral fuel assemblies. For FNCBP = 1 (recommended for the B & W-type design), the return flow of natural circulation passes through the core barrel/baffle annulus. The sensitivity study performed for the Zion plant (Westinghouse design) showed that the selection of the flow configuration could affect the containment failure time significantly. When the return flow is allowed to pass through the core barrel/baffle annulus, the containment could fail early by about 5 hours.

The MAAP guidance document [4] states that, "for most plants, the core/upper plenum natural circulation configuration parameter should be set to the default value of zero." No sensitivity study is recommended. However, for "B&W plants and perhaps some others which have significant flow area through the core baffle and through the core former plates," it is recommended that the configuration parameter be set to 1 and sensitivity calculation be performed for a high pressure station blackout sequence.

Table E.4 Effect of Natural Circulation Model Parameters

Model Parameter No/Name	Value Used	Reactor Vessel Failure, Hr.	Containment Failure, Hr.	In-Vessel Cladding Oxidation, %	Remarks
Base Case	-	4.0	36.8	25	
59 VFSEP	0.25	3.98	36.9	26	
9 HTSTAG	100	4.29	45.0	26	Delay Containment Failure
	5000	3.94	36.5	26	
10 FAOUT	0.1	3.95	36.4	28	
	0.5	4.05	45.2	27	Delay Containment Failure
54 FNCBP	1	3.80	31.4	24	Hasten Containment Failure
53 FFRICR	0.05	4.05	37.1	26	
	0.2	3.97	37.0	25	
57 FFRICX	0 1	4.05	41.7	25	Delay Containment Failure
	1	4.15	41.9	28	Delay Containment Failure
	0.25	3.99	30.4	26	Hasten Containment Failure
	-0.1	4.21	45.1	24	Delay Containment Failure
	-1	3.95	39.8	24	
56 NSAMP	1	3.88	38.1	25	
	20	4.07	38.4	25	

See Table E.3 for Model Description.

We believe that the above MAAP guidance is vague. No specific criterion is given either to define the core-baffle configuration or to assess the relative resistance of the through-core-baffle flow. In view of the importance of this parameter on containment failure time given by the MAAP sensitivity study [3], we suggest that a clear guidance be provided for all PWR plants. A sensitivity study should be performed in IPEs if there is any uncertainty on the flow pattern for a given reactor vessel design.

5 Debris Dispersal and Distribution in Containment

The dispersal of debris at the time of reactor vessel failure and its subsequent distribution in the containment will directly affect the containment's performance. These parameters are particularly important for high-pressure sequences under which direct containment heating (DCH) is a potential contributor to the failure of the containment. Table E.5 shows the model parameters of MAAP applicable to the dispersal and distribution of debris in the containment. They cover the initial vessel failure size, ablation rate, RPV failure time, and debris entrainment. All the parameters, except the initial size of the RPV failure (XRPVO), were included in the sensitivity study for the station blackout sequence [1]; their effects are summarized in Table E.6.

Table E.5 MAAP Parameters Involved With Debris Dispersal and Distribution

Model Parameter No/Name	Sensitivity Study, Ref. [3]		Guidance Document, Ref. [4]	
	Base Case	Variation	Best Estimate	Uncertainty Analysis
1 FRCOEF	0.005	0.001, 0.1	0.005	None
3 TTRX	60 S	30, 1000	Note 1	Note 2
24 TTENTR	0.5 S	0.1, 10	0.5	None
31 FENTR	0.33	0.2, 100	Note 3	None
34 NVP	1	10	1	None
XRPVO	-	-	Note 4	Note 4

Parameter Description:
FRCOEF: Friction coefficient used in calculating the reactor vessel ablation
TTRX: Delay time of the RPV lower-plenum failure
TTENTR: Time constant for debris transport from the cavity in high-pressure sequences
FENTR: Multiplier used for flooding calculation
NVP: Number of openings in RPV lower plenum that fail and discharge debris
XRPVO: Initial radius of failure in RPV lower plenum

Note:
1. 60 s for plants with penetrations; 1800 s for plants with no penetrations
2. Larger delay times are recommended for some high-pressure sequences and small break LOCA.
3. A value of 1.0 for most plants with a Zion-like instrument tunnel. This value may be reduced for other plant-specific cavity configurations.
4. Radius of penetration tubes and no uncertainty analysis. For plant with no penetrations, a value of 25 cm is recommended; and 1 cm and 50 cm for the uncertainty analysis.

In the MAAP analysis, the failure time of the lower head after contact with core debris is specified by the model parameter TTRX. The selection of the delay time depends on whether or not the lower plenum contains penetrations. The MAAP guidance document recommends a delay time of 60 seconds for plants with penetrations, and 1800 seconds for plants with no penetrations. An uncertainty analysis using longer delay times is

Table E.6 Effects of Model Parameters Described in Table E.5

Model Parameter	Value Used	Reactor Vessel Failure, Hr	Containment Failure, Hr	In-Vessel Cladding Oxidation, %	Remarks
(Base Case)		4.0	36.8	25	
FRCOEF	0.001	4.0	36.5	25	
	0.1	4.0	43.8	25	
TTRX	30	4.0	36.3	25	
	1,000	4.27	45.3	26	Late Containment Failure
TTENTR	0.1	4.0	36.8	25	
	10	4.0	42.6	25	
FENTR	0.2	4.0	37.0	25	
	100	4.0	>72	25	No containment failure in 72 hrs.
NVP	10	4.0	43.9	25	

suggested for some sequences. In the sensitivity study performed for the Zion plant, which has penetrations, containment failure was delayed by about 9 hours when the RPV failure time was postponed from 60 seconds (base case) to 1000 seconds.

A large value of the flooding multiplier (FENTR = 100) was used in the sensitivity study [1], which resulted in a considerable delay in the containment's failure time. Because the MAAP guidance document recommends the multiplier to be 1.0 or less, depending on the configuration of the cavity, this analysis may not be realistic.

Table E.6 shows that some large values of parameters, such as the friction coefficient, entrainment time constant, and number of penetrations, could also yield a later failure time.

These values are not recommended in the MAAP guidance document.

6 Debris Coolability in Containment

Following RPV failure, a large portion of core debris is relocated into the reactor cavity. Depending on the accident scenario, water could flow into the cavity before or after reactor vessel failure. The potential quenching of the debris due to corium/water interaction affects the extent of concrete erosion, generation of combustible gases, and the rate of containment pressurization. These issues are plant-specific, as they depend on the specific configuration of the cavity and water transport into the containment.

The uncertainty in the corium-concrete interaction depends on the uncertainties of the initial and boundary conditions computed by the code, such as the temperature and mass of the molten debris, the fraction of Zircaloy oxidation before vessel failure, and the quantity of water in the cavity. Many of these conditions are determined by the in-vessel melt progression, discussed in previous sections. In addition, the MAAP code has two model parameters, which can control heat transfer between the core debris and water. The two parameters were included in the sensitivity study [3], as shown in Tables E.7 and E.8. The results show that the debris film boiling coefficient (HTFB) has no significant effect on containment failure time nor on releases of fission products from the containment. However, the critical heat-flux parameter (FCHF) affects the failure time. An increase of the parameter's value from 0.14 (base case) to 0.3 delays containment failure by about 3 hours. This delay is probably due to the increased debris/water interaction, which rapidly cools the debris. Consequently, the corium-concrete interaction is reduced and less non-condensable gases are generated.

Table E.7 MAAP Model Parameters Involved With Debris Coolability

Model Parameter No/Name	Sensitivity Study, Ref.[3]		Guidance Document, Ref. [4]	
	Base Case	Variation	Best Estimate	Uncertainty Analysis
8 HTFB	300 W/M^2-K	100, 400	300	None
33 FCHF	0.14	0.12, 0.3	0.1	Note

Parameter Description:
HTFB: Coefficient for film boiling heat transfer
FCHF: Coefficient used in the formula for critical heat flux

Note: Reduce FCHF to 0.02 in the uncertainty analysis for a debris thickness of 25 cm or more. Increase the FCHF to 2.0 to make the atmosphere inert, if large burns are calculated to occur in the immediate period after vessel failure while the debris is being quenched.

Table E.8 Effect of Debris Coolability Parameters

Parameter	Value	Containment Failure, Hr.
(Base Case)		36.8
HTFB	100	36.7
	400	36.9
FCHF	0.12	36.2
	0.3	44.0

The MAAP guidance document does not recommend any uncertainty analysis for the film boiling coefficient (HTFB) because of its minor role on the corium/water interaction. For the critical heat-flux parameter (FCHF), the document recommends a value of 0.1 as the best estimate, based on the comparisons with experimental data [4]. Uncertainty analyses are recommended for cases in which the thickness of debris is 25 cm or more. For a thick debris bed, the parameter should be reduced to 0[illegible] limit heat transfer from the debris to the water. A reduction in the value of the parameter was not [illegible]d in the sensitivity study. We believe that if the critical heat flux parameter is small, it will significantly limit the cooling of the core debris. The guidance document also recommends a sensitivity analysis if hydrogen burns are predicted to occur in the immediate period after the vessel has failed, while the debris is being quenched. The recommended best estimate then is 2.0. Using this large value for the critical heat-flux calculation would increase steam generation and could, potentially, make the containment inert and prevent a hydrogen burn. This approach is non-conservative as far as combustion is concerned; however, it would predict a higher rate of pressurization in the containment.

The recent MAAP analysis of a small break LOCA sequence shows that about 170,000 Kg of water and 130,000 Kg of corium are in the reactor cavity after the penetration failure of the vessel. Because of the strong corium/water interaction (FCHF = 0.1), debris is rapidly quenched from the initial 2500 K to about 400 K within 1500 seconds. Although the quenched debris does not yield any non-condensible gases from concrete erosion, the steam generation produced by the debris/water interaction causes a pressurization rate of about 14 Pa/s in the containment. The reactor cavity water is completely boiled-off in about 28,400 seconds, and thereafter, MAAP predicts a dry cavity situation.

According to the MAAP analysis, the debris thickness is more than 25 cm for this small break LOCA sequence. Therefore, a sensitivity analysis was performed to limit the coolability of the debris, as specified in the NRC Generic Letter guidance [2]. The critical heat-flux parameter, FCHF, was reduced to 0.01 to assume a low corium/water interaction. In addition, the curb at the outlet of the cavity instrument tunnel was removed to allow water to flow from the lower compartment into the cavity. A flooded cavity was maintained for the entire transient. The results show that the temperature of the debris stays above 1850 K (i.e., an uncoolable configuration). Comparisons with the base case are shown in Table E.9. When the parameter FCHF is reduced, the debris/water interaction is decreased and, consequently, less steam generation and less pressurization are predicted. As a result of lower pressurization, the containment failure time is delayed by about 11 hours. A delay of containment failure allows a longer period of corium-concrete interaction, which in turn, results in a large release of gases from the concrete. The release of a large quantity of combustible gases is an important consideration for any accident-management strategy.

Table E.9 Debris Coolability Study

	Base Case	Sensitivity Study
FCHF	0.1	0.01
Cavity Configuration	Wet/Dry	Wet
Debris Temperature	Quenched Before Water Depletion	Above 1800 K
Average Containment Pressurization Rate	14 Pa/s prior to water depletion, 3.8 Pa/s due to corium/concrete interaction	2.6 Pa/s due to corium/concrete interaction
Concrete Erosion Distance, m	0.8	1.5
Gas Release From Concrete, Kg		
Steam	1,350	4,800
H_2	570	860
CO_2	5,700	19,000
CO	90,000	230,000
Containment Failure Time, S	92,718	134,136

Note: Concrete erosion and gas release are evaluated at the time of containment failure.

7 H_2/CO Combustion

Table E.10 summarizes the combustion parameters used in the MAAP code. The flame-flux multiplier (FLPHI), which represents all the uncertainties of the MAAP-computed flame speed, flame surface area, and gas density, is probably the most important parameter. This multiplier parameter has been determined by benchmark calculations against four series of experiments (WNRE, EPRI/ACUREX, VEGS, and NTS). At the second familiarization meeting [9], it was reported that the experimental data can be reasonably represented by using a flame-flux multiplier of 2 for quiescent conditions, and 10 for turbulent environments (i.e, when the containment's fans or sprays are turned on). For many cases, the MAAP combustion model underpredicts the burn duration with respect to the experiments when the recommended values of the flame flux multiplier are used. The MAAP model also underpredicts the combustion completeness by about 20% for some cases. Because the MAAP 3.0B combustion model was not included in the sensitivity study [3], and the MAAP analysis of a small break LOCA sequence [Appendix C] does not result in any combustion in the containment, the overall effect of the uncertainty of the flame-flux multiplier on containment performance cannot be assessed. In the MAAP guidance document [4], no recommendation is made to change the multiplier parameter for uncertainty analysis. However, a discussion of the MAAP model for ALWRs [10] suggests that if a sensitivity analysis is desired, a minimum value of 1 and a maximum value of 3 for quiescent cases are recommended. For turbulent cases, the range of the parameter should be expanded to include 3 and 12. Because of the importance of this parameter and the lack of any sensitivity study analysis, the same recommendations made by Plys and Astelford [10] for ALWRs are suggested for existing LWRs for accident sequences, in which combustion has an important contribution to the failure of containment.

Table E.10 Combustion Model Parameters

Parameter	Guidance Document	
No/Name/Description	Best Estimate	Uncertainty Analysis
36 SCALU Scale Factor on Computer Burn Velocities	1	None
60 TJBRN Gas Jet Temperature Required for Combustion to Occur	1060 K	Note 1
71 TAUTO Autoignition Temperature	983 K	Note 1
72 XSTIA Steam Mole Fraction to Make the Autoignition Inert	0.75	None
73 DXHIG Offset Concentration Used to Account for Unreliability in Ignition	0	Note 2
74 FLPHI Flame Flux Multiplier	Note 3	Note 4

Note:
1. If H_2 behavior is driven by jet-burning or auto-ignition, the two temperatures should be increased to 3000 K to terminate the effect.
2. In at least one station blackout sequence, in which no obvious ignition sources exist, a large value of DXHIG should be input.
3. The best estimate is 2 for no fans or sprays; 10 for fans or sprays.
4. Reductions in FLPHI below 1 can be used to model diffusion flames.

Uncertainty analysis for the jet-burning and auto-ignition temperatures are recommended in the MAAP guidance document which suggests that for sequences in which hydrogen behavior is driven by the jet-burning and/or auto-ignition effects, these effects are terminated by increasing the two input temperatures to test their impact on the containment's performance. Terminating these effects would allow the accumulation of H_2/CO in the containment until ignition criterion, based on concentrations, are met. This approach is a conservative one for the analysis of combustion behavior.

The reliability of the ignitors is a concern for some sequences, such as the station blackout without AC/DC power. Here, the MAAP guidance document recommends the use of a large value for the parameter DXHIG to test sensitivity to delays in the onset of burning. This approach also is a conservative one for the containment analysis of combustion behavior.

8 Summary

MAAP/PWR model parameters and some input parameters, which effect predictions of containment failure modes and containment performance, were reviewed. The review is based on 1) the PWR sensitivity study [3] performed for the station blackout sequence, 2) the MAAP guidance document [4], and 3) the MAAP analysis for a small break LOCA sequence [Appendix C]. The PWR sensitivity study includes most of the available MAAP model parameters, and covers a wide variation in their values. Only the DCH and combustion models were not considered in the sensitivity study. The MAAP guidance document recommends the best estimate values of these parameters and their ranges for a sensitivity study to use in IPEs, if needed. The discussions and recommendations given in the guidance document, in general, are adequate for IPEs. However, because of the importance of certain parameters and/or the lack of sensitivity analysis for these parameters, we recommend that the following also be considered in IPEs:

(1) Because of the importance of the model parameter FLPHI (flame flux multiplier) on the MAAP combustion model, and the lack of a sensitivity study with this parameter, we suggest that the flame flux multiplier is included in an uncertainty analysis for those sequences in which combustion plays an important role in the performance of the containment. The same values of the parameter recommended for ALWRs [10] could be used for IPEs.

(2) The MAAP sensitivity analysis performed for the Zion plant shows the importance of the flow path of in-vessel natural circulation on containment failure time. The recommendations for uncertainty analysis given by the MAAP guidance document is not clearly defined for all IPEs. We suggest that a specific criterion be developed for the selection of this parameter. The criterion should be based on the flow areas and flow resistances.

(3) The MAAP/PWR analyses indicate the importance of the latent heat of eutectic solution on hydrogen generation and containment failure-time. The maximum value (400 KJ/Kg) in the MAAP code is within the uncertainty range of the latent heat. Therefore, we suggest that this maximum value is included in the uncertainty analysis for IPEs.

In addition, this review noted that a parameter used in References 3 and 4 for sensitivity studies related to variation in fission product generation and release, also had a significant effect on containment failure time [3]. This parameter, FCRDR, allows the user to specify the conditions for which all remaining solid core debris is ejected when the vessel fails. The user specifies the fraction of original core mass, below which the remaining core is dumped into the reactor cavity. As indicated in the main report (Volume 1), we suggest that this parameter be varied also for the IPE analysis.

These recommendations are based, in large part, on information provided in the sensitivity study [3].

9 References

1. U.S. Nuclear Regulatory Commission, "Individual Plant Examination: Submittal Guidance," NUREG-1335, August 1989.

2. U.S. Nuclear Regulatory Commission, "Individual Plant Examination for Severe Accident Vulnerabilities," Generic Letter No. 80-20, November 1988.

3. G. Lowenhielm, Z.T. Mendozen, and J.M. Hall, MAAP 3.0B Sensitivity Analysis for PWR Station Blackout Sequences, EPRI NP-7192, January 1991.

4. M.A. Kenton and J.R. Gabor, Recommended Sensitivity Analyses for an Individual Plant Examination Using MAAP 3.0B, (Draft Report), Fabor, Kenton & Associates, Inc.

5. U.S. Nuclear Regulatory Commission, "Severe Accident Risks: An Assessment for U.S. Nuclear Plants, Summary Report," NUREG-1150, Second Draft for Peer Review, June 1989.

6. U.S. Nuclear Regulatory Commission, "Containment Performance Working Group Report," NUREG-1037, Draft report to comment, May 1985.

7. P. Hofmann, et. al., "Dissolution of solid UO_2 by Molten Zircaloy and its Modelling", Int. Symposium in Severe Accidents in Nuclear Power Plants, Sorrento, Italy, March 21-25, 1988.

8. Wu, Fauske & Associates, Inc., private communication, May 31, 1991.

9. MAAP Familiarization Meeting: Ex-Vessel Models, April 2-3, 1990, Rockville, Maryland.

10. M.G. Plys and R.D. Astleford, "Modifications for the Development of the MAAP-DOE code, Vol. III: A Mechanistic Model for Combustion in Integrated Accident Analysis, Task 3.4.5," DOE/ID-10216, Vol. III, Nov. 1988.

APPENDIX F
SENSITIVITY STUDIES

J. Valente

Table of Contents

1 Introduction

Appendix D compared the results of a loss of all electric power scenario for a BWR with a Mark I containment, using MAAP and MELCOR. This comparison shows that some of the most basic assumptions used in MAAP affect significant figures of merit. Among these assumptions are the amount of hydrogen produced in-vessel, the composition and physical state of the ejected core debris, the spreadability of this debris, and the heat transfer logic used to determine the coolability of the debris.

This appendix examines these issues, and ascertains whether by varying input parameters in MAAP we could obtain results which bound the inherent uncertainties. Some of the uncertainty is reflected in the predictions of alternative models such as MELCOR. MELCOR calculated earlier times for heatup of and failure of containment than MAAP. The physical form of the corium debris is at the root of much of the difference between these codes. MELCOR permits solid, as well as molten corium debris, whereas the debris is predicted to be nearly fully molten in MAAP. The previous study (Appendix D) indicated the possible variation in estimates we can observe from differences in this basic assumption.

One approach is to recommend that IPEs supported by MAAP be submitted with sensitivity studies on key input model parameters to demonstrate the variation in results. Several such parameters are investigated in this report. If such variation in input parameters is insufficient to cover the differences in outcomes between alternate severe accident analyses, model changes to the code also may be recommended.

This appendix has three attachments which provide the MAAP and MELCOR results in more detail.

2 MAAP Sensitivities

The MAAP model, as described in Appendix D, is taken as the base case. For each sensitivity case, one input parameter is varied and its effects are studied.

2.1 Two-Sided Clad Oxidation

Approximately half of the zircaloy in the core is in the fuel cladding. FAI ran a MAAP case where the input parameter FUMIN was set to the two-sided clad oxidation option. The result was an increase in H_2 generated in-vessel to 970 kg. The base case with single-sided clad oxidation produced 860 kg. Because the surface area of zircaloy is greater for the cladding than for the channel material, we might have expected more than this 13% increase in hydrogen generation For the MAAP runs, although the local channel blockage flag was chosen, a code error resulted in the no blockage model being used by MAAP for both the single- and double-sided cases.

Several phenomena contribute to these results. With greater oxidation, because of the larger surface area, greater oxidation energy is produced. This production results in a quicker heatup of the fuel cells and a faster vessel failure. The amount of increased zircaloy oxidation is affected not just by the surface area, but also by steam availability and relocation dynamics. It is the lack of steam from the lower plenum region due to the short time between lower core plate failure and vessel failure which is the dominant effect in the only mild increase in the in-vessel hydrogen production for the two-sided clad case.

The increased hydrogen production for the two-sided oxidation sensitivity run should reduce the time to containment failure. Unfortunately, this time cannot directly be compared because the sensitivity case had different options for containment modelling.

We should note that MELCOR predictions for in-vessel H_2 production range from 600 kg for the finer core nodalization to 1000 kg for the base case (see Section 3).

Table F.1 Two-Sided Oxidation

MAAP Clad Oxidation Surface Option	H_2 Produced In-Vessel Up To Vessel Failure Time (kg)	Time of Vessel Failure (Seconds)	Percent Clad and Channel Material Reacted In-Vessel
Base (Single Sided)	860	7765	28
2-Sided	970	7558	31

2.2 Composition of Corium

The MAAP guidance document [1] does not presently recommend varying the mass of the core support plate. However, Appendix D showed that there can be a considerable difference in relocated steel between MELCOR and MAAP. The BWR version of MAAP relocates the steel in the control blades, the lower core plate, and the ablated portion of the vessel lower head. This assumption excludes the steel in the upper fuel tie plate, the top guide, the lower fuel tie plate, and the control rod drive tubes, which amounts to a mass of about 50,000 kg for a commercial BWR. To observe the effect of varying the relocatable steel, the core support plate mass was varied. The effect on the time to containment failure was significant. Table F.2 shows increasing the steel mass increases the time to containment failure. The accompanying plots of Attachment 1 show that the corium temperature on the drywell floor is lowered when larger amounts of steel are added. This lower temperature reduces the concrete ablation and production of non-condensible gases.

These results imply that during the time before containment failure, the effect of the additional mass of steel in reducing concrete ablation is larger than the oxidation energy produced by the greater mass of metallic constituents (iron and chromium) in the corium. Indeed, for the two higher steel mass cases, there is little ablation to supply the necessary oxygen containing compounds (CO_2, H_2O) to the corium for oxidation. Even for cases where iron and chromium oxidation occur, the zircaloy is fully oxidized first. For the 60,000 kg of steel case, this results in no discernable oxidation of chromium until 50,000 seconds. Zirconium dioxide stopped being produced at about 30,000 seconds. These times are for masses in the pedestal.

Table F.2 Effects of Increased Core Plate Steel

Core Support Steel Plate Mass (kg)	Total Fe Mass Added to Cont. (kg)	Mass of Corium in Drywell/Pedestal (kg)	DW Concrete Ablation Depth (m)	Time DW Corium Is Above 1500 K (s)	Containment Failure Time (s)
10,000	15,000	163,000/83,000	0.4	15,000 to end of run	72,673
24,000	25,000	178,000/84,000	$6x10^{-2}$	20,000 to 60,000	85,916
60,000	30,000	182,000/85,000	$1x10^{-3}$	20,000 to 40,000	93,208

*DW = Drywell

The iron mass ejected from the vessel includes that portion of the steel from the core support plate that was predicted to melt. (This steel becomes molten through contact with the core cell above it.) Table F.2 shows that the iron mass in the containment has increased by only 15,000 kg, when the core plate mass increased from 10,000 to 60,000 kg. This difference, which is reflected in the mass of corium in the drywell, is sufficient to substantially change the concrete ablation history in this region. This can be observed by the values for time at which the corium in the drywell remains above the 1500 K ablation temperature, and the depth of concrete ablation (Table F.2).

2.3 Spreadability of Corium

As explained in the introduction, the physical form of the corium ejected from the vessel is a major modelling difference between MAAP and MELCOR. The ability of the corium to spread across the pedestal and drywell floor is affected by the physical state of the corium. In the MAAP base case, the corium was fully or nearly fully molten, and it was predicted to be distributed as 80% in the drywell and 20% in the pedestal. These ratios are determined by code logic based on options and floor area characteristics supplied by the user. Another case was run, following the MAAP guidance document [1], in which the area of the drywell floor was reduced to one-quarter of the initial value. (This area coupled with the pedestal floor area then approximately equaled the cavity floor area assumed in the MELCOR analysis). The revised MAAP results show more of the corium being retained in the pedestal region

(26% in the pedestal and 74% in the drywell). Note that the pedestal region as modeled in MAAP has a sunken floor in reference to the drywell floor. The effect of this change was to reduce the predicted containment failure time by about 12 hours to 42,021s. The early containment failure time is closer to the time of containment failure predicted by MELCOR.

2.4 Coolability of Corium

MAAP uses a homogeneous model for the corium pool in the containment. This model is very different from the model in MELCOR. As a result of the comparison for the Loss of All Electric Power scenario between the two codes, we found a large difference in time to containment failure. Parameters that may have contributed to the difference were reviewed, and the heat transfer coefficient between the corium pool and its crust were found to be important. This user-controlled input parameter affects the heat loss from the corium, and particularly the distribution of heat between the concrete surrounding the pool and the upper surface of the corium. As discussed in the description of the DECOMP subroutine in MAAP, the heat flux (q") out of corium pool surfaces is determined by the expression:

$$q'' = h[T_F - T_{F,m}] + q_v x_c \qquad (1)$$

where,

h = Convective heat transfer coefficient between corium pool and crust

T_F = Bulk temperature of the molten debris

$T_{F,m}$ = Melt temperature of debris and assumed temperature at pool-crust interface

q_v = Volumetric heat generation rate of corium

x_c = Thickness of crust

In equation (1), a change in the convective heat transfer coefficient will affect the heat transfer from the pool to the crust for all surfaces. Also, an energy balance on the crust determines its thickness, and as shown in equation (1) will affect the heat transfer from the outer surfaces of the corium crust.

For a small value of "h", the crust at the upper surface will be thicker than for a larger value of "h". By raising the value of "h", a greater amount of heat is transferred to the crust. To dissipate this heat, the crust thickness is reduced and its outer surface temperature increases. With a small thickness, less heat will be produced by the volumetric source term [$q_v x_c$]. However, the total heat loss from the outer surface is controlled by the atmospheric convective term, the radiation term to the concrete surrounding walls, and the temperatures of the heat transfer nodes.

There also is an effect on the crust surfaces in contact with the concrete. Again a higher "h" will be compensated for by an increased heat flux to the concrete. An increased heat flux will, in turn, lower the crust thickness. However, although the heat transfer driving potential (crust outer surface temperature in contact with the concrete) will rise, we may not see a change in the conductive heat transfer coefficient, i.e., the contact heat transfer coefficient between crust and concrete.

The result may be a smaller increase in the heat removed from the crust to concrete, than from crust to atmosphere because of a rise in "h". This would be governed by the $q_v x_c$ term in equation (1).

In mathematical notation:

$$\frac{\partial q''}{\partial h} = [T_F - T_{F,m}] + \frac{\partial (q_v\, x_c)}{\partial h} \tag{2}$$

To compare the heat split between the concrete ($_c$) and atmosphere ($_u$), the T_F - $T_{F,m}$ term would be the same.

$$\left.\frac{\partial q''}{\partial h}\right|_{u} = [T_F - T_{F,m}] + \frac{\partial (q_v\, x_c^{u})}{\partial h} \tag{3}$$

and

$$\left.\frac{\partial q''}{\partial h}\right|_{c} = [T_F - T_{F,m}] + \frac{\partial (q_v\, x_c^{c})}{\partial h} \tag{4}$$

Equations (3) and (4) show that $\frac{\partial q''}{\partial h}$ will be equal if the crust thickness changes are the same. However, this should not be true for the reasons explained.

Hence, increasing "h" should result in a greater initial transient heat loss from the corium pool and a quicker rise in concrete and atmospheric temperatures. Further, it should result in a greater percentage rise in the heat loss upward versus downwards or sideways (although, this may be small). Based on the above discussion we would expect that increasing the value of "h" will increase the generation of non-condensable gas, possibly raise chemical reaction energy in the corium pool, and increase the heat transfer to the atmosphere.

As shown in Table F.3, increasing the value of "h" substantially decreased the time to containment failure. The primary cause was an increase in the generation rate of non-condensible gas from core-concrete-interaction (CCI). In particular, the drywell concrete now undergoes substantial ablation because the higher "h" allowed a sustainable ablation temperature in the drywell floor.

3 MELCOR Sensitivity

We conducted a sensitivity study based on increasing the number of core nodes to investigate its effects on the timing of in-vessel phenomena and H_2 production. A 5x7 active fuel zone mesh was created from the 3x5 configuration of the base case. The two inner rings of the base case and the two upper fuel containing horizontal rows of cells were each split in half for the 5x7 configuration. First, fuel melting had been predicted in this region. Numerous input changes were needed to incorporate this new mesh.

Table F.3

Heat Transfer Coefficient J/S-K-m^2	Time of Containment Failure (TOF) (s)	DW Temperature at TOF (K)	Concrete Ablated at TOF DW/Pd (m)	Global H_2 Mass at TOF (kg)
1,000	85,916	710	.6x10^{-2}/0.72	1250
10,000	66,816	680	0.28/0.66	1500

TOF = Time of Containment Failure
Pd = Pedestal

3.1 Enhanced Core Nodalization

Increasing the number of core nodes gave interesting results:

1) The in-vessel H_2 production dropped.
2) The time between the failure of the core support plate and vessel failure dropped significantly.

The second of these effects is because of the unique geometric configuration of the lower plenum. Essentially, with an equal corium mass located in a volumetrically smaller cell, more of the penetration surface area will be in contact with the corium. This is because the corium is not permitted to spread radially across ring boundaries. The lowest lower plenum cell contains the corium available for penetration attack. The amount of corium initially relocated to the lower plenum is the same for both cases, because even though the 5 x 7 run has less total core mass in its interior rings, a greater percentage of the cladding has melted in the ring that fails first.

In the version of MELCOR we used, when the corium relocates, only a small amount of the particulate debris passes by the lower intact core to attack the core support plate. For the 5 x 7 core, the amount relocated to a given core support plate ring is smaller than for the 3 x 5 core. Because this results in boil-off of the water above the plate, this action affects both further core heating and relocation, as well as hydrogen production. The Zr available for oxidation is either in an intact geometry or has a distorted surface area due to candling. The output from the

MELCOR runs suggests that channel material can remain in some of the axially higher regions of the core after the fuel clad has relocated.

In both cases, however, it is the same geometrically located material, ring 2 (R2) in the 3 x 5 core, and R3 in the 5 x 7 core, that first fails the plate. In the 5 x 7 core, the amount of zirconium in conglomerate form is greater at the plate failure time. Both cases show about 600 kg of H_2 produced up to the plate failure times, but because of the difference in time between plate failure and vessel failure, and possibly the surface area of zirconium available in conglomerate form, the 3 x 5 core produces far greater in-vessel H_2. None or very little zirconium has been transported to the lower plenum at the time of vessel failure, therefore, H_2 continues to be produced above the plate. The lack of a corium spreadability model in the lower plenum is the dominant phenomena that should be investigated for both its direct effect on vessel failure time and its synergistic effect on hydrogen production. It is not realistic to assume that no corium spreading will occur outside the immediate region of plate failure. Perfect spreading of the debris may not occur either. MELCOR does allow the modeler to adjust the vessel penetration characteristics and the height of the lowest lower plenum cell. These could be used to tune the surface area of the vessel penetration attack and heat transfer characteristics, if desired. However, any such tuning would be based on altering some physical parameters to match an estimate of the degree of corium spreadability in the lower plenum.

4 Conclusions and Recommendations

The basic assumptions of the corium's physical properties, especially solid vs. liquid form, have a major impact on the time to containment failure. Of the four sensitivity cases conducted with MAAP, the assumption regarding corium spreadability has the greatest effect. By reducing the spread of the corium to an area closer to that used in MELCOR, we can obtain relatively close agreement in containment failure times predicted by the two codes. The MELCOR floor area available for CCI was twice the pedestal area of MAAP. In the MAAP sensitivity study a similar floor surface area resulted in a containment failure time of 42,000 s, which is only 40% larger than the failure time of approximately 30,000 s predicted by MELCOR. This input parameter variation is recommended in the guidance document [1], and BNL strongly agrees with this recommendation.

The sensitivity of the MAAP results to the corium pool-to-crust heat transfer coefficient, "h", also is strong. An order of magnitude increase in "h" reduced the time to containment failure by about 25%.

In MAAP, when UO_2 and Zr are expelled from the Reactor Pressure Vessel (RPV), the assumption of a homogenous corium pool allows close and total contact between the UO_2 and Zr. An equilibrium constant is calculated for the reaction:

$$UO_2 + Zr \rightarrow U + ZrO_2$$

which results in a chemical reduction of UO_2. In this way, a substantial amount of $Zr\ O_2$ is created at the time of vessel failure. With this assumption, MAAP assures that nearly all the Zr will be oxidized.

Table F.4 Comparison of Key Timing Events

		3x5	5x7
Core Uncovery	(s)	2500	2900
Clad Perforation	(s)	4060	4576
H_2 Generated	(s)	4000	4500
Clad Melt	(s)	5000	5500
Fuel Relocated	(s)	5000	5500
Fuel on Core Support Plate	(s)	5500	5600
Core Support Plate Failure	R1(s)	9800	8000
	R2(s)	6500	8800
	R3(s)	15,500	7400
Vessel Failure	R1(s)	9910	8099
	R2(s)	12,077	8755
	R3(s)		7458
Cavity Receives Mass	(s)	14,900	11,400
Concrete Attack	(s)	20,000	11,400
Containment Failure Time	(s)	31,820	27,241
Initial Corium Mass Relocated to Lower Plenum (kg)		29,000	29,000
Mass of Corium in L.P. at time of Vessel Failure (kg)		100,000	29,000
Water in Lower Plenum at TOF (tons)		21	41
Wetwell Airspace Temp. at TOF (K)		350	350
Drywell Airspace Temp. at TOF (K)		1300	975
DW Pressure at TOF (psia)		130	130
H_2 produced in vessel at the time of vessel failure (kg)		1000	600
Mass of H_2 Produced in vessel at TOF (kg)		1140	760

Note: Ri = i^{th} ring

The oxidation of the uranium will then occur based on the availability of H_2O and CO_2 released from concrete ablation. From 20,000 to 50,000 s, the base case shows little uranium oxidation (about 20,000 kg), while the sensitivity case shows nearly four times this value (80,000 kg). Thus, though the amount of oxidized Zr in the two cases is similar, the chemical energy released is higher for the sensitivity case because of the oxidation of uranium. The threshold of ablation in MAAP is therefore important. In MAAP, there is no release of free water in the concrete until the ablation temperature is reached, but substantial ex-vessel zirconium oxidation is guaranteed without steam being available.

If a case shows insufficient corium energy to produce ablation, parameters which can affect corium spreadability and corium heat flux should be varied to determine their effects. Therefore, there is a need, to reduce the spreadability of the corium, and possibly at the same time varying the value of "h" to initiate concrete ablation. The former sensitivity should capture most of the concern over ablation, however.

In-vessel oxidation of zirconium is enhanced by two-sided oxidation; the effects will be very dependent on the accident under investigation. For the station blackout scenario that we investigated, it is important. However, MAAP's increase in hydrogen with two-sided oxidation did not substantially change containment challenge time. The major effect is the amount of water in the lower plenum which is made available to the zirconium remaining in the core. Because of MAAP's rather short time predictions for the time between lower core plate failure and vessel failure, little of this water is available for H_2 generation in-vessel. Therefore, to compensate for the possibility of more steaming from lower plenum water, BNL recommends the use of the no-blockage model and single-sided clad oxidation for the base case. A lower estimate for in-vessel hydrogen generation can be obtained using the local blockage model and the single-sided clad oxidation surface, a higher estimate can be obtained using no local blockage and a double-sided clad oxidation surface.

The MAAP sensitivity case for core support plate steel showed a monotonic trend in the time to containment failure. Increasing the steel increases the time to failure. There was little effect on vessel failure time or in-vessel H_2 production. The difference in containment failure time is related to ablation of drywell concrete for the 10,000 kg case and lack of ablation in the 24,000 kg case. The lower steel mass resulted in significant H_2 production and ablation of the concrete in the drywell. In both the 24,000 kg and 60,000 kg case, the amount of ablation was small. Still, somewhat more H_2 is produced for the 24,000 kg case, and the corium is hotter over most of the time span of interest. Therefore, any altering of the chemical reactions or increased corium mass are insufficient to compensate for the lowering the effective long term corium temperature, when the steel mass of the core plate is increased. The use of the true steel mass of the plate, as recommended in the guidance document, [1] is appropriate with the CCI model presently used.

The oxidation of the metals composing the corium pool on the concrete is much different for MAAP and MELCOR. The ejection sequence of the available metals in the RPV is important in this regard. The effect on oxidation energy is strong. There are periods of time in the MELCOR calculation during which the oxidation energy is greater (by almost an order of magnitude) than the decay heat. In MAAP, decay heat always dominates. MAAP's low oxidation energy may need further investigation.

Summarizing, the sensitivity runs discussed above have resulted in the following recommendations:

- For in-vessel hydrogen generation in a BWR, assuming the base case is calculated with single-sided clad oxidation and no local blockage, BNL recommends two sensitivity calculations; one with the two-sided oxidation and no local blockage, and one with single-sided oxidation with local blockage.

- For core-concrete interaction (CCI) modeling in a BWR, BNL recommends a base case assuming only one-quarter of the drywell floor area is available for concrete attack. A sensitivity is recommended in which all the drywell floor is available for attack.

5 References

1. Kenton, M.A. and Gabor, J.R., "Recommended Sensitivity Analyses for an Individual Plant Examination Using MAAP 3.0B," Gabor, Kenton and Associates, Inc.

ATTACHMENT 1

Fauske & Associates, Inc.

May 31, 1991

Dr. J. Valente
Safety & Risk Evaluation Division
Brookhaven National Laboratory
Building 130
Upton, Long Island, NY 11973

SUBJECT: MAAP SENSITIVITY STUDIES FOR THE MELCOR/MAAP COMPARISON

Dear Dr. Valente:

Enclosed are the results of MAAP sensitivity studies and a floppy disk which contains four modified subroutines from BWR MAAP 3.0B revsion 7.0 for the MAAP/MELCOR comparison. Five cases were run and compared here. The figures of merit of the original case is also attached for comparison. Differences among the cases are described below.

Case 0 (BNL_SBO)
The original case.

Case 1 (BNL_MCSP0)
The core plate mass was increased to 60,000 kg from 24,000 kg in the original case.

Case 2 (BNL_MCSP1)
The core plate mass was reduced to 10,000 kg from 24,000 kg in the original case.

Case 3 (BNL_HT4)
The corium-crust heat transfer coefficient was increased to 10,000 (J/(SEC*K*M**2) from 1000 (J/(SEC*K*M**2)) in the original case.

Case 4 (BNL_DW0)
The pedestal floor elevation was raised to drive the debris to the drywell. The drywell liner was changed as an adiabatic wall. The drywell floor area was set equal to the pedestal floor area, which is about one quarter of the original drywell floor area.

Case 5:(BNL_DW1)
This is essentially same as case 4 (BNL_DW0) except that two sided oxidation model was used (FUMIN=2) on hydrogen generation.

16W070 West 83rd Street • Burr Ridge, Illinois 60521 • (708) 323-8750
Telefax (708) 986-5481

Case 1 and 2 are the sensitivity studies of the core plate steel mass. The results showed that adding more steel in the core plate increased the debris mass in the containment. Because the additional steel mass was served as heat sink in the debris, the debris temperature and concrete attacking rate were decreased which caused containment failure later.

Case 3 is the sensitivity study of the corium-crust heat transfer coefficient. Containment failure time was sooner in this case because the debris temperature in the drywell was above the concrete melting temperature to cause strong concrete attack.

Case 4 is the sensitivity study of the debris spreading in the containment. Debris was forced to stay in the drywell with small floor area. Less heat loss from debris to the gas caused strong concrete attack and earlier containment failure.

If you have questions regarding this transmittal, please do not hesitate to call me at (708) 887-5243 or Marty Plys at (708) 887-5207.

Sincerely yours,

Toby Wu
Method Development Group

cc: R. J. Hammersley
M. G. Plys

CASE 6 BNL-ADWF4
= BNL-SBO but with ADWF = 33 m² = 1/4 Drywell Floor

core plate mass vs time for 3 core plate mass cases (MCSPT=10,000, BNL-SBO, MCSPT=60,000)

Corium Crust & Pool parameters for SB o/H = 10000 Case

ZWV	Water Level in RV
TS1HS1	T OF INNER PD WALL
TS1HS2	T OF INNER DW WALL
TS1HS3	T OF DRYWELL FLOOR
TS1HS4	T OF TORUS ROOM WALL
THS1P(1)	T OF INNER PD WALL
THS2P(1)	T OF INNER DW WALL
THS3P(1)	T OF DRYWELL FLOOR
TCNPD(1)	T OF CONCRETE IN PD
TCNDW(1)	T OF CONCRETE IN DW
TWPS	WATER TEMP IN PS
TSATPS	SAT TEMP IN PS
TLCMLP	CORIUM TEMP IN LP
T11OP	MAX CORE NODE TEMP
UCMLP	CORIUM ENERGY IN LP
TWDW	WATER TEMP IN DW
MWDW	WATER MASS IN DW
MCMTDW	CORIUM MASS IN DW
MCMDW(1)	U OF MASS OF CORIUM IN DW
MCMDW(2)	UO2 MASS OF CORIUM IN DW
MCMDW(3)	C MASS OF CORIUM IN DW
MCMDW(4)	ZR MASS OF CORIUM IN DW
MCMDW(5)	ZRO2 MASS OF CORIUM IN DW
MCMDW(6)	CR MASS OF CORIUM IN DW
MCMDW(7)	CR203 MASS OF CORIUM IN DW
MCMDW(8)	FE MASS OF CORIUM IN DW
NF02DW	MOLE FRAC 02 IN DW
NFSTDW	MOLE FRAC STEAM IN DW
NFN2DW	MOLE FRAC N2 IN DW
TWPD	WATER TEMP IN PD
MWPD	WATER MASS IN PD
XWPD	WATER HEIGHT IN PD
MCMTPD	CORIUM MASS IN PD
NF02PD	MOLE FRAC 02 IN PD
NFC2PD	MOLE FRAC CO2 IN PD
NFSTPD	MOLE FRAC STEAM IN PD
NFC0PD	MOLE FRAC CO IN PD
NFN2PD	MOLE FRAC N2 IN PD
MCMPD(1)	U MASS OF CORIUM IN PD
MCMPD(2)	UO2 MASS OF CORIUM IN PD
MCMPD(3)	C MASS OF CORIUM IN PD
MCMPD(4)	ZR MASS OF CORIUM IN PD
MCMPD(5)	ZR02 MASS OF CORIUM IN PD
MCMPD(6)	CR MASS OF CORIUM IN PD
MCMPD(7)	CR203 MASS OF CORIUM IN PD

MCMPD(8)	FE MASS OF CORIUM IN PD
MCMTWW	CORIUM MASS IN WW
NFN2WW	MOLE FRAC N2 IN WW
MCMWW(1)	U MASS OF CORIUM IN WW
MCMWW(2)	UO2 MASS OF CORIUM IN WW
MCMWW(3)	C MASS OF CORIUM IN WW
MCMWW(4)	ZR MASS OF CORIUM IN WW
MCMWW(5)	ZRO2 MASS OF CORIUM IN WW
MCMWW(6)	CR MASS OF CORIUM IN WW
MCMWW(7)	CR203 MASS OF CORIUM IN WW
MCMWW(8)	FE MASS OF CORIUM IN WW
MFPREX(1)	MASS NOBLES EX-VSL
MFPREX(2)	MASS CSI/RBI EX-VSL
MFPREX(3)	MASS TEO2 EX-VSL
MFPREX(4)	MASS SRO EX-VSL
MFPREX(5)	MASS MOO2 EX-VSL
MFPREX(6)	MASS CSOH EX-VSL
MFPREX(7)	MASS BAO EX-VSL
MFPREX(8)	MASS LANTHANDS EX-VSL
MFPREX(9)	MASS CEO2 EX-VSL
MFPREX(10)	MASS SB EX-VSL
MFPREX(11)	MASS TE2 EX-VSL
MFPREX(12)	MASS UO2+ EX-VSL
MFPRIN(1)	MASS NOBLES IN-VSL
MFPRIN(2)	MASS CSI/RBI IN-VSL
MFPRIN(3)	MASS TE02 IN-VSL
MFPRIN(4)	MASS SRO IN-VSL
MFPRIN(5)	MASS M002 IN-VSL
MFPRIN(6)	MASS CSOH IN-VSL
MFPRIN(7)	MASS BAO IN-VSL
MFPRIN(8)	MASS LANTHANDS IN-VSL
MFPRIN(9)	MASS CEO2 IN-VSL
MFPRIN(10)	MASS SB IN-VSL
WWDCCR	WATER FLOW RATE FROM DC TO CORE
WSTCR	STEAM FLOW RATE FROM CORE
XWB	WATER HEIGHT IN B COMPT

Table 4-3

DESCRIPTION OF BWR PLOT FILES

First Plot File - Primary System (Default File #41)

TIME	Time since accident initiation.
PPS	Pressure in the primary system.
QCORE	Total core power.
TGPS	Average temperature of gas in the primary system.
TWLP	Temperature of water in the lower plenum.
TWSH	Temperature of water in the shroud.
WCORI	Core inlet flow rate.
WSTBRK	Steam flow rate through the break (lower plenum).
WFLSH	Flashing rate in the shroud.
WFLLP	Flashing rate in the lower plenum.
WFLPS	Flashing rate in the core.
MGLOBE	Global mass balance on water.
WWLOCA	Water flow rate through LOCA.
MWSH	Mass of water in the shroud.
WJETO	Total flow rate from downcomer to lower plenum.
MWLPP	Mass of water in the lower plenum.
MWPSP	Mass of water in the core.
MSTPS	Mass of steam in the primary system.
MU2CT	Mass of UO_2 in the core.
MLCMLP	Mass of molten corium in the lower plenum.
XHCMLP	Height of corium in the lower plenum.
MCRUST	Mass of corium in frozen crust (lower plenum).
XWJET	Height of water in the jet pumps (ref. to bottom of vessel).
XWCOR	Height of water in the core (ref. to bottom of vessel).
XWSH	Height of water in the shroud (ref. to bottom of vessel).
TIMRAT	Ratio of accident time to CPU time.
QDECAY	Decay power.
WWBRK	Flowrate of water through the lower head failure.

Table 4-3 (Continued)

DESCRIPTION OF BWR PLOT FILES

Second Plot File - Heatup (Default File #42)

TIME	Time since accident initiation.
WSCOR	Steam flow rate out of the core.
WH2COR	Hydrogen flow rate out of the core.
MWBYP	Mass of water in the core bypass region.
TCORO	Temperature of core outlet gases.
XW(1)	Boiled up water level in radial region 1 (ref. to bottom of core).
XW(2)	Boiled up water level in radial region 2 (ref. to bottom of core).
XW(3)	Boiled up water level in radial region 3 (ref. to bottom of core).
XW(4)	Boiled up water level in radial region 4 (ref. to bottom of core).
XW(5)	Boiled up water level in radial region 5 (ref. to bottom of core).
T11OP	Maximum temperature in core.
T15P	Average core temperature.
WECCSS	Core spray flow rate.
WECCSI	ECCS injection flow rate.
WSTRV	Flow rate of steam through the relief valves.
XHLPCI	Net positive suction head at LPCI pump.
XHLPCS	Net positive suction head at LPCS pump.
XHHPCS	Net positive suction head at HPCS pump.
XHRCIC	Net positive suction head at RCIC pump.
XHHPCI	Net positive suction head at HPCI pump.
PDWWW	Pressure difference between drywell and wetwell.
VLCSTP	Volume of water in the condensate storage tank.

Table 4-3 (Continued)

DESCRIPTION OF BWR PLOT FILES

Fourth Plot File - Pedestal and Wetwell (Default File #44)

TIME	Time since accident initiation.
NFH2WW	Mole fraction of H_2 in the wetwell.
PWW	Pressure in the wetwell.
TFLWW	Flame temperature in the wetwell.
TGWW	Temperature of gas in the wetwell.
TCMWW	Temperature of corium in the wetwell.
NFO2WW	Mole fraction of O_2 in the wetwell.
NFC2WW	Mole fraction of CO_2 in the wetwell.
NFSTWW	Mole fraction of steam in the wetwell.
NFCOWW	Mole fraction of CO in the wetwell.
MU2WWP	Mass of UO_2 in the wetwell.
PPD	Pressure in the pedestal.
TCMPD	Temperature of corium in the pedestal.
TGPD	Temperature of gar in the pedestal.
MU2PDP	Mass of UO_2 in the pedestal.
NFH2PD	Mole fraction of H_2 in the pedestal.
XCNPDP	Concrete ablation thickness in the pedestal.
MWPDPP	Mass of water in the pedestal.
MWSP	Mass of water in the suppression pool.
TWSP	Temperature of water in the suppression pool.
XSPWW	Level of water on the wetwell side of the suppression pool.
XSPDW	Level of water on the drywell side of the suppression pool (downcomer).
TETSP	Temperature of torus shell (Mark I).
THS2P(1)	Temperature of gas in torus room (Mark I).
THS2(1)	Temperature of heat sink #2 (node 1).

Table 4-3 (Continued)

DESCRIPTION OF BWR PLOT FILES

Fifth Plot File (Continued)

FMCSID	Fraction of CsI in the drywell and pedestal.
FMCSIW	Fraction of CsI in the wetwell.
FMCSIR	Fraction of CsI released from containment.
MFPREX(3)	Mass of Group 3 fission products released ex-vessel.
MFPREX(4)	Mass of Group 4 fission products released ex-vessel.
MFPREX(5)	Mass of Group 5 fission products released ex-vessel.
MFPREX(6)	Mass of Group 6 fission products released ex-vessel.
MFPREX(7)	Mass of Group 7 fission products released ex-vessel.
MFPREX(8)	Mass of Group 8 fission products released ex-vessel.
MFPREX(9)	Mass of Group 9 fission products released ex-vessel.
MFPREX(10)	Mass of Group 10 fission products released ex-vessel.
MFPREX(11)	Mass of Group 11 fission products released ex-vessel.
MFPREX(12)	Mass of Group 12 fission products released ex-vessel.

Table 4-3 (Continued)

DESCRIPTION OF BWR PLOT FILES

Seventh Plot File - Mark III Only (Default File #47)

TIME	Time since accident initiation
NFH2CA	Mole fraction of H_2 in compartment A.
PCA	Pressure in compartment A.
TFLCA	Flame temperature in compartment A.
TGCA	Temperature of gas in compartment A.
NFO2CA	Mole fraction of O_2 in compartment A.
NFC2CA	Mole fraction of CO_2 in compartment A.
NFSTCA	Mole fraction of steam in compartment A.
HFCOCA	Mole fraction of CO in compartment A.
NFH2CB	Mole fraction of H_2 in compartment B.
PCB	Pressure in compartment B.
TFLCB	Flame temperature in compartment B.
TGCB	Temperature of gas in compartment B.
NFO2CB	Mole fraction of O_2 in compartment B.
NHC2CB	Mole fraction of CO_2 in compartment B.
NFSTCB	Mole fraction of steam in compartment B.
NFCOCB	Mole fraction of CO in compartment B.
MWCBP	Mass of water in compartment B.

Table 4-3 (Continued)

DESCRIPTION OF BWR PLOT FILES

Auxiliary Building Output File (Continued)

WRB9	Same from node 9 to 10.
WRB10	Same from node 10.
FMTOTP1	Fraction of the fission product group 1 released from the primary containment.
FMTOTP2	Same for group 2.
FMTOTP3	Same for group 3.
FMTOTP4	Same for group 4.
FMTOTP5	Same for group 5.
FMTOTP6	Same for group 6.
FMSGTP1	Fraction of fission product group 1 drawn into the SGTS.
FMSGTP2	Fraction of fission product group 2 drawn into the SGTS.
FMSGTP3	Fraction of fission product group 3 drawn into the SGTS.
FMSGTP4	Fraction of fission product group 4 drawn into the SGTS.
FMSGTP5	Fraction of fission product group 5 drawn into the SGTS.
FMSGTP6	Fraction of fission product group 6 drawn into the SGTS.
FMENVP1	Fraction of fission product group 1 released to the environment (not through SGTS*).
FMENVP2	Fraction of fission product group 2 released to the environment (not through SGTS*).
FMENVP3	Fraction of fission product group 3 released to the environment (not through SGTS*).
FMENVP4	Fraction of fission product group 4 released to the environment (not through SGTS*).

*Note that the fractional releases from the SGTS system to the environment are obtained by multiplying the fraction of each group drawn into the SGTS system by the assumed filter efficiency.

```
NUMERICAL    PERFORMANCE    FIGURES    OF    MERIT
----------------------------------------------------

TIME (SEC) . . . . . . . . . . . . . . .    144002.2        CASE Ø

FRACTION OF CLAD REACTED IN VESSEL . .        0.2762
CONCRETE AEROSOL GENERATED (KG). . . .        528.5

UO2 MASS IN PEDESTAL (KG). . . . . . .      32884.4
UO2 MASS IN DRYWELL (KG) . . . . . . .     136499.7

TIME OF CORE UNCOVERY (SEC). . . . . .       1897.7
TIME OF VESSEL FAILURE (SEC) . . . . .       7764.8
TIME OF CONTAINMENT FAILURE (SEC). . .      85916.2

CSI MASS BALANCE (KG)

    INITIAL MASS . . . . . . . . . . .      38.2155
    IN CORE. . . . . . . . . . . . . .       0.0000
    IN CORIUM. . . . . . . . . . . . .       0.5605
    IN PRIMARY SYSTEM. . . . . . . . .       8.3677
    IN CONTAINMENT . . . . . . . . . .      22.0989
    TOTAL IN-VESSEL RELEASED . . . . .      37.3001
    TOTAL EX-VESSEL RELEASED . . . . .       0.3549
    RELEASED FROM CONTAINMENT. . . . .       7.1882

SRO MASS BALANCE (KG)

    INITIAL MASS . . . . . . . . . . .     103.4367
    IN CORE. . . . . . . . . . . . . .       0.0000
    IN CORIUM. . . . . . . . . . . . .     103.1911
    IN PRIMARY SYSTEM. . . . . . . . .       0.0621
    IN CONTAINMENT . . . . . . . . . .       0.2029
    TOTAL IN-VESSEL RELEASED . . . . .       0.0700
    TOTAL EX-VESSEL RELEASED . . . . .       0.1950
    RELEASED FROM CONTAINMENT. . . . .       0.0000


FORTRAN STOP
$ delete BNL_SBO_inp.dat;*
$ delete BNL_SBO_par.dat;*
$!
$ node = "M3300"
$ if "FALSE".eqs."FALSE" then logoff/full
  WUTOBY       job terminated at  9-APR-1991 10:10:43.43

  Accounting information:
  Buffered I/O count:            622     Peak working set size:   1395
  Direct I/O count:            12755     Peak page file size:     4600
  Page faults:                  2176     Mounted volumes:            0
  Charged CPU time:    0 00:00:41.54     Elapsed time:     0 00:51:11.18
```

CASE 1

MCSPT = 60,000 kg

```
NUMERICAL   PERFORMANCE   FIGURES   OF   MERIT

TIME (SEC) . . . . . . . . . . . . . .          144002.8

FRACTION OF CLAD REACTED IN VESSEL . .            0.2789
CONCRETE AEROSOL GENERATED (KG). . . .            430.2

UO2 MASS IN PEDESTAL (KG). . . . . . .          32424.2
UO2 MASS IN DRYWELL (KG) . . . . . . .         136959.6

TIME OF CORE UNCOVERY (SEC). . . . . .           1897.7
TIME OF VESSEL FAILURE (SEC) . . . . .           7764.4
TIME OF CONTAINMENT FAILURE (SEC). . .          93208.0

CSI MASS BALANCE (KG)

     INITIAL MASS . . . . . . . . . . .          38.2155
     IN CORE. . . . . . . . . . . . . .           0.0000
     IN CORIUM. . . . . . . . . . . . .           0.5763
     IN PRIMARY SYSTEM. . . . . . . . .           9.0641
     IN CONTAINMENT . . . . . . . . . .          22.0491
     TOTAL IN-VESSEL RELEASED . . . . .          37.3025
     TOTAL EX-VESSEL RELEASED . . . . .           0.3365
     RELEASED FROM CONTAINMENT. . . . .           6.5257

SRO MASS BALANCE (KG)

     INITIAL MASS . . . . . . . . . . .         103.4367
     IN CORE. . . . . . . . . . . . . .           0.0000
     IN CORIUM. . . . . . . . . . . . .         103.2213
     IN PRIMARY SYSTEM. . . . . . . . .           0.0621
     IN CONTAINMENT . . . . . . . . . .           0.1742
     TOTAL IN-VESSEL RELEASED . . . . .           0.0700
     TOTAL EX-VESSEL RELEASED . . . . .           0.1663
     RELEASED FROM CONTAINMENT. . . . .           0.0001

FORTRAN STOP
$ delete BNL_MCSPO_inp.dat;*
$ delete BNL_MCSPO_par.dat;*
$!
$ node = "N780"
$ if "FALSE".eqs."FALSE" then logoff/full
  WUTOBY        job terminated at 31-MAY-1991 11:54:00.89

  Accounting information:
  Buffered I/O count:             619     Peak working set size:  1288
  Direct I/O count:             13076     Peak page file size:    4600
  Page faults:                   2254     Mounted volumes:           0
  Charged CPU time:     0 00:00:45.55     Elapsed time:     0 01:03:02.02
```

MAAP-MELCOR: BWR SBO. MCSPT = 60.000 KG
BNL_MCSPO_43.PLT LINE

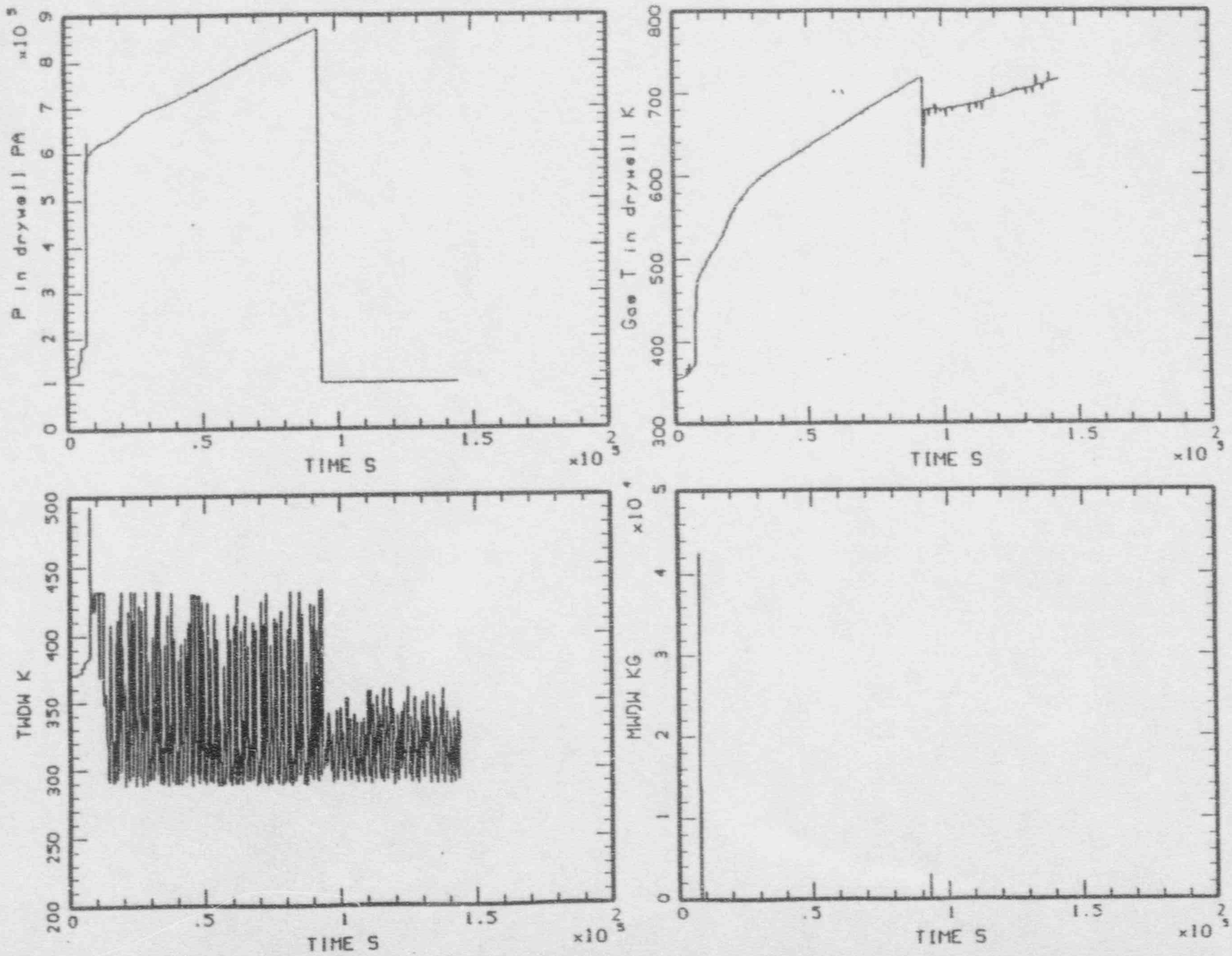

MAAP-MELCOR: BWR SBO. MCSPT = 60,000 KG
BNL_MCSPO_43.PLT LINE

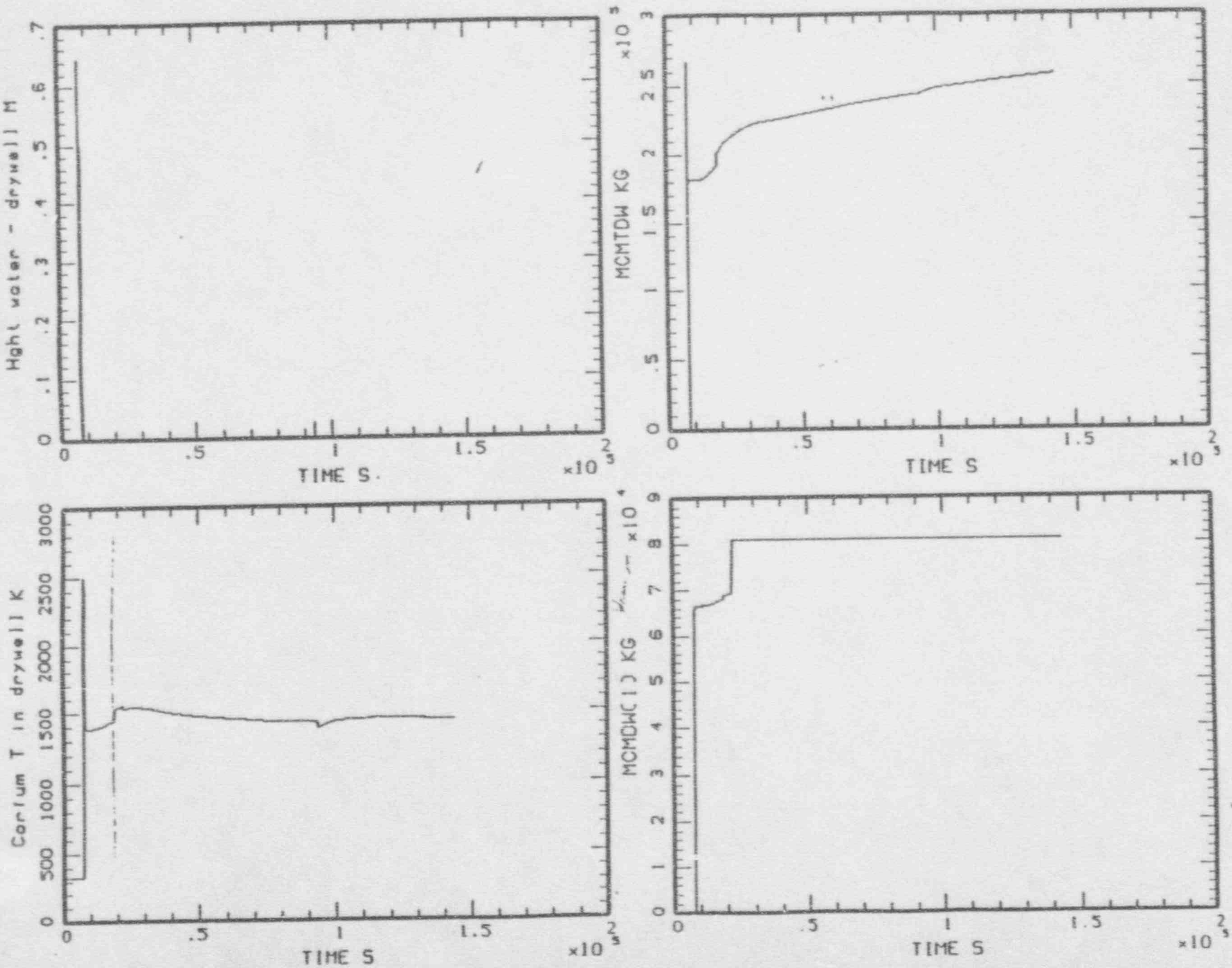

MAAP-MELCOR: BWR SBO, MCSPT = 60,000 KG
BNL_MCSPO_43.PLT LINE

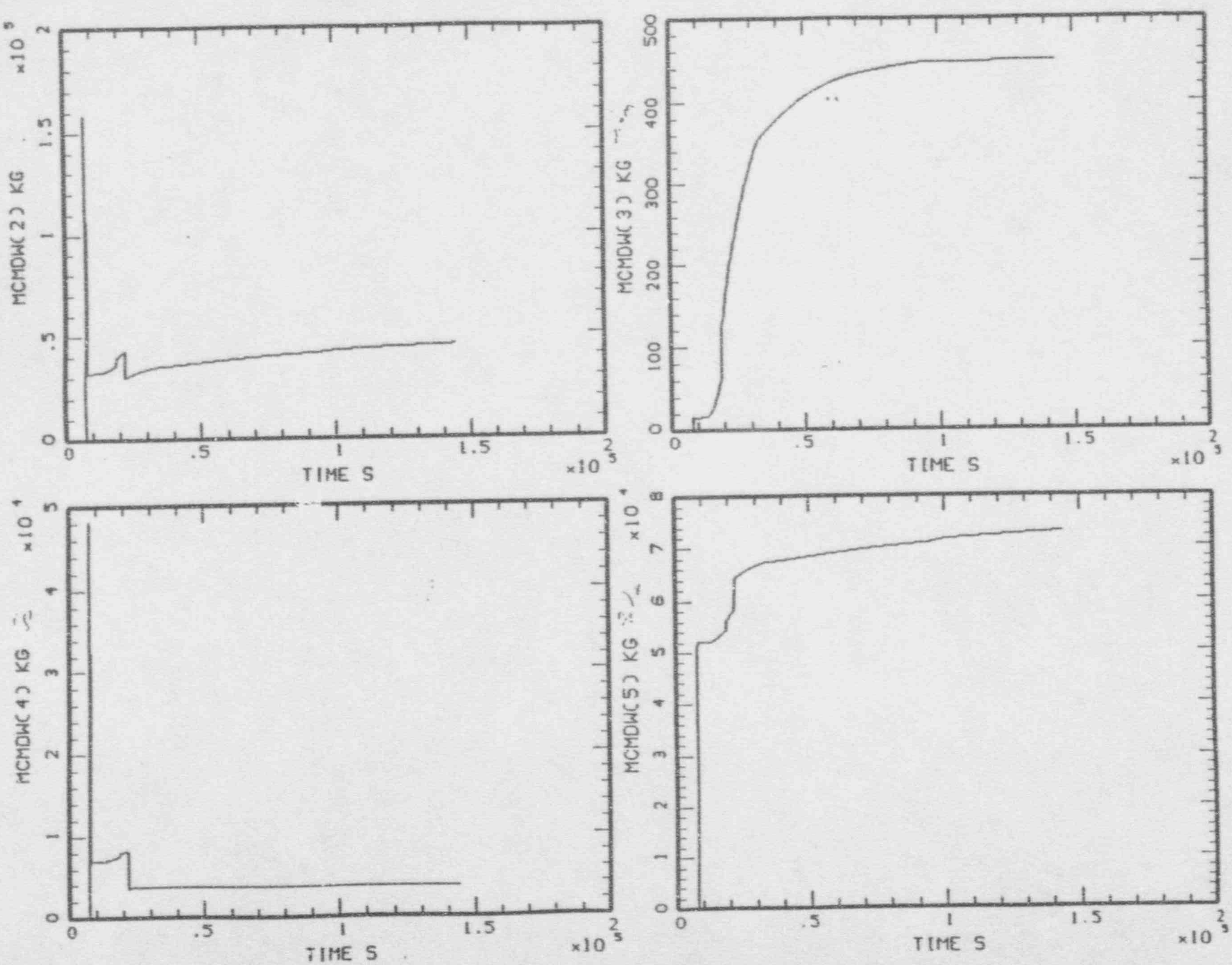

MAAP-MELCOR: BWR SBO, MCSPT = 60,000 KG
BNL_MCSPO_43.PLT LINE

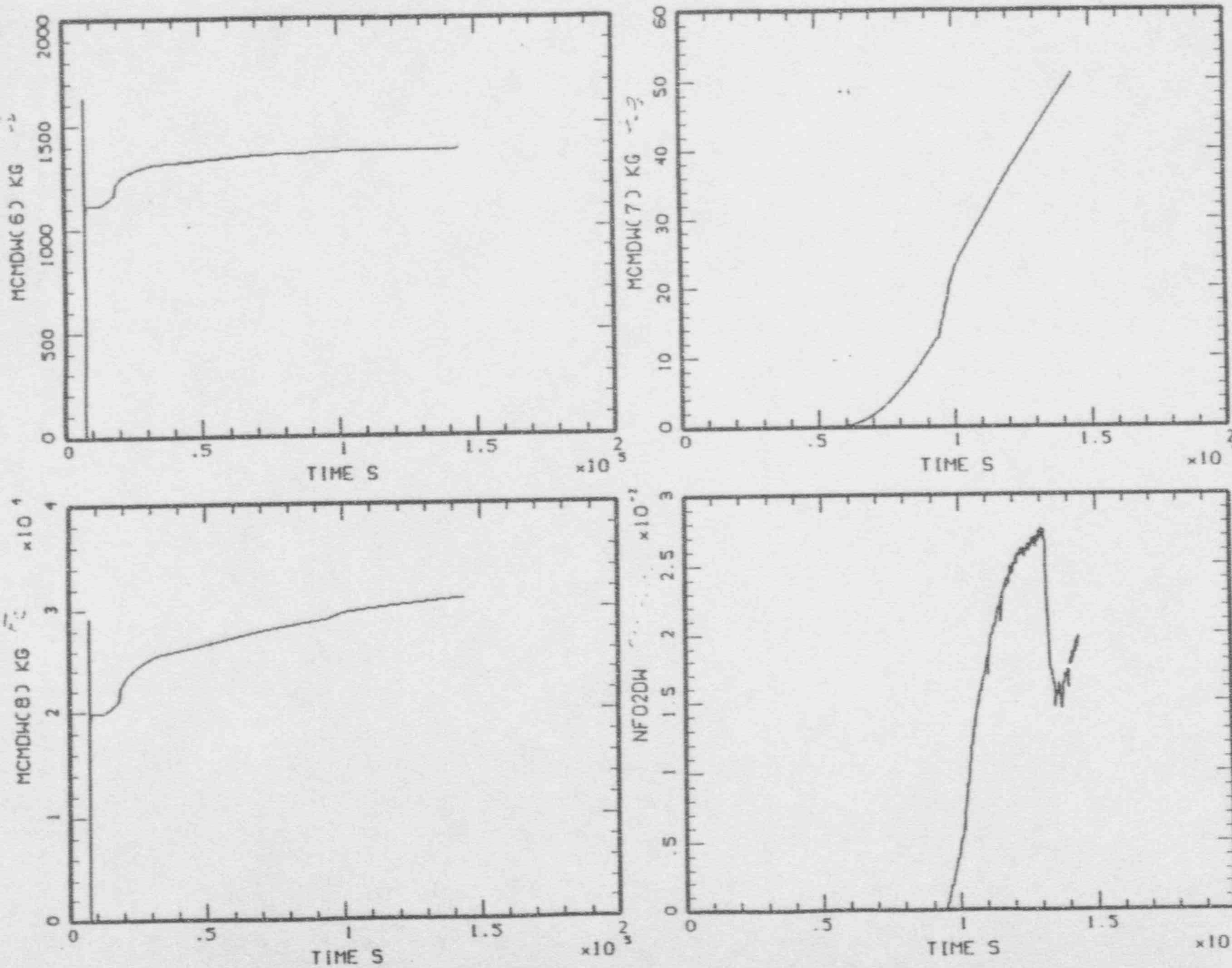

MAAP-MELCOR' BWR SBO, MCSPT = 60,000 KG
BNL_MCSPO_43.PLT LINE

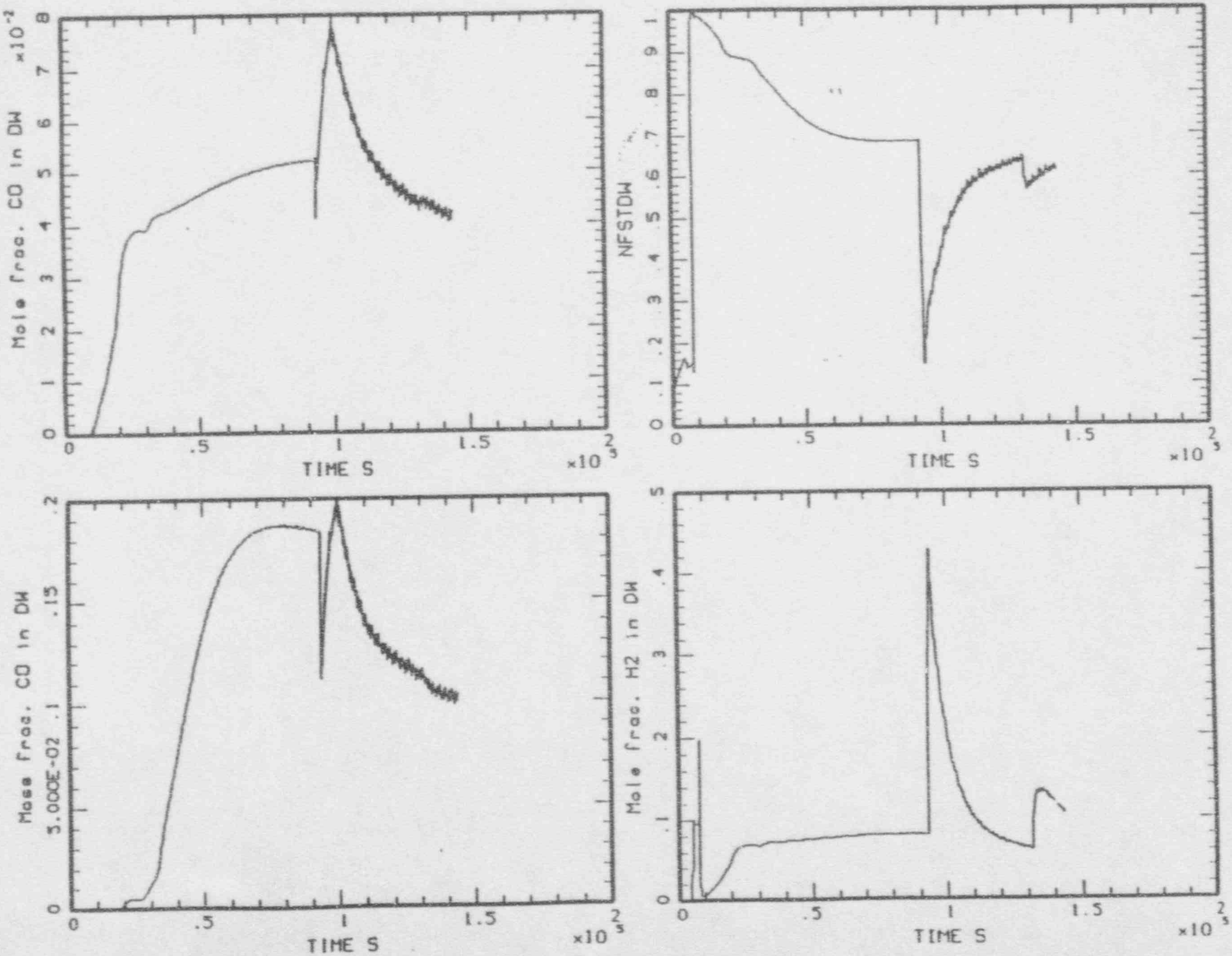

MAAP-MELCOR: BWR SBO, MCSPT = 60,000 KG
BNL_MCSPO_43.PLT LINE

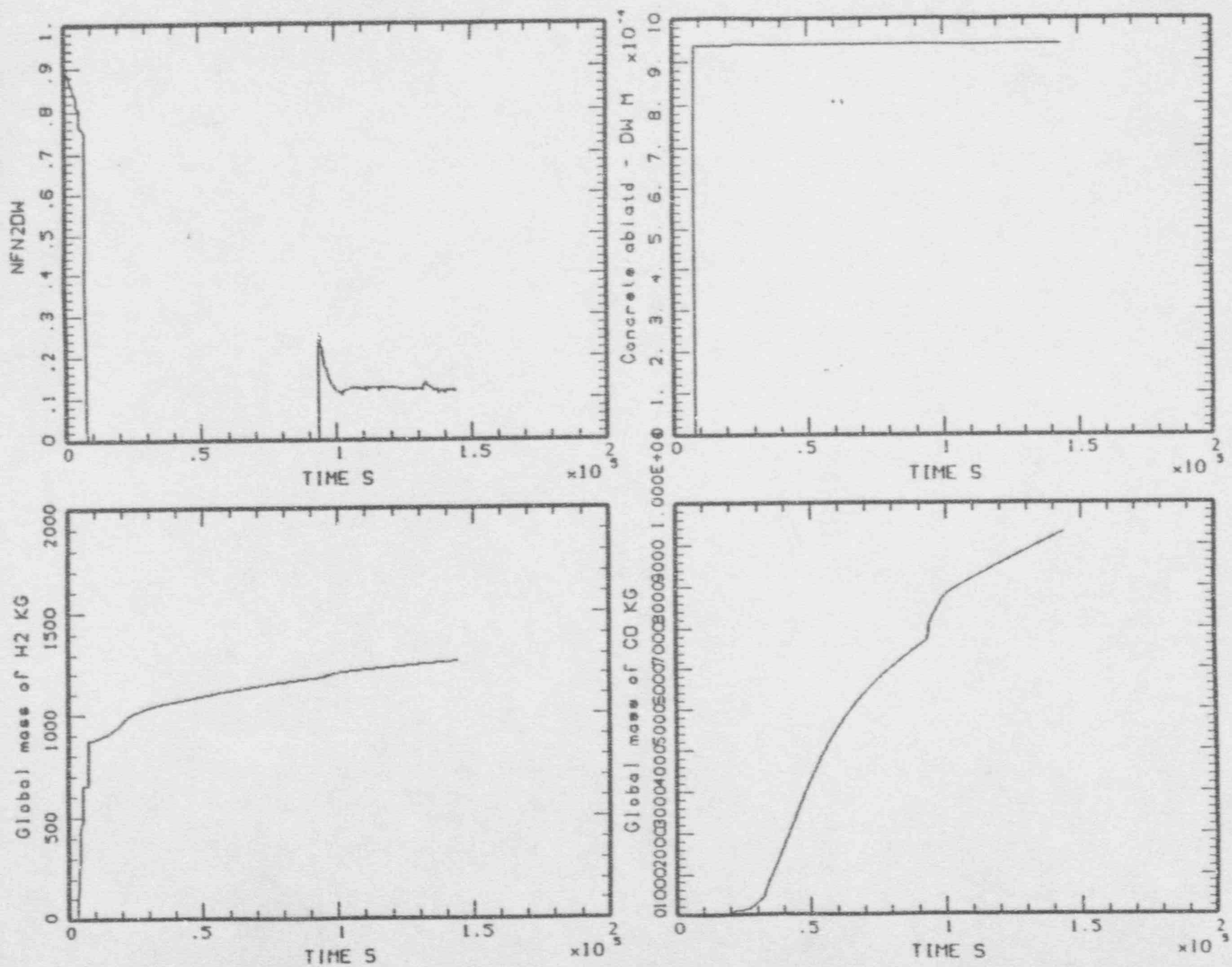

MAAP-MELCOR: BWR SBO. MCSPT = 60,000 KG
BNL_MCSPO_44.PLT LINE

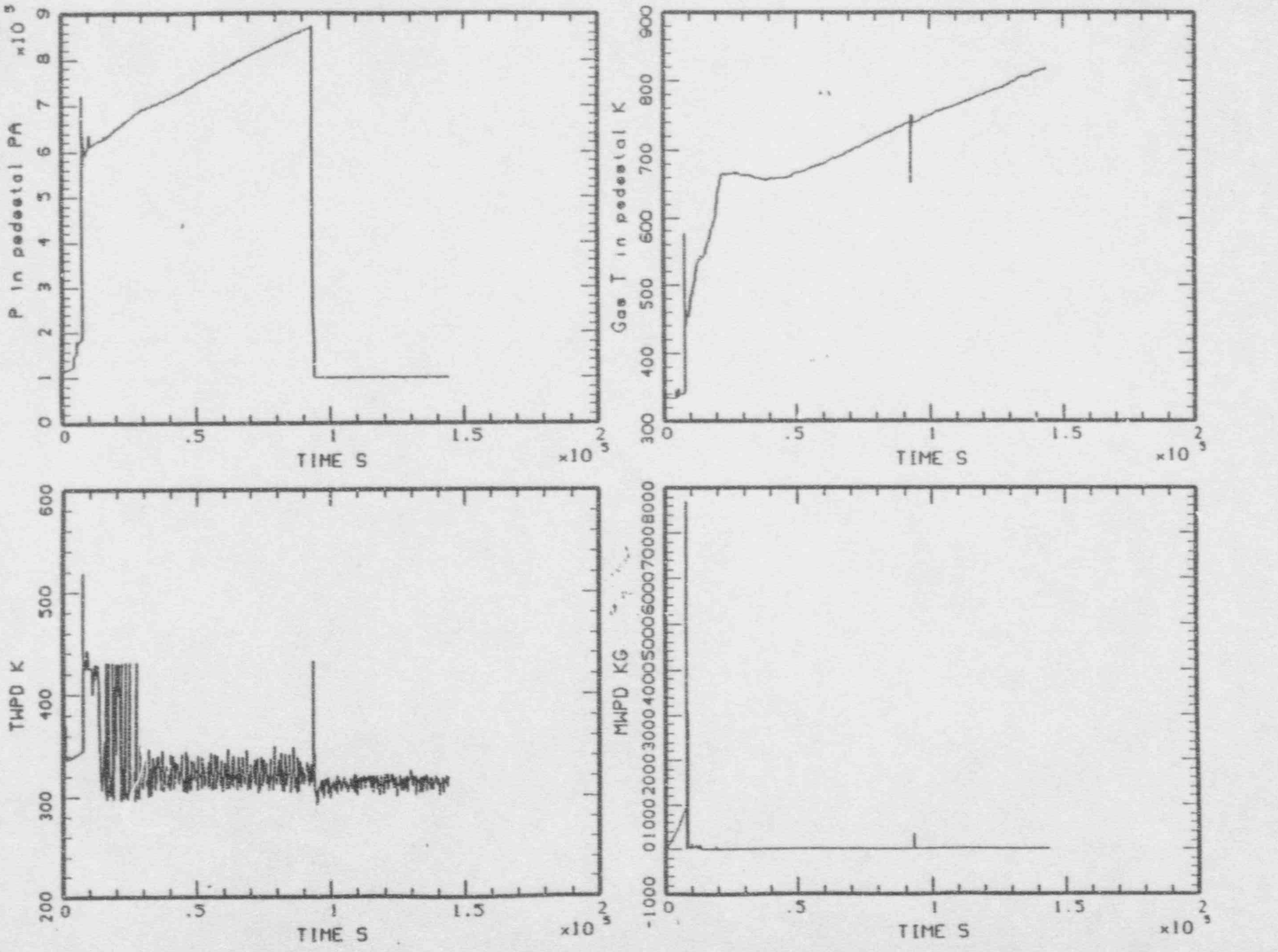

MAAP-MELCOR: BWR SBO, MCSPT = 60.000 KG
BNL_MCSPO_44.PLT LINE

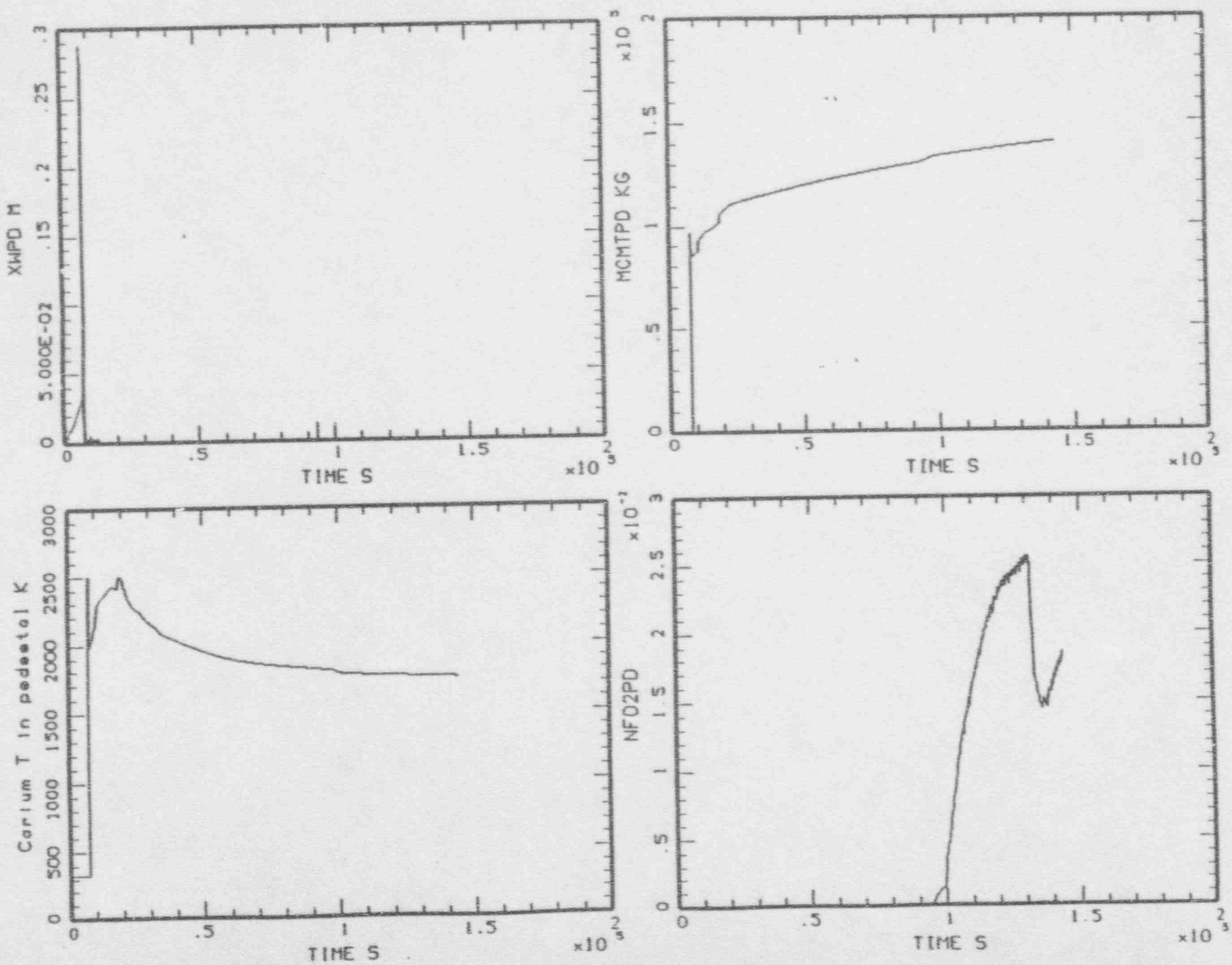

MAAP-MELCOR: BWR SBO, MCSPT = 60,000 KG
BNL_MCSPO_44.PLT LINE

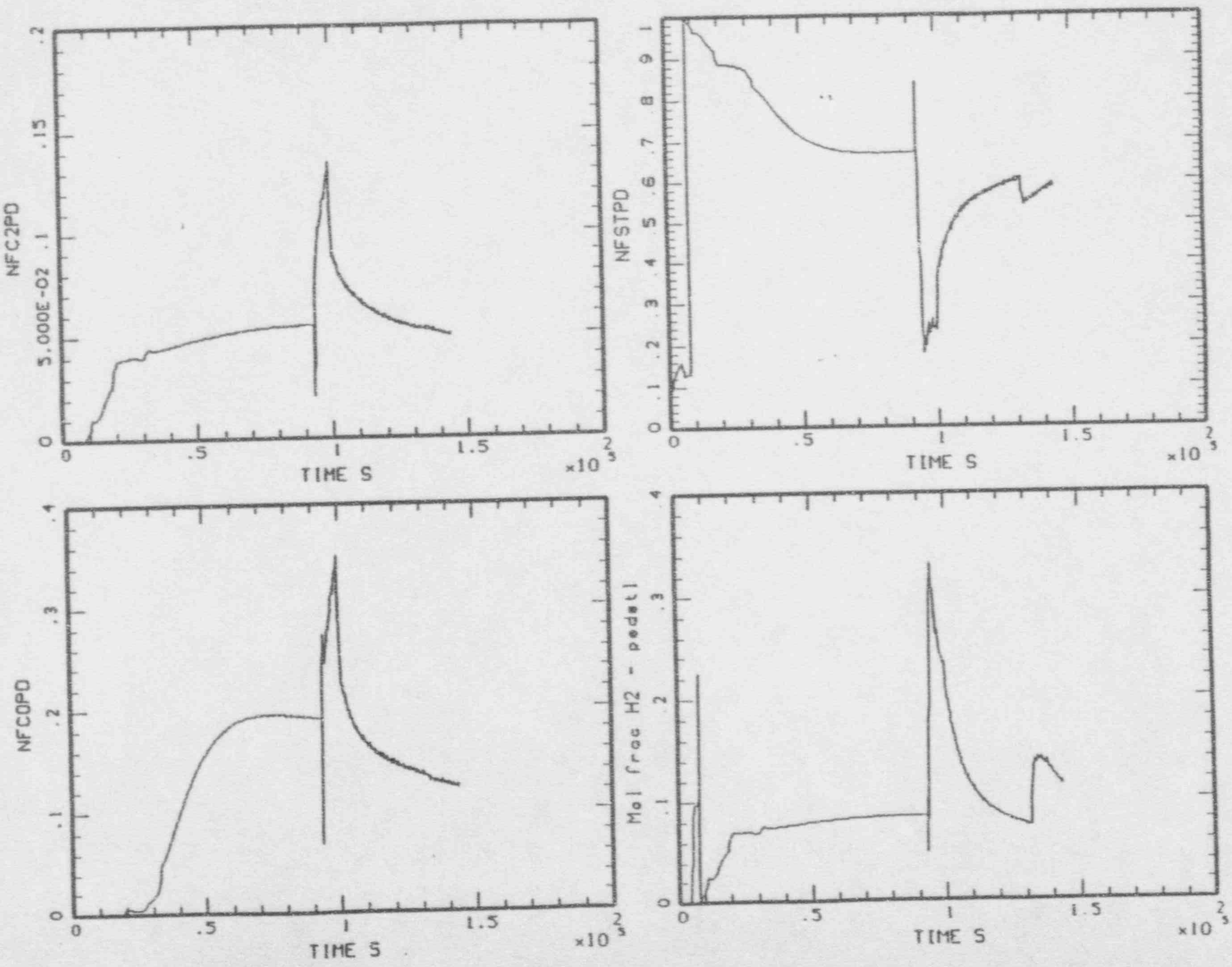

MAAP-MELCOR: BWR SBO, MCSPT = 60,000 KG
BNL_MCSPO_44.PLT LINE

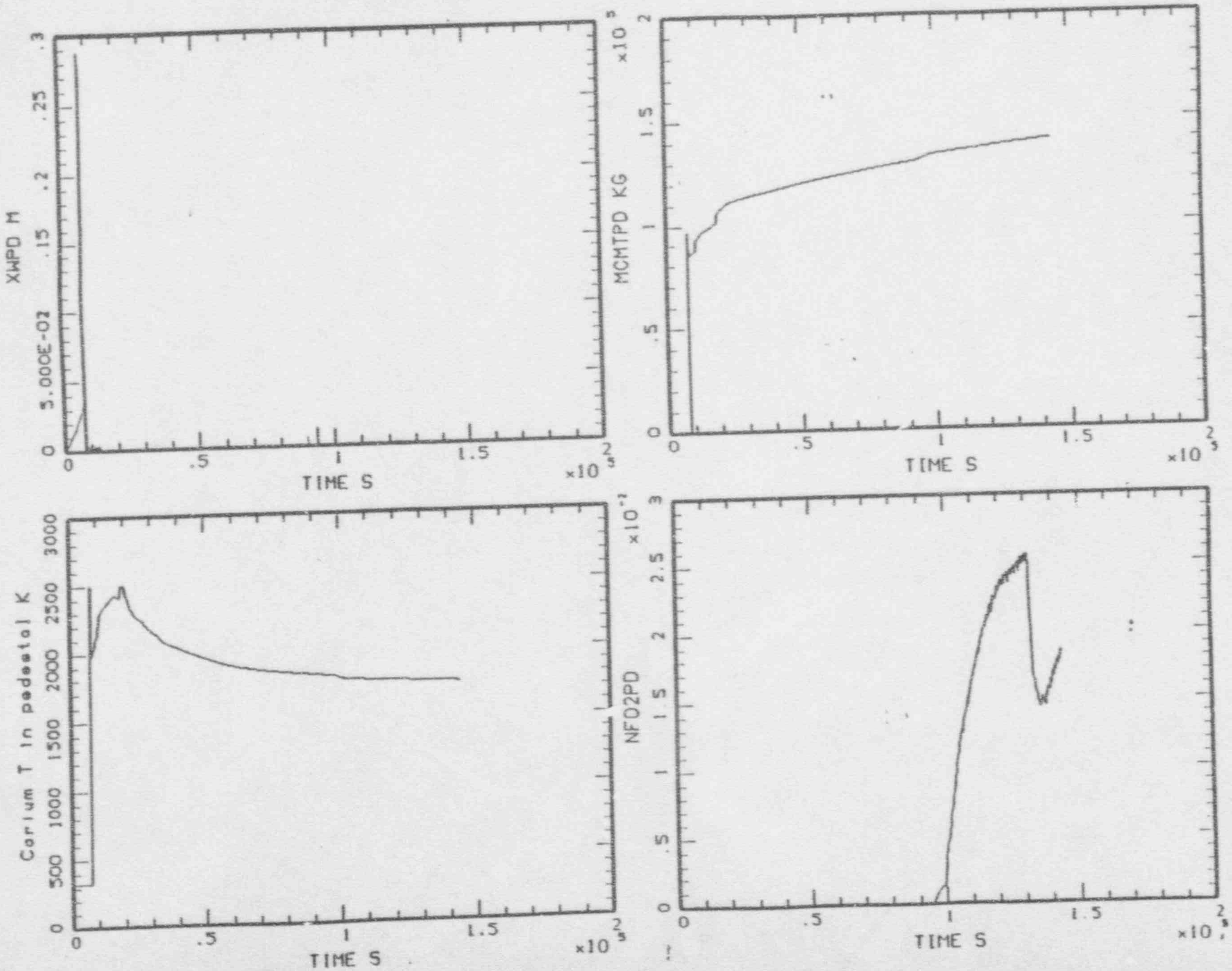

MAAP-MELCOR: BWR SBO, MCSPT = 60,000 KG
BNL_MCSPO_44.PLT LINE

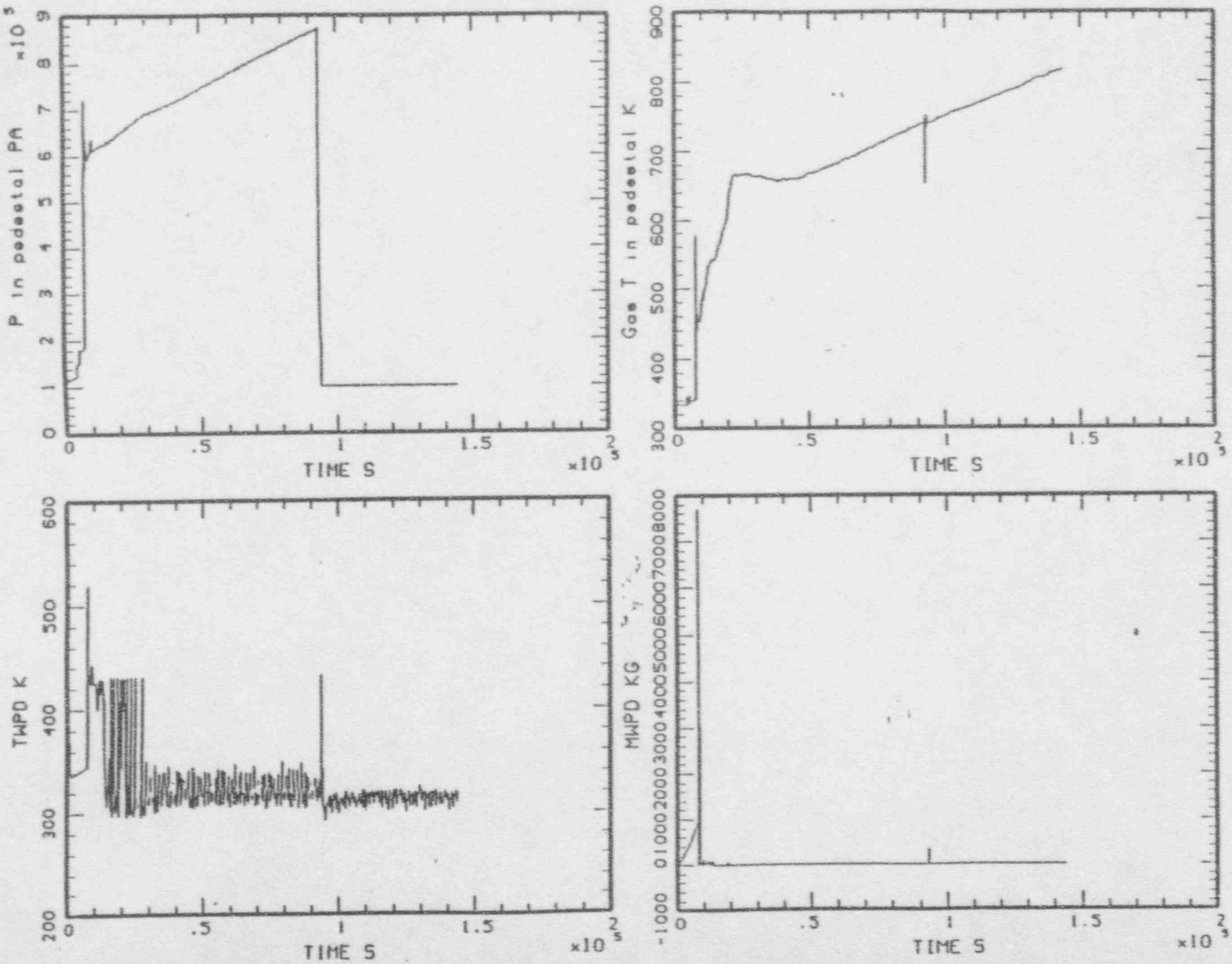

MAAP-MELCOR: BWR SBO, MCSPT = 60.000 KG
BNL_MCSPO_43.PLT LINE

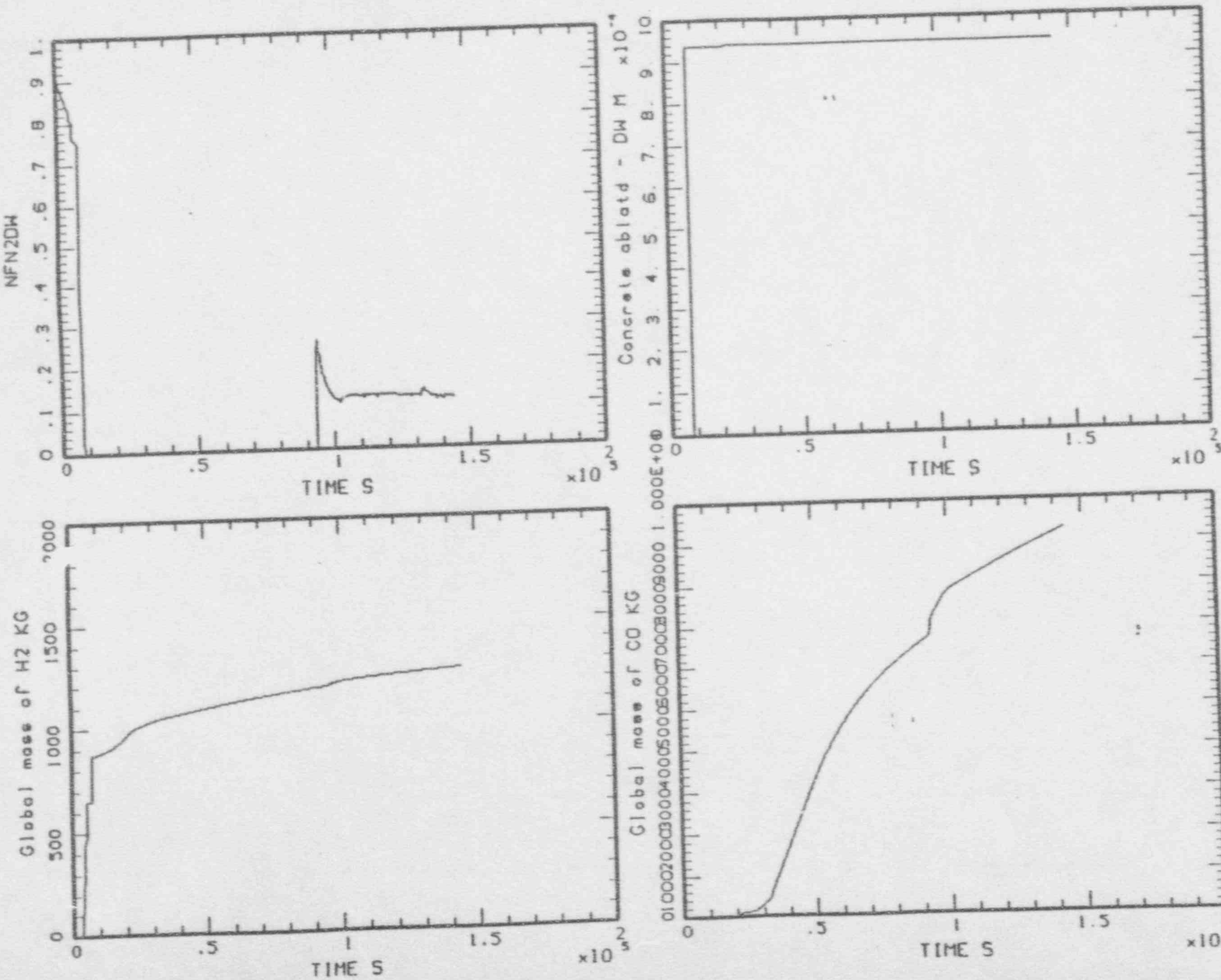

MAAP-MELCOR: BWR SBO, MCSPT = 60,000 KG
BNL_MCSPO_44.PLT LINE

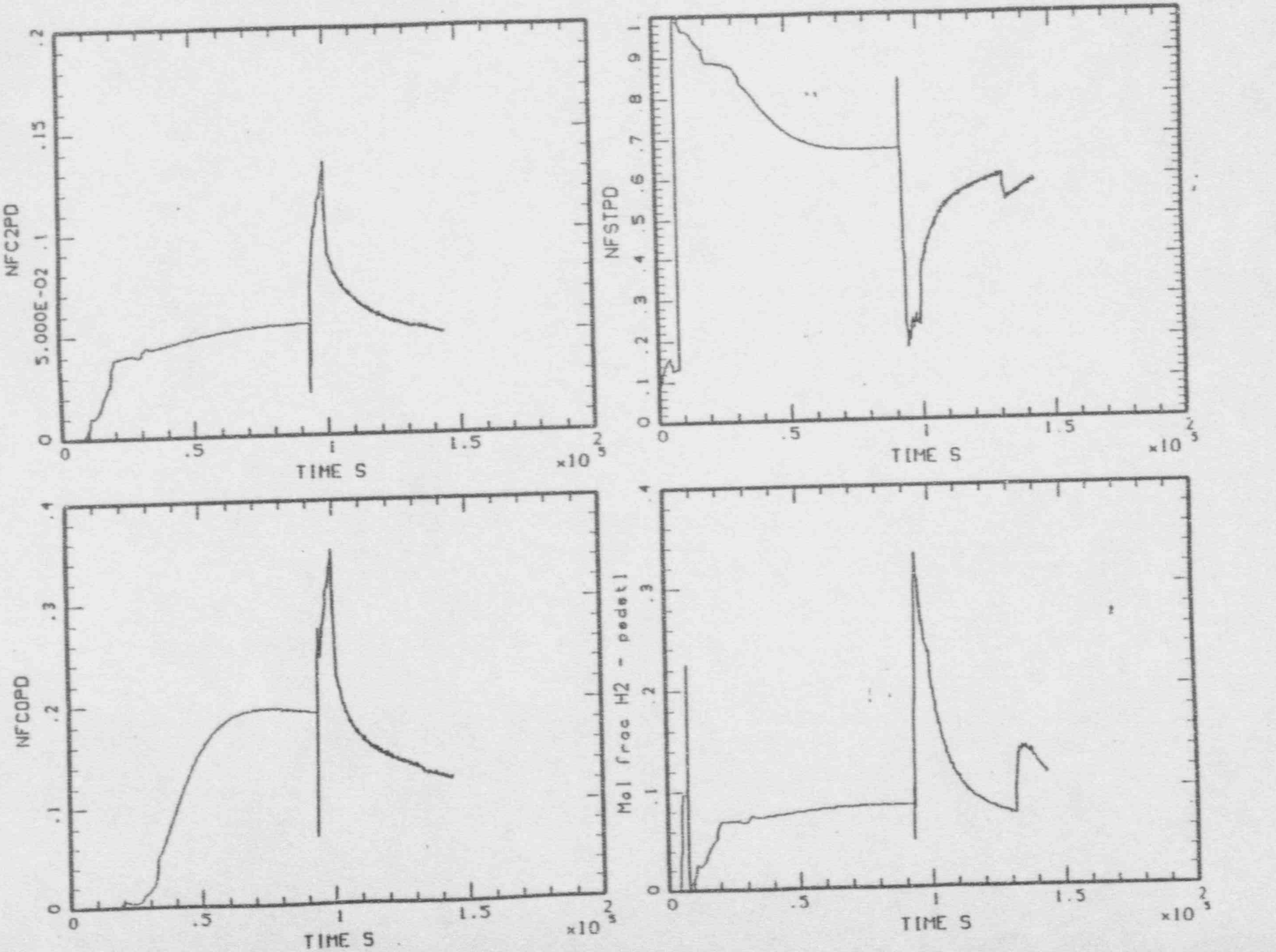

MAAP-MELCOR: BWR SBO, MCSPT = 60,000 KG
BNL_MCSPO_44.PLT LINE

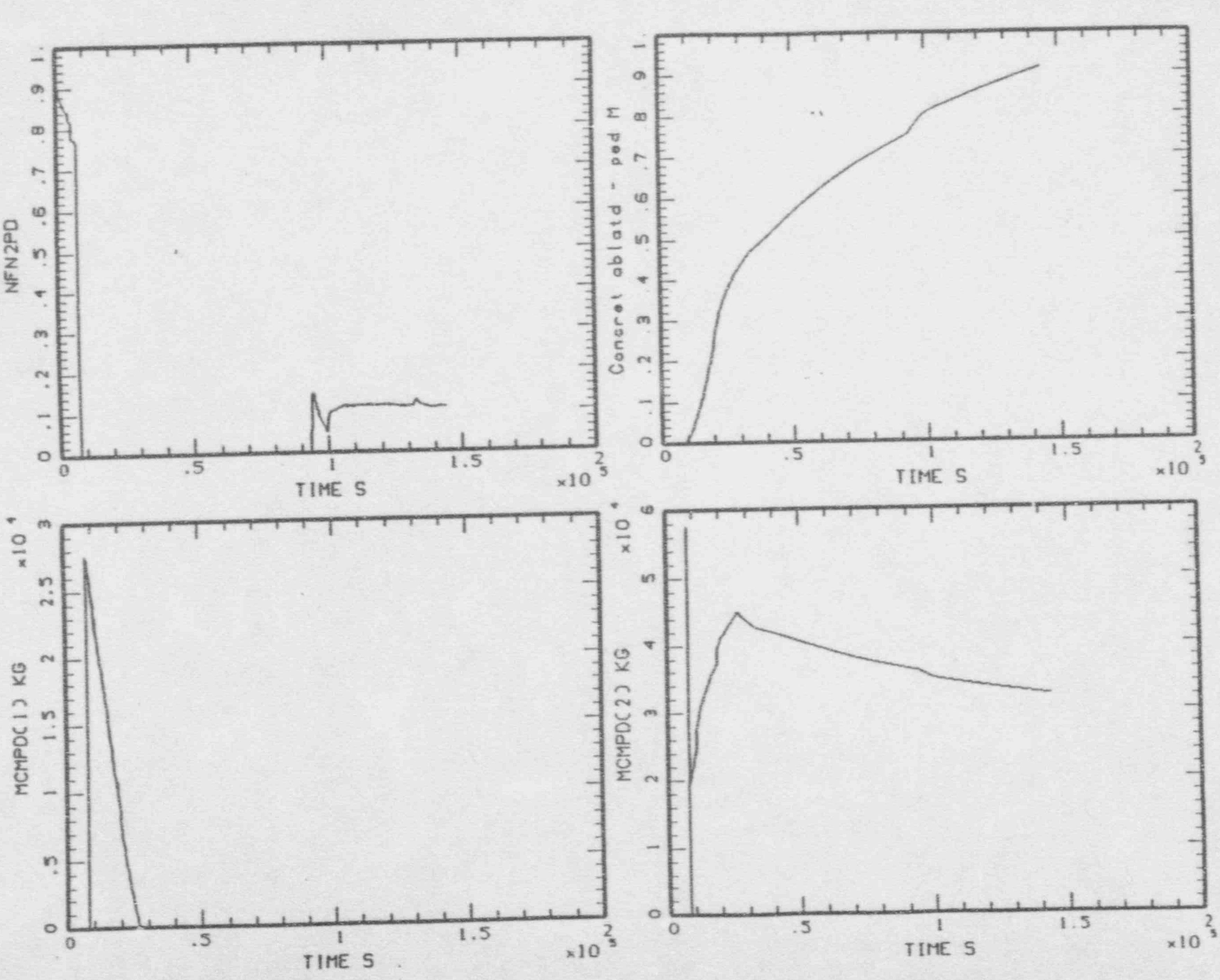

MAAP-MELCOR: BWR SBO. MCSPT = 60,000 KG
BNL_MCSPO_44.PLT LINE

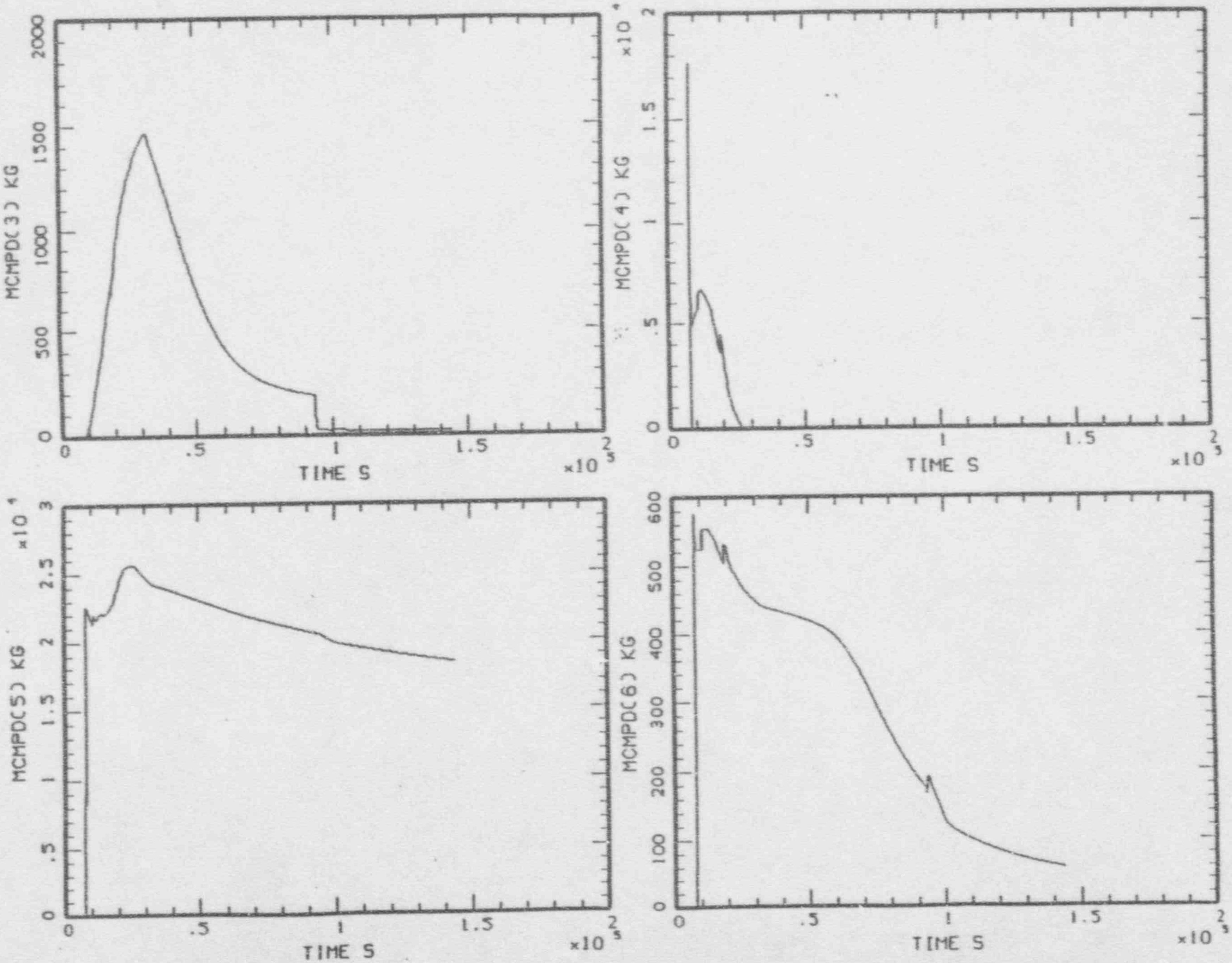

MAAP-MELCOR: BWR SBO, MCSPT = 60,000 KG
BNL_MCSPO_44.PLT LINE

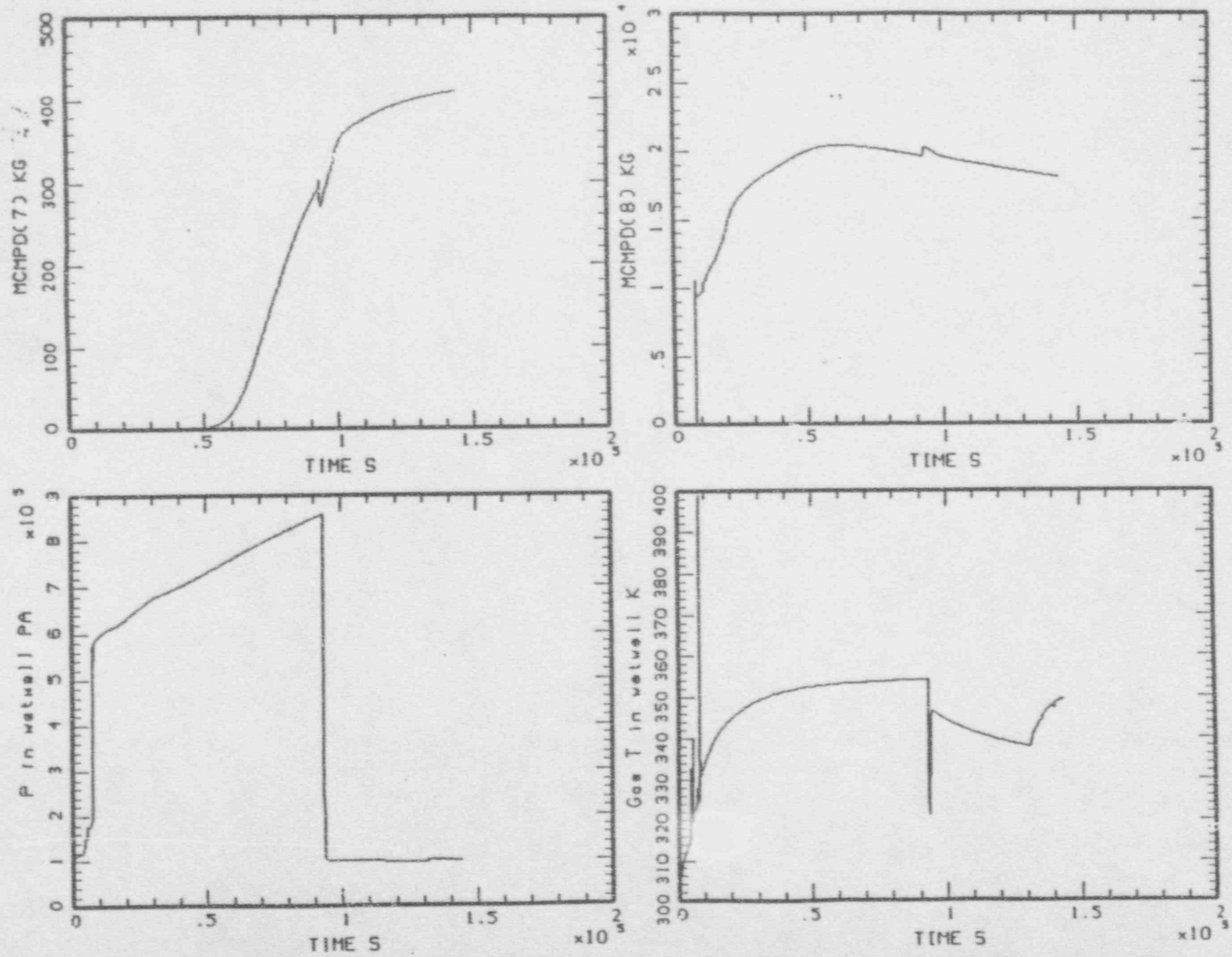

CASE 2

MCSPT = 10,000 kg

NUMERICAL PERFORMANCE FIGURES OF MERIT

TIME (SEC)	144015.5
FRACTION OF CLAD REACTED IN VESSEL . .	0.2737
CONCRETE AEROSOL GENERATED (KG). . . .	892.4
UO2 MASS IN PEDESTAL (KG).	31753.0
UO2 MASS IN DRYWELL (KG)	137634.1
TIME OF CORE UNCOVERY (SEC).	1897.7
TIME OF VESSEL FAILURE (SEC)	7765.4
TIME OF CONTAINMENT FAILURE (SEC). . .	72673.4
CSI MASS BALANCE (KG)	
INITIAL MASS	38 [illegible] 5
IN CORE.	0.0000
IN CORIUM.	0.3288
IN PRIMARY SYSTEM.	6.6409
IN CONTAINMENT	21.7703
TOTAL IN-VESSEL RELEASED	37.3004
TOTAL EX-VESSEL RELEASED	0.5865
RELEASED FROM CONTAINMENT.	9.4752
SRO MASS BALANCE (KG)	
INITIAL MASS	103.4367
IN CORE.	0.0000
IN CORIUM.	103.1137
IN PRIMARY SYSTEM.	0.0621
IN CONTAINMENT	0.2806
TOTAL IN-VESSEL RELEASED	0.0700
TOTAL EX-VESSEL RELEASED	0.2728
RELEASED FROM CONTAINMENT.	0.0001

```
FORTRAN STOP
$ delete BNL_MCSP1_inp.dat;*
$ delete BNL_MCSP1_par.dat;*
$!
$ node = "N780"
$ if "FALSE".eqs."FALSE" then logoff/full
  WUTOBY         job terminated at 31-MAY-1991 14:30:10.80

  Accounting information:
  Buffered I/O count:            668     Peak working set size:   1344
  Direct I/O count:            12179     Peak page file size:     4600
  Page faults:                  2140     Mounted volumes:            0
  Charged CPU time:    0 00:00:44.75     Elapsed time:     0 01:30:09.49
```

MAAP-MELCOR: BWR SBO, MCSPT = 10,000 KG
BNL_MCSPI_43.PLT LINE

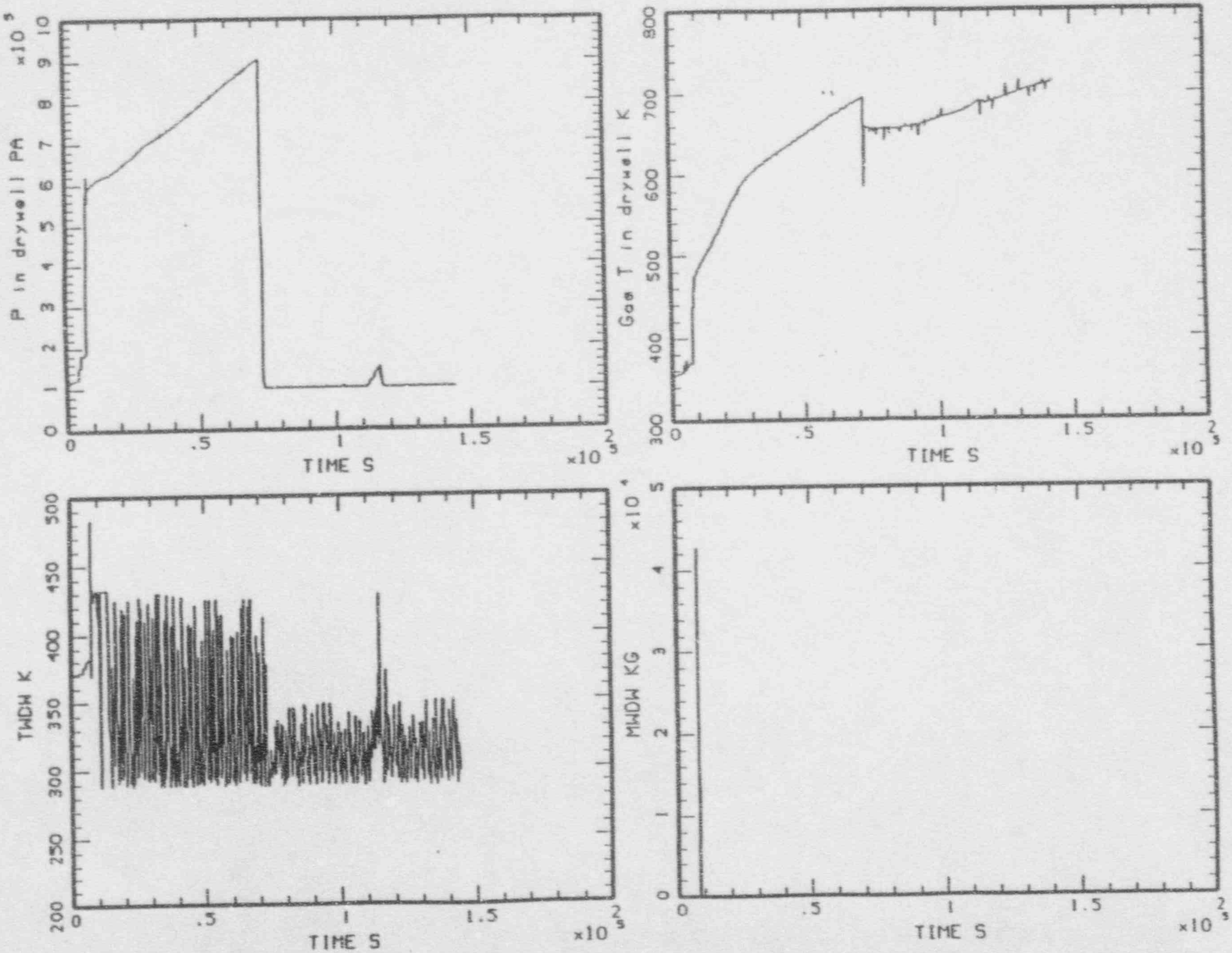

MAAP-MELCOR: BWR SBO, MCSPT = 10,000 KG
BNL_MCSP1_43.PLT LINE

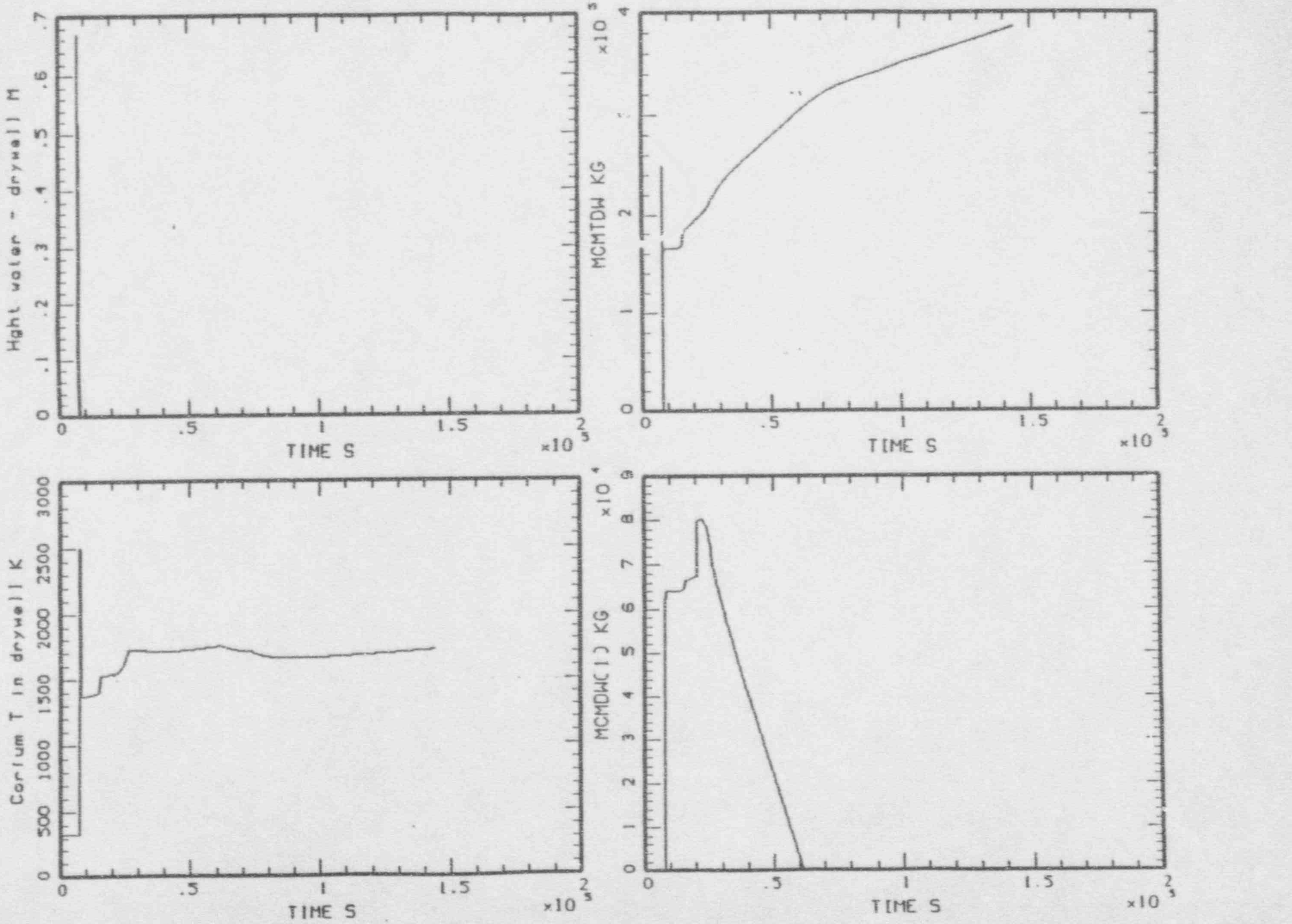

MAAP-MELCOR: BWR SBO. MCSPT = 10.000 KG
BNL_MCSP1_43.PLT LINE

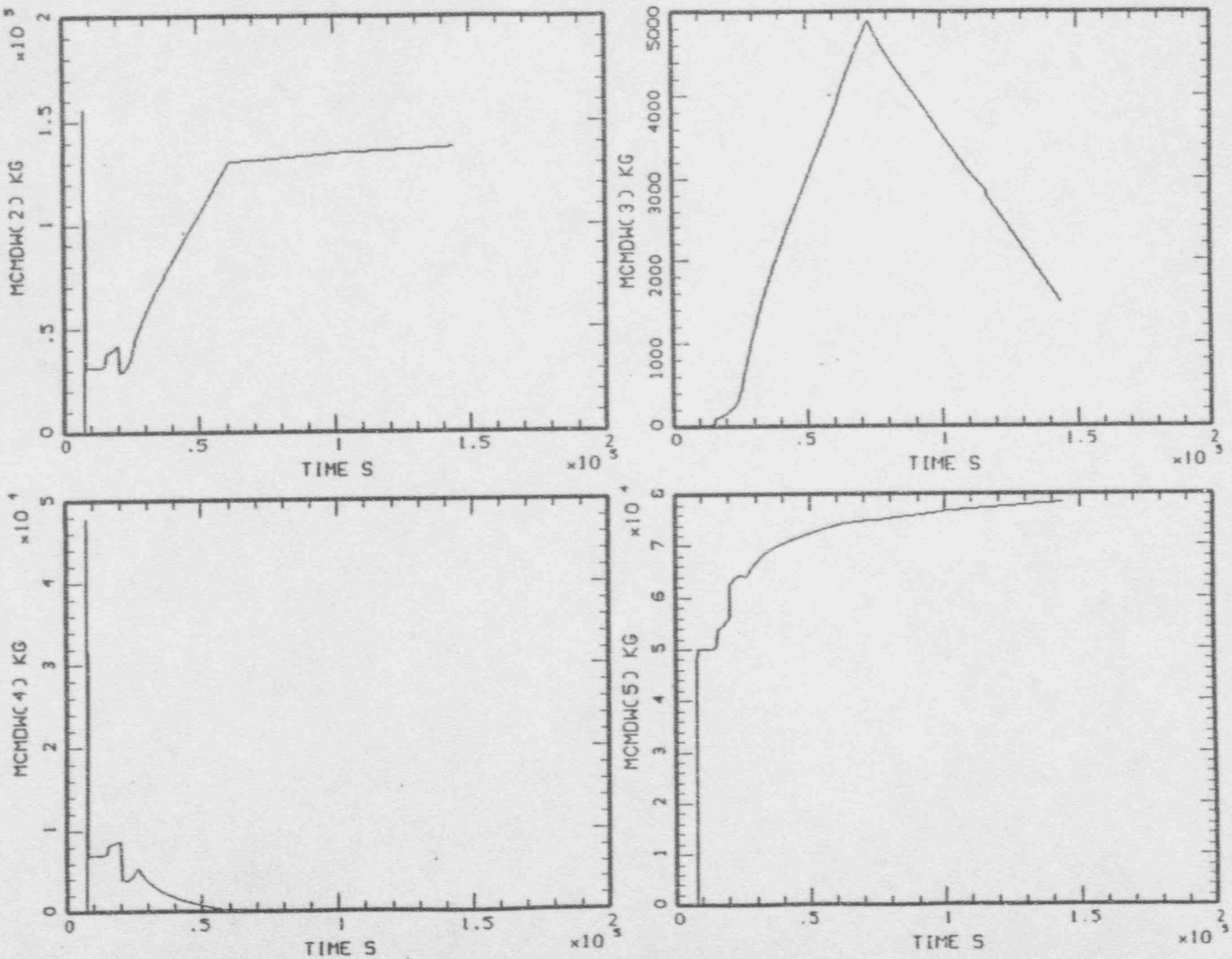

MAAP-MELCOR: BWR SBO. MCSPT = 10.000 KG
BNL_MCSP1_43.PLT LINE

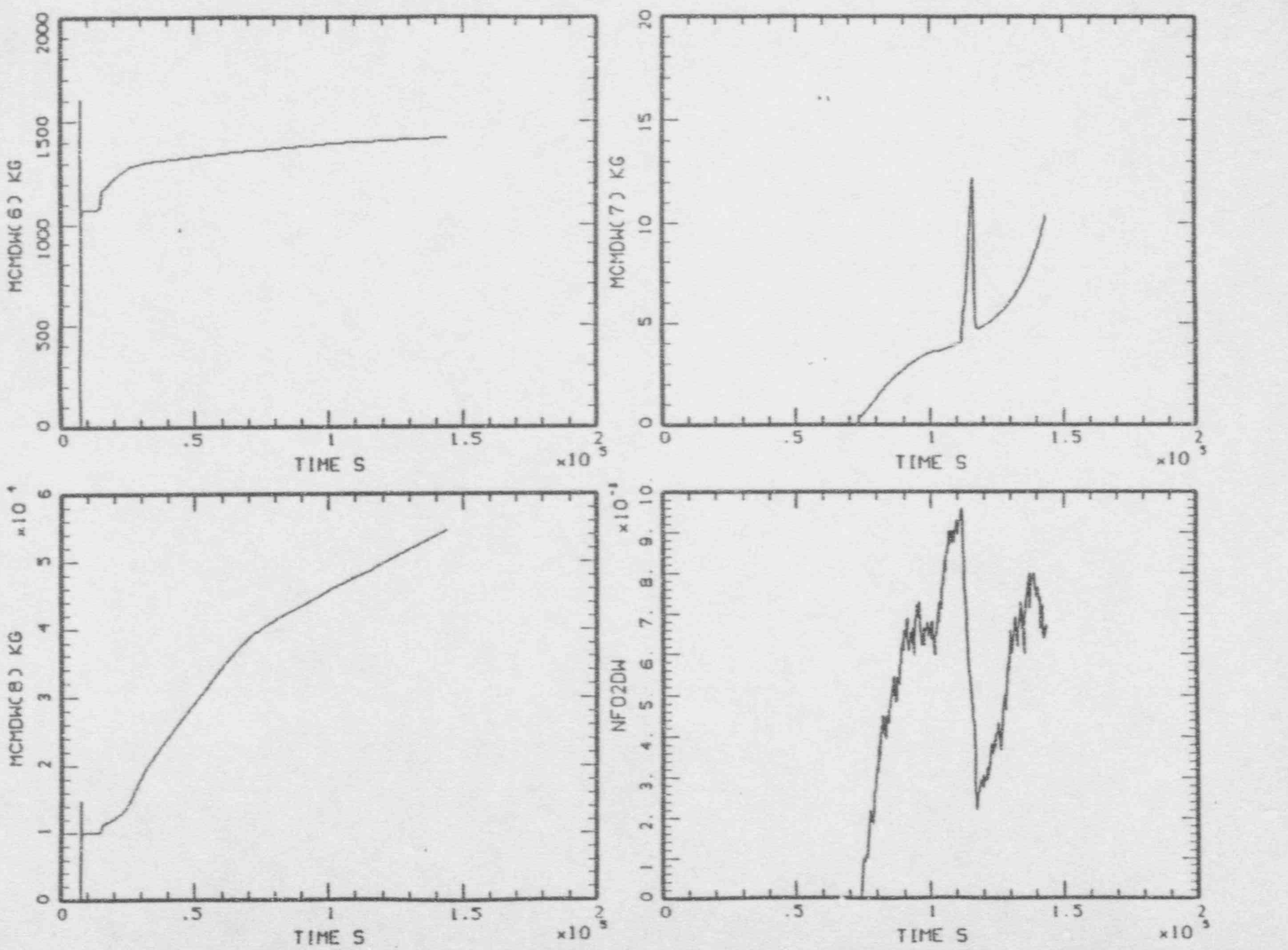

MAAP-MELCOR: BWR SBO. MCSPT = 10.000 KG
BNL_MCSP1_43.PLT LINE

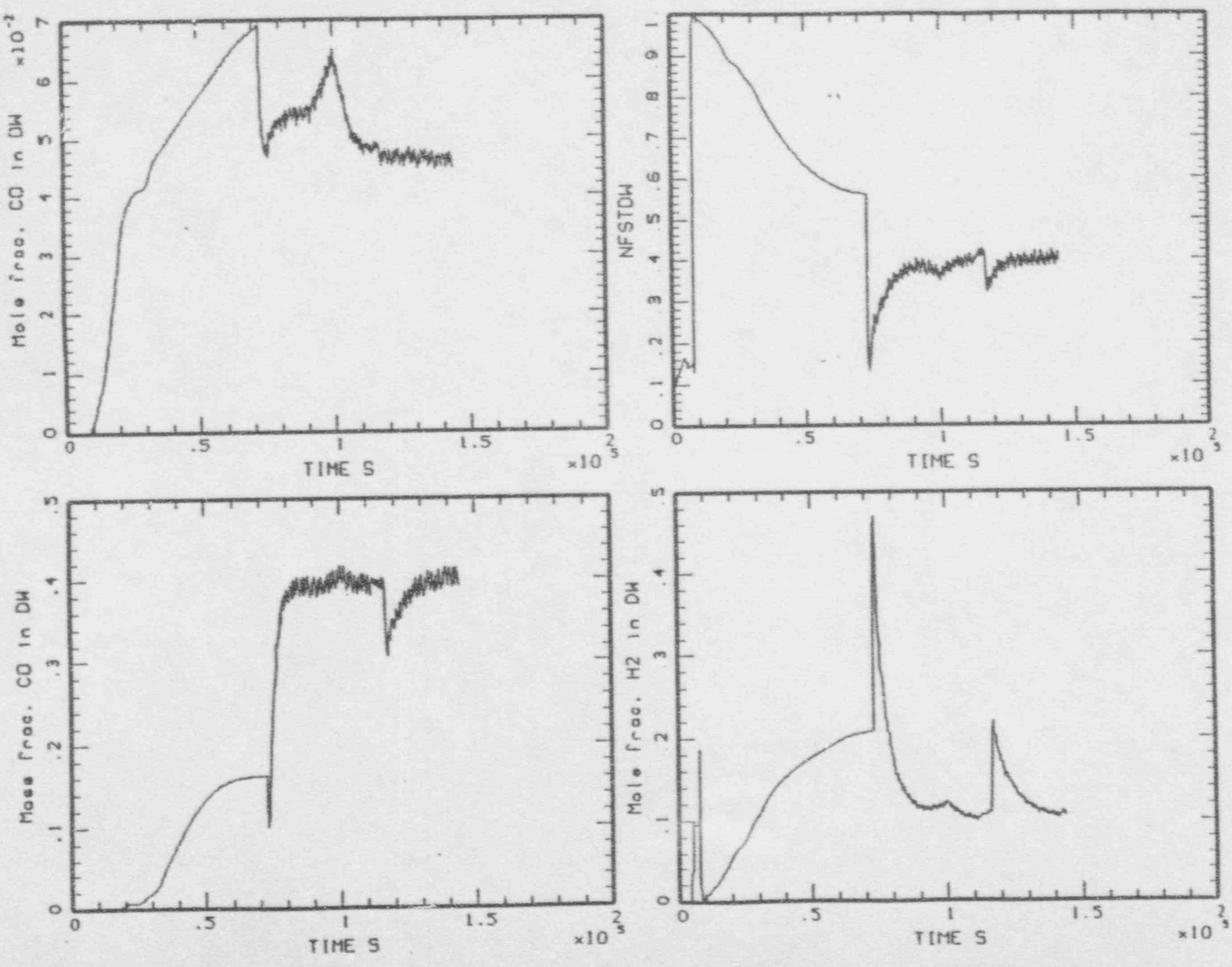

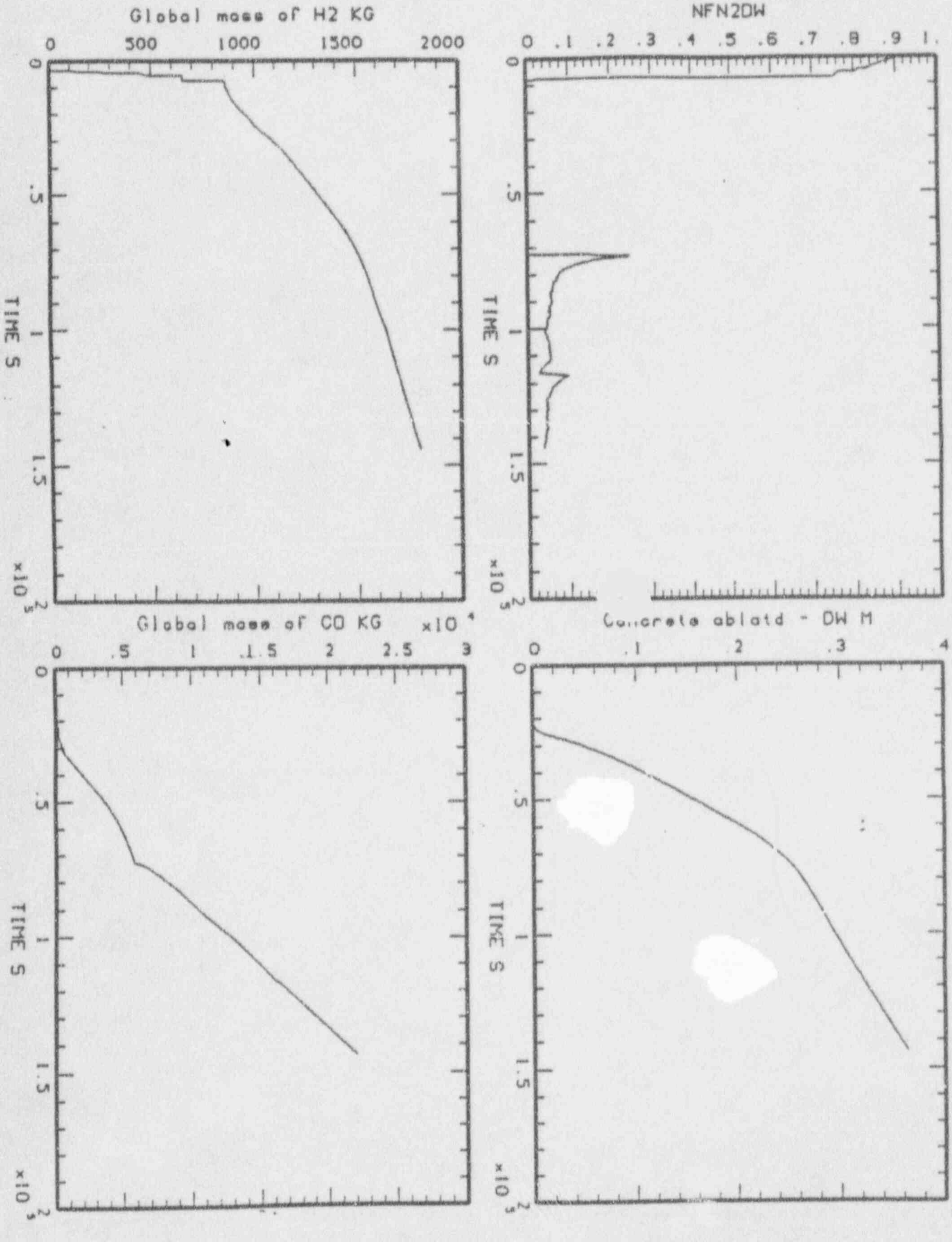

MAAP-MELCOR' BWR SBO. MCSPT = 10.000 KG
BNL_MCSP1_43.PLT LINE

MAAP-MELCOR: BWR SBO. MCSPT = 10.000 KG
BNL_MCSPI_44.PLT LINE

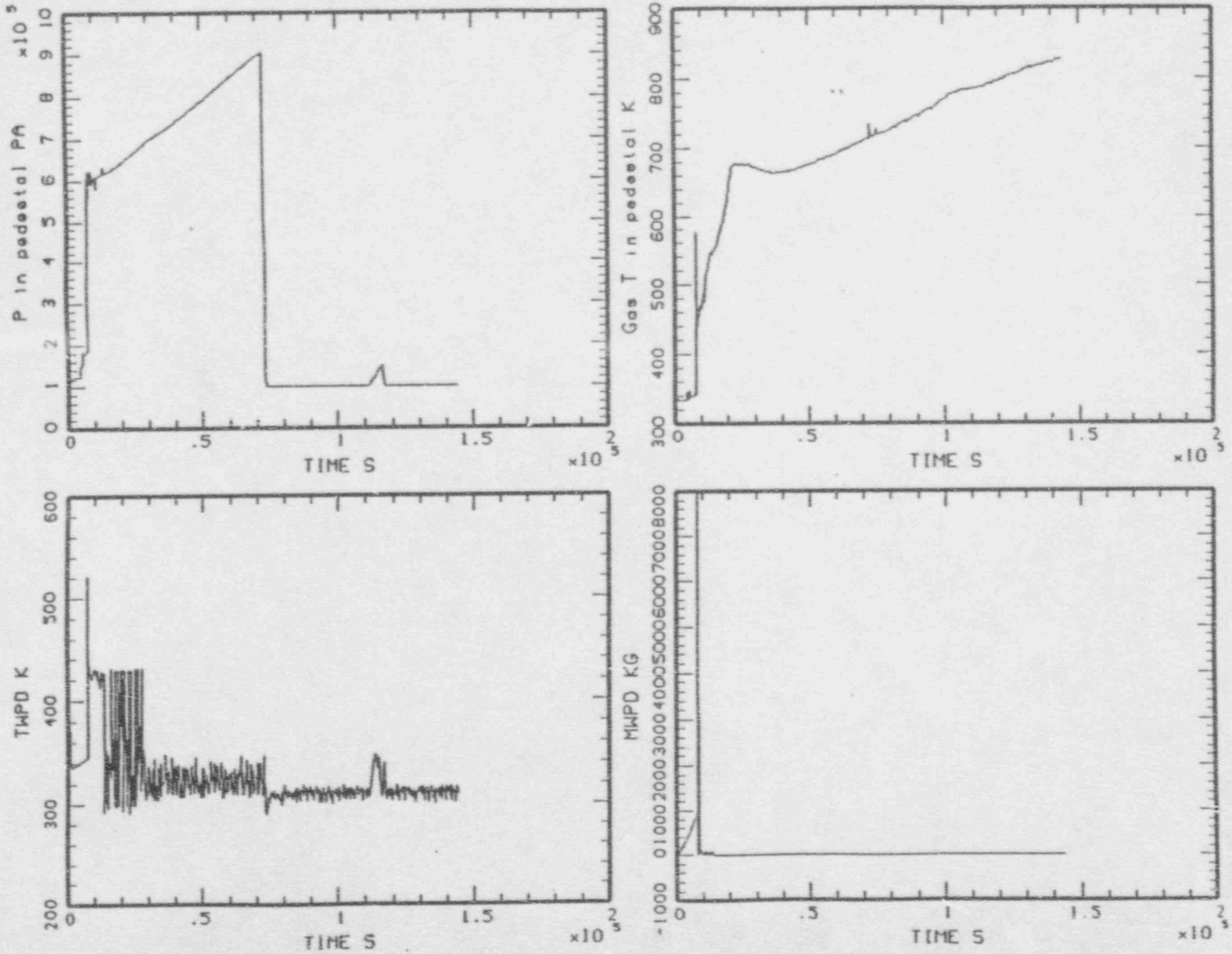

MAAP-MELCOR: BWR SBO, MCSPT = 10,000 KG
BNL_MCSP1_44.PLT LINE

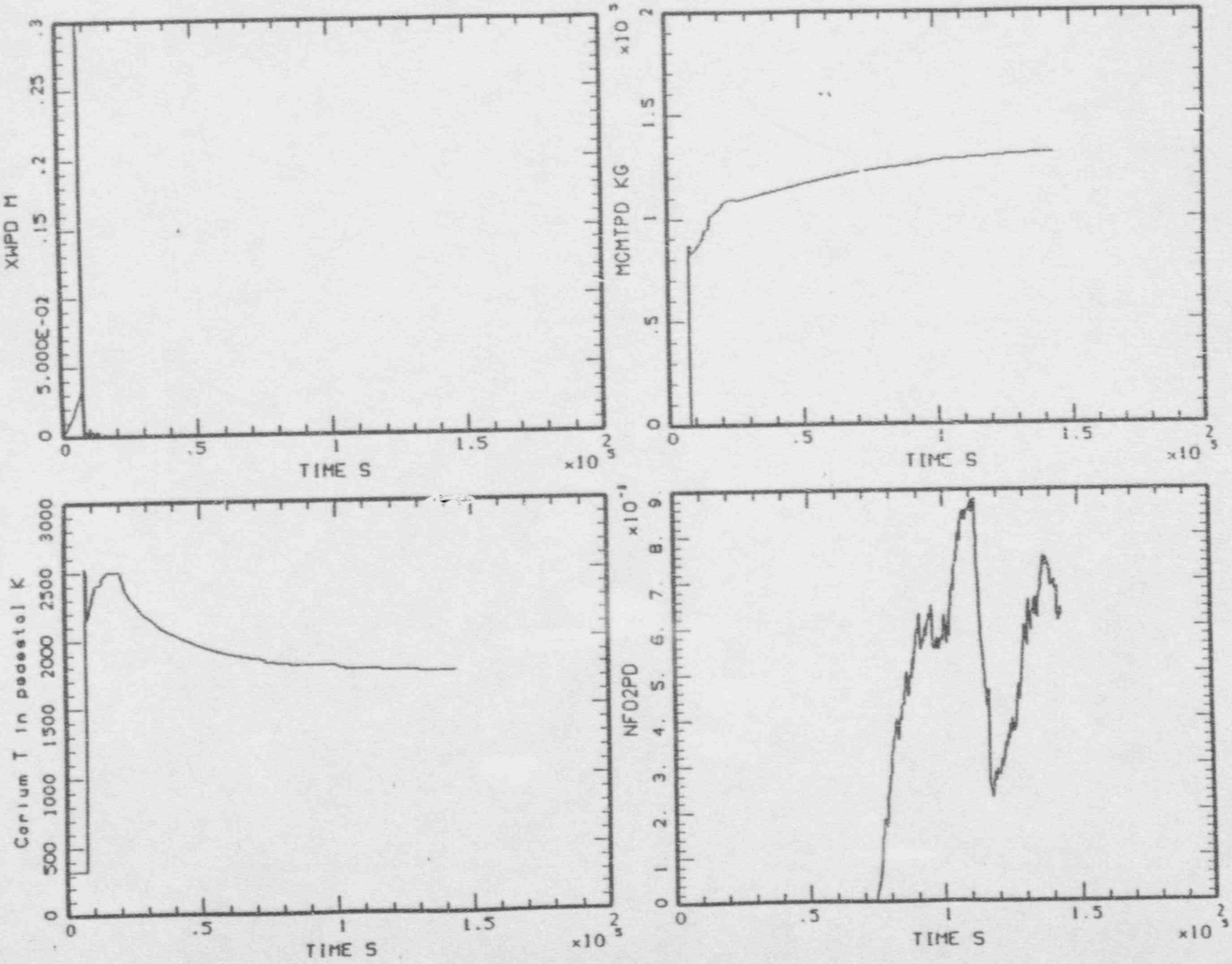

MAAP-MELCOR: BWR SBO, MCSPT = 10,000 KG
BNL_MCSP1_44.PLT LINE

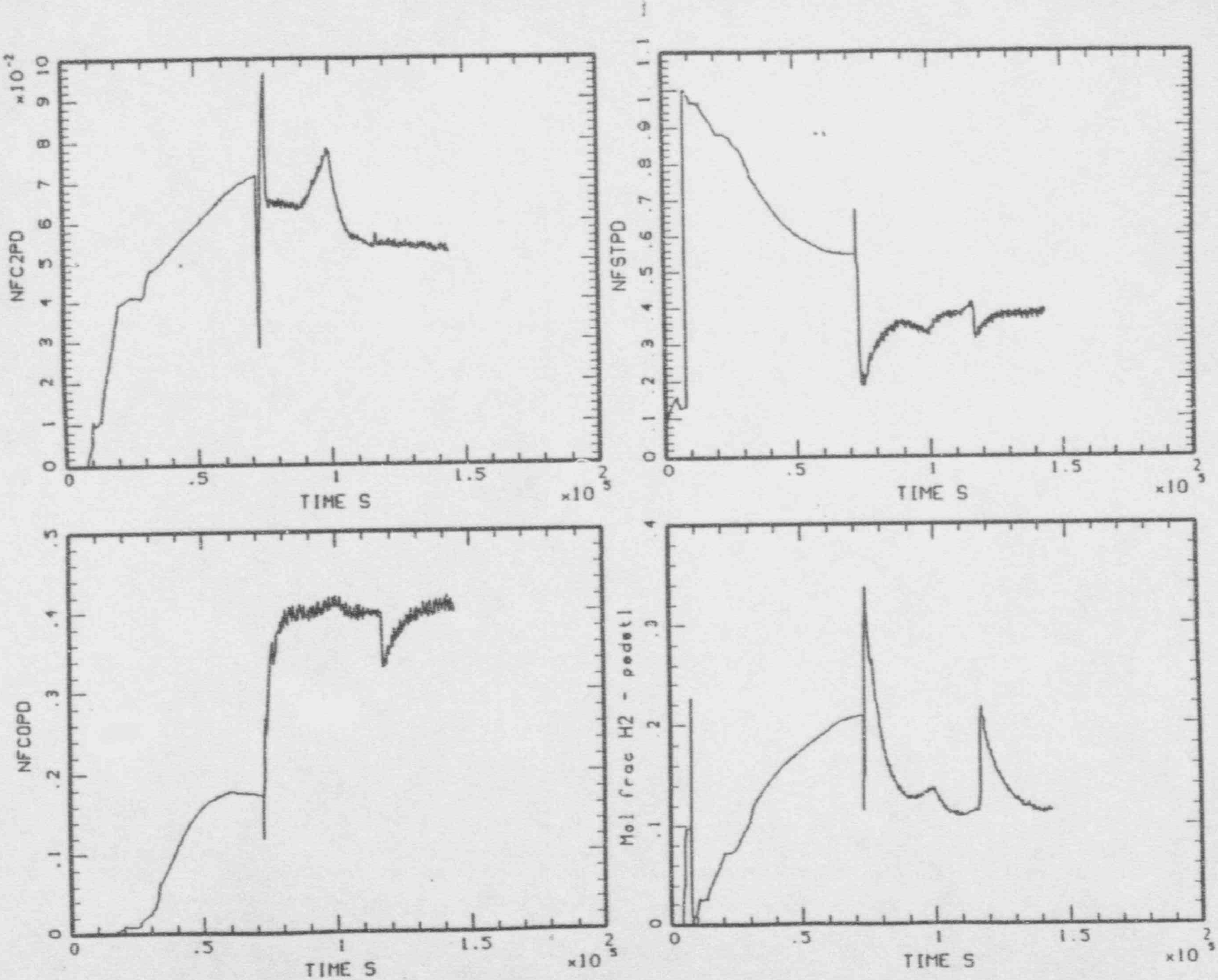

MAAP-MELCOR: BWR SBO, MCSPT = 10.000 KG
BNL_MCSP1_44.PLT LINE

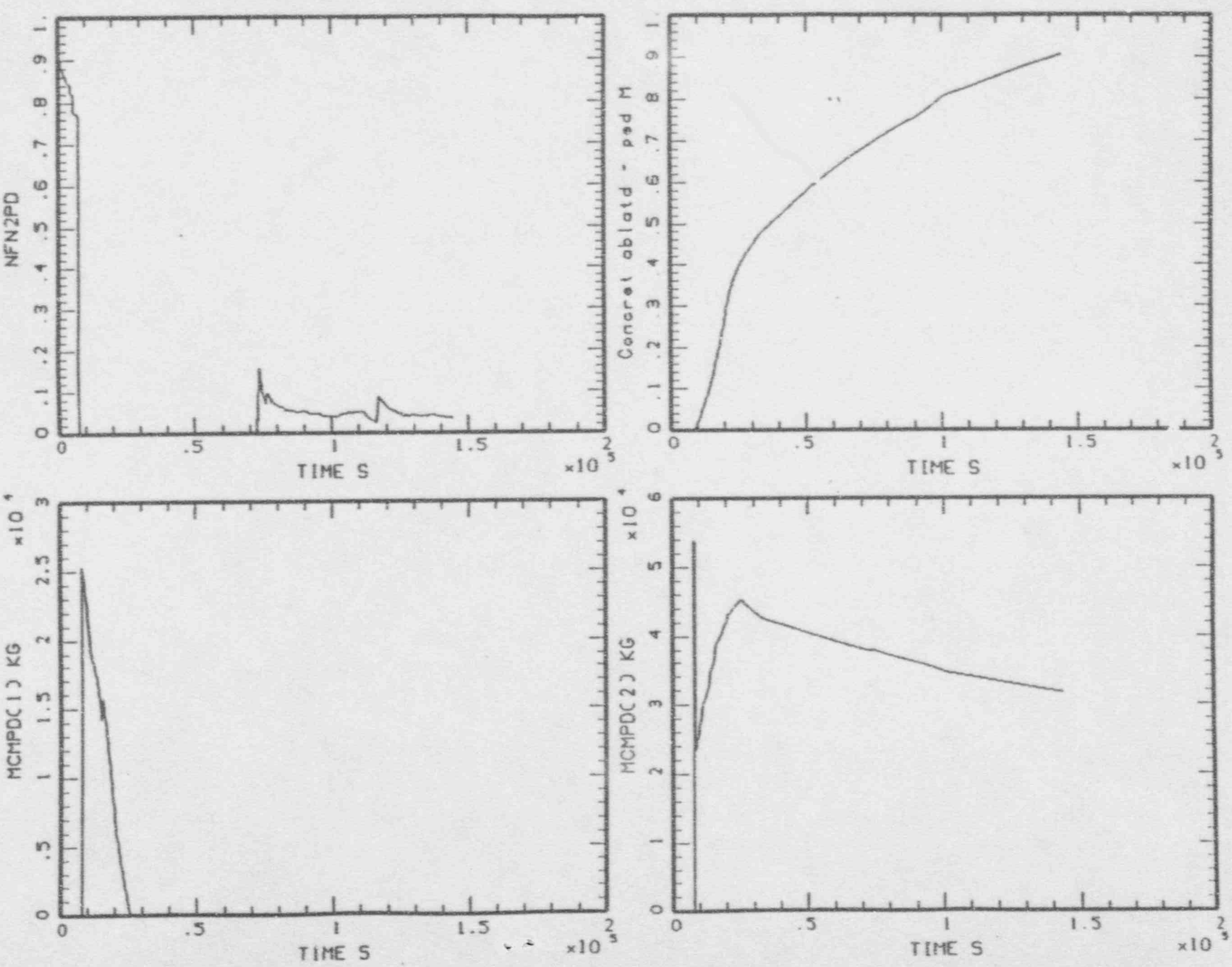

MAAP-MELCOR: BWR SBO. MCSPT = 10.000 KG
BNL_MCSP1.44.PLT LINE

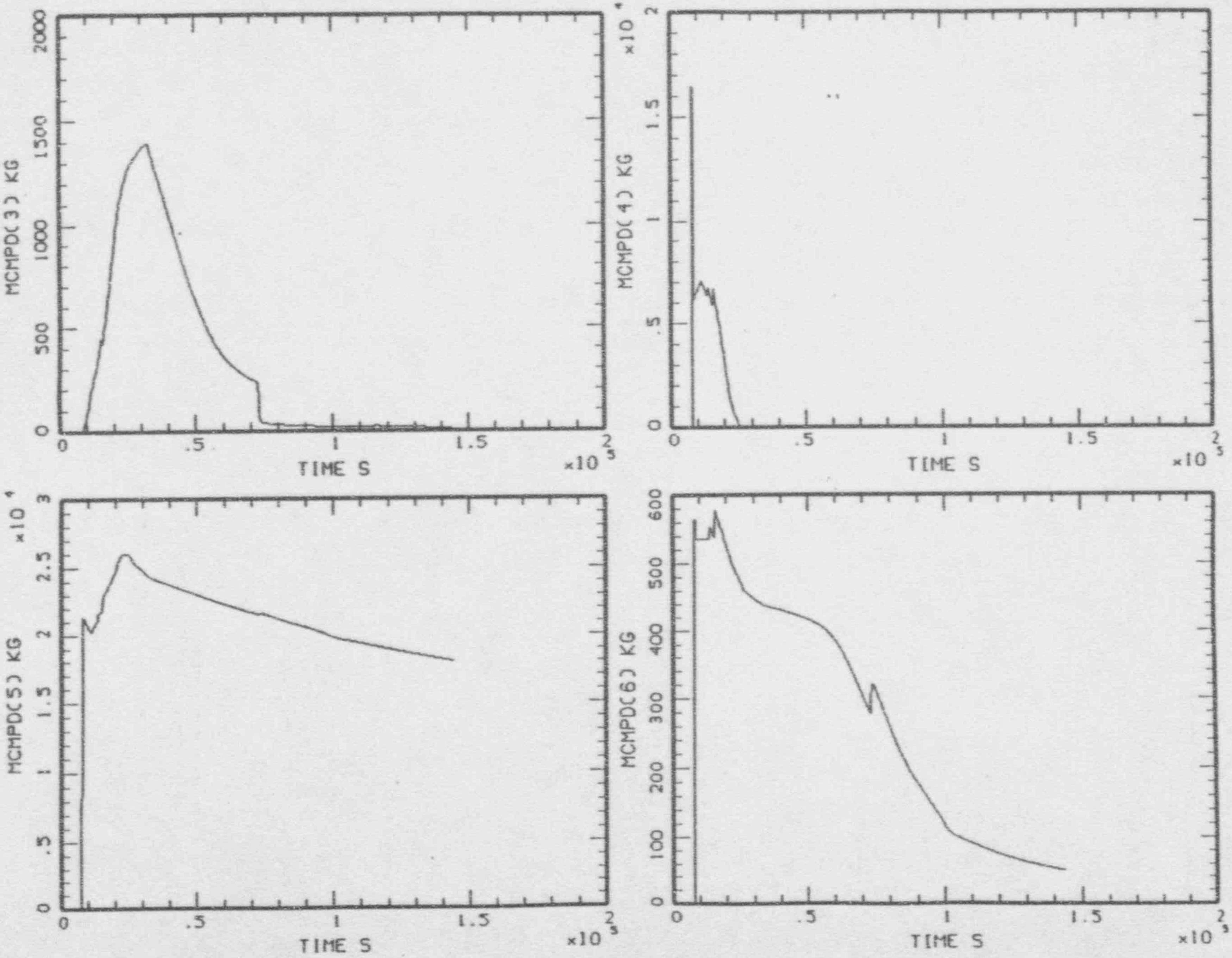

MAAP-MELCOR: BWR SBO. MCSPT = 10.000 KG
BNL_MCSP1_44.PLT LINE

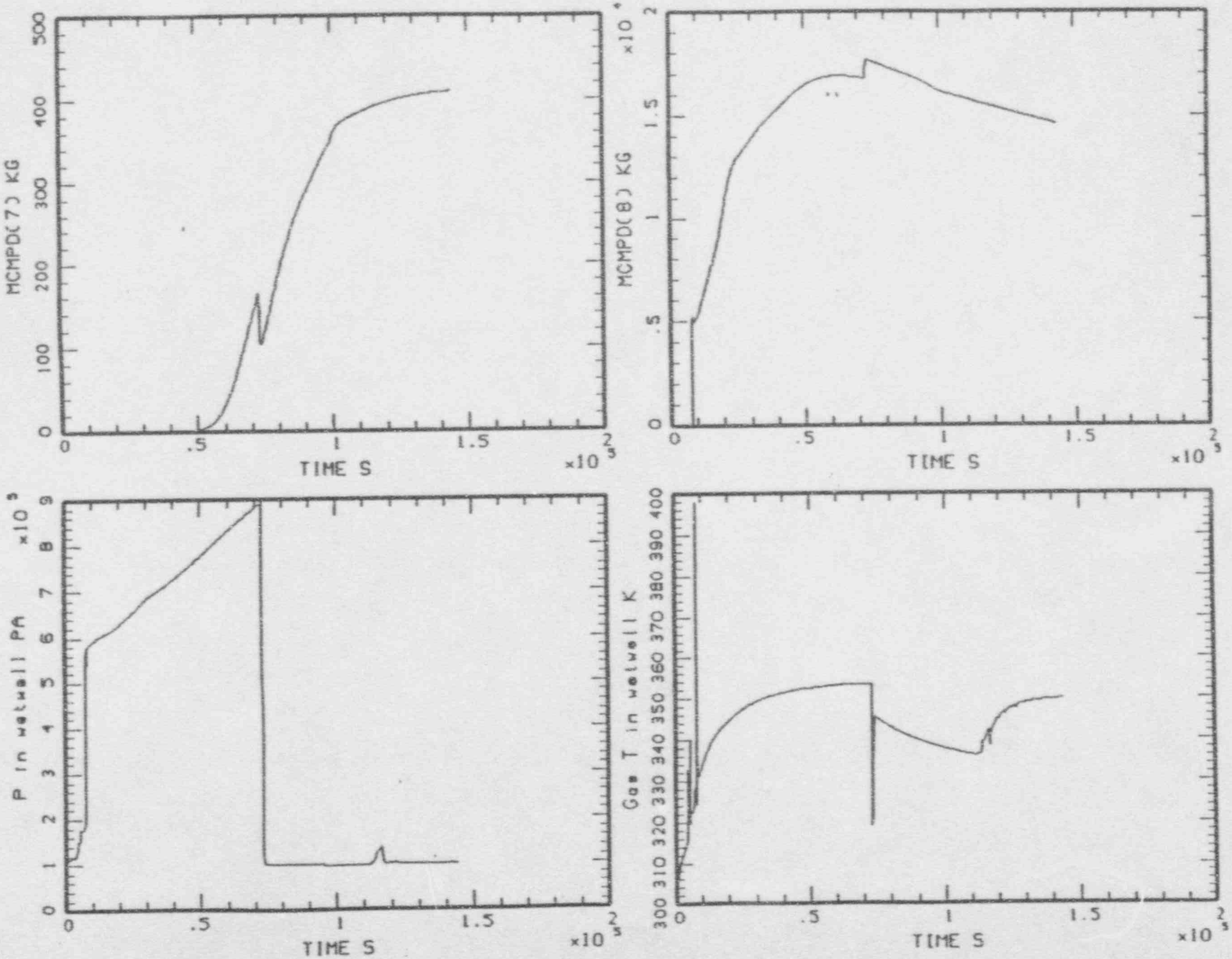

Case 3

HTCMCR = 1000.

NUMERICAL PERFORMANCE FIGURES OF MERIT

TIME (SEC)	144018.3
FRACTION OF CLAD REACTED IN VESSEL . .	0.2627
CONCRETE AEROSOL GENERATED (KG). . . .	615.6
UO2 MASS IN PEDESTAL (KG).	29016.2
UO2 MASS IN DRYWELL (KG)	140400.7
TIME OF CORE UNCOVERY (SEC).	1897.7
TIME OF VESSEL FAILURE (SEC)	6315.5
TIME OF CONTAINMENT FAILURE (SEC). . .	66815.?

CSI MASS BALANCE (KG)

INITIAL MASS	38.2155
IN CORE.	0.0000
IN CORIUM.	0.4950
IN PRIMARY SYSTEM.	6.7745
IN CONTAINMENT	19.5566
TOTAL IN-VESSEL RELEASED	36.3263
TOTAL EX-VESSEL RELEASED	1.3943
RELEASED FROM CONTAINMENT.	11.3914

SRO MASS BALANCE (KG)

INITIAL MASS	103.4367
IN CORE.	0.0000
IN CORIUM.	103.2158
IN PRIMARY SYSTEM.	0.0542
IN CONTAINMENT	0.2110
TOTAL IN-VESSEL RELEASED	0.0652
TOTAL EX-VESSEL RELEASED	0.2001
RELEASED FROM CONTAINMENT.	0.0001

```
FORTRAN STOP
$ delete BNL_HT4_inp.dat;*
$ delete BNL_HT4_par.dat;*
$!
$ node = "M3300"
$ if "FALSE".eqs."FALSE" then logoff/full
  WUTOBY        job terminated at  9-APR-1991 09:19:29.83

  Accounting information:
  Buffered I/O count:           655    Peak working set size:   1421
  Direct I/O count:           13417    Peak page file size:     4600
  Page faults:                 2123    Mounted volumes:            0
  Charged CPU time:   0 00:00:45.88    Elapsed time:     0 01:06:16.76
```

MAAP-MELCOR: BWR SBO/H=10000
BNL_HT4_43.PLT LINE

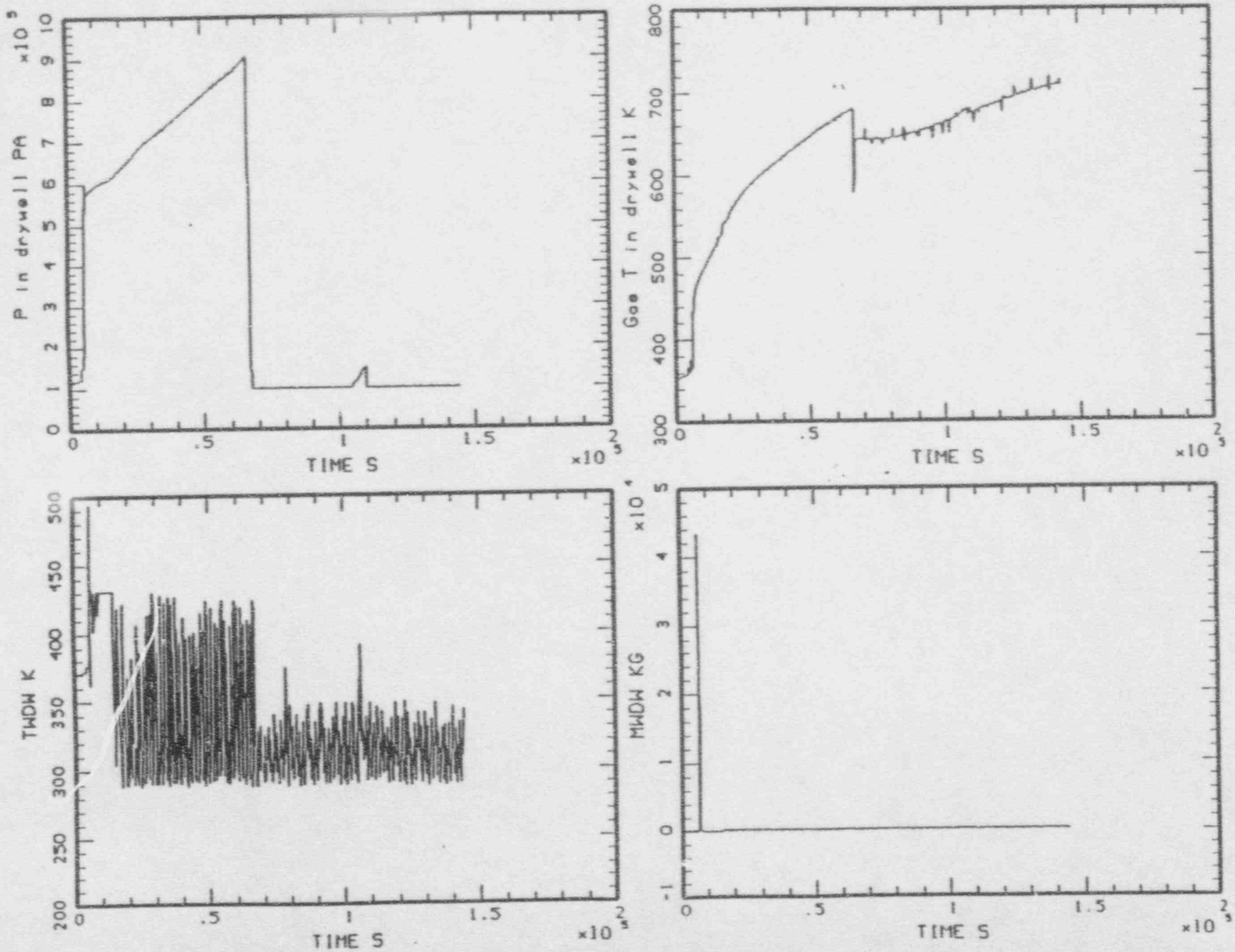

MAAP-MELCOR: BWR SBO/H=10000
BNL_HT4_43.PLT LINE

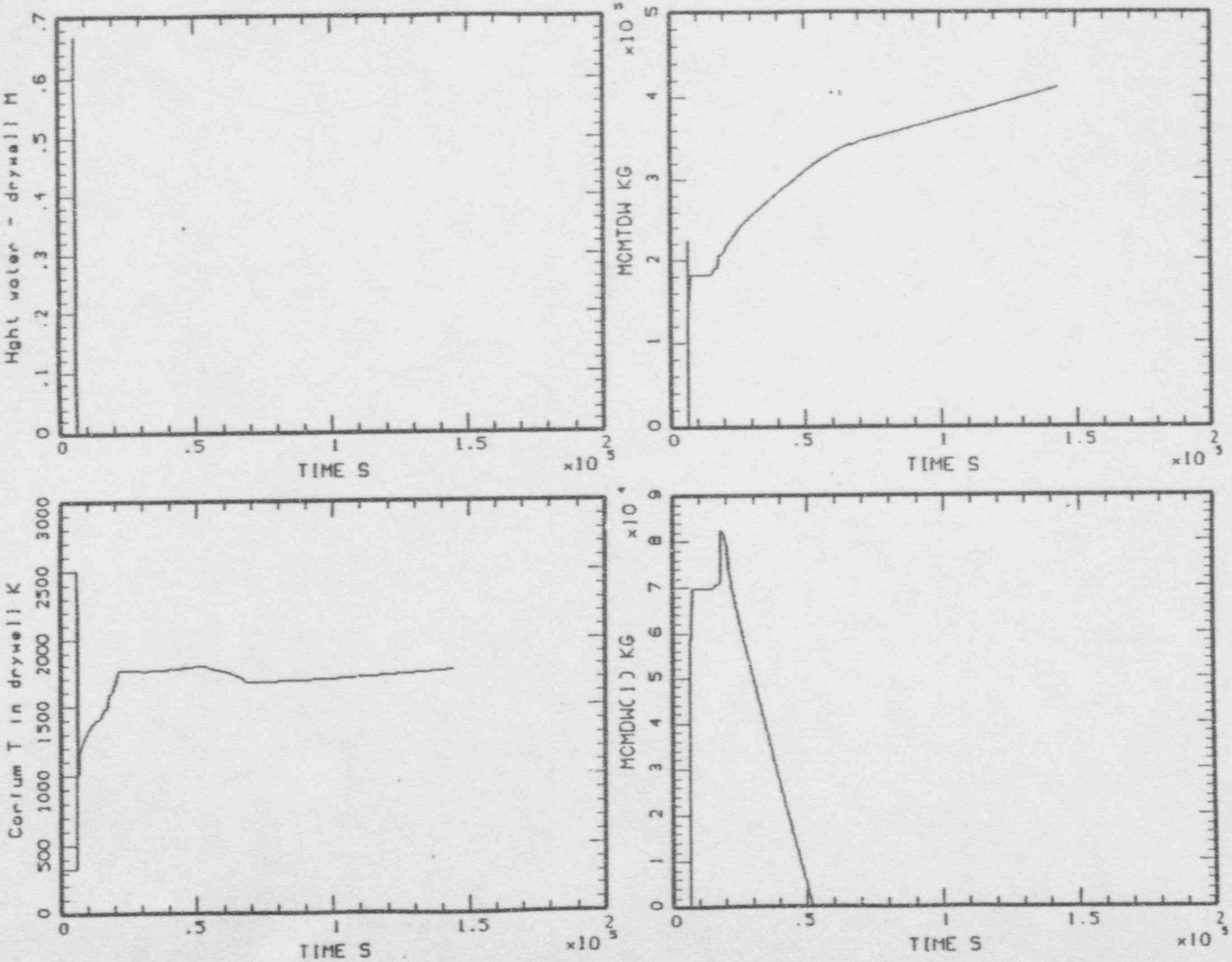

MAAP-MELCOR: BWR SBO/H=10000
BNL_HT4_43.PLT LINE

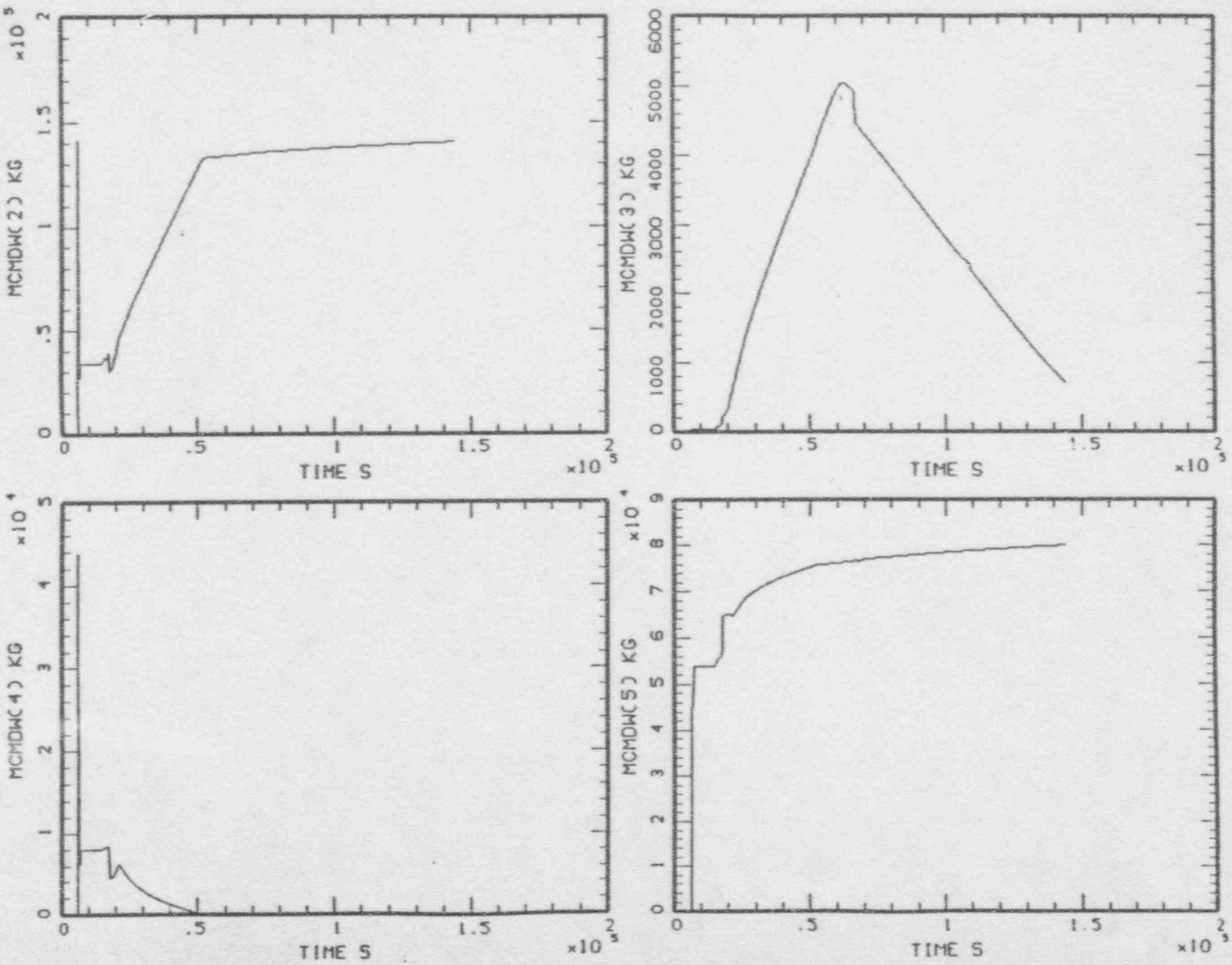

MAAP-MELCOR: BWR SBO/H=10000
BNL_HT4_43.PLT LINE

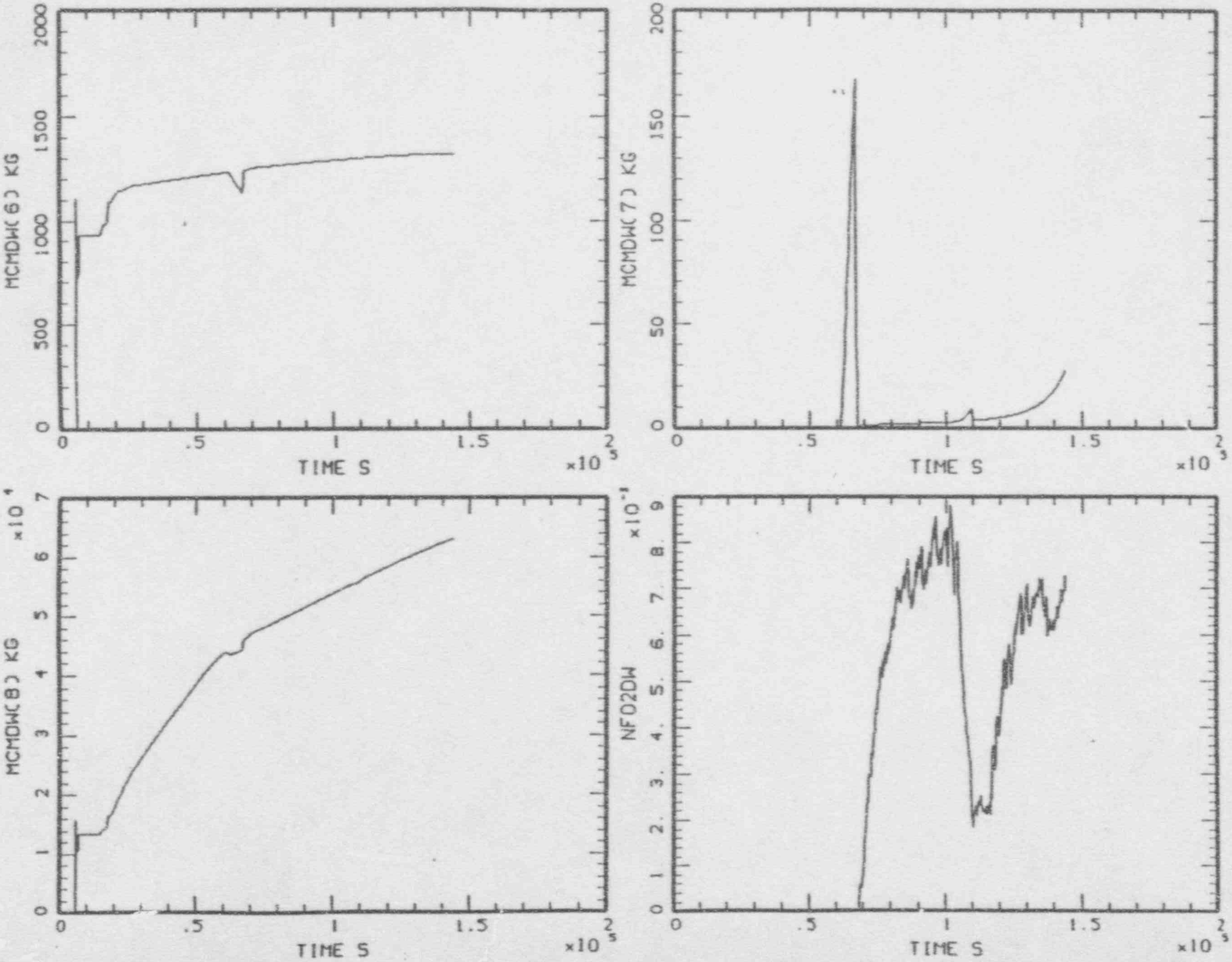

MAAP-MELCOR: BWR SBO/H=10000
BNL_HT4_43.PLT LINE

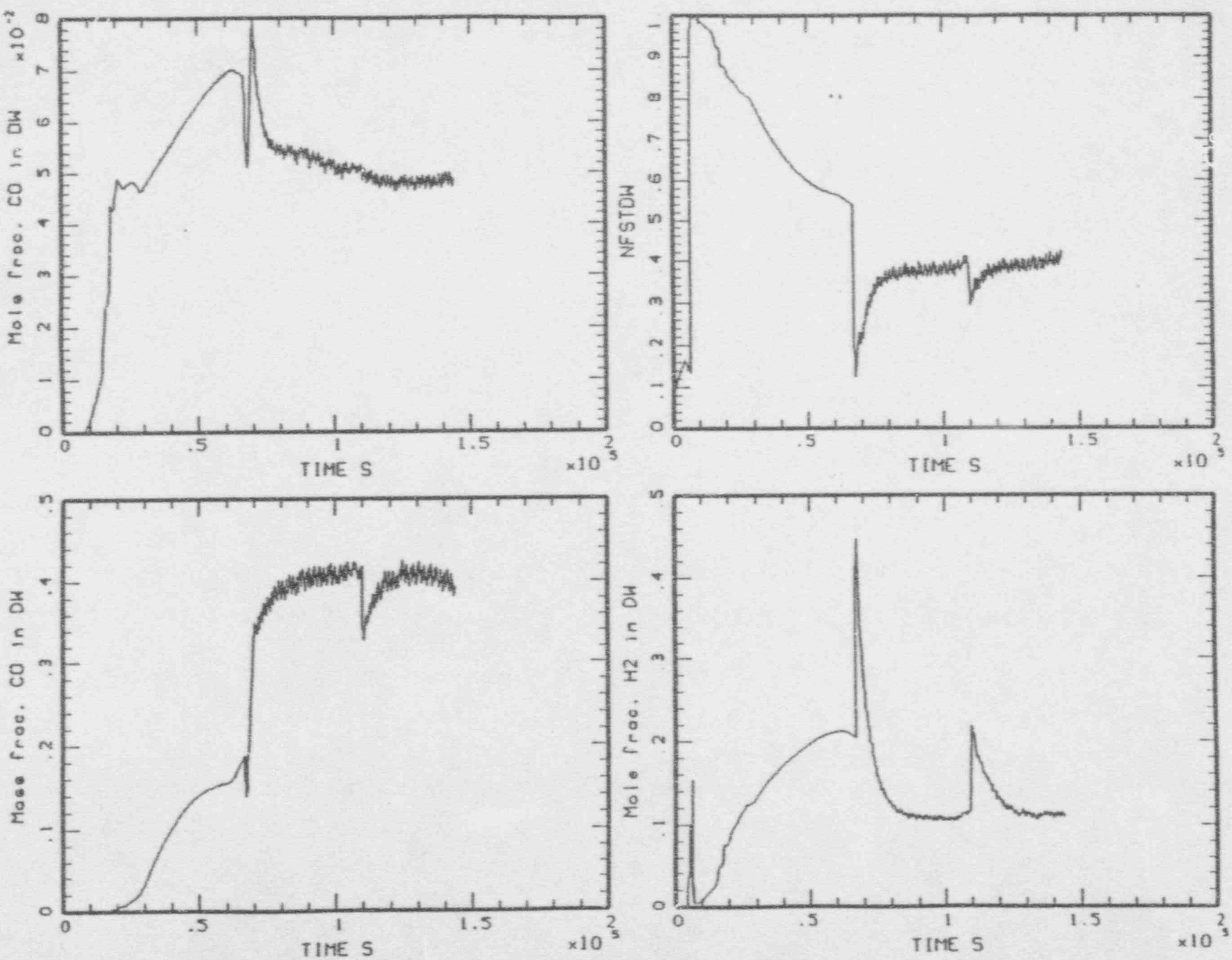

MAAP-MELCOR: BWR SBO/H=10000
BNL_HT4_43.PLT LINE

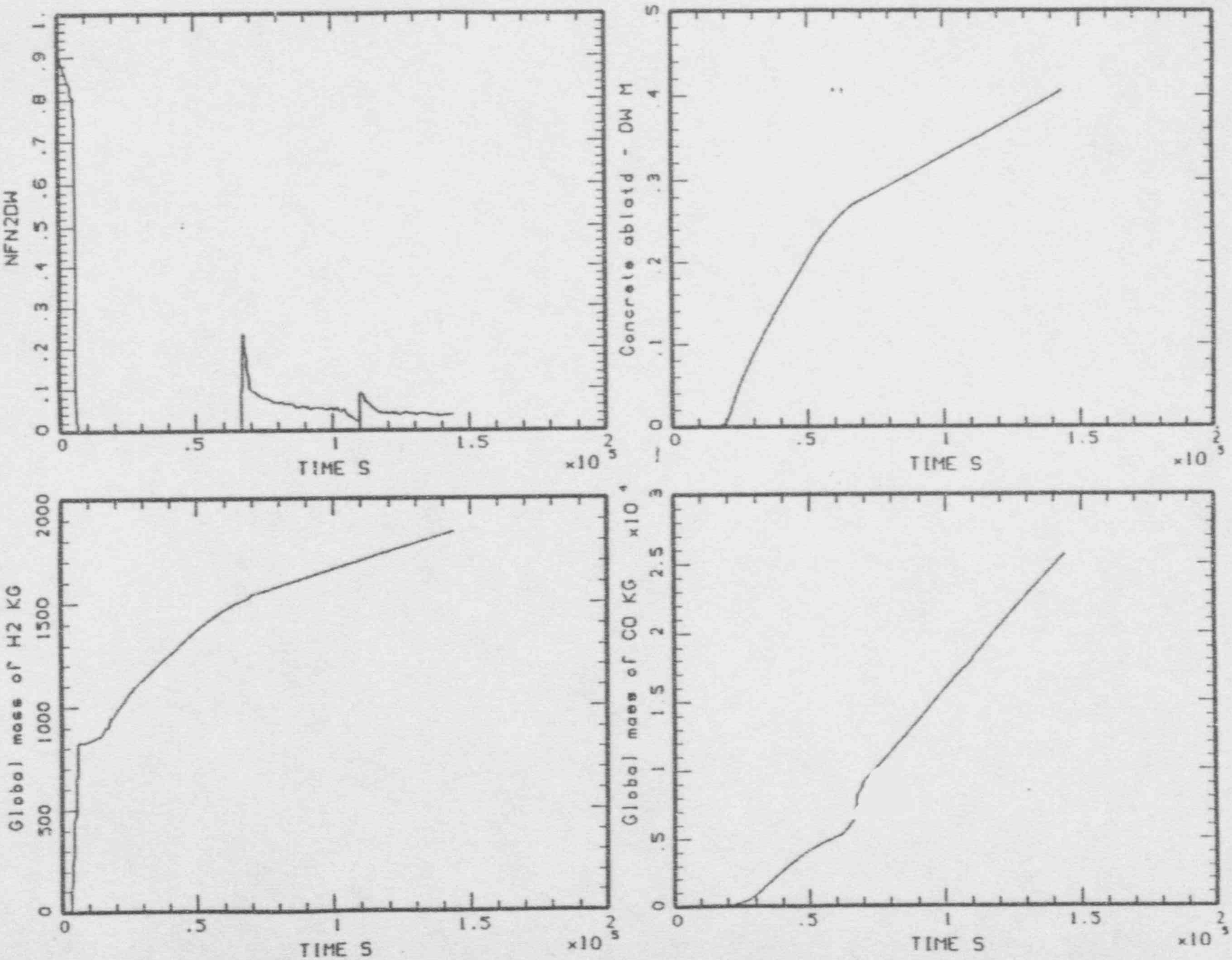

MAAP-MELCOR: BWR SBO/H=10000
BNL_HT4_44.PLT LINE

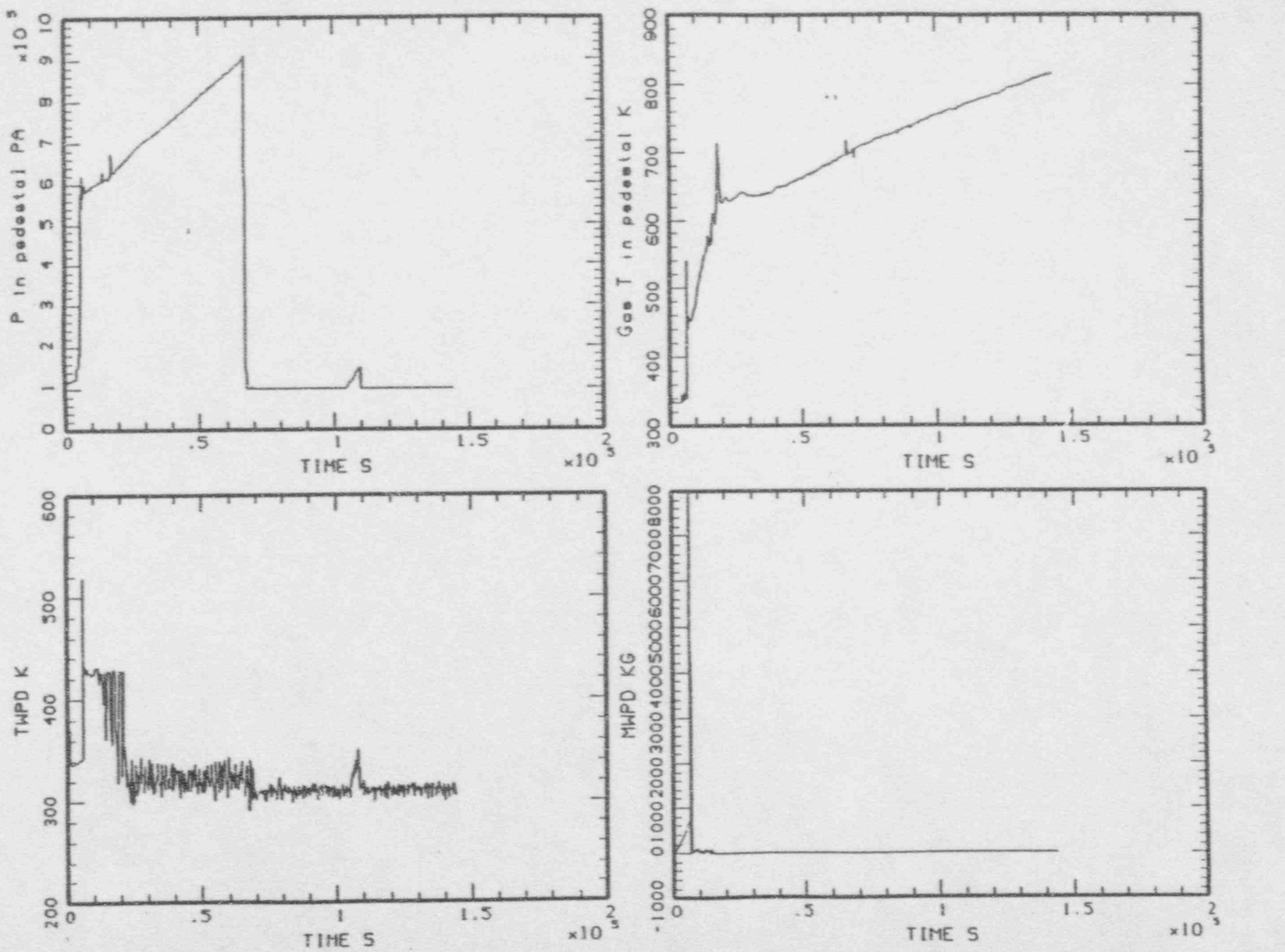

MAAP-MELCOR: BWR SBO/H=10000
BNL_HT4_44.PLT LINE

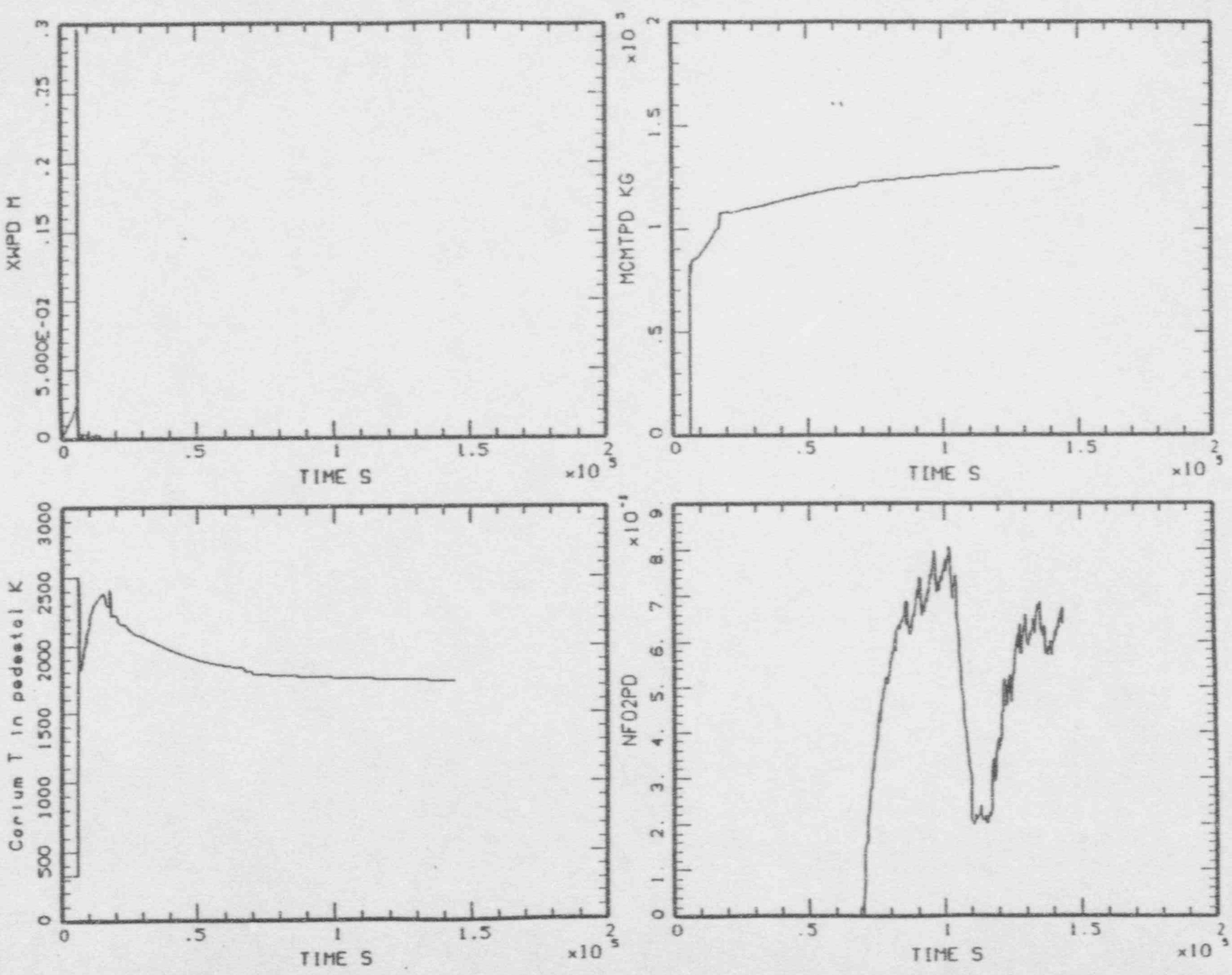

MAAP-MELCOR: BWR SBO/H=10000
BNL_HT4_44.PLT LINE

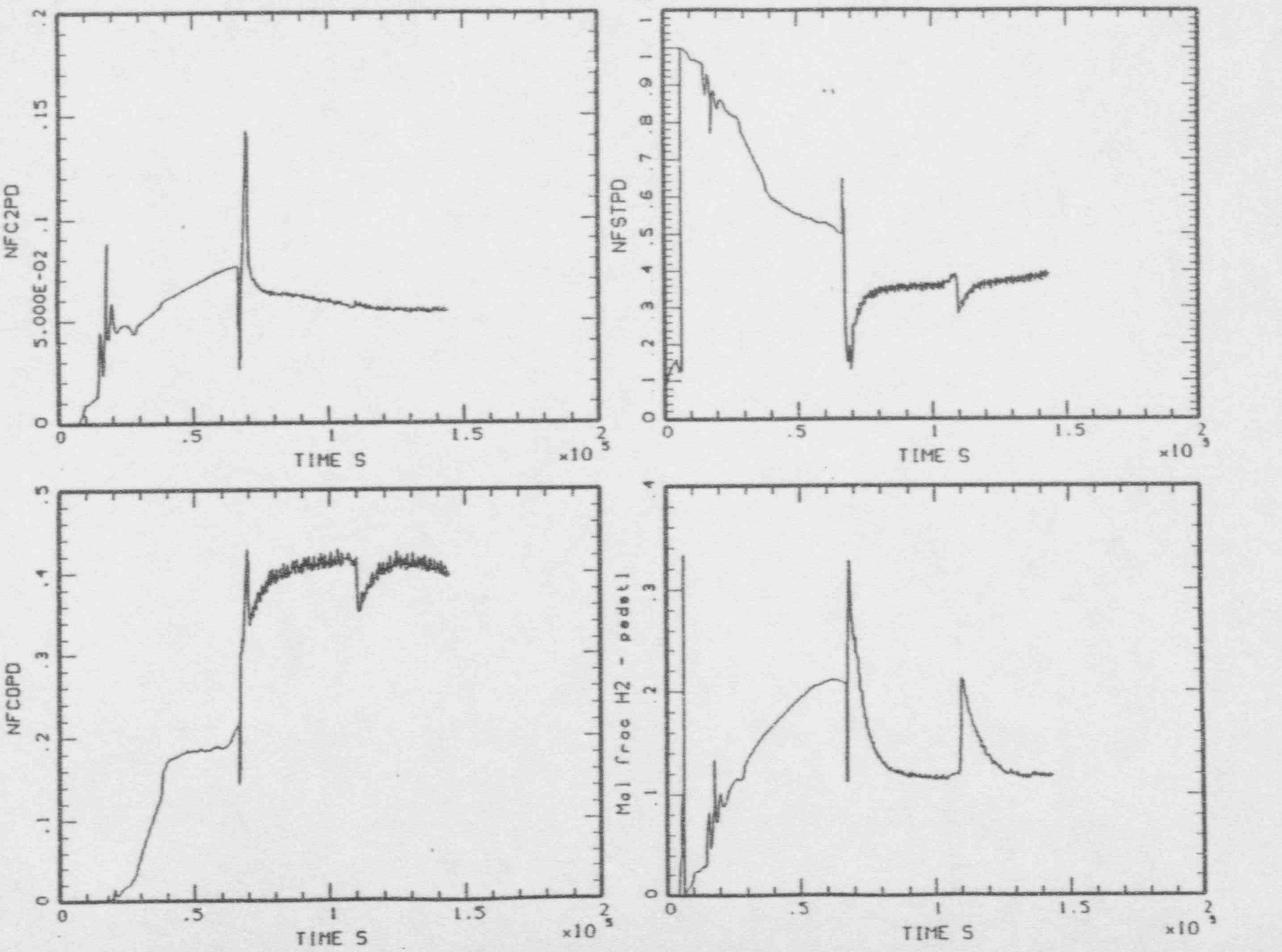

MAAP-MELCOR: BWR SBO/H=10000
BNL_HT4_44.PLT LINE

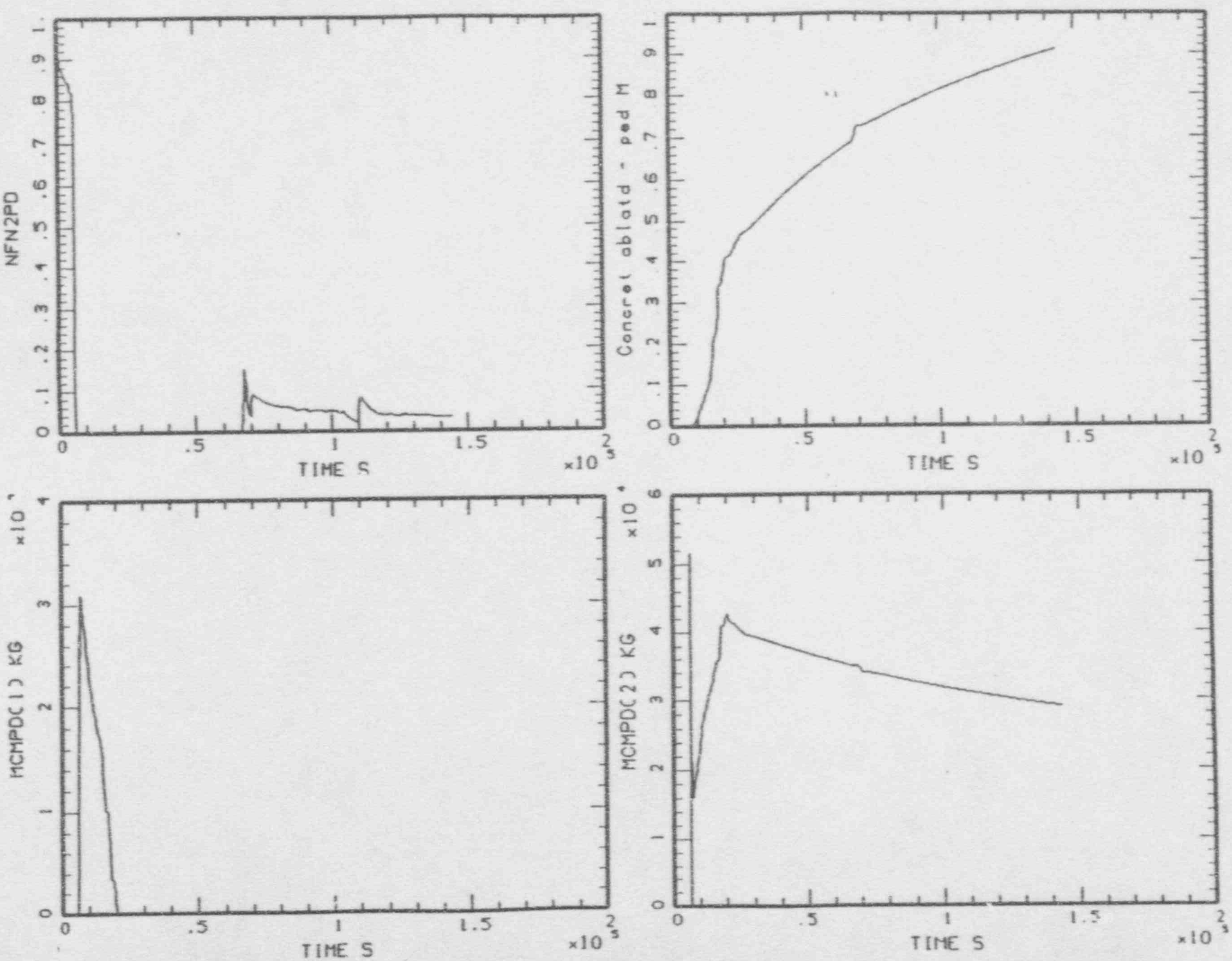

MAAP-MELCOR: BWR SBO/H=10000
BNL_HT4_44.PLT LINE

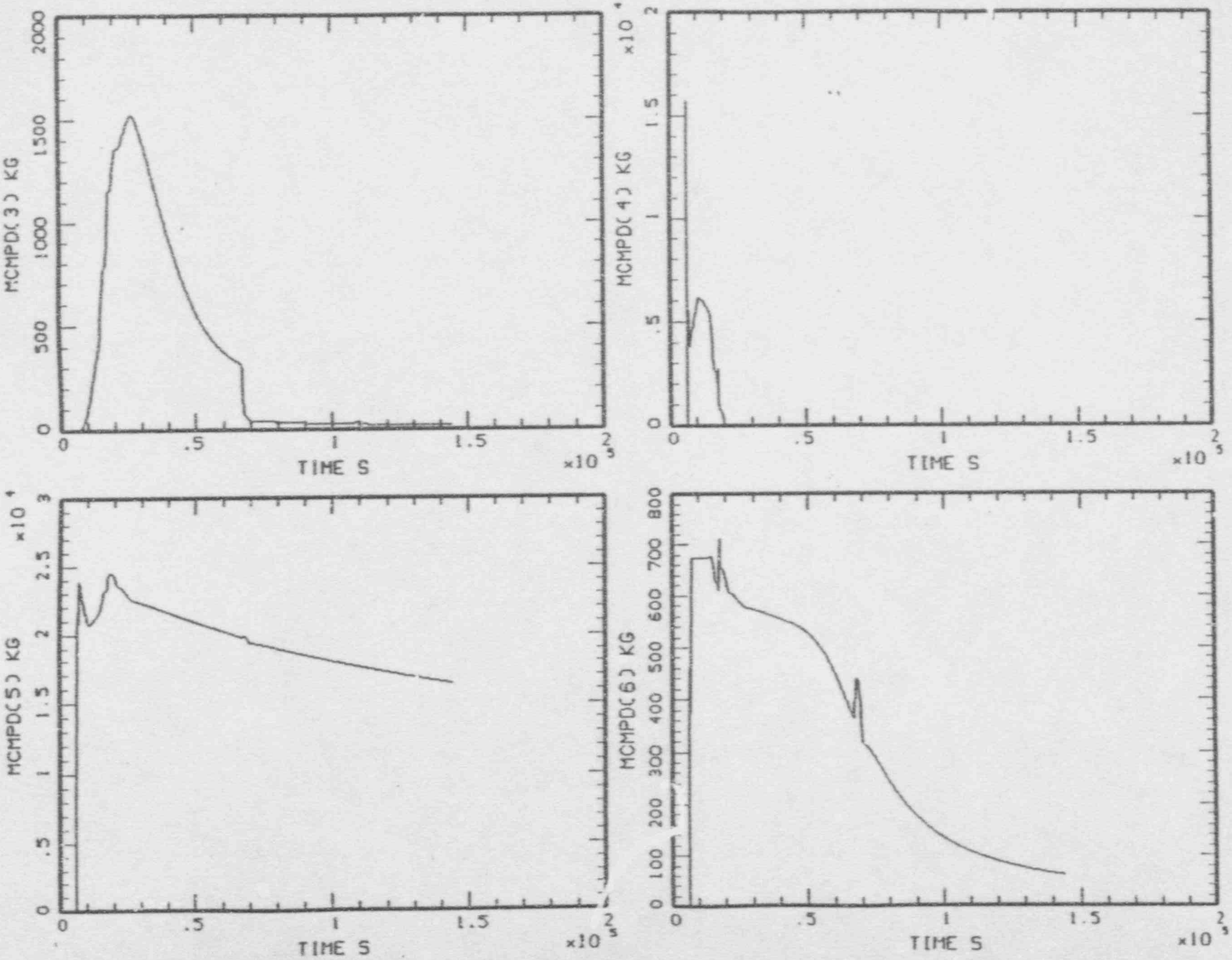

MAAP-MELCOR: BWR SBO/H=10000
BNL_HT4_44.PLT LINE

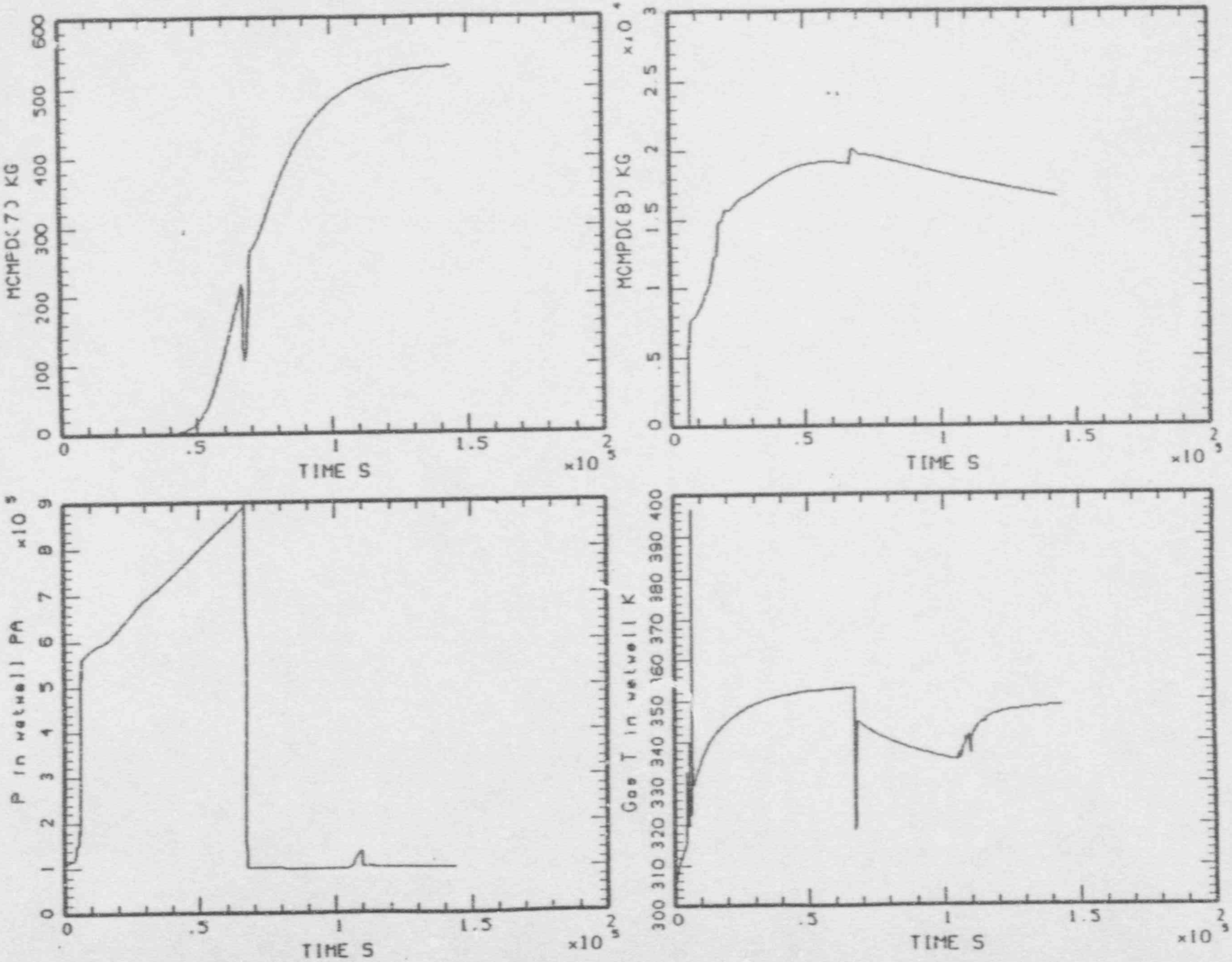

BNL_HT4_78.PLT LINE

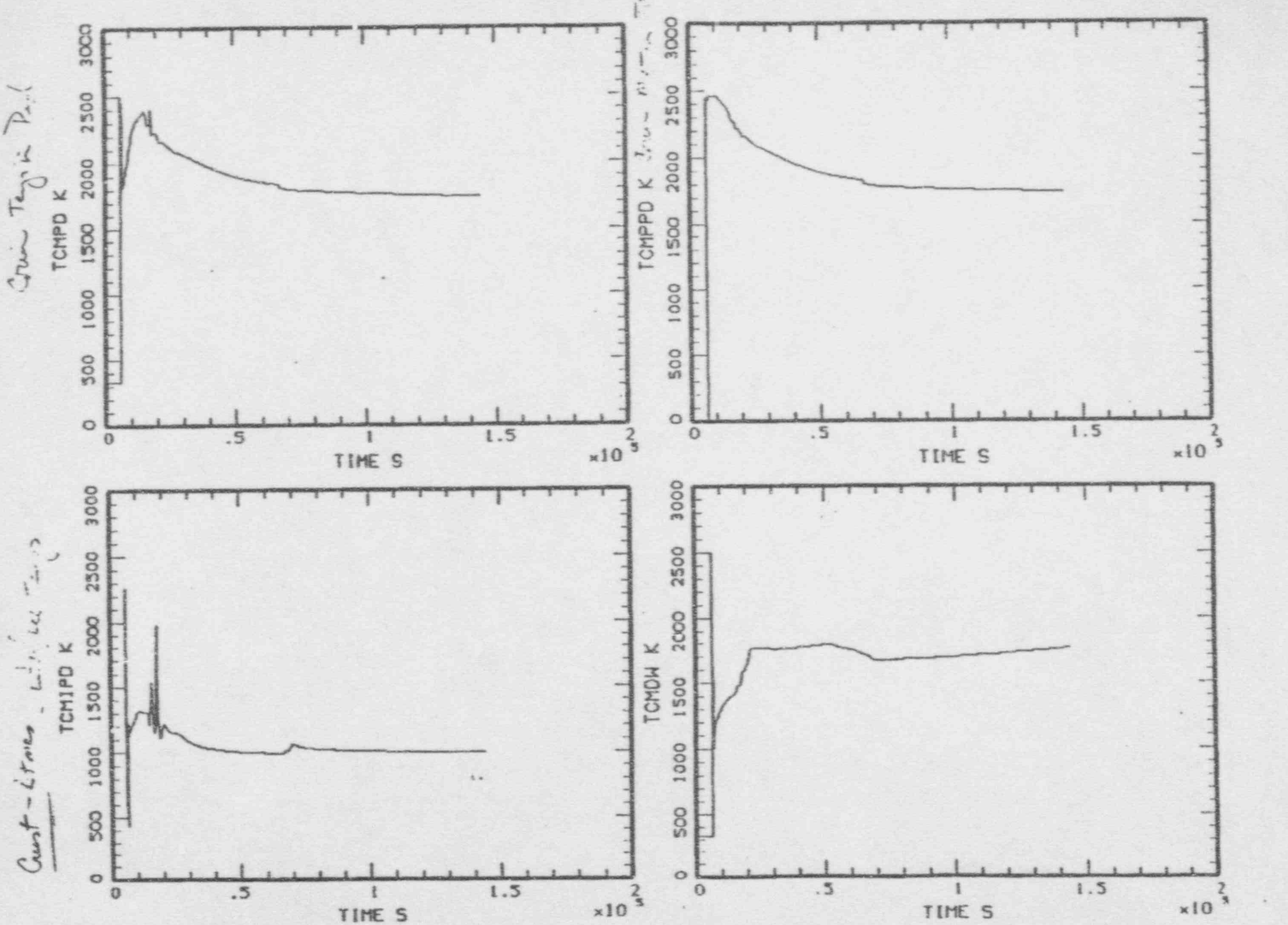

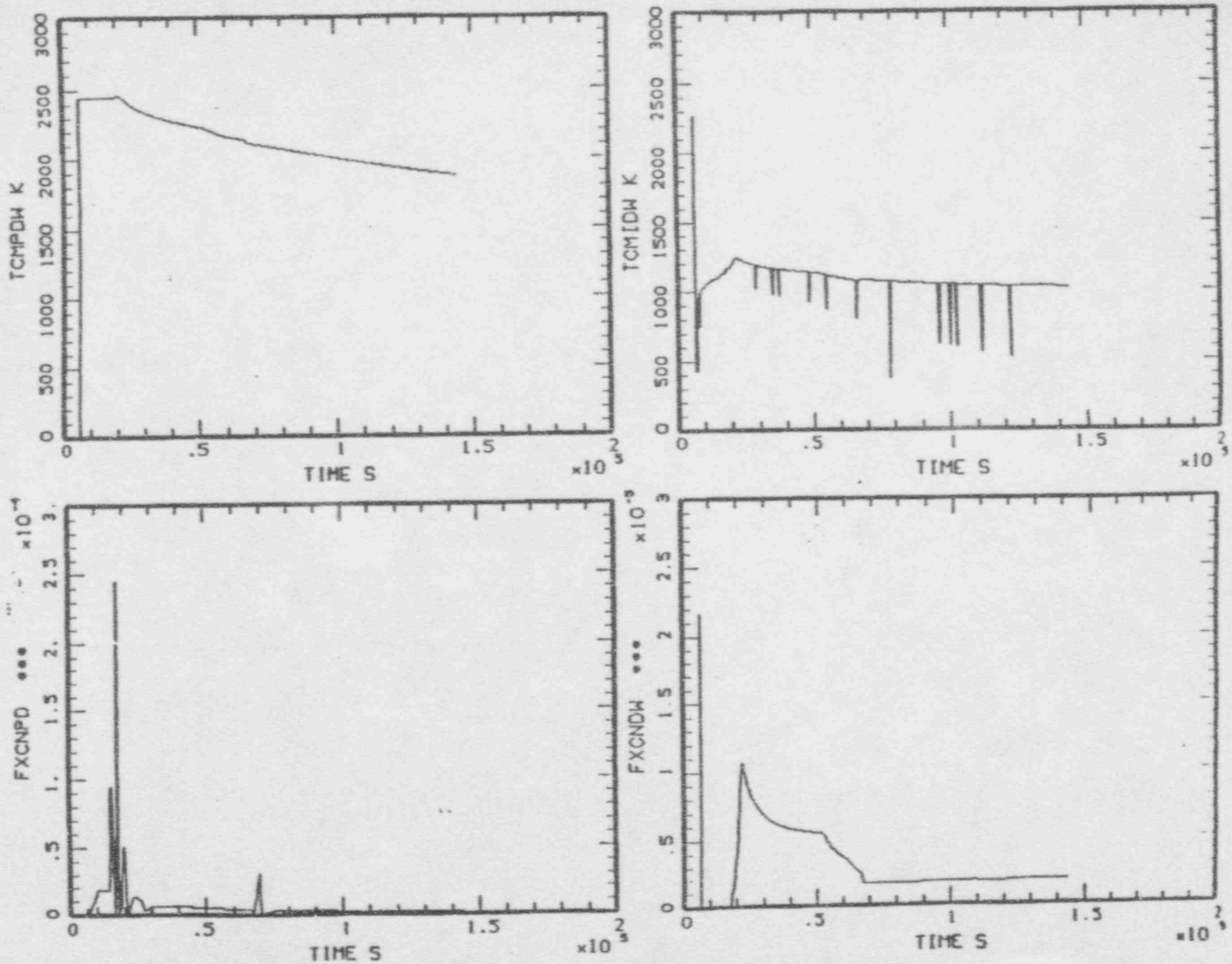
TCMPDW K
0
500
1000
1500
2000
2500
3000
0
.5
1
1.5
2
×10^5
TIME S
TCMIDW K
0
500
1000
1500
2000
2500
3000
0
.5
1
1.5
2
×10^5
TIME S
FXCNPD ***
×10^-4
0
.5
1.
1.5
2.
2.5
3.
0
.5
1
1.5
2
×10^5
TIME S
FXCNDW ***
×10^-3
0
.5
1
1.5
2
2.5
3
0
.5
1
1.5
2
×10^5
TIME S

BNL_H14_78.PLT LINE

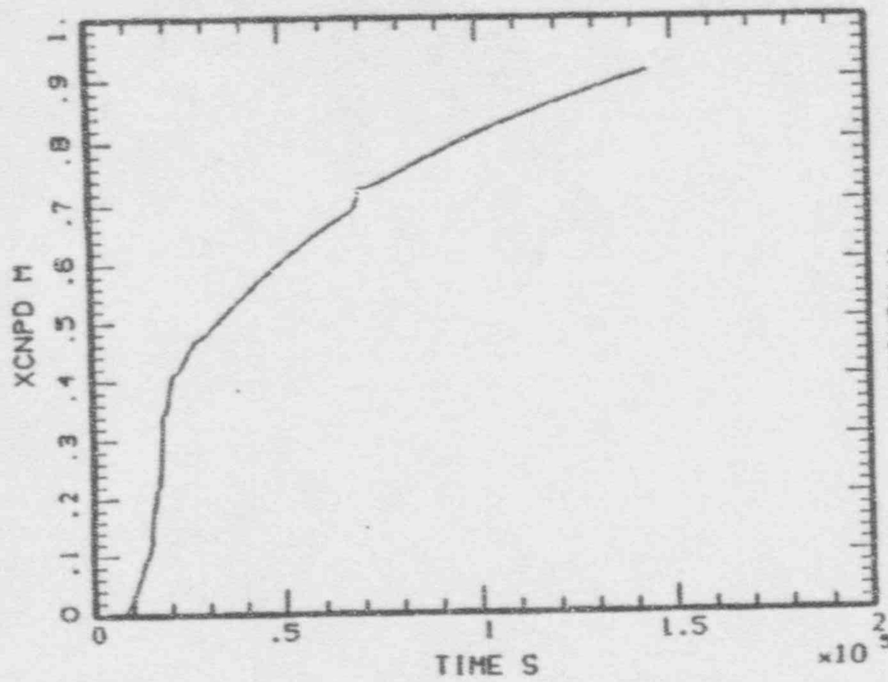

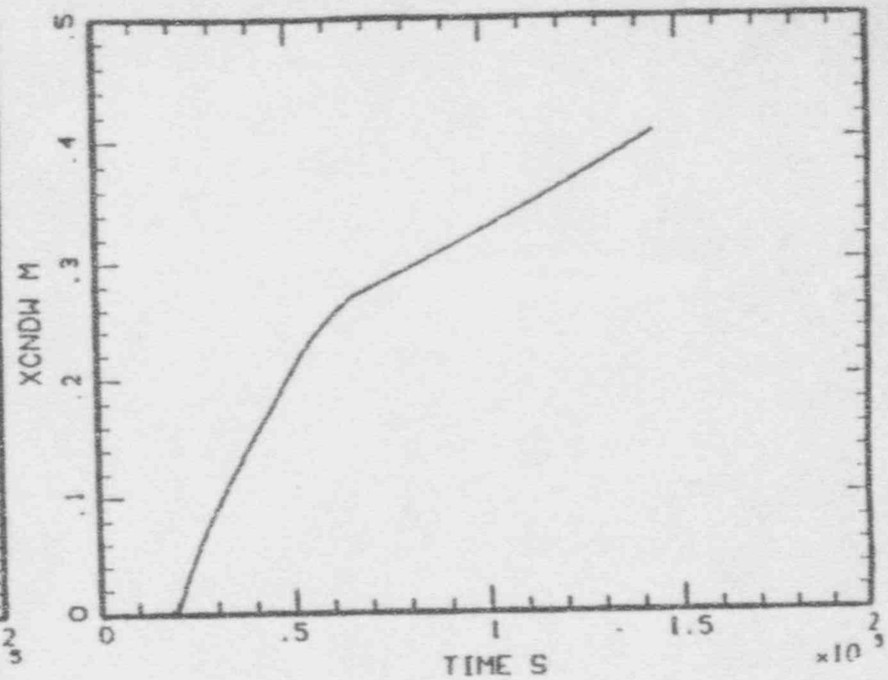

_2DUA1:[WUTOBY.BNL5]BNL_DWO.FOMA;1 9-APR-1991 16:13

CASE 4

~ 1/4 ADWF

```
NUMERICAL    PERFORMANCE    FIGURES    OF    MERIT

TIME (SEC) . . . . . . . . . . . . . .           144005.6

FRACTION OF CLAD REACTED IN VESSEL . .             0.2872
CONCRETE AEROSOL GENERATED (KG). . . .             2859.3

UO2 MASS IN PEDESTAL (KG). . . . . . .              343.1
UO2 MASS IN DRYWELL (KG) . . . . . . .           169040.2

TIME OF CORE UNCOVERY (SEC). . . . . .             1906.6
TIME OF VESSEL FAILURE (SEC) . . . . .             8021.2
TIME OF CONTAINMENT FAILURE (SEC). . .            40785.6

CSI MASS BALANCE (KG)

    INITIAL MASS . . . . . . . . . . .            38.2155
    IN CORE. . . . . . . . . . . . . .             0.0000
    IN CORIUM. . . . . . . . . . . . .             0.0360
    IN PRIMARY SYSTEM. . . . . . . . .             8.7112
    IN CONTAINMENT . . . . . . . . . .            22.6639
    TOTAL IN-VESSEL RELEASED . . . . .            37.3837
    TOTAL EX-VESSEL RELEASED . . . . .             0.7959
    RELEASED FROM CONTAINMENT. . . . .             6.8042

SRO MASS BALANCE (KG)

    INITIAL MASS . . . . . . . . . . .           103.4367
    IN CORE. . . . . . . . . . . . . .             0.0000
    IN CORIUM. . . . . . . . . . . . .           102.8088
    IN PRIMARY SYSTEM. . . . . . . . .             0.0562
    IN CONTAINMENT . . . . . . . . . .             0.5730
    TOTAL IN-VESSEL RELEASED . . . . .             0.0617
    TOTAL EX-VESSEL RELEASED . . . . .             0.5795
    RELEASED FROM CONTAINMENT. . . . .             0.0120

FORTRAN STOP
$ delete BNL_DWO_inp.dat;*
$ delete BNL_DWO_par.dat;*
$!
$ node = "M3300"
$ if "FALSE".eqs."FALSE" then logoff/full
  WUTOBY        job terminated at  9-APR-1991 13:06:39.40

  Accounting information:
  Buffered I/O count:            677    Peak working set size:   1420
  Direct I/O count:            12963    Peak page file size:     4600
  Page faults:                  2121    Mounted volumes:            0
  Charged CPU time:    0 00:00:46.99    Elapsed time:    0 01:03:54.55
```

MAAP-MELCOR: BWR SBO/DW
BNL_DWO_43.PLT LINE

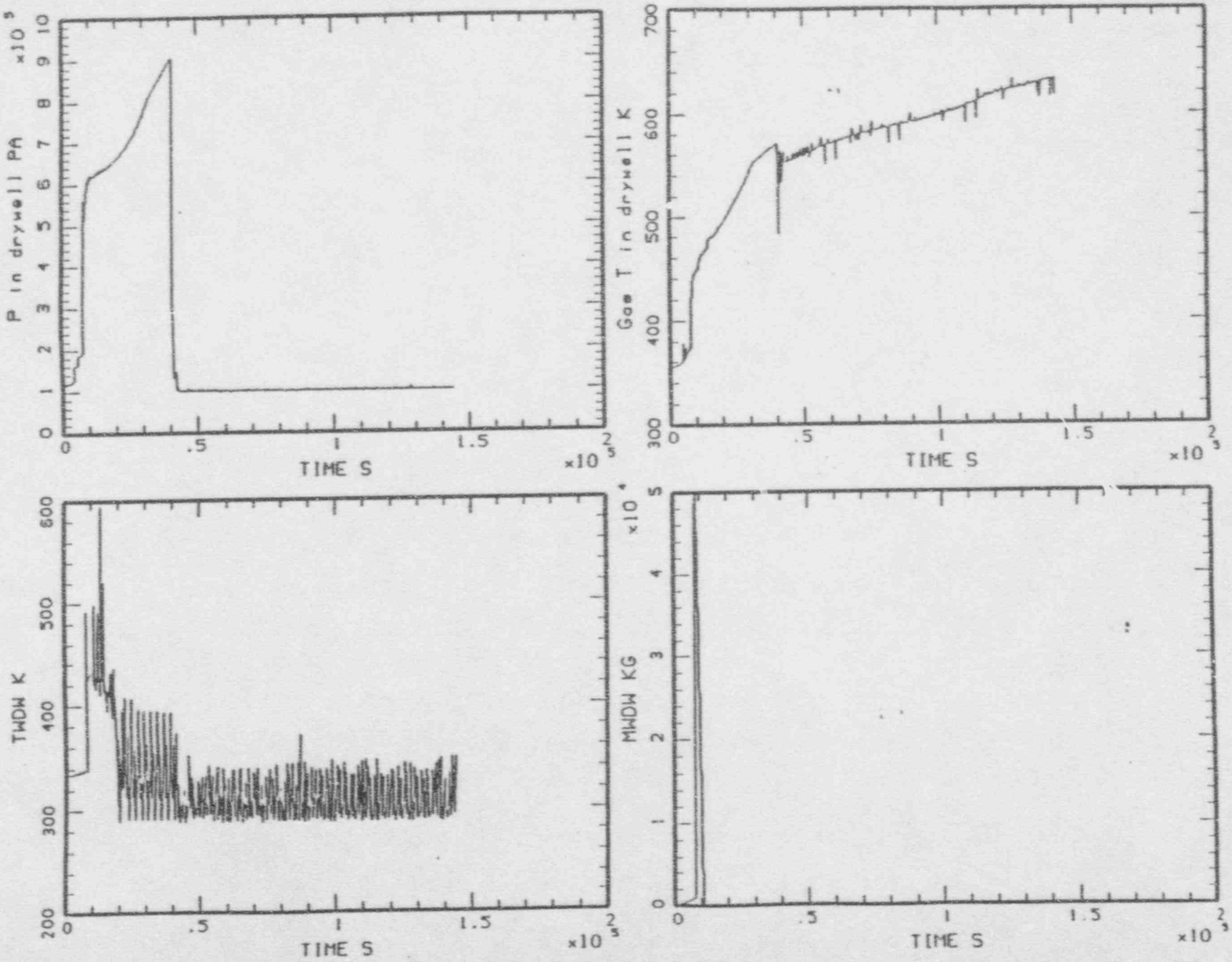

MAAP-MELCOR: BWR SBO/DW
BNL_DWO_43.PLT LINE

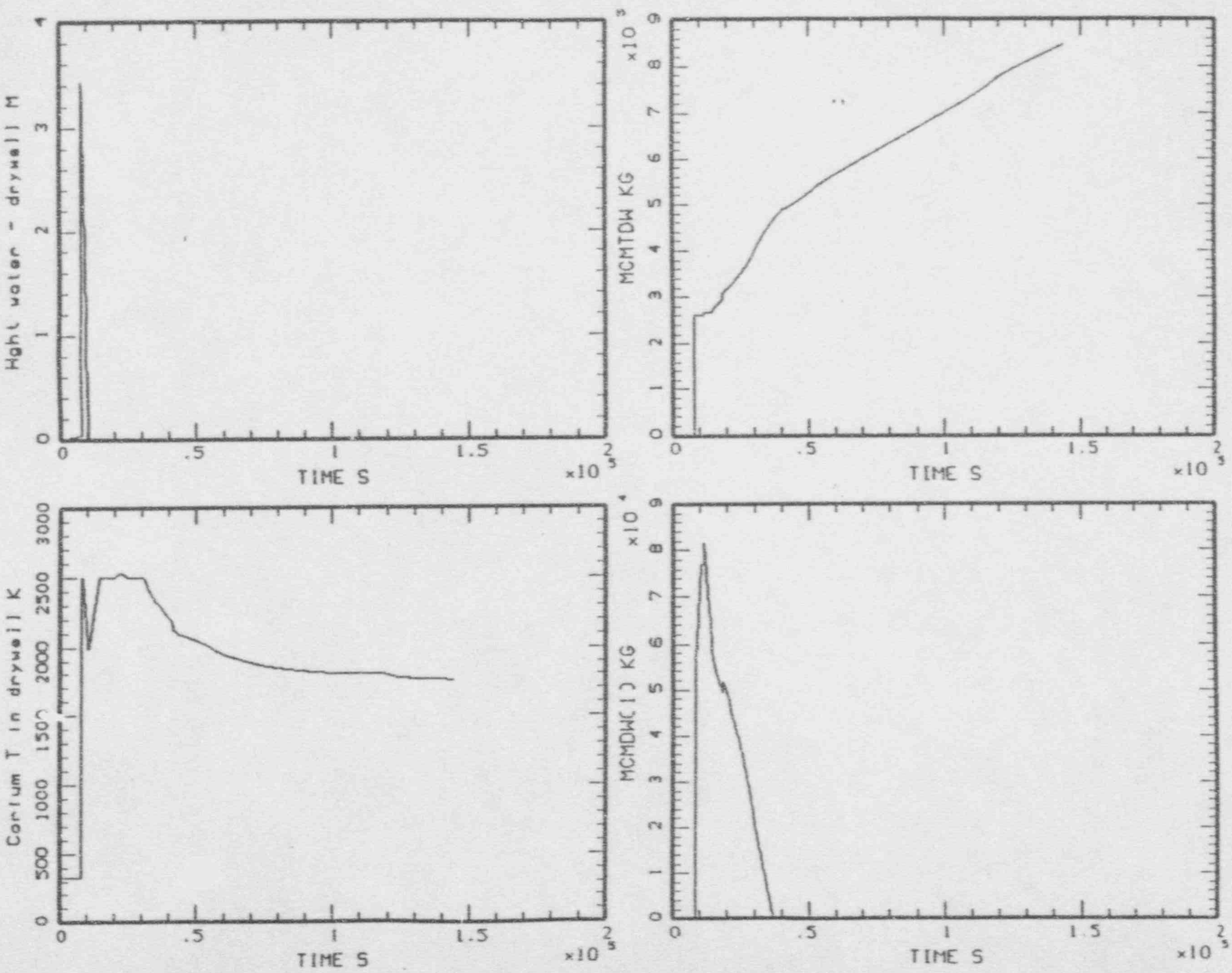

MAAP-MELCOR: BWR SBO/DW
BNL_DWO_43.PLT LINE

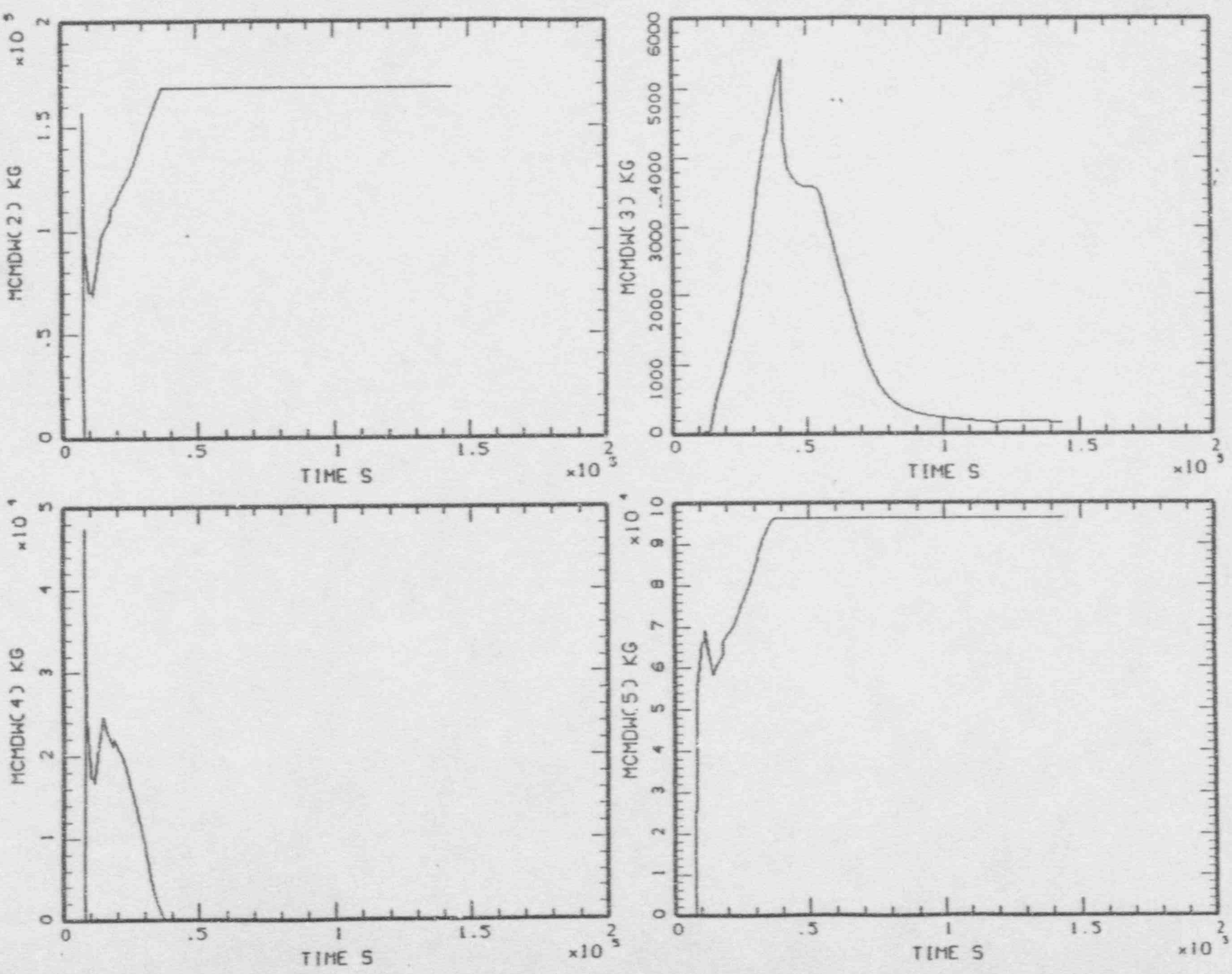

MAAP-MELCOR: BWR SBO/DW
BNL_DWO_43.PLT LINE

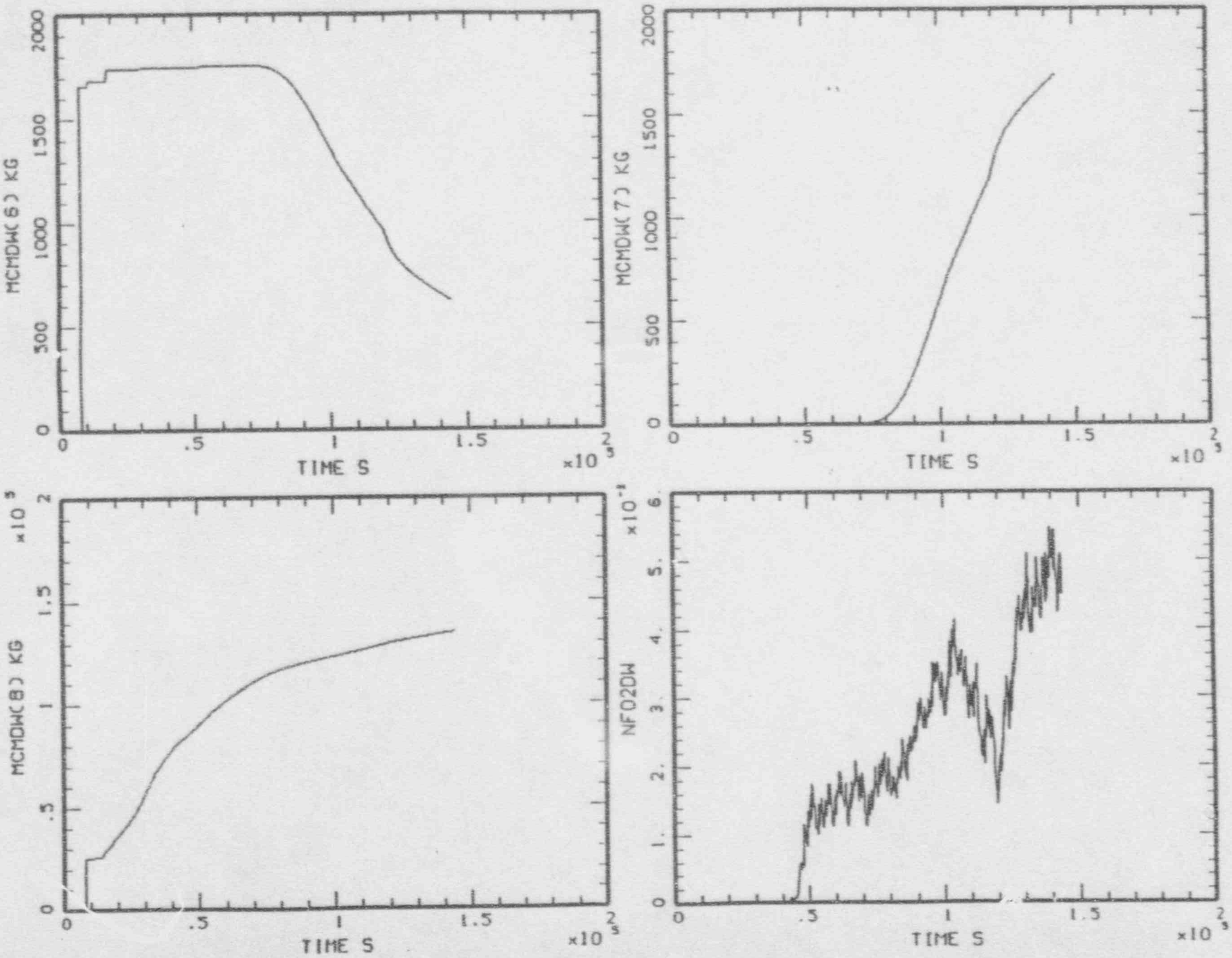

MAAP-MELCOR: BWR SBO/DW
BNL_DWO_43.PLT LINE

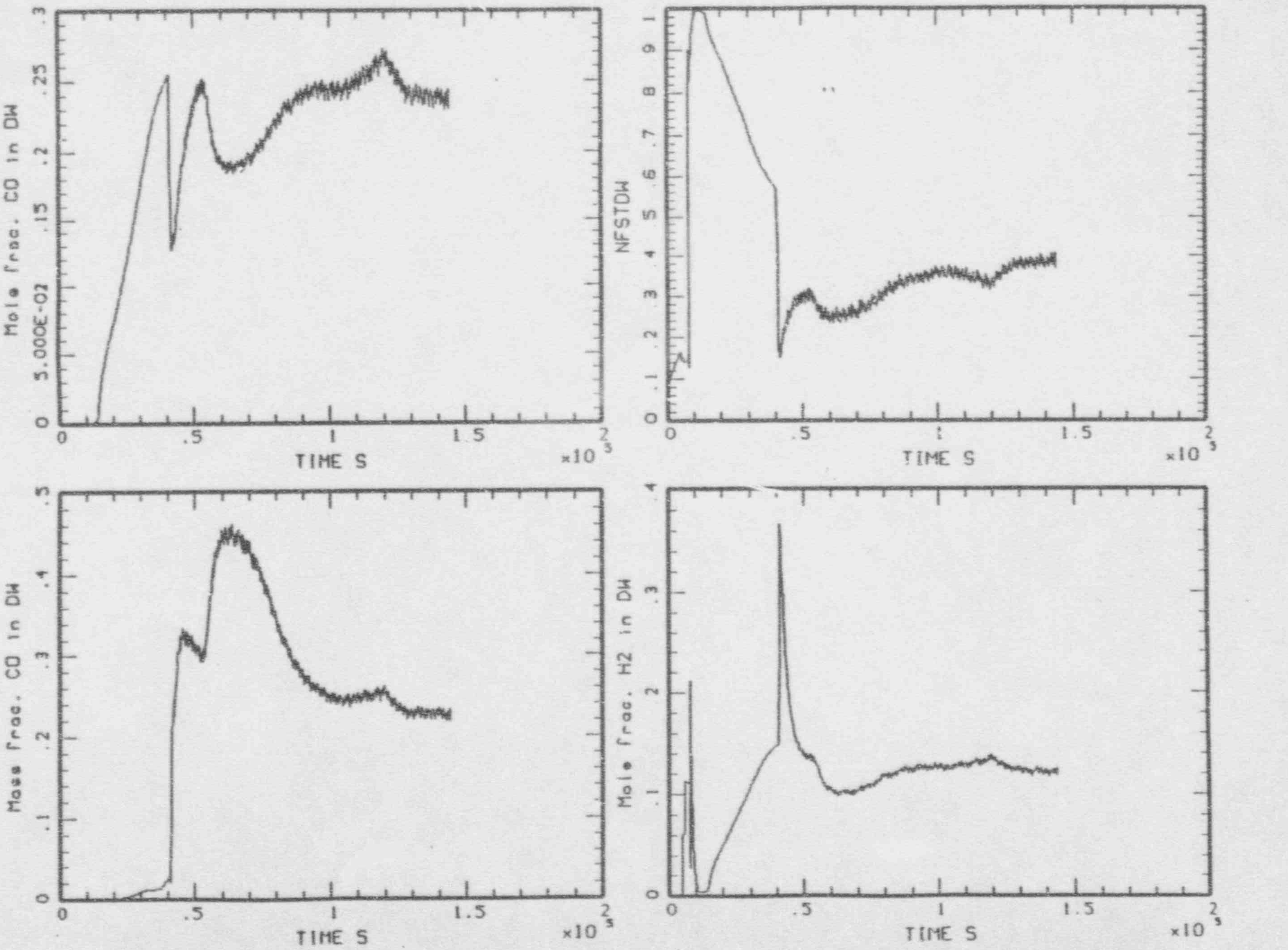

MAAP-MELCOR: BWR SBO/DW
BNL_DWO_43.PLT LINE

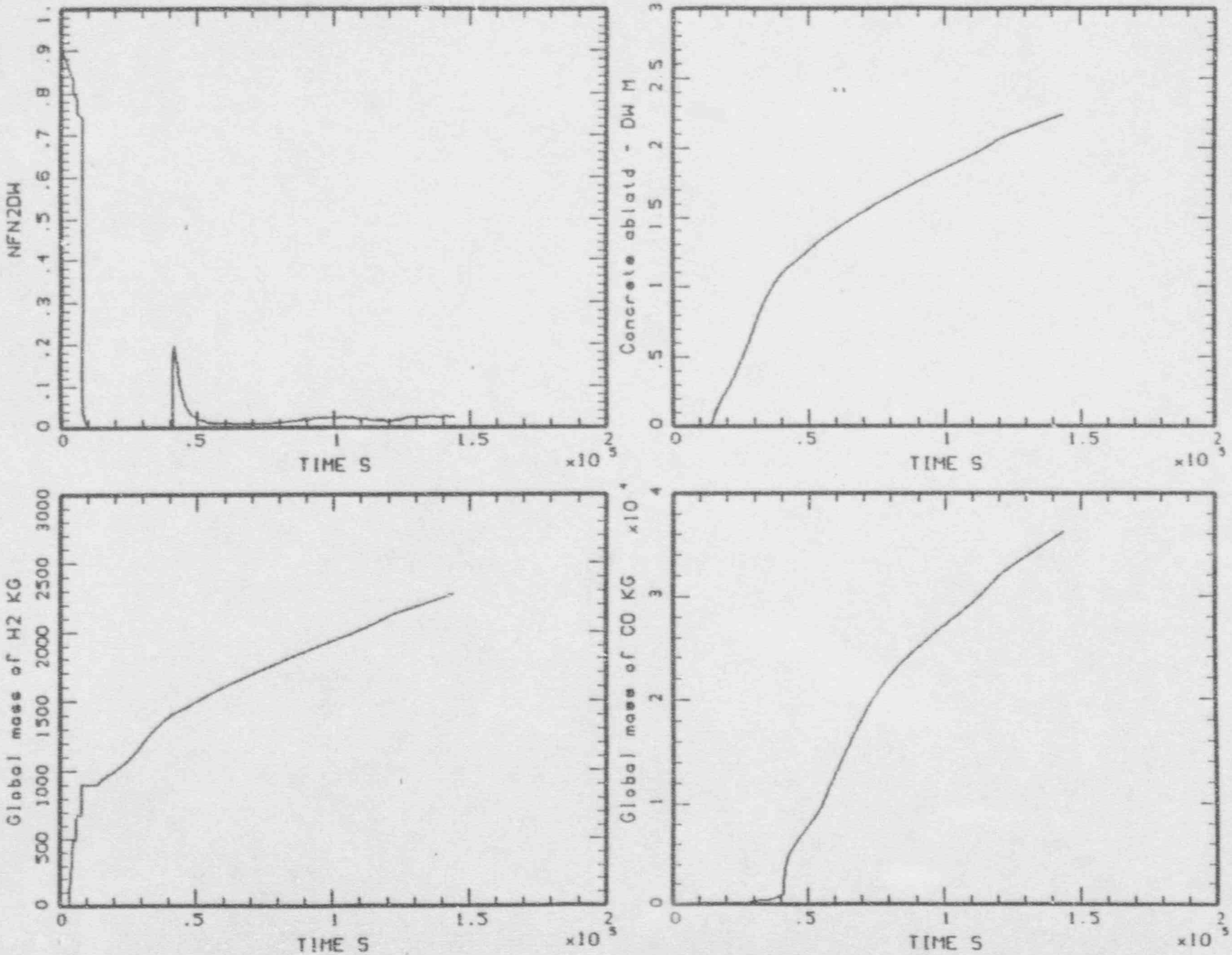

MAAP-MELCOR: BWR SBO/DW
BNL_DWO_44.PLT LINE

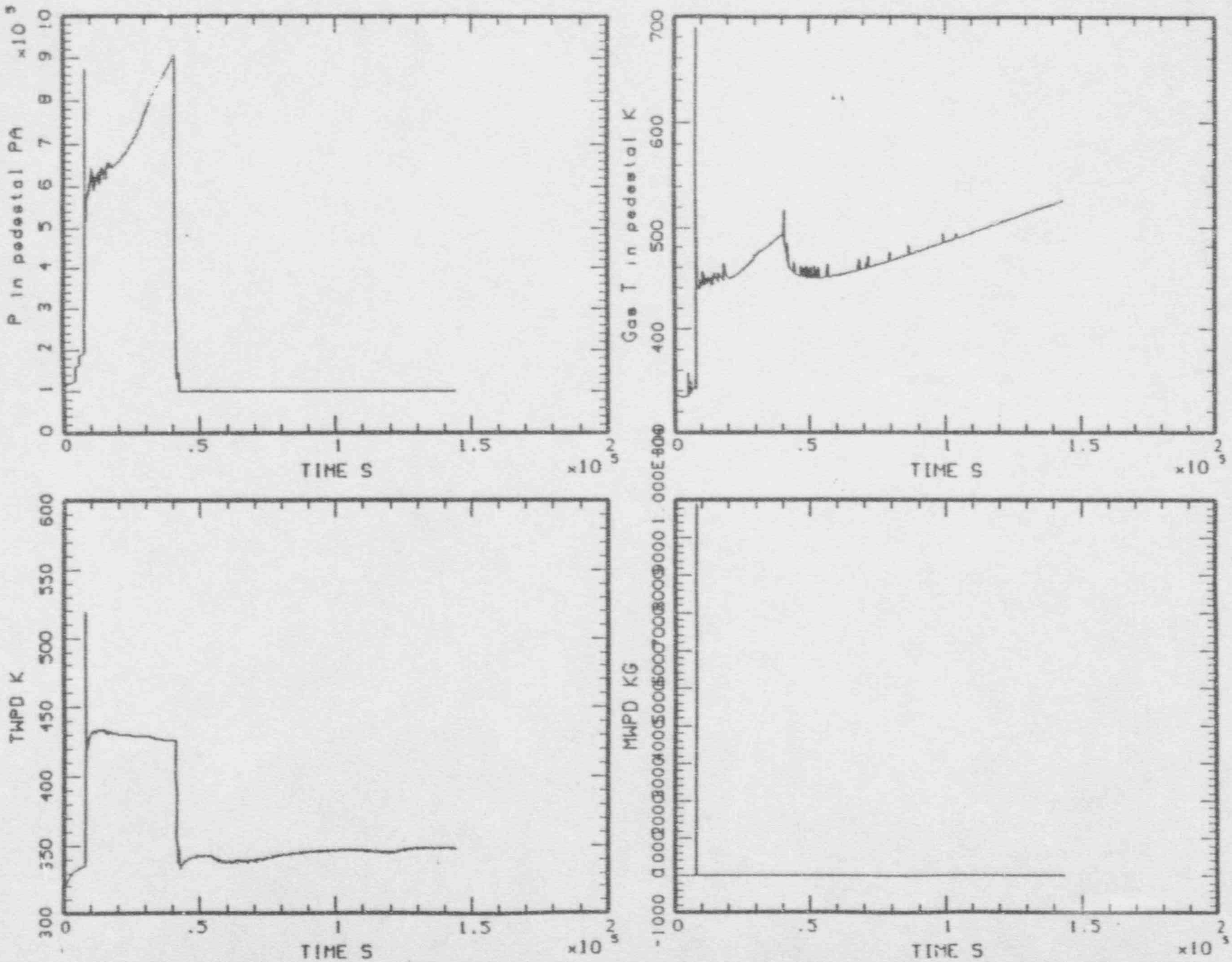

MAAP-MELCOR: BWR SBO/DW
BNL_DWO_44.PLT LINE

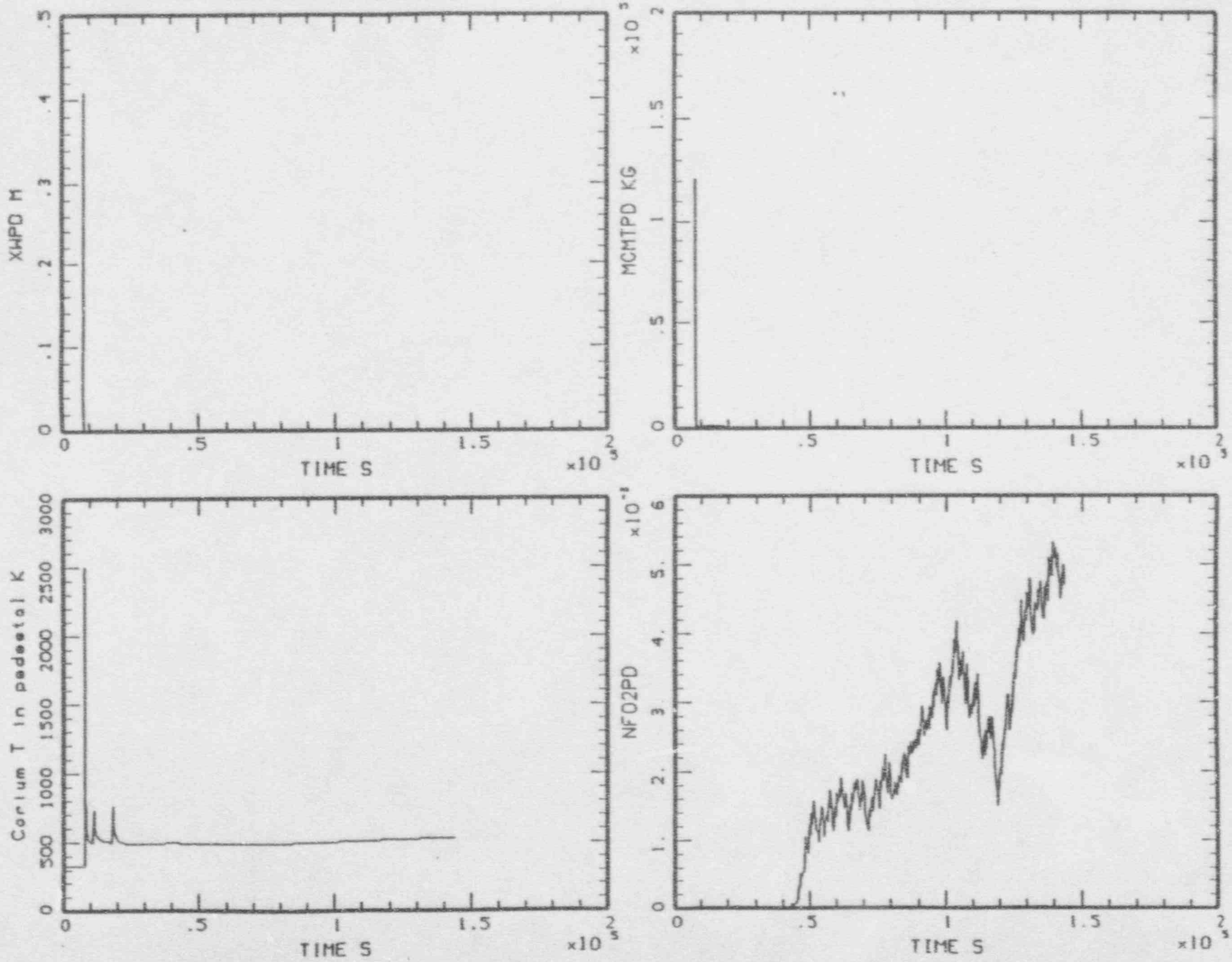

MAAP-MELCOR: BWR SBO/DW
BNL_DWO_44.PLT LINE

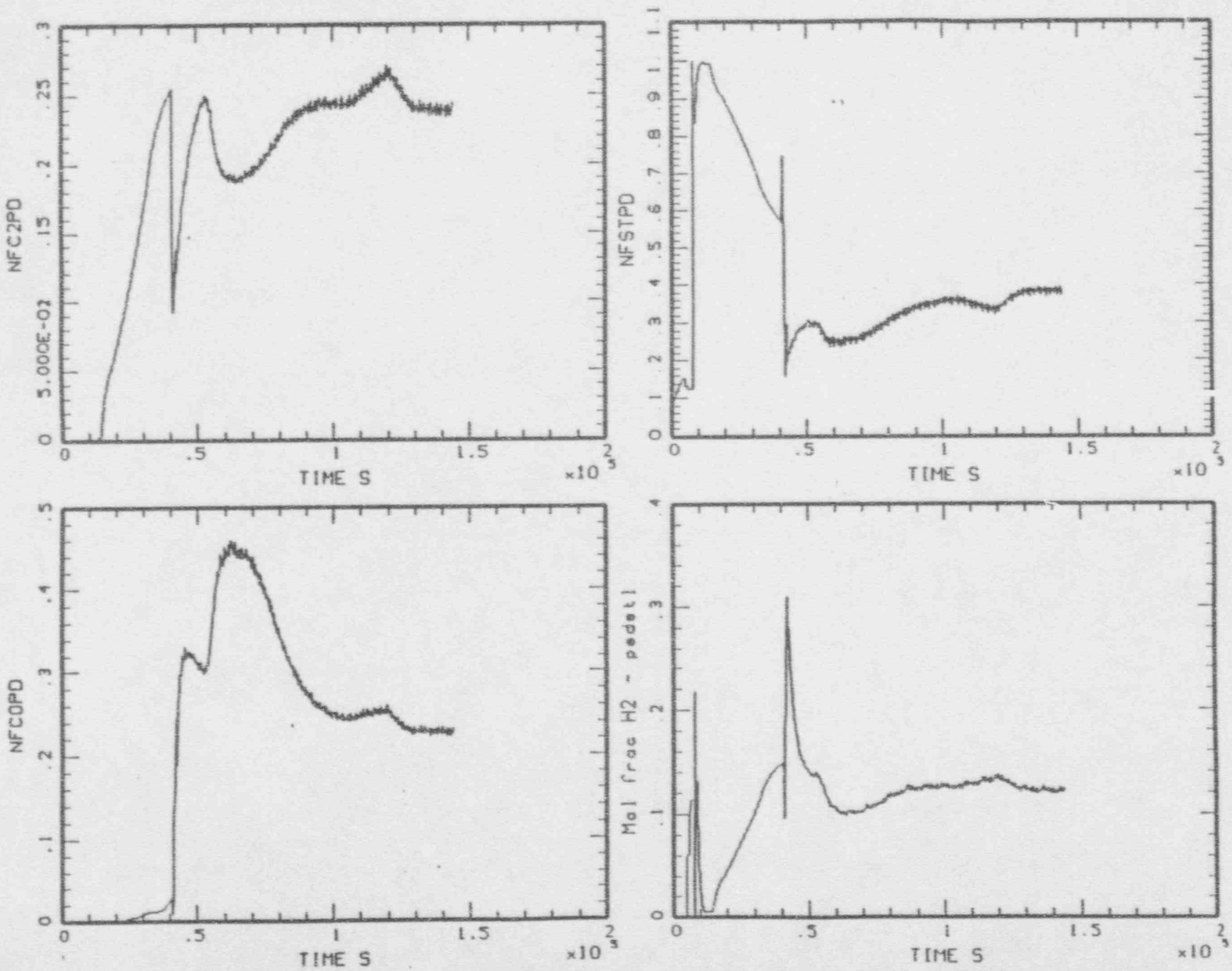

MAAP-MELCOR: BWR SBO/DW
BNL_DWO_44.PLT LINE

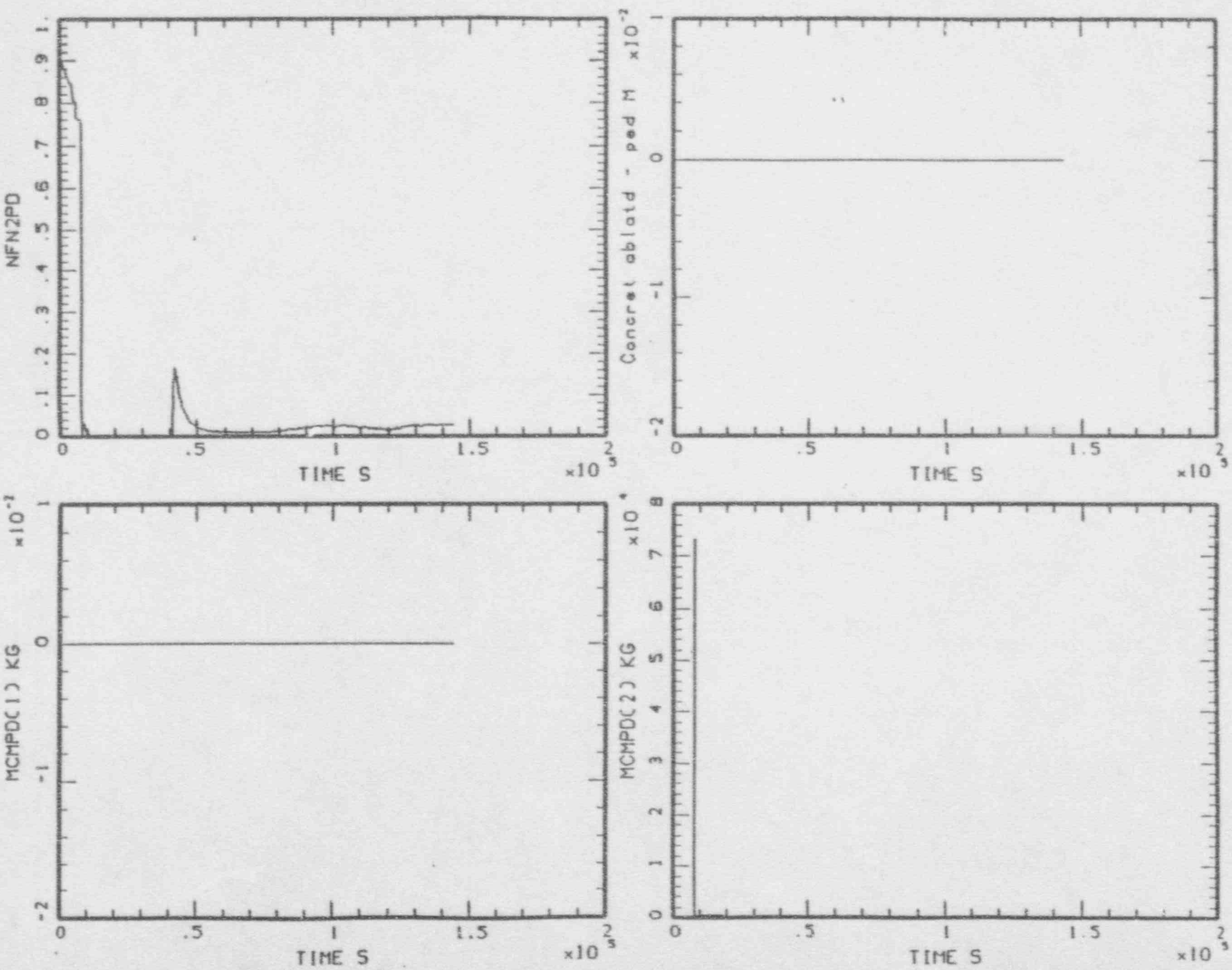

NUMERICAL PERFORMANCE FIGURES OF MERIT

CASE 5

FUMIN = 2.Ø

TIME (SEC)	144014.8
FRACTION OF CLAD REACTED IN VESSEL . .	0.3108
CONCRETE AEROSOL GENERATED (KG). . . .	2801.0
UO2 MASS IN PEDESTAL (KG).	356.6
UO2 MASS IN DRYWELL (KG)	169027.4
TIME OF CORE UNCOVERY (SEC).	1906.6
TIME OF VESSEL FAILURE (SEC)	7558.2
TIME OF CONTAINMENT FAILURE (SEC). . .	38165.7
CSI MASS BALANCE (KG)	
INITIAL MASS	38.2155
IN CORE.	0.0000
IN CORIUM.	0.0270
IN PRIMARY SYSTEM.	8.4881
IN CONTAINMENT	20.6878
TOTAL IN-VESSEL RELEASED	37.3060
TOTAL EX-VESSEL RELEASED	0.8827
RELEASED FROM CONTAINMENT.	9.0128
SRO MASS BALANCE (KG)	
INITIAL MASS	103.4367
IN CORE.	0.0000
IN CORIUM.	103.0068
IN PRIMARY SYSTEM.	0.0956
IN CONTAINMENT	0.5567
TOTAL IN-VESSEL RELEASED	0.1056
TOTAL EX-VESSEL RELEASED	0.5642
RELEASED FROM CONTAINMENT.	0.0175

```
FORTRAN STOP
$ delete BNL_DW1_inp.dat;*
$ delete BNL_DW1_par.dat;*
$!
$ node = "M3300"
$ if "FALSE".eqs."FALSE" then logoff/full
  WUTOBY       job terminated at  1-MAY-1991 12:52:39.78

  Accounting information:
  Buffered I/O count:          681     Peak working set size:  1282
  Direct I/O count:          11963     Peak page file size:    4600
  Page faults:                2167     Mounted volumes:           0
  Charged CPU time:     0 00:00:39.77  Elapsed time:     0 01:11:29.64
```

MAAP-MELCOR: BWR SBO/PD2
BNL_DW1_43.PLT LINE

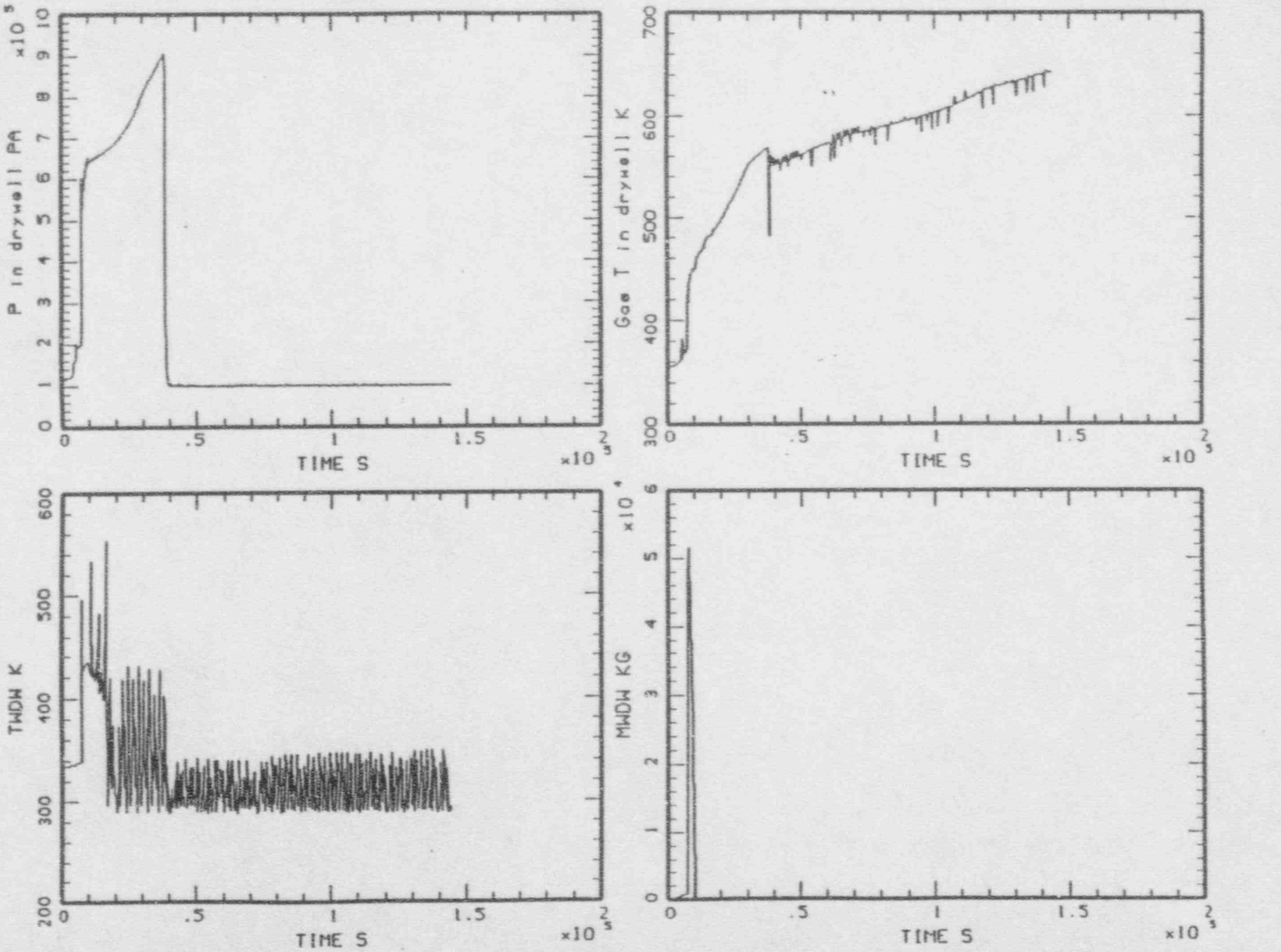

MAAP-MELCOR: BWR SBO/PD2
BNL_DWI_43.PLT LINE

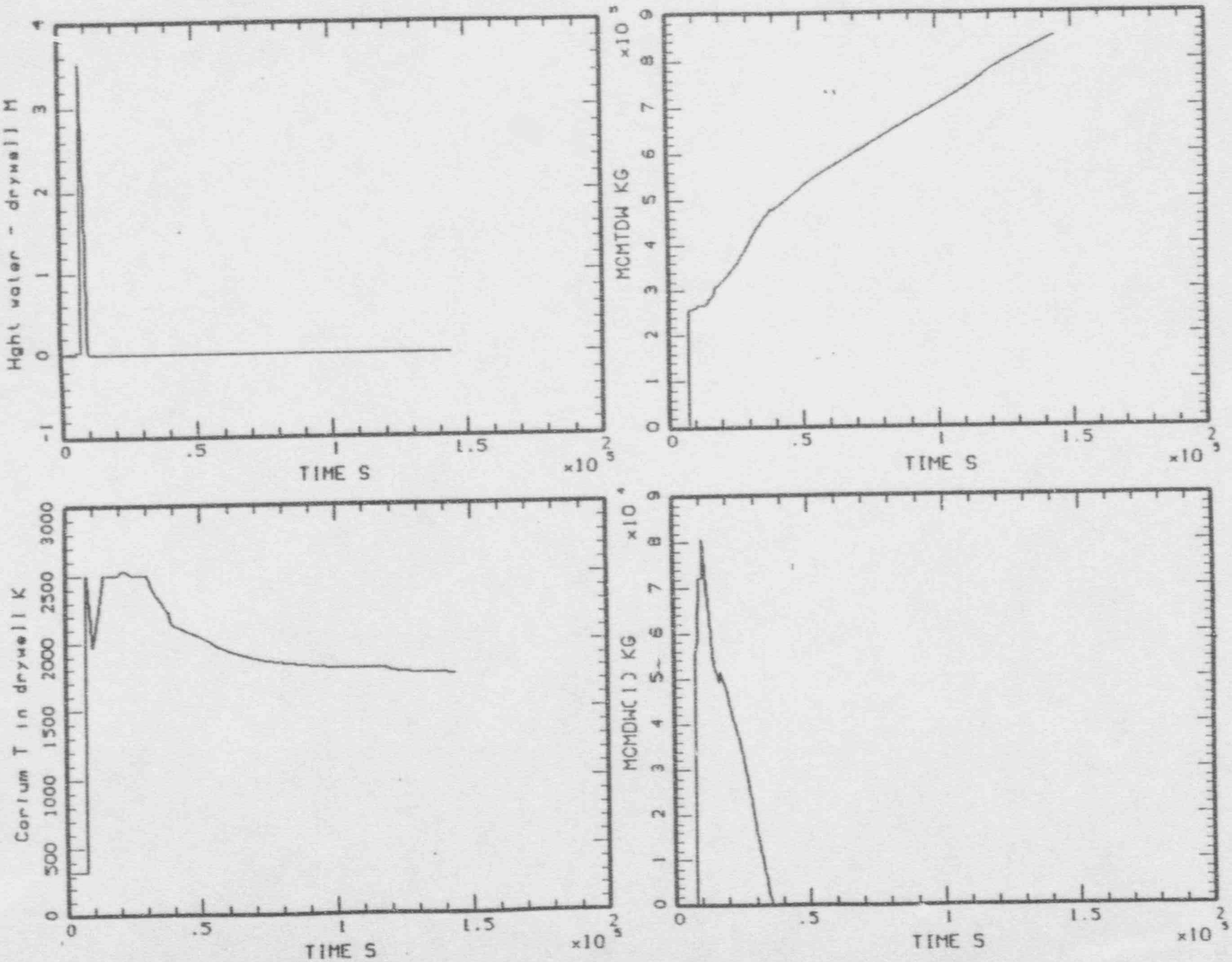

MAAP-MELCOR: BWR SBO/PD2
BNL_DW1_43.PLT LINE

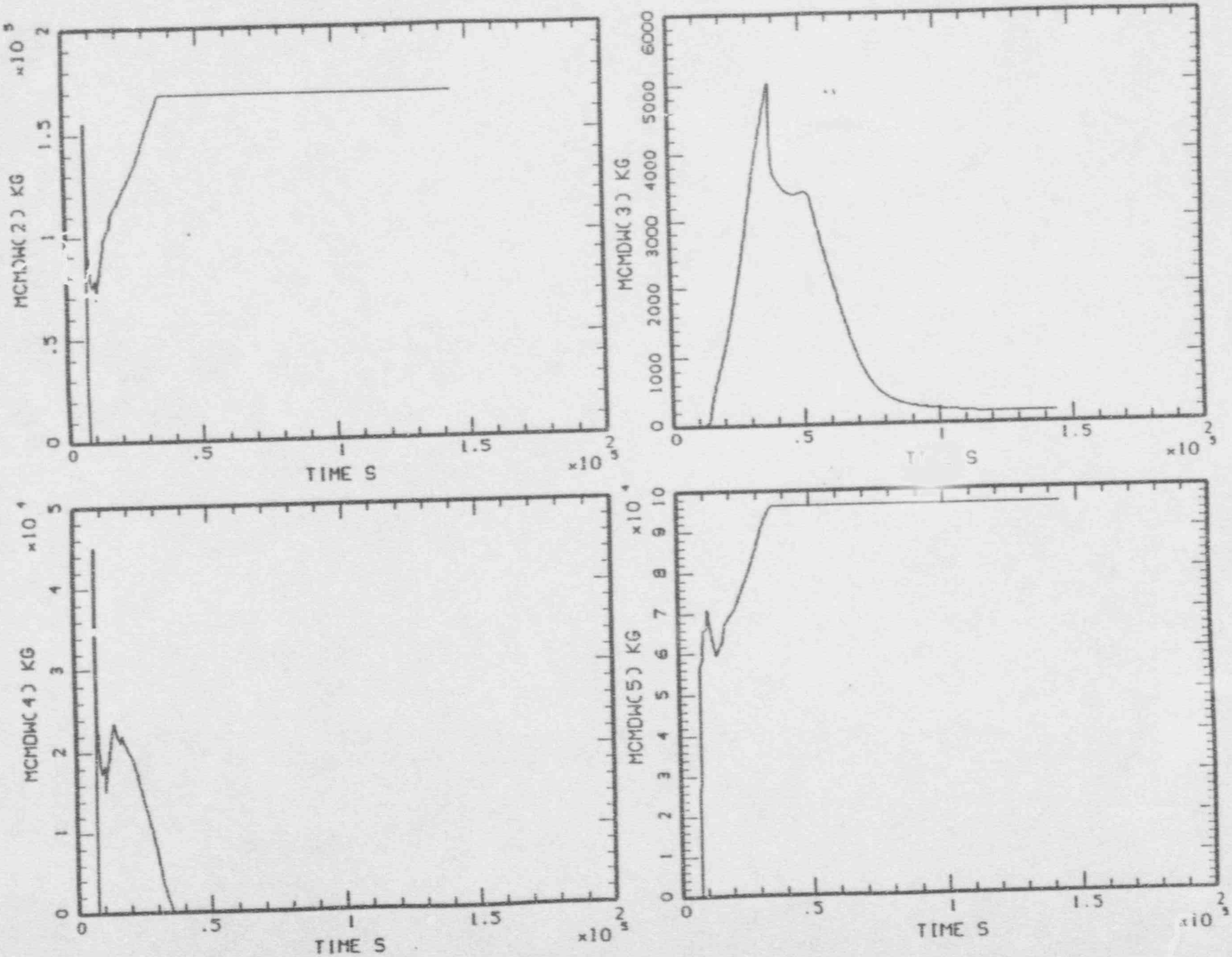

MAAP-MELCOR: BWR SBO/PD2
BNL_DWI_43.PLT LINE

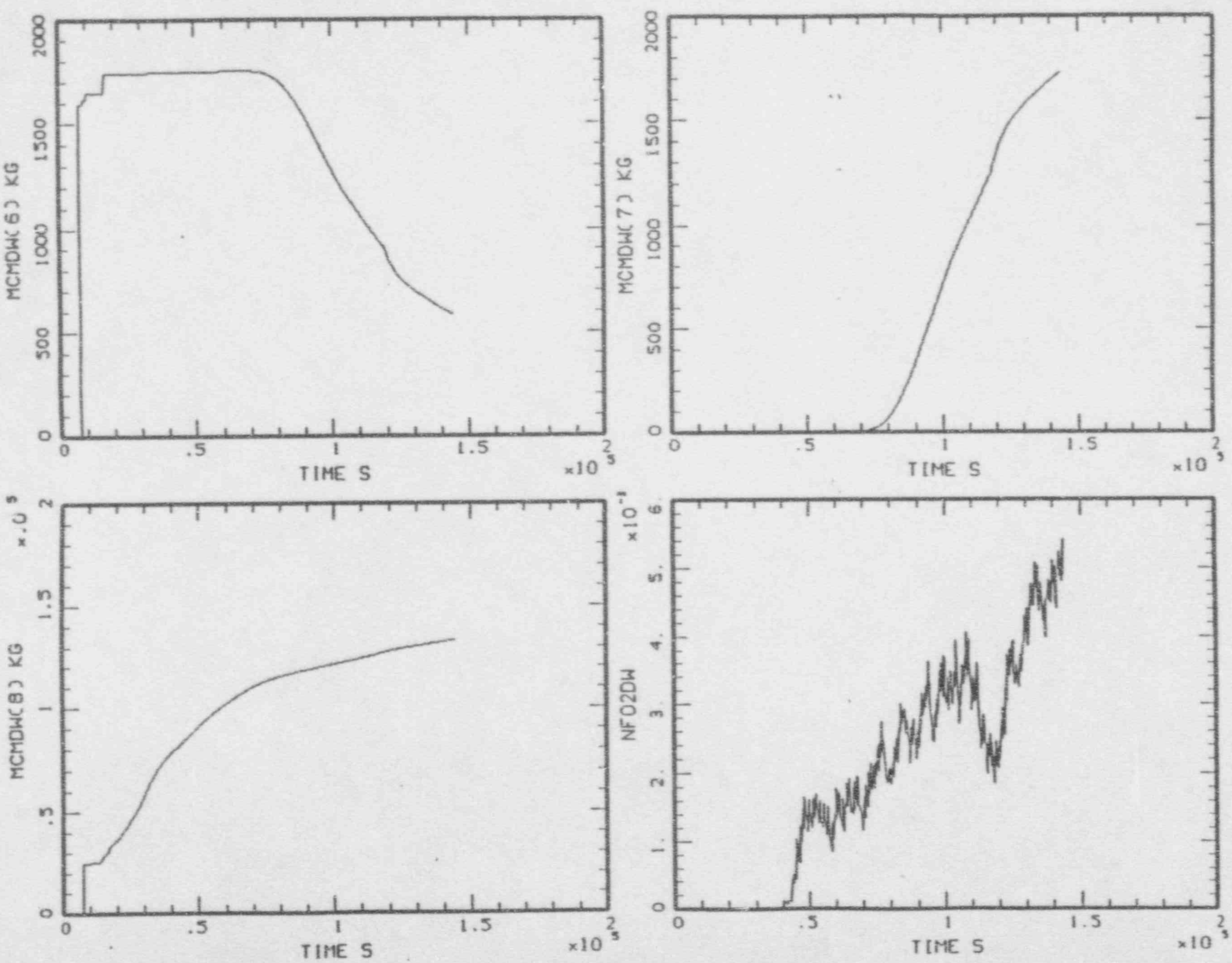

MAAP-MELCOR: BWR SBO/PD2
BNL_DWL_43.PLT LINE

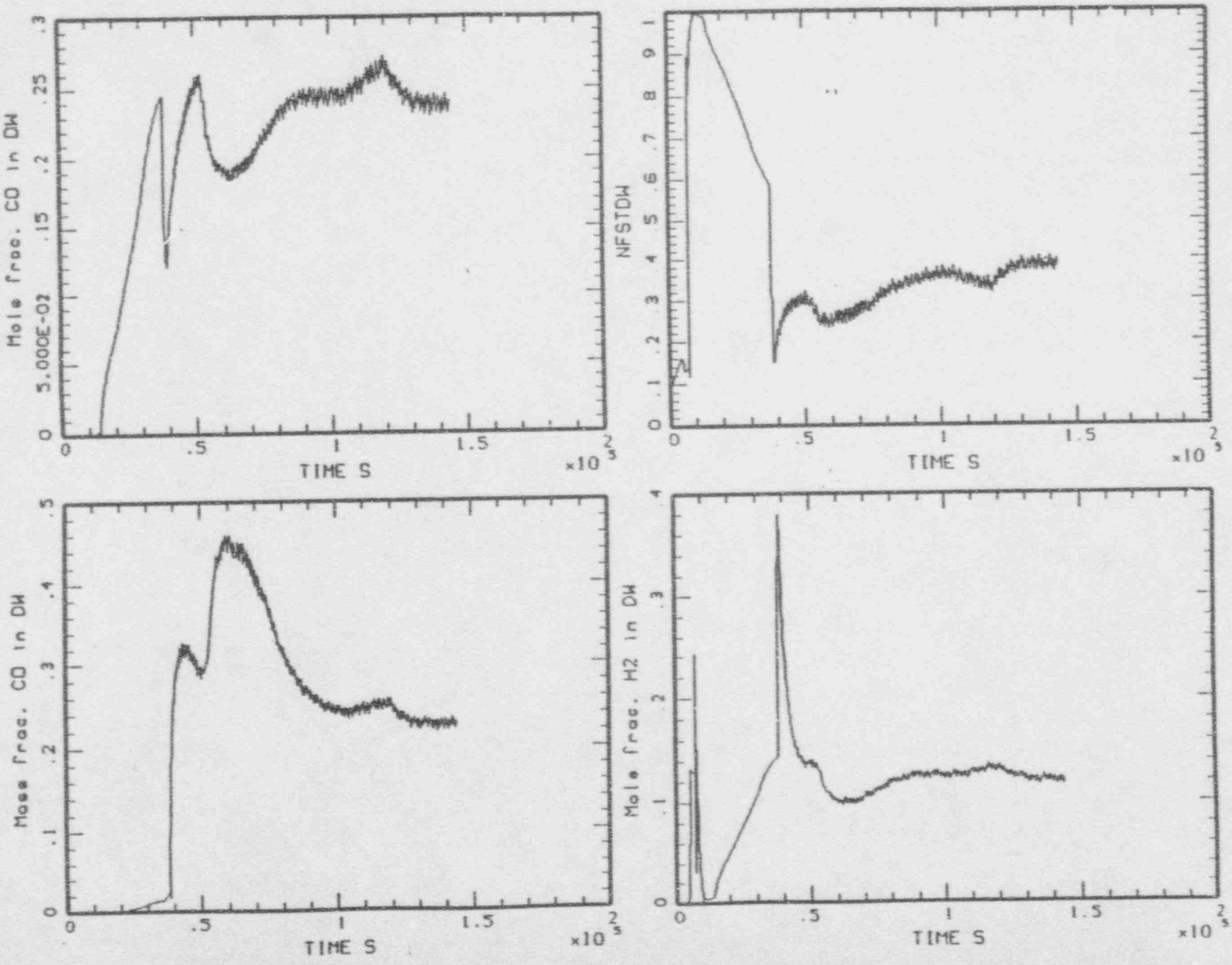

MAAP-MELCOR: BWR SBO/PD2
BNL_DWI_43.PLT LINE

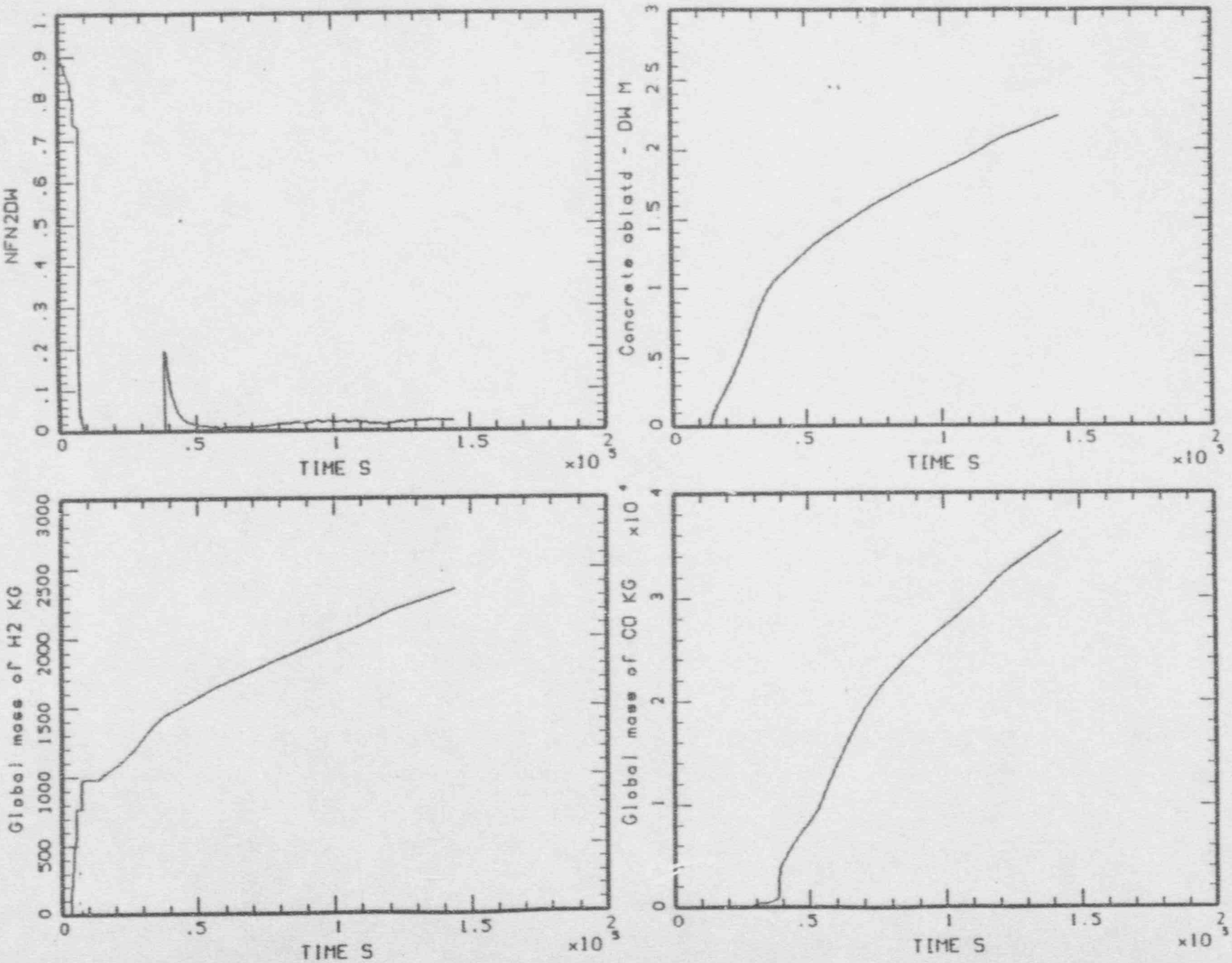

MAAP-MELCOR: BWR SBO/PD2
BNL_DWI_44.PLT LINE

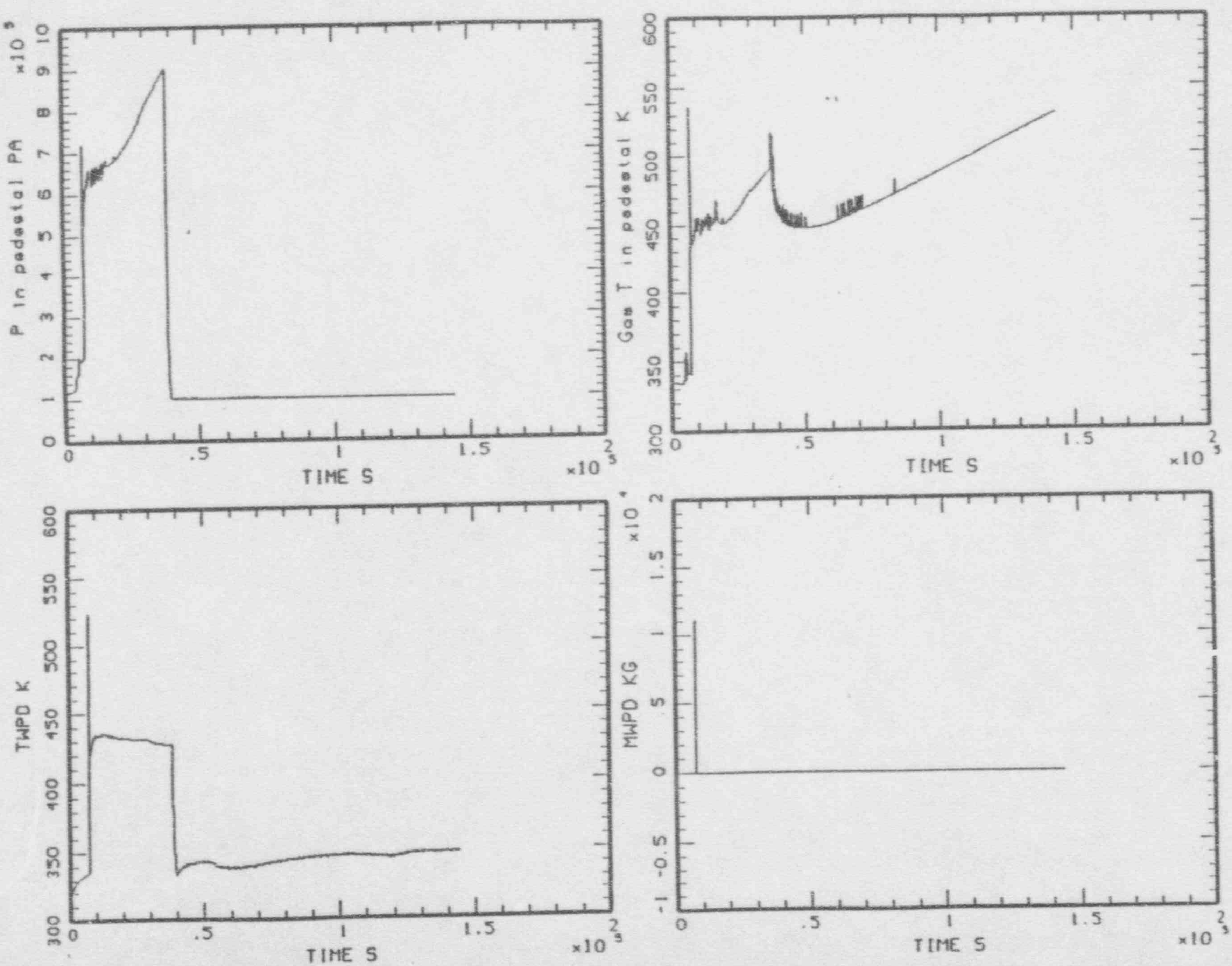

MAAP-MELCOR: BWR SBO/PD2
BNL_DW1_44.PLT LINE

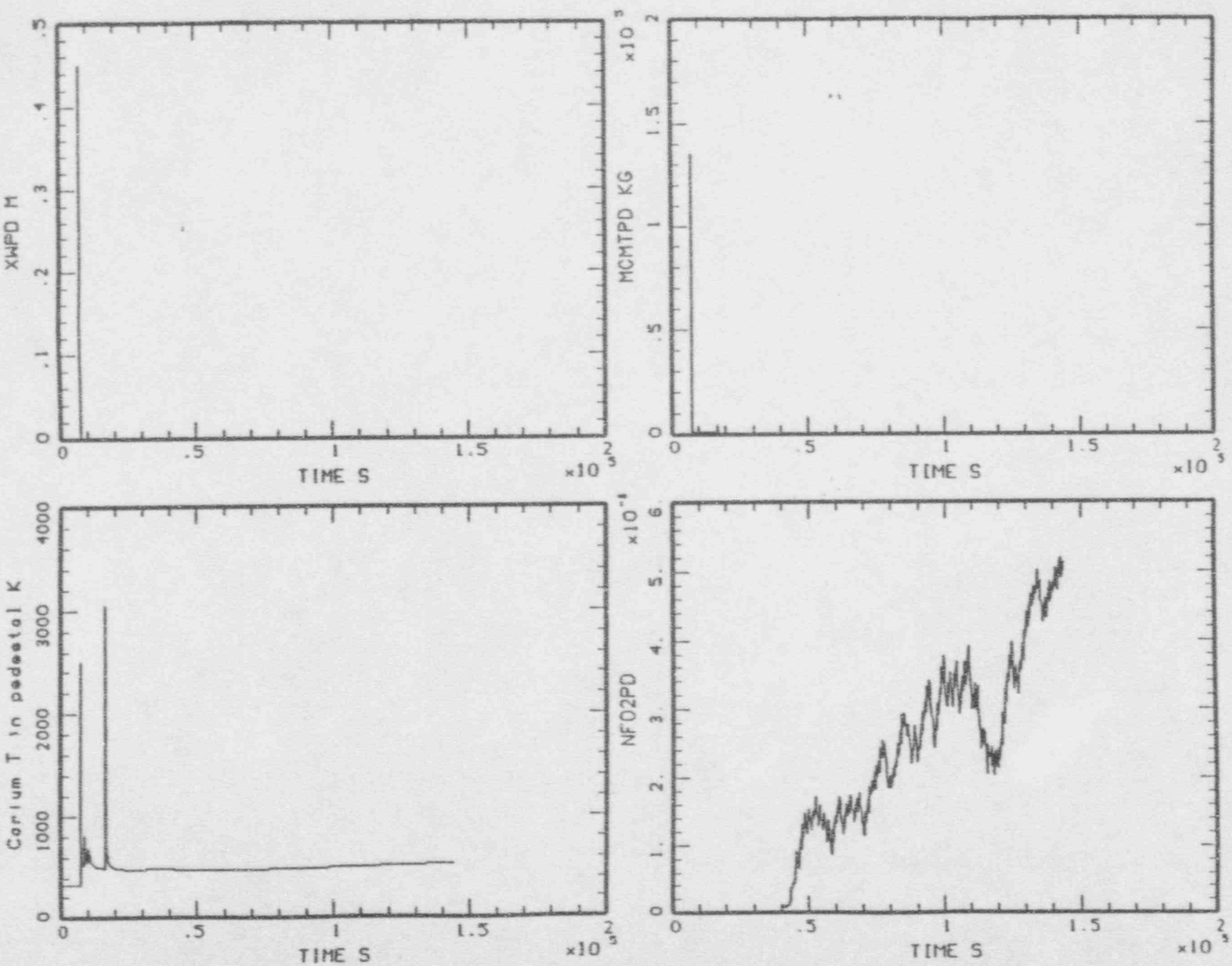

MAAP-MELCOR: BWR SBO/PD2
BNL_DW1_44.PLT LINE

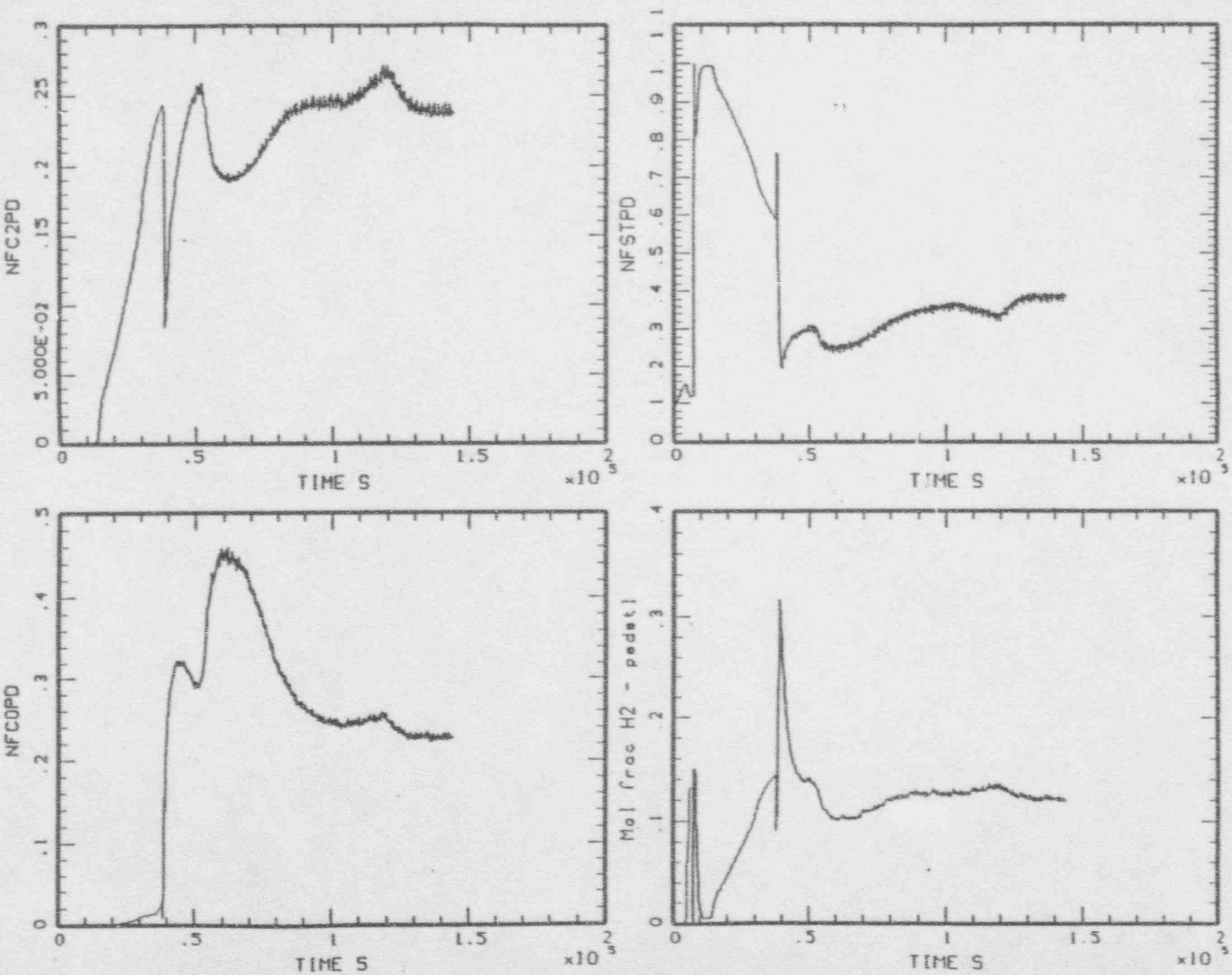

MAAP-MELCOR: BWR SBO/PD2
BNL_DW1_44.PLT LINE

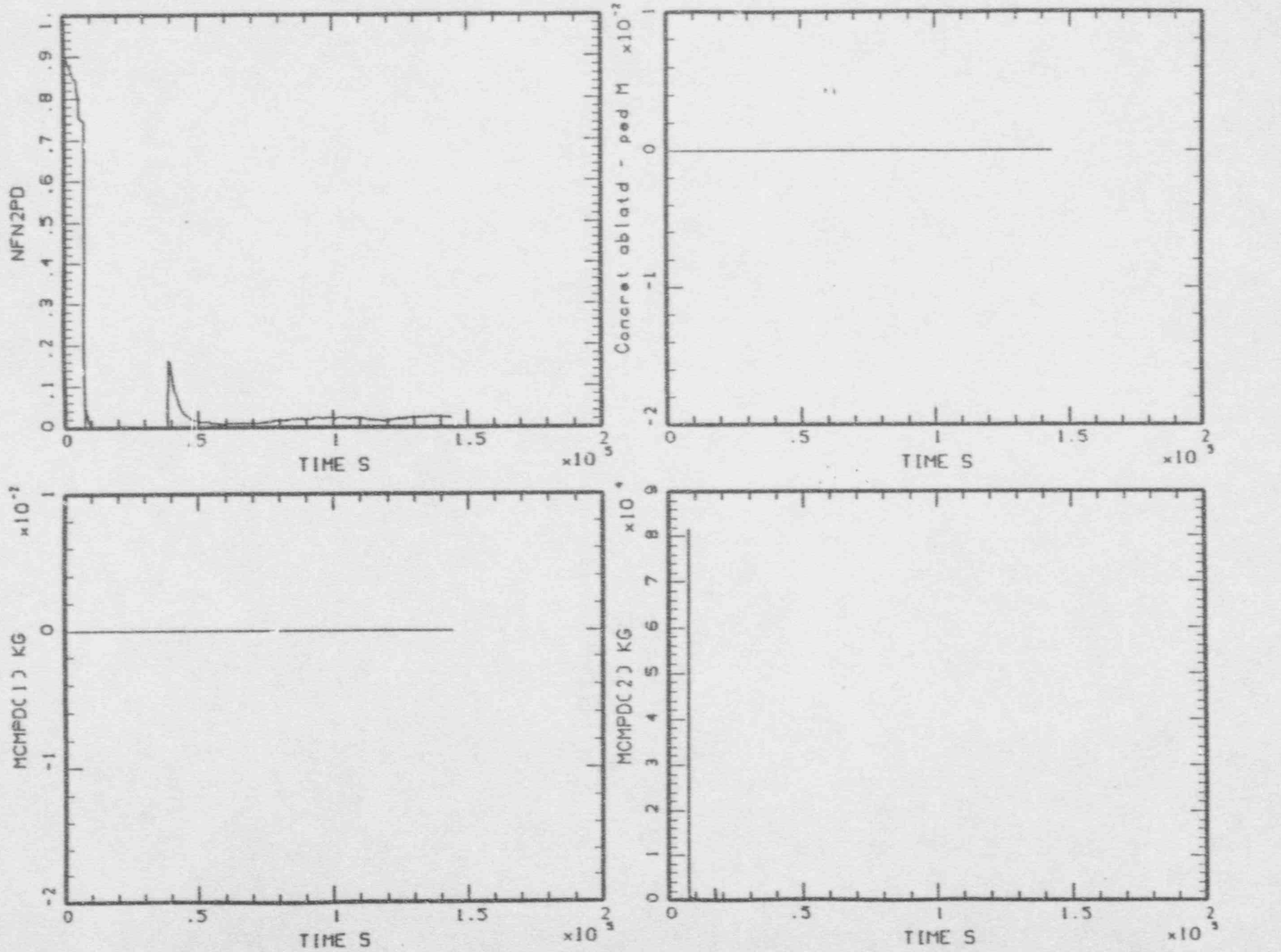

ADWF = 33 m² (132 m²)

NUMERICAL PERFORMANCE FIGURES OF MERIT

TIME (SEC)	144017.1
FRACTION OF CLAD REACTED IN VESSEL . .	0.2666
CONCRETE AEROSOL GENERATED (KG). . . .	2298.9
UO2 MASS IN PEDESTAL (KG).	43457.2
UO2 MASS IN DRYWELL (KG)	125921.4
TIME OF CORE UNCOVERY (SEC).	1908.9
TIME OF VESSEL FAILURE (SEC)	7402.8
TIME OF CONTAINMENT FAILURE (SEC). . .	42021.8

CSI MASS BALANCE (KG)

INITIAL MASS	38.2155
IN CORE.	0.0000
IN CORIUM.	0.0334
IN PRIMARY SYSTEM.	4.5731
IN CONTAINMENT	11.6522
TOTAL IN-VESSEL RELEASED	37.2041
TOTAL EX-VESSEL RELEASED	0.9780
RELEASED FROM CONTAINMENT.	21.9565

SRO MASS BALANCE (KG)

INITIAL MASS	103.4367
IN CORE.	0.0000
IN CORIUM.	102.7941
IN PRIMARY SYSTEM.	0.0630
IN CONTAINMENT	0.6098
TOTAL IN-VESSEL RELEASED	0.0715
TOTAL EX-VESSEL RELEASED	0.6058
RELEASED FROM CONTAINMENT.	0.0045

```
FORTRAN STOP
$ delete BNL_ADWF4_inp.dat;*
$ delete BNL_ADWF4_par.dat;*
$!
$ node = "N780"
$ if "FALSE".eqs."FALSE" then logoff/full
  WUTOBY        job terminated at  5-JUN-1991 19:01:33.44

  Accounting information:
  Buffered I/O count:          669    Peak working set size:  1515
  Direct I/O count:          13406    Peak page file size:    4600
  Page faults:                2163    Mounted volumes:           0
  Charged CPU time:  0 00:00:45.17    Elapsed time:    0 01:57:21.04
```

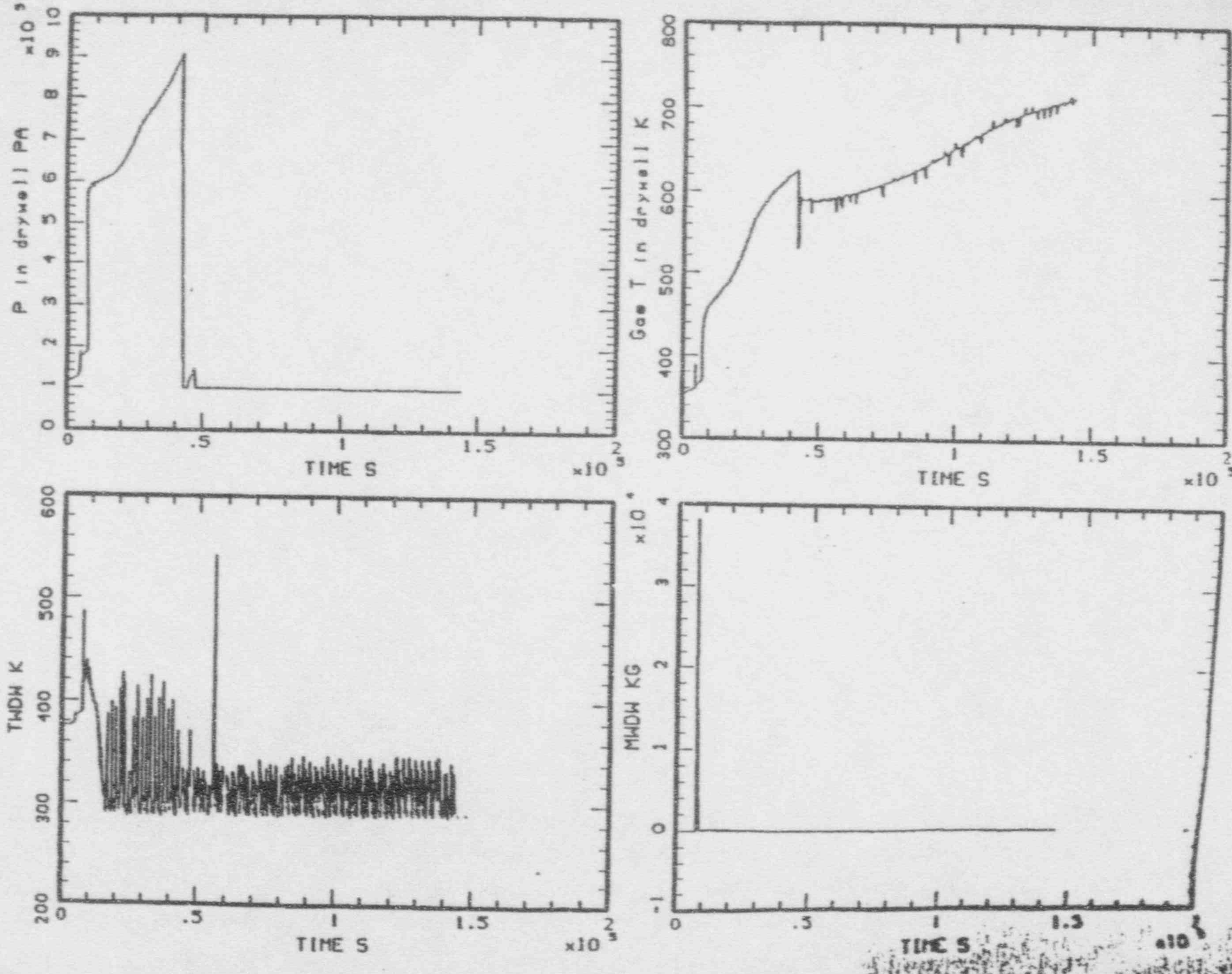
P in drywell PA
×10^5
TIME S
×10^3
Gas T in drywell K
TIME S
×10^3
TWDW K
TIME S
×10^3
MWDW KG
×10^4
TIME S
×10^3

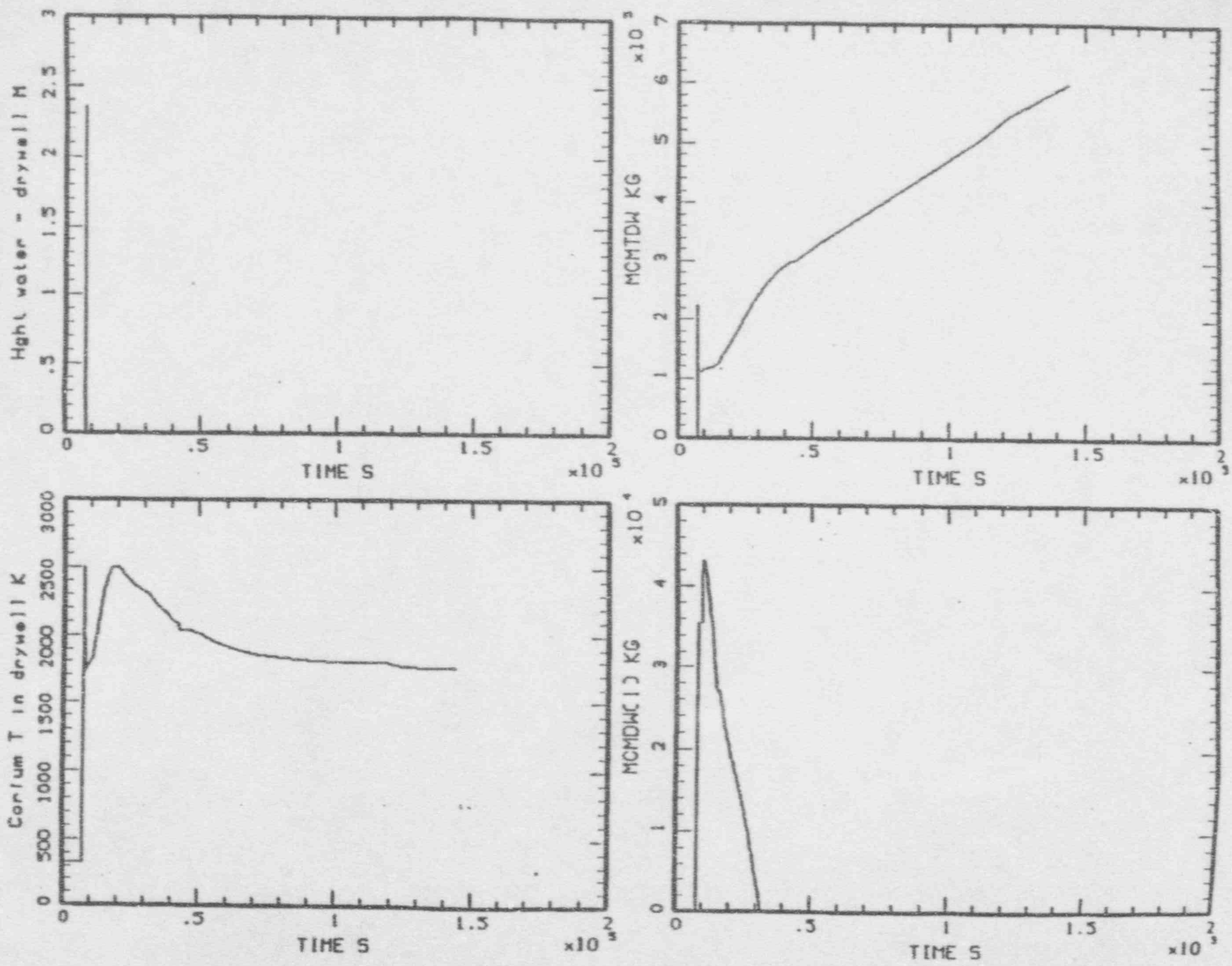
Hght water - drywell M
TIME S
x10^3
MCMTDW KG
x10^3
TIME S
x10^3
Corium T in drywell K
TIME S
x10^3
MCMDWC(1) KG
x10^4
TIME S
x10^3

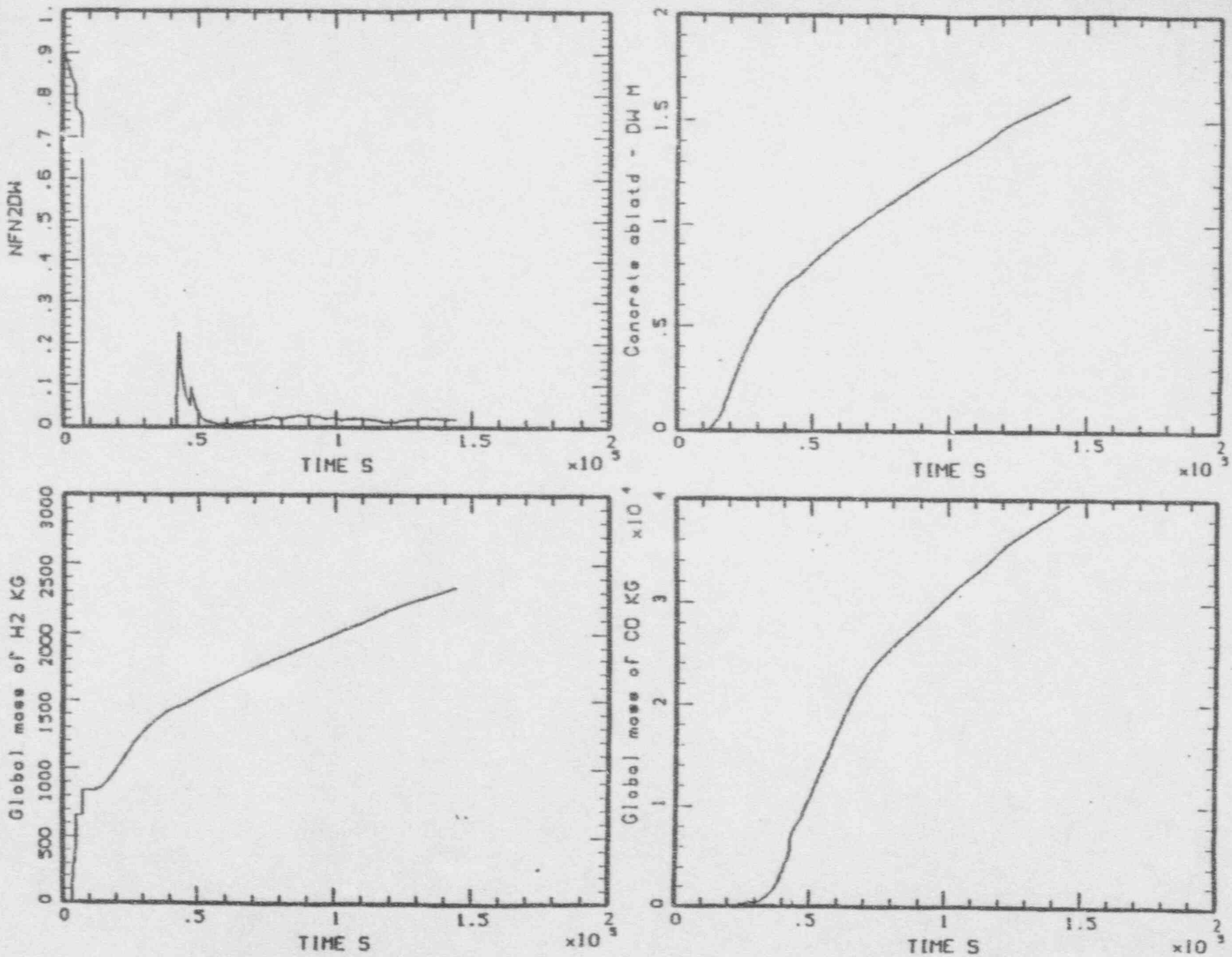
NFN2DW
TIME S
×10^3
Concrete ablatd - DW M
TIME S
×10^3
Global mass of H2 KG
TIME S
×10^3
Global mass of CO KG
×10^4
TIME S
×10^3

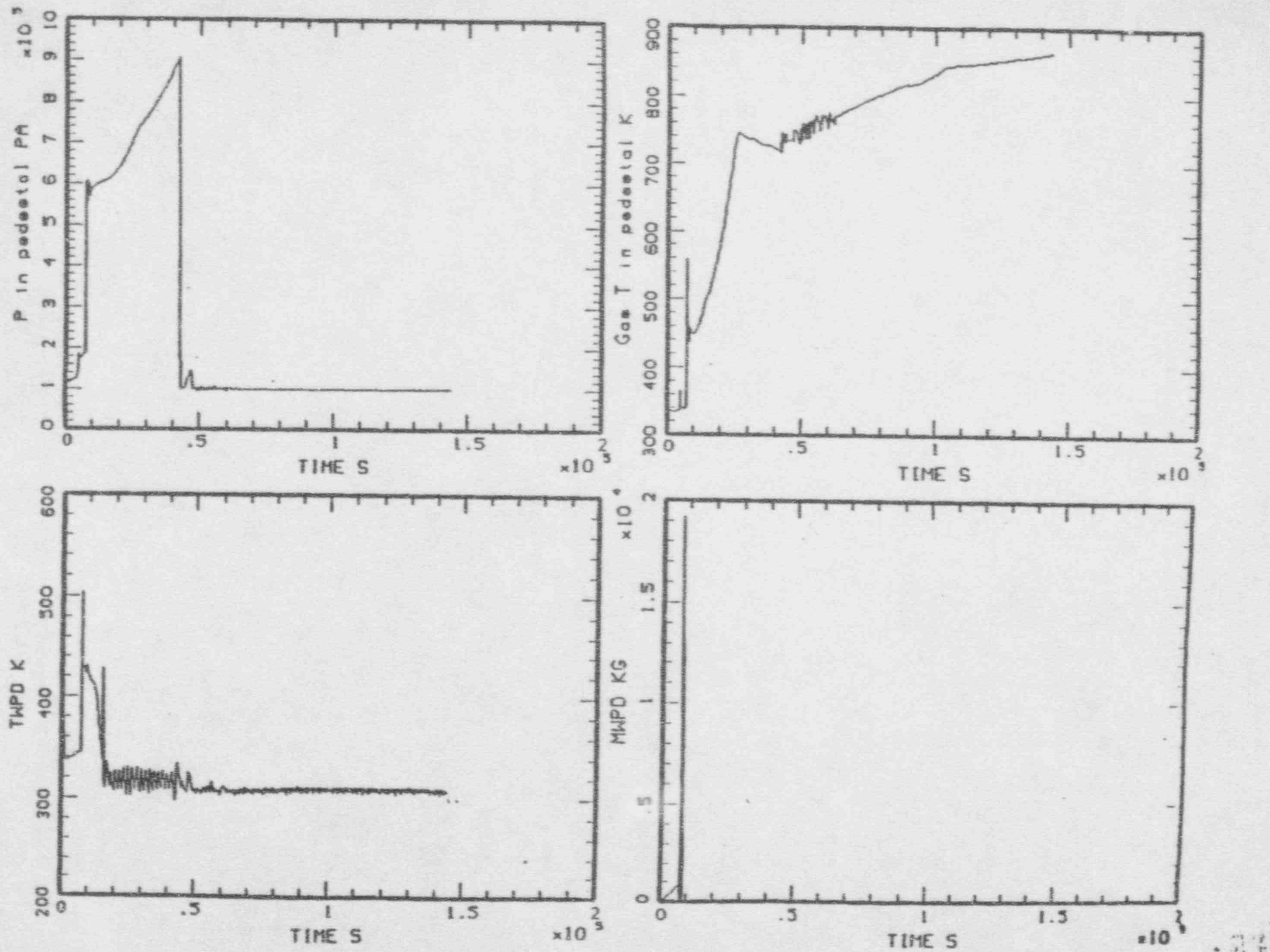
P in pedestal PA
×10³
Gas T in pedestal K
TWPD K
MWPD KG
×10⁴
TIME S
×10³
0
.5
1
1.5
2

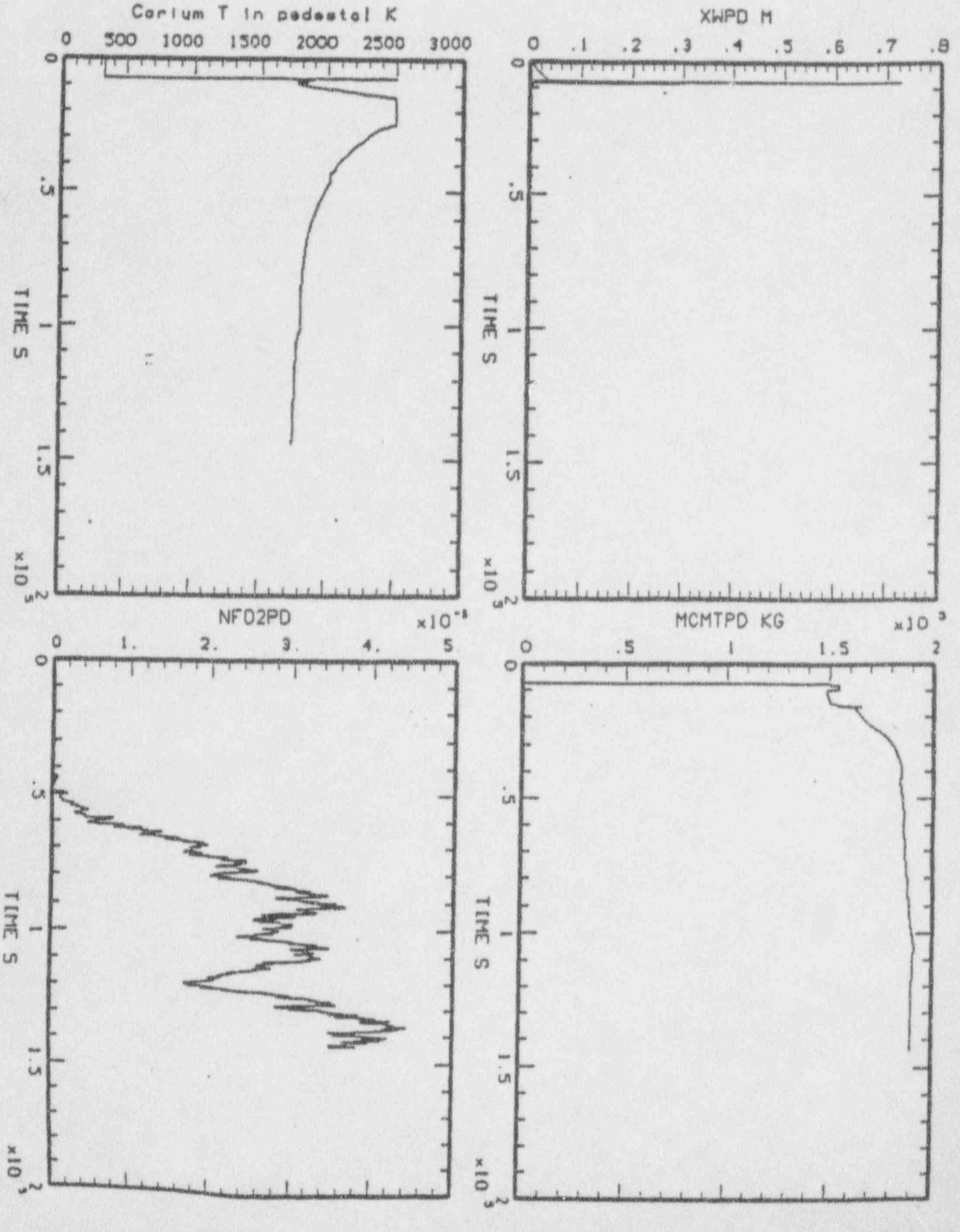
Corium T in pedestal K
0 500 1000 1500 2000 2500 3000
TIME S
0 .5 1 1.5 2
×10^5
XWPD M
0 .1 .2 .3 .4 .5 .6 .7 .8
TIME S
0 .5 1 1.5 2
×10^5
NFO2PD
×10^-3
0 1. 2. 3. 4. 5
TIME S
0 .5 1 1.5 2
×10^3
MCMTPD KG
×10^3
0 .5 1 1.5 2
TIME S
0 .5 1 1.5 2
×10^3

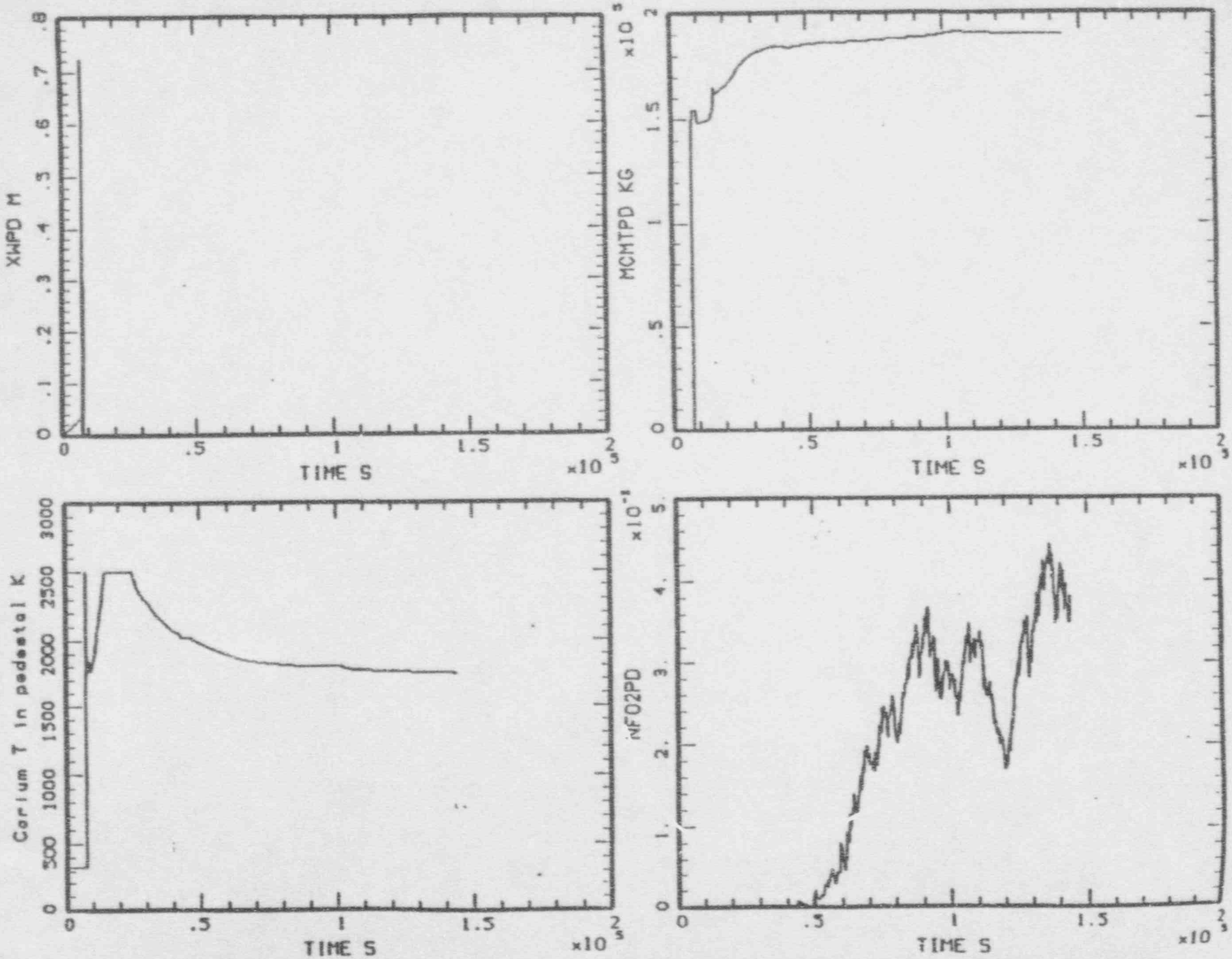
XWPD M
TIME S
×10^5
MCMTPD KG
×10^3
TIME S
×10^5
Corium T in pedestal K
TIME S
×10^5
ṅFO2PD
×10^-1
TIME S
×10^5

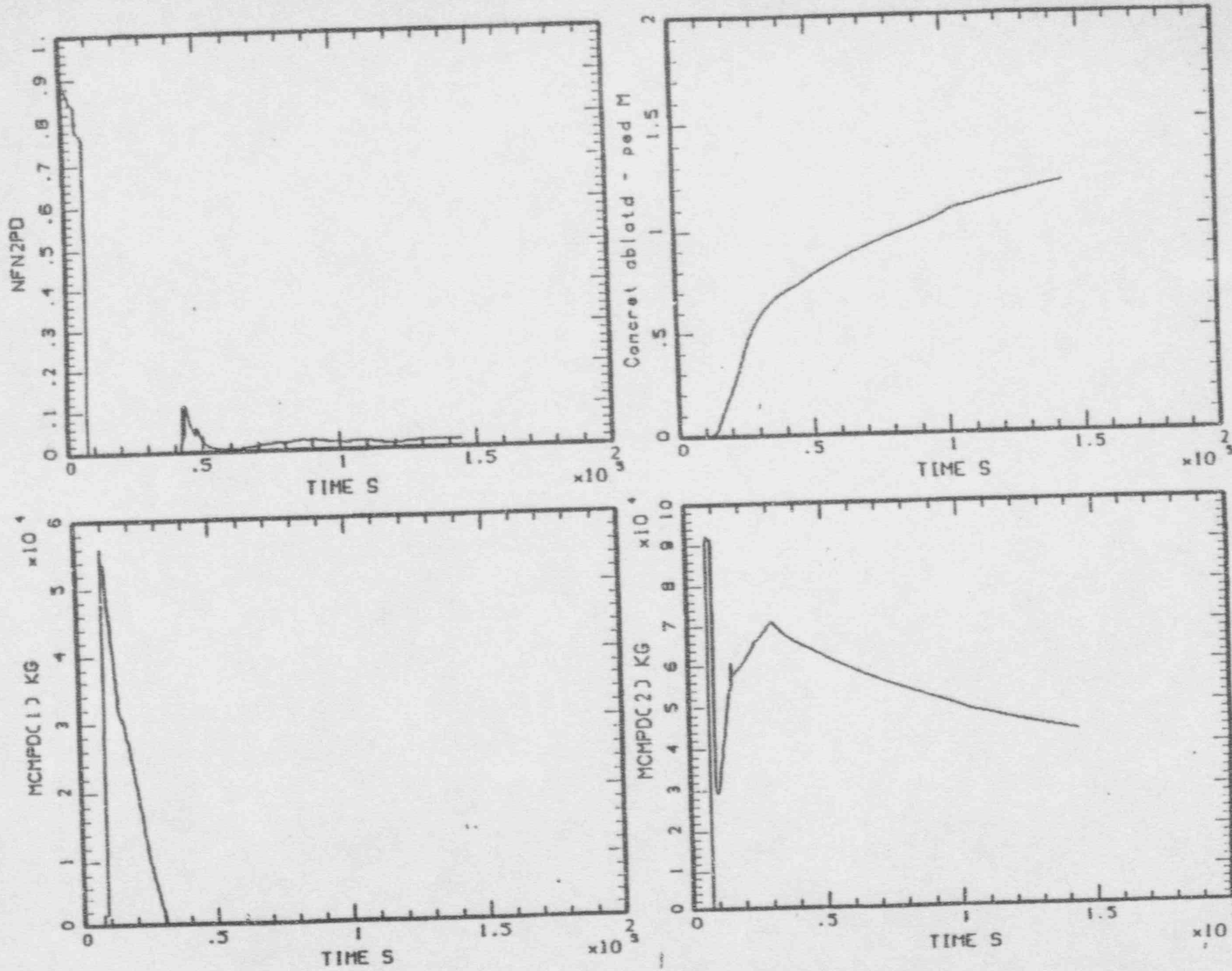
NFN2PD
0 .1 .2 .3 .4 .5 .6 .7 .8 .9 1.
TIME S
0 .5 1 1.5 2
x10 3
Concret ablatd - ped M
0 .5 1 1.5 2
MCMPDC(1) KG
x10 4
0 1 2 3 4 5 6
MCMPDC(2) KG
x10 4
0 1 2 3 4 5 6 7 8 9 10

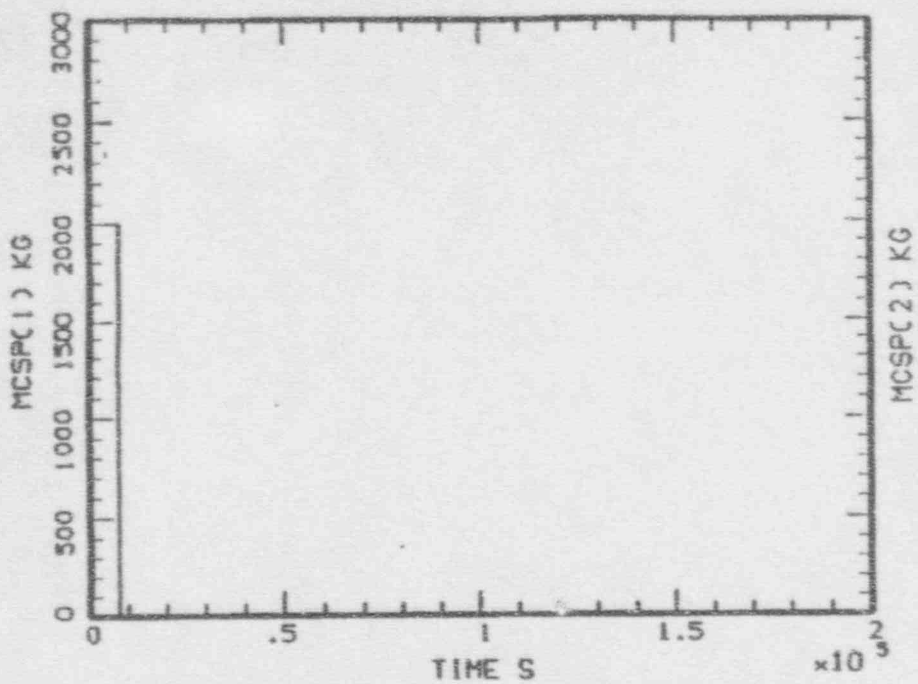
MCSP(1) KG
0
500
1000
1500
2000
2500
3000
0
.5
1
1.5
2
TIME S
x10^5

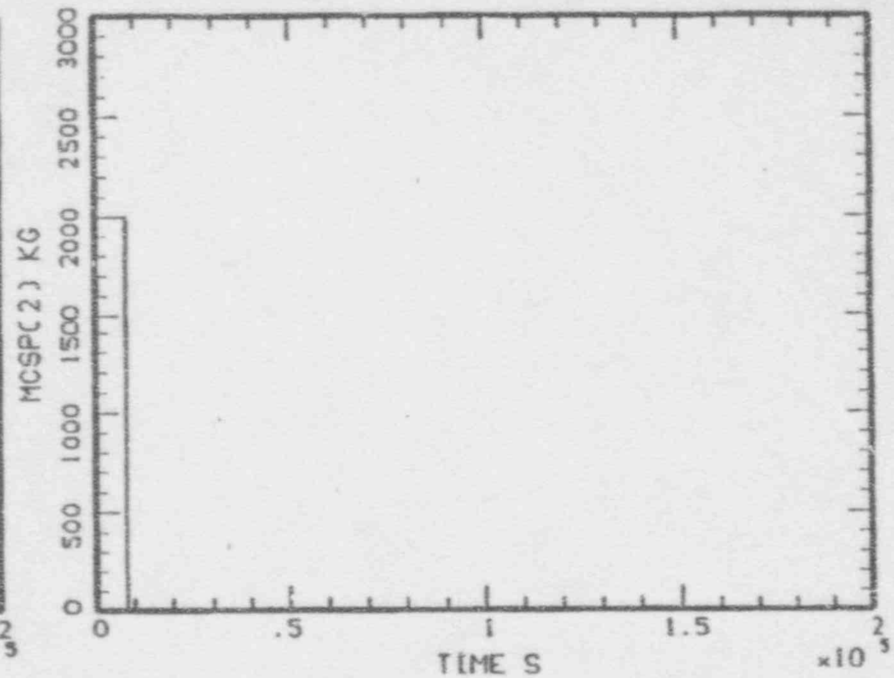
MCSP(2) KG
0
500
1000
1500
2000
2500
3000
0
.5
1
1.5
2
TIME S
x10^5

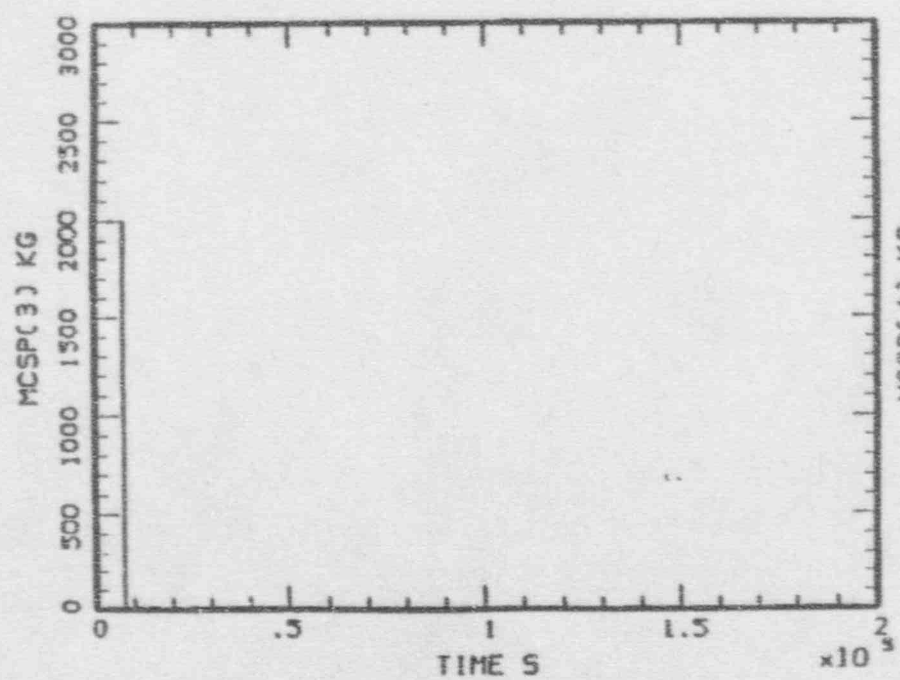
MCSP(3) KG
0
500
1000
1500
2000
2500
3000
0
.5
1
1.5
2
TIME S
x10^5

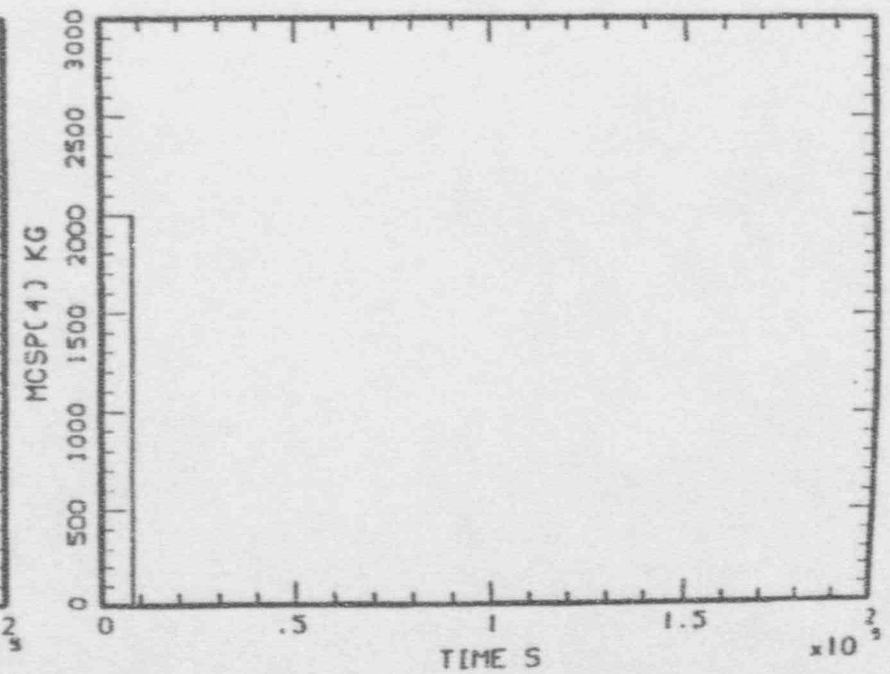
MCSP(4) KG
0
500
1000
1500
2000
2500
3000
0
.5
1
1.5
2
TIME S
x10^5

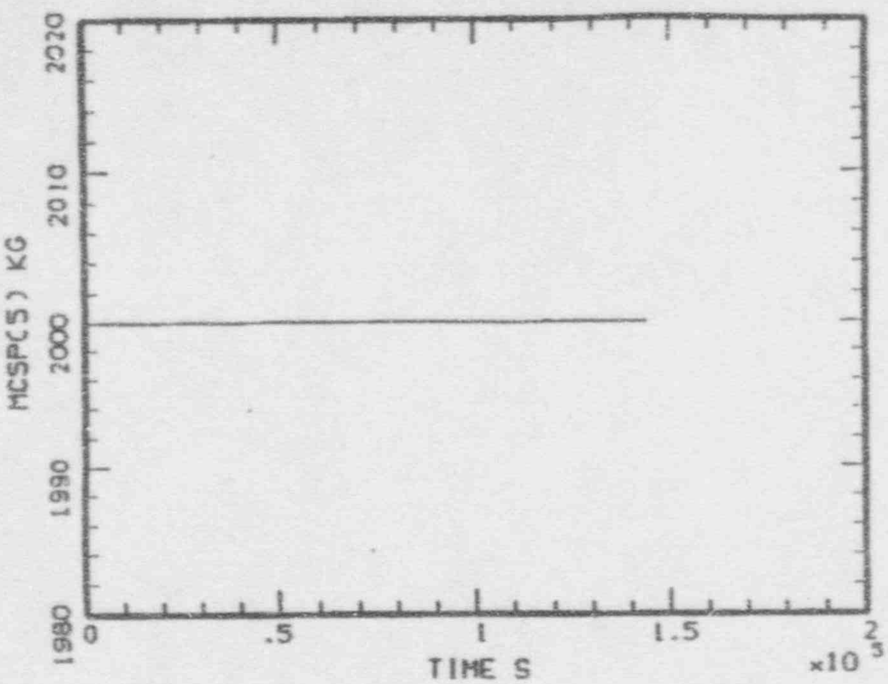
2020
2010
2000
1990
1980
MCSP(5) KG
0
.5
1
1.5
2
TIME S
x10 3

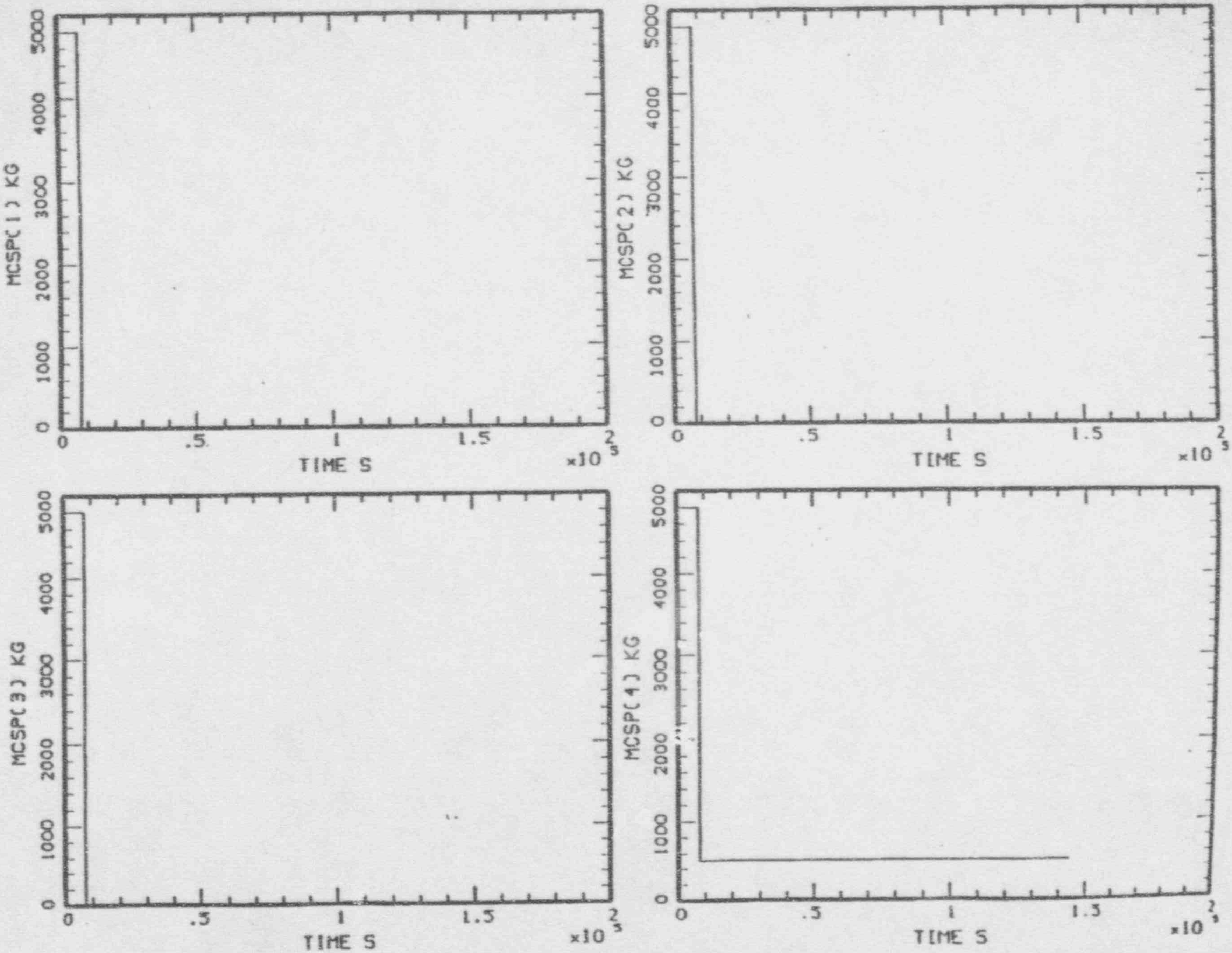
MCSP(1) KG
0
1000
2000
3000
4000
5000
0
.5
1
1.5
2
×10^5
TIME S
MCSP(2) KG
0
1000
2000
3000
4000
5000
0
.5
1
1.5
2
×10^5
TIME S
MCSP(3) KG
0
1000
2000
3000
4000
5000
0
.5
1
1.5
2
×10^5
TIME S
MCSP(4) KG
0
1000
2000
3000
4000
5000
0
.5
1
1.5
2
×10^5
TIME S

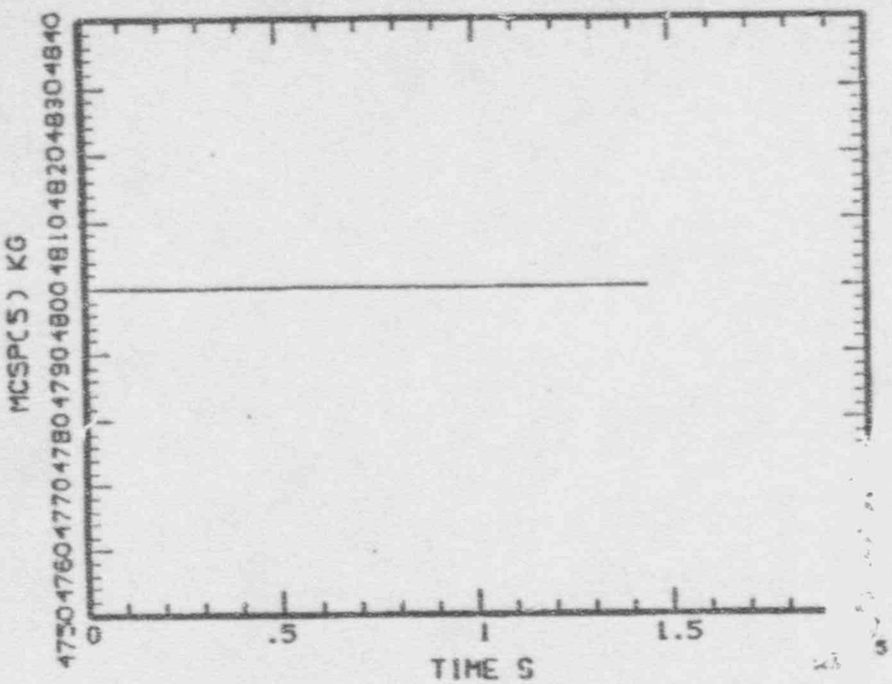
MCSP(5) KG
4750
4760
4770
4780
4790
4800
4810
4820
4830
4840
0
.5
1
1.5
TIME S

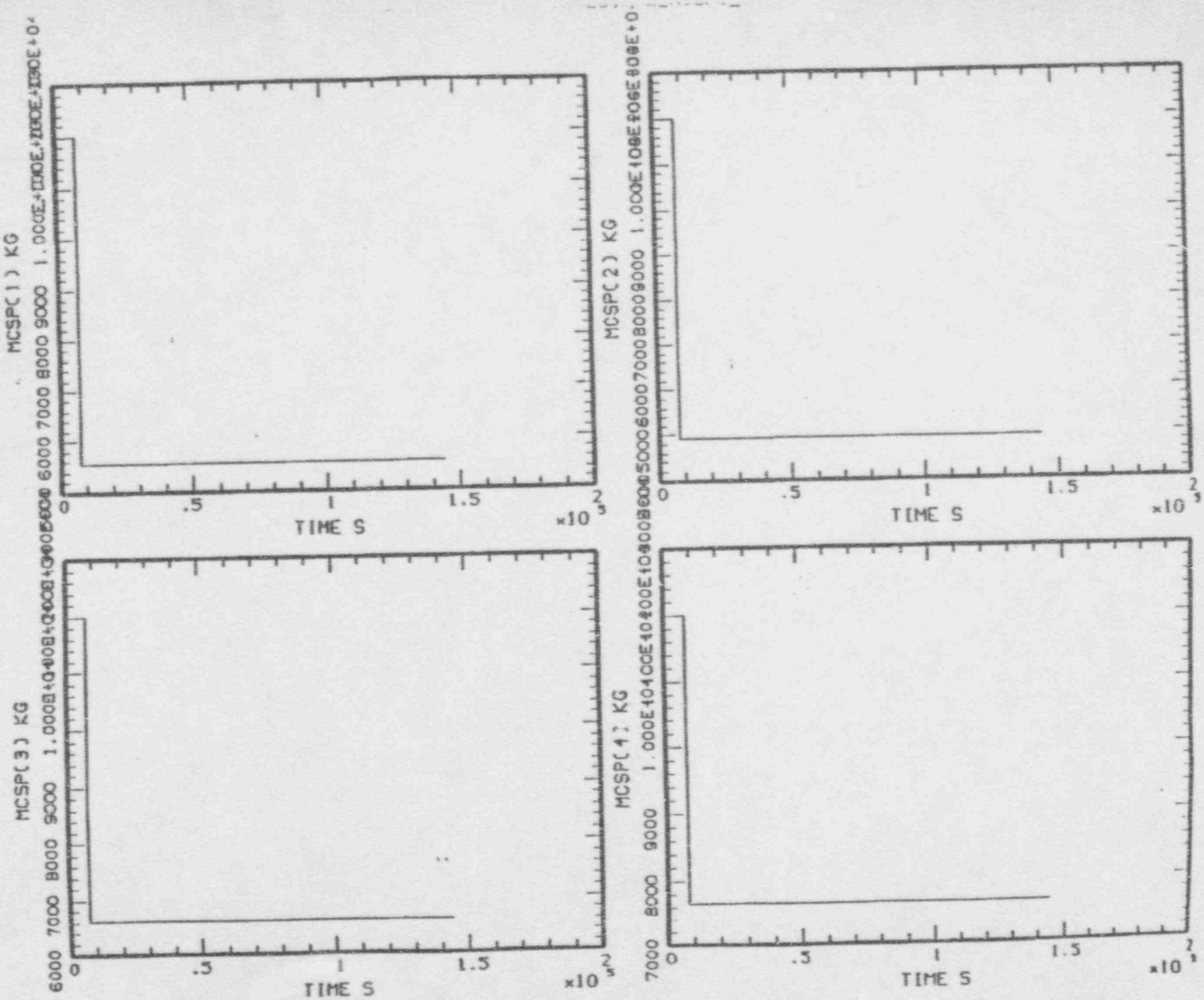
MCSP(1) KG
6000 7000 8000 9000
TIME S
0 .5 1 1.5 2
x10^5
MCSP(2) KG
TIME S
0 .5 1 1.5 2
x10^5
MCSP(3) KG
6000 7000 8000 9000
TIME S
0 .5 1 1.5 2
x10^5
MCSP(4) KG
7000 8000 9000
TIME S
0 .5 1 1.5 2
x10^5

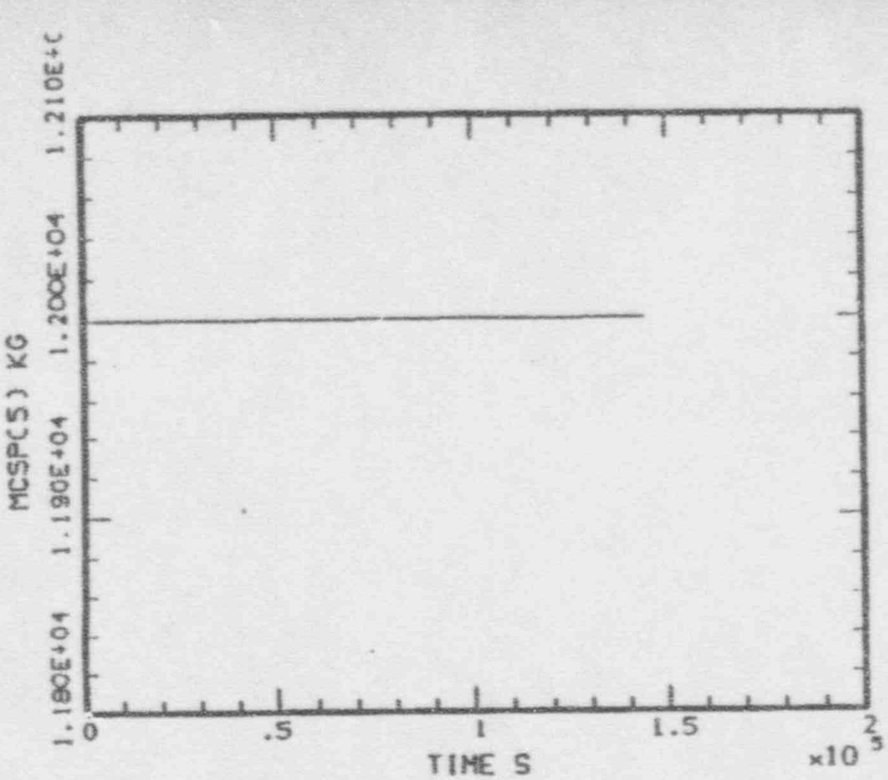
MCSP(5) KG
1.180E+04
1.190E+04
1.200E+04
1.210E+0
0
.5
1
1.5
2
x10^5
TIME S

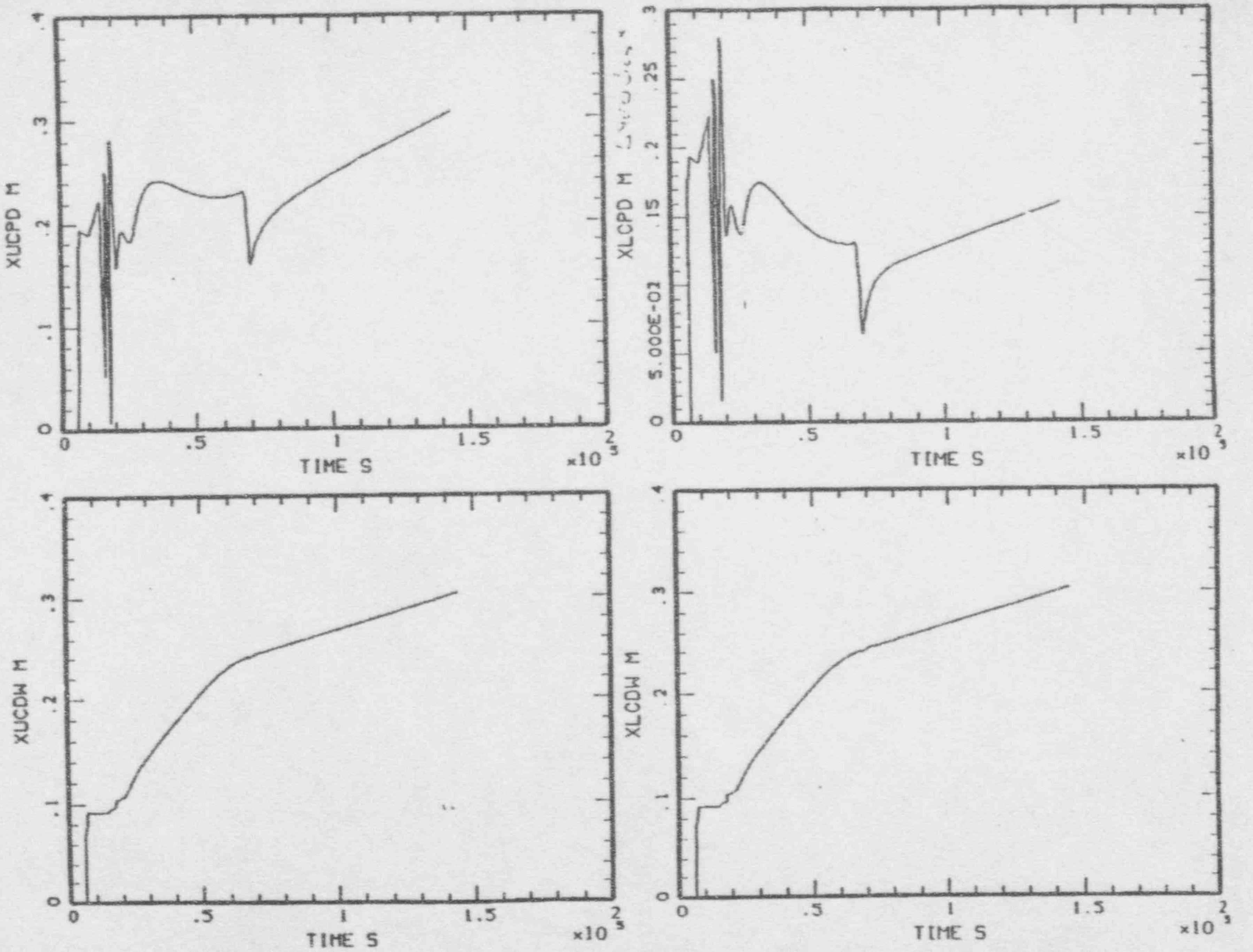
XUCPD M
XLCPD M
XUCDW M
XLCDW M
TIME S
×10^3
5.000E-02

ATTACHMENT 2

MELCOR FINE CORE NODALIZATION

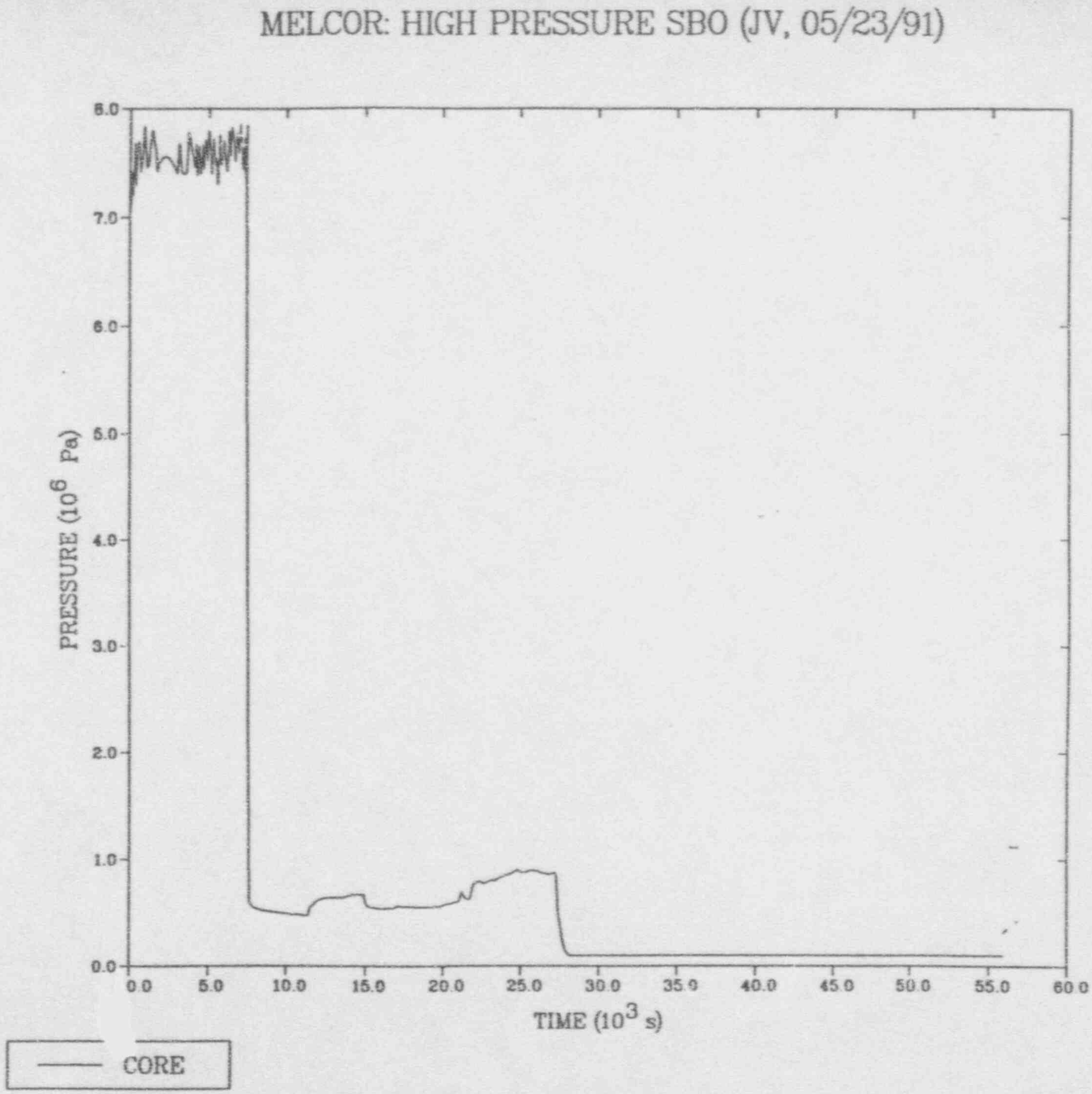
MELCOR: HIGH PRESSURE SBO (JV, 05/23/91)
PRESSURE (10^6 Pa)
8.0
7.0
6.0
5.0
4.0
3.0
2.0
1.0
0.0
0.0
5.0
10.0
15.0
20.0
25.0
30.0
35.0
40.0
45.0
50.0
55.0
60.0
TIME (10^3 s)
CORE

MELCOR: HIGH PRESSURE SBO (JV, 05/23/91)

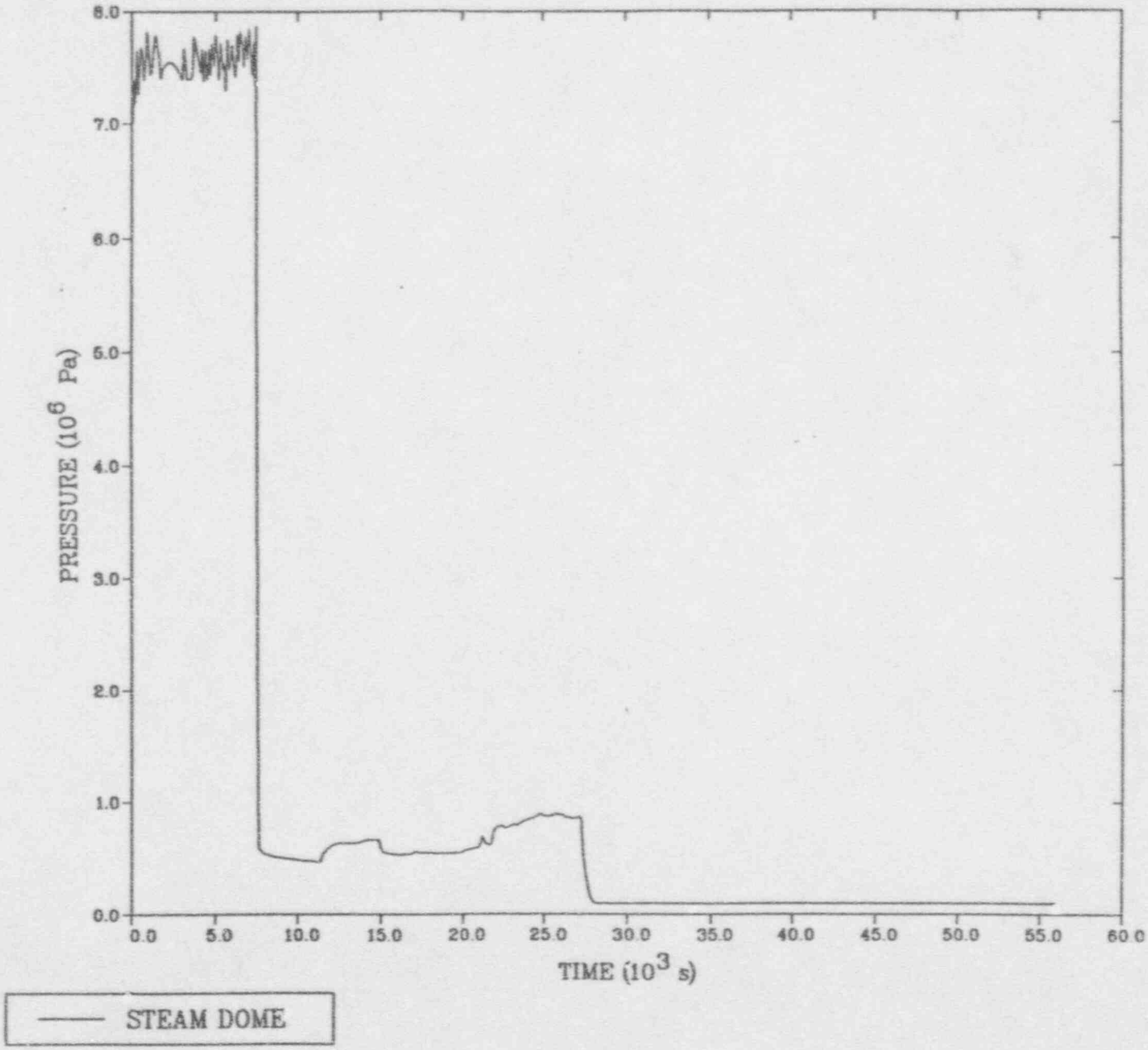

MELCOR: HIGH PRESSURE SBO (JV, 05/23/91)

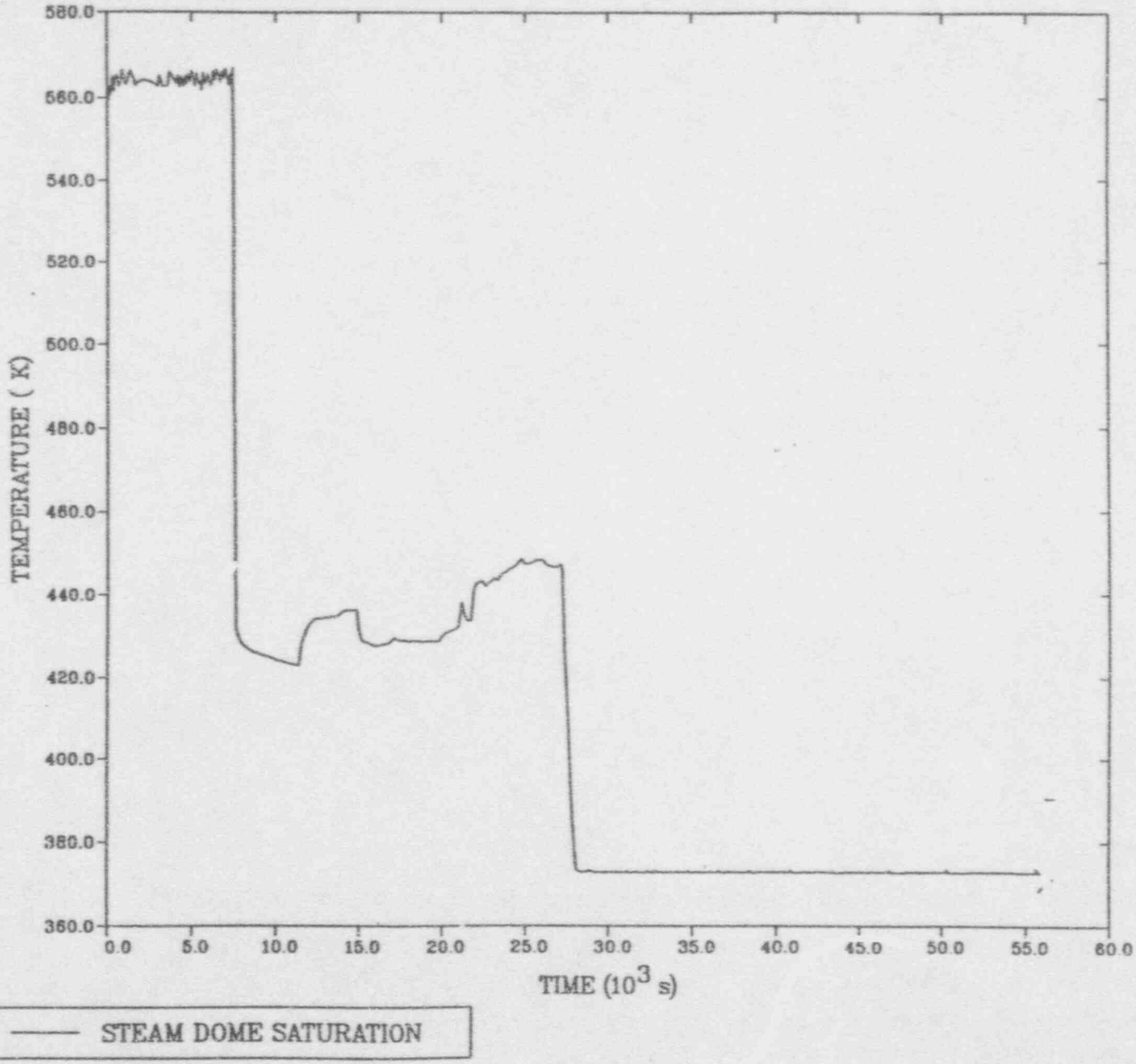

MELCOR: HIGH PRESSURE SBO (JV, 05/23/91)

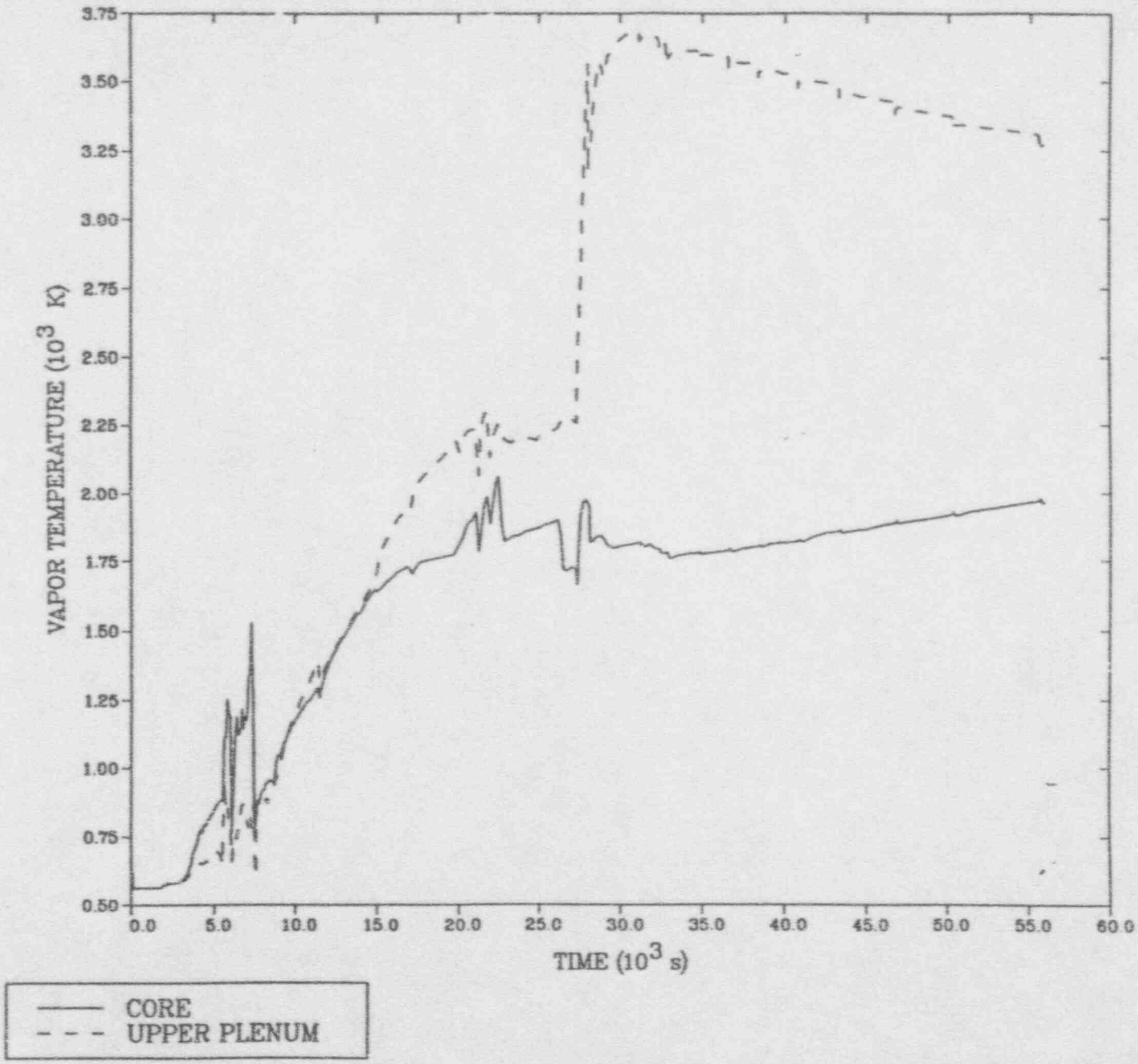

MELCOR: HIGH PRESSURE SBO (JV, 05/23/91)

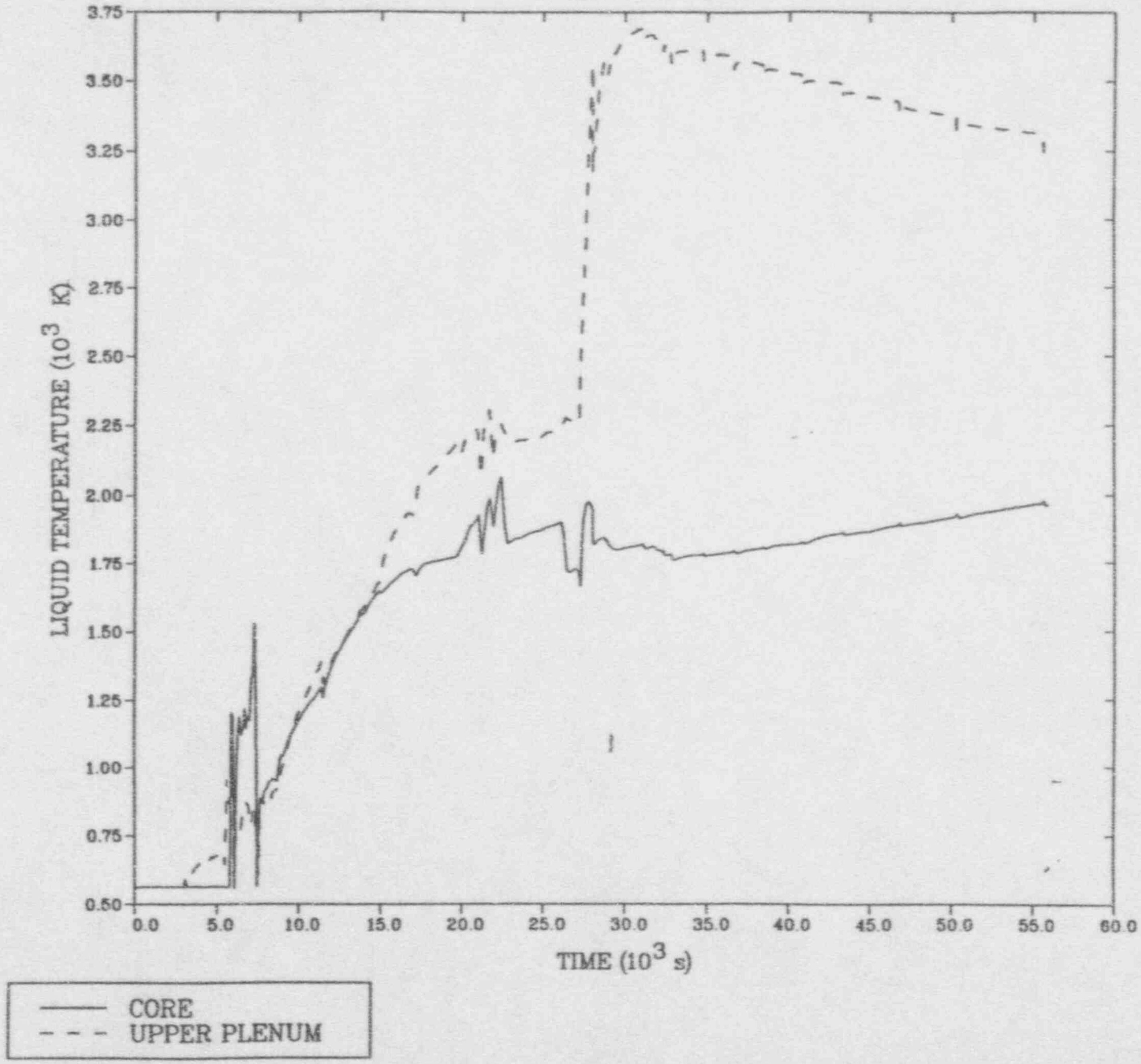

MELCOR: HIGH PRESSURE SBO (JV, 05/23/91)

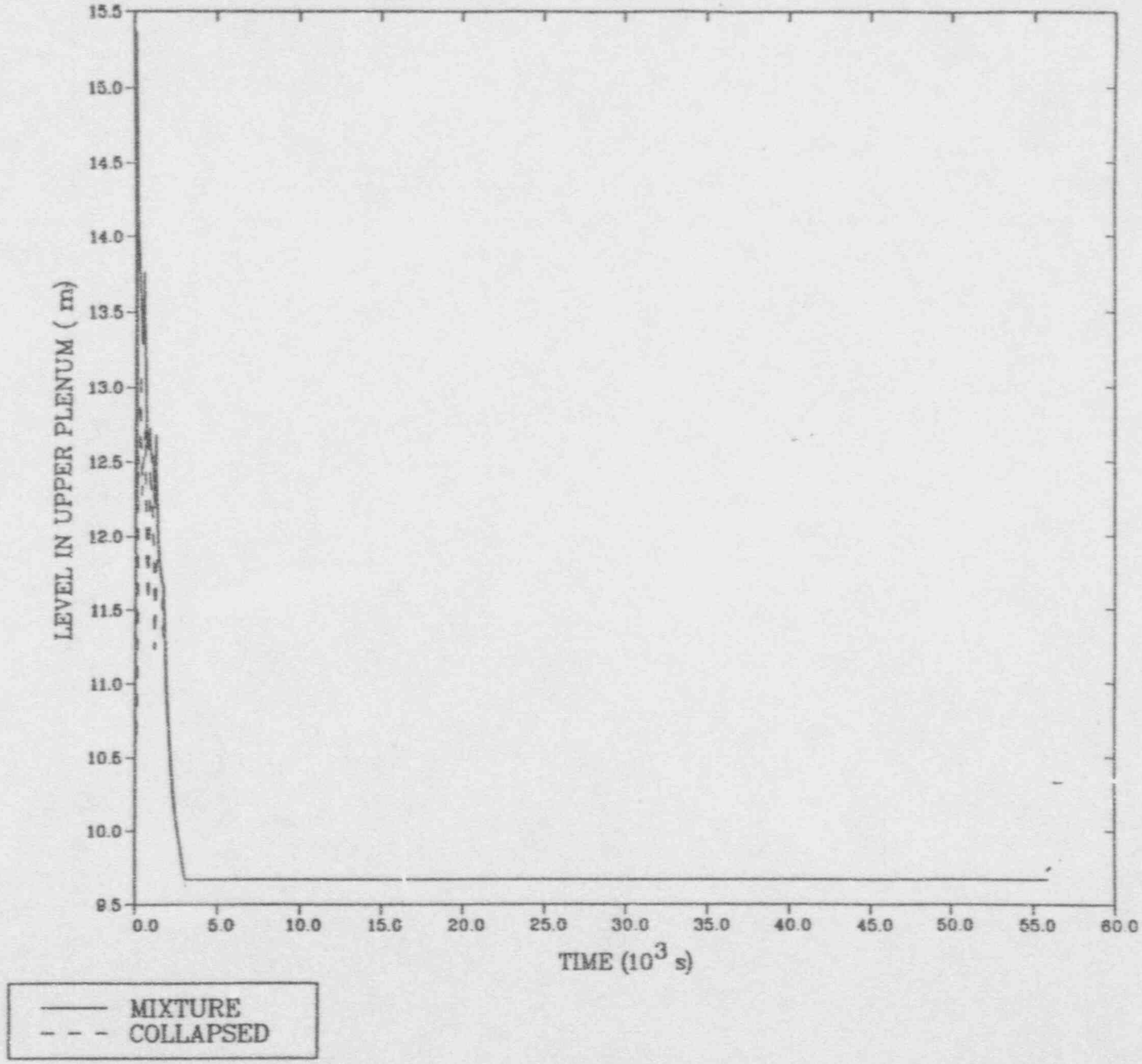

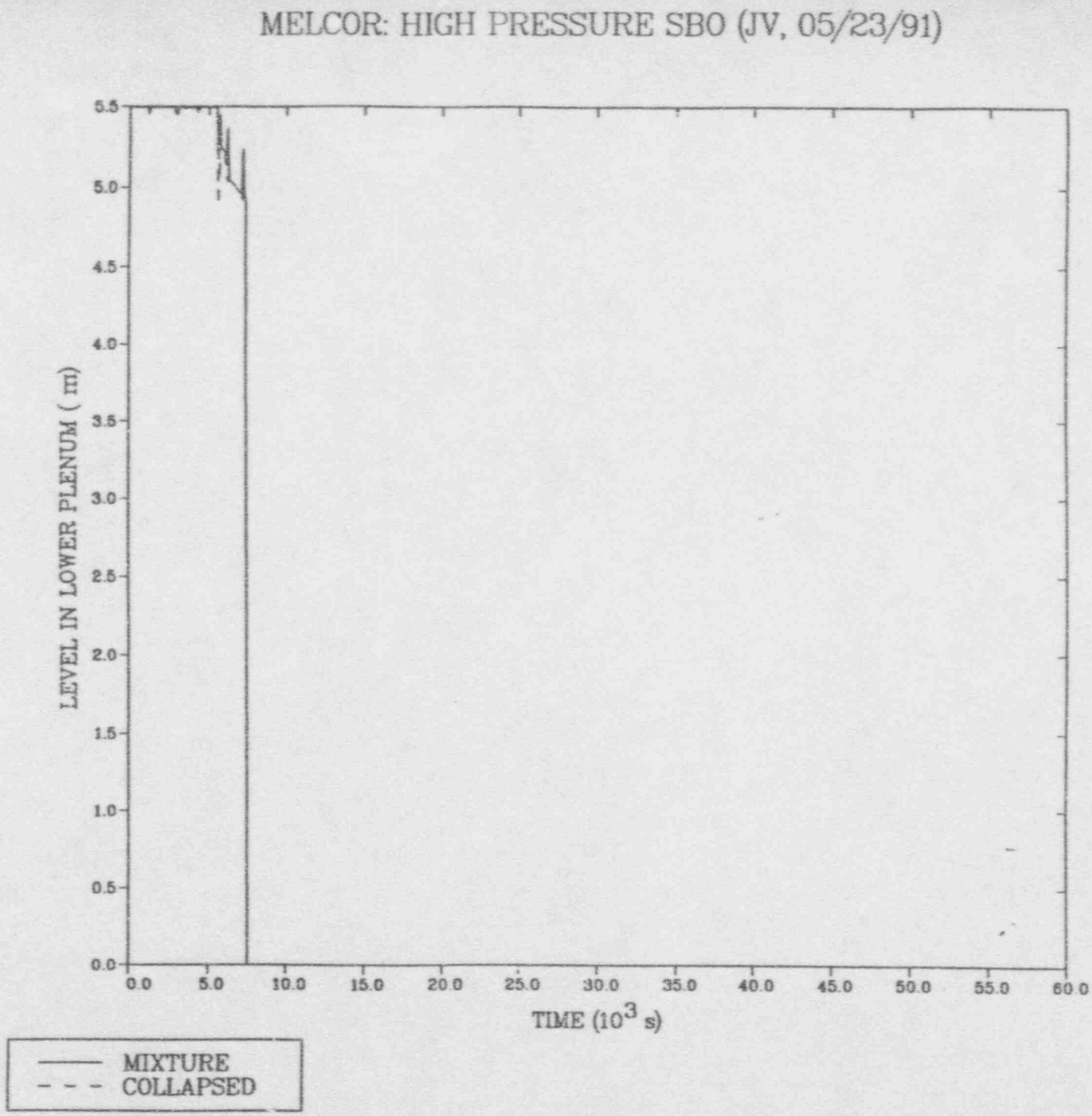
MELCOR: HIGH PRESSURE SBO (JV, 05/23/91)
LEVEL IN LOWER PLENUM (m)
TIME (10^3 s)
0.0
0.5
1.0
1.5
2.0
2.5
3.0
3.5
4.0
4.5
5.0
5.5
5.0
10.0
15.0
20.0
25.0
30.0
35.0
40.0
45.0
50.0
55.0
60.0
MIXTURE
COLLAPSED

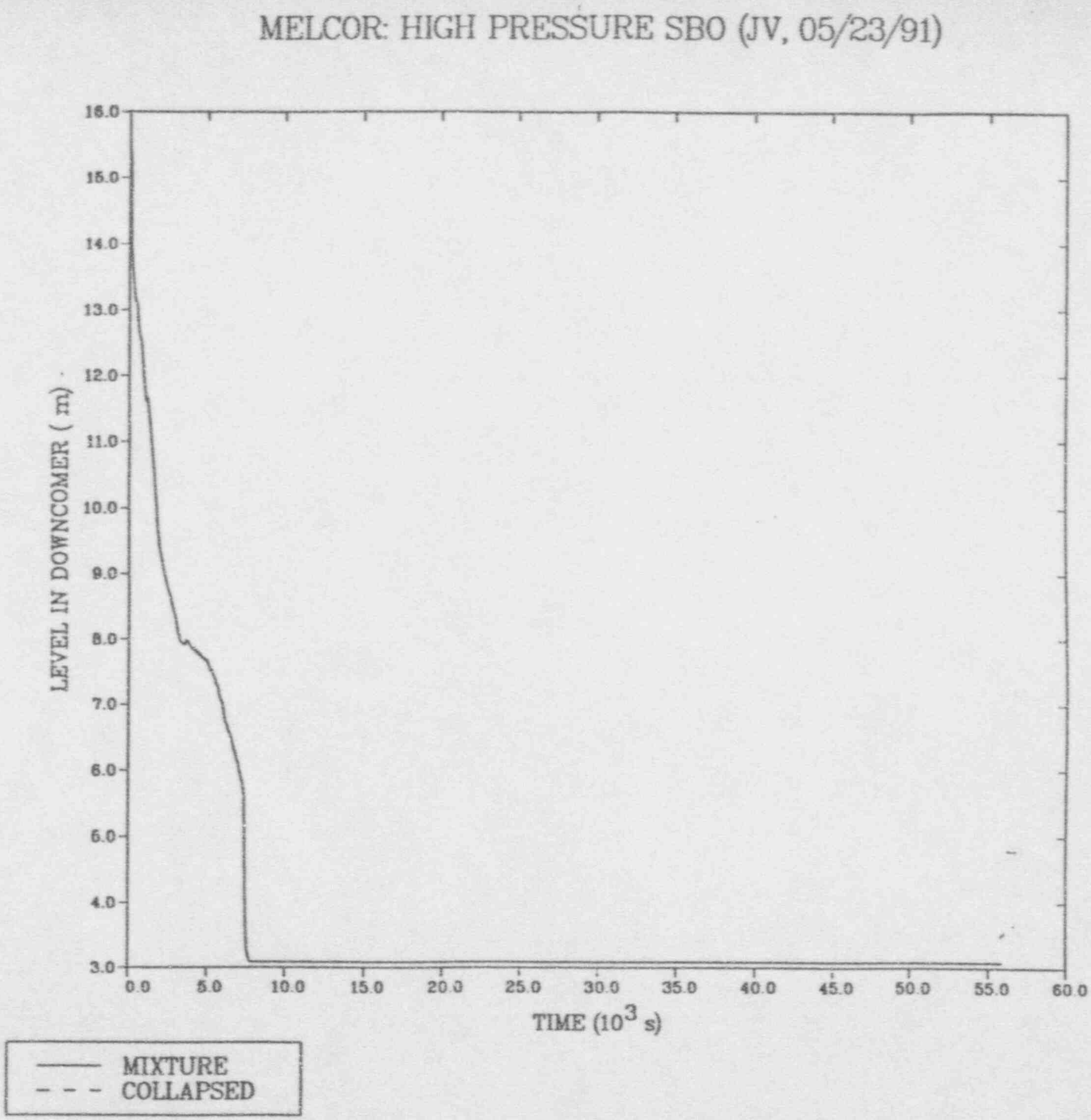
MELCOR: HIGH PRESSURE SBO (JV, 05/23/91)
LEVEL IN DOWNCOMER (m)
TIME (10^3 s)
16.0
15.0
14.0
13.0
12.0
11.0
10.0
9.0
8.0
7.0
6.0
5.0
4.0
3.0
0.0
5.0
10.0
15.0
20.0
25.0
30.0
35.0
40.0
45.0
50.0
55.0
60.0
MIXTURE
COLLAPSED

MELCOR: HIGH PRESSURE SBO (JV, 05/23/91)

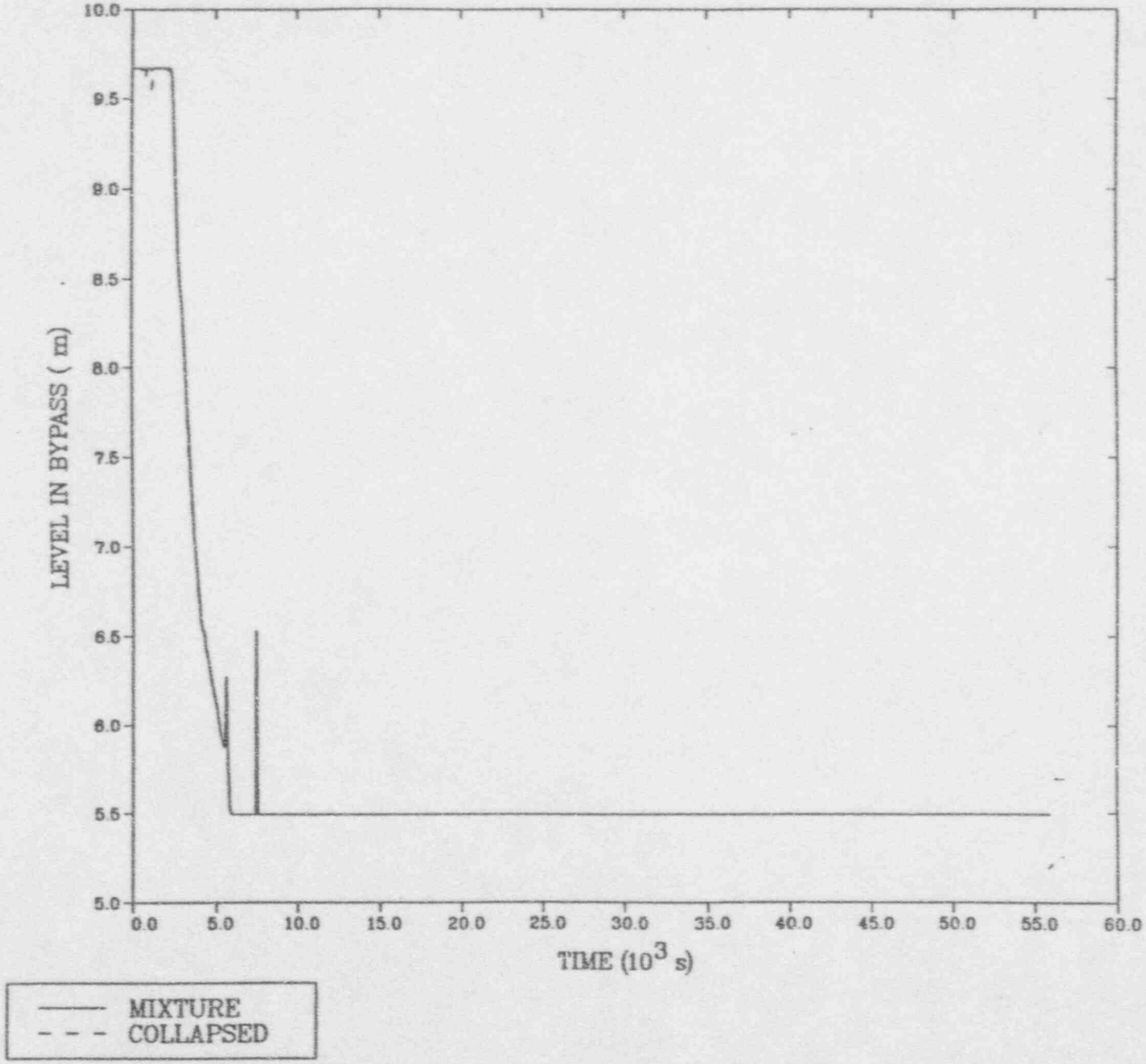

MELCOR: HIGH PRESSURE SBO (JV, 05/23/91)

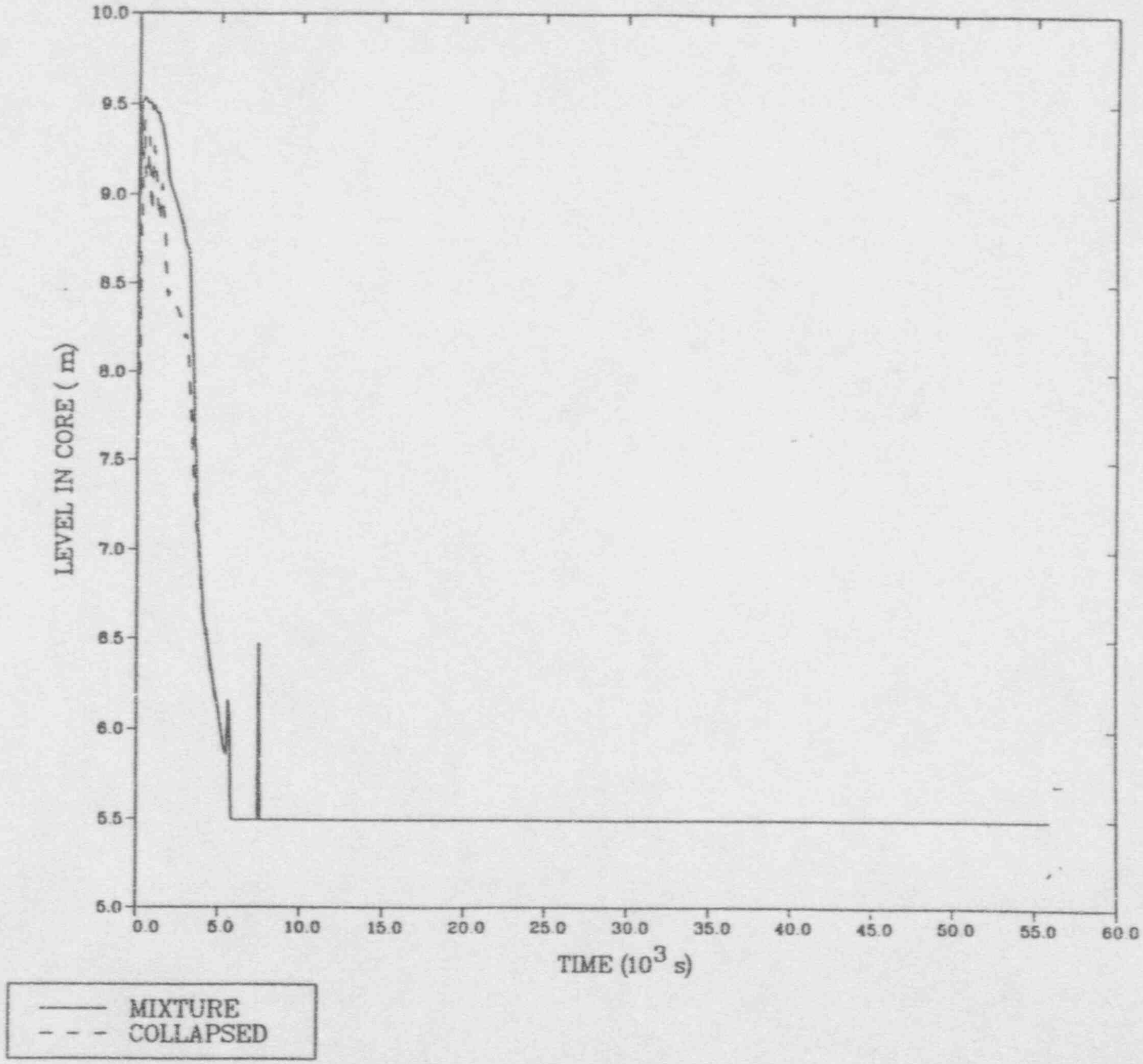

MELCOR: HIGH PRESSURE SBO (JV, 05/23/91)

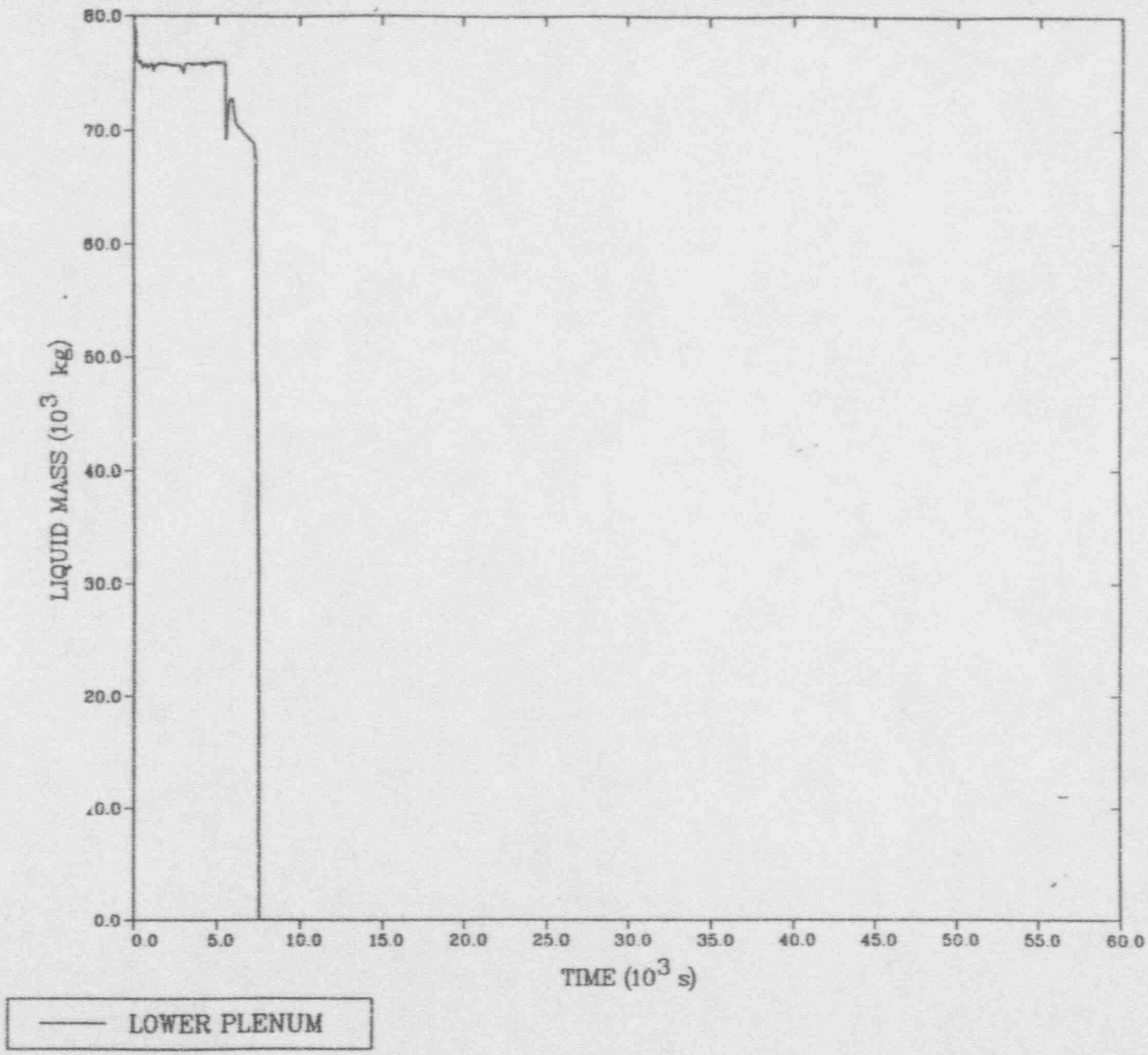

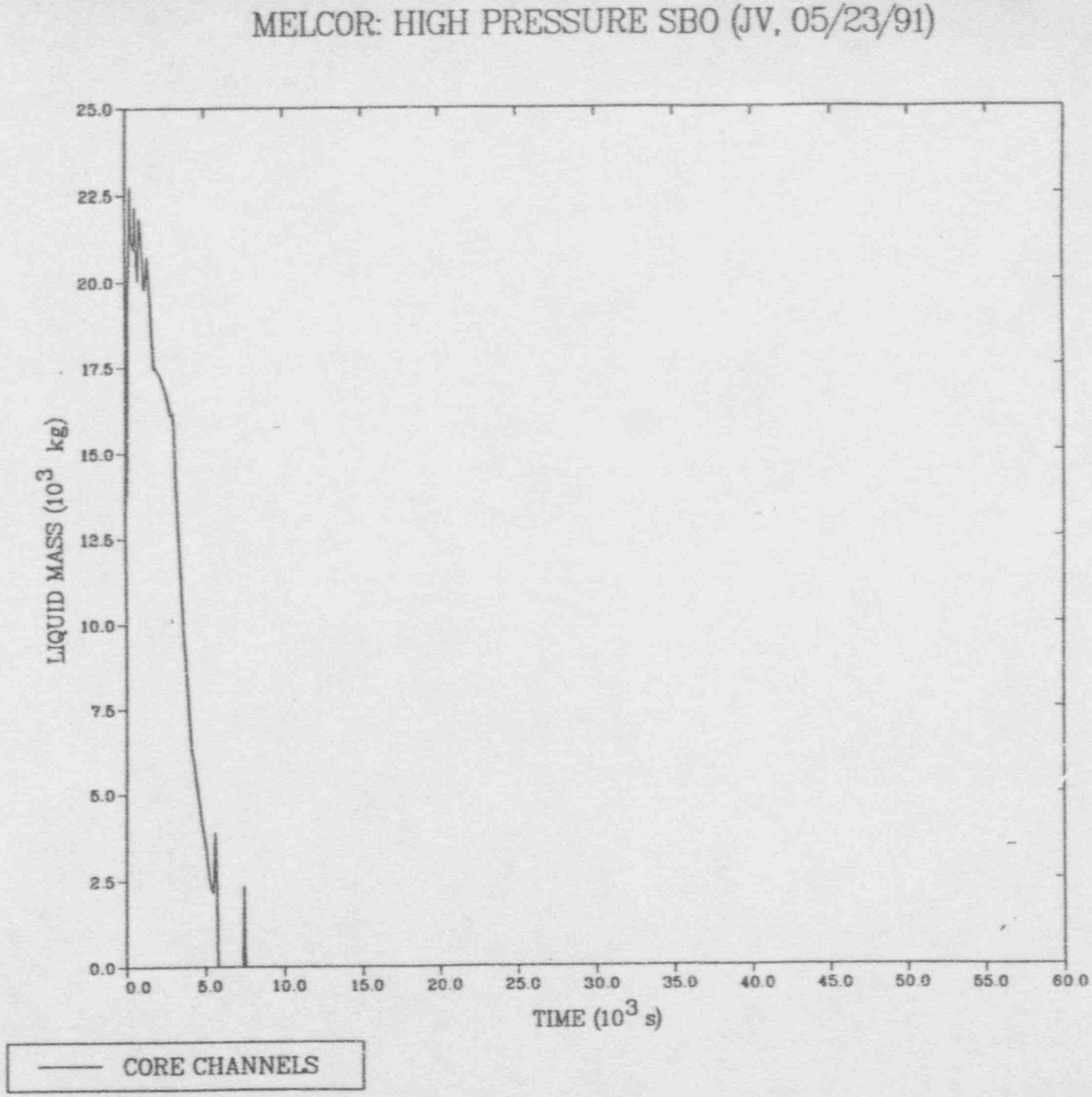
MELCOR: HIGH PRESSURE SBO (JV, 05/23/91)
LIQUID MASS (10^3 kg)
25.0
22.5
20.0
17.5
15.0
12.5
10.0
7.5
5.0
2.5
0.0
5.0
10.0
15.0
20.0
25.0
30.0
35.0
40.0
45.0
50.0
55.0
60.0
TIME (10^3 s)
CORE CHANNELS

MELCOR: HIGH PRESSURE SBO (JV, 05/23/91)

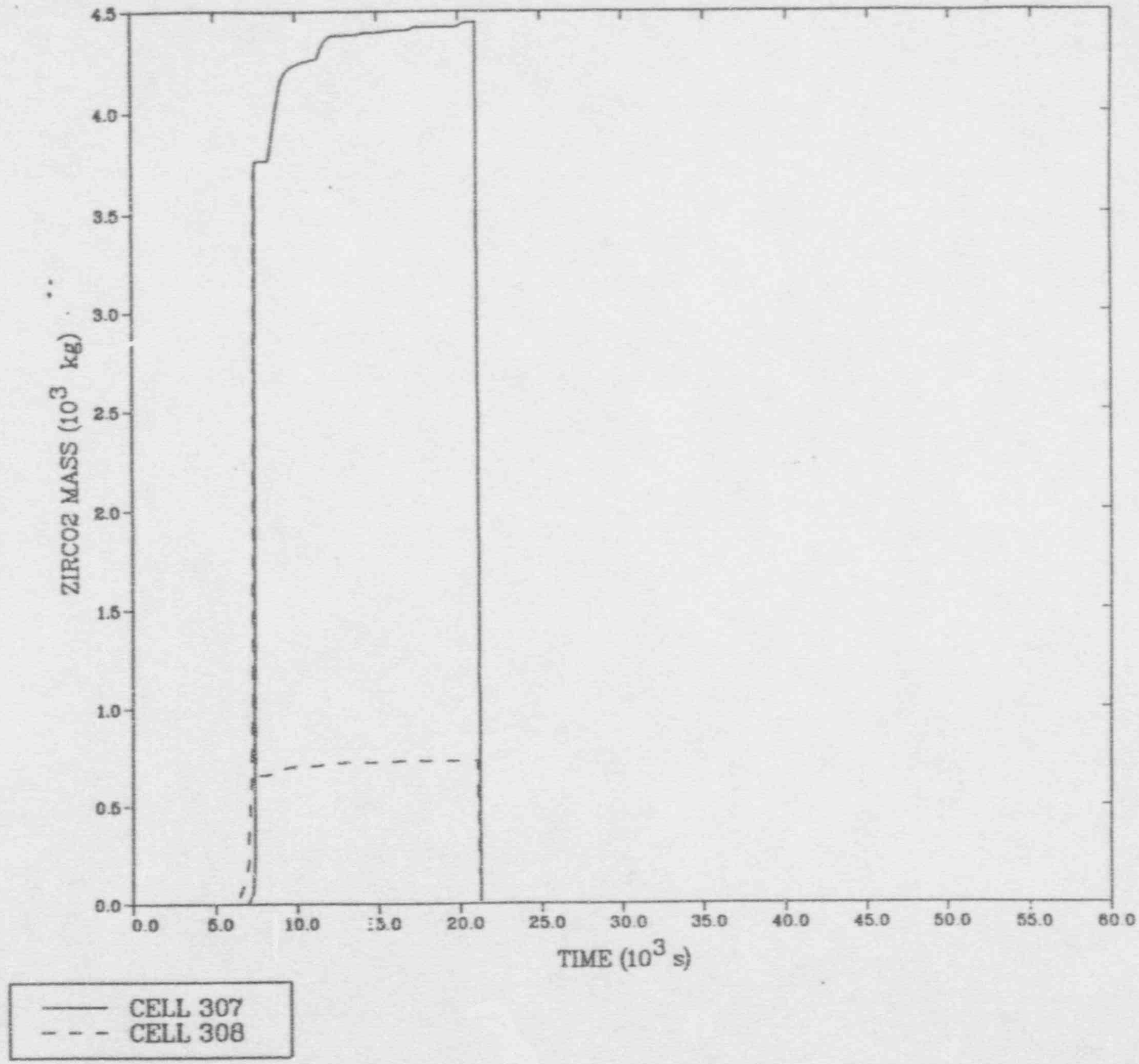

MELCOR: HIGH PRESSURE SBO

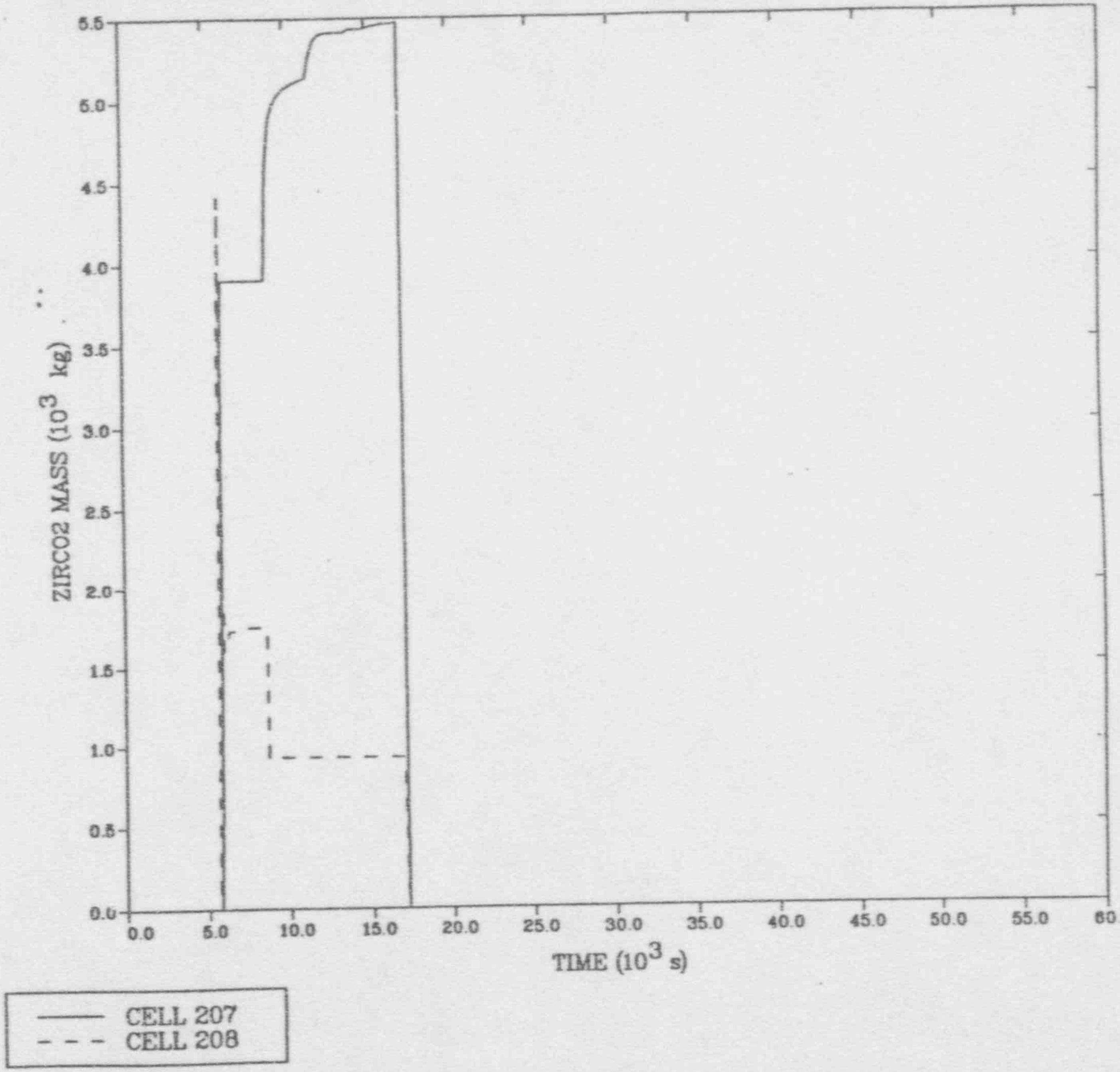

MELCOR: HIGH PRESSURE SBO (JV, 05/23/91)

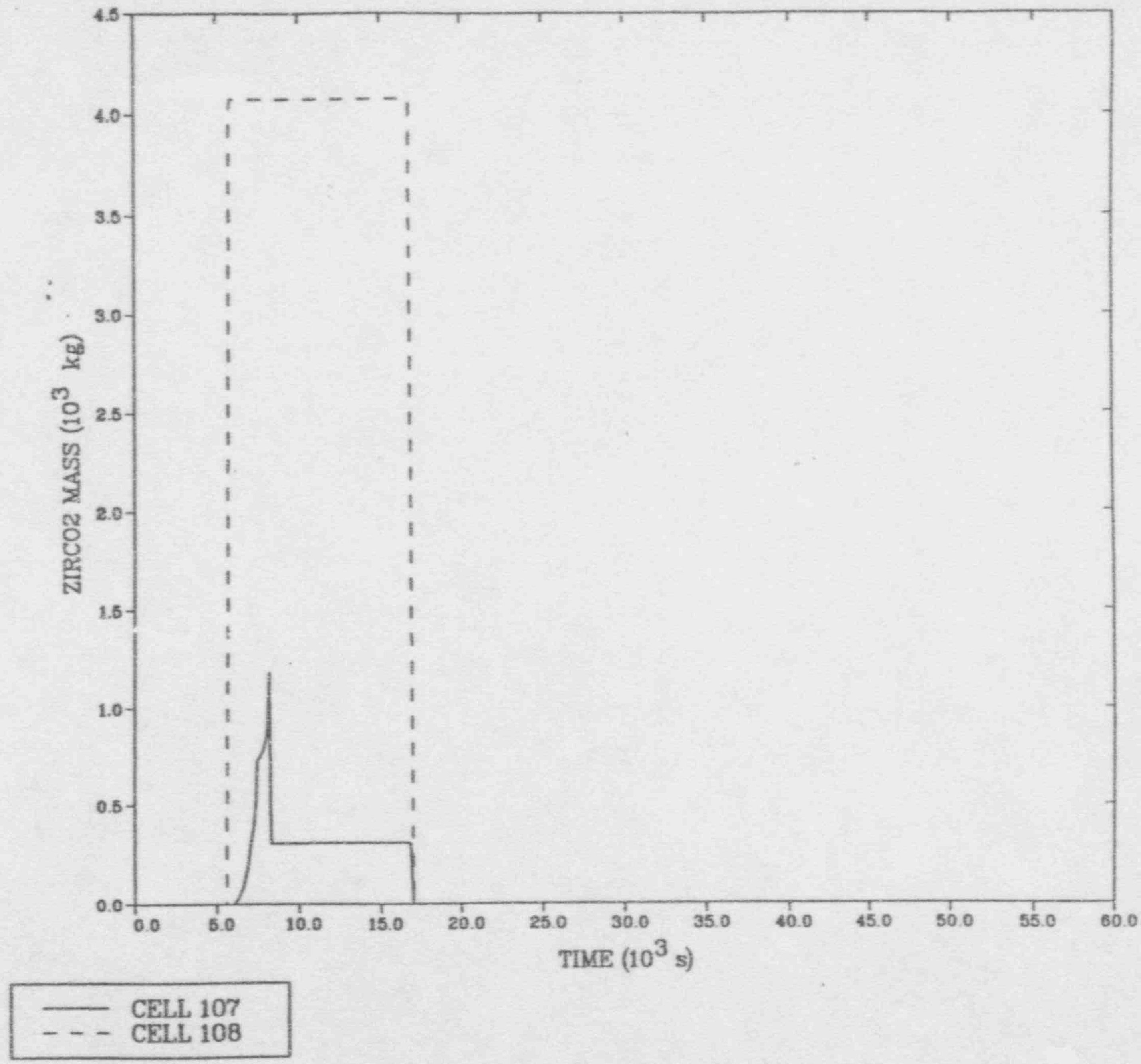

MELCOR: HIGH PRESSURE SBO (JV, 05/23/91)

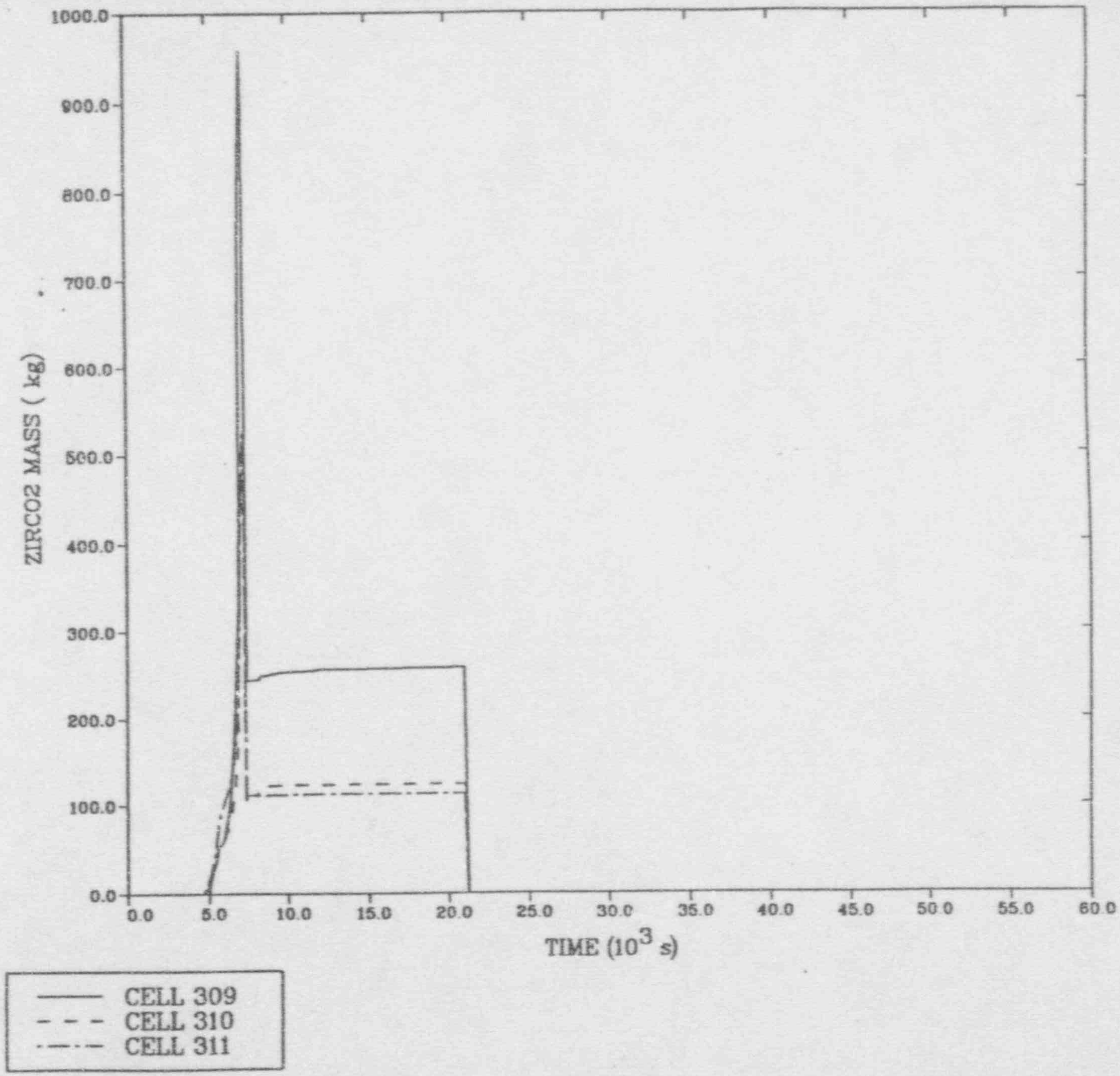

MELCOR: HIGH PRESSURE SBO (JV, 05/23/91)

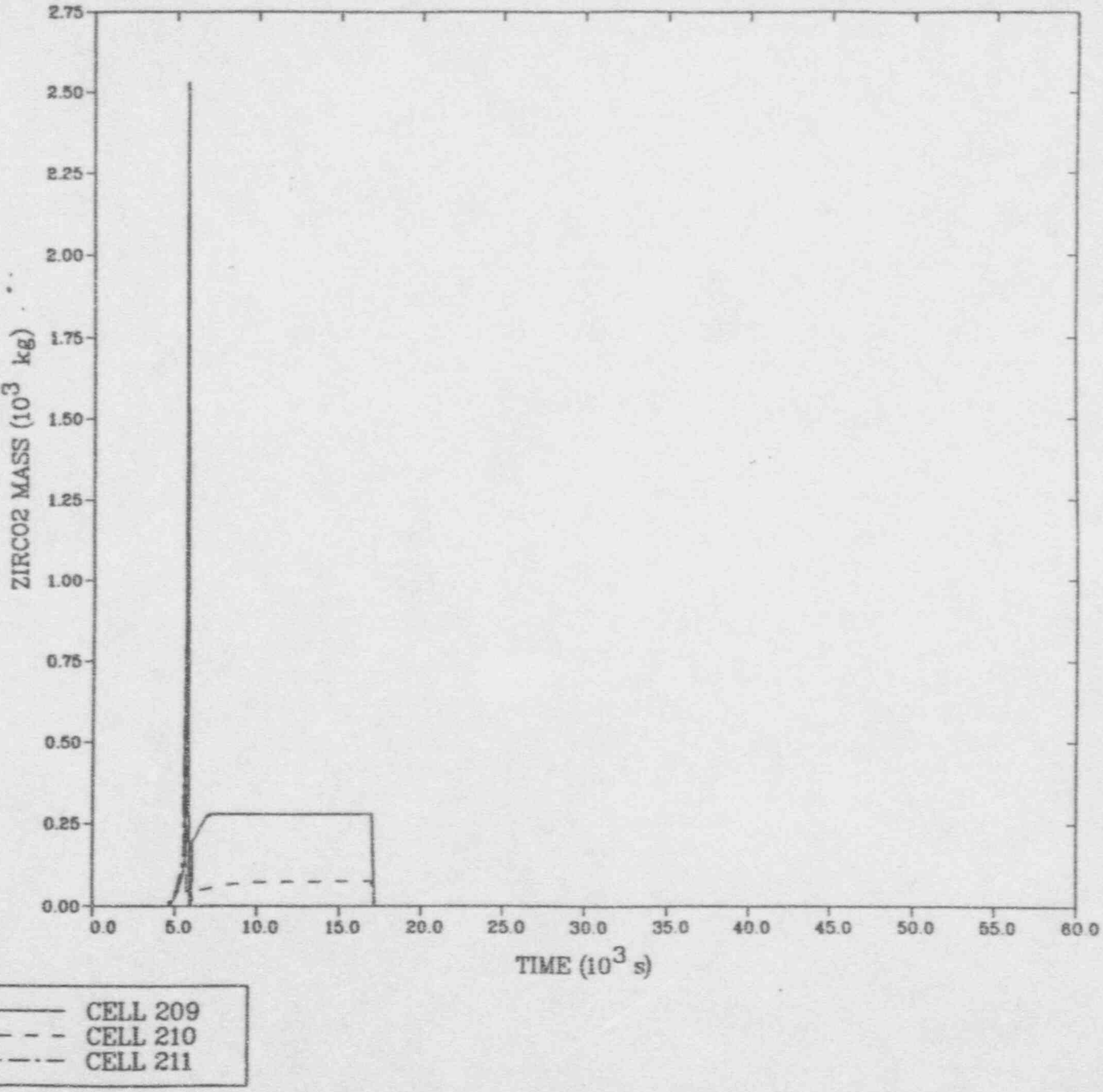

MELCOR: HIGH PRESSURE SBO

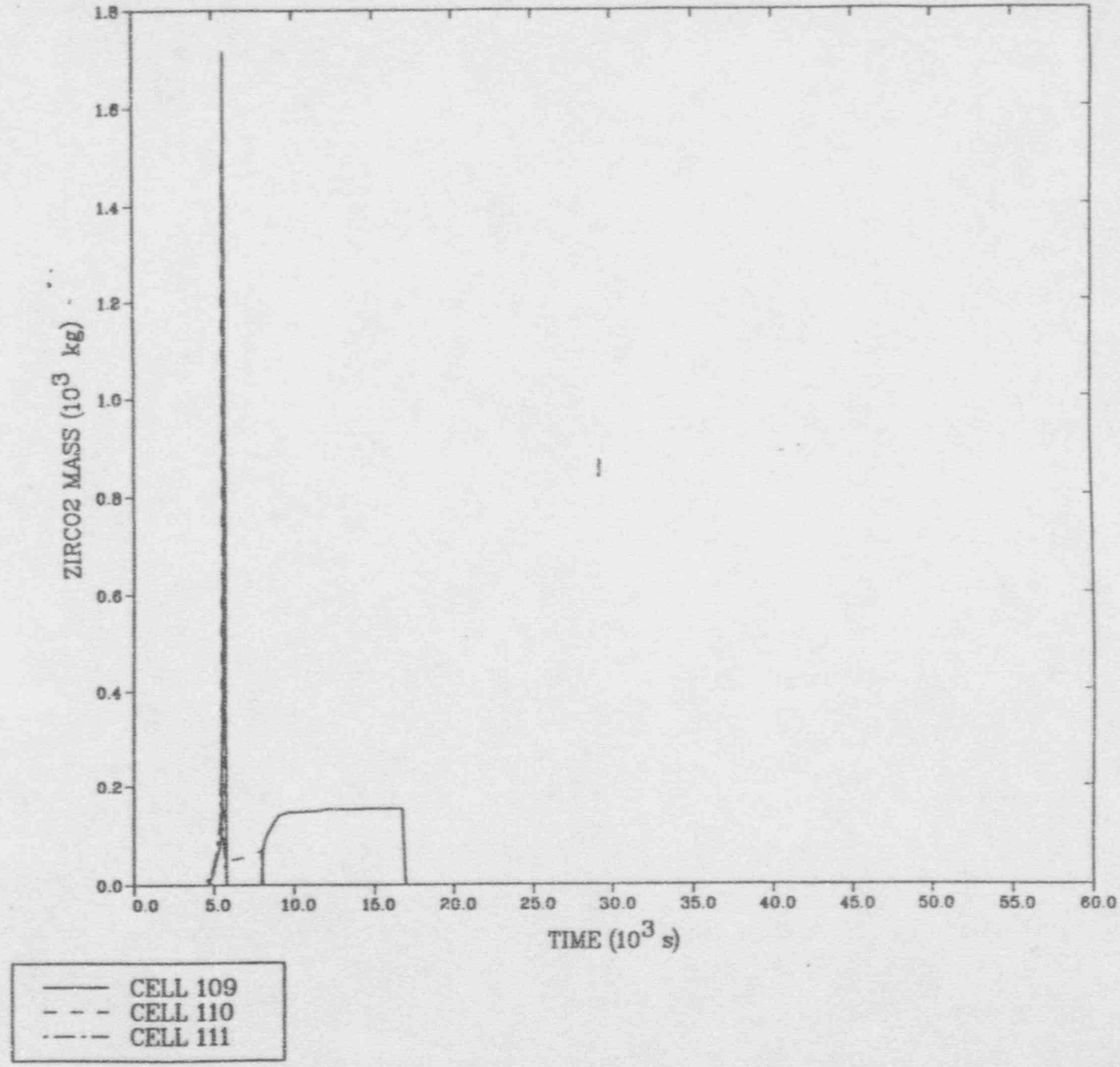

MELCOR: HIGH PRESSURE SBO (JV, 05/28/91)

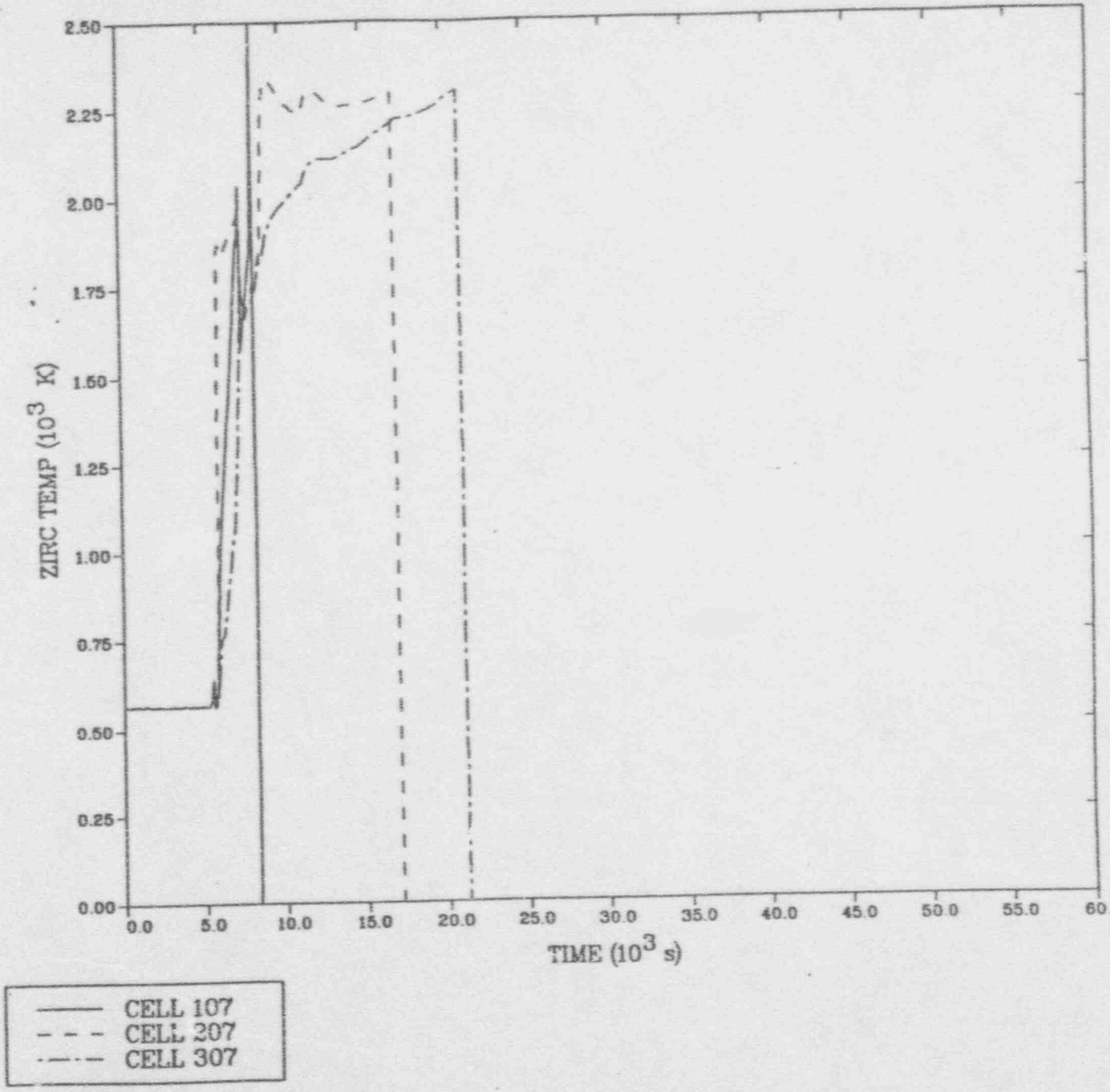

MELCOR: HIGH PRESSURE SBO (JV, 05/23/91)

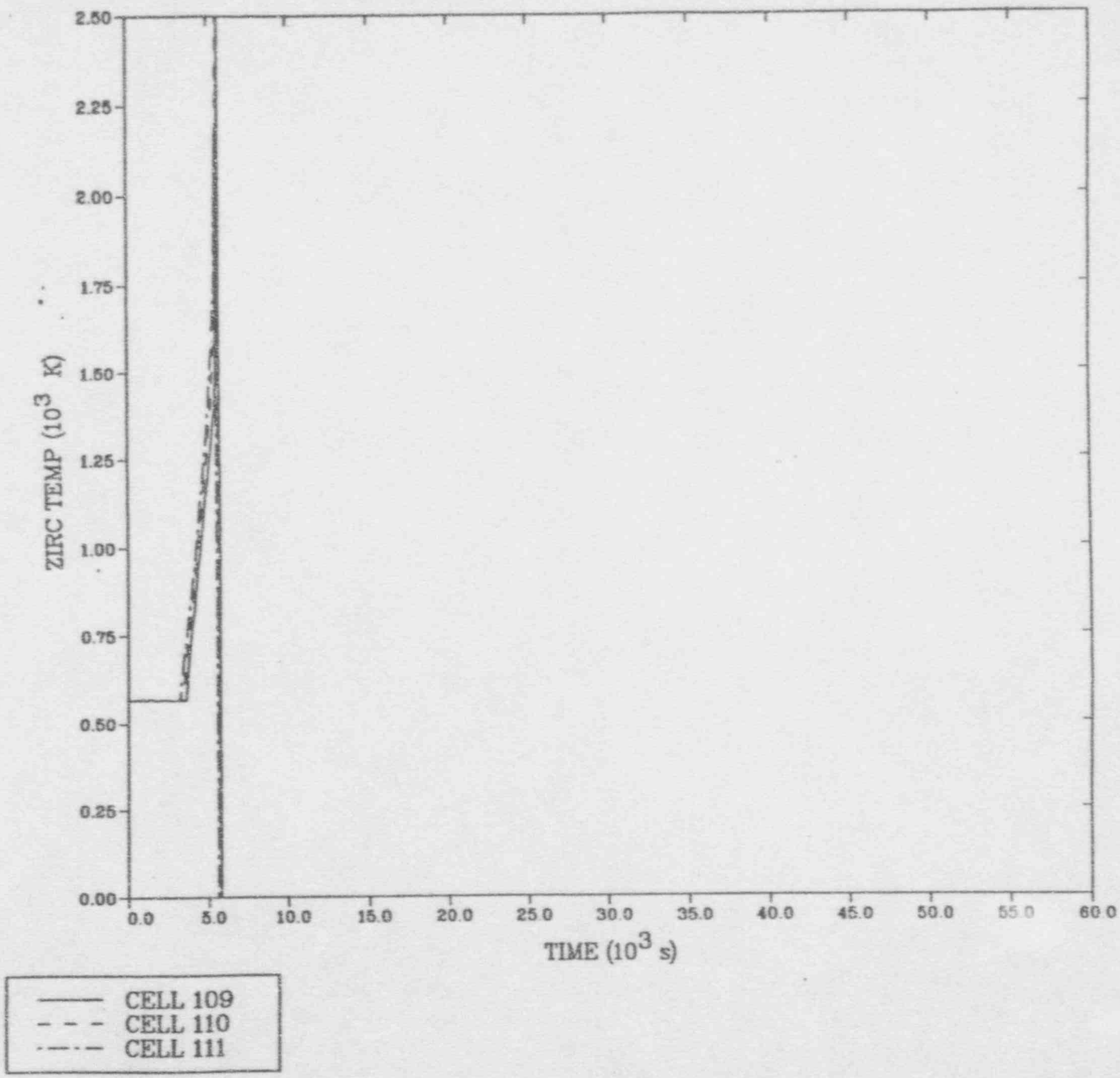

MELCOR: HIGH PRESSURE SBO (JV, 05/23/91)

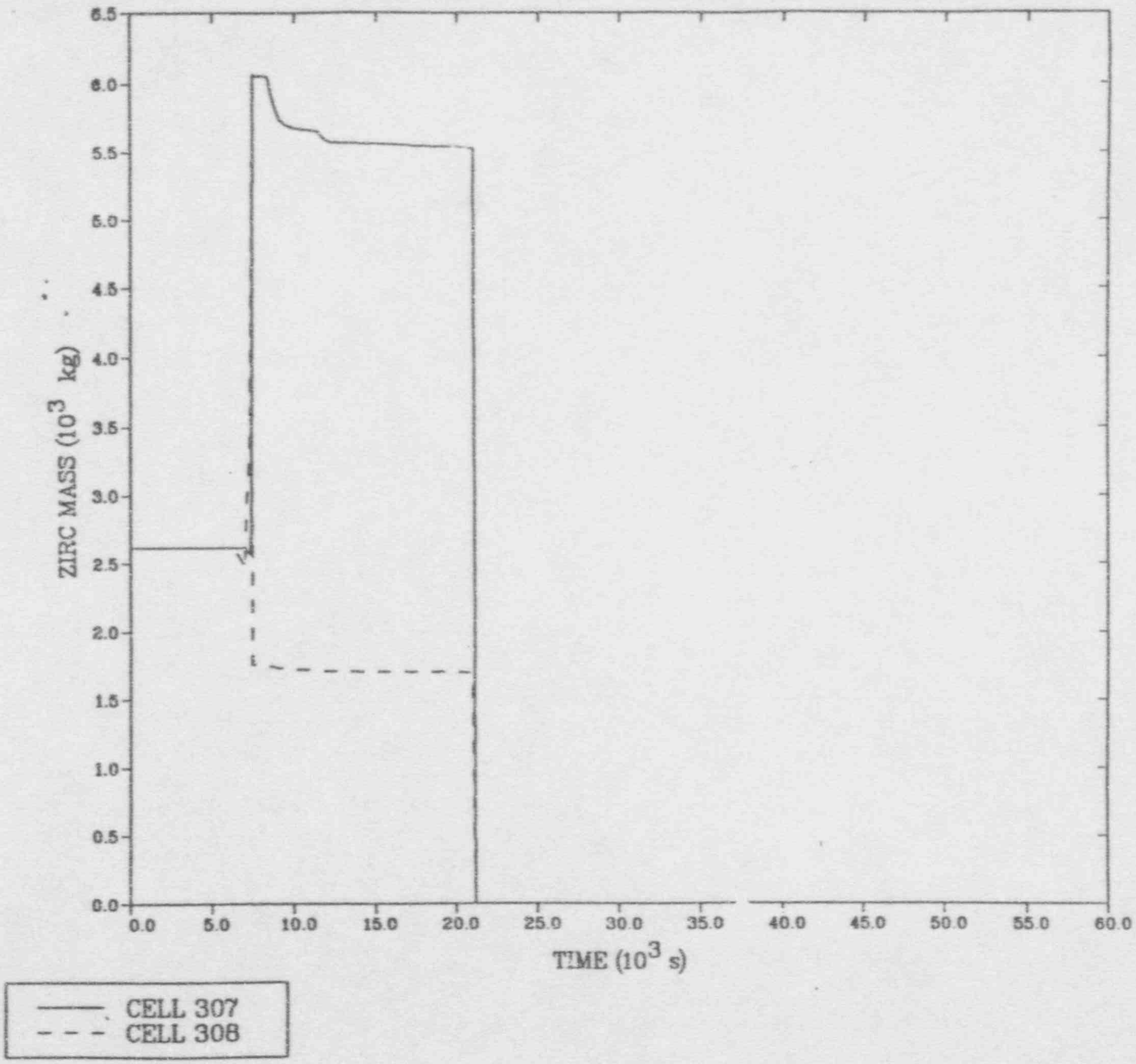

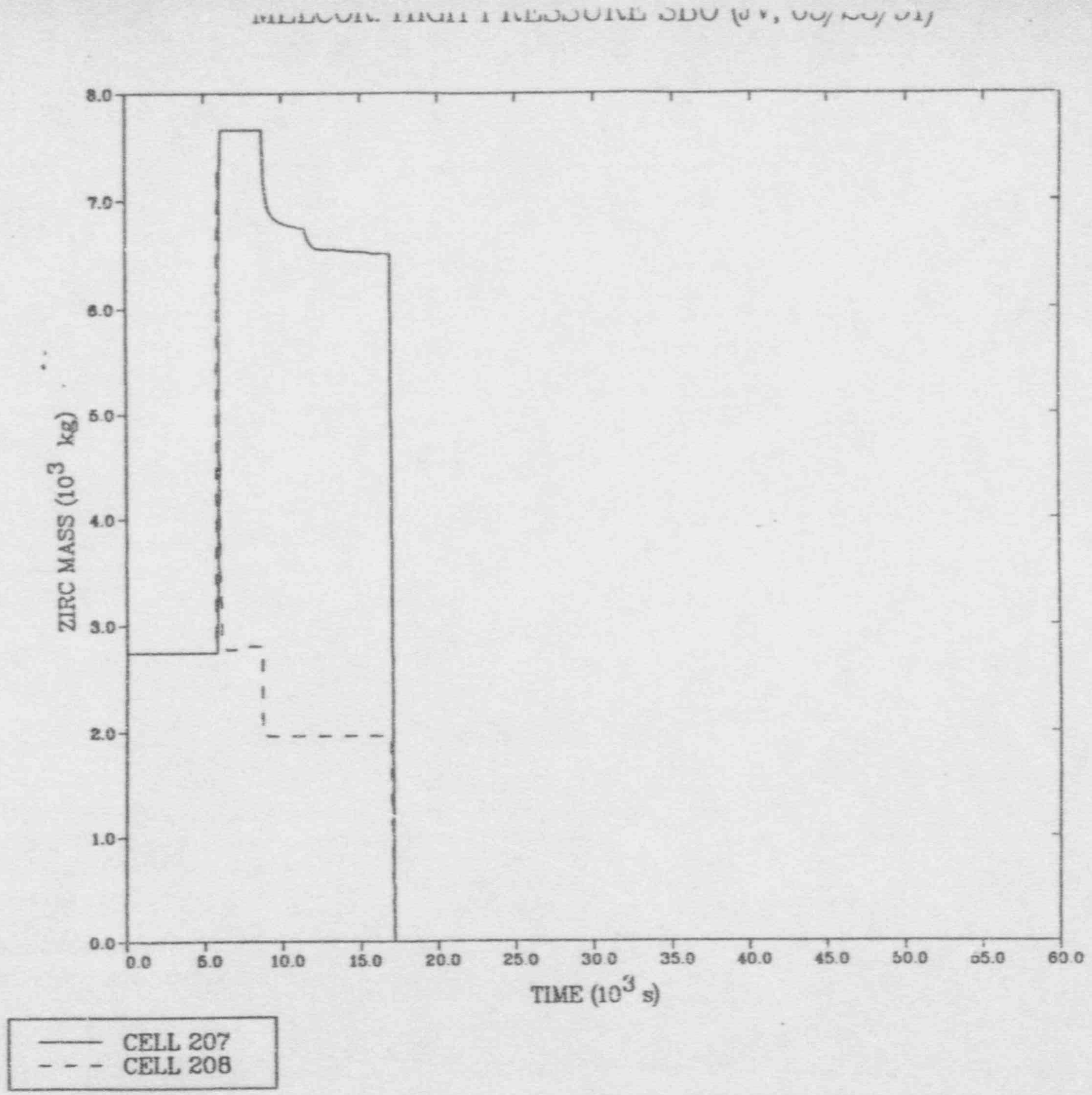
ZIRC MASS (10^3 kg)
8.0
7.0
6.0
5.0
4.0
3.0
2.0
1.0
0.0
0.0
5.0
10.0
15.0
20.0
25.0
30.0
35.0
40.0
45.0
50.0
55.0
60.0
TIME (10^3 s)
CELL 207
CELL 208

MELCOR: HIGH PRESSURE SBO (JV, 05/23/91)

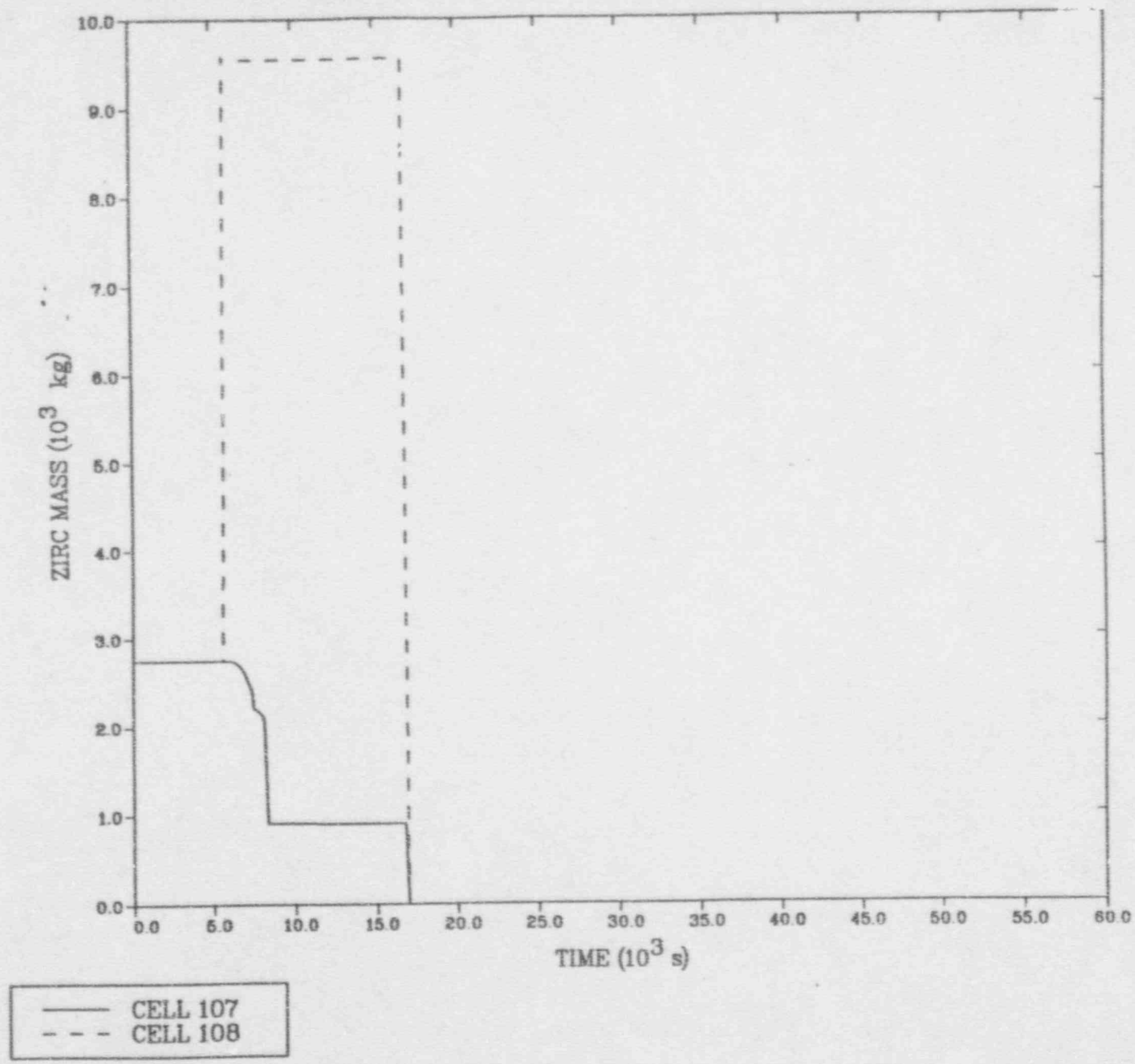

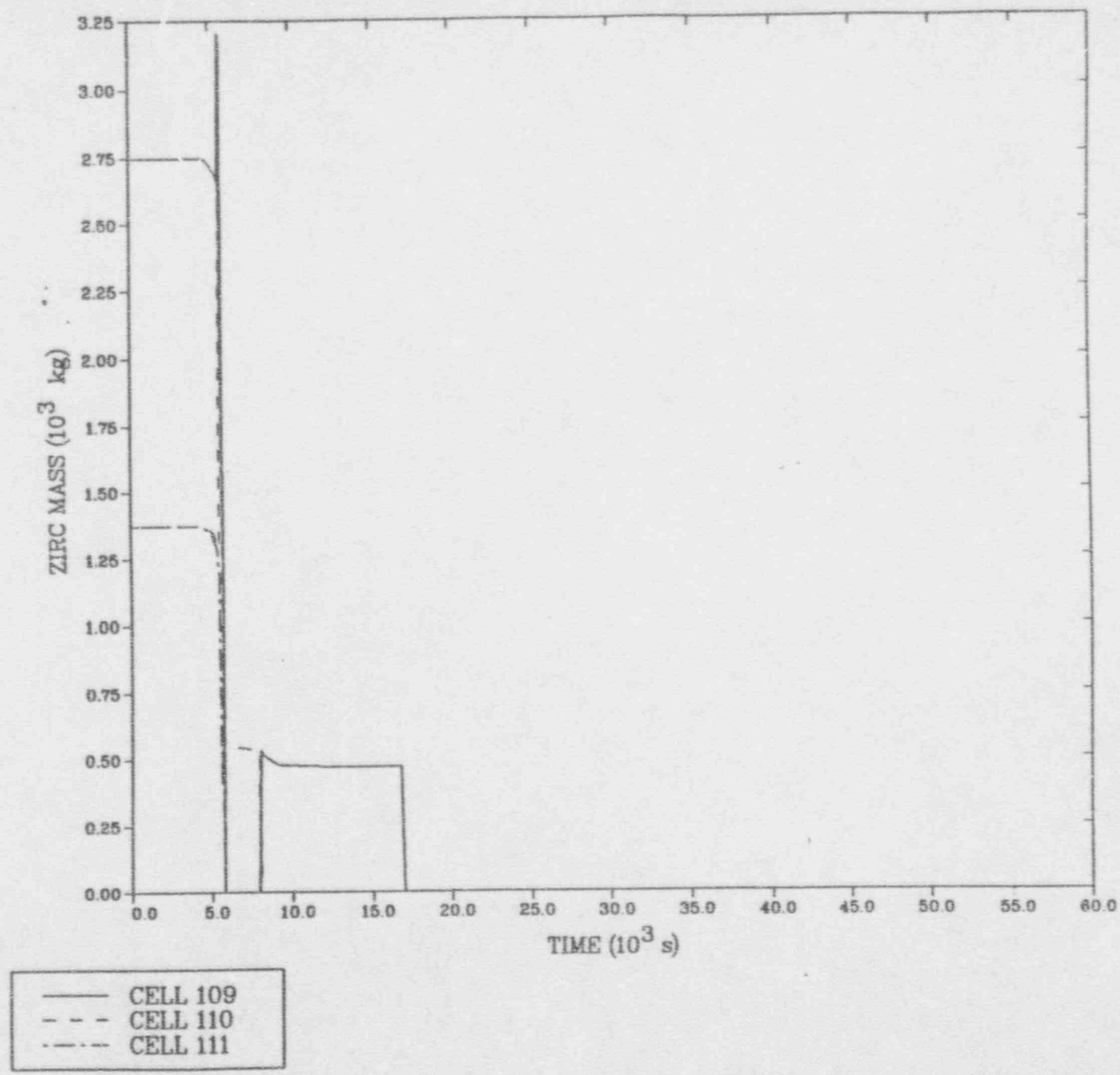

ZIRC MASS (10^3 kg)
3.25
3.00
2.75
2.50
2.25
2.00
1.75
1.50
1.25
1.00
0.75
0.50
0.25
0.00
0.0
5.0
10.0
15.0
20.0
25.0
30.0
35.0
40.0
45.0
50.0
55.0
60.0
TIME (10^3 s)
CELL 109
CELL 110
CELL 111

MELCOR: HIGH PRESSURE SBO

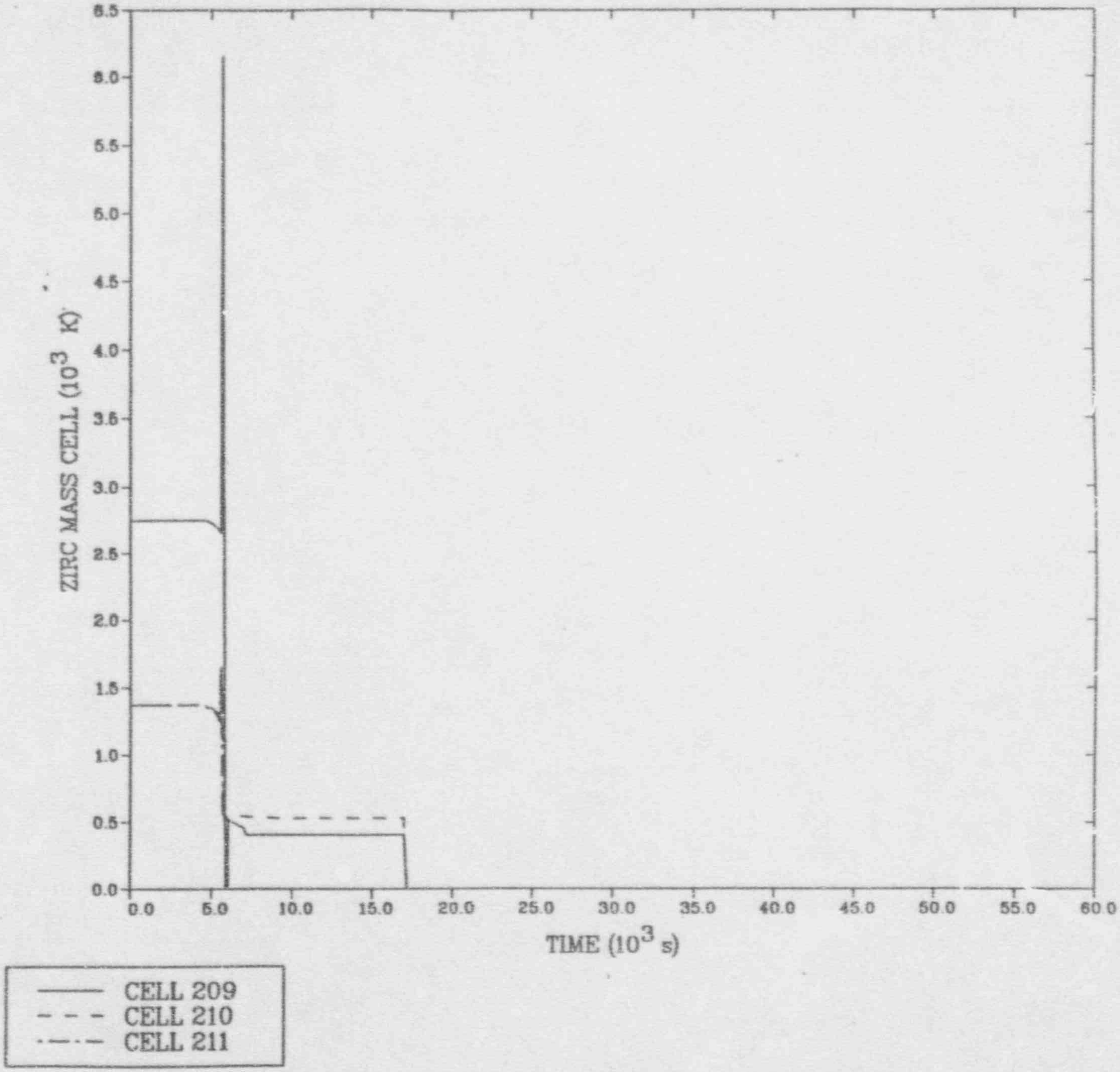

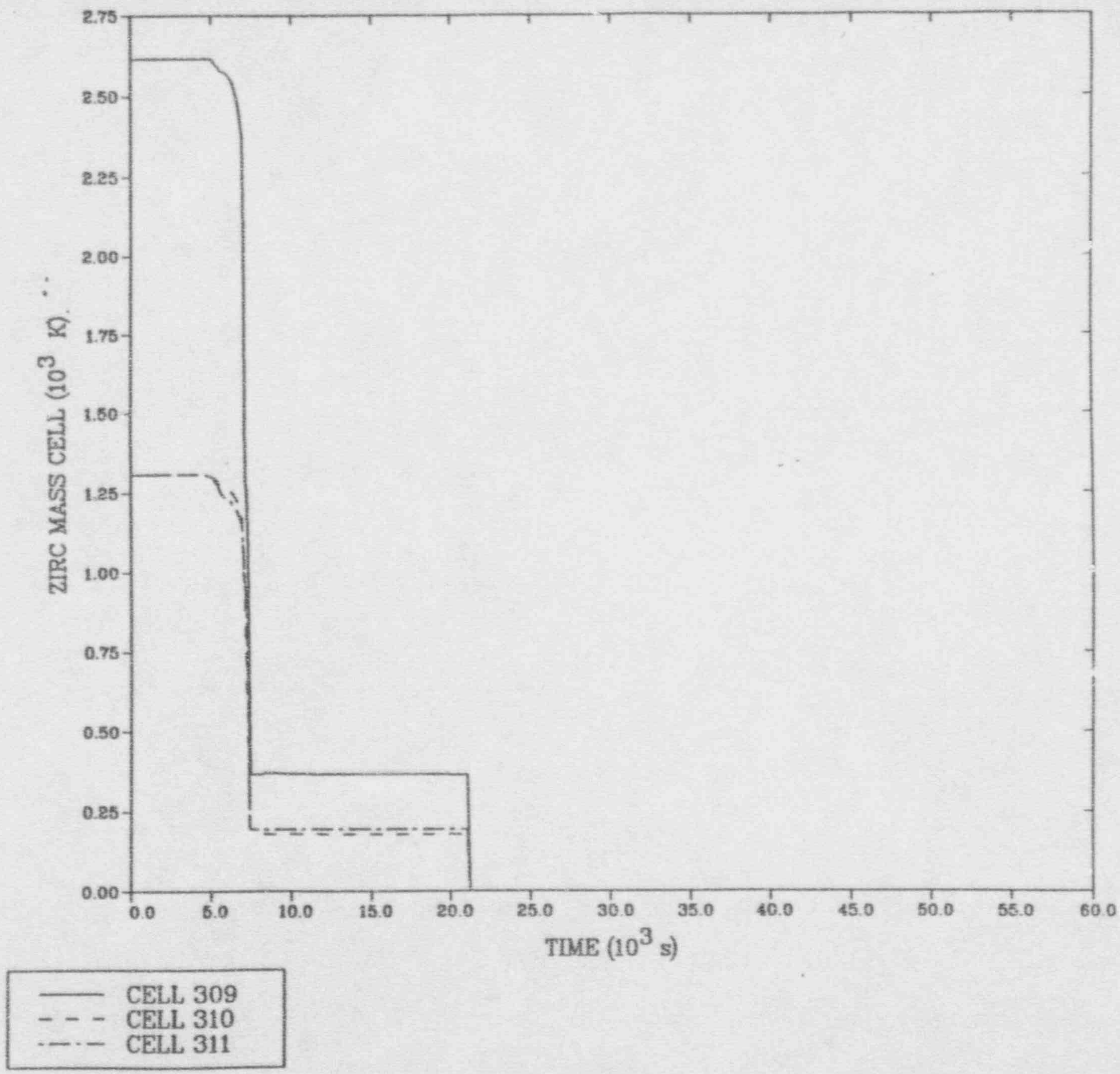
2.75
2.50
2.25
2.00
1.75
1.50
1.25
1.00
0.75
0.50
0.25
0.00
ZIRC MASS CELL (10^3 K)
0.0
5.0
10.0
15.0
20.0
25.0
30.0
35.0
40.0
45.0
50.0
55.0
60.0
TIME (10^3 s)
CELL 309
CELL 310
CELL 311

MELCOR: HIGH PRESSURE SBO

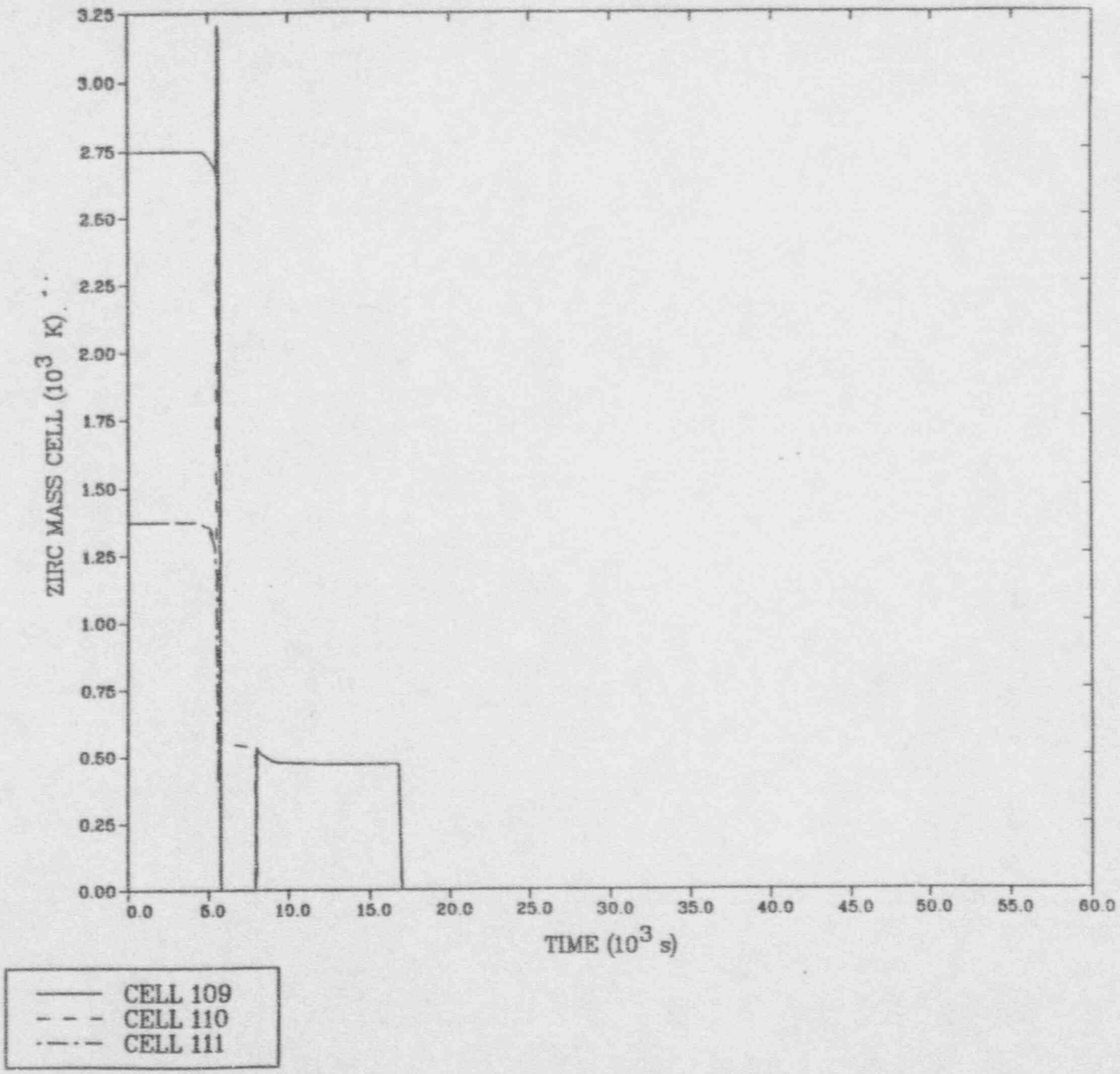

MELCOR: HIGH PRESSURE SBO (JV, 05/23/91)

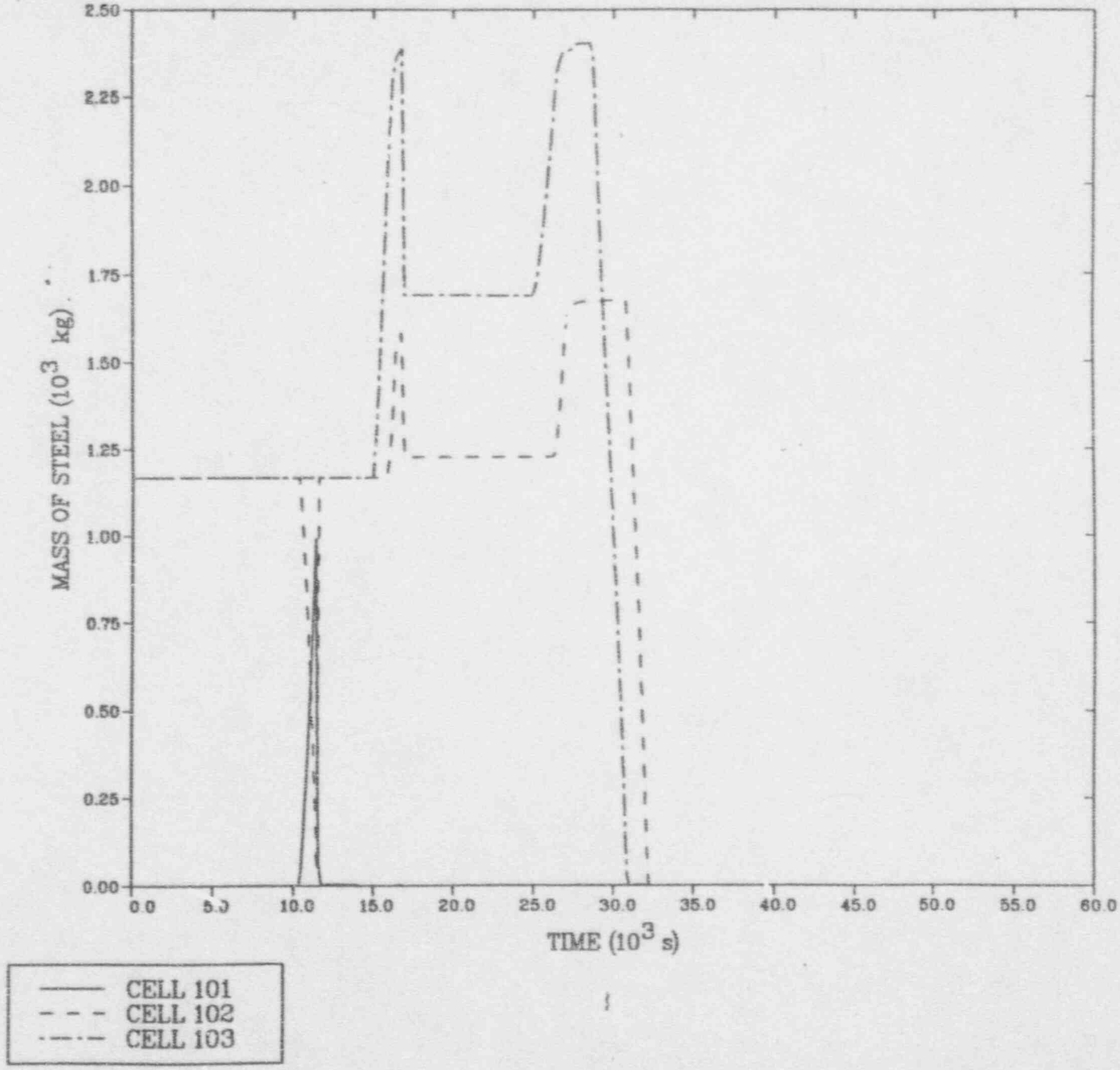

MELCOR: HIGH PRESSURE SBO (JV, 05/23/91)

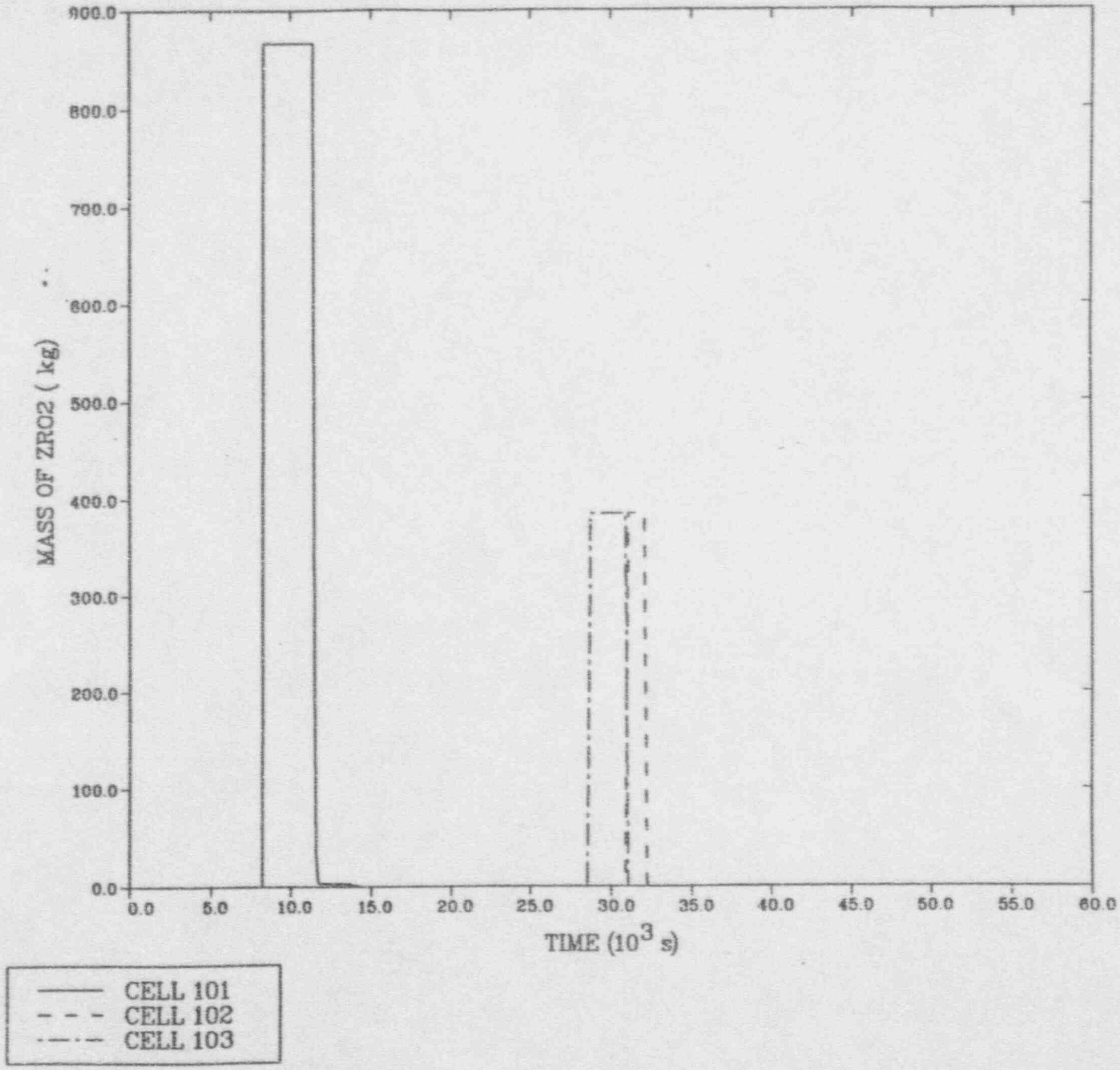

MELCOR: HIGH PRESSURE SBO (JV, 05/23/91)

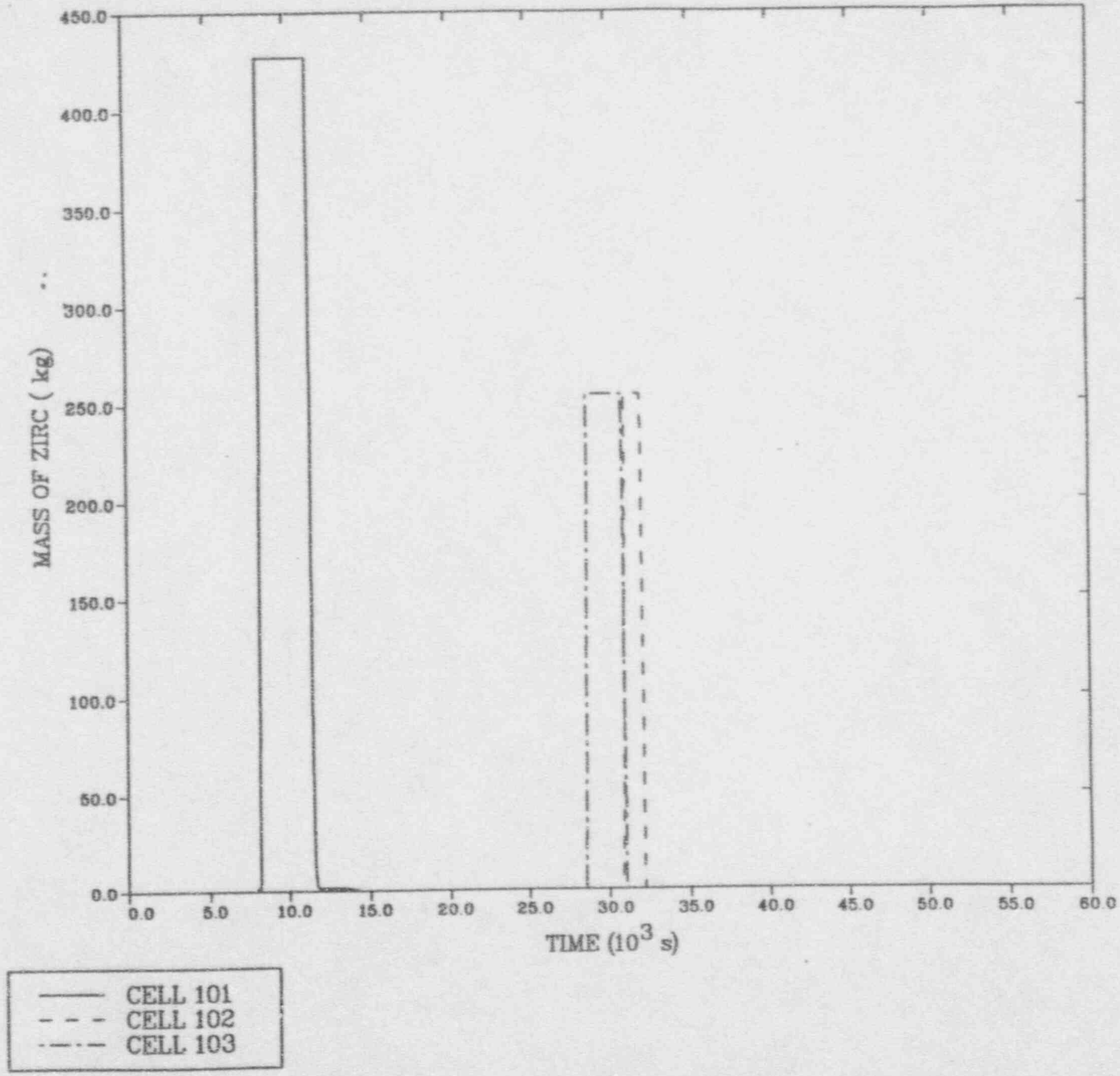

MELCOR: HIGH PRESSURE SBO (JV, 05/23/91)

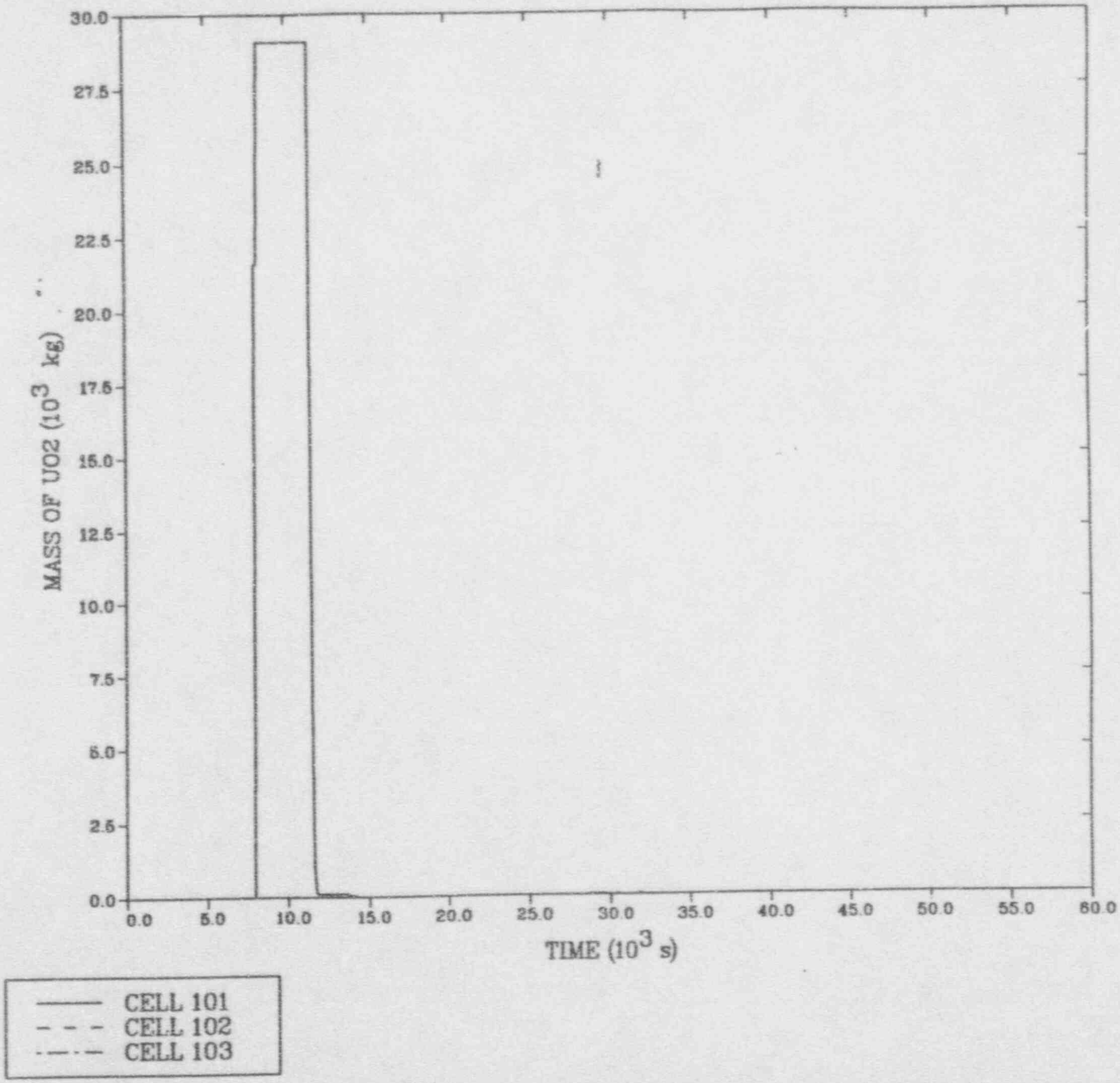

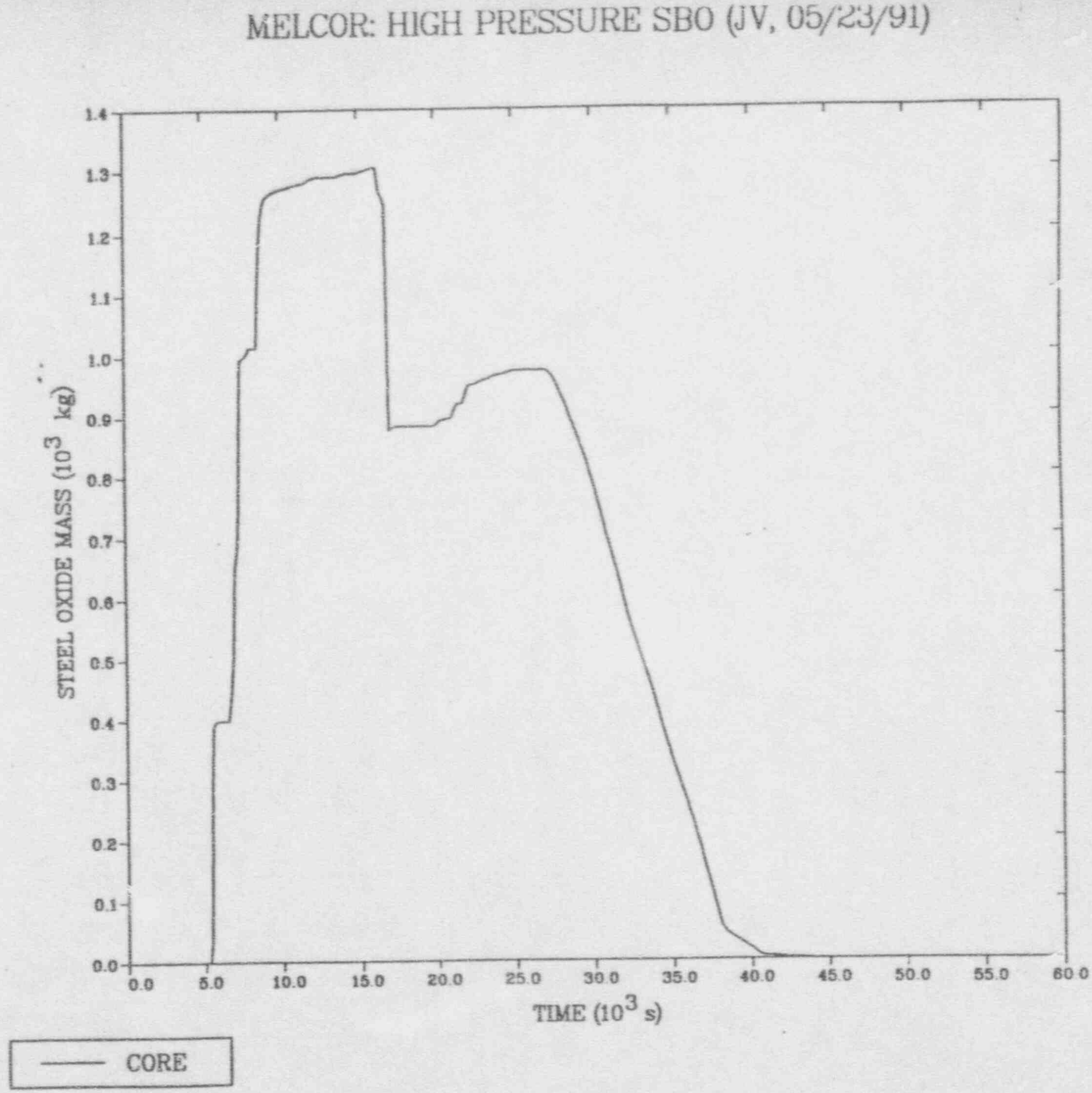

MELCOR: HIGH PRESSURE SBO (JV, 05/23/91)
STEEL OXIDE MASS (10^3 kg)
1.4
1.3
1.2
1.1
1.0
0.9
0.8
0.7
0.6
0.5
0.4
0.3
0.2
0.1
0.0
0.0
5.0
10.0
15.0
20.0
25.0
30.0
35.0
40.0
45.0
50.0
55.0
60.0
TIME (10^3 s)
CORE

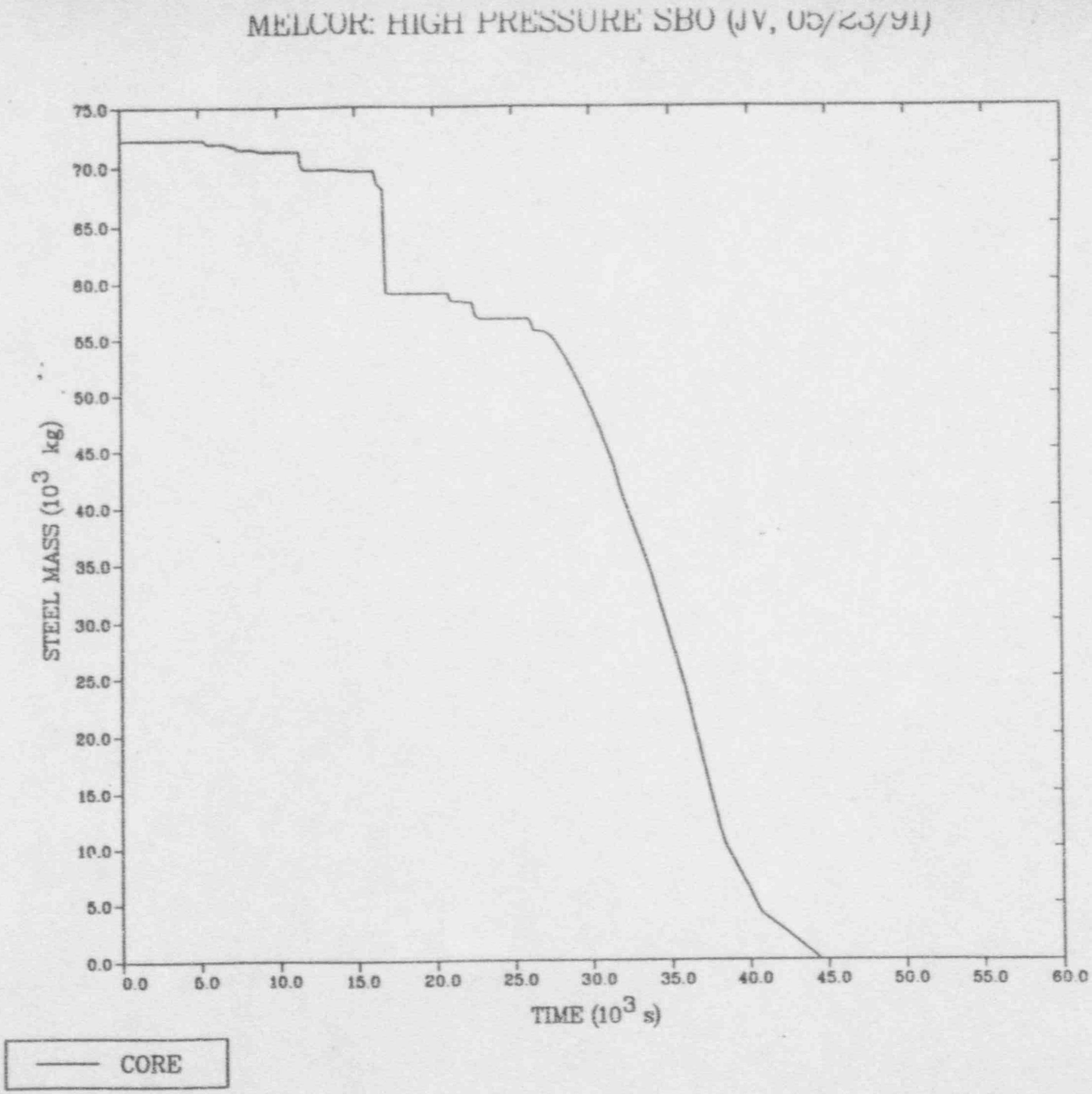
MELCOR: HIGH PRESSURE SBO (JV, 05/23/91)
STEEL MASS (10^3 kg)
75.0
70.0
65.0
60.0
55.0
50.0
45.0
40.0
35.0
30.0
25.0
20.0
15.0
10.0
5.0
0.0
0.0
5.0
10.0
15.0
20.0
25.0
30.0
35.0
40.0
45.0
50.0
55.0
60.0
TIME (10^3 s)
CORE

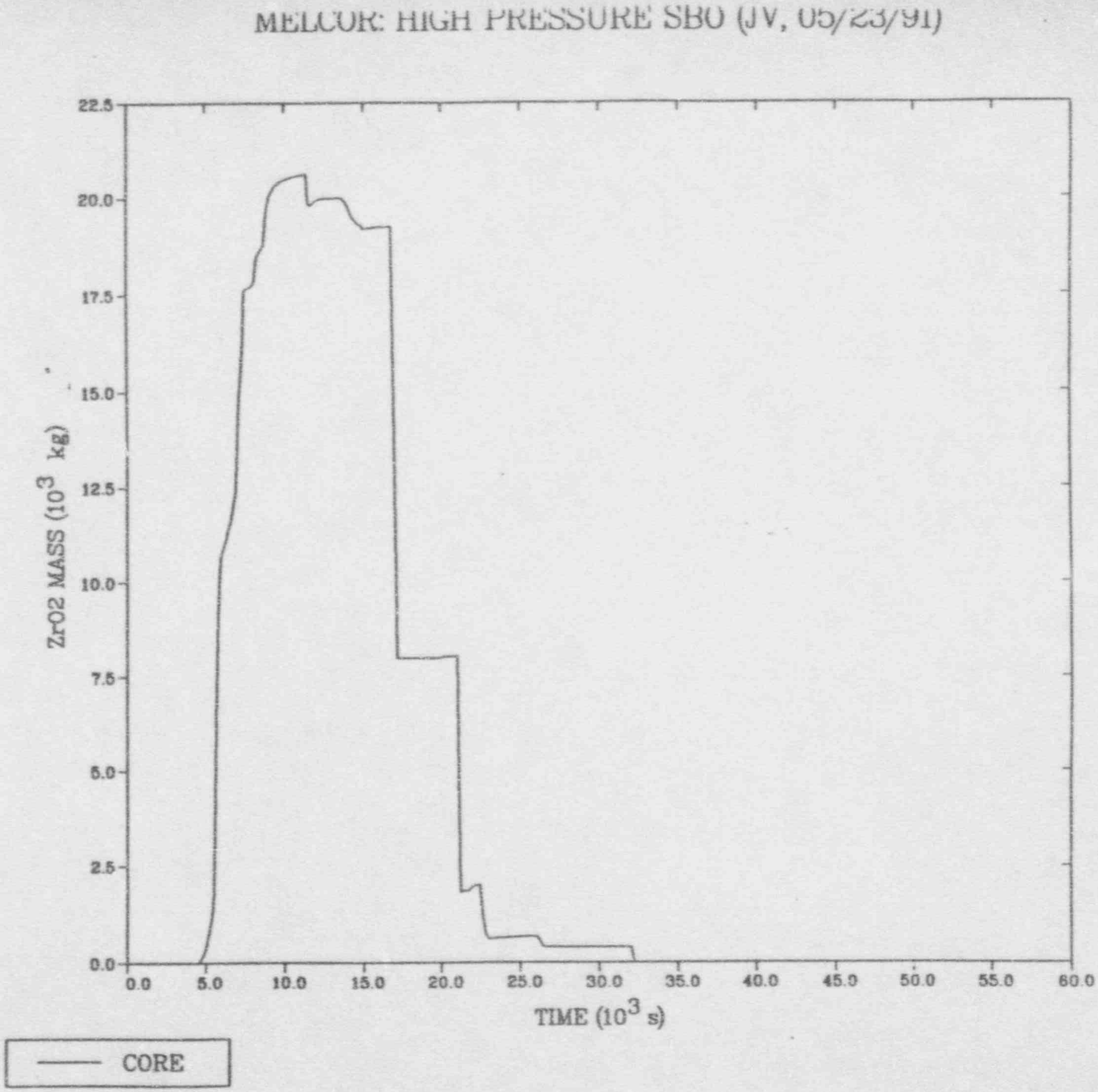
MELCOR: HIGH PRESSURE SBO (JV, 05/23/91)
ZrO2 MASS (10^3 kg)
22.5
20.0
17.5
15.0
12.5
10.0
7.5
5.0
2.5
0.0
0.0
5.0
10.0
15.0
20.0
25.0
30.0
35.0
40.0
45.0
50.0
55.0
60.0
TIME (10^3 s)
CORE

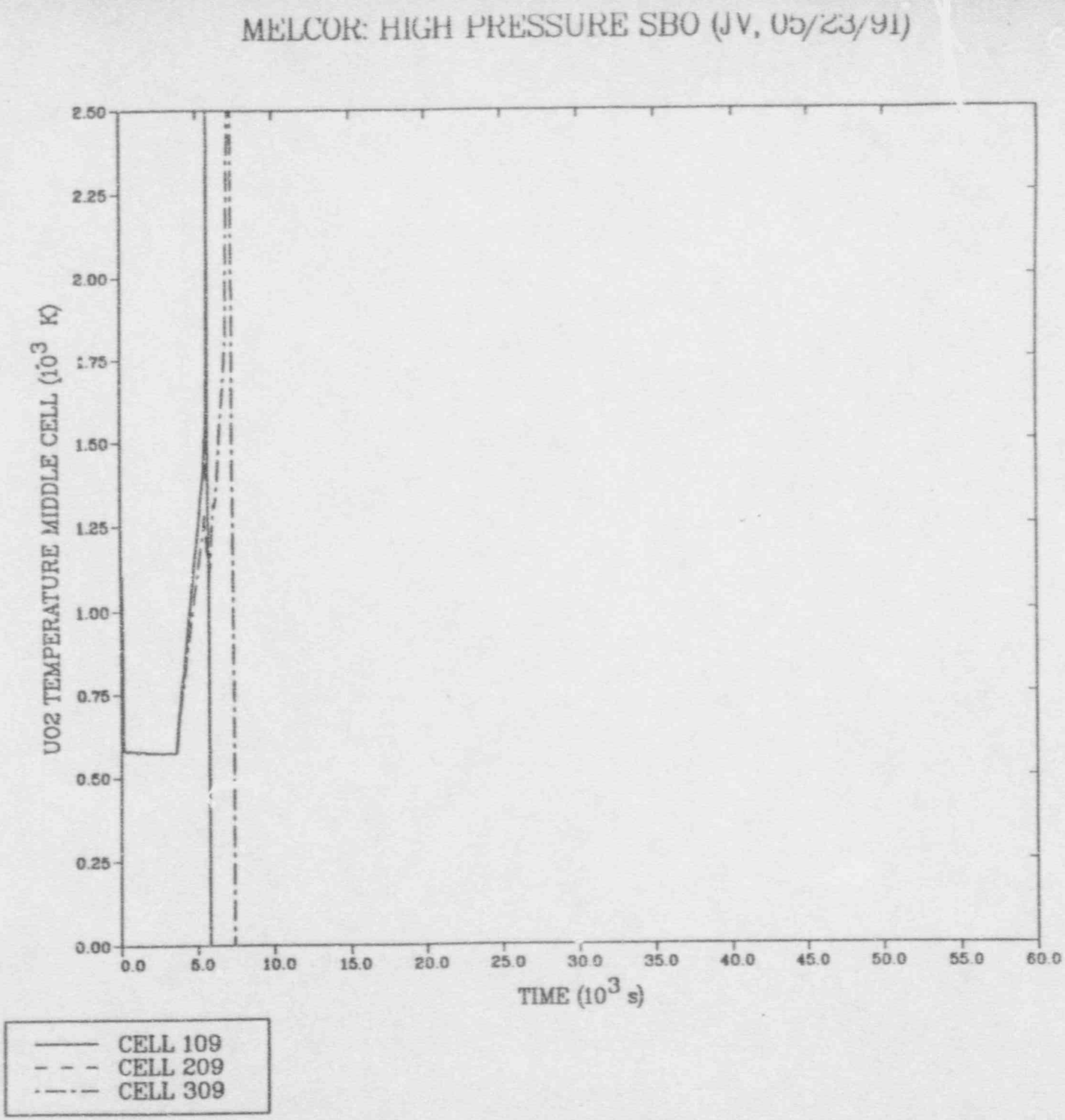

MELCOR: HIGH PRESSURE SBO (JV, 05/23/91)
UO2 TEMPERATURE MIDDLE CELL (10^3 K)
TIME (10^3 s)
0.00
0.25
0.50
0.75
1.00
1.25
1.50
1.75
2.00
2.25
2.50
0.0
5.0
10.0
15.0
20.0
25.0
30.0
35.0
40.0
45.0
50.0
55.0
60.0
CELL 109
CELL 209
CELL 309

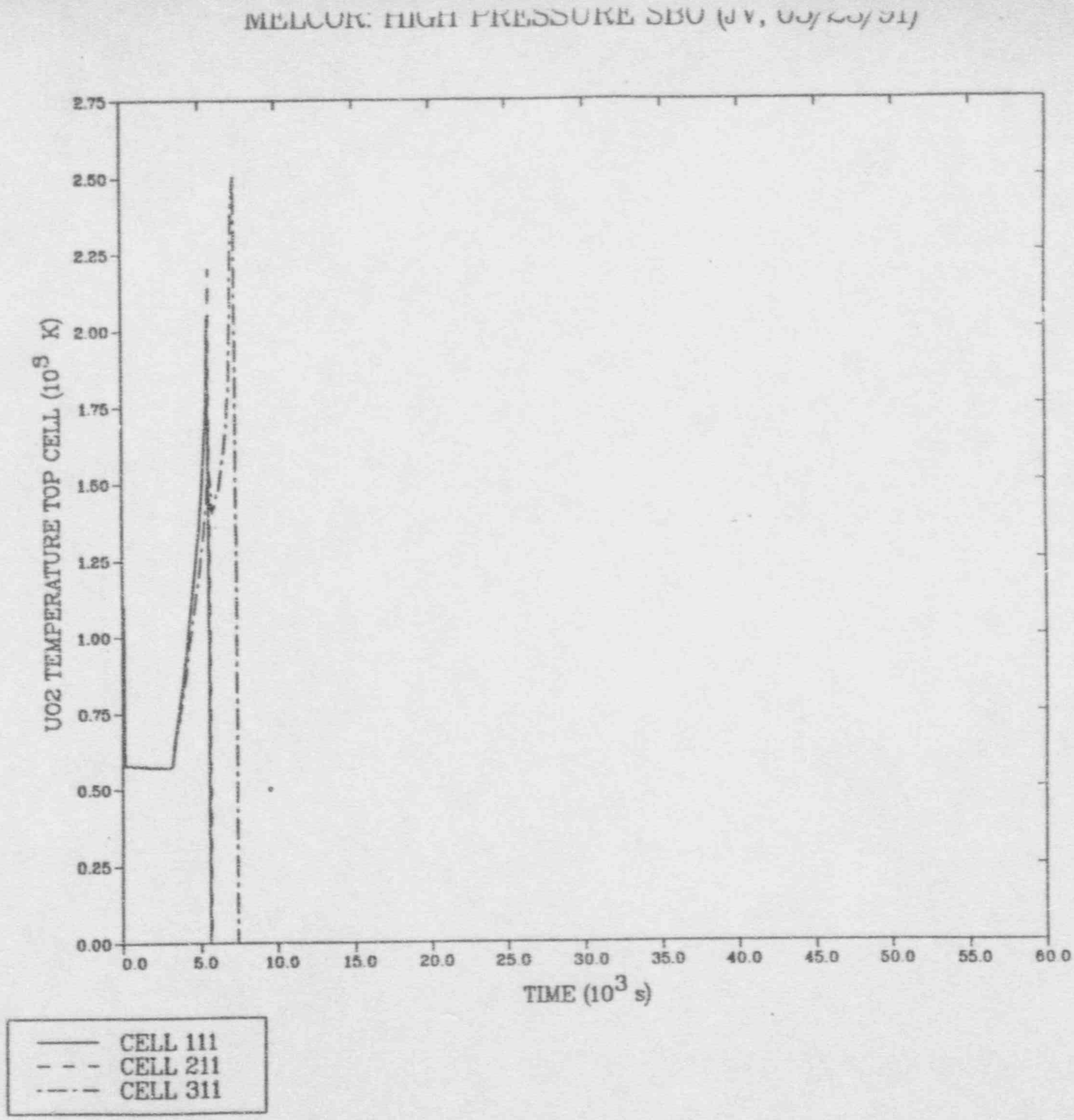
MELCOR: HIGH PRESSURE SBO (JV, 05/23/91)
UO2 TEMPERATURE TOP CELL (10^3 K)
0.00
0.25
0.50
0.75
1.00
1.25
1.50
1.75
2.00
2.25
2.50
2.75
0.0
5.0
10.0
15.0
20.0
25.0
30.0
35.0
40.0
45.0
50.0
55.0
60.0
TIME (10^3 s)
CELL 111
CELL 211
CELL 311

MELCOR: HIGH PRESSURE SBO (3V, 05/23/91)

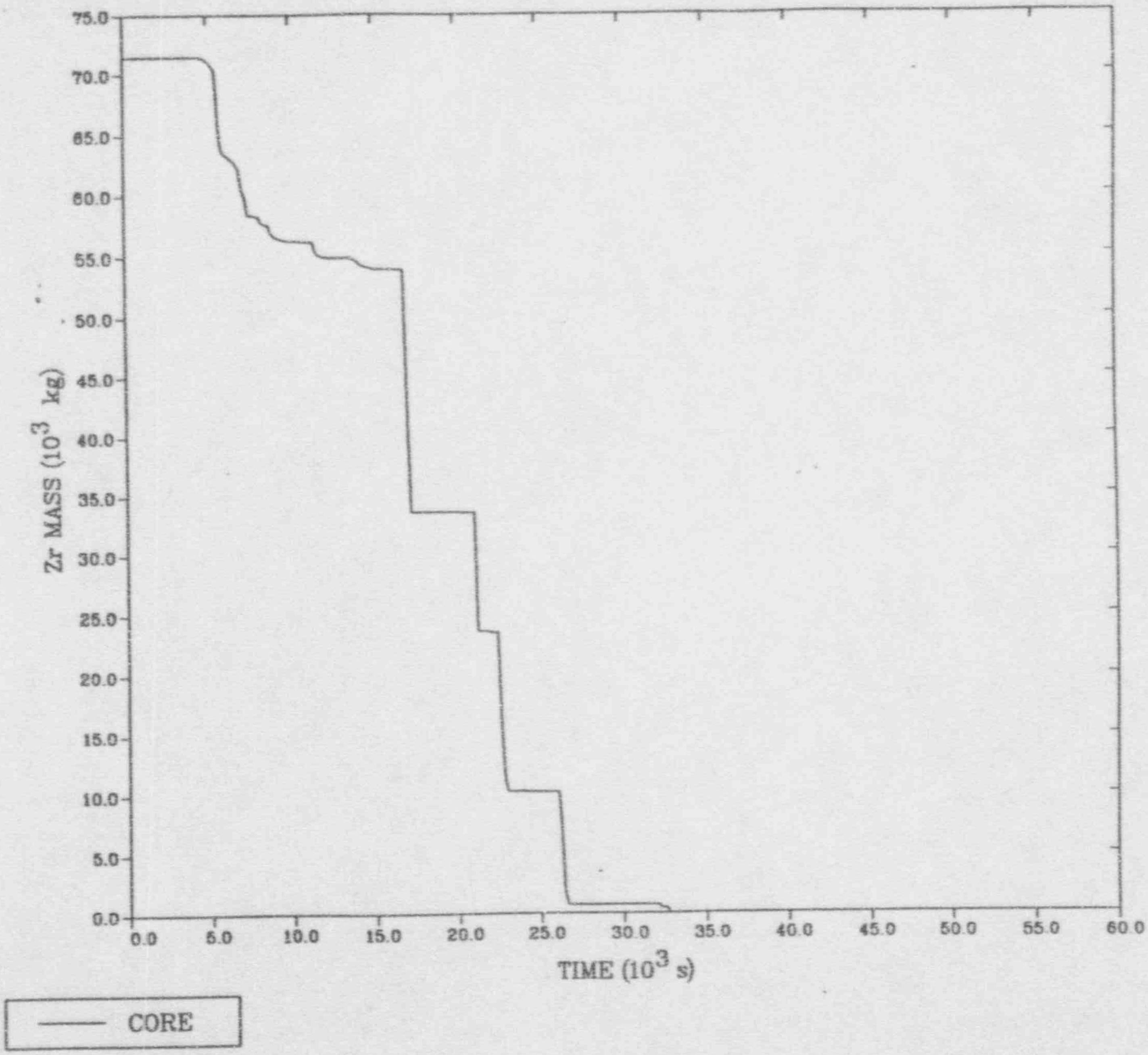

MELCOR: HIGH PRESSURE SBO (JV, 05/23/91)

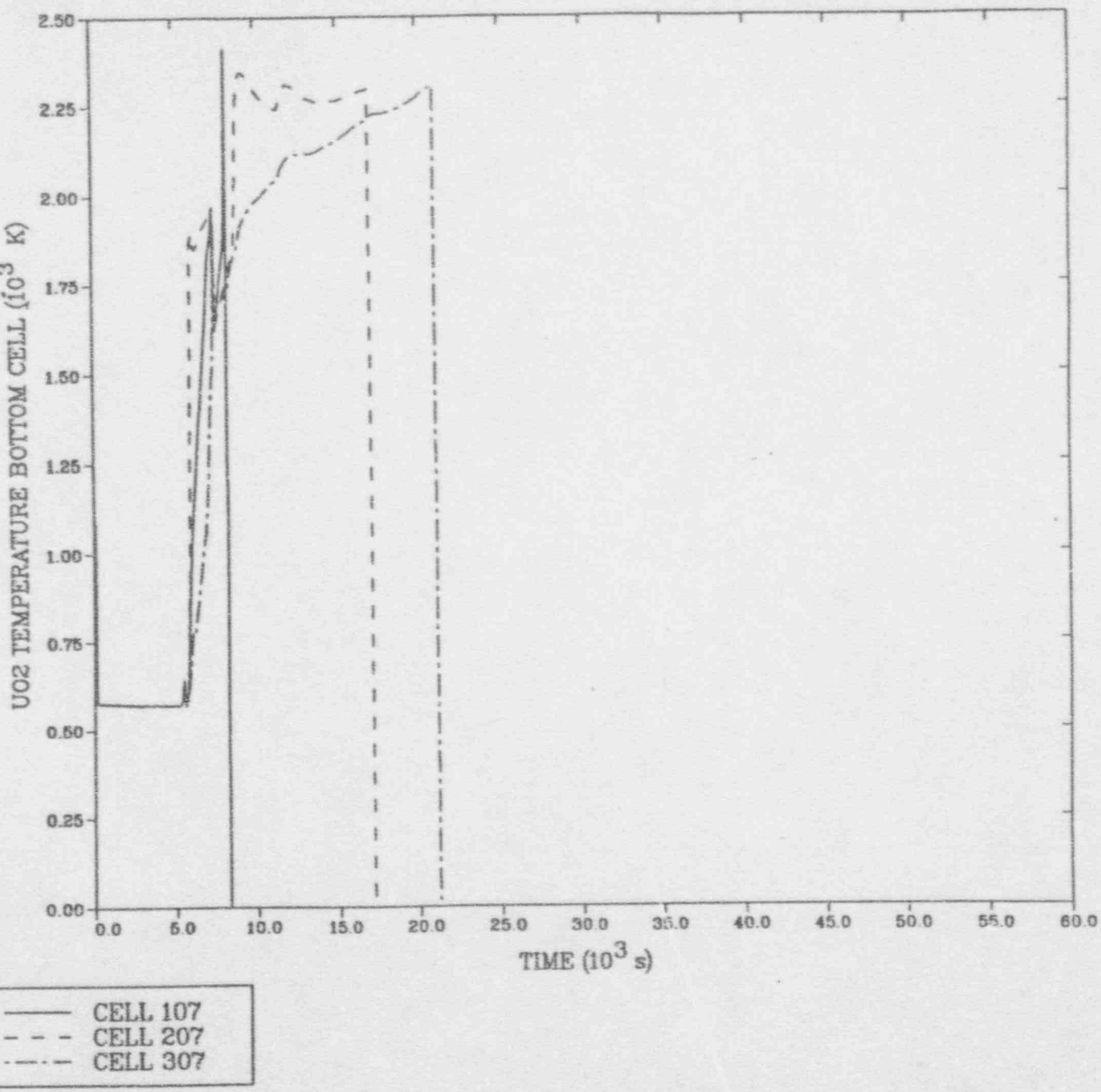

MELCOR: HIGH PRESSURE SBO (JV, 05/23/91)

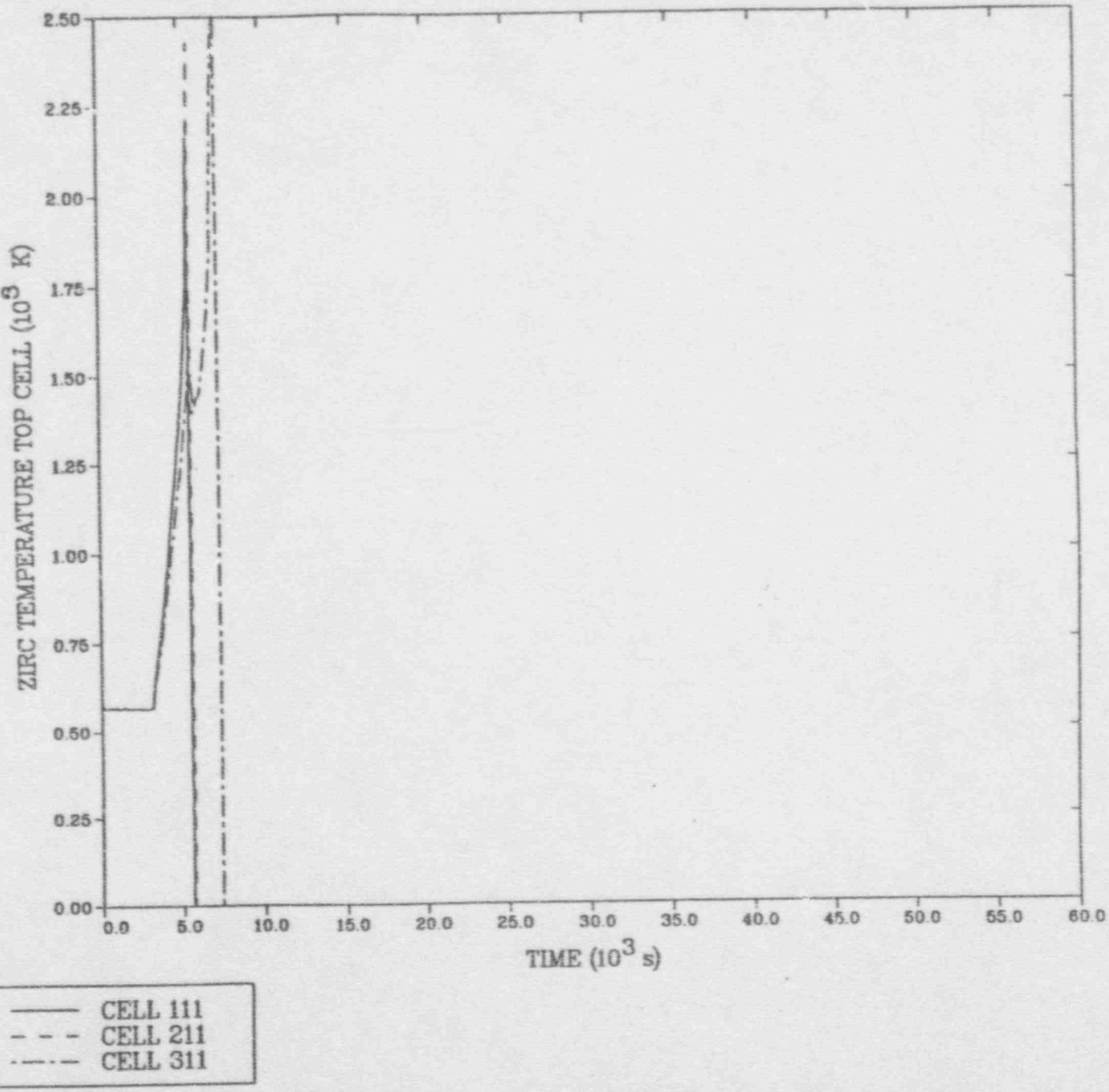

MELCOR: HIGH PRESSURE SBO (JV, 05/23/91)

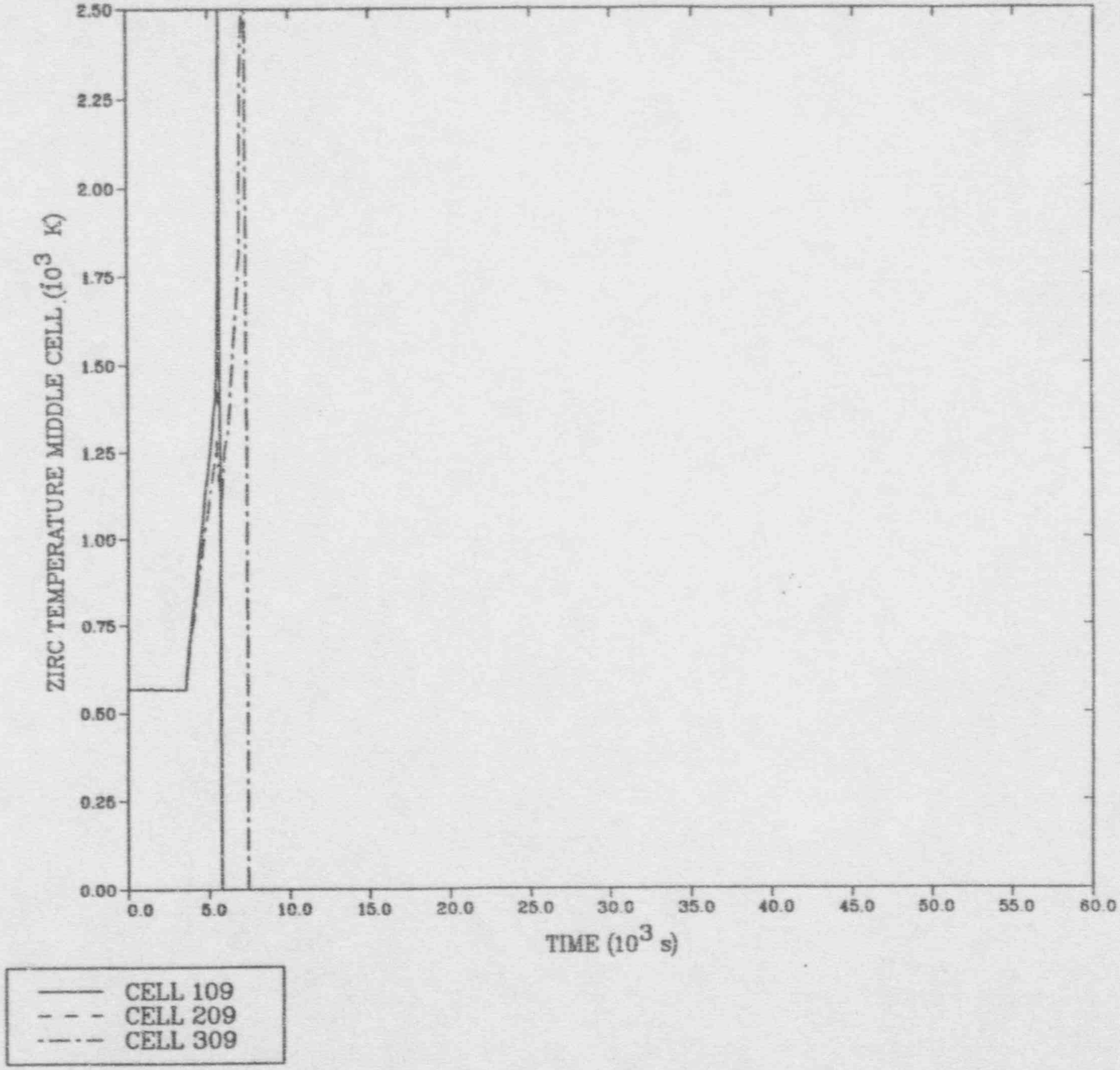

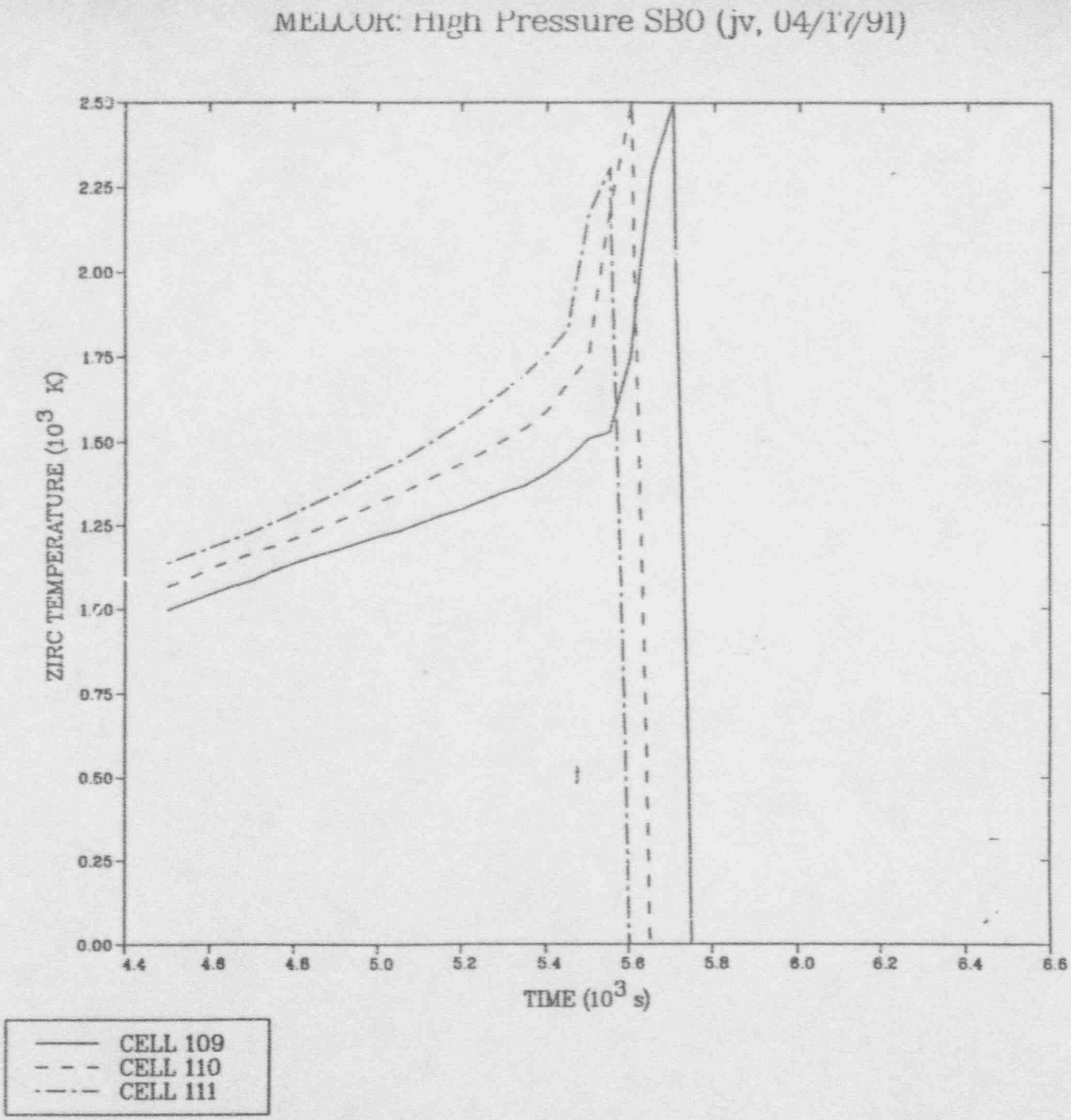
MELCOR: High Pressure SBO (jv, 04/17/91)
ZIRC TEMPERATURE (10^3 K)
TIME (10^3 s)
2.50
2.25
2.00
1.75
1.50
1.25
1.00
0.75
0.50
0.25
0.00
4.4
4.6
4.8
5.0
5.2
5.4
5.6
5.8
6.0
6.2
6.4
6.6
CELL 109
CELL 110
CELL 111

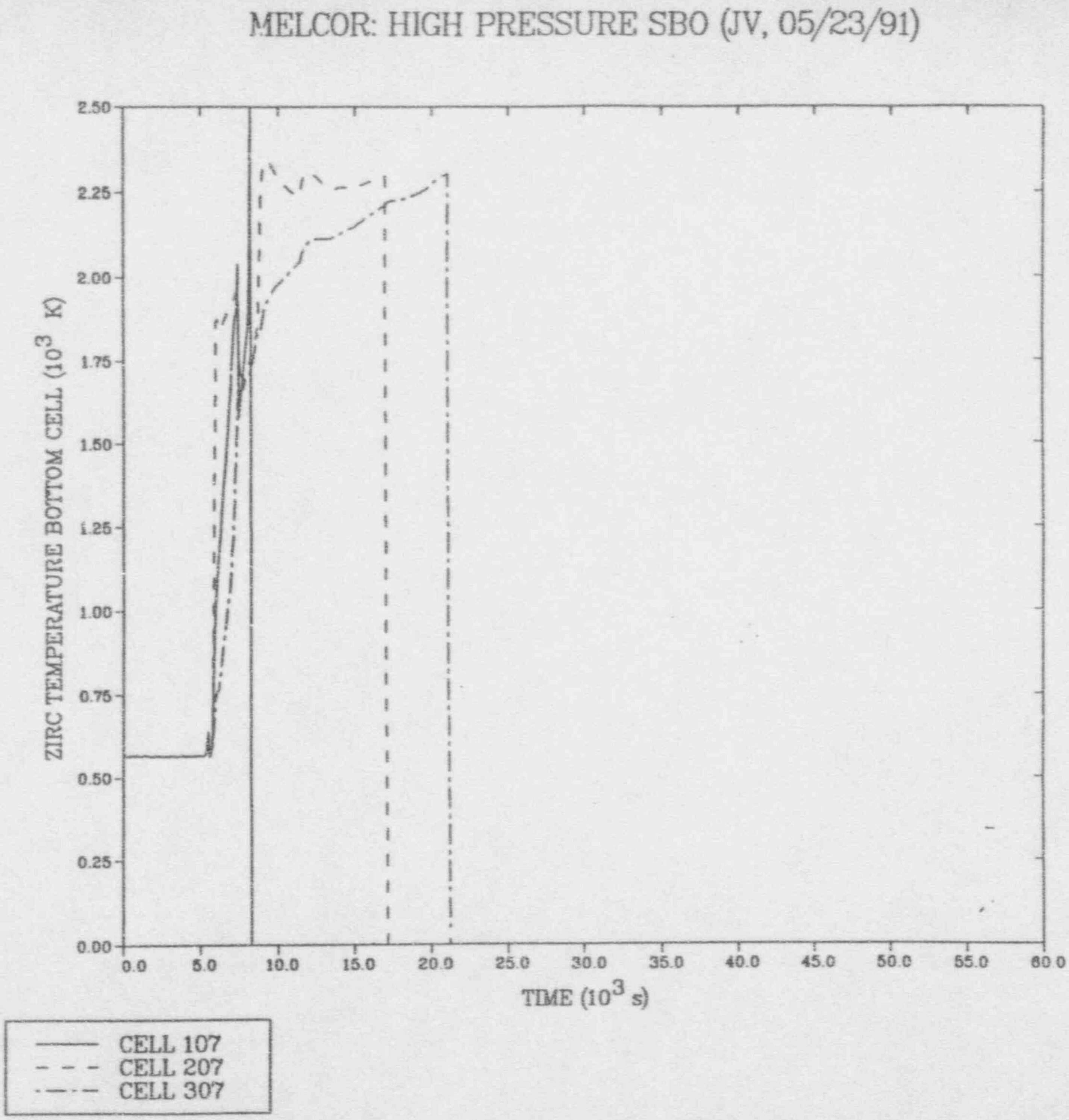
MELCOR: HIGH PRESSURE SBO (JV, 05/23/91)
ZIRC TEMPERATURE BOTTOM CELL (10^3 K)
2.50
2.25
2.00
1.75
1.50
1.25
1.00
0.75
0.50
0.25
0.00
0.0
5.0
10.0
15.0
20.0
25.0
30.0
35.0
40.0
45.0
50.0
55.0
60.0
TIME (10^3 s)
CELL 107
CELL 207
CELL 307

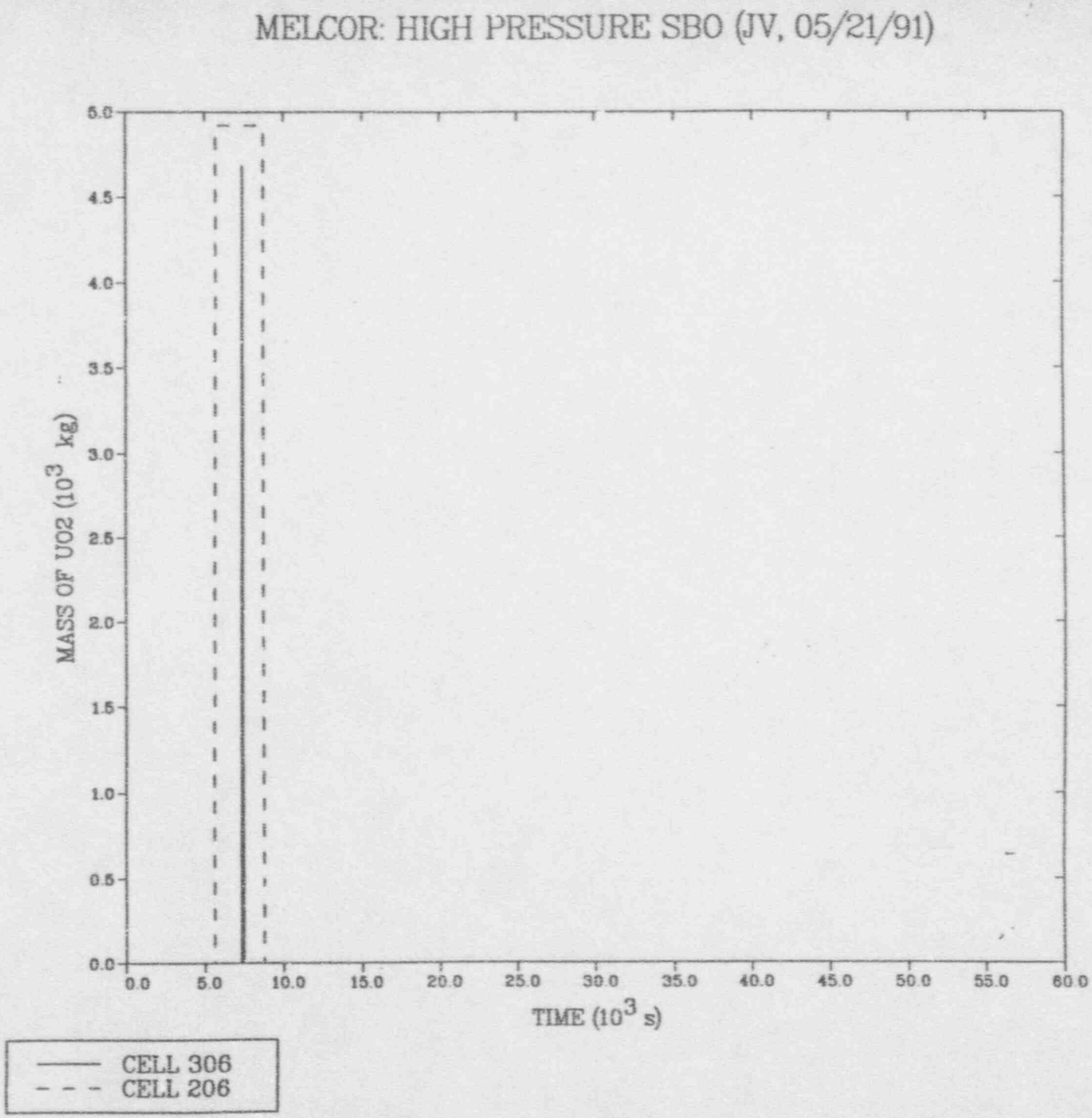
MELCOR: HIGH PRESSURE SBO (JV, 05/21/91)
MASS OF UO2 (10^3 kg)
0.0
0.5
1.0
1.5
2.0
2.5
3.0
3.5
4.0
4.5
5.0
0.0
5.0
10.0
15.0
20.0
25.0
30.0
35.0
40.0
45.0
50.0
55.0
60.0
TIME (10^3 s)
CELL 306
CELL 206

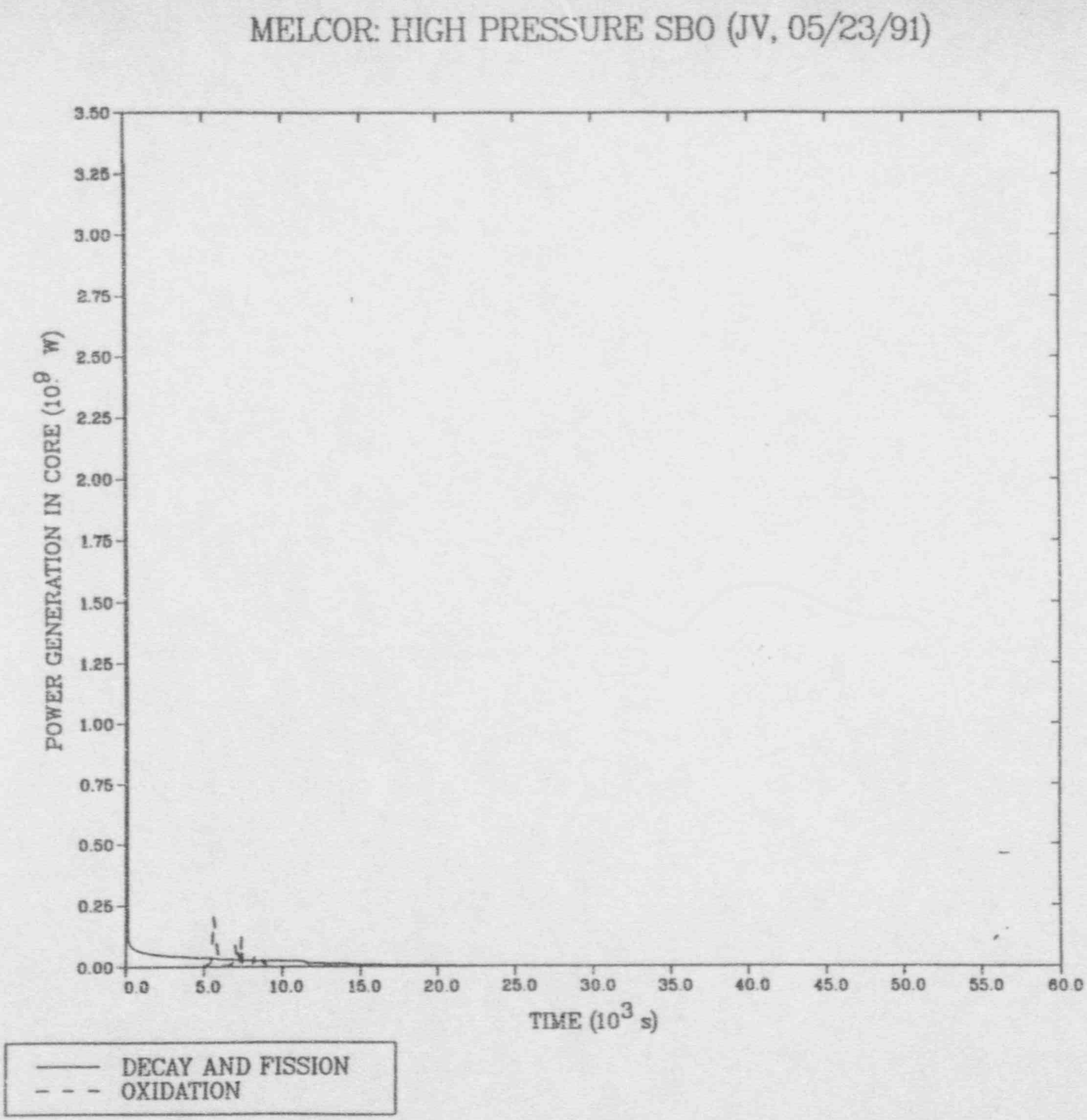

MELCOR: HIGH PRESSURE SBO (JV, 05/23/91)
POWER GENERATION IN CORE (10^9 W)
3.50
3.25
3.00
2.75
2.50
2.25
2.00
1.75
1.50
1.25
1.00
0.75
0.50
0.25
0.00
0.0
5.0
10.0
15.0
20.0
25.0
30.0
35.0
40.0
45.0
50.0
55.0
60.0
TIME (10^3 s)
DECAY AND FISSION
OXIDATION

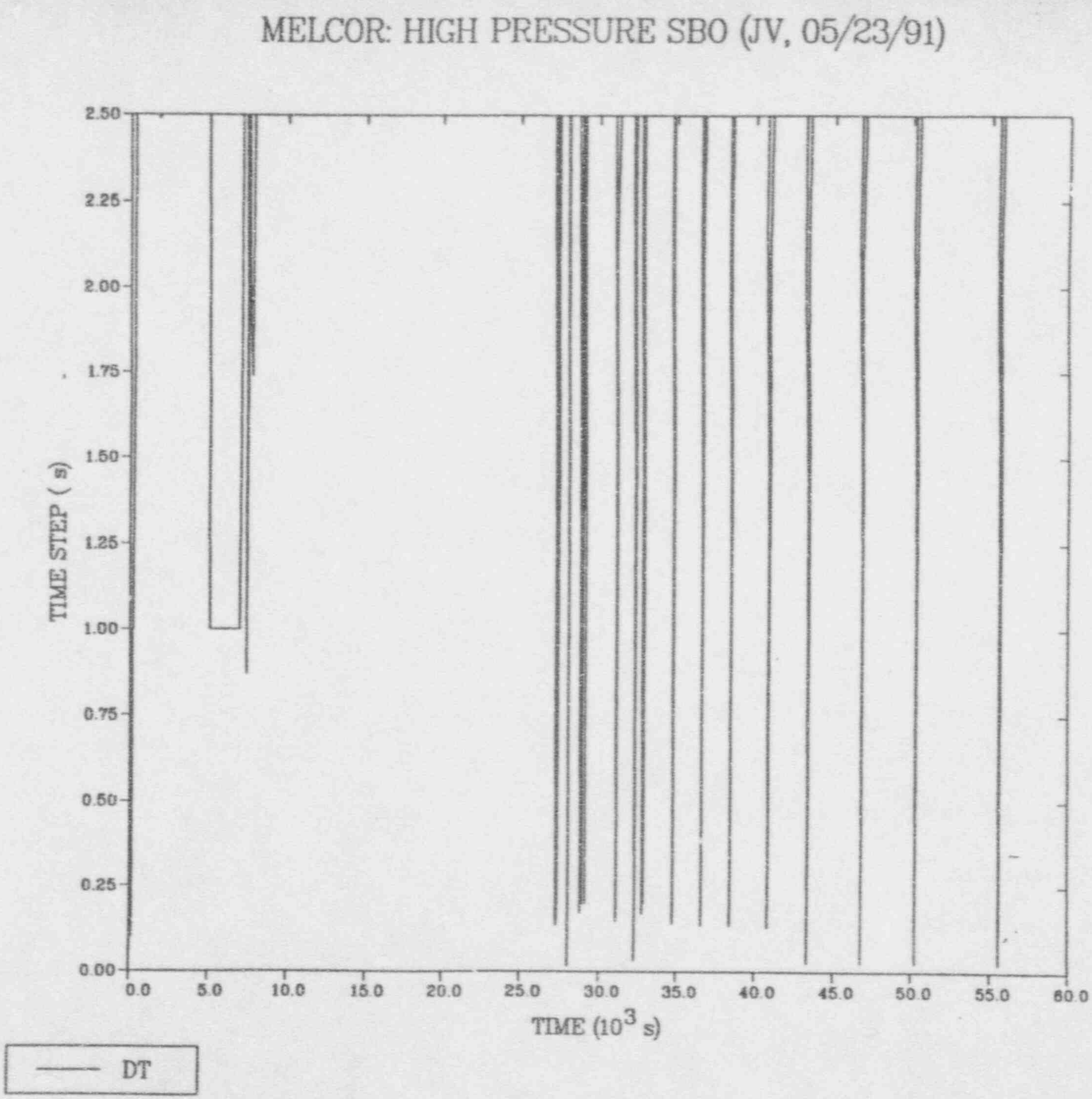
MELCOR: HIGH PRESSURE SBO (JV, 05/23/91)
2.50
2.25
2.00
1.75
1.50
1.25
1.00
0.75
0.50
0.25
0.00
TIME STEP (s)
0.0
5.0
10.0
15.0
20.0
25.0
30.0
35.0
40.0
45.0
50.0
55.0
60.0
TIME (10^3 s)
DT

MELCOR: HIGH PRESSURE SBO (JV, 05/23/91)

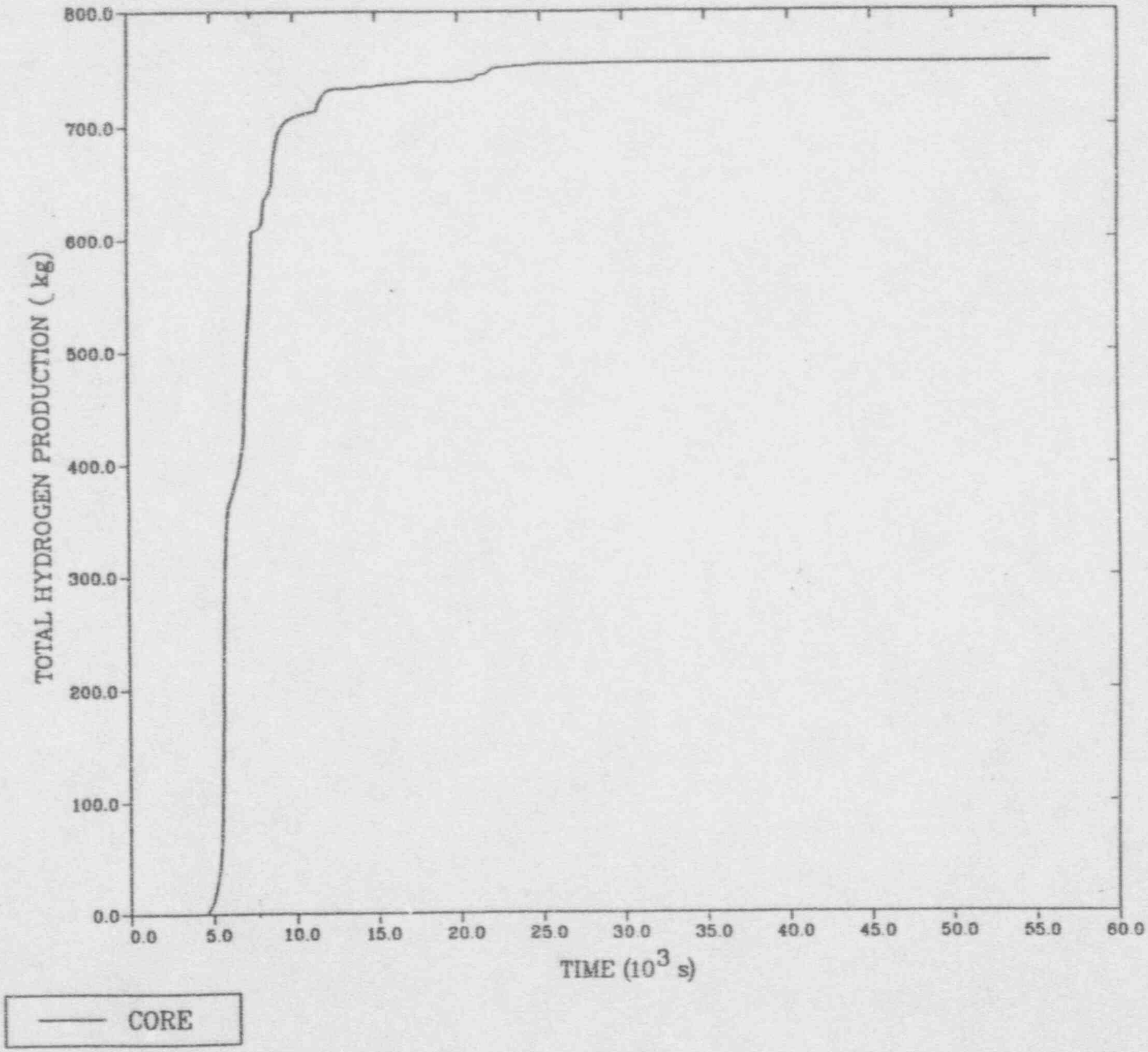

MELCOR: HIGH PRESSURE SBO (JV, 05/23/91)

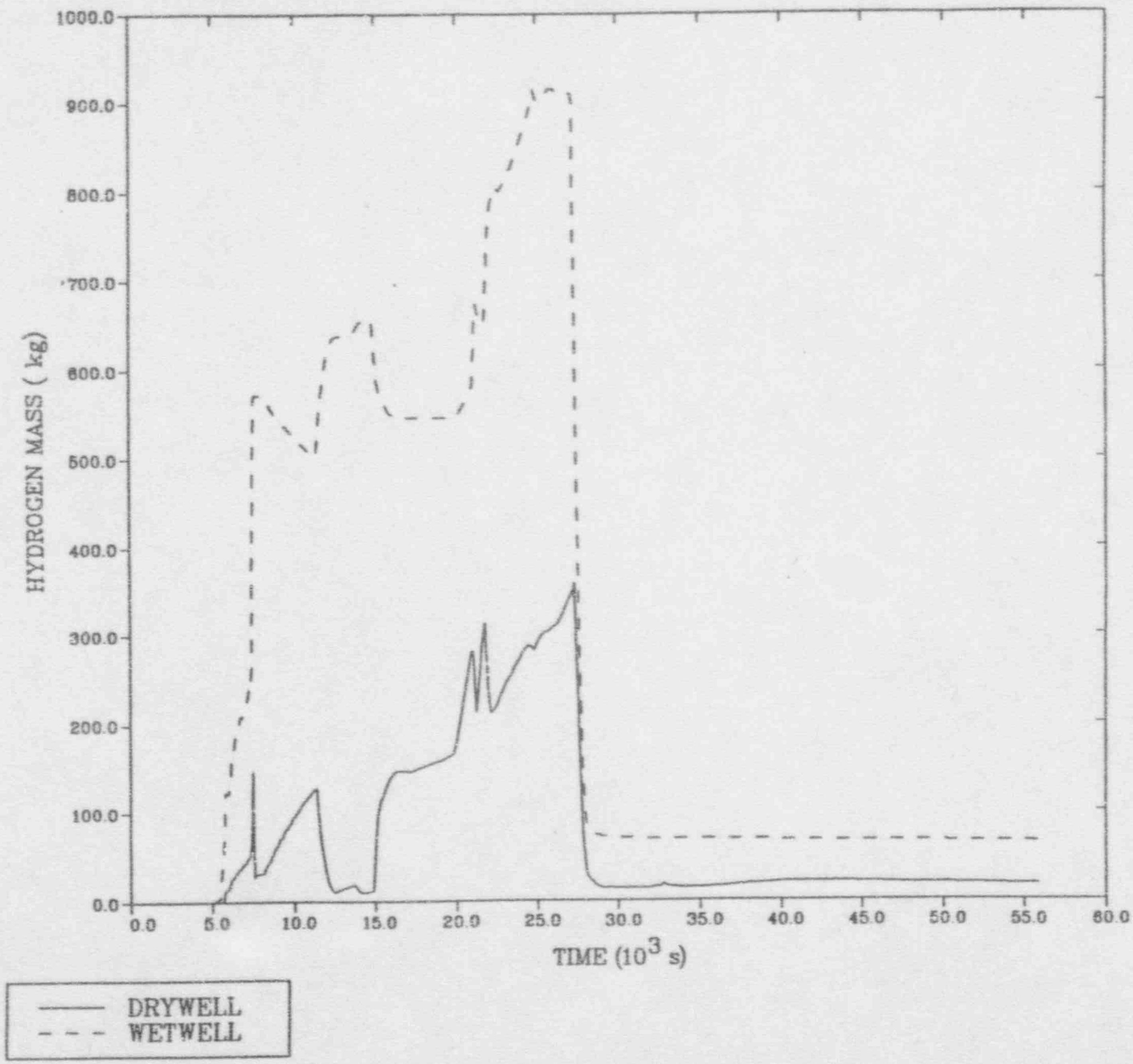

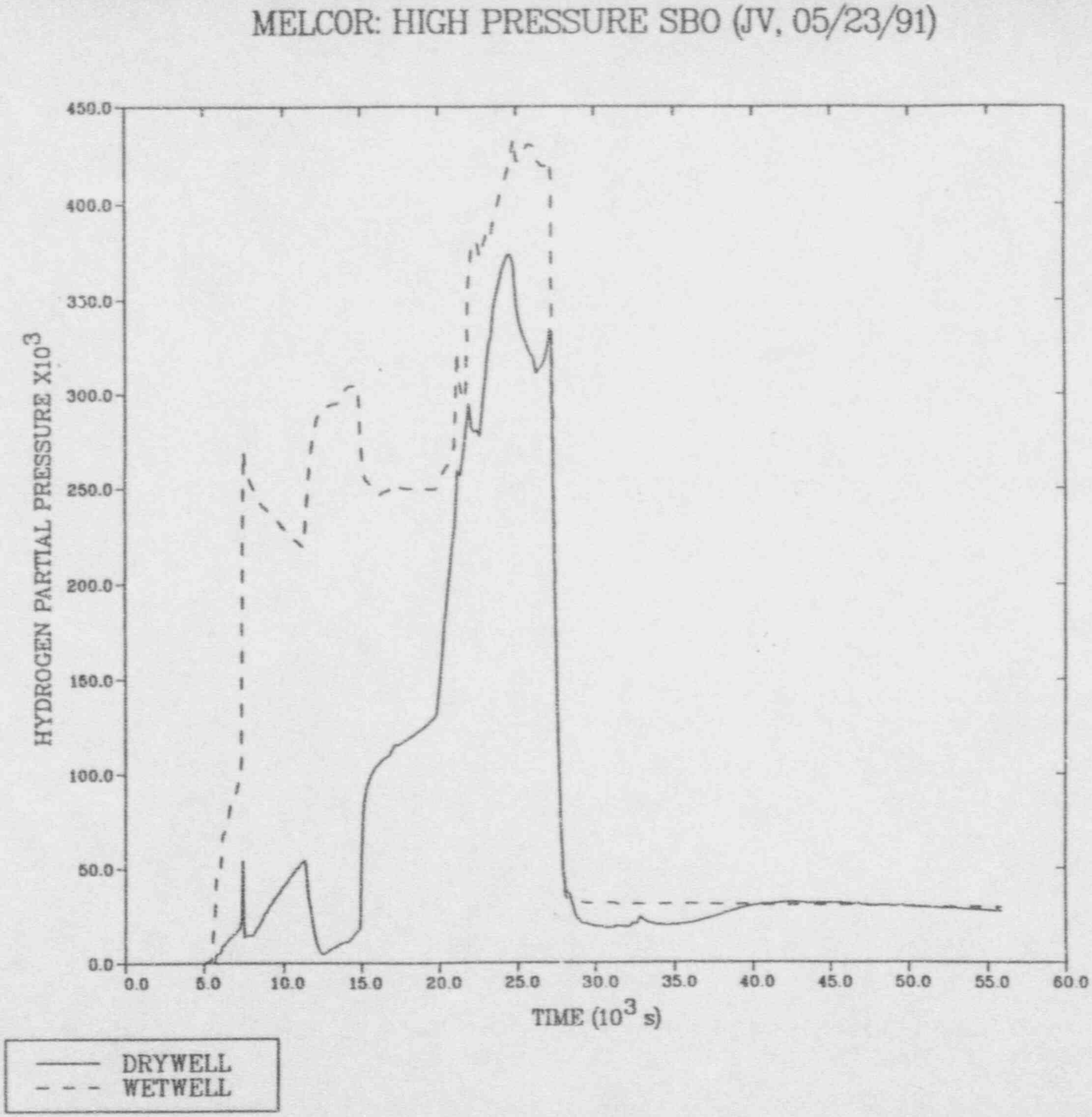

MELCOR: HIGH PRESSURE SBO (JV, 05/23/91)
HYDROGEN PARTIAL PRESSURE X10^3
TIME (10^3 s)
0.0
50.0
100.0
150.0
200.0
250.0
300.0
350.0
400.0
450.0
5.0
10.0
15.0
20.0
25.0
30.0
35.0
40.0
45.0
50.0
55.0
60.0
DRYWELL
WETWELL

MELCOR: HIGH PRESSURE SBO (JV, 05/23/91)

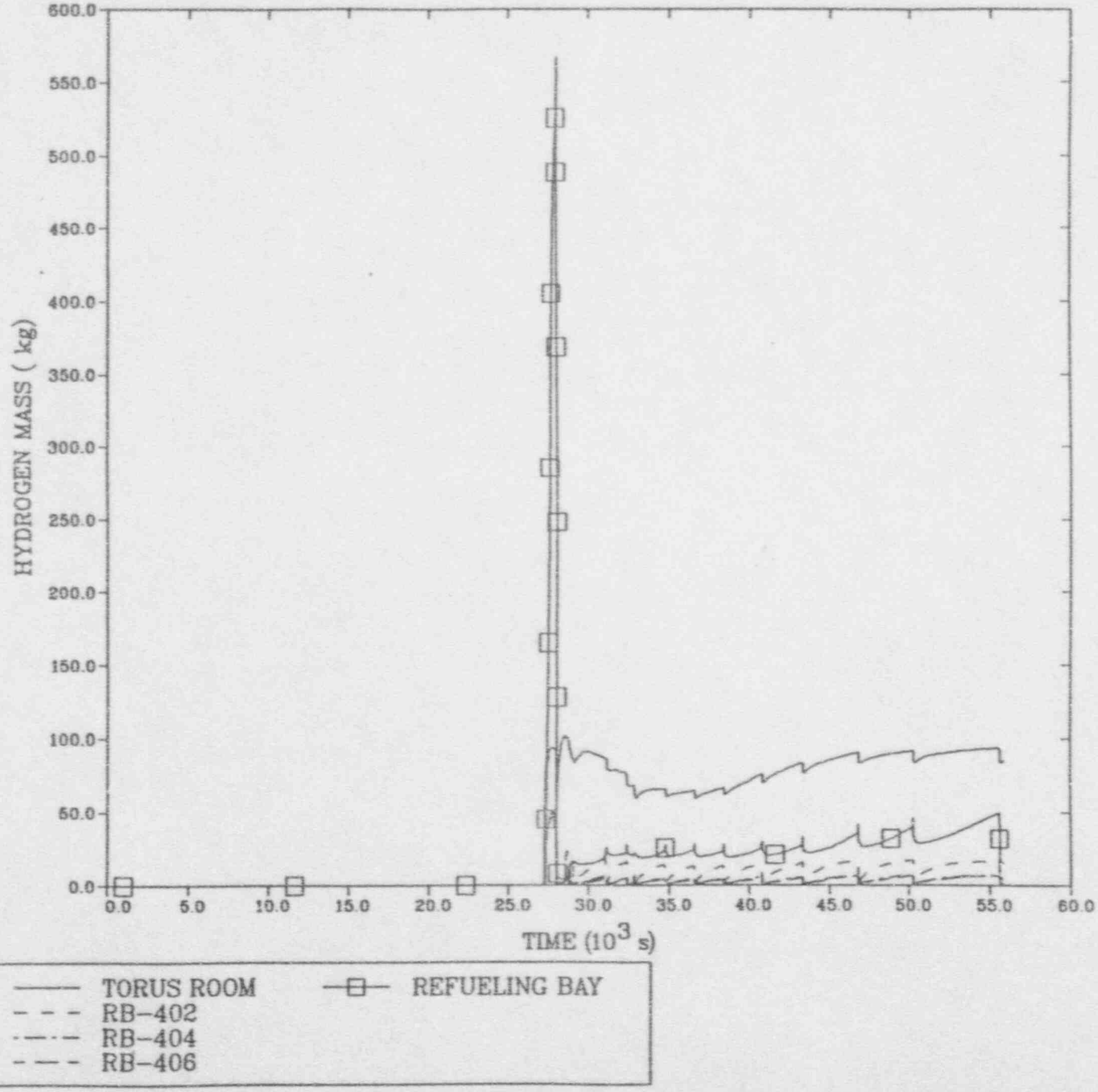

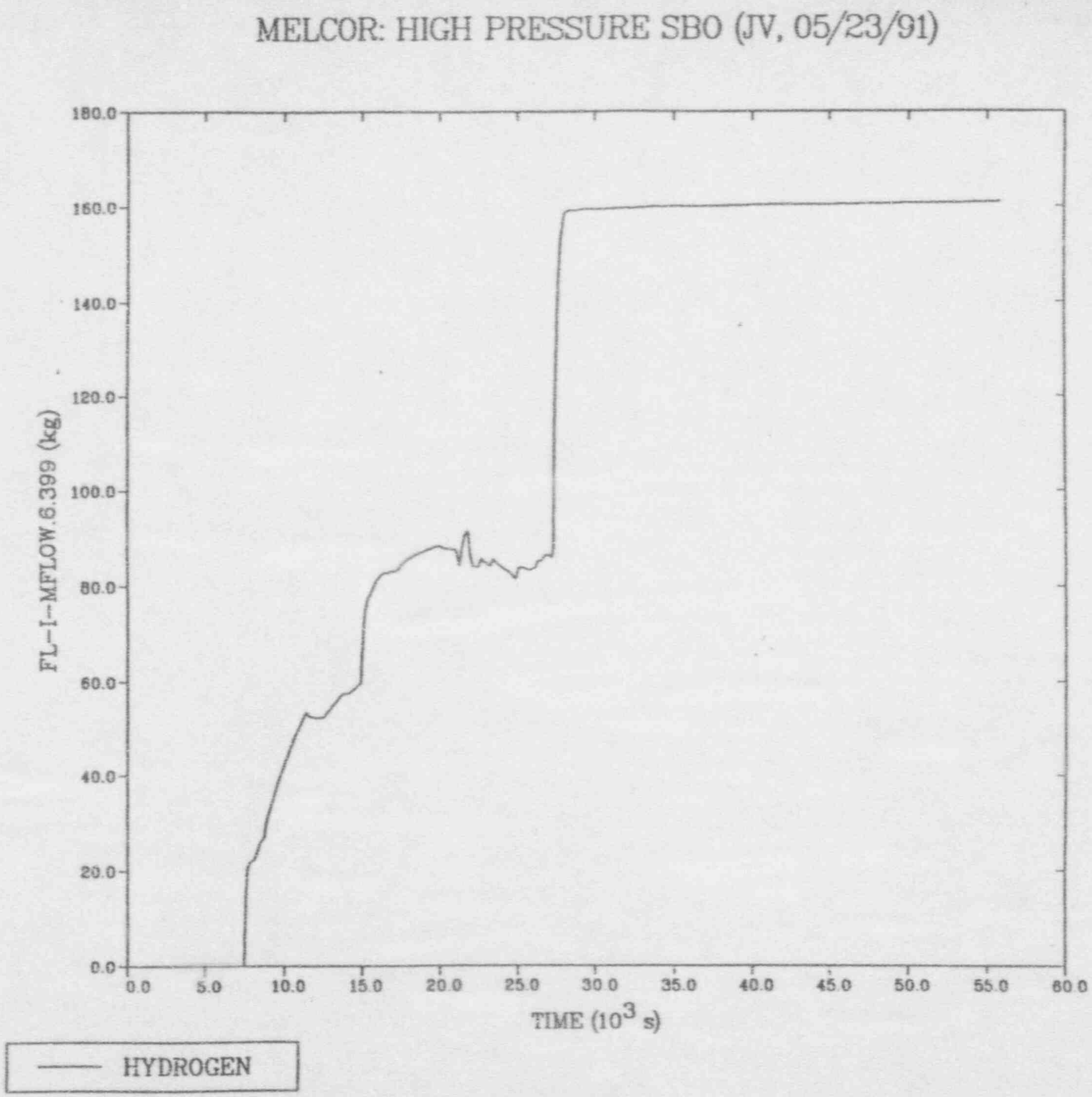
MELCOR: HIGH PRESSURE SBO (JV, 05/23/91)
FL-I--MFLOW.6.399 (kg)
0.0
20.0
40.0
60.0
80.0
100.0
120.0
140.0
160.0
180.0
0.0
5.0
10.0
15.0
20.0
25.0
30.0
35.0
40.0
45.0
50.0
55.0
60.0
TIME (10^3 s)
HYDROGEN

MELCOR: HIGH PRESSURE SBO (JV, 05/23/91)

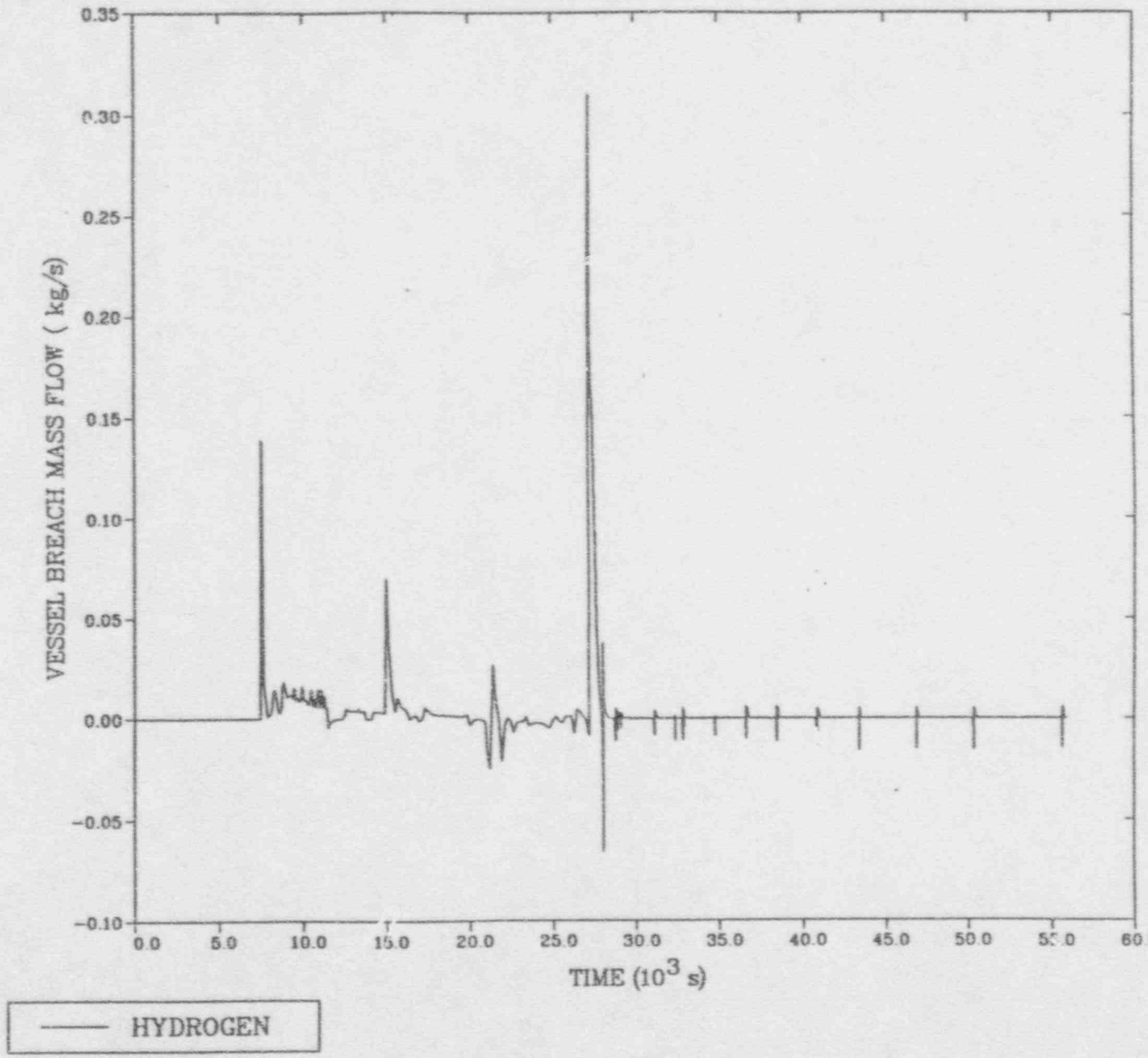

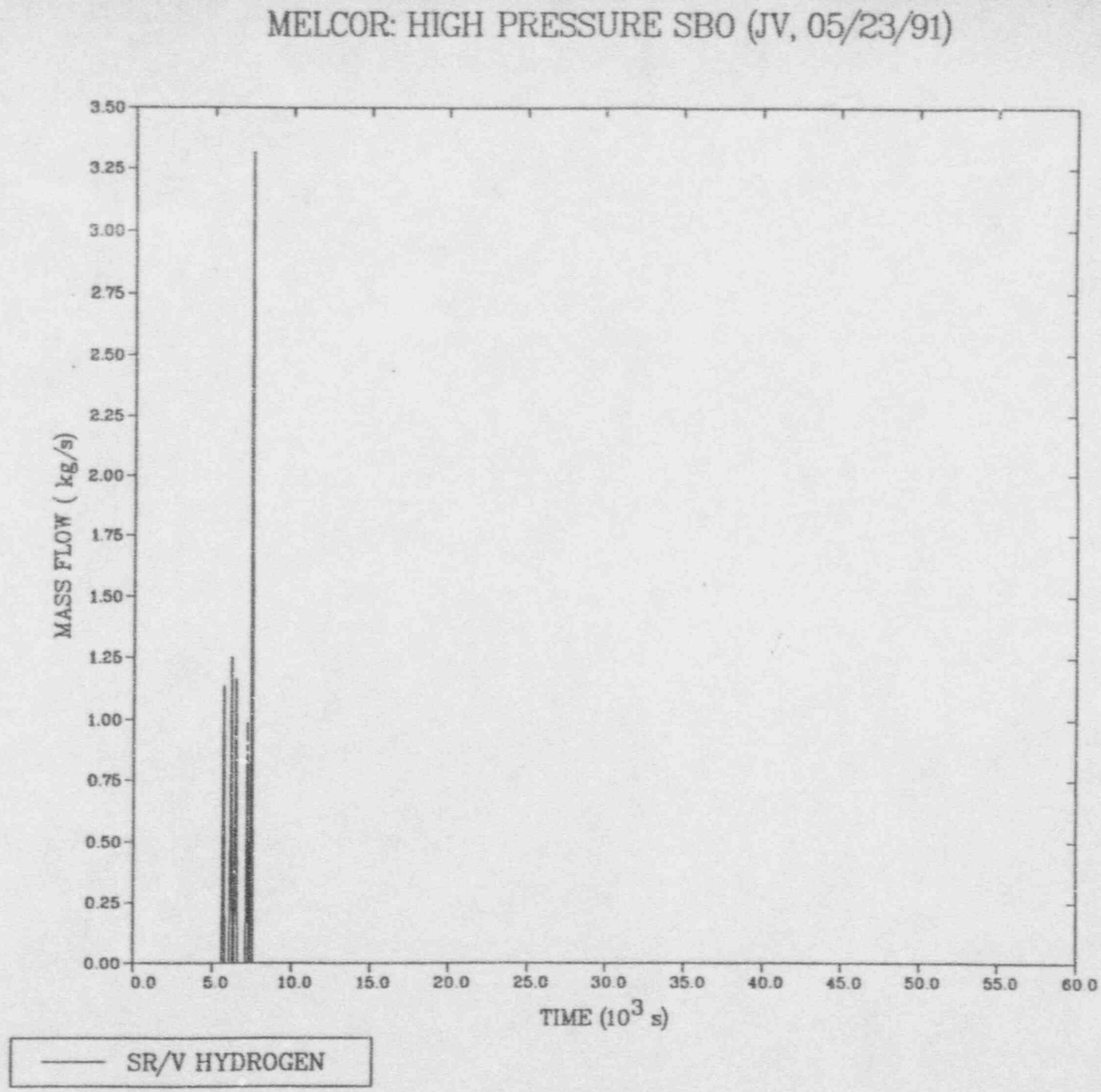
MELCOR: HIGH PRESSURE SBO (JV, 05/23/91)
MASS FLOW (kg/s)
3.50
3.25
3.00
2.75
2.50
2.25
2.00
1.75
1.50
1.25
1.00
0.75
0.50
0.25
0.00
0.0
5.0
10.0
15.0
20.0
25.0
30.0
35.0
40.0
45.0
50.0
55.0
60.0
TIME (10^3 s)
SR/V HYDROGEN

MELCOR: HIGH PRESSURE SBO (JV, 05/23/91)

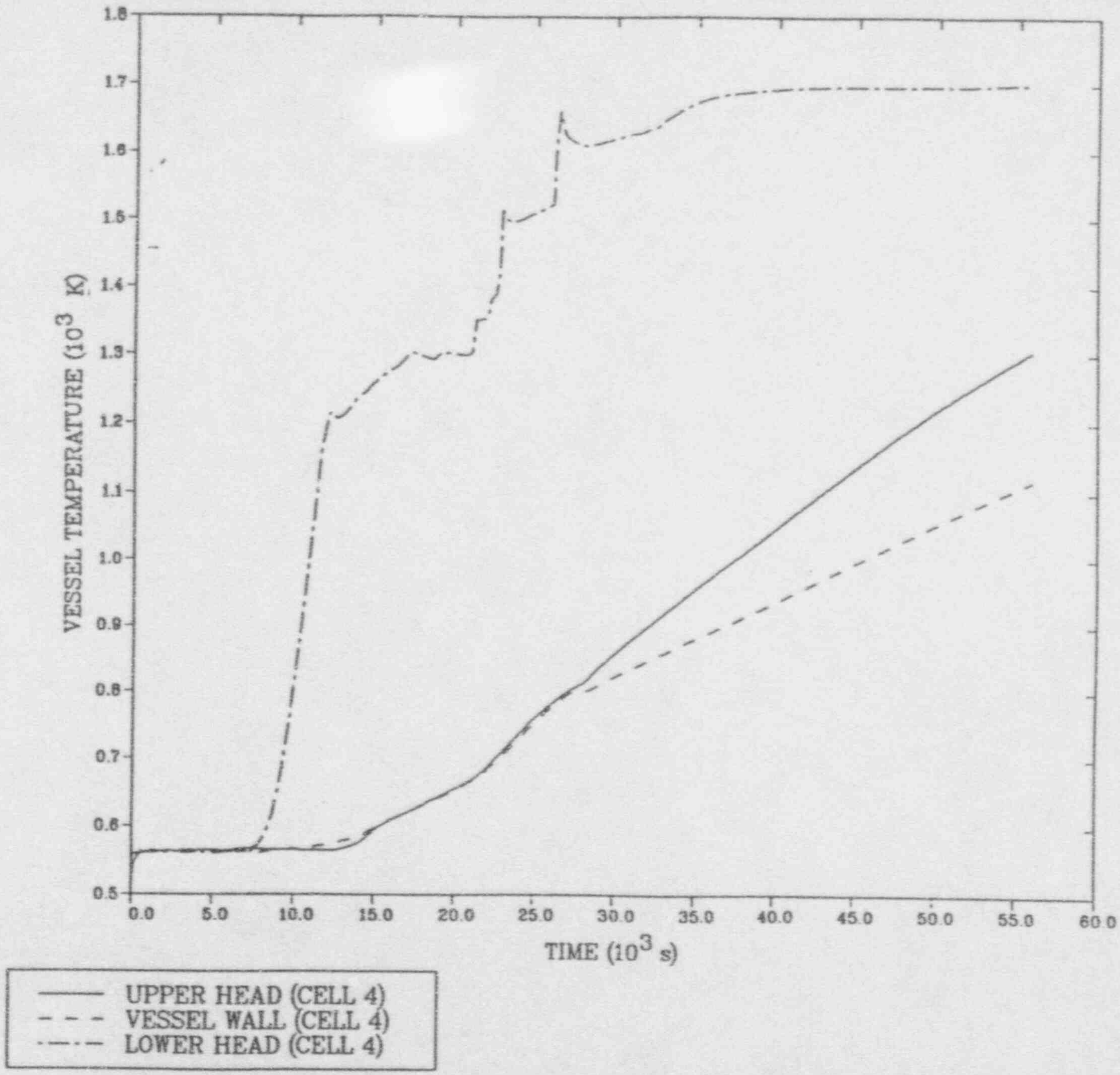

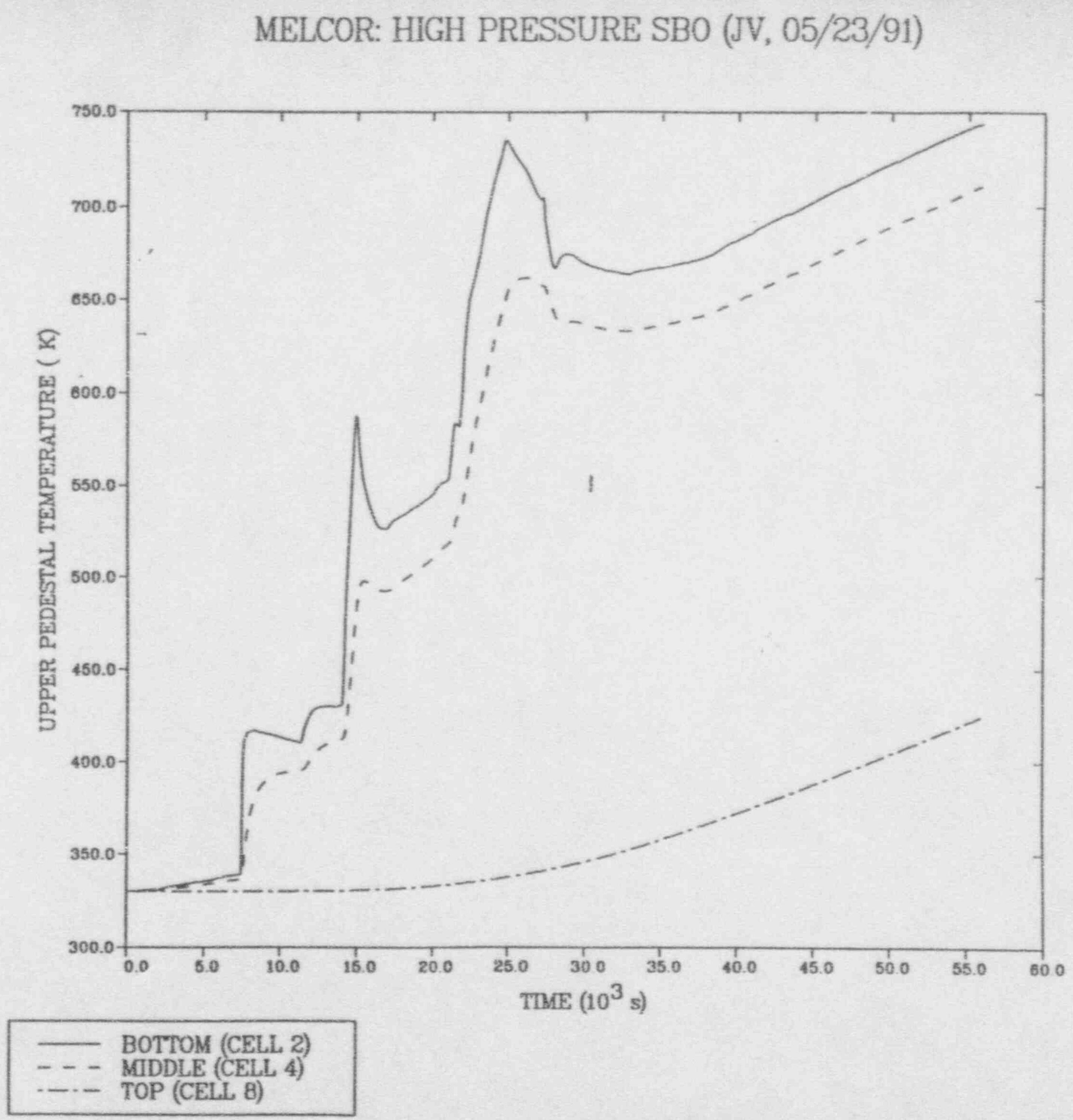

MELCOR: HIGH PRESSURE SBO (JV, 05/23/91)
UPPER PEDESTAL TEMPERATURE (K)
750.0
700.0
650.0
600.0
550.0
500.0
450.0
400.0
350.0
300.0
0.0
5.0
10.0
15.0
20.0
25.0
30.0
35.0
40.0
45.0
50.0
55.0
60.0
TIME (10^3 s)
BOTTOM (CELL 2)
MIDDLE (CELL 4)
TOP (CELL 8)

MELCOR: HIGH PRESSURE SBO (JV, 05/23/91)

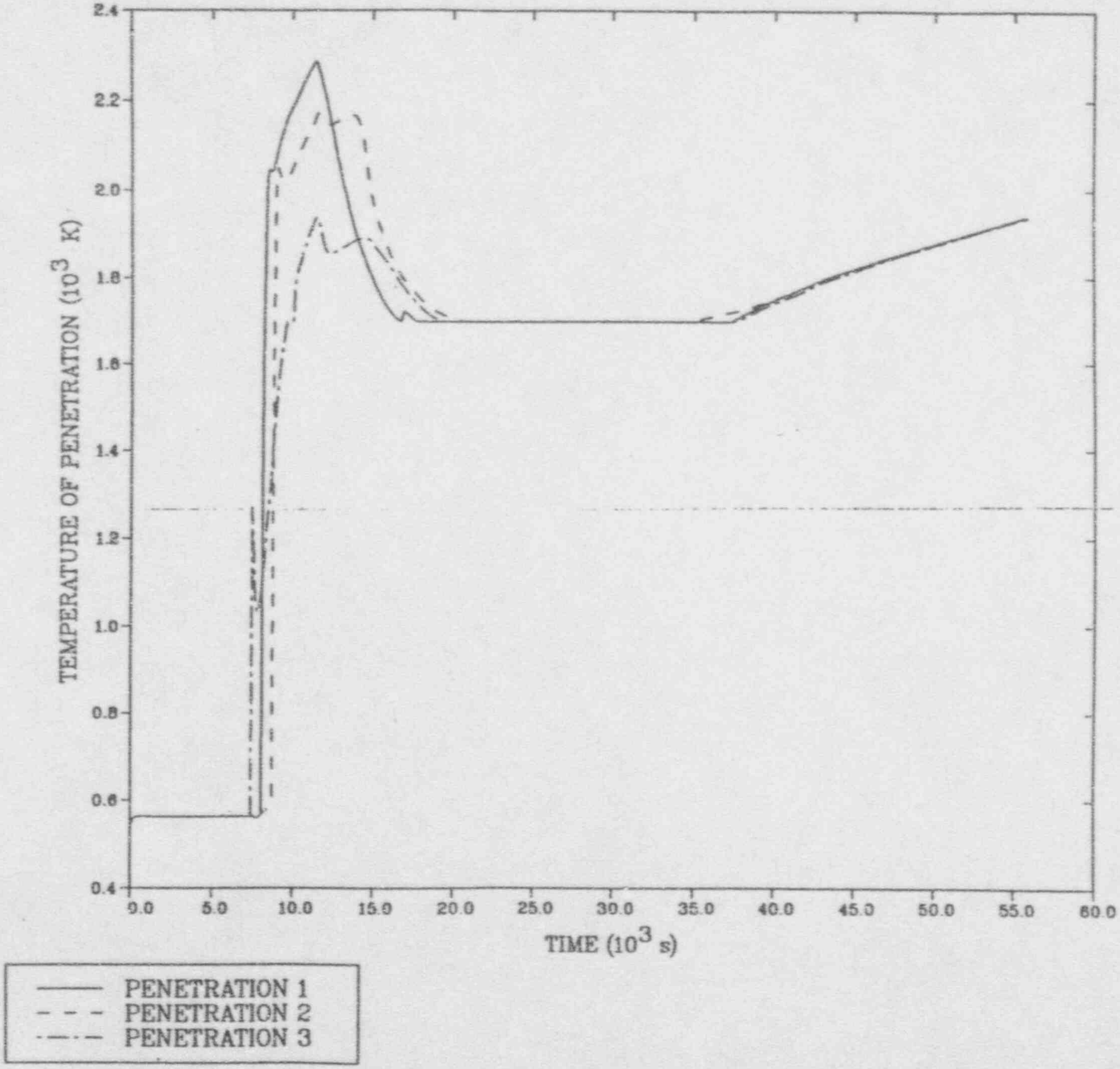

MELCOR: HIGH PRESSURE SBO (JV, 05/23/91)

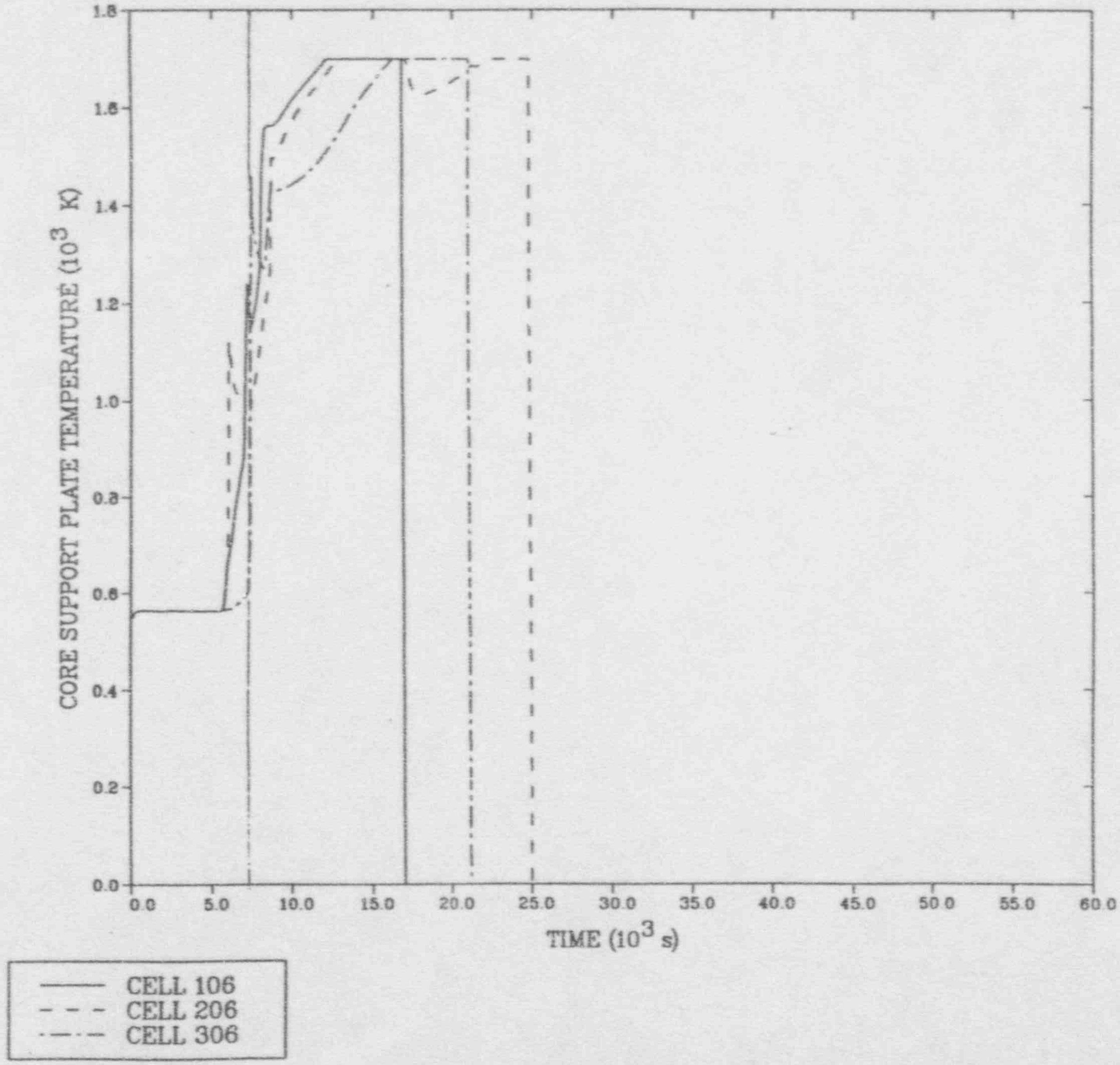

MELCOR: HIGH PRESSURE SBO (JV, 05/23/91)

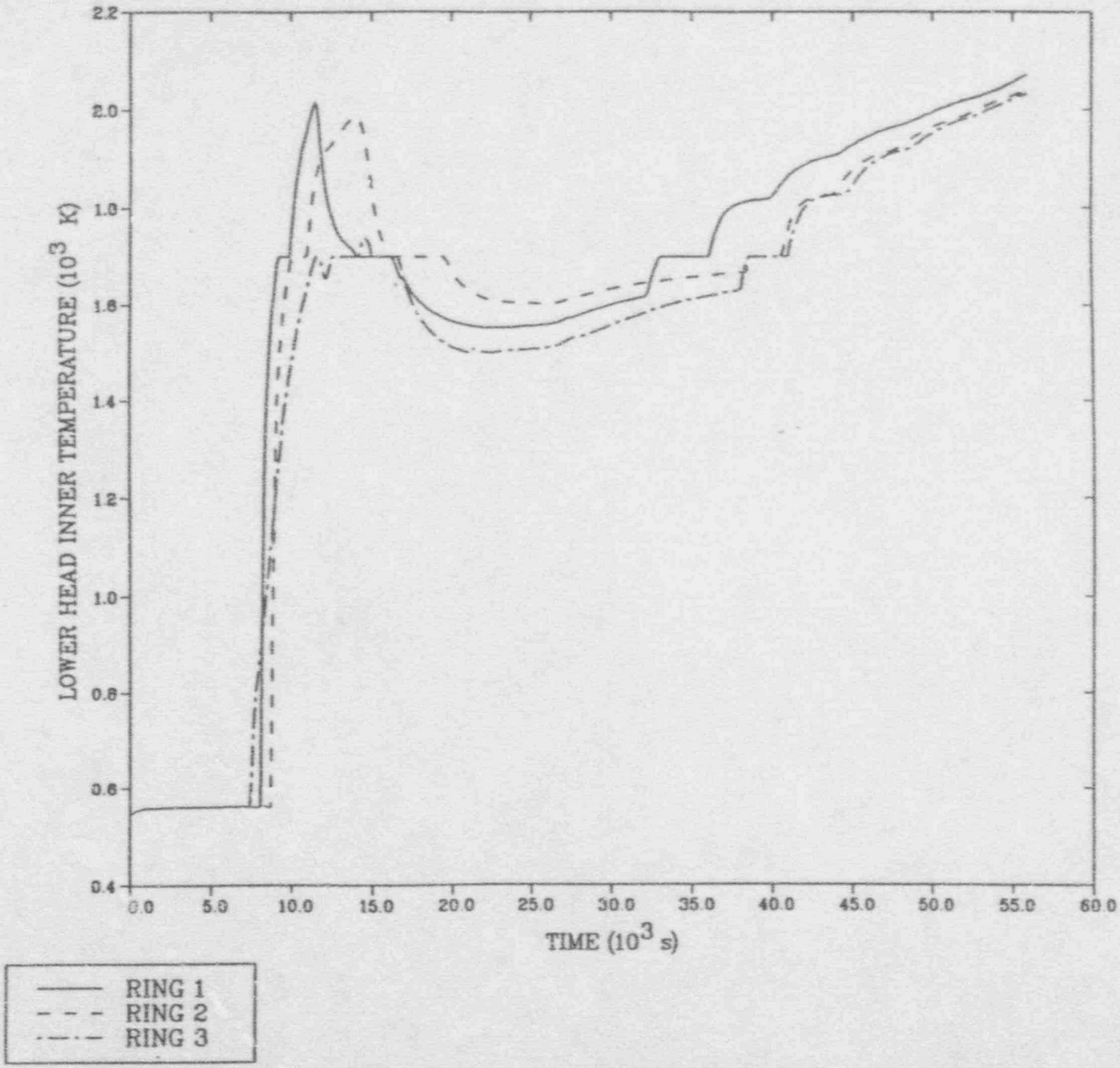

MELCOR: HIGH PRESSURE SBO (JV, 05/23/91)

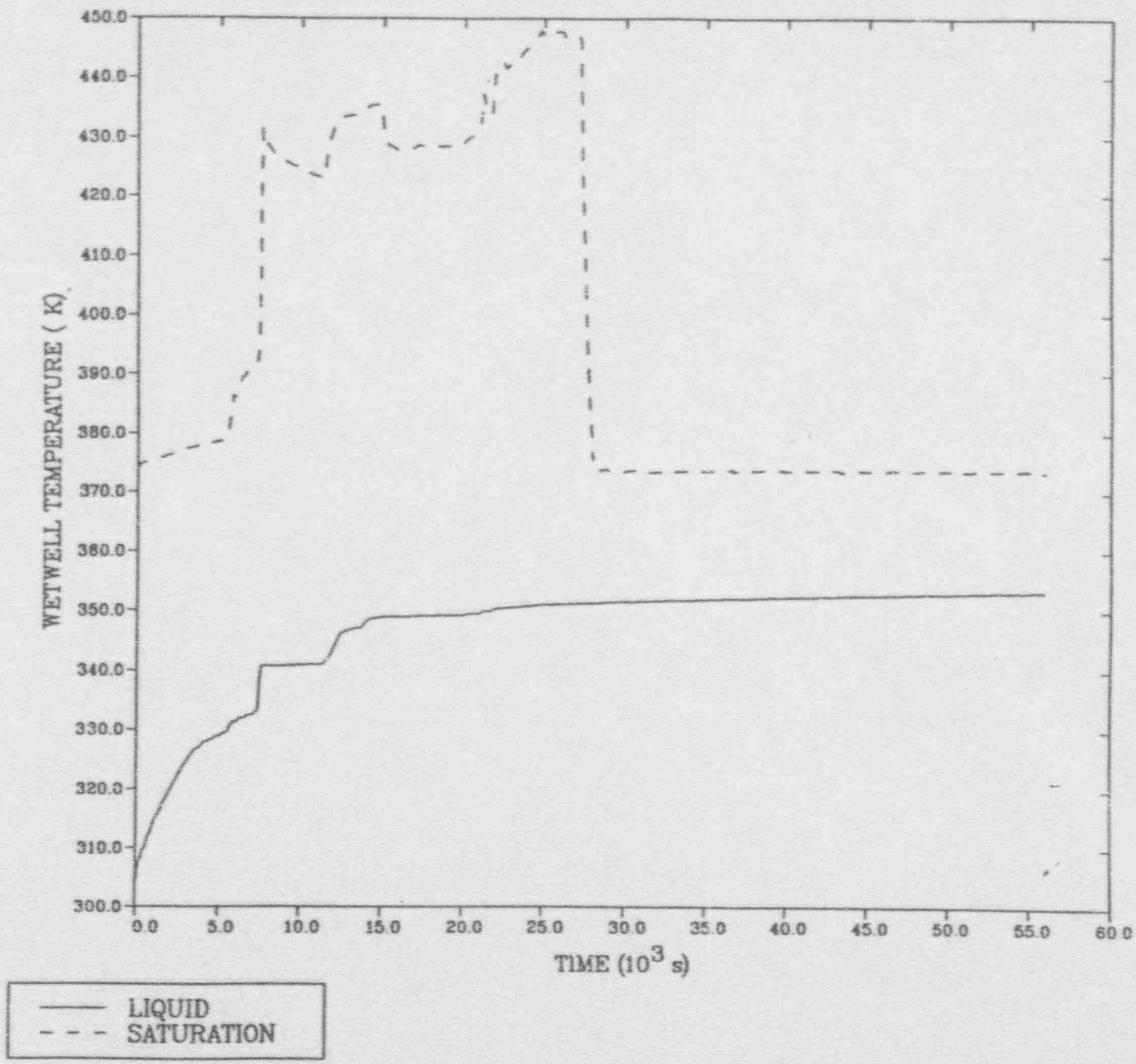

MELCOR: HIGH PRESSURE SBO (JV, 05/23/91)

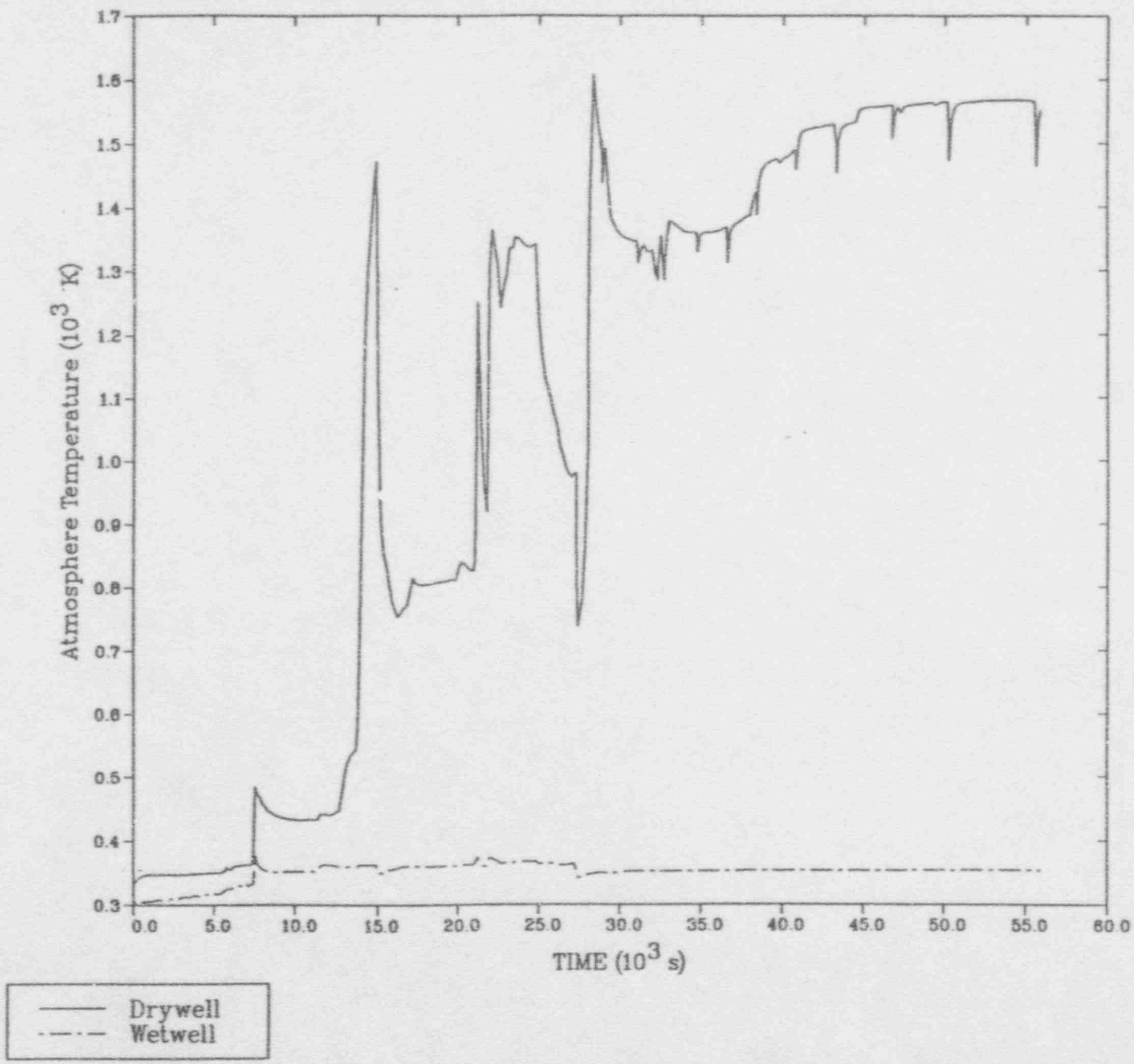

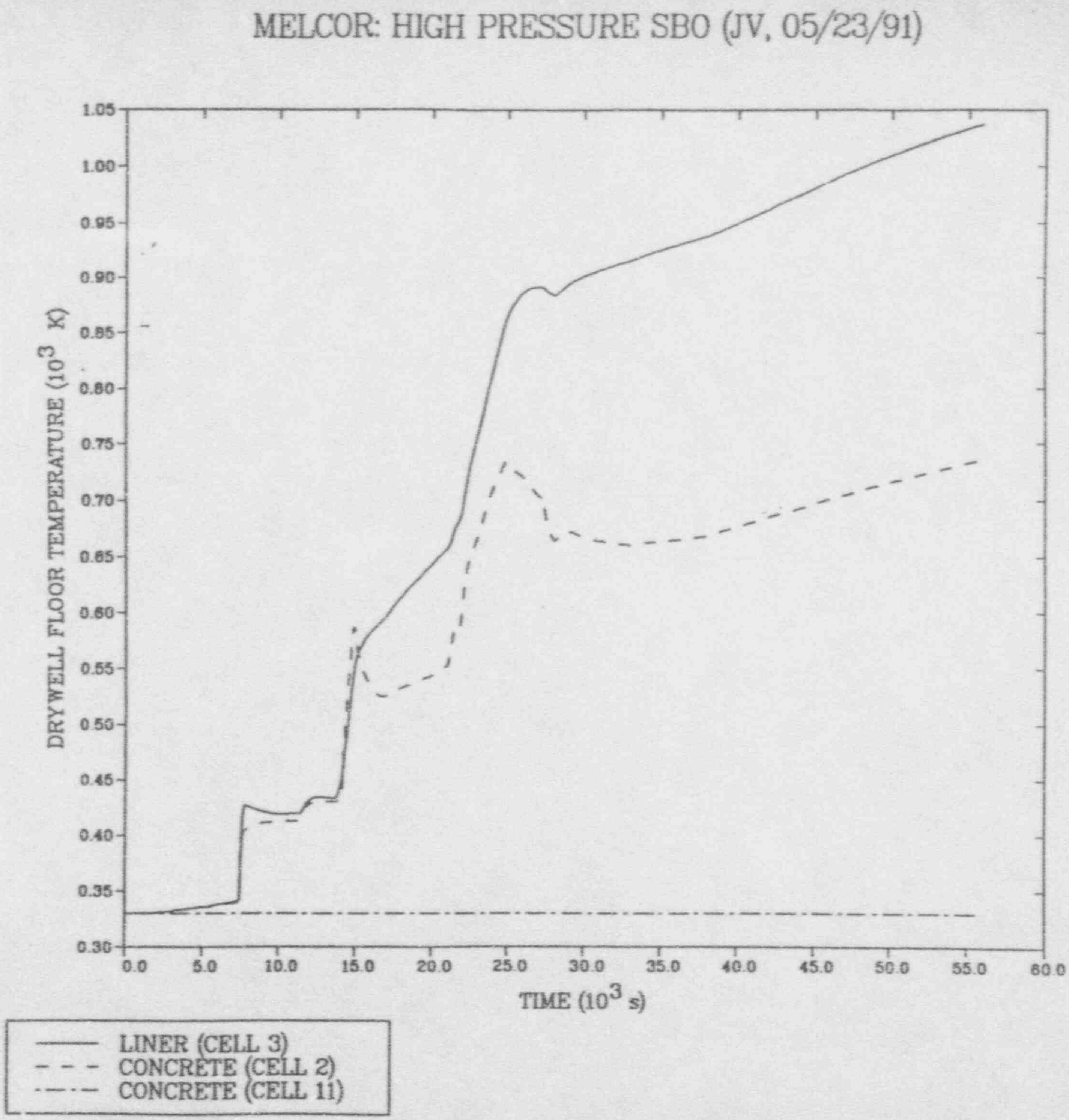
MELCOR: HIGH PRESSURE SBO (JV, 05/23/91)
DRYWELL FLOOR TEMPERATURE (10^3 K)
1.05
1.00
0.95
0.90
0.85
0.80
0.75
0.70
0.65
0.60
0.55
0.50
0.45
0.40
0.35
0.30
0.0
5.0
10.0
15.0
20.0
25.0
30.0
35.0
40.0
45.0
50.0
55.0
60.0
TIME (10^3 s)
LINER (CELL 3)
CONCRETE (CELL 2)
CONCRETE (CELL 11)

MELCOR: HIGH PRESSURE SBO (JV, 05/23/91)

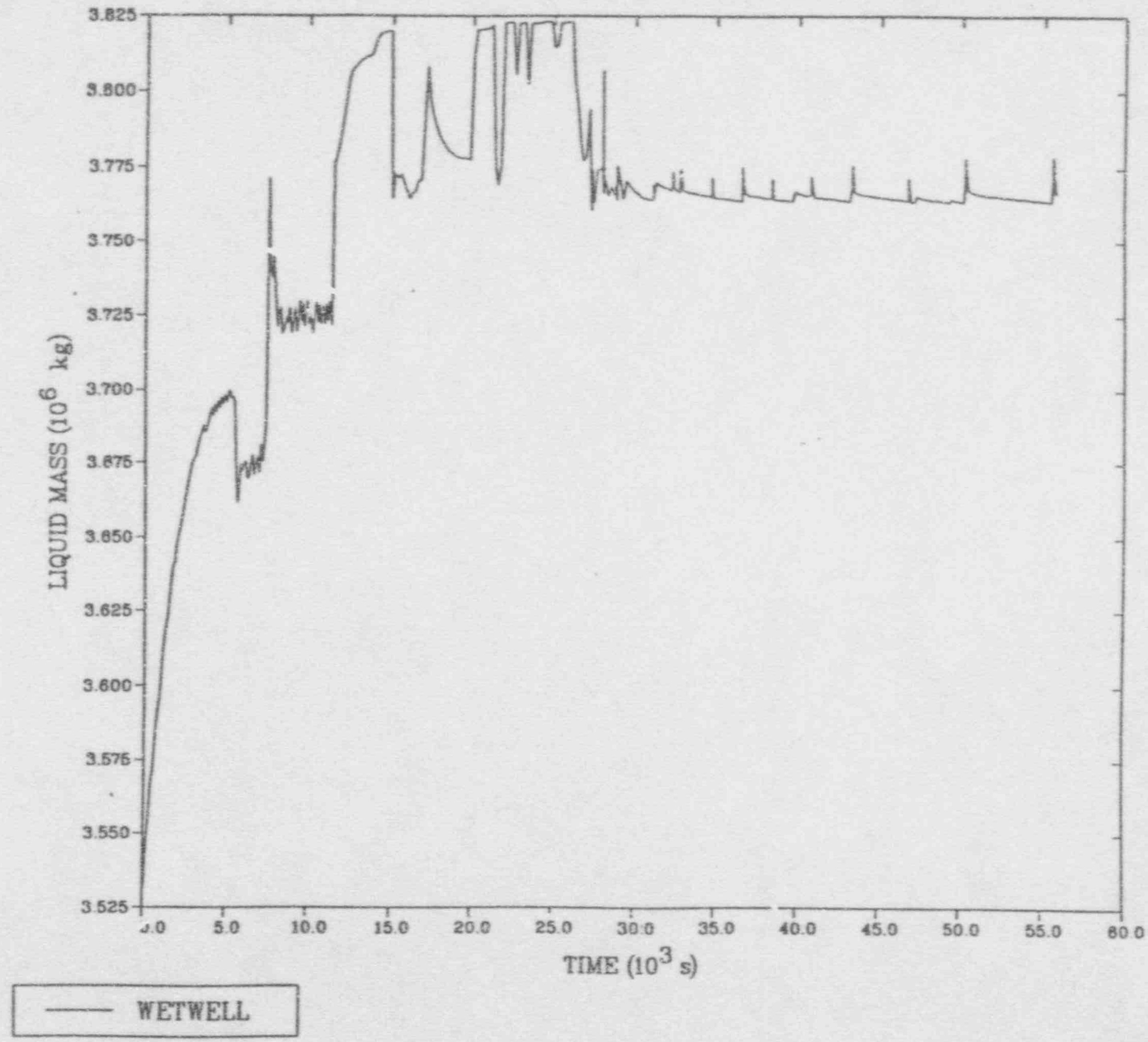

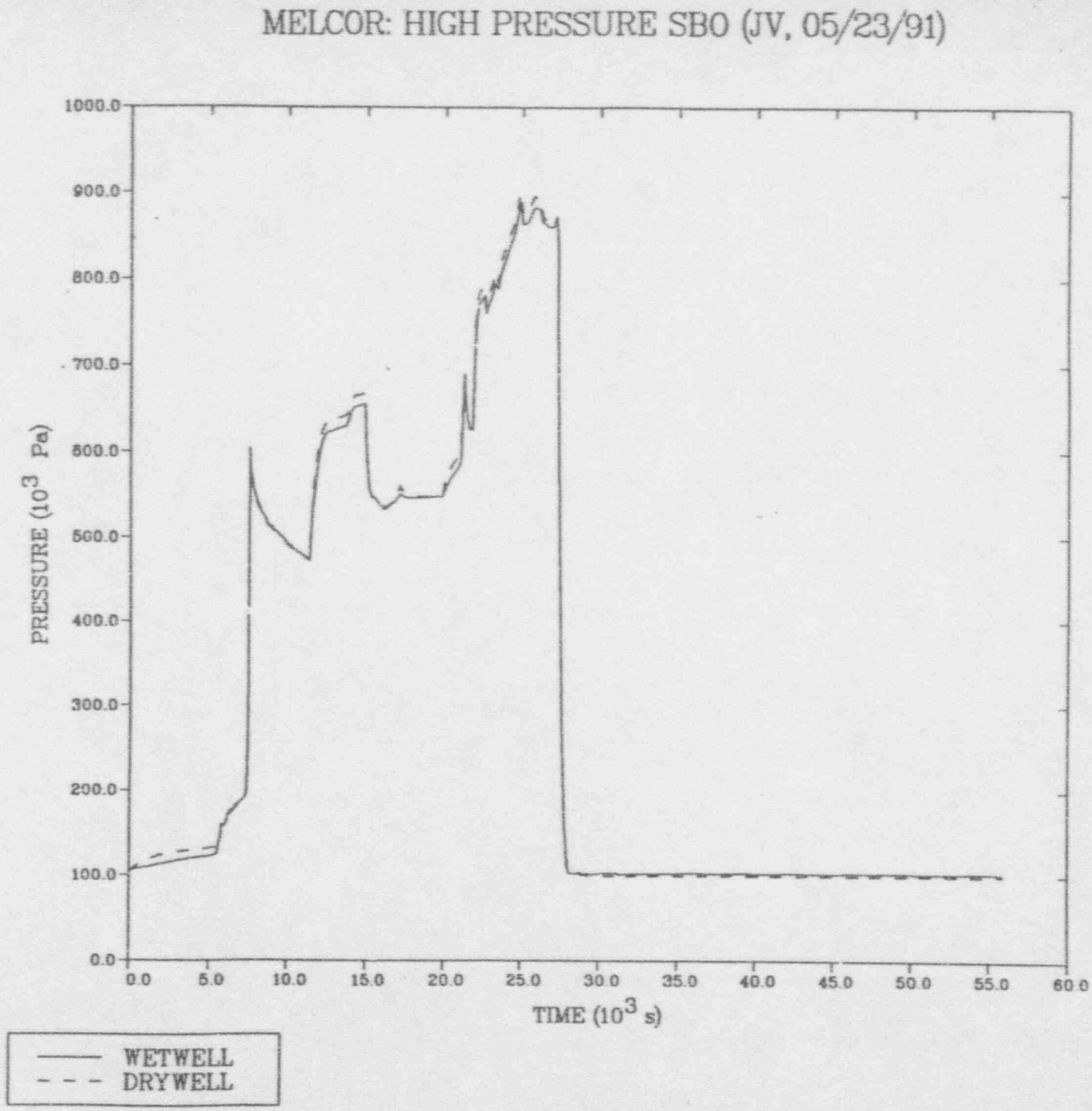
MELCOR: HIGH PRESSURE SBO (JV, 05/23/91)
1000.0
900.0
800.0
700.0
600.0
500.0
400.0
300.0
200.0
100.0
0.0
PRESSURE (10^3 Pa)
0.0
5.0
10.0
15.0
20.0
25.0
30.0
35.0
40.0
45.0
50.0
55.0
60.0
TIME (10^3 s)
WETWELL
DRYWELL

MELCOR: HIGH PRESSURE SBO (JV, 05/23/91)

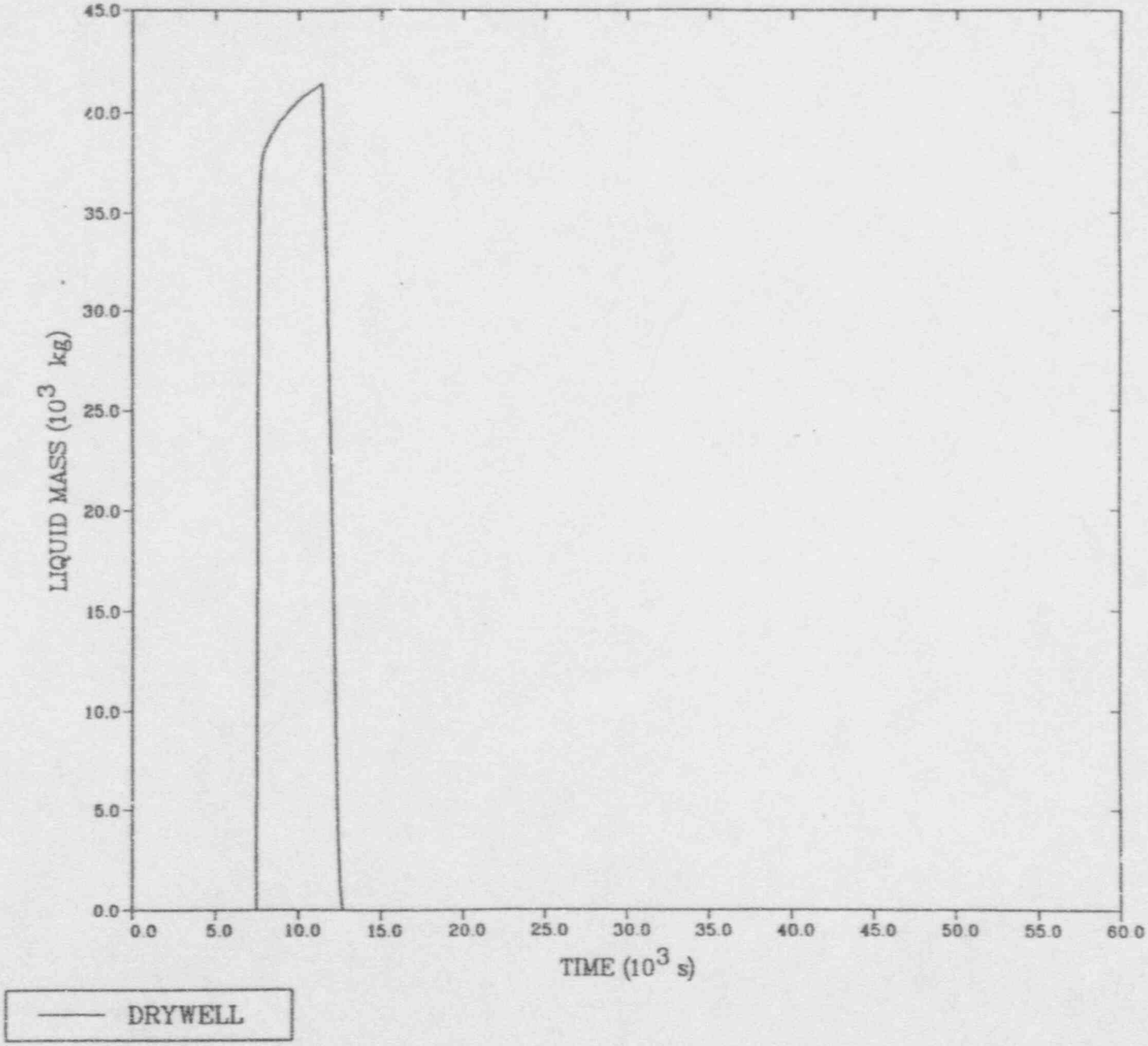

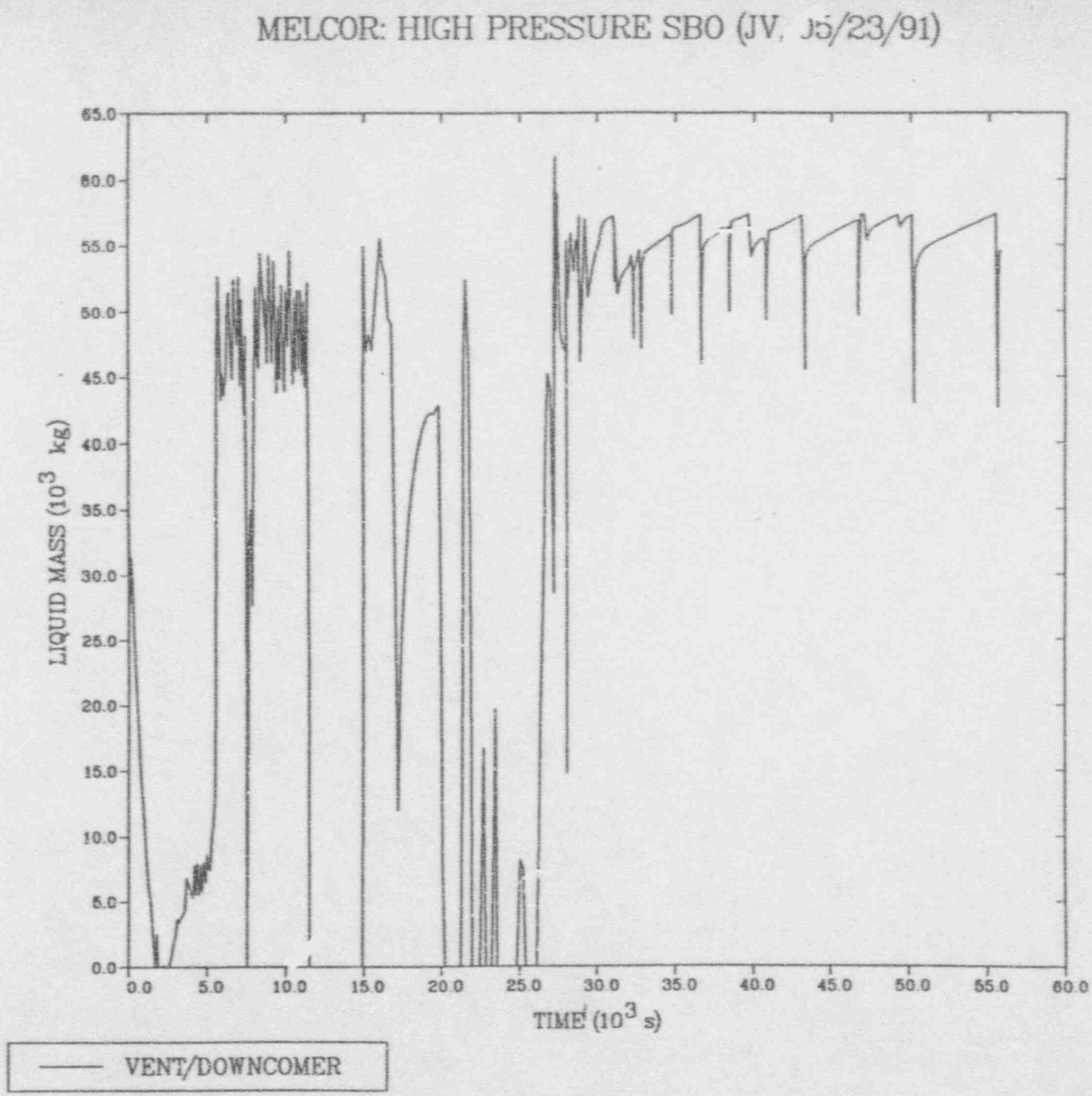
MELCOR: HIGH PRESSURE SBO (JV, J5/23/91)
LIQUID MASS (10^3 kg)
TIME (10^3 s)
0.0
5.0
10.0
15.0
20.0
25.0
30.0
35.0
40.0
45.0
50.0
55.0
60.0
65.0
VENT/DOWNCOMER

MELCOR: High Pressure SBO (LN, 04/17/91)

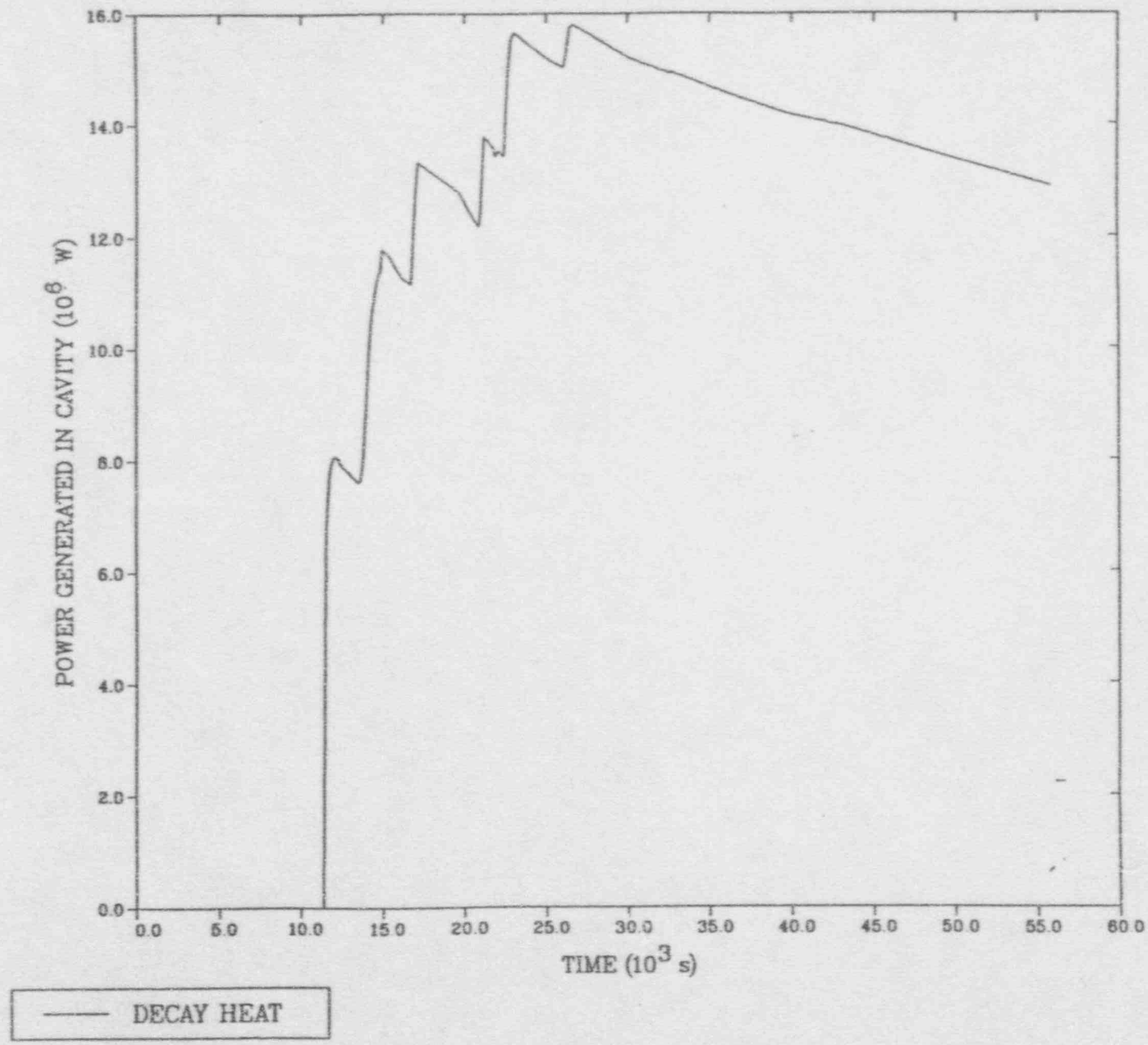

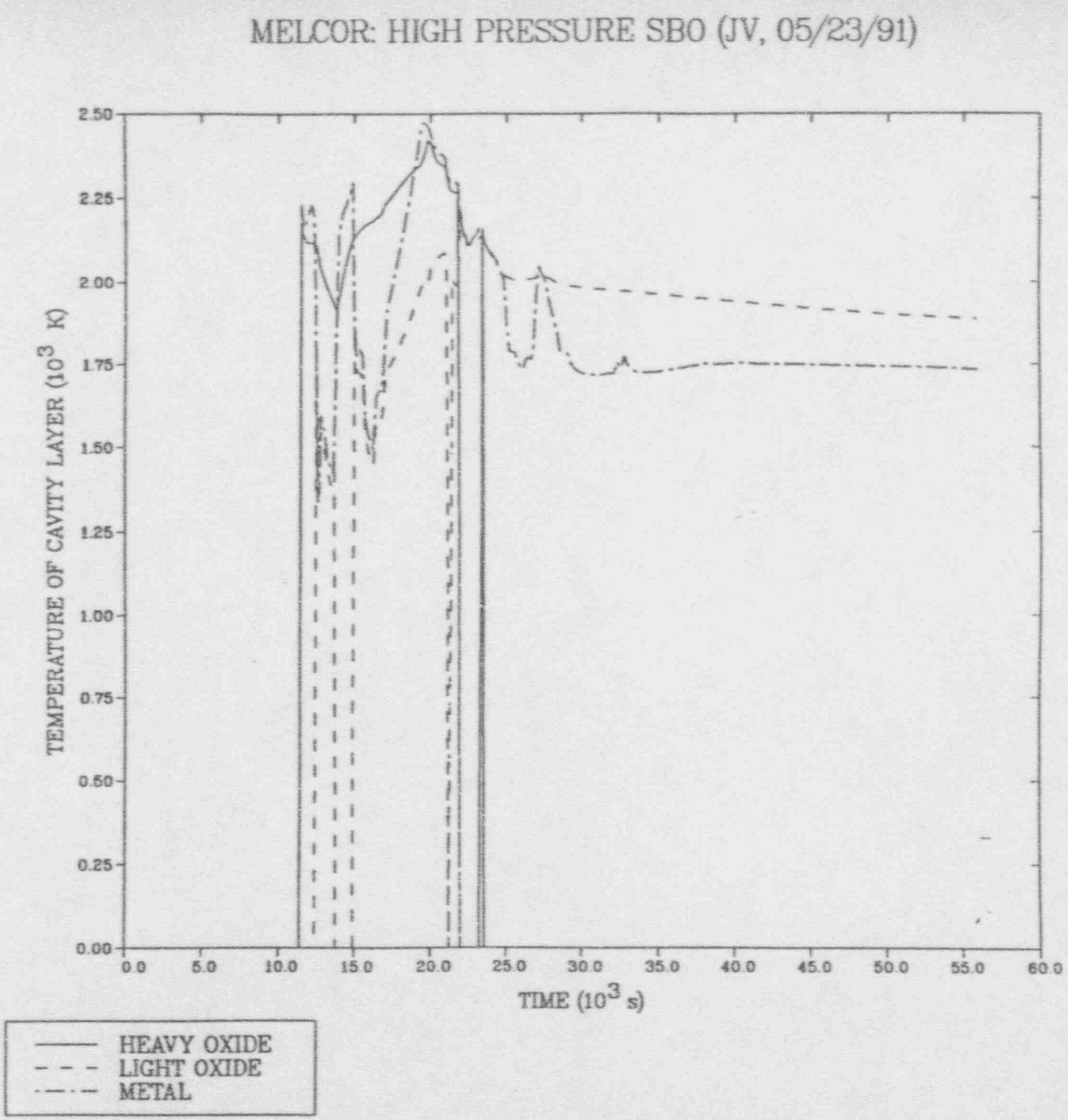

MELCOR: HIGH PRESSURE SBO (JV, 05/23/91)
TEMPERATURE OF CAVITY LAYER (10^3 K)
2.50
2.25
2.00
1.75
1.50
1.25
1.00
0.75
0.50
0.25
0.00
0.0
5.0
10.0
15.0
20.0
25.0
30.0
35.0
40.0
45.0
50.0
55.0
60.0
TIME (10^3 s)
HEAVY OXIDE
LIGHT OXIDE
METAL

MELCOR: HIGH PRESSURE SBO (JV, 05/23/91)

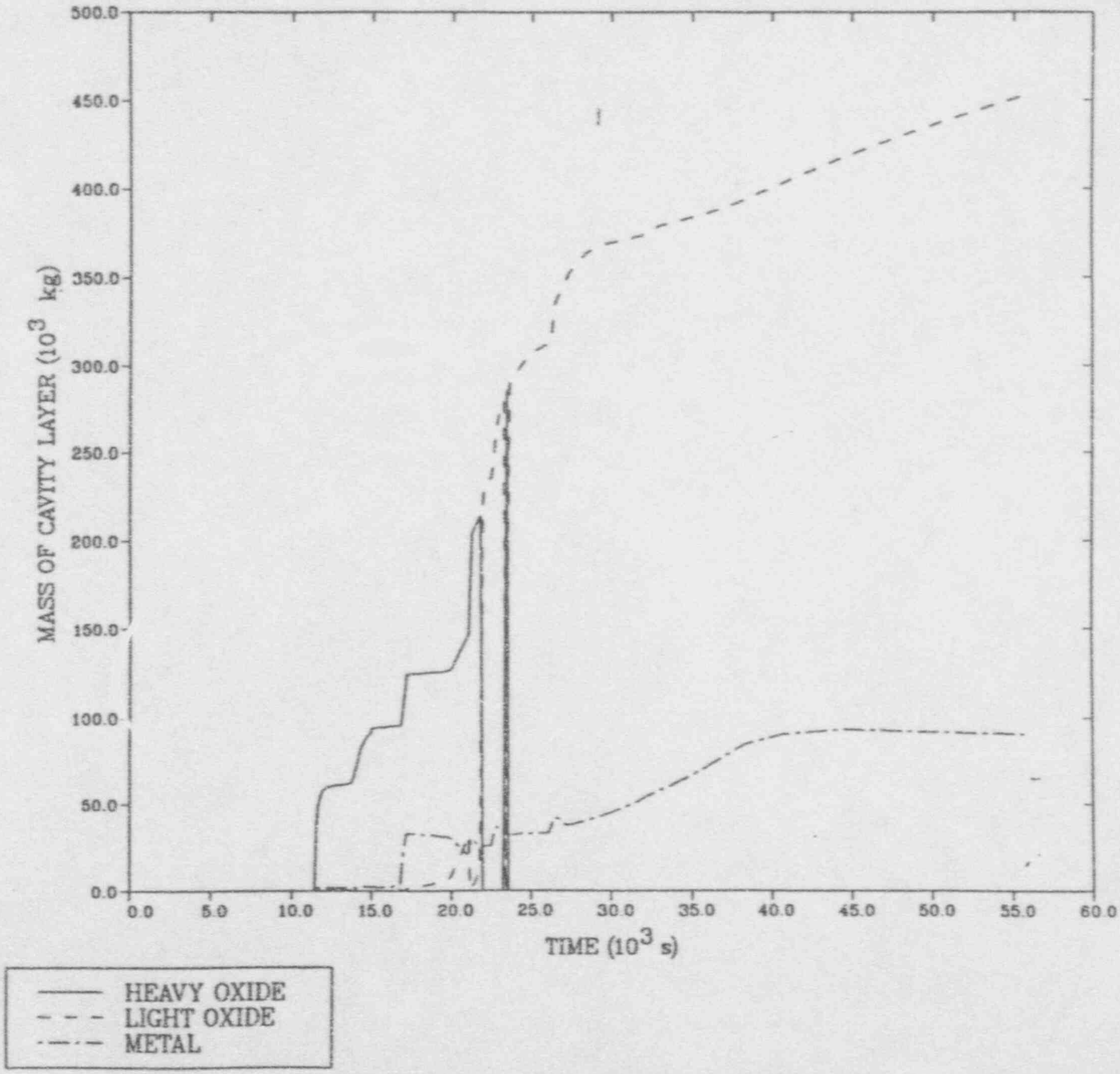

MELCOR: HIGH PRESSURE SBO (JV, 05/23/91)

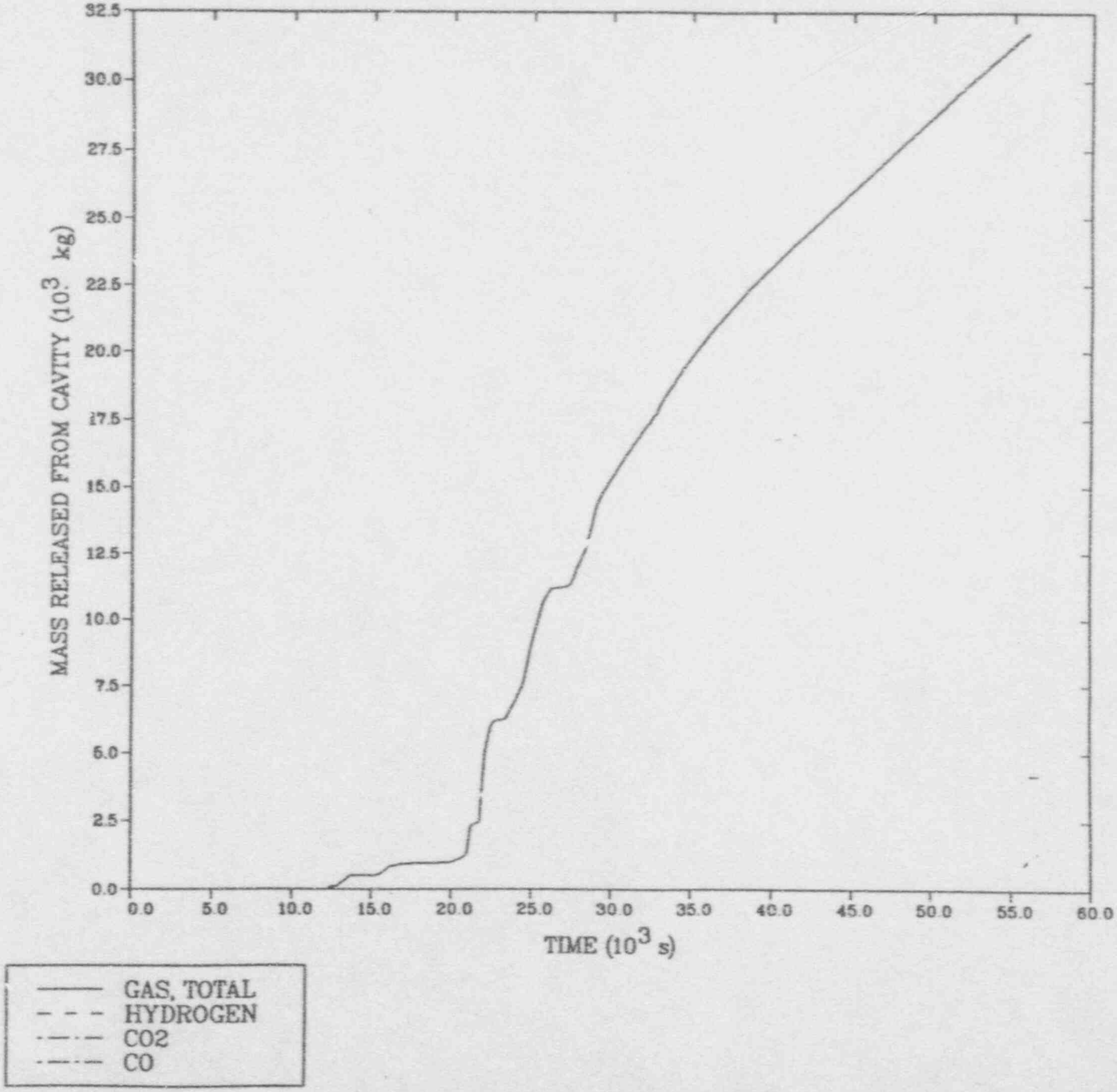

ATTACHMENT 3

CHEMICAL POWER IN CAVITY

APPROXIMATE OVERALL ENERGY BUDGET FOR DEBRIS
(SEE MANUAL FOR EXPLANATION AND CAVEATS)

```
INTERNAL (DECAY) SOURCE         (W) =  1.215E+07
CHEMICAL REACTION SOURCE        (W) =  9.884E+07

HEAT LOSS TO CONCRETE           (W) =  6.497E+07
HEATUP OF ABLATION PRODUCTS     (W) =  3.875E+07
HEAT LOSS FROM SURFACE          (W) =  3.139E+06
  (TO SURROUNDINGS)

CHANGE IN POOL ENTHALPY         (W) =  2.010E+07
  (SUMMATION OF M*DH/DT)
```

NUMERICAL CHECKS ON MASS AND ENERGY CONSERVATION

```
RELATIVE ERROR IN MASS      =     9.68781E-13              RELATIVE ERROR IN E
```

```
lt-A menu, Alt-H help : DIRECT    : Capture Off            : Prn Off :   6:43:23

MELCOR OUTPUT    B1  F 133        5482 BLKS 91/05/18 LINE    51543 OF  168815
==>                                                                   BROWSE
```

```
                                        CORCON VERSION 2.04.(+)          ME
TIME =  20988.63         CAVITY  0  CAVITY 1        ASSOCIATED WITH USER VO
                                   * * * * G A S   G E N E R A T I O N *
```

GAS EXITING POOL (INCLUDES FILM AND COOLANT)

	GENERATION RATE		CUMULATIVE RELEAS	
SPECIES	MASS (KG/S)	MOLES (1/S)	MASS (KG)	MOLES
C(G)	0.00000E+00	0.00000E+00	0.00000E+00	0.0000
CH4	0.00000E+00	0.00000E+00	0.00000E+00	0.0000
CO	8.07225E-01	2.88188E+01	1.00590E+03	3.5911
CO2	4.10368E-04	9.32447E-03	4.53728E+01	1.0309
C2H2	0.00000E+00	0.00000E+00	0.00000E+00	0.0000
C2H4	0.00000E+00	0.00000E+00	0.00000E+00	0.0000
C2H6	0.00000E+00	0.00000E+00	0.00000E+00	0.0000
H	0.00000E+00	0.00000E+00	0.00000E+00	0.0000
H2	1.45582E-01	7.22206E+01	2.17344E+02	1.0782
H2O	3.41056E-04	1.89316E-02	1.31192E+01	7.2823
N	0.00000E+00	0.00000E+00	0.00000E+00	0.000

MAAP-MELCOR: BWR SBO (03/10/91)
bnl_sbo_43.plt LINE

P 37

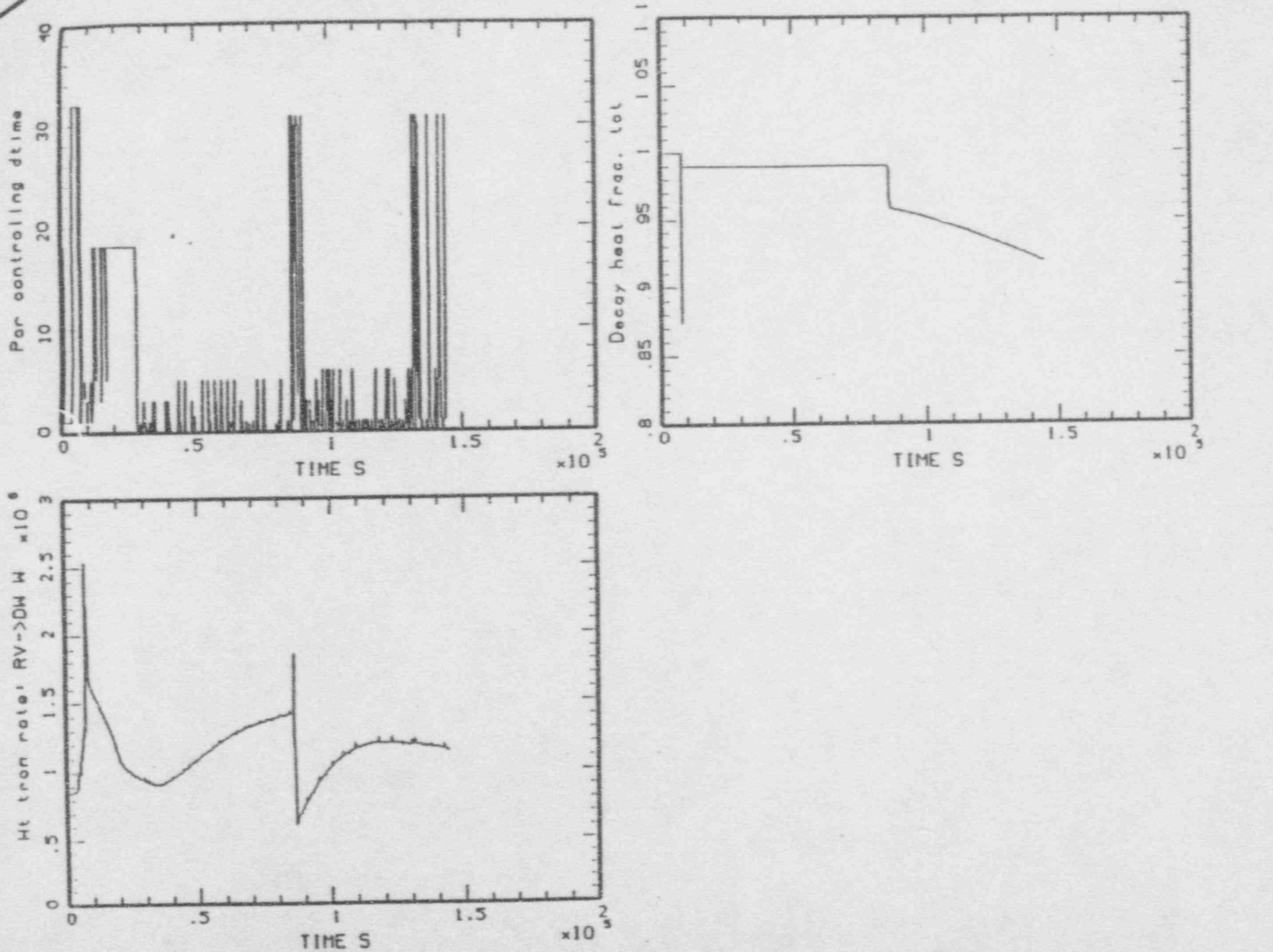

ESTIMATION, UNCERTAINTY ANALYSIS, AND SENSITIVITY ANALYSIS: DIRECTIONS FOR RMIEP

Robert G. Easterling
Floyd W. Spencer
Kathleen V. Diegert

Statistics, Computing, and Human Factors Division
Sandia National Laboratories
Albuquerque, New Mexico 87110

January 4, 1985

APPENDIX D

Use of the Maximus Methodology for Confidence Bound Calculations in Fault Trees--Trial Problem

Introduction

To demonstrate the use of the Maximus Methodology [3] for confidence bound calculations in fault trees, a dominant accident sequence from the Interim Reliability Evaluation Program: Analysis of the Arkansas Nuclear One-Unit 1 Nuclear Power Plant [1] was chosen for analyses. The sequence chosen was the $B(1.2)D_1C$ sequence, which denotes a reactor coolant pump seal rupture or a rupture in the RCS piping in the range of .38" to 1.2" (B(1.2)) followed by failure of the high pressure injection system (D_1) and reactor building spray injection system (C).

The Maximus Methodology was developed for system reliabilities modeled by block diagrams. Block diagrams are generally not as extensive as fault tree models for nuclear plant accident sequences. This trial problem was initiated to answer the question--Can Maximus still be used and if so with what modifications?

In this paper, the calculation of confidence bounds in several cases will be considered. The cases illustrate the distinction between data-based and data-free estimates as outlined in the guidelines [2] for the PRA Methods Develoment Program. In case 1, the estimates given for each event are treated as being data-based and recovery is not considered. Case 2 is like case 1 in the treatment of event data, but the probability of recovery (as subjectively determined) is added. In case 3, the probability of the accident sequence is considered as being estimated by both data-based and subjectively-based estimates with recovery probabilities also considered as subjectively determined. The consideration of recovery is an explicit recognition that even though a particular accident sequence may occur it will not necessarily lead to core melt. Human intervention may restore things if done correctly and in a timely manner. The recovery action, however, takes place after the accident sequence has occurred.

Case 3 reflects the most realistic situation for accident sequences in that some of the basic event probability estimates are data based, some are subjectively determined, and recovery is included. However, the other cases are worth considering as they may be applied at intermediate steps, and it is the first case that is comparable to the uncertainty analysis done in reference 1. For all the cases, the information available was in the form of point estimates and error factors, as well as the associations of events whose probabilities were considered as being estimated from the same data base. For the example problems considered here, those estimates considered as data based are translated into pseudo-data by finding the occurrences in demands (or operating time) that gives the same point estimate and gives the error factor times the point estimate as a 95% upper statistical confidence bound. If the probability of the event is considered to be subjectively estimated, the interval ℓ, u, where ℓ = (point estimate/error factor) and u = (point estimate · error factor) is taken as the subjective interval and the point estimate is taken as the nominal value in carrying out the uncertainty analysis as described in Reference 2. The above procedure of converting to pseudo-data is not being recommended. It is used here to obtain "data" for the sake of illustration.

In the accident sequence considered, B(1.2) is the initiating event and D_1C represents the hardware and system failures that are modeled in the fault tree. The event B(1.2) has an estimated occurrence rate of .02/reactor year. For illustration purposes, we will derive the overall uncertainties in each case by considering the failure rate of B(1.2) as a constant and also considering it as having been estimated by 2 occurrences in 100 reactor years.

Case 1. All probabilities considered as data based--no recovery

This problem was originally approached by considering the dominant 500 cut sets for the sequence of reference 1. The estimated occurrence rate from the 500 cut sets is approximately 98% of the estimate that would result considering the top 1,355 cut sets. The 500 dominant cut sets are comprised of 135 different basic events. In order to represent D_1C in a series-parallel arrangement, the 500 cut sets were examined in a factored form. The series-parallel arrangement derived from this factored form is given in Figure 1. The numbers inside the boxes are the number of serial basic events that comprise that segment of the sequence. Although constructed from considering the dominant 500 cut sets, the system of Figure 1 has 1,289 cut sets. This is because the representation of the system is block form introduced cut sets not in the original 500. These additional cut sets were then verified to be actual cut sets of the system.

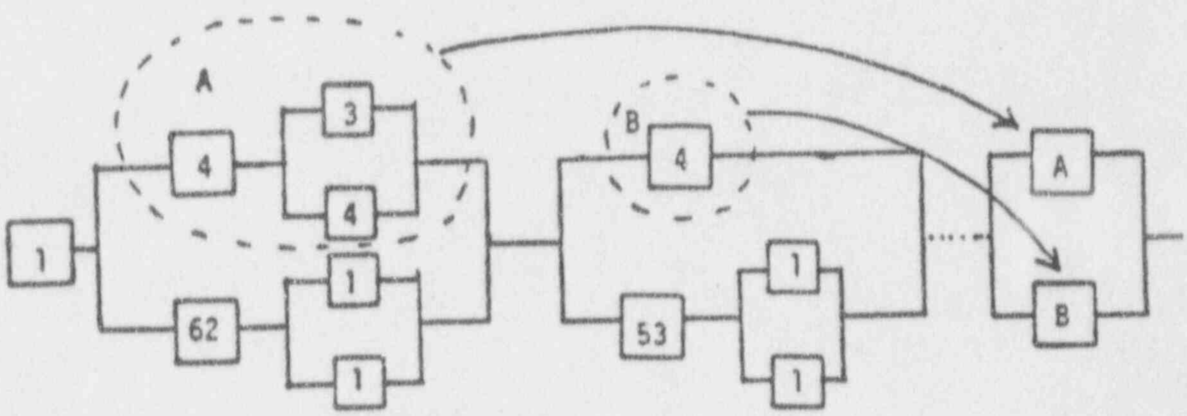

Figure 1. A series-parallel representation of the dominant cut sets of $B(1.2)D_1C$. The A and B terms are repetitions of the same group of components with the same structure.

In Appendix C of reference 1, dominant minimal cut sets in terms of independent subtrees were given. The series-parallel arrangement implied by the configuration given in Appendix C is consistent with that shown in Figure 1, except that the parallel arrangements of Figure 1 contain single events that were not included in reference 1. By considering both the independent subtrees given in reference 1 and the elements included in the top 500 cut sets, the representation of Figure 2 is obtained. In Figure 2, each block is one or more basic events in series and those blocks labeled the same are repeats of the same chain of events. The blocks labeled P, Q, a, and b represent events not listed in reference 1 but contained in the top 500 cut sets. As the total contribution of these were small and they had very little effect on the uncertainty calculations, they are left out of the present analysis.

The events contained in each block are enumerated in the Appendix in Table A2. Those blocks (A through O) that were derived from reference 1 are documented by inclusion in the Appendix of the appropriate table from that reference. Also added to the tables are identifiers for the population type. Those events whose probabilities are estimated from the same data sources have the same population type identifier. In order not to double or multiple the same data in the overall uncertainty estimate, the available data is divided among those events to which the data apply (see Reference 3). In this example, pseudo-data are constructed by finding the number of occurrences in time that would give the same point estimate and for which the 95% upper confidence bound equals the point estimate times the error factor. The intent is to illustrate the analysis with statistical data that correspond, at least roughly, to the subjective estimates and uncertainty assessments in Reference 1. This gives rise to the following two equations (for the Poisson-type data, these are exact; for binomial-type data, these are based on very good approximations):

$$f/T = \hat{P}$$

$$\frac{\chi^2(2f + 2;\ .95)}{2T} = \hat{p} \cdot EF\ .$$

Here, $\chi^2(df;\ \alpha)$ denotes the α percentile of the chi-square distribution with df degrees of freedom. The values f and T are the pseudo data of f occurrences in T time (or demands) and p and EF are the given point estimate and error factor.

By substituting the first equation into the second, the T values cancel and f is the solution of:

$$\chi^2(2f + 2;\ .95)/f = 2 \cdot EF\ .$$

The solution of the above equation when EF = 3 is f = 2.20 and when EF = 10, f is .37. The denominator (demand or time) is calculated in each case by dividing f by the point estimate.

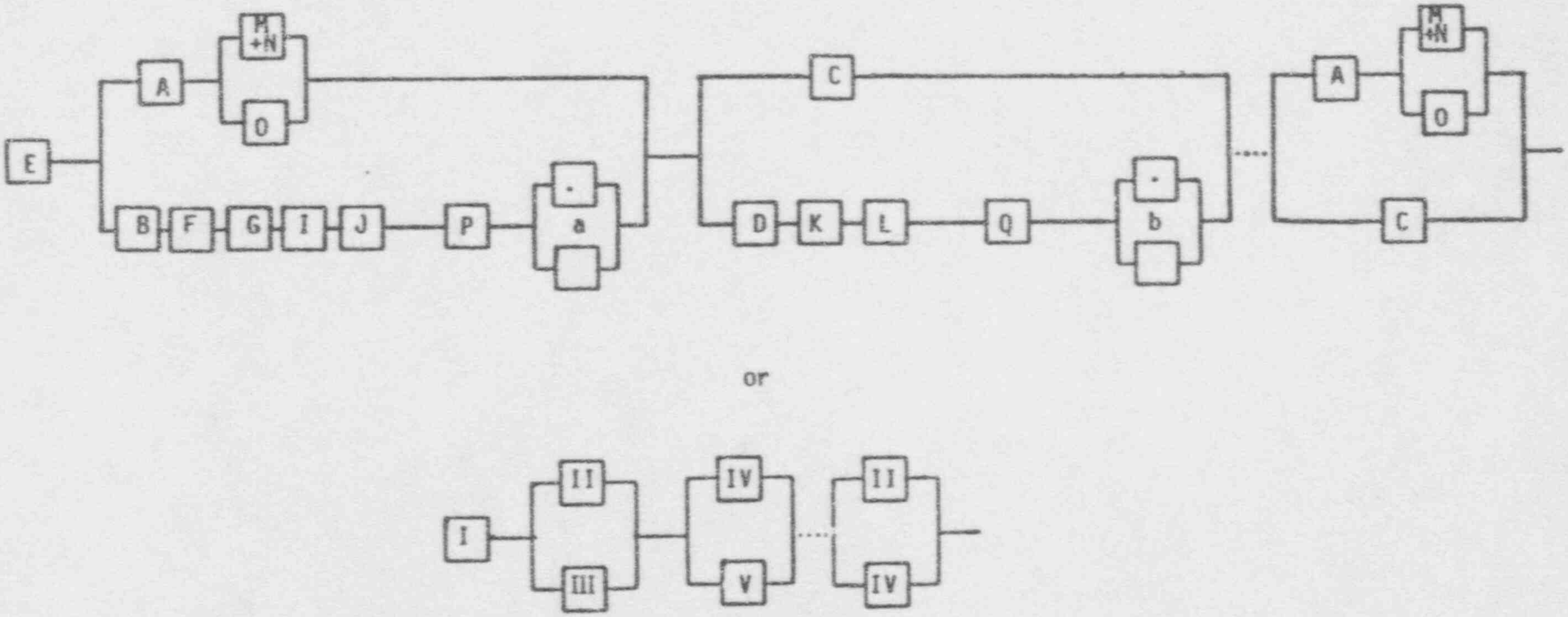

Figure 2. Series-parallel arrangement for B(1.2)D_1C. Each block is one or more basic events in series. Those blocks labeled the same represent the same event.

The various population types and derived pseudo-data are given in Table A3. Some of the population types have events that have different point estimates. This situation is taken to reflect the case where a rate λ is estimated for all the events of interest, but the actual rate for a particular event i is λt_i. In the Poisson case, if λ is estimated by f occurrences in T time, then the estimate of λt is equivalent to f occurrences in time T/t. To handle those population types that had different point estimates within them, the largest point estimate is taken as the λ estimate and smaller point estimates have associated with them a time factor for adjustment. For example, consider that two event probabilities, one estimated at 1.1(-3) and one at 3.3(-3), are considered to be from the same population type. Both have error factors of 3 so that we take f = 2.2. Using the larger of the two as reflecting the λ to be estimated, we take T = 2.2/3.3(-3) = 667 as the applicable data. If 3.3(-3) is the estimate for λ, then 1.1(-3) must correspond to an estimate of $\lambda/3$. Therefore, if we divide the applicable data between the two events, giving 1.1 failures in 333.3 time units for estimating each λ independently, this is equivalent to using 1.1 failures in 1,000 time units for estimating $\lambda/3$. And, thus, the time factor of the second event would be given as 3. The various factors by which times are adjusted are given in Table A4 in the Appendix.

The Maximus method for calculating confidence bounds was applied to the system of Figure 2. The effective number of tests was calculated and combined with the total failure estimate to calculate the effective number of failures. The last parallel arrangement (Branches II and IV in Figure 2) was not originally considered in deriving the effective number of tests because it does not represent an independent subsystem but rather is included in the system to represent an additional cut set not present in the parallel-series arrangement. The effective tests for the two branches (II and IV) derived from the first part of the system when combined in a parallel arrangement exceed that originally calculated for the system. Therefore, this cut set does not affect the effective failure number calculation.

Computer Program

There currently exists a Fortran program that calculates effective data for series-parallel systems given component data and using the Maximus methodology. Figure 3 is an example output of this program for the system under consideration here. The inputs to the program are the system description and the component data. In this example, each of the components (events) from the same population type are labeled with the same alphabetic character. Differences in the numeric value following the alphabetic character are needed because of the potentially different test quantities to be assigned in the unpooling process.

The system equation is recursive, where each set of parentheses encloses a subsystem which may contain other subsystems. For example, in the system description of Figure 3, subsystem 1, which is represented as (1*a2b2c2c2g2j1), is a series (denoted by the "*") subsystem representing the independent subtree labeled LPI1408B-VCC-LF in the ANO analysis. Subsystem 1 is itself an element of the subsystem labeled 16 in the description. Subsystem 16 combines subsystem 1 in series with subsystem 14, which is the subsystem that combines the parallel arrangement of M+N and O of Figure 2.

From Figure 3, it is seen that the overall effective data are roughly 1.2 failures in 1,430 tests. This analysis does not include the additional cut sets represented by the parallel arrangement of II with IV appended to the system in Figure 2. If we combine those systems from Figure 3 that make up the added cut sets (subsystems 16 and 3), the effective n far exceeds 1,430. Therefore, 1,430 is used as the overall system effective test size and the overall system point estimate of 9.2(-4) gives the effective data of roughly 1.3 failures in 1,430 tests. The upper 95% confidence limit on the sequence occurrence rate, based on 1.3 failures in 1,430 tests is 3.7(-3).

If the point estimate divided into the upper 95% bound is taken to be the error factor, then the error factor from this data would be 4.0. Contrast this with the error factor of 3 that is given in the ANO report. However, note that the lower 95% bound on 1.3 failures in 1,430 tests is given by 8.3(-5) and if the point estimate divided by this lower limit is taken to be the error factor, then 11 ($\approx 9.2 \div .83$) would be taken as the error factor.

In the methodology used for the ANO report, the distribution on the top event would not have a lognormal distribtuion, and, therefore, the error factor determination could suffer from inconsistencies similar to those discussed above. It would make more sense to compare the results of these two methods by looking directly at the uncertainty intervals. Uncertainty intervals from the ANO report method are not directly available but from the values given in Table 8-4 of reference 1, we can infer that the median of the derived distribution was 1.25(-3). With this value and an error factor of 3, the upper 95th percentile must have been approximately 3.75(-3) as compared to 3.7(-3) derived from the Maximus methodology. Thus, the two methods produce upper uncertainty bounds that are virtually the same in this particular example. However, there is a vast difference in the interpretations from the methods. By use of the Maximus methodology, statistical confidence bounds are stressed. That is, one is asking how high the probability of the sequence D_1C might be and still be consistent with the available data on the individual events. The degree of "consistency" is determined by the confidence level. On the other hand, a Monte Carlo method such as used in ANO, requires the placement of distribution functions on each of the individual event probabilities. These distribution functions do not correspond to anything that we have specifically modeled, and therefore, they reflect an added mathematical level that is often referred to as the "analyst degree-of-belief."

The above analysis reflects only the D_1C portion of the sequence. If the .02/reactor year occurrence rate for B(1.2) is considered as constant, then the overall uncertainty analysis would correspond to that of 1.3 failures in 71,400 reactor years. The lower and upper 95% bounds are then given by 1.7(-6) and 7.3(-5), respectively.

If the .02/reactor year rate is considered as coming from 2 occurrences in 100 years, the effective overall data is .61 occurrences in 33,200 reactor years (see Reference 3 for combining algorithm) and the lower 95% confidence limit is 1.9(-7) ~~and the upper 95% confidence limit is 1.9(-7)~~ and the upper 95% confidence limit is 1.2(-4).

SUBSYSTEM		EQUIVALENT FAILURES	EQUIVALENT TESTS	MLE OF RELIABILITY
A 1		1.3678	163.30	0.9916
MIN 12		0.4837	14.60	0.9669
O 13		0.2489	17.80	0.9860
14		0.0786	169.72	0.9995
16	II	1.4428	163.30	0.9912
B 2		0.8107	35.70	0.9773
F 6		0.3735	35.70	0.9895
G 7		0.3699	35.70	0.9896
I 8		0.2782	55.70	0.9950
J 9		0.1760	35.70	0.9951
17	III	1.8718	35.70	0.9476
15	II par III	0.6608	1426.54	0.9995
C 3	IV	1.1048	131.90	0.9916
D 4		0.8084	33.30	0.9757
K 10		0.2987	59.60	0.9950
L 11		0.1642	33.30	0.9951
19	V	1.1306	33.30	0.9660
18	IV par V	0.4062	1428.38	0.9997
0		1.2089	426.54	0.9992

Current system description is:

```
(0*e1(15+(16*(1*a2b2c2c2g2j1)(14+(12*a5a5a6b4b4b4b4ce2e2e2f1f1g5j4j414o2ptu1
(13*a7a7b5b5c3e3e3e3f2g4j5j515o3)))(17*(2*a1b1deeeeeeeefg1g1j1ou)
(6*ab1c1g1j)(7*ab1g1j)(8*a3b1j11o1)(9*a1b1eeejk)))(18+(3*a8b3c4c4g3j3)
(19*(4*a9bd1e4e4e4e4e4e4e4f3ggj212o4u2)(10*a4bj213o5)(11*a9be4e4e4j2k))))
```

COMPONENT	FAILURES	TESTS	Test factor - see Table A4
a	0.3406	103.20	
a1	0.1135	103.20	3
a2	0.4653	423.00	3
a3	0.0106	105.60	33
a4	0.0106	105.60	33
a5	0.0317	28.80	3
a6	0.0950	28.80	
a7	0.0409	37.20	3
a8	0.3340	303.60	3
a9	0.1162	105.60	3
b	0.1192	59.60	
b1	0.1114	55.70	
b2	0.5990	299.50	
b3	0.4024	201.20	
b4	0.0348	17.40	
b5	0.0726	36.30	
c	0.0022	21.80	
c1	0.0176	175.70	
c2	0.0278	278.10	
c3	0.0027	27.20	

Figure 3. Output from Maximus Method Code for B(1.2)D_1C Sequence

Press return to continue

c4	1.0609	10609.00	
d	0.1928	35.70	
d1	0.1798	33.30	
e	0.0036	35.70	
e1	2.1133	21133.00	
e2	0.0016	16.00	
e3	0.0020	20.00	
e4	0.0033	33.30	
f	2.1672	21671.50	
f1	0.0016	15.90	
f2	0.0019	19.20	
f3	0.0278	277.50	
g	0.1365	33.30	
g1	0.1464	35.70	
g2	0.6695	163.30	
g3	0.5408	131.90	
g4	0.0730	17.80	
g5	0.0599	14.60	
j	0.1189	118.90	
j1	0.6434	643.40	

Press return to continue

j2	0.1223	122.30	
j3	0.4191	419.10	
j4	0.0378	37.80	
j5	0.0520	50.20	
k	1.1000	2037.00	
l	0.9675	261.50	
l1	0.4396	261.36	2.2
l2	0.5206	140.70	
l3	0.2394	140.80	2.2
l4	0.0167	16.65	3.7
l5	0.0203	20.35	3.7
o	1.3370	3109.40	
o1	0.6856	3109.30	1.95
o2	0.0041	18.53	1.95
o3	0.0045	22.58	2.15
o4	0.1115	259.20	
o5	0.0571	259.20	1.95
p	2.2000	2200.00	
t	0.3680	46.00	
u	0.0435	217.40	9

Press return to continue

u1	0.0036	18.00	9
u2	0.3229	179.40	
v	2.1990	733.00	

Figure 3 (Continued)

The data for each of the components (events) in Figure 3 result from the unpooling process. The algorithm used for unpooling is presented in the Appendix.

Case 2. Recovery Added

Some of the failure events in D_1C can be "recovered," or corrected, thus preventing the sequence from progressing to core melt. Thus, it is more "realistic" to incorporate recovery events and their probabilities into the models.

Of more interest than whether a given sequence, such as $B(1.2)D_1C$, occurs is the case that it occurs and is not recovered from, thus leading to a severe consequence such as core melt. Case 2 considers the event of the accident sequence occurring and no recovery taking place. In probabilistic notation, the parameter of interest is written as follows:

$$Pr(B(1.2)D_1C \text{ and no recovery}) = Pr(\text{no recovery}|B(1.2)D_1C) \cdot Pr(B(1.2)D_1C) ,$$

where $Pr(A|B)$ denotes the conditional probability of A when B is known to have occurred. For uncertainty analysis, if $Pr(\text{no recovery}|B(1.2)D_1C)$ was considered to be a known constant, then the effective number of tests (or effective time) derived for the uncertainty analysis of $Pr(B(1.2)D_1C)$ would be divided by the value of $Pr(\text{no recovery}|B(1.2)D_1C)$ to give the effective test size for the estimate of $Pr(B(1.2)D_1C \text{ and no recovery})$. Because estimated recovery probabilities will most likely be subjective in nature (i.e., not directly data based) and the uncertainty in recovery factors will be treated by an interval analysis, $Pr(\text{no recovery}|B(1.2)D_1C)$ is treated as being constant. Its value is calculated by the ratio, $Pr(B(1.2)D_1C \text{ and no recovery})/Pr(B(1.2)D_1C)$.

The conditional probability of no-recovery for $B(1.2)D_1C$ in reference 1 was calculated to be .22. This value was arrived at by calculating the probability of nonrecovery for each subtree and then taking the probability of nonrecovery for a cut set to be the minimum probability of nonrecovery amongst the subtrees represented in the cut set. This is the procedure that would be followed on the original fault tree instead of on the cut sets from the independent subtrees.

Using the value of .22 for the probability of nonrecovery and the effective data of 1.31 failures in 1,430 tests from case 1, we get that the uncertainty bounds for the estimate of D_1C, considering recovery would be based on 1.31 failures in 1430/.22 = 6500 tests. If the initiating event rate is included in the analysis as having a value of .02, then the uncertainty bounds are based on 1.3 failures in 324,000 reactor years. In this case, the lower and upper 95% confidence bounds are given by 3.7(-7) and 1.6(-5), respectively.

If the initiating event rate is considered as 2 occurrences in 100 reactor years, then the uncertainty bounds are based on .61 failures in 151,000 reactor years and the confidence limits are given by 4.1(-8) for the lower 95% limit and 2.7(-5) for the upper 95% confidence limit.

The recovery model is such that for any given minimal cut set the probability of nonrecovery is the minimum of the probabilities of nonrecovery amongst the individual terms of the cut set. For the D_1C sequence, as approximated by the system of Figure 2, the nonrecovery for subtrees A, C, and E are 1. Therefore, a very good approximation to the probability of D_1C including recovery is obtained by modeling each of the basic events of subsystems III and V from Figure 2 as a parallel arrangement of the basic event with the event of no recovery for that basic event. The uncertainty analysis in this case is easily accomplished by altering the test quantities for those events in III and V by dividing the old test quantities by the probability of nonrecovery for that event. This was done with the data in Figure 3. The effective test quantity for the parallel arrangement of II with III (from Figure 2) was 7690 and that from the parallel arrangement of IV with V was 5790. These were derived without re-unpooling the data for the new system. If the unpooling algorithm was followed specific to the new model, the effective test quantity would be greater than 5790 but less than 7690. The suggested method that gives an effective test quantity of 6500 is roughly in the range that would be obtained if the Maximus methodology was rerun for the parallel-series system discussed above that closely approximates the model with recovery.

Case 3. Overall uncertainty analysis amongst subjective- and data-based estimates

Cases 1 and 2 provide the bases for calculating uncertainty intervals when some of the estimates are subjective and some are data based. In this section, they are combined to demonstrate a complete analysis using the Maximus methodology combined with other features of the guidelines (Reference 2). For this example, five of the population types from the analysis of case 1 were chosen randomly to be considered as subjective estimates. The data types chosen to be subjective were those labeled a, f, j, ℓ, and o in Table A3.

The set up and recommended display for uncertainty analysis contained in the Guidelines (Reference 2) is briefly reviewed. Assume the parameter of interest, Prob(B(1.2)D_1C and no recovery), is expressed as a function, $f(\underline{\theta}, \underline{\omega})$, where $\underline{\omega}$ is a vector of parameters subjectively estimated and $\underline{\theta}$ is a vector of parameters for which data are available for estimation purposes. In the present example, $\underline{\omega}$ contains not only the parameters from population types labeled a, f, j, ℓ, and o, but also all recovery factors.

We define $\eta_\ell(\underline{\omega})$ and $\eta_u(\underline{\omega})$ to be the lower and upper 95% statistical confidence limits based on $\underline{\theta}$ evaluated at a specific $\underline{\omega}$. With this notation, the quantities of interest for an uncertainty display are the overall extremes,

$$L = \min_{\underline{\omega}} \eta_\ell(\underline{\omega}) \ , \qquad U = \max_{\underline{\omega}} \eta_u(\underline{\omega}) \ ,$$

the differences in point estimates over the range of subjectively determined estimates,

$$\min_{\underline{\omega}} f(\underline{\theta}^*, \underline{\omega}) \quad \text{and} \quad \max_{\underline{\omega}} f(\underline{\theta}^*, \underline{\omega}) ,$$

where $\underline{\theta}^*$ represents the point estimates from the data. Also of interest are the data uncertainty interval at the nominal subjective points,

$$\eta_\ell(\underline{\omega}^*) \quad \text{and} \quad \eta_u(\underline{\omega}^*) ,$$

and, of course, the overall nominal assessment, $f(\underline{\theta}^*, \underline{\omega}^*)$.

The basis for calculating the lower and upper bounds using the Maximus methodology has been given in cases 1 and 2. For the purposes of this example, the probability of nonrecovery factors (n) are taken to range over $(n/2, 2 \cdot n)$ unless $2n > 1$ in which case the upper limit is 1. The other subjectively determined types are assumed to range over $(p/EF, p \cdot EF)$, where p is the nominal point estimate and EF is the error factor given for that population type. The recovery factors are given in Table A2, taken from the ANO report (Reference 1).

Since $f(\underline{\theta}, \underline{\omega})$ is an increasing function with respect to each component of the vector $\underline{\omega}$, the minimum and maximum of $f(\underline{\theta}^*, \underline{\omega})$ is easily calculated by substituting the minimums for all the components of $\underline{\omega}$. Thus, all the events of types a, f, j, ℓ, and o are evaluated at their point estimate divided by the error factor and all the probabilities of nonrecovery are halved. For example, consider the subtree labeled A. Subtree A has 6 events (See Table A2) of which the events LPI6164-BOO-LF and 6164B-CBL-LF are considered as subjectively determined, and, therefore, lower estimates for them are taken to be (1E-3)/3 and (1.1E-3)/3. The lower estimate for subtree A then becomes 7.0(-3). The probability of nonrecovery is taken to be .5 for the lower bound analysis since the original probability of nonrecovery was taken to be 1 (see footnote in Table A2).

When the Maximus methodology is applied in order to calculate $\min_{\omega} \eta_\ell(\underline{\omega})$, the approach of cases 1 and 2 are used where the subjectively determined estimates have been evaluated at their lower points. Thus, subtree A would be modeled as having 4 events for which data are available, but the point estimate for the subtree would be taken to be 7(-3), thus reflecting the impact of the subjectively determined estimates. This can be done because the Lindstrom-Madden method for determining effective test quantities depends only on the number of tests in the components. The effective failures is then determined by the point estimate times the effective test quantity.

Table 1 presents the results of such an analysis. These results are also graphically presented in Figure 4. It is worthwhile here to discuss the interpretation of the display in Figure 4. The nominal point estimate is represented by the slash in the box. The overall uncertainty (allowing the subjectively based paramaeter estimates to be anywhere in their range, combined with 95% statistical confidence bounds on the data-based estimates) is represented by the end marks. If the uncertainty surrounding the data-based estimates were eliminated, the total uncertainty interval would shrink down to the endpoints of the box. If the ranges (uncertainty) around the subjectively determined estimates were eliminated, leaving only the data-based uncertainty, the interval would be given by the "*s".

The incorporation of the estimate for the initiating rate in the uncertainty analysis is just as it was in the previous cases. Table 2 and Figure 5 reflect the total uncertainty on the estimate of the occurrence rate for $B(1.2)D_1C$ including recovery.

Summary

The purpose of this exercise was to demonstrate the feasibility of using the Maximus methodology for calculating statistical confidence bounds for fault tree sequences. The analysis was done incorporating all the factors that will be present in applying the methodology to the La Salle PRA. These factors include a mixture of subjectively-based and data-based estimates and recovery factors, including uncertainty in the recovery factors. When compared to the uncertainty interval generated by placing distributions on all parameters and performing a Monte Carlo analysis, the Maximus methodology produced an upper 95% confidence limit that was in the same range (perhaps a little smaller). An exact comparison is difficult because of the practice of converting uncertainty analysis results to error factors.

In the process of applying the Maximus methodology, an algorithm was developed for the unpooling of data used to estimate several parameters. The unpooling of the data is accomplished in a manner as not to be overly conservative. The algorithm is presented in the appendix. The existing Maximus code was altered during this exercise so there would be no absolute constraints on the size of the system or the number of components (units) that could be input to the Maximus method program.

The Maximus methodology applies to parallel-series configurations. For systems that are more general than parallel-series, the Maximus methodology can be used with some modifications. However, the closer the configuration from the fault tree is to a parallel-series arrangment, the easier it is to implement the Maximus method. For this reason, the expression of the sequences in terms of independent subtrees greatly facilitates the implementation.

Table 1. Combination of Subjective- and Data-Based Uncertainties for Estimate of Probability of D_1C

	Without Recovery	Prob. of Nonrecovery	With Recovery
Nominal point	9.2(-4)	.22	2.0(-4)
$\min_{\omega} f(\underline{\theta}^*, \underline{\omega})$	6.1(-4)	.14	8.5(-5)
$\max_{\omega} f(\underline{\theta}^*, \omega)$	2.3(-3)	.22	5.2(-4)
$\eta_\ell(\omega^*)$	8.3(-5)	.22	1.8(-5)
$\eta_u(\omega^*)$	3.7(-3)	.22	8.1(-4)
based on	1.3 failures/ 1420 tests		1.3 failures/ 6450 tests
L	3.5(-5)	.14	4.8(-6)
based on	1.04 failures/ 1690 tests		1.04 failures/ 12200 tests
U	6.9(-3)	.22	1.5(-3)
based on	2.3 failures/ 980 tests		2.3 failures/ 4450 tests

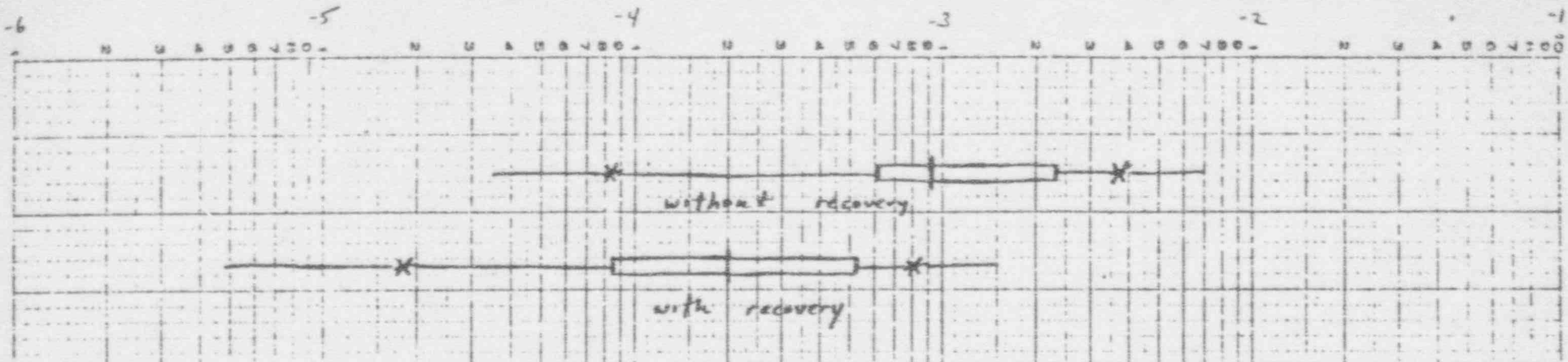

Figure 4. Uncertainty presentation for the D,C sequence.

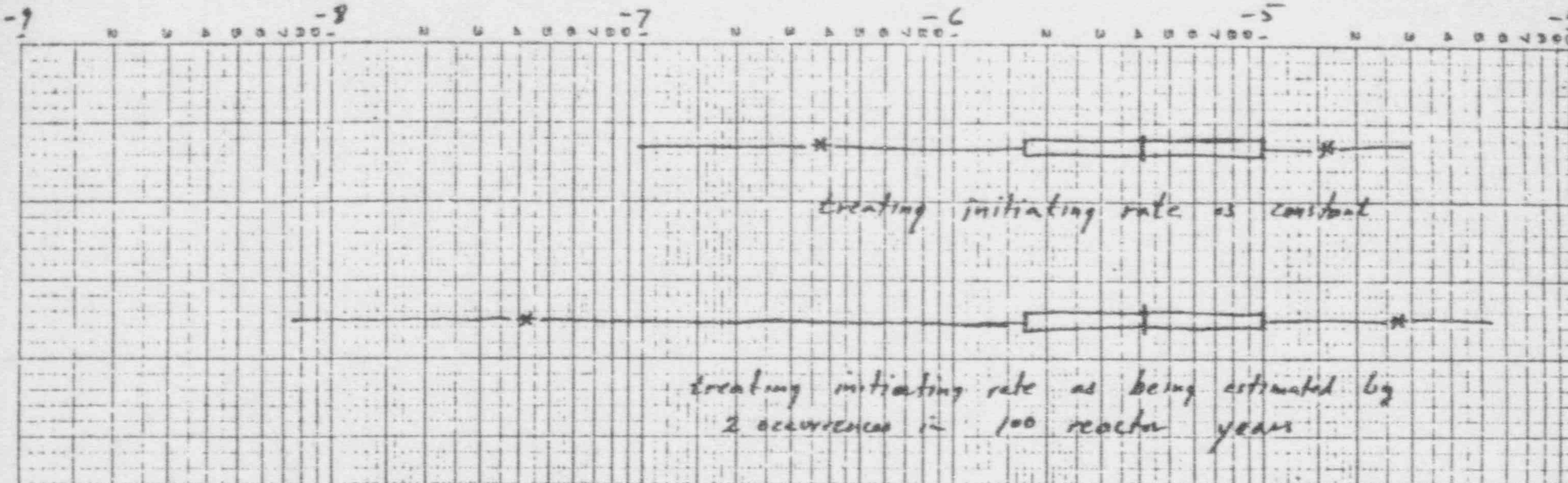

Figure 5.

Total uncertainty presentation for $B(1.2)D_2C$, (including recovery).

APPENDIX

Data

Table A1 is representation of $B(1.2)D_1C$ in terms of independent subtrees that is given in reference 1. The subtrees are labeled A-O to correspond with the labeling in this paper. Table A2 contains the individual elements that comprise the independent subtrees. Added to the tables are small letter designators (e.g., a, b, v, etc.) for population types. Thus, all events labeled a are considered to be estimated from the same data. In Table A3, the population types are enumerated, with the assumed data also given.

Those population types marked with '*' in Table A3 contain events with different point estimates. A listing of the different point estimates and the resulting T factors are given in Table A4. The T factors are necessary to adjust the equivalent test quantity in the unpooling process. For example, the 206 tests on population type u would be used to estimate a , but in two cases, the parameter applied in the model is /9. When the 206 tests are apportioned between the occurrence of λ and the two occurrences of $\lambda/9$, those quantities used for estimating $\lambda/9$ are increased by a factor of 9. This adjustment properly accounts for the data being used to estimate $\lambda/9$ rather than λ.

Table A1. LOCA Accident Sequence Cut Sets or $B(1.2)D_1C$

Initiating Event: B(1.2)   Initiating Event Frequency: .02/yr

Sequence Identifier: $B(1.2)D_1C$ (Sequence 26 on B(1.2) Event Tree, Figure A-1)

Total Sequence: $B(1.2)\bar{K}\bar{D}_1\bar{Y}C$

	Unavailability	Frequency
Sequence (without recovery)	1.E-3	2.E-5/yr
Sequence (with recovery)	2.2E-4	4.4E-6

Dominant Minimal Cut Sets	Unavailability w/o Recovery	Probability of Non-Recovery	Unavailability w/Recovery
(A) LPI1408B-VCC-LF*LF-SWS-VCH4B (B)	1.9E-4	.01	1.9E-6
(C) LPI1407A-VCC-LF*LF-SWS-VCK4A (D)	1.9E-4	.01	1.9E-6
(E) LF-LPI-L25	1E-4	1.	1E-4
(A) LPI1408B-VCC-LF*LF-SWS-S14 (F)	8.2E-5	.01	8.2E-7
(A) LPI1408B-VCC-LF*LF-SWS-S5 (G)	8.2E-5	.01	8.2E-7
(C) LPI1407A-VCC-LF*LPI1408B-VCC-LF (A)	6.7E-5	1.	6.7E-5
(A) LPI1408B-VCC-LF*LF-SWS-S2 (I)	4.1E-5	.05	2.1E-6
(A) LPI1408B-VCC-LF*LF-ECS-ROOM100 (J)	4.1E-5	.01	4.1E-7
(C) LPI1407A-VCC-LF*LF-SWS-S1 (K)	4.1E-5	.4	1.6E-5
(C) LPI1407A-VCC-LF*LF-ECS-ROOM99 (L)	4.1E-5	.01	4.1E-7
(M+N) (LF-RBI-B1+LF-RBI-B9) *LF-HPI-H14 (O) *LF-SWS-VCH4B (B)	1.1E-5	.01	1.1E-7

Table A2

Pipe (or Wire) Segment Local Fault: LPI1408B-VCC-LF (A)

System: Low Pressure

Sequence Considered: All denoting D_3, D_2, D_1, or C

Critical Time: 15 minutes*

Unavailability w/o Recovery: 8.4E-3

Unavailability w/ Recovery: 1.9E-3

Probability of Non-Recovery: 0.23

Sub-Event Name (See Appendix B)	Is it Recoverable?	Location of Recovery Action	q, w/o Rec.	P(NR)	q, w/ Rec.	Comments
LPI1408B-VCC-LF	Y	Local	g 4.1E-3	.25	1.1E-3	4E-3 recoverable, 1E-4 is not
LPI6164-BOO-LF	Y	Local	j 1E-3	.25	2.5E-4	
LPI6164-BOO-CC	Y	Control Room	b 2E-3	.1	2E-4	
6164B-CBL-LF	Y	Local	a 1.1E-3	.25	2.8E-4	
A-LPI-5	--	--	ε	--	ε	
A-LPI-7	--	--	ε	--	ε	
ESFU207-UCT-LF	Y	Control Room	c 1E-4	.1	1E-5	
ESFU232-UCT-LF	Y	Control Room	c 1E-4	.1	1E-5	

*For D_3 and D_1, the critical time is <5 min., and P(NR) for them is 1.0. Loss of suction to the HP pumps will fail them is less than 5 minutes.

Table A2
(Continued)

Pipe (or Wire) Segment Local Fault: LF-SWS-VCH4B (B)

System: Emergency Cooling

Sequence Considered: All denoting fault

Critical Time: > 70 minutes

Unavailability w/o Recovery: 2.3E-2

Unavailability w/Recovery: 2.3E-4

Probability of Non-Recovery: 0.01

Sub-Event Name (See Appendix B)	Is it Recoverable?	Location of Recovery Action	q, w/o Rec.	P(NR)	q, w/ Rec.	Comments
ECSCH4BA-CKV-LF	Y	Local	l 3.7E-3	.01	3.7E-5	For all, recovery
5254A-CBL-LF	Y	Local	a 1.1E-3	.01	1.1E-5	action is to
ECS5254A-BOO-LF	Y	Local	j 1E-3	.01	1E-5	manually start
ECS5254A-BOO-CC	Y	Local	b 2E-3	.01	2E-5	portable fans.
ECS5254A-B-AASF	Y	Local	d 5.4E-3	.01	5.4E-5	
A-ECS-2	Y	Local	o 4.3E-~~3~~4	.01	4.3E-~~8~~6	
A-ECS-15	-	---	ε	---	ε	
SWS608BX-XOC-LF	Y	Local	e 1E-4	.01	1E-6	
SWS3900X-XOC-LF	Y	Local	e 1E-4	.01	1E-6	
SWS606BX-XOC-LF	Y	Local	e 1E-4	.01	1E-6	
SWS3902X-XOC-LF	Y	Local	e 1E-4	.01	1E-6	
ECS602BX-XOC-LF	Y	Local	e 1E-4	.01	1E-6	
ECS604BX-~~X~~OC-LF (CC)	Y	Local	e 1E-4	.01	1E-6	
ECS601BX-XOC-LF	Y	Local	f 1E-4	.01	1E-6	
ECS6036A-DPC-LF (ECS6036A-BPC-LF)	Y	Local	g 4.1E-3 (4.1E-3)	.01	4.1E-5	
ECS600BX-XOC-LF	Y	Local	g e 1E-4	.01	1E-6	
R-HCP-VCH4B-2	Y	Local	u 2E-4	.01	2E-6	
ECS200BX-XOC-LF	Y	Local	e 1E-4	.01	1E-6	

Table A2
(Continued)

Pipe (or Wire) Segment Local Fault: LPI1407A-VCC-LF (C) System: Low Pressure

Sequence Considered: All denoting D_3, D_2, D_1, or C Critical Time: 15 minutes*

Unavailability w/o Recovery: 8.4E-3 Unavailability w/ Recovery: 1.9E-3

Probability of Non-Recovery: 0.23

Sub-Event Name (See Appendix B)	Is it Recoverable?	Location of Recovery Action	q, w/o Rec.	P(NR)	q, w/ Rec.	Comments
LPI1407A-VCC-LF	Y	Local	g 4.1E-3	.25	1.1E-3	4E-3 recoverable, 1E-4 is not
LPI5164A-BOO-LF	Y	Local	j 1E-3	.25	2.5E-4	
LPI5164A-BOO-LF CC?	Y	Control Room	b 2E-3	.1	2E-4	
5164A-CBL-LF	Y	Local	a 1.1E-3	.25	2.8E-4	
A-LPI-14	--	--	ϵ	--	ϵ	
A-LPI-12	--	--	ϵ	--	ϵ	
ESFU106-UCT-LF	Y	Control Room	c 1E-4	.1	1E-5	
ESFU132-UCT-LF	Y	Control Room	c 1E-4	.1	1E-5	

*For D_3 and D_1, the critical time is <5 min, and the P(NR) for them is 1.0. Loss of suction to the HP pumps will fail them in less than 5 minutes.

Table A2
(Continued)

Pipe (or Wire) Segment Local Fault: LF-SWS-VCH4A (D)

System: Emergency Cooling

Sequence Considered: All denoting fault

Critical Time: > 70 minutes

Unavailability w/o Recovery: 2.5E-2

Unavailability w/Recovery: 2.5E-4

Probability of Non-Recovery: 0.01

Sub-Event Name (See Appendix B)	Is it Recoverable?	Location of Recovery Action	q, w/o Rec.	P(NR)	q, w/ Rec.	Comments
ECSCH4AB-CWU-LF	Y	Local	ℓ 3.7E-3	.01	3.7E-5	For all, recovery action is to manually start portable fans.
6254B-CBL-LF	Y	Local	a 1.1E-3	.01	1.1E-5	
ECS6254B-B-AASF	Y	Local	d 5.4E-3	.01	5.4E-5	
ECS6254B-BOO-LF	Y	Local	j 1E-3	.01	1E-5	
ECS6254B-BOO-CC	Y	Local	b 2E-3	.01	2E-5	
A-ECS-3	Y	Local	o 4.3E-4	.01	4.3E-6	
R-HCP-VCH4A-3	Y	Local	u 1.8E-3	.01	1.8E-5	
ECS602AX-XOC-F	Y	Local	e 1E-4	.01	1E-6	
ECS604AX-CCC-LF	Y	Local	f 1E-4	.01	1E-6	
ECS601AX-XOC-LF	Y	Local	e 1E-4	.01	1E-6	
ECS6034B-DPC-LF	Y	Local	g 4.1E-3	.01	4.1E-5	
A-ECS-14	–	---	ε	--	ε	
ECS600AX-XOC-LF	Y	Local	e 1E-4	.01	1E-6	
ECS6034B-BPC-LF	Y	Local	g 4.1E-3	.01	4.1E-5	
ECS200AX-XOC-LF	Y	Local	e 1E-4	.01	1E-6	
SWS608AX-XOC-LF	Y	Local	e 1E-4	.01	1E-6	
SWS3903X-XOC-LF	Y	Local	e 1E-4	.01	1E-6	
SWS606AX-XOC-LF	Y	Local	e 1E-4	.01	1E-6	
SWS3905X-XOC-LF	Y	Local	e 1E-4	.01	1E-6	

Table A2
(Continued)

Pipe (or Wire) Segment Local Fault: LF-LPI-L25 (E)

System: Low Pressure

Sequence Considered: All denoting D_1, D_2, D_3, or C

Critical Time: 15 minutes

Unavailability w/o Recovery: 1E-4

Unavailability w/ Recovery: 1E-4

Probability of Non-Recovery: 1

Sub-Event Name (See Appendix B)	Is it Recoverable?	Location of Recovery Action	q, w/o Rec.	P(NR)	q, w/ Rec.	Comments
LPIOBW1X-XOC-LF	N	--	e 1E-4	1	1E-4	

Table A2
(Continued)

Pipe (or Wire) Segment Local Fault: LF-SWS-S14 (F)

System: Service Water

Sequence Considered: All LOSP

Critical Time: 30 min

Unavailability w/o Recovery: 1E-2

Unavailability w/Recovery: 9.3E-4

Probability of Non-Recovery: 0.09

Sub-Event Name (See Appendix B)	Is it Recoverable?	Location of Recovery Action	q, w/o Rec.	P(NR)	q, w/ Rec.	Comments
SWS3820A-VOO-LF	Y	Local	g 4E-3	.1	4E-4	
5181A-CBL-LF	Y	Local	a 3.3E-3	.1	3.3E-4	
SWS-5181A-BOO-LF	Y	Local	j 1E-3	.1	1E-4	
SWS-5181A-BOO-CC	Y	Control Room	b 2E-3	.05	1E-4	
ESFU113-UCT-LF	Y	Control Room	c 1E-4	.05	5E-6	

Table A2
(Continued)

Pipe (or Wire) Segment Local Fault: LF-SWS-S5 (G) System: Service Water

Sequence Considered: All LOSP Critical Time: 30 min

Unavailability w/o Recovery: 1E-2 Unavailability w/Recovery: 9.3E-4

Probability of Non-Recovery: 0.09

Sub-Event Name (See Appendix B)	Is it Recoverable?	Location of Recovery Action	q, w/o Rec.	P(NR)	q, w/ Rec.	Comments
SWS3643A-VOO-LF	Y	Local	g 4E-3	.1	4E-4	
5653A-CBL-LF	Y	Local	a 3.3E-3	.1	3.3E-4	
SWS5653A-BOO-LF	Y	Local	j 1E-3	.1	1E-4	
SWS5653A-BOO-CC	Y	Control Room	b 2E-3	.05	1E-4	
A-SWS-14	-	---	ϵ	---	ϵ	

Table A2
(Continued)

Pipe (or Wire) Segment Local Fault: LF-SWS-S2 (I)

System: Service Water

Sequence Considered: All LOSP

Critical Time: 30 minutes

Unavailability w/o Recovery: 5E-3

Unavailability w/Recovery: 4.6E-4

Probability of Non-Recovery: 0.09

Sub-Event Name (See Appendix B)	Is it Recoverable?	Location of Recovery Action	q, w/o Rec.	P(NR)	q, w/ Rec.	Comments
SWS001BX-COC-LF	--	---	ε	---	ε	
SWS002BX-COC-LF	--	---	ε	---	ε	
A-SWS-3	N	---	o 2.2E-4	1	2.2E-4	
SWSOP4BA-PMD-LF	Y	Control Room	l 1.7E-3	.05	8.5E-5	Start standby pump is recovery action
0303-CBL-LF	Y	Control Room	a 1E-4	.05	5E-6	
SWS0303A-BOO-LF	Y	Control Room	j 1E-3	.05	5E-5	
SWS0303A-BOO-CC	Y	Control Room	b 2E-3	.05	1E-4	

Table A2

(Continued)

Pipe (or Wire) Segment Local Fault: LF-ECS-ROOM 100 (J) System: Emergency Cooling

Sequence Considered: All denoting fault Critical Time: > 70 minutes

Unavailability w/o Recovery: 4.9E-3 Unavailability w/Recovery: 4.9E-5

Probability of Non-Recovery: 0.01

Sub-Event Name (See Appendix B)	Is it Recoverable?	Location of Recovery Action	q, w/o Rec.	P(NR)	q, w/ Rec.	Comments
ECSVC2BA-FAN-LF	Y	Local	k 5.4E-4	.01	5.4E-6	For all, recovery action is to manually start portable fans.
5246A-CBL-LF	Y	Local	a 1.1E-3	.01	1.1E-5	
ECS5246A-BOO-LF	Y	Local	j 1E-3	.01	1E-5	
ECS5246A-BOO-CC	Y	Local	b 2E-3	.01	2E-5	
A-ECS-11	-	---	ϵ	---	ϵ	
ECSC41BX-XOC-LF	Y	Local	e 1E-4	.01	1E-6	
ECSC44BX-XOC-LF	Y	Local	e 1E-4	.01	1E-6	
ECSC45BX-XOC-LF	Y	Local	e 1E-4	.01	1E-6	

Table A2

(Continued)

Pipe (or Wire) Segment Local Fault: LF-SWS-S1 (K)

System: Service Water

Sequence Considered: All LOSP

Critical Time: 30 minutes

Unavailability w/o Recovery: 5E-3

Unavailability w/Recovery: 2.2E-3

Probability of Non-Recovery: 0.44

Sub-Event Name (See Appendix B)	Is it Recoverable?	Location of Recovery Action	q, w/o Rec.	P(NR)	q, w/ Rec.	Comments
SWS001CX-COC-LF	--	---	ϵ	—	ϵ	
SWS002CX-COC-LF	--	---	ϵ	--	ϵ	
A-SWS-1	N	---	o 2.2E-4	1	2.2E-4	
SWSOP4CB-PMD-LF	N	---	l 1.7E-3	1	1.7E-3	
0402-CBL-LF	N	---	a 1E-4	1	1E-4	
SWS0402B-BOO-LF	Y	Local	j 1E-3	.1	1E-4	
SWS0402B-BOO-CC	Y	Control Room	b 2E-3	.05	1E-4	

Table A2

Failure Probabilities, With Recovery, of Support System Faults

Pipe (or Wire) Segment Local Fault: LF-ECS-ROOM 99 (L)

System: Emergency Cooling

Sequence Considered: All denoting fault

Critical Time: > 70 minutes

Unavailability w/o Recovery: 4.9E-3

Unavailability w/Recovery: 4.9E-5

Probability of Non-Recovery: 0.01

Sub-Event Name (See Appendix B)	Is it Recoverable?	Location of Recovery Action	q, w/o Rec.	P(NR)	q, w/ Rec.	Comments
ECSC2DB-FAN-LF	Y	Local	k 5.4E-4	.01	5.4E-6	All subfaults are recoverable by the use of portable fans.
6246B-CBL-LF	Y	Local	a 1.1E-3	.01	1.1E-5	
ECS6246B-BOO-LF	Y	Local	j 1E-3	.01	1E-5	
ECS6246B-BOO-CC	Y	Local	b 2E-3	.01	2E-5	
A-ECS-8	-	---	ϵ	--	ϵ	
ECSC41DX-XOC-LF	Y	Local	e 1E-4	.01	1E-6	
ECSC44DX-XOC-LF	Y	Local	e 1E-4	.01	1E-6	
ECSC45DX-XOC-LF	Y	Local	e 1E-4	.01	1E-6	

Table A2

(Continued)

Pipe (or Wire) Segment Local Fault: LF-RBI-B1 + LF-RBI-B9 (M+N) System: Reactor Building Injection/Recirculation

Sequence Considered: All denoting C or F Critical Time: 70 minutes

Unavailability w/o Recovery: 3.4E-2 Unavailability w/ Recovery: 4.1E-3

Probability of Non-Recovery: 0.12

Sub-Event Name (See Appendix B)	Is it Recoverable?	Location of Recovery Action	q, w/o Rec.	P(NR)	q, w/ Rec.	Comments
2400B-VCC-LF	Y	Local	g 4.1E-3	.1	5E-4	Crit Time = 30 min, 4E-3 recoverable, 1E-4 is not
6171X-CBL-LF	Y	Local	a 3.3E-3	.1	3.3E-4	
6171X-B00-LF	Y	Local	j 1E-3	.1	1E-4	
6171X-B00-CC	Y	Control Room	b 2E-3	.05	1E-4	
A-RBI-5	--	--	ε	--	ε	
A-1104.05-0	Y	Local	p 1E-3	.03	3E-5	

Table A2

(Continued)

Pipe (or Wire) Segment Local Fault: LF-RBI-B1 + LF-RBI-B9 (Cont.) (M+N) System:

Sequence Considered: Critical Time:

Unavailability w/o Recovery: Unavailability w/ Recovery:

Probability of Non-Recovery:

Sub-Event Name (See Appendix B)	Is it Recoverable?	Location of Recovery Action	q, w/o Rec.	P(NR)	q, w/ Rec.	Comments
BS48X-CCC-LF	N	--	f 1E-4	1	1E-4	
BW6BX-CCC-LF	N	--	f 1E-4	1	1E-4	
A-RBI-1	N	--	o 2.2E-4	1	2.2E-4	
BS1BX-XOC-LF	N	--	e 1E-4	1	1E-4	
BW5BX-XOC-LF	N	--	e 1E-4	1	1E-4	
0404X-CBL-LF	N	--	a 1.1E-3	1	1.1E-3	
0035B-PMD-LF	N	--	l 1E-3	1	1E-3	
021BX-XOC-LF	N	--	e 1E-4	1	1E-4	
3805B-NCC-LF	Y	Local	v 3E-3	.01	3E-5	Crit Time > 70 min

Table A2

(Continued)

Pipe (or Wire) Segment Local Fault: LF-RBI-B1 + LF-RBI-B9 (Cont.) (M+N) System:

Sequence Considered: Critical Time:

Unavailability w/o Recovery: Unavailability w/ Recovery:

Probability of Non-Recovery:

Sub-Event Name (See Appendix B)	Is it Recoverable?	Location of Recovery Action	q, w/o Rec.	P(NR)	q, w/ Rec.	Comments
3805B-NCC-CC	Y	Control Room	b 2E-3	.01	2E-5	Crit Time > 70 min
0404B-BOO-LF	Y	Local	j 1E-3	.03	3E-5	
0404B-BOO-CC	Y	Control Room	b 2E-3	.01	2E-5	
U239-UCT-LF	Y	Control Room	c 1E-4	.01	1E-6	
R-HCP-021B-8	Y	Local	u 2E-4	.01	2E-6	Crit Time > 70 min
R-110405-5-21B	Y	Local	t 8E-3	.01	8E-5	Crit Time > 70 min
2B32B-CBL-LF	Y	Local	a 1.1E-3	.03	3.3E-5	
SWS2B32B-BOO-CC	Y	Control Room	b 2E-3	.01	2E-5	
Y02-120-LF	N	--		--		
IEA06BB-TFM-LF	N	--		--		

Table A2

(Continued)

Pipe (or Wire) Segment Local Fault: LF-RBI-B1 + LF-RBI-B9 (Cont.) (M+N) System:

Sequence Considered: Critical Time:

Unavailability w/o Recovery: Unavailability w/ Recovery:

Probability of Non-Recovery:

Sub-Event Name (See Appendix B)	Is it Recoverable?	Location of Recovery Action	q, w/o Rec.	P(NR)	q, w/ Rec.	Comments
IEA6143BB-CBL-LF	N	--	ε	--	ε	
IEA052BB-BCO-LF	Y	--	ε	--	ε	
IEA6193BB-BCO-LF	Y	--	ε	--	ε	

Table A2

(Continued)

Pipe (or Wire) Segment Local Fault: LF-HPI-H14 (o)

System: High Pressure

Sequence Considered: All denoting D_3, D_1, or H_1

Critical Time: 60 minutes

Unavailability w/o Recovery: 1.4E-2

Unavailability w/ Recovery: 3.2E-3

Probability of Non-Recovery: 0.23

Sub-Event Name (See Appendix B)	Is it Recoverable?	Location of Recovery Action	q, w/o Rec.	P(NR)	q, w/ Rec.	Comments
HPIV19CX-CCC-LF	N	--	f 1E-4	1	1E-4	
HPIV20CX-XOC	N	--	e 1E-4	1	1E-4	
A-HPI-4	N	--	o 2E-4	1	2E-4	
A-HPI-5	--	--	ε	--	ε	
A-HPI-6	--	--	ε	--	ε	
HPIV18CX-XOC-LF	N	--	ε 1E-4	1	1E-4	
HPIP36CB-PMD-LF	N	--	ℓ 1E-3	1	1E-3	
A406B-CBL-LF	N	--	a 1.1E-3	1	1.1E-3	
HPIA406B-BOO-LF	Y	Local	j 1E-3	.05	5E-5	
HPIA406B-BOO-CC	Y	Control Room	b 2E-3	.03	6E-5	

Table A2

(Continued)

Pipe (or Wire) Segment Local Fault: LF-HPI-H14 (Cont.) (o)

System:

Sequence Considered:

Critical Time:

Unavailability w/o Recovery:

Unavailability w/ Recovery:

Probability of Non-Recovery:

Sub-Event Name (See Appendix B)	Is it Recoverable?	Location of Recovery Action	q, w/o Rec.	P(NR)	q, w/ Rec.	Comments
ESFU201-UCT-LF	Y	Control Room	c 1E-4	.03	3E-5	
SWS018CX-XOC-LF	N	--	e 1E-4	1	1E-4	
6214B-CBL-LF	Y	Local	a 1.1E-3	.03	3.3E-5	Recovery time is 60 minutes for rest of sub-events
SWS6214B-BOO-LF	Y	Local	j 1E-3	.03	3E-5	
SWS6214B-BOO-CC	Y	Control Room	b 2E-3	.01	2E-5	
SWS3810B-VCC-LF	Y	Local	g 4.1E-3	.03	1.3E-4	4E-3 recoverable, 1E-4 is not

Table A3. "Population Type" Data

Pop. Type	File No.	Point Estimate	Error Factor	Equiv. Failures	Equiv. Tests	Total Number of Occurrences	Blocks (# Occurrences)
*a	1	3.3(-3)	3	2.20	667	15	A,B,C,D,F,G,I,J,K,L,M+N(3),O(2)
b	2	2.0(-3)	3	2.20	1100	16	A,B,C,D,F,G,I,J,K,L,M+N(4),O(2)
c	3	1.0(-4)	3	2.20	22000	7	A(2),C(2),F,M+N,O
d	4	5.4(-3)	10	.37	69	2	B,D
e	5	1.0(-4)	3	2.20	22000	29	B(8),D(8),E,J(3),L(3),M+N(3),O(3)
f	6	1.0(-4)	3	2.20	22000	5	B,D,M+N(2),O
g	8	4.1(-3)	3	2.20	537	10	A,B(2),C,D(2),F,G,M+N,O
j	11	1.0(-3)	3	2.20	2200	14	A,B,C,D,F,G,I,J,K,L,M+N(2),O(2)
k	12	5.4(-4)	3	2.20	4074	2	J,L
*l	13	3.7(-3)	3	2.20	595	6	B,D,I,K,M+N,O
*o	26	4.3(-4)	3	2.20	5116	6	B,D,I,K,M+N,O
p	28	1.0(-3)	3	2.20	2200	1	M+N
t	40	8.0(-3)	10	.37	46	1	M+N
*u	41	1.8(-3)	10	.37	206	3	B,D,M+N
v	47	3.0(-3)	3	2.20	733	1	M+N

* These types have individual point estimates within the type that differ.
See Table A4 for applicable adjustment factors.

Table A4. Population Types With Mixed Point Estimates With Appropriate Test Factors

	Point Estimates--Blocks of Occurrence		
Pop. Type	Base	Other	T Factor
a	3.3(-3) F,G,M+N	1.1(-3) A,B,C,D,J,L,M+N(2),O(2)	3
		1(-4) I,K	33
	3.7(-3) B,D	1.7(-3) I,K	2.2
		1(-3) M+N,O	3.7
o	4.3(-4) B,D	2.2(-4) I,K,M+N	1.95
		2(-4) O	2.15
u	1.8(-3) D	2(-4) B,M+N	9

Unpooling Algorithm

The proposed unpooling scheme unpools each of the data-type populations, compares the test quantities that result to the existing unpooled types, makes adjustments in the current type if necessary, and then moves to the next data type. The process is elaborated on here and illustrated using the D_1C sequence and data from the main report.

Step 1. The system under consideration is broken into series subsystems for which an equivalent test quantity will be recorded and updated with the addition of each population type. Initially, the equivalent test quantity for each subsystem is treated as missing or unassigned. Also calculated at this step is the failure probability for each subsystem. Three values will be used for unpooling purposes.

Example. For the $B(1.2)D_1C$ sequence, the system to be considered is given in Figure A1. The blocks are labeled with the leading block label used in the body of the report.

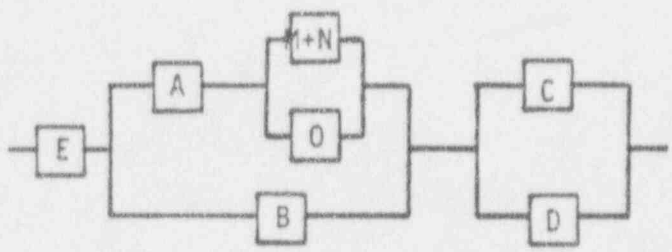

Point Estimates

A - 8.38(-3)
B - 5.24(-2)
C - 8.38(-3)
D - 3.40(-2)
E - 1.00(-4)
M+N - 3.31(-2)
O - 1.39(-2)

B includes B,F,G,I,J from Figure 2
D includes D,K,L from Figure 2

Figure A1. Overall system in terms of branches for which equivalent test quantities are needed.

Step 2. All data types that appear only once in the total system are assigned and the minimum test quantity for each segment is recorded.

Example. Population types p, t, and v occur singly, all in the M+N branch. Therefore, branch M+N now has a minimum test quantity of 46 from the component of type t.

Step 3. All the data types that have more than one occurrence are ordered according to the number of tests divided by the sum of the reciprocals of the T factors for each occurrence. This represents the quantity that will apply to each occurrence of a population type if a split is done to make each occurrence have the same amount of applicable data. This ordering will be used for purposes of unpooling.

Example. For the $B(1.2)D_1C$ sequence, the ordering is d, g, b, a, u, j, [illegible], e, o, k, c, and f. Population type d is considered first as there are, in general, less "data" for each of the occurrences (69/2 = [illegible]5). Population type g is next with approximately (537/10 = 53.7 test quantities that can be assigned to each occurrence. Notice that for type a, [illegible] of the unpooled values will be times a factor of 3, 2 will be times a factor of 33, and 3 will be at the base value (factor of 1). Thus, [illegible] so that every occurrence has the same amount of data, the 667 test quantity is divided by $10 \cdot 1/3 + 2 \cdot 1/33 + 3 = 6.39$, to give 104.3 tests to each occurrence.

Step 4. The individual population types are unpooled for each population type in the order determined by step 3. The unpooling is done in such a way as to maximize the effective overall test quantity incorporating the given component with the already unpooled data and the minimum test quantities that apply to each subsystem. Subsystems that have no minimum test quantities as yet assigned are treated as constants.

Example 1. Population type d is the first type to be unpooled, as determined from step 3. Only the subsystem M+N has a test quantity associated with it from the data types with a single occurrence considered in step 2. Considering the point estimate for subsystem O as a constant, the test size of 46 from M+N is equivalent to a test size of 3309 (= 46/1.39(-2)) for the system of M+N in parallel with O. The test size of 3309 would then also apply to the whole subsystem containing A, M+N, and O. If n of the 69 tests on population type d were assigned to the occurrence in subsystem B, then the equivalent test quantity for that combination would be given by 8.84(-3) x 3309 = 29.3 failures in 3309 tests combined in parallel with $5.24(-2) \cdot n$ failures in n tests. The effective test quantity for the other parallel branch is (69 - n)/8.38(-3) since subsystem C is treated as a constant. Since the effective test quantity increases with n in the first case and decreases with n in the second, the minimum of the two will be maximized when the two expressions above are equal. This occurs when n = 35.7, therefore, population type d is unpooled by considering 35.7 tests in subsystem B and 33.3 tests in subsystem D. The equivalent test quantities are now 3309 for M+N, 35.7 for B, and 33.3 for D. The rest of the subsystems would still be considered as constants (having no equivalent test quantities).

Example 2. It will be instructive to also consider the next population type g here at step 4. There are occurrences of population type g in all but subsystem E. There are single occurrences of type g in subsystems A, M+N, O, and C and there are four occurrences in subsystem B and two occurrences in subsystem D. Let n_A, n_B, ... denote the unpooled test quantity for subsystems A, B, ... The total test quantity is 537, and thus, we want to assign the test quantities such that $n_A + n_{M+N} + n_O + n_C + 4 \cdot n_B + 2 \cdot n_D = 537$, and the overall equivalent system test size is maximized. At this stage, we are not concerned with the equivalent test quantities that have already been assigned to the subsystems in which population type g appears. We perform the optimization problem for g and then compare the equivalent test quantities for g alone to those already assigned and make appropriate adjustments in step 5. The solution of the problem for allocating g is $n_A = 168.4$, $n_B = 35.4$, $n_C = 109.6$, $n_D = 42.6$, $n_{M+N} = 14.5$, and $n_O = 17.7$, with an equivalent system test size of 1450.

A specific method for solving the above problem is not being recommended. The above solution was obtained by programming the Maximus rules for parallel systems on a desk calculator and iterating intelligently to obtain the solution.

Notice in the solution for g that $n_D = 42.6$, but from the unpooling of population type d, the equivalent test size for subsystem D was 33.3. This difference forms the basis for the next step.

Step 5. If, for a specific population type in step 4, any of the equivalent tests for a subsystem exceed the equivalent test quantity already assigned to that subsystem and there is some other subsystem in which the current population type is minimum, then rework step 4, but first allocating the existing equivalent test size to those subsystems where this value was less than that calculated in step 4.

Example. In step 4 for population type g $n_D = 42.6$, which exceeds the existing test size of subsystem D of 33.3 and in all the other subsystems the assignment from type g is the minimum. Therefore, n_D is set to 33.3 and the allocation of the remaining 537 - 2(33.3) = 470.4 is done for population type g as was done originally in step 4. The result of this step is that $n_A = 163.3$, $n_B = 35.7$, $n_C = 131.9$, $n_D = 33.3$, $n_{M+N} = 14.6$, and $n_O = 17.8$. These are the values used in the overall analysis and are reflected in the allocations of Figure 3.

Step 6. Return to step 4 (and 5) for the next population type.

For all the remaining population types in the example followed, the effective numbers for each branch all exceed that assigned in determining the allocation for type g. Therefore, the combination of data types d and g determine effective quantities for each branch.

The unpooling algorithm as presented is meant to give the flavor of a systematic way to look at the unpooling question. The algorithm has not been completely defined in that the method of optimization for steps 4 and 5 is not specified. In practice, a stepwise method may be the easiest to implement. The different population types that determine the equivalent test quantities may interact to such an extent that the whole procedure would have to be reapplied. For example, in the D_1C case considered here, population types d and g are the determining population types. However, the first time through the algorithm the d population was unpooled assuming some of the subsystem branches were constant. Once population type g was unpooled, one would need to reexamine the unpooling of type d again, and so on between the two, in order to converge to an "optimal" unpooling.

In the case worked here, an equivalent system test quantity of 1427 was obtained, but it is known from g alone that 1450 is an upper bound. Thus, the iterations between population types d and g seemed unnecessary.

REFERENCES

1. Kolb, G. J.; et al., Interim Reliability Evaluation Program: Analysis of the Arkansas Nuclear One--Unit 1 Power Plant, Vol. 1 and 2, NUREG/CR-2787, SAND82-0978, Sandia National Laboratories, June 1982.

2. Methodology and Guidelines for Uncertainty and Sensitivity Analysis--Tasks 2 and 3 of PRA Methods Development Program, Division 7223, Sandia National Laboratories, 7/6/84.

3. Spencer, F. W., and Easterling, R. G., Lower Confidence Bounds on System Reliability Using Component Data: The Maximus Methodology, SAND84-1199C, Conference on Reliability and Quality Control, University of Missouri-Columbia, June, 1984.